

16th International Symposium on
District Heating and Cooling,
DHC2018, 9–12 September 2018,
Hamburg, Germany

Edited by Ingo Weidlich

Volume 149, Pages 1-642 (September 2018)



Preface

The International Symposium on District Heating and Cooling (DHC) has over the years developed into one of the most well-reputed events world-wide for the communication of academic research in the field of DHC. This Symposium has been the world's meeting place for district heating and cooling experts for more than 30 years now and has steadily been gaining greater significance, particularly in relation to the environmental challenges faced by many countries around the world. In fact, DHC has positioned itself as a vital element for a sustainable energy future. Under the wing of the International Energy Agency's research programme on District Heating and Cooling (IEA DHC), the Symposium is truly global since 2016. The Symposium presents new developments and best practices available on DHC in different countries.

In 2018, the 16th International Symposium on District Heating and Cooling is hosted by the HafenCity University Hamburg. District Heating has a strong history in Hamburg, since it was first implemented in 1893. Today the district heating network of Hamburg has a length of 812 km with 460.000 connected residential units. 8 Power plants have a district heating output of 5TWh per year. Ongoing discussion on ownership models for the district energy grids in Hamburg makes the related topics more visible to the public than in other cities. Furthermore, Hamburg is one of Germany's leading cities for innovation in district energy generation, distribution and sector coupling. Trends of the energy transition in Germany are challenging for Hamburg as well as for many other cities. These trends can be observed also worldwide.

On behalf of the ExCo and the organizers of the Symposium we want to express our sincere thanks to the members of the Scientific Committee, the Local Organizing Committee and the members of the Advisory Committee for their valuable contribution. Through a tough selection process, 66 high quality papers resulted out of the 160 submitted abstracts, and are to be presented at this Symposium and published open access in this edition of Energy Procedia. Of course we also thank the individual authors for their contribution with Abstracts, Papers and Posters and the regular participants of the Symposium.

The international and interdisciplinary approach and its quality assurance makes the Symposium a high level vibrant hub for communication and networking of DHC experts and scholars from the established and aspiring DHC-countries world-wide.

On behalf of the Executive Committee of IEADHC, the Chairman of the Scientific Committee wants to express a special thanks to all the committees, key note speakers, organizers, administrative staff and supporters for their excellent performance to make the 16th International Symposium on District Heating and Cooling a reality.

Ingo Weidlich, Guest Editor
Chairman of the Scientific Committee

Research Topics

A. Urban energy systems, planning and development

How does city planning influence the development of district heating and cooling systems and vice versa? Papers in this section explore district heating and cooling as a driving force for city planning and development including development of large or regional heat networks.

B. Resource efficiency and environmental performance

How can district heating and cooling contribute to an efficient and low carbon energy supply? Papers in this section will consider performance and environmental issues in district heating and cooling, including the integration of renewables, primary energy savings, reduction of CO₂ emissions, combined heat and power and the use of thermal storage.

C. Key elements in District Heating and Cooling systems

What are the new developments in district heating and cooling technology? Papers in this section consider steps towards the next generation of district heating and cooling. They focus on improving current district heating and cooling solutions and key elements of the technology: for example, piping systems, sub stations and metering techniques. This area includes issues regarding cost reduction, the increase of service life, demand side management and low temperature technologies.

D. Customer relations and market issues

How do customers interact with district energy companies and what is the role of the district energy customers in general? Papers in this area focus on business and infrastructure management and development. A special focus lies on how the challenges for establishing district heating and cooling in an economically viable way can be overcome.

E. Policy and regulation

What policies and regulatory framework can be deployed to assist the establishment and evolution of efficient district heating and cooling networks? How flexible is district heating and cooling to different regulatory environments? What aspects work universally and to what extent do national and regional elements affect the potential of this technology?

F. Open Arena, District Heating and Cooling

What other research can forward the success of district heating and cooling? In line with the broad and multidisciplinary approach needed to overcome the sectors challenges, the organizers offer the opportunity to submit abstracts that do not fit into the above categories but still bear relevance for a successful future of district heating and cooling.

Committees

Scientific Committee

Martin Achmus, Leibniz University of Hannover, GERMANY
Gatis Bazbauers, Riga Technical University, LATVIA
Dagnija Blumberga, Riga Technical University, LATVIA
Anatolijs Borodinecs, Riga Technical University, LATVIA
Clemens Felsmann, Technical University of Dresden, GERMANY
Lars Gullev, VEKS, DENMARK
Stefan Holler, HAWKS University, GERMANY
Heiko Huther, AGFW, GERMANY
Anton Ianakiev, Nottingham Trent University, UK
Oliver Kastner, ISFH, GERMANY
Kyung Min Kim, Korea District Heating Corp., KOREA
Bruno Lacarriere, IMT Atlantique, FRANCE
Henrik Lund, Aalborg University, DENMARK
Natasa Nord, NTNU, NORWAY
Olafur Petur Palsson, University of Iceland, ICELAND
Irene Peters, HafenCity University, GERMANY
Peter Riederer, Scientific Center CSTB, FRANCE
Rolf Ulseth, IEA – DHC, NORWAY
Dietrich Schmidt, IEE, GERMANY
Andres Siirde, Tallin University of Technology, ESTONIA
Svend Svendsen, DTU, DENMARK
Sanna Syri, Aalto University, FINLAND
Thorsten Urbaneck, Chemnitz University, GERMANY
Ingo Weidlich, HafenCity University, GERMANY
Robin Wiltshire, Heatmatters, UK
Jianjun Xia, Tsinghua University, CHINA
Nazdaneh Yarahmadi, RISE, SWEDEN

Advisory Committee

Michael Hübner, bmvit, AUSTRIA
Ralf-Roman Schmidt, Austrian Institute of Technology, AUSTRIA
Raymond Boulter, Canmet Energy Natural Resources Canada, CANADA
Lars Gullev, West Copenhagen Heating Transmission Company, DENMARK
Liu Rong, China District Heating Association, CHINA
Jianjun Xia, Tsinghua University, CHINA
Jari Kostama, Finnish Energy, FINLAND
Sihem-Tasca Guernouti, Cerema, FRANCE
Sylvie Leveaux, Cerema, FRANCE
Carsten Magass, Project Management Jülich, GERMANY
Heiko Huther, German Efficiency Association for Heating and Cooling, GERMANY
Kyung Min Kim, Korean District Heating Corp., KOREA
Heidi M. Juhler, Norsk Fjernvarme, NORWAY
Rune Volla, Research Council of Norway, NORWAY
Sofia Andersson, Swedish Energy Agency, SWEDEN

Lina Enskog Broman, Swedenergy, SWEDEN
Robin Wiltshire, Building Research Establishment, UK

Local Organization Committee

Ingo Weidlich, HafenCity University, GERMANY
Irene Peters, HafenCity University, GERMANY
Maria Grajcar, HafenCity University, GERMANY
Gersena Banushi, HafenCity University, GERMANY
Noriko Kakue, HafenCity University, GERMANY
Comfort Mosha, HafenCity University, GERMANY
Johanna Cortes, HafenCity University, GERMANY
Clarisa Mazzara, HafenCity University, GERMANY
Juliana Webel de Lima, HafenCity University, GERMANY
Abdullah Khisraw, HafenCity University, GERMANY
Lucia Doyle, HafenCity University, GERMANY



Available online at www.sciencedirect.com

ScienceDirect

Energy Procedia 149 (2018) 5–14

Energy

Procedia

www.elsevier.com/locate/procedia

16th International Symposium on District Heating and Cooling, DHC2018,
9–12 September 2018, Hamburg, Germany

Performance monitoring of rural district heating systems

Dominikus Buecker^{a,*}, Peter Jell^b, Rafael Botsch^a

^a*Hochschule Rosenheim, Hochschulstr. 1, 83024 Rosenheim, Germany*

^b*Seestrasse 31, 83254 Breitbrunn, Germany*

Abstract

The performance of six small scale district heating systems (DHS) in Upper Bavaria has been monitored over a 12 months' period with the aim to identify typical optimization potentials and to develop a standardized approach to performance monitoring. Extensive operational data were analyzed and Key Performance Indicators (KPIs) were assessed. KPIs show strong fluctuation and variation between different DHS. Main potentials were found in the control of the DHS, component sizing, and grid temperatures. Further standardization of performance monitoring is required and will be addressed in a follow-up study which was started in January 2018.

© 2018 The Authors. Published by Elsevier Ltd.

This is an open access article under the CC BY-NC-ND license (<https://creativecommons.org/licenses/by-nc-nd/4.0/>)

Selection and peer-review under responsibility of the scientific committee of the 16th International Symposium on District Heating and Cooling, DHC2018.

Keywords: performance monitoring; district heating; optimization; efficiency

* Corresponding author. Tel.: +49-8031-805-2652; fax: +49-8031-805-2688.

E-mail address: dominikus.buecker@fh-rosenheim.de

1. Introduction

The operation of district heating systems (DHS) is based on a complex interaction of different heat sources with multiple heat consumers. Many parameters need to be managed dynamically within the overall operational strategy to achieve optimum DHS performance and reliability. Prioritization of heat sources, control of main and distribution pumps, operation of heat storage systems as well as monitoring and control of the system temperatures are only a few examples for operational aspects that have a direct influence on performance of the DHS and the durability of its components. Therefore, knowledge of the dynamic behavior of the DHS and close monitoring of the key operational indicators is vital for efficient operation of the system.

In today's DHS, many operational parameters are being recorded already. However, these values provide only little insight into the operating conditions when they are analyzed separately. In addition, many parameters are recorded as accumulated or time-averaged values only. In these cases, unsatisfying annual key figures might indicate weaknesses, but may not reveal the real cause and optimization potential. Systematic and continuous processing and evaluation of recorded data and a standard operating procedure to identify weaknesses and optimization potentials are missing in most large and virtually all smaller DHS. A survey amongst the operators of the DHS participating in the present study, revealed the following main reasons for insufficient performance monitoring of small scale DHS:

- DHS have grown over time and may have changed in structure both on the heat production and heat consumption side, making operation of the DHS more and more complex
- Data acquisition may be insufficient to ensure effective monitoring of DHS operation
- Staff may be lacking to perform required data acquisition and data analysis tasks
- Know-how for data analysis may be missing
- Standard operating procedures for an effective performance monitoring may be missing

Monitoring the relevant operating parameters with a sufficient frequency and the use of standard operating procedures for analyzing the recorded operational data is key to identify optimization potentials. Subsequently, suitable measures can be developed to permanently improve the performance of the system.

In view of this, the MoNa project ("MoNa – Monitoring von Nahwärmenetzen") was initiated at the University of Applied Sciences Rosenheim in 2014. The main goal of the study was to develop a standardized approach towards performance monitoring and thus to facilitate performance monitoring of small scale DHS. Six rural district heating systems in Upper Bavaria have been investigated, monitoring their performance over a 12 months' period. To this end, a set of key performance indicators (KPI) were assembled to compare the performance of the systems and minimum requirements for measurement and data acquisition were defined to assess the KPIs.

During the monitoring period, extensive operational data were recorded using the equipment present in the DHS. The data were then validated and analyzed, the KPIs were calculated over different time intervals and further operational data were taken into account to identify further optimization potentials. These potentials were then categorized to identify typical optimization potentials of small scale rural DHS.

2. Investigated DHS

The six DHS considered in the study are located in communities of 1,000 to 20,000 inhabitants in mostly rural areas in Upper Bavaria. All DHS provide heat to a mix of residential, commercial, and sometimes public customers. Four of the DHS use wood chips as a main source of energy, three of the DHS have combined heat and power (CHP) plants. Table 1 gives an overview of essential characteristics of the investigated DHS.

Table 1. Characteristics of the investigated DHS.

DHS	Network length [km]	Installed thermal capacity [MW]	Energy sources	CHP
A	3.2	3.7	Wood chips, fuel oil	No
B	7.4	3.7	Wood chips, fuel oil	No
C	1.6	1.7	Wood chips, fuel oil, natural gas, solar heat	No
D	1.0	2.2	Wood chips, palm oil, fuel oil	Yes
E	11.4	4.0	Natural gas, biomethane, biogas, power-to-heat	Yes
F	2.8	1.5	Natural gas, biogas	Yes

3. Key performance indicators

A set of key performance indicators was assembled to assess performance of the DHS. The set includes parameters indicating efficiencies as well as criteria describing environmental impact and security of supply. The following performance indicators were assessed:

- Primary Energy Factor (PEF), indicating the ratio of primary energy used to heat delivered according to AGFW 309-1 [1],
- Efficiencies of heat distribution and heat generation,
- Heat consumption,
- Auxiliary power consumption,
- Reliability of main heat generators (in terms of hours of unplanned outages),
- Labor input (man-hours per year for operation and maintenance),
- Regional origin of energy sources (distance between sourcing and consumption of the energy sources),
- Degree of fulfilment of the German Renewable Energies Heating Act (EEWärmeG),
- CO₂ Emission.

While all of the above-mentioned criteria appear to be important for the assessment of the performance of DHS, reliable values could not be established for some of them. “Labor input”, for instance is difficult to be determined in a standardized way and values for this KPI may not be established through metering data. Other criteria, like the degree of fulfilment of the EEWärmeG may have a local importance but may not be relevant on an international scale. In the following sections, exemplary results for some of the most important KPIs will be presented, with the chosen time scale being monthly values over a 12-month period. Certainly, in future standardized monitoring campaigns, many more KPIs will be assessed in varying time scales. In this respect, this work is only a first step towards the formulation of requirements for monitoring campaigns. A larger follow-up project, “Nemo” [2], was started by the University of Applied Sciences Rosenheim and the AGFW – der Energieeffizienzverband für Wärme, Kälte und KWK e. V. (AGFW) in 2018 with the goal to establish detailed standards and requirements for performance monitoring of DHS, see also [3].

4. Measurement Requirements

In order to evaluate the KPIs and to show their fluctuations over time, metering data need to be recorded and analyzed during the monitoring campaign. The required measurement equipment has been defined by “minimum measurement requirements” including metering points, measured variables, and metering intervals.

In general, more metering points, higher metering frequencies, and higher accuracies of measurement will lead to better results in the evaluation of the DHS performance, identification of weaknesses and optimization potentials. For this reason, all available data and all existing metering points should be included in the monitoring campaign. Nevertheless, technology levels of existing DHS with respect to metering equipment vary greatly and effective monitoring is also possible with limited metering equipment. Table 2 gives an overview of the most important metering points in a monitoring campaign. Metering points which are crucial for the energy balance from heat source to grid injection are considered as “essential”. In some cases, certain metering points can be replaced by smart balancing. In addition, differential pressure gauges across the main grid and subnets, and the main electricity meter are considered essential because they are important for understanding the overall operational strategy and the consumption of auxiliary electric energy. Metering points which give important information on the performance of the DHS and its components, but which are not necessary for setting up the basic balances are considered as “recommended”. In many cases, some of these metering points will not exist or at least not be accessible by the monitoring system.

Table 2. Most important metering points in a monitoring campaign.

Component	Essential	Recommended
Heat source (heat generator)	Heat meter (incl. temperature and flow)	Fuel meter Status signals
Thermal energy storage	Temperature gauge	Heat meter (incl. temperature and flow)
Main grid / Subnet	Differential pressure gauge Heat meter (incl. temperature and flow)	Index circuit measurement (differential pressure) Status signals
Network /subnet pump		Power meter
Customer		Heat meter (incl. temperature and flow) Differential pressure (primary site)

To determine the required frequency of measurement, the monitoring objective needs to be defined. If only yearly or monthly values of the KPIs are investigated, the frequency of measurement can be chosen accordingly. This, however, will not facilitate detection of events taking place on shorter time levels, such as charging/discharging the thermal energy storage, fluctuation of temperatures and flows, intermittent operation of components etc. To enable this kind of event detection, the rate of change of the KPIs needs to be assessed in more detail. The highest rates of change can be expected for KPIs directly reacting on control commands of the DHS and the substations. Considering the KPIs discussed in this report, these are the primary energy factor, efficiencies of generation, heat consumption, auxiliary power consumption, and CO₂ emissions. To recognize all significant changes in these parameters, a 15-minute interval was chosen for the measurement of all parameters relevant for these KPIs. This interval has proven to enable detection of most of the events relevant during operation of the DHS. However, in subsequent analysis, even higher frequencies of measurements have shown to be required. One example of such analysis is the evaluation of charging and discharging rates of a thermal energy storage (TES) based on temperature measurements [3].

Additional metering points exceeding the parameters listed in Table 1 are not necessary for a minimum standard data acquisition concept, but may help to gain better results on the operating conditions and optimization potentials of the DHS and thus improve the quality of the monitoring campaign.

5. Monitoring results

Table 3 reports yearly values of key parameters of the investigated DHS calculated from metering data monitored in the current campaign. With the yearly heat consumption ranging from 2,600 to 11,300 MWh, the investigated DHS are significantly smaller than the average of 46,605 MWh per DHS and year that is reported by AGFW for the 1.405 German DHS considered in the AGFW 2016 survey [4]. The same holds true for the heat consumption density, with an average value of 3,140 kWh/(m·a) reported by AGFW and values ranging from 636 to 3,030 kWh/(m·a) for the DHS investigated in this study. The main reason for the low heat consumption density is the rural character of the DHS. The heat loss per network length of most of the investigated DHS is well below the average of 53.1 W/m which can be derived from the values reported by AGFW. With most of the investigated systems having been commissioned after 2000, the technology level and condition of the piping can be assumed to be above average. Combining the low heat consumption density with small heat losses per network length yields values of the relative heat loss which correspond very well to the values reported by AGFW. Empirical data for small DHS are scarce. Nevertheless, the values given in Table 3 appear to correspond well with other published data, see [5-10]. CO₂ emission data were calculated according to [11] with the allocation of CO₂ between heat and power production based on their respective exergetic value.

Table 3. Yearly values of key parameters of the investigated DHS monitored in the current campaign. Negative calculated values of primary energy factors are the result of the underlying allocation method for CHP plants. These values are set to zero according to [11]

DHS	Heat production [MWh]	Heat consumption [MWh]	Heat consumption density [kWh/(m·a)]	Relative heat loss [% of production]	Heat loss per network length [W/m]	Primary energy factor [-]	CO ₂ emission per heat consumption [g/kWh]
A	6,651	5,696	1,798	14.4	34.4	0.33	5.5
B	5,491	4,708	636	14.3	12.1	0.36	28.5
C	2,946	2,618	1,689	11.1	24.2	0.82	119.0
D	3,430	2,882	3,030	16.0	65.8	0 (-1.01)	15.0
E	13,452	11,293	994	16.0	21.7	0.49	107.0
F	4,405	3,822	1,362	13.2	23.7	0.41	264.0

5.1. Heat consumption

As mentioned above, heat consumption densities of the considered DHS represent typical values for smaller rural DHS. Fig. 1 shows monthly totals of heat consumption, normalized on the maximum monthly heat consumption of the respective DHS.

The heat consumption curves for DHS A, B, C, and E are very similar, showing typical time progressions for systems dominated by space heating demand. Maxima are reached in January or February and minima are reached in July or August with minimum values ranging from 10 % to 20 % of the peak demand. DHS D and F, however, show different seasonal progressions of heat demand, caused by atypical consumers like open-air public pools (DHS F) and process heat (DHS D). It is obvious, that atypical consumers will have a significant effect on the seasonal progression of heat demand in smaller DHS.

With regard to a future standardization of performance monitoring, the following values should be considered:

- Temporal location of maximum and minimum monthly and daily heat loads
- Ratio of maximum to minimum monthly heat consumption.

While these parameters will give a good indication on the structure of heat demand, changing them is difficult from an operator's perspective. Seasonal levelling of heat demand requires either large seasonal thermal energy storage systems or the integration of atypical heat consumers whose availability is outside the operator's sphere of influence.

On a smaller time scale, however, optimising the DHS may be easier. For example, ratios of minimum and maximum daily heat consumption in a week's turn may indicate the necessity of a TES and may even give a first estimate on the required storage capacity.

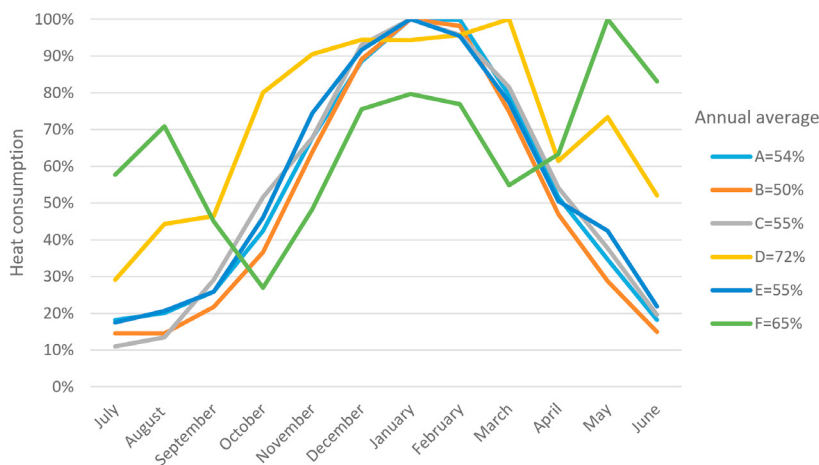


Fig. 1. Monthly totals of heat consumption, normalized on maximum monthly heat consumption of the respective DHS. July 2014 to June 2015.

5.2. Primary energy factor

The German Renewable Energies Act (EEG) introduces the Primary Energy Factor (PEF) as a means to compare the specific consumption of (non-renewable) primary energy of different energy systems. A high value of the PEF indicates a high specific consumption of non-renewable primary energy. The PEF not only accounts for the non-renewable part of the primary energy source itself but also for the consumption of non-renewable primary energy in the upstream processes. As an example, the PEF of natural gas or fuel oil is 1.1, while the PEF of wood-based fuels is 0.2. For heat supplied by a district heating system, the PEF may be calculated according to AGF 309-1 [1]. The value depends basically on the mix of energy sources used and the efficiencies of heat generation and distribution. In the case of CHP production, the fuel consumption of the plant has to be allocated to heat and power production, respectively, using a prescribed allocation method.

According to legislation, the PEF has to be calculated as annual value. In DHS with a high contribution of heat from CHPs fuelled by renewable energy sources such as biogas, biomethane or palm oil, the PEF will be very low or may even turn negative as a result of the allocation method. In these cases, the PEF is set to zero.

Fig. 2 shows the PEF of the six DHS as monthly values, keeping the negative values where applicable. The DHS using CHP (D, E, F) show very low values of the PEF, but also considerable variations over time. The reason for the high variations for DHS E and F is the use of fossil fuel based boilers for peak demand and back-up, making the actual dispatch of the CHP plant and boiler a crucial criterion for the system's performance with respect to primary energy efficiency. For DHS D, the relatively high value of the PEF in Summer is a consequence of the detrimental part load operation of the CHP in times of low heat demand.

DHS A and B, using wood as base load energy source, show relatively low values of the PEF with only little variations over the course of the year. The wood-chip fuelled boiler of DHS B is severely oversized, leading to detrimental intermittent operation in spring and fall. The effect of this behaviour shows as a small peak in March. However, to reliably detect these intermittencies, higher resolutions in time are required, see [3].

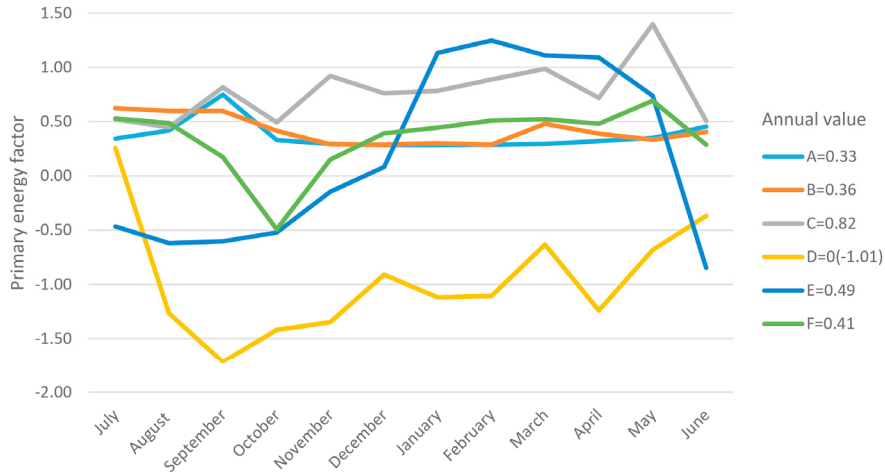


Fig. 2. Monthly and annual values of the primary energy factor, calculated based on [1]. July 2014 to June 2015. According to [1], official PEF have to be calculated as annual values and negative annual values have to be set to zero. DHS D, E, and F use CHP.

DHS C shows rather high values of the PEF, especially when considering that it uses wood chips as energy source for the main heat generator and additionally integrates large rooftop solar thermal heat installations. The reasons for this are manifold, with two long unplanned outage periods of the wood-chip burner in November and May being one part of the problem and the complex hydraulic set-up of the DHS with a partly inefficient integration of solar thermal heat being another, see section 5.4.2 for details.

With respect to a standardized monitoring campaign, primary energy efficiency is an important criterion for the performance of DHS and should therefore be monitored closely. However, obtaining short term values of this parameter may be difficult since it requires knowledge of the fuel consumption of all heat generators as well as heat consumption and – if applicable – power production, all of these values determined for every period in consideration.

Besides their effect on the PEF in DHS C, unplanned outages of the main components are also a crucial criterion for the performance of DHS and should always be considered in a monitoring campaign.

5.3. Heat distribution efficiency and thermal losses

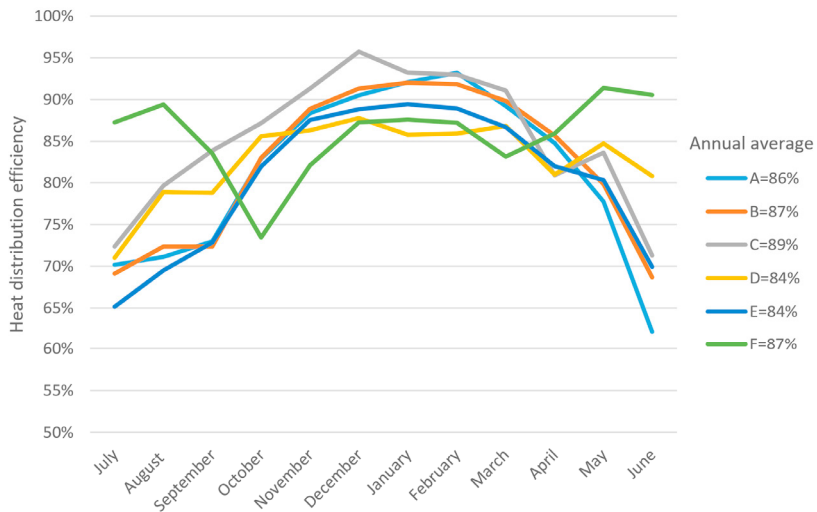


Fig. 3. Monthly and annual values of the heat distribution efficiency. July 2014 to June 2015.

Heat distribution efficiency is defined as ratio of total heat consumption of the consumers to heat supplied to the grid by the heat generators. Heat losses, on the other hand, are calculated as the difference between heat supplied to the grid and total heat consumed. Both KPIs are important criteria for judging on the quality of heat distribution.

As shown in Fig. 3, annual average heat distribution efficiencies of the investigated DHS are high, ranging from 84 % to 89 %. As expected, efficiencies are highest in winter when the heat load is high. The systems D and F, facing smaller seasonal variation in heat demand, can retain better efficiencies even in summer.

Fig. 4 shows heat losses of the DHS, given as percentage of the heat supplied by the heat generators and divided by the network length. The result is the specific relative heat loss of the DHS. This diagram gives a better view on the technology level of the piping used. DHS D, using old pipes with poor thermal insulation shows high specific heat losses. However, since the total Network length is small and heat consumption density is high, the heat distribution efficiency is still good, as can be seen from Figure 3. DHS E, however, due to its high network length, needs very low specific heat losses to reach acceptable heat distribution efficiencies. Ranking of different DHS with respect to their heat distribution efficiencies and heat losses is ambiguous, however, since parameters like supply, return, and ambient temperatures, network length and pipe diameter, heat consumption density and linear heat density are decisive boundary conditions and need to be accounted for, see also [12].

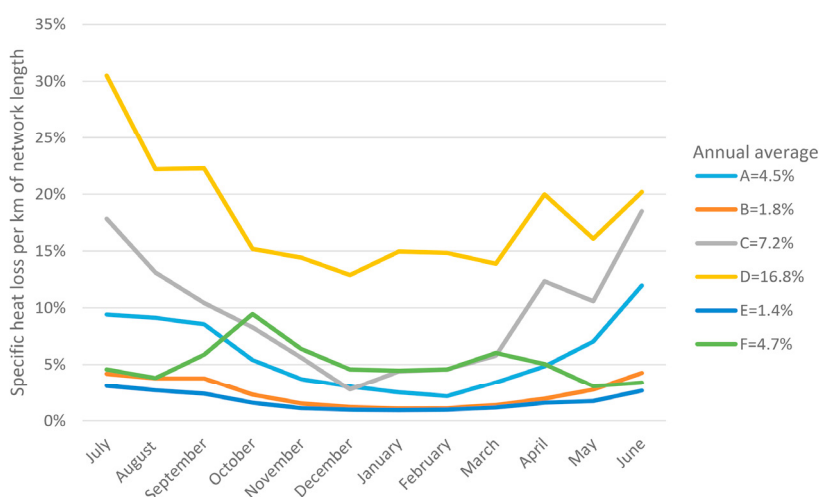


Fig. 4. Monthly and annual values of the relative specific heat loss as percentage of heat supplied to the grid by the heat generators, divided by the network length. July 2014 to June 2015.

Annual values of heat losses can be calculated based on data used for financial settlement. Many heat meters log monthly values so that monthly heat losses can be calculated when collecting these data from all substations and comparing them to metering data from the heat generators. This procedure is obviously very time-consuming so that it should be applied only if there is a particular interest in knowing the seasonal variation of heat losses. The calculation of shorter term values for heat losses requires that all substations be equipped with online metering. In this case, calculation of heat losses is easy and should be part of the monitoring campaign. The results of this analysis can be used, for instance, to optimize heat losses by adapting the grid temperatures in particular seasons or in times of low demand.

5.4. Typical optimization potentials

In the course of the study, a total of 46 optimization potentials have been identified by analysing the extensive metering data, with the individual number identified potentials for each DHS ranging from five to thirteen. The potentials were assigned to four different categories and a total of eleven sub-categories and were rated as either “high potential / urgent need for action” and “medium potential” depending on their impact on performance of the DHS or their potential to shorten lifetime of critical components. A “high potential / urgent need for action” rating was assigned to

- Components operating at efficiencies at least 30 % below best practice for more than three days. Examples:
 - Fixed speed pumps,
 - Wood-chip boilers with high intermitting frequencies,
 - Solar heating systems with very little or no feed-in during solar radiation,
- Thermal energy systems utilizing less than 50 % of their nominal capacity for more than three months,

- Flow temperatures below contractual value or return temperatures more than 10 K above contractual value, or temperature spreads below 10 K for more than three days,
- Significantly increased slag production in wood burners,
- Failure of supply.

A “medium” potential was assigned to components or operational states with a significant lack of efficiency compared to best practice that were not rated as “high potential / urgent need for action”. Multiple optimization potentials could be identified for each of the DHS.

An overview of the identified potentials is shown in Fig. 5. Each red block represents a DHS with a high optimization potential in the respective sub-category, while each yellow block represents a DHS with medium potential. Green blocks represent DHS with no potential in the corresponding sub-category. If a certain category is not relevant for all DHS, the according spaces are left blank.

Category		Potential: high medium small					
Components	Oversized	■	■	■	■	■	■
	Undersized	■	■	■	■	■	■
	Technically obsolete	■	■	■	■	■	■
	Susceptible to outages	■	■	■	■	■	■
Control and dynamics	Distributed feed-in	■	■	■			
	Heat generators	■	■	■	■	■	■
	Network pumps	■	■	■	■	■	■
	Thermal energy storage	■	■	■	■	■	■
Grid temperatures	Flow temperature	■	■	■	■	■	■
	Return temperature	■	■	■	■	■	■
Solid fuels	Fluctuating fuel quality	■	■	■	■		

Fig. 5. Incidence of optimization potentials according to categories. Red blocks represent DHS with high optimization potential, yellow blocks represent DHS with medium optimization potential. Green blocks represent DHS without optimization potential in a specific category. If a category is not relevant for all of the DHS, spaces are left blank.

As expected, component sizing is an issue in small scale DHS, where there is often just one dedicated base load heat generator and one or two central pumps. Also, both flow and return temperatures will always play a central role in optimizing DHS. Surprisingly, however, most of the optimization potentials with a significant impact on the performance of the DHS were identified in the “control and dynamics” category. Four DHS were either using inefficient or even ineffective control mechanisms for the network differential pressure, and all DHS using decentralized heat generation had problems with their hydraulic integration. In DHS with more than two heat generators, their coordination was sometimes found to be inefficient, leading to increased cost of heat generation. Also, controlling the thermal energy storage system to effectively support efficient operation is not an easy task and may cause difficulties for the operator. Many of these specific optimization potentials may not be captured by analyzing annual values of the KPIs only, but may easily be identified in a continuous monitoring campaign where the time progression of the metering data is tracked and analyzed systematically.

5.4.1. Newer DHS with wood-chip heat generator and gas-fueled backup boiler

Many small scale DHS combine a wood-chip heat generator as base load heat source with a gas-fueled boiler for peak demand and backup. Two of the systems investigated in this study (A, B) use this setup. Both DHS were commissioned within the last ten years.

The base load heat generator of DHS B is oversized due to false estimation of total heat demand of the DHS. In combination with an inefficient operating regime of the thermal energy storage, this leads to a detrimental intermittent operation, especially in fall and spring. In consequence, the boiler efficiency is poor and molten slag is formed in the combustion chamber, increasing the cost for maintenance and repair. Detection of this effect requires metering frequencies of a few minutes or smaller. In preparation of the follow-up project Nemo, new KPIs are defined that can be used to identify this optimization potential [3].

No other weaknesses with “high potential” or “urgent need for action” were detected in these two DHS, indicating that this setup can work efficiently if current technology is used and the system is designed properly.

5.4.2. DHS with wood-chip heat generator, gas-fueled backup boiler, and a significant contribution of solar heat

DHS C comprises a wood-chip heat generator for base load supply and a gas boiler for peak demand and backup. In addition, rooftop solar thermal systems with a total collector area of 716 m² are integrated. The grid is operated with the flow temperature fluctuating between 25 °C and 95 °C. Decentral heat pumps are used to raise the temperature to the level required by the individual buildings. The aim of this complex setup is to maximize contribution from solar heat. The system has been monitored

in great detail from 2012 to 2015 in a research project funded by the German Federal Ministry of Economic Affairs and Technology (“Monitoring NES”, funding code 0327400V) [13]. In this period, major optimization potentials of the DHS could be detected. The contribution of solar heat was very low, reaching only 25 % of the expected value. A main problem was caused by the undersized pumps of the solar energy systems being unable to overcome the differential pressure necessary for direct injection to the grid. In addition, at times of low heat demand and high solar radiation, increasing flow temperatures caused the distribution grid flow to virtually stop, preventing the injection of solar heat. The wood chip boiler was also facing different problems. In the beginning of the Monitoring NES project, the boiler showed intermittent operation with up to 170 starts per day due to fluctuations in heat demand and solar heat injection [13]. This issue could be rectified by adding a TES. Poor hydraulic balancing between wood and gas boiler additionally restrained the operating hours of the wood boiler.

With these problems solved, the boiler performance was expected to increase in the monitoring period 2014/2015 which was considered in the MoNa project. Nevertheless, two long periods of unplanned outages occurred. The boiler uses a custom-made configuration combining a combustion chamber initially designed for 400 kW with increased heat transfer surfaces to enable a total heat output of 500 kW. The setup works well with high-quality sieved and dried wood chops or pellets. In 2014 and 2015, however, lower-quality fuel was tested to increase cost-effectiveness. This led to significant problems with melting slag and finally to long outages for repair in November 2014 and in Mai 2015. The effect shows clearly in the respective peaks of the primary energy factor in Fig. 2.

Detailed monitoring results for this DHS and conclusions on the design and operation of such complex systems are given in the final report on the Monitoring NES project [13].

5.4.3. DHS with CHP

DHS D, E, and F all use CHP plants as baseload heat generators. System D is a local heat distribution grid supplying a larger facility consisting of a total of 36 heat consumers. It uses two palm-oil-fueled plants, two oil-fueled boilers and a wood-chip boiler. The system has developed from three separate boiler houses that have been connected by a distribution grid and has grown significantly over the last few decades. Some of the components are outdated and no higher-level process control system is in place. Optimization potentials that were detected include fixed speed pumps in the main boiler house, undefined hydraulic pressure and flow distribution in the grid due to decentral unregulated pumps in the auxiliary boiler houses, lack of process control, fluctuating return flow temperature with temperature spreads below 10 K over long periods. In consequence, auxiliary power consumption and heat losses are high while security of supply and component efficiencies are low.

Systems E uses a total of nine heat generators, including six CHP plants (2 x biogas, 2 x biomethane, 2 x natural gas), two gas boilers and one power-to-heat module. Both natural-gas-driven CHPs and one boiler are located in an auxiliary boiler house. The piping is at a higher technology level compared to System D. A higher-level control system is missing. Optimization potentials that were detected include oversized fixed speed pumps, outdated gas boilers with low efficiencies, undefined dispatch order of the individual heat generators, lack of process control, insufficient use of the power-to-heat unit, insufficient use of the TES, high return flow temperatures.

For both Systems D and E, the optimization potentials that were detected are rooted in the overly complex structure and the partially outdated components, combined with a lack of process control.

System F is a smaller DHS using 2 CHPs (one natural gas and one biogas) and two natural gas boilers. The heat consumption is dominated by an open-air public pool and public schools, with a few apartment buildings and single-family homes. Main optimization potentials include excessive drops in the flow temperature during summer, when the public pool starts to heat up the water and a hydraulic short circuit at the end of the main loop caused by a defective volume control valve.

6. Conclusion

The MoNa project was completed successfully and should be seen as a first step towards a systematic and standardized performance monitoring of DHS. While the investigated smaller rural DHS show good performance with respect to some of the most important KPIs such as heat distribution efficiency, the investigated systems also show significant optimization potentials. Although small scale DHS appear to be less complex and easier to control than large urban networks, many of the identified optimization potentials belong to the “control and dynamics” category. Lack of high-level control systems, overly complex structures even in presumably small systems, and outdated or badly designed components can be considered as main sources for insufficient performance in the investigated systems.

It should be noted that in most cases the operators were aware of a general lack of efficiency and effectiveness of their systems, but could not identify the underlying problems. By analyzing the dynamic operation of the DHS, performance monitoring helps to reveal the causes. Since performance monitoring has proven to be an effective way of identifying optimization potentials of DHS, a further dissemination should be aimed at.

To this end, standard operating procedures to ensure quality and usability should be developed and monitoring cost should be reduced further to make this method available for all sizes of DHS. This is addressed in a follow-up project, “Nemo” [2], funded by the German Federal Ministry of Economic Affairs and Technology (funding code 03ET1538A), that was started in January 2018. 15 – 20 DHS will be monitored over a 24-month’s period and all aspects of standardized performance monitoring will be approached systematically with the aim to develop guidelines and standard operating procedures.

7. Acknowledgements

The MoNa project was funded by Saatinvest GmbH & Co. KG (Brannenburg) and B&O Gruppe (Bad Aibling).

References

- [1] AGFW | Der Energieeffizienzverband für Wärme, Kälte und KWK e. V. (ed.): *Arbeitsblatt FW 309 Teil 1 - Energetische Bewertung von Fernwärme – Bestimmung der spezifischen Primärenergiefaktoren für Fernwärmeversorgungssysteme (Energy Performance of District Heating – Determination of the specific primary energy factors in district heating supply)*. (2014) Frankfurt, AGFW Verlag.
- [2] Bückler D, Hager M, Wieser R: „EnEff:Wärme – Nemo: Wärmenetze im energetischen Monitoring“, in AGFW | Der Energieeffizienzverband für Wärme, Kälte und KWK e. V. (ed.): *Fernwärme + KWK – durch Forschung fit für die Zukunft*. (2018) Frankfurt, AGFW Verlag.
- [3] Schuster S, Bückler D: Key Performance Indicators for Thermal Energy Storage in District Heating Systems. Accepted for publication in EuroHeat&Power International III/2018.
- [4] AGFW | Der Energieeffizienzverband für Wärme, Kälte und KWK e. V. (ed.): *AGFW Hauptbericht 2016*. (2017) Frankfurt, AGFW Verlag.
- [5] Vesterlund M, Sandberg J, Lindblom B, Dahl J: *Evaluation of losses in district heating system, a case study*. Proceedings of ECOS 2013, July 16-19, Guilin, China
- [6] Çomaklı K, Yüksel B, Çomaklı Ö. *Evaluation of energy and exergy losses in district heating network*. Appl Therm Eng 2004;24:1009-17.
- [7] Bohm B. *Experimental Determination of Heat Losses from Buried District Heating Pipes in Normal Operation*. Heat Transfer Eng 2001;22:41-51.
- [8] Lindenberger D, Bruckner T, Groscurth H-, Kümmel R. *Optimization of solar district heating systems: seasonal storage, heat pumps, and cogeneration*. Energy 2000;25:591-608.
- [9] Dalla Rosa A, Christensen JE. *Low-energy district heating in energy-efficient building areas*. Energy 2011;36:6890-9.
- [10] Berge A, Adl-Zarrabi B, Hagentoft C-E: Assessing the thermal performance of district heating twin pipes with vacuum insulation panels. Energy Procedia 78 (2015) 382 - 387
- [11] AGFW | Der Energieeffizienzverband für Wärme, Kälte und KWK e. V. (ed.): *Arbeitsblatt FW 309 Teil 6 - Energetische Bewertung von Fernwärme - Bestimmung spezifischer CO₂-Emissionsfaktoren - Energy Performance of District Heating - Determination of specific CO₂ Emission factors*. (2016) Frankfurt, AGFW Verlag.
- [12] Masatin V, Latôšev E, Volkova A: Evaluation factor for district heating network heat loss with respect to network geometry. Energy Procedia 95 (2016) 279 – 285
- [13] Wambsganß M, Spindler U, Alscher F, Botsch R, Hauck-Bauer E: *Monitoring – eine Militärbrache auf dem Weg zur Nullenergiestadt. Abschlussbericht zum Forschungsvorhaben Monitoring NES, Förderkennzeichen 0327400V, EnEff:Stadt*. (2015) Hochschule Rosenheim.



16th International Symposium on District Heating and Cooling, DHC2018,
9–12 September 2018, Hamburg, Germany

Operational optimization of energy systems, 25 years – established and promising use cases

Peter Stange*, Anja Matthees, Thomas Sander

*TU Dresden, Institute of Power Engineering, Chair of Building Energy Systems and Heat Supply,
Helmholtzstraße 14, Dresden, 01069, Germany*

Abstract

The operation of complex energy systems for the supply of heat and electricity leads to several questions regarding their optimal control, e.g. when to use which generator, when to load or unload energy storages or when to buy or sell energy. Usually it is a complex task to answer these questions with the aim of optimizing a specific objective and respecting all arising physical, technical and economic constraints.

Since 25 years we are solving this problem for an energy provider of a medium-sized city with the aim of minimizing the operational costs. For this purpose, an own modelled mixed-integer linear optimization problem (MILP) has to be solved in association to the continuous operation of the energy system. The model includes but is not limited to several combined heat and power generators, heat accumulators, steam generators and auxiliary coolers.

In this presentation we will give an outline about the wide range of given conditions that are successfully implemented for this application. Further we show our approach to generate realistic heat demand and power consumption forecasts which are both essential preconditions for obtaining reliable optimization results.

In addition to the well – established MILP model in this specific use case we will outline some further promising applications of mathematical optimization in the context of energy systems. This includes the more precise modelling of energy storages, the computation of the optimal design of energy systems and the consideration of different or multiple targets in optimization. Moreover, we outline the problem of uncertain boundary conditions due to the growing amount of temporally hard to predict energy production and demand.

© 2018 The Authors. Published by Elsevier Ltd.

This is an open access article under the CC BY-NC-ND license (<https://creativecommons.org/licenses/by-nc-nd/4.0/>)

Selection and peer-review under responsibility of the scientific committee of the 16th International Symposium on District Heating and Cooling, DHC2018.

* Corresponding author. Tel.: +49-351-463-32308; fax: +49-351-463-37076.

E-mail address: peter.stange@tu-dresden.de

Keywords: optimization of operation; mixed-integer linear programming; energy supply; district heating; demand forecast;

1. Introduction

The optimal operation of heat generators for satisfying the demand of a district heating system depends on numerous influences. Typical supply systems consist of various plants in combination with heat accumulators and further relevant components. In most applications at least some of the generators are combined heat and power (CHP) units. Due to the complexity of actual supply systems it is usually not possible to compute the optimal operation with the objective of optimizing a special criterion, for example, the operational costs, straightforward.

The aim of this paper is to show our approach by means of a specific use case. It applies well known existing methods for performing operational optimization in combination with a demand forecasting algorithm. In section 2 some details about the case of application that is mainly considered in this paper is shown. In addition, we will outline the historical development of the algorithm that is currently used for the forecast of energy demand and for the optimization of operation. Section 3 is focused on the optimization method. We give a brief introduction to the underlying model. Further we will describe how the operational optimization is used by the energy provider. In sections 4 we describe the method that is used for the forecast of the heat and electricity demand of the supply network. In the following we will outline some additional problems and applications that are related to the previously described methods and which are interesting for future developments. Finally, we give a short summary in section 6.

2. Past developments

A method for operational optimization in combination with a demand forecasting algorithm is developed and continuously improved and adapted in cooperation with a local district heating provider. The considered energy supply system provides heat to 40 % of the buildings of a city with more than 200.000 inhabitants. Therefore a district heating network with a length of approximately 300 km is used.

In the following some major steps of the past developments of the operational optimization during its long time of successful application in this use case are highlighted. In the late 70's first algorithms were applied on a mainframe to support the operational planning. At that time the calculation was executed on the basis of a fixed order of operations. It was not possible to consider the combined generation of heat and electricity in one framework. For that reason, the electricity production was preset and the main focus was to improve the usage of the heat accumulator and the heating plants. This algorithm was only used for a daily optimization. In the 80's combined methods of dynamic optimization and linear programming were developed and applied. The program was transferred to a PC in 1987. Due to the availability of more powerful computers some years later it was possible to perform the first yearly optimizations for long-term planning purposes.

25 years ago, in 1993 the algorithm was significantly improved. Starting from that time it was possible to optimize the operation for the combined problem of heat and electricity supply. Soon after, the first version of the demand forecasting algorithm was introduced. In the following years the optimization model as well as the forecasting algorithm were further developed. In addition, the first basic graphic user interface was created. The next major developments took place in 1999. Due to the flexibilisation of the electricity market it was necessary to decrease the discretization in time of the model from one hour to fifteen minutes. Furthermore, the problem was reformulated as a mixed-integer linear optimization problem (MILP) and solved by branch-and-bound algorithms. In the following years the model was improved and adapted to the changing demands of the energy provider. Since 2006 GAMS [1] was used as the algebraic modelling environment and CPLEX [2] for solving the MILP. This software combination is still in use today. Since that time the optimization problem was continuously adapted to changing requirements. Most of the developments were related to electricity and gas trading. Furthermore, an interface was introduced which made it possible to combine our optimization algorithm with external forecast software that is used for energy trading purposes. The demand forecast algorithm was refined and brought to the actual state.

An extensive update of the characteristic equations that are used to model the existing energy system was recently performed in 2017/18. Furthermore, models of additional CHP units that will possibly be introduced in the future were developed.

3. Optimization of operation

3.1. Problem description

The main task of the energy provider is to supply the heat and the electricity that is required by the customers and to fulfill energy trading contracts. For this purpose, in our case of application the energy supply system consists of a number of different combined heat and power units, heating plants, steam generators, auxiliary coolers and heat accumulators. The major consideration in our use case is how to operate the generators and accumulators to fulfill the demand of heat and power with the aim of minimizing the operational costs. Further related problems are the determination of optimal periods for revisions of system components, the estimation of fuel consumption for longer periods and how to participate advantageous at the electricity exchange.

To answer these questions we developed a model that is highly adapted to the given conditions in our case of application. To show the complexity of the problem some of the arising constraints are mentioned in the following.

As described before the energy supply system consists of a number of different components. For each of those components a number of technical constraints must be considered. Depending on the component these are, for example, different kinds of limitations, like the minimal and the maximal output of energy, maximal charging and discharging power, limited storage capacities, a limited number of allowed restarts and limited load changes. Further constraints result from the coefficients of efficiency and from more complex correlations to describe energy transformations between fuel, heat and power. The internal consumption of electricity and steam must be regarded. Further important conditions which must be satisfied are energy balance equations for heat, for electricity, for steam and for different kinds of combustibles. Among others these equations ensure that the energy demand is satisfied, that trading contracts are fulfilled and that the transformation from fuel to heat and power is correct. They guarantee that the content of the heat accumulators is accurate in each time step as well as across time respecting thermal losses, charging and discharging processes. Additional constraints that can be specified are the time dependent availability and the minimal and maximal period of operation or break of single system components. Furthermore, several logical conditions, e.g., describing states or processes, which sometimes depend on and influence multiple components need to be considered.

3.2. Mathematical formulation

The practical optimization problem that is described in the previous subsection is formulated as a mixed-integer linear program. Due to its complexity only an outline of the optimization model which is used in our application is given in the following.

For modelling purposes some general specifications were made:

- The optimization period is discretized in time by a step size of 15 minutes. This step size is a suitable compromise between runtime requirements, availability of predicted data and sufficient accuracy of the results for their practical application.
- All arising types of energy including heat, electricity, steam and fuel are considered as an amount of energy per time step.
- The spatial distribution between producers and customers is ignored which coincides with the fact that the demand data forming the basis of our forecast model is directly measured at the location of the producers.

In the following the components of the MILP are briefly introduced.

Objective function and variables

In our case of application the objective of the optimization of operation is the minimization of the operational costs

$$\min z(x_j) = \min \sum_{i=1}^m K_i(x_j) \quad (1)$$

that depend on the variables x_j , where $j = 1, \dots, n$. The linearized terms $K_i(x_j)$ in equation (1) represent the proportionate costs (or income, if $K_i(x_j) < 0$) for:

- Consumption of combustibles
- Starting processes of CHP units
- CHP cogeneration bonus
- System usage charges
- Costs and income from power trading
- Fictive costs which are necessary for modelling reasons

It is possible to define multiple different electricity trading contracts. They can either be directly included in the objective function and in the corresponding balance equations or they can be handled independently from the optimization process, e.g., by external software. Due to the formulation as a MILP the variables x_j in equation (1) can be separated into continuous and integer variables, whereas most of the latter ones are binary in our application. Continuous variables mostly represent energy, power or utilization ratios. The integer variables are mainly used to describe if a certain process is in progress or to describe switching states. Further, they are necessary to formulate logical conditions and they are needed for the piecewise linear approximation of essential non-linear relations. Details about building integer programming models can be found, e.g., in [3] and [4]. Obviously, most of the variables are time dependent. That means they occur as often as the number of time steps of the optimization period. This leads to a large problem size of the resulting MILP. For example, for optimizing the operation of the period of one day with a step size of 15 minutes a typical problem consists of about a few hundred continuous and a few thousand binary variables after reduction by the solver. The number of reduced variables varies significantly due to several conditions, e.g., if a generator is available or not by external definition.

Constraints

In section 3.1. different actual conditions that must be respected were already outlined. In the MILP they all need to be represented as linear constraints in the form of equalities, inequalities or simply as direct lower or upper bounds of variables. Since there is a large number of variables and due to the fact that most of the numerous constraints are valid in each time step of the optimization period, the dimension of the matrices defining these constraints become large.

Some of the most important equality constraints of the optimization model are the balance equations which, e.g., safeguard that the amount of supplied energy equals the demand. In the case of heat and electricity these equations are the interfaces between the optimization and the forecast algorithm described in section 4. They must be valid in each time step of the optimization period so they multiply occur in the part of equality constraints in (2). In the following the balance equation for heat is shown. Therein the different terms of heating power depend on the optimization variables which are time-depending itself. For the reason of a better readability these dependencies are not illustrated in

$$\sum_{prod} \dot{Q}_{prod} + \sum_S \dot{Q}_{S,dis} + \dot{Q}_{err,+} = \dot{Q}_{demand} + \sum_S \dot{Q}_{S,ch} + \sum_{ac} \dot{Q}_{ac} + \dot{Q}_{err,-}$$

where $\sum_{prod} \dot{Q}_{prod}$ is the sum of the thermal output of all producers, $\sum_S \dot{Q}_{S,ch}$ and $\sum_S \dot{Q}_{S,dis}$ represent the thermal power for charging and discharging the heat accumulators, $\sum_{ac} \dot{Q}_{ac}$ is the sum of heat that is extracted from the heating network by the auxiliary coolers, \dot{Q}_{demand} is the forecast of the heat demand of the customers that must be satisfied, $\dot{Q}_{err,+}$ and $\dot{Q}_{err,-}$ are error terms. These error terms are weighted with extreme high costs in the objective function so that they become zero in almost all cases. They are included for the purpose of safeguarding the solvability of the optimization problem even if the balance equation can't be satisfied for some reason, e.g., due to an extremely high difference between forecasted and actual demand or due to a breakdown. In such a case the error terms give a feedback about the under- or oversupply occurring in the system.

Another typical condition that needs to be formulated as a linear constraint is the identification of a process or a state. For example, if the thermal output of a heat plant is greater than zero this must imply that a binary variable which indicates if the plant is active or not is equal to one. Further problems that need to be formulated in the MILP are, e.g., the piecewise linear approximation of non-linear relations and the representation of discontinuous values. The latter problem occurs quite often in the context of a value that is either zero or it is bounded by a certain interval with a lower bound greater than zero. The presentation of the whole MILP that is used to solve the operational optimization problem is beyond the scope of this presentation. Typical formulations for representing a wide range of general constraints in the context of MILP are given, e.g., in [3].

For the formulation of the MILP we use GAMS as an algebraic development environment. The solution of the problem is performed by the solver CPLEX.

3.3. Application of optimization

The previously described optimization model is used for different purposes that occur in our case of application. The main difference between these problems is the length of the optimization period that is mainly determined by the purpose of the computation. Two typical applications are outlined in the following.

Iterative optimization of operation

Similar to a model predictive control, the optimization problem is successively solved to determine the best possible operation of the components of the energy system in real time. In the standard case the optimization is repeated after a time step of 15 minutes. In the case of sudden actual changes regarding electricity trading or balancing power requirements the iterative optimization is performed more frequent. One step of the iterative process is performed as follows:

Step 1: Data is collected from the underlying database to adapt the constraints of the MILP to the actual conditions of the system. This data includes:

- States, conditions and limitations of the energy system which are results of the preceding operation (e.g. temperatures, state of charge of the heat accumulators, state of operation of the single producers).
- The availability of components regarding the actual optimization period. It is either defined beforehand as a result of a daily optimization process or it is given in the short term by the operator of the system.
- The demand of heat and electricity that is forecasted in every iteration by the algorithm described in section 4. It is based on updated external data like outside temperature, global radiation, wind speed, differences between previous forecasts and actual measurements and others.
- Constraints regarding electricity trading based on the daily optimization and on continuous updated external input.

Step 2: The optimization problem is solved for a predefined optimization period. In our use case we consider a period of 8 hours divided into 32 time steps. Since the result of the optimization is used in a real time process the computational time must be limited. One advantage of the formulation as a mixed-integer linear problem is that it is possible to stop the calculation after reaching a predefined accuracy or after a predefined time. If the latter case occurs the value of the gap, which describes the maximal possible distance to the global optimum, is used to decide if the result of the optimization is usable. If not the operation of the system must be set by a predefined alternative method for this time step.

For operational purposes a further refinement regarding the size of the time step is necessary. In a post processing calculation the result of the optimization with a discretization of 15 minutes is converted into time steps of one minute. This computation respects the constraints of the system. It allows to react on short-term discrepancies between data that was used in the optimization and actual values.

Step 3: The result of step 2 is used to operate the energy supply system until the following optimization is performed. Furthermore, the database is updated regarding to the recent computation from step 2 as well as regarding to actual measurements. The entire iterative process runs automatically and is manually monitored.

Optimization for planning processes

One example for a planning process in the context of our use case is the estimation of fuel consumption throughout the year. This is a basis for signing contracts of purchase of combustibles. A further result of this long-term view is the determination of time periods that are well suited for longer revisions of the generators. In principle, the optimization must be performed for a period of one year in this case. Typically, this yearly consideration must be repeated respecting different assumptions for the energy demand and for the expected prices of fuel and electrical energy. Since the number of variables and constraints becomes huge if the whole period of one year is considered in its totality the problem is divided into smaller sub-problems of shorter length in time. These sub-problems are optimized nearly independently of each other with the only interfaces being some boundary conditions, i.e., the amount of energy stored in the heat accumulators and the state of operation of the generators at the end and at the beginning of each period. In our use case, due to the dimension of the generators and heat accumulators, it turned out that as long as the optimization periods of the sub-problems are not too short and as long as the constraints which are valid across time are carefully considered the discrepancy between the result of this splitting approach and the global optimal result for one year is negligible. This result was validated by comparisons with long-term computations and with splitting approaches where the optimization periods overlapped to determine the interfaces between the separate calculations.

Additionally, those planning processes are performed regularly throughout the year for shorter optimization periods ranging from one day to two weeks. They are considering actual trends and forecasts of prices and demand data as well as actual restrictions of the system. These computations are made to determine the medium-term usage of the generators with respect to current conditions and form the basis for the iterative optimization described before. The optimization of operation for daily planning is further used for variants calculations which are essential for fixing electricity trading contracts.

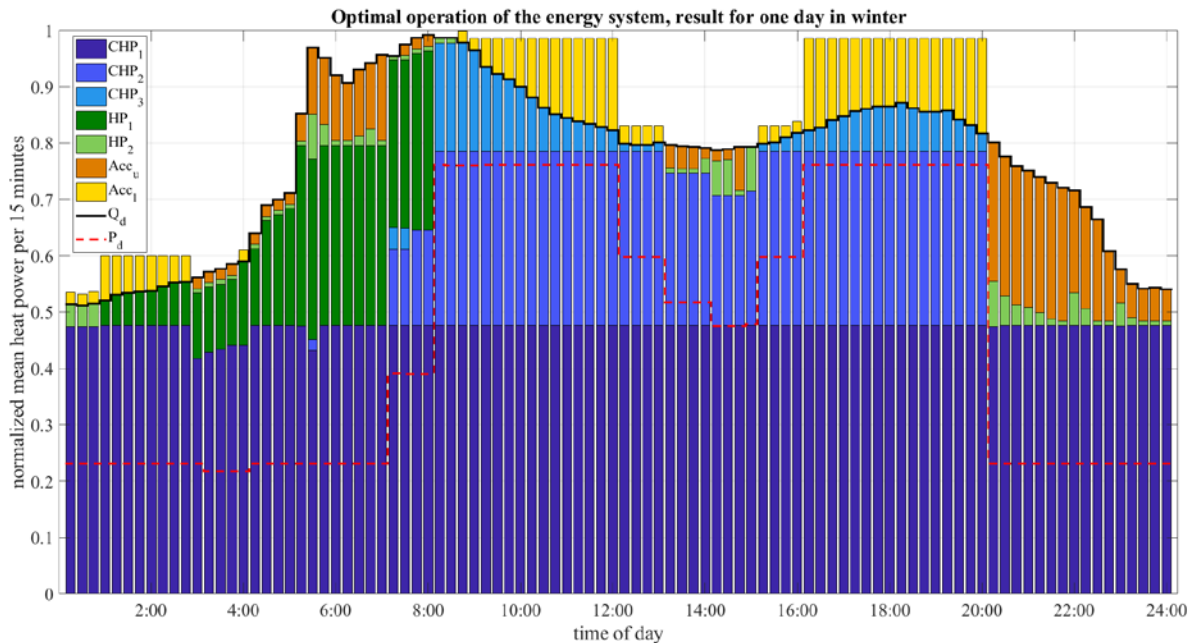


Fig. 1. Optimal operation of the energy system on a winter day. Black line: heat demand of the district heating network. Red dotted line: electricity demand defined by multiple trading contracts. Blue bars: heat generation by CHP plants. Green bars: heat plants. Orange bar: unloading power of the heat accumulator. Yellow bar: loading power of the heat accumulator.

3.4. Exemplary results of the optimization

In figure 1 the result of the operational optimization for one day in winter is shown. In this case the heat demand was forecasted by the method described in the following section 4. The electricity demand consists of different trading contracts that need to be fulfilled. For reasons of anonymisation the original values were normalized and detailed system data can't be given. The blue colored bars shown in the figure represent the mean heat power per 15 minutes of the different CHP units. The green bars represent this value for the heat plants. The usage of the heat accumulator is illustrated in orange and yellow where bars above the demand line represent loading and bars below it represent unloading processes. Additional units which are not used, e.g., auxiliary coolers and a biomass plant are not shown.

Obviously the base load is compensated by the biggest CHP unit. Due to the reason that this unit is fueled by coal it is the most cost-efficient plant that is available, although costs for CO₂ emissions are included in the calculation. Only in a few time steps between three and four o'clock the heating power of unit CHP₁ is reduced slightly due to the minimal electricity demand and the corresponding low income (prices are not illustrated). During daytime the generation of electricity is economically favorable. For this reason, CHP₂ and CHP₃, both fueled by gas, are used. The surplus heat that is generated within this period is stored in the heat accumulator.

In contrast, as long as the electricity demand is on a low level heat is produced by the heat plants HP₁ and HP₂ as it is the case in the morning. Since the maximal power of HP₁ is larger compared to HP₂ the first one is preferably used to fulfill larger heat demands above the base load. Alternatively to the instant generation by plants heat is taken out of the heat accumulator as is the case in the evening.

4. Forecast of heat and electricity demand

One of the most essential prerequisites for reliable and useful results of the optimization of operation in the context of this application is the precise forecast of heat and electricity demand of the customers. Several fundamental constraints of the optimization problem, e.g., the balance equations for heat and power, are defined by these values. Obviously it is impossible to determine the demand by a deterministic method. For this reason, we are using a data-driven regression model to forecast the future load based on measured data from preceding years.

One approach in this case is to build a model that approximates the measured data depending on a number of known explanatory influences first. Applying this model to a new combination of these explanatory data will then lead to the corresponding prediction of the modeled value. Several approaches for solving this kind of problem are known and well developed. Some of the most popular ones are multiple linear regression (MLR), see, e.g., [5], artificial neural networks, see [6] for an energy related application, Gaussian processes [7] and classical time series analysis with or without explanatory influence (ARIMA, ARIMAX), see [8].

In the following we outline our model that combines methods of multiple linear regression and time series analysis. In our use case we need to predict the demand of heat and electricity of the customers of the supplied network. In both cases we almost use the same forecasting method. For that reasons it will be shown for the case of heat demand prediction only. The basic approach of our forecast model is classical multiple linear regression

$$\dot{Q} = k_1 + \sum_{i=2}^n k_i X_i \quad (2)$$

where \dot{Q} is the predicted heat demand, k_i are the regression coefficients and X_i are the explanatory variables. Since the computation of the coefficients of regression is pretty straightforward by the method of least squares the key problem is to determine and to transform the explanatory variables.

During the years of application it turned out that one of the main influences for the demand of heat is the time of the day. For that reason we don't use one single model (2) for our prediction. Instead we categorize the data respecting to the time of the day. For this purpose the latter is divided into time frames of fifteen minutes. For each of those time steps a separate regression model consisting of the same kind of external influences is calculated in the form

$$\dot{Q}_\tau = k_{1,\tau} + \sum_{i=2}^n k_{i,\tau} X_{i,\tau} \quad (3)$$

where $\tau \in \{1, \dots, 96\}$ denotes the time frame of the day ($\tau = 1$: 0:00 – 0:15 am, $\tau = 2$: 0:15 – 0:30 am, ...).

Another important influence factor for the heat demand is the outside temperature which therefore must be used in several ways to define some of the explanatory variables. First of all, the heat demand directly depends on the temperature. This dependency is non-linear, which is caused, e.g., by the heating limit and the maximal available heating power. For that reason we use a transformation that allows to describe this relation in the MLR model (3) piecewise linear as a polygonal chain. In addition, the temperature appears in further explanatory terms as a factor which is multiplied by other influencing data, like wind speed, global radiation and the day of the week. This represents its dominant influence compared to several other explanatory variables. Additionally, the daily mean of the outside temperature and the value of the temperature of the day before within the same time frame are used as explanatory variables. The quality of the forecast of the temperature is essential for a realistic demand forecast. In our case of application it is provided as well as all other relevant weather data by a commercial meteorological service.

In addition to the temperature related terms further explanatory variables in equation (3) are, for example, wind speed, global radiation and logical terms that distinguish working days, weekends and public holidays. A periodic function describes the different heating behavior between summer, winter and transitional period. For each time frame the MLR model for predicting the heat demand in our application consists of $n = 36$ explanatory variables which are not all explicitly named in this work. The mathematical MLR approach for predicting the electrical demand is the same as for the case of heat load. But it differs in its explanatory variables. In the case of forecasting the electrical demand the outside temperature is almost negligible. Instead a number of social factors, e.g., school holidays, bridging days, New Year and the periods around Easter and Christmas have a significant influence to the electricity demand. For that reason they have to be considered as explanatory terms which are transformed to logical values.

The previously described MLR method (3) can further be refined by a time series analysis of the residual values:

$$R_{\tau}^t = Q_{\tau,for}^t - Q_{\tau,act}^t \quad (4)$$

In equation (4) the upper index t denotes continuously the number of the day. The index ‘act’ denotes the actual value whereas ‘for’ denotes the forecasted one. The time dependent residual R_{τ}^t can be described by a seasonal ARIMA method. In our case of application it is approximated by a second order autoregressive model with a seasonal autoregressive component of order one and a seasonality of seven days:

$$R_{\tau}^t = a_1 R_{\tau}^{t-1} + a_2 R_{\tau}^{t-2} + s_1 R_{\tau}^{t-7} - a_1 s_1 R_{\tau}^{t-8} - a_2 s_1 R_{\tau}^{t-9} \quad (5)$$

where a_1 , a_2 , s_1 denote the model coefficients and R_{τ}^t represent the residual at the corresponding day t and time frame τ . The use of this ARIMA approach (5) allows the extension of the MLR method by explanatory variables corresponding to recent differences between the forecasted and the measured data:

$$\dot{Q}_{\tau}^t = k_{1,\tau} + \sum_{i=2}^n k_{i,\tau} X_{i,\tau}^t - (a_1 R_{\tau}^{t-1} + a_2 R_{\tau}^{t-2} + s_1 R_{\tau}^{t-7} - a_1 s_1 R_{\tau}^{t-8} - a_2 s_1 R_{\tau}^{t-9}). \quad (6)$$

Finally, the MLR model is extended by an autoregressive component of the residual of the heat load regarding its value at the actual time frame and at the preceding one. This model refinement safeguards a certain kind of coherence between the separate models for each time frame:

$$\dot{Q}_{\tau}^t = k_{1,\tau} + \sum_{i=2}^n k_{i,\tau} X_{i,\tau}^t - (a_1 R_{\tau}^{t-1} + a_2 R_{\tau}^{t-2} + s_1 R_{\tau}^{t-7} - a_1 s_1 R_{\tau}^{t-8} - a_2 s_1 R_{\tau}^{t-9}) - c_1 R_{\tau-1}^t \quad (7)$$

In table 1 two performance indicators, cf. [9], are given to show the reliability of the forecast of heat and electricity demand. These results are based on recent data from our case of application. The demand values were normalized regarding its corresponding maximal value in the measured data for the reason of anonymisation. In the case of ‘1 day – discretization’ daily sums of the demand data, in the case of ‘1 hour’ hourly sums of the demand data and in the case of ‘15 minutes’ the direct values of the demand data were analyzed. For a better comparison the mean absolute error is always related to a step size of 15 minutes. In this example the forecast algorithm was performed once a day. That means the refinement described by equation (7) could not be applied. Nevertheless, the value of the coefficients of determination R^2 is greater than 0.91 in all cases. In addition, the consistent low mean absolute error which is between 1.9 % and 3.8 % of the maximal demand verifies the very good performance of our forecasting method.

Table 1. Performance indicators for the quality of the demand forecast

period	discretization	Heat demand forecast		Electricity demand forecast	
		\emptyset MAE	R ²	\emptyset MAE	R ²
19.3. – 26.3.2018	15 minutes	0.028	0.914	0.038	0.918
11.1. – 15.5.2018	15 minutes	0.029	0.963	0.032	0.949
11.1. – 15.5.2018	1 hour	0.028	0.968	0.030	0.956
11.1. – 15.5.2018	1 day	0.019	0.981	0.021	0.974

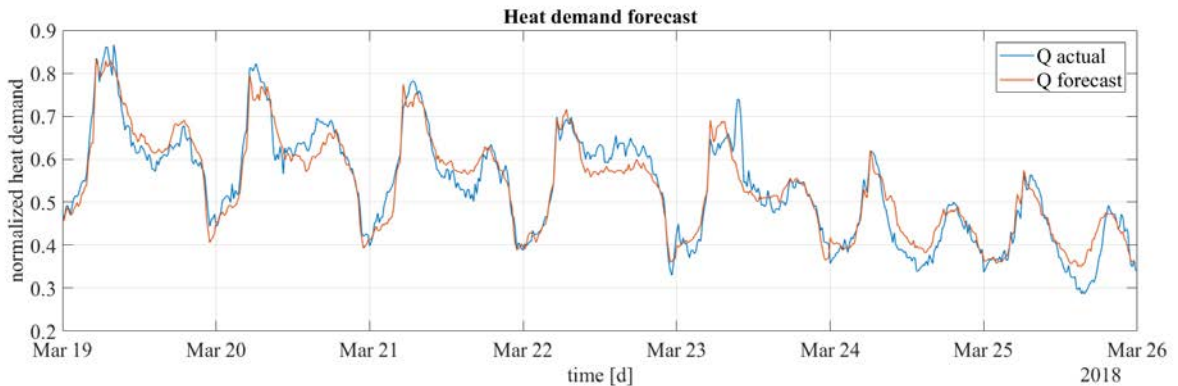


Fig. 2. Measured and forecasted heat demand of the district heating network in our case of application.

In figure 2 the predicted and measured heat demand is illustrated for one week. It can be seen that especially the typical shape of the curve throughout the time of the day is met very well by the prediction. The underestimation on March 22 could be explained by the temperature forecast which was too high for these hours. The unusual peak in the measurement on March 23 is probably an exception since it doesn't typically occur on Friday. The overestimation on Sunday and Wednesday afternoon can't be explained by the explanatory factors that we use in our model.

5. Related applications and future developments

5.1. Optimization under uncertainties

The optimization method can't lead to optimal results as long as the demand forecast isn't accurate. Even worse than performing a sub-optimal operation is the possibility that one or more constraints can't be satisfied if the demand of heat or electricity doesn't meet the forecast. If this case occurs there is a risk of an undersupply of the district heating network or of an excess production of heat which somehow needs to be dissipated. In [10], general linear optimization problems from the NETLIB library [11] were analyzed regarding this issue. In one example it is shown that an uncertainty of 0.1 % in the parameters leads to a violation of the constraints by as much as 450 % when the solution of the original undisturbed problem is applied to the disturbed system.

In practice an exact forecast is impossible to give. For that reason it is necessary that the energy provider conservatively apply the optimization of operation, e.g., by keeping additional heat ready in the accumulators for the case that the demand is much higher than expected or in contrast by avoiding a maximal state of charge in addition with running the auxiliary coolers at their maximal power. This will influence the quality of the solution regarding their optimality. For that reason further statistical analyses of the forecasting model should be performed. Based on those results methods of robust optimization should be developed and introduced to our algorithm for computing the best possible operation regarding uncertainties.

5.2. Alternative optimization criterions

At the moment the reduction of operational costs is the only criterion which is used as an objective for the optimization. If the operational optimization is applied on a different application maybe alternative optimization goals become more or equally important. Some alternative criterions which could be considered in the optimization are for example, the degree of self-sufficiency, the primary energy factor, investment costs, life cycles of system components or emissions. Depending on the kind and number of objectives it is necessary to formulate the appropriate objective functions and possibly to consider the problem by methods of multi-objective optimization, see [12].

5.3. Optimization of system design and system extension

In most cases it is not trivial to decide how to design a new or how to extend an existing energy supply system such that it is optimal regarding a predefined goal. Speaking about the reduction of operational and investment costs it is possible to use the previously described optimization method within a variants calculation of different setups of system components. In a post-processing step the operational costs can be merged with the investment costs and a subsequent investment calculation could be performed. However, if there is a huge number of possible setups it may happen that there are too many variants to optimize. Another special case of interest in the context of system extension is to determine if and how the installation of solar thermal systems in combination with corresponding heat accumulators are suited to improve the operation of existing district heating networks. For solving such problems we develop an optimization algorithm for the optimal design that includes the different optional components which may be installed as decision variables. The key problem in this case is the formulation as a MILP since it is a complicated task to keep the constraints linear.

6. Summary

We introduced a case of application in which methods of operational optimization are successfully used over the last decades. For this example, we outlined the major steps of the developing process of the applied algorithms. Some aspects of the operational optimization problem are briefly shown. At first we described the wide range of actual conditions that need to be considered in our use case. Thereafter, we have shown some basic mathematical formulations for the constraints as well as for the objective function of the MILP. In addition, a reliable forecasting algorithm that is applied to provide the heat and electricity demand data as an important prerequisite for the optimization is presented. This method is based on easy to use approaches of multiple linear regression and time series analysis. Finally, we briefly outlined a choice of problems which are important to consider for the further development of our optimization method.

7. References

- [1] GAMS Development Corporation. General Algebraic Modeling System (GAMS) Release 24.2.1. Washington, DC, USA, (2013)
- [2] IBM ILOG CPLEX Optimization Studio, <https://www.ibm.com/analytics/data-science/prescriptive-analytics/cplex-optimizer>, (2018)
- [3] H.P. Williams, "Model Building in Mathematical Programming", 5th. ed., *John Wiley & Sons, Inc.*, (2013)
- [4] J. Kallrath, "Gemischt-Ganzzahlige Optimierung. Modellierung in der Praxis", *Vieweg*, Wiesbaden, (2002)
- [5] J. Fox, "Applied Regression Analysis, Linear Models, and Related Methods", *SAGE Publications*, Thousand Oaks, (1997)
- [6] S.A. Kalogirou, M. Bojic, "Artificial neural networks for the prediction of the energy consumption of a passive solar building", *Energy*, 25(5), (2000): 479-491
- [7] S. Roberts, M. Osborne, M. Ebdon, S. Reece, N. Gibson, S. Aigrain, "Gaussian processes for time-series modelling", *Philosophical Transactions of the Royal Society of London A: Mathematical, Physical and Engineering Sciences*, *The Royal Society*, (2013)
- [8] G.E.P. Box, G. M. Jenkins, G.C. Reinsel, "Time series analysis: forecasting and control", 4th. ed., *Wiley Series in Probability and Statistics*, *John Wiley and Sons, Inc.*, (2008)
- [9] C.W. Dawson, R.J. Abraham, L.M. See, "HydroTest: A web-based toolbox of evaluation metrics for the standardized assessment of hydrological forecasts", *Environmental Modelling and Software*, 22, 1034 -1052, 10.1016/j.envsoft.2006.06.008, (2007)
- [10] A. Ben-Tal, L. El Ghaoui, A. Nemirovski. "Robust Optimization" *Princeton Series in Appl. Mathematics*, *Princeton University Press*, (2009)
- [11] Netlib Repository, www.netlib.org. (2018)
- [12] M. Ehrgott, "Multicriteria Optimization", *Lecture Notes in Economic and Mathematical Systems* 491, *Springer Verlag*, (2000)



16th International Symposium on District Heating and Cooling, DHC2018,
9–12 September 2018, Hamburg, Germany

Urban Energy Systems and the Transition to Zero Carbon – Research and Case Studies from the USA and Europe

Brendan Shaffer^b, Robert Flores^b, Scott Samuelson^b, Mark Anderson^{a*}, Richard Mizzi^a,
Ellie Kuitunen^a

^a*Arup, 13 Fitzroy Street, London W1T 4BQ, United Kingdom*

^b*Advanced Power and Energy Program (APEP), University of California, Irvine, Irvine, CA 92697-3550, United States*

Abstract

Local community interests in achieving carbon neutral energy supplies continues to rise whether these are cities, counties, universities, aggregated communities, or businesses themselves. Continued growth in this interest will be necessary to meet global carbon reduction targets. This paper considers some of the drivers and challenges faced by different communities in the USA and Europe, using the authors' experience of different projects and initiatives to illustrate the points. The challenges identified include technical aspects of integrating existing systems with new renewable energy generation; short term financial pressures surpassing longer term environmental considerations; the inability to compare health, wellbeing and other social indicators with financial and environmental aspects; the difficulty in balancing the need for a viable business case with the needs of multiple stakeholders; and the need for transformational digital systems to become part of smart energy systems. An in-depth case study is provided for the University of California, Irvine campus which aims to reach carbon neutrality by 2025. The case study demonstrates the technical challenges of combining existing combined heat and power (CHP) systems with heating and cooling networks with local renewables. The results reveal that existing and new CHP and community thermal and power networks systems will need to operate in a much more dynamic fashion, which has implications on economics (reduced capacity factor, higher operating and maintenance costs) as well as on emission rates. This represents a challenge but innovative strategies are emerging to manage these dynamics including the use of thermal energy storage, experimental utility tariffs, improved part load operation of CHP systems, and the emergence of carbon capture techniques utilizing molten carbonate fuel cells.

© 2018 The Authors. Published by Elsevier Ltd.

This is an open access article under the CC BY-NC-ND license (<https://creativecommons.org/licenses/by-nc-nd/4.0/>)

Selection and peer-review under responsibility of the scientific committee of the 16th International Symposium on District Heating and Cooling, DHC2018.

* Corresponding author. Tel.: +44161 602 9373

E-mail address: mark.anderson@arup.com

Keywords: Low carbon energy systems, Combined heat and power, CHP, Microgrids, Advanced Energy Communities

1. Introduction

Interests in achieving affordable, secure and sustainable, energy supplies, as captured by the ‘energy trilemma’, continue to rise whether these are cities, counties, universities, aggregated communities, or businesses themselves. Continued growth in this interest will be necessary to meet global carbon reduction targets. In the United States of America (USA), local institutions such as universities are acting as leaders in meeting the carbon reduction commitments of international agreements such as the 2015 Paris Agreement. In the United Kingdom (UK), electricity supplies are decarbonising, but heating still has a long way to go, with the majority of industry and buildings heated using individual gas boilers. This paper examines the drivers (section 2) and challenges (section 3) faced by selected communities in the USA and Europe in their journey towards carbon reduction or carbon neutrality. Finally, an in-depth case study about the technical challenges faced by one of the communities, the University of California, Irvine (UCI) campus, but with applicability to the other examples considered in the paper, is provided in section 4.

2. Drivers

2.1. Universities in the USA striving towards carbon neutrality

Universities across the USA have set ambitious targets to reduce their carbon footprint. In 2013, the University of California (UC) adopted the University of California 2025 Carbon Neutrality Initiative which commits all ten campuses to the goal of climate neutrality by 2025 for all buildings and fleet vehicles [1]. This aggressive goal requires significant planning and investment to achieve. To date, UC has focused on four scoping areas: 1) establishing itself as a registered ‘energy service provider’ such that it can manage the supply of wholesale electricity, i.e. purchasing electricity from large, regional renewable power plants and supplying the UC campuses; 2) deploying energy efficiency and on-site renewables across the campuses; 3) biogas procurement given that several of the campuses have on-site combined heat and power (CHP) plants; and 4) managing the participation of the UC in California’s cap-and-trade program whereby offsets can contribute to further carbon reductions.

2.2. UK Government support for the decarbonisation of heat

In the UK, the Heat Network Delivery Unit (HNDU) was established in 2013 to support local authorities in carrying out early stage energy masterplanning and more detailed heat network feasibility studies. Over 200 unique projects have so far been supported across 140 local authorities [2]. The HNDU does not only offer financial contributions, but has in-house technical expertise to review the work of consultants working on the studies. This is designed to ensure a consistent quality of outputs, even in the absence of the relevant technical skills within the local authorities accessing the funding. To further help address the ‘heat’ challenge, the UK Government has pledged £320 million of capital investment for projects through the Heat Network Investment Project (HNIP) to kick-start the development of low carbon heat networks at a larger scale. Some of the schemes which have benefitted from the HNDU funding are now reaching commercialisation stages, with HNIP grant funding and loans available for public and private organisations developing them.

Arup has worked with a number of local authorities and Government organisations across the UK, investigating the potential for developing new heat networks. The authors’ experience is particularly in the northern areas of the country.

3. Challenges

3.1. Challenge 1: Technical integration

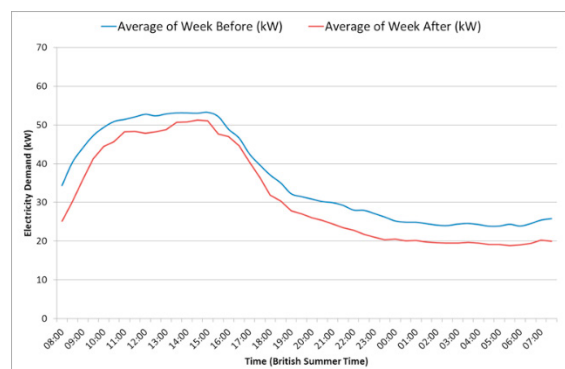


Fig. 1. Short-term results of simple energy reduction campaign

Carbon neutrality does not come without the technical challenges of integrating existing, often carbon intensive, systems with new renewable systems. Arup has worked with UK university estates in developing strategic energy developments and carbon management plans. The basic energy investment hierarchy of first to reduce losses, then to improve efficiencies, and finally to invest in low and zero carbon generation, is a principle adopted by organisations. However, the low cost, quick return on investment opportunities, i.e. ‘low hanging fruit’, have often been achieved. Greater demand side efficiencies are likely to exist but interventions can be disruptive to business continuity, requiring long-term commitment to renovation programmes. The renovation programmes, such as the roll-out of improvements to building fabric and glazing, are often

costly with long returns on investment.

The replacement of aging energy generation and distribution infrastructure with for example high efficiency boiler plant, heat pumps, CHP and heat networks can be justified on the grounds of business continuity and supply security. Again, these are costly long-term ventures, often with marginal financial returns. They are usually investigated comparatively alongside the potential to integrate renewable technologies like solar PV, wind turbines, biomass, geothermal, and heat pumps.

Whether interventions are deeper demand-side efficiencies or main plant and distribution system replacements, the objective will be to minimize where necessary the usually encountered consequential impacts imposed on the estates’ systems by the interventions. Consequential impacts of these interventions potentially consist of business operational changes, disruptions and costly end-use renovation. Knock-on effects can be both physical and more temporal in nature and include for example spatial constraints, thermal matching of generation to demand, utility connection constraints, life-cycle business case development, design, procurement, and delivery timeframes.

Technical challenges are further examined through the UCI case study presented in section 4 of this paper.

3.2. Challenge 2: Short term commercial pressures vs. longer term environmental aspirations

Local authorities in the UK typically express a strong desire for financial viability, even at the cost of environmental performance at least during the initial operating life-cycle. This has resulted in many schemes choosing to use a ‘tried and tested’ technology, gas-fired CHP engine, with the premise that this will be replaced at the end of its useful lifetime with a lower to zero carbon technology. As the lifetime of the CHP engine is expected to be 15 to 20 years, and during this time it is expected that carbon savings compared to the counterfactual case are expected to diminish and probably cease completely due to the decarbonisation of the electricity grid, therefore currently only incremental steps are currently being taken towards reducing carbon emissions.

In 2017, Manchester City Council appointed a lead developer to act as the Council’s delivery partner to completely redevelop a part of the city called Northern Gateway. The redevelopment is expected to involve the building of approximately 10,000 new homes across 120 ha of land over a 15-year period. As this is a complete redevelopment of a large urban area, there is significant potential to utilise local resources and break the tried and tested mould by including mine, sewage, and river water as heat sources with heat pumps upgrading to utilizable temperatures. However, these technologies are likely to be more expensive and/or require more extensive analysis feasibility stages. The scheme needs to receive buy-in from Manchester City Council, the private developer/operator and the incumbent electricity Distribution Network Operator (DNO); this is expected to be achieved by opting for a low-risk and low-

cost technology solution, such as gas CHP energy centres serving phased clusters of district heating. While this solution can be considered as benign or ‘vanilla’, it is by no means without competition from the more ‘business as usual’ options including building by building all-electric solutions considered by some to be unencumbered by troublesome forward planning and interference from disruptive emerging technologies and innovative business operating models.

There is, however, more hope for decarbonisation in the long-term, with one potential solution being the replacement of natural gas (predominantly methane) with hydrogen. UK gas network operators are showing an increasing amount of interest in repurposing their existing networks to switch to accommodate hydrogen. Arup was recently appointed to manage a £25 million innovation programme for the Department for Business, Energy and Industrial Strategy (BEIS) to demonstrate and de-risk the use of hydrogen for heating in UK homes and businesses. The project will establish if it is technically possible, safe and convenient to replace methane with hydrogen in residential and commercial buildings and gas appliances. This will enable the government to determine whether to proceed to a community trial. The programme will run over three years, finishing in 2021, and involve the development of hydrogen-ready appliances and the required quality assurance.

3.3. Challenge 3: Fuel poverty and social value

As well as financial viability, addressing fuel poverty is a key consideration for several local authorities. One UK local authority that has taken concrete steps towards addressing fuel poverty is Leeds City Council, which is taking steps to convert existing social housing tower blocks from having electric heaters to wet heating systems. The supply of reasonably-priced heat through the city’s heat network is thought to significantly lower the tenants’ heating bills, thus having a wider impact on the health and wellbeing of the residents.

However, many schemes suffer from the over-emphasis of financial indicators used to optimise the scheme. Knowsley Council is planning to develop a heat network to supply heat and power to one of its key industrial employment areas. The employment area is surrounded by a deprived neighbourhood. The feasibility of expanding the industrial heat network to also supply nearby schools and social housing was investigated. However, the studies found that such an extension would have a negative impact on the scheme’s finances. The Council therefore chose not to take this option further. If the true value of the connection could be understood (and monetised if necessary), then the wider benefits of the extension could allow the scheme expansion to go ahead, bringing affordable heat not just to businesses but also individuals living in the area. A similar example was found in Calderdale, where near-by social housing was left out of the proposed scheme due to financial considerations, even though this was indicated by the Council as being a key driver at the start.

3.4. Challenge 4: Big visions and collaboration

Finding economies of scale can be aided by bringing together collective interests in a bigger vision than simply serving one’s own interests. Districts by their nature consist of multiple stakeholders of public and private estates; it is not uncommon for public administrators to view their jurisdiction altruistically in this way. Often this view is shared by forward-thinking district stakeholder organisations who see advantage in a collective approach particularly when they have an opportunity to contribute and potentially earn revenue from the process. The collaborative approach applied to a district energy vision can make good use of sharing the outputs from a number of energy producer surpluses with district networked consumers. The district energy networked vision has led to the rise of the ‘prosumer’, meaning that network connected stakeholders have the capacity to both produce, consume and share energy at times that suit their needs. However, this arrangement while simple in concept requires there to be a common network integrator or administrator with the task of balancing production and consumption in a predetermined way to fulfil the business case requirements of the investment model.

Corridor Manchester (also known as Oxford Road Corridor) is a 240 hectare area home to an exceptional group of knowledge-intensive organisations and businesses, operating in the areas of health, higher education, creative industries, advanced materials, low carbon, digital and financial services.

A Corridor-wide Transmission Network is proposed whereby heat producers provide heat to this network in addition to supplying their own heat needs.

This Transmission Network SPV will trade heat between the stakeholders, both those that require heat (consumers) and those that have heat to sell (producers). The modelling carried out as part of a feasibility study showed that there is a potential ‘over availability’ of heat supply in the scenario where all main producers are operating at full output.

The potential for over availability is a similar situation to standing reserve generators on the UK National Grid electricity network. The over availability is mitigated through only calling on (dispatching) suppliers to meet the demand (plus a margin for redundancy), and contract with suppliers to increase the margin by standing reserve payments. This is a balancing and settlement arrangement to be managed by the Transmission Network SPV not dissimilar to the ELEXON for the UK electricity network. The characteristics of electricity (and the same is anticipated for Transmission Network heat) mean it is almost inevitable that quantities of energy generated and consumed will deviate from the quantities for which contracts have been struck in advance. Consequently, central arrangements are required to:

- meter the quantities produced and consumed by each party;
- compare these with the quantities covered by bilateral contracts; and
- provide financial settlement for the differences (known as ‘imbalances’).

These functions are collectively referred to as ‘imbalance settlement’. These arrangements will be included up front in the Transmission Network contracts: contracts for heat supply from producers and contracts for heat consumed by consumers. These will firmly test the willingness for participation in the Corridor scheme before monies are committed to the scheme.

Constraints to the collaborative district networked model are ultimately complex. Early consideration should be given to stakeholder retention/commitment, long phasing timeframes, monopoly positions, public body leadership, as well as Internet of Things (IoT)/Information and Communications Technology (ICT) dispatch and administration limitations.

3.5. Challenge 5: Digitisation and IoT

Smart grids and demand side management are essential elements of the affordable, efficient and low carbon energy future that international climate change agreements imply.

We are pleased to see a significant increase in the volume and ambition of developers to explore ‘smart’ energy projects. It is essential that our urban energy and utility infrastructure employs smart networks of power and heat for better integration of distributed energy generation and demand response to avoid the wasteful ‘business as usual’ approach to urban regeneration. Such systems used in conjunction with ‘time of generation/use’ energy pricing and building management systems will help future proof how we generate, use and control energy.

ICT is recognized as being a key player against climate change. Arup has worked on leading edge global urban energy infrastructure projects, including the EU supported DIMMER [3] project with the aim of integrating BIM and district level 3D models with real-time data from sensors and user feedback. This allowed real-time feedback about energy-related behaviours to be provided. The data also enabled the analysis and visualisation of energy-related information for applications such as energy and cost-analysis, tariff planning and evaluation, failure identification and maintenance and energy information sharing. The project demonstrated a reduction in both energy consumption and carbon emissions, as well as a more efficient utilization and maintenance of the energy distribution network based on the behaviour and demand of the energy consumers.

Turin’s heat network is fed by three Combined Cycle Gas Turbine (CCGT) Plants (total of 1200 MWe), heat only boilers, (more than 1000 MWth) and thermal energy storage (12500 m³). A schematic of the area of focus of the heat network for the DIMMER project is shown in Fig. 2.

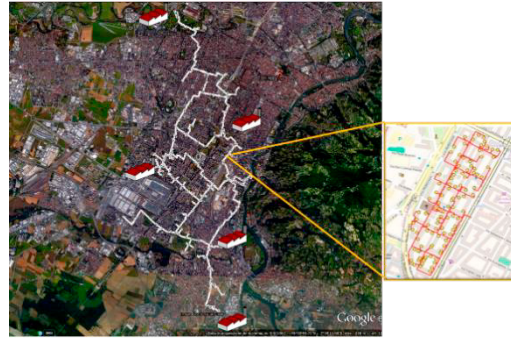


Fig. 2. Schematic of the Turin heat network and the area of focus in the DIMMER project

One of the aims of the DIMMER project was to develop control policies for increasing energy efficiency in district heating networks. The Turin city heat network was used as a demonstrator district, where temperatures and mass flow rates at the heat exchangers were monitored.

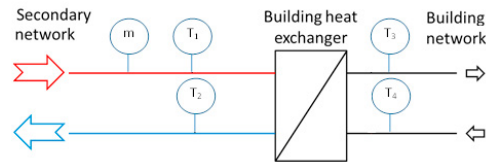


Fig. 3. Monitoring of heat networks

Rescheduling of heat demands can lead to a reduction of peak heat demand resulting in greater exploitation of CHP and reduced heat generation by boilers. Primary energy consumption thus decreases due the increased efficiency of generation.

The thermal behaviour of the buildings connected with the network was evaluated to establish possible variations in the heat request profile that would benefit the network, with the acceptability of the internal building temperatures as a constraint for the new scheduling.

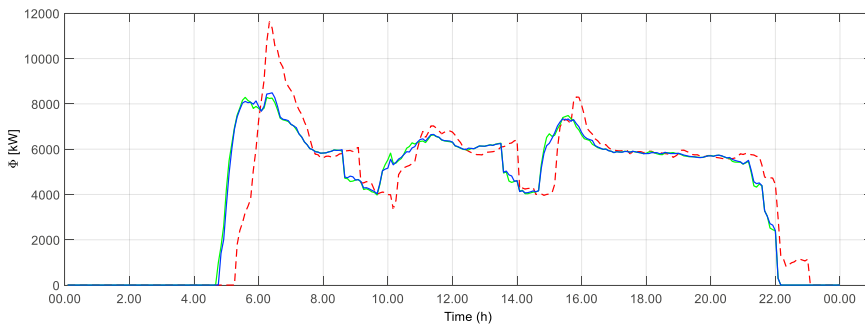


Fig. 4. Effect of the rescheduling of heat demands

A tool for optimal operation of district heating networks was developed. In the modelling, where the indoor temperature in buildings decreases below the acceptable values, an additional thermal flux is supplied to these buildings. Nevertheless, due to the larger exploitation of cogeneration which is obtained through rescheduling, primary energy consumption is expected to decrease despite the additional heat request. Other modelling constraints were applied: a limit on the maximum indoor temperature; and a limit on the equivalent time corresponding to temperature deviation as a result of rescheduling.

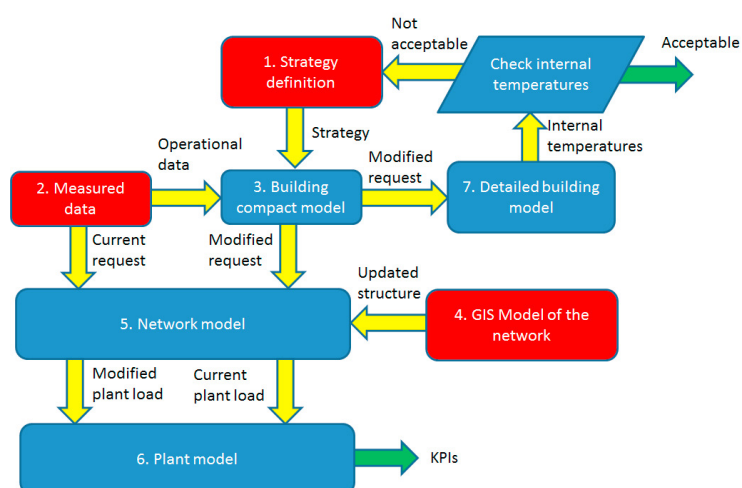


Fig. 5. Tool for optimal operation of district heating networks

Three cases, corresponding to different numbers of buildings for which schedules can be modified, were considered. All cases resulted in a decrease in primary energy savings due to more efficient cogeneration compared to boiler operation. As the numbers of buildings increases, the results showed that greater savings could be realised, with diminishing returns observed.

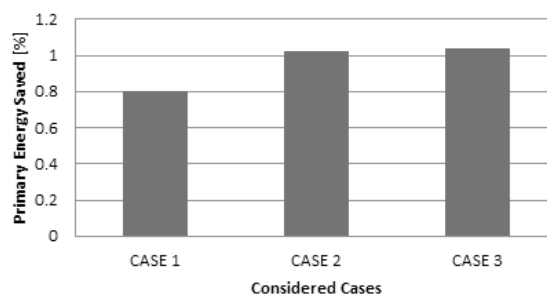


Fig. 6. Energy saving in the three cases considered in the DIMMER project

A radical change is necessary in the way we all consider and interact with energy. At the heart of this is how we treat data ownership and administer energy buying and selling. Transactional energy systems modelling is required in order to bringer about greater penetration of renewable distributed generation. Blockchain ledgers enabling localized balancing and Peer2Peer transactions of generation and demand are seen as a possible answer to the need for widespread change.

4. Case Study: University of California, Irvine (USA)

Of the ten campuses, this paper focuses on the UCI campus as a selected case study for several reasons: 1) deployment of deep energy efficiency measures; 2) fully functional microgrid capabilities; 3) large deployment of on-site solar photovoltaic; 4) zero-emission shuttle bus fleet (includes battery electric and fuel cell electric buses); and 5) integrated efforts by university facilities management and university research programs to study the decarbonization pathways most suitable through demonstration projects and modeling, e.g. demonstration of power-to-gas technology for pipeline injection, microgrid smart charging demonstration, etc.

The UCI microgrid serves a daytime community of more than 50,000 and consists of the following assets: 1) a central microgrid controller with islanding/resynchronization capability; 2) a 1.5 km underground utility tunnel loop connected to the central plant providing a district heating and cooling system that incorporates a large cooling thermal energy storage tank (17,000 m³ / 212 MWh thermal); 3) a single point of interconnection to the electric utility at the UCI Substation with two 15 MVA transformers; 4) ten 12 kV circuits and additional switching substations; 5) nearly

4 MW of solar power; 6) a 2 MW-0.5 MWh battery; 7) a 19 MW natural gas fired CHP plant; and 8) various distributed energy resources (DER) including: a) EV charging at multiple parking locations; b) 60 kW electrolyzer for producing hydrogen for pipeline injection; c) hydrogen fueling for fuel cell vehicles; d) two-axis tracking concentrating solar photovoltaic systems (CPV); e) advanced building energy efficiency measures; and f) advanced building monitoring and control. These resources are summarized in Fig. 7.

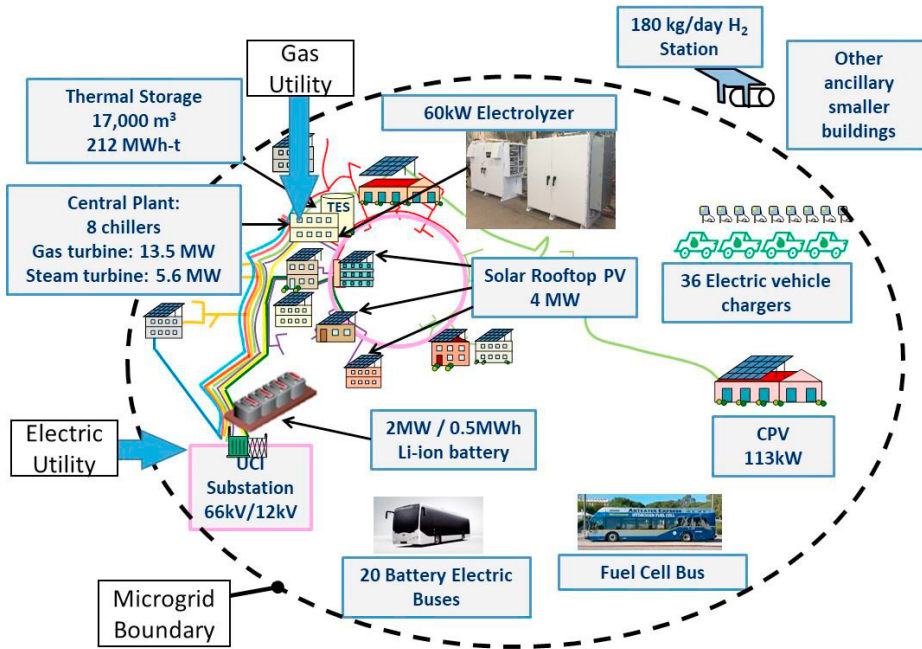


Fig. 7. University of California, Irvine microgrid

In 2016, UCI updated their 2014 Climate Action Plan [1]. The plan identified several specific target areas that map to the UC wide four scoping areas. Fig. 8 shows the carbon reductions to be achieved in each target area such that the 2025 goal is met. The specific target area of offsite renewable procurement maps the first scoping area. Most of the specific target areas of map to the second UC wide scoping area, i.e., continued deep energy efficiency measures (EEM), onsite renewable deployment, fleet energy efficiency/replacement, and optimized microgrid operations. The biogas procurement target area applies to the third UC wide area, and the specific target area responsible for the largest carbon reductions is the carbon offsets, which applies to the fourth UC wide scoping area.

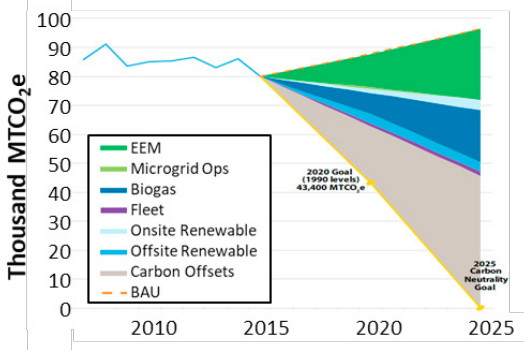


Fig. 8. UC Irvine climate action plan [1]

To date, the most successful programs across the different target areas at UCI have been (as previously mentioned in the selection justification):

- deployment of deep EEM
- fully functional microgrid capabilities
- zero-emission shuttle bus fleet (includes battery electric and fuel cell electric buses)
- large deployment of on-site solar photovoltaic

In addition to those successful programs applicable to each target area, UCI, as well as the UC system as a whole, has utilized the valuable research expertise contained in these institutions to inform the planning with UCI evolving this a step further through close interaction with the university facilities management to deploy actual demonstrations in addition to the typical modeling activities, e.g., demonstration of power-to-gas technology for pipeline injection, microgrid smart charging demonstration, etc.

The deployment of deep EEM resulted in the UCI campus achieving the greatest electric and thermal energy use reductions per square foot of building space in the UC system. In the past few years, these programs achieved 10% reduced energy use despite adding 93,000 m² of building space. UCI is also participating in the Better Buildings Challenge through the US Department of Energy with a goal to reduce site/source energy consumption by 20% by 2020. The laboratories contribute one third of total campus carbon emissions motivating UCI to develop the SmartLabs program, which focuses on EEMs in lab spaces. Although UCI continues to further its EEMs, these measures will be far from sufficient in meeting the 2025 UC goal of zero carbon as shown in Fig. 8.

The development of fully functional microgrid capabilities, i.e., islanding from and reconnection to the utility grid, occurred over three previous research contracts conducted in collaboration with university facilities management [refs]. The implementation of the microgrid controller was initially difficult to justify financially, thus requiring the research funds. However, reliability concerns have grown in recent years leading to further campus support. Analyses completed in these research contracts [2][4] showed significant value in deployment of a microgrid controller that enabled islanding and reconnection. These analyses were conducted with the Smart Grid Computational Tool [5] and resulted in very high benefit-cost ratios that were driven by the high default “value of service” for electricity provided to commercial customers (\$295.70/kWh) in the tool. Although this tool showed very high values of service, the reality was that campus business operations did not have a method of accounting for the indirect cost of possible future outages using a metric like the “value of service” rather only direct costs were considered. Therefore, it took time for the campus to appreciate the value of this additional capability.

UCI recently entered into a lease-to-own agreement with BYD for 20 BYD K9M battery electric buses to become the first all-electric fleet in the USA [6]. The UCI bus fleet also employs a fuel cell electric bus. The BYD Iron-Phosphate battery that powers the K9M has a 12-year warranty. The charging of the battery electric buses occurs via chargers connected to the UCI microgrid. This charging occurs during the night, boosting the gas turbine capacity factor. This mode of operation reduces electricity costs, but not carbon emissions. Therefore, the university is actively exploring options for building out 1MW of solar paired with a 1 MWh battery on a nearby parking structure for storing the electricity for overnight charging. The total daily energy consumption of the battery electric bus fleet is approximately 1 MWh.

UCI has 893 kW of fixed panel PV installed on the rooftops of 12 buildings and an additional 3 MW installed on three parking structures. These systems are owned and operated by third party providers with the electricity purchased by UCI through power purchase agreements. The capacity factor for the rooftop panels, in operation since 2008, was 0.187 in 2012, which is reasonable, given the coastal climate. There is potential for 22 MW of dual axis tracking CPV and 15 MW fixed panel PV based on available campus property [7]. Although the campus solar resources are still at a low penetration (3.5%), they are already causing operational challenges with the gas turbine such that no additional on-site solar can be installed without installing complementary technology deployment (e.g., electric energy storage, power-to-gas, additional thermal energy storage, etc.) that enables absorption of the solar power since curtailment is not possible due to the power purchase agreements. The gas turbine operational issues primarily occur due to the minimum turndown (7.5 MW) of the gas turbine to remain in emissions compliance with the local air quality management district ([NO_x] < 2ppmv and [CO] < 3ppmv, both corrected to 15% O₂) and the current inability of the UCI microgrid to export to the utility (inadvertent export interconnection agreement

with utility). These operational issues occur only several times per year during periods of low electric demand and high solar irradiation, which occurs in the winter.

The CHP plant (13.5 MW gas turbine, a heat recovery steam generator (HRSG), and a 5.5 MW steam turbine) represents a major challenge in decarbonization in that it is fueled by natural gas and provides nearly all the energy needs for the microgrid, which makes it the largest contributor to carbon emissions. The CHP plant provides 99% of the heating loads on the campus through the high temperature water district heating system and 96% of the electrical needs on campus, which also embody the cooling needs. The balance of the electrical needs is served by solar resources (3.5%) and utility import (0.5%). This also makes the CHP plant the largest contributor to carbon emissions. The CHP plant presents a challenge in directly decarbonizing its fuel due to the price premium on biogas. Current price premiums for biomethane vary between 40% and 120% [8]. If current prices for natural gas at UCI are used and these biogas price premiums assumed, then biogas prices between \$7/GJ and \$12/GJ could be expected, which yields electricity price increases of 45% and 150%, respectively, due to the electrical efficiency of the CHP plant (~30%). Increasing electricity prices by this much is undesirable to the campus, and the UCI climate action plan specifies that only 25% of natural gas consumption will be replaced with biomethane by 2025 in order to limit cost increases. UCI will receive this biomethane from various projects being developed by the University of California, which currently includes two landfill gas projects outside the state of California.

The CHP plant faces two challenges: 1) the turndown limit impedes further onsite solar deployment and 2) cost increases associated with biogas replacement of natural gas. Various solutions to these challenges are being investigated in collaboration with university facilities management. These include: 1) utility export and sale of power generated with natural gas, 2) increased gas turbine turndown, 3) battery energy storage, 4) larger TES, 5) implementing power-to-gas, and 6) carbon capture using molten carbonate fuel cells.

To quantitatively evaluate the various decarbonization options, an integrated UCI Energy System model was formulated [9]. This model is based on the methodology developed in the Holistic Grid Resource Integration and Deployment (HiGRID) tool [7], [10], and includes several key aspects noted here. First, the model enables comparison of onsite (local) renewable integration and offsite (regional) renewable integration. Second, the thermal energy storage tank is utilized such that cooling costs are minimized. The maximum and minimum power levels of the gas turbine and steam turbine are 13.5/7.5 MW and 5.5/0.5 MW, respectively. Load and generation are balanced at each time step (1 hr). The dynamics of the heat recovery steam generator were captured using output from a physical model [11].

Fig. 9 shows the modeling results conducted for various future scenarios. These scenarios include a regional (Reg) wind only case wherein wind from regional wind farms is imported via the UC energy service provider and assumes the utility requires that the imported wind be absorbed by UCI in real time without export). Regional solar is also simulated, and when compared to regional wind, lower renewable penetration for a given capacity results due to the diurnal nature of solar generation profiles. Varying levels of energy storage are examined with the default discharge duration being 4 hours. Onsite (local) solar PV is also analyzed. When compared to regional wind and solar, the regional wind enables more renewable penetration (energy basis) for a given installed capacity, which translates to lower cost and less curtailment. This suggests that purchasing offsite renewable power is more effective. A major conclusion is that achieving a renewable penetration greater than 50% without increased gas turbine flexibility will be impossible. Increased gas turbine flexibility is represented by the “GT+9MW turndown” case where the turndown limit has been reduced to 4.5 MW from 7.5 MW. Energy storage (even 12-hour duration storage) does not enable renewable penetrations past 48%. Even with additional gas turbine flexibility, nearly 60 MW of onsite PV would need to be deployed (recall that there is only enough UCI space for 15MW PV). Utility export is also evaluated and illustrates that enabling a peak export of 4MW could enable the same increase in renewable penetration that 10 MW of energy storage could. Although some benefit from deploying different renewables is possible, these curves cannot simply be added together since renewable sources will interact when deployed together with the qualification that wind and solar, when deployed together, typically result in less curtailment [7].

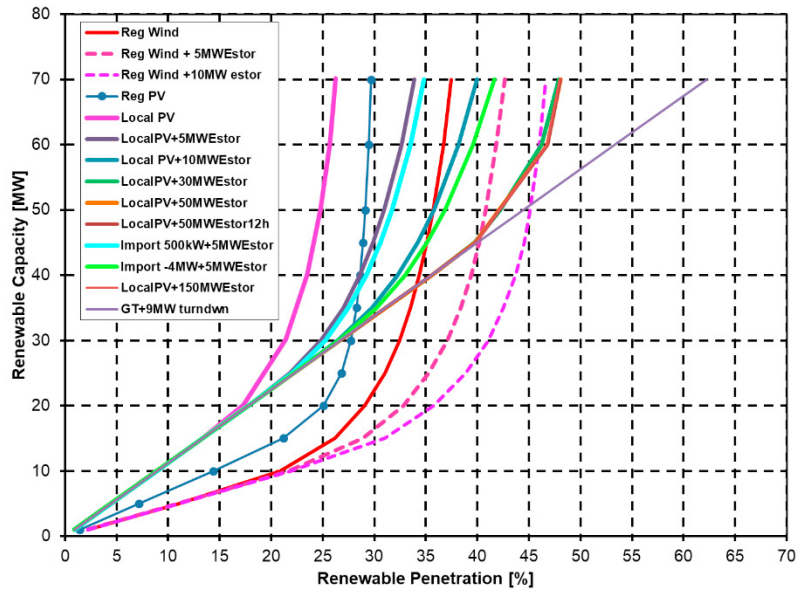


Fig. 9. Renewable capacity required to achieve a given renewable penetration (energy basis) on the UCI Microgrid based on UCI Energy System model analyses [7], [9]

To summarize, the CHP plant ultimately represents a baseload resource given its turndown limit, is fueled by natural gas, and is responsible for most of UCI's current energy needs. Decarbonization of this resource will be achieved in part by switching to biomethane as fuel. The rest of the carbon reductions will occur through purchasing of offsets through the California cap-and-trade market. This currently represents the most cost-effective path for UCI to decarbonize by 2025. Applied research continues on the UCI Microgrid to examine advanced energy system integration methods including power-to-gas, carbon capture using molten carbonate fuel cells, and increased gas turbine turndown.

Work towards improving gas turbine turndown have focused on boosting part load performance. Typical gas turbine designs allow for turndown of up to 40% prior to experiencing significantly degraded fuel conversion efficiency. Even if pollutant control measures could be implemented to ensure compliance with air quality standards, low efficiency at part load operation can begin to negate the greenhouse gas benefits of additional renewable energy resources. In order to better understand the maximum efficiency potential at part load operation, an optimization model was developed to simulate the steady state performance of a gas turbine using thermodynamic principles and both compressor and turbine performance maps. By using an exhaustive search method over the compressor map, the maximum part load efficiency at a discrete power setting was determined, as seen in Fig. 10. Note that the two modes of operation considered were constant and variable speed operation. Using conventional gear boxes and electrical generator sets, only the constant speed operation is compatible when synchronized with the electrical grid. Under this mode of operation, part load efficiency can be boosted by changing both inlet guide vane angle to reduce mass flow through the engine, and by increasing the firing temperature inside the combustor. Much larger part load efficiency gains can be achieved by allowing variable speed operation, allowing the compressor to operate at lower pressure ratio, reducing the back-work ratio, or the percent of turbine power used to operate the compressor. Note that this method would require the use of unconventional hardware, such as a constant-variable transmission connected to a constant speed generator, a variable frequency AC – DC – constant frequency AC conversion, or a two-spool gas turbine. Although technically feasible, many of these options are likely to reduce the maximum efficiency achieved at full load. Further analysis of the impact of boosting part load efficiency on achieving carbon neutrality is being conducted using an optimization model [12].

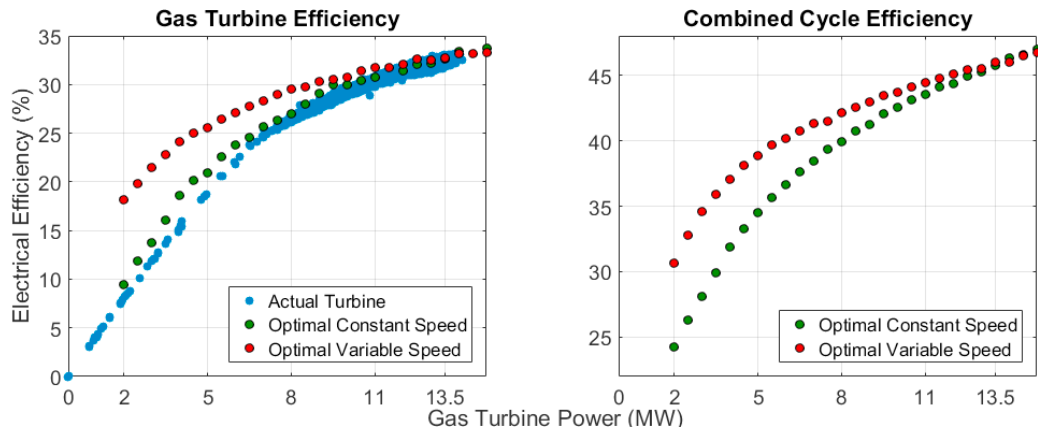


Fig. 10. Optimal part load efficiency for the simple cycle gas turbine and combined cycle power plant located at UCI

In addition to reducing greenhouse gas emissions through improved gas turbine efficiency, other methods of reducing emissions are being explored through the use of a molten carbonate fuel cell (MCFC). Since the carbonate ion (CO_3^{2-}) primary charge carrier across the fuel cell electrolyte requires CO_2 to form, and the exhaust stream of the fuel compartment consists primarily of water and CO_2 , MCFC supplied with gas turbine exhaust gas can be operated to concentrate and capture greenhouse gas emissions. As opposed to conventional amine carbon capture technology, carbon capture through an MCFC would increase plant output. Initial results based on the electrochemical properties of a 250 kW MCFC stack are shown in Fig. 11. Note the required fuel cell surface area to capture between 25% and 95% of carbon emissions when varying fuel cell current density and the gas turbine is operating at full power. Note also that 95% carbon emissions would require novel exhaust flow through the fuel cells to ensure that CO_2 starvation does not occur in any fuel cell. In addition to the required area, the points of lowest carbon capture cost are highlighted for each level of carbon capture, with the associated stack number used to label the point. Although the labels indicate partial stack numbers, further analysis that the ideal stack number is found when rounding the fractional stack number (i.e. 23.4 to 24 stacks). In general, the results indicate that approximately 350 kW and 450 kW of MCFC are required for each MW of gas turbine operation at 33% efficiency when reducing carbon emissions by 75% and 95% respectively. These values do not include the cost of purifying the CO_2 rich stream to storage standards, which can reduce MCFC output by over 30%.

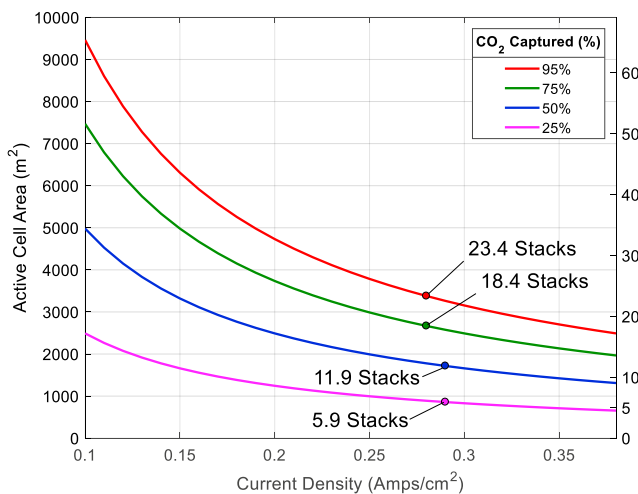


Fig. 11. MCFC surface area required for various levels of carbon capture, along with the point of minimum cost of carbon capture

5. Discussion and Conclusions

The discussion provided in this paper highlighted a number of challenges faced by communities attempting to curb their carbon emissions through the implementation of energy efficient systems such as district heating and cooling. It is the authors' experience that there is a need for the following measures and interventions which would aid the communities in their journey towards lower carbon emissions:

1. **Technical integration.** Be aware of the potential consequential impacts of integrating certain intervention options. Look for opportunities that do not simply align to single project bottom-line but bring about benefits of improving long-term resilience and business continuity. Prepare for future changes by identifying enablement opportunities.
2. **Short term commercial pressures vs. longer term environmental aspirations.** It seems that the incremental steps that the UK local authorities are able to make within their short-term budgetary constraints are not enough to meet the longer term international and UK Government targets. A longer term vision and matching financial arrangements would be needed to allow local authorities to embark on truly low to zero carbon projects.
3. **Fuel poverty and social value.** There is currently a limited understanding of the social value of energy infrastructure, while the commercial and environmental benefits can be more easily compared. More work is, therefore, needed to understand and quantify the social impact of energy infrastructure. This would allow different technologies and network options to be compared using a wider set of criteria than financial/environmental performance alone, and justify the additional investment required for schemes with potential wider social benefits.
4. **Big visions and collaboration.** It is mandatory for public authorities to develop the strategic vision for communities, district community stakeholders are often brought together and willingly align their thinking around energy infrastructure development. However, moving from the visionary strategic cases towards the development of the technical, financial and commercial opportunities it is often seen that misalignment to the vision begins to creep. This is mainly due to perceived complexities of the prosumer operational model and differences in stakeholder programme and agenda objectives. The intention for the greater good to be served by the strategic vision is right and proper, however, it should be acknowledged that significant limitations will exist when attempting to move forward. The full potential of zero carbon transitional projects will not be achieved without a long term commitment to a non-monopolistic public entity with clear governance structure and the responsibility to procure the operation of community scale energy infrastructure [13].
5. **Digitisation and IoT.** The experience shown in the DIMMER project has shown how real-time data analytics and algorithms for better control and intervention analysis can bring about significant change at the district level. In short, smart micro-grids and demand side response are increasingly being proved to be achievable today. With the advent of innovative transactional mechanism such as blockchain and Peer2Peer trading, greater penetration of distributed renewables and the prosumer economy is set to flourish. If the incumbent utility companies are to survive as going concerns they will need to transition their businesses quickly. Electricity DNOs will need to go beyond the distribution system operator model and perhaps widen their operations to include multi-vector network operations (heat, cooling, power and fuels).

The experience of the authors articulated by the collection of cases presented in this paper has demonstrated that the transition of communities, made up of estates owners, campuses, districts and public/municipal authorities, to a zero carbon future is faced with significant challenges and opportunities. One thing is clear, some challenges are not technological but are small 'p' political in nature. However, technology interventions aided by innovative transactional business and operational models are inhibited by short-termism and a tendency to default to the 'business as usual' model. Addressing the key challenges of long project timeframes, investment risks profile and operational responsibility lie at the heart of why we are not transitioning at the rate we know is possible and that the planet needs us to.

References

- [1] University of California Irvine, “UCI Climate Action Plan.” 2016.
- [2] C. Marnay, L. Liu, J. Yu, D. Zhang, J. Mauzy, B. Shaffer, X. Dong, W. Agate, S. Vitiello, G. Ren, C. Yao, X. Hong, X. Wang, J. Song, T. Wang, L. Wu, J. Zhao, N. Karali, G. He, K. Clampitt, R. J. Yinger, H. Zhu, L. Zhao, S. Samuelsen, D. Smith, J. Kumar, F. Jiao, D. Zou, J. Zhang, M. Xiao, S. Tang, Z. Li, X. Li, T. S. Yan, L. Zhu, and X. Liu, “White Paper on Benefit Analysis of Smart Grid Projects,” 2016.
- [3] District Information Modeling and Management for Energy Reduction, https://cordis.europa.eu/project/rcn/110900_en.html
- [4] N. Karali, B. Shaffer, K. Clampitt, A. Zhu, R. Yinger, and C. Marnay, “Benefits Analysis of Irvine Smart Grid Projects,” in 2016 Grid of the Future Symposium - CIGRE/EPRI, 2016.
- [5] US Department of Energy, “Smart Grid Computational Tool.” 2011.
- [6] MassTransit, “BYD to Convert University Bus Fleet Into Nation’s First All-Electric Shuttle Service,” 2018. [Online]. Available: http://www.masstransitmag.com/press_release/12409185/byd-to-convert-university-bus-fleet-into-nations-first-all-electric-shuttle-service.
- [7] S. Samuelsen, F. Mueller, and J. Eichman, “Piloting the Integration and Utilization of Renewables to Achieve a Flexible and Secure Energy Infrastructure,” 2013.
- [8] C. Herbes, L. Braun, and D. Rube, “Pricing of Biomethane Products Targeted at Private Households in Germany—Product Attributes and Providers’ Pricing Strategies,” *Energies*, vol. 9, no. 4, p. 252, Mar. 2016.
- [9] B. Shaffer, B. Tarroja, and G. S. Samuelsen, “Advancing Toward Sustainability Goals at the University of California, Irvine,” in International Conference on Energy Sustainability, 2014.
- [10] J. D. Eichman, F. Mueller, B. Tarroja, L. S. Schell, and S. Samuelsen, “Exploration of the integration of renewable resources into California’s electric system using the Holistic Grid Resource Integration and Deployment (HiGRID) tool,” *Energy*, vol. 50, pp. 353–363, 2013.
- [11] A.-T. V. Do, “Performance and Controls of Gas Turbine-Driven Combined Cooling Heating and Power Systems for Economic Dispatch,” University of California, Irvine, 2013.
- [12] R. Flores and J. Brouwer, “Optimal Design of a Distributed Energy Resource System That Minimizes Cost While Reducing Carbon Emissions,” ASME 2017 11th International Conference on Energy Sustainability collocated with the ASME 2017 Power Conference Joint With ICOPE-17, the ASME 2017 15th International Conference on Fuel Cell Science, Engineering and Technology, and the ASME 2017 Nuclear Forum. American Society of Mechanical Engineers, 2017.
- [13] Knowsley Metropolitan Borough Council – KBP Energy Co. Detailed Project Development and Outline Business Case. 2018.



16th International Symposium on District Heating and Cooling, DHC2018,
9–12 September 2018, Hamburg, Germany

Assessment methodology for urban excess heat recovery solutions in energy-efficient District Heating Networks

Manuel Andrés^{a,*}, María Regidor^a, Andrés Macía^a, Ali Vasallo^a, Kristina Lygnerud^b

^aCARTIF Technology Centre, Energy Division. Parque Tecnológico de Boecillo, 205, 47151, Boecillo, Valladolid (Spain)

^bIVL Svenska Miljöinstitutet, Valhallavägen, 81, 114 26 Stockholm (Sweden)

Abstract

A large amount of low-temperature urban excess heat sources are available to play a fundamental role in the decarbonisation of the heating sector and the present and future of District Heating Networks (DHNs). This work, in the context of the ReUseHeat project, defines a performance assessment procedure applied to four advanced heat recovery solutions from data centres, hospital cooling systems, sewage water networks and underground stations. Key Performance Indicators are defined to allow for integral evaluation in line with the Smart Cities Information System guidelines. The proposed methodology will sustain reliable demonstration results and facilitate replication towards more energy-efficient DHNs.

© 2018 The Authors. Published by Elsevier Ltd.

This is an open access article under the CC BY-NC-ND license (<https://creativecommons.org/licenses/by-nc-nd/4.0/>)

Selection and peer-review under responsibility of the scientific committee of the 16th International Symposium on District Heating and Cooling, DHC2018.

Keywords: waste heat, heat recovery, urban infrastructures, performance assessment, Measurement & Verification, District Heating Networks

1. Introduction

Heating and Cooling is the biggest energy sector in the European Union (EU), accounting for around 50% of its total final energy consumption [1]. Despite the increase on the share of Renewable Energy Sources (RES) within the

* Corresponding author. Tel.: +34-983-546-504

E-mail address: manand@cartif.es

energy system, the European Commission (EC) strongly pursues to achieve further decarbonisation of this sector, which led, in 2016, to the publication of the EU Strategy on Heating and Cooling [2]. The Strategy includes a number of actions concerning four groups, namely: (i) renovation of the building stock, (ii) increase of the RES share, (iii) recovery of waste energy, and (iv) enhancement of the users' awareness and involvement. Within this context, District Heating and Cooling (DHC) solutions play a major role, allowing for synergies with waste heat sources to provide a more secure, renewable and affordable energy supply while displacing fossil fuels.

There are many examples of District Heating Networks (DHN) integrating waste heat recovery from industrial processes (e.g. [3-5]) and/or including RES generation technologies (e.g. [6-7]), but there is still also a large amount of unexplored waste heat available at urban level from different sources.

These unconventional urban waste/excess heat sources are normally low-enthalpy (around 20-40°C) and available in all cities. Therefore, due to the proximity to the end users, such sources could be effectively exploited to provide heating and cooling both through individual systems as well as DHC networks.

According to the definition of 4th Generation DHN provided by Lund et al. [8], future DHNs will have to supply low-temperature heat for space heating and domestic hot water (DHW) to energy-renovated existing buildings and new low-energy buildings. In such a perspective, urban excess heat sources are expected to play a fundamental role to cover the global thermal energy demand, considering that the temperature levels at which they are available could be easily upgraded to fulfil the end-use requirements.

The roadmap to this transition must be prepared. While, it has been already fully demonstrated that DH fed by RES is technically and economically viable in certain scenarios, the fact that urban waste heat sources can be integrated into existing heating and cooling systems still has to be demonstrated. If feasibility proofs can be provided today, future lower temperature heating demand will be more easily satisfied by urban waste heat sources.

In this context, the ReUseHeat European project aims to provide answers to the open issues regarding urban waste heat recovery investments, demonstrating the techno-economic viability of four large scale systems enabling recovery and reuse of different non-conventional sources at urban level (from data centres, sewage water networks, underground railway stations and hospitals), in four cities covering different climate and energy markets [9].

Demonstration unavoidably requires defining a proper evaluation framework in order to consistently prove successful performance and viability of the proposed concepts. This work presents the elaboration of an assessment methodology adapted from common energy-efficiency projects to the particular specifications of urban waste heat recovery interventions. It will rely on a set of Key Performance Indicators (KPIs) to allow for the comparison of the solutions' performance with a baseline scenario, with the final purpose to facilitate future replication and upscaling of efficient and viable urban waste heat recovery projects.

Nomenclature

CHP	Combined Heat and Power
COP	Coefficient of performance
DH	District Heating
DHC	District Heating and Cooling
DHN	District Heating Network
DHW	Domestic Hot Water
GHG	Greenhouse Gas
HP	Heat pump
IPMVP	International Performance Measurement and Verification Protocol
KPI	Key Performance Indicator
M&V	Measurement and Verification
HX	Heat exchanger
RES	Renewable Energy Source
SCIS	Smart Cities Information System
WC	Water-Cooled
WWTP	Waste Water Treatment Plant

reversible heat pump, a DHW tank and an electric boiler as back-up equipment. The estimated available temperature in the low temperature side of the HX varies depending on the season, being around 26 °C in summer and 12 °C in winter. Such moderate temperature levels are also based on a hybrid heating/cooling operation at network level with possible efficient load compensation among different buildings. In addition, they enable high-efficient operation of the end-use heat pumps, which otherwise will not be possible. Two different operating modes (at building level) should be considered:

- During the heating mode, end-use heat pumps will take the heat from the low-temperature network. Therefore, the return pipe of the LTDH network will be colder than the supply, thus extracting heat from the tank in the WWTP and cooling down the temperature of the outflow sent to the sea.
- During the cooling mode, the reverse situation will occur: end-use heat pumps will reject heat to the low-temperature network. Therefore, the return pipe of the LTDH network will be warmer than the supply, thus injecting heat to the tank in the WWTP and slightly increasing the temperature of the outflow sent to the sea.

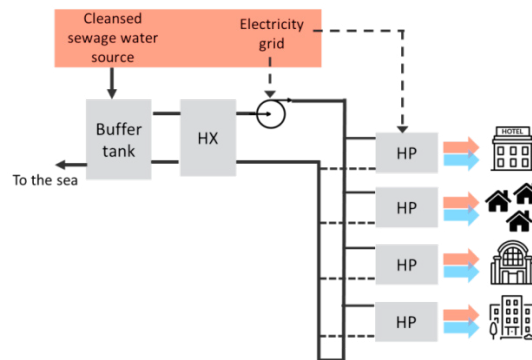


Fig. 2. Conceptual diagram of the heat recovery solution from sewage water in Nice

2.3. Waste heat recovery from cooling systems in tertiary buildings

Tertiary buildings (offices, commercial buildings, hospitals, etc.) often present important cooling demands throughout the whole year, particularly in Southern countries. Heat removed from indoor spaces is normally rejected to the environment by conventional cooling systems, but it represents a low-temperature waste heat source of great potential to meet other surrounding heating demands.

Figure 3 shows the conceptual diagram of a case waste heat recovery from a hospital's cooling system in Madrid (Spain).

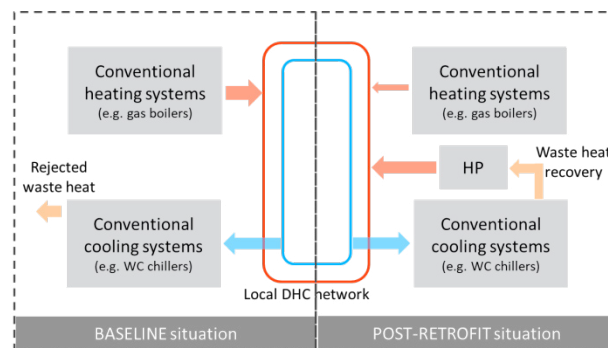


Fig. 3. Conceptual diagram of the heat recovery solution from a hospital's cooling system in Madrid

The hospital buildings are served by a local DHC network. In a baseline scenario, heat and cold production is performed by conventional equipment (gas boilers and water-cooled chillers individually connected to closed-loop cooling towers, respectively). The heat recovery intervention is based on a booster heat pump unit connected to the condensation circuit of the cooling generation plant. The heat rejected by the chillers is captured, thermally

upgraded and injected to the heating supply. Particularly, the heat pump hot sink will be connected to the return pipe of the local DHN and used for preheating the water flowing into the district heating boilers. For the proper functioning of the facility, the targeted temperature available in the heat dissipation must be around 30 °C, aiming to reach 75 °C in the district heating flowing water.

Electric energy is currently needed by the chillers and the cooling tower fans. By implementing the heat recovery solution, it is expected to get a decrease in the cooling towers consumption and an additional need in the heat pump and maybe in the target chiller (due to a slightly higher condensation temperature). In the end, the amount of primary energy used as well as some water additives is expected to be reduced after the heat recovery intervention.

2.4. Waste heat recovery from underground railway stations

Underground railway transport systems in large cities comprise relevant excess heat sources at urban level. Train brakes energy use is ultimately rejected as heat into the tunnels and waiting platforms, which are also affected by heat gains from a great number of transport users [14]. Additionally, technical rooms with electric equipment for traction, lighting, HVAC systems, etc. are particularly interesting hot spots.

Figure 4 shows the conceptual diagram of a case waste heat recovery from an underground railway station in Bucharest (Romania).

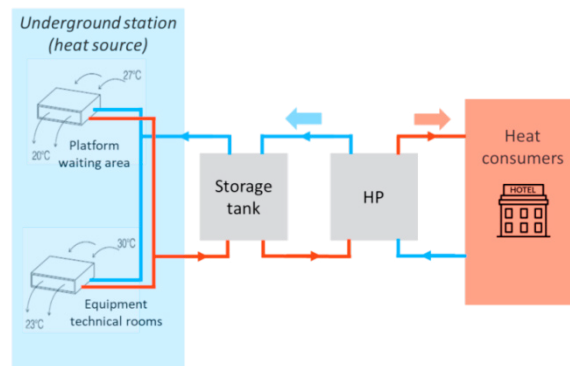


Fig. 4. Conceptual diagram of the heat recovery solution from an underground railway station in Bucharest

The solution exploits that heat released in an underground station in order to supply a heating demand in a nearby area. A booster heat pump will be used for a temperature upgrade so that the heat recovery could be directly injected into the Bucharest citywide DHN or into a separate/private heat supply system.

Some previous heat recovery experiences in underground transport systems reported in literature [15, 16] are based on HXs directly placed within existing ventilation shafts. Here, specifically, the heat capture is performed through a set of fan-coils distributed in two different spaces to be conditioned: the waiting platform and technical rooms. These fan coils, acting as cooling terminal units, provide heat up their water return pipes due to the heat dissipation. They are connected to a thermal storage tank and the heat pump, which provides upgraded energy to preheat the water flow supplied to the end consumers for space heating and/or DHW provision.

Beside the subsequent reduction of the energy consumption for heating purposes at the demand side facilities, there will be benefits linked to thermal comfort gains within the underground spaces and, above all, benefits for the transport system operator and owner of the underground infrastructure. These will be associated to the reduction of the electricity use for HVAC systems at the underground facilities.

3. General evaluation methodology

Based on the preconditions of the case studies described above, the definition of the evaluation framework is provided next. This approach relies on existing methodologies and definitions that are commonly used in similar energy-efficient retrofitting interventions, aiming to adapt to the particular cases of urban excess heat recovery, as well as extend the scope of the evaluation to account for other dimensions of its potential impact. A twofold objective is addressed:

- Savings verification, which must be based on proper measurements and a consistent methodology for data-processing comparing baseline and post-retrofit scenarios. This will define the M&V plan.
- Extended assessment of impacts and performance, since there will be many other relevant variables, parameters, etc. besides what can be strictly defined as ‘savings’.

Both aspects are treated from four different perspectives, namely: energetic, environmental, economic and social; and they will be condensed into a set of KPIs and auxiliary measurements.

3.1. Savings Measurement and Verification (M&V)

The present evaluation methodology takes the International Performance Measurement and Verification Protocol (IPMVP) [17] as the basis for the assessment of the targeted urban excess heat recovery solutions. Although this kind of technical interventions are not specifically addressed within the most commonly-used existing protocols, IPMVP has been considered as the most suitable one for this purpose, on account of its simplicity, adaptability and broader scope, including explicit consideration of economic aspects.

The overall assessment methodology mainly relies on the comparison of the baseline and post-retrofit situations according to the definition of a measurement or evaluation boundary. Particular specifications apply depending on the availability of monitored data.

- Missing real data for the baseline scenario requires the development and calibration of a simulation model. The calibration will be based on values measured during the post-retrofit period. Then, the heat recovery is removed from the model, and simulations are performed to estimate the theoretical performance of the baseline scenario, considering typical reference energy systems and their performance curves/maps.
- If real data from both baseline and reporting periods are available, fair comparable reference conditions must be guaranteed. Energy use will be correlated to relevant independent variables (weather, use patterns, etc.) based on regression and/or detailed simulation models. These will be used to estimate the performance profile of the target systems under such comparable conditions.

Concerning the characterization of the measurement boundary for the targeted urban excess heat recovery solutions, it is a recurrent matter that such actions involve modifications in cooling systems, capturing the released low-temperature heat and upgrading it through a heat pump afterwards with the aim of reaching the targeted temperature for space heating and/or DHW supply. Then, they will have relevant impacts both at ‘source’ and ‘load’ levels. Considering this Figure 5 shows the proposed general definition of the measurement boundary.

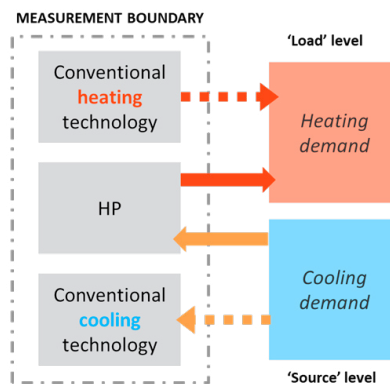


Fig. 5. Measurement boundary for energy savings evaluation.

3.2. Key Performance Indicators (KPIs)

An appropriate definition of indicators is recommended for a consistent evaluation of energy retrofiting projects. They allow both the assessment of the technical intervention at issue and potential similar implementation actions. This section tackles the definition of energetic and economic KPIs aiming to support the IPMVP approach. SCIS

guidelines [18] have also helped to select proper environmental and social indicators that complete a comprehensive assessment of the targeted solutions. Table 1 presents the proposed list of KPIs.

3.2.1. Energy indicators

Within the scope of non-conventional urban excess heat recovery interventions, energy is the main target dimension of the proposed evaluation methodology. EN stands for ENergy indicators in Table 1.

- Useful and final energy demands constitute the first step to enable the calculation of primary energy use and savings, which will then derive the main environmental and economic figures. Fixed conversion coefficients from European databases (e.g. [19]) will be used in a first simplified approach for all demo cases. Further specific analyses based on variable coefficients depending on the season, on the differences in national energy mixes, etc. can be also addressed for more detailed evaluation.
- Energy savings will be quantified in terms of primary energy in order to allow a fair comparison. It should be noted that different energy sources (fuel and electricity) can be used before and after the interventions.
- Energy efficiency quantification is based on the performance assessment of the heat pump (which is the central component of most of the solutions). Both heating and cooling HP performance are included, since useful effects will be obtained with both the HP source and sink heat flows.
- The relative importance of the energy supply coming from excess heat is of particular interest for this kind of solutions. Then, the degree the non-fossil energy supply is also considered.

3.2.2. Environmental indicators

Linked to the positive energy impact, environmental benefits can be derived. The main expectation of these heat recovery projects is to reduce the greenhouse gas (GHG) emissions associated to the energy use for heating and cooling. ENV stands for ENVironmental indicators in Table 1. Regarding this relation between energy and environmental savings, GHG savings (commonly expressed in terms of equivalent tCO₂ avoided), must be calculated from primary energy savings according to contrasted values for the ‘emission factors’. To this purpose, [19] is proposed as a reference, so that a common contrasted approach for all the interventions can be followed.

3.2.3. Economic indicators

Economic benefits are also a direct consequence from energy savings. It can be easily stated that the less energy consumed, the less cost, either for the energy supplier or the end-user, depending on the level at which the savings are achieved. The economic assessment begins with the definition of a baseline which is established by the initial invoices, as well as the required investments for the energy retrofitting project. Then, the evaluation of the economic benefits is challenging because it requires taking into account a comparison with the costs associated to the energy consumed if the intervention or the project had not been implemented.

In this sense, ‘cost savings’ and ‘cost avoidance’ should be differentiated in this context. The term ‘cost savings’ involves that the energy costs in the post-retrofit situation will be lower than those within the baseline period; however, it does not take into account changes in factors that determine energy use (e.g. changes in site activities, effects of independent variables such as production or weather, etc.), or price risks such as changes to energy contracts or tariff rates. Then, cost savings can be achieved due to influencing factors even if the target facilities are the same or even deteriorated in comparison to the baseline situation. On the other hand, the term ‘cost avoidance’ does include the effect of such influencing factors and accounts for the economic costs avoided in respect to a situation in which the energy intervention had not been undertaken. Thus, ‘cost avoidance’ is a more appropriate term according to the present evaluation approach and thus, it will be used from now on.

Although the cost avoidance to be achieved by the excess heat recovery project is the main objective of the evaluation from an economic perspective, a breakdown of this concept is of great relevance for a proper analysis of the investments. Additionally, other aspects should be considered when addressing the economic feasibility of similar actions (e.g. return of the investment). EC stands for EConomic indicators in Table 1.

3.2.4. Social indicators

The last dimension of the evaluation approach refers to social aspects. In the context of energy efficiency projects this social dimension is of much more importance when there is a direct involvement of the end user or a direct

impact on the price that he/she pays for a given service (normally the energy supply). In this regard, urban excess heat recovery concepts tackled here does not imply such a direct and evident techno-economic impact on the end users, changes related to comfort conditions or in the energy price they pay for the energy supply. On the contrary, positive impacts are more focused on the excess heat owners and the operator of the heat recovery facilities, who will contribute to improve energy efficiency (in global terms) and will benefit from a business model linked to the provision of energy as a service. Therefore, the evaluation of social impact, being understood as the impact on the everyday people perception of the services that they receive, on the end-user satisfaction, etc., is considered as a secondary aspect of the proposed assessment methodology, with the exception of cases oriented to increase the end-users interaction, similar to the above-introduced heat recovery from sewage water system case, where it is foreseen to develop a dashboard aiming at stimulating user participation.

3.2.4.1. Social evaluation scope and suggested indicators

Despite of the previous arguments, it is intended to provide some social insight focused on those people directly interacting with the heat source and/or the heat recovery facility itself. The proposed KPIs include definitions to quantify the relevance of urban excess heat recovery projects and increase social awareness to energy efficiency and environmentally clean initiatives, as well as to evaluate people perception of the quality of the services that they receive (e.g. thermal comfort, secure supply, reliable service, etc.). S stands for Social indicators in Table 1.

3.2.4.2. Social evaluation procedures

Social evaluation is proposed to be based on the following procedures:

- Survey method: This is the main procedure for the evaluation of the social acceptance since it provides the subjective perspective of the owners. It is based on a question/answer process. The selection of relevant surveys and the definition of the related questionnaires should be addressed during evaluation.
- Analysis of participation in social media and software platforms on behalf of end-users or interested stakeholders.
- Measurements: Social acceptance should be completed with an objective point of view. Data from the monitoring system will be used for assessing real parameters, such as comfort conditions or energy consumption. Comparison of both survey and measurements will provide a better knowledge of the real situation.

Table 1. Definition of Key Performance Indicators (KPIs)

Name	Category	Units	Description
EN01	Energy	kWh/yr; %	Primary energy savings
EN02	Energy	kWh/yr	Useful energy demand: heating
EN03	Energy	kWh/yr	Useful energy demand: cooling
EN04	Energy	kWh/yr	Final energy demand: fuel
EN05	Energy	kWh/yr	Final energy demand: electricity
EN06	Energy	%	Degree of Primary energy supply based on RES/excess heat recovery
EN07	Energy	-	Seasonal COP of the HP (cooling performance)
EN08	Energy	-	Seasonal COP of the HP (heating performance)
EN09	Energy	-	“Total heating and cooling useful energy” to “Electric consumption” ratio
ENV01	Environmental	tCO ₂ /yr; %	GHG emissions reduction
ENV02	Environmental	tCO ₂ /yr	Total GHG emissions
EC01	Economic	€	Cost avoidance
EC02	Economic	€	Total costs (along the facility lifetime)
EC03	Economic	€; €/kW	Capital expenditure (CAPEX)
EC04	Economic	€; €/yr	Operating expenditure (OPEX)
EC05	Economic	€/yr	Energy costs: fuel
EC06	Economic	€/yr	Energy costs: electricity

EC07	Economic	€/yr	Maintenance costs
EC08	Economic	€/yr	Financing costs
EC09	Economic	yr	Payback time
EC10	Economic	%	Return of Investment (RoI)
EC11	Economic	%	Internal Rate of Return (IRR)
EC12	Economic	€	Net Present Value (NPV)
EC13	Economic	n. of jobs	Job creation
S01	Social	n; %	People that are positive about the project
S02	Social	n (Likert scale)	Degree of people satisfaction
S03	Social	PPD; PMV	Average comfort perception
S04	Social	Tweets, web visits	Presence in social media

As a general remark, it should be noted that absolute units have been only considered so far within the KPI lists. However, providing many of these indicators in specific terms (i.e. as ratios in respect to a given characteristic parameter of the demo case) is considered of great importance within the proposed assessment methodology. For this reason, relevant characteristic features for each specific heat recovery solution should be identified, contributing to enable future comparison studies on similar projects as well as replicability analyses.

3.3. Monitoring requirements

A general guidance to set the basis on the variables to be measured is provided since design and technical details must be given in each specific case. Table 2 presents a list of the main variables that will be required for the evaluation of the intervention both within the ‘after’ and ‘before’ scenarios. These parameters must be in line with the conceptual diagrams presented previously for the measurement boundary.

Table 2. Main variables to be measured

Variable	Use/Contribution to	Data source
Fuel consumption	- Final energy consumption of conventional heating system	- Smart meters - Energy bills
Electricity consumption	- Final energy consumption of conventional HVAC equipment (e.g. boilers, chillers, cooling tower fans, water pumps) - Final energy consumption of the HP during post-retrofit period - Power of the HP contributing to COP calculation	- Smart meters - Energy bills
Fluid energy flow	- End-use (useful) thermal energy demand as dependent variable of energy models - Input/output thermal energy flows in the HP contributing to COP calculation	Smart meters
Fluid temperature	- Indirect measurement for fluid energy flow determination - Surveillance and control systems	Smart meters
Fluid mass flow rate	- Indirect measurement for fluid energy flow determination - Water consumption - Surveillance and control systems	Smart meters
Air temperature	- Excess heat source temperature characterization - Thermal comfort conditions - Surveillance and control systems	Smart meters

In addition, the assessment methodology must determine a reference requirement in terms of the monitoring sampling rate for the aforementioned variables. This will enable to check the system behavior as well as meet the data resolution required for control and surveillance purposes. Hence, a 15-minute period is considered as the reference sampling rate requirement for those variables registered by smart sensors/meters. However, exceptions

to this rule could be accounted for within the detailed specifications and also regarding such variables coming from other data sources (e.g. energy bills for baseline characterization).

4. Conclusion

This work focuses on the evaluation of projects based on heat recovery from urban low-temperature heat sources and proposes a broad assessment methodology essentially addressing energy, economic, environmental and social aspects. A general set of KPIs adapted to this particular kind of projects as well as the most relevant metering requirements have been defined. The proposed methodology is presented on the basis of four representative case studies targeting the heat recovery from data centres, hospitals' cooling systems, sewage water and underground stations, which are being developed within the ongoing European ReUseHeat project. This will allow setting the basis for replication and upscaling of urban waste heat recovery, facilitating future investments in this field.

Acknowledgements

This work has been developed within the ReUseHeat project, which has received funding from the EU's Horizon 2020 Research and Innovation Program under Grant Agreement n°767429.

References

- [1] Fleiter, Tobias et al. "Mapping and analyses of the current and future (2020-2030) heating/cooling fuel deployment (fossil/renewables)" (2016) European Commission. Directorate General for Energy.
- [2] COM (2016) 51 final, "An EU Strategy on Heating and Cooling", <https://ec.europa.eu/energy/en/topics/energy-efficiency/heating-and-cooling>
- [3] Bühler, Fabian, Petrović, Stefan, Karlsson, Kenneth and Elmegaard, Brian. "Industrial excess heat for district heating in Denmark". *Applied Energy*, 205, (2017): 991-1001
- [4] Fang, Hao, Xia, Jianjun, Zhu, Kan, Su, Yingbo, and Jiang, Yi. "Industrial waste heat utilization for low temperature district heating". *Energy policy*, 62, (2013): 236-246.
- [5] Sun, Fangtian, Cheng, Lijao, Fu, Lin, and Gao, Junwei. "New low temperature industrial waste heat district heating system based on natural gas fired boilers with absorption heat exchangers". *Applied Thermal Engineering*, 125, (2017):1437-1445.
- [6] Soloha, Raimonda, Pakere, Ieva, and Blumberga, Dagnija. "Solar energy use in district heating systems. A case study in Latvia". *Energy*, 137, (2017): 586-594.
- [7] Oktay Zuhail, Aslan, Asiye. "Geothermal district heating in Turkey: The Gonen case study" *Geothermics* 36 (2007): 167-182
- [8] Lund Henrik, Werner Sven, Wiltshire Robin, Svendsen Sven, Thorsen Jan Eric, Hyelplund Frede, Mathiesen Brian Vad. "4th Generation District Heating (4GDH) – Integrating smart thermal grids into future sustainable energy systems", *Energy* 68 (2014): 1-11.
- [9] European Commission. "Recovery of Urban Excess Heat – ReUseHeat". (2017) Grant Agreement number: 767429. H2020-EE-2016-2017/H2020-EE-2017-RIA-IA
- [10] Culha, Oguzhan., Gunerhan, Huseyin, Biyik, Emrah, Ekren, Orhan, and Hepbasli, Arif. "Heat exchanger applications in wastewater source heat pumps for buildings: A key review". *Energy and Buildings*, 104 (2015): 215-232.
- [11] Guo, Xiaofeng, and Hendel, Martin. "Urban water networks as an alternative source for district heating and emergency heat-wave cooling". *Energy* 145 (2018): 79-87
- [12] Wahlroos, Mikko, Pärssinen, Matti, Rinne, Samuli, Syri, Sanna, and Manner, Jukka. "Future views on waste heat utilization—Case of data centres in Northern Europe". *Renewable and Sustainable Energy Reviews*, 82 (2018):1749-1764.
- [13] Ebrahimi, Khosrow, Jones, Gerard F., and Fleischer, Amy. S. "A review of data centre cooling technology, operating conditions and the corresponding low-grade waste heat recovery opportunities". *Renewable and Sustainable Energy Reviews*, 31 (2014): 622-638.
- [14] Revesz, Akos, Chaer, Issa, Thompson, Joylon, Mavroulidou, Maria, Gunn, Mike, and Maidment, Graeme. "Ground source heat pumps and their interactions with underground railway tunnels in an urban environment: A review". *Applied Thermal Engineering*, 93 (2016): 147-154.
- [15] Gilbey, M. J., Duffy, S., and Thompson, J. A. "The potential for heat recovery from London underground stations and tunnels". In: *Proceedings of CIBSE technology and symposium*. (2011) DeMontfort University.
- [16] D'Appolonia. "D4.1. Report on KPI values". Combined Efficiency Large Scale Integrated Urban Systems – CELSIUS project (2014) Grant Agreement number: 314441. FP7-ENERGY-SMARTCITIES-2012
- [17] Efficiency Valuation Organization (EVO). "International Performance Measurement and Verification Protocol. Core Concepts" (2016). EVO 10000 – 1:2016.
- [18] Garrido, Antonio; Etmnan, Ghazal; Möller, Sebastian. "Smart Cities Information System. Key Performance Indicator Guide". Version 2.0. (2017) Available at: <https://smartcities-infosystem.eu/library/resources/scis-essential-monitoring-guides>
- [19] Koffi, B., Cerutti, A., Duerr, M., Iancu, A., Kona, A., and Janssens-Maenhout, G. "CoM Default Emission Factors for the Member States of the European Union" (2017). European Commission, Joint Research Centre (JRC)



16th International Symposium on District Heating and Cooling, DHC2018,
9–12 September 2018, Hamburg, Germany

Resulting Effects On Decentralized Feed-In Into District Heating Networks – A Simulation Study

S. Paulick^a, C. Schroth^a, S. Guddusch^a, K. Rühling^{a,*}

^a*Technische Universität Dresden, Institute of Power Engineering,
Professorship of Building Energy Systems and Heat Supply, 01062 Dresden, Germany*

Abstract

This paper presents latest results and outcomes of a research project with focus on the thermo-hydraulic impact of decentralized feed-in in existing network structures with the resulting requirements for components like pressure maintenance, pipes as well as on the net control strategy. Furthermore, the implementation of central heat storages and their operation mode as part of the network control is considered. As a result, the simulation study provides detailed insights in flow conditions, with which requirements for system components in the network can be derived.

© 2018 The Authors. Published by Elsevier Ltd.

This is an open access article under the CC BY-NC-ND license (<https://creativecommons.org/licenses/by-nc-nd/4.0/>)

Selection and peer-review under responsibility of the scientific committee of the 16th International Symposium on District Heating and Cooling, DHC2018.

Keywords: DH simulation; decentralized feed-in, solar thermal, distributed generation

* Corresponding author. Tel.: +49-351-463-34440; fax: +49-351-463-37076.
E-mail address: sven.paulick@tu-dresden.de

1. Introduction

This paper presents the latest results of the research project “Prognose der Auswirkungen dezentraler Einbindung von Wärme aus erneuerbaren Energien und anderen Wärmeerzeugern in Fernwärmenetze (*DELFIN*)”, based on the previous research project *DEZENTRAL* [1]. The project partners are *Solites*¹ and *AGFW*².

The results of *DEZENTRAL* have shown in detail, which effects occur when decentralized heat feeds-in into district heating networks. Flow reversal in parts of the net branches, moving supply frontier or full supply of the decentralized producers can occur. The current project focusses on the impact in the network itself according to thermo-hydraulic effects and the consequent, alternating thermal stress of the pipes. Moreover, statements will be made about conditions when feed-in should be avoided according to network stability. Finally, requirements for the feed-in pumps of the decentralized producers concerning to the location and local conditions in the network will be derived. A further aspect is the integration of a central thermal storage in the network. To prevent stagnation of installed solar thermal plants, the storage operation shall lead to a network load relief to decrease the stress in the network. Additionally, a subsequent unloading can lead to a longer offline period of the central heat producer.

The simulation study focusses on two representative district heating networks, combined with two different weather locations to generalize the results for a wide field of application. Decentralized heat producers (DCP) are considered in terms of solar thermal plants and combined heat and power units (CHP). A variation of decentralized heat producer according to size and position is part of the investigation as well as different operation modes of the central heat storage.

This paper presents the latest results of the simulation study just as the principle of consumer, decentralized producer and storage modeling. Results of solar fraction, storage operation, and requirements for pressure maintenance as well as first insights on the flow conditions will be presented and discussed.

Nomenclature

Symbols			Abbreviations		Indices	
h	Hour	h	C	consumer	a	ambient
H	heating period	0 / 1	CHP	combined heat and power	i, j	index
\dot{m}	mass flow	kg/s	CP	central heat producer	in	input / feed-in
Q	Heat	kWh	DCP	decentralized heat producer	l	lower
\dot{Q}	heat flow	W			loss	losses
SF	solar fraction	%			max	maximum
V	volume	m ³			net	network
W	working day	0 / 1			off	offline
ϑ	celsius temperature	°C			RL	return line
					SL	supply line
					ST	storage
					T	type
					u	upper

¹ Steinbeis Research Institute for Solar and Sustainable Thermal Energy Systems

² AGFW - Der Energieeffizienzverband für Wärme, Kälte und KWK e.V.

2. Simulation

2.1. Simulation Tools

The simulation study is realised by a coupling of two different simulation tools. For the thermo-hydraulic simulation of the district heating network, TRNSYS-TUD is used, as an in-house development on base of the Transient System Simulation Tool (TRNSYS). The advantage of TRNSYS-TUD is the developed thermo-hydraulic solver, adopted for the usage of district heating networks in [2] and [3] and further developed in the project *DEZENTRAL* [1]. It leads, especially for larger meshed networks, to adequate time taken for the simulation. The modeling of the consumer, decentralized heat producer and the storage is realised in the modeling language Modelica. Modelica, as a second simulation tool, has on the one hand the possibility to read in large MATLAB-Files and on the other hand diverse functionalities for dynamic simulation. The coupling of both simulation tools is realised with the Functional Mock-up Interface (FMI), a tool independent standard for co-simulation [4]. The coupling works on a so-called Master-Slave-Technology. The models of the simulation tools represent the slaves, whereas the master controls the data exchange between the slaves on each simulation time steps. Fig. 1 shows the principle for the here mentioned simulation study. The used FMI-Master is an in-house development that enables the communication to TRNSYS-TUD.

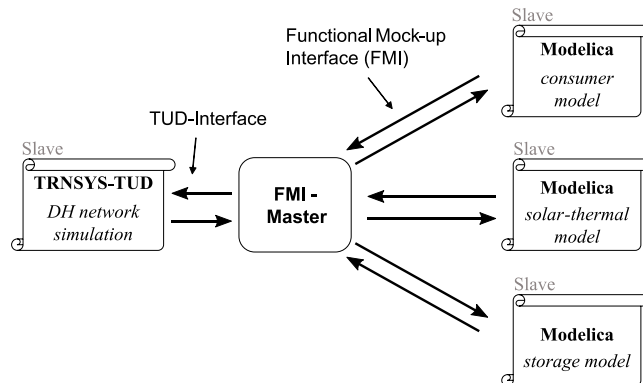


Fig. 1: Schema of the coupling between TRNSYS-TUD and Modelica via FMI-Master

2.2. Considered District Heating Networks

Two different district heating networks are the research objects in this simulation study. The first is a 3rd generation-, radial DH network (following IEA-DHC Annex X classification), called Net G. The main characteristics are:

- installed load of 2.2 MW with a length of 2.65 km
- 51 consumers with a load range of 5.0 kW to 72.0 kW

Up to five distributed decentralized heat producers (DCP) - in terms of solar thermal plants with each 100 m² gross area - are considered in Net G. A prospective integration of combined heat and power (CHP) units is planned. The second network is a 2nd generation-, meshed DH network, called Net B with the following main characteristics:

- installed load of 83 MW with a length of 41 km
- 485 consumers with a load range of 22 kW to 14.000 kW
- four meshes
- additional booster pump, installed in the return line

The simulation study for Net B focusses on the integration of up to 24 DCP in terms of solar thermal plants in the network. Three different sizes of gross area are installed with 500 m², 1000 m² and 5000 m², which are distributed in the network (compare Fig. 2). The sizes correlate with the respective consumer at the location according to the installed

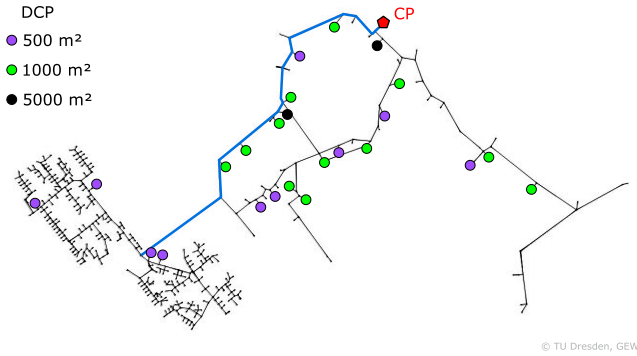


Fig. 2: Structure of the 2nd generation network - Net B - with central heat producer (CP) and decentralized heat producer (DCP) according to size of collector gross area; blue marked example segment

load of $\dot{Q}_{Ci} > 500 \text{ kW}$, $> 1000 \text{ kW}$ and $> 5000 \text{ kW}$. Similar to Net G, decentralized CHP units will prospectively considered.

The simulation study focusses on the two different weather data locations Würzburg and Potsdam (Germany), as regions with different radiation. The data source is Deutscher Wetterdienst (DWD), so original measured data is used for year 2015.

2.3. Consumer Modeling

Individual load profiles are crucial for a DH network simulation to prevent overestimated simultaneity in the network. The previous project *DEZENTRAL* used an adopted Typical-Day Method following VDI 4655 [5]. Measured data of consumer were adopted to specific weather data, and heat load profiles scaled to a given peak load. A detailed description can be found in [6].

This method was a pre-processing work and time-consuming for larger networks. Therefore, a new method was developed to enable online calculation of the heat load and return line temperature during the simulation. The procedure bases on linear regression models for 24 types of buildings (for Net B) and two types of buildings for Net G. As data source, hourly measured data for heat load and return line temperature of one or two years as well as the respective weather data was considered. The data sources for the Net B are not from this original network, but from different unknown networks. This fact is a major advantage, because it allows using these regression models in several different DH network simulations.

The heat load of each building type \dot{Q}_{Ti} mainly depends on the ambient temperature ϑ_a , the distinction of the working day W (working or a non-working day), the distinction of the heating period H (heating or non-heating period) and the hour of the day h , see equation (1). The return line temperature ϑ_{RLi} of each building type additionally depends on the supply temperature at the consumer ϑ_{SLi} as well as on the current heat load of the respective consumer \dot{Q}_{Ci} , see equation (2).

$$\dot{Q}_{Ti} = f(\vartheta_a, \vartheta_a^2, W, H, h) \quad (1)$$

$$\vartheta_{RLi} = f(\vartheta_a, \vartheta_a^2, W, H, h, \vartheta_{SLi}, \dot{Q}_{Ci}) \quad (2)$$

As a result, a set of regression coefficients were derived for each building type dependent on the hour of the day h and the heating period H . During the simulation, in each time step the relevant regression coefficients are used together with the other influencing parameters to calculate the heat load and return line temperature of each building type. Finally, the heat load for each consumer \dot{Q}_{Ci} is scaled to the installed heat load of the connection point of the consumer. The distribution of the different regression models in the network was realised, for example in Net B, by information of the network operator about the type of consumer (e.g. residential building, industry).

2.4. Decentralized Heat Producer

Two types of decentralized heat producers (DCP) are considered in the simulation study – solar thermal plants and combined heat and power units. The installed load differs according to network and location within. Currently only solar thermal plants are implemented in the network, however the integration of the CHP units is planned.

The model for the solar thermal plants developed the project partner *Solites*. It is based on an *EXCEL*-Tool and was transferred into the modeling language Modelica for coupling with the network simulation TRNSYS-TUD (see part 2.1). The model contains the calculation of the insolation towards the inclined plane, the collector and the required components like heat exchanger and pipes. As an input, the supply and return line temperature at the feed-in point as well as the temperature set point is required. The resulting feed-in heat to the network is given finally for each time step. All solar thermal plants are designed to reach the highest amount of heat, e.g. a 30° tilted collector with southern orientation. Further details on the characteristics of the solar thermal plants are described in [5].

2.5. Heat Storage Integration

The integration of a heat storage can be an element to reduce the impact of decentralized feed-in heat in the district heating network. Moreover, an excess of heat in the network due to feed-in, for example on summer days, can be used to load the storage for later unloading if necessary. Furthermore, the integration of heat storages in the network (central or decentral) can prevent stagnation of the solar thermal plants and can lead to a more efficient operation of the network, as well as of the solar thermal plants.

In this simulation study, one heat storage at the central heat producer is considered with different operation modes. The stagnation of all solar thermal plants installed is permitted, that means that a surplus of heat in the network will directly load the storage. For first investigations, the heat storage is considered here only per energy balance sheet without thermal losses. Three storage operation modes (SO) were implemented, distinguished by the way of unloading:

- SO-P: permanent unloading allowed if necessary
- SO-D: daily unloading allowed between 08:00 PM and 08:00 AM if necessary
- SO-W: weekly unloading allowed between Friday 08:00 PM and Monday 08:00 AM

The loading of the storage is allowed at all times. For first investigations, the size is unlimited to get an overview of the required storage volume demand. Loading of the storage occurs when a flow reversal in the supply line at the central heat producer is present due to an excess of heat in the network. In that case, the heat into the storage $\dot{Q}_{ST,in}$ is calculated with the net mass flow \dot{m}_{net} and the temperature difference of the supply line ϑ_{SL} and return line ϑ_{RL} , (compare Fig. 3). A detailed description how loading and unloading is integrated in the network simulation, is given in [7].

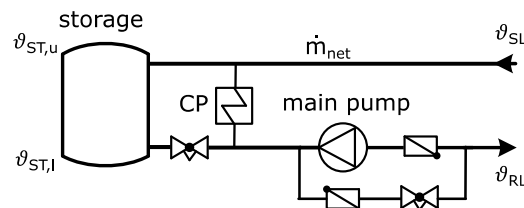


Fig. 3: Heat storage integration at central heat producer (CP); case of flow reversal displayed

The maximum volume of the storage is the result of the maximum amount of heat in the storage, due to an exceed of heat in the network caused by decentralized feed-in. The maximum volume is calculated with the highest amount of heat in the storage over the considered period. For the calculation, the difference of the upper storage temperature $\vartheta_{ST,u}$ and the lower temperature $\vartheta_{ST,l}$ with the respective specific heat capacity and density is used.

3. Results

3.1. Feed-In Results

For both considered networks, simulations have been made with feed-in in terms of solar thermal plants for both networks. One of the main evaluation parameters is the solar fraction SF , defined as ratio of solar heat input by DCP $\sum Q_{DCPi}$ to the sum of consumer demand $\sum Q_{Ci}$ and heat losses Q_{loss} of the network, see equation (3).

$$SF = \frac{\sum Q_{DCPi}}{\sum Q_{Ci} + Q_{loss}} \tag{3}$$

In Fig. 4, the sum of DCP annual solar-thermal input $\sum Q_{DCP}$ and the solar fraction SF are shown for the considered plants in both networks according to the location.

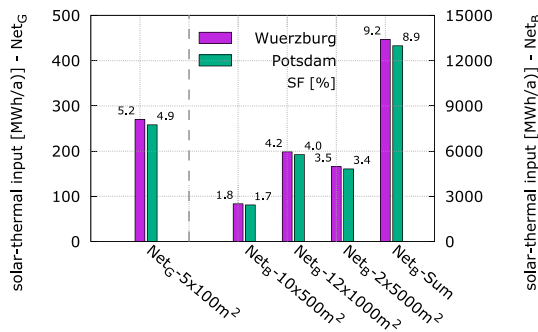


Fig. 4: Solar-thermal input and solar fraction of all considered thermal plants according to location and network

In Net G, a solar fraction of around 5 % was reached at both locations. The specific annual solar-thermal input leads to 515 kWh/(m²·a) for Potsdam and 540 kWh/(m²·a) for Würzburg. In Net B, none of the variants with only one size of collector area reaches a solar fraction of 5 %. However, the head load in the network is much higher. If all solar thermal plants are installed (27.000 m²), a solar fraction of around 9 % can be reached with a specific annual solar-thermal input of 480 kWh/(m²·a) for Potsdam and 497 kWh/(m²·a) for Würzburg.

These results show that the amount and size of installed solar-thermal plants leads to a solar fraction that is realistic and feasible for existing networks for the future. Moreover, the specific annual solar-thermal input is around 500 kWh/(m²·a), which stands for a high gain and makes it suitable for the investigations in this project regarding the thermo-hydraulic impact of feed-in.

The annual solar fraction is an important parameter for the overall evaluation. However, the solar-thermal input fluctuates significantly over the year. Fig. 5 present the monthly solar fraction for both networks with all variations of installed solar thermal plants, here only for Würzburg. It can be seen, that the solar fraction has a high fluctuation

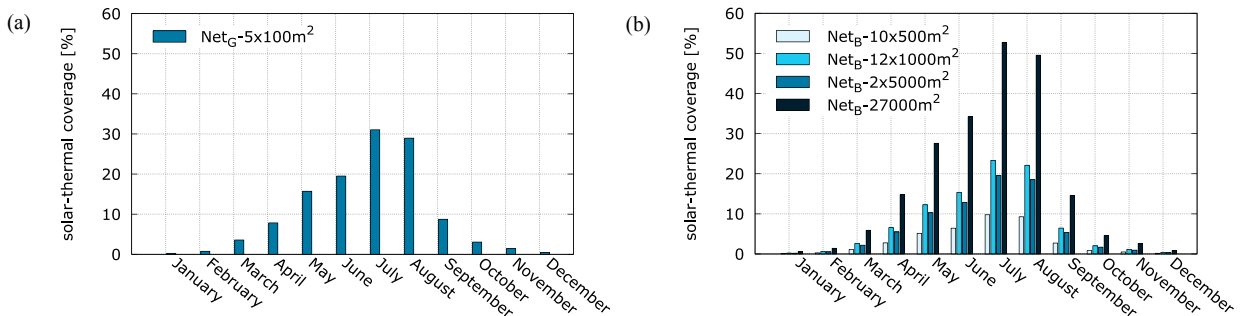


Fig. 5: Monthly solar fraction for Net G (a) and Net B (b) according to installed solar-thermal area for Würzburg

during the year and can reach more than 50 % in summer time for Net B, depending on the amount of solar thermal plants.

3.2. Heat Storage Operation

The main parameters of interest for the heat storage operation are the maximum required volume of the storage tank $V_{ST,max}$ as well as the possibly offline time of the central heat producer $\sum h_{CP,off}$ depending on the operation mode (compare part 2.5). In Table 1, the results are compared for Net G and Net B for the location of Würzburg. For both Networks, the results are given for the maximum amount of solar thermal plants in the network (Net G - 500 m²; Net B - 27.000 m² in total).

Table 1: Results of storage operation modes for both networks according to operation mode (Würzburg)

		Net G			Net B		
		SO-P	SO-D	SO-W	SO-P	SO-D	SO-W
$V_{ST,max}$	[m ³]	38	38	98	3.661	3.661	16.627
$\sum h_{CP,off}$	[h]	596	523	556	1.477	1.375	1.387
$\sum h_{DCP,in}$	[h]	1.636	1.636	1.636	1.724	1.724	1.724

The required size of storage strongly depends on the operation mode. For weekly mode (SO-W), the maximum required storage tank volume is 2.5 times larger than for the other modes (Net G), and 4.5 times larger in Net B. The sizes for permanent and daily mode do not defer, because in both modes the unloading cannot reach the subsequent loading period to extend the necessary size. The offline time of the central heat producer $\sum h_{CP,off}$ has the highest value at permanent operation, which can be explained by the time of allowed unloading. The operation modes SO-D and SO-W allow unloading at 08:00 PM where the demand is commonly higher than in the afternoon with mode SO-P. This leads to a faster unloading of the storage. The value $\sum h_{DCP,in}$ is the total time where decentralized heat producer (DCP) feed-in. It is equal in all operation modes due to same boundary conditions of the solar thermal plants. However, the value for Net B is lower than expected according to the solar fraction ratio (compare Fig. 4).

In Fig. 6 the progress of weekly storage operation (SO-W) is presented for Net B on eight summer days with all solar thermal plants installed. On each day, an excess of heat due to DCP occurs while the central heat producer goes offline. From Friday 20:00 PM to Monday 08:00 AM the heat storage is unloading with reloading in between. That

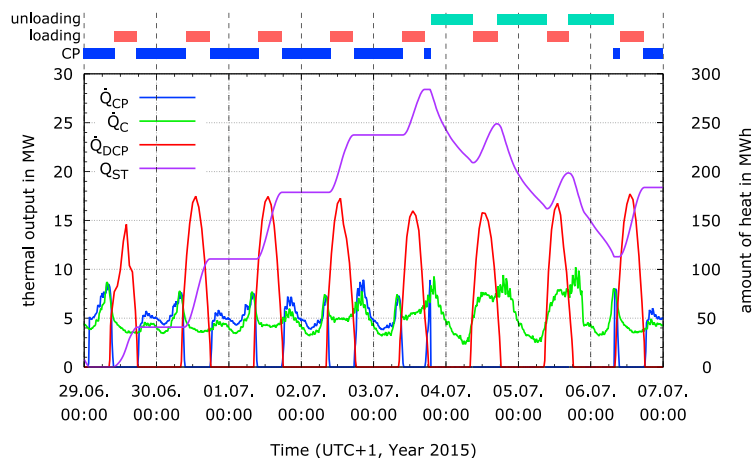


Fig. 6: Example for weekly storage operation mode (SO-W), Net B, Würzburg; 8 days from Monday 0:00 AM to Monday 0:00 PM

means that the central heat producer is offline for 36 consecutive hours. A further unloading would be possible according to the storage level, however, the weekly operation mode (SO-W) does not allow.

3.3. Pressure Maintenance

The pressure maintenance of the network is observed pursuant to possibly significant changes between operation without and with integrated decentralized heat producers. From solar thermal plants, fast pressure changes in the plant are well-known. On how far pressure maintenance in district heating networks is influenced by decentralized feed-in, is observed in this simulation study. Therefore, changes in the mass of the network fluid are considered over time and compared with each other. The volume of the network is set to be constant, that means that no thermal expansions of the pipes are considered.

First Investigations with Net B (compare Fig. 2) with all solar thermal plants installed (27.000 m²) has shown differences between the masses of the network with and without DCP, however not significantly. A few major deviations occur in times when DCP feed-in and network temperatures are higher, so in spring and autumn month. A second point of investigation was the change of mass within one simulation time step, which means 15 minutes in real. Here almost no deviations occur. Just the maximum value is higher in the version without DCP.

The first investigations have shown that an installation of decentralized heat producer in the network have no negative influence on the pressure maintenance. There are indications that with DCP the effort can be decreased, however further investigations are necessary.

3.4. Thermo-hydraulic Effects

The focus on the simulation study are the resulting effects of decentralized feed-in into district heating networks. Therefore, insights in flow conditions are observed according to pressure, mass flow and temperatures. The following example presents the results of a segment in Net B (compare Fig. 7 (left), and in total Fig. 2). However, these effects occur not only in meshed networks like Net B, but also in radial networks like Net G. On anytime decentralized feed-in appears, the following effects might occur depending on heat load conditions in the network.

Starting from the central heat producer (CP), eight decentralized heat producers (DCP) with different sizes are located along the segment (see Fig. 7 (left)). On each of the DCP a consumer is coupled behind, as well as further

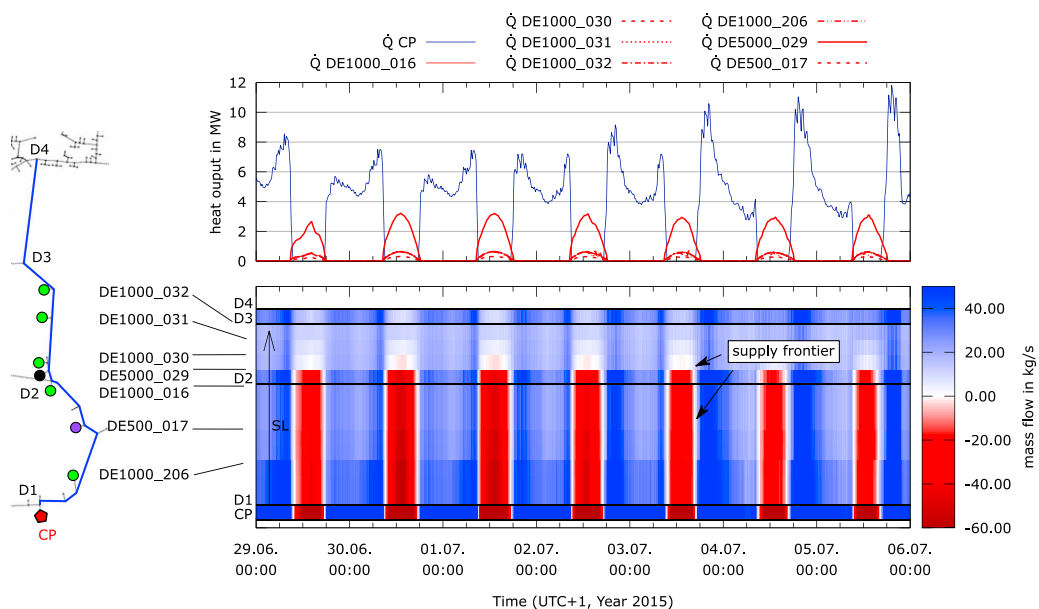


Fig. 7: Heat flow profiles and mass flow distribution for observed segment; summer week all DCP installed in network; Net B; Würzburg

ones along the segment. The network diversions D1..D3 are points where the observed segment enters or leaves a mesh, D4 is a network diversion where the net splits. In Fig. 7 (top) the progression of the heat flows for a representative summer week with high solar gains is shown. The heat load $\dot{Q}_{DCP,i}$ of all decentralized heat producers are given, as well as the heat provided by the central heat producer \dot{Q}_{CP} . The central heat producer is on every day for several hours offline, as seen in moments of $\dot{Q}_{CP} = 0 \text{ kW}$. Here a full supply of the DCP occurs in the whole network. In Fig. 7 (bottom) the time-equivalent diagram shows the distribution of the mass flow in the supply line over the length of the observed segment. The position of the DCP, diversions and central heat producer (CP) are marked along the y-axis. The blue colour implies mass flow in positive direction to the supply line (normal operation). The red colour indicates negative mass flow that means a flow reversal in the pipes occurs due to an excess of heat in parts of the segment. The transition between both conditions is marked in white. Here the flow velocity goes down to around zero, which is called a supply frontier (see the marked hint in Fig. 7 (bottom)).

In this example, on all seven days a flow reversal occurs between DE5000_029 and the central heat producer (CP) during daytime. At this time, from DE5000_029 to the end of the segment, a positive mass flow occurs. This means that part of the heat flow of the large plant with 5000 m² goes further along the Segment due to a demand of consumer and most of the heat goes back to the central producer with the heat storage, due to an excess of heat. The following DCP until the end of the segment (D4) provide the heat, necessary for the demand in this direction. Between the diversions D3 and D4 the mass flow significantly increases. Here one of the meshes ends, and the pipe supplies the subsequent network, as can be seen in Fig. 7 (left) and Fig. 2. During night, the mass flow is fully positive along the segment as expected due to no feed-in of DCP.

These alternating mass flow leads to alternating temperature profiles in the pipes. This is the main reason for thermal stress. Fig. 8 shows the time-equivalent temperature distribution of supply and return line. Examples of supply frontier zones are marked. The temperatures at these points are lower, compared to parts with feed-in. As the supply frontier is moving over time, an alternating thermal stress occurs at each pipe section. As a reaction of the supply frontier, higher fluctuation of the temperature can also be seen in the return line.

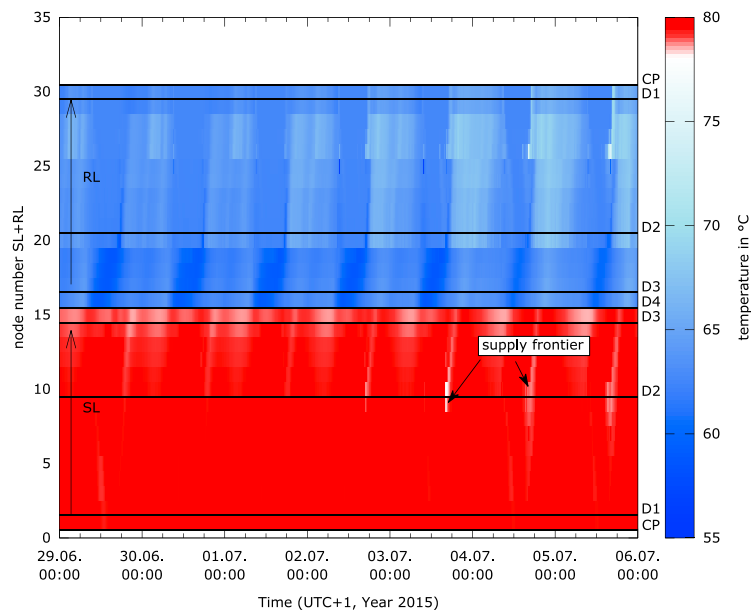


Fig. 8: Temperature distribution for observed segment; Net B, summer week; Würzburg

4. Conclusion and Outlook

The simulation study of the research project *DELFIN* gives an overview what kind of resulting effects can occur when decentralized heat producer feed-in into district heating networks. Moreover, first statements about the components pressure maintenance and heat storages were derived. The integration of a heat storage was discussed and several operation modes were investigated. As a result, a necessary size of the heat storage tank as well as the amount of possibly offline times of the central heat producer were determined according to the amount of decentralized heat producer and the storage operation mode. Furthermore, insights into the flow conditions of a representative segment of a meshed network have shown how decentralized heat feed-in influences the conditions in the pipes.

As a next step, pressure conditions in the network will be investigated in detail. Especially the requirements for feed-in pumps are in focus of the investigations. Statements shall be derived which generation of feed-in pumps are needed to ensure feed-in under conditions treated here and what are the challenges for the operation of feed-in and main pump. Furthermore, the topic of thermal stress will be treated in detail. Finally, the influence of decentralized feed-in to the net control strategy will be discussed.

Acknowledgements

This project was founded by the Federal Ministry for Economic Affairs and Energy (FKZ: 03ET1358B).

References

- [1] Heymann M., Rühling K., Felsmann C. "Integration of Solar Thermal Systems into District Heating – DH System Simulation" *Energy Procedia*, 116, (2017), Seoul, doi:<https://doi.org/10.1016/j.egypro.2017.05.086>
- [2] Felsmann C., Dittmann A., Richter W., Rühling K., Gnüchtel S., Sander T., Rhein M., Wirths A., Robbi S., Haas D., Eckstädt E., Knorr M., Meinenbach A., Gross S., Rothmann R. "Zusammenfassung LowEx Fernwärme: Multilevel District Heating." *FKZ: 0327400B, TU Dresden*, (2011)
- [3] Robbi S. "LowEx-Fernwärme – Vergleichende Bewertung von Maßnahmen für eine effiziente, multifunktionale Fernwärmeversorgung" PhD theses, *TU Dresden*, (2013)
- [4] Blochwitz T., Otter M., Arnold M., Bausch C., Clauß C., Elmqvist H., Junghanns A., Mauss J., Monteiro M., Neidhold T., Neumerkel D., Olsson H., Peetz J.-V., Wolf S. "The Functional Mockup Interface for Tool independent Exchange of Simulation Models" *8th International Modelica Conference 2011*, Dresden
- [5] VDI 4655 "Reference load profiles of single-family and multi-family houses for the use of CHP systems." *VDI, Verein Deutscher Ingenieure e.V.*, (2008)
- [6] Heymann M., Kretschmar T., Rosemann T., Rühling K. "Integration of Solar Thermal Systems into District Heating" *2nd International District Heating Conference*, (2014), Hamburg
- [7] Paulick S., Rühling K. "Effects On Decentralized Feed-In Into District Heating Networks – A Simulation Study" *5th International Solar District Heating Conference*, (2018), Graz



16th International Symposium on District Heating and Cooling, DHC2018,
9–12 September 2018, Hamburg, Germany

Forecasting District Heating Demand using Machine Learning Algorithms

Etienne Saloux^{a,*}, José A. Candanedo^a

^aCanmetENERGY, Natural Resources Canada, 1615 Boulevard Lionel Boulet, Varennes (QC) J3X 1P7, Canada

Abstract

Short-term forecasting of thermal energy demand is critical to optimally manage on-site renewable energy generation and the charge and discharge of energy storage devices in district heating and cooling (DHC) systems. As part of a larger study on advanced predictive control for a solar district heating system with 52 homes – the Drake Landing Solar Community (DLSC) – this paper investigates the use of Machine Learning algorithms to predict the aggregated heating load of the community.

In this study, the initial approach to estimate the heating load of the DLSC employed a piecewise linear regression based on the outdoor air temperature. Such an approach yields significant errors, in particular when weather forecasts are used instead of actual outdoor air temperature measurements. It has been found that Machine Learning algorithms, such as decision trees, can significantly improve the accuracy of predicted heating loads by incorporating the effect of additional influencing factors (e.g., time of the day, day of the week, solar radiation, etc.). In this study, the predicted heating demand obtained from different algorithms are compared under two different scenarios; (a) by using actual weather conditions from measured data; (b) by using weather forecasts. The potential implementation of such models for control purposes is discussed.

© 2018 The Authors. Published by Elsevier Ltd.

This is an open access article under the CC BY-NC-ND license (<https://creativecommons.org/licenses/by-nc-nd/4.0/>)

Selection and peer-review under responsibility of the scientific committee of the 16th International Symposium on District Heating and Cooling, DHC2018.

Keywords: solar community; heating demand prediction; Machine Learning algorithms; weather forecast.

* Corresponding author. Tel.: +1-450-652-0862; fax: +1-450-652-0999.

E-mail address: etienne.saloux@canada.ca

1. Introduction

Optimal energy management – including renewable energy generation, energy storage and demand-side strategies – is essential in the development of sustainable district heating systems [1]. Energy management requires an optimal control of the equipment that can be achieved through predictive control, whereby weather forecasts and other pieces of information (e.g., occupancy forecasts) are used to predict the system performance in advance (e.g., a few hours ahead) and to adjust the operation accordingly. The advantages of such approach have already been demonstrated in the past [2]. The present work investigates different modelling methods for the short-term forecasting (hours to days in advance) of the load of a solar community.

1.1. The Drake Landing Solar Community

In Canada, the Drake Landing Solar Community (DLSC) has a solar district heating system that provides space heating to a community of 52 residential houses by using solar energy [3]. This system has been in operation since 2007 and achieved remarkable performance by an appropriate management of solar energy that can be stored either at short-term – for immediate use and over the next few hours – or long-term – for future use later in the year – using seasonal borehole thermal energy storage (BTES). A schematic of this system is shown in Fig. 1.

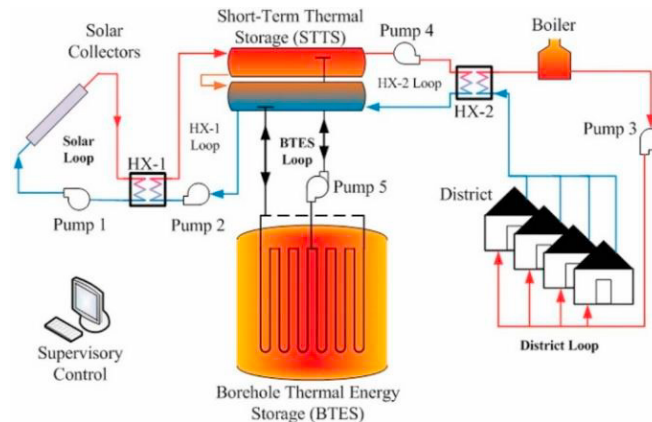


Fig. 1. Schematic of the Drake Landing Solar Community district heating system [3].

In this system, solar energy is harvested by means of solar thermal collectors and transferred to a short-term thermal storage (STTS), composed of two hot water tanks with a total volume of 240 m³ (120 m³ each). The STTS can then provide heat to the community when required; natural gas boilers are turned on when the stored solar energy does not suffice to fulfill the heating demand. On the other hand, if there is enough thermal energy in the STTS, a fraction of this energy can be transferred to the seasonal BTES for later use during the cold months of the year. After the first five years of operation, the solar fraction of this system – i.e., the fraction of the community heating demand satisfied by solar energy – has been consistently higher than 90%. In the period 2015-16 the solar fraction reached the maximum value of 100%; in other words, only solar energy was used to provide space heating to the community.

A detailed monitoring system records hundred variables (including temperatures, flow rates and electric power) at 10-min intervals. In particular, this monitoring system measures the water flow rate in the district loop that carries thermal energy to the houses as well as the temperature of water that is supplied and returns from the homes.

1.2. Forecasting the district heating demand

This study is part of a larger project, aiming at implementing predictive control to improve, or at least to maintain, the high level of performance of this solar district heating system. Reducing electric energy use by circulation pumps is of particular interest. To this purpose, it is essential to be able to predict the heating demand (either energy or power)

a few hours ahead in order to adapt the system operation consequently. Different approaches can be used to model this community. Simple models (such as linear regressions as a function of the outdoor air temperature), can be readily developed, but they might be not accurate enough, especially for short-term predictions. Data-driven models and machine learning techniques represent an untapped opportunity to develop models that are accurate, robust and account for effects that are not necessarily measured (for instance, the occupancy).

Within this context, the use of machine learning algorithms to predict building heating demand in buildings has already been investigated in the past. Artificial Neural Networks (ANN) and Support Vector Machines (SVM) are two of the most widely used techniques and their applications have been reviewed by Mat-Daut et al. [4] and Ahmad et al. [5]. Decision Trees (DT) are suitable as well to forecast energy consumption [6]. In addition to these techniques, Wang and Srinivasan investigated the capabilities of ensemble models for building energy use prediction [7], where multiple integrated algorithms are used to improve the performance of the model. Conversely, such an approach is highly dependent on the available data. The selection of model inputs may significantly affect model development and accuracy; Raza and Khosravi reviewed model inputs for smart grid and building load forecasting [8].

1.3. Objective of the present work

The objective of this paper is to develop models that predict the aggregated heating demand of the community by using machine learning techniques, and to compare the results with predictions from traditional linear regression models. Three machine learning techniques have been considered in this paper:

- Decision trees,
- Support vector machines,
- Artificial neural networks.

Since this work is developed for predictive control applications, it is essential that the model estimate the district heating demand accurately not only with recorded weather conditions, but also with weather forecasts. Thus, the model accuracy is assessed under two different scenarios:

- By using actual weather conditions from recorded data,
- By using actual weather forecasts from meteorological services.

The scope of this study is to assess the use of machine learning for district heating demand forecasting, rather than improving existing algorithms. The paper is organized as follows. Firstly, the modelling approach is discussed and an overview of the considered algorithms is presented. Secondly, the methodology is described, including the selection of training, validation and test periods and the use of weather measured data and forecasts. The accuracy of the different models is then investigated and compared. Possible model applications are finally discussed.

Nomenclature

ANN	Artificial Neural Network
BTES	Borehole Thermal Energy Storage
DLSC	Drake Landing Solar Community
DT	Decision Tree
OAT	Outdoor Air Temperature
NWH	Non-working hours
RMSE	Root Mean Square Error
SR	Solar Radiation
STTS	Short-Term Thermal energy Storage
SVM	Support Vector Machine
TOD	Time of the Day
WEND	Week-END

2. Modelling approach: linear regressions and machine learning algorithms

The district heating demand of the DLSC (the output variable) was calculated by using the water flow rate in the district loop (Fig. 1) and the temperature difference between supply and return. This section presents a conceptual summary of the models investigated for predicting the community heating demand. The considered models are: (a) linear regressions (used as the reference model); (b) decision trees; (c) support vector machines; and (d) artificial neural networks.

2.1. Input variables

The heating demand of a building depends on several variables. Weather conditions, mainly outdoor air temperature (heat losses through the building envelope), solar radiation (solar gains through windows, heating the building envelope) and outdoor air humidity, highly affects the energy consumption. Other variables, such as the occupant behaviour (temperature setpoint, internal heat gains, left ‘open’ windows, etc.), can also play an important role [9].

In this study, the aggregated heating load (kW) of the community was estimated by using as inputs one or more of the following variables: the outdoor air temperature, the horizontal solar radiation and occupant behavior related variables (Table 1). Weather conditions are measured on-site; weather forecasts are available from meteorological services [10].

In contrast with weather, there is no measured occupancy data. Two methods to account for occupancy were tested.

- a) The operation time is divided into working hours (i.e., people at their workplace) and non-working hours (i.e., people at home). For the purposes of this study, working hours are assumed to be from 8:00 to 18:00, Monday to Friday. This approach corresponds to a binary description of occupancy (the variable NWH may be either 0 or 1).
- b) The days of the week are divided into workdays (Monday-Friday) and weekends (the variable WEND is 0 or 1). Furthermore, the hour of the day (TOD), ranging from 0 to 23, was used as an additional input variable.

Table 1. Machine learning model inputs.

Model input	Variable	Unit	Value
Outdoor air temperature	OAT	°C	various
Horizontal solar radiation	SR	W/m ²	various
Non-working hours	NWH	-	[0, 1]
Time of the day	TOD	hr	[0, 1, 2, ..., 23]
Weekend	WEND	-	[0, 1]

2.2. Linear regression model

In general, linear regression models are quite simple, a fact which makes them attractive for control applications. However, the accuracy of these models is often quite low.

This study considered linear regressions with minimal and maximal values using a 2-hr “rolling” outdoor temperature (i.e., moving average of the last 2 hours) as their only input. Two separate linear regressions were used to calculate the heating demand: one for the flow rate and another for the temperature difference between supply and return. In this approach, solar radiation and occupancy effects were neglected. This simple model serves as the reference model.

2.3. Decision trees

Decision trees (DTs) use a binary classification process where the model inputs (i.e., outdoor air temperature, solar radiation, occupancy) are successively used to classify operation modes that predict a specific value of the model output (i.e., the heating load). Firstly, the main modes of operation are used to split the “trunk” into the main branches;

the categorization is subsequently refined as more conditions are incorporated, in a manner akin to the branches, twigs and leaves of a tree.

The complexity of DTs can be handled by using minimal “leaf size” constraints, i.e., a minimal number of observations that provide the same model output. For similar reasons, trees can be “pruned” to avoid overfitting. Pruning consists in judiciously removing branches that do not have a significant impact on the model accuracy.

2.4. Support vector machines

Support vector machines (SVMs) are generally used to solve non-linear problems and rely on structural risk minimization [11]. The principle is to find the optimal boundaries (hyperplanes) that maximize the distance between data points of distinct groups. In a non-linear problem, a SVM considers a Kernel distribution to optimize the margin. In this work, a Gaussian radial basis function has been used.

2.5. Artificial neural networks

Artificial neural networks mimic a human neural system and the process of learning [4] to determine appropriate connections between input(s) and output(s). These connections are constructed by means of neurons contained in hidden layer(s) [12]. The information transfer between input(s), neurons and output(s) is regulated by using appropriate weights. Meanwhile, at each neuron, the information undergoes a mathematical transformation (activation function). Such structure results in many connection possibilities. The model training consists in adjusting the values of the weights in order to match output predictions and targets (e.g., measurements) [12]. Weight optimization can be carried out by calculating the error between predictions and targets, and then adapting the weights via propagation learning methods.

This study employed a feedforward ANN, in which the information moves unidirectionally from input(s) to output(s). It contains a single hidden layer of 10 neurons. A tan-sigmoid activation function was selected; the Levenberg-Marquardt method was used for the backpropagation learning.

3. Methodology: model training, validation and test

Data-driven models require training (or calibration). By their nature they are subject to overfitting – a model that performs very well with the training dataset may perform poorly with a different one. To avoid this issue, models must be validated with a different dataset. For machine learning algorithms, the dataset used to “feed” the model is generally divided into “training” and “validation” periods; the training procedure evaluates the model accuracy in both periods. Once the model has been trained and is ready-to-use, a third dataset may be selected to test the model under yet different conditions. The selection of training, validation and test periods is described in this section.

3.1. Weather measured data

In this study, the models were trained by using measurements collected at 10-min intervals during two years of operation of the DLSC, from July 2015 to June 2017. This training-validation dataset was then randomly divided, 70% was used for training and 30% for validation. Furthermore, the accuracy of models was also tested by using an additional dataset corresponding to measurements for the next seven months (July 2017 to January 2018).

3.2. Weather forecast data

In addition to the on-site measurements, the models were tested with weather forecast data. The Canadian Meteorological Centre provides hourly forecasts up to 48-hour ahead, updated four times per day. In other words, every six hours a new forecast is released with 48 values per variable. The software tool CanMETEO [9] was used to facilitate the data retrieval and to store forecasts over several months. This method enables assessing the impact of under- and over-estimations of weather conditions (outdoor temperature, solar radiation) on the heating demand. It is

worth mentioning that overall, the outdoor temperature is quite well predicted (standard deviation of 2.2°C) while the intermittency of solar radiation makes it more difficult to forecast [13].

Machine learning models were tested using the recorded weather forecasts, ranging from July 2017 to January 2018. To match the time step of the recorded measurements, the hourly forecasts were linearly interpolated at 10-min intervals. Note that, due to technical issues (e.g., failures in the network), the forecast database is incomplete and does not cover the entire period. However, since four forecasts are released every day, several predictions exist for the same moment in time; this represents an equivalent period of around 3 years' worth of forecast data. Moreover, considering that weather forecasts are likely to be more accurate over the short-term (for example, only a few hours ahead), the model accuracy was calculated for two forecast horizons: 6-hr and 48-hr.

4. Results: model accuracy and district heating load forecasts

This section discusses the accuracy of the different models. The impact of model inputs is assessed by using both weather data recorded on-site and weather forecasts. The accuracy of the different models is evaluated by comparing their Root Mean Square Error (RMSE) with the value obtained from linear regressions (reference model). Scatter plots of heating load vs temperature are then examined. Finally, the influence of weather forecasts on short-term forecasting is discussed.

4.1. Comparison between model accuracy and impact of model inputs

OAT as the only input. The simplest modelling approach consists in using the outdoor air temperature (OAT) as the only model input (Fig. 2, top). Results with recorded data and weather forecasts are shown. In both cases, machine learning methods improve the accuracy of the results. Since in general short-term weather forecasts are more accurate, the models using 6-hr forecasts tend to outperform slightly those using 48-hr ahead forecasts.

OAT and SR as inputs. When solar radiation (SR) is included as an additional model input (Fig. 2, bottom), the accuracy is better when recorded data is used, but not necessarily with weather forecasts 48-hr ahead. This may be due to solar radiation forecasts that are not always accurate and the resulting error propagation. Again, shorter forecast horizons (6-hr) improve the accuracy.

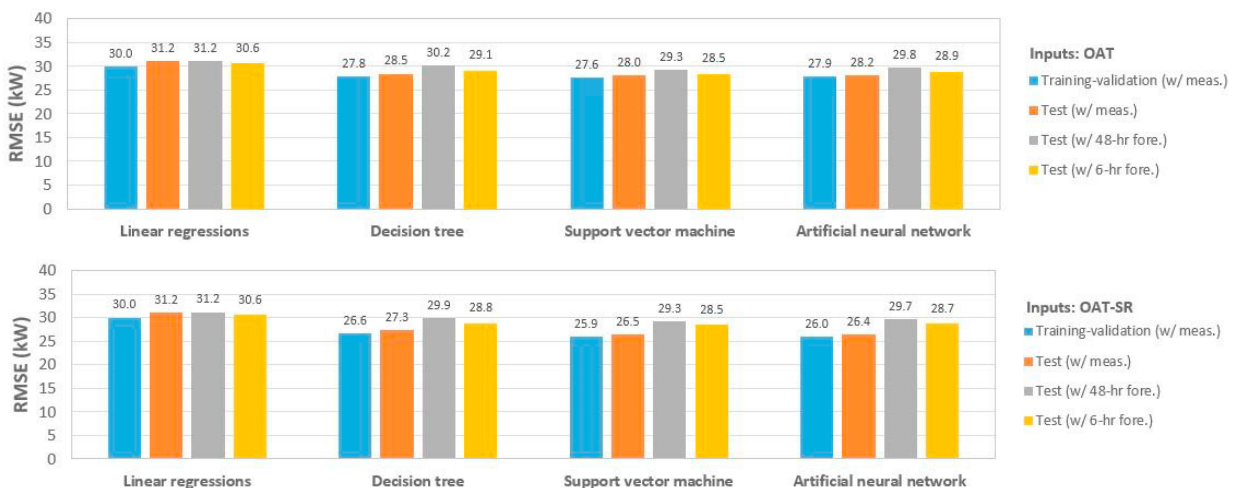


Fig. 2. Model accuracy (RMSE) using weather condition measurements and forecasts, with OAT (top) and OAT-SR (bottom) as inputs.

OAT, SR and occupancy index as inputs. The effect of occupancy was examined according to the models described above: (a) working- and non-working-hours" (NWH); (b) the time of the day (TOD) and whether or not the current

time is a weekend (WEND). Using NWH has a low impact on the model accuracy. Such an approach is equivalent to applying models for two operation modes and may explain the small difference compared with OAT-SR.

The detailed TOD-WEND model significantly decreases the RMSE with on-site measurements, especially for the training-validation period. Since these “occupancy” forecasts only depend on the day and the time of the day, they can be considered as “perfect”; the deviation may come from model overfitting. In general, except in the case of the SVM, 6-hr predictions provide similar results for OAT-SR-NWH and OAT-SR-TOD-WEND.

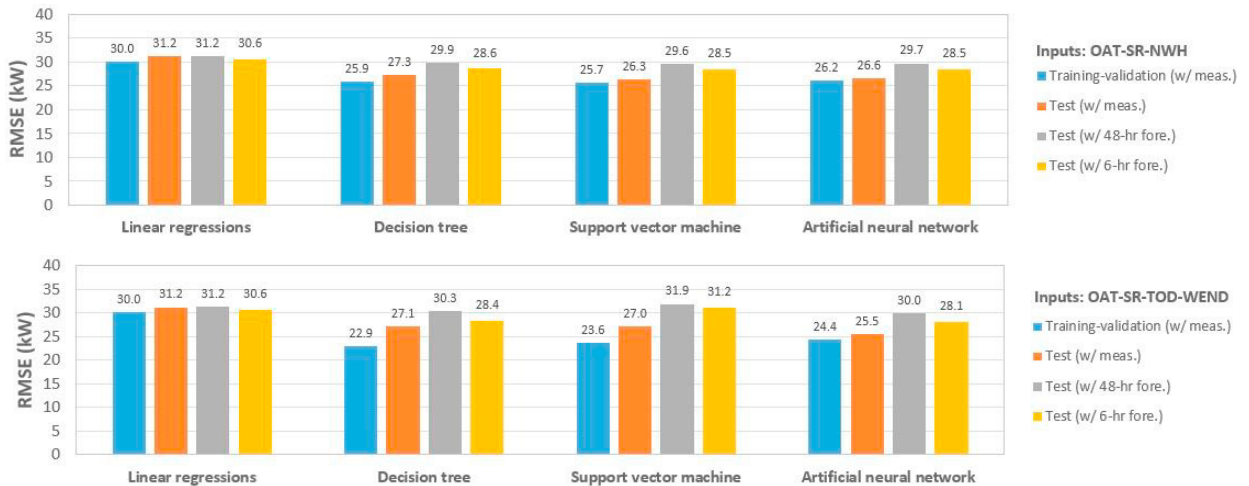


Fig. 3. Model accuracy (RMSE) using weather condition measurements and forecasts, with OAT-SR-NWH (top) and OAT-SR-TOD-WEND (bottom) as inputs.

In terms of algorithms, similar results were obtained with all the methods (DT, SVM and ANN). The main difference occurs for the SVM with OAT-SR-TOD-WEND as model inputs, in which the accuracy for weather forecasts is lower than with linear regressions. This might be because the SVM model struggles with the complexity of the TOD-WEND model (i.e. 24 values for both workdays and weekend). The RMSE improvement obtained by using machine learning techniques in comparison with linear regression is summarized in Table 2.

Table 2. RMSE improvement obtained by using machine learning techniques.

Model input	RMSE improvement		
	w/ meas.	w/ 48-hr fore.	w/ 6-hr fore.
OAT	7.3% – 10.1%	3.3% – 6.0%	5.0% – 7.0%
OAT-SR	11.3% – 15.3%	4.1% – 6.1%	5.8% – 6.8%
OAT-SR-NWH	12.4% – 15.5%	4.1% – 5.2%	6.5% – 7.0%
OAT-SR-TOD-WEND	13.0% – 23.9%	2.9% – 3.9%*	7.2% – 8.3%*

* The SVM is excluded from the calculations

4.2. District heating load forecasts

Scatter plots of heating load vs outdoor temperature, obtained using linear regressions, DT, SVM and ANN, have been shown in Fig. 4. Using linear regressions for both flow rate and temperature difference makes the reference model approximately follow a linear regression, whose “width” may be attributed to the 2-hr rolling outdoor air temperature.

The machine learning models considered OAT-SR-NWH as inputs. Therefore, for a given outdoor air temperature, the heating load might vary due to solar and internal heat gains (this results in a wider range of potential heating demands for a given outdoor temperature).

In the DT model, the binary classification process is limited by the “leaf size”, which reduces the number of possible heating demand values. Despite some negative values, the SVM and ANN models appear to predict the general trends of heating load variations appropriately.

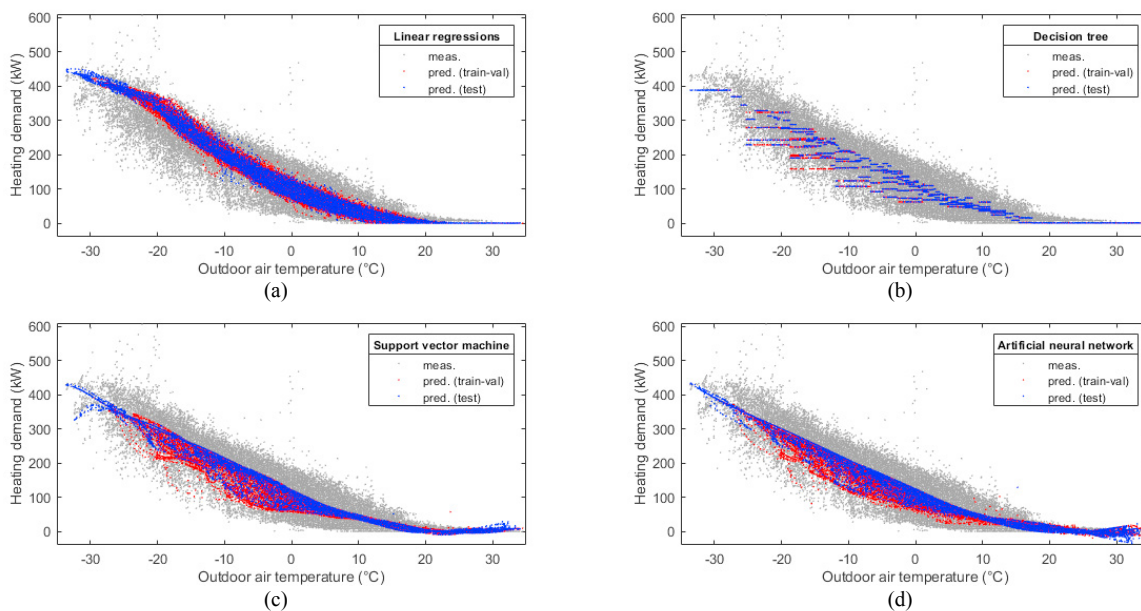


Fig. 4. District heating demand using (a) linear regressions, (b) decision tree, (c) support vector machine and (d) artificial neural network for the training, validation and test periods with measured weather conditions and OAT-SR-NWH as inputs.

Fig. 5 shows changes in heating demand with time. Measurements and model outputs using weather measurements are shown with solid lines; model outputs using weather forecasts (up to 48-hr and 6-hr ahead) are shown with markers. The selected period corresponds to 5 days in mid-January in which the ambient temperature decreased from 0°C down to -30°C, and then increased back, up to 0°C. During this period, the expected solar radiation was overestimated (1st day), well predicted (2nd-5th days) and underestimated (3rd day).

As shown in this figure, linear regressions capture the main trends but not necessarily short-term fluctuations (Jan 11-13). Machine learning algorithms allow accounting for these fluctuations, at both 6-hr and 48-hr ahead (similar results were obtained for DT and SVM). Moreover, on Jan 9, the solar radiation overestimation coincides with higher outdoor air temperature predictions and results in a clear underestimation of the heating demand. On Jan 10, weather conditions are well-predicted 6-hr ahead, which leads to accurate district heating demand predictions. Overall, machine learning models are accurate enough to be used for load forecasting.

5. Discussion: model applications and future work

Machine learning algorithms appear to provide accurate predictions for the community heating demand, even if, for the considered case study, accuracy gains are relatively small compared with a simple linear regression model. In particular, machine learning methods help predict short-term load fluctuations that might be very useful for control applications. Moreover, occupancy, and at a lesser extent solar radiation, appear to have a modest impact on the heating demand of this 52-unit residential community. This might be partially explained by a possibly low number of occupants (low internal gains), their individual behaviour (e.g., identical temperature setpoint during the daytime and nighttime) and their effect on the aggregated demand (individual effect, relatively to 52 homes). Furthermore, the configuration of the community, located on two east-west streets, might reduce solar gains (e.g., low window-to-wall ratio). Nevertheless, one should keep in mind that the strength of machine learning methods lies in their reproducibility

in other cases where occupancy and solar radiation may have a significant influence on the district heating demand that may not be predicted accurately using simple linear relations.

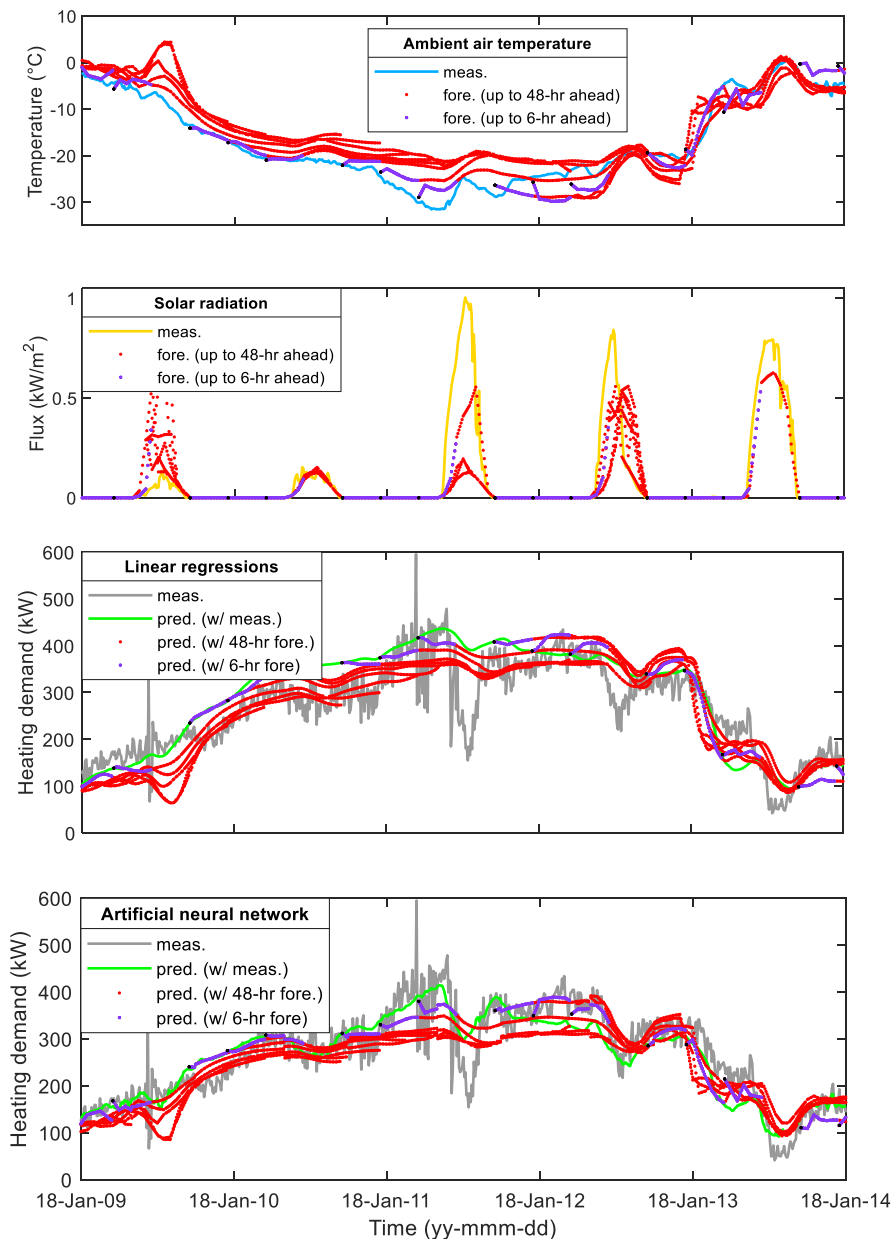


Fig. 5. Measured and forecasted outdoor air temperature, horizontal solar radiation and heating demand using linear regressions, artificial neural network (from top to bottom) and OAT-SR-NWH as inputs.

As part of a larger study on predictive controls in the DLSC, this paper represents a first step towards a ready-to-use and efficient machine learning algorithm to forecast the heating demand. Moreover, a detailed analysis of the model parameters for the three techniques used in this work might help improve the model accuracy. For example, the parametric analysis could investigate DT minimal leaf sizes and pruning, kernel distributions in SVM or the number of hidden layers and neurons in ANN. Dedicated models for the occupancy may also be developed while other

Artificial Intelligence (AI) algorithms could be analyzed. These include ensemble of trees, Gaussian process regression models and non-linear autoregressive artificial neural networks (with or without exogenous inputs). Regarding control applications, simulation parameters could also be investigated. In particular, the size of the time steps (e.g., 1-hr or 3-hr instead of 10-min) has significant impact, especially for autoregressive approaches, and is critical to account for short-term fluctuations.

6. Conclusions

This paper has discussed and assessed the use of machine learning algorithms to forecast the heating demand of the Drake Landing Solar Community. Decision trees, support vector machines and artificial neural networks have been considered and evaluated under two specific conditions: (a) using measured weather conditions and (b) using weather forecasts retrieved from meteorological services. Furthermore, different model inputs have been considered – outdoor air temperature, solar radiation and two occupancy models – and their influence on model accuracy has been evaluated. It has been found that all machine learning algorithms improve the accuracy of heating demand predictions – albeit modestly – when weather forecasts are considered, especially in the short-term (6-hr ahead) when forecasts are more accurate. Machine learning techniques capture short-term fluctuations, which are essential for control applications. It has also been found that the impact of occupancy (and solar radiation to some extent), is relatively low on this community demand and might be explained by the studied community configuration and occupant behaviour. Further research on these techniques (including auto-regressive methods and different time steps) will help in the development of appropriate data-driven models for control applications.

Acknowledgments

The financial support of Natural Resources Canada through the Office of Energy Research and Development is gratefully acknowledged. The authors also want to thank their colleagues from CanmetENERGY, in particular Doug McClenahan and Lucio Mesquita, for sharing their experience of Drake Landing and providing data. Their help was greatly appreciated. Internal and external reviewers are also acknowledged for their feedback.

References

- [1] Lund H, Werner S, Wiltshire R, et al. "4th Generation District Heating (4GDH): Integrating smart thermal grids into future sustainable energy systems." *Energy* 68 (2014): 1–11.
- [2] Quintana HJ and Kummert M. "Optimized control strategies for solar district heating systems." *J Build Perform Simul* 8 (2015): 79–96.
- [3] Sibbitt B, McClenahan D, Djebbar R, et al. "The Performance of a High Solar Fraction Seasonal Storage District Heating System – Five Years of Operation." *Energy Procedia* 30 (2012): 856–865.
- [4] Mat Daut MA, Hassan MY, Abdullah H, et al. "Building electrical energy consumption forecasting analysis using conventional and artificial intelligence methods: A review." *Renew Sustain Energy Rev* 70 (2017): 1108–1118.
- [5] Ahmad AS, Hassan MY, Abdullah MP, et al. "A review on applications of ANN and SVM for building electrical energy consumption forecasting." *Renew Sustain Energy Rev* 33 (2014): 102–109.
- [6] Johansson C, Bergkvist M, Geysen D, et al. "Operational Demand Forecasting In District Heating Systems Using Ensembles Of Online Machine Learning Algorithms." *Energy Procedia* 116 (2017): 208–216.
- [7] Wang Z and Srinivasan RS. "A review of artificial intelligence based building energy use prediction: Contrasting the capabilities of single and ensemble prediction models." *Renew Sustain Energy Rev* 75 (2017): 796–808.
- [8] Raza MQ and Khosravi A. "A review on artificial intelligence based load demand forecasting techniques for smart grid and buildings." *Renew Sustain Energy Rev* 50 (2015): 1352–1372.
- [9] O'Brien W and Gunay HB. "The contextual factors contributing to occupants' adaptive comfort behaviors in offices – A review and proposed modeling framework." *Build Environ* 77 (2014): 77–87.
- [10] Natural Resources Canada. CanMETEO, English / French., <https://www.nrcan.gc.ca/energy/software-tools/19908> (2017).
- [11] Lazos D, Sproul AB and Kay M. "Optimisation of energy management in commercial buildings with weather forecasting inputs: A review." *Renew Sustain Energy Rev* 39 (2014): 587–603.
- [12] Platon R, Dehkordi VR and Martel J. "Hourly prediction of a building's electricity consumption using case-based reasoning, artificial neural networks and principal component analysis." *Energy Build* 92 (2015): 10–18.
- [13] Candanedo JA, Saloux E, Hardy J-M, et al. "Preliminary Assessment of a Weather Forecast Tool for Building Operation." *5th International High Performance Buildings Conference* (2018) Purdue, July 9-12.



16th International Symposium on District Heating and Cooling, DHC2018,
9–12 September 2018, Hamburg, Germany

Optimal Temperature Control of Large Scale District Heating Networks

R. Bavière^{a,*}, M. Vallée^a

^aCEA, LITEN, 17 rue des Martyrs, F-38054 Grenoble, France

Abstract

The present paper synthesizes four years of research conducted by our team in collaboration with CCIAG, the operating company of the Grenoble large scale district heating network. This research focused on the design of a model predictive controller that optimizes the distribution of heat by an appropriate scheduling of supply temperatures and differential pressure at the production level. The controller relies on a heat load prediction covering a 24 h anticipation horizon combined with a constrained optimization problem. More specifically, our research was divided in four topics. First, we proposed and assessed various day-ahead load prediction models. An original feature of our work is to explicitly account for the network storage effect resulting from supply temperature variations. Second, we formulated a linear problem consisting of an objective function reflecting the production costs and a set of constraints representing, inter alia, the heat transport dynamics. In our solution, some of the parameters (e.g. producer-consumer temperature transportation delay) of the optimization program are periodically updated using dynamic simulation. Third, a fast fluid-dynamic simulation code based on a reduced-order model was designed and assessed. Finally, the developed models were all implemented and assembled in a decision support software tool called PEGASE. We proved the feasibility of running our controller in real-time for a large-scale DHN and the proposed solution is currently being evaluated by CCIAG.

© 2018 The Authors. Published by Elsevier Ltd.

This is an open access article under the CC BY-NC-ND license (<https://creativecommons.org/licenses/by-nc-nd/4.0/>)

Selection and peer-review under responsibility of the scientific committee of the 16th International Symposium on District Heating and Cooling, DHC2018.

* Corresponding author. Tel.: +00-33-4-38-78-20-61

E-mail address: roland.baviere@cea.fr

Keywords: High-Temperature DH; Operational Optimization; Model-Predictive Control; Heat Load Prediction

1. Introduction

Large scale District Heating Network (DHN) operated at variable supply temperature are installed in several large European cities, and more than 50 % of the heat delivered by French DHN is over 110 °C. Because of their size and complexity, operational optimization of these systems can lead to significant energy and cost savings.

As an example, the Grenoble urban district is equipped with the second largest DHN in France. The system delivers annually 900 GWh of heat to more than 1000 buildings, through a 150 km two-pipe network. The heat carrier fluid is pressurized water operated at a supply temperature ranging from 105 °C to 180 °C. The DHN is fed by 3 main supply units sourced by waste, biomass, coal, natural gas and heating oil. The renewable and recovery energy share amounted 60 % in the energy mix during the 2016-2017 heating season. Heat consumers are indirectly connected to the network by a sub-station (SST). The SSTs used in Grenoble are mainly composed of a heat exchanger, a control valve located on the primary side and a regulator controlling the secondary supply temperature using the aforementioned valve. In such a system, optimization even by a few percent leads to significant costs savings.

Energy load of large scale DHN such as the one in Grenoble is generally supplied by numerous generators relying on various fuels so that production costs depends largely on the load variations. On the other hand, large scale distribution networks are subject to complex dynamic behaviors originating from the variability of the demand and from significant temperature transportation delay between production and consumption. If the network supply temperature is variable the aforementioned transportation delay goes hand and hand with a thermal storage effect. Developing an appropriate temperature controller capable of mastering this so-called “network storage effect” paves the way to intelligent heat distribution accounting for the flexibility natively offered by such a large-scale DHN.

The present paper summarizes four years of research conducted by our team in collaboration with CCIAG, the operating company of the Grenoble DHN, to develop and assess a model-predictive controller to optimize the distribution of heat. The following section gives an overview of preexisting supply temperature controllers along with their limitations when an application to a large scale DHN is considered.

1.1. Related works

The approach traditionally used to determine the supply temperature of a DHN relies on heuristic methods, i.e. a formalization of common sense, simple logic or expert judgement. The single or even multi-variables (e.g. external temperature, hour of the day ...) heating curve is an application of such a method. Though simple to implement and robust with respect to production or demand uncertainties, the efficiency of such method is always limited when applied to a system comprising several sources, variable energy purchase prices and energy storage capacity. This is partly due to the fact that anticipative control strategies are difficult if not impossible to formulate in this framework. Another difficulty is that production goals may be multiple and conflicting (e.g. power and heat generation in combined heat-and-power units).

To overcome the aforementioned difficulties, a Model Predictive Controller (MPC) is an attractive alternative. An MPC is generally composed of a load prediction module and an optimization procedure used to determine the best possible path for control variables, i.e. the one minimizing an objective function while meeting different technical and operational constraints. Depending on the formulation of the quantitative objective to minimize, operating costs and/or CO₂ content of the delivered heat may be significantly improved.

However, formulating a general MPC for a DHN is a complex task, and most previous works only consider some parts of the problem. In particular, numerous studies deal with production optimization only, i.e. they address the unit commitment and load dispatch problem without considering distribution of heat. Several works also consider optimizing the supply temperature, in order to reduce heat losses and to leverage the network storage effect. For instance, the Finite Impulse Response method has been proposed to linearize a dynamic distribution network model, which can be used to solve a linear optimization problem [1]. While theoretically sound, this method is often impractical since it requires a prohibitive number of dynamic network model simulations at each optimization step. As an example, in the Grenoble case, deploying this MPC solution with a 24h prediction horizon and 15 minutes step

would require several hundreds of dynamic network simulations at each step. This would only be possible with a very low accuracy modeling, yielding non-exploitable control trajectories as a result.

Another possible approach consists in modeling, formulating and solving a dynamic optimization problem using dynamic programming. Following this method, it is possible to solve a short-term production planning problem for a DHN using a two-steps optimization procedure including production and distribution variables [2]. However, due to prohibitive computational costs, the network representation only includes few consumers. Other studies [3] can reach a result only under the restrictive assumption that the network mass flow rate is independent of the supply temperature. As a conclusion, no method is currently available for performing a model-predictive control of the supply temperature to leverage the network storage effect in large-scale DHN, where it is most useful. The work we conducted over the last four year demonstrates such a solution on a real-world DHN.

1.2. Structure of the paper

The rest of this paper is organized as follows. In section 2 we give an overview of the model predictive controller we developed. In section 3 we consider a load prediction model explicitly taking into account the network storage effect resulting from varying supply temperatures. In section 4, we present a novel fast-fluid dynamic network simulation model we introduced for addressing operational optimization in large-scale DHN. In section 5, we briefly describe the optimization model used in our model-predictive controller. In section 6, we report on the implementation of the controller for evaluation in an industrial environment. Finally in section 7 we present some results and conclude in section 8.

Nomenclature

α_k	Commitment factor for supply unit k [–]		
α	Commitment factor vector for all supply unit [–]		
$A_{1 \rightarrow 3}, A'_{1 \rightarrow 3}$	Load prediction coefficients (in equations (2) and (3))		
A_c	Parameter of differential pressure law for consumer c [Pa]		
B_c	Parameter of differential pressure law for consumer c [Pa/kg · s]		
Cal	Calendar information (day and hour within a week) [–]		
ΔP	Differential pressure at the load following plant of the network [Pa]		
F_T	Supply temperature modulation term [–]		
H_o	Anticipation horizon [s]		
$I_{k,c}$	Proportion of hot fluid consumed by c originating from supply unit k [–]		
\dot{Q}	Heating power [W]		
\dot{m}	Mass flow-rate [kg/s]		
N	Number of [–]		
T_{amb}	Ambiant temperature around the distribution pipes [°C]		
$T_{in,c}$	Primary inlet temperature at consumer level [°C]		
$T_{ins,c}$	Secondary inlet temperature at consumer level [°C]		
$T_{outs-sp,c}$	Secondary outlet set-point temperature at consumer level [°C]		
T_{S_k}	Supply temperature of unit k [°C]		
$\tau_{k,c}$	Temperature transportation delay between supply unit k and consumer c [s]		
$Th_{k,c}$	Thermal time constant between supply unit k and consumer c [s]		
$VOL_{k,c}$	Equivalent volume of flow path between supply unit k and consumer c [m^3]		
Wea	Weather prediction (temperature, wind speed, solar irradiance)		
\dot{W}_{pmp}	Mechanical pumping power [W]		
c	consumer	dmd	heat demand
k	supply unit	tot	total
$prod$	produced		

2. Overview of the model-predictive controller

The model-predictive controller we developed in the case of the large-scale Grenoble DHN is a generalization of the work presented in [4]. As depicted in Fig. 1, the overall functioning of the controller combines a dynamic simulation step and an optimization step. To reach an acceptable computational efficiency, and similarly to other work, the optimization step relies on a Mixed Integer Linear Programming (MILP) formulation. However, because of inherent non-linear dynamics of the DHN, we also perform a dynamic network simulation in order to provide updated inputs to the MILP optimizer at each optimization step. An example of such input variable is the transportation delay between the producers and the consumers. Since the outputs of the optimizer, i.e. the path for the supply temperatures and differential pressure control variables can alter the dynamic behavior of the network, we introduced iterations between the dynamic simulations and the optimizer.

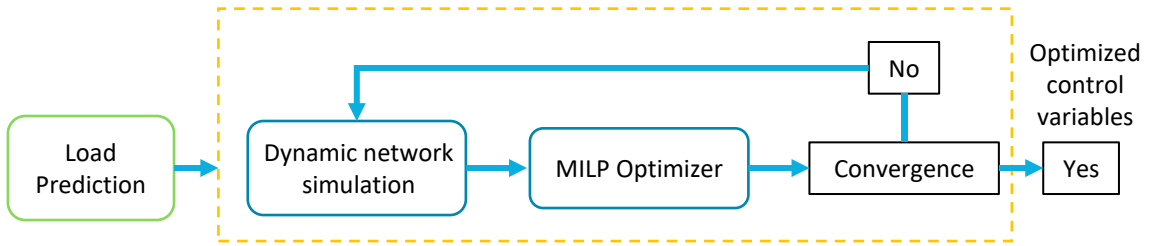


Fig. 1. General functioning of the model-predictive controller.

A key contribution of the work presented here is the generalization of the work presented in [4] to a large-scale DHN. In the following sections, we give an overview of the steps taken to improve the previously proposed solution. In particular, two key contributions are the improved load prediction taking the network storage effect into account, and the fast-fluid dynamic network simulation model.

3. Load Prediction including the network storage effect

The network storage effect is one of the key characteristics of the type of DHN we consider. Because of their large volume and varying supply temperatures, a significant amount of energy can be stored within the network itself, and introduce indirect dependencies between the actual demand and the heat injected in the network at each time. In this section, we highlight on the impact of taking into account the network storage effect when predicting the load of the network.

In [4], we show that a relation between the total demand $\dot{Q}_{dmd,tot}$, i.e. the sum of the individual demands at the consumer level, and the heat injected in the network $\dot{Q}_{prod,tot}$ at each time t can be expressed as:

$$\dot{Q}_{prod,tot}(t) = \sum_{k=1..N_k} \dot{Q}_k(t) = \dot{Q}_{dmd,tot}(t) \cdot [1 + F_T(t)] - \dot{W}_{pmp}(t) \quad (1)$$

In Eq. (1), k is the supply unit index, F_T is a modulation term that depends on past and present values of supply temperature and \dot{W}_{pmp} is the pumping work. It is important to note that in Eq. (1), \dot{Q}_{dmd} can in general not be measured directly, as it would require all consumers of the network to be equipped with real-time consumption measurement. On the contrary, all other terms can be derived from measures at the heating plants.

We note \tilde{X} the predicted value of the sample variable X for future times. Various methods can be found in the literature for estimating $\tilde{Q}_{prod,tot}$. In our work, similarly to [5], we consider a simple linear model combining data on predicted weather forecast, calendar information and past values of $\dot{Q}_{prod,tot}$. However, the originality of our work is that we not only consider direct estimation of $\tilde{Q}_{prod,tot}$ but also indirect estimation based on Eq. (1). In particular, we consider that $\tilde{Q}_{prod,tot}$ can also be estimated as the right hand-side of Eq. (1) where $\dot{Q}_{dmd,tot}$ is replaced by $\tilde{Q}_{dmd,tot}$ and F_T and \dot{W}_{pmp} can be accurately estimated for future times based on the planned supply temperature and differential pressure set points, which are controlled by the DHN operator.

Table 1 presents a comparison of the two alternative models we consider. This comparison is based on historical data from the CCIAG network in Grenoble, between 18/11/2013 00:00 and 17/03/2014 00:00, with a granularity of 1 hour. In order to focus on the respective quality of both models, we used the actual weather measurements (i.e. perfect weather forecast) as well as the actual values of supply temperature and differential pressure (i.e. perfect control of planned set-points). Each model then estimates the value of $\tilde{Q}_{prod,tot}$ for each hour based on vector $\mathbf{Wea}(t) = [\mathbf{Wea}(t-1), \mathbf{Wea}(t)]$ of current and predicted weather conditions at time t , on vector $\tilde{Q}_{prod,tot}^{past}(t) = [\tilde{Q}_{prod,tot}(t-1), \dots, \tilde{Q}_{prod,tot}(t-24)]$ of past values of $\tilde{Q}_{prod,tot}$ and on vector $\mathbf{Cal}(t)$ denoting the current day and hour of the week. In the direct estimation model, regression coefficients are computed directly for the relation:

$$\tilde{Q}_{prod,tot} = A_1 \cdot \mathbf{Wea} + A_2 \cdot \tilde{Q}_{prod,tot}^{past} + A_3 \cdot \mathbf{Cal} \quad (2)$$

In the indirect estimation model, coefficient are computed for $\tilde{Q}_{dmd,tot}$, before computing $\tilde{Q}_{prod,tot}$ using Eq. (1).

$$\tilde{Q}_{dmd,tot} = A'_1 \cdot \mathbf{Wea} + A'_2 \cdot \tilde{Q}_{prod,tot}^{past} + A'_3 \cdot \mathbf{Cal} \quad (3)$$

Table 1. Comparison of the direct and indirect load prediction models.

Model	MAE (MW)	RMSE (MW)
Direct estimation of $\tilde{Q}_{prod,tot}$	11.27	8.90
Indirect estimation of $\tilde{Q}_{prod,tot}$ from $\tilde{Q}_{dmd,tot}$	6.58	8.40

To ease the numerical vs. experimental cross-comparison, we used two common metrics namely the Mean Absolute Error (MAE) and the Root Mean Squared Error (RMSE). As it can be expected, considering the network storage effect in the prediction brings significant improvement in the load prediction accuracy, so that the MAE in the indirect estimation is almost half the MAE of the direct estimation. Indeed, the variables considered in the models are related to the actual demand, but can in general not reflect the control decisions taken by the DHN operators, especially if they are subject to specific rules (i.e. not only a heating curve). In the following, we consider a load prediction based on the indirect estimation model.

4. Fast fluid-dynamic simulation of the distribution network

As introduced in section 2, a dynamic simulation is necessary to account for the non-linear behavior of a DHN. This is for instance the case for the temperature transportation delay between producers and consumers. The dynamic simulation must therefore be able to simulate heat transport in a DHN.

In [4], we use a classical approach based on a one dimensional fluid dynamic model and a full physical representation of the network including pipes, fittings, pumps etc ... The distribution network is represented using a collection of nodes and edges and the physical behavior is modelled using mass, energy and momentum balance equations.

In the case of large scale systems, i.e. amounting several tens of thousands of nodes or edges, such an approach has proven to lead to excessive simulation times when used in an online operational optimization application, even with commercially available software. To circumvent this problem, aggregation methods [6-7] have been developed to progressively reduce the topological complexity of the model while tentatively conserving the most important physical properties of the original network. However, as pointed in [8], this aggregation process requires human decisions taken by an experienced researcher. More recently, Guelpa et al. [9] designed and evaluated a model based on Proper Orthogonal Decomposition combined with Radial Basis function for a large-scale network, and demonstrated encouraging results. In the present research program, we formulated and assessed another variation of reduced network model, hereafter referred as RNM.

4.1. Formulation of the Reduced Network Model for large-scale DHN

The proposed RNM firstly relies on the assumption that the fluid transported from supply unit k to consumer c flows through an equivalent virtual single pipe. The determination of the virtual pipes properties will be dealt with at the end of this section. It is well known that the temperature transport through a single pipe can be efficiently computed using the method of characteristics. We further assume that we can linearly combine the contributions from the various supply units. This reasoning leads to the following equation, linking the network temperature at the consumer level $T_{in,c}$ to the past values of the supply temperature TS_k at the production level:

$$T_{in,c} = \sum_{k=1..N_k} I_{k,c} \cdot \left\{ T_{amb} + [TS_k(t - \tau_{k,c}) - T_{amb}] \cdot e^{-\tau_{k,c}/Tth_{k,c}} \right\} \quad (4)$$

where $I_{k,c}$ is the proportion of hot fluid consumed by consumer c originating from supply unit k , T_{amb} is the ambient temperature surrounding the distribution pipes, and $\tau_{k,c}$ and $Tth_{k,c}$ respectively stand for the transportation delay and the mean thermal time constant of the flow-path between supply unit k and consumer c . In Eq. (4), $\tau_{k,c}$ is evaluated using a predefined equivalent volume denoted $VOL_{k,c}$ and the recent history of the total network mass flow-rate denoted \dot{m}_{tot} .

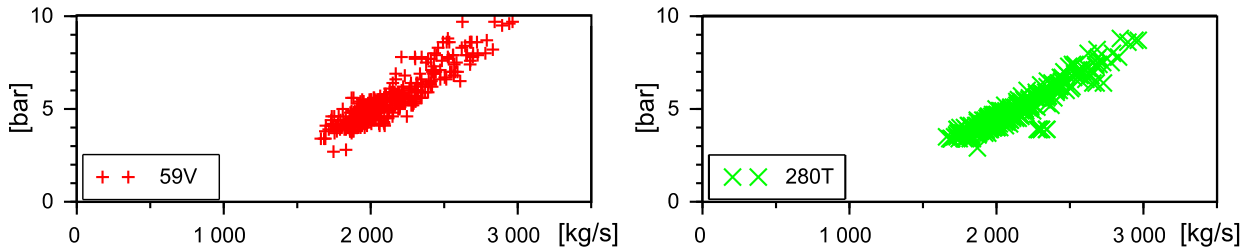


Fig. 2. $\Delta P - \Delta P_c$ as a function of the total network mass flow-rate \dot{m}_{tot} for the two consumers “59V” (left) and “280T” (right) – experimental results for operating condition $\alpha = [0.3; 0.38; 0.32]$ (see equation (7) for the definition of α).

By observing the experimental evolutions of the differential pressure (see Fig. 2), we then assume that the value at consumer c , i.e. ΔP_c , can be computed using the following simple linear relation:

$$\Delta P - \Delta P_c = A_c + B_c \cdot \dot{m}_{tot} \quad (5)$$

where ΔP is the differential pressure imposed in the load following plant of the network and A_c and B_c are parameters of the law.

Then, a sub-station model is required to link the clients’ heat consumption to the network mass flow-rate. Inputs of the model are the secondary inlet and the outlet set-point temperatures (respectively denoted $T_{ins,c}$ and $T_{outs-sp,c}$), as well as the heat demand \dot{Q}_c and the primary differential pressure at the consumer level. We compute the thermal behavior of the heat-exchanger using a conventional logarithmic mean temperature difference formulation valid for a counter-flow configuration. As in [10], our model explicitly represents the hydraulic regime where the client’s heat request is not satisfied. From a computational point of view, our model is expressed by a non-linear function F_{SST} (see below) which is solved for variable \dot{m}_c , i.e. the primary mass-flow-rate for consumer c :

$$F_{SST}(\dot{m}_c, T_{in,c}, T_{ins,c}, T_{outs-sp,c}, \dot{Q}_c, \Delta P_c) = 0 \quad (6)$$

F_{SST} is solved for each consumer and their respective contribution are summed to compute the total network mass flow-rate \dot{m}_{tot} . Since \dot{m}_{tot} is both an input for Eq. (4) and (5) and a result of the calculation procedure, we use an iterative procedure associated to a termination criteria based on numerical increments to solve the RNM.

To be accurate, the RNM must be properly parametrized; in particular the values for $I_{k,c}$, $Tth_{k,c}$, $VOL_{k,c}$, A_c and B_c must be fixed. To do so, we rely on simulations carried with an off-line higher-order static model comprising an

exhaustive description of the Grenoble network in terms of pipes, dimensions, materials etc... For each operating condition, we determine and store an independent set of parameters for quick inline retrieval. In our work, the operating conditions of the network are primarily described using the commitment factor vector α :

$$\alpha = [\alpha_1 \dots \alpha_{N_k}] \quad \text{with} \quad \alpha_k = \dot{m}_k / \dot{m}_{tot} \quad (7)$$

where \dot{m}_k stands for the mass flow-rate heated by supply unit k . Thus, the possible operating conditions of the network are scanned using a collection of discrete values of α . The cardinality of this collection depends on the number of supply units in the network and on the size of the discretization step. To establish the RNM of the Grenoble DHN containing 3 supply units, we relied of several thousands of independent parameters sets for the RNM.

4.2. Validation of the RNM

The accuracy of the proposed RNM model has been evaluated by cross-comparing experimental and numerical results. The numerical results were obtained by simulating a past heating season, from November to late March. The measured values of the supply temperatures, of the differential pressure for the load following plant and of the commitment factors were used as boundary conditions for the simulation. The clients' heat demand and secondary temperatures were estimated and imposed as boundary conditions in the simulation.

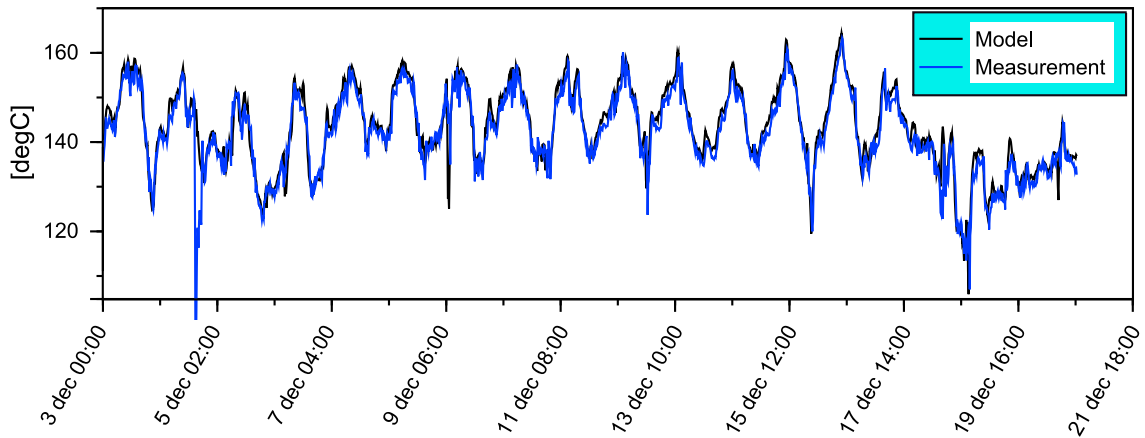


Fig. 3. Numerical vs. Experimental cross-comparison of the network temperature for consumer “95V”.

Fig. 3 shows an extract of the obtained result. The scores obtained over the heating season for the 7 consumers monitored in terms of temperature and differential pressure, namely “13V”, “95V”, “13EY”, “1LT”, “219T”, “280T” and “240N”, are summarized in Table 2. As can be seen in Table 2, the accuracy is acceptable for $T_{in,c}$ but only partly satisfying for ΔP_c . We are thus currently working to improve the accuracy of the RNM model for ΔP_c .

Table 2. Temperature and differential pressure accuracy of the RNM for 7 consumers.

		“13V”	“95V”	“13EY”	“1LT”	“219T”	“280T”	“240N”
ΔP_c (bar)	MAE - RMSE	0.86 – 0.49	0.94 – 0.51	1.03 – 0.56	1.24 – 0.72	0.59 – 0.36	0.61 – 0.39	1.11 – 0.42
$T_{in,c}$ (°C)	MAE - RMSE	2.05 – 1.4	2.05 – 1.31	3.13 – 2.17	2.04 – 1.19	2.22 – 1.09	1.13 – 0.78	3.48 – 2.31

5. The MILP optimization problem

In the case of a large-scale DHN, we use a MILP formulation similar to the one described in [4], with two notable changes we introduced to cope with large-scale DHN.

The first change is on the critical conditions to supply heat demand. We recall here that the critical conditions are the network operating conditions ($T_{in,c}$, ΔP_c) at the consumer level below which the heat demand cannot be fulfilled. To limit the number of constraints and the size of the optimization problem, these inequality constraints are only written for a reduced set of consumers, called representative consumers. Implicitly, our controller considers that if the operating conditions of the network exceed the critical conditions for all representative consumers, then this will be the case for all the consumers of the network. In practical terms, we can consider up to one hundred representative consumers without significantly increasing the computational burden.

The second change is on the linearized distribution network model, in which the modulation term $F_T(t)$ is dynamically constructed based on the RNM presented in section 4.

6. Implementation of the controller

In order to be properly evaluated in an industrial context, the proposed controller has been implemented and deployed as a decision-support software at the Grenoble DHN operator. The implementation is based on a dedicated model-predictive control platform called PEGASE. PEGASE provides the key features for:

- Retrieving data from a Supervisory Control And Data Acquisition (SCADA) or equivalent industrial automation environment, using standard protocols;
- Sequencing the execution of heterogeneous dynamic simulation models, based on the Functional Mock-up Interface (FMI) standard [11];
- Performing dedicated computations (e.g. load prediction, MILP optimization), at scheduled time steps;
- Presenting the evolution of the control program, using graphs as well as dedicated Human-Machine Interface using the Qt/QML framework

PEGASE has been designed on top of a FMI-compliant co-simulation platform provided by L3S company [12], especially by introducing support for (1) managing receding time horizon at each MPC iteration (2) interfacing with open-source and commercial MILP Solvers. The receding time horizon, as illustrated in [4], involves performing the whole optimization process described in Fig. 1 at regular time intervals, in order to cope with prediction uncertainties. While this concept is absent from the original co-simulation platform, it has been introduced with the use of vector variables representing time series over a given horizon. The interface with various solvers has been implemented using dedicated C++ code, which performs the formulation of the MILP problem at each iteration and communicates with existing MILP solvers.

7. Results and discussion

7.1. Verification of the linear model

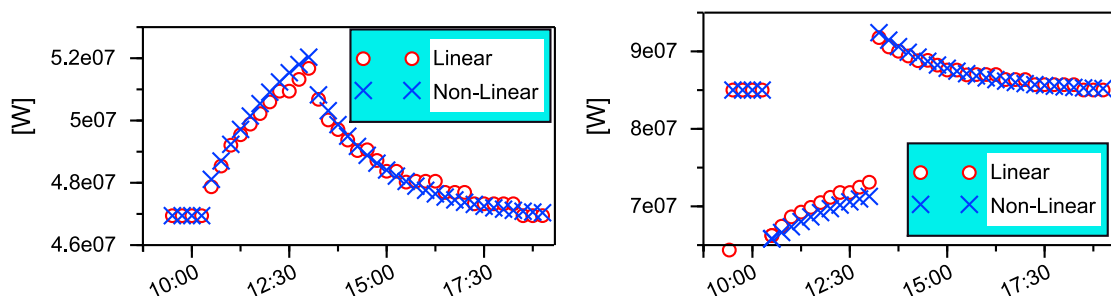


Fig. 4. Heating power of supply units n° 1 (left) and 2 (right): comparison between the linear and a non-linear network model for a simulation scenario where supply temperature of unit n°2 is temporarily decreased while the remaining boundary conditions are kept constant.

Before implementing the linear model within the MILP controller, we verified it by comparing its result to that of a non-linear network model. 30 analytical scenarios were simulated to that end. Figure 4 presents typical results obtained during this verification step for a scenario where all boundary conditions are kept constant except for the temperature of supply unit n° 2, which is temporarily decreased by 15 °C. As can be seen on the graph, the agreement between the linear and non-linear model is acceptable for control purposes.

7.2. Verification of the optimal controller

We then verified the behavior of the controller for different elementary simulation scenario. We present an example of obtained result in Figure 5, which corresponds to a simulation scenario where the heat production costs are constant except during the 5:00 to 5:45 time slot where they are increased by 20 %. We note that the controller anticipates the production cost perturbation by increasing the supply temperature thereby storing heat directly into the distribution network. It is also worth mentioning that the controller selects a supply temperature always above the critical temperature at the consumer level. We recall that the critical conditions are the operating conditions at the consumer level below which the demand cannot be fulfilled. To ease the verification process, we considered identical critical conditions for all representative consumers (see section 5 for more details) and we only plot the critical temperature corresponding to a differential pressure of 1 bar.

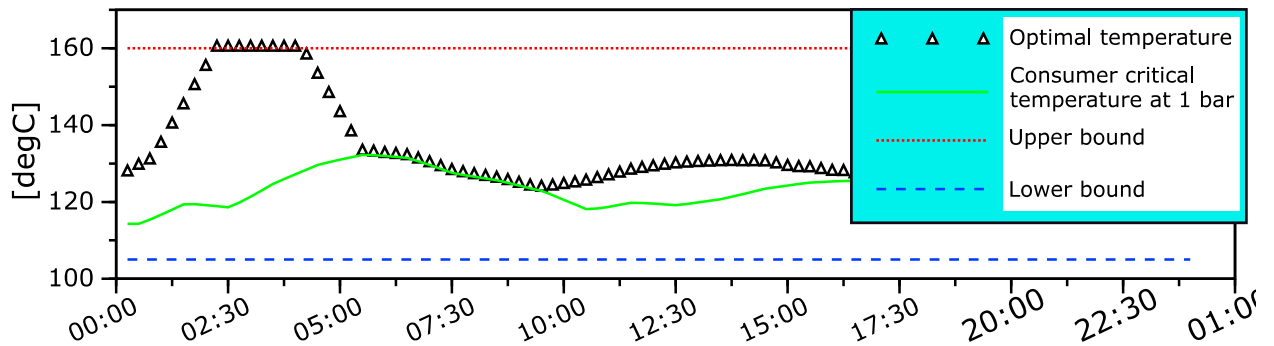


Fig. 5. Temperature for supply unit n°3 computed by the optimal controller for a simulation scenario where thermal production costs are temporarily increased by 20 % during the 5:00 → 5:45 time-slot.

7.3. Numerical performances

As an example on the case of the Grenoble DHN, the controller is run every 15 min and takes only a few seconds on a standard laptop (26 Ghz quad-core processor, 16 Go Random-access Memory RAM). The RNM takes around 10 ms per time-step to compute the evolution of relevant state variables at 789 consumers (i.e. around 75% of the network consumers, the remaining 25% being smaller and not monitored). The optimization problem contains around 2,5k continuous variables and more than 11k constraints and is solved in less than 3s by an open source solver, although it is well-known that a commercial solver would be much faster. It is worth mentioning that the problem was built considering 50 representative consumers.

Our approach and implementation demonstrates not only the feasibility of running our controller in real-time for a large-scale DHN, but also the feasibility of performing detailed yearly simulations including MPC for evaluation and dimensioning purpose.

8. Conclusions

In this paper we present a framework for optimal temperature control of large-scale DHN with multiple supply points. More precisely, we first present a load prediction model explicitly taking into account the network storage effect resulting from varying supply temperatures. We then describe and assess a novel fast-fluid dynamic network

simulation model we introduced for addressing operational optimization in large-scale DHN. We then briefly describe the optimization model used in our model-predictive controller. We also report on the implementation of the controller within the so-called PEGASE software. We demonstrated that the accuracy and numerical performances of our controller were sufficient to consider testing it in real-life conditions. Our solution is therefore currently being tested on the Grenoble DHN (see Fig. 6).

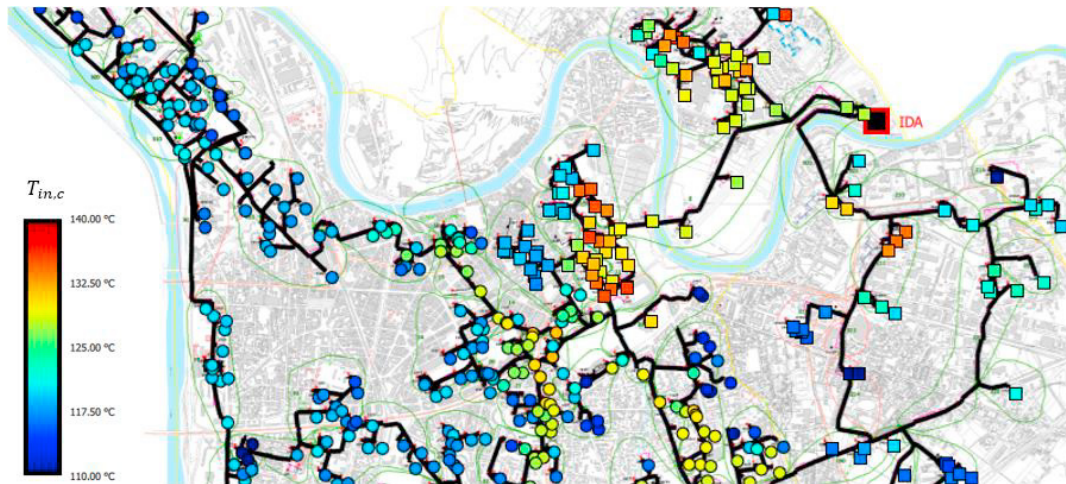


Fig. 6. Screenshot of the PEGASE software Human-Machine Interface showing the network temperature at the consumer level: zoom on the northern part of the Grenoble DHN.

Acknowledgements

This research work was funded by CCIAG, our industrial partner in the project. The authors sincerely wish to thank Elise Le Goff, Ana Tempass-De-Soussa, Nicolas Giraud and Philippe Clotot for the many stimulating exchanges and for providing real-life data from the Grenoble network.

References

- [1] Nielsen T. S., Madsen H., "Control of supply temperature in district heating systems with multiple supply points", *Proc. ECOS* (2005): 1071-1079
- [2] Schweiger G., Larsson P.-O, Magnusson F., Lauenburg P., Velut S. "District Heating and cooling systems – Framework for Modelica-based simulation and dynamic optimization", *Energy* 137 (2017): 566-578
- [3] Gu W., Wang J., Lu S., Luo Z., Wu C., "Optimal operation for integrated energy system considering thermal inertia of district heating network and buildings", *Applied Energy* 199 (2017) 234-246
- [4] Giraud L., Merabet M., Bavière R., Vallée M. "Optimal Control of District Heating Systems using Dynamic Simulation and Mixed Integer Linear Programming", *Proc. 12th International Modelica Conference* (2017): 141-150
- [5] Dotzauer E. "Simple model for prediction of loads in district-heating systems" *Applied Energy* 73 (2002): 277-284.
- [6] Larsen H.V., Palsen H., Bohm B. and Ravn H.V., "Aggregated dynamic simulation model of district heating heating networks" *Energy Conversion and Management* 43 (2002): 995-1019.
- [7] Loewen A., Wigbels M., Althaus W., Augusiak A., Renski A., "Structural simplification of complex DH-networks" *Euroheat & Power* (2001):46–50.
- [8] Larsen H.V., Bohm B. and Wigbels M., "A comparison of aggregated models for simulation and operational optimization of district heating networks" *Energy Conversion and Management* 45 (2004): 1119-1139.
- [9] Guelpa E., Toro C., Sciacovelli A., Melli R., Sciubba E., Verda V., "Optimal operation of large-scale district heating networks through fast fluid-dynamic simulation", *Energy* 102 (2016): 586-595.
- [10] Giraud L., Bavière R., Paulus C., Vallée M., Robin J.-F., « Dynamic modelling, Experimental Validation and Simulation of a Virtual District Heating Network », *Proc. ECOS* (2015)
- [11]: <http://fmi-standard.org/>, accessed in May 2018
- [12]: <https://web.1-3s.com/>, accessed in May 2018



16th International Symposium on District Heating and Cooling, DHC2018,
9–12 September 2018, Hamburg, Germany

Optimal conditions for accelerated thermal ageing of district heating pipes

A. Vega^{a,*}, N. Yarahmadi^a, I. Jakubowicz^a

^a*RISE Research Institutes of Sweden, Gibraltargatan 35, Gothenburg, 412 79, Sweden*

Abstract

Technical lifetime prediction of polymeric materials is often based on accelerated ageing tests at elevated temperatures. Samples are exposed to relatively high temperatures to accelerate the natural degradation processes. For district heating pipes, accelerated thermal ageing is the ordinary method used to determine the lifetime of pipes. According to the Standard EN 253:2009 + A1:2013, the district heating pipes shall be subjected to an accelerated thermal ageing for a long period of time at 160 °C or 170 °C. The lifetime is determined by extrapolation using the Arrhenius relationship. However, papers published recently have questioned this method, especially the high temperatures used for ageing of the pipes and the use of Arrhenius equation to describe the complicated degradation mechanisms, which can result in the erroneous estimation of the technical lifetime.

Our investigation has shown the complexity of the pipe's degradation mechanisms. The behaviour of mechanical shear strength at elevated temperatures ($T > 130$ °C), suggests an alteration rather than an acceleration of the degradation mechanisms. Accelerated ageing tests should reproduce the proper natural ageing mechanisms. The analyses of PUR's thermal conductivity and its chemical structure by FTIR confirmed the degradation patterns.

© 2018 The Authors. Published by Elsevier Ltd.

This is an open access article under the CC BY-NC-ND license (<https://creativecommons.org/licenses/by-nc-nd/4.0/>)

Selection and peer-review under responsibility of the scientific committee of the 16th International Symposium on District Heating and Cooling, DHC2018.

Keywords: Degradation mechanisms; district heating pipes; rigid polyurethane foam; accelerated ageing

* Corresponding author. Tel.: +46 10 516 58 57; fax: +46 31 16 12 95.

E-mail address: alberto.vega@ri.se

1. Introduction

New elements have been introduced to the district heating (DH) systems looking for more sustainable networks. Integration of renewable energies into the DH networks is a reality which has been possible due to the use of better insulation materials in new buildings. In the last years, a new generation of DH technology has been discussed. The 4th generation of DH system (4GDH) integrates different energy systems and operate at lower temperatures in combination with low-energy buildings. It means smarter distribution networks looking for synergies between several energy sources [1]. This development seems like a natural and needed improvement of DH networks to become more efficient. However, the current DH networks should be improved to deal with future issues. Today, there is almost 600 000 km of distribution pipes from older generations, especially from the third generation, around the world today [2]. A big challenge is to understand the DH pipes' deterioration which would be helpful for the urban and energy planning activities for the future.

The standard method used today for lifetime prediction of DH pipes is based on accelerated thermal ageing at relatively high temperatures and evaluation of the mechanical shear strength during the ageing period. Then, an Arrhenius relationship is applied to extrapolate the results to the average operating temperature. Recently, researchers have pointed out that thermal ageing at relatively elevated temperatures alters the degradation mechanisms rather than accelerate them as mentioned in [3,4]

The first part of our investigation focused on the degradation mechanisms of rigid polyurethane (PUR) foam [5]. The main aim of the second part was to understand the degradation mechanisms of PUR in DH pipes aged artificially. We studied the ageing effects on the pipes' mechanical and thermal performances, which are of vital importance for the correct functionality of the DH networks. Non-standard methods were used to measure both thermal and mechanical properties. Fourier Transform Infrared (FTIR) analyses were performed to study the changes of PUR chemical composition and the ageing effects.

2. Experiments

Four DH pipes were instrumented with thermoelements type K and transient plane sources (TPS) sensors for measurements of temperature and thermal conductivity, respectively. The pipes were placed in a controlled temperature chamber at 23 °C. Three pipes were connected to controllers to heat up the service steel pipe to the corresponding ageing temperatures, 130, 150 and 170 °C. The remaining pipe was kept at room temperature, and the reference measurements were performed on it.

The SP plug method, described in [6], was used to measure the pipes' mechanical shear strength. The pipes could cool down to room temperature first before the mechanical tests were performed. Three samples were taken from each pipe, every test occasion.

A TPS method was used to measure the thermal conductivity of the pipes. The measurements were performed first at the ageing temperature and then before the mechanical test at room temperature. The TPS method is a standard method [7], but it is not generally applied for pipe application and in the DHPs' branch. In this case, two TPS sensors were installed in each pipe at two different distances from the steel service pipe, 5 and 30 mm, respectively.

Some PUR samples collected from the aged DHPs were selected to a more in-depth analysis of their chemical structure using the attenuated total reflection (ATR) technique in an FTIR equipment. The samples had a thickness of approximately 2 mm.

3. Results

The mechanical tests were performed firstly after 1, 2, 3, 6, 8, 15, 21 and 30 days, after this period every 30 days. The SP plug method evaluates the residual shear strength between PUR and the steel service pipe. During the first stage of ageing, the mechanical strength dropped down to a local minimum and then it went up to a maximum point. The change's rate depends on the ageing temperature, occurring faster at higher temperatures. After the local maximum was reached for every ageing temperature, the mechanical strength tended to decrease to zero. However, the pipe aged at 130 °C showed another behaviour after 10 000 hours. The strength dropped to 65 – 70 % of the original value and remained constant for an extended period. Interestingly, this result means that a linear Arrhenius

relationship cannot be applied to calculate the DHP lifetime, as the standard EN253 describes [8]. The results were normalised using the first values obtained after 24 h and are shown in Fig. 1.

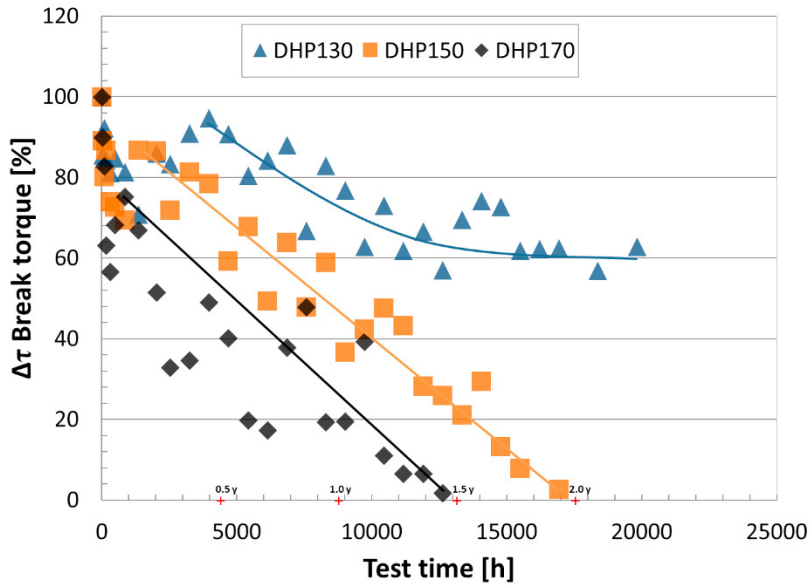


Fig. 1. Mechanical shear strength measured by the SP plug method.

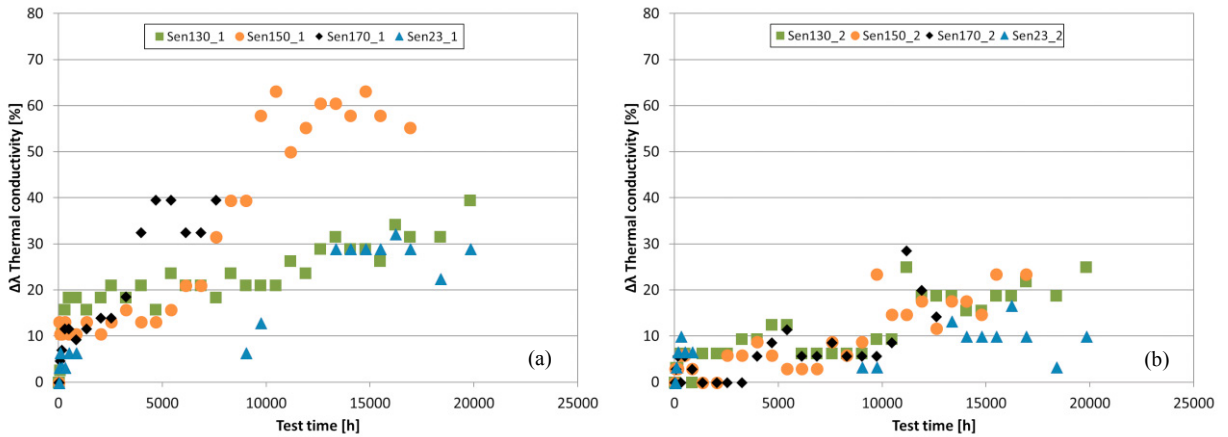


Fig. 2. Thermal conductivity measurements. (a) $\Delta\lambda$ measured by the sensor positioned at 5 mm and (b) 30 mm in each pipe.

Table 1. Temperatures measured by the TPS sensors at their locations, 5 and 30 mm from the steel service pipe.

Ageing temperature (°C)	Temperature at 5 mm (°C)	Temperature at 30 mm (°C)
130	97-100	55-60
150	112-114	67-71
170	130-141	76-86

The thermal conductivity (λ) was measured first at the corresponding ageing temperatures and then at room temperature, by TPS sensors located at two different distances from the steel service pipe, which means that the PUR foam was exposed to lower temperatures at these locations than the chosen ageing temperatures as shown in Table 1.

Following the change of this property at different temperatures was possible. The curves in Fig. 2 behave similarly, but the λ values increased rapidly at temperatures higher than 130 °C. It is well-known that λ values for DH pipes are affected mainly due to gas transport, depending on the foam morphology and the HDPE casing pipe [4]. The gas exchange process seemed to be the dominant mechanisms at the places where the temperature was not higher than 100 °C. However, another process might be activated besides gas diffusion at $T > 130$ °C. Alteration of the cell morphology and losses of cyclopentane, due to thermo-oxidative degradation, may cause deterioration of the insulation performance at these temperatures.

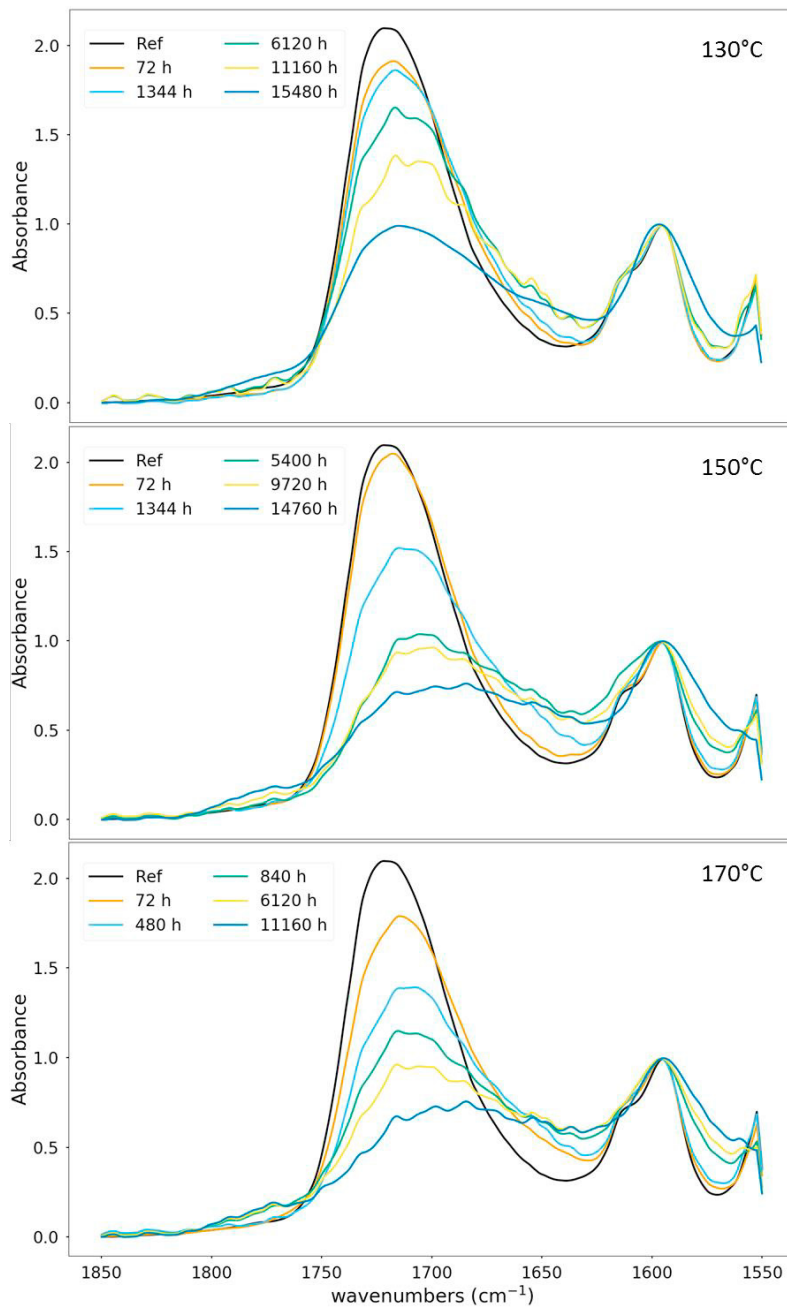


Fig. 3. FTIR spectra showing the new carbonyl peaks formed because of oxidation processes.

Ageing caused changes in the chemical structure of the foam, which affect the mechanical and thermal performance of the pipes. These changes were identified using FTIR spectroscopy, pointing out the most interesting peaks. In Fig. 3, a part of the FTIR spectra shows the loss of urethane (C=O) group around 1712 cm^{-1} . This change was mainly due to thermo-oxidative degradation. This phenomenon is temperature-dependent, occurring very rapidly at higher temperatures. Also, a new carbonyl group appeared in the range $1760 - 1790\text{ cm}^{-1}$ as a result of the oxidation process [4].

4. Conclusion

Accelerated thermal ageing of DH pipes at elevated temperatures was performed, observing the activation of different degradation mechanisms and deterioration of the pipes' performance. It seemed to be a combination of several processes, that hardly can be described by a linear Arrhenius relationship, as proposed in the European Standard EN253. For this reason, the lifetime prediction becomes a complex task due to the different factors that affect the measurements.

Additionally, all tests performed in this study demonstrate that the degradation mechanisms at high ageing temperatures, $T > 130\text{ °C}$, differed significantly from the results obtained at lower temperatures. It means that some ageing processes activated at high temperatures are unusual for the normal operation of DH networks and can lead to an incorrect estimation of the pipes' lifetime.

An improved ageing methodology is needed to obtain reliable lifetime prediction, which can have a significant impact on the general urban planning in a city. It includes decisions for new systems and replacement or extension of the existing systems. It is essential not only for the energy companies but also for social, educational and cultural infrastructures.

References

- [1] H. Lund, S. Werner, R. Wiltshire, S. Svendsen, J.E. Thorsen, F. Hvelplund, B.V. Mathiesen, 4th Generation District Heating (4GDH). Integrating smart thermal grids into future sustainable energy systems., *Energy*. 68 (2014) 1–11. doi:10.1016/j.energy.2014.02.089.
- [2] S. Fredriksen, S. Werner, *District heating and cooling*, 2013.
- [3] A. Leuteritz, K.-D. Döring, T. Lampke, I. Kuehnert, Accelerated ageing of plastic jacket pipes for district heating, *Polym. Test*. 51 (2016) 142–147.
- [4] A. Vega, N. Yarahmadi, I. Jakubowicz, Determination of the long-term performance of district heating pipes through accelerated ageing, *Polym. Degrad. Stab*. 153 (2018) 15–22. doi:10.1016/j.polymdegradstab.2018.04.003.
- [5] N. Yarahmadi, A. Vega, I. Jakubowicz, Accelerated ageing and degradation characteristics of rigid polyurethane foam, *Polym. Degrad. Stab*. 138 (2017) 192–200.
- [6] J.H. Sällström, O. Ramnäs, S. Sällberg, Status Assessments of District Heating Pipes, in: *13th Int. Symp. Dist. Heat. Cool.*, Copenhagen, 2012.
- [7] EN22007, *Plastics – Determination of thermal conductivity and thermal diffusivity – Part 1: General principles (ISO 22007-1:2017)*, Brussels, 2014.
- [8] EN253, *District heating pipes -Preinsulated bonded pipe systems for directly buried hot water networks -Pipe assembly of steel service pipe, polyurethane thermal insulation and outer casing of polyethylene*, Brussels, 2009.



16th International Symposium on District Heating and Cooling, DHC2018,
9–12 September 2018, Hamburg, Germany

Analyses of Axial Displacement Measurements from a Monitored District Heating Pipeline System

S. Hay^a, F. A. Villalobos^b, I. Weidlich^c, I. Wolf^d

^aAGFW | Energy efficiency association for heating, cooling and CHP, Stresemannallee 30, Frankfurt am Main, 60596, Germany

^bCatholic University of Concepción, Alonso de Ribera 2850, Concepción, Chile

^cHafenCity University, Überseesallee 16, Hamburg, 20457, Germany

^denercity Netzgesellschaft mbH, Auf der Papenburg 18, Hannover, 30459, Germany

Abstract

The need for understanding the response of district heating piping systems on temperature-driven loads to improve life-time analysis has led to the development of a monitoring programme. This programme includes the design of the connection of an instrumented section of piping within an operating district heating network. The design complies with the current European district heating recommendations and standards [1, 4]. There are different conditions under testing and minor differences in design of the sections causing different friction resistance in the bedding soil. The pipes' axial displacements are recorded in six positions along each of the sections of the pipeline. For the first time axial displacements of four similar buried preinsulated bonded pipes were measured under defined on-site conditions. This experimental setup allowed preliminary results of axial displacements, which are relevant for the district heating design, operation and maintenance. The contribution focusses on the results of the first period of operation, where a defined start-up procedure is performed (temperature increase up to 90 °C, held constant for 60 days). Afterwards the operating temperature was reduced down to the ambient temperature. The start-up procedure was repeated once before starting the cyclic-operating procedure up to 140 °C. The measured maximum pipes' axial displacements at operating temperature of 90 °C were around 25 mm in the bows of the monitored pipelines. The measurement results are between estimated values using current recommendation procedures (23 mm) and commercial computer programs (31 mm). In addition, residual displacements at ambient temperature level were measured. The impact of unloading-reloading cycles on pipe deformation behaviour will be a future research focus of the ongoing monitoring programme. The results of the four sections will be presented in a comparative way and a forecast on the cyclic-operating procedure will be given here.

© 2018 The Authors. Published by Elsevier Ltd.

This is an open access article under the CC BY-NC-ND license (<https://creativecommons.org/licenses/by-nc-nd/4.0/>)

Selection and peer-review under responsibility of the scientific committee of the 16th International Symposium on District Heating and Cooling, DHC2018.

* Stefan Hay. Tel.: +49-69-6304-345, fax: +49-69-6304-455.

E-mail address: s.hay@agfw.de

Keywords: district heating, buried preinsulated bonded pipes, pipe soil interaction monitoring, axial displacement

1. Introduction and Design

The monitored pipeline sections are based on four identical sections with constant coverage height of 0.8 m. Fig. 1 is a scheme of the all monitored pipeline sections. It shows the four sections having the same length properties ($length_I = 5\text{ m}$, $length_{II} = 41\text{ m}$). At the end of every section fixed point construction (here: execution as a concrete block) prevents mutual interference between the sections. During the design process the axial displacements as well as the relevant static conditions of the buried preinsulated bonded pipes of the monitored pipeline sections has been calculated according to European district heating recommendation and standard EN 13941 [1] with the calculation program sisKMR [2]. The four sections differ from each other due to different casing pipe connections, the number of casing pipe connections per section and the bedding material used. Table 1 shows the differences.

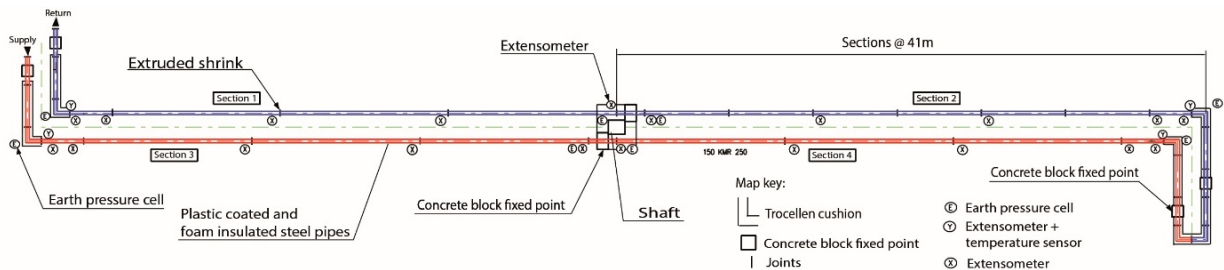


Fig. 1: Scheme of the monitored pipeline sections, showing fixed points, joints and cushions

Table 1. Differences between sections 1-4 (bedding material, type and number of jacket pipe connections).

Section	Bedding Soil Type	Type of Joints	Number of Joints
1	Sand	Extruded shrink	5
2	Sand	Plastic shrink-on sleeves	8
3	Sand	Plastic shrink-on sleeves	5
4	Sand / Gravel	Plastic shrink-on sleeves	5

To measure the soil-pipe interaction, the four sections are equipped with the same number of extensometers (axial displacement sensors, deviations in the measurement result $\pm 0.1\text{ mm}$). The positioning of the measuring sensors is carried out in the same way for all sections (see fig. 1). In all sections, the last joint in front of the bows of the monitored pipelines is not filled with foam. The resulting cavities are used to install measurement equipment, consisting of an extensometer sensor and a temperature sensor, which are fixed at the steel medium pipe. Due to the variation of the bedding soil as well as the variations of joints (system and number) it can be assumed that the frictional forces between the pipeline and the surrounding soil develop differently in the four sections. This has an effect on the axial displacement of the sections as well as on the stress of the insulated pipes. For the dimensioning of insulated pipes, assumptions are made for the degree of compaction and the coefficient of friction μ on the basis of the bedding soil used. Depending on the type of joints and the conditions during the assembly process of the joints, an increase of the diameter of the pipe segment can occur. Both the increase of diameter in the region of the joints and the deviations of the friction conditions resulting from the bedding situation are not included in the calculation. These, however, affect the stress of buried insulated pipes and are necessary for a deeper understanding of the construction as well as more detailed predictions regarding the service life in district heating systems.

1.1. Research objectives and related operations

In the dimensioning process of insulated pipes in district heating systems, the fatigue check is based on the Palmgren-Miner approach according to the current recommendations and standards [1, 3]. In these norms and standards, real temperature loads are converted into the equivalent number of full temperature cycles (FTCs) and limited to a certain number of presupposed FTCs. According to the dimensioning of the monitored pipeline section [1, 3], the 250 FTCs used for material fatigue are generated in total in six different operating phases (phase 0: defined start-up procedure 1 FTC; phase 1 to 4: 50 FTCs per phase; phase 5: 49 FTCs) during the entire monitoring programme. The connection to the district heating network of the utility company inetz GmbH (located at Chemnitz, Germany) and the regulation of the supply temperature in accordance with the defined operating program are made via a specially designed connecting station in the measuring container. According to the intended mode of operation of the respective operating phase, the supply temperature between 60 °C and 140 °C is regulated by the connecting station. After completion of the research operation, parts of the pipelines will be subjected to destructive tests in material testing institutes. In order to verify the material degradation due to the 250 FTCs, the initial values of the delivered material were determined on a brand new straight 12 m pipe (DN 150) according to EN 253 [4]. The comparison of the determined material parameters, before and after the load, enables to quantify the degradation of the material on the basis of the applied load. In this paper the results of phase 0 are presented and interpreted. The operating phase 0 can be subdivided into the following 3 partial operating phases.

Sub-operating phase 01 (SOP01): In operating phase 0, the research measuring section was first filled via the return line of the heating network. Subsequently, the operating temperature of the monitored pipeline sections was raised to 90 °C with a gradient of 5 K/h. The operating temperature 90 °C was held constant over 61 days.

Sub-operation phase 02 (SOP02): Subsequently, the heat supply was interrupted for a period of 30 days and the monitored pipeline sections cool down to the temperature level of the surrounding soil via natural convection.

Sub-operating phase 03 (SOP03): In the last sub-phase of operating phase 0, the monitored pipeline sections were reheated to an operating temperature of 90 °C. Initially, the minimum operating temperature was set via the connecting station while the target temperature of 90 °C was subsequently realized with a gradient of 5 K/h. The operating temperature of 90 °C was held constant for another 30 days.

After completion of the entire monitoring programme, it will be possible to compare different modes of operation and, based on this to assess their influence on the service life time of the monitored pipeline sections. Based on the results, it can be expected that improved approaches will be incorporated into the calculation of material fatigue.

2. Diameter measurements and geotechnical investigations

2.1. Diameter increase of the joints

To determine the influence of the increase of diameter of the various joints or number of joints, the peripheries of the joints were measured and documented after the installation. In fig. 2, the embedded extrusion sleeve is shown during the assembly process of section 1. At the construction site, this joint is adapted to the preinsulated pipes and welded by means of polyethylene (PE) welding. As shown in fig. 2, production-related PE circular welds are created at both ends of the sleeve, as well as a PE longitudinal weld in the middle of the joint. Depending on the diameter of the insulated pipes, these PE welds lead to an increase in diameter at the joints. The diameter in the middle of the jacket pipe connection is 250 mm and thus 3.6 mm smaller than the outside diameter of the insulated pipe (253.6 mm). The circular PE welds cause a diameter, which are between 259.4 mm and 267.4 mm and thus compared to the outer diameter of the insulated pipe to a diameter increase between 5.8 mm and 13.8 mm.



Fig. 2: Embedded extrusion sleeve section 1 after the production of the PE welds and the foaming process

In the same way as for section 1, the geometrical parameters of the remaining joints of sections 2 to 4, which were designed as shrink-on sleeve joints with additional shrink sleeves, were documented after their assembly. For sections 2 to 4, the same diameter (283.4 mm) was measured for all shrink sleeves. The installed shrink sleeves have a 29.8 mm larger outer diameter compared to the insulated pipes (253.6 mm).

2.2. Results of geotechnical investigations

Fig. 3 shows the particle size distribution of the bedding materials for the sections 1 to 3 (blue) and section 4 (purple). These bedding materials are oriented towards permissible limit curves of the current draft standard for the construction of buried preinsulated bonded pipes - prEN 13941-2, 2016 [5]. It can be seen that the bedding material of section 4 consist of 50% coarse grain fraction (higher than 1 mm). On the other hand, in the case of sections 1 to 3, 60% of the bedding is sand (grain size lower than 0.2 mm).

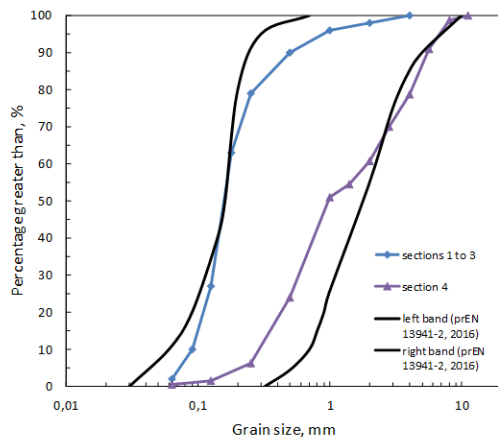


Fig. 3: Grain size distribution of the bedding materials in section 1 to 3, and in section 4 following prEN13941-2, 2016 [5]

The bedding materials used were examined both in the laboratory and in the field with regard to their properties and the installation situation in order to determine the relevant parameters for the interpretation of the measurement results. In the laboratory experiments characteristic mechanical parameters of the soil as well as the relative density were determined. Friction coefficients $\mu_{\max} = 0.504$ and $\mu_{\text{residual}} = 0.415$ were determined for the bedding material of the section 1 to 3 for the relative density of 0.4. For section 4, the maximum coefficient of friction is $\mu_{\max} = 0.468$ and a residual friction value of $\mu_{\text{residual}} = 0.429$ was determined for the same relative density of 0.4 [6].

3. Measurement results of the operating phase 0

3.1. Section 3

The section 3 corresponds to the conventional construction of insulated pipes for district heating in Germany and thus forms a reference route to real district heating networks. Consequently, section 3 is best suited for a detailed analysis and presentation of the measurement results. In fig. 4, the measurement results from the entire operating phase 0 for section 3 are shown. Fig. 4 clearly shows the three partial operating phases based on the temperature and displacement measurements.

Before the first filling on April 27, 2017, the measuring sensors were zeroed. Subsequently, section 3 was put into operation in accordance with the starting process described in SOP01 and operated according to the operating criterion of phase 0 (SOP01, SOP02, SOP03). Regarding the curve progression of the axial displacements in fig. 4 it can be noted that they qualitatively follow the curve progression of the operating temperature of section 3. Besides that the measured displacements increase over the sections length. Correspondingly, displacements are at a minimum of 1.5 m from the fixed point (in the middle of the monitored pipe sections, measured on S311.5 sensor). The sensor on the steel medium pipe (S3140), which is 40 m away from the fixed point, measures the largest axial

displacements and reaches a maximum value of 25.8 mm in operating phase 0. The measured axial displacements on the steel medium pipe (S3140) are approx. 1.5 mm larger than those on the adjacent measuring point (S3139,4) on the PE jacket of the insulated pipe which has a distance of 39.4 m to the fixed point in the middle.

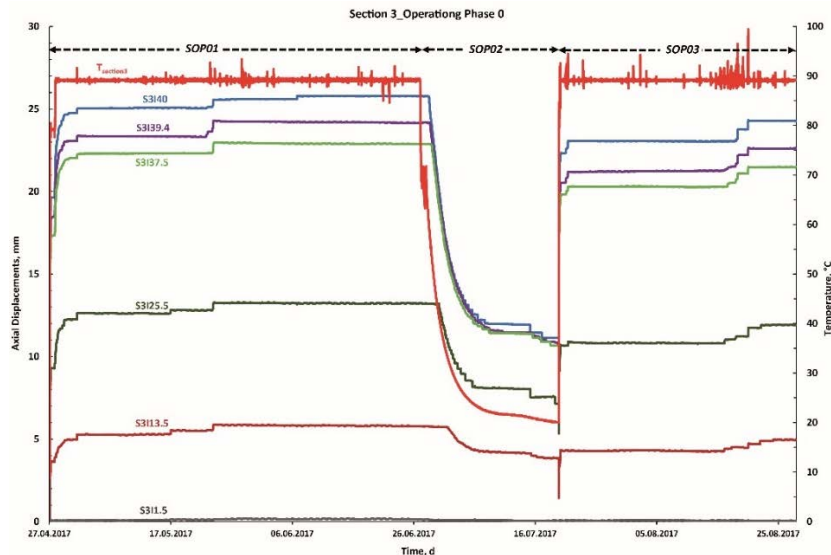


Fig 4: Measuring results of section 3, temperature and axial displacements versus time

In the SOP01, which lasts from April 27 to June 27, 2017, the measurements of the axial displacements seem to have larger changes at a total of three times: Mai 01, Mai 17, and Mai 24, 2017. Looking more closely at these times, it can be stated that minor positive temperature increases between 2 K and 5 K on Mai 01 and Mai 24, 2017 cause axial displacements at all six extensometers. The associated displacements range between 0.2 mm and 0.6 mm. On Mai 17, 2017 axial displacements occur at the sensors S3113.5 and S3125.5. Compared with the axial displacements in the first 72 h of the SPP01 (the displacements increase from 0 mm to 20 mm) these measured displacements are significantly smaller. Temperature reductions in the comparable amplitude between 2 K and 5 K show no measurable axial displacements.

Fig. 5 (see p. 6) shows the first 72 h of the defined starting procedure and the associated measurement results of section 3. As can be seen in Fig. 5, the operating temperature during the filling process suddenly increases from about 10 °C to about 65 °C. Due to the minimum possible temperature level at this time, the temperature of the sections were first raised to 80 °C and then at the intended rate of temperature change of 5 K/h to 90 °C which were reached after 24 h. Fig. 5 shows the detailed course of the axial displacements during the first 72 hours of operation. It can be seen that after reaching the target temperature of 90 °C (after 24 h), a large part of the axial displacements are formed. In addition, fig. 5 shows that creep processes occur after 24 h without any further increases in the track temperature, which almost completely stop after 72 h.

Table 2 (see p.6) shows the measurement results at selected times of the extensometer sensors and the supply temperature - measured on steel medium pipe - of section 3. The first value of the displacement measurement in table 2 indicates the absolute axial displacement of the measuring point (specified in mm) in each case at the time of measurement. The bracketed values represent the percentage of the displacement achieved at the time of measurement, relative to the maximum value of the axial displacement that this measuring point reaches after 61 d.

The tabular overview once again confirms the results already described in fig. 5. Table 2 shows for section 3, that after one operating hour axial displacements occur, which are 50% of the maximum value in operating phase 0. The track temperature at 62.3 °C is still below the target temperature. Looking at the track temperatures in table 2 the measurement results with max. 89.2 °C are still below the set point temperature of 90 °C, while the temperature sensors of the sections measure the temperature of the steel (outside of the steel medium pipe). The associated temperature deviation is reflected in the temperature measurement results shown. After one day, the axial

displacements increased to over 80% measured at sensors further away than 13.5 m from the fixed point in the middle. The measuring point S3I13.5 has even smaller displacements with 67%. On the S3I1.5 sensor, very small displacements have been measured over the entire period of observation. In the following 2 days, the axial displacements increase at constant supply temperature to over 90%. These creep processes can also be clearly seen in fig. 5. On the basis of a tabular overview, it is also clear that the creeping processes are largely completed after 72 h (3d).

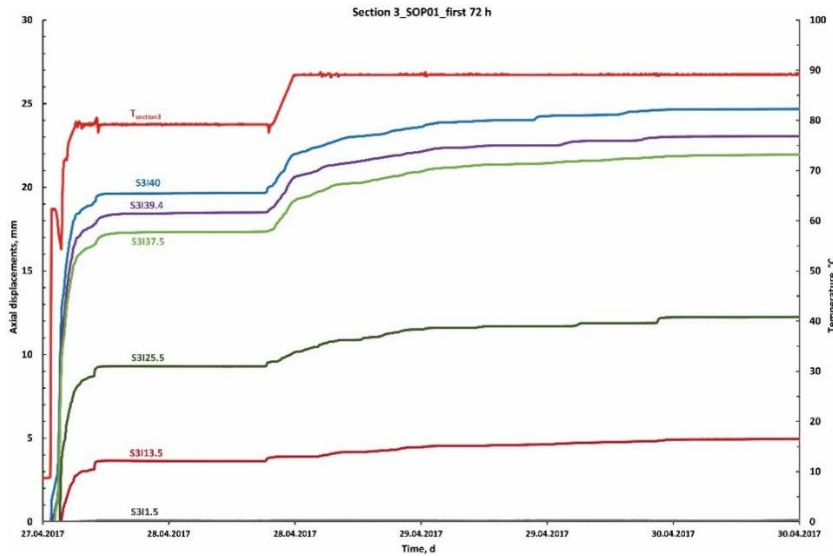


Fig. 5: Measuring results SOP01 (first 3 days of operation), temperature and axial displacements versus time

Table 2. Measurement results of section 3 at selected points in SOP01

Time	T _{Section3} [°C]	S3I1.5 [mm]	S3I13.5 [mm] (%)	S3I25.5 [mm] (%)	S3I37.5 [mm] (%)	S3I39.4 [mm] (%)	S3I40 [mm] (%)
1h	62.3	0.0	0.4 (7)	4.0 (30)	10.1 (44)	11.3 (47)	13.0 (50)
1d	89.2	0.0	3.9 (67)	10.3 (84)	19.4 (85)	20.8 (86)	22.1 (86)
2d	89.1	0.0	4.7 (81)	11.7 (89)	21.5 (94)	22.5 (93)	24.3 (94)
3d	89.1	0.1	5.0 (86)	12.3 (93)	22.0 (96)	23.0 (95)	24.7 (96)
4d	89.1	0.1	5.0 (86)	12.3 (93)	22.0 (96)	23.1 (95)	24.8 (96)
61d	89	0.1	5.8 (100)	13.2 (100)	22.9 (100)	24.2 (100)	25.8 (100)

Fig. 6 (see p. 7) shows the cooling behavior of section 3 and the associated displacements. After the monitored pipe sections were put out of operation on June 27, 2017 by turning off the flow pump, further temperature increases were measured in the course of the temperature. These are also shown in fig. 6 and are due to flow processes that result from the pressure and temperature differences to the connected district heating network. As a result, the manual shut-off valves were closed on June 28, 2017 and the monitored pipe sections were thus completely disconnected from the heating network. Afterwards, the operating temperatures of section 3 - as shown in fig. 6 - declined.

Initially, a temperature drop of 30 K is necessary before section 3 starts to shift back towards 0-position. In an analogous manner to the starting process, the sensors with the greatest distance to the fixed point also begin to reverse the axial displacement when the temperature is decreased. Thus, the values of the sensors S3I40, S3I39.4 and S3I37.5 have reduced to less than 20 mm before the sensors 25.5 m and 13.5 m start to move. Until July 06, 2017, the displacements have receded to less than 13 mm.

In table 3 (see p.7), in an analogous manner as in table 2, the axial displacements of the measuring points of section 3 at the respective times are given. The results presented in table 3 demonstrate that the first reduction in

axial displacement at S3I40 occurs after 36 hours, in conjunction with a 29.9 K reduction in track temperature. 24 hours later, the section temperature cooled by further 12.5 K and as a result, the displacements of the sensors S3I40, S3I39.4 and S3I37.5 are reduced to approximately 90%. On the sensors S3I25.5 and S3I13.5, no reduction of the displacements occurred at this time. The numerical values show that the axial displacements in SOP02 are reduced to approximately 45% of the maximum measurement result of the respective sensor (at 90 °C). The tabular overview uses the numerical values to clarify the results already derived from fig. 6.

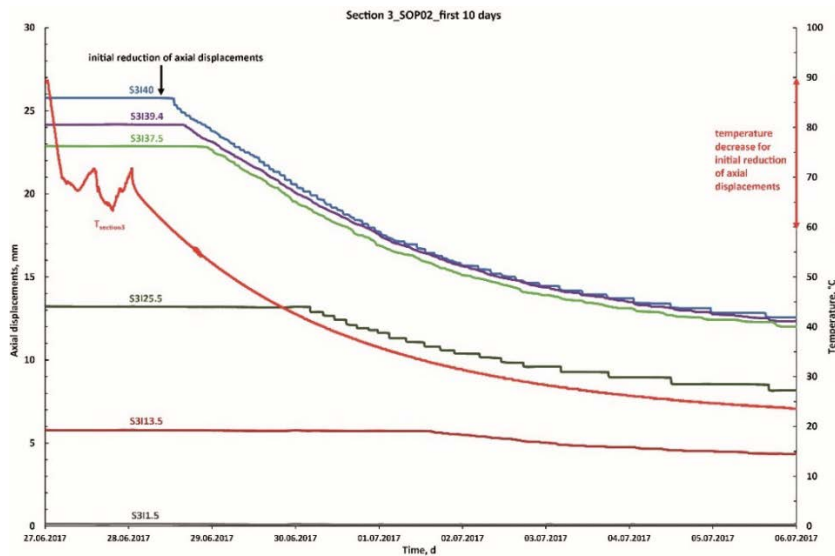


Fig. 6: Measuring results SOP02 (first 10 days), axial displacements and decrease of supply temperature versus time

Table 3. Measurement results of section 3 at selected point in SOP02

Time	T _{Section3} [°C]	S3I1.5 [mm]	S3I13.5 [mm] (%)	S3I25.5 [mm] (%)	S3I37.5 [mm] (%)	S3I39.4 [mm] (%)	S3I40 [mm] (%)
61d	89	0.1	5.8 (100)	13.2 (100)	22.9 (100)	24.2 (100)	25.8 (100)
61.5d	70.8	0.1	5.8 (100)	13.2 (100)	22.9 (100)	24.2 (100)	25.8 (100)
62.5d	59.1	0.1	5.8 (100)	13.2 (100)	22.9 (100)	24.2 (100)	25.5 (99)
63.5d	46.6	0.0	5.8 (100)	13.2 (100)	21.0 (92)	21.5 (89)	22.2 (86)
64.5d	38.5	0.1	5.7 (98)	12.4 (94)	18.1 (79)	18.6 (77)	19.0 (74)
77.5d	21.6	0.1	4.2 (72)	8.0 (61)	11.4 (50)	11.5 (48)	11.9 (46)
84d	20.1	0.1	3.8 (66)	7.1 (54)	10.7 (47)	10.7 (44)	11.1 (46)

The defined reheating procedure to the supply temperature of 90 °C in SOP03 starts on July 20, 2017 on the basis of the corresponding residual axial displacements of the different measuring points in section 3 (see p.8, fig.7). The supply temperature of the monitored pipe sections is determined by the temperature level of the return line of the district heating system, which varies between 75 °C and 93 °C during the day on July 20, 2017. It is only in the late afternoon that it is possible to compensate for the network-related temperature fluctuations in such a way that the control regulates the defined operating state (90 °C) with the temperature change rate of 5 K/h. As shown in fig. 7, most of the axial displacements occur within the first 12 hours after the section restarts. As a result of temperature fluctuations on July 21, 2017 a further increase in the axial displacements is observed. It cannot be ruled out that without these temperature pulses, the axial displacements could have reached a stationary state after only 24 h.

Table 4 (see p. 8) shows the absolute values of the axial displacements as well as the percentage values related to the maximum measured value of the respective sensor (after 61 d) at selected times of SOP03. It can be seen that the measurement results increase within the first hour after reheating section 3 to about 70% of the maximum displacements. Compared with the same period during the first start (SOP01), the measurement results (84.05 d) are thus about 20% above the displacements after 1 hour, whereby the supply temperature at the time shown in table 4 is

20 K higher. Two days after restart, both the supply temperature and the axial displacements have reached a stable state. The axial displacements have been set at a level of 90% of the maximum displacements in SOP01. Regarding fig. 7 and table 4, it should be noted that the axial displacements - compared to the startup process of SOP01 – form in a similar speed but the creep processes observed in SOP01 hardly take place or stop after only 48 hours.

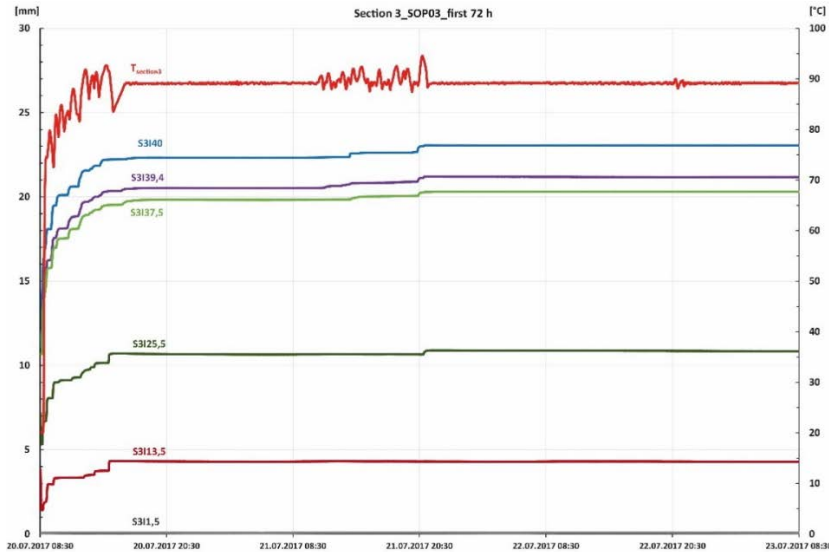


Fig. 7: Measuring results SOP03 first 72 hours of the reoperation, axial displacements and supply temperature

Table 4. Measurement results of section 3 at selected point in SOP03

Time	T _{Section3} [°C]	S311.5 [mm]	S3113.5 [mm] (%)	S3125.5 [mm] (%)	S3137.5 [mm] (%)	S3139.4 [mm] (%)	S3140 [mm] (%)
84d	20.1	0.1	3.8 (66)	7.1 (54)	10.7 (47)	10.7 (44)	11.1 (46)
84.05d	79.1	0.1	2.9 (50)	8.1 (61)	15.8 (69)	16.3 (67)	18.1 (70)
85d	89.2	0.1	4.3 (74)	10.7 (81)	19.8 (86)	20.5 (85)	22.3 (86)
86d	89.1	0.1	4.3 (74)	10.9 (83)	20.3 (89)	21.2 (88)	23.1 (90)
91d	89.2	0.1	4.3 (74)	10.8 (82)	20.3 (89)	21.2 (88)	23.1 (90)
123d	89.1	0.1	5.0 (86)	11.9 (90)	21.5 (94)	22.2 (92)	24.3 (94)

In the period between July 21 and August 16, 2017, the supply temperatures of sections 3 are subject to fluctuations, which in some cases are to be quantified as more than 5 K. Nevertheless, no further displacements occur during this period. This suggests that after the reheating procedure (SOP03) of the operating phase 0, very stable stationary states have been already formed at the beginning. In mid-August 2017, the operating temperature deviates up to 10 K in places from the set point temperature of 90 °C. These generate a further increase in the displacement measurements. Due to the time overlay, it can be demonstrated that the axial displacements - shown in fig. 4 (see p. 5) - are due to the temperature pulses at the end of August 2017 and that otherwise the defined termination criterion for operating phase 0 ($\Delta l \rightarrow 0$) was met. On the basis of this, it was decided to move to cyclic operation phase 1 on August 27, 2017.

3.2 Comparison between the measurement results of all sections and the calculations of design

The curve progression of temperatures and axial displacements shown on the results of section 3 are also reflected qualitatively in the curve progressions of sections 1, 2, and 4. In the following, the previously described extreme positions of the three partial operating phases are compared and set in relation to the calculation results of the static design. During the dimensioning, the axial displacements were determined according to the laying and

operating temperatures according to the valid calculation formulas regarding [1]. The influences of the different bedding soils are essentially taken into account in the calculation on the basis of the coefficient of friction μ . It was assumed that a friction coefficient $\mu = 0.4$ was achieved for the sand bedding of sections 1, 2 and 3, and realistic results for section 4 with a higher coefficient of friction $\mu = 0.5$.

Table 5 shows the calculation results with sisKMR [2] based on [1] with the different friction values for the measurement points at 90 °C track temperature (see Calculation1 and Calculation2). The maximum axial displacements of the various sections of the monitored pipe sections after 61 days before the lowering of the operating temperature are included as percentages based on the calculation results 1 with the friction coefficient $\mu = 0.4$ in table 5. The values in brackets of table 5 refer to the results of calculation 2, in which the friction coefficient is $\mu = 0.5$. The representation selected in table 5 enables us to compare the measurement results of the individual sensors of the different sections at the same measuring points.

Table 5. Measurement results after 61 days of operation of all sections in percent referred to the results of calculations

Section	T _{Section}	SI1.5	SI13.5	SI25.5	SI37.5	SI39.4	SI40
1	88 °C	30% (50%)	64% (88%)	72% (92%)	72% (85%)	76% (89%)	74% (87%)
2	88.8 °C	133% (200%)	65% (89%)	69% (88%)	73% (86%)	73% (86%)	77 (90)
3	89 °C	17% (255)	66% (91%)	72% (92%)	79% (93%)	78% (92%)	82 (96)
4	87.8 °C	0 (0)	40% (55%)	59% (75%)	66% (78%)	72% (84%)	73 (86)
Calculation1 ($\mu=0,4$)	90 °C	0.6 mm	8.8 mm	18.3 mm	29.0 mm	30.9 mm	31.4
Calculation2 ($\mu=0,5$)	90 °C	0.4 mm	6.4 mm	14.4 mm	24.5 mm	26.4 mm	26.9

It can be stated that the calculation results of calculation 2 with the higher coefficient of friction are closer to the measurement results of all partial sections. The deviations between the measurement results of the sections and the calculation results of calculation 2 are sometimes even less than 10%. In addition, the measurement results of the sections 1, 2 and 3 are usually less than 10% from each other. For section 4, the deviations from the measurement results of the other sections at the measuring points 40 m and 39.4 m are also in the range of 10% deviation. Between the measuring points 37.5 m and 1.5 m, these deviations increase to more than 25%.

Table 6. Measurement results after 84 days of operation of all sections in percent referred to the results of calculations

Section	T _{Section}	SI1.5	SI13.5	SI25.5	SI37.5	SI39.4	SI40
1	20,6 °C	33% (33%)	97% (75%)	103% (74%)	126% (87%)	145% (102%)	155% (109%)
2	20 °C	200% (200%)	132% (102%)	153% (110%)	138% (95%)	187% (132%)	203% (143%)
3	20,1 °C	33% (33%)	103% (79%)	118% (85%)	155% (107%)	151% (106%)	156% (110%)
4	20,8 °C	0,0	76% (58%)	90% (64%)	139% (96%)	151% (106%)	177% (125%)
Calculation1 ($\mu=0,4$)	10 °C	0.3 mm	3.7 mm	6.0 mm	6.9 mm	7.1 mm	7.1 mm
Calculation2 ($\mu=0,5$)	10 °C	0.3 mm	4.8 mm	8.4 mm	10 mm	10.1 mm	10.1 mm

Table 6 shows - in the same way as table 5 - the calculation results with sisKMR [2] based on [1] with the different friction values for the measuring points at 10 °C section temperature - for the state of a cooled pipe. Based on the numbers in table 6, the measurement results of the individual sensors of the different sections will be compared at the same measuring points. In summary, first it can be stated that both in the calculation results as well as in the measurement results of the four sections, the states do not shift back to 0-position and there is a residual displacement. In addition, it should be noted temperatures of the sections at the specified measuring time are 10 K above the temperature assumptions of the calculation. It is therefore not surprising that the residual displacements of the sections are usually larger than those of the calculations. The tabular overview also makes it clear that the deviations of the residual displacements of the sections to the calculation results also increase with increasing length of the sections. Unlike the presentation in table 5, the results of SOP02 (see table 6) are much more different. This can be seen particularly clearly on Section 2.

In table 7 the sensors' maximum measured results in SOP03 referred to the maximum value – measured at the end of SOP01 - are shown. Except S2I1.5 no sensor achieved the maximum axial displacement of SOP01. As shown in table 7 the differences in the results per section decreases with the total length of the sections. The results of axial displacement in SOP03 are in the range of 90% of the maximum in SOP01.

Table 7. Comparison sensors axial displacement SOP03 with maximum measurements SOP01

Section	SI11.5	SI13.5	SI25.5	SI37.5	SI39.4	SI40
1	50%	75%	81%	90%	91%	90%
2	100%	84%	89%	91%	92%	94%
3	56%	86%	90%	94%	93%	94%
4	0	74%	76%	86%	85%	92%

4. Conclusions

In this paper the axial displacements of four monitored pipeline sections achieved during the first period of operation at 90 °C were presented. The measuring results in SOP01 and SOP03 are showing that the predominant share of axial displacements were achieved during the first 24 h of operation caused by the temperature increase. Up to 72 h extend creeping was noted before steady stress conditions in the pipe-soil interaction were achieved. Small temperature increases could disturb this steady stress conditions and cause an increase of the measured displacement. Temperature decreases in the same range do not lead to a reduction of the axial displacements. It was shown that in the beginning of SOP02 an initial temperature decrease of 30 K is needed to disturb the steady stress conditions in the pipe-soil interaction and that the insulated pipe do not shift back to 0-position. The measured residual displacement was in the range of 40% of their maximum values. Starting from the residual displacements in SOP03 smaller displacements were achieved. Although the supply temperature in SOP03 differs more from the set temperature the measurements are more stable compared with the results of SOP01 which indicate on more stable pipe-soil stress conditions.

The results of the geotechnical investigations provide us with higher friction values compared to the standards. The diameter of the joints are compared to the diameter of the insulated pipes only 15 mm higher. Regarding the calculations referred to the results of the measurements larger compliance with higher friction coefficient $\mu = 0.5$ was achieved. This is in line with the results of the geotechnical investigations. Nevertheless, there is still a deviation around 10% between the measurement results and the result of calculation 2. This could be due to the diameter increase of the joints. The minor differences in the design of the sections have not caused a significant deviation in the measuring results during the operating phase 0. It is expected that in operating phase 1 the higher temperatures and the cyclic procedures will enlarge the resistance in bedding soil. This should lead to a higher differences in the measuring results of the axial displacements of the four sections. On the basis of the presented measurement results it could be shown that the pipelines are exposed to a very high initial load due to the starting process. This should be verified in further researches and taken into account in the pipe deformation behavior as well as in the material fatigue of buried preinsulated bonded pipes.

Acknowledgements

This work is part of ongoing research programmes on district heating by AGFW for the development and improvement of pipeline networks. The authors are especially grateful to the BMWi German Federal Ministry of Economics and Energy for the funding support to these ongoing research programmes (funding code: 03ET13335).

References

- [1] EN 13941 (2010). Design and installation of preinsulated bonded pipe systems for district heating. European CEN, Brussels.
- [2] sisKMR (2016). District heating pipe stress analysis software. Version 24.9.0. GEF Ingenieur AG, Leimen, Germany.
- [3] AGFW FW 401 (2007). Installation and calculation of preinsulated bonded pipes for district heating networks. Part 10: Static design; basics of stress analysis. AGFW, Frankfurt am Main.
- [4] EN 253 (2015). District heating pipes - Preinsulated bonded pipe systems for directly buried hot water networks - Pipe assembly of steel service pipe, polyurethane thermal insulation and outer casing of polyethylene. European CEN, Brussels.
- [5] prEN 13941 (2016). District heating pipes – Design and installation of thermal insulated bonded single and twin pipe systems for directly buried hot water networks: Part 1: Design. Part 2: Installation. European CEN, Brussels.
- [6] IGtH (2015). Geotechnische Untersuchung des Bettungsmaterial der FW-Langzeitmessstelle. Institute for Geotechnical Engineering Leibniz University Hannover, Hannover.



16th International Symposium on District Heating and Cooling, DHC2018,
9–12 September 2018, Hamburg, Germany

Power Generation System for Using Unused Energy in District Heating Pipelines

Kyung Min KIM^{a,*}, Mun Sei OH^a, Sung Yong PARK^a

^a*Korea District Heating Corp., 92 Gigok-ro, Yongin, Gyeonggi, 17099, Korea*

Abstract

When the hot water for district heating (DH) is supplied through a thermal grid, a pressure differential control valve (PDCV) in a substation protects the users' equipment from the high pressure water and helps to supply DH water to long distance. It also controls the constant temperature and adjusts the constant pressure in the thermal grid. However, cavitation occurs in PDCV due to the use of high pressure DH water. It causes frequent failures, many problems and energy losses. It makes a complaint to both the operator and the user. In order to solve these problems, we have introduced the hydroelectric power generation method to replace PDCV with hydraulic turbine, convert the unused differential pressure within a DH pipe into electricity. When a differential pressure power generation system is operated in the user's substation, power generation of about 10 to 20 MWh and reduction of carbon dioxide emission to about 7 tons can be seen for a year. It is possible to install more than 3,000 out of about 10,000 of the district heating in Korea. It can grow into a new energy business model. It is also calculated that the DH plant has a power saving effect. The cost of the DH pump power can reduce by more than 3%, and the efficiency of CHP plant can increase by more than 0.3% because 10% defective of PDCV is decreased.

© 2018 The Authors. Published by Elsevier Ltd.

This is an open access article under the CC BY-NC-ND license (<https://creativecommons.org/licenses/by-nc-nd/4.0/>)

Selection and peer-review under responsibility of the scientific committee of the 16th International Symposium on District Heating and Cooling, DHC2018.

Keywords: Hydroelectric Power; pressure differential; unused energy; thermal grid; district heating system

* Corresponding author. Tel.: +82-32-80149645; fax: +82-31-282-6037.

E-mail address: kimkm@kdhc.co.kr

1. Introduction

Here introduce the paper, and put a nomenclature if necessary, in a box with the same font size as the rest of the paper. The paragraphs continue from here and are only separated by headings, subheadings, images and formulae. The section headings are arranged by numbers, bold and 10 pt. Here follows further instructions for authors. The changing global energy situation faces various challenges in providing the energy infrastructure needed to meet the electricity, heating and cooling needs of an energy-driven world. District heating and cooling (DHC) and smart thermal grid make up the backbones of the efficient, reliable and resilient infrastructure that supports the heating and cooling of buildings in many cities, communities, hospitals, airports and campuses as a best practice approach for low-carbon energy supply [1].

District heating (DH) is the process of replacing the heat (hot water) produced in a concentrated large-scale heat production facility (such as a cogeneration plant) instead of having separate heat production facilities (such as gas boilers, etc.) in buildings. Because district heating uses centralized high-efficiency heat production facilities, it is economical, easy to operate and manage, and is environmentally friendly [2]. DHC systems have the multiple benefits, such as greenhouse gas emissions reductions, air pollution reductions, energy-efficiency improvements, use of local and renewable resources, resilience and energy access, and green economy. Despite DHC's many benefits, there are significant untapped and unused potentials [3]. Thus, many researches have been studied the potentials. An example is to use an abandoned energy that has been utilized industrially but has not been used yet. This is because the use of fossil fuels decreases as the amount of unused energy is increased.

DH network as a thermal grid with pipelines is used to transfer the heat less than 120 degrees Celsius. However, as shown in Figs. 1 and 2, due to the pressure drop of the fluid in the DH pipelines, the fluid conveyed through the DH pipelines has a hot water pressure difference depending on the distance. A pressure differential control valve (PDCV) is used to supply a constant flow rate from the hot water pressure differential and to protect the users' equipment from the high pressure fluid. Another role of the PDCV is to regulate the pressure at each point so that the fluid can be supplied remotely.

However, in the case of the use of high-pressure fluid of 6 bar or more, cavitation occurs in the PDCV [4]. It causes frequent failure, many problems of supplying hot water, and energy losses. They make a complaint to operator and the user. If the PDCV is not operated, stable operation of the DH system in a substation will be impossible, shortening the lifespan of the user's devices and abnormal temperature operation of the temperature control valve (TCV) caused by uneven flow and pressure. This failure can result in a large amount of heat loss, causing the valves to be replaced or replaced periodically.

Currently, national studies in Korea are conducted to overcome the limitations of such PDCV and to reduce field problems, and to generate new energy business by generating electric power from the unused pressure energy in the DH pipelines using the hydraulic turbine power generation system. Hydraulic power generation using the pressure differential is one of the small hydropower, which is a low-maintenance, economical power generation system with high energy density without greenhouse gas emissions. When installed in the position of the PDCV in the user's substation, the initial investment cost is low because the civil work cost is not spent differently from the river small hydraulic power generation. In addition, it does not affect the surrounding ecosystem.

In this paper, we will introduce the hydraulic power generation system of the district heating system in the user's substation.



Fig. 1. Schematic diagram of district heating system.

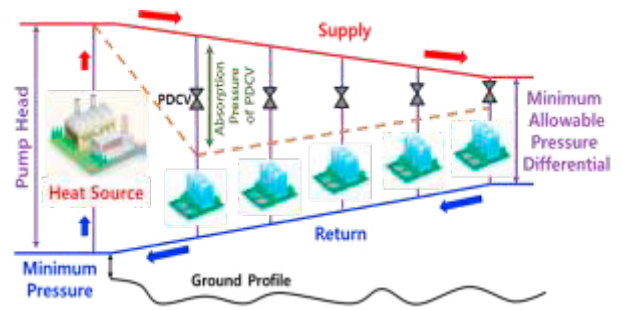


Fig. 2. Schematic of pressure distribution system in district heating.

Nomenclature

P_e	output power per unit time (kW)
g	gravitational acceleration (m/s ²)
ρ	water density (kg/m ³)
η	efficiency of power generation system (%)
H_e	effective head drop (m)
Q	flow rate (m ³ /s)
Q_r	hydraulic turbine design flow (m ³ /s)
P_i	hydraulic power generation (kW)
P_1	partial output power (kW)
P_2	based output power (kW)
L_f	operation rate of power generation system (%)
C	facility capacity (kW)
E_a	annual power generation amount (kWh)

2. Technology and Market Trends

After two oil crises in the 1970s, the Korea government invested heavily in the development of small-scale hydropower technologies. In early 1990, it standardized the aberrations to the standard range according to the head drop (the difference in elevation) and flow rate, and reduced the construction cost of water turbines by mass production. Thereby, it improved economic efficiency and supported resource development. In recent years, as a countermeasure against global warming, the use of small-scale hydropower, such as micro hydropower and pico hydropower, is under way in accordance with the trend of strengthening the use of renewable energy [5].

Market and technology trends show that related markets are growing, including a case study of the US power plant production in Portland. According to DOE's the small hydropower market, the market size of micro- and pico-hydropower will be 29.35 billion won in 2022. Japan is actively promoting the development of small hydropower, which has excellent characteristics in terms of energy safety and environment, focusing on NEDO for technology preoccupation. To focus on eco-friendly development, strategic technology is being developed considering cost factors.

In recent, because of construction and integration into local environments, the installation of micro and pico hydropower systems is increasing in many locations of the world, especially in remote areas where other energy sources are not viable or not economically attractive. Between micro and pico hydropower systems, particularly interesting for the potential of integration at urban and building scale are hydro power systems in pipelines, though power generation from fluid flow confined is not a new concept. In-pipe hydro systems can operate across a wide range of head and flow conditions inside most common piping materials such as steel, ductile iron, concrete, or any material that can be mated with steel pipe, providing clean, baseload energy without the intermittency of wind and solar and without environmental repercussion [6].

Moreover, all cities are served by pressured piping grids systems to supply water where it is needed for drinking, industrial use, while drain and sewage systems are usually gravity fed. Both hold untapped energy deriving from abundant pressure, and drinking water processors and industrial manufacturers typically install pressure reduction valves – hydraulic devices that maintain preset pressure ranges – to relieve the excess pressure and release it as waste heat. Theoretically, all systems that employ pressure reducing devices could replace them with in pipe generators, maintaining the same control on water flow and pressure whilst producing usable electricity [6].

Another large potential energy source lies in the piping systems of single buildings, both for tap water supply, drainage and cooling and heating circuits, with particular regard to large building such as commercial and residential high-rises or shopping malls. In particular, skyscrapers require large amounts of pressure to supply water to the

higher floors, and the excess pressure in the lower section is usually wasted via pressure reduction valves and could be harvested for powering buildings appliances [6].

This technology is an urban energy harvesting technology that maximizes the efficiency of transmission and distribution of electricity by shortening the production and the use of the electricity. Thus, it is a national energy saving technology in terms of leakage prevention and unused energy utilization. Harvesting, rectifying, and storing of the surplus hydraulic pressure and the flow velocity caused by the altitude difference are applied to the urban power infrastructure. In a similar technology, a small turbine generator is installed in a water supply pipe coming into an apartment complex, and electricity is generated by using the energy of water and the pressure of water. In this case, the power generation capacity is about 100 watts of micro hydropower, respectively. In this paper, a differential pressure power generation system that replaces the PDCV can be classified into a pico hydropower (less than 5 kW). The size based subdivision represent an average size reference as there is no global agreement among different countries on the classification of hydropower systems according to the installed power, with the consequence that the definition of micro and pico hydropower spans a very wide range of plants sizes [7].

In particular, in 2015 the city of Portland made the news by installing ‘Lucidpipe Power System’ in one of its main water lines: the four 42” vertical axis turbines total 200kW Power and are expected to generate an average of 1100MWh each year serving approximately 150 homes [6]. Korea’s example is the application of a 10kW micro hydroelectric power plant to the sewage treatment facility - ‘Kiheung respia’ in 2013 [8].

Hitachi Energy Recovery System uses a vertical axis Francis turbine with integrated electric generator to provide a compact assembly, already tested in the Iwatsuki office of Fuji Xerox (2 units outputting 2.4kW each with 25m water head) and in Koyo Paper (9.6kW with 40m head) and NGK Spark Plug (6.0kW and 25m head) factories [6]. In Korea, the Lotte E&C developed micro-hydroelectric power generation system [9] in Korea to generate electric power using the sink of the water filling the underground water tank in the apartment complex. Both 9kW and 3.5kW generators are installed in the apartment. 2,520kWh of electricity can be produced each month.

For single habitation unit applications, reduced space and water head requirements become paramount for any integration of energy harvesting devices in existing piping systems without impeding water flow. These machines have little energy output – less than 1W – and are best suitable for powering metering and control devices or small lighting systems. Scientists from HSG-IMIT and IMTEK developed an automatic remote water meter powered by an energy harvester able to generate up to 720mW when using a flow rate of 20 liter/min, corresponding to a fully opened water tap. This way it is possible to add metering devices anywhere in existing piping systems without the need for electric and data connections since the devices is self-powered and transmits data via Wi-Fi, and to integrate water monitoring to any building automation system or to other internet of things devices with positive effect on water consumption and energy reduction. The energy harvester itself I based on an impeller wheel directly coupled with an electromagnetic energy transducer, constituted by a two pole magnet and three induction coils along with a battery [10].

In summary, it is possible to apply both waterworks and district heating pipelines to high-rise buildings (more than 80,000 in 2014) with high water pressure in Korea, and it is advantageous that not only energy saving but also prediction and quick recovery of drain pipe leaks are possible. Therefore, it will be possible to develop the market through technological preemption through this technology.

3. Power System Configuration

Fig. 3 shows the heat supply system of the district heating. The system is divided into DH supply and return pipes from a heat source plant (hereinafter referred to as a "primary side") and user’s equipment (hereinafter referred to as a "secondary side"), based on heat exchangers. The DH hot water generated in the plant is kept in a constant pressure less than 1 bar between the DH supply pipe and the DH return pipe while passing through the PDCV in the user's substation. In other words, by maintaining a constant pressure in response to pressure fluctuations, it has a function to safely maintain the heat exchanger, the valves for heating and hot water control, the heating and cooling piping, and the fittings.

It is a hydraulic power generation system to place a hydraulic turbine at the position of the above mentioned PDCV. The hydrodynamic differential power generation system is shown in Fig. 4. The hydraulic turbine reduces

the pressure of the primary DH supply pipe and converts the reduced pressure energy to electric energy. The generated electricity is used for driving the secondary side pump. Thus, it reduces the electricity cost of pump and the energy loss for transferring the electricity to the grid.

In pipe hydro power systems can be divided in two main designs, internal system and external system. An internal system is that the runner is wholly inside the pipe section and only the generator protrudes from the conduit. An external system is that the runner is contained in a secondary conduit that bypasses the main one. In this study, the hydraulic power system is an external system. The external systems do not depend so strictly on pipe size since the runner is enclosed in a dedicated conduit, and allow for even greater flexibility. Their main drawback is the need for larger vaults to accommodate the turbine and generator assembly, making them less ideal for retrofit intervention on existing water infrastructures [6].

The system consists of two parts: hydroelectric power generation system which converts pressure energy into electric energy; energy storage system (ESS) and power supply system which converts the generated electricity, supplies it to pump, or stores it in energy storage system.

In order to increase the economic efficiency, this system is designed to have four functions. First, it serves as a PDCV through the hydraulic turbine. Second, it can replace the flowmeter by measuring the rotation speed. Third, through the power conversion device, it can replace TCV. Last, a power supply device acts as a pump inverter to utilize the generated electricity. In this way, we intend to increase competitiveness through multi-function of differential pressure control, flow measurement, temperature control and pump inverter.

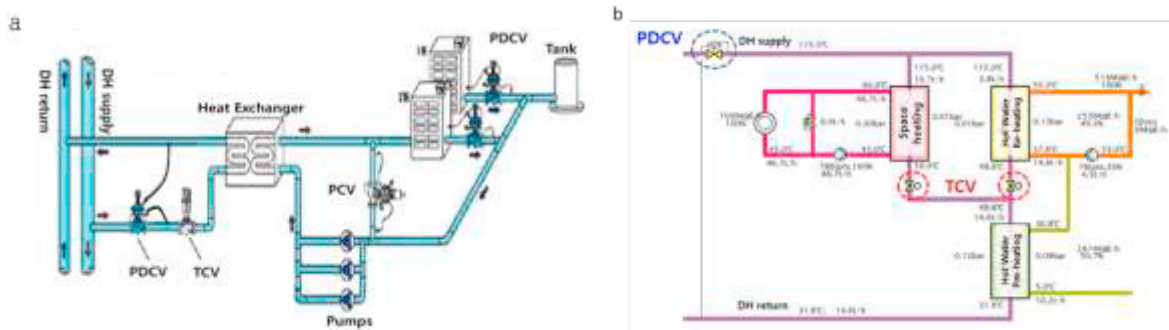


Fig. 3. Schematic of district heating system in a substation; (a) Pipelines and pressure control values, (b) Temperature and flowrate at each location.

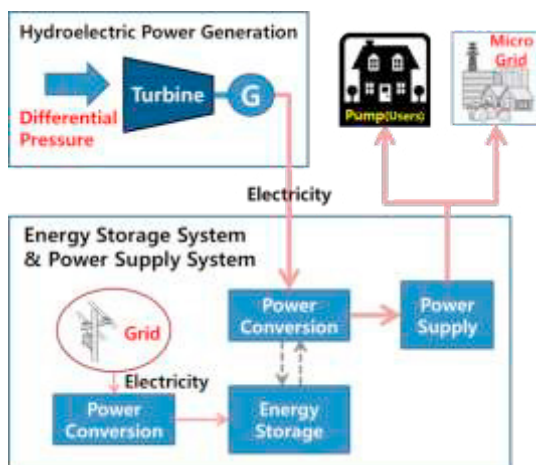


Fig. 4. Concept of hydraulic power generation system.

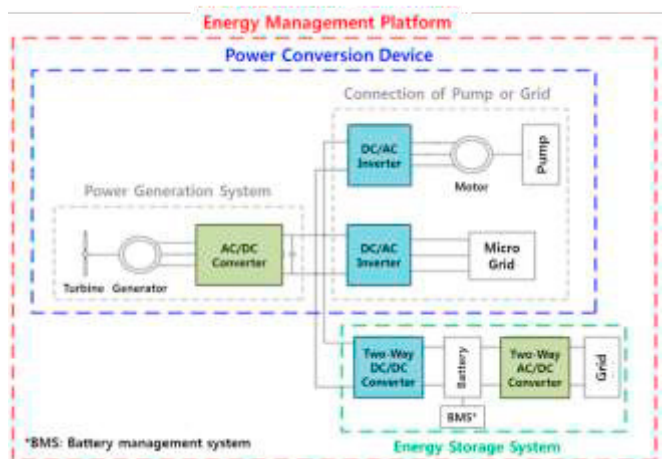


Fig. 5. Hydropower management platform.

The capacity of the hydraulic turbine to convert the differential pressure within the DH pipe into electricity is designed to be 5kW. Since the hydraulic characteristics of the hydraulic turbine are high pressure difference and low flow rate, they are selected as volumetric hydro turbines suitable for high pressure drop. The ESS and power supply are shown in Fig. 5 developed the internal system.

The average power generation amount per unit time (P_e) in the user's substation can be expressed as (1), and the facility capacity (C) as (2), the annual average operation rate (L_f) as (3), the annual power generation amount (E_a) as (4) [9]. The operation rate refers to the ratio between the time of power generation and the year (8,760 hours), assuming that the total power generation during the year is developed only at the maximum output (capacity).

$$P_e = \rho g H_e \eta \left(\int_0^{Q_r} Q P(Q) dQ + Q_r \int_{Q_r}^{\infty} P(Q) dQ \right) = P_1 + P_2 \tag{1}$$

$$C = \rho g H_e Q_r \eta \tag{2}$$

$$L_f = (P_1 + P_2) / C \tag{3}$$

$$E_a = 8,760 C L_f \tag{4}$$

4. Results and Discussion

Fig. 6 is the actual flow rate for one year supplied to the apartment house located in Bundang, Gyeonggi, Korea. The annual flow rate was 0.07 ~ 38.8m³/hr. The variation is due to the weather (outside temperature) and life pattern, and the same tendency is observed in the other regions. The annual flow rate was reduced during the summer season due to seasonal factors and increased during the winter season. The daily fluctuation range was 8 ~ 15m³/hr, and the daily fluctuation was also very large.

Seasonal factors have an important influence on the estimation of design capacity of hydraulic turbine. In other words, small hydropower cannot be generated during the period when the flow rate is lower than the design flow rate. If the design flow rate is set at a low value in order to increase the operation rate, it becomes disadvantageous in terms of annual power generation amount. Therefore, the selection of the aberration and flow control system that can operate in a relatively large flow rate range is very important for the application to the DH substation. At the same time, annual flow variation characteristics of the flow rate should be considered for designing the optimal hydraulic power generation system using differential pressure.

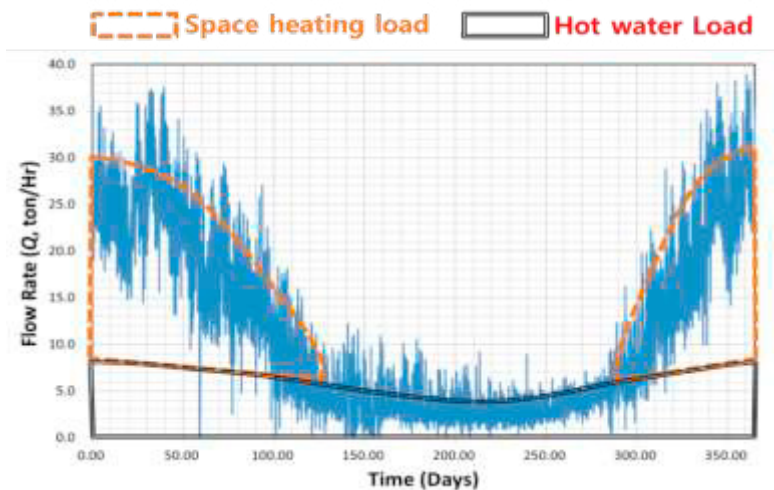


Fig. 6. Actual flow rate (Q) in a year.

The design flow rate is an important factor for selecting power generation capacity and hydraulic turbine. It is necessary to select a design flow rate value in order to maximize the power generation amount in a flow condition with a large variation range. Thus, we can select to separate a 5kW hydraulic turbine into 1.5kW for hot water load and 3.5kW for space heating load in order to increase the operation rate.

When selecting 3.5kW hydraulic turbine, flow rate and supply pressure in Figs. 6 and 7 were used. The design flow range for the spacing heating load is 0 ~ 27m³/hr except 8m³/hr for hot water load. Therefore, considering the frequency, the design flow rate (Q_s) for the spacing heating load is 17m³/hr and the minimum flow rate is 5m³/hr. At this time, the total power generation capacity (C) of two hydraulic turbines is 3 ~ 5kW, and the operation rate (L_f) of each turbine is 30% for spacing heating load and 80% for hot water load.

When a hydraulic power generation system are operated, it is considered that there will be a power generation of about 10 ~ 20MWh and a carbon dioxide emission reduction effect of about 7 tons when installing more than 3,000 of the 10,000 local DH substations. Also, it is expected that the power cost will be reduced even on the heat source side. Typically, when the PDCV is 10% defective, the cost of the DH pump power will increase by more than 3%, and the efficiency of CHP plant will be reduced by more than 0.3% because of decreasing the return temperature of DH water.

Fig. 8 is an example for pressure map at the locations of substations in DH supply area in Seoul, Korea. We are measuring and calculating the pressure on the supply pipes and the return pipes at the substations as shown in as shown in Fig. 8(a). The pressure data will be changed to pressure map for calculating hydraulic power generation as shown in Fig. 8(b). These data will be used for technology commercialization with small business partners.

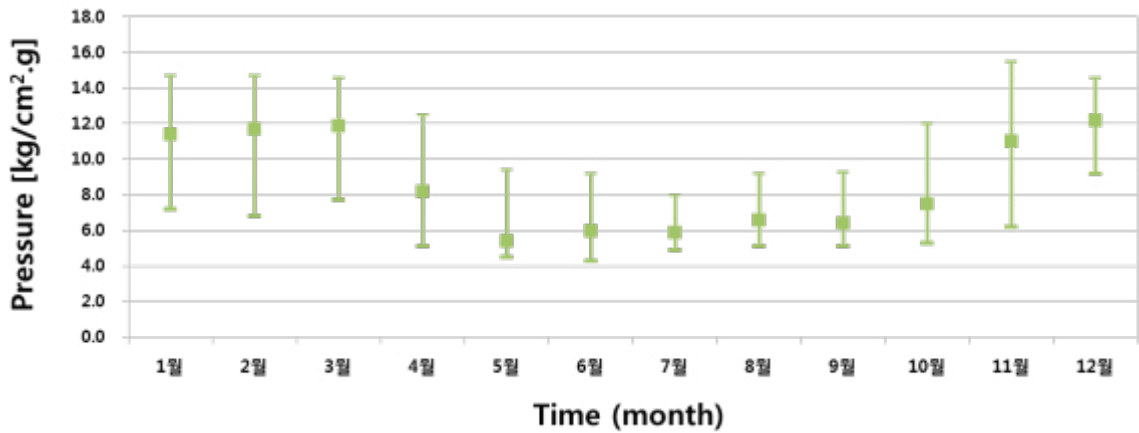


Fig. 7. Variation of supply pressure (Q) in a year.

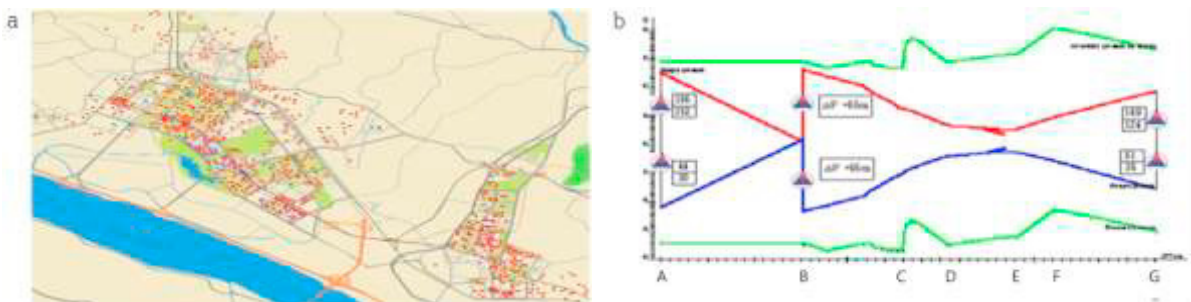


Fig. 8. Substaion locations and pressure map for hydraulic power generation in Seoul, Korea (a) The locations of substations (=a legend red dots) in DH supply area; (b) An example of pressure map at certain location

5. Conclusions

When the hot water for district heating (DH) is supplied through a thermal grid, a pressure differential control valve (PDCV) in a substation protects the users' equipment from the high pressure water. PDCV helps to supply DH water to long distance. It also controls the constant temperature and adjusts the constant pressure in the thermal grid. However, cavitation occurs in PDCV due to the use of high pressure DH water. It causes frequent failures, many problems and energy losses. It makes a complaint to both the operator and the user.

In order to solve these problems, the hydroelectric power generation method to replace PDCV with hydraulic turbine was introduced in this paper. This system converts the unused differential pressure within a DH pipe into electricity and uses electricity as the power of the closest pump.

When a differential pressure power generation system is operated in the user's substation, power generation of about 10 to 20 MWh and reduction of carbon dioxide emission to about 7 tons can be seen for a year. It is possible to install more than 3,000 out of about 10,000 of the district heating in Korea. It can grow into a new energy business model. It is also calculated that the DH plant has a power saving effect. The cost of the DH pump power can reduce by more than 3%, and the efficiency of CHP plant can increase by more than 0.3% because 10% defective of PDCV is decreased.

Acknowledgements

This work was supported by the Renewable Energy Program of the Korea Institute of Energy Technology Evaluation and Planning (KETEP) granted financial resource from the Ministry of Trade, Industry & Energy, Republic of Korea (No.20172020108970).

References

- [1] L. Rao, A. Chittum, M. King, and T. Yoon. "Governance models and strategic decision-making processes for deploying thermal grids." IEA-DHC Annex XI Final Report (2017).
- [2] Y. M. Ahn. "New climate change regime & DHC in Korea" 1st ed., E-square (2016): 15-25.
- [3] L. Mastny. "District energy: unlocking the potential of energy efficiency and renewable energy." United Nations Environment Programme (2015).
- [4] P. Q. Johansson. "Buildings and district heating, DK: Lund University." Ph. D. Dissertation (2011).
- [5] R. Uribe-Martinez, Rocio, P. W. O'Connor, and M. M. Johanson. "2014 Hydropower market report." the U.S. Department of Energy (2015).
- [6] G. T. Lee. "Micro power generation system in mass residence area and method therefore." KR: Patent No. 10-1200550 (2010).
- [7] M. Casini. "Harvesting energy from in-pipe hydro systems at urban and building scale." IJSGCE, No. 9 (2015): 316-327.
- [8] D. H. Na. "Feasibility study on the construction of small hydro-power plants at the discharge point of Gumi sewage treatment plant." KR: Kumoh National Institute of Technology, Ph. D. Dissertation (2010).
- [9] K. J. Chae. "Micro-hydropower system with a semi-kaplan turbine for sewage treatment plant application: Kiheung resopia case study." JKSEE, Vol. 35, No. 5 (2013): 363-370.
- [10] D. Hoffmann, A. Willmann, R. Gopfert, P. Becker, B. Folkmer, and Y. Manoli. "Energy harvesting from fluid flow in water pipelines for smart metering applications." JPCS, Vol. 476 (2013): 1-5.



16th International Symposium on District Heating and Cooling, DHC2018,
9–12 September 2018, Hamburg, Germany

Techno economic analysis of thermochemical energy storage and transport system utilizing “Zeolite Boiler”: case study in Sweden

Shoma Fujii^{a*}, Yuichiro Kanematsu^b, Yasunori Kikuchi^b, Takao Nakagaki^a,

Justin NW Chiu^c, Viktoria Martin^c

^aDepartment of Modern Mechanical Engineering, Waseda University, 3-4-1 Okubo, Shinjuku-ku, Tokyo 169-8555, Japan

^bPresidential Endowed Chair for “Platinum Society”, The University of Tokyo, 7-3-1 Hongo, Bunkyo-ku, Tokyo 113-8656, Japan

^cDepartment of Energy Technology, Royal Institute of Technology, 10044, Stockholm, Sweden

Abstract

Thermochemical energy storage and transport system utilizing zeolite steam adsorption and desorption cycle is one of the methods to resolve the mismatch between industrial surplus heat and heat demands. To generate 60 °C hot water utilizing zeolite 13X, zeolite boiler employing moving bed and indirect heat exchanger was developed. Pressurized water is heated up and flash steam is injected into the zeolite bed for adsorption. A quasi – 2D model solving heat and mass conservation equations was developed, leading to a performance characterization of this zeolite boiler. The developed simulation model was used to predict performance of a heat charging device employing moving bed as well. Based on this calculation, a case study, heat transporting between a local steel works and a hotel was examined and all corresponding cost were fixed. The Levelized Cost of Energy (LCOE) results in around 60 €/MWh which is comparable cost against conventional pellet boiler. Sensitivity analysis showed both of cheaper transportation cost and larger zeolite capacity on the one trailer give a comparable impact on the LCOE.

© 2018 The Authors. Published by Elsevier Ltd.

This is an open access article under the CC BY-NC-ND license (<https://creativecommons.org/licenses/by-nc-nd/4.0/>)

Selection and peer-review under responsibility of the scientific committee of the 16th International Symposium on District Heating and Cooling, DHC2018.

Keywords: Thermochemical energy storage, Adsorption, Techno-Economic analysis, Industrial surplus heat, District heating

* Corresponding author

E-mail address: shoma@fuji.waseda.jp

Around 20% of final energy consumption in the industrial sector in Sweden is exhausted as surplus heat [1]. To reach the sustainable goal, effective use of this industrial surplus heat plays a vital role. Regarding the energy use in Sweden, half of the primary energy supply in the residential and service sector is used for heating, mainly as district heating [2]. Reutilization of this industrial surplus heat in the district heating system will reduce both the primary energy supply and the corresponding CO₂ emission. However, in Sweden, only 8% of district heating source was converted from the waste heat in 2013 [2]. To use this surplus heat effectively, thermochemical energy storage and transport system utilizing zeolite 13X steam adsorption and desorption cycle is one of the methods that effectively supply industrial surplus heat to the users. Many fixed bed type devices discharging and charging heat have been developed [3], [4] and several economic analyses have been reported [5]. However, the batch process requires additional labor cost due to frequent transportation of costly containers and cannot supply heat continuously.

Considering these aspects, we have reported the concept of a moving bed zeolite boiler supplying pressurized steam up to 0.2 MPa continuously in an indirect contact heat exchanger [6]. This zeolite boiler adsorbs steam from an existing boiler and generates higher amount of adsorption heat, with this, zeolite boiler reduces the fuel consumption of the existed boiler. In this study, an additional conceptual design of both heat discharging and charging device to supply 60 °C hot tap water is also shown. The numerical simulation models for the heat discharging and charging device were developed to predict the performance of each of the components. Based on these calculations, a case study for heat transportation between a local steel works and a hotel was examined and the Levelized Cost of Energy (LCOE) was evaluated.

Nomenclature

Symbols		Subscript	
c_p	specific heat capacity	J/(kg·K)	0 initial
d	diameter	m	a ambient
D	diffusivity	m ² /s	ax axial
k_{LDF}	overall mass transfer coefficient	1/s	b bed
n_{bt}	number of tubes	-	bt boiler tube
p	pressure	Pa	c chamber
q	adsorption amount	kg _{water} /kg _{zeolite}	eff effective
r	adsorption rate	kg/s	eq equilibrium
R_g	gas constant	J/(mol·K)	g gas
T	temperature	K	kn knudsen
u	velocity	m/s	L length of chamber
W	adsorption volume	mL/g	m molecular
x	axial distance	m	max maximum
α	heat transfer coefficient	W/(m ² ·K)	o outer
ΔH	adsorption heat	kJ/kg	p particle
ε	porosity	-	s steam
λ	thermal conductivity	W/(m·K)	w water
μ	viscosity	Pa·s	z zeolite
ρ	density	kg/m ³	
τ	tortuosity	-	
ϕ	relative humidity	-	
Re	Reynolds number	-	
Pr	Prandtl number	-	
Nu	Nusselt number	-	
CAPEX	Capital Expenditure	€	
OPEX	Operating expenses	€/y	
LCOE	Levelized cost of energy	€/MWh	

2. Main System Components

Thermochemical energy storage and transport system utilizing zeolite can be divided into three steps: charging, transportation and discharging. In this section, charging and discharging devices are called “Heat Charger” and “Zeolite Boiler”. The processes were numerically modeled and validated based on experimental results of equilibrium water adsorption in the zeolite 13X.

2.1 Discharging in the “Zeolite Boiler”

As a steam generator utilizing zeolite, zeolite boiler employing moving bed and indirect heat exchanger has been developed [6], as shown in Fig.1 (a1). The zeolite boiler consists of a non-pressurized chamber and an indirect multi-tubular heat exchanger, which is a vertically mounted counter-flow type reactor. Zeolite is poured into the chamber from the top and flows downward adsorbing injected steam. Adsorbed steam is injected from the top of heat exchanger and zeolite adsorbs injected steam and accompanying adsorption heat is transferred to the heat exchanger in the chamber. Water is supplied from the bottom of the heat exchanger and flows upward with increasing temperature. Although the moving bed reactor has benefits in supplying heat continuously, zeolite would be clogged in adsorbing liquid water in moving bed due to wetting of the zeolite particles, so water vapor is supplied to discharge the stored heat. In order to generate adsorbed steam by the zeolite boiler itself, a new type of zeolite boiler was designed as shown in Fig. 1 (a2).

The water pressurized up to 1.1 MPa is introduced from the bottom of the heat exchanger and is heated up to around 184 °C corresponding to the saturated temperature under 1.1 MPa. The pressurized water is depressurized to the ambient condition, and a part of the water is flashed and injected from the top. The drain water at 100 °C is mixed to the water at the ambient temperature to control the temperature in the water tank. The process of this system was modelled in the commercial process simulator Aspen HYSYS®, and a process flow diagram in generating 3100 kg/h of hot tap water is shown in Fig. 2.

Assuming in the numerical model that the zeolite boiler is an axially symmetric reactor without radial distribution, this zeolite boiler can be simplified to quasi-two-dimensional steady state model which has only axial temperature and steam concentration distribution and radially heat exchange between zeolite bed-water through the tube wall, and heat leakage between zeolite bed-ambient air through the insulated chamber wall. Other assumptions are shown as follows:

1. the chamber is packed with zeolite uniformly
2. the gas inside the chamber is treated as the ideal gas
3. steady-state heat and mass transfer with constant flow rate of zeolite

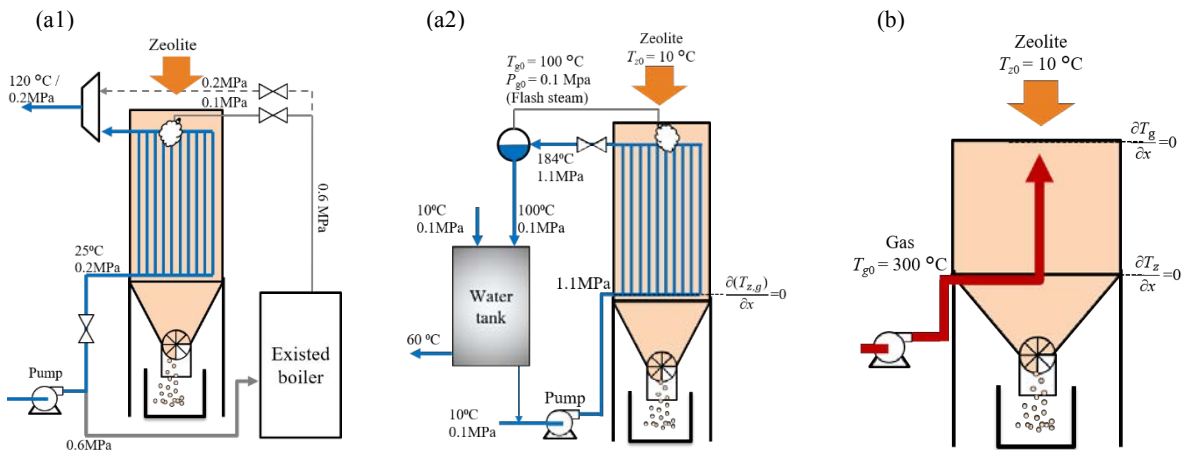


Fig.1 Schematic of a novel design (a1) Zeolite Boiler operated with existed boiler, (a2) Zeolite boiler injecting flash steam and (b) Heat Charger

Based on these assumptions, governing equations as shown in Table 1 were solved with a commercial CFD program, COMSOL Multiphysics® 5.3. The water mass flow rate is set firstly and determines the injection steam and drain water mass flow according to the flash rate under 1.1 MPa. Zeolite mass flow is adjusted until the outlet temperature of water reaches 184 °C. The water mass flow rate is changed by 100 kg/h step and repeat above procedure to seek the condition with minimum zeolite mass flow rate.

The heat transfer coefficient between zeolite and gas was given by Ranz Marshall [7] shown in Eq (11)

$$Nu = 2.0 + 0.6Re_p^{0.5}Pr^{0.333} \quad (11)$$

The heat transfer between zeolite bed and the wall of boiler tube and the chamber wall was shown in Eq. (12) and (13) [8].

Table 1. Governing equation of zeolite boiler and heat charger

Mass balance of zeolite	
	$\frac{\partial}{\partial x}(\rho_z u_z) = \rho_{z0} r \quad (1)$
Continuous equation	
(Zeolite boiler)	$\frac{\partial}{\partial x}(\rho_g u_g) = -\rho_{z0} r, \text{ B.C: } u_g = u_{g0} (x = 0 \text{ mm}) \quad (2)$
(Heat charger)	$\frac{\partial}{\partial x}(-\rho_g u_g) = -\rho_{z0} r, \text{ B.C: } u_g = u_{g0} (x = x_L) \quad (3)$
Energy balance (Zeolite)	
(Zeolite boiler)	$\frac{\partial}{\partial x}(\rho_z u_z c_{pz} T_z) = \frac{\partial}{\partial x}(\lambda_{z\text{-eff}} \frac{\partial T_z}{\partial x}) - \frac{4d_{bt,o} n_{bt} \alpha_{zw}}{d_c^2} (T_z - T_w) - \frac{4\alpha_{za}}{d_c} (T_z - T_a) - \frac{6(1 - \varepsilon_b) \alpha_{gz}}{d_c} (T_z - T_g) + \rho_{z0} r \Delta H \quad (4)$ B.C: $T_z = T_{z0} (x = 0 \text{ mm}), \frac{\partial T_z}{\partial x} = 0 (x = x_L)$
(Heat charger)	$\frac{\partial}{\partial x}(\rho_z u_z c_{pz} T_z) = \frac{\partial}{\partial x}(\lambda_{z\text{-eff}} \frac{\partial T_z}{\partial x}) - \frac{4\alpha_{za}}{d_c} (T_z - T_a) - \frac{6(1 - \varepsilon_b) \alpha_{gz}}{d_c} (T_z - T_g) + \rho_{z0} r \Delta H \quad (5)$ B.C: $T_z = T_{z0} (x = 0 \text{ mm}), \frac{\partial T_z}{\partial x} = 0 (x = x_L)$
Energy balance (Gas)	
(Zeolite boiler)	$\frac{\partial}{\partial x}(\rho_g u_g c_{pg} T_g) = \frac{\partial}{\partial x}(\lambda_{\text{avg}} \frac{\partial T_g}{\partial x}) - \frac{4d_{bt,o} n_{bt} \alpha_{gw}}{d_c^2} (T_g - T_w) - \frac{4\alpha_{za}}{d_c} (T_g - T_a) - \frac{6(1 - \varepsilon_b) \alpha_{gz}}{d_c} (T_g - T_z) \quad (6)$ B.C: $T_g = T_{g0} (x = 0 \text{ mm}), \frac{\partial T_g}{\partial x} = 0 (x = x_L)$
(Heat charger)	$\frac{\partial}{\partial x}(-\rho_g u_g c_{pg} T_g) = \frac{\partial}{\partial x}(\lambda_{\text{avg}} \frac{\partial T_g}{\partial x}) - \frac{4\alpha_{za}}{d_c} (T_g - T_a) - \frac{6(1 - \varepsilon_b) \alpha_{gz}}{d_c} (T_g - T_z) \quad (7)$ B.C: $\frac{\partial T_g}{\partial x} = 0 (x = 0 \text{ mm}), T_g = T_{g0} (x = x_L)$
Energy balance (Water)	
(Zeolite boiler)	$\frac{\partial}{\partial x}(-\rho_w u_w c_{pw} T_w) = \frac{4d_{bt,o} n_{bt} \alpha_{zw}}{d_c^2} (T_z - T_w) + \frac{4d_{bt,o} n_{bt} \alpha_{gw}}{d_c^2} (T_g - T_w) \quad (8)$ B.C: $T_w = T_{w0} (x = 0 \text{ mm}), \frac{\partial T_w}{\partial x} = 0 (x = x_L)$
Momentum equation	
(Zeolite boiler)	$\frac{\partial P}{\partial x} = \frac{150\mu_g u_g}{d_p^2} \cdot \frac{(1 - \varepsilon_b)^2}{\varepsilon_b^3} + \frac{1.75\rho_g u_g^2}{d_p} \cdot \frac{1 - \varepsilon_b}{\varepsilon_b^3}, \text{ B.C: } p = p_0 (x = x_L) \quad (9)$
(Heat charger)	$\frac{\partial P}{\partial x} = -\frac{150\mu_g u_g}{d_p^2} \cdot \frac{(1 - \varepsilon_b)^2}{\varepsilon_b^3} + \frac{1.75\rho_g u_g^2}{d_p} \cdot \frac{1 - \varepsilon_b}{\varepsilon_b^3}, \text{ B.C: } p = p_0 (x = 0 \text{ mm}) \quad (10)$

Table 2. Physical properties (Comsol, 2017)

Density of zeolite	[kg/m ³]	$\rho_{z0} = 721^*$
Porosity of zeolite bed	[-]	$\varepsilon_b = 0.4^*$
Porosity of zeolite particle	[-]	$\varepsilon_p = 0.3^*$
Heat capacity	[J/(kg·K)]	
		$c_{pz0} = -0.002198 \times T_z^2 + 3.1897 \times T_z + 33.8205^*$
		$c_{pz} = \frac{c_{pz0} + (q - q_0) + c_{pw}}{1 + (q - q_0)}$
		$c_{ps} = 13604 - 90.4304 \times T_g + 0.2774 \times T_g^2 - 4.2126 \times 10^{-4} \times T_g^3 + 3.1837 \times 10^{-7} \times T_g^4 - 9.5615 \times 10^{-11} \times T_g^5$
		$c_{pa} = 1047 - 0.3726 \times T_g + 9.4530 \times 10^{-4} \times T_g^2 - 6.0241 \times 10^{-7} \times T_g^3 + 1.2859 \times 10^{-10} \times T_g^4$
		$c_{pw} = 12010 - 80.4073 \times T_w + 0.3099 \times T_w^2 - 5.3819 \times 10^{-4} \times T_w^3 + 3.6254 \times 10^{-7} \times T_w^4$
Thermal conductivity	[W/(m·K)]	
		$\lambda_{z_eff} = 0.06171 + 3.2779 \times 10^{-4} \times T_z + 2.5641 \times 10^{-8} \times T_z^2^*$
		$\lambda_s = 1.3173 \times 10^{-4} + 5.1497 \times 10^{-5} \times T_g + 3.8965 \times 10^{-8} \times T_g^2 - 1.3681 \times 10^{-11} \times T_g^3$
		$\lambda_s = -0.002276 + 1.1548 \times 10^{-4} \times T_g - 7.9025 \times 10^{-8} \times T_g^2 + 4.1170 \times 10^{-11} \times T_g^3 - 7.4836 \times 10^{-15} \times T_g^4$
		$\lambda_w = -0.8691 + 0.0089 \times T_w - 1.5837 \times 10^{-5} \times T_w^2 + 7.9754 \times 10^{-9} \times T_w^3$
Viscosity	[Pa·s]	
		$\mu_s = -1.4202 \times 10^{-6} + 3.8346 \times 10^{-8} \times T_g - 3.8522 \times 10^{-12} \times T_g^2 + 2.1020 \times 10^{-15} \times T_g^3$
		$\mu_a = -8.3828 \times 10^{-7} + 8.3572 \times 10^{-8} \times T_g - 7.6943 \times 10^{-11} \times T_g^2 + 4.6437 \times 10^{-14} \times T_g^3 - 1.0659 \times 10^{-17} \times T_g^4$

* Experimentally obtained values

$$\text{(Zeolite particle – wall)} \quad a_{zw} = \frac{2.12\lambda_{eff0}}{d_p} \quad (12)$$

$$\text{(Gas – wall)} \quad Nu = 0.6Re_p^{0.5}Pr^{0.333} \quad (13)$$

The axial thermal conductivity of the zeolite was assumed to be equal to the effective thermal conductivity of zeolite under stagnant condition. The axial thermal conductivity of gas phase was shown in Eq. (14) [8].

$$\frac{1}{Re_p Pr} = \frac{0.73\varepsilon_b}{Re_p Pr} + \frac{0.5}{\left(1 + \frac{9.7\varepsilon_b}{Re_p Pr}\right)} \quad (14)$$

Heat loss from the wall can be calculated using overall heat transfer resistance consists of heat transfer between zeolite bed and chamber wall, thermal conduction inside 2.0 mm of the stainless wall (thermal conductivity of stainless: 16.7 W/(m·K)) and 25 mm of glass wool for thermal insulation (thermal conductivity of glass wool: 0.05 W/(m·K)) and natural convection from the surface of thermal insulating material which is assumed to be 10 W/(m·K).

Adsorption rate r in the eq. (1) - (5) can be described as follows;

$$r = k_{LDF}(q_{eq} - q) \quad (15)$$

Overall mass transfer coefficient k_{LDF} based on the linear driving force model [9] can be described as follows, it is based on the assumption that resistance of external film and micro pore diffusion are negligible, i.e. only macro pore diffusion was considered.

$$\frac{1}{k_{LDF}} = \frac{(d_p/2)^2}{15(1 - \varepsilon_b)\varepsilon_p D_{eff}} \cdot \frac{\rho_z R_g T_z q_{eq}}{p_s} \quad (16)$$

The effective diffusivity is composed of both the molecular and Knudsen diffusion as shown in eq. (17).

$$\frac{1}{D_{eff}} = \tau \left(\frac{1}{D_m} + \frac{1}{D_{kn}} \right) \tag{17}$$

The pore diameter and the tortuosity of this zeolite 13X were assumed to be 181 nm and 4.0, respectively. Other physical properties were summarized in Table 2. The specific heat capacity and stagnant effective thermal conductivity of dried zeolite were obtained by the adiabatic calorimetry and hotwired method in the range of temperature of 0 - 300°C and 20 - 300°C, respectively. The gas phase thermal conductivity and viscosity were treated as the mixed gas [10], [11].

2.2 Charging in the “Heat Charger”

The charging device (Heat charger) employs a counter flow type moving bed reactor similar to the design of the zeolite boiler, as shown in Fig. 1(b). Zeolite is supplied from the top and moves downwards. Reversely, heated gas is introduced from the bottom of the chamber and goes upwards. This heat charger is simpler than zeolite boiler because of no heat exchanger inside the chamber, only considering heat transfer between zeolite - hot gas, axial effective thermal conductivity and heat loss from the wall. A quasi-2D model with the governing equations presented in Table. 1 has been developed. The same assumptions as in the zeolite boiler model were considered. The heat transfer and kinetic model were set as the same as the zeolite boiler as shown in Eq. (11) - (17).

2.3 Equilibrium adsorption amount

In the modelling of both the zeolite boiler and the heat charger, it is critical to validate the equilibrium sorption characteristics of zeolite 13X. For this, a fixed bed experimental test was conducted. A stainless steel 3/4-inch tube was employed as an outlet diameter of the reactor, and 4.92 g of zeolite was diluted with 59.5 g of alumina ball which is inert to the water vapor because adsorption heat can be moderated leading to faster experimental procedure. Firstly, the reactor temperature is kept constant, and humidified air of which vapor pressure is controlled by bubbler system is introduced. The outlet vapor pressure decreases rapidly because water vapor in the humidified air is adsorbed by the zeolite. After all the zeolite in the reactor reaches equilibrium, outlet vapor pressure begins to increase. When the outlet vapor pressure reaches the same pressure as at the inlet, the whole zeolite in the reactor is completely saturated, and temperatures of the reactor wall and the inlet gas are cooled down. Due to temperature decrease, zeolite can adsorb additional steam along the equilibrium line. Here the vapor pressure change is measured experimentally. Several series of experiments were conducted under 4.2 – 8.0 kPa of vapor pressure and temperature between 45 – 250 °C.

Fig. 3 shows the results of equilibrium adsorption amount. For the equilibrium adsorption model, Sips equation was selected in this study, however, at the higher relative humidity area, equilibrium adsorption amount is rapidly

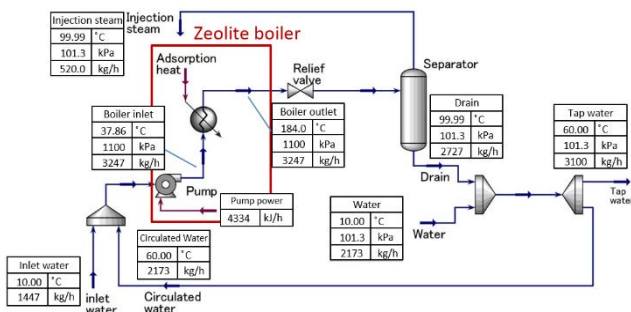


Fig. 2 Process flow diagram of “Zeolite boiler”

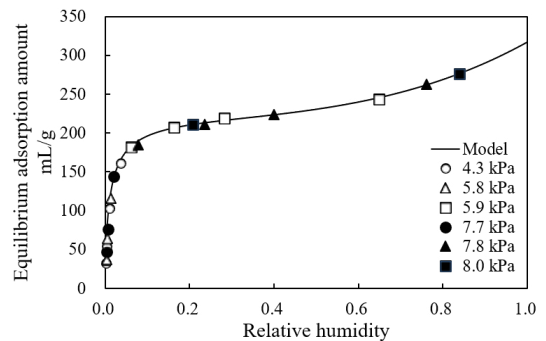


Fig. 3 Result of equilibrium adsorption amount

increased due to capillary effect. However, the conventional adsorption equilibrium models (e.g. Langmuir, Sips, Dubinin-Astakov and others) cannot simulate this capillary effect. To simulate this, Excess Surface Work (ESW) model based on the chemical potential should be employed [12], however, to simplify, a combined equilibrium adsorption model of Sips and Freundlich, Eq. (18), is used in this study.

$$W = \frac{W_{\max} (b\phi)^{1/n}}{1+(b\phi)^{1/n}} + K\phi^m \tag{18}$$

Sorption specific parameters (b , n , W_{\max} , K , m) were fitted to the experimental data utilizing a non-linear square fitting where $W_{\max} = 232.20$ mL/g, $n = 1.27$, $b = 85.4$, $K = 91.4$ and $m = 3.23$. Fig. 3 shows the comparison between experimental data and the calculated data and good agreement of this model was obtained.

3. Case study of techno economic analysis in Sweden

A case study in Sweden was conducted utilizing the zeolite boiler and the heat charger. The cost of equipment in each station was estimated mainly from the cost estimation handbook for chemical engineering plant [13]. The Chemical Engineering Plant Cost Index (2000: 394.1, 2016: 556.8) [14], [15], the price level index by OECD (Japan: 106, Sweden 119) [16] and SDRs per Currency unit (Japan:0.006, Euro: 0.826, SEK:0.085) [17] were used to convert the Japanese price in 2000 to current Swedish price. We assumed that the zeolite is regenerated by the waste heat from a local steel works, and transported to a vicinal hotel currently using the pellet boiler to generate the hot tap water around 60 °C.

3.1 Heat discharging planning

From October to April, demand of hot tap water at 60°C is over 4000 kg/h in the hotel. This flow rate was calculated by the enthalpy of hot water for the averaged hourly heat demand during the months. In other months, heat demand decreases; demand of hot tap water in May, June, August and September are 3100, 1800, 1500 and 2500 kg/h, respectively. In this study, for 8 months from October to May, zeolite boiler generates 3100 kg/h of hot tap water corresponding to the maximum demand of hot tap water of May for the baseload. Other months except July, zeolite boiler supplies all heat demand of the hotel and hot water is supplied to the tank which can adapt to heat demand fluctuation. In July, heat demand in Sweden drastically decreases and heat transporting is assumed to suspend. Therefore, the heat charging station of the local steel works operates for 11 months per year. Residual (initial) adsorption amount of the inlet zeolite was set as 0.01 kg_{water}/kg_{zeolite} according to the heat charging step mentioned below.

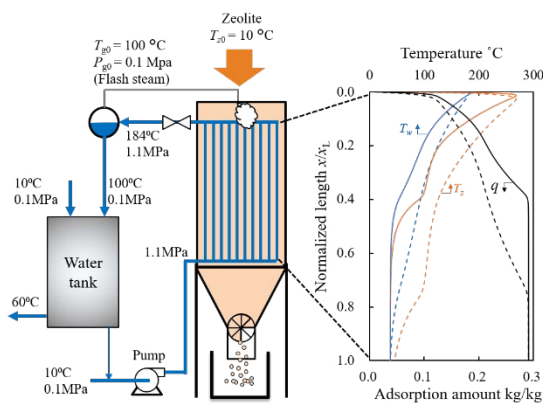


Fig.4 Result of “Zeolite boiler”

Hot water flow: 3100 kg/h, Zeolite flow:1850 kg/h
 Solid line: $x_L = 1.0$ m
 Dotted line: $x_L = 0.5$ m

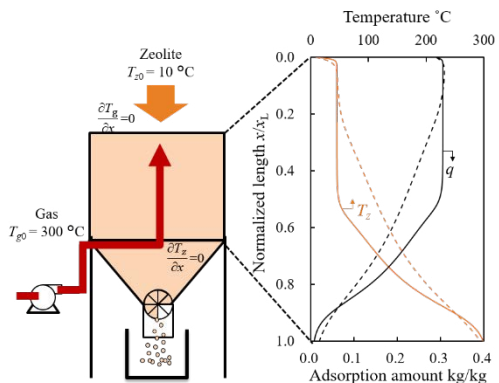


Fig. 5 Result of heat charger

Zeolite flow: 1850 kg/h
 Solid line: $(x_L, d_c) = (1.0 \text{ m}, 2.0 \text{ m})$
 Dotted line: $(x_L, d_c) = (0.1 \text{ m}, 2.5 \text{ m})$

The diameter of chamber is set as 1.5 m, which is roughly the same diameter as normal hot water boiler, and heat exchange tubes with 15.9 mm of outer diameter and 1.2 mm thickness are assumed to form the tube bundle with 60 ° and 1.25 pitch staggered array inside the zeolite boiler. With the given pitch and tube length, heat transfer area is determined. The length of heat exchanger was tested 0.5 and 1.0 m on the condition of 1850 kg/h zeolite. Figure 4 shows the temperature and adsorption amount distribution in the zeolite boiler on normalized axis. The temperature around the top of the chamber rapidly increases (rises up), and the temperature of zeolite drops down accompanying with heating the water and approaches the temperature of water at the middle section of the chamber. The result shown in Fig. 4 indicates that the heat exchanger with 1.0 m has sufficient length to transfer the adsorption heat. The heat transfer area of this configuration is 210 m². Other conditions are shown in Table 1. The cost of these equipment was estimated from on Saito [13]. A conveyor belt was selected to transport the zeolite from the container to the top of the zeolite boiler, and its cost was estimated referring the same literature. A zeolite discharger at the bottom of the chamber employs a rotary valve, and its cost was estimated as 750,000 JPY [18]. The required power of the water pump is calculated by the process flow diagram on Aspen HYSYS, shown in Fig. 2. All results are summarized in Table 3.

3.2 Heat charging planning

There are several temperature levels of waste heat in the local steel works. The heat at 560 °C is the largest amount of surplus heat from there and is selected as the heat source for this system. The process flow diagram of the heat charging system was built in Aspen HYSYS. The surplus heat is recovered by ambient air that is heated up from 10 to 300 °C thorough the heat exchanger of which overall heat transfer coefficient and heat transfer area are estimated as 35 W/(m²·K) and 53.3 m², respectively. The cost of the heat exchanger was estimated based on the cost handbook [13]. Figure 5 shows the temperature and adsorption distribution in the heat charger with 0.34 m in height on normalized axis on the condition of 1850 kg/h zeolite. The sorption amount increases around the top due to vapor pressure increase by desorption. The zeolite temperature around the bottom of chamber rapidly increases, and the ultimate adsorption amount reaches the target value of 0.01 kg_{water}/kg_{zeolite}. In order to synchronize with the operation of zeolite boiler, the heat charger with 2.0 m in diameter and 0.34 m in height was reasonable because the longer heat charger (0.8 m in height and 1.5 m in diameter) had over 20 kPa pressure loss leading to around 5 times higher OPEX. On the other hand, the shorter heat charger (0.1 m in height and 2.5 m in diameter) was not feasible because it cannot achieve the target ultimate adsorption amount. All results are summarized in Table 3.

3.3 Transportation

A standard 24 ft container was assumed to transport the zeolite. The maximum capacity of dried zeolite was determined as 17.0 ton, which is equivalent to 21.8 ton using the same container for the return trip of the zeolite saturated with water. Transportation cost is taken to be 750 SEK/hour. The required transportation time is rounded off to the whole hour. In this system, only storage material is transported, i.e. zeolite can be transported at any time as long as there is zeolite available, so transportation cost can be reduced if more trips are done in an hour. Regenerated zeolite is transported to the hotel and is unloaded there, then the saturated zeolite is transported back to the charging station to the local steel works site. This round-trip transportation is repeated in accordance with heat demand. The distance between the hotel and the local steel work industry is 6.7 km. In this study, zeolite transportation is assumed to be operated on a round trip basis performed within an hour and the transportation commences only when the containers hold the full payload. The exemplified operation diagram for 55 hours is shown in Fig. 6. In this case, the

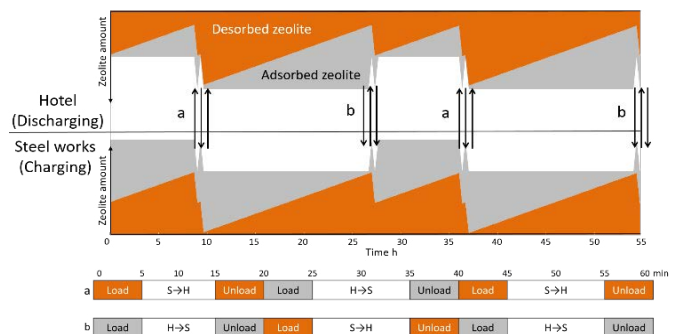


Fig. 6 Operation diagram

zeolite boiler generates 3100 kg/h of hot tap water continuously. On the discharging site, spare zeolites for additional 4 hours of operation is made available in case of unforeseen need. The total amount of zeolite requires 76 ton considering imbalance of the demand and supply side operations and total price of zeolite is taken at 2500 €/ton [19]. Table 3 summarizes the operation modes for each of the heat transportation cycle throughout the year. The number of cycles in August is about 65% of January-May and October-December because of lower heat demand in

Table 3. Calculation conditions for charge (Heat charger), discharge (Zeolite boiler) and number of cycles

		Jan – May, Oct - Dec	Jun	Aug	Sep
Zeolite Boiler	Zeolite mass flow rate kg/h	1850	1350	1200	1600
	Tap water mass flow kg/h	3100	1800	1500	2500
	Injection steam mass flow kg/h	520	329	297	435
	Supplied water mass flow kg/h	3247	2054	1856	2717
	Pump power kW	1.2	0.76	0.69	1.0
	Reduced heat MWh/month	120	70	55	95
Heat charger	Volumetric m ³ /min at 10 °C	115	79	71	98
	Pressure drop kPa	4.6	2.5	2.1	3.5
Transportation	Cycles/month	73	53	47	63

Summer.

3.4 Levelized Cost of Energy

The interest rate, the life time of each equipment and the electricity price are assumed to be 2.0%, 15 years and 0.65 SEK/kWh respectively. Maintenance factor was set at 2.0% of all CAPEX exclude zeolite. The life time and maintenance factor of Zeolite 13X are set as 25 years and 0.5%, respectively. Total heat output by zeolite boiler is 1182 MWh/year. LCOE resulted in 60.9 €/MWh, which is a comparable cost against conventional pellet boiler (approximately 60 €/MWh). Fig. 7 shows the cost breakdown of this system. The inventories shown in deep and light colors are categorized as Capital expenditure (CAPEX) and Operating expenses (OPEX). Transportation cost accounts for 53% of the total cost due to high number of cycles. In the CAPEX, cost of storage material and heat exchanger inside the zeolite boiler account for 41% and 16% of CAPEX, respectively.

The sensitivity analysis was conducted for transportation, transported capacity and zeolite price. Fig. 8 shows the result of sensitivity analysis in which all variables are normalized based on the base scenario. Both cheaper transportation cost and larger zeolite capacity on the one trailer give a comparable impact on the LCOE, which implies that developing the zeolite with a higher storage density is an effective solution to reduce LCOE, for instance, 1.5 times higher storage density leads 18% reduction in LCOE.

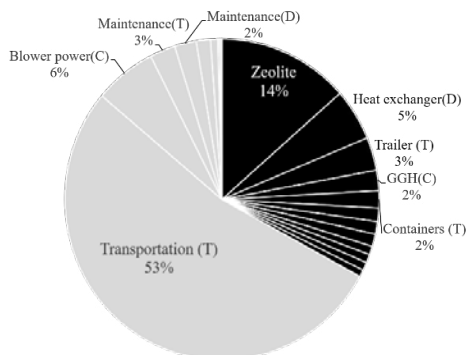


Fig. 7 Result of economic analysis (C, D and T represent charging, discharging and transportation)

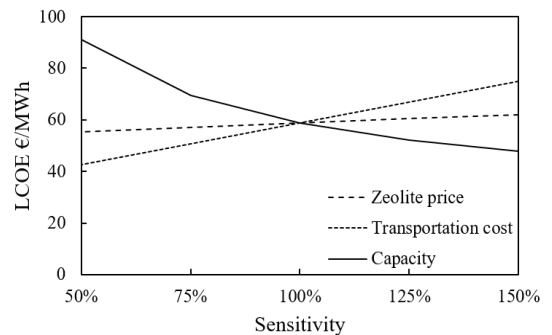


Fig. 8 Result of sensitive analysis

4. Conclusion

In this study, a case study of techno economic analysis of thermochemical energy storage and transport system utilizing zeolite 13X steam adsorption and desorption cycle in Sweden was conducted. The heat and material balance of system was designed in Aspen HYSYS and under the boundary condition given by the system analysis, the heat discharging and charging devices were modelled and computed reflecting the experimental result of adsorption and desorption.

The zeolite boiler employing moving bed and indirect heat exchanger supplying around 60 °C hot water was designed as a heat discharging device in the system. The zeolite boiler generates pressurized water and flash steam is injected into the chamber. Also, the design of heat charger employing a counter flow type moving bed reactor similar to the design of zeolite boiler was made. The zeolite boiler and heat charger were modeled as a quasi-two-dimensional steady state model and computed numerically based on experimental results of water equilibrium adsorption amount of zeolite 13X to predict the performance.

The LCOE of a case study transporting heat between a local steel works and vicinal hotel resulted in 60.9 €/MWh, which was comparable cost against conventional pellet boiler. From the sensitivity analysis, both cheaper transportation cost and larger zeolite capacity on the one trailer give a comparable impact on the LCOE, for instance, 1.5 times higher storage density leads 18% reducing in LCOE.

Acknowledgements,

The authors acknowledge the support of Shinko Sugar Mill Co., Ltd. and Japan Boiler Association and would like to express our gratitude.

References

- [1] Miró L, Sarah B, Cabeza L F. Mapping and discussing Industrial Waste Heat (IWH) potentials for different countries. *Renewable and Sustainable Energy Reviews* 2015; 51: 847-855.
- [2] Swedish Energy Agency. Energy in Sweden 2015 2015
- [3] Hauer A. ADSORPTION SYSTEMS FOR TES—DESIGN AND DEMONSTRATION PROJECTS. In: Paksoy H.Ö. (eds) Thermal Energy Storage for Sustainable Energy Consumption. *NATO Science Series (Mathematics, Physics and Chemistry)*, Springer, Dordrecht; 2007; 234.
- [4] Nakaso K, Tanaka Y, Eshima S, Kobayashi S, Fukai J. Performance of a novel steam generation system using a water-zeolite pair for effective use of waste heat from the iron and steel making process. *ISIJ International* 2015; 55.2: 448-456.
- [5] Krönauer A, Lävemann E, Brückner S, Hauer A, Mobile sorption heat storage in industrial waste heat recovery. *Energy Procedia* 2015; 73: 272-280
- [6] Fujii S, Nakaibayashi K, Kanematsu Y, Kikuchi Y, Nakagaki T. Development of zeolite boiler in thermochemical energy storage and transport system utilizing unused heat from sugar mill. *14th International Conference on Energy Storage, EnerSTOCK2018* 2018
- [7] Ranz W. E, Marshall W. R. Evaporation from drops. *Chemical Engineering Progress* 1952; 48(3): 141-146.
- [8] Dixon A G, David L Cresswell, Theoretical prediction of effective heat transfer parameters in packed beds. *AIChE Journal* 1979; 25.4: 663-676.
- [9] Gorbach A, Stegmaier M, Eigenberger G. Measurement and modeling of water vapor adsorption on zeolite 4A—Equilibria and kinetics. *Adsorption* 2004; 10(1): 29-46.
- [10] Mason E. A, S C Saxena. Approximate formula for the thermal conductivity of gas mixtures. *The Physics of fluids* 1958; 1.5: 361-369.
- [11] Wilke, C. R. A viscosity equation for gas mixtures. *The journal of chemical physics* 1950; 18.4: 517-519.
- [12] Adolphs J, Setzer M J. A model to describe adsorption isotherms. *Journal of Colloid and interface science* 1996; 180.1: 70-76.
- [13] Saito Y. Cost estimation handbook for chemical engineers. *Kogyo chosakai* 2000 (in Japanese).
- [14] Vatavuk W M. Updating the CE plant cost index. *Chemical Engineering* 2002; 109.1: 62-70.
- [15] CURRENT ECONOMIC TRENDS – MARCH 2016, (online), available from <<http://www.chemengonline.com/current-economic-trends-march-2016/?printmode=1>> (accessed on Oct, 2017).
- [16] Price level indices, (online), available from <<https://data.oecd.org/price/price-level-indices.htm>> (accessed on Oct, 2017).
- [17] SDRs per Currency unit (online), available from <https://www.imf.org/external/np/fin/data/rms_mth.aspx?SelectDate=2017-11-30&reportType=SDRCV> (accessed on Nov, 2017).
- [18] AISHIN rotary valves, (online), available from <http://www.mekatoro.net/mechatro_parts/vol3/pdf/P09-105.html> (accessed on Oct, 2017)
- [19] Scapino L, Zondag H A, Van Bael J, Diriken J and Rindt C C. Energy density and storage capacity cost comparison of conceptual solid and liquid sorption seasonal heat storage systems for low-temperature space heating. *Renewable and Sustainable Energy Reviews* 2017; 76: 1314-1331.



16th International Symposium on District Heating and Cooling, DHC2018,
9–12 September 2018, Hamburg, Germany

Thermal grid system and its field test in multiple buildings with individual heating and cooling facility

Masaki Nakao^{a*}, Minako Nabeshima^a, Youichi Kobayashi^b, Masashi Ishinada^a

^a Osaka City University, 3-3-138 Sugimoto-cho, Sumiyoshi-ku, Osaka, Osaka 558-8585, Japan

^b Yasui Architects and Engineers, inc., 2-4-7 Shima-machi, Chuo-ku, Osaka, Osaka 540-0034, Japan

Abstract

A thermal grid system (TGS) has been developed for addition to district multiple buildings in order to reduce their primary energy consumption and CO₂ emissions. The TGS consists of double-loop piping and routers, which use control valves and grid pumps to switch the route of water flow. The TGS and a high-efficiency heat source unit with a cooling capacity of 5% of the total heat source units were installed in the building group of aged absorption chilling and heating units. CO₂ emissions after installation decreased by 42% in the summer of 2015 compared to 2014 before introducing the TGS.

© 2018 The Authors. Published by Elsevier Ltd.

This is an open access article under the CC BY-NC-ND license (<https://creativecommons.org/licenses/by-nc-nd/4.0/>)

Selection and peer-review under responsibility of the scientific committee of the 16th International Symposium on District Heating and Cooling, DHC2018.

Keywords: Thermal grid system; Router; Dual-loop piping; Optimal operation; Air conditioning; Heat source unit

1. Introduction

Approximately 40% of the energy consumed in Japanese office buildings is used in air conditioning. As such,

* Corresponding author. Tel.: +81-6-6605-2993; fax: +81-6-6605-2993.

E-mail address: nakao@urban.eng.osaka-cu.ac.jp

optimal operation and energy savings are indispensable in air conditioning systems in order to realize a low-carbon society. Although district heating and cooling (DHC) can contribute to energy savings in air conditioning systems, DHC is not prevalent in Japan. Instead, individual air conditioning systems are installed in almost all buildings. The heat source units used in air conditioning systems in many buildings are outdated and have low unit performance, resulting in low efficiency of air conditioning systems. In addition, most air conditioning systems in office buildings in Japan are being operated most of the time under extremely inefficient conditions with low partial load efficiency.

We have developed the TGS in order to solve the abovementioned problems with existing air conditioning systems. The TGS, also referred to as a smart grid, interchanges heat with chilled water in the summer and interchanges hot water in the winter between two or more buildings in order to reduce energy consumption. In other words, the TGS is defined as a system that routes between individual air conditioning units and heat sources in order to minimize the air conditioning energy consumption of multiple buildings. The energy bus system of [1], 4th Generation District Heating (4GDH) of [2], the extended energy hub approach of [4], and the bidirectional district energy system of [5] are also bidirectional thermal energy network models. Although the interactivity is also the same in the present paper, we attempt to conserve energy across multiple building groups with an existing independent heat source. In addition, although the thermal energy system of [1] and [5] is a heat source water network, the TGS in the present paper is a network of cold water and hot water. On the other hand, the optimal calculation method described herein is based on [3]. In the model of [3], mass flow and water temperature are taken into consideration as basic variables for expressing heat flow, pressure loss, and heat loss in piping segments.

Symbols:

AC	air conditioning unit
AR	gas-fired absorption chilling and heating unit
R, R1...R15	chilling unit or heat source unit
Re1...Re4	receiving pattern of heat
RL-1	left-hand side of the return loop
RL-2	right-hand side of the return loop
Se1...Se4	sending pattern of heat
SL-1	left-hand side of the supply loop
SL-2	right-hand side of the supply loop
TR	centrifugal chilling unit, such as a turbo refrigerator or heat pump chilling and heating unit

2. Thermal Grid System

The purpose of the TGS is to flexibly change the flow pattern and to realize optimum operation by connecting heat sources and loads with double-loop piping of comparatively small diameter. When the TGS is applied to an existing city district, the following effects can be expected (Fig. 1).

(1) Priority operation of high-efficiency heat source units

Just by updating some existing heat source units to new high-efficiency units in the area, it is possible to supply the heat produced by a high-efficiency heat source to all buildings connected by piping. Furthermore, it is possible to lower the operation rate of old low-efficiency heat sources.

(2) Volume reduction of total heat source units

(3) Improvement in the load factor of heat source units

By reducing the number of heat source units for operation, it is possible to move from low-efficiency low-load operation to high-efficiency high-load operation.

(4) Improvement of the reliability of the heat supply for important buildings

2.1 Construction of the TGS

The TGS connect nodes, such as multiple buildings and heat sources, by double-loop piping, and routers that transport chilled water in summer or hot water in winter, as well as heat in both directions between the connected nodes. A router consists of a control valve that switches the direction of heat transport and a grid pump that drives the heat flow. Routers can connect heat sources and demands.

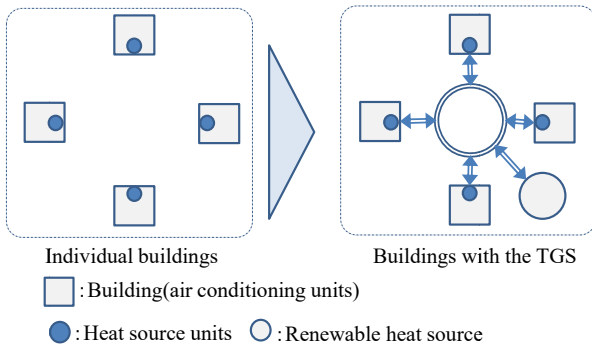


Fig. 1. Before and after introduction of the TGS

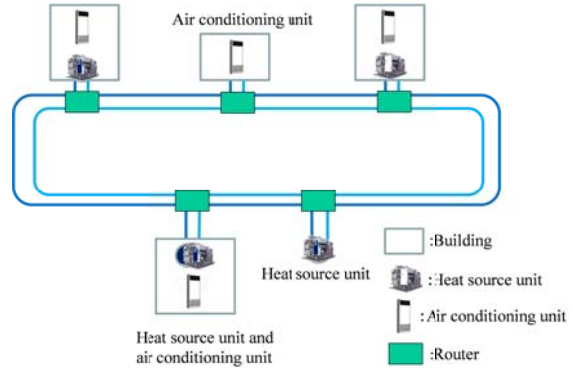


Fig. 2. Basic concept of the TGS

2.2 Configuration of the optimal operation system

(1) Piping network model

A mathematical model for calculating energy consumption is necessary for optimal operation of the TGS. In this model, the mass flow rate and water temperature are taken into consideration as basic variables to express the heat flow rate, pressure, and heat loss of piping segments. For details of the model, refer to [3].

(2) Model of heat source unit

An approximate model of the heat source unit is obtained from measured values of input energy and cooling capacity.

(3) Optimal operation

The overall flow of the optimal operation system is shown in Fig. 3.

(a) Present thermal load is given by local Energy Management System(EMS).

(b) One hour prediction of thermal load is conducted hourly, every day, using information such as the present thermal load, the room usage schedule input by the operator and the weather forecast.

(c) An optimization program is executed hourly based on the load prediction data to determine the flow pattern and the heat source to be operated. This optimal operation is performed when an optimal solution is obtained.

Selection of the flow pattern and the heat source unit is realized by operation of the valve and the pump.

(d) Local EMS control the capacity of heat source, room air temperature and grid pumps for the routing.

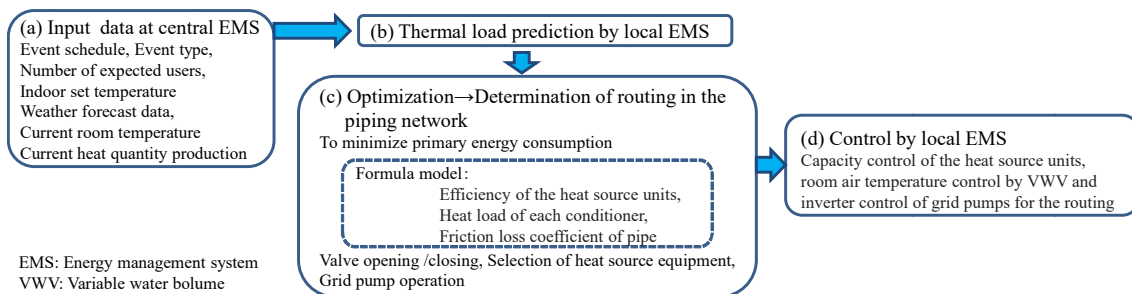


Fig. 3. Optimal operation

3. Router configuration and functions

3.1 Router function

The router connects the heat source, the air conditioning unit, and the double-loop piping and switches the flow path of the TGS. The heat source and the air conditioning unit are composed of seven electrically operated switching valves and a grid pump to change the flow rate by inverter control. The selection of the heat source unit and switching of the router are determined by the optimization program. There are 128 (= 2⁷) combinations of valve

opening/closing states, because there are seven valves for pipes in each building. In addition, there are four patterns ($= 2 \times 2$), i.e., whether to use an air conditioning unit, and whether to use a heat source unit. Moreover, we need to consider, whether to supply water to a supply loop or a return loop, as well as whether to receive water from the supply loop or from the return loop. Furthermore, we must consider the direction of water flow, whether to the right or the left in case of supplying water, and from the right or the left in case of receiving water.

As a result, there are 32 ($= 2 \times 2 \times 2 \times 2 \times 2 \times 2$) combinations of flow routes. However, since half of the combinations are not practical, there are actually 16 modes. Finally, by adding two modes, “individual operation” and “stop”, to the 16 modes, we have 18 modes of useful flow patterns. Figure 4 summarizes the flow routes from a functional aspect, and Table 1 lists the useful combinations of router functions.

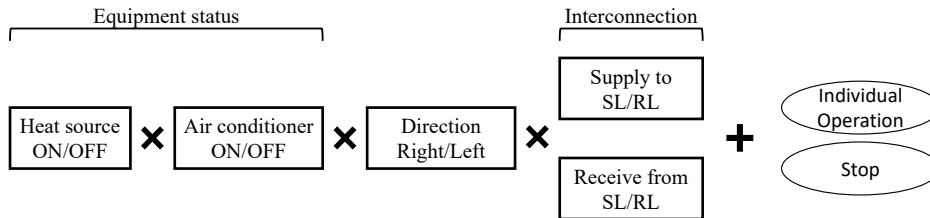


Fig. 4. Combinations of flow routes

Table 1 Functions of the router

R	AC	Supply		Demand		None
		Send to supply loop	Send to return loop	Receive from supply loop	Receive from return loop	
ON	ON	Se1 RL-1=>SL RL-2=>SL	Se2 RL-1=>RL-2 RL-2=>RL-1	Re1 SL=>RL-1 SL=>RL-2	Re2 RL-1=>RL-2 RL-2=>RL-1	Individual operation
ON	OFF	Se3 RL-1=>SL RL-2=>SL	Se4 RL-1=>RL-2 RL-2=>RL-1	—	—	—
OFF	ON	—	—	Re3 SL=>RL-1 SL=>RL-2	Re4 RL-1=>RL-2 RL-2=>RL-1	—
OFF	OFF	—	—	—	—	Stop

For example, in Se1, both the heat source unit and the air conditioning unit are used, and water is received from the return loop(RL) and supplied to the supply loop(SL). In addition, in Re4, the air conditioning unit is used, but the heat source unit is not used, and water is received from the return loop and sent to the return loop. Hence, a thermal cascade can be realized to save energy by supplying the chilled return water for reuse in another building. This happens when the temperature difference between the supply and the return water is small. For each of these conditions, we distinguish between the left- and right-hand sides of the return loop. The expression RL-1=>RL-2 indicates that water is taken from the left-hand side return loop to the building and is sent to the right-hand side return loop.

3.2 Router configuration

Table 2 shows the open/closed states of the valves. Figures 5 through 13 show the flow routes. In order to prevent short circuiting of piping due to excessive flow rates, the valve of the loop piping is open. In other words, it is also possible to open the valve of the loop piping and allow bypass, even with the same flow path pattern. In these figures, the thick line shows the piping in which chilled water actually flows, and dotted lines indicate bypassed piping. In addition, black icons indicate closed valves, and white icons indicate open valves. The simplified diagram at the upper right of the flow pattern diagram was adapted to the expression of a piping network in the reference [3].

The routing patterns are more limited than the total number of combinations of flow routes from the viewpoint of practicality. For operation, the switching table of valves that realize patterns is programmed in a local energy management system (EMS).

Table 2 Valve states

pattern	Se1		Se2		Se3		Se4		Re1		Re2		Re3		Re4		None	
	RL-1	RL-2	RL-1	RL-2	RL-1	RL-2	RL-1	RL-2	SL	SL	RL-1	RL-2	SL	SL	RL-1	RL-2	IO	Stop
=>	=>	=>	=>	=>	=>	=>	=>	=>	=>	=>	=>	=>	=>	=>	=>	=>		
SL	SL	RL-2	RL-1	SL	SL	RL-2	RL-1	RL-1	RL-1	RL-2	RL-2	RL-1	RL-1	RL-2	RL-2	RL-1		
V-1	O	O	X	X	O	O	X	X	O	O	X	X	O	O	X	X	X	X
V-2	X	X	X	O	X	X	X	O	X	X	X	O	X	X	O	X	X	X
V-3	X	X	O	b	X	X	O	b	X	X	O	X	X	X	X	O	X	X
V-4	b	b	O	X	b	b	O	X	X	X	O	X	X	X	X	O	X	X
V-5	O	O	b	O	O	O	b	O	O	O	X	O	O	O	O	X	X	X
V-6	O	X	b	b	O	X	b	b	O	X	b	b	O	X	b	b	X	O
V-7	O	O	O	O	O	O	O	O	X	X	X	X	X	X	X	X	O	O
V-AC	O	O	O	O	b	b	b	b	O	O	O	O	O	O	O	O	O	X

b: (bypass) when the cooling water flowing in the pipe exceeds a certain volume, the valve will be open in order to allow bypass, O: valve open, X: valve closed, =>: heat flow, IO: individual operation, Stop: heat source units and air conditioning units of a building re stopped

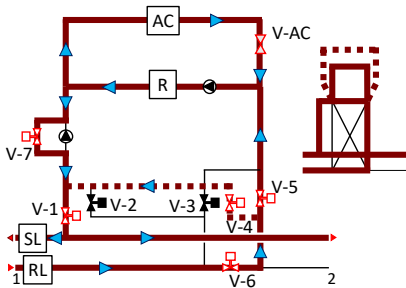


Fig. 5 Se1: RL-1=>SL flow pattern

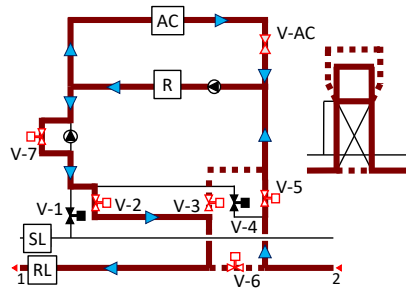


Fig. 6 Se2: RL-2=>RL-1 flow pattern

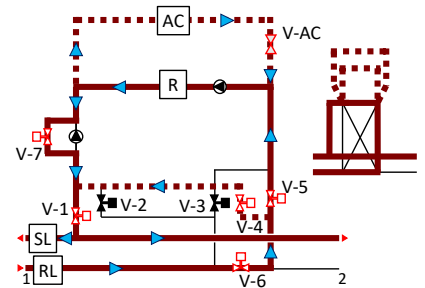


Fig. 7 Se3: RL-1=>SL flow pattern

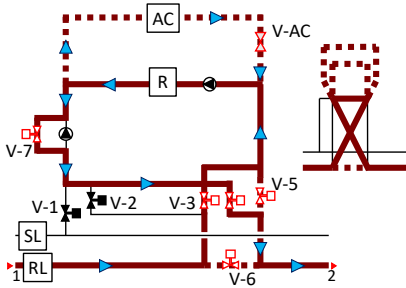


Fig. 8 Se4: RL-1=>RL-2 flow pattern

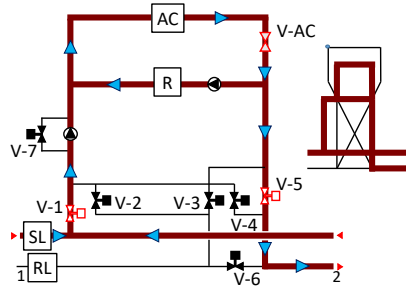


Fig. 9 Re1: SL=>RL-2 flow pattern

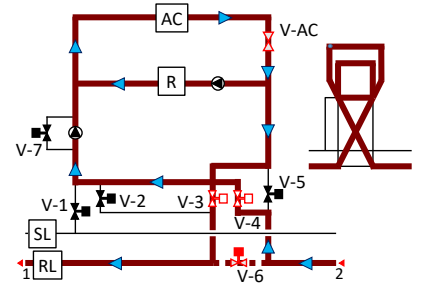


Fig. 10 Re2: RL-2=>RL-1 flow pattern

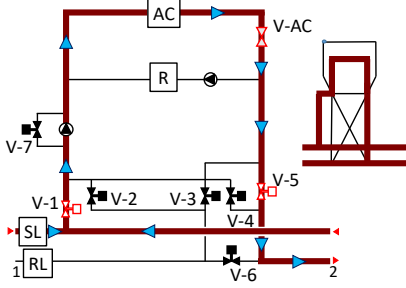


Fig. 11 Re3: SL=>RL-2 flow pattern

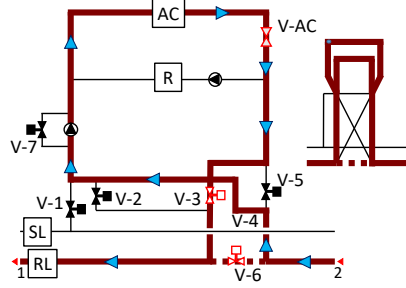


Fig. 12 Re4: RL-2=>RL-1 flow pattern

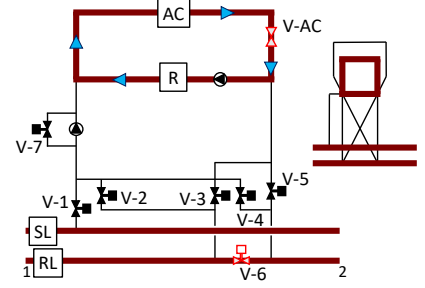


Fig. 13 Individual Operation flow pattern

4. Outline of the demonstration field

4.1 Buildings and facilities of the demonstration field

The Osaka International Trade Fair Exhibition Hall, which was opened in 1985, is used as the demonstration field in the present study. The total floor area is 132,709 m², and the total exhibition area is 72,978 m². Each air

conditioning facility in the building is a central heat source system, with individual operation for each building, as shown in Fig. 14. Table 3 lists all of the heat source units that are existent. Except for Building 4, which has heat pump chilling and heating units, all of the buildings have gas absorption chilling and heating units. The six buildings have a total of 15 existent, older heat source units with a total cooling capacity of 28 MW. Buildings 1, 2, and 3 are facilities that prioritize economy, such as one heat source unit per building. Building 4 is equipped with four heat pump chillers. Building 5, which has two absorption chilling and heating units (R14 and R15), and Building 6, which has five absorption chilling and heating units (R5 to R9), are each multi-unit operation controlled. The heat source units of Buildings 1 and 2 are installed in the machine room of a separate building.

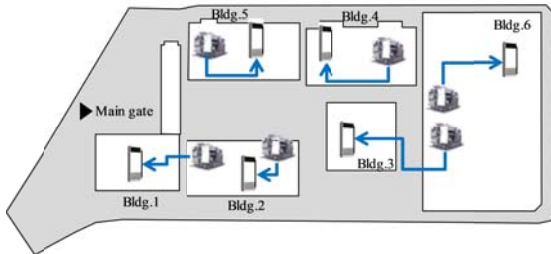


Fig. 14. Before introducing the TGS

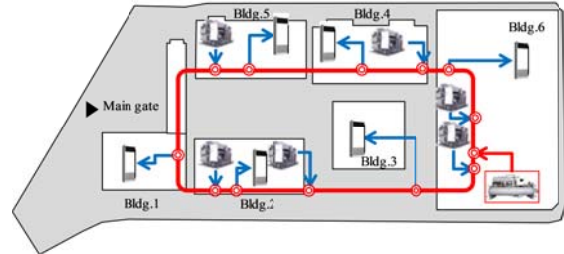


Fig. 15. After introducing the TGS

Table 3 Heat source unit specifications

Building	Unit number	Heat source	Cooling capacity	Rated COP
			kW	-
Bldg.1	R3	AR	2,109	1.03
Bldg.2	R1	AR	2,812	1.03
Bldg.3	R2	AR	2,109	1.03
Bldg.4	R10–R13	Heat pump TR	358	3.2
Bldg.5	R14	AR	1,933	1.02
	R15	AR	984	1.03
Bldg.6	R7	AR	3,515	1.03
	R8	AR	3,515	1.03
	R9	AR	1,054	1.03
	R5	AR	4,393	1.03
	R6	AR	4,393	1.03
	R4	High-efficiency TR	1,758	6.19

4.2 Application of the TGS

We introduced the TGS to six existing buildings in the Osaka Exhibition Hall. Double-loop piping with an inner diameter of 204.7 mm was connected to units of six buildings via routers. A high-efficiency heat source unit (R4) with a capacity of 5% of the total cooling capacity was added to the TGS. This unit has a higher coefficient of performance (COP) than the existing absorption chilling and heating units. The test field after introducing the TGS is shown in Fig. 15.

The piping network model for optimal operation is quoted from the reference [3]. In this model, the mass flow rates and temperatures of water are considered to be basic variables expressing heat flow rates as well as pressure loss and heat loss in piping segments. Figure 16 shows the configuration of this model. Solid lines denote piping segments for water supply and return flows, and broken lines denote piping segments for water bypass flows. Outside loop is designated as the supply loop, and inside loop is designated as the return loop. The inner box R means heat source unit and the outer box AC means air conditioning system. Red numbers identify piping segments, and blue numbers identify piping junctions.

5. Measured energy consumption in summer cooling operation before and after introduction of the TGS

We selected the same exhibition fair held in the summer of 2014 and 2015 for comparison. The city gas and electricity usage data were compared for the same dates for the exhibition fairs in 2014 and 2015, before and after introduction of the TGS. The cooling loads in 2014 and 2015 were estimated to be similar, but not identical.

As shown in Table 4, electricity consumption decreased by 7% and gas consumption decreased by 56% in 2015.

Total CO₂ emissions decreased by approximately 42%. The reasons for this decrease are that the highly efficient R4 supplied 80% of the total heat and the number of ARs decreased. The power consumption of the cooling tower pump for the ARs decreased drastically after introduction of the TGS.

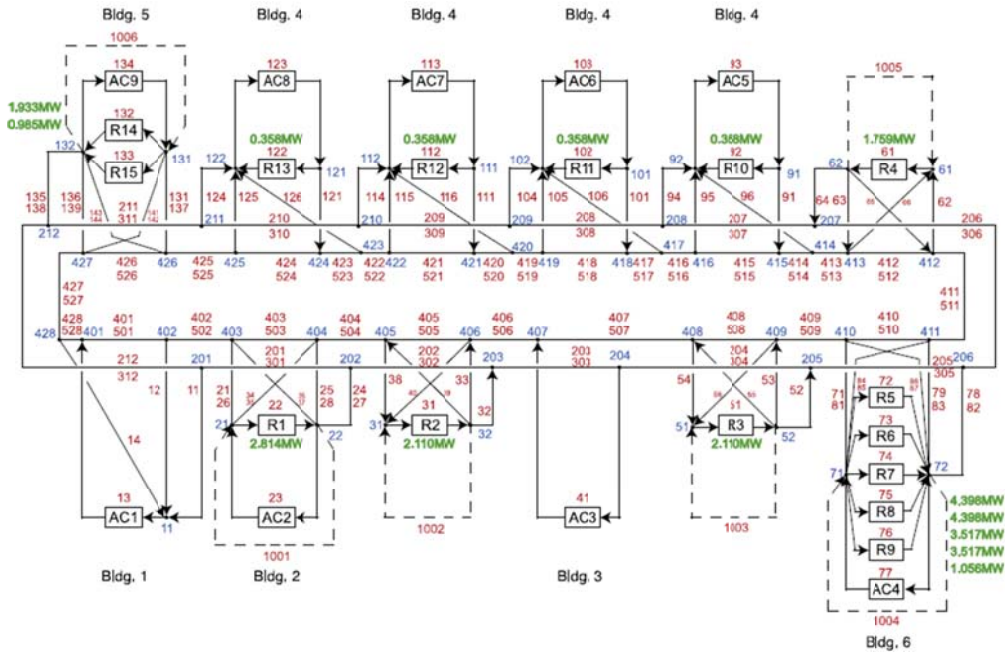


Fig. 16. Configuration of the heat supply system with a piping network [3]

Table 4 Effects of the TGS (energy consumptions of 2014 and 2015)

	Electricity			Gas			CO ₂ Emissions		
	2014	2015	Reduction rate	2014	2015	Reduction rate	2014	2015	Reduction rate
	kWh	kWh	%	m ³	m ³	%	t-CO ₂	t-CO ₂	%
July	61,331	43,597	-28.9	28,167	8,962	-68.2	90.5	39.0	-56.9
August	64,803	70,830	9.3	32,673	17,271	-47.1	102.2	69.5	-32.0
September	52,590	51,732	-1.6	22,748	10,338	-54.6	74.3	45.6	-38.7
Total	178,723	166,159	-7	83,587	36,571	-56.3	267	154	-42.3

CO₂ emission factor Electricity: 0.000423 t-CO₂/kWh, Gas:0.002291 t-CO₂/Nm³

The energy consumption value actually measured in the summer of 2015 after applying the thermal grid was compared with the measured value at the same exhibition event in the summer of 2014 before applying the thermal grid (Table 5). Since the climatic conditions such as the outside air temperature are different, the cooling load is not equal in the compared years. However, reliability of the comparison is high, as electricity and gas consumption of each building is measured. The CO₂ emissions on 25th July in 2015 decreased by approximately 63.5%. The example of the optimal calculation result for the day in 2015 is shown in Figs.17 and 18. Figure 17 shows the heat source facilities and buildings in use. Figure 18 shows chilled water flow and temperature level by optimal operation of the TGS.

Table 5 Energy consumption and CO₂ emissions of the same event compared before and after introduction of the TGS

Year	Date	Temperature Outside/Indoor	Bldg.	Consumption		CO ₂ emissions (t-CO ₂)			
				Gas (Nm ³)	Electricity (kWh)	Gas	Electricity	Total	Difference
2014	26 th July	33.3/—°C	6	4146	6691	9.5	2.83	12.33	-7.83
2015	25 th July	29.9/26.8°C	4	677	1,385	3.26	1.24	4.5	(-63.5%)
			5	748	1,530				

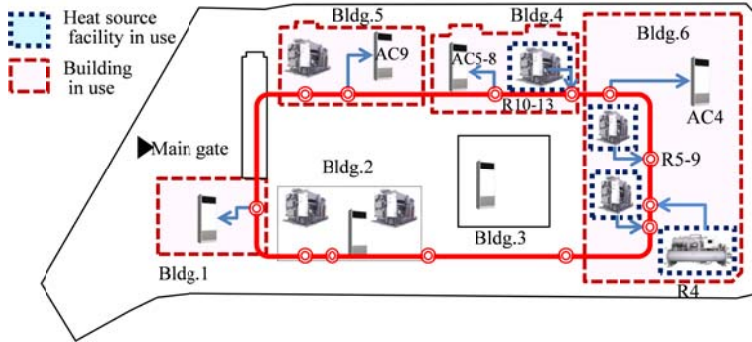


Fig. 17. Optimal operation state of heat source units after applying the TGS for event J on 25th July, 2015

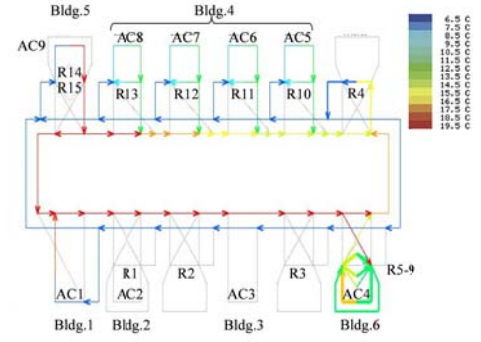


Fig. 18. Heat supply flow by optimal operation of the TGS

6. Energy consumption of actual TGS operation and estimated individual operations under the same demands

We assumed that the demand for individual operation was equal to the demand during TGS operation. The actual consumption during TGS operation was compared with the estimated value for individual operation of several heat source models (Table.6). The models for individual operation do not include the high-efficiency heat source unit (R4).

Table 6 Comparison on CO₂ emissions of Actual TGS and models without TGS

Individual operation model	Electricity consumption of Pumps, fans and auxiliary unit	Electricity consumption of air-cooled heatpump units	Gas consumption of absorption heating and chilling unit	CO ₂ emissions t-CO ₂ /Cooling period	Reduction rate based on model A
Model A (EXIST)	Rated value 38	Constant COP=3.2(rated value) 5	Actual COP of existing units with partial load rate 129	172	0.00
Model B (EXIST+IUC)	Same as above 38	Same as above 5	Actual constant COP of existing units with ideal multi unit control 91	134	0.22
Model C (HAR)	Same as above 38	Same as above 5	High COP1.4 of absorption heating and chilling units with partial load rate 68	111	0.35
Model D (HAR+IUC)	Same as above 38	Same as above 5	High constant COP 1.4 of absorption heating and chilling units with ideal multi unit control 60	103	0.40
Model E (HTB)	Same as above 38	All heat source units are replaced with high efficiency turbo units 36		74	0.57
Model F (HTB+IUC)	Same as above 38	All heat source units are replaced with high efficiency turbo units and ideally controlled at constant COP(6.19) 14		52	0.70
Model G (HTB+IUC)	Actual measured value of the TGS 18	All heat source units are replaced with high efficiency turbo units and ideally operated at constant COP(6.19) 14		32	0.81
Actual measured value of TGS	Actual measured value 18	Actual measured value 22	Actual measured value 12	53	0.69

EXIST: existing heat source units, IUC: ideal multi-unit control, HAR: AR with the high COP 1.4, HTB: high efficiency turbo

Models A and B use approximate expressions of the measured COP value for existing heat source units (Fig. 19). Models C and D use the highest value 1.4 of COP for ARs. Models E and F use a high-efficiency heat source unit (TR) with a COP rated at 6.19. The COPs of Models A, C, and E varied with partial load. The COPs of Models B, D, and F are assumed to be constant and equal to the ideal value for multi-unit control (Fig. 20).

The electricity consumption of pumps, fans, and auxiliary units of ARs were assumed to be the same as rated value, even when the cooling load was small. Their electricity consumption in Model G is set to be the same as that under the TGS operation.

In these models, we calculated the CO₂ emissions based on the gas and electricity consumption. Figure 21 shows the estimated value for Model A from July 15th to September 27th, excluding the date of building unused day, date of data loss and manual operation day. Since Model A consists of individually operated heat source units (AR) that

have deteriorated over time, the model emits more CO₂ than TGS operation, which includes a high-efficiency heat source unit with 5% of the total capacity. Figure 22 shows the actual CO₂ emissions during TGS operation.

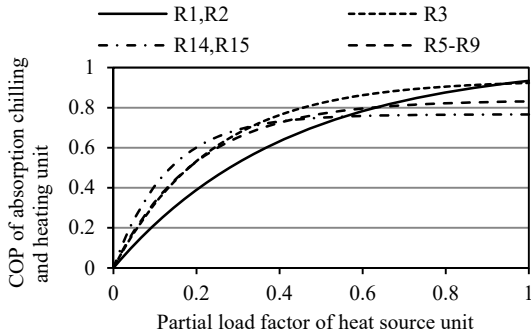


Fig. 19. Measured COPs of older existing ARs

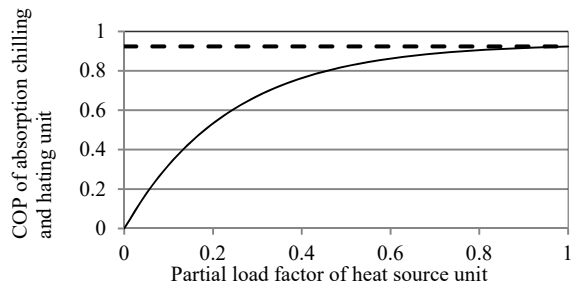


Fig. 20. Actual (solid line) and ideal multi-unit control(dashed line) COPs

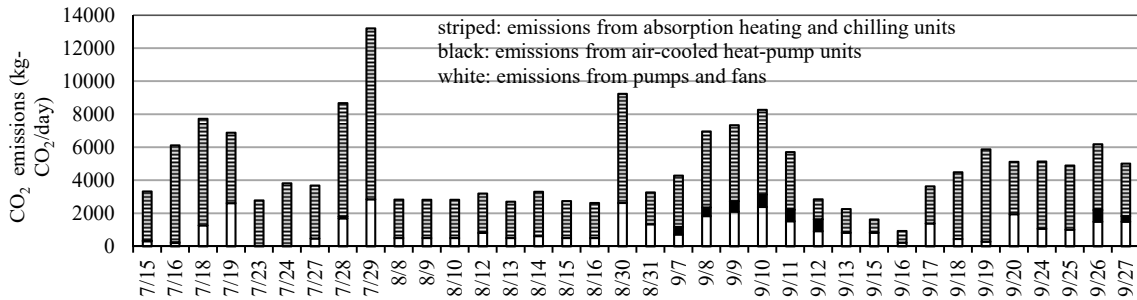


Fig. 21. CO₂ emissions for Model A

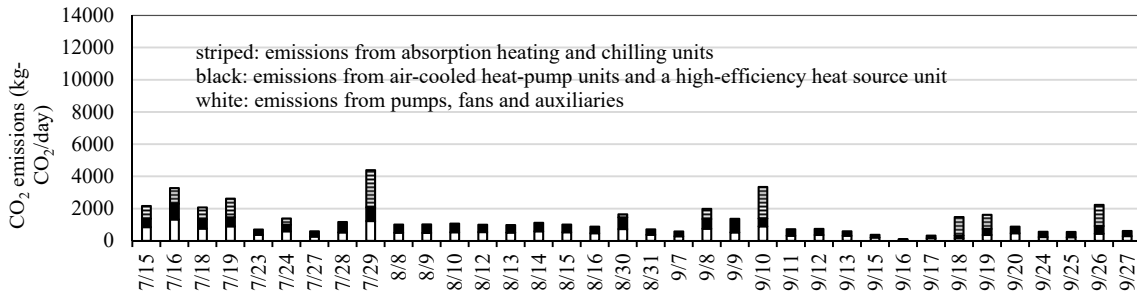


Fig. 22. Actual CO₂ emissions during TGS operation

The CO₂ emissions of all models are shown in Fig. 23, which clarified the following.

- (1) The CO₂ reduction effect of Model F was 70%, as compared to Model A.
- (2) The CO₂ reduction effect of Model B, which used the ideal number-of-units control operation, was 22%, as compared to Model A.
- (3) The heat source unit of Model D provides only 11% reduction in CO₂ emissions as compared to Model C. Introducing a thermal grid to a building group having a high-COP heat source unit will have only a small effect.
- (4) By replacing the heat source units of Model A with high-efficiency heat source units in Model E, CO₂ emissions were reduced by 57%. Furthermore, the CO₂ emissions under maximum-COP operation (Model F) were 54 t-CO₂, which was approximately the same as the actual amount of emissions of 53 t-CO₂.
- (5) The CO₂ emissions of Model F were approximately the same as the measured results for the TGS, but the composition of the CO₂ emissions of the heat source unit differs from that of the pumps and fans.
- (6) Since an inverter pump was installed in the TGS, the power consumption of pumps and fans was changed. The electricity consumption of pumps and fans for Model G was made the same as that for Model F. The CO₂ emissions of Model F were approximately 40% lower than the actual operating CO₂ emissions of the TGS. Electricity consumption of Pumps, fans and auxiliary unit of Model F are rated value. CO₂ emissions of Model

G is smaller than that of Model F, as Model G uses the actual measured value of the TGS which electricity consumption of Pumps, fans and auxiliary unit become small by applying inverter control.

The effect of CO₂ reduction by the TGS was apparent. The reductions in CO₂ emissions from Model A to Model B, from Model C to Model D, and from Model E to Model F are brought by the introduction of the ideal TGS. The CO₂ reduction from Model A to Model C and that from Model C to Model E are brought by the introduction of the high-efficiency heat source unit.

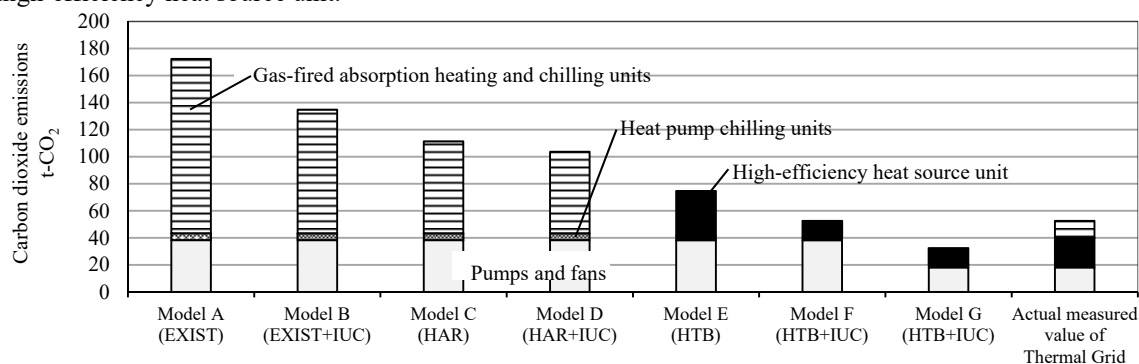


Fig. 23. CO₂ emissions of each model

7. Conclusions

The composition of the TGS and the functions of the routers included therein were shown. There are eight basic flow patterns, including a flow pattern from the return to the next supply, which is a cascade of a usable pattern.

The TGS and a high-efficiency heat source unit with a cooling capacity of 5% of the total heat source units were installed in a building group having old absorption-type chilling and heating units. After introduction of the TGS, CO₂ emissions in 2015 decreased by 42%, as compared to 2014 before introduction of the TGS.

We estimated the CO₂ emissions of various models with the same demand as that of TGS under actual operation. Compared to a model in individually operated old heat source units, the actual CO₂ emissions during operation of the TGS with a high-efficiency heat source unit having a cooling capacity of 5% was estimated to reduce CO₂ emissions by 69%.

Acknowledgements

The present study was conducted through the “Regional Energy Network Gathering Existing Energy Resources Through Rail Network” project and the “Demonstration project promoting green communities through waste heat utilization” as part of the Low Carbon Technology Research and Development Program of the Ministry of the Environment of Japan.

The authors would like to thank Mr. Nagahiro and Mr. Isozaki of SSCA and Dr. Onojima and Mr. Nakamura of Obayashi Corp. of the design and construction project team of the TGS for their helpful comments and fruitful discussions.

References

- [1] Hai Wang, Hua Meng, Weiding Long, “A District Energy Planning Method with Mutual Interconnection and Interchange of Thermal Grids”, *Procedia Engineering* 205 (2017) 1412–1419
- [2] Henrik Lund, Sven Werner, Robin Wiltshire, Svend Svendsen, Jan Eric Thorsen, Frede Hvelplund, Brian Vad Mathiesen, “4th Generation District Heating (4GDH) Integrating smart thermal grids into future sustainable energy systems”, *Energy* 68 (2014) 1–11
- [3] Ryohei Yokoyama, Hiroyuki Kitano, Tetsuya Wakui, “Optimal operation of heat supply systems with piping network”, *Energy* 137 (2017) 888–897
- [4] Getnet Tadesse Ayele, Pierrick Haurant, Bjorn Laumert, Bruno Lacarriere, “An extended energy hub approach for load flow analysis of highly coupled district energy networks: Illustration with electricity and heating”, *Applied Energy* 212(2018) 850–867
- [5] Felix Bünning, Michael Wetter, Marcus Fuchs, Dirk Müller, “Bidirectional low temperature district energy systems with agent-based control: Performance comparison and operation optimization”, *Applied Energy* 209 (2018) 502–515



16th International Symposium on District Heating and Cooling, DHC2018,
9–12 September 2018, Hamburg, Germany

High Resolution Heating Load Profiles for Simulation and Analysis of Small Scale Energy Systems

Anna Kallert*, Robert Egelkamp and Dietrich Schmidt

Fraunhofer Institute for Energy Economics and Energy System Technology, Königstor 59, DE-34119 Kassel, Germany

Abstract

In the analysis of energy systems such as local low temperature district heating (LTDH) systems, not only the properties of the supply system but also the characteristics of the buildings and the behavior of its inhabitants, have an influence on the overall energy demand. In particular in the case of decreasing supply temperatures, it is becoming increasingly important to consider the different energy demands in residential buildings, which differ in terms of their quantity and occurrence over time.

In this context detailed energy demand profiles for different demands in buildings can be used for the analysis of demand and supply. Hence, as part of this paper an approach for the creation of stochastic user profiles is presented using a VBA tool, which provides the main basis for the generation of heating load profiles (HLP). The tool generates randomized profiles of electricity and DHW demand as well as body heat profiles depending on the number and behavior of the inhabitants. Using a simulation software the profiles are then used to create HLP for different building energy classes. The outcome of this work is a generally applicable approach for the generation of scale able HLP, which can be used for e.g. the analysis or design of complex energy systems such as LTDH supply schemes.

To demonstrate the application of the developed method and the influences of random user profiles on the overall energy demand, examples of applications are shown. Furthermore, possible applications in future research projects are indicated.

© 2018 The Authors. Published by Elsevier Ltd.

This is an open access article under the CC BY-NC-ND license (<https://creativecommons.org/licenses/by-nc-nd/4.0/>)

Selection and peer-review under responsibility of the scientific committee of the 16th International Symposium on District Heating and Cooling, DHC2018.

Keywords: Randomized user profiles; Demand side modelling; Low temperature district heating supply; Assessment and planning issues

* Corresponding author. Tel.: +49 561 804-1876

E-mail address: anna.kallert@iee.fraunhofer.de

1. Introduction

When analyzing small-scale energy systems such as low temperature district heating (LTDH) systems, not only the properties of the supply system but also the characteristics of the buildings and its inhabitants have a major impact on the overall thermal energy demand. This is especially true when the supply temperature in the heating network decreases due to the increased use of low temperature sources like renewable energies [1] and thus the influence of the demand e.g. space heating (SH) or domestic hot water (DHW) increases. Due to this interrelationship, the effects of simultaneity are becoming more and more important, in particular with innovative low-temperature supply solutions, and should always be taken into account when e.g. dimensioning the energy supply system.

In principle, three relevant types of energy demand occur in residential buildings: electricity, DHW as well as SH demand. Usually there are interactions of the individual demands. In addition, between two households, these demands may differ considerably in terms of their amount and temporal occurrence [2]. In particular in an early stage of planning, when e.g. measured data is not available, energy demand profiles for domestic housing offer great potentials for the analysis of demand conditions [3–5]. In this context, the application of high resolution heating load profiles taking randomized user behavior into account offers prospects for accurate analysis of small-scale energy systems. For detailed holistic energy analysis of energy systems the following aspects are of major importance:

- When are how many residents at home?
- When are how many of those residents active, meaning not asleep?
- When is which electricity demand caused by appliances?
- When is which thermal energy needed?
- When is how much DHW used?

For the analysis of complex energy systems all aspects need to be considered simultaneously since they are influencing each other and have a significant influence on the overall thermal energy demand [6].

In the course of the evaluation and simulation of energy systems in particular building supply, the application of different kinds of profiles is common. Frequently demand profiles are mainly taken from standardization (e.g. VDI 4655 [7]) for the analysis of building supply. Furthermore, measured load profiles or synthetic profiles generated by building simulation are used [1, 5]. Representing individual cases an aggregation of those profiles to larger units could lead to wrong outcomes compared to energy statistics. Standardized load profiles in turn represent statistical data but they are often only valid for energy systems larger than 800 households [8].

Richardson et al. [2, 9] introduced models combining occupancy, light usage and appliances electricity demand. Similar approaches can be found in [5, 10] and [11, 12]. A detailed review of modeling of end-use energy is e.g. found in [6].

The outcome of the literature research demonstrated that most of the profiles respectively models mainly cover electricity demand, any other single energy demand or do not consider occupancy. Moreover, the research showed that the stochastic end-energy modeling is an appropriate method to meet the described requirements mentioned before.

Hence, the work presented in this paper is targeted on the creation of stochastic user profiles, which provide the main basis for the generation of heating load profiles (HLP) for different building energy classes. The outcome of this work is a generally valid approach for the generation of scalable HLP. The profiles can e.g. be used for the analysis or design of complex energy systems such as LTDH supply schemes. To demonstrate the application of the developed method and the influences of random user profiles on the overall end-energy demand, examples of applications are shown.

2. Generation of high resolution heat load profiles for accurate analysis of small scale energy systems

As part of this section the process of creating the HLP is described, which can e.g. be used for the demand-side modelling or the analysis of local low temperature district heating systems as part of simulation studies. Basically the generation of the HLP takes place in two steps (see Fig. 1). In the first step, randomized demand profiles of high resolution are generated using the tool “Profile Maker”. The tool creates electricity and DHW demand profiles as well

as body heat profiles depending on the number and behavior of the inhabitants (occupancy) automatically (section 2.1). For the creation of the HLP (SH and DHW preparation), the generated profiles are implemented in a building simulation model in a second step (section 2.2). To generate heating load profiles for different building energy standards, the simulation model comprises a building typology and user classes.

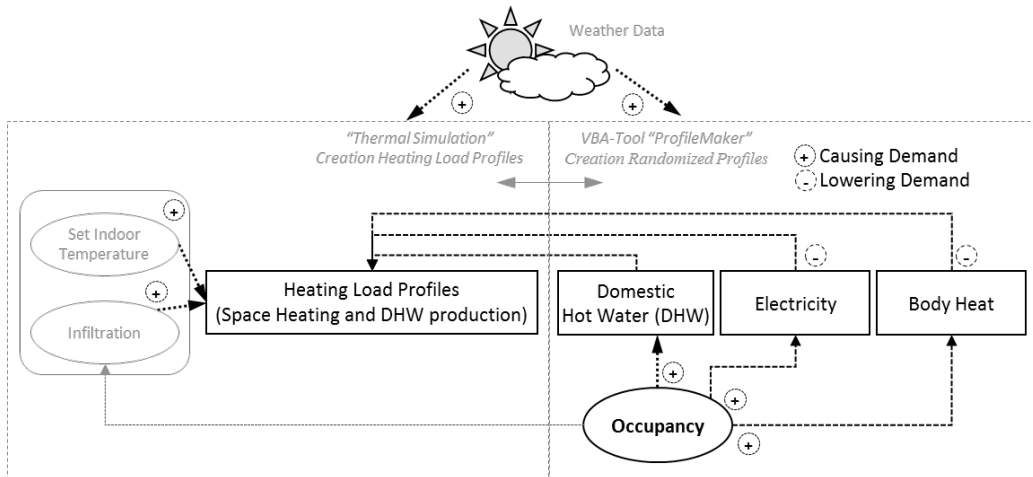


Fig. 1. Principle of the method for the creating of heating load profiles and representation of the interaction of the different demand user profiles causing or lowering the energy demand of the buildings.

When creating the profiles, the influencing factors for causing respectively reducing demand and the interactions between these factors are considered. For the creation of the profiles, climate data from [13], infiltration and set-point indoor temperatures are used.

2.1. The “ProfileMaker” – a VBA tool for the generation of randomized user profiles

For the detailed demand-side modeling taking randomized user behavior into account, the tool “ProfileMaker” was created. The tool generates profiles for electricity and DHW demand as well as for the emitted body heat to the room air. When generating the randomized profiles, the presence and activity of “inhabitants of a housing unit” (e.g. dwelling) are taken into account. The resolution of the profiles is on an hourly basis. Furthermore a distinction is made between “working day” and “weekend”. The tool is programmed using the script language “Visual Basic for Applications” (VBA). The user profiles can be applied as an input for a simulation environment (e.g. TRNSYS [15]) and in this way be used for thermal building simulation. Furthermore, the VBA-tool offers the possibility to evaluate heating load profiles and to determine the simultaneity factor. This function is used in the calculation example presented in section 3.

When creating the user profiles the probabilistic approach of the Markov Chain technique is applied. Simplified, the technique can be described as a mathematical process that predicts the next state of a system via probability functions (for a comprehensive explanation of the technology, please refer to literature e.g. [14]). This property can be used to predict, for example, whether DHW tapping will take place or a resident is not home. In order to achieve realistic results, it is important to define a realistic value for the possible states (e.g. DHW tap volume from standardization). As the characteristics of the demand profiles often differ statistically, a calibration of the probability functions is carried out to avoid logical errors and to link the profiles [15].

The main working principle of the VBA-tool is shown in the flowchart presented in Fig. 2. Accordingly, a new stochastic profile for one day is created each time the tool respectively the script is run. In this way, profiles can be generated for only one day or for an entire year. For example, to address an entire year, 365 profiles are aggregated.

Before this process starts, the number of occupants representing between 1 and 5 inhabitants is determined by the user of the tool. Furthermore, the starting month and the number of days are selected. If no starting month is selected

the process starts in January and runs over the year until the given day or the end of the year is reached. After all required parameters are defined, a loop over the days starts.

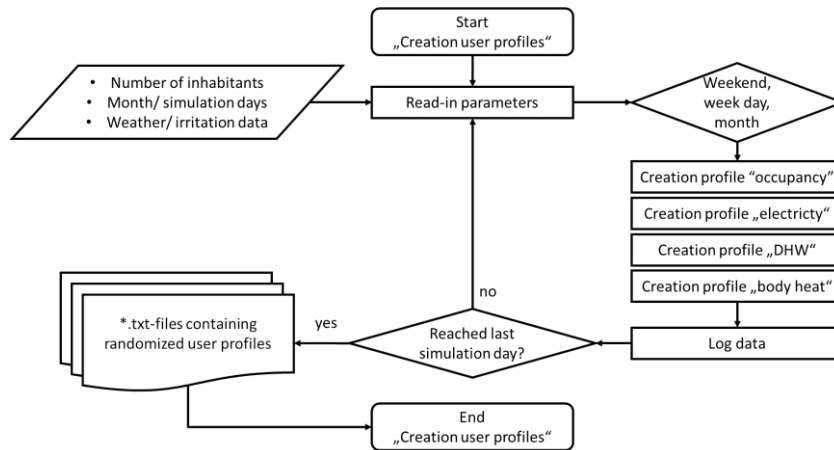


Fig. 2. Main working principle (flow chart) of the “ProfileMaker” for the generation of the randomized user profiles.

In the first step of the loop, it is determined whether it is a weekday or weekend. Based on this information, a randomized occupancy profile of hourly resolution is created. For the representation of the occupancy, approaches from [16] are used. As part of the profiles it is distinguished if the inhabitants are “at home” or “not at home”. In addition, it is distinguished whether the residents are “inactive” (sleeping) or “active” (e.g. doing housework or reading). Since the approaches from the original model are validated for the UK, the model has been modified so that it can also be applied to Germany [15].

In the next step, the profiles for electricity demand, DHW demand and body heat are created depending on the number of active residents calculated before. To avoid logical errors in the process of profile generation (e.g. DHW water is tapped when no inhabitant is at home), calibration functions were used to link the profiles to the function of the other profiles within the VBA-script [15].

When generating randomized electrical demand profiles for residential buildings, it is generally distinguished in two categories of electrical devices: devices that run independently of the inhabitants’ influence (e.g. refrigerator) and devices that are actively switched on and off by the inhabitants (e.g. television). The principle of switching the devices on and off was derived from the approaches found in Richardson et al. [2, 9] and implemented in the VBA tool. To create stochastic DHW tapping profiles in addition to the electricity demand a probability function for the tapping of water was added to the VBA tool. The basic principle was derived from the method for the generation of electricity profiles. The DHW demand profiles are divided into four possible types of tapping (loads). The four DHW loads representing draw-off events for showering, bathing as well as small and medium DHW tapping (e.g. for hand washing and body hygiene) are defined and implemented in the model (see Table 1). Since the daily DHW demand per person must be known in order to create the profiles for varying number of residents, different tap volumes in accordance with values that can be found in literature (e.g. German standardization [16] or [18]) were added.

Table 1. DHW demand data in accordance with [16,18].

		Shower	Bath	Tap S	Tap M
Frequency	[n/day]	0.5	0.03	7	3
Duration	[min]	5	10	1	1
Draw-off volume	[l/min]	8	14	1	6
Daily draw-off volume	[l/day]	20	5	7	18

Next to the tapping profiles, the creation of randomized profiles reflecting the emitted body heat to the room air is implemented in the VBA-tool. When creating the profiles, the degree of activity of the "occupants" is taken into account in order to determine the emitted body heat to the room. To indicate values for specific body heat emitted by a person values from the literature are used [17, 18].

At the end of a loop in the simulation the data calculated by the different probability functions are logged to an EXCEL-file. If the last day of the simulation, which was specified at the beginning of the process, is reached, the simulation ends and the generated user profile is written in a *.txt file. As a result of the approach presented here, the VBA-tool "ProfileMaker" creates holistic as well as stochastic user profiles based on statistical data.

Using the VBA- tool, an example profile set is created for a random day on February 2nd (Fig. 3).

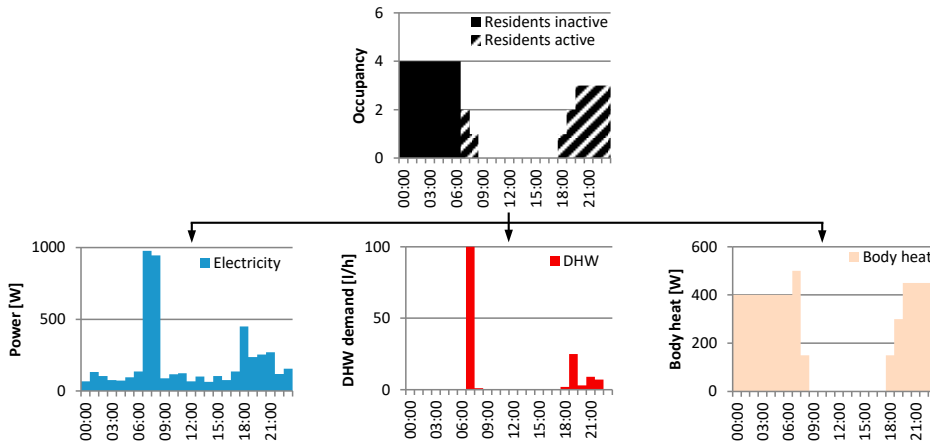


Fig. 3. Examples for electricity, space heating (SH) and domestic hot water (DHW) demand for random day February 2nd [6].

The figure illustrates how the presence and activity of occupants, as a function of time of day, influences the generated user profiles and how they influence each other. Due to the absence of all residents between 09:00 and 18:00, no tapping processes are occurring and no internal gains are caused by body heat during that period. Since some appliances run on continuous operation, the electricity profile has a base load, which is independent of the occupancy profile. With increased activity of the residents, in particular the electricity and the DHW profile react with a significant increase in demand. Such DHW peak loads are typically found in the morning and in the evening.

2.2. Generation of heating load profiles for space heating and domestic hot water

To demonstrate the application of stochastic user profiles in thermal simulation programs in general and for the generation of the heating load profiles (SH and DHW) a model of a building group is used, which was created with TRNSYS [19, 20]. When generating the heating load profiles the simulation program is only used to determine the room set-point temperature and to model the characteristics of the building envelope. In this way, the properties of the opaque and transparent components of the envelope as well as the corresponding thermal losses and gains are taken into account.

Like most the thermal simulation programs, TRNSYS also offers the possibility of using user-specific parameters. The definition and input of the parameters is usually detailed and therefore time-consuming. DHW or electricity profiles are read in as lists, interaction with the user or the interaction of the profiles are not taken into account sufficiently. But it is precisely this relationship that is becoming increasingly relevant against the background of decreasing supply temperatures and when effects of simultaneity are taken into account [5, 15].

To calculate heating load profiles for new buildings as well as for existing buildings, a typology of residential buildings was developed and used to parameterize the buildings in the simulation model. The data of the typology are derived from [21] and [20]. As part of this typology, four building age classes are used to reflect the standards of new buildings (built in 2016) as well as buildings representing the German building stock (see Table 2).

Table 2. Properties of the individual buildings (building age classes) used for the determination of thermal behavior [15, 21].

	Unit	Built before 1978 (-1978)	Built after 1978 (1978+)	Built after 1995 (1995+)	New buildings (new)	
Heated living space	m ²	149.48	153.82	151.67	153.52	
Base of the building	m ²	97.13	80.8	92.34	96	
Number of floors	-	1.72	1.6	1.61	2	
Clear room height	m	2.5	2.5	2.5	2.5	
Total roof surface	m ²	121.07	115.14	118.32	113.2	
Total window surface	m ²	29.27	28.59	36.43	53.25	
Door area	m ²	2	2	2	2	
U-value (respectively k-value)	Base slab	W/(m ² K)	1.18	0.58	0.33	0.245
	Exterior wall	W/(m ² K)	1.08	0.46	0.28	0.196
	Window	W/(m ² K)	2.35	2.62	1.51	1.1
	Door	W/(m ² K)	3	3	2	1.4
	Roof	W/(m ² K)	0.73	0.41	0.28	0.14

In addition to different building energy standards (building age classes), three different user types (user classes) are implemented in the simulation model: "average", "saver" and "waster" (see Table 3). The basic properties of these user classes are derived from [22]. The main difference between the user types is the set room temperature. "Average" and "saver" are also equipped with night setback, which means that the room temperature is lowered by 3 °C for seven hours during the night [15]. Furthermore, the user profiles are assigned to the user types according to the number of residents.

Table 3. Definition of user classes in accordance with [15, 22].

	Unit	User type "average"	User type "saver"	User type "waster"
Number of residents	[n]	3-4	1-2	5
Room temperature	[° C]	21	19	22
Night setback	[-]	Yes	Yes	No

Since the infiltration has a decisive influence on the thermal energy demand of the buildings, different air exchange rates are regarded taking into account the type of the user (user class) and the building energy standards (building age class). To determine the air exchange rates values from [23] were used and interpolated (see Table 4) [15].

Table 4. Air exchange rates of the different building age classes in dependency of the amount of the heating demand (interpolated according to [23]) [15].

Building age class	Unit	User type "average"	User type "saver"	User type "waster"
(-1978)	1/h	1.0	0.7	1.5
(1978+)	1/h	0.9	0.6	1.3
(1995+)	1/h	0.7	0.4	1.1
(new)	1/h	0.6	0.3	1.0

To visualize the application, the user profiles generated by the "ProfileMaker" have been implemented in a TRNSYS model [20] which includes buildings of different building ages. Due to this implementation, the presence and activity as well as the electricity profiles lead to internal gains in the buildings causing an impact on the SH

demand. The tapped volume of DHW specified by the user profile is converted into a heating load in the simulation model.

Using the simulation software, HLP for each combination of building type and number of residents were determined. Examples of these profiles, separated into heating load for DHW preparation and for SH, are shown in Fig. 4 and Fig. 5. It should be noted that these figures are intended to lead to a better understanding of the created HLP and are not results of an analytic comparison of different profiles.

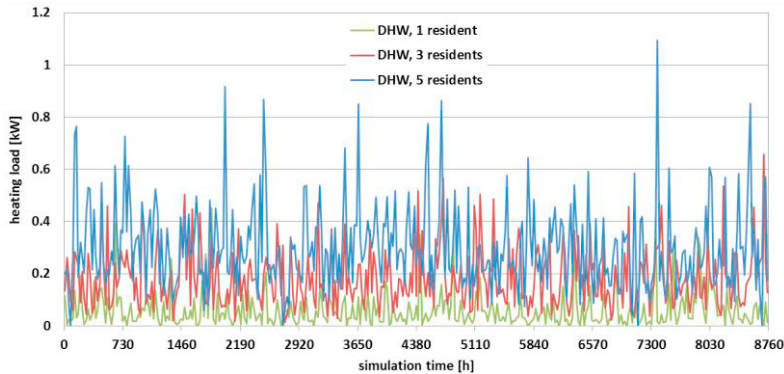


Fig. 4. Heating load for DHW preparation over simulation time for different user profiles.

As shown in Fig. 4 the user profiles reflecting the number of residents have a major impact on the heating load for DHW preparation. Further calculations showed that the heating load of DHW scales almost linearly with the number of inhabitants.

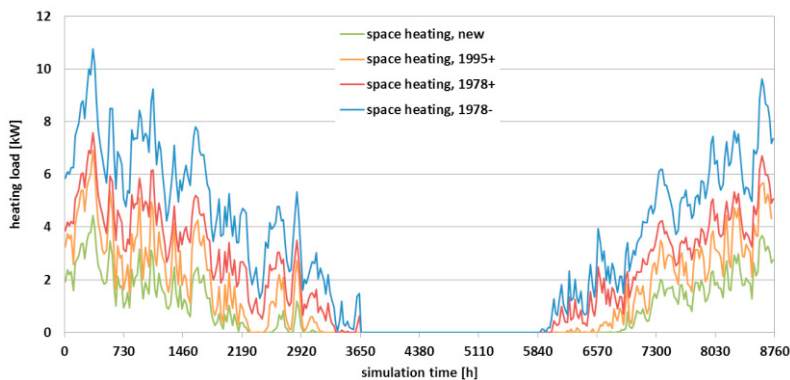


Fig. 5. Heating load for space heating (SH) over simulation time for different building ages.

In contrast, the heating load caused by SH demand depends largely on the building age class and correspondingly on the insulation standard of the building. In addition, the seasonal effect of the weather data [13] has a significant influence on the heating load of SH. Furthermore, the share of DHW demand in total demand increases with the insulation standard of a building so that the DHW demand is more important in newer buildings.

To check the plausibility of the simulation results, they were compared with the literature values from [21]. The result shows a good concordance with the values from the literature.

The method of HLP generation presented here is characterized by realistic but also varying load profiles taking the user behavior but also the properties of the buildings (building age class) into account. Because of these characteristics, the approach developed here can be applied to a variety of other applications in thermal network evaluation and simulation. A main advantage of the developed method is the stochastic approach and the consideration of simultaneity effects, which allow the accumulation of the HLP to a supply area of any size. In contrast, when static profiles are

summed up for the thermal simulation of larger supply systems, unrealistically high heating load peaks occur. In addition, it is conceivable to use the heating load profiles for heating load prediction to test control or supply strategies (e.g. feed-in of fluctuating, renewable energies).

3. Application example - Analysis of a small energy system using randomized user profiles

Besides the creation of stochastic user profiles, the "ProfileMaker" offers the possibility to evaluate the heating load profiles generated by the simulation. This is done automatically since TRNSYS can write the generated HLP values directly into the VBA tool.

This function is used to demonstrate the performance of the approach presented in this paper to calculate the heating demand for SH and DHW preparation for an exemplary supply system (building group) by using the "ProfileMaker" and the simulation model. As part of this example, load profiles for ten buildings (in this exemplary case build before 1978 with an area A_N of 119.6 m²) representing a supply area are generated for a random day on February 2nd.

Table 5. Example inputs for demand profile generation using the ProfileMaker and TRNSYS [20].

Assumption for the calculation of heat demand		User type "saver"	User type "average"	User type "waster"
Number of profiles	[-]	3	5	2
Inhabitants	[-]	2	4	5
Temperature	[°C]	19	21	22
Heat exchange rate	[1/h]	0.7	1	1.5
Night setback	[-]	yes	yes	no

The corresponding building properties used for this calculation are found in Table 2. Furthermore, the different user classes "saver", "average" and "waster" are assigned to the buildings (see also Table 3 and Table 4). Based on these information the tool calculates the installed heating power of the examined supply area (here ten buildings), the maximum required heating capacity and the simultaneity. The heating load for SH and DHW is shown in Fig. 6.

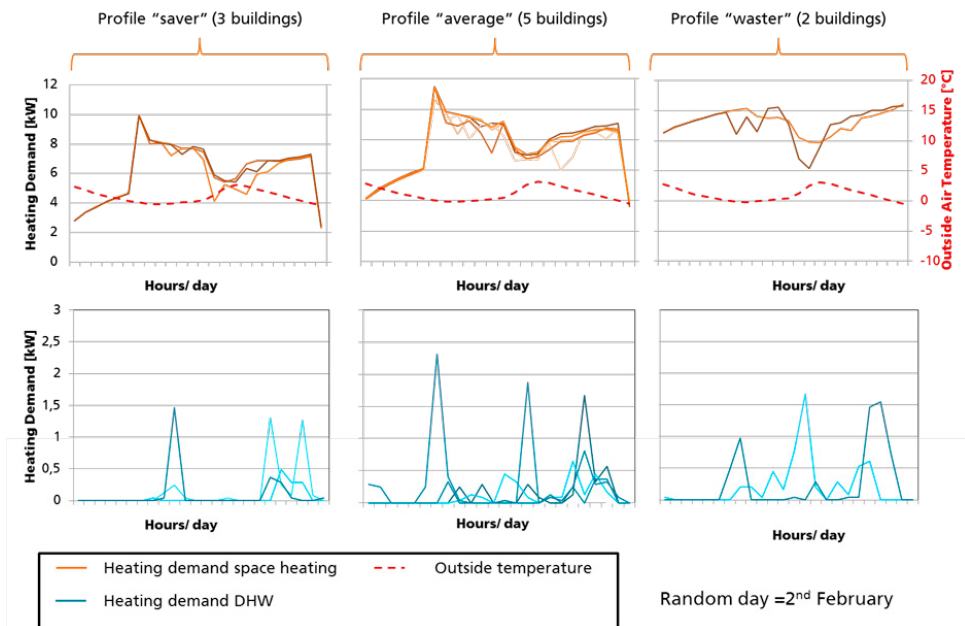


Fig. 6. Exemplary heating demand profiles (SH and DHW) for the random day February 2nd.

The orange lines represent the demand for SH. It appears that the heating demand varies depending on the type of selected randomized user profile. In particular, the influence of night set-back reduction in the profiles "saver" and "average. Furthermore, the influence of the outdoor temperature, represented by the red dashed lines, on the energy requirement is noticeable. The blue lines represent the variation of the DHW demand. Over the course of the day the peaks of the tapping is varying. In this way, different tapping events caused by different uses (e.g. showering or cooking) are illustrated.

Based on the calculated installed heating power of 146.8 kW and the maximum heating power of 141.5 kW for the building group, the tool determines a simultaneity factor of 0.9. In principle, this calculation can be used to select and to dimension a suitable supply solution taking into account the user behavior and the building characteristics. This is an advantage especially at low supply temperatures.

It should be noted that only one day was selected for the example to illustrate the effects (mutual influence of demands). For example, if a year-round evaluation is targeted, the profiles are aggregated.

The result of this calculation demonstrate that the developed approach for the generation of load profiles taking randomized user behavior into account can be used for e.g. the dimensioning of a small local heating network. In particular in an early stage of planning or if measured data are not available, prediction of user behavior using randomized user profiles offers opportunities for the analysis or design of energy systems.

4. Conclusions and outlook

For the analysis and dynamic simulation of small scale energy system such as local district heating networks high resolution energy demand profiles offer great potentials, in particular when the supply temperature in the heating network decreases.

Hence, a VBA-tool for the generation of user profiles considering random user behavior has been developed. The user profiles generated by the tool called "Profile Maker" comprise stochastic profiles for the occupancy of buildings by active and inactive residents as well as profiles for the use of electrical appliances and DHW. The user profiles were used to generate heating load profiles (space heating and DHW) which represent the heating load of a building over one year at a temporal resolution of one hour. These heating load profiles, which differ according to user types and building age classes, allow a diverse mapping of the thermal demand of buildings, taking into account the effect of simultaneity. Due to the stochastic and holistic approach of the profile generation, the heating load profiles can be summed up to realistic and arbitrarily large demand profiles representing e.g. the demand of a district heating supply system. This is an advantage, as extrapolating static profiles for larger residential areas can lead to unrealistically high peak loads. In this way the generated profiles can be used for a detailed heating load prediction in order to develop, test or evaluate supply strategies.

The approach presented here can be applied for design and optimization of innovative system solutions based on LTDH supply in future research. Moreover the method is adaptable for application in projects dealing with aspects of sector coupling, demand-side management or hybrid energy networks.

Acknowledgements

The authors warmly thank the German Federal Ministry for Economic Affairs and Energy (BMWi) for the received financial support. Furthermore, the authors wish to thank Mr. Thies Blaese as well as the members of the international cooperation project of the "IEA DHC Annex TS1 – Low Temperature District Heating" for the valuable input.

References

- [1] D. Schmidt and A. Kallert, "Future low temperature district heating design guidebook: Final Report of IEA DHC Annex TS1 - Low Temperature District Heating for Future Energy Systems," Frankfurt am Main, Germany, 2017.
- [2] I. Richardson, M. Thomson, and D. Infield, "A high-resolution domestic building occupancy model for energy demand simulations," *Energy and Buildings*, vol. 40, no. 8, pp. 1560–1566, 2008.
- [3] J. Widén *et al.*, "Constructing load profiles for household electricity and hot water from time-use data—

- Modelling approach and validation,” *Energy and Buildings*, vol. 41, no. 7, pp. 753–768, 2009.
- [4] E. Ampatzis and I. Knight, “Modelling the effect of realistic domestic energy demand profiles and internal gains on the predicted performance of solar thermal systems,” *Energy and Buildings*, vol. 55, pp. 285–298, 2012.
- [5] D. Fischer *et al.*, “Stochastic Modelling and Simulation of Energy Flows for Residential Areas,” VDE-Kongress 2014 - Smart Cities – Intelligente Lösungen für das Leben in der Zukunft, Frankfurt am Main (Germany), 2014.
- [6] A. Kallert and T. Blaese, “Implementation of random user behavior in building simulation: Demand profile modeling for accurate analysis of small scale energy systems: Contribution to the IEA DHC Annex TS1 Subtask C report,” Fraunhofer IBP, Internal working document, 2016.
- [7] VDI 4655, “Referenzlastprofile von Ein- und Mehrfamilienhäusern für den Einsatz von KWK-Anlagen,” Verein Deutscher Ingenieure (VDI), Berlin (Germany), 2008.
- [8] J. von Appen, J. Haack, and M. Braun, “Erzeugung zeitlich hochaufgelöster Stromlastprofile für verschiedene Haushaltstypen,” *Power and Energy Student Summit (PESS)*, 2014.
- [9] I. Richardson, M. Thomson, D. Infield, and C. Clifford, “Domestic electricity use: A high-resolution energy demand model,” *Energy and Buildings*, vol. 42, no. 10, pp. 1878–1887, 2010.
- [10] J. Widén and E. Wäckelgård, “A high-resolution stochastic model of domestic activity patterns and electricity demand,” *Applied Energy*, vol. 87, no. 6, pp. 1880–1892, 2010.
- [11] J. Page, D. Robinson, N. Morel, and J.-L. Scartezzini, “A generalised stochastic model for the simulation of occupant presence,” *Energy and Buildings*, vol. 40, no. 2, pp. 83–98, 2008.
- [12] L. G. Swan and V. I. Ugursal, “Modeling of end-use energy consumption in the residential sector: A review of modeling techniques,” *Renewable and Sustainable Energy Reviews*, vol. 13, no. 8, pp. 1819–1835, 2009.
- [13] Meteotest, *Einstrahlungsdaten für jeden Ort des Planeten*. [Online] Available: <http://www.meteonorm.com/de/>.
- [14] K.-H. Waldmann and U. M. Stocker, *Stochastische Modelle: Eine anwendungsorientierte Einführung*, 2nd ed., 2014.
- [15] A. Kallert, “Modelling and simulation of low-temperature district heating systems for the development of an exergy-based assessment method,” Dissertation, Technische Universität München, Munich (Germany), to be published in 2018.
- [16] VDI 2067, “Wirtschaftlichkeit gebäudetechnischer Anlagen - Grundlagen und Kostenberechnung,” Verein Deutscher Ingenieure (VDI), 2012.
- [17] L. Garby, M. S. Kurzer, O. Lammert, and L. Nielsen, “Energy expenditure during sleep in men and women: evaporative and sensible heat losses,” *Human nutrition. Clinical nutrition*, pp. 25–233.
- [18] DIN EN ISO 7730, “Ergonomics of the thermal environment - Analytical determination and interpretation of thermal comfort using calculation of the PMV and PPD indices and local thermal comfort criteria,”
- [19] TRNSYS, “Volume 5 - Multizone Building modeling with Type56 and TRNBuild,” 2005.
- [20] TRNSYS17, *TRNSYS17*. [Online] Available: <http://sel.me.wisc.edu/trnsys/features/features.html>.
- [21] T. Loga, B. Stein, N. Diefenbach, and R. Born, “Deutsche Wohngebäudetypologie: Beispielhafte Maßnahmen Beispielhafte Maßnahmen zur Verbesserung der Energieeffizienz von typischen Wohngebäuden: 2nd ed. Darmstadt,” 2015.
- [22] T. Loga, M. Großklos, and J. Knissel, “Der Einfluss des Gebäudestandards und des Nutzerverhaltens auf die Heizkosten: Konsequenzen für die verbrauchsabhängige Abrechnung,” Institut Wohnen und Umwelt, Darmstadt, 2003.
- [23] DIN V 18599-2:2012-06, “Energy efficiency of buildings - Calculation of the net, final and primary energy demand for heating, cooling, ventilation, domestic hot water and lighting - Supplement 2: Description of the application of values from DIN V 18599 for the certification according to the act on the promotion of renewable energies in the heat sector (EEWärmeG),” DIN Deutsches Institut für Normung e.V.



16th International Symposium on District Heating and Cooling, DHC2018,
9–12 September 2018, Hamburg, Germany

A Study of District Heating Systems with Solar Thermal Based Prosumers

Danhong Wang^{a,b,*}, Kristina Orehounig^b, Jan Carmeliet^a

^aChair of Building Physics, Swiss Federal Institute of Technology, Zurich (ETHZ), 8001, Switzerland

^bUrban Energy Systems Laboratory, Empa, Dübendorf, 8600, Switzerland

Abstract

The integration of heat production from solar energy technologies can be realized by feeding in energy both at centralized or at multiple decentralized locations from the consumer side. As distribution networks serve as thermal transmission grids, the interaction between the energy feed in (i.e. production) and withdrawal (i.e. consumption) at multiple locations within distribution networks should be incorporated. Modelling the interactions between these subsystems is challenging. This paper aims to study the potential of district heating system with solar thermal based prosumers, by developing a modelling framework for design and simulation of such networks. Quantitative comparisons are made on the system performances, by addressing key technical configurations and constraints of thermal networks and temperature dynamics of energy sources.

In this paper, a comprehensive design and simulation model is built to assess the performance of different scenarios of district heating system designs with solar thermal based prosumers. Design variations are carried out by selection of different buildings in the district as prosumers. The simulation model framework is setup in Matlab, with hourly time step. The distribution network model is formulated as a thermal hydraulic model representing detailed information on thermal and hydraulic losses on each pipe. It enables bidirectional flow from multiple sources integrated into the district heating network. Energy conversion technologies (solar thermal collectors) and heat demand are connected with the network model as source and sink. A natural gas boiler acts as an additional base load heat source. The design and simulation framework is applied to an artificial case study, composed of 20 buildings with mixed building stocks including office and residential buildings.

© 2018 The Authors. Published by Elsevier Ltd.

This is an open access article under the CC BY-NC-ND license (<https://creativecommons.org/licenses/by-nc-nd/4.0/>)

Selection and peer-review under responsibility of the scientific committee of the 16th International Symposium on District Heating and Cooling, DHC2018.

Keywords: district heating system design; decentralised integration; bidirectional flow

1. Introduction

Buildings contribute a significant amount of energy consumptions in urban environments. In Switzerland, around 30% of the total energy consumption is used to cover space heating, domestic hot water demands, air-conditioning in buildings [1]. District heating networks are a promising solution, together with multi-energy systems and thermal networks for sufficiently provide energy for buildings at a district scale, as opposed to heating systems installed locally at individual building level. It also has the potential to employ low exergy heat sources, such as waste heat from industrial process or cooling load, geothermal heat, solar energy, to be integrated and utilized by individual buildings collectively in a more energy efficient and effective way.

In recent years, attention has arisen to the concept of “prosumer” in district heating networks, a concept which was originally invented for power grids. A prosumer in energy systems is defined as a unit/member which both consumes and produces energy in the form of electricity or heat [2]. The integration of renewable energy sources in districts is often difficult due to limited local available resources, geospatial limitation and topographical constraints. By including the idea of prosumers, it allows us to enlarge system design boundaries, to incorporate new system configurations with multiple energy sources from decentralized locations. Brange et al. conducted a comprehensive analysis of the technical and environmental performance by introducing prosumers to existing district heating systems [3], and Hassine et al. investigated on different supply scenarios for solar assisted district heating networks and the energy performance respectively [4]. For both cases, solar energy integration works as auxiliary heat sources to existing networks. However, little focus has been put on designing of a district heating network system with prosumers or decentralized sources, and system configurations, with necessary components and operation strategies are rarely discussed.

This paper aims to deepen the knowledge by applying a holistic approach for the design and ideal operation of a district heating system with multiple prosumers, which utilize energy from rooftop mounted solar thermal collectors. Key system configuration compared with conventional district heating systems are addressed. A novel design configuration with decentralized pumps at substation (prosumer) is implemented, which allows for bi-directional flow to withdraw from or feed-in to the network. To further assess the energy performance of different design scenarios, a simulation model is built based on a multi time step steady-state thermal hydraulic model. Potential operational strategies are additionally applied and discussed accordingly.

The design and simulation process is applied on an artificial case study comprising 20 buildings with mixed building usage including office and residential buildings. Performance indicators regarding the distribution networks and the system as a whole are identified, including network thermal losses and pumping power, system solar fraction for multiple design cases.

Nomenclature

A	Incidence Matrix
d_{ij}	Pipe inner diameter
f_D	Friction Factor
L_{ij}	Pipe length
T_{in}	Inlet temperature
T_{out}	Outlet temperature
T_{amb}	Ambient temperature
T_g	Ground Temperature
$\mathbf{m}s$	Matrix of mass flow rate for all source/sink
\mathbf{m}	Matrix of mass flow rate in the network
$\dot{m}_{i,j}$	Mass flow rate at pipe
Re	Reynolds number
ρ	Water density
ϵ	Pipe roughness

2. Methodology

2.1. System Configuration

District Heating System (DHS) are composed of 3 subsystems, 1) heat production, 2) distribution networks, and 3) multiple consumers. For traditional networks, heating production is normally placed at a centralized location. By switching from traditional network layouts to a prosumer based system, the distribution network is responsible for transmitting energy from multiple sources which are sparsely distributed at decentralized locations.

The network configuration of this study is shown in figure 1(a). A prosumer is a building unit with rooftop mounted solar thermal collectors. A natural gas boiler acts as an additional base load heat source at a centralized location. A long term storage tank is located at the centralized location to be charged when there is surplus energy feed into the network during low energy demand periods, which happens especially in summer time.

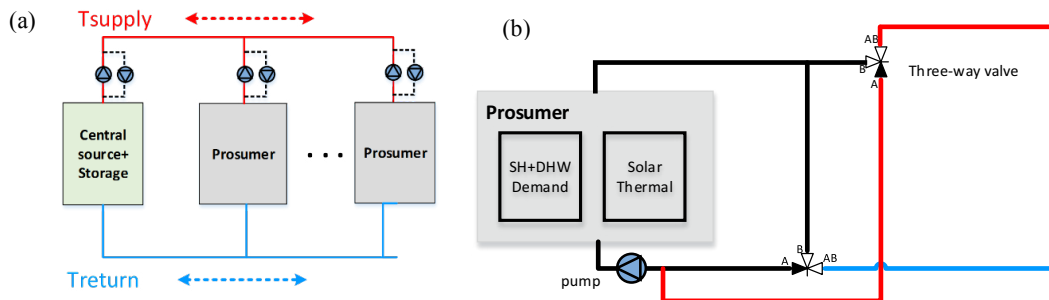


Fig. 1. (a) Schematics of network configuration; (b) Schematics of substation configuration with decentralized pump.

Pumps are located at both the centralized source side and at the prosumer side. Therefore, the flow direction in the distribution network might change due to different states of the prosumers (consume or produce). The operation strategy at the building side is to consume the solar energy from rooftop locally and feed-in the surplus energy (if there is any) to the network through a heat exchanger. Therefore, depending on the demand and solar profiles, by utilizing two three-way-valves (as shown in figure 1.b), the water flow direction can be controlled with one single pump. When the substation withdraws heat from the network, the flow is pumped from the hot pipeline (supply pipe) to the cold pipeline (return pipe) through a heat exchanger. When the substation feeds in heat to the network, water from the cold pipeline is pumped to the hot pipeline. Therefore, the pressure cone along the distribution pipeline would also change due to flow direction at each time step. The above mentioned design and operation of the substation configuration has been applied to some Swiss case studies and also implemented for test cases [5]. An agent based control model has been investigated for bidirectional flow district heating and cooling systems with multiple distributed heating and cooling sources in the system [6]. How to effectively control and operate such a substation with bi-directional pumping is still under substantial research effort for future large scale applications. Unfortunately, not so much scientific publications could be found other than research from industry at the moment.

2.2. Modelling framework

2.2.1 Network Model

To investigate the thermal and hydraulic behaviour of the pipe and network design with prosumers, a modelling framework is built in Matlab for pipe design and to simulate network performance with the prosumers conditions in terms of its thermal and hydraulic behavior.

A branch typology is selected as a network layout which is structured by graph theory in matrix format. A directed graph is used for network connections and the direction indicates the sign convention of each edge property. The end

node of the branch represent source or sink of the network, while nodes in between represents network connection as a diverter, or mixer when there are more than two connections. The modelling effort for this particular design case is challenging due to the change of flow direction in different time steps. At each new time step, the flow streams from multiple sources at distributed locations are tracked and a new graph matrix is updated to incorporate the flow directions.

During network simulation, major variables accounting for thermal and hydraulic properties are incorporated as graph properties, displayed below: (Note that the direction of edge indicates the sign convention of pipe mass flow rate).

- Edge properties (at edge $i \rightarrow j$): pipe length L_{ij} , pipe mass flow rate \dot{m}_{ij} , pipe characteristics (such as thermal conductivity, roughness, etc)
- Node properties (at node i): temperature T_i , pressure P_i , consumption (+)/produce (-) mass flow rate \dot{m}_s

For the balance of the network mass flow rate, the mass conservation at each node is represented by a linear system of equation in (1), where \mathbf{A} is the incidence matrix of the network graph defined above. Hydraulic losses due to pipe friction is reformulated from Darcy-Weisbach equation, representing the quadratic correlation of pressure drop with respect to circular pipe mass flow rate (2). f_D is the friction factor, calculated by equation (3) and (4), dependent on the flow regime for laminar or turbulent flow.

$$\mathbf{A} \times \dot{\mathbf{m}} = \dot{\mathbf{m}} \mathbf{s} \quad (1)$$

$$\Delta P_{ij} = f_D \cdot \frac{8L_{ij}}{\rho \cdot \pi^2 \cdot d_{ij}^5} \cdot \dot{m}_{ij}^2 \quad (2)$$

$$f_D = \frac{64}{Re} \text{ (laminar flow regime)} \quad (3)$$

$$\frac{1}{f_D} = -2 \log \left(\frac{\epsilon/d_{ij}}{3.7} + \frac{5.74}{Re^{0.9}} \right) \text{ (turbulent flow regime)} \quad (4)$$

Thermal balance is calculated after hydraulic balance when the flow direction is determined and the upstream flow is identified. For each pipe, outlet temperature T_{out} is calculated by equation (5) with respect to inlet temperature T_{in} , where k_{ij} is the thermal transfer coefficient, and T_g is the ground temperature. Since the district heating network model incorporates multiple energy sources at central and decentralized locations, thermal flow mixing from multiple flow streams is represented at each network mixing node (6).

$$T_{out} = T_g + (T_{in} - T_g) \cdot e^{-\frac{k_{ij} \cdot L_{ij}}{\dot{m}_{ij} \cdot c_p}} \quad (5)$$

$$\dot{m}_{mix} T_{mix} = \sum_i^n \dot{m}_i T_i \quad (6)$$

2.2.2 Prosumer with the substitution model

The substitution model incorporates the solar thermal collector model and the demand model. As described previously in substitution configuration design, the operation strategy at the building side is to consume the solar energy from rooftop locally and feed-in the surplus energy to the network through heat exchanger. The secondary loop of the substitution is not represented by a thermal simulation model, however represented by energy balance calculation. Heating demand by consumers is calculated by aggregated space heating and domestic hot water demand. Available solar energy at a targeted supply temperature is calculated, which is in this case, the district heating design supply temperature. Flat plate collector efficiency η_{col} is an operational parameter, which depends on the mean flow temperature, ambient temperature, and solar radiation, calculated by equation (8).

$$\dot{Q}_{solar_ava} = \eta_{col} \cdot Area_{col} \cdot I_{solar} \quad (7)$$

$$\eta_{col} = c_0 - c_1 \cdot \frac{T_{in} - T_{air}}{I_{solar}} - c_2 \cdot \frac{(T_{in} - T_{air})^2}{I_{solar}} \quad (8)$$

By identifying the states of each prosumer, the flowrate for withdrawal or feed in to the network $\dot{m}S_i$ is calculated with a fixed temperature difference at the prosumer according to equation (9), which is dependent on the adopted control strategy.

$$\dot{m}S_i = \frac{Q_{demand} - Q_{solar_ava}}{c_p \cdot \Delta T} \quad (9)$$

3. Case study and analysis

3.1. System Configuration

In this study, the modelling framework is applied to an artificial case study, to demonstrate the design and operation process. The artificial case is selected to design a solar thermal based district heating system with prosumers. As solar irradiation profiles do not vary notably from building to building. To demonstrate the potential benefits of districts with prosumers, where there is share of extra thermal energy from neighbour buildings through the network, the case district is intentionally selected with mixed building types with different load patterns, eg office buildings and residential buildings. Demand profiles are generated by dynamic building simulation tool Energyplus for the 20 selected buildings [7]. Figure 2.a displays the schematics of the designed network layout and connections of building types with two separate branches of residential building and office buildings. The network layout generated by Matlab is shown in figure 2.b, where the line thickness represents the relative size of designed pipe diameter system. Pipe length and node numbers are also indicated.

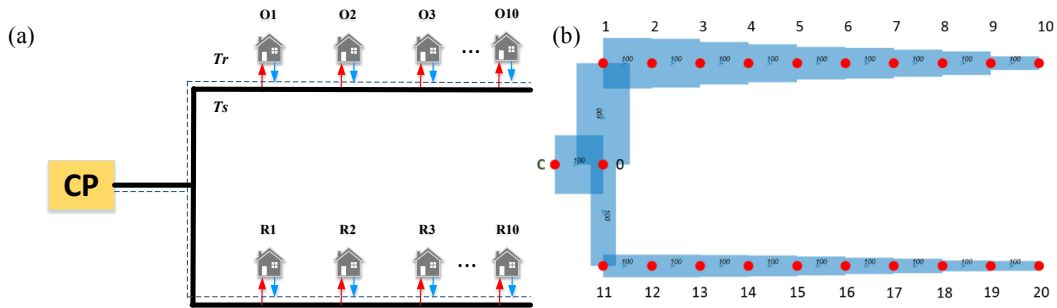


Fig. 2. (a) Schematics of network layout; (b) network structure generated by Matlab code with node number and pipe length indicated

Figure 3 shows hourly demand profiles and available solar energy (after conversion) on the rooftop for 4 representative buildings (office building 1,2, residential building 1,2), for a typical winter week (a) and a summer week(b). By analysing the hourly profiles of the districts in terms of heating load and solar energy available on the rooftop, it shows there is potential for feed-in to the network as prosumers in the wintertime, particularly by residential buildings. In summer time, when there is only domestic hot water demand, there is usually abundant solar energy to feed in to the network and be transmitted to the central location for storage.

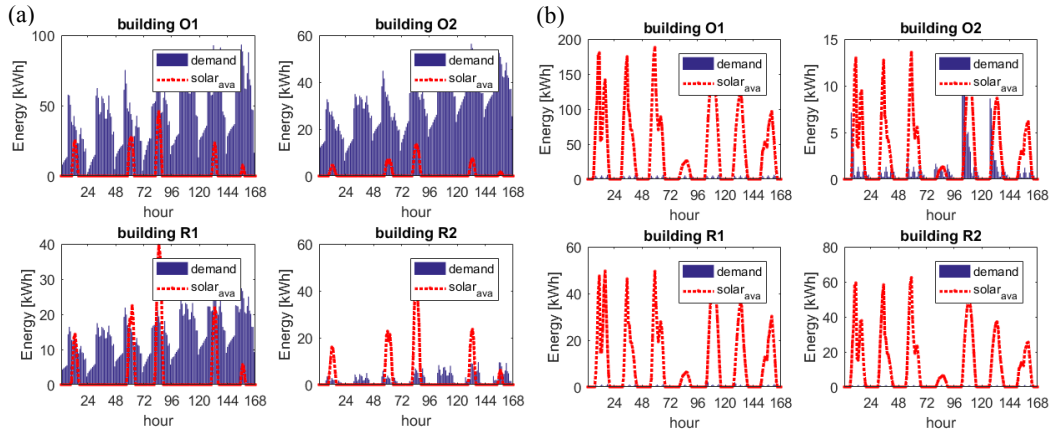


Fig. 3. (a) Winter week hourly demand and available solar energy profile; (b) Summer week hourly demand and available solar energy profile.

3.2 Simulation Scenarios

To investigate on the energy performance of the demonstrated case, simulation of the network model with hourly resolution for a year is carried out for two sets of design scenarios. Operation conditions and key parameters for the analysis are shown in figure 4.

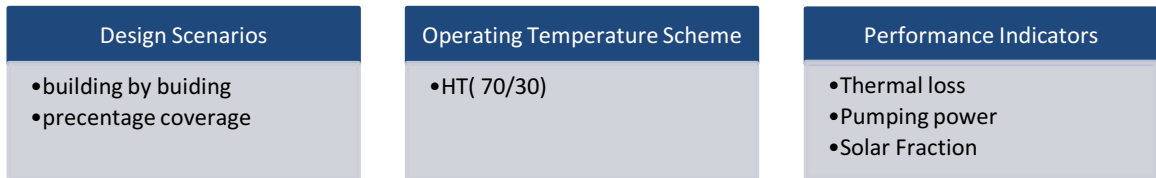


Fig. 4. Workflow of design scenarios and analysis.

The total area of east and south facing rooftop area on each building is identified as total installation capacity.

The two sets of design scenarios include:

- building by building scenarios: only one building is selected to install solar collector with full coverage of rooftop capacity as a prosumer (20 scenarios with 20 building options)
- percentage coverage scenarios: every building is selected but installed collectors vary from 10% to 100% of total rooftop capacity (10 scenarios)

The designed operating temperature is 70 /30 ° C for the hot and cold pipeline respectively. As the thermal losses from the cold pipeline is negligible, thermal losses of the cold pipeline are not calculated. As mass flowrate in the cold pipeline is identical with the hot pipeline with opposite flow direction. The pressure distribution along the cold pipeline could easily be derived with the simulation results from the hot pipeline.

For each system design scenario, hydraulic calculation are used to derive peak flowrates on each pipe segment of the network. Therefore, the final pipe diameter is designed to guarantee the maximum flow rate less than 2 m/s for each design case. Designed pipe diameter and corresponding pipe characteristics are shown in table 1 for one design scenario with full rooftop (east south facing) coverage on each building. Total installed area is 1860 m² for 20 buildings. The flat plat solar thermal collector is selected from commercially available design with conversion factor c_0 equal to 0.854, and loss coefficient c_1 and c_2 equal to 4.06 and 0.0090 W/(m²K).

Table 1. Designed pipe parameters

Pipe No.	From Node	To Node	Length (m)	Inner Diameter (mm)	Heat Transfer Coefficient (W/mK)	Roughness (mm)
1	C	0	100	65	0.2405	0.2
2	0	1	100	59	0.2321	0.2
3	0	11	100	28	0.1887	0.2
4	1	2	100	56	0.2279	0.2
5	2	3	100	54	0.2251	0.2
6	3	4	100	47	0.2153	0.2
7	4	5	100	42	0.2083	0.2
8	5	6	100	36	0.1999	0.2
9	6	7	100	34	0.1971	0.2
10	7	8	100	30	0.1915	0.2
11	8	9	100	26	0.1859	0.2
12	9	10	100	15	0.1705	0.2
13	11	12	100	25	0.1845	0.2
14	12	13	100	25	0.1845	0.2
15	13	14	100	24	0.1831	0.2
16	14	15	100	23	0.1817	0.2
17	15	16	100	21	0.1789	0.2
18	16	17	100	18	0.1747	0.2
19	17	18	100	16	0.1719	0.2
20	18	19	100	12	0.1663	0.2
21	19	20	100	11	0.1649	0.2

3.4 Results and discussion

Thermal loss and pumping power are calculated at each hourly time step for the designed cases as network performance indicators. Annual heat loss and pumping energy are shown in figure 5 for all design scenarios. By installing more decentralized solar area from prosumers thermal losses of the network reduce. That is mainly due to shorter travel distance of heat flow when heat sources are at more decentralized locations, closer to the consumer’s side. This effect should have more significant impact with a larger network size. However, more solar area installation results also in more active pumping from multiple decentralized sources. For a small area of installation, there is no obvious correlation for the pumping power. A reason could be that among this range of design (solar area), the trade-off between active pumping and shorter transmission distance with less hydraulic losses is taking an effect. However, with larger solar installed area, particular in summer, when most energy is pumped from prosumers to the central storage, the pumping power is increasing significantly with respect to total installed area. In this study, only one operation temperature with particular control strategy is adopted, to operate the networks more efficiently in the future, optimal control strategies and operation temperature could be further investigated.

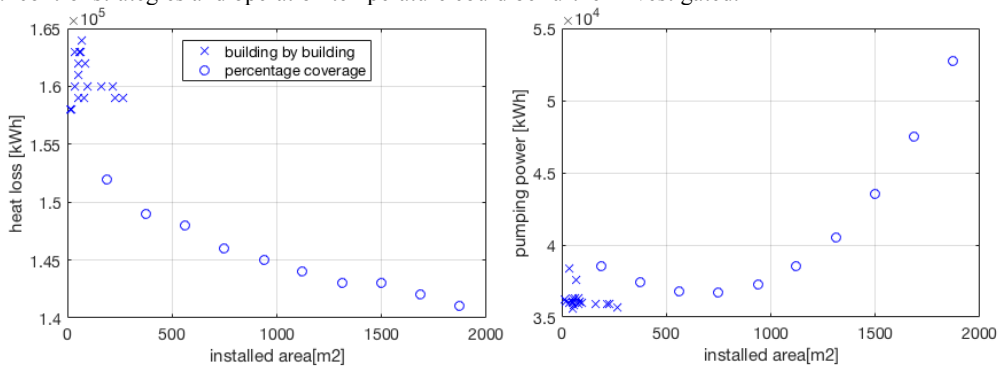


Fig. 5. Annual Thermal heat loss and pumping energy for different design scenarios.

For system performance analysis, solar fraction quantifies the amount of total energy demand covered by solar energy, calculated by equation (10):

$$SF = \frac{Q_{solar\ utilized}}{Q_{demand}} \quad (10)$$

Figure 6 shows the solar fraction value for both sets of scenarios explained above (not accounting the potentials of thermal storage). It shows significant correlation for system solar fraction with respect to the installed rooftop area. With full coverage of all 20 buildings installation capacity, solar fraction could reach around 15%. By observing closely on the selection of building by building scenario, physical location where solar thermal collectors are installed does not play a role in this small district for overall system solar fraction. For larger case study with different heat load density, the decision for prosumer's selection under design might contribute a different result.

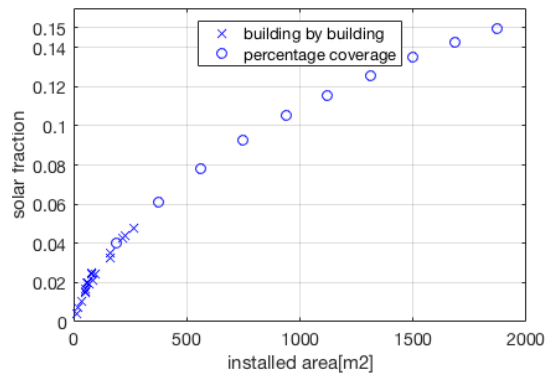


Fig. 6. Annual system solar fraction for different design scenarios.

4. Conclusion and outlook

This paper introduces the value chain of design prosumer based district heating systems with solar thermal collectors. Key system configurations are addressed to allow for bidirectional flow at the substation, by operating decentralized pumps. To further quantify network performance under design scenarios, a thermal-hydraulic model is built to simulate the network behavior for the whole year with hourly time step. A small district with mixed building stocks as a case study is investigated to demonstrate the process. Simulation results show that network pumping power and thermal losses are not so sensitive to the locations of prosumers in a small district. It is beneficial by introducing more prosumers in the network to reduce thermal losses of the network, which has a negative effect on the pumping power. To increase system efficiency of this network type, it requires better operation and control of the networks with prosumers, which should be substantially investigated in the future.

It is certain that not all districts with decentralized renewable potential would be suitable for a district heating system with prosumers. For energy system planners and decision makers, it is of paramount importance to evaluate which type of district and load profiles could potentially benefit in terms of self-sufficiency, cost and many other evaluation criteria. The modelling framework could be further extended by incorporating short and long term storage technologies in the system design as a next step.

For large scale adoption and implementations of the concept in the future, challenges remain concerning various perspectives, such as the optimal control of multiply decentralized, economic drives and political regulations. A pricing mechanism should be set up to incentive the adoption of technologies among different stakeholders such as utility companies and building owners.

Acknowledgements

This research has been financially supported by CTI within the SCCER FEEB&D (CTI.1155000149) and by SNF within the SNF project (Renewable powered district heating networks Nr.165978).

References:

- [1] S. F. O. of E. SFOE, “Energy in buildings,” 2018.
- [2] Nikolina Šajn, “Briefing European Parliamentary Research Service,” 2016.
- [3] L. Brand, A. Calvén, J. Englund, H. Landersjö, and P. Lauenburg, “Smart district heating networks – A simulation study of prosumers’ impact on technical parameters in distribution networks,” *Appl. Energy*, vol. 129, pp. 39–48, 2014.
- [4] I. Ben Hassine and U. Eicker, “Impact of load structure variation and solar thermal energy integration on an existing district heating network,” *Appl. Therm. Eng.*, vol. 50, no. 2, pp. 1437–1446, 2013.
- [5] P. Kräuchi, M. Kolb, T. Gautschi, U.-P. Menti, and M. Sulzer, “Modellbildung Für Thermische Arealvernetzung Mit IDA-ICE,” in *Fifth German-Austrian IBPSA Conference*.
- [6] F. Bünning, M. Wetter, M. Fuchs, and D. Müller, “Bidirectional low temperature district energy systems with agent-based control: Performance comparison and operation optimization,” 2017.
- [7] Georgios Mavromatidis, “Model-based Design of Distributed Urban Energy Systems under Uncertainty,” ETH Zurich, 2017.



16th International Symposium on District Heating and Cooling, DHC2018,
9–12 September 2018, Hamburg, Germany

Impact of distribution and transmission investment costs of district heating systems on district heating potential

Mostafa Fallahnejad^{a,*}, Michael Hartner^a, Lukas Kranzl^a, Sara Fritz^b

^aEnergy Economics Group, Technische Universität Wien, Gusshausstrasse 25-29/370-3, 1040 Vienna, Austria

^bInstitute für Energie- und Umweltforschung Heidelberg GmbH, Im Weiher 10, 69121 Heidelberg, Germany

Abstract

In this paper, we use a heat density map (HDM) and a plot ratio map to propose a GIS-based method for determining potential DH areas with specific focus on district heating (DH) grid costs. The DH areas are determined via performing sensitivity analyses on the HDM under consideration of predefined upper bound of the average distribution costs. The approach additionally allows for estimation of length and diameter of transmission lines and their associated costs. The outputs are GIS layers that illustrate areas that are economically viable for construction of DH as well as the cost-minimal transmission lines connecting these regions to each other. The impacts of key input parameters like grid costs ceiling and market share on potential and on expansion and extension of the DH systems were studied for the case study of Vienna. The results showed that the increase of DH market share in DH areas under a certain grid cost ceiling significantly reduce average grid costs. In addition, it was revealed that the expansion of DH system without increasing the market share in the DH areas does not effectively increase the share of DH from the total heat demand and leads to higher average grid costs. These results call for policy interventions like spatial heat planning, zoning and implementation of district heating priority areas.

© 2018 The Authors. Published by Elsevier Ltd.

This is an open access article under the CC BY-NC-ND license (<https://creativecommons.org/licenses/by-nc-nd/4.0/>)

Selection and peer-review under responsibility of the scientific committee of the 16th International Symposium on District Heating and Cooling, DHC2018.

Keywords: District heating potential; Grid investment costs; Heat density map; Plot ratio

* Corresponding author. Tel.: +43-1-58801-370374; fax: +43-1-58801-370397.

E-mail address: fallahnejad@eeg.tuwien.ac.at

1. Introduction

The investments in district heating (DH) infrastructures help to integrate diverse renewable and low-carbon energy sources and reduce the dependency on a single energy source. Especially with the 4th generation of DH system, due to its low working temperature, it is possible to supply heat, either directly or indirectly, with a wide range of energy sources such as geothermal, solar, wind, biomass, excess heat etc. [1]. However, the initial investment in the DH grid is usually associated with uncertainty regarding future heat sales and the potentially achievable connection rate of DH. In this paper, the DH grid investments are studied from various perspectives such as grid cost ceiling, investment periods, DH market share and expected levels of the energy saving in future due to building retrofitting and renovation. In addition, the impact of these parameters on DH potential and connection of remote areas to the DH grid is studied as well.

Nomenclature

A	Set of all coherent areas
AF	Annuity factor
C	Set of pipeline dimension steps
$C_{1,T}, C_{2,T}$	Construction costs constant [€/m] and Construction costs coefficient [€/m ²]
Cap _{ij}	Required capacity in the pipeline connecting area <i>i</i> to <i>j</i> [MW]
$c_{dist}, c_{trans}, c_{grid}$	Average specific costs of distribution grid, transmission grid and both of them [€/MWh]
c_{grid_max}	Specific grid cost ceiling [€/MWh]
c_{dist_max}	Specific distribution grid cost ceiling [€/MWh]
d_a	Pipe diameter [m]
D_t	Annual heat demand in year “ <i>t</i> ”
<i>e</i>	Plot ratio
FLH	Full load hours
G	Coherent area with highest DH heat demand
Inv _T	Investment in year “ <i>T</i> ”
L	Total trench length [m]
l_{ij}	Border-to-border distance of area <i>i</i> and area <i>j</i>
<i>m</i>	Investment period [years]
MS ₀ , MS _{<i>m</i>}	DH market share at the beginning (year “0”) and the end (year “ <i>m</i> ”) of the investment period
<i>n</i>	Depreciation time
PowStep	Capacity of a pipeline for a give dimension
q_i	Boolean variable determining if the coherent area <i>i</i> is part of DH system or not
Q_t	Heat demand supplied by DH in year “ <i>t</i> ”
<i>r</i>	Interest rate
S	Ratio of accumulated energy savings
SPCTL _{ij}	Specific cost of transmission line connecting area <i>i</i> to area <i>j</i>
TLC _{ij}	Annualized specific cost of transmission line connecting area <i>i</i> to area <i>j</i>
TLB _{ij}	Boolean variable showing if transmission line from area <i>i</i> to <i>j</i> should be built
<i>w</i>	Effective width of distribution pipeline [1/m]
y_{ij}	Boolean variable determining if there is a line from coherent area <i>i</i> to coherent area <i>j</i>

The connection of buildings to the DH grid via long pipes not only is expensive, but also increases the heat losses. Therefore, the linear heat density (transferred heat per length of pipeline) is considered as a key elements in the assessment of DH distribution grid costs [2–4]. The linear heat density was traditionally quantified based on empirical data. Another method is to estimate the pipeline length based on street routes and subsequently, calculate the linear heat density. This method was used in [5–8]. This is done by determining shortest street pathway required to connect all buildings in an area. The method uses computer algorithms and can be easily implemented. However, it requires detailed georeferenced data and long processing time for larger areas like a city. The method may also ignore waterways, highways, or physical barriers if they exist in the study area. Furthermore, a 100% connection rate of buildings to the DH system, even if realized in the future, usually does not occur at once in practice – an important issue that should be considered in investment decisions. In addition, the implementation of method for lower connection rates is also difficult to implement and may lead to inaccurate results. Persson and Werner proposed an analytical approach for estimating the linear heat density using the concept of effective width [9]. They addressed the limitations caused by lack of empirical data for tuning the results. Later on, they used the method for

estimating the distribution cost of district heating based on heat demand and plot ratio and demonstrated the competitiveness of DH in inner city areas for several European cities [10]. Since then, the approach has been applied widely in different study areas [11–15]. The advantage of this method is its easy implementation and application for large regions as well as the higher calculation speed.

The determination of potential DH areas can be used for either construction of new DH systems or extension of them. In that sense, the GIS methods provide a good insight to study areas and have been used frequently by researchers and energy planners [3,12,16–18]. The GIS methods used for estimation of DH potential can be divided into 3 main categories. In the first category, the heat sources and sinks are indicated with a very local focus in order to precisely determine the expansion and extension potentials. In this way, the major heat consumers such as shops, hospitals, hotels, offices etc. are determined and the DH potential calculated. For example, Finney et al. determined the existing and emerging heat sources and sinks and subsequently, depending to their vicinity to the existing DH infrastructure, calculated the potential for expansion of DH system via separate network as well as for the extension of the existing networks [19]. In the second category, a heat demand threshold is used for the determination of areas with DH potential [16]. In other words, it is assumed that the DH supply of all dense areas with a heating demand of above a certain level is economically viable. This method can be additionally used to determine the suitable technology for heat supply depending on the heat density, as done in [17]. The third category, calculates the distribution costs using the concept of effective width, as proposed by Persson and Werner [10], and compares them with other heat supply options. For instance, Nielsen and Möller divided the grid investment into distribution grid and transmission grid investment [4]. For the distribution costs, they used the analytical approach based on the concept of effective width. For the transmission lines, on the other hand, they calculated the costs based on required capacity and shortest path between the center of a potential DH area and center of the closest existing DH system to that area. Finally, areas that had the total cost of lower than individual supply options, were considered as potential DH expansion areas.

The strength and weakness found in above enumerated methods are explained in the following. Having a detailed local focus and determining heat sources and sinks with the intention of providing a reliable, accurate result for a given case study, is highly beneficial for making concrete investment decisions (category 1). However, this process requires a very detailed information about the suppliers and consumers and replicating it in other regions requires almost the same amount of effort. The introduction of the heat density threshold for determination potential DH areas, as was done in category 2, is much easier to apply to larger areas and requires less processing time. However, sometimes the obtained regions are close to each other and interconnection of these regions may economically justify the supply of heat to their surrounding areas with DH as well. In other words, it may underestimate the existing potential. Furthermore, the small zones are prone to demand reduction, which can risk the investment for connecting them to the DH grid. In comparison to the category 2, category 3 provides a brighter picture from pre-feasibility study of implementing DH systems. However, it should be noted that implementation of DH system in new areas is a time consuming procedure and the uncertainties regarding heat saving actions and the expected future market share should be included in the study. Additionally, it should be noted that having common transmission line corridor between several potential areas, instead of building multiple parallel lines, could improve the feasibility of connecting more potential areas to the DH system. This leads to a better estimation of required pipeline diameter and as a result, reduction of costs of heat losses in transmission lines.

Consequently, this paper proposes a method for determining DH potential with respect to investment periods, expected future market share of DH system, expected level of energy savings. Additionally, the cost-optimum transmission lines and their capacities for connecting the coherent areas are determined. The method is applied to the case study of Vienna and the obtained results are illustrated in GIS-layers.

2. Approach

For the economic assessment of investment in DH system, both marginal heat generation costs and heating grid investments must be studied [2]. However, to simplify the problem and focus on grid investments, we introduce a parameter as grid cost ceiling (c_{grid_max}). This parameter implies that the marginal heat generation costs have been studied separately and to keep the DH system competitive, the grid costs may not exceed this cost ceiling. Additionally, the DH grid costs (c_{grid}) is split up into distribution grid capital costs (c_{dist}) and transmission grid capital costs (c_{trans}). This is shown in Eq. (1).

$$c_{grid} = c_{dist} + c_{trans} \quad [€/MWh] \quad S.t.: c_{grid} \leq c_{grid_max} ; c_{dist} \leq c_{dist_max} \quad (1)$$

The main input data for this study are a heat density map (HDM) and a plot ratio map. These data are obtained from the preliminary version of European HDM and plot ratio map provided by Hotmaps project [20]. Both the HDM and plot ratio map have a resolution of 100x100m. Each cell of these maps is referred as a pixel in this work.

2.1. Distribution costs

One of important means to reach the EU targets for reduction of greenhouse gases is improving the efficiency and decreasing energy use in buildings [21]. In term of heat consumption, this lead to implementing measures for energy-efficient thermal envelope retrofit of existing buildings and constructing new buildings with higher thermal insulation levels. These measurements have direct impact on heat demand and influence investments in DH systems. Considering an investment period of “ m ” consecutive years on DH grid, the annual heat demand in t^{th} year of investment (D_t) is calculated using the heat density map from the first year of investment and the ratio of accumulated energy saving (S) at the last year of investment (Eq. (2)).

$$D_t = D_0 \cdot \sqrt[m]{(1-S)^t} \quad (2)$$

$$0 \leq S \leq 1 \quad ; \quad t \in \{0, 1, 2, \dots, m\}$$

The reduction of heat consumption in European buildings in the future, can potentially affect the capital costs and consequently, the market share of DH. Therefore, the current market share as well as the targeted market share at the end of investment period should be included in the investment calculation. In this paper, the term “market share” is referred to “market share within DH areas” unless it is clearly stated. Accordingly, the expected heat demand that should be supplied by DH in each year (Q_t) and in each pixel is calculated based on the DH market share at the beginning of the investment period (MS_0) and the expected market share at the last year of investment (MS_m):

$$Q_t = D_t \cdot \left[MS_0 + t \cdot \frac{MS_m - MS_0}{m} \right] \quad (3)$$

The distribution grid investment required in each pixel of the HDM is calculated using the proposed method by Persson & Werner [10] with additional considerations regarding the investment period. The study area is categorized in three groups (inner city areas, outer city areas and park areas) based on the plot ratio value. Subsequently, the linear heat density (L) is calculated using the concept of effective width (w) in Eq. (4). Afterwards, the average pipe diameters in distribution grid is estimated Eq. (5). Finally, the distribution grid investment in year T is calculated by Eq. (6).

$$L = 1/w = 1 / (61.8 \cdot e^{-0.15}) \quad (4)$$

$$d_a = 0.0486 \cdot \ln(Q_t / L) + 0.0007 \quad (5)$$

$$Inv_T = \frac{C_{1,T} + C_{2,T} \cdot d_a}{\left(\sum_{t=0}^m \frac{Q_{T+t}}{(1+r)^t} + \sum_{t=m+1}^n \frac{Q_{T+m}}{(1+r)^t} \right) / L} \quad (6)$$

The parameters used in Eq. (4-6) are as follows: Q_t is part of annual heat demand (D_t) that is supplied by DH in year t [GJ/a], C_1 is the construction cost constant [€/m], C_2 is the construction cost coefficient [€/m²], d_a is the average pipe diameter [m], L is the total trench length [m]. C_1 and C_2 are set according to the plot ratio, r is interest rate and n is depreciation time.

As it is shown in Eq. (3), it is possible that the market share at the end of investment period (MS_m) decreases or remains equal to the beginning of the investment period. The DH system should be capable to cover the DH demand (Q_t) at all times of the investment period. Therefore, for the calculation of the investments and potentials, the highest annual DH demand during the investment period (Q_{max}) should be considered. For the calculation of distribution grid capital costs in Eq. (6), the annual DH demand is considered to remain constant after the last year of investment period. This assumption is made in order to focus on the investment period only.

2.2. Determination of coherent areas

Pixels with low heat demand have high distribution costs and therefore, it is not economic to connect them to the DH system. We define a pixel demand threshold of 1GWh/km² for removing such pixels. By eliminating these pixels from the map, we obtain groups of pixels that are attached to each other. Each set of these attached pixels constitute small zones that in this paper, are referred as “coherent areas”. Afterwards, the distribution costs in each coherent area are calculated and the ones with costs of below the upper bound (c_{dist_max}) are extracted. Subsequently, the pixel threshold is increased with a small step (0.1GWh/km²) and the previous step is repeated. This process is continued until no pixel above the threshold remains. The result would be a set of coherent areas, all with distribution costs of bellow the defined distribution cost ceiling. Fig. 1 shows the flowchart of these steps.

In practice, determination of coherent areas starts by selecting regions with higher heat densities. Here, this process is done the other way around in order to speed up the calculation process. It should be noted that this has no influence on determination of coherent areas since the distribution cost upper bound is considered in each loop.

2.3. Transmission line model

Transmission lines connect coherent areas to each other and constitute one connected DH grid. The analysis of two or more detached DH systems is not in the scope of this study. The aim of this step is to connect as much coherent areas as possible without exceeding grid cost ceiling (c_{grid_max}). The connected coherent areas that constitute the DH system are referred as “**economic coherent areas**” in this paper. The determination of economic coherent areas as well as the cost-minimal transmission lines and their capacities are determined in an optimization procedure. This is done by introducing a prize-collecting spanning tree problem.

In the first step, the border-to-border distances of coherent areas (l) from each other should be calculated. The coherent areas are labeled from one to N (Eq. (7)). Considering “N” coherent areas, this will give an NxN distance matrix. The transmission pipeline capacities ($PowStep$) and their specific costs are obtained from Table 1. The pipeline specific costs are annualized over the lifetime of the system. The coherent area with highest DH heat demand (G) is considered as the only available heat source. It produces the heat for itself and all other economic coherent areas.

$$A = \{1, 2, \dots, N\} \quad (7)$$

The prize-collecting spanning tree problem is defined so that the objective would be to maximize the difference between the revenue from heat sales in economic coherent areas and the costs imposed by construction of transmission lines (Eq. (8)).

$$\max c_{grid_max} * \sum_i Q_{max,i} * q_i - \sum_i \sum_j TLC_{ij} * l_{ij} * y_{ij} \quad \forall (i, j) \in A \quad (8)$$

Here, A is the set of all coherent areas; $Q_{max,i}$ is the highest heat demand that is supplied by DH in area i through the investment period; q_i is a Boolean variable determining if the coherent area i is part of DH system or not; TLC is the annualized specific cost of transmission line connecting area i to area j ; l_{ij} is the the border-to-border distance of area i and area j ; y_{ij} is a Boolean variable determining if there is a line from coherent area i to coherent area j .

The objective function, on the one hand, maximize the supplied heat by DH and on the other hand, finds the cost-optimum combination of the pipelines. The objective function is subject to three groups of constraints: 1) minimum spanning tree (MST) related constraints 2) pipeline capacity related constraints 3) economic constraints. These groups are explained in detail in the followings.

2.3.1. Minimum spanning tree (MST) related constraints

The coherent areas and transmission lines can be considered as a graph. The aim of using MST constraints is to connect all economic coherent areas with minimum number of transmission lines. In order to achieve this goal, the number of transmission lines should be just below the number of economic coherent areas (Eq. (9)). This rule should be true for any subset of the graph and no loop should exist in the final tree (Eq. (10)). Here, it is assumed that between two coherent areas, the heat can only flow in one direction (Eq. (11)). Since the number of economic coherent areas is not clear before the optimization, additional constraints are required as well. There must be one transmission line entering to an economic coherent area (Eq. (12)). On the other hand, a transmission line can be drawn from a coherent area, only if one transmission lines has been entered to it (Eq. (13)). Also, a transmission line

can be constructed between two “economic” coherent areas (Eq. (14)). Self-loops should not exist in the graph (Eq. (15)). The Eq. (16) makes sure that the coherent area G is one of the economical areas.

$$\sum_i \sum_j y_{ij} = \sum_i q_i - 1 \quad \forall (i, j) \in A \tag{9}$$

$$\sum_i \sum_j y_{ij} \leq |S| - 1 \quad \forall S \subseteq A ; \forall (i, j) \in A : i \in S, j \in S \tag{10}$$

$$y_{ij} + y_{ji} \leq 1 \quad \forall (i, j) \in A \tag{11}$$

$$q_i \leq \sum_j y_{ij} \quad \forall i \in A - \{G\} ; \forall j \in A \tag{12}$$

$$y_{ij} \leq \sum_h y_{jh} \quad \forall i \in A - \{G\} ; \forall (j, h) \in A \tag{13}$$

$$2 * (y_{ij} + y_{ji}) \leq q_i + q_j \quad \forall (i, j) \in A \tag{14}$$

$$y_{ii} = 0 \quad \forall i \in A \tag{15}$$

$$q_G = 1 \tag{16}$$

2.3.2. Pipeline capacity related constraints

The required capacity in MW in a pipeline (Cap) is calculated by dividing the total annual energy demand transferred through that pipeline (in MWh per year) by 3000 full-load hours (FLH). The capacities depend on the existence of the pipelines (y_{ij}) and the demand in the economic coherent areas (Q_{max,i}*q_i). The capacities of pipelines are bounded so that the solver can converge faster (Eq. (17-22)).

$$Cap_{ij} \geq y_{ij} * Q_{max,j} / FLH \quad \forall (i, j) \in A \tag{17}$$

$$Cap_{ij} \leq (\sum_h Q_{max,h} - \sum_r (y_{ri} * Q_{max,r})) / FLH \quad \forall (i, j) \in A ; \forall h \in A - \{G, i\} ; \forall r \in A - \{G\} \tag{18}$$

$$Cap_{ij} - y_{ij} * Q_{max,G} \leq 0 \quad \forall (i, j) \in A \tag{19}$$

$$\sum_j Cap_{ij} - \sum_j Cap_{ji} = q_i * Q_{max,i} / FLH \quad \forall i \in A ; \forall j \in A - \{G\} \tag{20}$$

$$\sum_j Cap_{ij} = (\sum_j q_j * Q_{max,j}) / FLH \quad \forall j \in A - \{G\} \tag{21}$$

$$Cap_{ii} = 0 \quad \forall i \in A \tag{22}$$

Table 1. Total cost of transmission pipes including projecting, field work, pipe work, materials, and digging, based on [4] with 55°C temperature difference.

Step (C)	Dimension DN	Capacity [MW] (PowStep)	Specific Cost [EUR/m] (SPCTL)
0	32	0.2	195
1	40	0.3	206
2	50	0.6	220
3	65	1.2	240
4	80	1.9	261
5	100	3.6	288
6	125	6.1	323
7	150	9.8	357
8	200	20	426
9	300	45	564
10	400	75	701
11	500	125	839
12	600	190	976

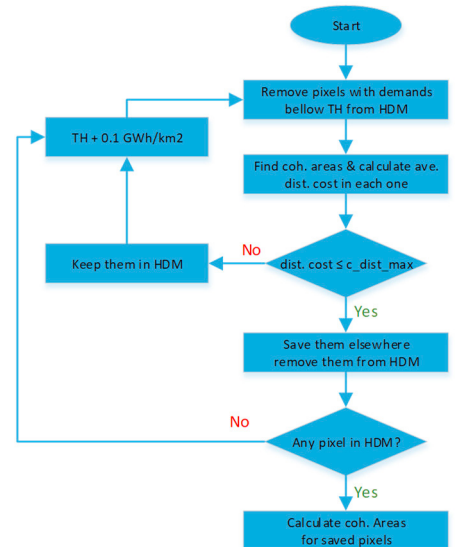


Fig. 1. Flowchart of determination of coherent areas (TH: threshold)

2.3.3. Economic constraints

The distribution grid cost of economic coherent areas are included in total grid costs. Transmission lines costs, on the other hand, are calculated in the optimization model. Based on the required capacity in a pipeline (Cap), a suitable step from table 1 should be chosen. Here, the steps are labeled from 1 to 12 (Eq. (23)). Accordingly, the pipe capacity (PowStep) and the specific annualized transmission line costs (TLC) are calculated. The transmission line Boolean variable (TLB) is used to find the right cost and capacity of pipelines (Eq. (24-28)). The grid cost ceiling also should not be exceeded. This condition is fulfilled by Eq. (29).

$$C = \{1, 2, 3, \dots, 12\} \tag{23}$$

$$TLC_{ij} = AF * \sum_k TLB_{ijk} * (SPCTL_k - SPCTL_{k-1}) \quad \forall (i, j) \in A ; \forall k \in C - \{0\} \tag{24}$$

$$TLB_{ijk} \leq y_{ij} \quad \forall (i, j) \in A ; \forall k \in C \quad (25)$$

$$TLB_{ij(k+1)} \leq TLB_{ijk} \quad \forall (i, j) \in A ; \forall k \in C - \{0, last_step\} \quad (26)$$

$$0 \leq Cap_{ij} - \sum_k ((PowStep_k - PowStep_{k-1}) * TLB_{ij(k+1)}) \quad \forall (i, j) \in A ; \forall k \in C - \{0, last_step\} \quad (27)$$

$$0 \leq \sum_k (PowStep_k - PowStep_{k-1}) * TLB_{ijk} - Cap_{ij} \quad \forall (i, j) \in A ; \forall k \in C - \{0\} \quad (28)$$

$$0 \leq \sum_i (q_i * Q_{max,i} * (c_{grid_max} - c_{dist})) - \sum_i \sum_j (TLC_{ij} * l_{ij}) \quad \forall (i, j) \in A \quad (29)$$

3. Parametrization

A key input parameter of the model is the DH grid cost ceiling (c_{grid_max}). For the case study of Vienna, we study the DH grid cost ceilings from 8 EUR/MWh to 17 EUR/MWh. In this study, the ratio of distribution grid cost ceiling (c_{dist_max}) to grid cost ceiling (c_{grid_max}) was set empirically by running sensitivity analyses on this ratio for various regions across Europe. The sensitivity analyses revealed that the factor of 0.95 provides a good balance between inclusion of coherent areas in DH system and connecting remote coherent areas to the DH system (Eq. (30)). As the results from [6] shows, this value may reduce to approximately 0.85 if street routes instead of the Euclidean distances are used for the transmission line corridors.

$$c_{dist_max} = 0.95 \cdot c_{grid_max} \quad (30)$$

In the last years, the share of district heating from the total heat demand in Vienna has been around 30% [22]. This is equivalent to 36% market share within DH areas [23]. The model is run for various expected market share increases over the investment period from 2018 until 2030 ranging from 40% to 90%. Additionally, the total heat demand reduction due to building retrofitting and higher thermal efficiency of newly constructed buildings is considered. This is reflected in the ratio of accumulated energy saving (S) with 5%, 10% and 15% heat demand reduction in 2030 compared to 2018. A discount rate of 5% and depreciation time of 30 years are considered in the calculations. Table 2 shows the summary of the input parameters and scenarios.

4. Results

Here, the outputs are depicted in GIS layers and the impacts of market share and energy savings are presented.

4.1. GIS Layers

Fig. 2a shows the HDM of Vienna at the beginning of the investment period. As it can be seen in the map, the heat density is at highest in the center and decreases as going toward the suburbs. Fig. 2b illustrates the impact of the expected market share at the end of the investment period (MS_m) on the expansion of DH system. It can be seen that the establishment of DH in the suburban areas only at high market shares (>70%) is economically feasible. The expected accumulated energy saving at the end of the investment period (S), however, has a reverse impact on the expansion of the DH (Fig. 2c). In other words, the higher the energy saving measurements, the less suburban areas can be supplied by DH at a certain grid cost threshold.

Finally, Fig. 2d shows some of coherent areas and transmission pipelines from a closer look. Additionally, the required capacity for the transmission pipelines are shown. Based on this capacity, a suitable pipe dimension is selected and accordingly, the pipeline costs are calculated in the model.

4.2. Impact of market share and energy savings

Fig. 3 provides a summary of obtained results from various scenarios. In the figure, the points represent the calculated average grid costs obtained from the model under a certain scenario. The red lines in Fig. 3a and 3b show the current status in Vienna, i.e. the 30% of the total heat demand that is supplied by DH system.

In the Fig. 3a, the focus is on the impact of the market share on the calculated specific grid cost. As it can be seen, under a certain grid cost ceiling (eg. $c_{grid_max} = 14$ EUR/MWh), as the market share at the end of the investment period (MS_m) increases, the specific grid costs decrease. At the same time, the share of total heat demand supplied by DH system, increases dramatically. The figure also highlights the importance of achieving a high market share. For instance, at the cost of less than 8 EUR/MWh, it is possible to supply more than 60% of total heat demand

if the market share of 90% is reached. In the Fig. 3b, the focus is on the impact of the grid cost ceiling on the calculated specific grid costs. As it can be seen, higher grid cost ceilings, do not necessarily lead to the increase of supplied heat with DH. Considering the section 2.2, increase of the grid cost ceiling has a direct impact on areal expansion of the coherent areas. However, areal expansion of DH areas without increasing the market shares, has low impact on the increase of the share of total heat demand supplied by DH. This trend can be seen in Fig. 3b. It can be concluded that, the increase of the market share within a DH area, has a higher impact on increase of the heat supply by DH compared to the expansion of the DH grids to the suburban areas. This has also high impact on the reduction of specific grid costs. These can be realized by policy interventions like spatial heat planning, zoning and implementation of district heating priority areas [24].

Fig. 3c depicts the impact of expected accumulated energy saving on the specific grid costs. It can be concluded from the graph that the increase of the accumulated energy saving, leads to slight increase of the average grid costs and decrease of the share of total heat demand that is supplied with the DH system.

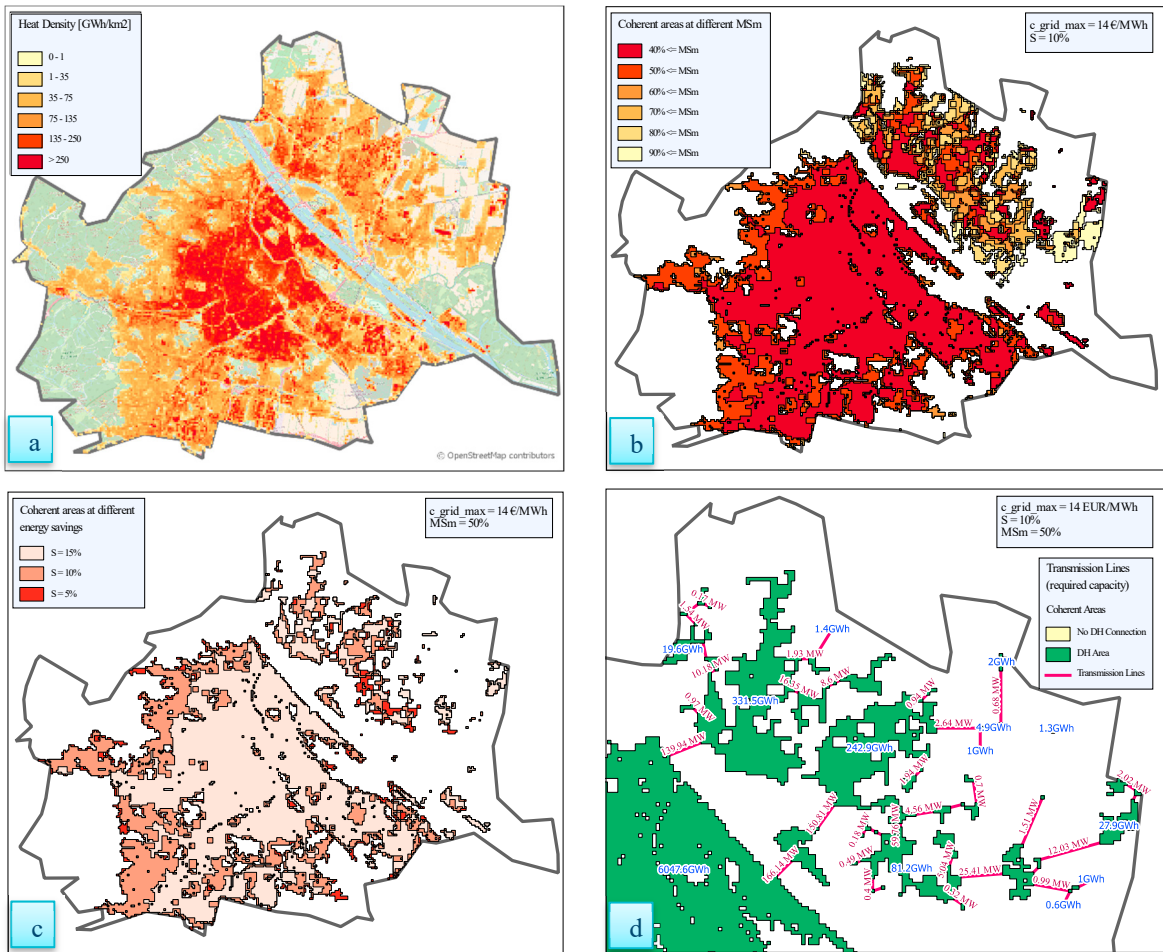


Fig. 2. (a) Heat density map of Vienna; (b) Coherent areas at various expected market share at the end of investment period (MS_m); (c) Coherent areas at various expected accumulated energy saving (S); (d) Optimum pipeline connection and required pipeline capacity

5. Discussion

In order to construct a DH network, the technical aspects such as water flow, heat losses and ground elevation should be simulated and optimized in detail. However, the purpose of this article is not to design the distribution and transmission grids, but rather to develop a method for estimation of the cost-optimal size and cost of the grid on a

regional scale and calculate the DH potential. The approach can be applied to any urban and rural area to examine different DH grid investment strategies. The outputs of the approach do not limit to a DH potential value; but also reveal the investment strategy that can lead to higher heat supply with DH system at the same average grid costs. The optimization model not only determines economic coherent areas for connection to the DH grid, but also identifies the cost-minimal transmission line passages and required pipeline sizes. Furthermore, the output GIS layers provide an intuitive illustration and perspective to an investment plan.

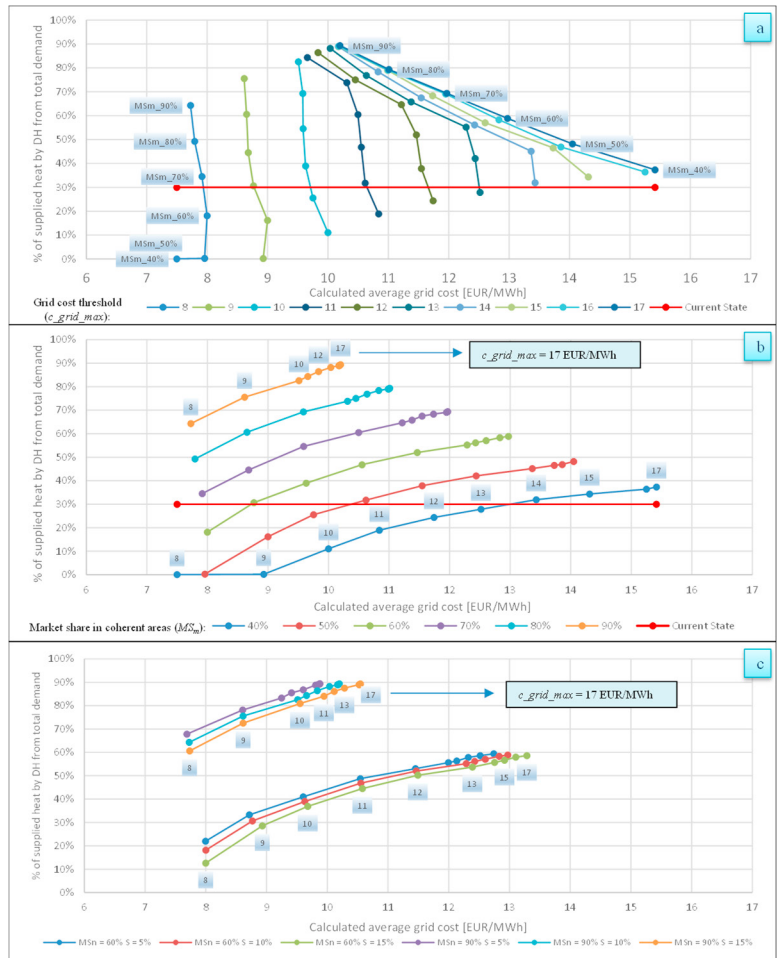


Fig. 3. (a) Impact of market share at the end of investment period (MS_m) on obtained average grid costs and on percentage of the total heat demand supplied by DH in last year of investment for different c_{grid_max} levels; (b) Impact of grid cost ceilings (c_{grid_max}) on calculated average grid costs and on percentage of the total heat demand supplied by DH in last year of investment at different market share levels (MS_m); (c) Impact of expected accumulated energy saving (S) on the specific grid costs and on percentage of the total heat demand supplied by DH in last year of investment

6. Conclusion

In this paper, a HDM and a plot ratio map were used for the study of DH potentials. Distribution grid costs in each pixel of the HDM were calculated and the coherent areas with an average distribution grid cost of below the distribution grid cost ceiling were determined. Subsequently, via an optimization model, the economic coherent areas were determined and the optimum corridors for connecting these areas as well as the capacity of transmission pipelines were calculated. The method allows for consideration of DH market share and accumulated energy saving for the calculation of grid costs and DH potentials.

The proposed method was applied to the case study of Vienna and various scenarios were examined. The results showed that the increase of grid cost ceiling leads to expansion of the coherent areas to suburban areas and accordingly, increases of the share of total heat demand supplied by DH. However, this trend slows down as the grid cost ceiling rises. Increase of the market share at coherent areas, on the other hand, leads to reduction of average grid costs and has a high impact on growing the share of supplied heat by DH from total heat demand. In other

words, higher DH market share can contribute to boost the competitiveness of DH systems. Finally, the increase of the accumulated energy saving leads to a slight increase of the average grid costs and decrease of the share of total heat demand that is supplied with the DH system. Overall, the results are backing the call for policy interventions like spatial heat planning, zoning and implementation of district heating priority areas.

References

- [1] Lund H, Werner S, Wiltshire R, Svendsen S, Thorsen JE, Hvelplund F, et al. 4th Generation District Heating (4GDH). *Energy* 2014;68:1–11. doi:10.1016/j.energy.2014.02.089.
- [2] Reidhav C, Werner S. Profitability of sparse district heating. *Appl Energy* 2008;85:867–77. doi:10.1016/j.apenergy.2008.01.006.
- [3] Andrews DD, Krook-Riekkola A, Tzimas E, Serpa J, Carlsson J, Pardo-Garcia N, et al. Background Report on EU-27 District Heating and Cooling Potentials, Barriers, Best Practice and Measures of Promotion. Luxembourg: Publications Office of the European Union; 2012.
- [4] Nielsen S, Möller B. GIS based analysis of future district heating potential in Denmark. *Energy* 2013;57:458–68. doi:10.1016/j.energy.2013.05.041.
- [5] Eikmeier B, Klobasa M, Toro F, Menzler G. Potenzialerhebung von Kraft-Wärme- Kopplung in Nordrhein-Westfalen. Ministerium für Klimaschutz, Umwelt, Landwirtschaft, Natur-und Verbraucherschutz des Landes Nordrhein-Westfalen; 2011.
- [6] Nielsen S. A geographic method for high resolution spatial heat planning. *Energy* 2014;67:351–62. doi:10.1016/j.energy.2013.12.011.
- [7] Unternährer J, Moret S, Joost S, Maréchal F. Spatial clustering for district heating integration in urban energy systems: Application to geothermal energy. *Appl Energy* 2017;190:749–63. doi:10.1016/j.apenergy.2016.12.136.
- [8] Nielsen S, Grundahl L. District Heating Expansion Potential with Low-Temperature and End-Use Heat Savings. *Energies* 2018;11:277. doi:10.3390/en11020277.
- [9] Persson U, Werner S. Effective Width: The Relative Demand for District Heating Pipe Lengths in City Areas. 12th Int. Symp. Dist. Heat. Cool. Tallinn Est. Sept. 5th Sept. 7th 2010, Tallinn University of Technology; 2010, p. 128–131.
- [10] Persson U, Werner S. Heat distribution and the future competitiveness of district heating. *Appl Energy* 2011;88:568–76. doi:10.1016/j.apenergy.2010.09.020.
- [11] Persson U. District heating in future Europe: Modelling expansion potentials and mapping heat synergy regions. Doctoral thesis. Chalmers University of Technology, 2015.
- [12] Müller A, Büchele R, Kranzl L, Totsching G, Mauthner F, Heimrath R, et al. Solarenergie und Wärmenetze: Optionen und Barrieren in einer langfristigen, integrativen Sichtweise (Solargrids). Technische Universität Wien, Institut für Energiesysteme und elektrische Antriebe, Energy Economics Group; 2014.
- [13] Möller B, Werner S. STRATEGO D 2.2: Quantifying the Potential for District Heating and Cooling in EU Member States. University of Flensburg; 2016.
- [14] Leurent M, Da Costa P, Jasserand F, Rämä M, Persson U. Cost and climate savings through nuclear district heating in a French urban area. *Energy Policy* 2018;115:616–30. doi:10.1016/j.enpol.2018.01.043.
- [15] Leurent M, Da Costa P, Rämä M, Persson U, Jasserand F. Cost-benefit analysis of district heating systems using heat from nuclear plants in seven European countries. *Energy* 2018;149:454–72. doi:10.1016/j.energy.2018.01.149.
- [16] Gils HC, Cofala J, Wagner F, Schöpp W. GIS-based assessment of the district heating potential in the USA. *Energy* 2013;58:318–29. doi:10.1016/j.energy.2013.06.028.
- [17] Connolly D, Lund H, Mathiesen BV, Werner S, Möller B, Persson U, et al. Heat Roadmap Europe: Combining district heating with heat savings to decarbonise the EU energy system. *Energy Policy* 2014;65:475–89. doi:10.1016/j.enpol.2013.10.035.
- [18] Artur Wyrwa, Yi-kuang Chen. Mapping Urban Heat Demand with the Use of GIS-Based Tools. *Energies* 2017;10:720. doi:10.3390/en10050720.
- [19] Finney KN, Sharifi VN, Swithenbank J, Nolan A, White S, Ogdan S. Developments to an existing city-wide district energy network – Part I: Identification of potential expansions using heat mapping. *Energy Convers Manag* 2012;62:165–75. doi:10.1016/j.enconman.2012.03.006.
- [20] Pezzutto S. Hotmaps D2.3 WP2 Report – Open Data Set for the EU28. 2018.
- [21] Truong NL, Doodoo A, Gustavsson L. Effects of heat and electricity saving measures in district-heated multistory residential buildings. *Appl Energy* 2014;118:57–67. doi:10.1016/j.apenergy.2013.12.009.
- [22] Energiebilanzen. Stat AUSTRIA n.d. https://www.statistik.at/wcm/idc/idcplg?IdcService=GET_PDF_FILE&RevisionSelectionMethod=LatestReleased&dDocName=022717 (accessed May 8, 2018).
- [23] Fortschrittsbericht über die Umsetzung des Klimaschutzprogramms (KliP) der Stadt Wien n.d.:252.
- [24] Büchele R. Policies for RES-H/C: Results of the quantitative assessment (D4.2) n.d.:159.



16th International Symposium on District Heating and Cooling, DHC2018,
9–12 September 2018, Hamburg, Germany

Impact of Different Design Guidelines on the Total Distribution Costs of 4th Generation District Heating Networks

Isabelle Best*, Janybek Orozaliev, Klaus Vajen

University of Kassel, Institute of Thermal Engineering, Department Solar and Systems Engineering, Kurt-Wolters-Str. 3, 34125 Kassel, Germany

Abstract

When it comes to the design of new district heating networks, different design guidelines of different countries and pipe manufactures occur. All guidelines are aiming to restrict the specific pressure drop per meter pipe length to avoid uneconomic network operation. This paper evaluates the impact of different design guidelines from Sweden, Germany and Austria, as well as pipe manufacture recommendations on the total distribution costs. The analysis was conducted for a 4th generation district heating network for a new housing development (3 km trench length). The resulting district heating networks were compared in terms of total distribution costs. The results state that designing small networks at maximum heat load by allowing high specific pressure drops of 300 Pa/m shows the most economic results in terms of capital costs and variable costs. Compared to 70 to 100 Pa/m recommendations, 6 – 8 % investment costs for transportation pipes can be saved designing the network with 300 Pa/m pressure drops of short duration. Regarding distribution heat loss costs, the smaller the average diameter of the network the lower the heat distribution losses. Optimal network design leads to a 7 % heat loss reduction for the whole network. Furthermore, the paper compares total costs of the networks designed for two different design temperatures: 70°C supply with 40 °C return and 40°C supply temperature with 25 °C return. In terms of total distribution costs, both networks are very similar, which shows that ultra-low temperature networks have no economic disadvantages compared to state of the art 70°C networks, as often believed.

© 2018 The Authors. Published by Elsevier Ltd.

This is an open access article under the CC BY-NC-ND license (<https://creativecommons.org/licenses/by-nc-nd/4.0/>)

Selection and peer-review under responsibility of the scientific committee of the 16th International Symposium on District Heating and Cooling, DHC2018.

Keywords: Ultra-Low-Temperature District Heating, Heat Distribution Costs, Small District Heating Networks

*Isabelle Best Tel.: +0049 561 804 2508

E-mail address: solar@uni-kassel.de

1. Introduction

Various investigations have been conducted in the field of low-temperature district heating questioning design and operating temperatures of district heating-based heat supply systems. The studies investigated technological solutions, cost reduction potentials, and challenges specifically for low heat demand density areas. To name few: in [1] the IEA DHC CHP Annex VIII discussed and evaluated techniques for the reduction of piping costs and heat losses from heat distribution among others. Also in [2] the IEA DHC CHP Annex V addressed various research questions ranging from system engineering regarding substation design through energy-efficient DH networks to concepts and technologies for the new generation of DH systems. In [3] Tol and Svendsen demonstrated a new method to design district heating networks achieving smaller pipe diameters taking simultaneity of the heat consumers involved into account. Furthermore, Lund and Mohammadi in [4] pointed out that a higher insulation standard is the most feasible solution for 4th generation DH systems. When it comes to ultra-low-temperature district heating, several research questions arise regarding the domestic hot water preparation due to very low DH supply temperatures of 35 °C – 45 °C. Lund et al. in [5] compared three different alternative concepts for DH temperature level on a long-term energy system perspective. The study stated that a low-temperature DH of 55/25°C shows the lowest costs for DH systems in Denmark. Best et al. stated in [6] that ultra-low-temperature district heating ensures important improvement of heat distribution efficiency, favorable conditions for renewable heat integration while showing no economic disadvantage compared to low-temperature district heating. No study directly assessed the impact of design guideline on the total heat distribution costs and comparing low-temperature district heating networks of 70°C/40°C with ultra-low temperature district heating networks of 40°C/25°C, which is necessary to provide more general recommendations regarding the realization of new small networks for districts with low heat demands. In this study, the economic impact of different existing design guidelines on the total heat distribution costs is evaluated for new building developments. Therefore, four design approaches have been applied for network dimensioning and compared within an economic evaluation. Generally, a lower temperature level and temperature difference between supply and return line lead to higher volume flow rates. Consequently, the required transportation pipe diameters are affected. Energy utilities and plant operators fear increased auxiliary energy demand and high investment for heat distribution infrastructure. This study compares two exemplary networks of same length differing in terms of design and operating temperature. It aims at quantitative evaluation of the impact of design approach and temperature design on the total distribution costs of DH network.

Nomenclature

AGFW	German District Heating Association
CHP	Combined heat and power
DH	District heating
DHA	District heating agency
DHC	District heating and cooling
DHW	Domestic hot water
DIN	Deutsches Institut für Normung e.V.
DN	Nominal diameter
IEA	International Energy Agency
LTDH	Low temperature district heating
SH	Space heating
ULTDH	Ultra-low temperature district heating
ÖKL	Austrian board of trustees for Agricultural and Rural Development
VDI	Verein Deutscher Ingenieure

2. Description of Case Study

2.1. New building development in sub-urban areas

In this study a housing development in a rural to suburban area was determined showing a high share of single family houses and row houses. The new development has 133 buildings with around 260 accommodation units. One accommodation unit has 115 m² dwelling area in average. The buildings show a specific space heating (SH) demand of below 50 kWh/(m²·a) according to the German low-energy building standard of the Energy Saving Ordinance 2016 [7]. The domestic hot water (DHW) demand was calculated taking a DHW consumption of 40 l/(Pers·d) at tapping temperature of 45 °C as basis. A total heat demand of around 1.8 GWh/a results, thereof 23 % is due to DHW demand and 77 % due to SH demand. Two case studies were determined distinguishing between the DH network design and network operating temperature: Ultra-Low Temperature district heating (ULTDH) network design temperature with 40°C supply 25 °C return (40 °C/25 °C); Low-Temperature district heating (LTDH) network design temperature with 70 °C supply 40 °C return (70 °C/40 °C). An indirect coupling of DH network and system engineering was assumed consisting of following main components for each building: house substation with heat exchanger unit for floor heating system, hot water tank with external heat exchanger for DHW supply. The DH network is separated into three main branches. The resulting pipe route length sums up to 2.89 km.

2.2. Network Design Method

A calculation tool was developed, which computes the nominal diameter (DN) for each pipe section according to the underlying design recommendation. The design recommendations limit the flow velocity in order to ensure a specific pressure drop. The pipe surface roughness was set to 0.01 mm representing new smooth pipes. The inner diameter is computed to meet the peak load of connected buildings. The generally known correlations of Blasius and Prandl are used to compute the friction factor depending on the flow conditions [8]. The nominal diameter calculation is performed iteratively. If the specific pressure drop recommendation is exceeded, a higher nominal diameter is chosen. For both case studies the networks were designed for the maximum heat load taking simultaneity into account. The connecting rate for SH was determined based on peak heating load for each building according to DIN EN 12831 [9]. Additional connecting rate for DHW supply was computed applying the German norm DIN 4708 [10–12]. A simultaneity of 1 for SH was assumed due to the thermal inertia of floor heating systems and the high building standard. Regarding the DHW supply, the simultaneity correlation based on DIN 4708 was applied [10–12]. The heat loss rate was computed based on Wallentén in [13] taking two buried insulated pipes (supply and return line) as basis. The seasonal varying ambient temperature of Kassel (Germany) on an hourly basis was used to calculate the average heat loss rate of the network. Therefore, each pipe section of transportation pipe and house lead-in pipes (DN and insulation thickness) was considered. For Kassel an average ambient temperature of 9.8 °C was determined. The supply and return temperatures were kept constant over the year for heat loss calculation.

3. Design guidelines

To evaluate the effect of the chosen design guideline, it has been differentiated between four design guidelines. According to Nussbaum et al. [14] different design approaches exist, which are shown in Figure 1. Depending on the inner diameter, a flow velocity is recommended, which limits the specific pressure drop over the pipe length. A threshold of maximum specific pressure drop of 100 - 150 Pa/m is common in order to avoid increased pump energy demand and corrosion [15]. Swedish and Austrian (board of trustees for Agricultural and Rural Development -ÖKL) recommendations allow higher flow velocities causing pressure drops of up to 200 and 350 Pa/m respectively [16]. Additionally, the piping manufacturer's recommendations (Isoplus) were used in this study (marked in green). The Isoplus flow velocity recommendation shows flow velocities from 0.5 to 1.3 m/s for DN 20 to DN 200 resulting in specific pressure drops below 100 Pa/m [17]. It is assumed that the maximum heat load occurs less than 200 hours per year (pump operating hours to meet 80 % - 100 % of the heat load). According to the connected rate, a volume flow and the corresponding pipe diameter were computed for each branch.

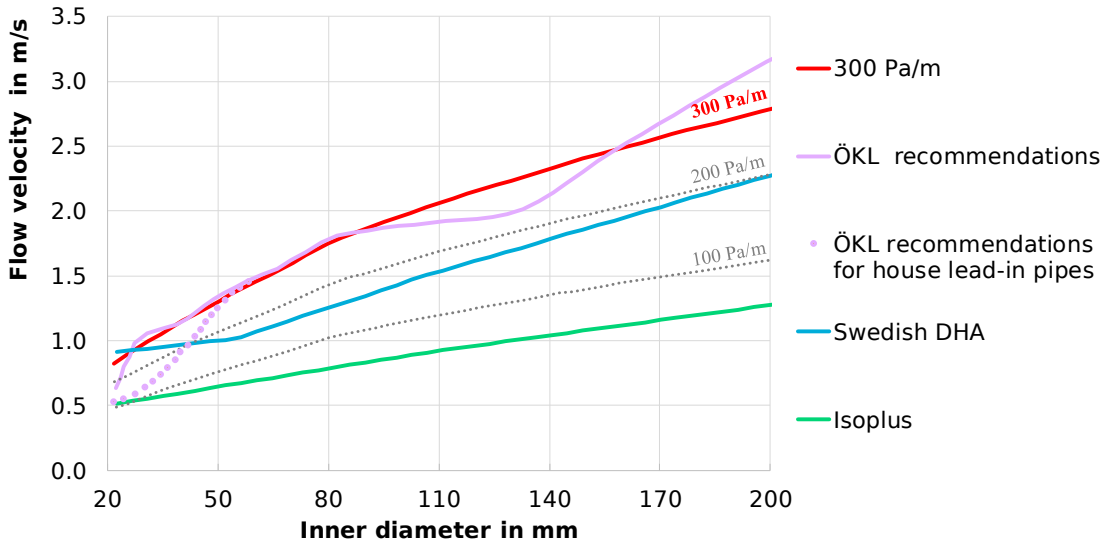


Figure 1: Design flow velocity curves as a function of inner diameter

4. Data for Cost Assessment

In order to evaluate the economic effect of different network designs, total network construction costs were considered. Table 1 gives an overview about the assumed costs. Total construction costs usually cover the pipe material costs, installation/ pipe laying costs and civil engineering costs, surface restoration costs and incidental construction costs. The surface restoration and civil engineering costs highly depend on the conditions of the construction site. Nast et al. [18] published costs for unmade terrain and rigid pipes for new building developments representing a medium cost approach. The specific construction costs range from 190 €/m_{trench} for DN 20 to 410 €/m_{trench} for DN 150. This medium cost approach was also approved by Klöpsch et al. [19] and can still be considered valid in 2018 according to the German District Heating Association AGFW. Nevertheless, there is an optimization potential according to Manderfeld et al. [20], who showed that specifically in rural areas the construction costs can be reduced using for example flexible pipes. This study assumed the medium cost approach of Nast et al. [18], because the costs should be calculated for new developments in Germany with standard rigid pipes.

Table 1: Data for Cost Assessment

Component	Specific Costs	Reference
Piping	190 €/m _{trench} (DN 25) – 410 €/m _{trench} (DN 150)	Nast et al. [18]
Pumps	3.300 €/unit – 3.500 €/unit	Manufacturer [21]
Substations	4.000 €/unit incl. water tank	Stuible et al. [22]
House lead-in costs incl. house connecting pipes	3.600 €/unit	Stuible et al. [22] & information of utility
Maintenance costs for distribution infrastructure	0.5 % of investment	German guideline VDI 2067 [23]
Maintenance costs substations	3.0 % of investment	German guideline VDI 2067 [23]
Planning costs	14 % of investment for transportation pipes and substations	German regulation HOAI [24]
Electricity tariff	0.17 €/kWh (major customer), 0.24 €/kWh (non-time-based customer)	Statistics for Germany 2017 [25]
Assumed variable costs	0.05 €/kWh	assumption

Furthermore, the additional costs for higher insulation standards were considered on the experience of pipe manufacturers. With reference to standard insulation, the higher insulation (class 2) results in 7 to 13 % higher construction costs, while the highest insulation standard (class 3) results in 16 % to 30 % higher specific construction costs [26]. The investment appraisal of the DH system was conducted pre-defining the investment period to the economic lifetime or operating time of the components and distribution infrastructure, which was set to 30 years for the distribution infrastructure and 15 years for substations. An annuity method was applied setting the interest rate to 5.6 %, representing a known hurdle rate (minimum rate of return the company will accept) from energy utilities. The capital costs are thus shown as present value (discounted value). The electricity costs were set constant due to many insecurities for a forecast.

5. Results

5.1. Case Study 1 – Impact of Network Design on Transportation Pipes of ULTDH

Based on the network dimensioning approach a nominal diameter for each pipe section was calculated depending on design guidelines. The DH network consist of approx. 55 % transportation pipes and 45 % of house-lead in pipes. The house lead-in pipe costs (house connecting pipes) are covered by a fix amount (see Table 1). In consequence, the design guidelines affect only the transportation pipe costs. Figure 2 (a) shows the resulting transportation pipe diameter distribution. The bar chart shows compared to the Isoplus standard through the Swedish and Austrian recommendations representing higher permitted flow velocities, an increase in share of DN 25 to DN 32, resulting in smaller average pipe diameters. The average transportation pipe diameter of the network design Isoplus is DN 65 for the given DH network. In comparison to this, the Swedish and Austrian (ÖKL) design guidelines result in an average pipe diameter of DN 50 respectively.

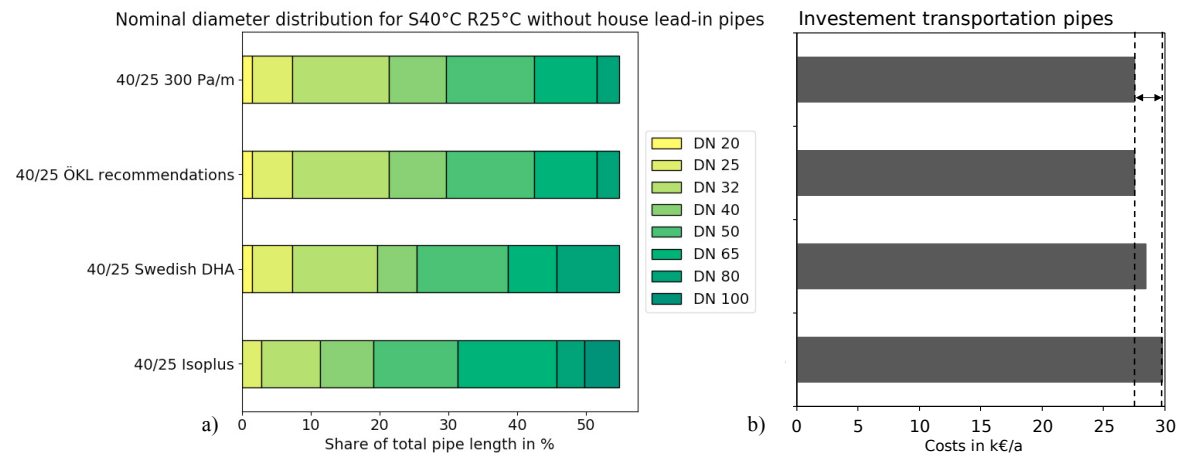


Figure 2: Nominal Diameter distribution of different network designs for ULTDH 40 °C/25 °C (a, left); corresponding investment rate (discounted value) for transportation pipes of different network designs (b, right)

The average network construction costs of range from Isoplus 244 €/m_{trench}, Swedish DHA of 233 €/m_{trench} to ÖKL 226 €/m_{trench}. Thereby the Swedish DHA design guideline already leads to a total investment cost reduction of 4.5 %. Applying the ÖKL guidelines or simply a pressure drop limitation of 70 – 100 Pa/m (Isoplus) (see Figure 2 (b)).

5.2. Case Study 1 - Total Distribution Costs ULTDH

The total distribution costs consist of capital costs, pressure loss costs, heat loss costs, and maintenance costs. The capital costs include investment for transportation pipes, house-in lead costs and house connecting pipes, substations, and pumps. The pressure loss costs indicate the electricity consumption by the network pumps. The maximum needed volume flow and corresponding maximum pressure drop for the different network designs are given in Table 2. The

numbers represent the pressure drop of each branch, because each branch is assumed to have an own pump. Therefore, for each DH branch a high efficiency network pump was designed according to the calculated pressure drop and needed volume flow. For the determination of the annual electricity consumption, the heat load characteristic of the building development was taken as basis at constant operating temperatures. Furthermore, it was assumed that the pumps are controlled as a function of differential pressure. For the highest total pressure drop of 3.8 bar, the total nominal electrical pump power is 3.2 kW. This results in an electricity consumption of 8.7 MWh/a for year-round network operation and causes pressure loss costs of 1.5 k€/a.

Next to the pressure loss costs, the heat loss costs determine the variable costs. Table 3 shows the total average heat loss rate of network designs. The heat loss rate causes heat loss costs of 9.4 – 10 k€/a, which represents seven times of pressure loss costs. The results state a maximum average heat loss rate reduction of 5.9 % applying network design guidelines with ≥ 300 Pa/m. Furthermore, installing piping of highest insulation class reduces the yearly heat distribution losses about around 22 %. This results in cost savings of around 2.0 k€/a compared to standard insulation irrespective of the applied design guideline.

Table 2: Maximum pressure drop and greatest volume flow according to network design at design temperatures 40 °C/25 °C

Network design	Maximum pressure drop for each branch in bar	Total pressure drop in bar	Maximum needed volume flow in m ³ /h
300 Pa/m	1.3 / 1.8 / 0.7	3.8	17.1 / 21.7 / 24.1
ÖKL	1.3 / 1.8 / 0.7	3.8	17.1 / 21.7 / 24.1
Swedish DHA	1.1 / 1.1 / 0.7	2.9	17.1 / 21.7 / 24.1
Isoplus	0.5 / 0.7 / 0.4	1.6	17.1 / 21.7 / 24.1

Table 3: Total average heat loss rate and heat loss costs at variable costs of 0.05/kWh

Network design	Total average heat loss rate for standard insulation in kW	Total average heat loss rate for third insulation class in kW	Heat loss costs for standard insulation in k€/a	Heat loss costs for third insulation class in k€/a
300 Pa/m	21.5	16.9	9.4	7.4
ÖKL	21.5	16.9	9.4	7.4
Swedish DHA	21.9	17.2	9.6	7.5
Isoplus	22.8	17.8	10	7.8
Highest Saving through different network design	5.9 %	5.1 %	0.6 k€/a	0.4 k€/a

The total distribution costs are shown for the standard insulation class (see Figure 3). The bar chart shows the overall distribution heat costs for each network design. The investment of transportation pipes represents 20 % of the total heat distribution costs. 53 % of the total distribution costs are due to investment for house lead-in (including house connecting pipes) and substations. Investment for network pumps play a subordinated role. The variable costs represent around 8 % of the total heat distribution costs and cover the heat loss costs as well as the pressure loss costs (electricity consumption of pumps). The heat loss costs amount to 87 % of the variable costs and determine the variable costs mainly. Thus, the pressure loss costs amount to around 1 % of total heat distribution costs and are insignificant even in case of ULTDH. The overall distribution costs decrease slightly with higher accepted flow velocity. The most important change was stated for the ÖKL network design and the upper pressure drop limit of 300 Pa/m. However, the impact of the design guideline affects the investment of transportation pipes only. Thus, the impact of design optimization towards smaller pipe diameters on the total heat distribution costs is restricted. In total, permitting specific pressure drops of 300 Pa/m saves 2.2 % of total heat distribution costs compared to design recommendations

of 70 – 100 Pa/m (see Figure 3). For the given assumptions, this is a yearly saving of 3.3 k€/a. This applies specifically for small networks and small pipe diameters.

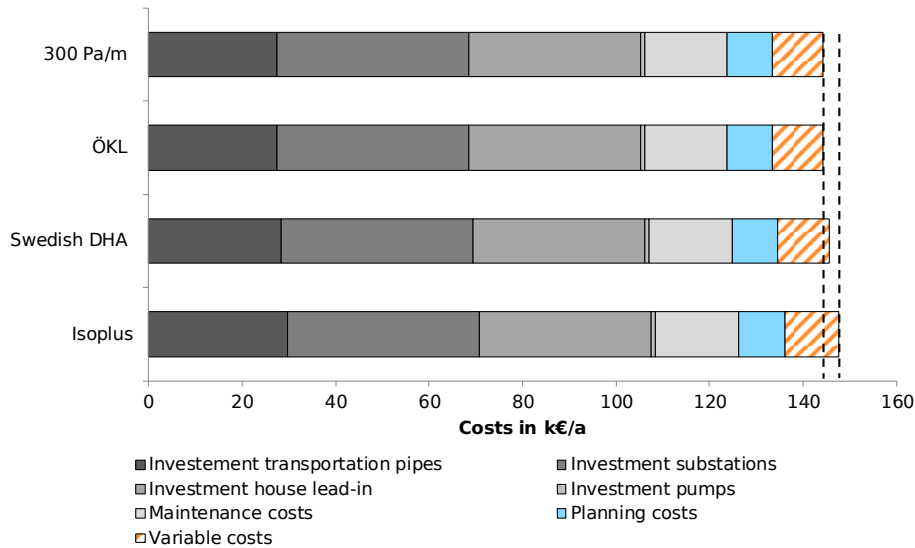


Figure 3: Total distribution costs of different network designs for ULTDH

The impact increases with higher pipe diameters due to the proportionally higher network construction costs of diameters greater than DN 65. An increase of insulation class to the highest insulation class decreases the heat loss costs about 22 %. On the other hand, the investment of transportation pipes would increase about 26 % that results in an overall distribution cost increase of 4.6 %.

5.3. Case Study 2 – Impact of Network Design on Transportation Pipes of LTDH

Analogously to the first case study, a nominal diameter for each pipe section was calculated depending on design guideline flow velocity restriction. Figure 4 (a) shows the resulting transportation pipe diameter distribution for LTDH. The bar chart shows a significantly higher share of DN 20 to DN 32 in comparison with ULTDH network. This is mainly because of the higher temperature difference between supply and return (30 K). This leads to lower needed volume flows to meet heat load resulting in smaller pipe diameters. Following the Isoplus guideline, the total investment for transportation pipes is 27 k€/a (discounted value), which is 3 k€/a less than in terms of the ULTDH network. The Isoplus DH network design shows an average pipe diameter of DN 50, while the Swedish DHA, the ÖKL guideline, and 300 Pa/m design lead to DN 40. The average network construction costs of range from Isoplus 221 €/m_{trench}, to Swedish DHA 211 €/m_{trench}, to ÖKL 208 €/m_{trench}. It can therefore be concluded that permitting pressure drops of 300 Pa/m leads to an average pipe diameter reduction of one DN size for small networks. The Swedish DHA design guideline already leads to an investment cost reduction of 4.5 %. Along the design guidelines a maximum investment cost saving of 6.1 % was calculated.

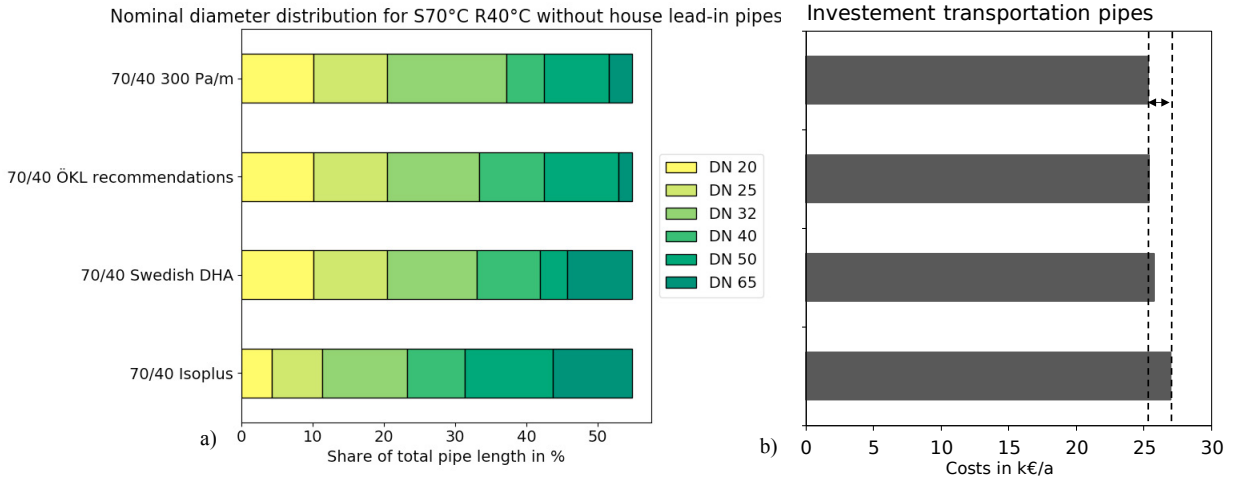


Figure 4: Nominal Diameter distribution of different network designs for LTDH 70 °C/40 °C (a, left); corresponding investment rate (discounted value) for transportation pipes of different network designs (b, right)

5.4. Case Study 2 - Total Distribution Costs LTDH

The total distribution costs were calculated analogously to the ULTDH case study (see Table 4). The LTDH network needs at peak load a total maximum volume flow of 31 m³/h. The nominal electrical pump power was calculated according to the maximum pressure drop of each network branch. Along the network designs, the maximum pressure drop is nearly tripled. However, the maximum pressure drop occurs at peak load only. The pressure drop follows the heat load, leading to much lower average pressure drops in the main time of the year. For the ÖKL design, a total nominal electrical pump power of 1.7 kW is needed, which leads to pressure loss costs of 0.73 k€/a. Thus, the pressure loss costs of LTDH are halved compared to the ULTDH, which is due to the higher design temperature difference between supply and return.

Table 4: Maximum pressure drop and greatest volume flow according to network design at design temperatures 70 °C/40 °C

Network design	Maximum pressure drop for each branch in bar	Total pressure drop in bar	Maximum needed volume flow in m ³ /h
300 Pa/m	1.5 / 1.3 / 0.8	3.6	8.6 / 10.9 / 12.1
ÖKL	1.1 / 1.3 / 0.8	3.2	8.6 / 10.9 / 12.1
Swedish DHA	0.9 / 1.1 / 0.7	2.7	8.6 / 10.9 / 12.1
Isoplus	0.4 / 0.6 / 0.3	1.3	8.6 / 10.9 / 12.1

Table 5: Total average heat loss rate and heat loss costs at variable costs of 0.05/kWh

Network design	Total average heat loss rate for standard insulation in kW	Total average heat loss rate for third insulation class in kW	Heat loss costs for standard insulation in k€/a	Heat loss costs for third insulation class in k€/a
300 Pa/m	39.1	31.1	17.1	13.6
ÖKL	39.5	31.4	17.3	13.7
Swedish DHA	40	31.6	17.5	13.8
Isoplus	42.1	33.1	18.4	14.5
Highest Saving through different network design	6.9 %	5.9 %	1.3 k€/a	0.9 k€/a

However, the average heat loss rate increases significantly compared to LTDH (see Table 5). It varies from 39.1 to 42.1 kW depending on the network design guideline. Applying ÖKL design recommendations reduces the average

heat loss rate about 6.9 % compared to the Isoplus design. The resulting heat loss costs range from 17.1 k€/a to 18.4 k€/a, which means heat loss costs are twice as high compared to ULTDH. Furthermore, installing piping of highest insulation class reduces the yearly heat distribution losses about around 21 %. This results in cost savings of approx. 3.5 – 3.9 k€/a compared to standard insulation. The total distribution costs of LTDH are shown for the standard insulation class (see Figure 5). The bar chart shows the overall distribution heat costs for each network design. At the first glance, the overall distribution costs decrease slightly with higher accepted flow velocity analogously to ULTDH. However, the investment of transportation pipes represents 18 % of the total heat distribution costs and the share of variable costs is 13 %. The total distribution costs range from 148.6 k€/a to 151.9 k€/a, which is app. a 3 % increase compared to ULTDH. Permitting max. specific pressure drops of 300 Pa/m saves 2.1 % of total heat distribution costs compared to design recommendations of 70 – 100 Pa/m (Isoplus). For the given assumptions, this is a yearly saving

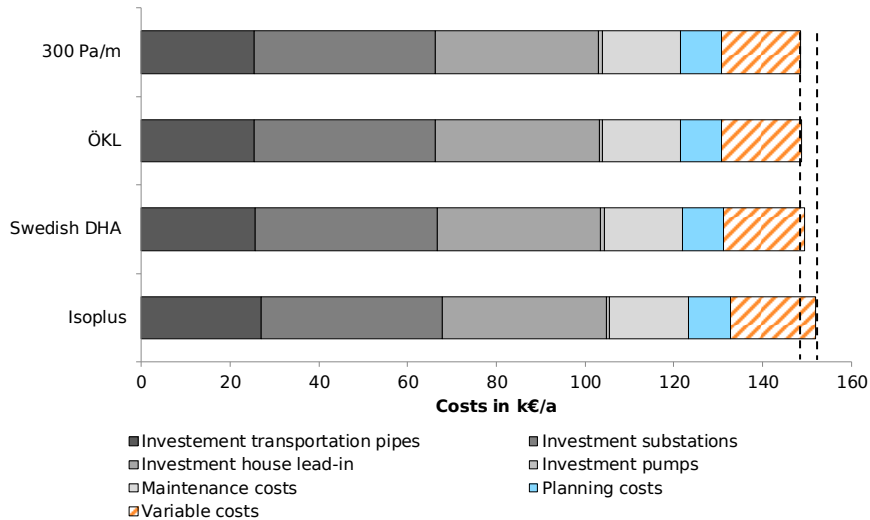


Figure 5: Total distribution costs of different network designs for LTDH

of 3.2 k€/a. An increase of insulation class to the highest insulation class reduces the heat loss costs about 20 %. On the other hand, the investment of transportation pipes increases about 26 % leading to an overall distribution costs increase of 2.6 %. Nevertheless, the results demonstrate that the impact of diameter optimization is restricted because it affects the transportation pipes only. The cost share of house lead-in (including house connecting pipes) and substations represents 68 % of the total fix costs. These large elements of distribution costs need to be reduced to achieve a significant overall distribution costs reduction.

6. Summary and Discussion

This study aimed at analyzing the impact of design recommendations on total distribution costs of small networks of 4th generation DH. The economic assessment was conducted taking a new building development comprising of 133 buildings as a case study. The building development shows a high share of single family and row houses representing a rural to suburban area. The impact of the guidelines was analyzed on two DH network types of different design and operating temperature. First, the impact of design guideline on the investment of transportation pipes was assessed. The results stated that allowing high specific pressure drops of ≥ 300 Pa/m at maximum heat load leads to transportation pipe investment savings of 6 – 8 % compared to 70 to 100 Pa/m recommendations. In terms of total heat distribution costs, the design guideline has little effect. This is preliminary due to the high share of house lead-in costs and substations costs, that represent 68 % of fix costs. The house lead-in pipes are covered by a fix amount, which is independent of the design guidelines. In consequence, the design guidelines affect the transportation pipes primarily. Thus, the impact of design optimization towards smaller pipe diameters on the total heat distribution costs is restricted. Nevertheless, the results show that next to investment savings the variable costs in terms of heat loss costs are reduced about 7 %. The comparison of ULTDH network (case study 1) with LTDH network (case study 2) stated, that ULTDH leads to slightly lower total distribution costs due to lower heat loss rate of the network. The

pressure loss costs achieve 1 % of the overall distribution costs, thus they have no significant impact on the economics of distribution networks. It has been shown, that ULTDH networks have no economic disadvantages compared to state of the art LTDH networks, as often believed. This study assessed only the impact of different DH network designs on heat distribution costs. It was not aimed at investigating the total heat supply system. Thus, ULTDH and LTDH were compared in terms of distribution costs, without central heat supply units and in case of ULTDH supplementary heating units in buildings to meet the DHW set temperatures.

Acknowledgements

The project partners greatly acknowledge the financial support of the project by the German Federal Ministry of Economic Affairs and Energy. (FKZ: 03ET1336C).

References

- [1] Zinko H, Bøhm B, Kristjansson H, Ottosson U, Sipilä K. District heating distribution in areas with low heat demand density. International Energy Agency Implementing Agreement on District Heating and Cooling. IEA-Report, IEA DHC Annex VIII. 1704-05-02-01-005 8DHC-08-03; 2008.
- [2] Rosa AD, Li H, Svendsen S, Werner S, Persson U, Ruehling K et al. Toward 4th Generation District Heating Final Report: Experience and Potential of Low-Temperature District Heating. IEA DHC CHP Annex X Final Report; 2014.
- [3] Tol HJ, Svendsen S. Improving the dimensioning of piping networks and network layouts in low-energy district heating systems connected to low-energy buildings: A case study in Roskilde, Denmark. *Energy* 2012;38(1):276–90.
- [4] Lund R, Mohammadi S. Choice of insulation standard for pipe networks in 4th generation district heating systems. *Applied Thermal Engineering* 2016;98:256–64.
- [5] Lund R, Østergaard DS, Yang X, Mathiesen BV. Comparison of Low-temperature District Heating Concepts in a Long-Term Energy System Perspective. *International Journal of Sustainable Energy Planning and Management* 2017;12(0):5–18.
- [6] Best I, Orozaliev J, Vajen K. Economic comparison of low-temperature and ultra-low-temperature district heating for new building developments with low heat demand densities in Germany. *International Journal of Sustainable Energy Planning and Management* 2018(Vol. 16):45–60.
- [7] GRE Gesellschaft für Rationelle Energieverwendung e. V. Energieeinsparverordnung 2016. Düsseldorf: Bau+Technik GmbH; 2016.
- [8] Böswirth L, Bschorer S, Buck T. Technische Strömungslehre: Lehr- und Übungsbuch. 10th ed. Wiesbaden: Springer Vieweg. 978-3-658-05668-1; 2014.
- [9] Deutsches Institut für Normung e. V. Heating system in buildings - Method for calculation of the design heat load - Supplement 2: Simplified method for calculation of the design heat load and the heat generator capacity(12831 Beiblatt 2): Beuth Verlag GmbH; 2012.
- [10] Deutsches Institut für Normung e. V. Zentrale Wassererwärmungsanlagen Begriffe und Berechnungsgrundlagen(4708 Teil 1). Berlin: Beuth Verlag GmbH; 1994.
- [11] Deutsches Institut für Normung e. V. Zentrale Wassererwärmungsanlagen Regeln zur Leistungsprüfung von Wassererwärmern für Wohngebäude(Teil 3). Berlin: Beuth Verlag GmbH; 1994.
- [12] Deutsches Institut für Normung e. V. Zentrale Wassererwärmungsanlagen Zentrale Wassererwärmungsanlagen Regeln zur Ermittlung des Wärmebedarfs zur Erwärmung von Trinkwasser in Wohngebäuden(4708 Teil 2). Berlin: Beuth Verlag GmbH; 1994.
- [13] Wallentén P. Steady-state heat loss from insulated pipes. *Byggnadsfysik LTH: Lunds Tekniska Högskola*; 1991.
- [14] Nussbaumer T, Thalmann S. Status Report on District Heating Systems in IEA Countries. prepared for the International Energy Agency IEA Bioenergy Task 32 and Swiss Federal Office of Energy ISBN: 3-908705-28-2; 2014.
- [15] Frederiksen S, Werner S. District Heating and Cooling. Lund: Studentlitteratur. 978-91-44-08530-2; 2013.
- [16] ÖKL-Arbeitskreis Landwirtschaftsbau. Planung von Biomasseheizwerken und Nahwärmenetzen(67). Wien: Österreichisches Kuratorium für Landtechnik und Landentwicklung; 2016.
- [17] ISOPLUS. Planungshandbuch: Kapitel Starre Verbundsysteme. [May 25, 2018].
- [18] Nast M, Ragwitz M, Schulz W, Bürger V, Leprich U, Klinski S. Ergänzende Untersuchungen und vertiefende Analysen zu möglichen Ausgestaltungsvarianten eines Wärmegesetzes: Ausarbeitung im Auftrag des Bundesministeriums für Umwelt, Naturschutz und Reaktorsicherheit; 2009.
- [19] Klöpsch M, Besier R, Wagner A. Reicht für Kunststoffantelrohre die Standarddämmung?: Wirtschaftliche Dämmung von KMR. *Euro Heat & Power* 2009(12):46–54.
- [20] Manderfeld M, Jentsch A, Pohlh A, Dötsch C, Richter S, Bohn K. Abschlussbericht Forschungsvorhaben Fernwärme in der Fläche RDH (Rural District Heating) : Ermittlung des Fernwärmepotentials unter Berücksichtigung der neuester Verlegeverfahren und unterschiedlicher Energiedarangebote in der Fläche der Bundesrepublik Deutschland; 2008.
- [21] wilo. high efficiency pumps: Stratos 40/ 1-16 PN 6/10, Stratos GIGA 50/ 1-20/1,2, operating mode dp-v. [2017].
- [22] Stuible A, Zech D, Wülbeck H-F, Sperber E, Nast M, Hartmann H et al. Evaluierung von Einzelmaßnahmen zur Nutzung erneuerbarer Energien im Wärmemarkt (Marktanreizprogramm) für den Zeitraum 2012 bis 2014: Evaluierung des Förderjahres 2014; 2016.
- [23] Verein Deutscher Ingenieure e. V. Economic Efficiency of building - Fundamentals and economic calculation VDI 2067 Blatt 1(2067): Beuth Verlag GmbH; 2012.
- [24] Bundesministerium für Wirtschaft und Energie. Verordnung über die Honorare für Architekten und Ingenieurleistungen (Honorarordnung für Architekten und Ingenieure - HOAI): Beuth Verlag GmbH; 2013.
- [25] Statista GmbH. statista: Strompreise für Haushaltskunden. [January 16, 2018]; Available from: de.statista.com.
- [26] thermaflex. detailed data about network construction costs based on project experiences; 2018.



16th International Symposium on District Heating and Cooling, DHC2018,
9–12 September 2018, Hamburg, Germany

Anthropogenic impact of Moscow district heating system on urban environment

G.G. Alexandrov, A.S. Ginzburg*

A.M. Obukhov Institute of Atmospheric Physics Russian Academy of Sciences, Pyzhevsky per., 3, Moscow, 119017, Russian Federation

Abstract

Moscow City district heating system is the largest in the world and study of its impact on urban environment is important for understanding and managing possibilities for increasing energy demand efficiency within large urban agglomerations. This research estimated and analyzed carbon and thermal emissions of the Moscow district heating system.

Moscow City district heating system is the largest in the world and understanding of its anthropogenic impact on environment, such as CO₂ emissions or thermal emissions, is important for understanding and managing possibilities within different urban agglomerations. The heat supply system of Moscow differs from its counterparts in European cities. It is unique in terms of its scale and is generally comparable to individual EU nations in terms of major characteristics. For example, in 2012, the total length of pipelines in Moscow was 16,323 km and the associated contractual thermal load was 19 GW, which exceeds the corresponding aggregate figures for Finland (roughly 13,600 km and 18.5 GW, respectively).

In this study authors present the analysis, based on official data of energy use for district heating, which is intended to show “end-user” CO₂ and thermal emissions, that represent the consumers and not producers. This research estimates and analyze CO₂ emissions and thermal emissions of the Moscow district heating system at the Moscow Administrative Districts level and shows that CO₂ emissions for districts vary from 1.16 to 6.74 Mt CO₂/year and mean annual thermal emissions vary from 23 to 75 W/m².

© 2018 The Authors. Published by Elsevier Ltd.

This is an open access article under the CC BY-NC-ND license (<https://creativecommons.org/licenses/by-nc-nd/4.0/>)

Selection and peer-review under responsibility of the scientific committee of the 16th International Symposium on District Heating and Cooling, DHC2018.

Keywords: District heating system, urban environment, heat fluxes, carbon emission

* Corresponding author. Tel.: +7-910-423-1434.

E-mail address: gin@ifaran.ru

1. Introduction.

Cities are the main global source of greenhouse gases, as well as of thermal, gas and aerosol pollution of the atmosphere. Studies show that 70% of global greenhouse gas emissions occur precisely at the expense of cities [1]. In metropolitan areas located at the mid latitudes of the Northern Hemisphere - Europe, Russia, the United States, Canada - the largest source of anthropogenic heat fluxes and greenhouse gases are heat supply systems along with urban transport.

The influence of the largest in the world Moscow district heating system (DHS) on the ecology and climate of the metropolis deserves special attention. These studies allow us to assess the relationship between energy consumption in the city and its climatic characteristics. Investigating this relationship for urban agglomerations is important due to the expected climate change and the urban environment, including an increase of extreme weather events. Only if this relationship is considered, it is possible to provide energy efficient heat supply to Moscow and sustainable development of urban infrastructure.

From the different aspects of the impact of the city's energy supply on climatic and ecological characteristics, this article looks at two main types of Moscow DHS impact on the city's ecological and climatic system: anthropogenic heat fluxes (AHF) and carbon dioxide emissions (i.e., carbon footprint).

The project "Analysis of the regional climate change impact on energy consumption of municipal services of megalopolises of Russia", supported by the Russian Scientific Foundation is carried out by the authors of the article together with other scientists of the Institute of Atmospheric Physics and the Moscow Power Engineering Institute. The project is aimed to identify the main factors of interrelationship between climatic and energy processes in the urbanized areas of urban agglomerations of Russia, and, first, the Moscow agglomeration.

In previous works authors with colloquies analyzed anthropogenic heat fluxes for cities agglomerations based on per capita energy consumption data [7, 11], impact of climate change on total Moscow’s energy consumption during the heating season [9], as well as impact of urbanization and global warming on total energy consumption in some large cities [10].

This article focused on thermal and carbon emissions in Moscow’s atmosphere caused by district heating system and distribution of thermal and carbon footprint among Moscow city districts. This could be done by using "final heat consumer" approach, and not only data of city thermal power plants energy production. This approach allows us to compare the ecological footprint of different districts of the city within 2011 Moscow city boundaries, using the official data provided by Moscow city department of fuel and energy on the heat supply of the administrative districts of the city.

Also, it allows to compare the distribution of anthropogenic heat fluxes within the city calculated by two different approaches – first one based on per capita energy consumption, second one based on heat supply data.

As it is well known [2], half of all urban total energy consumption in EU cities is-used for space heating and cooling as it is shown on Fig. 1. Situation with energy demand for space heating in Moscow is very similar to EU, and less than 1 % of total energy demand is used for space cooling.

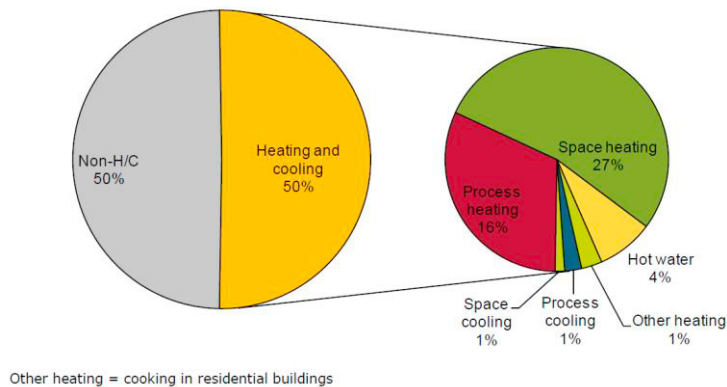


Figure 1. Heating and cooling demand in 2015 in the EU28 by end-use compared to total energy demand (adopted from [2])

2. Moscow basic information

An ecological footprint of a heat supply system is a result of such characteristics of the city as area, population, infrastructure and climate. Let us present some basic information about Moscow:

- Moscow is the capital of Russian Federation and the most populous urban area on European continent. Besides, it is the major political, economic, cultural, and scientific center of Russia and Eastern Europe.
- Moscow is the northernmost and coldest megacity and metropolis on Earth. Moscow has a humid continental climate with long, cold winters usually lasting from mid-November through the end of March, and warm summers. Weather can fluctuate widely with temperatures ranging from $-25\text{ }^{\circ}\text{C}$ in the city and $-30\text{ }^{\circ}\text{C}$ in suburbs to above $5\text{ }^{\circ}\text{C}$ in the winter, and from 10 to $35\text{ }^{\circ}\text{C}$ in the summer. The lowest ever recorded temperature was $-42\text{ }^{\circ}\text{C}$ in January 1940. Snow, which is present for about five months a year, often begins to fall mid-October, while snow cover lies in November and melts in the beginning of April.
- The heating season in Moscow begins when the average daily temperature over the past five days is kept below $8\text{ }^{\circ}\text{C}$, and ends, respectively, when the average daily temperature over the past five days is kept above $8\text{ }^{\circ}\text{C}$. Over the past 10 years, the duration of the period with a daily temperature below $8\text{ }^{\circ}\text{C}$ was 214 days, and the average daily temperature of this period was $3.1\text{ }^{\circ}\text{C}$.
- A part of Moscow Oblast (region) territory was merged into Moscow on July 1, 2012; as a result, Moscow is no longer fully surrounded by Moscow Oblast and now also has a border with Kaluga Oblast. In this paper the area of the Moscow districts is assumed within 2011 Moscow boundaries.
- The area, population, population density and heat supply for ten Moscow districts are taken from [3], [4], [5] and presented in Table 1. The presented heat supply data in Table 1 as accurate for 01.01.2012 [5].

Table 1. Area, inhabitants, population density and mean annual heat supply of Moscow districts within 2011 city boundaries

Moscow administrative okrugs (Moscow districts)	Area (km ²)	Inhabitants	Population density (per km ²)	Heat supply (Gcal/h)
Central	66.18	757137	11441	4287.15
Northern	113.73	1141913	10041	3566.81
North-Eastern	101.88	1398481	13726	3757.73
Eastern	154.84	1489765	9622	3668.33
South-Eastern	117.56	1352303	11503	3983.04
Southern	131.77	1754613	13315	4338.68
South-Western	111.36	1407331	12637	3336.24
Western	153.03	1333813	8716	4160.88
North-Western	93.28	973629	10438	2292.27
Zelenogradsky	37.20	229926	6181	737.12
Moscow (2011)	1080.83	11838911	11203	34128.3

The area of two new Moscow districts – Novomoskovsky and Troitsky – almost twice large then area of whole “old” Moscow, but much less populated: approximately 250,000 inhabitants live there. The “new” Moscow is consisting of suburb and rural territories and relatively small towns, which can’t be taken as a part of megalopolis. The district heating system in these districts is not so developed as within “old” Moscow and is not united with it. The ecological footprint of the new Moscow districts could be a subject of future research. In this paper we consider the district heating system of the “old” Moscow only.

3. Moscow District Heating System (DHS)

According to International Energy Agency (IEA) statement (CHP/DH Country Profile: Russia, 2009) Russia has the largest and oldest district heating system in the world. It is more than 100 years old and comprising almost 500 combined heat and power stations, 200 000 km of district heating (DH) pipeline network and more than 65,000 boiler houses. Russia's municipal district heating systems are a legacy of the Soviet era on which most of the country's urban population has come to depend during the long and cold winter season [6]. Russian district heating systems in 2007 delivered of about 1,700 TWh. This amount almost 10 times larger than the other largest system, Ukraine (less than 200 TWh) and Poland (under 100 TWh) [6].

In Moscow, heat is mostly produced by large combined-heat-and power plants (CHPs). According to data of 2007, an installed heat capacity was 32 250 Gcal/h, producing 79.9 Million Gcal per year (77 % of Moscow heat supply), 70 district and local heating plants (DHPs and LHPs) with an installed heat capacity of 13 700 Gcal/h, producing 22.7 Million Gcal per year (22 % of Moscow heat supply), and 100 local boilers (LBs) producing less than 1 % of Moscow heat supply.

In 2012, the length of pipelines in Moscow was 16,323 km, and the associated contractual heat load was about 19 GW, exceeding the similar system in whole Finland (about 13,600 km and 18.5 GW, respectively).

Nowadays, JSC "Mosenergo" belong within Gazprom Energoholding LLC is the largest regional power generating company in the Russian Federation, owning 15 power plants in Moscow region with an installed heat capacity of 42,8 thousand Gcal/h and produces 80 % of Moscow heat supply.

JSC "Moscow Integrated Power Company" (MIPC or MOEK) belong within Gazprom Energoholding LLC is the infrastructure company, providing the heating and hot water supply for Moscow and several satellite cities. The activity of the company covers production, transport, distribution and sale of heat energy.

Moscow district heating system covers 96% of heat consumers using mostly natural gas as a fuel and very small amount of coal, diesel and mazut as shown at Fig. 2 [5].

Moscow DHS annually consumes about 31 million tonnes of oil equivalent (toe) of natural gas, about 250 thousand toe of coal and about the same amount of diesel and mazut.

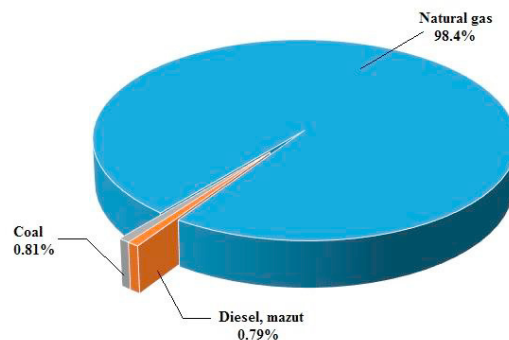


Figure 2. Moscow DHS fuel consumption chart

4. Moscow DHS heat and carbon emission

4.1. Anthropogenic heat fluxes

For the empirical assessment of total anthropogenic heat fluxes in urbanized areas, based on the analysis of national statistics on energy consumption, area and population of cities, the formula [7] is used:

$$Q_a = k \cdot PD \cdot EC \quad (1)$$

Where

Q_a is anthropogenic heat flux (W/m^2)

PD is urban population density (inhabitants/ km^2),

EC is energy consumption per capita in the country (kg o. e.),

$k = 1.325$ (see [7]).

Anthropogenic heat fluxes caused by space heating could be calculated using data of district heat supply [5] and next formula

$$AHF = G \cdot \frac{C_{GW}}{S} \quad (2)$$

Where

G is district heat supply (presented in Table 1),

S is district area (presented in Table 1),

C_{GW} is transfer coefficient from Gcal/h to kW (1 Gcal/h = 1162.22 kW).

The distribution of annual total anthropogenic heat fluxes and anthropogenic heat fluxes caused by DHS presented on Fig. 3 and 4 and in Table 2.

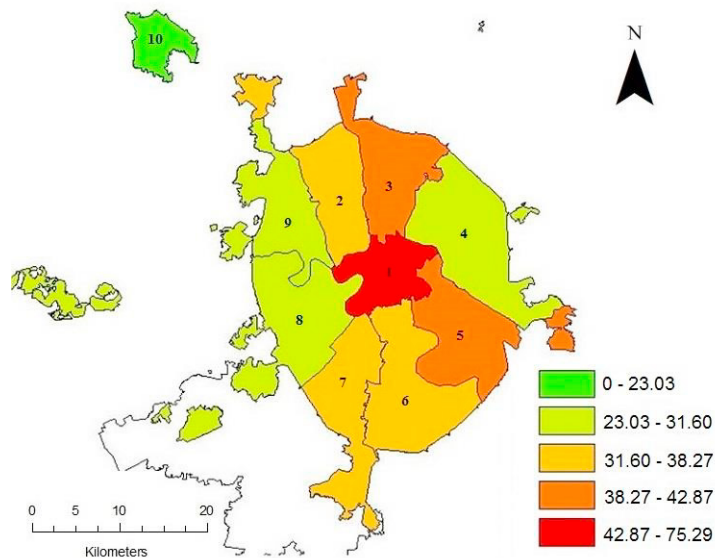


Figure 3. Total annual anthropogenic heat fluxes over Moscow districts calculated by formula (1).

(1 - Central district, 2 - Northern district, 3 - North-Eastern district, 4 - Eastern district, 5 - South-Eastern district, 6 - Southern district, 7 - South-Western district, 8 - Western district, 9 - North-Western district, 10 - Zelenogradsky district)

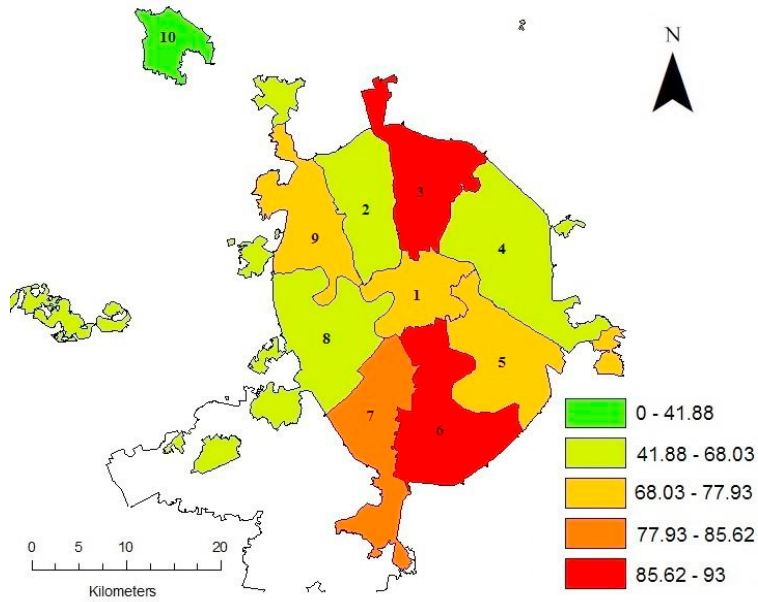


Figure 4. Anthropogenic heat fluxes over Moscow districts using Moscow DHS heat supply data. (1 - Central district, 2 - Northern district, 3 - North-Eastern district, 4 - Eastern district, 5 - South-Eastern district, 6 - Southern district, 7 - South-Western district, 8 - Western district, 9 - North-Western district, 10 - Zelenogradsky district)

Table 2. Anthropogenic heat fluxes (W/m^2) over Moscow districts and whole Moscow city calculated by formula (1) and estimated using Moscow DHS heat supply data.

Moscow districts	Formula (1)	DHS heating supply
Central	77.51	75.29
Northern	68.03	36.45
North-Eastern	93.00	42.87
Eastern	65.19	27.53
South-Eastern	77.93	39.38
Southern	90.21	38.27
South-Western	85.62	34.82
Western	59.05	31.60
North-Western	70.72	28.56
Zelenogradsky	41.88	23.03
Moscow (2011)	74.21	36.70

Fig. 3 and 4 as well as Table 2 show that average total emission of anthropogenic heat from the Moscow DHS approximately twice less than from all urban energy sources. The only within the Central district – Moscow “downtown” – almost whole AHF amount produced by heating of living and public spaces. For whole Moscow the picture is very similar to EU cities, where half of energy is using for space heating [2].

4.2. Carbon footprint.

To calculate anthropogenic carbon dioxide emissions caused of Moscow district heating system we use the data on the amount of combusted natural gas and the amount of heat supplied to administrative districts. In 2012, 29 billion cubic meters of natural gas were burnt in Moscow for heat supply.

According to [8], the coefficient for calculating CO₂ emissions from natural gas combustion is 1.85 t CO₂/m³. Using this coefficient, it is possible to estimate the total annual release of CO₂ into the atmosphere from burning natural gas for heating. In Moscow, where 29 billion cubic meters of natural gas are annually-burnt, this value is 53.65 Mt CO₂.

Using data on the amount of heat supplied to specific districts of Moscow [5], it is possible to estimate the amount of CO₂ emitted annually by each district – C_{DH} using the following formula:

$$C_{DH} = C \cdot \frac{G_{DH}}{G_t} \quad (3)$$

Where

G_{DH} is district heat supply in Gcal/h,

G_t is total Moscow heat supply (34,130 Gcal/h),

C is total annual Moscow CO₂ emission from district heating system (53.65 Mt CO₂).

Results of Moscow DHS carbon footprint calculations are presented on Fig. 5 and 6 as well in Table 3.

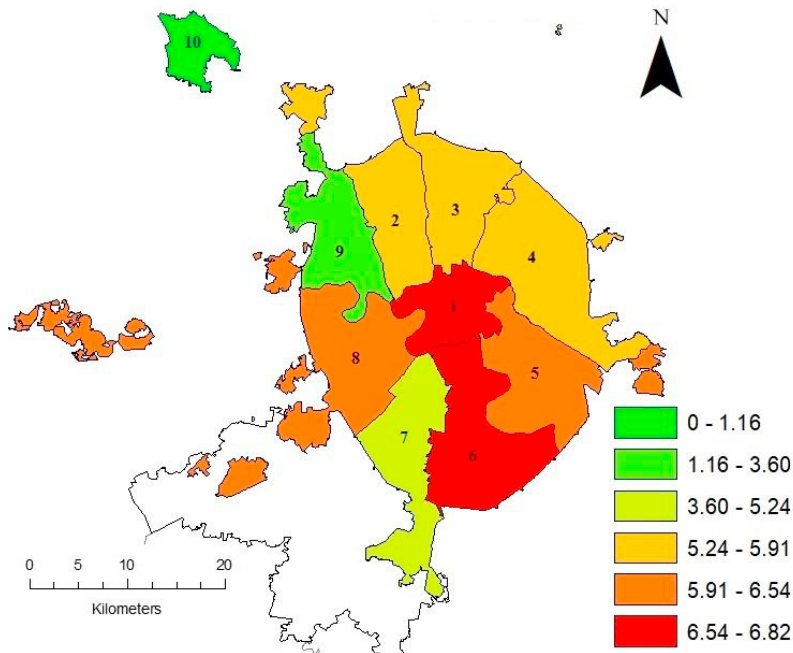
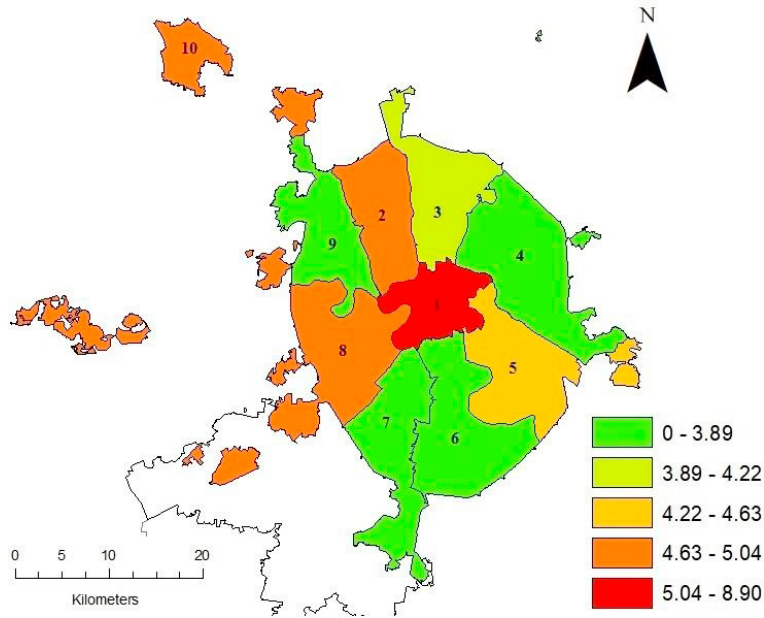


Figure 5. CO₂ emissions (Mt) per year.

(1 - Central district, 2 - Northern district, 3 - North-Eastern district, 4 - Eastern district, 5 - South-Eastern district, 6 - Southern district, 7 - South-Western district, 8 - Western district, 9 - North-Western district, 10 - Zelenogradsky district)

Figure 6. CO₂ emissions (t) per capita.

(1 - Central district, 2 - Northern district, 3 - North-Eastern district, 4 - Eastern district, 5 - South-Eastern district, 6 - Southern district, 7 - South-Western district, 8 - Western district, 9 - North-Western district, 10 - Zelenogradsky district)

Table 3. Moscow carbon footprint

Moscow districts	CO ₂ emissions (Mt)	CO ₂ emissions (t)
	per year	per capita
Central	6.74	8.90
Northern	5.61	4.91
North-Eastern	5.91	4.22
Eastern	5.77	3.87
South-Eastern	6.26	4.63
Southern	6.82	3.89
South-Western	5.24	3.73
Western	6.54	4.90
North-Western	3.60	3.70
Zelenogradsky	1.16	5.04
Moscow (2011)	53.65	4.53

5. Conclusions

The investigation shows the complicated picture of spatial distribution of annual anthropogenic fluxes (AHF) and CO₂ emission within the Moscow City (in 2011 boundaries).

It is shown that for total Moscow's emission of anthropogenic heat from the Moscow DHS is approximately twice less than from all urban energy sources. This situation is very similar to EU, where half of energy is using for space heating.

AHF distribution by Moscow between city districts shows that only in the Central district almost whole AHF amount produced by heating of living and public spaces. CO₂ emission from the Moscow DHS also show some particularity of Moscow Central district, where this emission per capita much higher than in other districts.

For the main belt of Moscow districts situated between Central district and Moscow ring road carbon footprint caused by DHS almost linearly depends on district population. It is very interesting that emission of carbon dioxide per capita from heat supply systems in different districts of Moscow is less, the higher the population density in these districts.

The needed energy demand and heating supply in Moscow, as well as in any large city, depends on global and regional climate changes, and the study of such dependencies and feedbacks is the main goal of analysis of the regional climate change impact on energy consumption of municipal services of large cities.

Hopefully, understanding of these dependencies and feedbacks can help Moscow municipal authorities improve heat supply system in Moscow and could be helpful for another Russian and not only Russian cities.

Acknowledgements

The presented paper describes results of studies performed within the framework of the project “Analysis of the regional climate change impact on energy consumption of municipal services of megalopolises of Russia” supported by Russian Scientific Foundation (Project No. 16-17-00114)

References

- [1]. Seto KC, Dhakal S, Bigio A, Blanco H, Delgado GC, Dewar D, Huang L, Inaba A, Kansal A, Lwasa S, McMahon JE, Müller DB, Murakami J, Nagendra H, Ramaswami A. Human Settlements, Infrastructure and Spatial Planning. In: Climate Change 2014: Mitigation of Climate Change. Contribution of Working Group III to the Fifth Assessment Report of the Intergovernmental Panel on Climate Change [Edenhofer, O., R. Pichs-Madruga, Y. Sokona, E. Farahani, S. Kadner, K. Seyboth, A. Adler, I. Baum, S. Brunner, P. Eickemeier, B. Kriemann, J. Savolainen, S. Schlömer, C. von Stechow, T. Zwickel and J.C. Minx (eds.)]. 2014. Cambridge University Press, Cambridge, United Kingdom and New York, NY, USA.
- [2]. Profile of heating and cooling demand in 2015. 2017. Available from www.heatroadmap.eu.
- [3]. https://en.wikipedia.org/wiki/Administrative_divisions_of_Moscow
- [4]. Federal State Statistic Service of Russian Federation: Moscow city. <http://www.gks.ru/dbscripts/munst/munst45/DBInet.cgi>
- [5]. Moscow city department of fuel and energy: The scheme of heat supply of the city of Moscow for the period till 2028 (in Russian). <http://depteh.mos.ru/legislation/scheme-of-development-of-engineering-infrastructure-of-the-city/the-scheme-of-heat-supply-of-the-city-of-moscow-for-the-period-up-to-2028/>
- [6]. International Energy Agency. CHP/DH Country Profile: Russia, 2009 <http://www.iea.org/media/topics/cleanenergytechnologies/chp/profiles/russia.pdf>
- [7]. Aleksandrov G.G., Belova I.N, Ginzburg A.S. Anthropogenic Heat Flows in the Capital Agglomerations of Russia and China Doklady Earth Sciences, 2014, Vol. 457, Part 1, pp. 849–853.
- [8]. National report of the Russian Federation on the inventory of anthropogenic emissions by sources and removals by sinks of greenhouse gases not controlled by the Montreal Protocol for 1990-2010, Moscow, 2012.
- [9]. Ginzburg A.S., Reshetar O.A., Belova I.N. Impact of Climatic Factors on Energy Consumption during the Heating Season. Thermal Engineering 2016; 63:9: 621–627.
- [10]. Klimenko V.V., A.S. Ginzburg, P.F. Demchenko, A.G. Tereshin, I.N. Belova, E.V. Kasilova. Impact of Urbanization and Climate Warming on Energy Consumption in Large Cities. Doklady Physics, 2016, Vol. 61, No. 10, pp. 521–525
- [11]. Alexandrov G.G., Belova I.N., Varentsov M.I., Dokukin S.A. Impacts of climate change on energy consumption of Russian cities in the winter period. Proc. SPIE 10466, 23rd International Symposium on Atmospheric and Ocean Optics: Atmospheric Physics, 104666K (30 November 2017); doi: 10.1117/12.2287766



16th International Symposium on District Heating and Cooling, DHC2018,
9–12 September 2018, Hamburg, Germany

District heating pipes buried in Temporarily Flowable Backfill Materials

Dominik Wolfrum*, Thomas Neidhart

Technical University of Eastern Bavaria at Regensburg, 93053 Regensburg, Germany

Abstract

It is state of technology in district heating systems to use sand as backfill material for district heating pipes (DHP). In conventional pipeline construction, Temporarily Flowable Backfill Materials (TFB) have been already used for backfilling the pipe zone. TFB consists of the excavated material, cement, water and optionally bentonite. Environmental and economic advantages are that the excavated material can be reused and that TFB requires no compaction. In order to embed district heating pipes in TFB, soil mechanical parameters of the TFB are required. Above all the resistance to temperature-induced axial displacement should be well-known in order to estimate the displacements of the DHP, as well as the stress distribution along the DHP. Compared to sand as a non-cohesive backfill TFB have remarkable adhesive contact stresses which result in considerable resistance forces. In this article, the contact behavior between TFB and DHP is described as well as the effect on the DHP statics. Therefore, the results of various laboratory tests are summarized and presented to understand the interface-resistance-characteristics (IRC) of the DHP/ TFB interface. Then, the deduced IRC was implemented in a computer program for some comparative calculations with sand and TFB. Finally, the results of cyclic loading are presented and discussed.

© 2018 The Authors. Published by Elsevier Ltd.

This is an open access article under the CC BY-NC-ND license (<https://creativecommons.org/licenses/by-nc-nd/4.0/>)

Selection and peer-review under responsibility of the scientific committee of the 16th International Symposium on District Heating and Cooling, DHC2018.

Keywords: distric heating, pipe static, thermal expansion, Temporarily Flowable Backfill Material, TFB, buried pipeline

* Corresponding author. Tel.: +49-941-943-9262

E-mail address: dominik2.wolfrum@oth-regensburg.de

1. Introduction

For the installation of buried district heating pipelines (DHP), it is state of technology to refill the pipe zone of the trench with sand. One possibility to reduce the costs of the installation is to use Temporarily Flowable Backfill Materials (TFB). The potential savings when installing a plastic jacket compound pipe with an outer diameter of 600 mm under a paved surface is up to $\approx 9\%$ [1]. For smaller diameters and unpaved surfaces, the saving potential can be even higher [1]. An ecological advantage of TFB is that the trench spoil can be reused directly on the construction site for the TFB production. This saves large transport distances for the disposal of the excavated material and the delivery of a new filling material. In addition, resources and disposal sites will be saved.

TFB is described in the German recommendation “Herstellung und Verwendung von zeitweise fließfähigen, selbstverdichtenden Verfüllbaustoffen im Erdbau” [2] (engl.: “Production and use of Temporarily Flowable, Self-Compacting Backfill materials in earthworks”) and is similar to the Controlled Low Strength Material (CLSM) [3]. For district heating systems, the reason for the low market development is that the standardized calculation procedures do not apply for TFB as bedding material [4]. For DHP the decisive influence on the static design of the system is the temperature-induced axial displacements. The buried pipe expands due to the increase of the temperature and causes contact shear stresses in the opposite direction of the displacement that hinder the free thermal expansion and reduce the displacements. It is important to know the contact forces between the bedding material and the pipe to be able to calculate the stress distribution and deformations of the pipe. Above all, the resistance to axial expansion of the pipeline is of decisive importance for the pipe static design. Therefore, the interface-resistance-characteristic (IRC) is needed, which can be determined by laboratory tests or by a full-scale test. The calculation concepts for buried DHP like in the European Standard EN 13941 [5] and in the German code of practice AGFW FW 401 [6] are only designed for non-bonding and non-cohesive materials with a simplified elastic-plastic IRC. As shown in the further article, the IRC of the TFB have considerable adhesive contact forces and so it strongly differs from the working line adopted in these calculation concepts. This means that the guidelines and standards cannot be used for the calculation of DHP with TFB as bedding material.

In the further article the laboratory experimental determination of the IRC and a rod-spring based calculation method is described and presented. The article is divided in following points:

- Characterization of TFB.
- Experimental investigation of the contact resistance and the IRC.
- Development of a rod-spring based system for the calculation of heating and cooling processes.
- Comparative calculations and presentation of various influences.

2. Characterization of Temporarily Flowable Backfill Materials

TFB is a bounded backfill and consists of spoil or aggregate, cement, water and optionally bentonite. The TFB can be produced in mobile mixing plants directly on the construction site next to the trench or in stationary mixing plants. The proportions of cement and bentonite are usually 25 kg/m^3 to 50 kg/m^3 and the water content of 400 kg/m^3 to 700 kg/m^3 . The composition is dependent on the initial material, e.g. the grain size distribution of the spoil and the required properties, e.g. compressive strength and can be adjusted accordingly. After mixing the TFB flows into all cavities and interstices solely under the influence of gravity and requires no additional compaction [2]. Due to chemical and physical reactions of the cement and bentonite, the material hardens and the TFB can be mechanically stressed. Compared to sand, TFB is a highly time-dependent material.

An important property of the TFB in pipeline construction is its re-excavation ability. According to the German recommendation for TFB [2], the uniaxial compressive strength after 28 days should be less than 0.3 N/mm^2 and the measure of the increase in strength f_z should be a maximum of 0.15 N/mm^2 in order to ensure long-term easy re-excavation ability.

The measure of the increase in strength is calculated using in formula [2]:

$$f_{TFB} = \frac{f_{TFB,t2} - f_{TFB,t1}}{\log\left(\frac{t_2}{t_1}\right)} \quad (1)$$

$f_{TFB,t1}$ is the uniaxial compressive strength at a sample age of $t_1 = 7 d$ and $f_{TFB,t2}$ is the compressive strength at a sample age of $t_2 \geq 56 d$. As an alternative to uniaxial compressive strength, the strength can be checked with the CBR-test.

3. Experimental determination of the contact resistance

3.1. Testing device Re-SIST

There are several laboratory tests to determine the interface-resistance-characteristic (IRC) between the soil and the material of the pipe surface, e.g. Direct Shear Test, Simple Shear Test, Ring Torsion Shear Test and Rod Shear Test [7]. As the material simulating the pipe surface, polyethylene is used, similar to the surface of the plastic jacket compound pipe.

Important boundary conditions for contact surface shear tests with TFB are that the contact between the TFB and the polyethylene must be established directly after the mixing process and since the properties of the TFB are strongly time-dependent, the test must be carried out with different sample ages. In order to be able to carry out a large number of tests, it is necessary to establish the contact and the preload externally outside the load frame. In addition, the IRC is dependent on the magnitude of the normal stress and the relative displacement between the TFB and the polyethylene. [8]

The decision was made against the Direct Shear Test and the Simple Shear Test, because the adjustment of a shear gap, the reduction of the shear surface and the deformation or distortion in the soil caused problems in these tests, which were confirmed by preliminary tests.

A test to determine the IRC is the Rod Shear Test in the ReSIST (Regensburger Stab-Interface-Scher-Test) device. Fig. 1.a shows a schematically sketch of the device. The ReSIST device consists of a cylindrical tube with square end plates at both ends. In the middle of this cylinder, a rod is placed through openings in the end plates that simulates the DHP. It should be noted that the rod has sufficient stiffness, so that no deformation occurs in the rod during the test. The space between the rod and the cylindrical tube is filled with the material to be examined. Via valves and a latex membrane, a lateral pressure can be applied to simulate different laying depth of the DHP. To reduce the end friction and for the dewatering by suitable water outlets a smooth drainage fleece covers the end plates. [3]

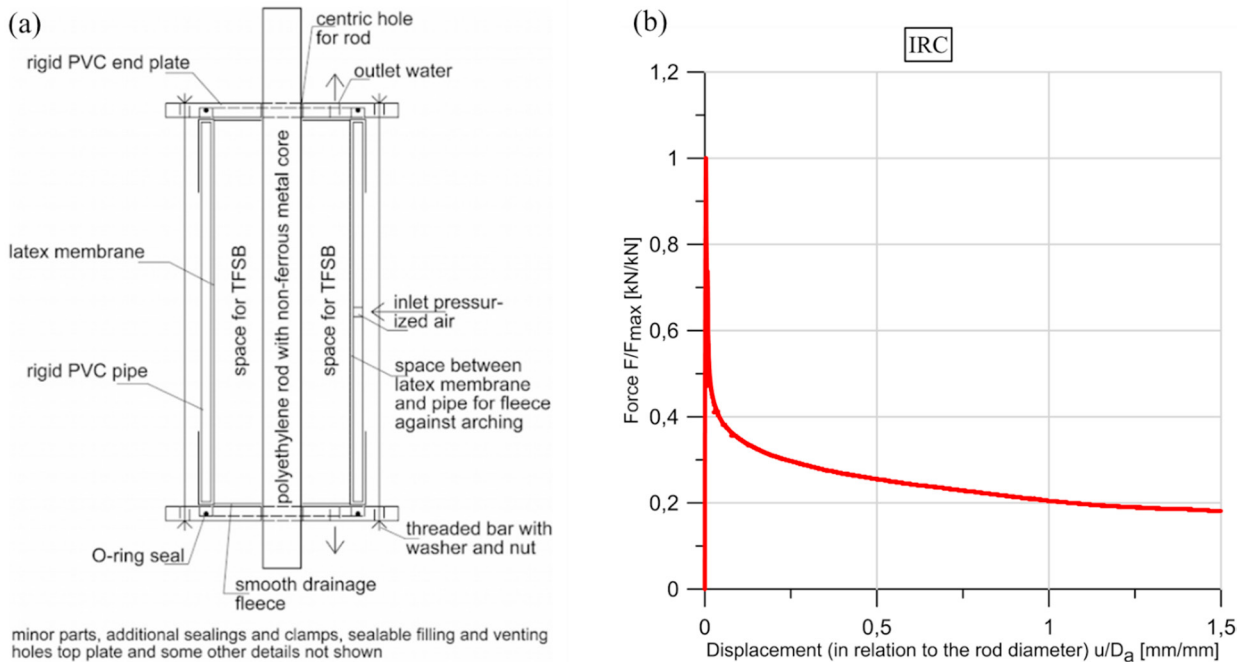


Fig. 1. (a) Re-SIST (Regensburger Stab-Interface-Scher-Test) device [3]; (b) Result of a ReSIST

On the day of testing, the ReSIST device is built into a load frame and the rod is pushed through the examined material with a constant speed, simultaneously measuring the required force and displacement. A disadvantage of this test is that the resistance is measured over the entire embedded length by a load cell at the top. To conclude from the measured force on a shear stress, the rod should neither compress nor deform radially. In addition, the normal stress vertically on the rod during the test and over the entire length of the embedded rod should be constant. Also the examined material should not deform or distort during the test. For small compressions in the rod, the test result can be adjusted with a correction algorithm by *Wagner* [8].

The test results of TFB as examined material and a rod with a polyethylene surface (see Fig. 1.b) show that a high displacement resistance (Peak) occurs with small displacement paths and decreases to a residual value with further displacement. The Peak value is due to adhesion forces between the TFB and the rod surface.

3.2. Testing device RIST

An alternative test that has been conducted is the Regensburger Interface-Ring-Torsion-Shear-Test (RIST). The TFB is filled into an annular test cell and loaded directly after filling with a polyethylene ring fixed on a load stamp (see Fig. 2.a). Through the stamp, a defined normal stress can be applied. At the bottom of the cell is a filter plate and openings with which the sample can be irrigated and drained. After a certain preload/ cure time, torsion is applied on the test cell and a shearing stress occurs between the polyethylene ring and the TFB. The torque, normal force, rotation and the settling is measured. The advantage of this tester is that the shear path is unlimited, the normal force can be regulated and measured directly via the stamp on the interface and the value of the normal force can be changed during the shearing process. Thus, it is also possible to simulate heating and cooling-related simultaneous axial and radial deformations of the pipe by simulating the axial displacement of the pipe via the torsional movement and the influence of the radial temperature expansion via the normal force.

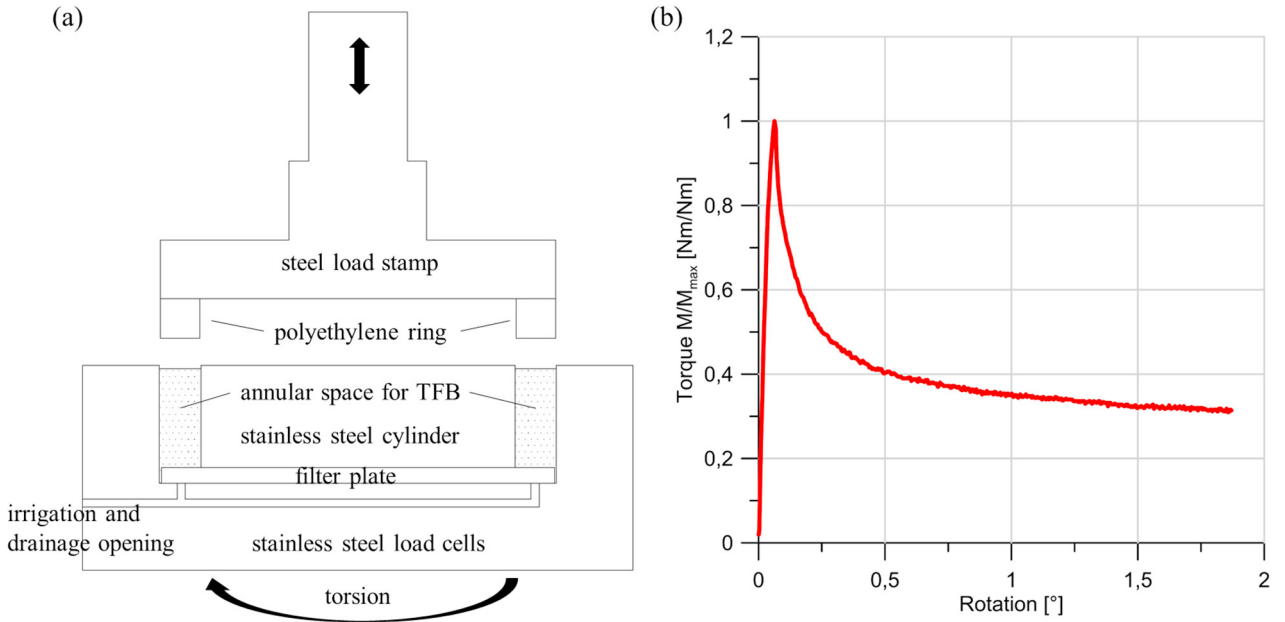


Fig. 2. (a) RIST (Regensburger Interface-Scher-Test) device; (b) Result of a RIST

Analogous to the results of the ReSIST, the results of the RIST also show the same course of the displacement-resistance-line. With small rotations, a maximum value of the torque occurs and decreases on further rotation to a residual value. From the torque and the contact surface, a shear stress τ can be calculated and from the rotation a middle displacement path u .

3.3. Conclusion

The following IRC of TFB and sand can be deduced from the test results of the ReSIST and RIST:

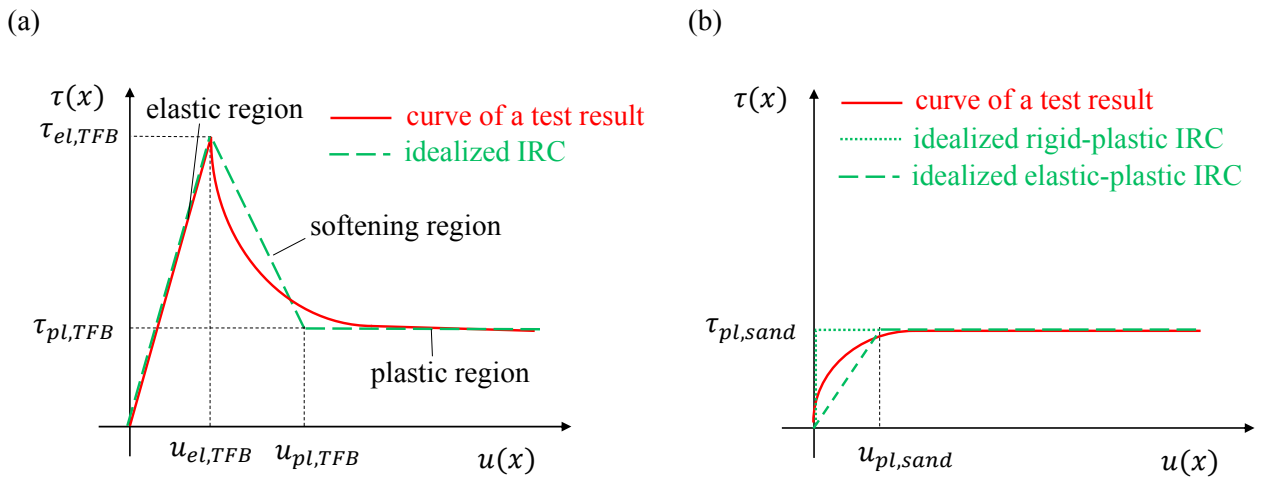


Fig. 3. (a) IRC of TFB and (b) IRC of sand for the first heating

The contact resistance between sand and the pipe surface can be idealized with a elastic-plastic IRC (see Fig. 3.b). Because the displacements $u_{pl,sand}$ are small compared to the maximum displacements of a buried DHP a rigid-plastic IRC can be accepted [9].

The idealized IRC of TFB for the first heating is divided into the following regions (see Fig. 3.a):

- Elastic region: The activatable shear stress increases with the shifts of the pipe up to a peak value (adhesion).
- Softening region: The shear stress decreases from the peak value to a residual value.
- Plastic region: The shear stress remains constant and is independent of the shift.

For calculating the cooling and reheating processes the results of the cyclic ReSIST of *Wagner* [8] concluded the following IRC:

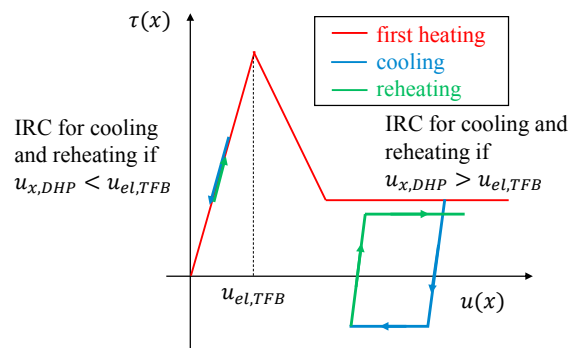


Fig. 4. Idealized IRC of TFB for the first heating, cooling and reheating processes

If the displacement $u_{x,DHP}$ at a considered point x of the DHP at the first heating is smaller than the displacement $u_{el,TFB}$ at the adhesion stress, the IRC behaves linear-elastic. If the adhesion stress and thus the displacement $u_{el,TFB}$ are exceeded, the IRC of cooling and reheating cycles behaves linear elastic-plastic (see Fig. 4).

4. Non-linear rod-spring based calculation method

The development of analytical equations and the calculations of pipe routes with bends, pipe kinks, changing the IRC due to uneven overlap height of the pipe or changing the parameters of the TFB is very work and time-intensive. For faster calculation and design of diverse pipe routes a rod-spring based system is developed.

The following load cases are decisive for the design of the pipes (see Fig. 8):

- First heating: At the first heating of the DHP, the maximum resistance of the IRC occurs and thus the stress distribution along the pipe is maximal.
- Cooling: During cooling, the pipe contracts and axial contact forces change the direction. This causes tensile stresses in the pipe. From difference of the stresses between the first heating and the cooling, the maximum stress range is determined.
- Reheating (after x cycles): As the contact forces decrease with the number of cycles, the shifts increase with the amount of reheating cycles. For the calculation an IRC will be taken, which occurs theoretically after endless reheating cycles and so, it is on the safe side of the pipe design.

Since the initial state of heating is required for the cooling calculation, a framework program must be used in which several construction states are programmable. In addition, the framework program must support non-linear spring models. Therefore a calculation concept was developed with the framework program RSTAB of the company Dlubal. In this program the pipe is modelled as a rod and the bedding material as springs. Since there are different

IRC for the heating and cooling calculation and the springs can only be activated or deactivated in the individual calculation stages, two nodes are created directly next to each other. In the heating or cooling calculation, one node with the respective spring characteristic is activated in each case. In Fig. 5 a sketch of the calculation process is presented.

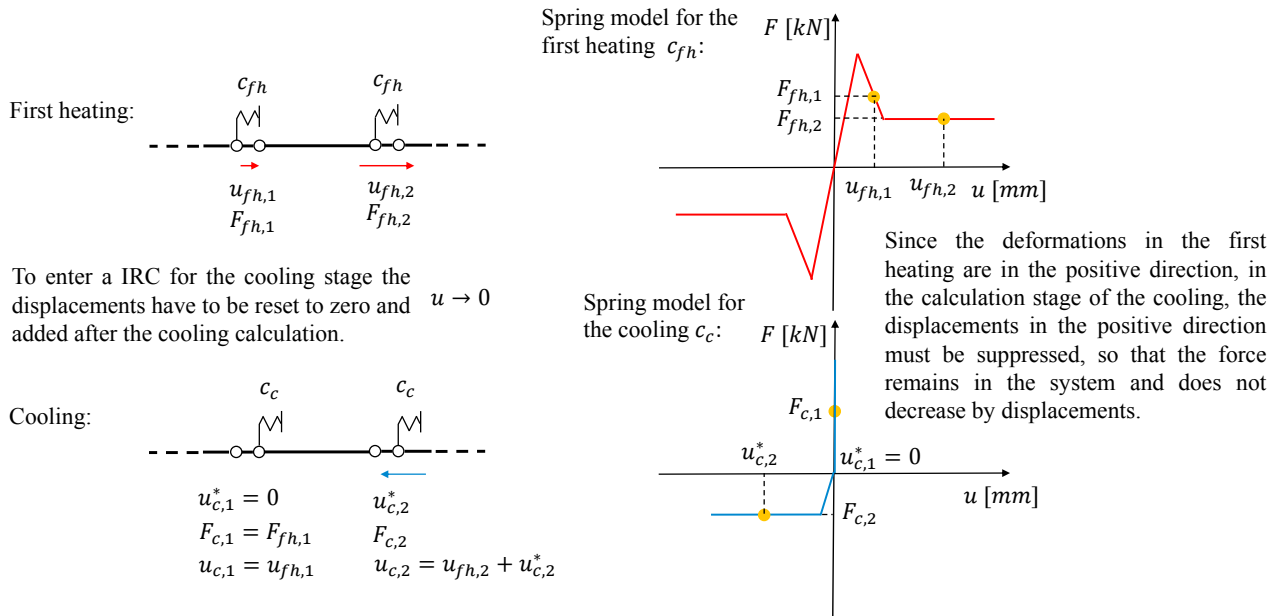


Fig. 5. Calculation concept of the first heating stage and the cooling stage

Reheating can be calculated independently of the other load cases. In the reheating stage, the softening component is not taken into account, since it is assumed that the contact forces with accumulated deformations approximate to the residual value. The size of residual value in the plastic region of the IRC is chosen to be on the safe side and so a minimum value has to be taken. At the first heating load a maximum for the residual value has to be chosen.

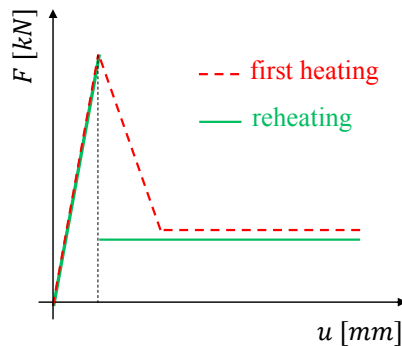


Fig. 6. IRC of TFB for the reheating stage compared with the IRC for the first heating

5. Comparative calculations

To illustrate the displacement and normal force characteristics of DHP, various examples are listed here. In the following calculations, the DHP is fixed against displacements at the standardized coordinate $x = 0$ and freely movable at the standardized coordinate $x = 1,0$. The influence and necessity of different load cases as well as the influences from the IRC are presented.

Influence of the adhesion on the displacement and normal force distribution for the first heating:

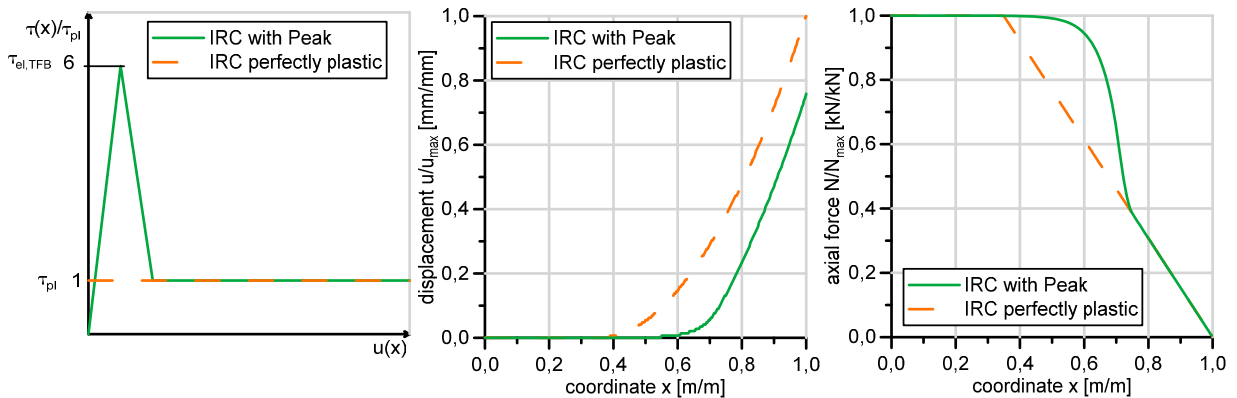


Fig. 7. IRC, displacement distribution and normal force distribution depending on the coordinate x of a IRC with Peak and of a perfectly plastic IRC (standardized).

Fig. 7 shows the differences between an IRC with a peak such as the idealized IRC of TFB and a perfectly plastic IRC like the IRC used in guidelines and standards for calculation in sand buried pipelines. The value of the plastic shear stress τ_{pl} of the TFB and Sand are not necessarily congruent. By the peak an additional work potential exist, that causes smaller displacements in the DHP and higher normal forces in parts along the DHP. The pipe length at which shifts occur is also shorter with the IRC with Peak than with the perfectly plastic IRC.

Displacement and normal force distribution during first heating, cooling and reheating:

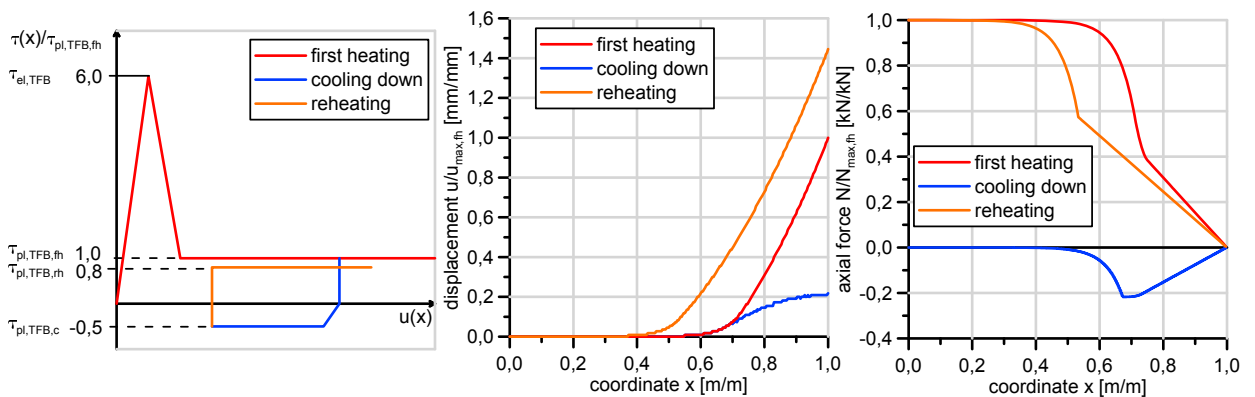


Fig. 8. IRC, displacement and normal force distribution for the first heating, cooling and reheating (standardized).

While the DHP is cooling down after the first heating, the pipe contracts and the displacements of the DHP decrease. In this region in which the displacements become smaller, the direction of the shear stresses turns and thus

tensile stresses occur. At the reheating process the displacements and the normal force distribution increase. If the temperature at the first heating and at the reheating process are the same, then the displacements at the reheating process are higher, because of the value of the plastic shear stress. This value is at the reheating smaller than at the first heating because of the radial influence and the accumulation of the displacements. As shown in Fig. 8 the maximum displacements occur in the reheating process, the maximum normal force distribution in the first heating and the biggest stress range between the first heating and the cooling.

6. Conclusion

Despite the environmental and economic advantages of the TFB, this material is still not used very often for backfilling the trench of DHP. The additional adhesive contact forces requires nonlinear calculations and actual calculation methods in standards do not apply for this. To develop a calculation method the IRC to temperature-induced axial displacement is of decisive importance. With the Rod Shear Test (ReSIST) or the Interface Ring Shear Test (RIST) the IRC of TFB can be investigated. For the heating and cooling processes a rod-spring based system is developed. With the activation or deactivation of two nodes next to each other, one spring can simulate the IRC of the TFB for heating and the other the IRC for cooling. With this method different DHP routes with the decisive load cases can be calculated. Because of the adhesion force of the TFB compared to sand as standard backfill material, TFB has additional work potential which leads to smaller displacements but partial higher normal forces along the pipe. The working line of the springs in radial directions are not described in this article, but must be considered for non-straight pipe sections.

Acknowledgements

This research was funded by the German Federal Ministry for Economic Affairs and Energy, support codes FKZ 03ET1063B and FKZ 03ET7531C. This support is greatly appreciated.

References

- [1] Schmitt, F., Caspar, J. u. Holler, S.: Bautechnische Entwicklungen von Fernwärme-Transportleitungen. Forschung und Entwicklung / AGFW, Bd. 32. Frankfurt am Main: AGFW 2015
- [2] FGSV (Hrsg.): H ZFSV - Hinweise für die Herstellung und Verwendung von zeitweise fließfähigen, selbstverdichtenden Verfüllbaustoffen im Erdbau. 2012
- [3] Wagner, B. u. Neidhart, T.: A new backfill material enhancing axial bedding of district heating pipes. In: Wuttke, F., Bauer, S. u. Sanchez, M. (Hrsg.): Energy Geotechnics. Proceedings of the 1st International Conference on Energy Geotechnics, ICEGT 2016, Kiel, Germany, 29-31 August 2016. London: CRC Press 2016, S. 105–112
- [4] Weidlich, I. u. Grajcar, M.: Expected potential of bound and recycled backfill material in low temperature district heating networks. Energy Procedia 128 (2017), S. 150–156
- [5] Entwurf prEN 13941-1:2016; 2016. *DIN EN 13941-1, Fernwärmerohre - Auslegung und Installation von gedämmten Einzel- und Doppelrohr-Verbundsystemen für direkt erdverlegte Heißwasser-Fernwärmenetze - Teil 1: Auslegung*
- [6] AGFW FW 401 - 10; 2007. *AGFW-FVGW Regelwerk, FW 401 Teil 10, Verlegung und Statik von Kunststoffmantelrohren (KMR) für Fernwärmenetze - Statische Auslegung; Grundlagen der Spannungsermittlung -*
- [7] Kishida, H. u. Uesugi, M.: Tests of interface between sand and steel in the simple shear apparatus. *Géotechnique* (1987) 37.1, S. 45–52
- [8] Wagner, B.: Ein Beitrag zur axialen Bettung von Kunststoffmantelrohren der Fernwärme in Zeitweise fließfähigen, selbstverdichtenden Verfüllbaustoffen (ZFSV). 2018
- [9] Beilke, O.: Interaktionsverhalten des Bauwerks "Fernwärmeleitung - Bettungsmaterial". Hannover: Eigenverlag 1993



16th International Symposium on District Heating and Cooling, DHC2018,
9–12 September 2018, Hamburg, Germany

Measurement-based modelling of large atmospheric heat storage tanks

A. Herwig^a, L. Umbreit^a, K. Rühling^{a*}

^a*Technische Universität Dresden, Institute of Power Engineering,
Professorship of Building Energy Systems and Heat Supply, 01062 Dresden, Germany*

Abstract

The presented research project uses an innovative measurement technology to investigate large atmospheric heat storage tanks with water as heat storage medium. For this type of heat storage tanks only a few scientific descriptions are available in literature. Measurement data combined with simulation results offer further insight into the temperature field. The findings enable assessment of thermal losses, improvements on load management and thereby reduction in of primary energy use.

© 2018 The Authors. Published by Elsevier Ltd.

This is an open access article under the CC BY-NC-ND license (<https://creativecommons.org/licenses/by-nc-nd/4.0/>)

Selection and peer-review under responsibility of the scientific committee of the 16th International Symposium on District Heating and Cooling, DHC2018.

Keywords: Large atmospheric heat storage tanks; distributed temperature sensing

1. Measurement Technology

In order to investigate their physical behaviour under real operation conditions four one-zone and two two-zone heat storage tanks at scales between 2,000 m³ and 43,000 m³ had been equipped with a distributed temperature sensing (DTS) measurement system. The DTS-measurement principle (Fig. 1) is based on the RAMAN-effect to gain precise information about the temperature distribution both in space and in time along one single glass fibre.

* Corresponding author. Tel.: +49-351-463-32375; fax: +49-351-463-37076.

E-mail address: karin.ruehling@tu-dresden.de

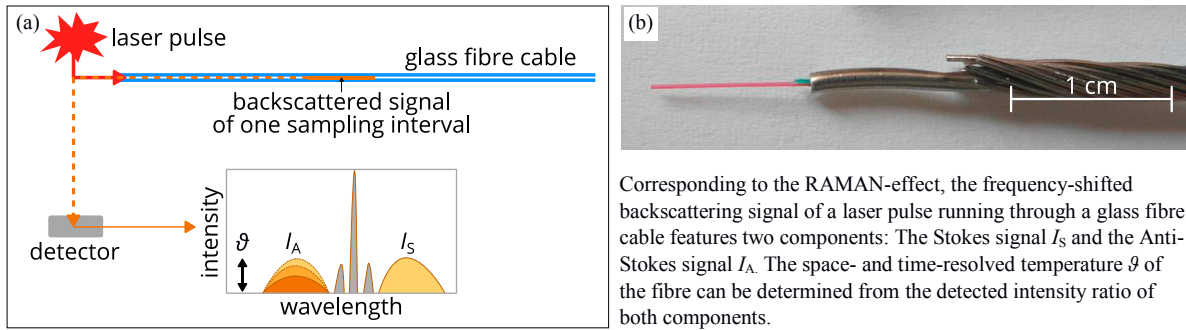


Fig. 1. (a) scheme of the DTS-measurement system; (b) glass fibre cable

The measurement data had been used to create animated visualizations that depict the operation mode of heat storage tanks in general [1]. Due to realizing an adapted measurement concept for each monitoring and developing appropriate analysis algorithms more detailed information can be revealed. Hence, different physical effects on thermal stratification within heat storage tanks can be proven.

2. One-zone atmospheric heat storage tanks

A common and widely realized type of large atmospheric heat storage tanks is based on the design of HEDBÄCK (Fig. 2). They are built as pressure-less standing steel cylinders with one radial diffuser at the bottom and one at the top of the storage volume. During the charging process, warm water is entering the tank through the top radial diffuser and cold water is leaving through the bottom radial diffuser. While discharging the flow is directed reversely. As both radial diffusers are concentric with the cylindrical surface of the storage tank they induce a radial free jet. In cases with well-defined charging and discharging temperatures a thermal stratification with a layer of high temperature above a layer of lower temperature is formed, with a thermocline in between. This heat storage tank design is optimized for capacities of up to several 10,000 m³. More than 100 of these heat storage tanks had been built during the past decades.

The grade of stratification inside the heat storage tank limits the amount of heat which can be discharged at the required supply temperature level. Therefore a good understanding of the main factors that have an impact on the stratification is important for both to give advice to improve operation management and to generate valid models of this type of heat storage tank. Main influences on thermal stratification within the heat storage tank had been mentioned in [2].

2.1. Measurement concept

The measurement concept includes the DTS-measurement system and additional operating data of the heat storage tank. As shown in Fig. 2 the DTS-system captures the temperature field vertically at four radial and two additional circumferential positions: R1, R2, R3=U3, R4 and U1 and U2. Supplementary operating data is available for 19 vertically aligned PT100 temperature sensors, supply temperature (ϑ_{D1}), return temperature (ϑ_{D2}), volume flow and pressure at the bottom of the heat storage tank. The temperature resolution of the DTS-measurement is limited by the random noise that can be reduced by averaging consecutive measurements. However, time resolution must be considered carefully. The presented work uses an average time of one minute. For this mean type the conditions inside the heat storage tank are assumed as sufficiently constant. As the focus in this study is set on the homogeneity of the temperature field in horizontal layers, temperature differences are formed at the same height between the six vertical positions. By the use of one-minute averages the DTS-system achieves a resolution, defined by the 1- σ standard deviation, of about 0.12 K for these horizontal temperature differences. The spatial resolution along the cable is 0.35 m.

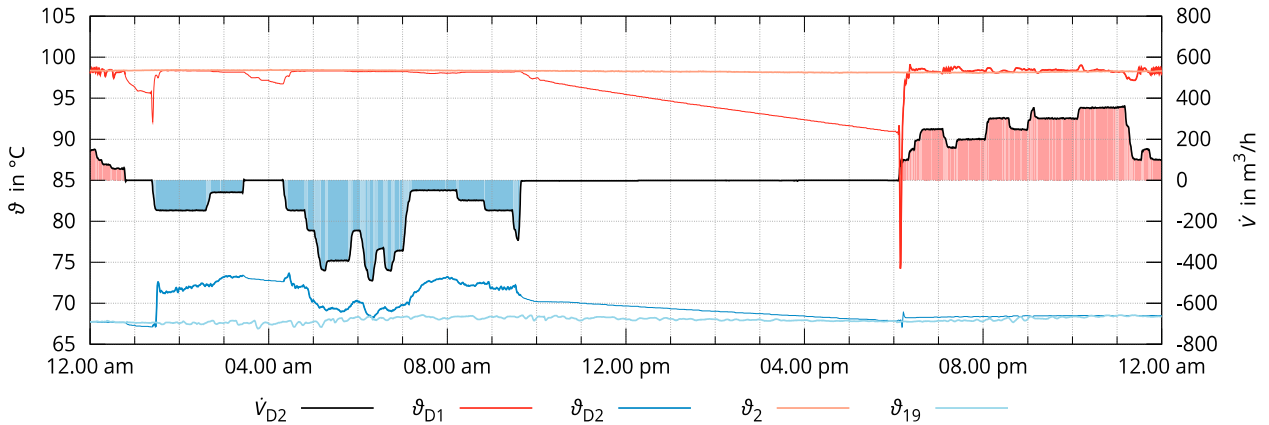


Fig. 3. operating data of the one-zone heat storage tank at 5 May 2016

At the beginning of the day, the heat storage tank is charged, followed by a short and a longer discharging phase, a standstill of about eight hours and a six-hour charging phase. During both charging and discharging almost 50 % of the design volume flow are reached.

Comparative to the measurement data of 5 May 5 2016, a reference day will be considered which is characterized by a standstill throughout the day. Hence, during the reference day there are no relevant influences of forced convective on the natural stratification.

The circumferential homogeneity of the temperature field is investigated based on the three positions U1 to U3. They are located at angles of 120° and have the same radial distance from the diffuser. In Fig. 4 (a) the solid lines to the right represent the temperatures at the three circumferential positions while the heat storage tank is discharged with the maximum volume flow of the day. Dashed lines to the left related to the scale at the x2-axis indicate the temperature differences to U3. The horizontal lines marked with D indicate the position of the two diffusers. The graph clearly shows that the temperature differences relative to U3 remain at very small scales over the entire height of the heat storage tank. These temperature differences are mostly caused by the random noise of the DTS-system.

A more detailed analysis with regard to the influence of the measurement noise of the DTS-system is possible comparing the data of 5 May 2016 to the reference day presented in the normal probability plot in Fig. 5 (a). In the normal probability plot normally distributed data arranges along a line of constant slope. For the reference day, the dataset of 816,461 circumferential temperature differences approximates a line of constant slope and thus the normal distribution very well (grey in Fig. 5 (a)). A state that can only be explained by the assumption that the temperature differences of the reference day are caused basically by the random noise of the DTS-system.

The 915,316 temperature differences obtained from the measurement data of 5 May 2016 are depicted in green (U1-U3) and orange (U2-U3) in Fig. 5 (a). In the bottom region of the figure, the green and orange data deviates

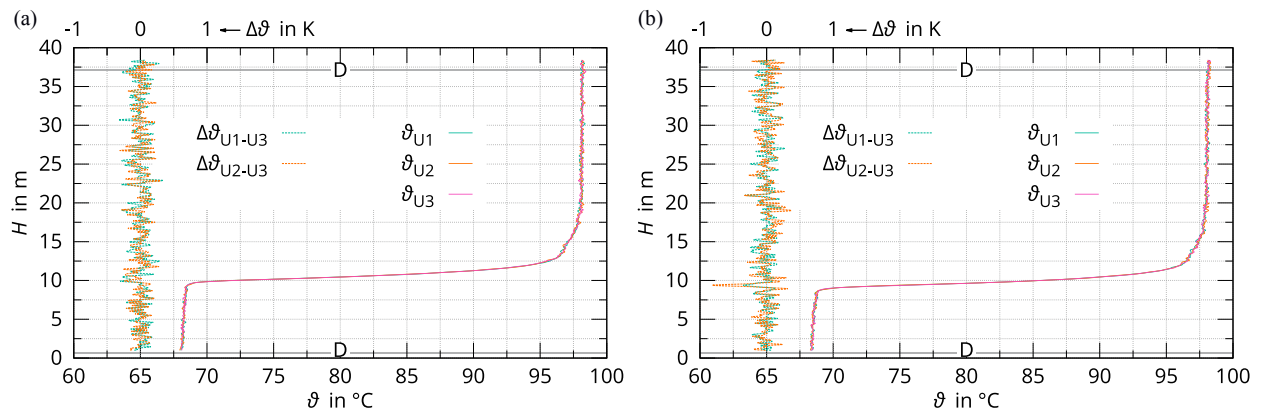


Fig. 4. temperature profile at the three circumferential positions and temperature difference to U3 at 5 May 2016; (a) during maximum volume flow at 06.18 am; (b) at maximum deviation in circumferential direction at 10.18 pm

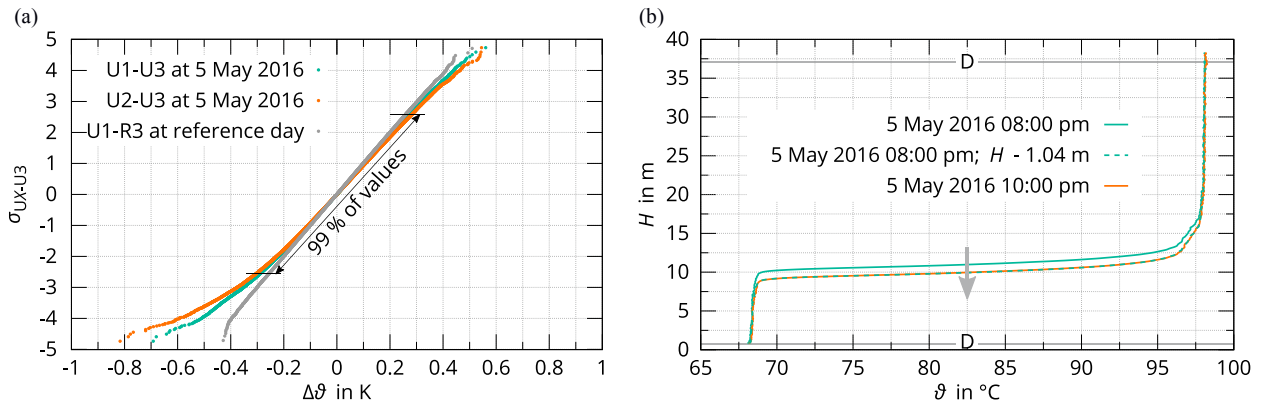


Fig. 5. (a) normal probability plot of temperature differences in circumferential direction, 5 May 2016 and reference day; (b) schematic sketch of calculating the volume flow from the vertical displacement of the temperature profile

from the reference case to larger temperature differences. For these values, the circumferential deviations can therefore not be explained solely by the measurement noise. The largest circumferential deviation of -0.82 K on 5 May 2016 is at 10.18 pm between U2 and U3. As shown in Fig. 4 (b), it occurs at the level of the thermocline, i.e. in the region of the largest vertical temperature gradient. In addition, the charging volume flow is at its maximum level during this time. Small vibrations of the thermocline of very few centimeters, possibly triggered from the relatively high volume flow, could already explain this deviation. Besides, even minimal errors in the vertical position assignment of the measurement setup can contribute.

Overall, however, there are only very few measurements which show deviations of more than ± 0.4 K and thus exceed the range expected solely because of the measurement noise. The maximum deviation in circumferential direction of -0.82 K is also very small compared to the temperature difference between hot and cold layer of about 30 K. This means that the investigated dataset is characterized by a very good circumferential homogeneity of the temperature field. This result confirms detailed investigations carried out on a similar heat storage tank in [1], [2].

The homogeneity of the temperature field in radial direction had been already proven for this heat storage tank in [3]. The temperature differences occurring in radial direction are slightly larger than the values found in circumferential direction. Nevertheless, radial differences that exceed the measurement noise are both rare and small compared to the temperature difference between the hot and the cold layer. Thus, very good homogeneity of the temperature field in horizontal layers can be assumed for the examined type of heat storage tank.

2.3. Calculating the volume flow from the vertical displacement speed of the temperature profile

The horizontal homogeneity of the temperature field discussed above is essential for the assumption that the temperature field during charging and discharging moves mainly vertically between the diffusers. This behavior is depicted for a time interval of two hours during a charging phase in Fig. 5 (b). The superposition of the two temperature profiles at 08.00 pm and 10.00 pm show a good congruence. Based on this consideration, it shall be investigated to which accuracy the charging and discharging volume flow can be calculated from the vertical displacement speed of the temperature profile multiplied by the cross sectional area of the storage tank. The study is based on the average temperature value of all six measured vertical temperature profiles to further reduce the measurement noise.

In Fig. 6, the green graph shows the volume flow calculated from the vertical displacement of the temperature profile of two consecutive DTS-measurements. The results show that the measured values of the volume flow sensor (black in Fig. 6) can be reproduced, but they are in superposition with a strong noise. This noise is a consequence of the random deviations of the DTS-system. Improved results can be obtained if the vertical displacement speed of the temperature profile is determined from two time steps that are separated by seven individual measurements. This leads to reduced statistical noise in the calculated vertical displacement speed of the temperature profiles and thus the calculated volume flow. In addition, for the orange curve, the moving average of the determined volume flow is

formed over five individual values. It has been found that this configuration shows the least deviation compared to the measured values. If the deviation between the black and the orange curve is related to the long-term average volume flow of the heat storage tank of 185 m³/h, the mean deviation between the measured volume flow and the volume flow determined from the temperature field is only 4.6 % for 5 May 2016. This method has practical advantages in order to verify whether the operation data is in accordance with the DTS-measurement data. Besides, in cases where there is no volume flow measurement device approximate values can be obtained.

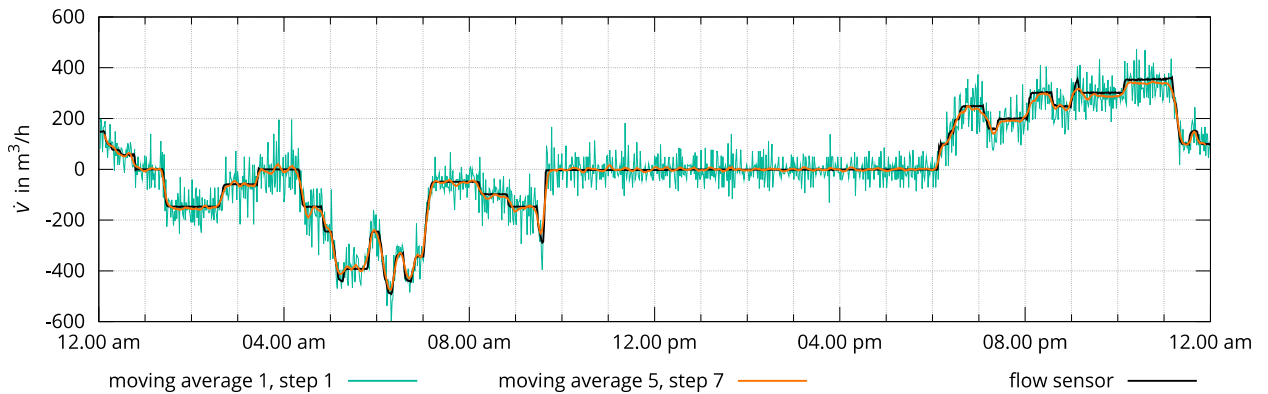


Fig. 6. calculated volume flow based on the vertical temperature profile compared to measured volume flow

3. Two-zone atmospheric heat storage tanks

The atmospheric two-zone heat storage tank is also based on HEDBÄCK and is shown as an example in Fig. 7 (not to scale). It has the same design features as the one-zone atmospheric heat storage tank, but is divided into two zones by an insulated, dome-shaped intermediate floor. The intermediate floor can be considered dimensionally stable.

The two storage zones each have two radial diffusers for charging and discharging. Moreover the two-zone heat storage tank features a vertical compensation pipe. This is an open ended pipe which serves as a hydraulic connection between the upper and lower storage zone. The length of the pipe and the amount of additional openings depend on constructive and functional requirements. The permanent exchange of fluid between the two storage zones is important for two reasons: The density changes occurring in the upper storage zone and the connected pipe system through charging and discharging have a direct effect on the filling level due to approximately constant fluid mass in the storage tank. In the lower storage zone, however, the volume is constant due to the fixed position and shape of the intermediate floor. Since there is no further expansion tank available for the heat storage tank, density changes occurring during charging and discharging of the lower storage zone must be compensated by a mass flow through the compensation pipe. Moreover, it serves as a safeguard against negative pressure or overpressure in the lower zone (e. g. as a result of operating errors).

On the other hand, the exchange of fluid between the two storage zones may encourage undesirable effects: The compensating pipe primarily conveys fluid from one storage zone to the other, or as a side effect within the upper storage zone itself in case of additional openings in the compensating pipe. Thus a flow in the immediate vicinity of the respective opening is induced when fluid leaves the compensation pipe. This fluid usually has not the same temperature as the surrounding fluid when entering the respective layer within a storage zone. Due to the inevitable convective mixing, the thermal stratification present in a storage zone can be negatively influenced.

Nevertheless, the hydraulic coupling of both storage zones has an important effect, which is an essential feature of the two-zone heat storage tank: The pressure level in the lower storage zone is sufficiently high to store water at temperatures above 100 °C. Currently, temperature levels of up to 130 °C are in use. These temperature levels do not mark the physical limits but meet the locally applicable safety measures. Consequently, the volume-specific heat capacity of the two-zone heat storage tank is higher compared to a one-zone heat storage tank of the same size. Thus, the higher total investment costs can be compensated with respect to the amount of stored energy.

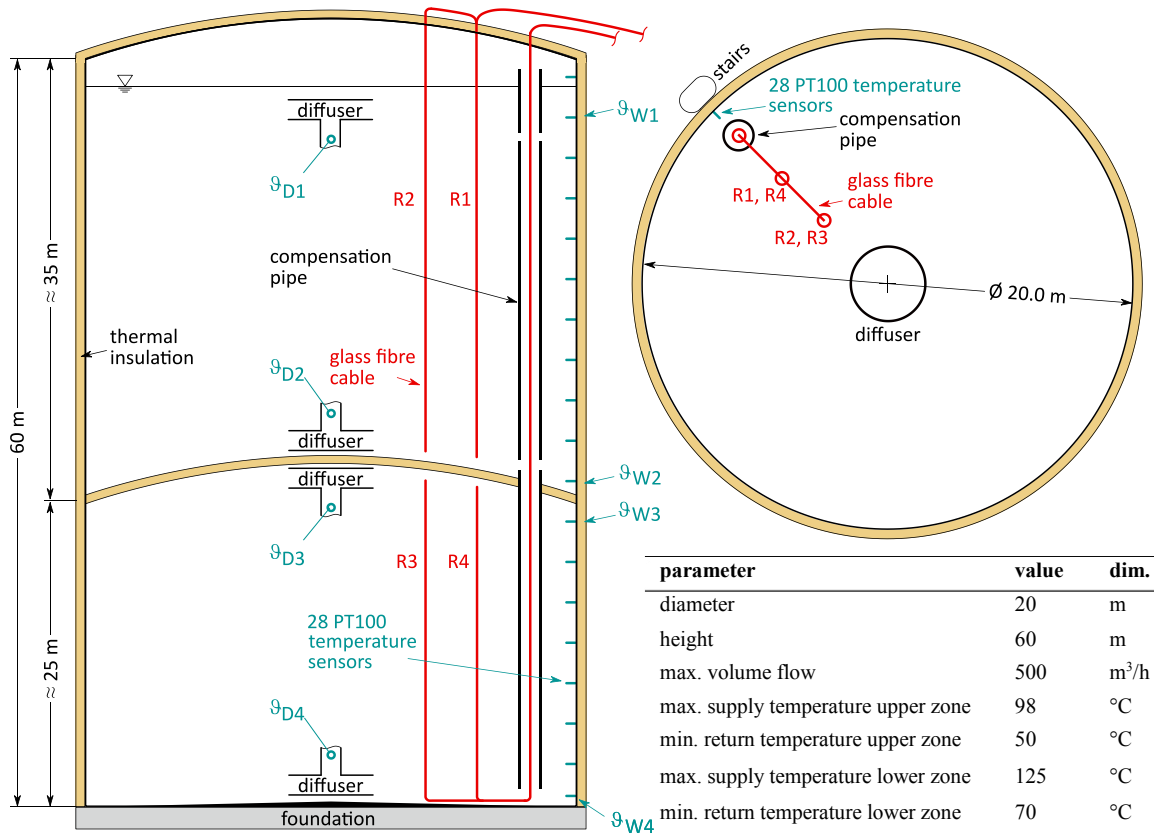


Fig. 7. measurement concept of the atmospheric two-zone heat storage tank and main design parameters

The constructive design of the two-zone atmospheric heat storage tank is not akin to that of the pressurized heat storage tank, since

- the maximum pressure level is not higher than with a one-zone heat storage tank of the same height
- the heat storage tank is operated as a displacement heat storage tank at atmospheric conditions and
- the intermediate floor experiences only a small pressure difference.

For atmospheric two-zone heat storage tanks there are two application possibilities: If heat is to be provided at two different temperature levels, both the lower and the upper storage zone can be used actively for heat storage which is the case for the study presented in this paper. The nominal operation of this heat storage tank had been described in [3]. Alternatively, the sole active operation of the lower storage zone is possible. The upper storage zone then serves as pressure load and may be used as water reservoir, for example.

3.1. Measurement concept

The measurement setup features vertical temperature profiles at two radial positions both in the upper and lower zone of the heat storage tank as well as in the compensation pipe (Fig. 7). The vertical temperature profiles at positions R1 and R4 had been captured at the same radial distance from the diffusers. The same applies to R2 and R3. For each zone, time-averaged means of 1 min had been calculated based on a physical time of 30 s due to alternating measurements on two cables. Supplementary operating data is available in 1-minute resolution for volume flow of the upper and lower zone, pressure at the bottom, supply and return temperatures for both the upper and lower zone and 28 vertically aligned PT100 sensors.

3.2. Radial homogeneity of the temperature field

To investigate radial homogeneity of the temperature field, two cases had been chosen: A reference case with no charging or discharging of the upper and lower zone as well and a case in nominal operation mode with thermal stratification and rather high volume flow in the two zones.

For the reference case the vertical temperature profiles at positions R1 for the upper zone and R4 for the lower zone are depicted in Fig. 8. The upper zone can be interpreted as almost completely discharged as most of the fluid up to a height of 50 m is at the temperature level of about 50 °C with a weakly pronounced thermocline in between. The lower zone is also at a low temperature level but thermal stratification is more pronounced. However, the superposition of the temperature profiles at four hour intervals show that there are no macroscopic changes in thermal stratification within both storage zones. Therefore, this case was used to determine the standard deviation of the measurement setup in order to reproduce the noise of the measurement as a comparison criterion for radial homogeneity. This was necessary because the standard deviation depends among others on the average time of the measurements, the length of the cable and the type of the cable. However, a brief estimate of the standard deviation according to the manufacturer's data sheet was not satisfying.

Under the precondition that there are no macroscopic changes in the temperature field between two time steps, i. e. one minute of physical time, temperature differences of consecutive measurements had been calculated along the two cables of the upper and lower zone. The standard deviation for the temperature differences is $\sigma = 0.26$ K for the upper zone and $\sigma = 0.31$ K for the lower zone (database for both values more than 300,000 values). These standard deviation are much larger than for the measurement setup of the one-zone heat storage tank presented above ($\sigma \approx 0.12$ K) because here the data base is different. The 1-min average data is based on alternating measurements for each cable (see section 3.1) meaning that for the same average time only half of the data is available. Furthermore, every vertical measuring section yields twice the information about the temperature due to constructive measures. Here, only one half of the available data had been used.

Subsequently, a case in nominal operation mode had been investigated, i. e. 07 October 2015. The operating data is depicted in Fig. 9. The upper zone gets charged at low and moderate volume flows with a standstill phase and a peak level of about 240 m³/h in between. The lower zone also gets charged throughout the day with a peak level of about 250 m³/h and a single peak value of 350 m³/h in between.

The evolution of the temperature field is shown in Fig. 10. The solid orange lines represent the temperature field in the heat storage tank whereas the dotted violet lines represent the temperature profile in the compensation pipe. The charging processes in both zones are shifting the temperature profiles downwards. In the lower zone the shape of the temperature profile remains stable, the coldest layer at the bottom is pushed out through the lower diffuser which is also indicated by the increase of the return temperature ϑ_{D4} in Fig. 9 (b) at 10.00 am. The temperature profile in the upper zone gets modified, especially the size of the thermocline is increasing.

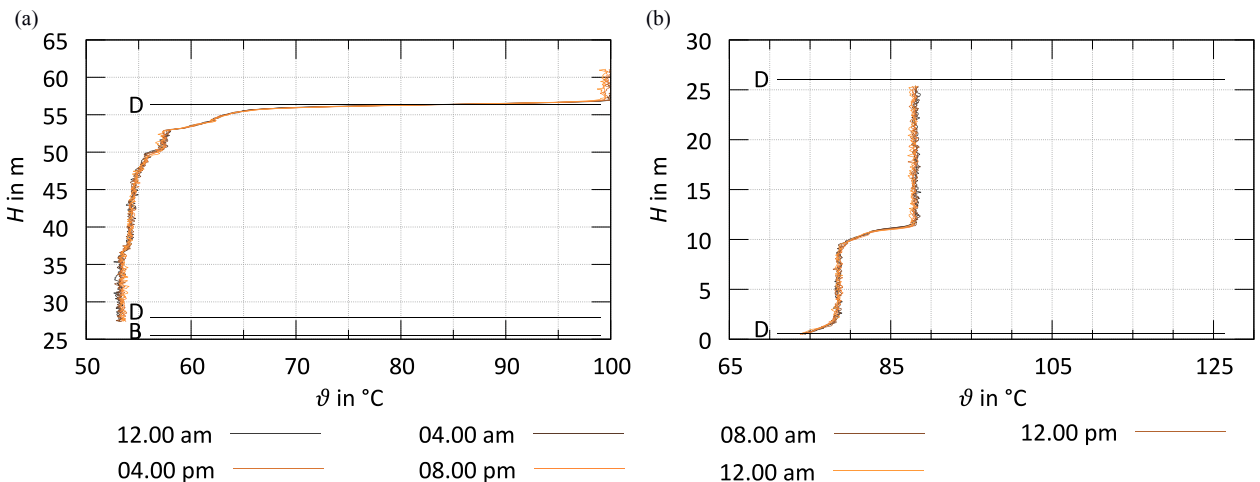


Fig. 8. temporal evolution of the temperature field for the reference case in the upper zone (a) and in the lower zone (b)

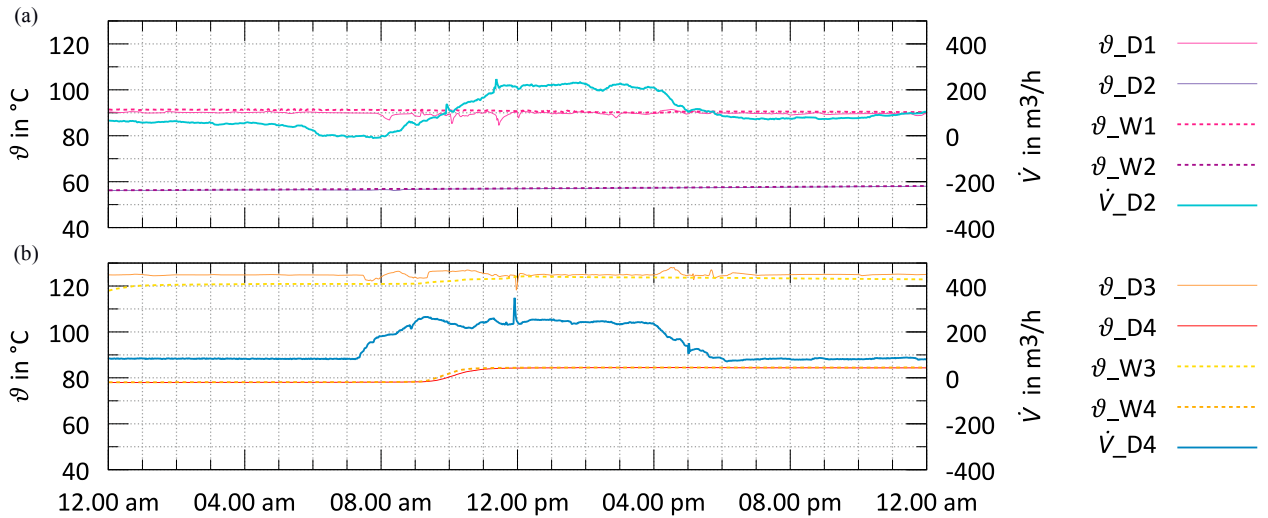


Fig. 9. operating data of the two-zone heat storage tank at 07 October 2015; (a) upper zone (b) lower zone

The temperature in the compensation pipe is decreasing from the bottom, where the temperature level is equal to the temperature of the coldest layer of the lower zone, to the first opening which is located at the bottom of the upper zone. The temperature profile is strongly convex, which is typical for a charging process in the lower zone inducing an upward directed mass flow to compensate volume expansion due to density changes. At the first opening fluid from the bottom of the upper zone is entering the compensation pipe. The mixing process in the compensation pipe within the upper zone is considered to be turbulent while the main flow direction is still upward which is indicated by the strongly irregular shaped temperature profiles e. g. Fig. 10 (a) 08.00 am and 04.00 pm. Animated visualizations of this operating regime show macroscopic fluctuations in time of the temperature profile in this area. Finally the fluid is leaving the compensation pipe through its top opening. The described process influences the thermal stratification within the upper zone as described in [3].

To investigate radial homogeneity the temperature differences $\vartheta_{R2} - \vartheta_{R1}$ for the upper zone and $\vartheta_{R3} - \vartheta_{R4}$ for the lower zone are depicted in the normal probability plot in Fig. 11. The solid line indicates the normal distribution

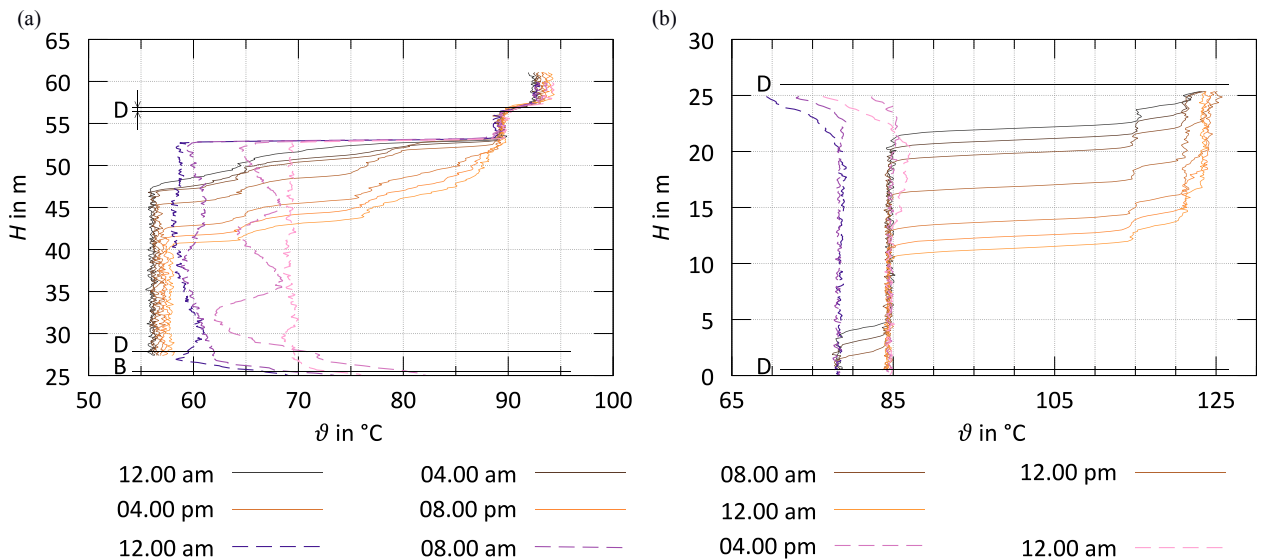


Fig. 10. temporal evolution of the temperature field in the upper zone (a) and in the lower zone (b); solid lines: temperature profiles within a storage zone; dashed lines: temperature profiles within the compensation pipe

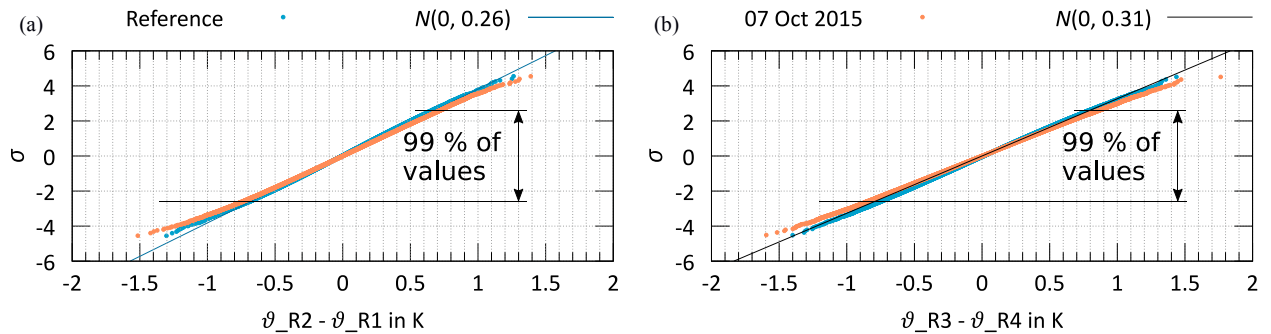


Fig. 11. normal probability plot of radial temperature differences for 07 October 2015 (a) upper zone (b) lower zone

with an expected value of $\mu = 0$ and the standard deviation for each zone. The blue dots in Fig. 11 represent temperature differences for the reference case. All evaluated temperature differences, with the exception of few outliers, are in the range of ± 1.4 K and stay close to the normal distribution for both the upper and the lower zone. Thus, they are part of the noise of the measurement system. The orange dots in Fig. 11 represent the data of the selected case in nominal operation mode. If the compensation pipe would have an influence on the radial homogeneity of the temperature field significant negative temperature differences would occur in the normal probability plot of the upper zone (Fig. 11 (a)) as the fluid in the compensation pipe has a higher temperature than in the surrounding fluid (Fig. 10 (a)). Especially for the period of high vertical displacement speed of the thermocline in the lower zone (Fig. 10 (b)) and turbulent mixing within the compensation pipe in the upper zone between 08.00 am and 04.00 pm visible effects are likely. But the determined temperature differences are very close to the reference case and to the normal distribution. Thus, it can be concluded that the compensation pipe does not affect significantly radial homogeneity in the two-zone heat storage tank although an influence on thermal stratification had been proven [3]. In the lower zone there are also no radial effects. The value at 1.78 K is considered as an outlier of the measurement system which cannot be explained further yet.

3.3. Conclusion

Hydraulic coupling of the upper and lower storage zone enables heat storage at temperature levels above 100 °C in the lower storage zone of a two-zone heat storage tank. Basically, there are two operating options: Heat can be provided either at two different temperature levels by using both zones actively for heat storage or the sole active operation of the lower storage zone is possible. In the presented case both zones are used actively, in the lower zone temperature levels of up to 130 °C are possible.

Despite an influence of the compensation pipe on thermal stratification had been proven in [3] the results presented in this paper show that the temperature field is homogeneous in radial direction. This had been confirmed for a reference day without charging or discharging and a case with significant change in the state of charge.

Acknowledgements

This research project is funded by German Bundesministerium für Wirtschaft und Energie (FKZ 03ET1322A).

References

- [1] Rühling K et al. Erhaltung der Marktfähigkeit von KWK Anlagen mittels Einbindung von Umweltenergie. Dresden (GER): TU Dresden, Institute of Power Engineering, Professorship of Building Energy Systems and Heat Supply; 2016. Report No.: ISBN: 3-89999-057-9. Contract No.: FKZ 0327831. Sponsored by BMWi (GER).
- [2] Herwig A, Rühling K. Fibre-Optic distributed temperature sensing of large hot water storage tanks. *14th International Symposium on District Heating and Cooling*; 2014 September 7-9; Stockholm, SE.
- [3] Umbreit L, Herwig A, Rühling K. Measurement-based description of the temperature distribution in large atmospheric heat storage tanks; *5th International Solar District Heating Conference*, 2018 April 11-12; Graz, A.



16th International Symposium on District Heating and Cooling, DHC2018,
9–12 September 2018, Hamburg, Germany

Improving operational efficiency of power plants through on-site calibration of flow sensors

Ulrich Müller^{1*}, Michael Dues², Waldemar Hübert¹, Christoph Rautenberg¹

¹OPTOLUTION Messtechnik GmbH, Gewerbestr. 18, Lörrach, 79539, Germany

²ILA R&D GmbH, Karl-Heinz-Beckurts-Straße 13, Jülich, 52428, Germany

Abstract

Growing industrial and legal need for precise heat and flow measurements in district heating facilities pushed the development and application of a technology for laser based on-site calibrations of large flow sensors. This calibration method works with direct flow velocity measurements along the pipe diameter through a custom made ball valve which is mountable during plant operations.

To accredit this calibration method an extensive uncertainty budget was created. The largest contribution to the uncertainty budget, the flow distribution in the relevant cross section of the pipe, was researched and quantified in an extensive project. The result of this project is a profile class model, where the resulting uncertainty of the measurement can be derived directly from the measurement itself.

The on-site calibration method is already deployed and executed in over 120 cases with a great variety in resulting flow sensor accuracies in within their operational conditions.

© 2018 The Authors. Published by Elsevier Ltd.

This is an open access article under the CC BY-NC-ND license (<https://creativecommons.org/licenses/by-nc-nd/4.0/>)

Selection and peer-review under responsibility of the scientific committee of the 16th International Symposium on District Heating and Cooling, DHC2018.

Keywords: flow measurement, innovative calibration technology, on-site calibration of flow sensors, flow sensor precision

* Corresponding author. Tel.: +49-7621-160-1515; fax: +49-7621-160-1526.

E-mail address: mueller@optolution.com

1. Motivation

A lot of operations and efficiency calculations for thermal power plants and district heating and cooling systems are based on measurements of large flow sensors (in this context greater than DN 150) and therefore, are strongly dependent on precise volume flow measuring data. These flow sensors (FS) are often used continuously for decades after an initial calibration at external test rigs under optimized conditions. An accredited recalibration of these FS within their actual operating conditions was not possible so far.

In the best case scenario those FS are unmounted and recalibrated on external test rigs. A large drawback of this procedure is the interruption of supply in addition to its already high costs. Furthermore, calibration conditions on test rigs can differ greatly from the actual operating conditions. These deviations are, for example

- Differences of the fluid parameters on test benches compared to supply systems, so e. g. large FS are calibrated on test benches with low temperature fluids and pressures
- Deviations from the well-known symmetrical flow conditions on test benches to the flow conditions in mounted state
- Long-term drifts, for example through abrasions (especially on orifices) and deposits and
- Deficiencies of the installation conditions (e. g. regarding the undisturbed lead-in length and/or grounding) of the FS.

So even if calibrated, the measurement uncertainty of the FS in operation remains fairly unknown.

More precisely measured values of FS may uncover hidden saving potentials and allow for more precise performance indicators, improving energy efficiency as well as day-to-day operations. A wide range of quality management objectives of district heating and cooling suppliers, namely higher accuracy of flow sensors for billing purposes, increased balancing certainty of energy flows and a verifiable quality of main benchmarks (e. g. primary energy factor, CO₂ balance, CHP ratio etc.), could be supported by more precise measurements of volume flow rates.

These reasons pushed the development of a technology for the on-site calibration of large FS independent of their measuring principle in the mounted state, without the need to interrupt supply and under its actual operating conditions.

2. Description of the technology

The on-site calibration (OSC) method is based on the optical measurement principle of Laser Doppler Velocimetry (LDV). Using this measurement technology, local flow velocities are measured across one or multiple paths along the pipe diameter. Applying a rotational integration to the measured velocity profile(s) a volume flow can be calculated to calibrate the FS.

The essential optical access to the flowing fluid is realized by welding a specially designed ball valve and subsequent hot-tapping without the need to interrupt fluid flow, which is an operational advantage compared to recalibration on external test rigs. Using a sleeve inset a special designed window is positioned and aligned to the interior surface of the pipe to ensure that the flow remains unaffected by the optical access [1], see also Figure 1a. The safety of this process is reviewed and certified by TÜV Rheinland, which guarantees that the optical access can be created within systems of up to PN40.

Further preparations for the OSC involve mounting of the pressure window flange with subsequent installation of the measurement equipment itself, which includes the laser probe on a traversing system. The velocity profile of the fluid flow is scanned through automated movements of the LDV probe along a fixed axis parallel to the pipe diameter, as seen in Figure 1b. During this velocity scan, the measurement values of the FS under test are logged with the highest possible temporal resolution.

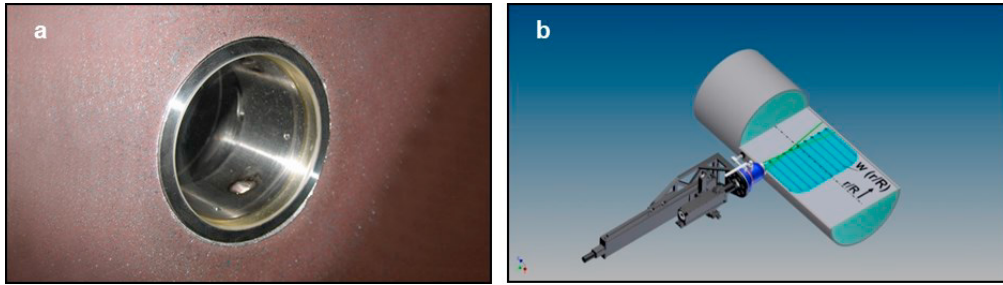


Figure 1: (a) Interior surface of the pipe with the inserted special window; (b) Demonstration of profile velocity ($w(r/R)$) measurement with LDV

To take the fluctuations of the volume flow rate during the measurement process into account the measured local velocity values are normalized with data of an additionally mounted ultrasonic clamp-on meter. This approach ensures the independence of the calibration from the FS under test, as neither linear error curves of the FS nor its correct temporal behavior can be guaranteed during the calibration. This case is especially relevant in calibrations during day-to-day operations, where the volume flow rate is fluctuating.

The normalization method is independent from the uncertainty and only reliant on the linearity characteristic of the device [2]. Therefore the used ultrasonic-clamp-on FS is special examined for this task. The measurement error of the FS is calculated through a comparison between the calculated LDV volume flow and a time averaged volume flow of the FS. The calibration procedure is repeated for different volume flow rates.

3. Measurement Uncertainties and Accreditation

Growing demand of the supply industry for reliable measurement values reinforced the need for a metrological accreditation of the OSC method. To achieve the credibility and traceability necessary for the demands of an accreditation according to the international standard ISO/IEC 17025 [3] a wide range of uncertainties from multiple sources needed to be quantified and put together in an extensive uncertainty budget as seen in Figure 2.

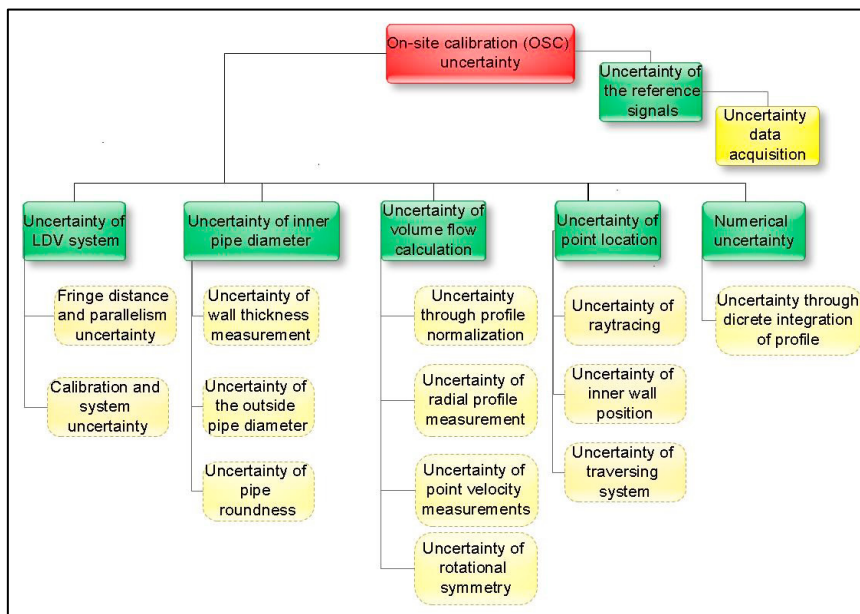


Figure 2: Overview about the different measurement uncertainties of the OSC method

Level of profile overlap:

$$K_D = \frac{1 + \left(\frac{r}{R}\right)_{\max}}{2} \quad \text{in \%} \quad (4)$$

with $\left(\frac{r}{R}\right)_{\max}$ the maximum penetration depth of the profile.

This key coefficient model was validated with more than 200 external measured velocity profiles with known volume flow rates. In consequence more than 95 % of the calculated volume flow rates fulfilled the acceptance criteria of two times of the standard deviation.

Figure 3 shows examples of the different profile classes compared to a fully developed profile acc. to GERSTEN & HERWIG [7]. Even though those velocity profiles are largely different compared to a fully developed turbulent profile one can still classify them from metrological point of view and give a good estimation of the induced volume flow bias and uncertainty contribution to the OSC method.

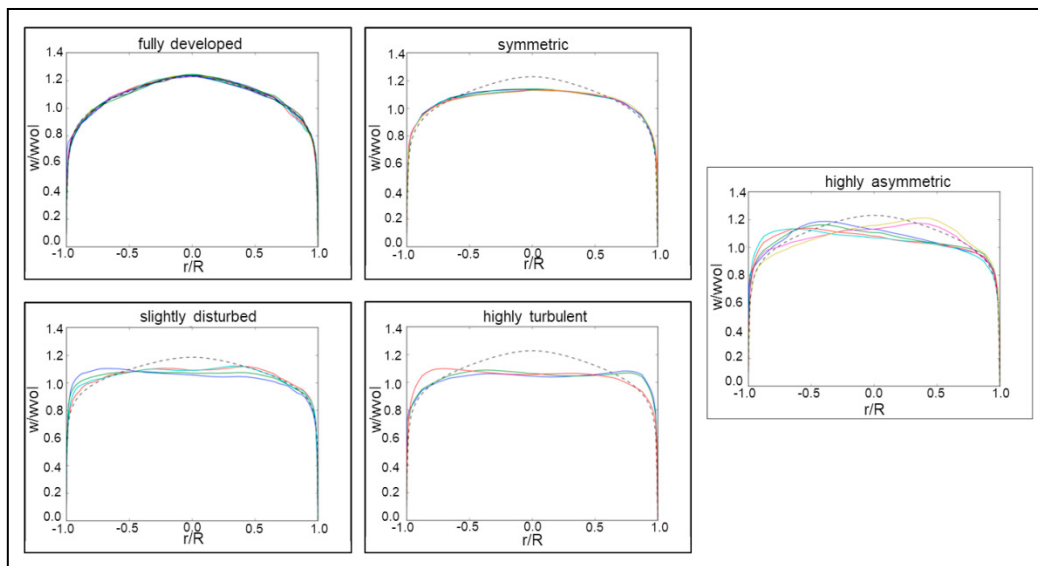


Figure 3: Examples of the different profile classes in contrast to a theoretical fully developed profile (GERSTEN & HERWIG)

In practice, the first three profile classes are most prominent for a carefully selected position of the optical access. The latter two profile classes appear mostly due to unexpected fluid distributions or due to restrictions in calibration positions inside power plants, forcing the OSC method to less favorable positions along the pipe system of the FS under test. As this classification method is based on the measurement itself, one cannot know beforehand how precise the measurement is going to be. Hence the position of the measuring path (the position of the welded ball valve) in regards to the flow situation is critical and must be chosen well.

The following Table 1 shows the achievable total measurement uncertainties for each one of these profile classes. The numbers are based on the measured value with a coverage factor of $k = 2$, expanding confidence interval to 95%. The minimum uncertainty for the profile class “fully developed” consists only the non-profile relevant contributions. For the combined uncertainties of all other profile classes the influence of the deviation from the rotation symmetry is the dominant contribution.

Table 1: Overview of the profile classes and their resulting measurement uncertainties

Profile class	Realistic measurement uncertainty (k = 2)
Profile class “fully developed”	0.7 %
Profile class “symmetric”	1.4 %
Profile class “slightly disturbed”	2.3 %
Profile class “highly turbulent”	2.7 %
Profile class “highly asymmetric”	4.2 %

In summary, it can be stated that the actual measurement uncertainty of the calibration strongly depends on the on-site flow conditions. On the basis of the on-site specific measurement uncertainty budget and metrologically traceable measurement tools, the calibration results are fully traceable to the national measurement standards of the German National Metrological Institute. This was one of the requirements for the accreditation as an on-site calibration laboratory according ISO/IEC 17025. The accreditation includes the following fluid conditions for the OSC method:

- Volume flow rate: 20 m³/h to 30'000 m³/h
- Fluid temperature: 5 °C to 150 °C
- Minimum bulk velocity: 0.3 m/s.

4. Benefits of the OSC technology and project examples

So far calibrations took place in a lot of power stations in Germany, Switzerland and Austria, with of a variety of motivations. The operating conditions of the measurements ranged from 50°C to 180°C of fluid temperatures, from 2 bars to 18 bar fluid pressure and pipes of sizes between DN 150 and DN 1000 (Figure 4a). There, the OSC measurements are useful auxiliary tools for heating grid planning and optimization processes, as well as input for FS lifetime logs for quality management purposes.

On another matter, OSC are often used as recalibration tool for flow sensors which were subsequently added as instrumentation to the grid lines. With those flow sensors often being ultra-sound clamp-on or other comparatively simple mountable instrumentation, they often lack the needed measurement precision. An additional calibration after mounting can decrease uncertainty of those flow sensors by a couple of percentages.

Another use of the OSC technology is the validation of FS precision in commercial practice between supplier and distributor of heat or water, where measurement errors have direct effects on accounting between the parties involved. E. g. one project covered calibrations of large water meters ranging from DN 500 up to DN 1200 within a large drinking water grid in Australia. An example of an OSC measurement situation on an underground water pipeline is given in Figure 4b. The distributor of the drinking water used the OSC method as there were found to be accounting discrepancies between the amount of water sold and the amount of water purchased, leading to accounting problems. The calibrations pointed out the flow sensors between supplier and distributor to be the dominating cause for the accounting mismatch.

Growing legal regulations and the increasing needs for more efficient and therefore more profitable operation lead to increasingly narrower design parameters of modern power plants. These design parameters and key factors range from thermic efficiency rates, CO₂ monitoring, primary energy factors to cogeneration proportion. But calculation of these factors can only be as exact as the least precise data source that goes into these calculations. As such, flow rate instrumentation often proves to be the most uncertain part in the calculation chains. In actual operational conditions the measurement uncertainty of flow sensors is often larger than given by their calibration certificates.

Further issues with flow sensor precision often arise during a demerger of grid lines and sourcing power plants, where formerly just internal measurement points of heat and flow become relevant accounting points. These heat

measurement points often were not initially designed to be precise measurement points but are suddenly subjected to be an important accounting measurement between two clients.

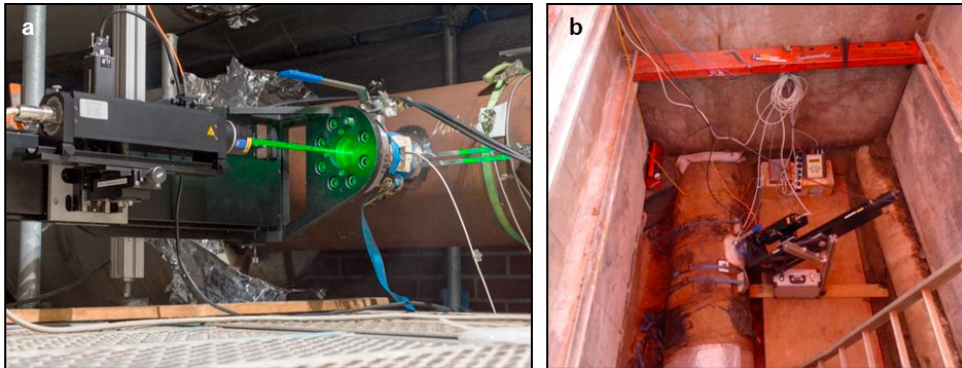


Figure 4: (a) OSC measurement equipment on a district heating pipe; (b) OSC measurement situation on an underground water pipeline

Generally speaking, the OSC technology is considered in cases where reliability and precision of FS is critical. It can support the calculation credibility of primary energy factors or CO₂ balance calculations indirectly through improved flow sensor data. The OSC method also helps in process control and optimization, as improved and therefore more reliable flow sensor readings help identifying bottlenecks and grid reserves. Therefore, while not being a direct planning tool for new construction projects or district heating grids, OSC can assist as auxiliary tool for decision making in special cases.

Normally, FS of large diameters (larger DN 150) are not covered by obligatory calibration. Additionally, there exist no legal national regulations in many European countries for periodical recalibrations of flow sensors these sizes in commercial practice. Thus the accuracy of FS remains entirely in the responsibility of the operators, where the large spectrum of operational conditions for FS often leads to inaccurate flow rate data.

Up to now, 123 large flow sensors were calibrated with the OSC method. The measurement errors of 25 flow sensors were greater than 4 % after subtraction of the inherent uncertainty of the OSC method. This means approximately 20 % of all inspected flow sensors show significant deviations from their initial test rig calibrations. The mean error of all tested flow sensors calculates to approximately -3.2 %. After subtracting the most typical uncertainty of the OSC method of 1.4 % (for profile class “symmetric”) a mean performance increase of 1.8 % is achieved. Transferred to accounting uncertainties in an exemplary case of a 50 MW measuring point at 150 heating days per year the OSC method would lead to a performance increase of 3'240 MWh per year. At an estimated price of 60 €/MWh the performance increase calculates to 194'400 €/year.

5. Summary

A new method to calibrate flow sensors under their operational conditions has been developed and already deployed in many different practical applications. Compared to other procedures of on-site checks of large flow meters within their operational conditions this method is directly traceable to national metrological standards, and therefore highly reliable in its measurement uncertainties and accreditable according to ISO/IEC 17025.

The nature of this laser optical calibration method is a direct fluid velocity profile measurement with the benefit of knowing the flow characteristics to a suitably sufficient degree to derive its own uncertainty budget. The installation of the necessary optical access requires no interruption of the supply. Depending on the flow conditions the combined uncertainty of this method ranges from 0.7 % up to 4.3 % in rare worst case practical scenarios. This method is highly suitable to improve flow sensor accuracy within cogeneration plants, district heating and cooling systems or also drinking water systems and thus very beneficial for optimization processes, calculations of performance indicators or accounting purposes. The OSC technology works seamlessly in conjunction of daily cogeneration plant operations as the calibration itself works within operation conditions and without the need to

interrupt supply. The OSC method also has the added benefit that it automatically calibrates the flow sensor at test points of day to day operations, where accuracy matters the most.

Acknowledgement

We would like to thank the German Federal Ministry of Economic Affairs and Energy for its continued support within the EnEff:Wärme project “On-site calibration of large flow meters in district heating systems” and the involved partners, the German National Metrological Institute Physikalisch-Technische Bundesanstalt, the Technical University of Berlin and the three representatives of industry, VATTENFALL Europe Heat Berlin GmbH, ILA R&D GmbH and OPTOLUTION Messtechnik GmbH.

Abbreviations

FS	Flow sensor
LDV	Laser Doppler velocimetry
OSC	On-site calibration

References

- [1] Dues, M.; Müller, U.; Kallweit, S., 2011. Method for measuring a flow, installation unit and measuring apparatus, Application: 30.11.2011. DE, *Patent Specification* EP 2 389 566 B1. 16.11.2016
- [2] ISO/TC 30/SC 5, ISO 3966:2008. Measurements of fluid flow in closed conduits – Velocity area method using Pitot static tubes. ISO Standard, 2008.
- [3] ISO/CASCO, DIN EN ISO/IEC 17025:2005. General requirements for the competence of testing and calibration laboratories. ISO Standard, 2005.
- [4] AGFW – Der Energieeffizienzverband für Wärme, Kälte und KWK e.V.. “EnEff. Wärme – Energieeffizienz in der Fernwärme durch Vor-Ort-Kalibrierung von Durchflussmessgeräten – Kopplung von laseroptischen und numerischen Verfahren”. Gemeinsamer Abschlussbericht der Partner ILA R&D GmbH, OPTOLUTION Messtechnik GmbH, Physikalische-Technische Bundesanstalt, Technische Universität Berlin, VATTENFALL Europe Wärme AG, *AGFW, Forschung und Entwicklung*, Heft 46, Frankfurt/Main, 2018.
- [5] Yeh, T., T. und Mattingly, G., E. Pipeflow downstream of a reducer and its effects on flowmeters. *J. Flow Measurements and Instrumentation*. 5 (1994), S. 181-187.
- [6] Russo, F. und Basse, N.T. 2016. Scaling of turbulence intensity for low-speed flow in smooth pipes. *Flow Measurements and Instrumentation*. 52 (2016) 101-114, 2016.
- [7] Gersten, K. 2005. Fully developed turbulent pipe flow. In Merzkirch, W. (Ed.) *Fluid Mechanics of Flow Metering*. Berlin Heidelberg, New York: Springer-Verlag, 2005.



16th International Symposium on District Heating and Cooling, DHC2018,
9–12 September 2018, Hamburg, Germany

Field experience with ULTDH substation for multifamily building

Jan Eric Thorsen^{a*}, Torben Ommen^b

^a*Danfoss A/S, Nordborgvej 81, 6430 Nordborg, Denmark*

^b*Department of Mechanical Engineering, Technical University of Denmark, Niels Koppels Allé, 2800 Kgs. Lyngby, Denmark*

Abstract

Ultra-low temperature district heating (ULTDH) substations may be an important enabler for integrating higher shares of renewables and waste heat in the district heating (DH) network. In the paper, we describe a concept and first experimental results for producing domestic hot water (DHW) at DH supply temperatures of 45°C. The substation utilises a heat pump for boosting the DH temperature up to approximately 60°C to an accumulation tank, after which the DHW can be produced on demand for temperatures up to 55°C. Additionally, the system included a separate heat pump to supply the DHW circulation heat demand. The DH accumulator tank provides load shift opportunities, which is important going towards the integrated, flexible and renewable based future energy system. The two heat pumps operate with a COP of approximately 5, which results in representative share of approximately 11-13 % electricity to supply the DHW including circulation.

© 2018 The Authors. Published by Elsevier Ltd.

This is an open access article under the CC BY-NC-ND license (<https://creativecommons.org/licenses/by-nc-nd/4.0/>)

Selection and peer-review under responsibility of the scientific committee of the 16th International Symposium on District Heating and Cooling, DHC2018.

Keywords: Heat Booster Station, Ultra Low Temperature District Heating, Load Shift, Heat Pump, 4th Generation District Heating

* Corresponding author. Tel.: +45 74882222; fax: +45 74 7449 0949

E-mail address: jet@danfoss.com

1. Introduction

To achieve the goal of 100 % renewable (RE) heat and power supply and increased energy efficiency, utilization of available RE resources is important. In this context, the benefits of ultra-low temperature district heating (ULTDH) are multiple. First, heat losses from the DH network can be reduced, which also becomes increasingly important in the future heat supply to low energy buildings, in order to keep relative and absolute network heat losses at an appropriate level. Second, ULTDH enables the use of a higher share of low temperature renewable energy resources such as solar, geothermal and industrial waste heat. If a heat pump is needed in order to utilize such heat sources, the low supply temperature allows significantly improved coefficient of performance (COP) of the utility plant [1]. Lowering the supply temperature may further facilitate individual customers to act as prosumers in case of waste heat generation at an appropriate temperature level. Moreover, ULTDH in local networks opens for possibility to connect new users to existing DH systems without large additional capacity investments. The ULTDH concept, with it the option of thermal and electric load shift, is one of the possible solutions going towards the 4 generation DH system [2].

The viability of low temperature district heating (LTDH) consumer with around 55 °C supply temperature has been proven and demonstrated in Denmark [3]. With it, it is possible to prepare DHW water at 50 °C without any additional energy source for boosting the temperature. However, the lower temperature heat sources down to 40-45 °C, which are sufficient for space heating most of the heating season and for floor heating in general, cannot be utilized directly in LTDH systems due to DHW temperature requirements. A reduction of supply temperature to 40 °C would in Denmark allow additional 10.000 TJ from waste heat sources, if solar thermal waste heat is excluded [4].

For these reasons, the ULTDH has attracted significant academic interest in recent years. Several studies show that the use of booster heat pumps allows reduced supply and return temperatures in the network and thereby provide a decrease in transmission losses and a different optimal relation between heat and pumping losses [5–7]. Assuming the ULTDH supply at 44 °C to originate from centralised heat pumps, the use of booster heat pumps results in an increase of 12 % in the overall performance compared to direct supply at above 60 °C [5]. By further improving the booster technology, the performance potential increase is approximately 17 % [8]. In case the DH was produced by CHP plants, the ULTDH resulted in a decrease of approximately 20 % compared to LTDH.

In order to take advantage of the multiple benefits of the ULTDH system, a substation was developed for multifamily buildings, based on a micro-booster concept for individual single-family houses [9,10]. The consumer DH unit boosts the temperature of the district heating water for DHW preparation and circulation, whereas the space heating is supplied directly by the ULTDH. In the paper, we present the integration methodology of the high efficiency heat pump as well as the layout of the substation. Further, the case study of the building and the implementation of the system is presented. The results show the first operational experience from the test installation site in Copenhagen, as part of the EnergyLab Nordhavn project.

2. Methods

2.1. The ULTDH concept

With the supply temperatures of DH below the needed temperature for producing DHW at 55°C by a direct heat exchange process, the temperature had to be raised or boosted. For this purpose, an electric driven heat pump was applied. In the developed heat booster station, this increase was obtained by use of heat pumps at the primary side, which utilized the supply of DH as the heat source. In cases where the DH network is used as the heat source, it is important that a significant amount of the heat originates from natural resources, such as heat pumps utilizing RE or solar thermal units, or waste heat, such as flue gas condensation, in order for the ULTDH system to exceed the performance of systems with LTDH. The conceptual layout of the system was chosen from a range of designs, in order to obtain the best thermodynamic performance of the HBS, and with it the highest coefficient of performance of the heat pump, for any DH supply between 35°C and 47°C [11].

2.2. The basic principles for the installed heat booster station

Due to capacity costs and the start-up dynamics of a heat pump, a tank for heat accumulation was introduced. The tank itself also enables load shifting in relation to electricity consumption as well as DH consumption. Due to legionella risks, it was decided to place the tank on the primary side and utilise an instantaneous heat exchanger for heating the DHW when tapped. The heat booster station (HBS) was designed and sized for operation in a multifamily building.

The overall concept of the HBS is shown in Fig. 1. Pls. note the system is simplified, which means systems related to heat pumps, control equipment and additional hydraulic and electric systems are not shown.

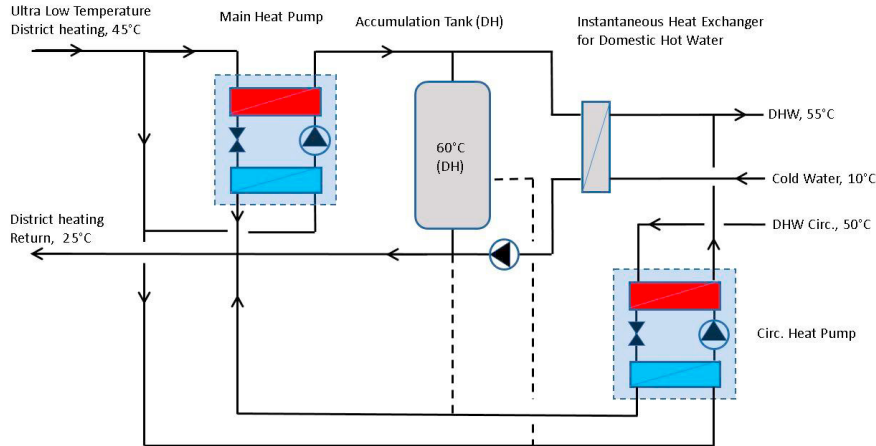


Fig. 1. Basic layout of the heat booster substation

The principle for the main heat pump is that the DH supply flow is split into two. The first part is led through the condenser of the heat pump, where it is heated or boosted to 60°C–65°C and let into the DH accumulation tank. The second part is led through the evaporator, where it's cooled down to e.g. 25°C and thus acts as the heat source for the heat pump.

To avoid the DHW circulation impacting the DH accumulation tank, by means of fast discharge and loss of the thermal stratification, a separate heat pump was applied for maintaining the DHW circulation temperature. The heat source was chosen to be the ULTDH supply, or from the bottom of the accumulation tank, in case the temperatures

are suitable. The buildings space heating circuit was operated in parallel to the DHW system and is not a part of the HBS.

2.3. Installation in the Building

The HBS unit was installed in Havnehuset located at the Nordhavn area of Copenhagen. The heat demand originated from supplying DHW and DHW circulation to 22 flats by 8 risers. 10 flats are in a 5-storey setup, and 12 flats are in a 3-storey setup, where the upper flats are in 2 storeys. The building is shown in Fig 2.



Fig. 2. Havnehuset located at the Nordhavn area of Copenhagen

The HBS consists of 4 parts; the prefabricated station or HBS module (including valves, meters, sensors, controllers, pump, pipes, heat exchanger for DHW and electrical cabinet), a prefabricated large heat pump (main) for the DH tank charging, a prefabricated (small) heat pump for the DHW circulation and two DH storage tanks of each 750 litres volume. The HBS concept can be realised with only one tank, but two was decided due to available space.



Fig. 3. (a) HBS installed in technical room; (b) Part of HBS unit with both tanks

The 4 modules are shown on Fig. 3. **Error! Reference source not found.**, where the heat pumps are placed in the front of the left figure.

For the purpose of the field evaluation, the HBS system was installed as add-on to the existing DHW system of the building. The existing space heating system was operated in the usual way, but supplied by ULTDH. For the sake of obtaining field experience, the ULTDH was established by a mixing loop, see Fig. 4.

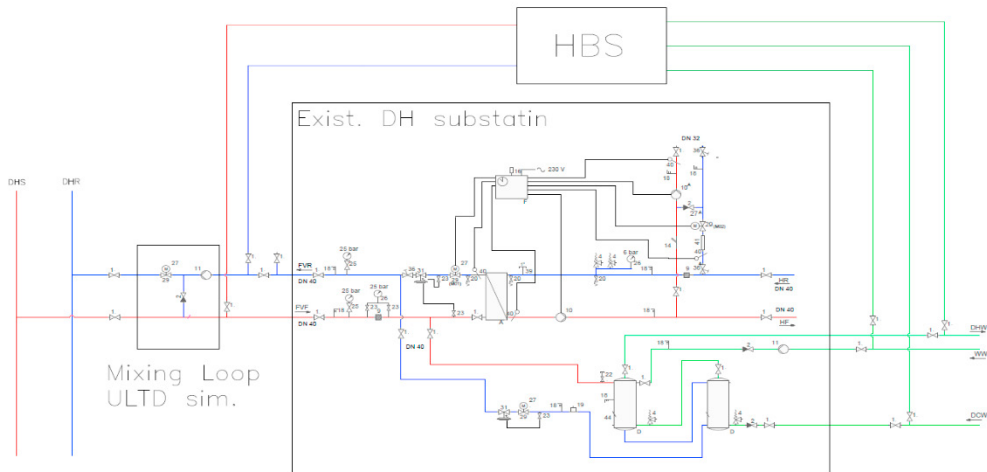
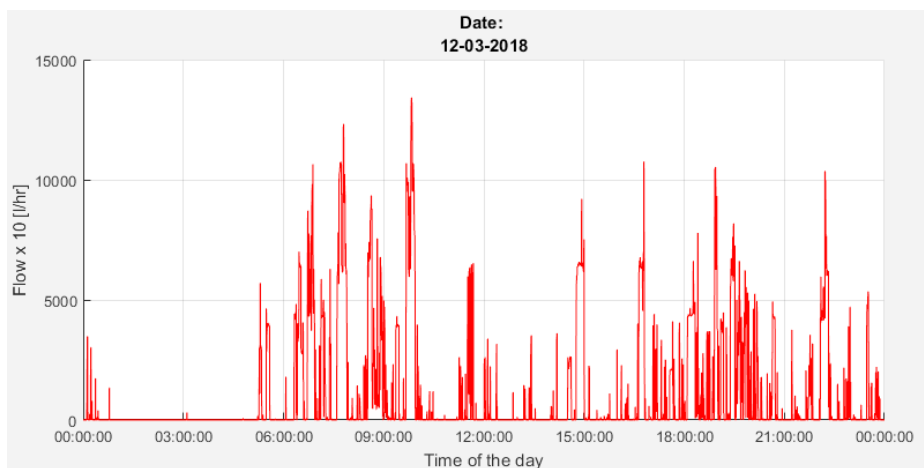


Fig. 4. HBS parallel integration into existing heating/DHW system

3. Results and discussion

3.1. Field Experience

The main field experience and operational data are presented and discussed in this section. The data is time varying and they are presented as plots with the time as the x-axis. The analysis was based on two months of operation, but data examples are specifically given for Monday 12.03.2018 and Sunday 18.03.2018. Fig. 5 shows the DHW tapping profile for two days. Maximum tapping flow is approx. 1,5 m³/hr, corresponding to a capacity of 78 kW. The HBS can keep the DHW temperature of approx. 55°C during all tapping's and no shortages of the DHW supply has been seen.



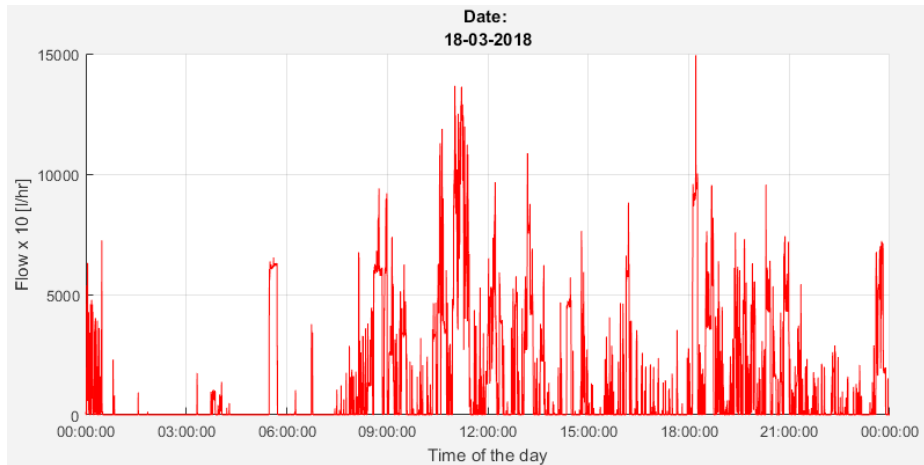


Fig. 5. DHW tapping during the day, a week day and a week-end day

It can be seen, that the amount of tapped DHW at 55°C was lower on the week days compared to the week-end days. In this example, for the week day it was 2.540 liters, where it was 2.905 liters in the week-end day. Further, during the week-day the tapping was more concentrated around the morning and evening hours, whereas the tapping was spread out during the week-end day and with a time delay in the morning.

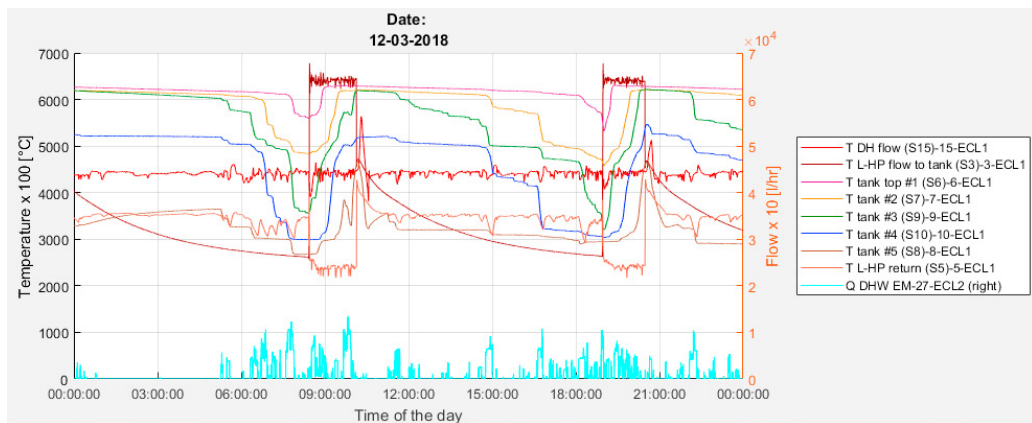


Fig. 6. Charging profile of HBS

The charging profile for the HBS of the 12.03.2018 can be seen on Fig. 6. The DH tanks were charged twice this day, at around 9 o'clock and 19 o'clock. When the tank top was below 56°C (T tank top #1) a charging was started and when the tank bottom temperature (T tank #5) was above 46°C, the charging was stopped. The main heat pump condenser boosts the charging temperature from approx. 45°C (T DH flow) to 63°C (T L-HP flow to tank), where the evaporator returns the DH water at a temperature of approx. 24°C (T L-HP return). The tapped DHW is shown as well (Q DHW). During charging of the DH tank, the flow through the condenser was approx. 730 l/hr, whereas the flow through the evaporator was 530 l/hr. DH temperatures in different vertical locations of the tank are shown as T tank top #1 to T tank #5.

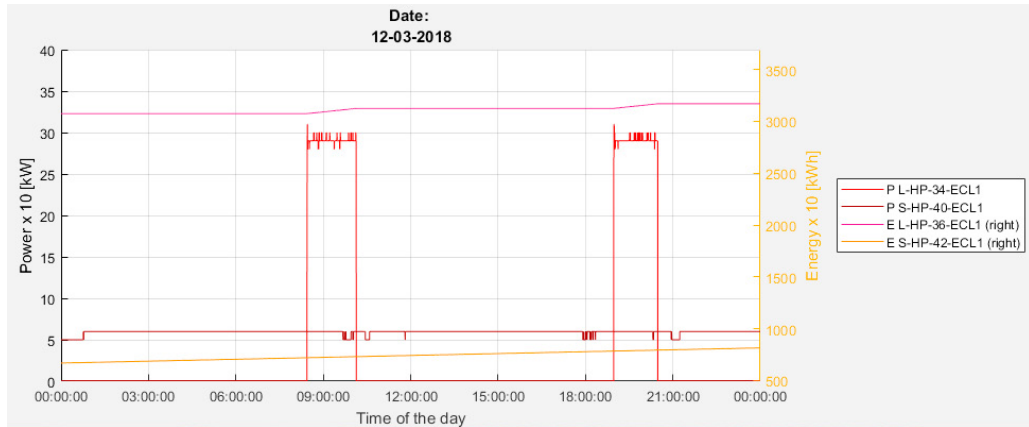


Fig. 7. Electric consumption of heat pumps

The electric power for operating the main heat pump was approx. 3 kW (P L-HP) and the power for operating the circulation (small) heat pump was 0,6 kW (P S-HP). The accumulated electric consumption for the two heat pumps are shown as well (E L-HP and E-S HP). The operation time of the main heat pump, based on the figures above, was 3,25 hr pr. day, resulting in consumption of 9,3 kWh, whereas the consumption for the small heat pump was 14,2 kWh. Totally the daily electric consumption this day was 23,5 kWh. On a yearly basis this adds up to 8.600 kWh of electricity.

The main heat pump condenser was boosting the temperature from 45°C to 63°C, at a flow of 730 l/hr. This corresponds to a capacity of 15 kW. With an electric consumption of 3 kW, the COP was 5,0, which is as expected. Other operational modes occur, e.g. when DH supply temperature or the HP evaporator outlet temperature is changed.

The small heat pump condenser was heating the DHW circulation temperature from 50°C to 55°C, at a circulation flow of 540 l/hr, this corresponds to a capacity of 3,1 kW. With an electric consumption of 0,6 kW, the COP was 5,2, which is as expected. Other operational modes occur.

Table 1. Essential performance of HBS based on two days

HBS data pr. Day	Monday 12.03.2018	Sunday 18.03.2018
Vol DHW [liters]	2.540	2.905
DHW Energy [kWh]	133	152
DHW Circ. Energy [kWh]	78,1	77,5
DH Energy [kWh]	181	204
Main HP Electric cons. [kWh]	9,3	11,7
Circ. HP Electric cons. [kWh]	14,2	14,2
Electric share [%]	11,1	11,3
DH weighted flow temp. [°C]	44,0	44,0
DH weighted return temp. [°C]	30,5	29,1
Energy Bal. (In – Out) [kWh]	-6,5	0,4

Table 1 includes the essential performance of the HBS for the two days. The main performance data relates to the share of electric consumption, which was approx. 11% of the used electric and DH energy, the DH inlet temperature of 44°C and DH return temperature of approx. 30°C. To understand the low electric share, it should be noted that e.g. out of 133kWh for DHW, the 49 kWh were boosted via the main heat pump condenser and the remaining 84kWh were directly from the DH supply. This also explains why the main heat pump electric consumption is lower than the circulation heat pump, even the DHW energy consumption is higher than the DHW circulation heat loss. The electric share depends on the use of DHW, in case of no DHW use at all, and still considering the tank to be charged, the electric share would be approx. 30%. In case the DH tank is not charged the electric share would correspond to the cop of the circulation heat pump, approximately 20%. In case of a low DHW consumption, e.g. one measured day of 1.318 liters of DHW, the electric share was 15,7%.

3.2. Load shift potential

Based on the field experience so far, the capacity during charging of the tank is 3,0 kW electric and 30 kW thermal from DH net. Based on 4 hrs. charging time pr. day, the load shift potential becomes:

Electric load shift potential:	12 kWh/day
DH load shift potential:	120 kWh/day

Comparing this to the heat demand pr. day of the building, which is in the design peak load range of 50 kW, and considering shifting this 5 hrs, the load shift potential for heating becomes 250 kWh/day, and this for peak load. On a yearly basis the average load shift potential is less than half, meaning that for a new building of this type, the load shift potential of DHW is in the same range as for the heating system. No load shift potential is present for the circulation heat pump, since its running continuously.

4. Conclusion

Based on the first field experience for the HBS, it can be concluded that the HBS unit is successfully installed, tested and operating. The DHW is produced at 55°C, DHW circulation is made at 50-55°C, with a DH supply temperature of approx. 45°C and a DH return temperature of approx. 30°C. The share of electric energy consumption for DHW and DHW circulation is 11-16%, depending on the measured DHW consumption. The representative electric share is around 11-13 %. The electric load shift potential is limited to approx. 12 kWh/day, whereas the DH load shift potential is approx. 120 kWh/day. On a yearly basis this is the same range as the load shift potential based on the buildings passive thermal capacity. The DH return temperature could be reduced further, e.g. by compromising the cop of the heat pumps and added heat pump capacity.

Acknowledgement

The work presented in this paper is a part of the Danish EUDP funded EnergyLab Nordhavn – New Urban Energy Infrastructures, is a lighthouse project which will continue until the year of 2019. The project will use Copenhagen's Nordhavn as a full-scale smart city energy lab, which main purpose is to do research and to develop and demonstrate future energy solutions of renewable energy. [www.energylabnordhavn.dk]

References

- [1] Ommen T, Markussen WB, Elmegaard B. Heat pumps in combined heat and power systems. *Energy* 2014;76:989–1000. doi:10.1016/j.energy.2014.09.016.
- [2] Lund H, Werner S, Wiltshire R, Svendsen S, Thorsen JE, Hvelplund F, et al. 4th Generation District Heating ({4GDH}). Integrating smart thermal grids into future sustainable energy systems. *Energy* 2014;68:1–11.

- [3] Christiansen CH, Dalla Rosa A, Brand M, Olsen PK, Thorsen JE. Results and experiences from a 2-year study with measurements on a low-temperature DH system for low energy buildings. *13th Int Symp Dist Heat Cool* 2012:87–94.
- [4] Bühler F, Fridolin M, Huang B, Andreassen JG, Elmegaard B. Mapping of low temperature heat sources in Denmark. *ECOS 2015 28th Int Conf Effic Cost, Optim Simul Environ Impact Energy Syst* 2015.
- [5] Ommen T, Thorsen JE, Markussen WB, Elmegaard B. Performance of ultra low temperature district heating systems with utility plant and booster heat pumps. *Energy* 2016. doi:10.1016/j.energy.2017.05.165.
- [6] Köfinger M, Basciotti D, Schmidt RR, Meissner E, Doczekal C, Giovannini A. Low temperature district heating in Austria: Energetic, ecologic and economic comparison of four case studies. *Energy* 2016;110:95–104. doi:10.1016/j.energy.2015.12.103.
- [7] Østergaard PA, Andersen AN. Booster heat pumps and central heat pumps in district heating. *Appl Energy* 2016;184:1374–88. doi:10.1016/j.apenergy.2016.02.144.
- [8] Zühlsdorf B, Meesenburg W, Ommen TS, Thorsen JE, Markussen WB, Elmegaard B. Improving the performance of booster heat pumps using zeotropic mixtures. *Energy* 2018;154. doi:10.1016/j.energy.2018.04.137.
- [9] Markussen M, Elmegaard B, Ommen T, Brand M, Eric Thorsen J, Iversen J. EUDP 11-I, J. nr. 64011-0076 Heat Pumps for Domestic Hot Water Preparation in Connection with Low Temperature District Heating. *J E* 2013.
- [10] Elmegaard B, Ommen TS, Markussen M, Iversen J. Integration of space heating and hot water supply in low temperature district heating. *Energy Build* 2015. doi:10.1016/j.enbuild.2015.09.003.
- [11] Ommen T, Elmegaard B. Exergetic evaluation of heat pump booster configurations in a low temperature district heating network. *Proc Ecos 2012 - 25th Int Conf Effic Cost, Optim Simul Environ Impact Energy Syst* 2012:1–14.



16th International Symposium on District Heating and Cooling, DHC2018,
9–12 September 2018, Hamburg, Germany

Evaluation of the return temperature reduction potential of optimized substation control

Tijs Van Oevelen^{a,b*}, Dirk Vanhoudt^{a,b}, Robbe Salenbien^{a,b}

^aVITO, Boeretang 200, Mol 2400, Belgium

^bEnergyVille, Energyville I, Thor Park 3800, Genk 3600, Belgium

Abstract

Network temperatures play a major role in the overall efficiency of district heating networks. Low network temperatures are desirable, because they allow high heat production efficiency and low network heat losses. Furthermore, low network temperatures benefit the injection of low-temperature renewable and excess heat sources. At the same time, a high temperature difference between supply and return pipes is desired to limit the network flow rate. This reduces pumping power and increases the network capacity. Whereas the network supply temperature is governed by the heat supply, the network return temperature is determined by the connected customers. This paper focuses on an approach for reducing the network return temperature by considering the control of district heating substations for space heating. Optimal heating control curves exist for the secondary-side supply temperature and flow rate that minimize the network return temperature of indirect substations. The goal is to investigate the impact of optimized control curves on the network return temperature, under various circumstances.

Using a steady-state model of an indirect substation connected to a radiator system, the optimal control strategy is calculated. Its performance is compared to that of traditional control using a pre-set heating curve. The results show that the biggest impact occurs in partial-load conditions, with a potential for reducing the network return temperature by up to 9.9 °C (average 6.0 °C) and primary flow rate reduction up to 14.7 % (average 7.6 %). A parametric analysis to evaluate the impact of the network supply temperature, heat demand and heating system design sizing is presented. It is concluded that the use of optimized substation control for space heating could significantly reduce the network return temperature and primary flow rate. This would benefit the overall energetic system performance of district heating grids.

© 2018 The Authors. Published by Elsevier Ltd.

This is an open access article under the CC BY-NC-ND license (<https://creativecommons.org/licenses/by-nc-nd/4.0/>)

Selection and peer-review under responsibility of the scientific committee of the 16th International Symposium on District Heating and Cooling, DHC2018.

* Corresponding author. Tel.: +32-14-335-152.

E-mail address: tijs.vanoevelen@vito.be

Keywords: Low-temperature district heating; space heating; optimal substation control

1. Introduction

In district heating, it is generally desirable to keep the return temperature of substations connected to the grid as low as possible, for various reasons. Low return temperatures benefit the heat production efficiency and injection of low-temperature renewable and excess heat sources, as well as help keeping the distribution heat losses low. Furthermore, lower return temperatures keep the network flow rate low, thereby reducing the pumping power and increasing the network heat transfer capacity. Practically, the return temperature is determined by the properties of the substation, building and thermal installation for space heating and domestic hot water preparation. Several approaches are possible to ensure a low return temperature: proper selection and installation of the thermal system components, high building insulation quality, and adequate control of the thermal systems.

Current space heating control of building substations usually consists of a heating curve that determines the setpoint for the secondary supply temperature based on the outdoor temperature. The installation is designed for specific operating conditions that occur at typical coldest-weather circumstances. This determines the fixed components of the heating system. The temperature program is tuned to deliver the right amount of heat under all outdoor temperature conditions. In many existing systems, the heat is emitted by means of radiators that are equipped with thermostatic radiator valves. These will close when the room temperature is higher than their setting, and thereby reduce the flow rate to that radiator. In summary, the secondary supply temperature is determined by the substation controller, whereas the secondary flow rate and return temperature are determined by the radiator valves. The temperature program is usually tuned to compensate as much as possible for the weather conditions, such that the thermostatic radiator valves are only required to limit the heat output when there are unexpected heat gains.

One of the downsides of the traditional approach is that it strives only towards one objective, *i.e.* satisfying the heat demand. Thereby, the impact of the space heating control on the return temperature of the district heating substation towards the grid is completely ignored. Nevertheless, it has been argued in the literature [1,2] that the secondary supply temperature setpoint can be optimized to minimize the network return temperature in indirectly connected substations. Practically, the secondary supply temperature needs to be higher than traditionally in order to reduce the return temperature. In order to supply the right amount of heat with an increased secondary supply temperature, a reduction of the secondary flow rate is required. There is a point at which the return temperature is minimal. In that case, the reduction of the secondary return temperature is balanced by the increase in the temperature gap across the heat exchanger.

Several researchers have investigated the use of optimized secondary supply temperature in substation space heating control. Ljunggren *et al.* [3] have analyzed the behavior and optimization of radiator temperature programs theoretically. Furthermore, they performed field tests to demonstrate the possibility of reducing the primary return temperature by optimized substation control in practice, using an adaptive control algorithm. A more advanced version of this control algorithm is presented in [4], involving regular tests with adapted secondary flow rate to find the optimal heating curve. This is then stored and regularly updated. During field tests described in [5], the improvement in houses with only radiators was 2.5 °C increased cooling, without noticeable impact on the users' thermal satisfaction. Gustafsson *et al.* [6,7] proposed an alternative control approach for district heating substations, using optimized secondary supply temperature setpoints considering the primary supply temperature. They concluded that control based on the primary supply temperature is superior to control based on outdoor temperature. It was estimated that their control approach could reduce the primary flow rate in the district heating network of Lulea by 7.4 %. Tunzi *et al.* [8] studied the optimal radiator supply and return temperatures in two scenarios: one minimizing the return temperature, and one minimizing the average of supply and return temperatures.

The objective of this paper is to estimate the potential for using optimized secondary supply temperature setpoints in the substation control to reduce the network return temperature. The results are compared to control using a traditional heating curve. A simple model is used for the evaluation of the improvement potential because a control system that is capable of determining the optimal secondary supply temperature in an operational substation does not yet exist. The details of the evaluation methodology are explained in Section 2. In Section 3, the results are presented and a discussion is provided in Section 4. The last section summarizes our main conclusions.

Nomenclature

A	Heat exchanger surface area
C	Model coefficient
c_p	Specific heat capacity
f	Oversizing factor
h	Heat transfer coefficient
k	Thermal conductivity heat exchanger plates
LMTD	Logarithmic-mean temperature difference
\dot{m}	Mass flow rate
n	Radiator model parameter
\dot{Q}	Heating power
q	Heat exchanger model parameter
T	Temperature
t	Heat exchanger plate thickness
UA	Heat transfer conductance

Subscripts

hex	Heat exchanger
p	Primary side
rad	Radiator
r	Return
s	Secondary side
s	Supply
0	Nominal design conditions
1	Actual (oversized) design conditions

2. Methodology

2.1. Model equations

The analysis is based on a simple steady-state model of an indirect building substation connected to a radiator heat emission system. The production of domestic hot water is not taken into account. For simplicity, the entire heat emission system is represented by one single radiator. This involves several implicit assumptions. For example, this assumes that the temperature in each room is the same and that the return temperature of each radiator is the same, *i.e.* the radiators are perfectly hydraulically balanced. Under those conditions, the heat output of all the radiators can be lumped together, and the entire system can be regarded as one big radiator heating a single room. Additionally, the heat loss from piping *etc.* are assumed to be negligible. This means that the heat transfer through the substation, radiators and piping are the same.

The logarithmic-mean temperature difference method is used to model the substation heat exchanger:

$$\dot{Q} = (UA)_{\text{hex}} \cdot \text{LMTD}_{\text{hex}} \quad (1)$$

where $LMTD_{hex}$ is defined as follows:

$$LMTD_{hex} = \left[(T_{ps} - T_{ss}) - (T_{pr} - T_{sr}) \right] / \ln \left(\frac{T_{ps} - T_{ss}}{T_{pr} - T_{sr}} \right) \quad (2)$$

The heat transfer conductance of the heat exchanger $(UA)_{hex}$ is determined by three heat transfer processes: convection heat transfer on both hot and cold sides and conduction heat transfer through the plate separating the flows, *i.e.*:

$$1/(UA)_{hex} = 1/(hA)_p + t/(kA) + 1/(hA)_s \quad (3)$$

Since high-conductive materials are used in heat exchanger plates, the conduction thermal resistance is generally negligible, so the model can be simplified.

$$1/(UA)_{hex} = 1/(hA)_p + 1/(hA)_s \quad (4)$$

The heat transfer coefficient on either side of the plate is not usually constant, but depends largely on the flow velocity, *i.e.* the flow rate. In general, an empirical correlation as follows holds for the heat transfer coefficient [3,9]:

$$h = C \cdot \dot{m}^q \quad (5)$$

where C and q are constants. It is possible to explicitly incorporate the dependence of $(UA)_{hex}$ on the primary and secondary flow rates into equation (4) when the same correlation (5) applies to both sides of the heat exchanger. Then, the substitution heat transfer can be calculated as follows:

$$\dot{Q} = C_{hex} / (\dot{m}_p^{-q} + \dot{m}_s^{-q}) \cdot LMTD_{hex} \quad (6)$$

A simple model for the steady-state radiator heat transfer is given by [3]:

$$\dot{Q} = C_{rad} \cdot LMTD_{rad}^n \quad (7)$$

Where C_{rad} and n are constant model parameters, and the logarithmic-mean temperature difference of the radiator is defined as follows:

$$LMTD_{rad} = (T_{ss} - T_{sr}) / \ln \left(\frac{T_{ss} - T_{room}}{T_{sr} - T_{room}} \right) \quad (8)$$

Conservation of energy on the primary and secondary side of the substation allows us to complete the model:

$$\dot{Q} = \dot{m}_p c_p (T_{ps} - T_{pr}) = \dot{m}_s c_p (T_{ss} - T_{sr}) \quad (9)$$

The full model is given by Equations (6), (7) and (9). The empirical coefficients C_{hex} , C_{rad} , q and n are considered constant parameters in this model. They are determined by the heating system installation. The parameter C_{hex} is representative of the thermal size of the substation heat exchanger. The flow rate dependence of the heat exchanger conductance UA_{hex} is represented by the coefficient q . A typical value for q is 0.7 [3]. The parameter C_{rad} represents the thermal size of the radiators. The nonlinear temperature dependence of the radiator heat transfer is governed by the coefficient n (typically about 1.3-1.4).

2.2. Calculation of the model parameters – Design calculation

Heating equipment is normally selected according to design conditions. Here, the same approach is followed. The design starts by choosing nominal temperatures $T_{ps,0}$, $T_{ss,0}$, $T_{sr,0}$, $T_{pr,0}$ and $T_{room,0}$, as well as the nominal heat supply Q_0 of the installation. In addition, the heat capacity c_p follows from the choice of heating medium, *i.e.* water; q and n are determined by the specific types of substation heat exchanger and radiators. The nominal flow rates $m_{p,0}$ and $m_{s,0}$ and thermal sizes of the heat exchanger $C_{hex,0}$ and radiators $C_{rad,0}$ can then be calculated from Equations (6), (7) and (9). The result is a consistent set of values that represent the nominal design conditions, identified by the subscript ‘0’.

Heating equipment is very often oversized. This can happen deliberately: *e.g.* to provide sufficient margin to cope with uncertainty in heat loss estimates, or when catalogue equipment doesn’t match well with the required size. Oversizing can also result as a side-effect from building renovations that improve the insulation quality – and thus reduce the heat losses – but leave the heating system unaltered. Heating systems can also be considered to be oversized during periods when the outdoor temperature is higher than the design outdoor temperature.

The goal is to evaluate the impact of oversized components on the potential of radiator supply temperature optimization. The effect of oversizing on the model parameters is clearly defined as follows. An oversized system is one that is capable of delivering more heat than the nominal system, at the same operating temperatures. This is defined by the oversizing factor f as follows: instead of being able to deliver the heat demand Q_0 , the oversized system is instead capable of delivering $(1+f)Q_0$. For example, if the oversizing factor is 100 % ($f = 1$), then the actual system can deliver double the amount of heat of the original system when the operating temperatures are kept the same.

The model parameters of the oversized system follow from the above approach with $(1+f)Q_0$ replacing Q_0 . The model parameters and variables corresponding to the oversized design are identified by the subscript '1'. The design sizing can be different for each of the components of the heating system. Then, the result of the design calculation is applied only to the parameter representing the targeted component. For example, if the radiator is oversized by a factor f_{rad} , then the parameter $C_{\text{rad},1}$ is taken from a design calculation where the requested heat output is $(1+f_{\text{rad}})Q_0$. Similarly, the substation heat exchanger oversizing factor f_{hex} determines the parameter $C_{\text{hex},1}$; and the secondary-side circulation pump oversizing factor f_s determines the parameter $m_{s,1}$. As a result of oversizing, the model parameters are not consistent with the nominal design temperatures. Therefore, the equations (6), (7) and (9) are used to solve for the actual design temperatures ($T_{\text{ss},1}$, $T_{\text{sr},1}$, $T_{\text{pr},1}$) and actual design primary flow rate ($m_{p,1}$).

During most of the heating season, the heat transfer capacity of the substation heat exchanger and the radiators is not fully utilized because the outdoor temperature is higher than the system is designed for. It is especially in those – often occurring – circumstances that the traditional heating curves behave sub-optimally with respect to return temperatures. Instead, by choosing a higher radiator supply temperature, the radiator return temperature can be lower for the same LMTD_{rad} , which is the parameter that determines the radiator heat output. Consequently, the radiator flow rate needs to be reduced, because of the increased temperature drop of the water through the radiator. As long as the radiator supply temperature doesn't approach the network supply temperature too closely, this will result in a reduced primary return temperature as well. Otherwise, the reduction in radiator return temperature will be offset by the increase of the temperature gap between the primary outlet and the secondary inlet of the substation heat exchanger. As a result of these physical system characteristics, there is an optimal radiator supply temperature that minimizes the primary return temperature, depending on the heat demand and operating temperatures T_{pr} and T_{room} .

2.3. Calculation of the control curves

The optimal secondary supply temperature T_{ss}^* depends on the heating system design and on the operating conditions. In each case, it is determined by the solution of the following minimization problem:

$$T_{\text{ss}}^* = \arg \min_{T_{\text{pr}}} T_{\text{pr}}(T_{\text{ss}}) \quad (10)$$

where the dependence of T_{pr} on T_{ss} is described by the model consisting of Equations (6), (7) and (9). The constant model parameters are either determined by the design ($C_{\text{hex},1}$, $C_{\text{rad},1}$, q , n , c_p) or by the operating conditions (Q , T_{ps} , T_{room}).

The performance of the heating system with optimized secondary supply temperature setpoint is compared to the performance of controlling this setpoint with a traditional heating curve. As a reference, a heating curve is used that perfectly compensates for the variations in outdoor temperature. This represents a situation where the heating curve is perfectly adjusted to the heat demand of the building. This implies that the system nominally operates with a constant secondary flow rate, in the absence of unexpected heat gains. This is a theoretical situation, because thermostatic radiator valves are needed in practice to limit the flow when there are internal or external heat gains.

An implicit assumption in these calculations is that the thermostatic radiator valves are behaving perfectly. Namely, that they succeed in controlling the secondary flow rate such that exactly the right amount of heat is emitted by the radiators and this constant over time.

3. Results

The study consists of several cases, where each time the performance of the optimized substation control is compared to the traditional control. In each case, the heat demand is varied between 0 % and 100 % of the nominal heat demand. The fixed model parameters are given in Table 1. Different cases related to the system temperatures and

the design sizing of the heating system components are considered. First, the impact of optimized substation control on a high-temperature case is evaluated. This is then repeated for a low-temperature case. Subsequently, the effect of oversizing the full heating system is studied. And finally, the oversizing of individual heating system components is considered.

Table 1. Fixed model parameters.

Parameter	q (-)	n (-)	c_p (J/(kg.K))
Value	0.7	1.33	4180

3.1. High-temperature case

The first case represents the situation in a typical high-temperature network. The radiators are sized to deliver the design heat demand at 80-60 °C. The primary-side temperatures of the substation heat exchanger are 95-63 °C at design conditions. The design room temperature is 20 °C.

The results for this case are depicted on Figure 1. Fig. 1(a) shows the temperatures (T_{ps} , T_{ss} , T_{sr} and T_{pr}) as a function of the relative heat demand, *i.e.* fraction of the design heat load. The corresponding primary and secondary flow rates are shown in Fig. 1(b). The dashed lines represent the traditional control curves, whereas the full lines represent the optimized control curves.

In the traditional control approach, the secondary supply temperature (red) varies approximately linearly with the heat demand. Furthermore, the temperature difference between radiator supply (red) and return (green) reduces proportionally to the relative heat demand (see Fig. 1(a)). This is consistent with the constant secondary flow rate, depicted in Fig. 1(b). Due to the large difference between the primary (black) and secondary (red) supply temperatures, the primary return temperature (green) is only slightly higher than the secondary return temperature (blue).

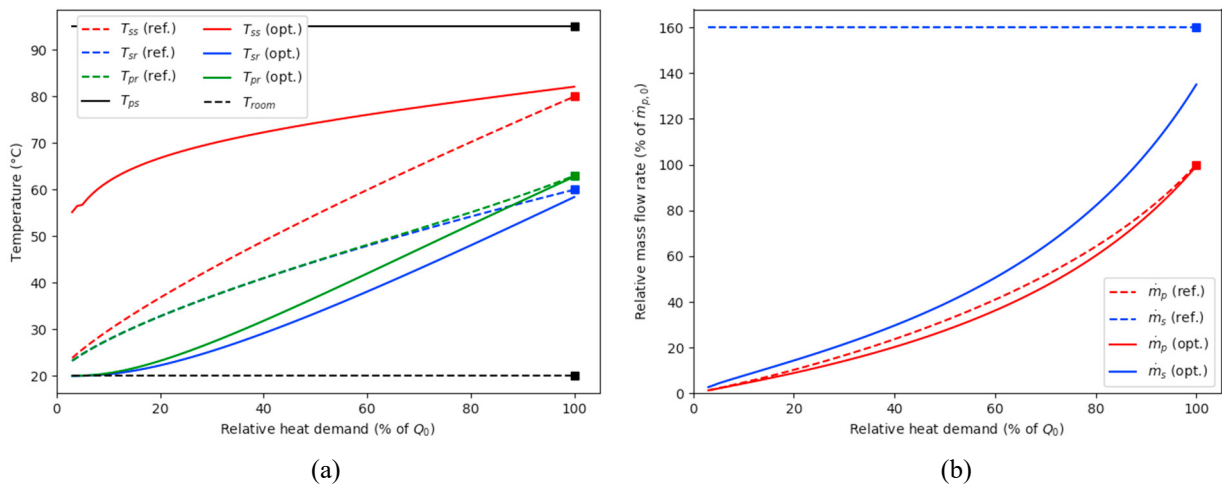


Fig. 1. (a) Temperatures and (b) flow rates for heat demand ranging from 0-100% (high-temperature case).

The optimized control curve for the secondary supply temperature deviates significantly from the traditional curve. It maintains a substantially higher temperature throughout the entire heating demand range. In order to supply the same amount of heat, the radiator return temperature needs to be lower than in the traditional control case. Correspondingly, the secondary flow rate also needs to be lower than in the traditional case. Fig. 1(b) shows that the secondary flow rate even needs a very large reduction when the heat demand is low. This may in practice be very challenging for thermostatic radiator valves to achieve and control smoothly. As a result of the reduction in the secondary return temperature, a reduction in the primary return temperature is obtained. However, the temperature gap between the primary and secondary return has increased as well due to the reduced secondary flow rate. In the

optimized control, these phenomena are exactly balanced, meaning that a further increase of T_{ss} would again increase T_{pr} instead of further reducing it.

The primary return temperature with optimized control (green, full line) is considerably lower than with traditional control (green, dashed line). This is summarized in Table 2, which lists the average return temperature and average primary flow rate over the entire heat demand range. On average, a return temperature reduction with 6.0 °C can be obtained. During times of low heat demand, the reduction is even higher (up to 9.9 °C). The lower return temperature benefits the heat production efficiency, the thermal network losses as well as the potential for renewable and excess heat usage in the grid. Furthermore, the primary flow rate also reduces with the optimized control, by 7.6 % on average (up to 14.7 %). This may lead to about 15-20% savings in pumping power consumption. It is concluded that optimized control could have a significant potential in this case.

Table 2. Control performance comparison of high-temperature case.

Control approach	Average return temperature (°C)	Average primary flow rate (% of $m_{p,0}$)
Traditional	44.6	38.4
Optimized (minimal T_{pr})	38.6	35.5

3.2. Low-temperature case

In new buildings and district heating grid developments, design temperatures are often lower than in existing grids, in order to reduce thermal network losses and improve conversion efficiency. An interesting question is whether the difference between traditional and optimized control is also significant in those situations. In the second case, the radiator design temperatures are 55-45 °C, while the primary-side design temperatures are 65-48 °C. The same design room temperature of 20 °C is assumed.

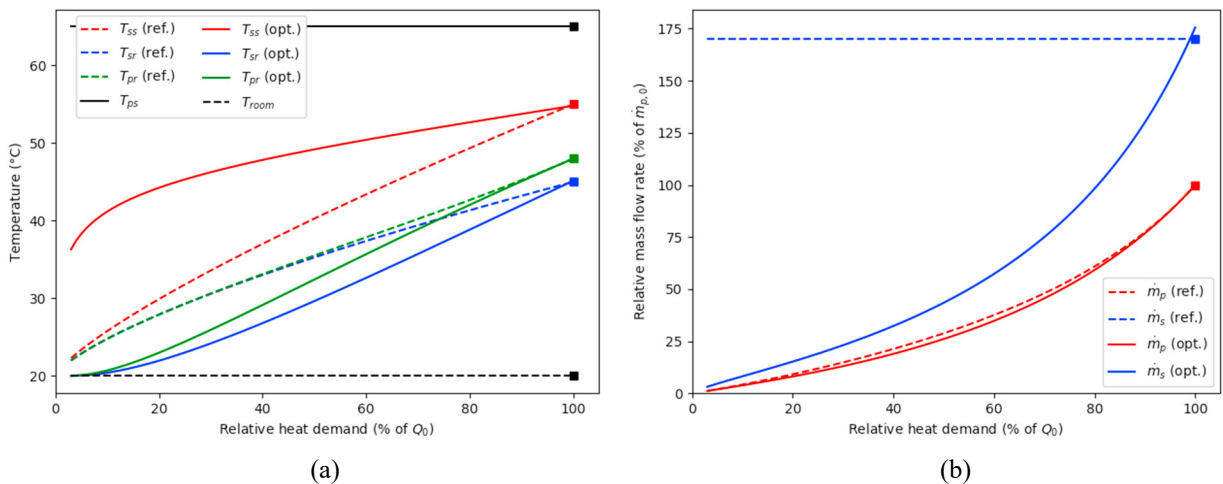


Fig. 2. (a) Temperatures and (b) flow rates for heat demand ranging from 0-100% (low-temperature case).

The control curves and results are shown in Figure 2. They are qualitatively very similar to the results of the high-temperature case. The quantitative results are summarized in Table 3. Optimized control on average leads to a 2.6 °C lower return temperature. The potential for return temperature reduction is clearly less than in the high-temperature case. This could be expected because the return temperature is already low with traditional control. The primary flow rate reduces by 4.4 % on average, which is also a lower reduction than in the high-temperature case. It is concluded that the use of optimized substation control brings more benefit in the case of traditional high-temperature grids than in newer low-temperature grids. However, even in the latter case the return temperature reduction potential is there, waiting to be unlocked.

Table 3. Control performance comparison of low-temperature case.

Control approach	Average return temperature (°C)	Average primary flow rate (% of $m_{p,0}$)
Traditional	35.7	36.2
Optimized (minimal T_{pr})	33.1	34.6

3.3. Oversizing of the full heating system

It is interesting to evaluate the impact of oversized heating system design on the return temperature reduction potential of optimized substation control curves. Indeed, practical systems are almost always oversized to some degree. Usually, all heating system components are equally oversized because the entire system is designed for a higher heat demand than actually occurs.

Table 4 summarizes the results of using different levels of oversizing for the heating system, for both control approaches and the two different temperature cases. In general, an oversizing of the heating system leads to a lower return temperature and a lower primary flow rate, in all cases. The most benefit is obtained with the first 50% of oversizing; the additional improvement from 50% to 100% is less. However, for higher degrees of oversizing, the improvement potential of the optimized control approach becomes higher. For example in the high-temperature case, the average return temperature reduction by using optimized control is respectively 6.0 °C, 7.9 °C and 8.4 °C when the heating system is 0 %, 50 % and 100 % oversized.

Further, notice that the combined effect of using optimized control and oversizing is larger than the individual effects. For example, starting from a nominal design with traditional control in the high-temperature case, the individual effect of optimized control is a return temperature reduction of 6.0 °C. Oversizing by 100 % reduces the return temperature by 9.8 °C. If both measures are applied together, the overall return temperature reduction reaches 18.2 °C on average. In other words, optimized substation control can make an oversizing of the heating system a lot more valuable, *i.e.* it almost adds the same amount of return temperature reduction as an oversizing by 100 %. To a lesser extent, it also applies to the low-temperature case.

Table 4. Control performance comparison with variation of heating system design sizing.

	Design sizing	Control approach	Average return temperature (°C)	Average primary flow rate (% of $m_{p,0}$)
High temperature (95-63/60-80 °C)	Nominal (0 % oversizing)	Traditional	44.6	38.4
		Optimized (minimal T_{pr})	38.6	35.5
	50% oversizing	Traditional	38.1	31.7
		Optimized (minimal T_{pr})	30.2	27.7
	100% oversizing	Traditional	34.8	29.2
		Optimized (minimal T_{pr})	26.4	25.2
Low temperature (65-48/45-55 °C)	Nominal (0 % oversizing)	Traditional	35.7	36.2
		Optimized (minimal T_{pr})	33.1	34.6
	50% oversizing	Traditional	31.4	28.8
		Optimized (minimal T_{pr})	27.7	26.1
	100% oversizing	Traditional	29.2	26.2
		Optimized (minimal T_{pr})	25.1	23.4

3.4. Oversizing of individual components

Practically, all components of the heating system are usually designed consistent with each other. This means that the oversizing factor f of all individual components is roughly the same. Instead, also the impact of oversizing individual components on the return temperature and the potential of optimized substation control in those situations

is interesting. This gives useful information about what aspects of the design deserve more attention and would benefit most from additional investments.

The following additional cases are now considered: a 100 % oversizing of the substation heat exchanger, a 100 % oversizing of the radiators and a combination of both. The last case resembles the oversizing of the full system except for the oversizing of the circulation pump. Notice that this difference appears only in the case of traditional control – where the secondary flow rate is fixed – but not in the case of optimized control – where the flow rate is determined by the optimization. These three cases have been simulated for both the high- and low-temperature situations. The results of the traditional and optimized control are compared in Table 5.

The results show that the impact of radiator oversizing is significantly larger than the impact of oversizing the substation heat exchanger. Almost all of the reduction in return temperature and primary flow rate in oversizing the full heating system is achieved by increasing the thermal size of the radiators alone. Not much additional impact is obtained by enlarging the substation heat exchanger. The reason for this is that the gap between the radiator outlet temperature and the room temperature is much bigger than the temperature gap on the return side of the substation heat exchanger. It is concluded that investments intended to reduce the network return temperature from building substations should be focused on the radiators.

Even with increased sizing of the radiators, a significant reduction of the return temperature by using optimized setpoints for the secondary supply temperature is still obtainable. In the high-temperature case, the average return temperature drops by 5.3 °C by applying the optimized control in the case of 100% radiator oversizing – compared to a drop of 6.0 °C for the nominally sized system. For the low-temperature case, the average return temperature reduction potential is 2.4 °C (100% radiator oversizing) – compared to 2.6 °C (nominal design). Thus, the potential for reducing the return temperature and the primary flow rate is almost unaffected by improving the design sizing of the radiators. The previous sub-section showed that the potential improvement even increases when the full heating system is oversized. This can be attributed to the increased secondary flow rate in that case (Table 4), as can be seen when comparing with oversizing the substation heat exchanger and radiators alone (Table 5).

Table 5. Control performance comparison with variation of individual heating components design sizing.

	Design sizing	Control approach	Average return temperature (°C)	Average primary flow rate (% of $m_{p,0}$)
High temperature (95-63/60-80 °C)	Nominal (0 % oversizing)	Traditional	44.6	38.4
		Optimized (minimal T_{pr})	38.6	35.5
	100% heat exchanger oversizing	Traditional	44.3	38.0
		Optimized (minimal T_{pr})	37.2	34.1
	100% radiator oversizing	Traditional	32.8	28.2
		Optimized (minimal T_{pr})	27.5	25.8
	100% heat exchanger + radiator oversizing	Traditional	32.6	27.8
		Optimized (minimal T_{pr})	26.4	25.2
Low temperature (65-48/45-55 °C)	Nominal (0 % oversizing)	Traditional	35.7	36.2
		Optimized (minimal T_{pr})	33.1	34.6
	100% heat exchanger oversizing	Traditional	35.3	35.3
		Optimized (minimal T_{pr})	32.0	32.8
	100% radiator oversizing	Traditional	28.4	25.5
		Optimized (minimal T_{pr})	26.0	24.2
	100% heat exchanger + radiator oversizing	Traditional	28.1	25.2
		Optimized (minimal T_{pr})	25.1	23.4

4. Conclusions

The secondary supply temperature of district heating substations is traditionally determined by a fixed heating curve depending on the outdoor temperature. However, when the space heating system is indirectly connected to the district heating network via a heat exchanger, there exists an optimal secondary supply temperature – and corresponding circulation flow rate – for which the primary return temperature is minimal. The corresponding primary return temperature could be up to 9.9 °C (6.0 °C on average) lower for the optimized control compared to the traditional control for a typical high-temperature design. This return temperature reduction is beneficial for the heat production efficiency, the thermal network losses and the potential for injection of renewable and excess heat sources. Furthermore, this reduction in return temperature is accompanied by a primary flow rate reduction of about 7.6 % on average. This increases the network flow capacity and could reduce the pumping power by approximately 15-20 %.

A sensitivity study has been performed to study the influence of certain parameters on the potential of optimized substation control to reduce the network return temperature. The following main observations have been made:

- The return temperature reduction potential is higher in high-temperature grids than in low-temperature grids, due to the closer temperature gap in the latter case.
- The potential benefits of optimized substation control increase with the size of the heating system. Optimized heating control increases the investment value of better performing heating systems, and *vice versa*.
- Most of the positive impact of oversizing the heating system is due to the radiators. The substation heat exchanger size has a smaller impact, whereas a too large circulation pump reduces the performance.
- The potential for return temperature reduction is relatively independent of the thermal sizing of the substation heat exchanger and radiators, so both can be applied simultaneously, without needing to choose.

Finally, it is concluded that optimized substation control is a promising technology to reduce network return temperatures in addition to efforts on proper design and installation of building-side heating equipment. Practical realization of this concept should be further investigated.

Acknowledgements

This work was done with the support of the European Union, the European Regional Development Fund ERDF, Flanders Innovation & Entrepreneurship and the Province of Limburg.

References

- [1] Frederiksen S. and Wollerstrand J., “Performance of district heating house station in altered operational modes.” *23rd UNICHAL Congress* (1987), Berlin.
- [2] Volla R., Ulseth R., Stang J., Frederiksen S., Johson A. and Besant R., “Efficient substations and installations (ESI).” *IEA District Heating and Cooling Project - annex IV* (1996).
- [3] Ljunggren P., Johansson P.-O. and Wollerstrand J., “Optimised space heating system operation with the aim of lowering the primary return temperature.” *The 11th International Symposium on District Heating and Cooling* (2008), Reykjavik.
- [4] Lauenburg P., ‘Improved supply of district heat to hydronic space heating systems.’ *Doctoral thesis*, Lund University (2009).
- [5] Lauenburg P. and Wollerstrand J., “Adaptive control of radiator systems for a lowest possible district heating return temperature.” *Energy and Buildings* 72 (2014), 132-140.
- [6] Gustafsson J., Delsing J. and van Deventer J., “Improved district heating substation efficiency with a new control strategy.” *Applied Energy* 87 (2010), 1996-2004.
- [7] Gustafsson J., Delsing J. and van Deventer J., “Experimental evaluation of radiator control based on primary supply temperature for district heating substations.” *Applied Energy* 88 (2011), 4945-4951.
- [8] Tunzi M., Ostergaard D. S., Svendsen S., Boukhanouf R. and Cooper E., “Method to investigate and plan the application of low temperature district heating to existing hydraulic radiator systems in existing buildings.” *Energy* 113 (2016), 413-421.
- [9] Lienhard J. H. IV and Lienhard J. H. V, *A heat transfer textbook, 4th edition* (2017), Phlogiston Press.



16th International Symposium on District Heating and Cooling, DHC2018,
9–12 September 2018, Hamburg, Germany

Seismic analysis of a district heating pipeline

Gersena Banushi^{a*}, Ingo Weidlich^a

^aHafenCity University, Überseesallee 16, Hamburg, 20457, Germany

Abstract

The effect of seismic loading is not contemplated in any of the current design standards of District Heating and Cooling (DHC) networks, since this technology has been originally adopted in northern Europe, characterized by low earthquake vulnerability. Nevertheless, an increasing number of countries, including those in seismic areas like Italy, Turkey, China, Japan, and Chile are using DHC solutions due to the higher energy efficiency, compared to individual heating systems.

Seismic regions are one of the most hostile environments for buried pipelines due to the effects of Transient Ground Deformation (TGD) caused by seismic wave propagation, and Permanent Ground Deformation (PGD), like faulting, landsliding, lateral spreading and buoyancy due to liquefaction.

Most of research publications on the seismic analysis and design of buried steel pipelines have been motivated by the need of safeguarding the integrity of hydrocarbon pipelines, and there are no actual studies on the seismic vulnerability of DHC pipelines. This highlights the need to carefully evaluate the seismic performance of DHC pipelines, considering their typical composite cross-section and soil-pipe interaction under service loading.

The present paper analyses the effect of diverse earthquake hazards on an operating District Heating (DH) pipe bend, usually susceptible to stress concentrations due to the greater flexibility, as well as the ability to accommodate thermal expansions, and absorb other externally-induced loading.

The response of the operating DH pipeline subjected to different seismic loading is evaluated taking into account the geometric and mechanical properties of the system, including the soil-pipeline interaction.

In conclusion, the obtained results give a better understanding on the seismic behavior of DH pipelines, highlighting important research ground for assessing their earthquake performance in operating conditions.

© 2018 The Authors. Published by Elsevier Ltd.

This is an open access article under the CC BY-NC-ND license (<https://creativecommons.org/licenses/by-nc-nd/4.0/>)

Selection and peer-review under responsibility of the scientific committee of the 16th International Symposium on District Heating and Cooling, DHC2018.

Keywords: Seismic analysis; Transient Ground Deformation; Permanent Ground Deformation; District Heating Pipeline

* Corresponding author

E-mail address: gersena.b@gmail.com

1. Introduction

District Heating and Cooling (DHC) consist of an underground pipe network connecting buildings in an urban area to centralized plants or a number of distributed heat producing units, allowing for heat recycling and renewable energy supply. Due to the higher energy efficiency, an increasing number of countries including those in seismic areas like Italy, Turkey, China, Japan, are adopting district heating solutions. The effect of seismic loading is not contemplated in any of the current design standards of DH networks, since this technology has been originally adopted in northern European countries, characterized by low earthquake vulnerability.

Seismic regions are one of the most hostile environments for buried pipelines due to the effects of Transient Ground Deformation (TGD) caused by seismic wave propagation, and Permanent Ground Deformation (PGD), like faulting, landsliding, lateral spreading and buoyancy due to liquefaction [1].

Most of research publications on the seismic analysis and design of buried steel pipelines have been motivated by the need of safeguarding the integrity of hydrocarbon pipelines [2], and there are no actual studies on the seismic vulnerability of DHC pipelines. This highlights the need to carefully evaluate the seismic performance of DHC pipelines, considering their typical composite cross-section and soil-pipe interaction under service loading.

To minimize heat losses, DHC pipes have a composite cross-section of three different material layers, including the steel pipe for the water supply, the insulation foam of polyurethane (PUR), and an outer coating of High Density Polyethylene (HDPE), interacting with the surrounding soil. The stiffness of the PUR foam and its constant adhesion to the steel pipe are essential to properly transmit at the HDPE coating the friction stresses from the surrounding soil.

The axial expansion of the operating pipeline, is counteracted by the soil friction at the outer HDPE coating interface, until the total friction reaction equilibrates the pipe axial force at the anchor point, where the thermal expansion is fully restrained. Moreover, the thermal expansion is counteracted at the bend by the lateral soil reaction, inducing high stress levels in this critical region, as schematically illustrated in Fig. 1. Additionally, the PUR insulation is very sensitive to axial shear stress and lateral pressures, inducing high stresses associated with material failure and loss of the bond; in a worse case, it can lose its insulation effect if the steel service pipe cracks and the foam is moistured. [3].

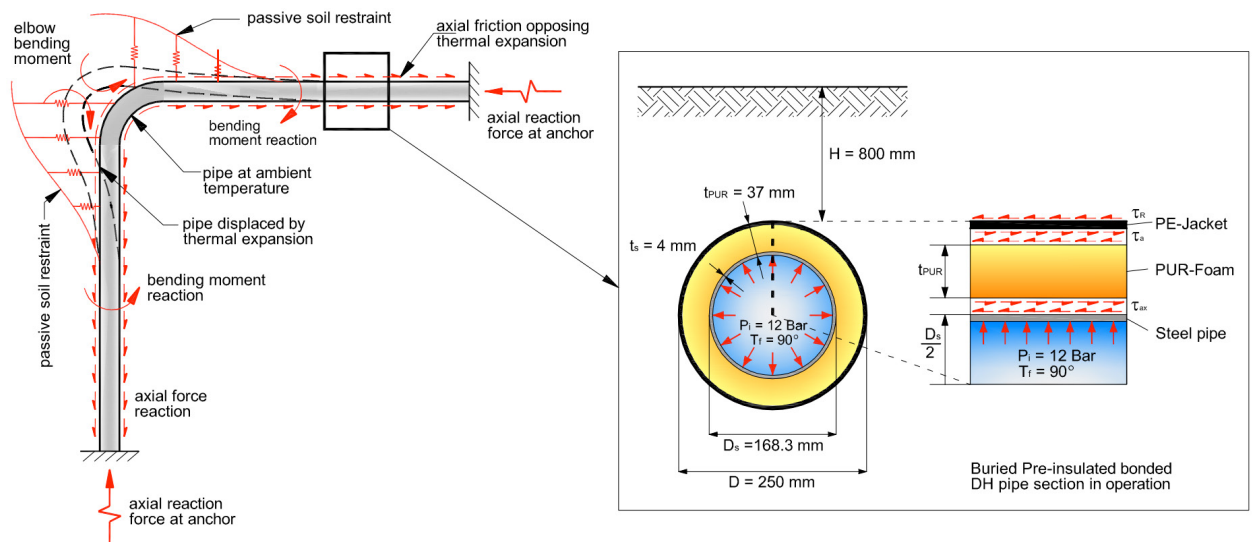


Fig. 1. Deformation of buried operating DH pipeline at the bend (adapted from [4] and [5])

Therefore, a correct design of DHC pipelines requires an accurate consideration of the elevated stresses and deformations due to the operating loads like internal pressure and temperature, as well as the evaluation of the soil-pipeline interaction.

Reported experimental research on the response of buried DH pipe systems subjected to ground movement is very limited, requiring further analysis of the soil-pipe interaction of buried DH pipes, while taking into account real operating conditions and modern pipe laying technologies [6-10]. On the other hand, the seismic response of buried pipelines has been investigated by many researchers in the last 50 years, using experimental investigations as well as simple analytical or more complex numerical approaches [11-17].

During extreme events like earthquakes, the pipeline needs to plastically stretch, bend and compress in order to accommodate local or global movement of the surrounding soil, requiring strain-based performance criteria for a safe and cost-effective pipeline design [18-19]. Evidently, stress-based performance limit states, like those recommended in European standard EN 13941 [20] or in the Eurocode 3 - Part 4-3 [21] are overconservative for pipelines constructed in harsh environments, like seismic regions.

The present paper analyses the effect of seismic induced ground movement on an operating District Heating (DH) pipe bend, typically susceptible to highest moments and stress concentrations due to the greater flexibility, as well as the ability to accommodate thermal expansions, and absorb other externally-induced loading. [22].

The response of the operating DH pipeline subjected to seismic loading is evaluated taking into account the geometric and mechanical properties of the system, including the soil-pipeline interaction. In conclusion, the obtained results give a better understanding on the seismic behaviour of DH pipelines, highlighting important research ground for assessing their earthquake performance in operating conditions.

Nomenclature

D_s	outer diameter of the steel pipe
t_s	thickness of the steel pipe
D	outer diameter of external HDPE coating
t_{PUR}	thickness of the PUR insulation
R_{bend}	radius of the pipe bend
L	length of the pipe legs
L_c	length of the expansion cushion at each bend leg
H	soil cover depth
E	elasticity modulus of the steel pipe
ν	Poisson's ratio of the steel pipe
σ_y	yield strength the steel pipe
α	linear thermal expansion coefficient of the steel pipe
ϕ	soil friction angle
γ	soil density
T_i, T_f	installation and operating temperature
P_i	operating internal pressure in the steel pipe
$U_g, \varepsilon_g, \lambda_g$	earthquake induced ground displacement, ground strain, and seismic wave length
F_R	soil friction reaction
P_u	maximum lateral soil reaction
k	elastic lateral soil stiffness
k_c	equivalent lateral stiffness in the pipe corner with expansion cushion
M_y	yielding moment of the steel pipe section

2. Methodology

This paper investigates the performance of preinsulated bonded DH pipelines, subjected to TGD due to seismic wave propagation. Clearly, this hazard affects DH networks, considerably more than does PGD, threatening mainly transmission hydrocarbon pipelines.

The investigated pipe bend DN 150/250 is composed of a central P235GH steel pipe of external diameter $D_s = 168.3$ mm and thickness $t_s = 4$ mm, a foam insulation of thickness $t_{PUR} = 37$ mm, and external plastic mantle with outer diameter $D = 250$ mm. The radius of the pipe bend is $R_{bend} = 1$ m, the length of the expansion cushion at the corner is $L_c = 2$ m, while the length of both bend legs is $L = 40$ m, anchored at the ends. The pipe is assumed buried in loose sand soil with a cover depth $H = 0.8$ m, as schematically illustrated in Fig. 1.

The soil-pipeline system subjected to seismic loading has been analyzed numerically within beam on Winkler foundation theory, using the finite element software ABAQUS/Standard [23].

The pipeline is modeled using the PIPE31 beam element type, allowing the possibility to specify external or internal pressure. The soil-pipeline interaction is modeled with the spring-like pipe-soil interaction elements PSI34, representing the soil reaction to the soil movement in the axial, lateral, and vertical direction. One edge of the element shares nodes with the underlying pipe element while the nodes on the other edge are assigned the far-field ground motion through the boundary conditions.

The P235GH steel pipe material model is defined within the von Mises plasticity theory with nonlinear hardening. The material parameters are determined as a function of the operating temperature T , according to EN 13941 [19]. The elasticity modulus, yield strength, and the linear thermal expansion coefficient at the operating temperature $T = 90^\circ\text{C}$ are $E = 208857$ MPa, $\sigma_y = 215.8$ MPa and $\alpha = 12.098 \cdot 10^{-06}$ 1/K respectively, while the Poisson's ratio is $\nu = 0.3$. A loose sand material is assumed as soil backfill, with the same properties reported in the calculation example of the German standard FW 401 [4], characterized by a friction angle $\phi = 32.5^\circ$, and a soil density $\gamma = 18$ kN/m³. The force-displacement relationship is considered bilinear elasto-plastic, and evaluated according to FW 401 [5]. Specifically, the calculated soil friction reaction is $F_R = 3944$ N/m, while the maximum lateral soil reaction is $P_u = 49750$ N/m, with an elastic lateral soil stiffness $k = 35$ MPa beyond the expansion cushion, where the equivalent elastic lateral stiffness is $k_c = 0.247$ MPa [5].

The seismic-induced ground movement is applied at the free nodes of the pipe-soil interaction elements, as a sinusoidal wave propagating horizontally in the direction of the longitudinal leg.

The numerical analysis for assessing the seismic performance of the operating DH pipeline are conducted in two consecutive steps. At first, a static analysis is performed to establish the stress and strain state in the soil-pipeline system in operating conditions with internal pressure $P_i = 12$ Bar, installation and service temperature $T_i = 10^\circ\text{C}$ and $T_f = 90^\circ\text{C}$, respectively. In the second step, a horizontal displacement is applied quasi-statically at the free nodes ends of the pipe-soil interaction elements, matching the sinusoidal pattern defined by:

$$U_g(x) = \varepsilon_g \left(\frac{\lambda_g}{2\pi} \right) \sin \left(\frac{2\pi y}{\lambda} \right) \quad (1)$$

where $\varepsilon_g = 0.0041$ is the soil strain and $\lambda = 500$ m is the seismic wave length. Thus, the maximum value of the ground displacement results $U_g = 0.33$ m

On each loading step, the global equilibrium equations are solved iteratively by the Newton-Raphson method permitting to assess the pipe and soil deformation state at each increment.

3. Results and discussion

This section presents the structural response of the buried DH pipeline evaluated using the proposed methodology. Firstly, the pipeline response is investigated in operating conditions, under the effect of internal pressure and temperature variation. Then the seismic performance of the pipeline is analyzed in terms of loading and deformations, for different values of the maximum seismic-induced ground displacement U_g , as discussed further in this section.

3.1. Structural response of the pipeline in operating conditions

The expansion of the operating pipeline is counteracted by the beneficial effect of the soil friction, and the bearing force on the transverse leg (Fig. 1). The maximum axial elongation of the pipeline in operation conditions,

calculated numerically (31.1 mm) is consistent with the theoretical value of the maximum axial elongation u_{max} , according to the formula reported in the standards FW 401 [5] and EN 13941 [20]:

$$u_{max} = \left(\alpha_T \Delta T + \frac{(1-2\nu) P_i D_s}{EA_s} \frac{P_i D_s}{4t_s} \right) \cdot L - \left(\frac{7}{10} \cdot \frac{F_R}{EA_s} \right) \cdot L^2 \approx 29.4 \text{ mm} \quad (2)$$

Clearly, the first addend in Eq. (2) indicates the pipeline expansion due to the positive temperature variation $\Delta T = 80^\circ\text{C}$, and internal pressure $P_i = 12 \text{ Bar}$, while the second negative term represents the pipeline contraction due to the soil resistance at the outer HDPE coating.

The aforementioned values of the maximum axial elongation are consistent with the estimations using the method proposed in [22, 24-26], considering the bend either rigid (30.8 mm) or flexible (31.4 mm).

The pipeline response in terms of longitudinal deformations does depend on the geometrical and mechanical parameters of the system, like the operating temperature T_f , the pipe length L , and the bend radius R_{bend} .

Clearly, the maximum longitudinal strain in operating conditions occurs at the elbow ($\epsilon_{max} = 0.42\%$, for $T_f = 90^\circ\text{C}$, $L = 40 \text{ m}$ and $R_{bend} = 1 \text{ m}$). A small parametric study has shown that the pipeline deformation is accentuated for greater operating temperatures ($\epsilon_{max} = 1.03\%$, for $T_f = 130^\circ\text{C}$), larger pipe length ($\epsilon_{max} = 0.91\%$, $L = 80 \text{ m}$), smaller bending radius ($\epsilon_{max} = 0.68\%$, for $R_{bend} = 0.5 \text{ m}$), all other parameters remaining the same, as shown in Fig. 2. These critical factors need to be carefully evaluated in the design phase in order to avoid excessive stress-strain concentration in the operating pipeline, associated with material damage.

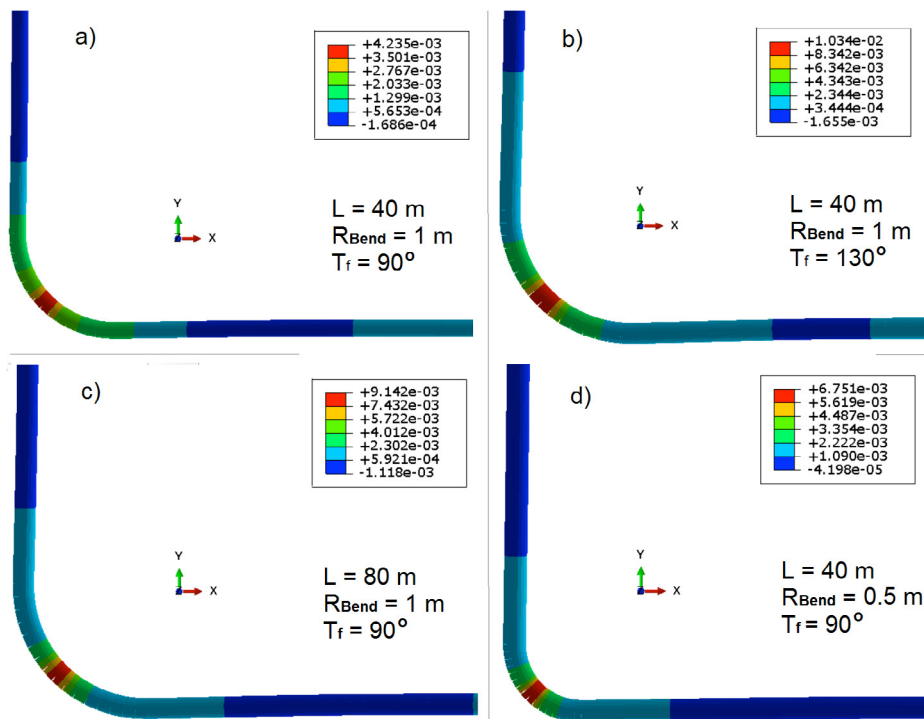


Fig. 2. Longitudinal strain contour and deformed shape of pipeline at the bend region, under operating conditions, for different values of the system parameters: a) $T_f = 90^\circ\text{C}$, $L = 40 \text{ m}$, $R_{bend} = 1 \text{ m}$; b) $T_f = 130^\circ\text{C}$, $L = 40 \text{ m}$, $R_{bend} = 1 \text{ m}$; c) $T_f = 90^\circ\text{C}$, $L = 80 \text{ m}$, $R_{bend} = 1 \text{ m}$; d) $T_f = 90^\circ\text{C}$, $L = 40 \text{ m}$, $R_{bend} = 0.5 \text{ m}$.

Evidently, the axial force in operating conditions is compressive and in the elastic range, with its magnitude increasing linearly along the pipeline from the bend region towards the anchor points, where it reaches its maximum

value (162507 N). The observed linear variation of the axial force beyond the bend region is caused by the constant soil friction ($F_R = 3944 \text{ N/m}$) opposing the thermal expansion. Instead, close to the bend, the pipe axial force decreases due to the bearing force on the transverse leg (Fig. 3a).

Conversely, the bending moment under service loads is maximum at the bend (22163 Nm), exceeding the yielding moment of the pipe section ($M_y = 18804 \text{ Nm}$), associated with plastic bending strains (Fig. 4), leading to compressive plastic longitudinal strains (-0.3%). The latter must be carefully verified in order to prevent the onset of local buckling limit state in the operating pipeline.

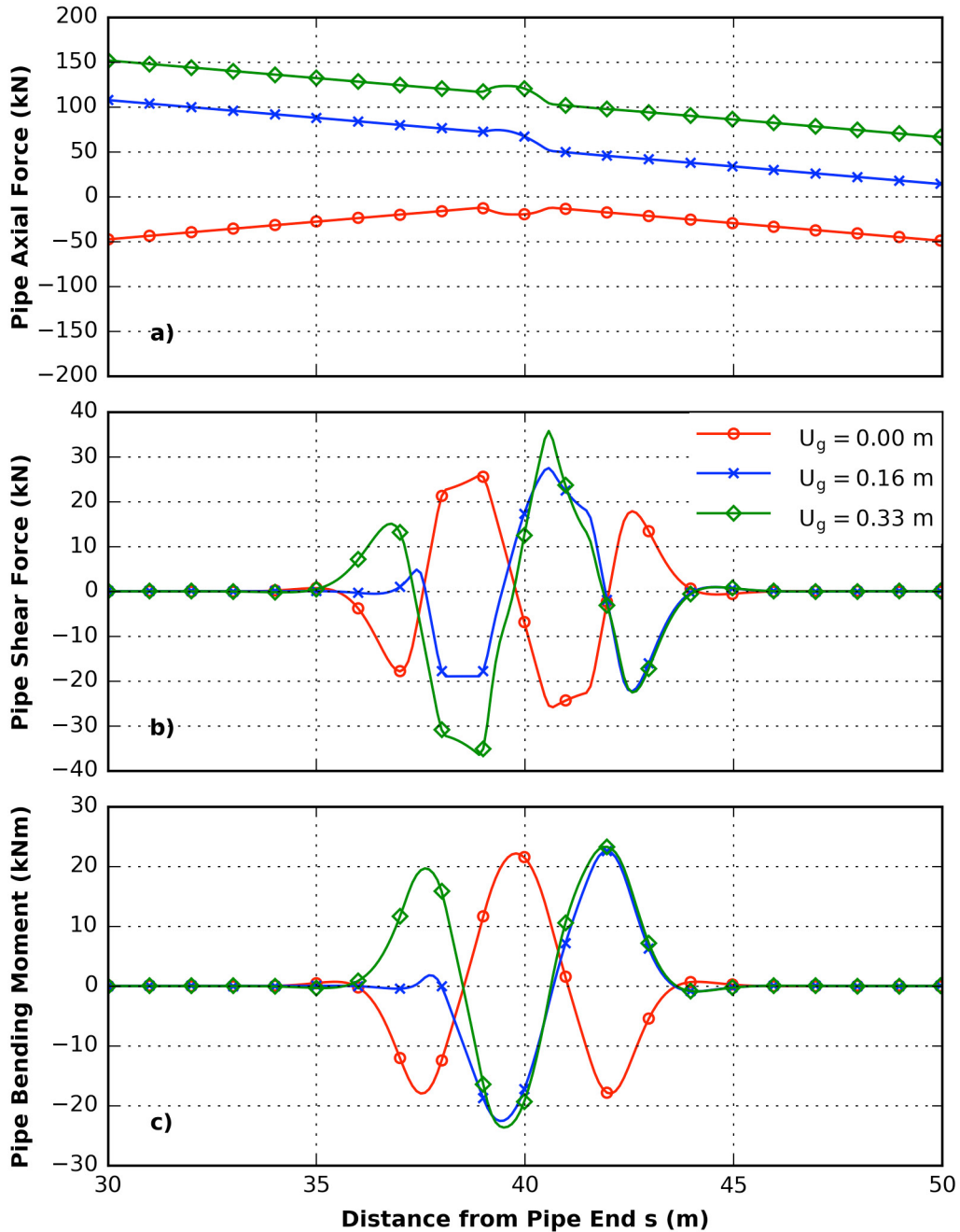


Fig. 3 Variation of the loads along the pipeline axis for different values of the ground displacement U_g : a) axial force; b) shear force; c) bending moment.

The bending moment decreases monotonically beyond the bend, inverting its direction until reaching two local peaks (17981 Nm) in the elastic range, located symmetrically at a distance of 2.5 m from the bend. Afterwards, the magnitude of the bending moment decreases rapidly to zero, so that beyond a distance of 5m from the bend, the pipeline undergoes only axial loading (Fig. 4).

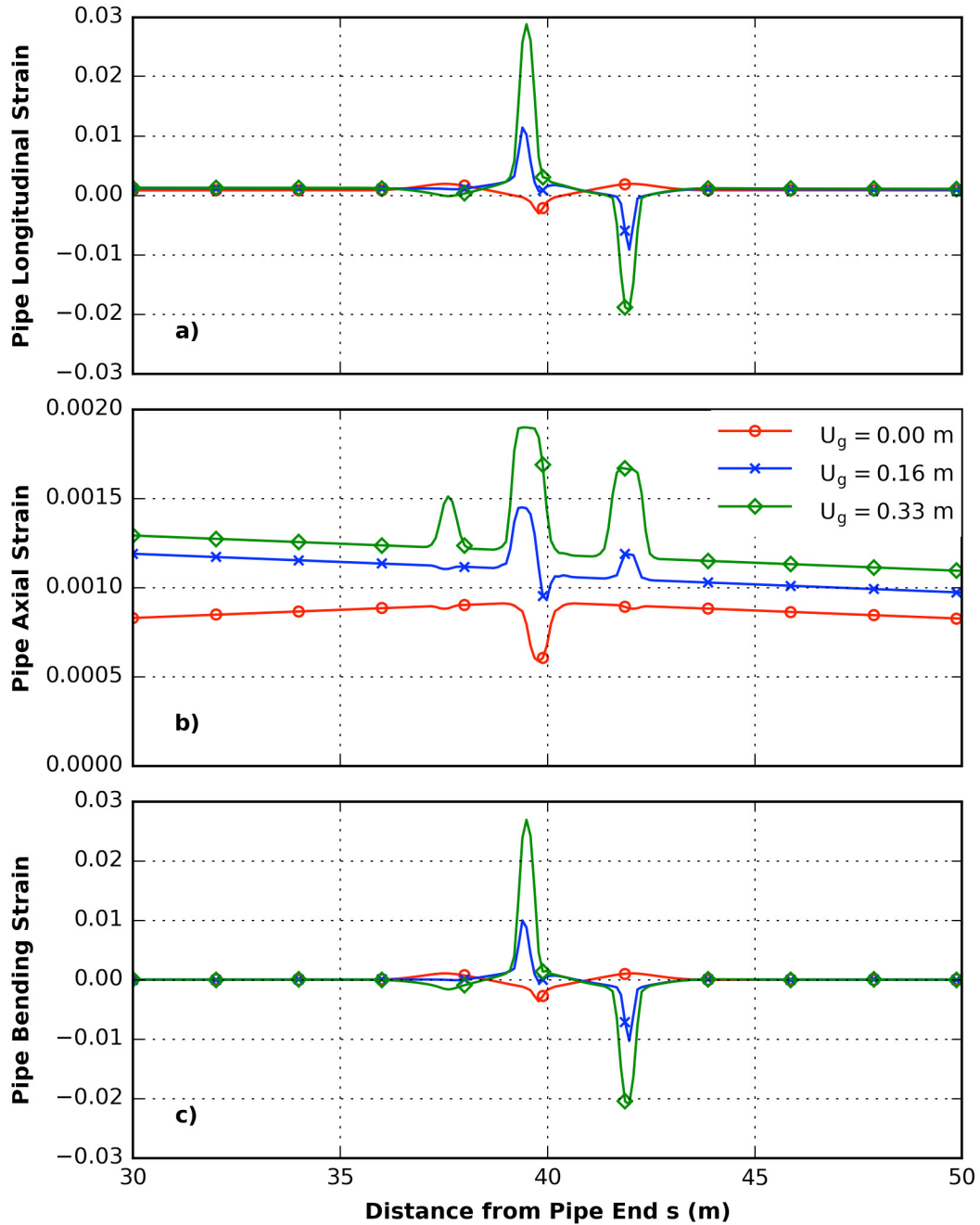


Fig. 4 Variation of the strains along the most stressed generator of the pipeline for different values of the ground displacement U_g : a) longitudinal strain; b) axial strain; c) bending strain.

3.2. Structural response of the pipeline in operating conditions

The seismic wave propagating parallel to one longitudinal leg, reverses the direction of the activated soil friction under service loads (Fig. 5), subjecting the pipeline to increasing tensile forces, as shown in Fig. 4 (a).

Evidently, pipe axial force varies linearly along the pipeline axis beyond the bend region, due to the soil friction reaction ($F_R = 3944 \text{ N/m}$), that is assumed constant throughout the analysis, despite the cyclic loading.

The pipe axial force is maximum at the anchor point in the longitudinal leg, parallel to the direction of the seismic wave propagation, decreasing linearly thereupon, until the bend region where it increases slightly, due to the lateral soil reaction in transverse leg. The linear variation of the axial force along the pipe axis is due to the soil friction reaction ($F_R = 3944 \text{ N/m}$), that is assumed constant throughout the analysis, despite the cyclic loading.

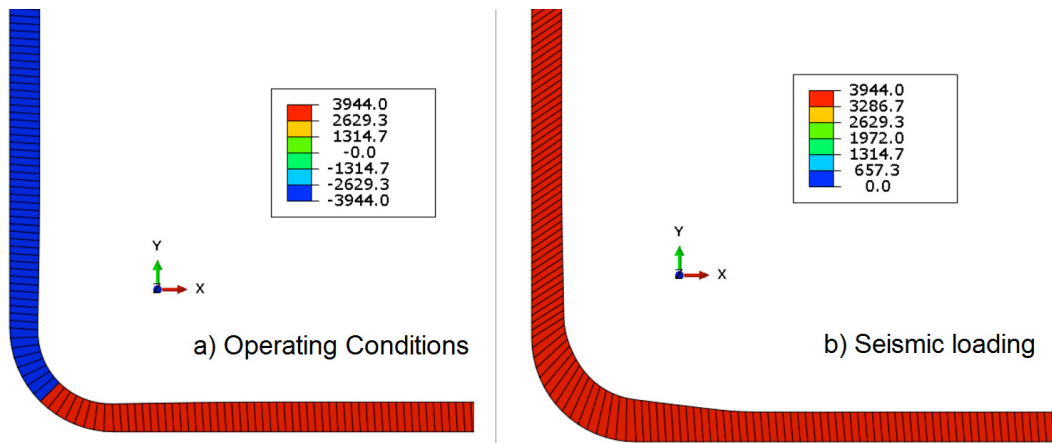


Fig. 5. Contour of the soil friction reaction along the pipeline (N/m): a) in operating conditions; b) under seismic loading.

The bending moment along the pipeline inverts its direction with respect to the operating conditions (Fig. 4), exceeding the elastic limit ($M_y = 18804 \text{ Nm}$), at the bending point in the transverse leg, located at 2.4 m from the bend. Consequently, two plastic hinges develop at these bending points during seismic loading, characterized by a localization of excessive bending and longitudinal strains, as shown in Fig. 4 and Fig. 6.

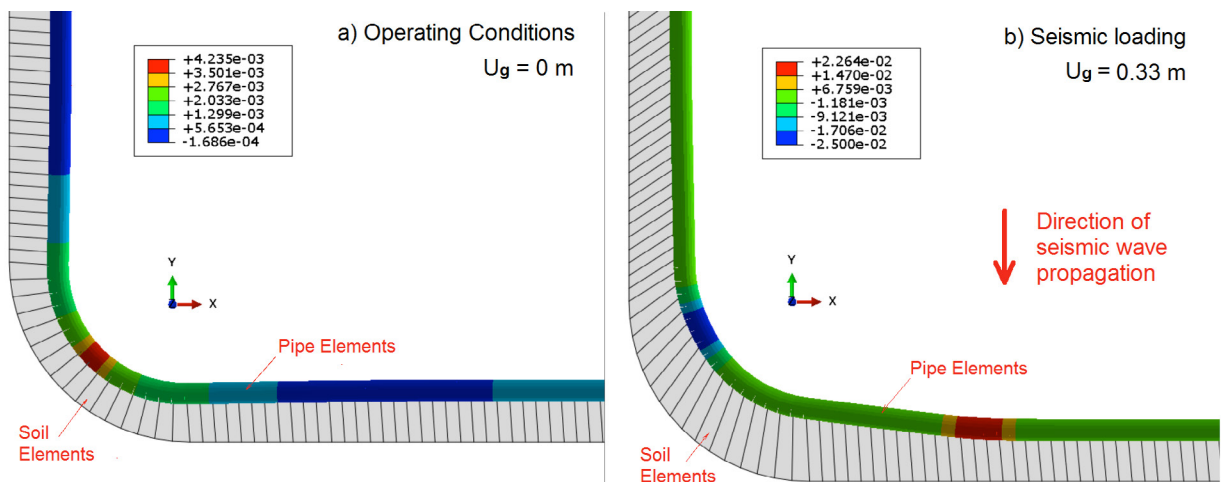


Fig. 6 Longitudinal strain contour and deformed shape of the pipeline at the bend region: a) in operating conditions; b) under seismic loading.

Particularly, the large compressive strains at the plastic hinges may lead to local buckling and consequent pipe failure, requiring proper mitigation measures in the design phase.

Furthermore, the axial strains vary linearly along the pipeline in the elastic range, apart two local peaks developing at the bending points (Fig. 4). The latter are produced by the interaction between bending and axial strains as a result of the elastoplastic response of the pipe section [27, 28]. Once the maximum longitudinal strain exceeds the yielding limit, axial strains increase locally so that the integral of the corresponding longitudinal stresses is equal to the continuously increasing axial force due to the ground displacement.

Evidently, the critical pipe region undergoing excessive plastic deformations is determined by the large bending moment, dissipating within a few pipe diameters around the bend (5 m), while beyond it the pipeline is subjected only to axial loading in the elastic range.

4. Conclusions

The present paper analyses the performance of an operating DH pipeline subjected to seismic loading within the finite element methodology, taking into account the geometric and mechanical properties of the system, including the soil-pipeline interaction.

The analyzed pipeline bend suffered plastic strains due to predominant bending induced by the imposed seismic ground displacement, leading to large compressive strains associated with local buckling in a brittle failure mode.

The pipeline performance depends on the geometrical and mechanical properties of the system, like the operating temperature, the pipe length, and the bend radius, requiring accurate evaluation in the design phase, in order to prevent material damage, under service and seismic loading.

Moreover, despite the simplistic assumptions regarding the adopted numerical model, including the representation of seismic loading as a sinusoidal wave, the obtained results give a better understanding on the earthquake response of operating DH pipelines. The latter is characterized by a cyclic soil-pipe interaction during seismic wave propagation (Fig. 7), requiring proper consideration in the engineering design practice.

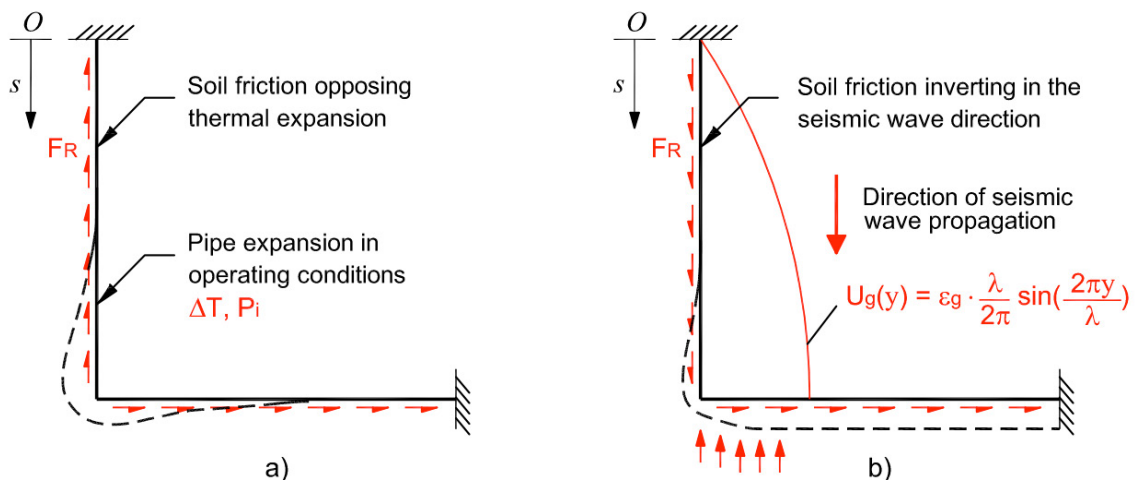


Fig. 7 Pipeline behaviour during: a) operating conditions; b) seismic ground deformation.

5. References

- [1] O'Rourke M.J. and Liu X. "Seismic design of buried and offshore pipelines". Monograph MCEER-12-MN04, Multidisciplinary Center for Earthquake Engineering Research, MCEER (2012).
- [2] Karamanos, S. A., Sarvanis, G. C., Keil, B. D., and Card, R. J. "Analysis and Design of Buried Steel Water Pipelines in Seismic Areas". *Journal of Pipeline Systems Engineering and Practice* 8(4) (2017).
- [3] Weidlich I., Illguth M., Banushi G. "Reserves in Axial Shear Strength of District Heating Pipes", International Scientific Conference on Environmental and Climate Technologies CONECT (2018).

- [4] American Lifeline Alliance, ALA. Guidelines for the design of buried steel pipe, (2001) Federal Emergency Management Agency, FEMA
- [5] FW401 - Teil 10 Verlegung und Statik von Kunststoffmantelrohren (KMR) für Fernwärmenetze. Arbeitsgemeinschaft Fernwärme, (2000) AGFW e.V.
- [6] Weidlich I. and Achmus M. "Measurement of normal pressures and friction forces acting on buried pipes subjected to cyclic axial displacements in laboratory experiments". *Geotechnical Testing Journal* 31(4) (2008): 334-343, doi: <https://doi.org/10.1520/GTJ100804>
- [7] Weidlich I. and Wijewickreme D. "Factors influencing soil friction forces on buried pipes used for district heating". *13th International Symposium on District Heating and Cooling* (2012).
- [8] Huber M. and Wijewickreme D. "Thermal influence on axial pullout resistance of buried district heating pipes". *14th International Symposium on District Heating and Cooling* (2014).
- [9] Gerlach T., Achmus M. and Narten M. "A numerical investigation on the bedding resistance of laterally displaced pipelines". *Simulia Community Conference* (2015).
- [10] Gerlach T. and Achmus M. "On the influence of thermally induced radial pipe extension on the axial friction resistance". *Energy Procedia*; 116 (2017): 351-364, doi: <https://doi.org/10.1016/j.egypro.2017.05.082>
- [11] Ha D., Abdoun T. H., O'Rourke M. J., Symans M. D., O'Rourke T. D., Palmer M. C. and Stewart H.E. "Centrifuge modeling of earthquake effects on buried High-Density PolyEthylene (HDPE) pipelines crossing fault zones" *Journal of Geotechnical and Geoenvironmental Engineering* 134(10) (2008): 1501-1515.
- [12] Karamanos S. A. et al. "Safety of buried steel pipelines under ground-induced deformations". RfCS project final report, RFSR-CT-2011-00027, (2015), doi: <https://bookshop.europa.eu/en/home/>.
- [13] Sarvanis G.C., Ferino J., Karamanos S.A., Vazouras P., Dakoulas P., Mecozzi E. and Demofonti G. "Soil-pipe interaction models for simulating the mechanical response of buried steel pipelines crossing active faults". *The 26th International Ocean and Polar Engineering Conference*; International Society of Offshore and Polar Engineers, ISOPE (2016).
- [14] Kouretzis G. P., Bouckovalas G. D. and Gantes C. J. "3-D shell analysis of cylindrical underground structures under seismic shear (S) wave action". *Soil Dynamics and Earthquake Engineering* 26(10) (2006): 909-921.
- [15] Saberi, M., H. Arabzadeh, and A. Keshavarz. "Numerical analysis of buried pipelines with right angle elbow under wave propagation." *Procedia Engineering* 14 (2011): 3260-3267.
- [16] Vazouras P., Karamanos S. A. and Dakoulas P. "Mechanical behavior of buried steel pipes crossing active strike-slip faults". *Soil Dynamics and Earthquake Engineering* 41(2012) 164-180.
- [17] Banushi G., Squeglia N., and Thiele K. "Innovative analysis of a buried operating pipeline subjected to strike-slip fault movement". *Soil Dynamics and Earthquake Engineering* 107 (2018): 234-249.
- [18] Barbas S.T. and Weir M.S. "Strain-based design methodology for seismic and arctic regions". *The Seventeenth International Offshore and Polar Engineering Conference*, International Society of Offshore and Polar Engineers, ISOPE (2007).
- [19] Guijt W. "Design considerations of high-temperature pipelines". *Proceedings of the ninth International Offshore and Polar Engineering Conference* (1999) 683–689.
- [20] EN 13941. "Design and installation of preinsulated bonded pipe systems for district heating". Beuth Verlag (2010).
- [21] CEN. "Eurocode 3 - Design of steel structures - Part 4-3: Silos, tanks and pipelines - Pipelines" (2002).
- [22] Goodling, E. C. "Buried piping—an analysis procedure update". *Proceedings international symposium on lifeline earthquake engineering*, ASME, PVP-77 (1983).
- [23] ABAQUS. (2014). User's guide, Simulia, Providence, RI.
- [24] Tung, T. K. and G. C. K. Yeh. "Thermal expansion of underground piping". *Pressure Vessels and Piping Conference*, ASME, PVP-65 (1982).
- [25] Yeh, G. C. K. "Hand calculation of seismic and thermal stresses in buried piping". *Earthquake behavior and safety of oil and gas storage facilities, buried pipelines and equipment*. PVP- 77 (1983).
- [26] American Society of Civil Engineers (ASCE), "Guidelines for the Seismic Design of Oil and Gas Pipeline Systems", *Committee on Gas and Liquid Fuel Lifelines*, ASCE (1984).
- [27] Karamitros, Dimitrios K., George D. Bouckovalas and George P. Kouretzis. "Stress analysis of buried steel pipelines at strike-slip fault crossings." *Soil Dynamics and Earthquake Engineering* 27.3 (2007): 200-211.
- [28] Banushi, G. and Squeglia N. "Seismic analysis of a buried operating steel pipeline with emphasis on the equivalent-boundary conditions". *Journal of Pipeline Systems Engineering and Practice* 9.3 (2018).



16th International Symposium on District Heating and Cooling, DHC2018,
9–12 September 2018, Hamburg, Germany

A machine learning approach to fault detection in district heating substations

Sara Månsson^{a,b,*}, Per-Olof Johansson Kallioniemi^a, Kerstin Sernhed^a, Marcus Thern^a

^aDepartment of Energy Sciences, Faculty of Engineering, Lund University, P.O. Box 118, SE-221 00 Lund, Sweden

^bVITO, Boeretang 200, BE-2400 MOL, Belgium

Abstract

The aim of this study is to develop a model capable of predicting the behavior of a district heating substation, including being able to distinguish datasets from well performing substations from datasets containing faults. The model developed in the study is based on machine learning algorithms and the model is trained on data from a Swedish district heating substation. A number of different models and input/output parameters are tested in the study. The results show that the model is capable of modelling the substation behavior, and that the fault detection capability of the model is high.

© 2018 The Authors. Published by Elsevier Ltd.

This is an open access article under the CC BY-NC-ND license (<https://creativecommons.org/licenses/by-nc-nd/4.0/>)

Selection and peer-review under responsibility of the scientific committee of the 16th International Symposium on District Heating and Cooling, DHC2018.

Keywords: District heating substations, fault detection, machine learning

1. Introduction

As the district heating (DH) systems are developing towards the 4th generation, it becomes increasingly important that the components of the systems are performing as well as possible [1]. In the existing DH systems, there are components that are poorly performing, and they need to be identified and addressed. One component that has been

* Corresponding author. Tel.: +46-46- 222 33 20.

E-mail address: sara.mansson@energy.lth.se

found to contain many faults is the DH substation located at the customers' installations [2]. Faults in substations could for example include valves that are stuck, fouled heat exchanger areas in the heat exchanger, malfunctioning temperature transmitters, but also wrong settings in the control system [3].

The faults in the substation cause poor cooling performance, which means that the heat from the DH system is not transferred in an optimal way in the customer substation. This leads to a need to increase either the flow or the supply temperature to be able to transfer the heat needed. This causes the energy efficiency of the entire DH system to decrease, especially if many of the substations are poorly performing [3]. Previous studies have shown that large shares of the substations in different DH systems are not performing well [4], [5], indicating that this is an issue that should be treated to as soon as possible in order to increase DH efficiency.

Historically, the most common way of detecting poorly performing substations has been to perform a manual analysis of customer data. This task can be extremely time consuming, due to the vast amount of data that is investigated when performing the analysis. Because of this, the substations with the largest heat demand in the DH system are normally prioritized when performing the analysis, leading to a large share of poorly performing substations being undetected. Therefore, well performing, automatic substation fault detection methods are needed.

The first step towards obtaining a well performing automatic fault detection method based on algorithms is to model the behavior of a substation in a good way. This can be done by identifying relationships between the measurements from the DH substation in order to establish patterns that occur when a substation is not performing optimally. Machine learning (ML) techniques have become one of the most used collection of techniques when modelling the relationship between different parameters. ML techniques are algorithms that are not specifically programmed; instead the purpose is to let the algorithms learn and improve from experience in order to obtain a well performing algorithm. Supervised learning techniques are a collection of ML methods that uses labeled data to train models that are used for a multitude of different problems, the most common ones being classification and regression modelling [6]. The labeled data consists of an input data set and an output data set, which both can contain one or more variables. During the training phase, both input and output data (labeled data) is presented to the model in order for it to learn the relationship between input and output data. When the training is finished, the model should be able to model the relationship well enough to be able to predict the labels of the output data when new, unlabeled input data is presented to the model [7]. Since the data from the district heating customers consist of numerical values, regression modelling should be used to predict the labels of the output values.

In this study, an ML regression model based on Gradient Boosting Regression (GBR) is used to predict the mass flow of one individual, well performing substation. The aim of the study is to develop a model that predicts the mass flow on an hourly basis, using as few input parameters as possible. When a good model has been obtained, a data set containing faults is introduced to the model in order to see if the model will make a different prediction for the faulty data set than for the data set that the model is created for

2. Background and related research

The heat demand in a building mainly originates from two different needs: the use of space heating and domestic hot water preparation [3]. These needs have to be met at all times, which means that the DH utilities need to make predictions about the heat demand in their systems in order to meet the customer demand. The prediction can be done for the entire system at once, as well as for the individual buildings in the system. Several studies have been conducted in the area, but the most recent studies focus mainly on statistical and ML prediction models. The statistical methods include Seasonal Auto-Regressive Integrated Moving Average (SARIMA) models, and Multiple Linear Regression (MLR) models, [8], [9], [10]. The neural network models are typically based on Boosting Regression (BR), Random Forest (RF), Support Vector Machines (SVM), Multi-Layer Perceptrons (MLPs), and k-Nearest Neighbor (k-NN) [11].

Dalipi et. al. described how different ML algorithms could be used to predict the heat load of a DH system using data from a waste incineration plant [12]. The authors compared three different ML algorithms (Support Vector Regression (SVR), Partial Least Squares (PLS), and RF) to each other in order to define a heat load forecaster that performs well in terms of low error and high accuracy. Fumo presented a review of the basics of building energy estimation, in which he mentioned two main approaches: forward (classical) approach and data-driven (inverse) approach [13]. The forward approach utilizes the already known mathematical equations describing the physical

relationships of a system and known inputs to predict an output parameter. In contrast, the data-driven approach consists of methods where measured variables are used as input for ML algorithms that uses the data to learn the behavior of the system.

Prediction methods have also been used in different contexts in order to detect anomalies in datasets. Araya et. al. presented a method that combined prediction-based and pattern-based classifiers to determine whether a consumption pattern was anomalous or not [14]. Chen et. al. described a statistical predictive method for detecting anomalies in building energy consumption [15]. The authors created a model of the baseline behavior of a building's energy consumption and calculated prediction intervals (PIs) for the mean and variance of the predicted data. The PIs described an estimate of an interval that future values should fall within. Future real values were considered as anomalies when their mean and/or variance fell outside the PIs. A similar approach was used in a study conducted by Baldacci et. al., where a prediction method using linear regression was used to detect anomalies in natural gas consumption [16].

The previous studies show that the most common techniques for prediction modelling in DH contexts are techniques that utilize patterns in existing DH data in order to identify important relationships between different variables. However, prediction methods have been used to detect anomalies in other energy-related research areas. The novelty of the work conducted in this study is that it combines the concepts of prediction modelling for forecasting in DH with the concepts of fault detection used in other fields.

3. Method

3.1. Data set

The data set used in this study consisted of hourly values during one year (November-November) from the primary side of one DH substation in a DH system in Sweden. The set originally contained hourly meter readings for one year for each measurement variable, but since some of these measurements were incomplete due to different reasons, the final number of instances was 8726. The variables, or features, that were included in the data set can be found in Table 1. $T_{out,24}$ refers to the average value of the outdoor temperature during the previous 24 hours.

Table 1. Features included in the data set.

Feature	Notation	Unit
Outdoor temperature	T_{out}	°C
Outdoor temperature, 24 hour average value	$T_{out,24}$	°C
Hour of the day	t	h
Supply temperature	T_s	°C
Return temperature	T_r	°C
Mass flow per hour	\dot{m}	m ³ /h

The data set was divided into one test set and one training set. The ratio between the number of meter readings in the training and test sets was 80/20.

3.2. Programming language

In this study, Python and the Scikit-learn package was used to conduct the modelling and fault detection. Python is an interpreted, object-oriented, high-level programming language, often used for data analysis and scientific computing. Python contains a wide range of different packages that can be used for these tasks, the Scikit-learn package being one of them. Scikit-learn is one of the most used packages for machine learning and provides a range of ML algorithms, including algorithms for regression, clustering, dimensionality reduction and preprocessing of features [17].

3.3. TPOT

Developing a machine learning algorithm can be a time consuming task, due to the fact that all data sets are unique and contain different challenges. There is almost always need for some sort of manual preprocessing of the data, to make sure that the data quality is sufficient. The variables (or features) may have to be modified in some way, e.g., scaling or introduction of polynomial features, and a well-performing predictor has to be chosen from the numerous methods that are available amongst the ML techniques [18].

In order to bypass some of the issues that traditionally arise when developing an ML model, a number of tools have been developed that allows the user to automate parts of the data analysis. One of these tools is the Tree-based Pipeline Optimization Tool (TPOT), which is an automated machine learning tool. TPOT is implemented in Python and creates combinations, or pipelines, of data transformations and machine learning models using genetic programming [18]. The tool optimizes the performance of the entire pipeline, using pre-existing algorithms in novel ways. Before using TPOT, the user must manually prepare the data for modelling by making sure that the data contains no missing or mislabeled values. TPOT then optimizes feature selection, feature preprocessing, feature construction, model selection, and parameter optimization. The last step of the ML process, the model validation, is carried out by the user.

3.4. Model Validation

The model validation can be carried out in a number of different ways. In this study, two different measures of difference between two variables were used: the coefficient of determination and the mean absolute error.

The coefficient of determination, or R² value, can be calculated using Equation 1. In the equation, SS_{res} is the sums of squares of the residuals, and SS_{tot} is the total sum of squares which is proportional to the variance of the data. The R² value is a number between zero and one, and a well performing model is expected to have a value close to one.

$$R^2 = 1 - \frac{SS_{res}}{SS_{tot}} \quad (1)$$

The mean absolute error, MAE, is the averaged sum of the absolute value of the residuals between actual values and predicted values can be calculated using equation 2. The MAE value for a well performing model is expected to be as close to zero as possible.

$$MAE = \frac{1}{n} \sum_{i=1}^n |(actual\ value)_i - (predicted\ value)_i| \quad (2)$$

3.5. Determining what TPOT pipeline to use

When running TPOT, it is important to make sure that the tool provides a well-functioning pipeline, with a model that captures the behavior of the substation well. In order to make sure that such a pipeline is obtained, TPOT was used on 16 different training sets and 16 different test sets to produce 16 different pipelines. The next step of the selection process was to introduce the obtained pipelines to the same training set, in order to be able to compare their performance for the same data. After fitting the pipelines to the labeled training data, they were introduced to the same test set and the R² and MAE values were then calculated. The resulting values are displayed in Table 2. The pipeline that had the highest R² value and the lowest MAE value for the test set was picked as the one to be further investigated in this study. The best performing pipeline was pipeline number 13 (highlighted in grey in Table 2), which had an R² value of 0.986 and an MAE of 0.100.

Table 2. R^2 and MAE values for the 16 different pipelines, used for the same test set. The best performing pipeline is highlighted in grey.

TPOT number	R^2	MAE
1	0.963	0.139
2	0.972	0.132
3	0.959	0.153
4	0.974	0.139
5	0.980	0.102
6	0.971	0.128
7	0.959	0.150
8	0.968	0.127
9	0.964	0.135
10	0.963	0.151
11	0.972	0.141
12	0.960	0.145
13	0.970	0.133
14	0.986	0.100
15	0.959	0.148
16	0.962	0.143

3.6. Final pipeline

The best performing pipeline, that was chosen to be further investigated in the study, consisted of two major components: pre-processing of data, and modelling, as illustrated in Fig. 2.

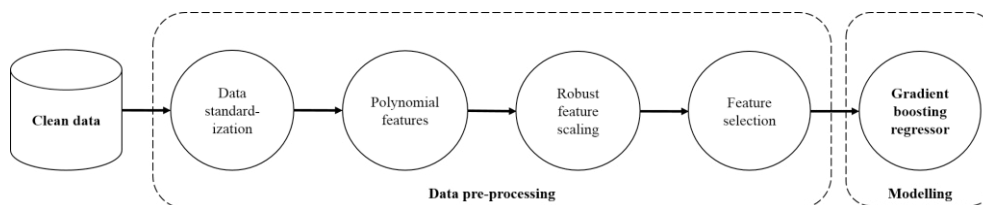


Fig. 1. Illustration of the TPOT pipeline

The first component, data pre-processing, consisted of four different steps. The first step consisted of a method for data standardization, which means that the features were standardized by removing their individual means and scaling to unit variance. This was done in order to make the distribution of the individual features look more or less like normally distributed data, since many machine learning algorithms (including the one used in this study) expects normally distributed data. If features of other distributions are introduced to the algorithms, there could be a risk of overestimating some features and excluding others that still would be useful in the next step.

In the second data pre-processing step, more features were generated. The generated features were polynomial and interaction terms of the original features. If the original features were labelled x_1 , x_2 , and so on, the additional features were generated as, e.g., the polynomial term x_1^2 , and the interaction term x_1x_2 . This kind of terms are normally introduced if no good model can be found when only using the original features. In this study, polynomial terms up to the second order of the original terms and first order of the interaction terms were included.

The next step of the data pre-processing scaled the features robustly, which means that all features, both the original and the generated ones, were standardized using a method that was robust to outliers. This was done in order to obtain a dataset where the ranges of the features were kept within the same limits. Similar feature ranges are important when modelling features that are normally measured in different units, e.g., when comparing the supply temperature to the flow rate per hour. Due to the different scales of the features, it might seem as if one feature is not varying as much as the other. This implies that the model should not put equal emphasis to the features' variation when fitting the model, causing a poorer fit of the data.

The last step consisted of a method for feature selection, where the features that were finally used to model the substation behavior were selected using the family-wise error rate. This meant that some of the features, either original or generated features, was not used to model the behavior of the substation. This is a common procedure in when using ML as a prediction tool, since it is important to keep the model as simple as possible. The features that were not contributing with new information to the model was therefore excluded.

The second main component of the pipeline was the regressor that predicted the behavior of the substation. The regressor was the Gradient Boosting Regressor (GBR). Gradient boosting is an iterative process, where regression models are added one by one to a so-called ensemble of methods. The model that is added in each iteration step is trained to minimize the regression error that the rest of the ensemble produces when modelling the data [19]. This means that in each iteration step, the added model improves the prediction ability of the ensemble. The final ensemble is obtained when a specified number of iterations has been performed. The number of iterations vary depending on how complex the data structure is, but in this study, 100 iterations was needed to obtain a model that did not improve significantly in terms of prediction ability when adding new models to the ensemble.

3.7. Test of variables

Since there are a number of plausible parameter combinations that could be used to model the substation behavior, a parameter test was conducted. In the test, the final pipeline was introduced to a number of different combinations of input and output parameters in order to see how well it could learn the substation behavior. The combinations were evaluated using the R^2 and MAE values.

The most promising combinations of the variable test are found in Table 3. The input/output combination that gave the highest R^2 value and the lowest MAE value was combination number 5 (highlighted in grey).

Table 3. Parameter combinations that were tested with the model. Combination number 5, highlighted in grey, obtained the best R^2 and MAE value.

Combination	Input parameters	Output parameters	R^2 value	MAE value
1	T_{out}, T_r, T_s, t	\dot{m}	0.9703	0.1337
2	$T_{out,24}, T_r, T_s, t$	\dot{m}	0.9555	0.2027
3	T_{out}, T_s, \dot{m}, t	T_r	0.8839	1.1091
4	$T_{out,24}, T_s, \dot{m}, t$	T_r	0.8903	1.0348
5	$T_{out,24}, T_{out}, T_s, t$	\dot{m}	0.9740	0.1301
6	$T_{out,24}, T_{out}, T_s, t$	T_r	0.8841	1.0555
7	$T_{out,24}, T_{out}, T_s, t$	T_r, \dot{m}	0.9296	0.5857
		T_r	0.8868	1.0412
		\dot{m}	0.9723	0.1301

3.8. Inducing faults

In order to test the fault detection potential of the model, the model was introduced to a dataset consisting of the parameters in the best performing parameter combination presented in section 3.7. To obtain a faulty dataset, two faults that are commonly known to occur in DH customer values were induced in the dataset from the well performing substation.

The first fault was related to communication problems between the meter and the DH utility's database, and occurs when the connection between the meter and the utility's database is lost. When this happens, many utilities choose to replace the missing meter reading with a fixed value. In this case, a value of 60 °C was inserted randomly in the data set for the supply temperature. Since this was an extremely low value comparing to the original dataset, another fault was also induced where the original value of the supply temperature was decreased by 10 %.

The second fault that was induced was a drifting meter fault, which can be described as a "...gradual change in output over a period of time which is unrelated to any change in input" [20]. The drifting meter fault was induced for two different meters: the outdoor temperature meter and the supply temperature meter. The fault was induced as a

gradually increasing addition to the original meter readings. For both variables, the maximum increase of the values was 1.08 °C.

In order to evaluate how the model performs when it was introduced to a dataset containing faults, the prediction performance of the model for the faulty dataset was compared to the prediction performance for the original dataset. The hourly residual between the real values and the predicted values for the faulty dataset was computed, as well as the hourly residual between the real values and the predicted values for the original dataset without faults. The cumulative sums of these residuals were also calculated using a rolling window that included the residuals from the last 24 hours.

4. Results

4.1. Model performance, well performing data set

Fig. 2 (a) displays the actual values obtained from the substation (blue dots), and the predicted values obtained from the model (red dots) as a function of time. As can be seen in the figure, the model is not able to capture all of the rapid changes that occur in a DH substation. However, the R^2 value of 0.986 is deemed to be good enough to continue with the model. Fig. 2 (b) displays the predicted values as a function of the real values. The relationship between the variables displays a more or less linear behavior, which is expected when a model that describes the main share of the variation in the original data has been obtained.

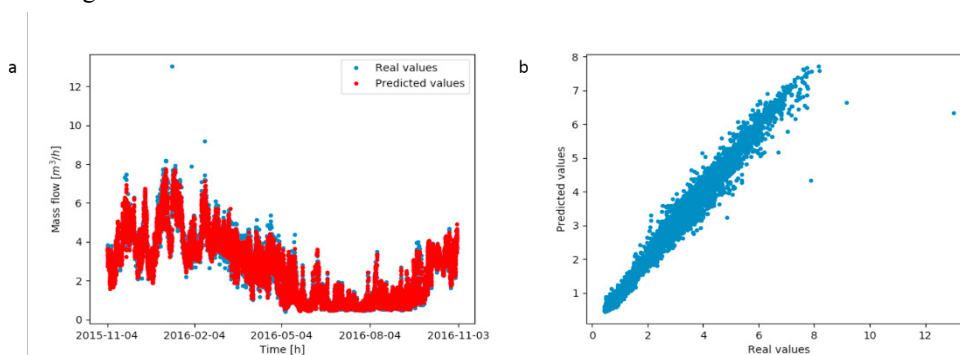


Fig. 2. (a) Real and predicted values for the entire data set. (b) Predicted values as a function of the real values.

4.2. Model performance, data sets containing faults

Fig. 3(a) displays two residuals: the residual between the real values and the predicted values for a well performing substation (blue line), and the residuals between the real values and the data where a communication fault has been induced (red line). Fig. 3(b) displays the cumulative sum over a 24 h interval of the same residuals. As can be seen from the residuals and the cumulative sum of the residuals, the residuals of the dataset containing faults deviate significantly from the residuals of the well performing dataset. This can especially be seen in Fig. 3 (b). The deviations were further investigated and were found to correspond to days where the 60 °C fault had been induced.

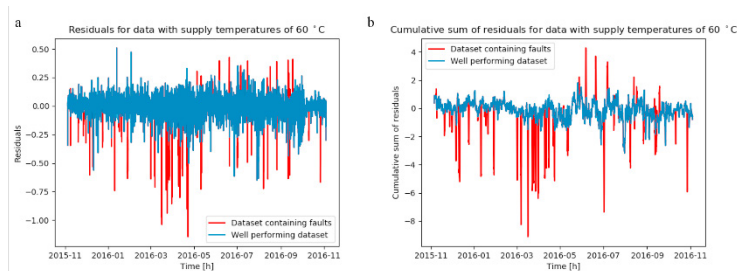


Fig. 3. (a) Residuals for data with supply temperatures of 60 °C. (b) Cumulative sum of residuals for data with supply temperature of 60 °C.

Fig. 4 (a) and (b) displays the residual and the cumulative sum of the residuals for the data where supply temperature instances have been decreased by 10 % (red lines). The figures also show the residual for the well performing dataset (blue lines). The difference between the residuals of the well performing dataset and the faulty dataset is not large, but the cumulative sum displays a larger difference.

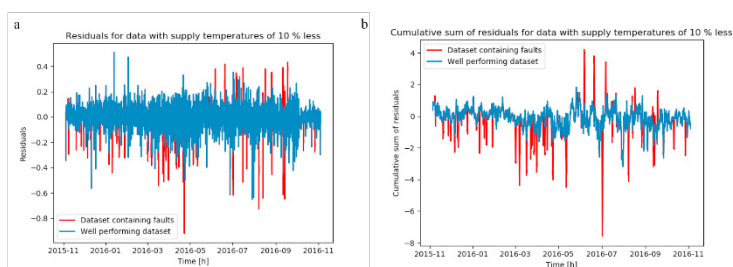


Fig. 4. (a) Residuals for data with supply temperatures that have been decreased by 10 %. (b) Cumulative sum of residuals for data with supply temperature that have been decreased by 10 %.

Fig. 5. displays the residual and cumulative sum of a dataset containing measurements from a drifting outdoor temperature meter (red lines), as well as the residual and cumulative sum for the well performing dataset (blue lines). For the residual, the deviation from the well performing dataset is not clearly visible, but the cumulative sum in Fig. 5. (b) displays a clear deviation approximately one month after the fault was induced in the data.

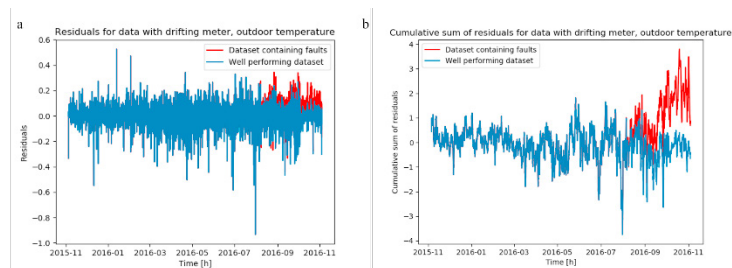


Fig. 5. (a) Residuals for data with drifting meter, outdoor temperature. (b) Cumulative sum of residuals for data with drifting meter, outdoor temperature.

Fig. 6. (a) displays the residuals for data induced with a drifting supply temperature meter (red line), and Fig. 6. (b) displays the cumulative sum of the residual (red line). In the same figures, the residual and cumulative sum of the residual for the well performing substation are displayed as well (blue lines). Here, there is no clear deviation from the residuals and cumulative sum of the well performing substation.

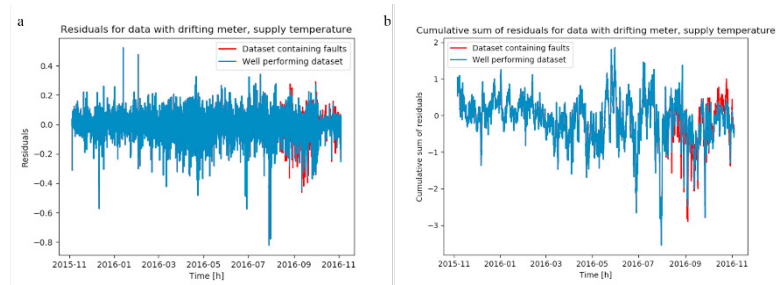


Fig. 6. (a) Residuals for data with drifting meter, supply temperature. (b) Cumulative sum of residuals for data with drifting meter, supply temperature.

5. Analysis and Discussion

The results of this study show that it is possible to model the behavior of a DH substation using machine learning algorithms, specifically using the Gradient Boosting Regressor. As can be seen the variable test, the model predictions were most accurate when having the flow rate as output parameter, and outdoor temperature, time of day, and supply temperature as input parameters. Fig. 2. (a) shows that the model manages to capture the main part of the substation's behavior, except for the most extreme values in the original dataset. This is confirmed by Fig. 2. (b), which displays the predicted values as a function of the real values. The values display a more or less linear relationship, which is expected (within a reasonable error limit) when a model is able to capture the largest part of the behavior of the output variable. The values that are deviating significantly from the linear behavior in Fig. 2. (b) are coupled to the most extreme values of the real dataset, which the model was not able to capture.

When testing the fault detection capability of the model, it is clear that different parameters have different impact on the model's performance. The fault representing communication error between the substation and the DH utility's database is clearly visible when comparing the residuals of the faulty dataset and the well performing dataset (Fig. 4 (a) and (b)). However, when comparing this to the faulty dataset containing an induced drifting supply temperature meter in Fig. 6., it is clear that the deviation from the original dataset is not as large. When comparing these conclusions to the results in Fig. 4. (a) and (b), it is clear that the residuals from the dataset containing supply temperature measurements that have been decreased by 10 % show a larger difference from the well performing substation than in the case of the drifting supply temperature meter. The deviation is not as large as for the data where 60 °C was induced, but this was expected since the 60 °C fault was extreme in this particular DH system and dataset.

Based on the figures presented in the results, the largest difficulty of obtaining a well performing fault detection method that works automatically will be to find an evaluation algorithm that can distinguish a sudden change in the residual and/or cumulative sum. When looking at Fig. 4. (b), it is clear that the deviations from the cumulative sum of the well performing dataset in most cases do not deviate significantly from the most extreme residuals from the well performing dataset. However, the most extreme deviations in the residual of the well performing dataset occur during summer, when the behavior of the substation will be different due to the fact that no space heating demand occur in the customer installation. When looking at the first part of the cumulative sum in Fig. 4. (b), from November until May, it is clear that the deviation from the residual of the well performing dataset is large, and it might be necessary to detect the deviations during heating season separately. One way of doing this could be to monitor the change of the residual and/or cumulative sum that the model produces continuously and flag a fault if a rapid change occurs.

The model is more sensitive to changes in measurements from the outdoor temperature meter. As can be seen in Fig. 5. (b), the cumulative sum of the residual of the faulty dataset deviates significantly from the residuals of the well performing dataset approximately one month after the fault is induced. The fault induced had a maximum value of 1.08 °C, and even though this can be considered as a small (and reasonable) change in the measurements of the outdoor temperature, the model responded clearly to the change. This is very promising for continued model development and fault detection studies.

6. Conclusion

In this study, a model for the flow rate in a DH substation has been created, using the outdoor temperature, supply temperature and time of day as input parameters. The model is based on a number of data pre-processing steps, as well as a regression method called Gradient Boosting Regressor. When introduced to datasets containing different faults, the model predictions change, which shows great promise for continued fault detection studies using this model.

Acknowledgements

This work is part of the TEMPO project which is funded by the European Union's Horizon 2020 Programme under Grant Agreement no. 768936.

References

- [1] H. Lund, S. Werner, R. Wiltshire, S. Svendsen, J. E. Thorsen, F. Hvelplund och B. Vad Mathiesen, "4th Generation District Heating (4GDH) - Integrating smart thermal grids into future sustainable energy systems," *Energy*, vol. 68, pp. 1-11, 2014.
- [2] H. Gadd, *To analyse measurements is to know!*, Lund: Lund University, 2014.
- [3] S. Frederiksen och S. Werner, *District heating and Cooling*, Lund: Studentlitteratur, 2013.
- [4] H. Gadd och S. Werner, "Achieving Low Return Temperature from District Heating Substations," *Applied Energy*, vol. 136, pp. 59-67, 2014.
- [5] H. Gadd och S. Werner, "Fault Detection in District Heating Substations," *Applied Energy*, vol. 157, pp. 51-59, 2015.
- [6] C. Sammut och G. I. Webb, "Supervised learning," i *Encyclopedia of Machine Learning and Data Mining*, Boston, Springer, 2017.
- [7] M. Mohri, A. Rostamizadeh och A. Talwalkar, *Foundations of machine learning*, Cambridge: MIT Press, 2012.
- [8] S. Grosswindhager, A. Voigt och M. Kozek, "Online short-term forecast of system heat load in district heating networks," i *Proceedings of the 31st International Symposium on Forecasting*, Prague, Czech Republic, 2011.
- [9] T. Fang och R. Lahdelma, "Evaluation of a multiple linear regression model and SARIMA model in forecasting heat demand for district heating system," *Applied energy*, vol. 179, pp. 544-552, 2016.
- [10] T. Catalina, V. Iordache och B. Caracaleanu, "Multiple regression model for fast prediction of heating energy demand," *Energy and buildings*, vol. 57, pp. 302-312, 2013.
- [11] H.-x. Zhao och F. Magoulés, "A review on the prediction of building energy consumption," *Renewable and sustainable energy reviews*, vol. 16, pp. 3586-3592, 2012.
- [12] F. Dalipi, S. Yildirim Yayilgan och A. Gebremedhin, "Data-Driven Machine-Learning Model in District Heating System for Heat Load Prediction: A Comparison Study," *Applied Computational Intelligence and Soft Computing*, vol. 2016, 2016.
- [13] N. Fumo, "A review on the basics of building energy estimation," *Renewable and sustainable energy reviews*, vol. 31, pp. 53-60, 2014.
- [14] A. D. B. K. Grolinger, H. F. ElYamani och M. A. Capretz, "An ensemble learning framework for anomaly detection in building energy consumption," *Energy and Buildings*, vol. 144, pp. 191-206, 2017.
- [15] B. Chen, M. Sinn, J. Ploennigs och A. Schumann, "Statistical Anomaly Detection in Mean and Variation," i *22nd International Conference on Pattern Recognition*, Stockholm, Sweden, 2014.
- [16] L. Baldacci, M. Golfarelli, D. Lombardi och F. Sami, "Natural gas consumption forecasting for anomaly detection," *Expert systems with applications*, vol. 62, pp. 190-201, 2016.
- [17] W. McKinney, *Python for data analysis - Data wrangling with Pandas, NumPy, and IPython*, O'Reilly, 2018.
- [18] R. S. Olson, R. J. Urbanowicz, P. C. Andrews, N. A. Lavender, L. C. Kidd och J. H. Moore, "Automating Biomedical Data Science Through Tree-Based Pipeline Optimization," i *European conference on the Applications of evolutionary computation*, 2016.
- [19] A. Natekin och A. Knoll, "Gradient boosting machines, a tutorial," *Frontiers in neurorobotics*, vol. 7, nr 21, 2013.
- [20] W. Bolton, *Newnes instrumentation & measurement pocket book*, Oxford: Newnes, 2000.



16th International Symposium on District Heating and Cooling, DHC2018,
9–12 September 2018, Hamburg, Germany

Towards understanding district heating substation behavior using robust first difference regression

Shiraz Farouq^{a,*}, Stefan Byttner^a, Henrik Gadd^b

^aHalmstad University, Department of Intelligent Systems and Digital Design,
Kristian IV:s väg 3, 301 18, Halmstad, Sweden

^bÖresundskraft AB, Sweden

Abstract

The behavior of a district heating (DH) substation has a social and operational context. The social context comes from its general usage pattern and personal requirements of building inhabitants. The operational context comes from its configuration settings which considers both the weather conditions and social requirements. The parameter estimating thermal energy demand response with respect to change in outdoor temperature conditions along with the strength of the relationship between these variables are two important measures of operational efficiency of a substation. In practice, they can be estimated using a regression model where the slope parameter measures the average response and R^2 measures the strength of the relationship. These measures are also important from a monitoring perspective. However, factors related to the social context of a building and the presence of unexplained outliers can make the estimation of these measures a challenging task. Social context of a data point in DH, in many cases appears as an outlier. Data efficiency is also required if these measures are to be estimated in a timely manner. Under these circumstances, methods that can isolate and reduce the effect of outliers in a principled and data efficient manner are required. We therefore propose to use Huber regression, a robust method based on M-estimator type loss function. This method can not only identify possible outliers present in the data of each substation but also reduce their effect on the estimated slope parameter. Moreover, substations that are comparable according to certain criteria, for instance, those with almost identical energy demand levels, should have relatively similar slopes. This provides an opportunity to observe deviating substations under the assumption that comparable substations should show homogeneity in their behavior. Furthermore, the slope parameter can be compared across time to observe if the dynamics of a substation has changed. Our analysis shows that Huber regression in combination with ordinary least squares can provide reliable estimates on the operational efficiency of DH substations.

© 2018 The Authors. Published by Elsevier Ltd.

This is an open access article under the CC BY-NC-ND license (<https://creativecommons.org/licenses/by-nc-nd/4.0/>)

Selection and peer-review under responsibility of the scientific committee of the 16th International Symposium on District Heating and Cooling, DHC2018.

* Corresponding author.

E-mail address: shiraz.farouq@hh.se

1876-6102 © 2018 The Authors. Published by Elsevier Ltd.

This is an open access article under the CC BY-NC-ND license (<https://creativecommons.org/licenses/by-nc-nd/4.0/>)

Selection and peer-review under responsibility of the scientific committee of the 16th International Symposium on District Heating and Cooling, DHC2018.

10.1016/j.egypro.2018.08.188

Keywords: district heating; energy demand response; robust regression; outliers

1. Introduction

Analysis of the substations is very important for improving the overall efficiency of the entire DH network. According to [1], two criteria, irregular oscillations in energy and flow, and low correlation between energy demand and outdoor temperature, may describe inefficient substation control settings. This paper, however, does not specify a particular measure to quantify these two criteria. In general, a simple way to observe operational efficiency of a substation is to measure its energy demand response to outdoor temperature changes and the strength of the relationship between these two variables. These can be estimated using a regression model. However, usage pattern of a building and individual requirements of its residents may appear as outliers in data. For instance, in many buildings, one can usually observe a surge in energy demand on Mondays and a substantial decrease during the weekends. This may pose a significant challenge for traditional methods such as the ordinary least squares (OLS) to efficiently and accurately estimate the operational efficiency measures of a substation, thus resulting in false alarms. Hence, we propose to use Huber regression [8], a robust method based on the M-estimator type loss function. The main reasoning behind the choice of this method is to isolate outliers and reduce their effect on the estimated response parameter without completely removing them. The use of robust regression methods is not common in the district heating literature. A mentionable work in this respect is [4].

From a statistical perspective, energy demand of a building is usually a combination of three processes. The first process is governed by outdoor temperature, the second by overall building usage pattern and the third by individual requirements of a resident. We assume that the primary process is a result of changes in outdoor temperature. In this situation OLS will try to fit all the three processes, doing justice to none. Robust regression on the other hand will fit the primary process while marking data from those secondary processes as outliers.

This paper investigates the following questions:

1. Do outliers detected through Huber regression explain the usage pattern of a building?
2. To what degree do outliers effect the strength of relation between energy demand and outdoor temperature?
3. Can changes in the parameter describing the relationship between energy demand response of a substation be explained by changes in return temperature and/or flow?
4. Do buildings belonging to the same building category, as marked by their owner company, show homogeneity of behavior in terms of their usage pattern?
5. In what ways does this analysis lead to identification of possible malfunctions and wrong configurations in DH substations?

The paper is organized as follows. An overview of on robust methods is provided in Section 2. In Section 3. we describe our methodology based on robust first difference regression. In Section 4. we describe details about the data. In Section 5. we present the results and show the corresponding visualizations. Finally, in Section 6. we present the summary of our findings and a discussion.

2. Robust methods

Prior assumptions form a basis for any statistical inference procedure. The most common such assumption is the normality of data generating process. Most statistical methods are sensitive to minor deviations from this assumption. For instance, OLS assumes that residual errors are normally distributed and homoscedastic. However, observations obtained in real-world, such as those from district heating substations, present a different picture. Missing values, sensor faults, equipment malfunction, misconfiguration, low time resolution and varying consumer behavior makes estimating the relationship between intrinsically linked variables such as energy demand and outdoor temperature quite difficult. It can be argued that a two step-procedure can solve this problem:

1. Apply certain rules for outlier rejection, for e.g., based on classical 3-sigma edit rule, to clean the data.
2. Use classical estimation and testing procedures on the remaining data.

There are several problems with the above procedure as mentioned in [2]. First, one needs to have parameter estimates, especially in a multiple regression case, before one can "cleanly" separate outliers. Second, the resulting dataset after applying outlier rejection rules may not reflect the actual distribution of the process. Third, classical rejection rules, in many cases, cannot cope with situations when one outlier can mask the other such that none of them is rejected.

It was argued in [3] that outlier diagnostics and robust regression have similar goals, but they proceed in the opposite order: *In a diagnostic setting, one first wants to identify the outliers and then fit the good data in the classical way, whereas the robust approach first fits a regression that does justice to the majority of the data and then discovers the outliers as those points having large residuals from the robust equation.* The philosophical arguments on which approach is better have different point of views. We believe that robust regression is a more principled approach towards outliers.

Robust regression methods, in general, rely on less restrictive assumptions. Not only can they detect the presence of outliers but also remove or dampen their effect on the estimated parameters. The M-estimators are class of robust regression methods based on maximum likelihood. Moreover, these methods are also called *winsorizing*, i.e., they do not completely remove the effect of an influencing outlier, but reduce it. This stands in contrast to other classes of robust methods such as least trimmed squares (LTS) [3,6] which remove the effect of outliers completely.

In a linear regression, the loss function increases quadratically with the increase of its residuals:

$$\rho(\mathbf{u}) = \sum_{i=1}^n u_i^2$$

Hence, the loss function is not robust to outliers. One approach to alleviate this problem is to use absolute value of the loss function:

$$\rho(\mathbf{u}) = \sum_{i=1}^n |u_i|$$

While this loss function achieves robustness, it is not differentiable. Huber proposed a robust alternative:

$$\rho(\mathbf{u};c) = \begin{cases} u_i^2 & \text{if } |u_i| \leq c \\ c(2|u_i| - c) & \text{if } |u_i| > c \end{cases} \quad (1)$$

The Huber loss function imposes a penalty on outliers: linear for large and quadratic for small. Hence, it does not completely remove the effect of outliers but reduces it. The parameter c controls the tradeoff between robustness and efficiency. Huber argued for $c=1.345$ on efficiency grounds if the underlying distribution is normal. The estimators obtained by minimizing the loss function (1) are called Huber estimators and belong to the class of M-estimators.

When dealing with robust regression, one also needs to be familiar with two important concepts: the *breakdown point* and the *leverage point*. Leverage points are outlying values in the x -direction that can inordinately affect the parameter estimates of a regression. These could be good or bad. A bad leverage point results in a large residual while a good leverage points is consistent with the regression line and may shrink certain confidence regions [3]. The concept of a breakdown point was introduced in [5], according to which, it is the smallest amount of data contamination that may cause an estimator to take on arbitrarily large aberrant values. It was shown in [6] that least median of squares (LMS) regression is robust up to 50% contamination. However, it was argued in [2] that the concept of a breakdown point should be taken cautiously. A high degree of contamination, especially in large samples, almost always must be interpreted as a mixture model.

While Huber M-estimator is robust in the y -direction, its breakdown point in the x -direction is $1/n$, which is similar to the OLS estimate. However, as we will discuss in the next section, this is not a concern for our analysis.

3. Methodology

In the context of this paper, robustness signifies insensitivity to small deviations from the assumptions as described in [2]. Moreover, as noted earlier, the breakdown point for Huber regression in the x -direction is $1/n$. For our analysis, however, this is not an issue since the x -direction consists of outdoor temperature readings. Since extreme outdoor conditions have not been observed for the period under consideration, the potential of having high leverage point is therefore unlikely. However, we need robustness in the y -direction and Huber regression provides that guarantee.

From a computational point of view, estimating energy demand response to the change in outdoor temperature requires a formulation of regression models. We consider two possible candidates. A simple linear regression model and the first difference version of it. Let's consider the first model:

$$y = a + bx + \epsilon$$

Here, a is the trend parameter which may contain building specific information and will therefore vary across substations even among similar building categories. Moreover, b is the slope parameter which measures the change in energy demand level of a substation when the outdoor temperature level changes. Furthermore, y and x represents energy demand and outdoor temperature levels, respectively, and ϵ represents residual errors. For comparing different substations having similar energy demands levels, one needs to consider the trend parameter a . A simple way around this is to remove it by de-trending the series using a first difference. First difference also acts as a high pass filter and is simple to compute than other similar techniques. It is also data efficient, since it does not require large amount of data. We need this filter since we want to identify and mark large deviating observations in the energy demand data. Moreover, if the data is non-stationary, i.e., its distribution changes over time, taking first difference reduces the problem. Furthermore, in our context, it is interpretable since we seek of how much energy demand response changes if the outdoor temperature changes by a single unit. Hence, the first difference regression model is given by:

$$\Delta y = \alpha \Delta x + \nu \quad (2)$$

Here α measures the average energy demand response Δy to unit change Δx in outdoor temperature and is the parameter of primary interest. Moreover, ν represents residual errors.

The Huber regression does not follow the distributional assumptions in the manner OLS does. Therefore R^2 obtained using Huber regression may not be informative in the current setting. Hence, in the context of our analysis, we used OLS after removing the outliers (which we assumed to be the result of secondary processes) to measure the strength of the relationship between Δy and Δx due to the primary process, i.e., the R^2 . Alternatively, robust covariance techniques can be used [2, 3].

The method is only applicable when outdoor temperature is below the level where space heating is required. The optimal value of α will depend on a number of factors including the social purpose of a building, its time constant, its envelope, and its energy demand requirements. There is no established range on what a good α should be even for a particular building category since no such studies are available in literature, especially in the context of entire district heating networks. A high α possibly means that a substation has to respond with higher energy demand for a unit decrease in outdoor temperature. For similar buildings, a higher α compared to others may signify energy losses due to insulation while a comparatively lower α may be due to better insulation. Differences in α may also be due to very different heat-load temperature curve settings. A very low α may signify problems in the substation as in these cases R^2 is also low. In certain cases, it may also signify that the first difference model is not appropriate for the particular substation.

We estimate Eq. (2) using Huber regression. Moreover, data efficiency, i.e., estimating parameters using minimal amount of data is important if timely information is required. Huber regression can isolate and efficiently compute regression parameters on small data sets. Hence, we undertake the analysis based on one-month data sets.

To further facilitate understanding on the behavior of a substation, we propose to visually relate α with other substation related variables: for instance, visualizing it together with return temperature and augmenting it with variables like volume and energy using different color-coded schemes.

4. Data

The data for this analysis was made available to us by Öresundskraft which provides district heating services to buildings in Helsingborg and Ängelholm (Sweden). Hence, we have data from around 11,000 substations in Helsingborg and 2,800 substations in Ängelholm. Each substation is associated with a building category like: public administration building, social services building, multi-dwelling building, small houses/villa, manufacturing industry etc. By far the most common building category is small house/villa with around 8,500 such buildings in Helsingborg and around 2,300 in Ängelholm. This study only focuses on the data from substations in Helsingborg. The category studied is “multi-dwelling” with around 800 buildings. The time resolution of the available data is 1 hour. Moreover, we only use data from the months of Jan 2016 and Jan 2017.

5. Results and visualizations

The y and x in Eq. (2) are computed as follows:

To remove any customer induced hourly trend, we sum the hourly energy demand E for each substation for the whole day, i.e.,

$$y_i = \sum_{i=0}^{23} E_i$$

The first difference between the $(j + 1)$ -th and the j -th day is then computed by:

$$\Delta y = y_{j+1} - y_j$$

Finally, the first difference of daily mean temperature is computed as:

$$\Delta x = \bar{x}_{j+1} - \bar{x}_j$$

Here, \bar{x}_{j+1} and \bar{x}_j are the mean temperatures for $(j + 1)$ -th and the j -th day, respectively.

We estimate Eq. (2) using Huber regression whose loss function is defined by Eq. (1). We chose $c=1.28$ based on discussion in [Chapter 3, 7]. Data for the months of Jan 2016 and Jan 2017 from buildings categorized as "Multi-dwelling" is used for analysis.

Since the intrinsic relation between energy demand and outdoor temperature is conceptually negative; hence when we say high α we mean its high *negative* value. Furthermore, α in this context signifies change in the total energy demand of a substation between two consecutive days if the mean temperature between those days change by 1°C. Hence, the unit of α is KWh/°C.

It can be observed from Fig. 1(a) and Fig. 1(b) that median R^2 obtained using OLS improves from 0.72 to 0.92 for the substations after removing the outliers identified by Huber regression. Moreover, half of these outliers can be explained by the weekday effect. For instance, it was observed that on Mondays, energy demand of a substation increases while on weekends it decreases compared to its average weekly energy demand. Fig. 1(c) shows the histogram of relative outliers in the substations identified by Huber regression. In Fig. 1(d), it can be observed that median relative outliers decrease from 0.43 to 0.20 after adjusting for the outliers associated with the weekday affect.

The above analysis therefore answers our first question on if certain outliers can be explained by the usage pattern of a building. It also answers our second question about the extent to which outliers effect the strength of relationship between energy demand and outdoor temperature. From the monitoring perspective, those substations which after adjusting for the outliers still show a low OLS R^2 can be considered to have wrong configuration or a malfunctioning equipment in line with the observation made in [1]. The irregular oscillations in energy demand as mentioned in [1] may be explained by high number of unexplained outliers. Consequently, a relatively high number

of unexplained outliers together with high return temperature in substation provides plausible basis for a deeper investigation.

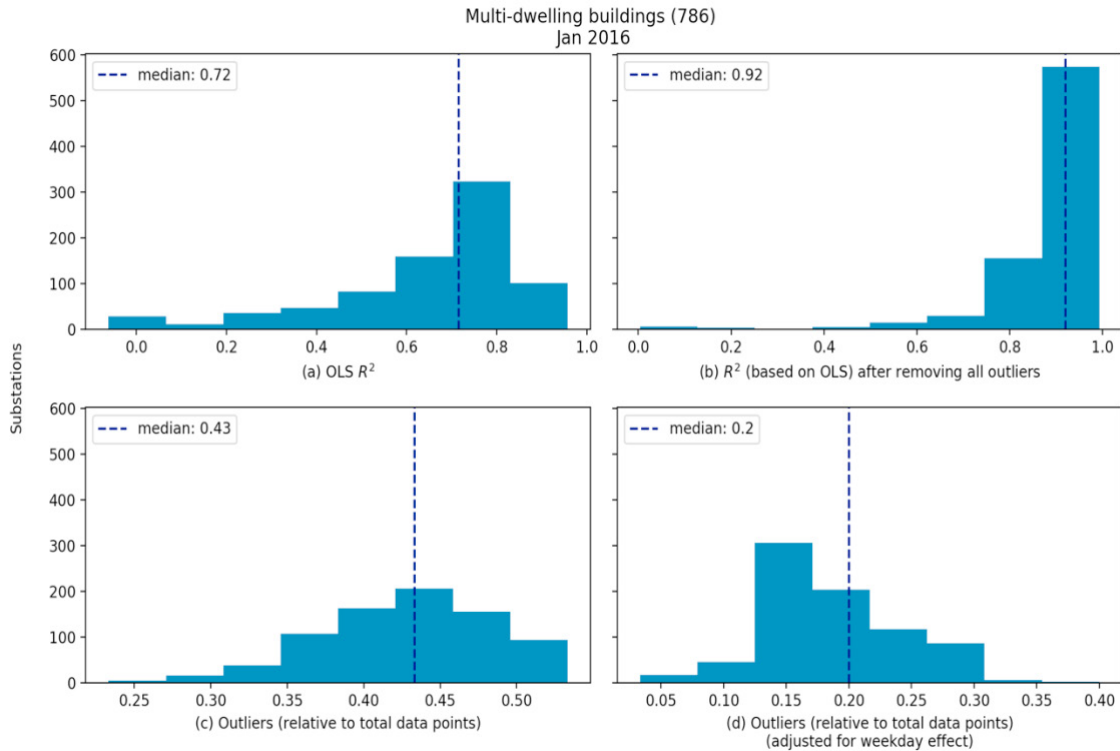


Fig. 1. Panel (a) shows the histogram of R^2 values calculated for substations using OLS. Panel (b) shows histogram of R^2 values calculated for the substations using OLS after removing the outliers identified by the Huber regression. Panel (c) shows the histogram of relative outliers identified by the Huber regression. Panel (d) shows the histogram of relative outliers after adjusting for the weekday effect.

In Fig. 2 and Fig. 3, we plot the return temperature against the estimated α parameters using data from Jan 2016 and Jan 2017 respectively. The return temperature is calculated by first taking its maximum recorded value on each day of the month and then taking their mean. Each blob represents one DH substation. The size of each blob is proportional to its average daily energy demand (left panel) and average daily volume demand (right panel) for that month. Therefore, the larger these demands are, the larger is the size of the blob. Blobs having similar colors are relatively similar in terms of energy demand (left panel) and volume demand (right panel). It is assumed that comparable substations should have similar energy and volume demands and temperature difference; hence consequently similar α . However, the variability in α among substations represented by the same color may be explained by a number of factors including their level of insulation, geographical location, and heat load-temperature curve setting. For instance, buildings located outside the city center that are exposed to winds are likely to have a higher α than those surrounded by other buildings.

One can also observe in Fig. 2 that for certain substations, α estimates, volume and energy demands are not in line with those of similar substations. For instance, substations marked as DH-1 and DH-2 fall into this category. These substations also show a higher return temperature. A comparative analysis of these substations in Jan 2017 shows that volume demand and return temperature for both DH-1 and DH-2 decreased; see Fig. 3. Moreover, the α for the two substations increased. This is a possible indication that the interaction between high return temperature and volume can decrease a substation's energy demand response to change in outdoor temperature. This answers our third question about how a change in α can be related to large changes in return temperature and/or flow.

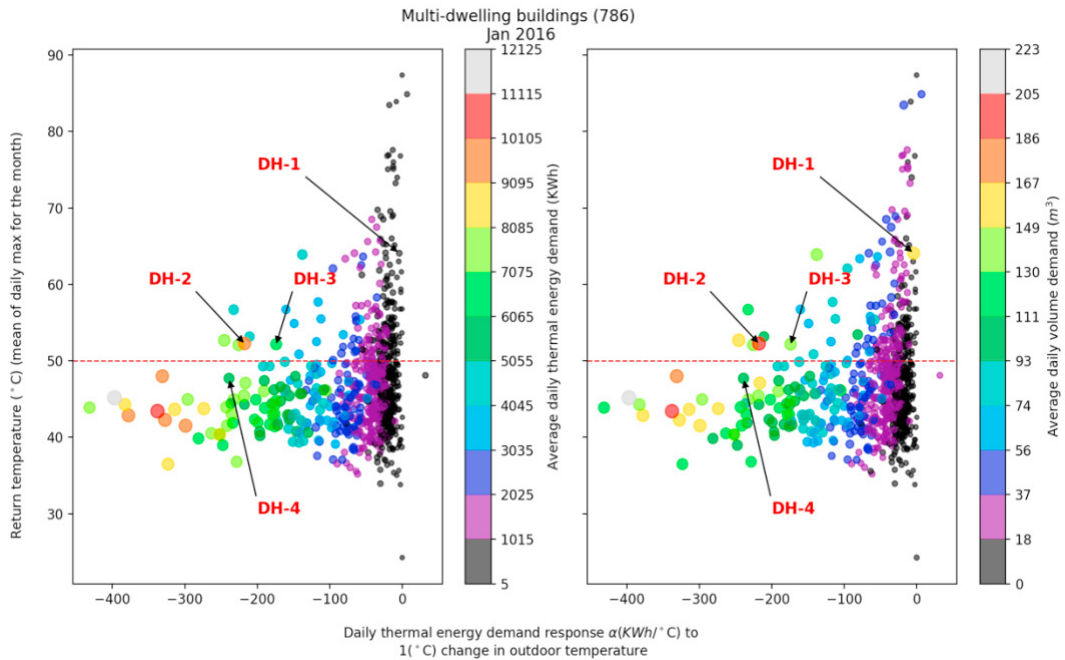


Fig. 2. Return temperature of substations are plotted against estimated parameter α computed for Jan 2016. Each blob represents one DH substation. Blobs of similar color are relatively similar in terms of energy demand (left panel) and volume demand (right panel).

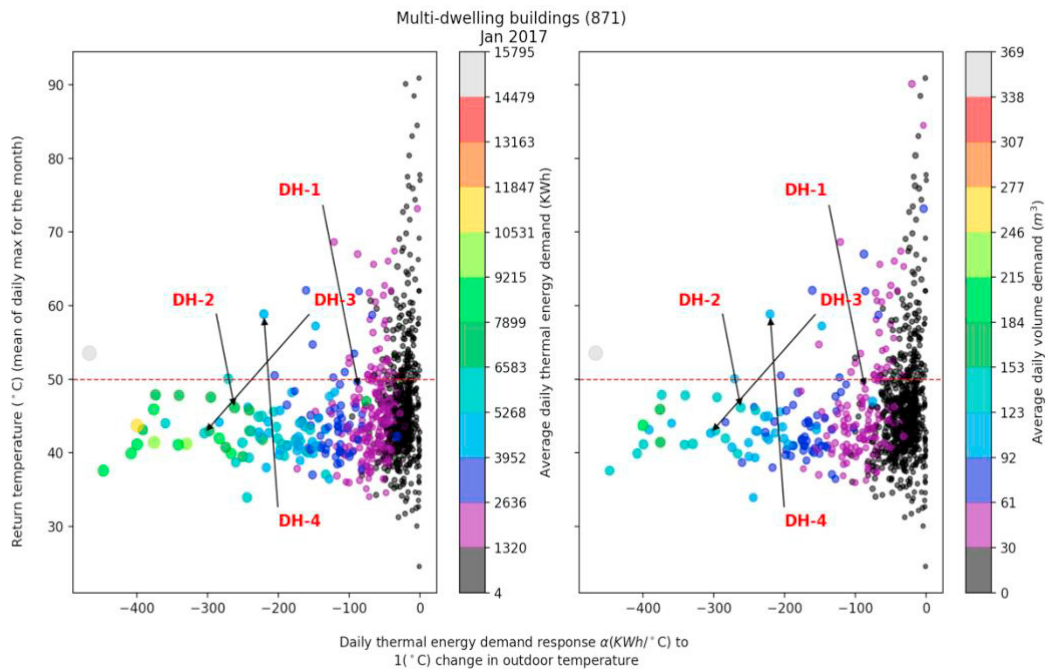


Fig. 3. Return temperature of substations are plotted against estimated parameter α computed for Jan 2017. Each blob represents one DH substation. Blobs of similar color are relatively similar in terms of energy demand (left panel) and volume demand (right panel).

The above analysis indicates that tracking α over time can be helpful from a monitoring perspective. This can be done in different ways. For instance, if one computes absolute change using $|\alpha_{2017} - \alpha_{2016}|$, then due to scale effect, the results will mostly detect deviations in large substations.

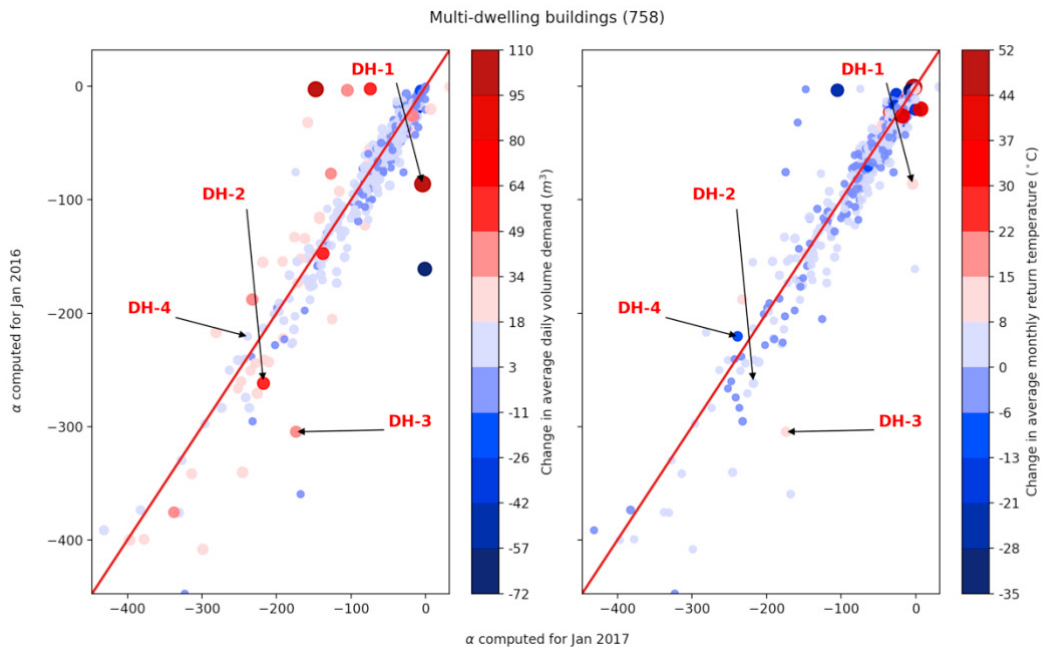


Fig. 4. Comparisons between α estimated for Jan 2016 and Jan 2017. Each blob represents one DH substation. The colors represent the corresponding change in volume (left panel) and change average return temperature (right panel) between the two months. The size of each blob is proportional to these changes.

A way around this is to calculate absolute relative change using $|\alpha_{2017} - \alpha_{2016}|/\alpha_{2017}$. Using this approach, we identified 18 out of 758 substations that showed an increase by a factor greater than $|\pm 1.0|$. Under the assumption that 20% is an acceptable variation in α , then quite a large number, i.e., 503 (66%) substations showed a variation of $|\pm 0.2|$. From a monitoring perspective, one can investigate substations that show a high change in α over time.

For illustrative purposes and to show how large changes in the estimates of α are reflected in changes in the return temperature and/or flow in DH substations, we plot their values estimated in Jan 2016 and Jan 2017 against each other in Fig. 4. Moreover, we color-code each substation with information about the estimated change in volume and return temperature between corresponding months. A diagonal line is drawn to observe how much the α has deviated in the absolute sense. Substations that lie far from the diagonal line, in many instances, also show an increased change in return temperature and/or volume. Clearly, substations marked as DH-1, DH-2 and DH-3 fall in this category.

In Fig. 5 and Fig. 6, we present details of the analysis for the substations marked earlier as DH-3 and DH-4. E and F on the top right boxes are the average daily energy and volume demand for the month, respectively. TR and TD are the average return temperature and temperature difference for that month. Here, we will answer the question related to if substations that belong to a particular building category show homogeneity in their usage pattern. It has been observed in literature that day of the week can affect energy demand of a building. Its effect, however, varies across substations even among similar category of buildings. Moreover, in certain instances, they appear as outliers which can then negatively affect the strength of relationship between Δy and Δx .

In Fig. 5, we show the results of Huber regression applied on the DH substation, marked as DH-3. The results are further augmented with information about which data points correspond to which days of the week: Mon, Sat-Sun and Tue-Fri. The Huber regression model marks many instances of Mon and Sat-Sun as outliers. One can also observe that in Jan 2016, the presence of outliers significantly reduced the value of α when OLS was used. Huber

regression on the other hand clearly seems to dampen their effect resulting in a higher value. One can also observe here that while its α increased in Jan 2017, its average daily volume demand and return temperature decreased in comparison to Jan 2016. This is similar to what we observed earlier in the case of substations marked as DH-1 and DH-2.

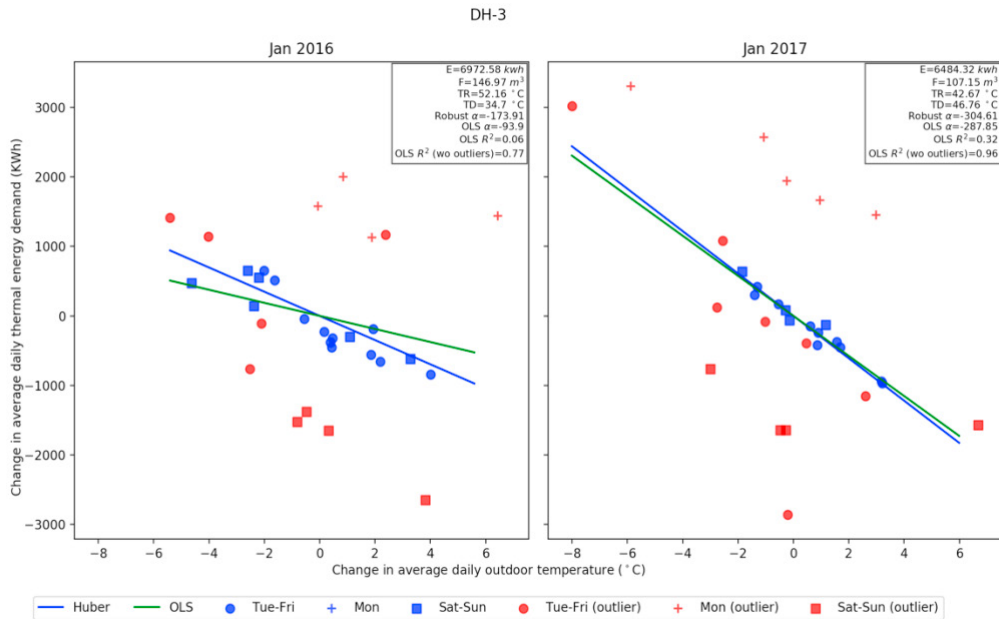


Fig. 5. Results from Huber and OLS regression for the substation marked as DH-3. There is a clear indication of energy demand drop during the weekend and a rise on Monday.

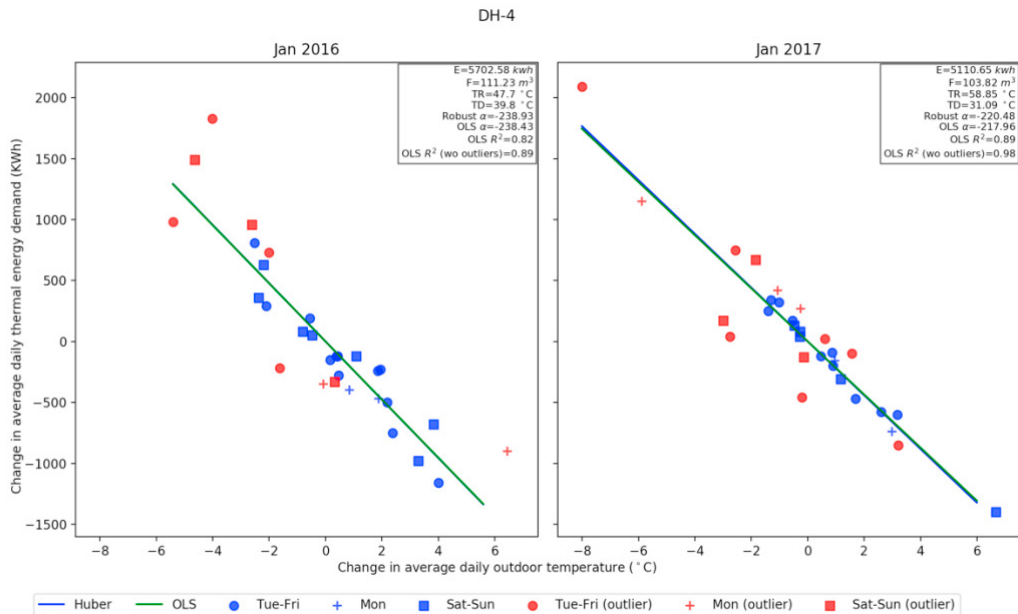


Fig. 6. Results from Huber and OLS regression for the substation marked as DH-4. No clear indication of weekday effect is present in this substation.

Fig. 6, however, presents a very different picture. The usage pattern due to weekdays is not prominent at all. Interestingly, while its α seems not to have changed much between Jan 2016 and Jan 2017 and the relation between energy demand response and change in outdoor temperature is strong, the return temperature in Jan 2017, however, increased significantly. The analysis does not seem to explain why this happened.

6. Summary and discussion

This study sought answers to five questions. Firstly, we found that half of the outliers detected by Huber regression when augmented with weekday information do show the usage pattern of that particular building. Secondly, the presence of outliers in many cases reduces the strength of relation between energy demand and outdoor temperature of a substation. Identifying and removing their presence and then estimating R^2 using OLS shows significant improvement in the relationship strength of these variables. Thirdly, we found that changes in the parameter α for many cases can be explained by a change in return temperature and/or flow of the substation. However, we also found instances where a conclusion could not be reached. Fourthly, certain substations have outliers which can be explained by the usage pattern of a building while others do not. Hence, the behavior of a substation seems to vary even within the same building category. Finally, from the monitoring perspective, a low OLS R^2 even after taking care of the outliers can suggest problems with substation configuration or equipment malfunction. Moreover, we found instances where a large change in α was accompanied with large changes in flow and return temperature. This gives a good reason to track this parameter over time to detect problems earlier.

In this study, we mainly studied the size effect, where DH substations with similar energy or volume demand levels are considered similar. Part of the reasoning is interpretability of the α estimates as the analysis retains its unit, i.e., KWh/°C. We did not introduce any classical standardization techniques such as z-scores which assumes no fat tails in the underlying distribution: if this is not the case, results of such scaling will not be reliable. Furthermore, techniques such as the 3-sigma rule were also not used to remove outliers since *it is an empirical fact that the best [outlier] rejection procedures do not quite reach the performance of the best robust procedures* [2, Chapter 1]. Hence using robust regression, we can isolate outliers in a principled way while acknowledging their presence as discussed in [2, 3].

Monitoring the behavior of district heating (DH) substations is a challenging task due to a number of reasons including low data resolution, lack of a reference, diverse social habits and unavailability of information about the secondary side of the system. Defining real outliers in a DH substation therefore becomes a challenge, since no standard situation can easily be defined. Therefore, augmenting additional information with α such as return temperature, energy and volume demand levels, and day of the week associated with the data point can shed additional insights.

A mathematical formulation together with its visualization are both important for understanding the system being modeled. This is especially true if the method is to be used by practitioners in the industry. We believe that following our analysis, district heating companies will be able to understand and monitor the behavior of substations in their network in an improved manner.

References

- [1] S. Werner and H. Gadd. "Fault detection in district heating substations". *Appl Energy*, 157:51–59, 2015.
- [2] Peter J. Huber and Elvezio M. Ronchetti. "Robust Statistics". Wiley, 2nd edition, 2009.
- [3] Peter J. Rousseeuw and Annick M. Leroy. "Robust Regression and Outlier Detection". Wiley, 1987.
- [4] J. Gustafsson F. Sandin and J. Delsing. "Fault detection with hourly district energy data - probabilistic methods and heuristics for automated detection and ranking of anomalies", *Fjärrsyn (Rapport 2013:27)*, 2013.
- [5] F. R. Hampel. "A general qualitative definition of robustness". *Annals of Mathematical Statistics*, 42:1887–1896, 1971.
- [6] Peter Rousseeuw. "Least median squares regression". *Journal of The American Statistical Association*, 79:871–880, 12 1984.
- [7] Rand Wilcox. "Introduction to Robust Estimation and Hypothesis Testing". Academic Press, 3rd Edition. 2011.
- [8] Peter J. Huber. "Robust Estimation of a Location Parameter". *Annals of Mathematical Statistics*. 35. 73-101, 1964.



16th International Symposium on District Heating and Cooling, DHC2018,
9–12 September 2018, Hamburg, Germany

Real-time grid optimisation through digitalisation – results of the STORM project

C. Johansson^a, D. Vanhoudt^{b,c}, J. Brage^a, D. Geysen^{b,c}

^a, NODA Intelligent Systems, Biblioteksgatan 4, Karlshamn, 374 35, Sweden

^bEnergyVille, Thor Park 8310, Genk, 3600, Belgium

^cVITO, Boeretang 200, Mol, 2400, Belgium

Abstract

The STORM controller is a platform for operational demand side management and has been developed since 2015 as part of the Horizon 2020 project STORM. The controller has been developed using state-of-the-art solutions based on machine learning and applied artificial intelligence, and it has already spawned results now being used in commercial smart heat grid projects throughout Europe. The results show significant benefits relating to peak load management, distribution balancing and market interaction mechanisms.

© 2018 The Authors. Published by Elsevier Ltd.

This is an open access article under the CC BY-NC-ND license (<https://creativecommons.org/licenses/by-nc-nd/4.0/>)

Selection and peer-review under responsibility of the scientific committee of the 16th International Symposium on District Heating and Cooling, DHC2018.

Keywords: digitalisation; demand side management; demonstration

1. Introduction

District heating and cooling has the potential to be a significant driving force in the creation of a sustainable European energy system. Heating in general represents more than 40 % of the total energy consumption in the EU, and more renewable generation can therefore have a considerable impact on greenhouse gas emissions in Europe [1]. Using district heating and cooling it is possible to introduce a larger share of excess heat and low-grade renewables, and this becomes increasingly pronounced as system temperatures decrease. However, the drawback is that many sources of excess heat or renewables are not as easy to control as traditional fossil-based energy sources. Excess heat is mostly harvested from industrial processes, and those industries are normally reluctant to adapt their processes just for the benefit of the district heating grid. Similarly, renewables originating from sources such as sun or wind are by

* Corresponding author

E-mail address: cj@noda.se

1876-6102 © 2018 The Authors. Published by Elsevier Ltd.

This is an open access article under the CC BY-NC-ND license (<https://creativecommons.org/licenses/by-nc-nd/4.0/>)

Selection and peer-review under responsibility of the scientific committee of the 16th International Symposium on District Heating and Cooling, DHC2018.

10.1016/j.egypro.2018.08.189

definition non-controllable. Even when comparing the operational flexibility of a biomass boiler with an oil burner, it is apparent that renewables are harder and more complex to manage. Nonetheless, there are strong environmental and financial incentives to increase their share in our energy systems. Therefore, if the source cannot easily be controlled, the sink must be more efficiently controlled to adapt to the source.

District heating and cooling, as well as most energy systems, are by design demand driven. The traditional way to manage these things is not to actually control that demand, but rather just to satisfy the demand without question. However, to truly optimise a demand-driven system, it would be expected that the ability to control the demand should be present, and that this ability would be increasingly important as the energy source becomes less and less controllable. This is the core idea behind demand side management systems, i.e. to introduce the ability to adapt demand to the operational constraints of the generation and distribution of energy [2].

When considering district heating and cooling in specific there is another large benefit relating to the ability to support smart electrical grids in hybrid solutions, e.g. through the use of heat pumps or combined heat and power generation. This expands the scope of district heating and cooling as a technology solution at the core of low emission energy systems on a global scale.

Considering the increased share of hard to control or even non-controllable energy source, in combination with the general hybridisation trend in energy systems, demand-side management in the form of smart network controllers can be expected to play an increasingly important role in the energy landscape of the future. The purpose of the STORM project (Horizon 2020 under grant agreement No 649743) is to provide a framework for such a network controller, including state-of-the-art algorithms for forecasting, planning and controlling the demand in existing as well as new district heating and cooling networks.

2. The STORM project

This paper describes and discusses results and conclusions from the Horizon 2020 STORM project. The purpose of STORM was to create a smart network controller for district heating and cooling networks, applicable in widely spread 3rd generation networks as well as in low-temperature innovative 4th generation networks [3]. The core idea of the project has been to build such a network controller based on self-learning algorithms and to deploy this in operational networks representing 3rd as well as 4th generation district heating and cooling systems. The project plan identified several specific objectives. The primary objective was to develop a generic network controller for district and cooling systems. Since the ambition was to build a generic controller it need to be self-learning, since it would be very hard to implement such a generic system if it was entirely reliant on human expert intervention. Another important objective was to demonstrate and quantify this generic ability. To do this, two very different demonstration sites were chosen, representing both a low-temperature 4th generation network and a more traditional network using common 3rd generation technology. A further project objective was to the develop business models required to enter the STORM controller on the market. Coupled to this effort was the work aiming at increasing awareness of digitalisation in district heating in general and smart network controllers such as STORM in particular. This has been achieved by several international dissemination efforts, public workshops and academic courses.

From a development perspective it has been a focus of the STORM project to build a modular and flexible system that allows for large-scale replicability. To facilitate this the STORM controller is based on an existing platform with extensive integration possibilities using open communication protocols and standard solutions. An important barrier for scalability is the complexity of deploying and tuning the parameters of such controllers. To tackle this problem the STORM controller focuses on self-learning and self-adaptive algorithms implemented as part of autonomous multi-agent technology. To retain a flexibility for optimisation requirements the STORM controller has focused on three use cases covering a significant range of expected operational scenarios; peak load management, market interaction and cell balancing. These concepts are further explained in the next section of this paper.

The STORM consortium is headed by VITO/Energyville (BE) acting as project coordinator. Further partners are NODA Intelligent Systems (SE), Mijwater (NL), Växjö Energi (SE), Euroheat & Power (BE) and Zuyd University (HL).

3. The STORM controller

At its core the STORM controller is a system for operational demand-side management, including abilities for heat load forecasting, real-time estimation of thermal flexibility available, operational optimisation and planning as well as mechanisms for distribution and coordination of control actions at building level. The overall STORM controller design is based on a concept that has evolved from research in multi-agent system technology during nearly twenty years [4, 5]. The core concept of that research is to combine traditional district heating engineering with modern information and communication technology. The basic idea is to combine the whole energy chain, including production, distribution and consumption, into a single coherent framework for operational optimisation [6]. A district heating or cooling system is basically a collection of separate control loop feedback systems, in which the overall operations are normally not directly coordinated in any way. These separate systems relate to system wide production and distribution processes as well as consumer level processes. To create a smart controller these separate processes are mapped to the three abilities of measuring, analysing and acting. Measuring relates to the ability to perceive ones' environment, while analysing relates to the ability to reach informed conclusions based on the perceived input and acting relates to the ability to act based on those conclusions. Together these three basic notions form the basis of what entails an intelligent system [7]. In the domain of the STORM controller, these three notions are realised through the Forecaster, Planner and Tracker modules in combination with the virtual distributed resource (vDER) agents.

3.1. Forecaster

The ability of predicting the future behavior of a district heating system in general and a 4th generation system in particular is key for increasing its energy efficiency. More specifically, an accurate forecast of the thermal load in the system is mandatory for optimizing the system controller. Existing research on thermal load forecasting in district heating ranges from models solely using historic load data up to more complex ones using additional parameters like occupancy, meteorological data or physical details of the building. All these approaches can be divided in two major classes: the forward and data-driven methods [8, 9]. In the first methods equations are used to describe the physical behavior of the system while in the latter the forecasted thermal load of the building is based on a model learned with historical data. These data-driven methods can be further subdivided in statistical and machine learning methods. In statistics, the complexity of these functions is often predetermined by the regression model whereas in machine learning this complexity is learned by the method itself [10]. As discussed in our related thermal load forecasting paper [11], the focus in this study is on data-driven methods. These have the advantage that there is no need for developing detailed physical models of the buildings and allows for a generic implementation for use in multiple district heating systems. Furthermore, the consumption forecasting capabilities of artificial neural networks (ANNs) has been compared with the results of using a physical model and it has been concluded that even with the use of a very detailed building model the results were comparable with ANNs [12].

A first version of the thermal load forecaster, extensively described in [13], consists of two machine learning approaches: an extremely randomized (extra) tree regressor (ETR) [14] and an Extreme Learning Machine (ELM) [15]. The following input features were used to train these models: timing information (hour of the day, day of the week and day of the year), weather information (forecasted outdoor temperature), historical thermal load (previous day and previous week). Using the mean absolute percentage error (MAPE) as a comparison metric, both algorithms gave similar results on average but varied depending on the input feature values. For example: when unseen input values were fed into the models, the accuracy of the ETR was lower than that of the ELM. This is because of the ETRs being unable to extrapolate predictions outside the span of the training data.

In a second version of the forecaster module we implemented an expert system able of combining multiple thermal load forecasting approaches, like the two discussed above, in a way that it always tracks the best forecast in the system [11]. It consists of a fixed share (FS) forecaster expert system, described by Herbster and Warmuth [16], combining eight individual experts into one forecast. The experts differentiate in both machine learning approach and number of input features used to train them [17]. The following techniques are used: linear regression (LR), ANNs [18], support vector machines (SVMs) [19] and ETRs in combination with three different feature sets, a first one solely taking into account timing information and an outdoor temperature forecast, the second one adding

historic thermal load information and the last one adding historic control signals. The FS system will assign weights to each expert in the system, the higher the accuracy of the expert the higher the impact it has on the combined forecast and vice versa. This adds robustness to the forecaster and reduces susceptibility to changes in the DHS.

At the time of writing version one of the forecaster is fully deployed in the operational system while version two is still in a testing phase.

3.2. Planner

The Planner module is responsible for the operational planning, which in practice means that it is an optimiser [20]. Furthermore, the Planner is also the part of the STORM controller that primarily interfaces with external processes, such as complementary optimisers, forecasters or market interaction signals. Similarly, like the other parts of the STORM controller the Planner is basically a container for implementing required behaviour and functionality. In the STORM project three basic control strategies for the Planner have been considered, relating to peak load management, market interaction and cell balancing.

3.2.1. Peak load management

Peak load management has been a core feature of demand side management efforts in district heating systems throughout the evolution of this type of technology [21]. This is a basic consequence of the fact that the heat load of most district heating systems is subject to large variations due to the fluctuating demands. A large portion of the peaks resulting from this behaviour is not physically required by the indoor climate in the connected buildings, but rather the results of sub-optimal controlling in the PI/PID circuits governing the substations throughout the grid. By overriding the individual controller in each building and coordinating their behaviour from a grid perspective it is possible to manage these type of peaks [22]. The primary incentive to do this is to avoid expensive peak load fuel with high environmental impact.

3.2.2. Market interaction

Market interaction as part of demand side management systems have been previously studied and found to add considerable benefit during short-term optimisation in operational settings [23]. In the generic case the Planner will try to synchronize the heat load demand in relation to high spot prices on the market. For a combined heat and power (CHP) system a higher heat demand will generate more power output from the physical process of generating both heat and power. A system for market interaction based on demand side management is flexible and can respond quickly to changes relating to operational conditions, and it is therefore suitable for intraday market optimisation.

The primary focus of the STORM project has been the CHP aspect, but market interaction in general can be applied to a number of scenarios such as margin cost optimisation or other mechanisms that can be expressed in time steps.

3.2.3. Cell balancing

Cell balancing is based on the notion that the energy demand should be balanced on a local level before a global level, i.e. the geographical location of the buildings within the grid is considered as part of the optimisation process. There are two primary reasons to strive for this [2]. Firstly, the shorter the distance between energy source and sink, the lower the amount of heat losses. Secondly, a local balance means lower demand from the higher-level transmission grid, which in turn means that that transmission grid can supply more local clusters using the same distribution constraints.

For the STORM project, cell balancing is of special interest due to the specific situation within one of the demonstrator grids, in which the network consists of several individual clusters connected through heat exchangers to a backbone network. However, it should be noted that the cell balancing control strategy generalises well into the more generic case of distribution optimisation within more common, hydraulically connected, grids. The most common scenario in the general case relates to narrow sections in the distribution grid, which can to a certain degree be overcome by using STORM technology.

3.3. Tracker

The STORM tracker serves to make the aggregated supply and demand of a large number of distributed energy resources, in STORM represented by the vDER agents, track a desired control plan generated by the planner module. To this end, it is necessary to perform model predictive control over a horizon of days at a resolution of a fraction of an hour. Distributed convex optimisation in the guise of the *alternating direction method of multipliers* (ADMM) offers a way to address the large-scale nature of the problem [24].

The implementation of ADMM in STORM follows [25] and [26], which addresses the problem of optimal power scheduling in a network of devices interconnected by local nets and provides a solution by means of the algorithm of *prox-average message passing*. The approach generalises the problem of optimal exchange in a star-shaped network of devices interconnected by a global net, the difference being the amount of bookkeeping necessary to describe the problem and its solution.

An earlier version of the tracker module featured a single step auction-based dispatch mechanism, in which the control actions were distributed independently within the grid each time step based on using the thermal inertia of the buildings as a currency. This market-like approach introduced a self-balancing mechanism in the tracking process. The ADMM approach developed in STORM expands on this concept by considering several time-steps, while still retaining the basic market analogy. In the ADMM-based tracker a variable converges to an optimal dual variable that can be interpreted as a set of optimal clearing prices between a number of resources. This analogy has previously been thoroughly investigated in several classical works [27, 28, 29, 30].

3.4. vDER

The virtual distributed energy resource (vDER), is a container for the software agent controlling the individual source of thermal flexibility. This is normally a building with a heating system but can basically be any entity controlling a thermal process, e.g. fridges and coolers at supermarkets or a storage tank in a building. The vDER module provides a structured way to integrate agent behaviour depending on specific requirements, including more complex behaviour, e.g. relating to prosumers or active market interaction.

The primary purpose of the vDER in relation to the STORM controller is to negotiate and implement control signals while ensuring quality of service within the underlying thermal process. In the case of a normal building, the vDER will want to implement as much control actions as possible, since this will result in financial and environmental benefits, but it wants to do this in way that doesn't cause any significant changes in the indoor climate of the building. There are several aspects of how to estimate quality of service in a building, but the primary tool for the vDER is either thermal models or indoor sensors or a combination of both. The vDER also needs to consider the operational behaviour in the substation, e.g. making sure that the valve for heating in the substation doesn't close completely during control actions since this might cause a perceived inconvenience if some tenant touches a cold radiator.

In the STORM controller each building is assigned a vDER. This vDER is then responsible for the real-time negotiation process with the Tracker in which the vDER's accept control actions in exchange for their thermal flexibility [31]. In this sense the vDER acts on a self-balancing market where it wants to buy as much control actions as possible using its thermal flexibility as currency. The objective of the vDER is to maximise the control action in relation to the given constraints of thermal flexibility. One notable thing about this process is that in essence it works like any other market, providing a self-balancing mechanism in that an actor cannot participate (i.e. buy control actions) if they have no available assets (i.e. available thermal flexibility). As long as the practical process of assessing the available thermal flexibility is sound, e.g. through thermal models and/or indoor sensors, the market mechanism as a whole ensures quality of service while acting to distribute control action among the vDERs in the most efficient fashion. Since the underlying process is basically a market process, it is convenient to attach actual financial instruments to the process. This design is specifically made in preparation for more advanced business models involving active pricing in demand-side management schemes, although it also benefits business models involving distributed small-scale energy generators or all-out prosumers.

4. Deployment

4.1. Access technology

Gaining access to relevant sensor and actuator devices is crucial for a system like the STORM controller. Since it is a demand-side management system, it obviously needs to interact with the controller devices located at the demand side. The market for heating controllers is diverse even though most of them work similarly. To achieve a high level of scalability, the STORM controller uses three main different types of access technology:

- Energy controller – one to one installation in small-scale or proof-of-concept contexts using either sensor override or single building automation controllers
- Building automation gateway – accessing several buildings through a single gateway using building automation protocols such as Modbus or BACnet
- IT based integration – integration into an existing network of buildings in larger scale projects, normally through techniques such as OPC, web services or similar solutions

The energy controller used in STORM is a retrofit solution based on sensor override, developed to facilitate cost-efficient access to heating controllers and building management systems. Sensor override means that the hardware is connected on the line of some sensor and then overrides the actual signal with an artificial signal during control actions. The most common situation is when overriding the outdoor temperature sensor in a building. This will make it possible to influence the behaviour of the heat demand. The retrofit solution used in STORM features sensors override as well as easy interfacing with the heat meter and additional sensory equipment for data collection in the substation.

The gateway solution uses as traditional heating controller to act as a communication bridge between the STORM controller and a set of buildings, and therefore creates a single point of access towards standard building automation protocols. Using a gateway like this creates access to the full range of sensors and actuators connected to the existing controller. Both the gateway and the existing controller needs to be re-programmed for this to work which adds a level of complexity compared to the sensor override solution. However, the benefit of using gateways is that this is well-known and accepted technology among building managers.

IT-based integration connects directly to an existing data management system or SCADA to create access to underlying control points. The platform used in the STORM project is currently available through several integration solutions such as OPC, AWS IoT, MQTT, Schneider Struxureware, Alfa Laval IQheat, Siemens and others. The software is of a modular design, which makes it relatively easy to add more integration solutions when needed.

Securing data in communication as well as during analysis and storage is a core part of the STORM controller and the underlying data management framework. The default system always uses the latest version of TLS/SSL as a cryptographic protocol to provide secure communication. Currently this is TLS 1.2 with SHA-256 RSA for certificate signature validation. Using TLS facilitates private and secure communication through symmetric cryptography, identity authentication and message integrity.

4.2. Demonstration sites

The STORM Controller has been tested in two different district heating networks. One demonstration site is traditional 3rd generation district heating system operated by Växjö Energy in the city of Rottne in Sweden. The other demonstration network is a low-temperature 4th generation district heating and cooling network operated by Mijwater in the city of Heerlen in The Netherlands.

The demonstration network in The Netherlands supply both heating and cooling using low temperatures based on geothermal energy through former mines filled with water. Depending on the depth of extraction, the water can be used for either heating or cooling. When used for heating the water has a temperature of about 28 °C while the cooling water is about 16 °C. The core network that carries the water to and from the mines is called the backbone. The backbone is connected to a set of clusters, to which the customers in turn are connected. Each customer can

either generate or consume energy, and the basic idea is to exchange energy within the cluster before extracting it from the backbone. Minimizing the distance between generation and consumption will decrease distribution losses and make the system more energy efficient in general. In Heerlen the buildings are integrated with the STORM controller through the use of a gateway.

Unlike the Heerlen network, the Rottne district heating system is a traditional system. The Rottne production site is based on 2.5 MW of biomass-based capacity, with an additional 3 MW peak load capacity. The peak load boiler uses RME biodiesel, so the environmental impact of the peak capacity is low. However, the biodiesel is expensive and the cost per generated MWh is higher than the price to customers. In Rottne the ten largest buildings are integrated with the STORM controller through the use of sensor override technology. These ten buildings comprise all multi-family buildings in Rottne and represent nearly a third of the total heat demand in Rottne. In addition to this the heat meter measuring the total output from all production is also integrated along with a specific sensor to measure the activity of the peak load boiler.

5. Evaluation methodology

The STORM controller is in essence a system for real-time demand side management, which basically means that the heat load profile is normally the focus of any evaluation. In addition to this the overall energy management is obviously also of interest, together with the quality of service in relation to operational temperatures in the individual substations as well as indoor climate.

The heat load analysis is based on hourly data. This can be done on other resolutions also obviously, but normally heat meter data is available hour by hour. Hourly data is also relevant since this is also the default time resolution for market interaction. The primary way to analyse control actions is to by creating a thermal demand signature, in which triplets of outdoor temperature, heat load and time of day are fitted to a virtual surface. This surface then becomes the reference to which active control triplets can be compared. From this perspective, the thermal demand signature can be seen as an extension of the normal energy signature of a building, albeit working in three dimensions rather than two and using hourly data instead of daily data. Similarly, if a set of data triplets belonging to a control action is below the reference surface the building is performing a successful discharge (i.e. reducing heat load), and if the data triplets are above the surface it is charging (i.e. increasing heat load). This virtual surface also provides a convenient reference set for the self-learning algorithm when evaluating the response impact of building.

Obviously, the data used to create the reference surface should not include any control actions, since this would warp the surface plot. Furthermore, it should be noted that it is not required to have a complete surface, covering all possible operational scenarios, to use this methodology. The creation of the surface is based on adaptive algorithms, and it will expand over time. As long as there is a statistically relevant surface area close in time and temperature to the control action in question, then that control action will have a reference by which it can be compared.

The surface method is primarily used for heat load analysis. For long term energy usage analysis traditional methods for normal-year corrections are used. For the evaluation in STORM this is done by using normal-year correction with energy signature analysis. Such analysis can also be done using normal-year correction with degree days. However, the energy signature method is mathematically sounder for individual buildings due to fewer assumptions involved and more transparent when employed.

The primary indicator for quality of service is the indoor temperature. In the Heerlen demonstrator indoor temperature sensors are available, which make it possible to follow the behaviour of the system closer. In the Rottne demonstrator no indoor sensors have been available. However, the system evaluates the thermal behaviour of the building using a thermal model of the building in combination with measurements from the substation secondary side which sets boundaries for the control algorithms involved. Also, the grid operator has been in recurrent contact with the building owners involved throughout the project and no complaints have been registered.

6. Results

Figure 1 shows an example of the impact of a control signal from the STORM controller in an individual building. As indicated by the letter A, a control signal is received which causes the building to raise the outdoor temperature signal to the heating controller. This will cause the valve to start closing slightly which in turn causes

the secondary supply temperature to decrease along with the secondary and primary return temperatures, as indicated by the letter B. At the end of this particular control action, the vDER realises that a rebound effect on the heat load is apparent which in turn causes it to perform a shorter control signal to even out the rollback behaviour, as indicated by the letter C.

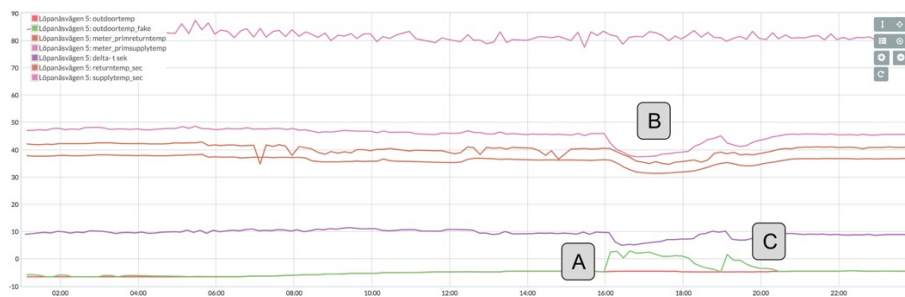


Fig. 1. An example of the response of a building receiving a control signal. Values on the y-axis are in °C.

Figure 2 shows the same data set, but with the instantaneous heat load measurements also included in the plot. For clarity, the heat load is shown in blue, while the rest of the values are greyed out. It is obvious that the heat load reacts clearly to the control signal and, in this case, it drops from about 150 kW to 75 kW during the initial parts of the control action. The rollback behaviour previously described is also apparent during the later parts of the control action.

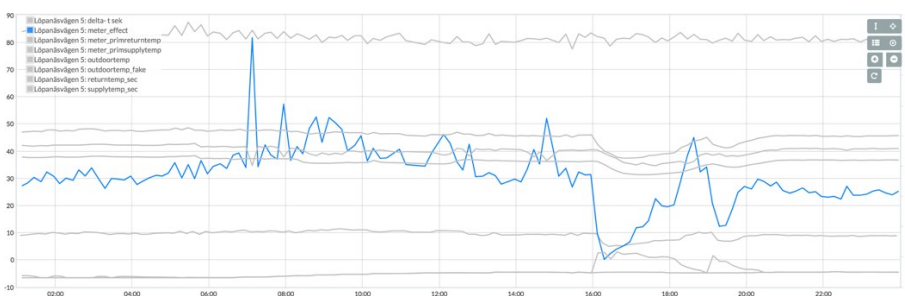


Fig. 2. The response of a building including the heat load (indicated on the right y-axis in kW)

When the STORM controller coordinates such control signals across a set of buildings it can achieve significant behavioural changes in the head load profile in the overall network, as is shown in Figure 3.



Fig. 3. Alternating between charging and discharging on grid level in the Rottne demonstrator. Values on the y-axis in kW.

The blue line in Figure 3 shows the controllable heat load (i.e. the sum of the heat load of the active vDER's in the grid), while the green line shows the total heat output from the production unit. Around 3am the vDER's are starting to charge, which is then followed by a discharge starting around 5am. It should be noted that in this example the total MWh output is more or less the same as the reference case, although the heat load profile during the night and morning has been significantly influenced. The behaviour shown in Figure 3 can be used by the grid operator as preparation for morning peaks (i.e. pre-charging before a discharge), but it is also applicable for market interaction (i.e. high spot prices lead to charging while low spot prices lead to discharging). It should be noted that the discharge and charge does not necessarily need to have a temporal connection like in this example. This is specifically true for market interaction where high and low spot prices might be spread out over the day.

Discharge			ODT	Charge		
Long	Medium	Short		Short	Medium	Long
	85	157	10°C			
54	134	248	5°C	192	100	
70	172	318	0°C			
	198	367	-5°C			
	28,89%	53,50%	10°C			
11,41%	28,00%	51,85%	5°C	40,15%	20,88%	
10,57%	25,95%	48,06%	0°C			
	23,45%	43,43%	-5°C			

Fig. 3. The static flexibility matrix for the Rottne demonstrator. Values in kW for available flexibility. The percentage is in relation to controllable load.

Figure 3 shows the flexibility matrix for the Rottne demonstrator. A flexibility matrix provides an estimation of the thermal flexibility at certain outdoor temperatures and during certain lengths in time. In essence, the flexibility matrix can be seen as an amount of energy which usage can be either extended in time or in intensity, i.e. if the intensity is high the control can only be sustained for a shorter period of time and vice versa. In this case short equals 1-3 hours, medium 4-6 hours and long equals more +6 hours. At the time of writing, much less charging has been performed which is reflected in the sparsity of the matrix on right side.

The flexibility matrix shows the amount of available flexibility based on statistical analyses of previous control actions. Exactly how this flexibility is then used depends on the operational situation in the specific grid as well as the control strategies are being deployed. As an example, in the Rottne case the last version of the STORM controller was fully deployed during the month of March 2018. During that month the total amount of discharge was about 23 MWh.

7. Conclusions

The STORM controller has been shown to work as intended in relation to peak load management and market interaction. Testing is still on-going in relation to cell-balancing, but the initial results are promising.

Due to the modular design of the system, the STORM controller has a very short time-to-market cycle. Indeed, parts of the STORM results are already deployed in commercial systems. This modularity and agile development process is a vital part of the success in any digitalisation effort.

It should be noted that the STORM project is still on-going, especially regarding cell-balancing and final results will be presented in the project deliverables related to the finalisation of the project.

Acknowledgements

The authors gratefully acknowledge the financial support for the STORM project by the European Commission. STORM was granted funding in the Horizon 2020 EE13 2014 call on 'Technology for District Heating and Cooling' under no. 649743.

References

- [1] “A European Strategy for Sustainable, Competitive and Secure Energy” *European Commission, Green Paper* (2006)
- [2] Vanhoudt, D., Claessens, B., Desmedt, J. and Johansson, C., “Status of H2020 STORM-project” *In proceedings of the 15th International Symposium on District Heating and Cooling, Republic of Korea* (2016)
- [3] Lund, H., Werner, S., Wiltshire, R., Svendsen, S., Thorsen, J.E., Hvelplund, F. and Vad Mathiesen, B. “4th Generation District Heating (4GDH) Integrating smart thermal grids into future sustainable energy systems” *Energy* 68, pp 1-11 (2014)
- [4] Wernstedt, F., “Multi-agent systems for district heating management” *Blekinge Institute of Technology Doctoral Dissertation Series No. 2005:10* (2005)
- [5] Johansson, C., “On Intelligent District Heating, Blekinge Institute of Technology” *Blekinge Institute of Technology Doctoral Dissertation Series No. 2014:07* (2014)
- [6] Wernstedt, F., Davidsson, P. and Johansson, C. “Demand Side Management in District Heating Systems” *In proceedings of the 6th International Conference on Autonomous Agents and Multiagent Systems, Honolulu, Hawaii* (2007)
- [7] Wechsler, G. “The measurement of adult intelligence” *Baltimore: Williams and Wilkins* (1944)
- [8] Xiang Zhao, H. and Magoulés, F. “A review on the prediction of building energy consumption”. *Renewable and Sustainable Energy Rev.* 16 (6) pp 3586-3592 (2012)
- [9] Fumo, N., “A review on the basics of building energy estimation” *Renewable and Sustainable Energy Rev.* 31 pp 53-60(2014)
- [10] Breiman, L., “Statistical modelling: the two cultures” *Statistical Science* 16 (3) pp 199-231 (2001)
- [11] Geysen, D., De Somer, O., Johansson, C., Brage, J. and Vanhoudt, D., “Operational thermal load forecasting in district heating networks using machine learning and expert advice” *Energy and Building, Vol. 162 pp 144-153* (2018)
- [12] Neto, A.H. and Fiorelli, F.A.S., “Comparison between detailed model simulation and artificial neural network for forecasting building energy consumption” *Energy Building* 40 (12) pp 2169-2176 (2008)
- [13] Johansson, C., Bergkvist, M., De Somer, O., Geysen, D., Lavesson, N. and Vanhoudt D., “Operational demand forecasting in district heating systems using ensembles of onlince machine learning algorithms” *In proceedings of the 15th International Symposium on District Heating and Cooling, Republic of Korea* (2016)
- [14] Wehenkel, L., Ernst, D. and Geurts, P., “Ensembles of extremely randomized trees and some generic applications” *In proceedings of Robust Methods for Power System State Estimation and Load Forecasting, RTE, France* (2006)
- [15] Huang, G.B., Zhu, Q.Y. and Siew, C.K., “Extreme learning machine: theory and applications” *Neurocomputing Vol. 70 Issues 1-3 pp 489-501* (2006)
- [16] Herbster, M. and Warmuth, M.K., “Tracking the best expert” *Machine Learning* 32 pp 151-178 (1998)
- [17] Suryanarayana, G., Lago, J., Geysen, D., Aleksiejuk, P. and Johansson, C., “Thermal load forecasting in district heating networks using deep learning and advanced feature selection methods” *Energy, ISSN 0360-5442* (2018)
- [18] Cochocki, A. and Unbehauen, R., “Neural Networks for Optimization and Signal Processing” *1st edition, John Wiley & Sons, Inc., New York, NY, USA* (1993)
- [19] Noble, W.S., “What is a support vector machine?” *Natural Biotechnology* 24 pp 1565-1567 (2006)
- [20] Johansson, C., Wernstedt, F. and Davidsson, P., “Combined Heat and Power Generation using Smart Heat Grid” *In proceedings of the 4th International Conference for Energy Systems, Suzhou, China* (2012)
- [21] Österlind, B. “Effektbegränsning av fjärrvärme” *Vol. 63:1982, Byggnadsnämnden* (1982) (in Swedish)
- [22] Johansson, C., Wernstedt, F. and Davidsson, P., “Deployment of Agent Based Load Control in District Heating Systems” *In proceedings of the 1st International Workshop on Agent Technologies for Energy Systems, Toronto, Canada* (2010)
- [23] Johansson, C., Wernstedt, F. and Davidsson, P., “Smart Heat Grid on an Intraday Power Market” *In proceedings of the 3rd International Workshop on Agent Technologies for Energy Systems, Valencia, Spain* (2012)
- [24] Boyd, S., Parikh, N., Chu, E., Peleato, B. and Eckstein, J., “Distributed optimisation and statistical learning via the alternating direction method of multipliers” *Foundations and Trends in Optimisation, Vol. 3, No. 1, pp 1-122* (2010)
- [25] Kraning, M., Chu, E., Lavaci, J. and Boyd, S., “Message passing for dynamic network energy management” *arXiv:1204.1106v1* (2012)
- [26] Kraning, M., Chu, E., Lavaci, J. and Boyd, S., “Dynamic network energy management via proximal message passing” *Foundations and Trends in Optimisation, Vol. 1, No. 2, pp 70-122* (2013)
- [27] Walras, L., “Éléments d’économie politique pure, ou, Théorie de la richesse sociale” *F. Rouge* (1896)
- [28] Arrow, K.J. and Debreu, G., “Existence of an equilibrium for a competitive economy” *Econometrica: Journal of the Econometric Society, Vol. 22, No. 3, pp 265-290* (1954)
- [29] Uzawa, H., “Market mechanisms and mathematical programming” *Econometrica: Journal of the Econometric Society, Vol. 28, No 4, pp 872-881* (1960)
- [30] Uzawa, H., “Walras’ tâtonnement in the theory of exchange” *The Review of Econometric Studies, Vol. 27, No 3, pp 182-194* (1960)
- [31] Johansson, C., Wernstedt, F. and Davidsson, P., “Distributed Thermal Storage Using Multiagent Systems” *In proceedings of the 1st International Conference on Agreement Technologies, Dubrovnik, Croatia* (2012)



16th International Symposium on District Heating and Cooling, DHC2018,
9–12 September 2018, Hamburg, Germany

Promotion of distributed energy systems integrated with district cooling systems considering uncertainties in energy market and policy in China

Qianzhou Du^a, Chengliao Cui^a, Ying Zhang^a, Chong Zhang^a, Wenjie Gang^{a*}
, Shengwei Wang^b

^aDepartment of Building Environment and Energy Application Engineering, Huazhong University of Science and Technology, Wuhan, 430074, China

^bDepartment of Building Services Engineering, the Hong Kong Polytechnic University, Hunghom, Kowloon, Hong Kong

Abstract

The distributed energy system has attracted increasing attentions due to its high efficiency and low pollution emissions. The Chinese government has planned to promote the application of distributed energy systems using natural gas to address the atmospheric pollution problem. However, considerable uncertainties exist in energy market and policy, which would significantly affect the economic performance of distributed energy systems and make the promotion challenging. Therefore, this study attempts to investigate the impacts of energy market and policy uncertainties by evaluating the economic performance of a distributed energy system integrated with a district cooling system serving a campus in the cooling dominated area of China. Uncertainties in the following factors are taken into account: the natural gas price, the electricity price, the feed-in tariff, the incentive from the government and the carbon tax. The payback period of the distributed energy system under various uncertainties is analysed. Results show that the economic performance of the distributed energy system is satisfactory when the ratio of natural gas price to the electricity price is less than 3. If the government plants to promote the DES, the incentive should be not less than 1300 CNY/kW or the carbon tax charged should be not less than 50 CNY/ton.

© 2018 The Authors. Published by Elsevier Ltd.

This is an open access article under the CC BY-NC-ND license (<https://creativecommons.org/licenses/by-nc-nd/4.0/>)

Selection and peer-review under responsibility of the scientific committee of the 16th International Symposium on District Heating and Cooling, DHC2018.

* Corresponding author. Tel.: +86-27-87792101; fax: +86-27-87792103.

E-mail address: gangwenjie@hust.edu.cn

1876-6102 © 2018 The Authors. Published by Elsevier Ltd.

This is an open access article under the CC BY-NC-ND license (<https://creativecommons.org/licenses/by-nc-nd/4.0/>)

Selection and peer-review under responsibility of the scientific committee of the 16th International Symposium on District Heating and Cooling, DHC2018.

10.1016/j.egypro.2018.08.190

Keywords: distributed energy system; district cooling system; uncertainty; energy market; energy policy; economic performance

1. Introduction

Distributed energy system (DES) integrates middle/small-scale on-site power generations with thermal energy production and/or storage devices to provide electricity, cooling and heating to end-users nearby [1]. It is regarded as an efficient, clean and reliable energy supply alternative and is attracting increasing attentions in recent decades [2, 3]. In China, the government has launched ten measures to address the pollution problem, one of which is to replace coal with natural gas for clean thermal energy supply [4]. The government plans to increase the energy consumption fraction of natural gas from 5.9% to 10% by 2020 [5]. In addition, the electrical and thermal demands keep rising due to the urbanization development [6]. Under this context, the DES based on natural gas can be an effective alternative to meet the electrical and thermal demands and improve the atmospheric environment by reducing pollution emissions [7].

DES using natural gas can generate cooling, heating and power on site and close to users. Without long distance transmission, which exists in central grid, and recover energy from exhaust gas or steam, the energy efficiency of DES is regarded to be high. The economic performance of DESs plays a significant role in the promotion of DESs. The short payback period and high benefits would attract more investment opportunities. However, large uncertainties exist in the energy markets and local policies, which would affect the economic performance of DESs. For instance, the natural gas price was fluctuated largely in 2017 due to the shortage of natural gas [8]. Even the domestic use of natural gas is limited and the local government has to implement rationing (less than i.e. 150 Nm³/household per month) for users [9]. Without considering these uncertainties in the economic performance, the investment can be risky and the promotion of DES can be challenging.

Energy policies determine the economic performance of DESs. Currently in China, energy policies associated to DES can be categorized into two types.

- i. Compensation for the first cost based on the installation capacity of the DES. During the installation of DESs, the local government will give financial support for investors of DESs and the value is calculated based on the capacity of the DES. For instance, the local government in Changsha announces that 2000 CNY/kW will be supported for the installation of DESs [10]. The incentive can be different in different cities (i.e. 3000 CNY/kW in Shanghai, 2000 CNY/kW in Beijing) [11].
- ii. High feed in tariff for the surplus electricity sent to the grid. The surplus electricity generated by DESs in some cities is permitted to be sent to the grid with a higher price than that for electricity generated from the coal fired plants. The difference is usually compensated by the government to the local utilities.

Another factor that affects the application of DES is the carbon tax, which is a fee imposed on the burning of carbon-based fuels (coal, oil, gas) [12]. It is regarded as the core policy aiming to reduce and eventually eliminate the use of fossil fuels. Many countries have been implemented carbon tax, such as Denmark, Finland [13], Australia [14], South Africa [15], New Zealand [16], etc. In China, the carbon tax is still controversial and not in use yet. However, it is proved that the carbon tax is an effective policy tool because it can reduce carbon emissions with a little negative impact on economic growth [17]. The impact of carbon tax on DESs should be considered because the DES using natural gas is regarded as a clean energy supply system.

It is therefore necessary to involve all these uncertainties in energy markets and policies during the development and promotion of DESs. This study quantifies the impacts of these uncertainties on the economic performance of the DESs, aiming to provide suggestions for the promotion of DESs in China. A DES integrated with district cooling systems (DES&DCS) serving a building cluster in cooling dominated areas of China is selected. By quantifying the

payback period of DES&DCS under various uncertainties, recommendations are summarized concerning the energy market and policies.

2. Method to evaluate impacts of energy market uncertainties

The methodology of this study is illustrated in Fig. 1. A DES&DCS serving a campus is selected to investigate the impacts of uncertainties in the energy markets and policies, based on historical cooling and electricity loads. The conventional system, which adopts the DCS for cooling supply and the grid is the only energy source (CES), is taken for comparison. Detailed steps are explained as follows.

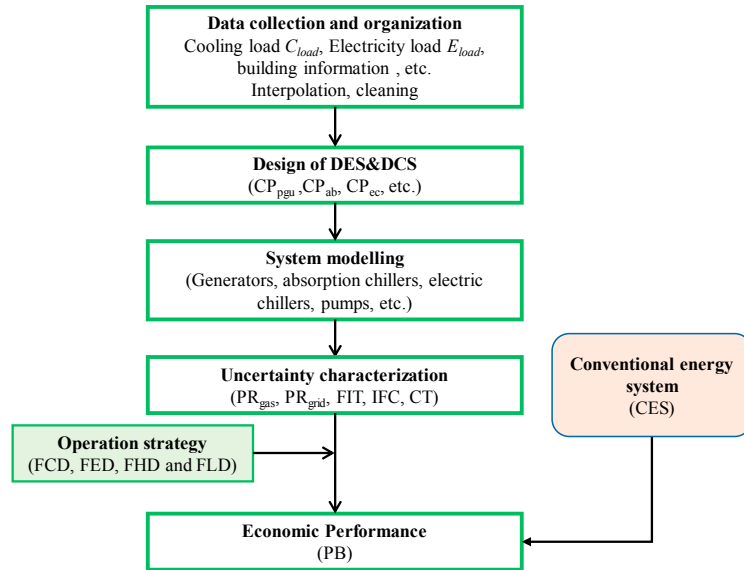


Fig. 1. The method to quantify the impacts of uncertainties in energy market and policy

(1) Data collection and organization

The annual hourly loads of buildings in a campus are collected. The electricity loads of each building are recorded by the meters of power utility. The cooling loads of each building are obtained from the building management systems (BMSs). The collected data are re-organized to keep consistent. The raw data from different BMSs have different resolutions. Some data are recorded every 15 minutes while others may be collected every 30 minutes. All these data are normalized into the same timescale, which is one hour in this study. For some BMSs, data during several hours or days may be lost or abnormal in certain periods due to various uncertainties and accidents in operation. The data therefore are carefully processed by interpolation and cleaning to ensure the consistence and completeness.

(2) DES&DCS design

The DES&DCS can be designed based on the collected electricity demand, cooling demands and the location of buildings. Absorption chillers meet partial cooling loads while the electric chillers complement to meet the excess cooling load. Based on the cooling and electricity demands, the numbers and capacities of power generator unit (PGU), absorption chillers, electric chillers, pumps and cooling towers can be designed. The hydraulic head of chilled water pumps in the DCS is calculated based on the loads of each building and the layout of the district/campus.

(3) System modelling

The performance of the DES&DCS is evaluated by modelling primary components including PGUs, absorption chillers, electric chillers, pumps, etc. The energy balance is expressed as Eq. 1. Where, Q_{gas} is energy from the primary energy (natural gas), Q_e is the energy used for power generation, Q_{tml} is the energy used for cooling, and Q_{waste} is the waste energy. The electrical efficiency η_{ele} and thermal efficiency η_{tml} is expressed in Eq. 2 and Eq. 3. The electrical efficiency η_{ele} depends on the partial loads (PL_{ele}) as shown in Eq. 4. Where, $\eta_{ele,full}$ is the electrical efficiency of generators at full loads and PL_e is the part electricity load ratio of generators. When the PL_{ele} is less than 30%, the generator will shut down to avoid operating with too low efficiency. The COP_{ec} (coefficient of performance) of electric chillers also follows a curve under different partial loads [18]. The cooling water and primary chilled water pumps work at a constant speed and efficiency. Variable-speed pumps are adopted in the secondary chilled water network and the required pressure varies with the cooling loads.

$$Q_{gas} = Q_{ele} + Q_{tml} + Q_{loss} \quad (1)$$

$$\eta_{ele} = Q_{ele} / Q_{gas} \quad (2)$$

$$\eta_{tml} = Q_{tml} / Q_{gas} \quad (3)$$

$$\eta_{ele} = \eta_{ele,full} \times (a_1 \times PL_{ele}^3 + a_2 \times PL_{ele}^2 + a_3 \times PL_{ele} + a_4) \quad (4)$$

(4) Control strategy

Four commonly-used strategies are selected and tested:

- Following the electricity demand method (FED)[19-21]: The generators operate to meet the electricity loads. If the cooling load exceeds the capacity of absorption chillers, electric chillers start.
- Following the cooling demand method (FCD)[19-21]: The generators operate to meet the cooling loads. If all the generators work at full loads but still cannot meet the cooling load, electric chillers start. The lacking/surplus electricity may be imported/exported from/to the grid.
- Following the electricity or cooling demand which requires generators to consume higher primary energy (FHD)[19]: The operation of generators switches between the FED and FCD, which meets the cooling or electricity demand always requiring higher primary energy. This strategy would make full use of the DES. When the generators operate to meet the cooling demand, surplus electricity arises. When the generators operate to meet the electricity demand, excessive heat would be wasted.
- Following one of the electricity or cooling demand which requires generators to consume lower primary energy (FLD): The operation of generators switches between the FED and FCD, which meets the cooling or electricity demand requiring less primary energy. This strategy will lead to neither cooling waste nor surplus electricity. It would always need to import electricity from the grid to meet the cooling and electricity demands.

(5) Evaluation criterion

To assess the economic performance of DES compared with the system that depending on the grid (CES), the payback period (PB) is calculated as shown in Eq. 5. It represents the time required for the DES to recover the additional first cost compared with CES. Where, ΔC_{cap} and ΔC_{opr} are the capital cost difference and annual operation cost difference between DES and CES, as shown in Eq. 6~7. Where, m and n is the number of equipment in CES and DES, PR_{gas} is the price of natural gas (CNY/Nm³), PR_{ele} and FIT are the prices of electricity and feed-in tariff (yuan/kWh), and E_{PGU} is the electricity generated by PGU (kWh), and CM_{PGU} is the maintenance cost coefficient (CNY/kWh). The equipment capital costs and other economic parameters are summarized in Table 1 [22-26].

$$PB = \frac{\Delta C_{cap}}{\Delta C_{opr}} \quad (5)$$

$$\Delta C_{cap} = \sum CAP_m \cdot C_{cap,m} - \sum CAP_n \cdot C_{cap,n} \quad (6)$$

$$\begin{aligned} \Delta C_{opr} &= C_{opr,CES} - C_{opr,DES} \\ &= (E_e + E_c) \cdot PR_{ele} - (F_{gas} \cdot PR_{gas} + E_{grid} \cdot PR_{ele} - E_{sell} \cdot FIT + E_{PGU} \cdot CM_{pgu}) \end{aligned} \quad (7)$$

Table 1. Parameters associated with the economic performance of DES&DCSs

Item	Parameter	value
Equipment capital cost (yuan/kW)	PGU	4800
	Absorption chiller	1200
	Electric chiller	970
Maintenance cost (yuan/kWh)	PGU and others	0.0394-0.0031ln(CAPPGU)
Carbon emission factor (kg/kWh) [26]	Natural gas	0.2
	electricity	0.997

(6) Uncertainty characterization

Uncertainties that affect the economic performance of the DES can be classified into three categories as follows.

Uncertainty in the energy markets: The source includes the natural gas price, the electricity price, and the price for surplus electricity sold to the grid. The benefits of the DES are determined by these three factors simultaneously instead of one factor. Therefore, the PBs under the uncertainties of these three factors are quantified.

Uncertainty in the incentives from the government: The incentives from the government are different from region to region and even from time to time. Therefore, the PBs under different incentives for the first cost are evaluated.

Uncertainty in the carbon tax. Currently the carbon tax varies in different countries. The uncertainty in the carbon tax is considered and its impact on the PB of DES is evaluated.

It is hard to get the probability function of the above uncertainty factors but it is possible to get the intervals. Therefore, the uncertainty quantification is conducted by sensitivity analysis.

3. A DES&DCS for a campus

The campus in the Hong Kong Polytechnic University is selected to investigate the performance of DESs considering uncertainties. Information for these buildings is shown in Table 2. The electricity load and cooling loads of the campus in 2015 are collected, as shown in Fig. 2. It shows that the campus needs cooling all the year because of the subtropical climate and the cooling loads in summer are much higher. The electricity loads have no apparent fluctuations in different months. The DES&DCS can be designed based on the peak cooling and electricity loads. In this study, the capacity of generators is designed to meet the peak electricity load and the demand resulting from the pumps serving the absorption chillers. The capacity of absorption chillers accordingly can be determined based on the exhaust gas from the generator. Electric chillers are selected to complement the absorption chillers to meet the left cooling loads. The schematic diagram of the DES&DCS is shown in Fig. 3.

Table 2. Buildings and gross floor areas

Phase	Area (m ²)	Phase	Area (m ²)
Phase 1	47270	Phase 6	12310
Phase 2	7980	Phase 7	25000
Phase 2A/B	24420	Phase 8	44000

Phase 3A	16780	PCD	10200
Phase 3B	23400	JCA	4800
Phase 4	19330	JCIT	15320
Phase 5	10080		

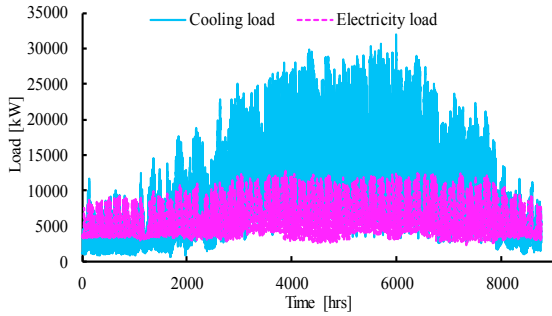


Fig. 2 Annual hourly electricity load and cooling load in 2015

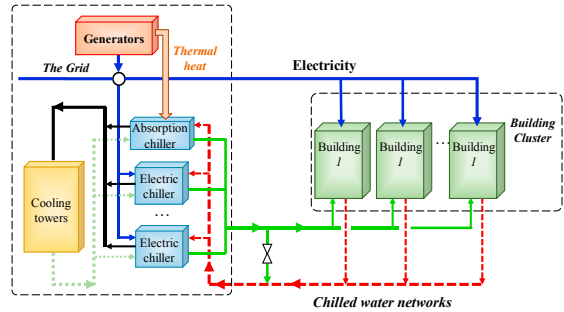


Fig. 3 Schematic diagram of the DES&DCS

4. Results and analysis

4.1. Impacts of uncertainty in the energy market

The uncertainty in the energy market includes the natural gas price, the electricity price and the feed-in tariff. These factors affect the economic performance simultaneously. The electricity price in different regions of China does not have very significant differences. However, the price of natural gas price can be very different, as shown in Table 3. It can be seen that the natural gas price ranges from 2.19 to 4.51 in different cities of China. Therefore, the ratio of the natural gas price to the electricity price (PRR) is used to quantify the uncertainty in energy market, which varies between 1 and 4. For the surplus electricity sent to the grid, the price also varies in different cities, even for different projects in one city. Therefore, the ratio of electricity price sold to the grid to that purchased from the grid (FR) is used to quantify the uncertainty.

Table 3 Natural gas prices in several cities of China

City	Residential	Industrial	Commercial	City	Residential	Industrial	Commercial
Urumqi	1.37	2.28	2.28	Shanghai	3.01	3.57	3.57
Xining	1.48	1.82	2.19	Hangzhou	3.11	3.28	3.28
Nanjing	2.51	2.99	2.99	Nanning	3.23	4.19	4.19
Wuhan	2.54	3.50	3.50	Guangzhou	3.46	4.26	4.26
Changchun	2.81	3.16	3.16	Shenzhen	3.51	4.51	4.51
Harbin	2.81	4.58	4.58	Beijing	2.29	3.23	3.23
Jinan	3.01	3.13	3.13	Tianjin	2.41	2.67	2.67

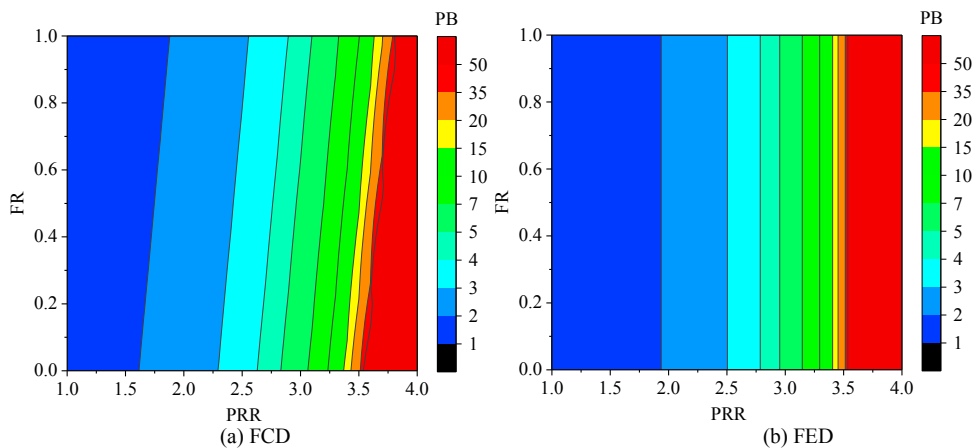
The PB of the DES&DCS controlled by FCD is shown in Table 4, considering the uncertainty in PRR and FR. It can be seen that the PB increases with the PRR and FR. When the PRR is less than 3, the investment can be paid back in 7 years. A higher FR results in a lower PB. Currently the utility company purchases the power from the coal-fired plants at a price of 0.35CNY/kWh, which corresponds to 0.35 for FR. The commonly-used FR for DESs in China is 0.8. It can be seen that if the FR is reduced from 0.8 to 0.3, the PB under different PRRs would be increased by 5% to 8%. It means that if the energy market is open and the DES has to compete with existing power plants to sell the

surplus electricity to the utility company, 5%~8% more time is required to get the investment paid back. Table 4 also shows that the PRR is more significant to the PB than the FR. When the PRR is over 3.4, the PB is not satisfactory and the DES is economically infeasible.

Table 4 PBs of the DES&DCS controlled by FCD considering the uncertainty in PRR and FR

PRR	FR										
	0	0.1	0.2	0.3	0.4	0.5	0.6	0.7	0.8	0.9	1
1	1.53	1.52	1.50	1.49	1.48	1.46	1.45	1.43	1.42	1.41	1.40
1.2	1.66	1.64	1.62	1.61	1.59	1.57	1.56	1.54	1.53	1.51	1.50
1.4	1.81	1.79	1.77	1.75	1.73	1.71	1.69	1.67	1.65	1.63	1.62
1.6	1.98	1.96	1.93	1.91	1.89	1.86	1.84	1.82	1.80	1.78	1.76
1.8	2.20	2.17	2.14	2.11	2.08	2.05	2.03	2.00	1.97	1.95	1.92
2	2.47	2.43	2.39	2.35	2.32	2.28	2.25	2.22	2.19	2.16	2.13
2.2	2.81	2.76	2.71	2.66	2.62	2.57	2.53	2.49	2.45	2.41	2.37
2.4	3.26	3.19	3.13	3.06	3.00	2.95	2.89	2.84	2.79	2.74	2.69
2.6	3.88	3.78	3.69	3.61	3.52	3.45	3.37	3.30	3.23	3.16	3.10
2.8	4.80	4.65	4.52	4.39	4.26	4.15	4.04	3.94	3.84	3.75	3.66
3	6.28	6.03	5.81	5.59	5.40	5.22	5.04	4.88	4.73	4.59	4.46
3.2	9.09	8.59	8.13	7.72	7.35	7.02	6.71	6.43	6.17	5.93	5.71
3.4	16.47	14.87	13.56	12.46	11.53	10.72	10.02	9.41	8.87	8.38	7.95
3.6	87.05	55.58	40.82	32.25	26.66	22.72	19.79	17.54	15.74	14.28	13.06
3.8	-26.49	-32.00	-40.41	-54.83	-85.24	-191.34	781.54	128.45	69.97	48.08	36.63
4	-11.49	-12.42	-13.52	-14.82	-16.40	-18.36	-20.85	-24.12	-28.61	-35.15	-45.58

The PBs of DES&DCS under different control strategies are shown in Fig. 4. The red colour represents that the DES is not applicable where the PB is either too long (more than 50 years) or negative. It can be seen that when the PRR is low (i.e., less than 2.5), the DES controlled under the FED and FHD has shorter PBs, which should be preferred. When the PRR is higher (i.e., more than 3), the FCD and FLD should be preferred. According to the results in Fig. 4, the feasibility of the DES and the optimal control strategy can be determined. When the PRR is over 3.5, the DES is not applicable under all the control methods.



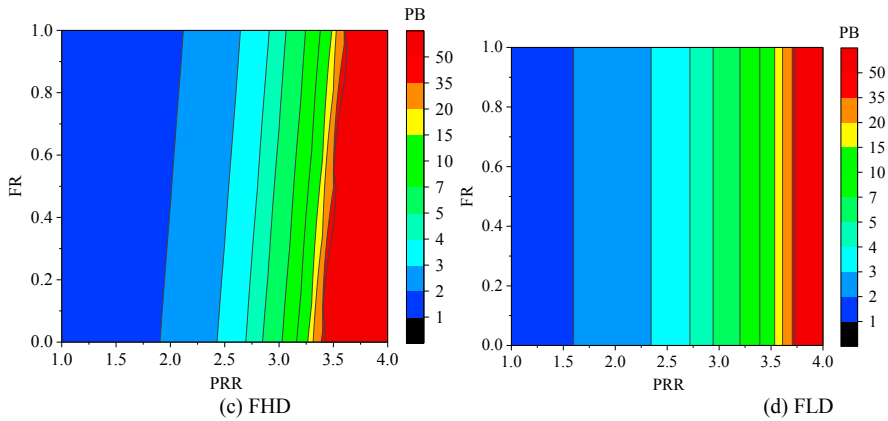


Fig. 4 PBs of the DES&DCS under four control strategies considering uncertainty in PRR and FR

4.2. Uncertainty in the incentives

The PB of the DES&DCS considering the incentives from the government is shown in Fig. 5. The PB of the base case without any incentive is evaluated based on a PRR of 3.5 and FR of 0.8, which currently are used in many projects. It shows that the PB is 11.3, 13.1, 20.1 and 25 years under FCD, FLD, FHD and FED. It means that FCD is recommended considering the economic performance of the DES&DCS. The PB under the FHD and FED is more than 20 years, which is not acceptable. The FCD and FLD can be used with a much smaller PB. With the incentives from the government, the PB is decreased significantly. When the incentive is 1300 CNY/kW, the PB can fall in 10 years under the FCD and FLD. When the incentive is 2500 CNY/kW (used in some areas of China), the PB under FCD, FLD, FHD and FED is 5.86, 6.78, 10.4 and 12.94 years, which is acceptable. It indicates that at least 1300 CNY/kW should be supported by the government to promote the DES if the natural gas price is not decreased.

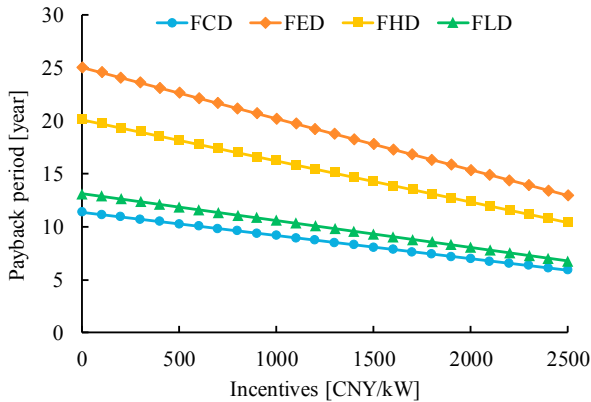


Fig. 5. PBs of the DES&DCS under different incentives

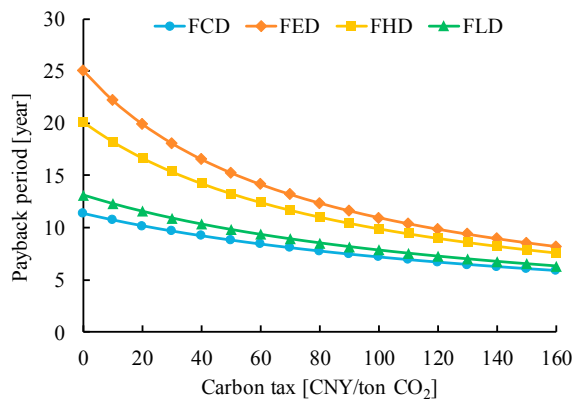


Fig. 6. PB of the DES&DCS under different carbon taxes

4.3. Uncertainty in the carbon tax

The effect of different carbon taxes on the PB of DESs is shown in Fig. 6. The range is determined by referring to existing carbon tax in other countries [13-15]. It shows that with the increase of carbon tax, the PB under the four control strategies decreases. It is because that the carbon emission of DESs using natural gas is lower than the CES depending on the grid primarily powered by coal in China. Additionally, the high efficiency of DESs will reduce the primary energy consumption. Fig. 6 shows that the PB can be less than 10 years for the DESs operated under FCD and FLD when the carbon tax is charged as 50 CNY/ton. When the carbon tax is over 120 CNY/ton, all the PBs of

the DESs under four control methods fall in 10 years. It means that when the government attempts to promote the DESs via carbon tax, the minimum charge should be not less than 50 CNY/ton.

5. Conclusions

The economic performance plays a significant role in the promotion of DESs and is concerned by both investors and users. However, large uncertainties exist in the energy market and policy, which would affect the economic performance and promotion of DESs. In this paper, uncertainty in the energy market and policy and their impacts on the promotion of DES are quantified. The conclusions are obtained as follows.

- 1) The natural gas price has a significant effect on the economic performance of DESs. When the PRR is more than 3, the investment of DES is hard to be beneficial. The feed-in tariff also affects the PB of DESs but not as important as the PRR. If the energy market is open and the price for the surplus electricity sent to the grid is the same as that utility company pays for other plants, the PB would increase by 5%–8%.
- 2) The optimal control strategy varies under different PRRs and FRs. FHD is recommended when the PRR is lower than 2.5. Otherwise, the FCD should be preferred.
- 3) The incentives from the government can help decrease the PB of DESs dramatically. If the investment needs to be paid back in 10 years, the incentive should be not less than 1300 CNY/kW.
- 4) If the government attempts to promote the DESs via carbon tax, the charge should be not less than 50 CNY/(ton CO₂)

Acknowledgement

The research presented in this paper is supported by the Early Career Research Scheme of Huazhong University of Science and Technology (NO. 300426110).

References

- [1] M.F. Akorede, H. Hizam, E. Poursmaeil. "Distributed energy resources and benefits to the environment." *Renewable and Sustainable Energy Reviews* 14 (2) (2010): 724-734.
- [2] K. Alanne, A. Saari. "Distributed energy generation and sustainable development." *Renewable and Sustainable Energy Reviews* 10 (6) (2006): 539-558.
- [3] Z. Ming, O. Shaojie, S. Hui, G. Yujian, Q. Qiqi. "Overall review of distributed energy development in China: Status quo, barriers and solutions." *Renewable and Sustainable Energy Reviews* 50 (2015): 1226-1238.
- [4] State Council. "Action plan for air pollution prevention." <http://www.gov.cn/zhengce/content/2013-09/13/content_4561.htm>.
- [5] State Council (The State Council of the People's Republic of China). "13th Five-Year Energy Development Plan." (2016) Beijing.
- [6] Y. Liu. "Exploring the relationship between urbanization and energy consumption in China using ARDL (autoregressive distributed lag) and FDM (factor decomposition model)." *Energy* 34 (11) (2009): 1846-1854.
- [7] J. Han, L. Ouyang, Y. Xu, R. Zeng, S. Kang, G. Zhang. "Current status of distributed energy system in China." *Renewable and Sustainable Energy Reviews* 55 (2016): 288-297.
- [8] Y. Qin, F. Tong, G. Yang, D.L. Mauzerall. "Challenges of using natural gas as a carbon mitigation option in China." *Energy Policy* 117 (2018): 457-462.
- [9] "Notice of Wuhan Gas Company informing customers." (2017) Hubei. <<http://zy.cnhubei.com/dongxiang/pOYRDF1100>>.
- [10] "Measures to Promote the Development of Natural Gas Distributed Energy." (2017) Changsha. <http://www.changsha.gov.cn/xxgk/gfxwj/szfbgt/201703/t20170314_1937978.html>.
- [11] R. Dong, J. Xu. "Impact of differentiated local subsidy policies on the development of distributed energy system." *Energy and Buildings* 101 (2015): 45-53.
- [12] "What's a carbon tax?" <<https://www.carbontax.org/whats-a-carbon-tax/>>.
- [13] M.S. Andersen. "Vikings and virtues: a decade of CO₂taxation." *Climate Policy* 4 (1) (2004): 13-24.

- [14] B. Fahimnia, J. Sarkis, A. Choudhary, A. Eshragh. "Tactical supply chain planning under a carbon tax policy scheme: A case study." *International Journal of Production Economics* 164 (2015): 206-215.
- [15] T. Alton, C. Arndt, R. Davies, F. Hartley, K. Makrelov, J. Thurlow, D. Ubogu. "Introducing carbon taxes in South Africa." *Applied Energy* 116 (2014): 344-354.
- [16] J. Creedy, C. Sleeman. "Carbon taxation, prices and welfare in New Zealand." *Ecological Economics* 57 (3) (2006): 333-345.
- [17] C. Lu, Q. Tong, X. Liu. "The impacts of carbon tax and complementary policies on Chinese economy." *Energy Policy* 38 (11) (2010): 7278-7285.
- [18] W. Gang, S. Wang, D. Gao, F. Xiao. "Performance assessment of district cooling systems for a new development district at planning stage." *Applied Energy* 140 (2015): 33-43.
- [19] L. Kang, J. Yang, Q. An, S. Deng, J. Zhao, H. Wang, Z. Li. "Effects of load following operational strategy on CCHP system with an auxiliary ground source heat pump considering carbon tax and electricity feed in tariff." *Applied Energy* 194 (2017): 454-466.
- [20] P.J. Mago, N. Fumo, L.M. Chamra. "Performance analysis of CCHP and CHP systems operating following the thermal and electric load." *International Journal of Energy Research* 33 (9) (2009): 852-864.
- [21] X. Song, L. Liu, T. Zhu, T. Zhang, Z. Wu. "Comparative analysis on operation strategies of CCHP system with cool thermal storage for a data center." *Applied Thermal Engineering* 108 (2016): 680-688.
- [22] J.-J. Wang, Y.-Y. Jing, C.-F. Zhang. "Optimization of capacity and operation for CCHP system by genetic algorithm." *Applied Energy* 87 (4) (2010): 1325-1335.
- [23] L. Wang, J. Lu, W. Wang, J. Ding. "Energy, environmental and economic evaluation of the CCHP systems for a remote island in south of China." *Applied Energy* 183 (2016): 874-883.
- [24] B. Yan, S. Xue, Y. Li, J. Duan, M. Zeng. "Gas-fired combined cooling, heating and power (CCHP) in Beijing: A techno-economic analysis." *Renewable and Sustainable Energy Reviews* 63 (2016): 118-131.
- [25] X. Zhang, H. Li, L. Liu, R. Zeng, G. Zhang. "Analysis of a feasible trigeneration system taking solar energy and biomass as co-feeds." *Energy Conversion and Management* 122 (2016): 74-84.
- [26] W. Ma, S. Fang, G. Liu. "Hybrid optimization method and seasonal operation strategy for distributed energy system integrating CCHP, photovoltaic and ground source heat pump." *Energy* 141 (2017): 1439-1455.



16th International Symposium on District Heating and Cooling, DHC2018,
9–12 September 2018, Hamburg, Germany

Combining a dynamic simulation tool and a multi-criteria decision aiding algorithm for improving existing District Heating

Mohamed Tahar Mabrouk^{a,b}, Pierrick Haurant^a, Vincent Dessarthe^c, Patrick Meyer^c,
Bruno Lacarrière^{a*}

^aIMT Atlantique, Department of Energy Systems and Environment, GEPEA, F-44307, Nantes, France

^bARMINES, 60 boulevard Saint-Michel, F-75272, Paris cedex 6, France

^cIMT Atlantique, Lab-STICC, Univ. Bretagne Loire, Technopôle Brest-Iroise, CS 83818, F-29238 Brest, France

Abstract

The work aims to evaluate the recovering potential of excess heat in the return pipe of a district heating (DH) for heating some substations.

The proposed method combines a DH simulation tool and a multi-criteria decision aiding algorithm. It is based on the analysis of the measured return temperatures at each sub-station in order to identify those with high potential of efficiency gains by using the return flow (with support of the supply pipe when needed). Combinations of substations from this set of eligible ones define potential scenarios of connection to the return pipe. The impacts of each scenario on the DH operational performance and the energy savings are evaluated with a detailed hydro-thermal model. The technical parameters and the energy efficiency are not the only points of view in the selection process “of best compromise” scenarios for the improvement of the DH, so that we propose a complex decision aiding process, involving multiple criteria, dealing with different points of view (economic, energy, technical...) and different decision makers. The evaluations of the scenarios on the criteria are summed up in a so-called performance table and aggregated by an outranking model (MR-Sort) to identify relevant scenarios.

This methodology is illustrated by the example of a part of the DH in Nantes (France). Interpretation of data from substations of a specific branch showed the potential of connecting some of them to the return pipe. Six scenarios were generated and evaluated with four criteria. Then, the Multi-criteria Decision Aiding method associated to two actors who have different priorities lead to not obvious results at a first glance.

© 2018 The Authors. Published by Elsevier Ltd.

This is an open access article under the CC BY-NC-ND license (<https://creativecommons.org/licenses/by-nc-nd/4.0/>)

Selection and peer-review under responsibility of the scientific committee of the 16th International Symposium on District Heating and Cooling, DHC2018.

Keywords: District heating, modelling, Return pipe, Multicriteria decision aiding

* Corresponding author. Tel.: +33 (0) 251 858 214

E-mail address: bruno.lacarriere@imt-atlantique.fr

1876-6102 © 2018 The Authors. Published by Elsevier Ltd.

This is an open access article under the CC BY-NC-ND license (<https://creativecommons.org/licenses/by-nc-nd/4.0/>)

Selection and peer-review under responsibility of the scientific committee of the 16th International Symposium on District Heating and Cooling, DHC2018.

10.1016/j.egypro.2018.08.191

Nomenclature

a	alternative
C	concordance index
c_p	specific heat capacity (J/kg)
d	diameter (m)
g_j	performance criterion j
C_h	class h
k	number of classes
b_h	separation profile between class h and class h+1
H	head (m)
L	length (m)
\dot{m}	mass flow rate (kg/s)
S	outranking relation
T	temperature (°C)
U	convection heat exchange coefficient (W/m ² /°C)

Subscripts

j	criterion index
h	class index
g	ground
in	inlet
out	outlet
p	pipe, primary
s	surrounding, secondary
w	water
0	nominal

1. Introduction

Low operational temperatures (supply and return) with high temperature differences are important conditions for increasing the efficiency of district heating (DH).

Low temperature has direct positive consequences on thermal losses and pumping cost [1, 2]. The reduction of operational temperatures also improves the efficiency of production energy systems and fosters the integration of renewable (solar thermal or heat pumps). In addition, low operational temperatures lead to a better energy efficiency as well as economic gains [3].

Despite its importance the management of temperatures is not simple to handle by DH operators due to various reasons among which the separated management and control of the DH and the secondary distribution networks in the buildings connected to the DH [4]. The secondary networks are designed, managed and controlled by independent operators what can lead to high return temperatures on the DH with limited possible actions for the DH operator. Temperature cascading is one of the possible solution for the DH operator to reduce the operational temperatures.

Temperature cascading aims to take advantage of return temperature complementary to the use of heat from the supply pipe when needed. This aims either to lower the global return temperature of the DH or to integrate new loads to the DH (low temperature loads). The implementation is done directly at the substation [5,6] or thanks to the loads management at the substation [7]. The optimal cascade functioning is conditioned to the different operational

temperatures of successive substations, as well as to an equilibrium between the loads requiring the use the supply pipe and the ones compatible with a connection to the return pipe [7]. In their study, Köfing et al.[6] compared different configuration for connecting additional low temperature substations to an existing DH. Their work demonstrates the interest of cascading with a decrease of the return temperature whatever the scenario. In their techno-economic analysis Flores et al. [1] evaluated the impact of the penetration rate of Low Temperature substations in conventional DH.

Most of these works are based on simulation tools for which different strategies can be implemented depending on the objectives (simulation, optimization, design, control...). Various works on pseudo-dynamic or dynamic simulations of DH have been carried out with tools dedicated to the modelling of complex energy systems such as TRNSYS, MODELICA, EnergyPlan... to study the whole system performance. Other works focusing more on the distribution used more detailed models based on different numerical schemes (e.g. [8-10]). This type of models generally requires important calculation times due to the level of complexity in the description of the systems. Simplified models can be used when the objective is at the same time to have a good representation of the whole system and to take into account physical variable like temperatures and mass flows [1].

Multi-Criteria Decision Aiding (MCDA) is the study of decision problems, methods and tools which may be used in order to assist one or more Decision Makers (DMs) in reaching a decision when faced with a set of decision alternatives, described via multiple, often conflicting, properties or criteria. Usually, three types of decision problems are put forward in this context [11]: the choice problem, which aims to recommend a subset of alternatives, as restricted as possible, containing the “satisfactory” ones; the sorting problem, whose goal is to assign each alternative into predefined preferentially ordered categories; and the ranking problem, which orders the alternatives by decreasing degree of preferences.

Various models have been proposed to support DMs facing a multi-criteria decision problem [12] and to represent their preferences. Roughly speaking, they originate from two methodological schools. First, in the outranking methodologies, any two alternatives are compared pair-wisely on basis of their evaluations on the set of criteria, according to a majority rule (see for example Roy, 1996 [11]). Second, methods based on multiattribute value theory aim to construct a numerical representation of the DM's preference on the set of alternatives. The main difference between these two methodological schools lies in the way in which the alternatives are compared and the type of information required from the DM. Outranking methods are preferred if the evaluations of the alternatives are primarily qualitative, if the DM would like to include a measure of imprecision about personal preferences in the model, and when a human-readable evaluation model is desired. Value-based methods can be favored if a compensatory behavior of the DM should be modeled, and when the evaluation of the alternatives should be summarized by a single value (as in the case of accounting, for instance). These methodologies are usually integrated in a more general decision aiding process, as described in [13].

In the context of DH systems, the *DMs* are the DH operator (called the *user* later), the consumers and the municipality (as the owner of the DH infrastructure), and the alternatives are the various scenarios to improve the district heating, while the evaluation criteria are the indicators or attributes used to evaluate the various scenarios.

The present work presents a methodology to provide the DMs involved in the DH management with the relevant information for selecting the substations of an existing DH to be connected to the return temperature. The methodology is based on the combination of the analysis of monitored data of the substations, the implementation of a MCDA method to identify the relevance of different scenarios (compounded of technical and non-technical data), and a dynamic hydro-thermal simulation of the DH to assess the energy performance of the different configurations tested.

2. Methodology

2.1. District heating network model

The DHN is represented by an oriented graph where each edge represents two pipes (supply and return) and nodes represents either production units or consumer substations. The model is based on a thermal and hydraulic modeling of pipes and heat exchangers at each node.

The hydraulic model calculates the pressure drops in the pipes and guaranties the mass balances at the nodes. Assuming the water flowing throughout the pipes to be incompressible with constant properties, the hydraulic head loss ΔH in a pipe between nodes i and j can be expressed by:

$$\Delta H = k_{ij} \dot{m}_{ij} |\dot{m}_{ij}| \quad (1)$$

With \dot{m}_{ij} the water mass flow rate in the pipe and k_{ij} the Darcy-Weisbach friction factor. The mass flow balance in each node is given by:

$$\sum_{j \in \{\text{Pr}(i)\}} \dot{m}_{ji} = \sum_{k \in \{\text{Su}(i)\}} \dot{m}_{ik} + \dot{m}_i \quad (2)$$

Where $\{\text{Pr}(i)\}$, $\{\text{Su}(i)\}$ are respectively the predecessors and the successors of the node i and \dot{m}_i is the mass flow rate going to the consumer or to the production unit depending on the node's type.

The thermal model here is a pseudo-dynamic model which takes into account the heat losses from the pipe to the ground. The temperature drops in the pipes are given by:

$$T_{w,out} = T_s + (T_{w,in} - T_s) e^{-\left(\frac{2\pi d g L_p U}{c_p \dot{m}}\right)} \quad (3)$$

The heat exchangers at each node are considered to be adiabatic. The transferred heat power can be calculated using the NTU method while the global heat transfer coefficient was characterized from real data. Then the variation of this coefficient from the nominal U_0 is :

$$\frac{U}{U_0} = C_1 + C_2 \left(\frac{\dot{m}_p}{\dot{m}_{p0}}\right)^\alpha + C_3 \left(\frac{\dot{m}_s}{\dot{m}_{s0}}\right)^\beta \quad (4)$$

Where \dot{m}_{p0} and \dot{m}_{s0} are nominal mass flow rate in the primary and secondary side of the heat exchanger and C_1 , C_2 , C_3 , α and β are constants. In this study, at the secondary side, return temperature are set constant whereas and supply temperatures are controlled based on the outdoor temperature using a linear control curve.

The equations are solved as a whole problem to model the district heating. The unknown variables of this problem are the hydraulic head at each node, the primary supply and return temperature at each node, the mass flow rates in the pipes and the primary and secondary side mass flow rates at the heat exchangers. The known variables are: the loads for all the substations, the power produced by all the production units except one of them (to ensure the energy conservation, this slack node correspond to the energy exchanges with the rest of the DH), the supply temperatures of the producers and return and supply temperatures at the secondary side of the substations. In the case of a substation connected to the return pipe, the mass flow rate $\dot{m}_{p,i}$ entering the heat exchanger is the sum of mass flow rate coming from the supply pipe and the return pipe. Then, the fraction of the mass flow rate from the return pipe over the total mass flow rate flowing in the return pipe is called α . The optimal fraction depends on the temperature of the water at the return pipe, the demand power at the substation and the supply temperature at the secondary side of the heat exchanger. These fractions are optimized at each time step in order to minimize the produced power.

2.2. Multi-criteria Decision Aiding

Among the possible outranking sorting methods, we choose Majority-Rule Sorting (MR-Sort) [15]. The method allows us to build an overall qualitative scale for the evaluation of the scenarios, while presenting a very readable and operational model. It handles very easily a mix of quantitative and qualitative evaluation scales on the criteria. The preferences of the DMs which are used in MR-Sort are represented here through criteria weights, which give the relative importance of criteria, a majority threshold which indicates the weight of a coalition of criteria in order to be considered sufficient and category limits, which are used to delimit the various categories. In more complex versions, veto and dictator profiles [15] are also considered, which allow to represent more precisely the preferential behavior of the DMs.

The basic version of MR-Sort is formalized as follows. Consider a finite set A of decision alternatives (here the scenarios), a finite set of evaluation criteria indexed by J and a set of category limits $B = \{B_1, \dots, B_{k-1}\}$. Each alternative and each category limit is a vector of evaluations with respect to all criteria. The evaluation with respect to criterion j can be viewed as a function $g_j: A \cup B \rightarrow \mathbb{R}$, where $g_j(a)$ denotes the evaluation of alternative $a \in A$ on criterion j and $g_j(b_h)$ denotes the evaluation of category limit $b_h, \forall h \in \{1, \dots, k-1\}$, on criterion j . The set of category limits are used to define a set of k categories $\{C_1, \dots, C_k\}$, ordered by their desirability, from C_1 being the worst category to C_k being the best one. Each category C_h is defined through its upper limit, b_h , and its lower limit, b_{h-1} , with the exception of the worst and best categories, which have only one limit. These categories represent the various levels of the qualitative scale on which the scenarios have to be evaluated. In this section, we assume, without loss of generality, that the performances are supposed to be such that a higher value denotes a better performance. This will not be the case in the final study. Furthermore the performances of the category limits are non-decreasing, i.e. $\forall j \in J, 1 < h < k: g_j(b_{h-1}) \leq g_j(b_h)$.

An alternative a is said to outrank a category limit b_{h-1} if and only if there is a sufficient coalition of criteria supporting the assertion “ a is at least as good as b_{h-1} ”. A coalition of criteria corresponds to a subset of criteria which “agree” on how an alternative compare to a category limit, either being at least as good or strictly worse. To measure this, we define for each criterion j a function $C_j: A \times B \rightarrow \{0,1\}$ which assesses whether criterion j supports that statement or not:

$$\forall j \in J, a \in A, 1 \leq h \leq k: C_j(a, b_{h-1}) = \begin{cases} 1, & \text{if } g_j(a) \geq g_j(b_{h-1}), \\ 0, & \text{otherwise} \end{cases} \quad (5)$$

To assess whether a coalition of criteria is in favor of the outranking or not, $\forall a \in A, 1 \leq h \leq k$, we first define the overall concordance as:

$$C(a, b_{h-1}) = \sum_{j \in J} w_j C_j(a, b_{h-1}) \quad (6)$$

where w_j is the weight of criterion j . The weights are defined so that they are positive and sum up to one. This overall concordance is then compared to a majority threshold λ extracted from the decision-maker's preferences along with the weights. As in this basic version we do not consider any veto rule here, the outranking relation S is then defined as:

$$aSb_{h-1} \Leftrightarrow C(a, b_{h-1}) \geq \lambda \quad (7)$$

If $C(a, b_{h-1}) < \lambda$, the coalition of criteria is not sufficient, the alternative does not outrank the frontier b_{h-1} and will therefore be assigned in a category lower than c_h .

Alternative a is assigned to the highest category it outranks, hence this rule can be written as:

$$a \in c_h \Leftrightarrow aSb_{h-1} \text{ and } aSb_h. \quad (8)$$

In order to model more accurately the preferential behavior of the DMs, several extensions of the MR-Sort model have been proposed in the literature. For example, [15] extended this approach in order to handle large performance

differences (resulting in what is called *dictator* and *veto* effects). These extensions lead to more flexible and more complex models as their number of parameters increases.

Several techniques have been proposed in the literature to determine the parameters of outranking-based multi-criteria sorting models. The DM could provide them directly, which is what we propose to do for the district heating problem presented hereafter. As an alternative, several authors have proposed to find the parameters of the model through the use of assignment examples.

3. Case study

Nantes’ district heating has been recently extended to link more than 380 substations with about 85 km of pipes in 2017 for only 22 km in 2012. It supplies heat to more than 16 000 dwellings and many public facilities (swimming pools, hospital, schools, museums...). The total capacity of heat production units hits 202 MW with an energy mix achieving 84 % of renewable and waste heat (Tab. 1).

Table 1. Nantes DH main production units.

Site	Number of units	Energy source	Technology	Capacity (MWth per unit)
Malakoff	2	Waste	Boiler	15
	2	Biomass (Wood)	Boiler	15
	3	Gas	Boiler	29
La Californie	3	Gas	Boiler	13
	2	Gas	CHP	8
	1	Biomass (Wood)	Boiler	8 (May 2019)

The aim of the study is to evaluate the ability of improving the efficiency of a network by implementing temperature cascades. In that view, a specific branch (Fig.1) of the network located in the East of Nantes Island has been selected since the return temperatures of most of its seven substations are usually over 60 °C: we can observe that the median, first and last quartile of return temperatures at Subs₆, Subs₄, Subs₃, Subs₂ and Subs₁ are between 62 °C and 75 °C (Fig. 2).

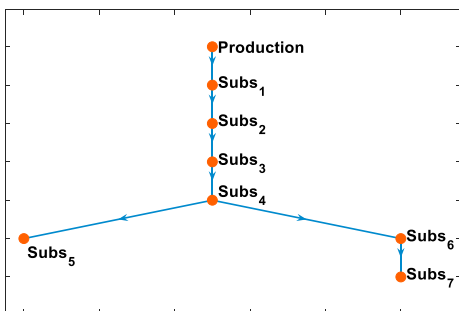


Fig. 1. Branch’s topology.

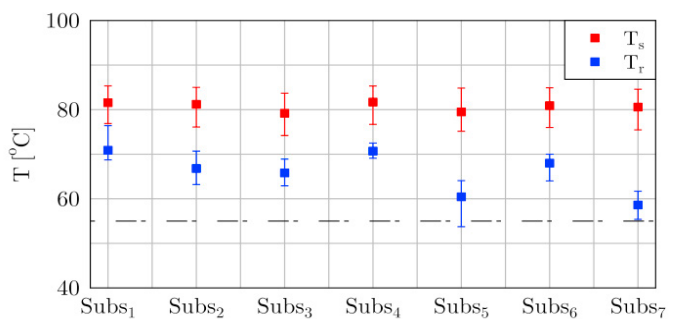


Fig. 2. Median and range between first and third quartile of supply and return temperatures in the branch.

These substations present high heat sources in their return pipe to be valorised, and particularly at Subs₆. We define the heat recovery potential as the difference between the power in the return pipe of a given substation at its functioning temperature and the power at a temperature of 55 °C. We can observe on figure 3 that for the Subs₆ the power varies from 80 kW to 200 kW in winter months, while the consumptions of Subs₄, Subs₃, Subs₂ and Subs₁ are always below 100 kW. It suggests that the high amount of heat available on the return pipe after subs₆ could be used by the other substations by connecting them both to the supply and the return pipe.

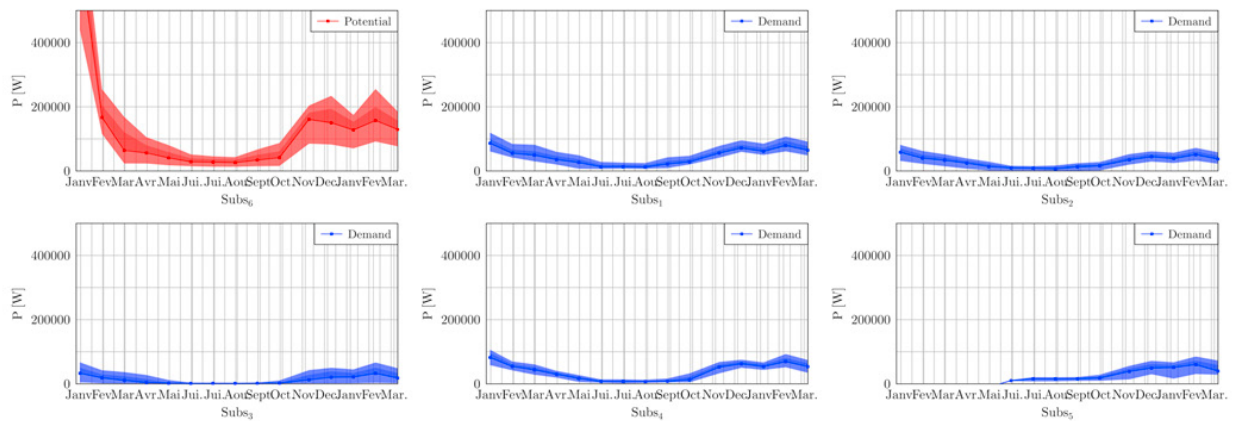


Fig. 3. Heat potential at subs₆ and heat consumptions at Subs₅, Subs₄, Subs₃, Subs₂ and Subs₁ (Median and range between 1st and 3rd quartile)

However, we cannot evaluate such a possibility only by summing the potential and the demands since the temperature cascade implies huge changes in the functioning of the branch and the substations themselves.

4. Results

For each scenario, the input data used in the simulation are demand powers in the substations and the outdoor temperature which is needed to calculate the secondary side supply temperatures using control curves. These data cover a period of 13 days in December/January 2018. The fraction of mass flow rate injected from the return pipe to the substation is calculated at each time step. As an illustration of the results obtained, the Figure 4 presents this fraction for a scenario where 3 substations are connected to the return pipe: Subs₄, Subs₂ and Subs₁. In these curves it is noticed that α in Subs₄ is always greater than those in the Subs₂ and Subs₁. This is due to the fact that Subs₄ is closer to the available heat in Subs₆ and that the temperature at the return pipe is lower as we get farther from Subs₆. This temperature drop is due to two phenomena: the heat losses in the pipes and the mixing with colder water at each substation.

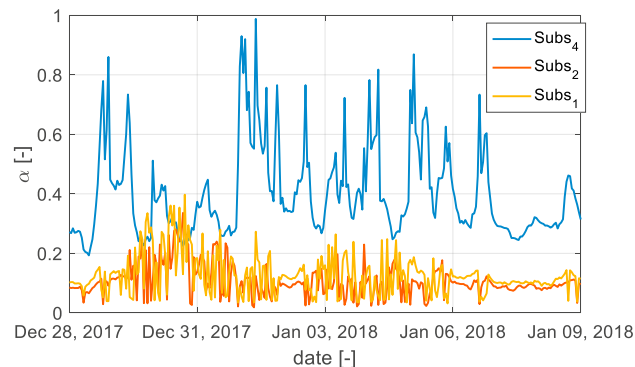


Fig. 4. Optimal fraction of the return mass flow rate injected to the substation

Two distinct decision makers are involved in the decision process of this case study: the *user* (the company that operates the secondary side of the heating network) and the *operator* (the company that operates the primary side of the network). Their goal is to evaluate each of the scenarios on a two-level qualitative scale (“bad”, “good”), i.e. each scenario will be assigned to one of the two ordered classes “bad” or “good” (in terms of the vocabulary of Section 2).

They agree on a set of 4 evaluation criteria of the scenarios (which represent energetic, economic and social perspectives of the problem):

- Criterion g_1 : Energy savings [MWh]. It is calculated as the difference between the energy produced by the production unit for each scenario and a reference case where there is not any substation connected to the return pipe.

- Criterion g_2 : Energy diagnostic of the substation consisting in the yearly energy consumption per heated surface. This criterion expresses the level of priority between connecting the substation to the return pipe and to retrofit the buildings connected to the given substation. For this criteria the results are presented with letters (inspired from the Energy Performance Certificate labels)

- Criterion g_3 : the connection cost. We do the assumption of a constant cost whatever the considered substation so that it is directly linked to the number of substations in the scenario.

- Criterion g_4 : the potential acceptance by the owners. This criterion formalizes the level of difficulty to convince the owners to accept modification in the infrastructure. In that view, we consider a scale from “-“ for strong resistance of the owners in the negotiations (e.g. multi-ownership buildings with many persons to convince), to “++” for low resistance (e.g. buildings owned by the municipality).

The evaluation of each scenario regarding the criteria are summed up in the Table 2:

Table 2. Performance table.

Scenario	Connected substations	g_1	g_2	g_3	g_4
1	Subs ₄	5.93	C	1	-
2	Subs ₄ , Subs ₂ , Subs ₁	6.21	B	3	-
3	Subs ₄ , Subs ₃	6.34	B	2	-
4	Subs ₂	4.73	A	1	-
5	Subs ₁	0.32	B	1	+
6	Subs ₃	0.56	C	1	++

The decision makers agree that criterion g_1 has to be maximized. Criterion g_2 is recoded on the following integer scale (A=1, B=2, C=3) and has to be minimized. Criterion g_3 has to be minimized, and finally, criterion g_4 is recoded on the following integer scale (-- = -1, neutral = 0, + = 1, ++ = 2), and has therefore to be maximized.

The *user* DM considers that a good value should be above 3MWh on criterion g_1 , below 2 on criterion g_2 , and below 3 on criterion g_3 . As he is not taking into account criterion g_4 when he evaluates the various scenarios, these evaluations are not important to him. This defines the separation profile between the categories “good” and “bad” for him. Besides, he cannot make a decision based on only one of the remaining three criteria. But if a scenario is good on criterion g_2 , then it is enough for him that it is good on either g_1 or g_3 to be considered on the overall as a good scenario. Finally, being good on g_1 and g_3 alone is not sufficient for him to evaluate the scenario as good. This defines the weights of the criteria, together with the majority threshold λ for this DM.

The *operator's* profile is a bit different. A good value on g_1 is above 2MWh, on g_2 below 2, on g_3 below 1, and on g_4 above 0. Again, this gives us the separation profile between the “good” and the “bad” classes. For him g_1 is clearly the most important criterion, and if a scenario is good on g_1 and either g_2 or g_4 , the scenario can be considered as good on the overall. If, however the scenario is not good on g_1 , then it should be good on the remaining 3 criteria to be evaluated as good. And finally, if a scenario is below 0.4 on g_1 , then it definitely cannot be considered as good on the overall, however good it has been evaluated on the remaining criteria. From these statements, we can deduce the weights of the criteria together with the majority threshold for this DM.

All in all, these preferential information lead to the preferential parameters of Tables 3 and 4.

Table 3. Weights, veto and majority threshold.

Decision maker	g_1	g_2	g_3	g_4	λ
User	0.25	0.50	0.25	0	0.75
Operator	0.40	0.20	0.10	0.30	0.60
Operator veto thresholds	0.40	NA	NA	NA	

Table 4. Separation profiles

Decision maker	g_1	g_2	g_3	g_4
User	3	2	3	0
Operator	2	2	2	0

For the user, the simple MR-Sort model described in Section 2 is applied to evaluate the scenarios. For the operator however, as the notion of veto has to be taken into account (no good scenario should be below 0.4 on g_1). Therefore, a classical extension of MR-Sort is used including this notion of veto. The results of the assignment are given in the following Table 5:

Table 5. Results of the assignment.

Decision maker\Scenario	1	2	3	4	5	6
User	"Bad"	"Good"	"Good"	"Good"	"Good"	"Bad"
Operator	"Bad"	"Good"	"Good"	"Good"	"Bad"	"Bad"

Consequently, a compromise decision would be to consider that scenarios 2, 3 and 4 are evaluated as "Good", as both decision makers agree. This decision aiding process should simplify their decision on which of these 3 scenarios should be implemented in practice, in order to improve the DH of this part of the city of Nantes.

It is interesting to notice that the reasons why these scenarios have been evaluated as "good" by the 2 DMs may not be the same for both of them. For example, scenario 4 has been evaluated as "good" for the *user* DM, because it is considered as good on g_2 and g_3 , which is sufficient for this DM. However, this same scenario is evaluated as "good" for the *operator* DM, because it is considered as good on the first 3 criteria, which again is sufficient for this DM. This underlines the importance of modeling the preferences of the DMs in such a process accurately, as the results depend a lot on the preferential parameters.

5. Conclusion

This work presents the interest of coupling MCDA methods with modelling tools for improving the existing DH by connecting relevant substations to the return pipe.

The MCDA method combines the information given by energy indicators by taking into account various criterion associated to divers actors who can have different points of view on the importance to be allocated to each indicator. The results show the coupled methods enable to identify strategies not obvious at a first glance and provide useful information for discussion between the different stakeholders. The proposed methodology in the example of a single branch is replicable to the whole DH as well as the list of criteria and points of view can be broaden depending of the case studied and the actors involved.

Acknowledgements

This project has received funding from the European Union's Horizon 2020 research and innovation program under grant agreement N° 731297. This document reflects only the author's view and the European Commission (Innovation

and Networks Executive Agency) is not responsible for any use that may be made of the information it contains. The authors are grateful to ERENA, the operator of Nantes district heating, for their collaboration in the EU programme MySMARTLife.

References

- [1] Castro Flores, J.F., Lacarrière, B. Chiu, J.N.W. and Martin. V. “Assessing the techno-economic impact of low temperature subnets in conventional district heating networks.” *Energy Procedia*, 116 :260–272, (2017). ISSN 18766102. doi : 10.1016/j.egypro.2017.05.073.
- [2] Xing, Yangang, Bagdanavicius, Audrius, Lannon, Simon, Pirouti, Marouf and Bassett, Thomas. “Low temperature district heating network planning with focus on distribution energy losses.” In International Conference on Applied Energy, (2012), Suzhou, China,
- [3] Frederiksen Svend and Werner., S. “District Heating and Cooling.” (2013) Lund, Studentlitteratur.
- [4] Gadd, Henrik and Werner, Sven. “Achieving low return temperatures from district heating substations.” *Applied Energy*, 136 (2014) 59–67.
- [5] Basciotti, Daniele, Köfing, Markus, Marguerite, Charlotte and Terreros. Olatz “Methodology for the Assessment of Temperature Reduction Potentials in District Heating Networks by Demand Side Measures and Cascading Solutions.” (2016) Aalborg, Denmark.
- [6] Markus Köfing, Daniele Basciotti, and Ralf-Roman Schmidt. “Reduction of return temperatures in urban district heating systems by the implementation of energy-cascades.” *Energy Procedia*, 116 (2017) :438–451.
- [7] Snoek, Chris Yang, Libing, Onno, Tom, Frederiksen, Svend and Korsman, Hans. “Optimization of District Heating Systems by Maximizing Building Heating System Temperature Difference.” Technical report, IEA SHC (1999).
- [8] Zheng, Jinfu, Zhigang Zhou, Jianing Zhao, et Jinda Wang. “Function Method for Dynamic Temperature Simulation of District Heating Network”. *Applied Thermal Engineering* 123 (2017): 682-88. <https://doi.org/10.1016/j.applthermaleng.2017.05.083>.
- [9] Zhou, Shou-jun, Mao-cheng Tian, You-en Zhao, et Min Guo. Dynamic Modeling of Thermal Conditions for Hot-Water District-Heating Networks. *Journal of Hydrodynamics*, Ser. B 26, no 4 (septembre 2014): 531-37. [https://doi.org/10.1016/S1001-6058\(14\)60060-3](https://doi.org/10.1016/S1001-6058(14)60060-3).
- [10] Gabrielaitiene, Irina, Benny Böhm, et Bengt Sunden. “Evaluation of Approaches for Modeling Temperature Wave Propagation in District Heating Pipelines”. *Heat Transfer Engineering* 29, no 1 (2008): 45-56. <https://doi.org/10.1080/01457630701677130>
- [11] Roy, B. “Multicriteria Methodology for Decision Aiding.” (1996) Kluwer Academic, Dordrecht.
- [12] Bouyssou, D., Marchant, T., Pirlot, M., Tsoukiàs, A. and Vincke., P. “Evaluation and decision models with multiple criteria: Stepping stones for the analyst.” *International Series in Operations Research and Management Science*, Volume 86. (2006) Boston, 1st edition.
- [13] Tsoukiàs, Alexis. “On the concept of decision aiding process: an operational perspective.” *Annals of Operations Research*, 154(1) (2007) 3 – 27.
- [14] Leroy, A., Mousseau, V. and Pirlot M. “Learning the parameters of a multiple criteria sorting method.” In R. Brafman, F. Roberts, and A. Tsoukiàs, editors, *Algorithmic Decision Theory*, volume 6992 (2011), 219–233. Springer.
- [15] Meyer, P., Olteanu, A. “Integrating large positive and negative performance differences into multicriteria majority-rule sorting models.” *Computers & Operations Research*, Volume 81, (2017) 216 – 230.



16th International Symposium on District Heating and Cooling, DHC2018,
9–12 September 2018, Hamburg, Germany

Analysis of possibilities to utilize excess heat of supermarkets as heat source for district heating

B. Zühlsdorf^{a*}, A. Riis Christiansen^b, F. Müller Holm^b, T. Funder-Kristensen^c,
B. Elmegaard^a

^a Technical University of Denmark, Nils Koppels Alle, Building 403, 2800 Kgs. Lyngby, Denmark

^b Viegand Maagøe AS, Nørre Farimgade 37, 1364 Copenhagen, Denmark

^c Danfoss A/S, Albuen 29, 6000 Kolding, Denmark

Abstract

The paper analyses the possibilities to recover excess heat from CO₂ supermarket refrigeration plants for supply to district heating networks. It was analyzed to operate the refrigeration system at an increased gascooler pressure to directly supply heat and to install a cascade heat pump to recover the heat from lower temperatures. Increasing the gascooler pressure appeared promising during summer, while the cascade heat pump showed higher COPs during colder periods. The investment for the cascade heat pump could be compensated within 4 years at district heating prices above 37 €/MWh.

© 2018 The Authors. Published by Elsevier Ltd.

This is an open access article under the CC BY-NC-ND license (<https://creativecommons.org/licenses/by-nc-nd/4.0/>)

Selection and peer-review under responsibility of the scientific committee of the 16th International Symposium on District Heating and Cooling, DHC2018.

Keywords: CO₂; District Heating; Excess Heat Recovery; Supermarket Refrigeration; Sector Coupling

1. Introduction

The advancements in district heating (DH) technologies are characterized by decreasing supply temperatures. The 4th generation of DH is described by supply temperatures between 40 °C to 70 °C, [1,2]. The 4th generation of DH

* Corresponding author. Tel.: +45 452 54103.

E-mail address: bezuhs@mek.dtu.dk

comprises low-temperature district heating (LTDH) and ultra-low-temperature district heating (ULTDH) networks. LTDH networks are designed with a supply temperature around 60 °C, which is just high enough for direct heat supply for domestic hot water. ULTDH networks operate at around 40 °C and are designed for direct supply of space heating, while the domestic hot water production requires a booster heat pump at the customer site.

The boundary conditions determine, which of the solutions constitutes the thermodynamic and economic optimum. Several studies have therefore compared various DH technologies under consideration of different conditions, such as consideration of existing network components, availability of heat sources, network layouts and other aspects [2–5].

Since the availability of heat sources for heat pump based district heating networks represents a key aspect with respect to their performance, different works in this field were carried out. Bühler et al. [6–8] have conducted economic analyses of the possibilities to use industrial excess heat from thermal processes for district heating. They considered spatiotemporal aspects and ensured the economic feasibility by comparisons to alternative heat sources for the DH network and to energy-efficiency measures, which would decrease the availability of industrial excess heat. Their studies outlined the general potential of excess heat recovery for DH purposes but also emphasized the importance of beneficial boundary conditions, such as short distances between heat source and customers and low integration cost.

Lund et al. [9] indicate, that the refrigeration systems of supermarkets represent another potential heat source for DH systems. These are rejecting excess heat to the ambience throughout the year and are typically located in close vicinity to areas with increased heating demands. While conventional refrigeration systems with e.g. R-404a, reject heat during a subcritical condensation just above the ambient temperatures, CO₂ systems reject the heat to a relatively large extent significantly above the ambient temperatures during desuperheating or transcritical gascooling processes. The increased temperature differences represent irreversibilities of CO₂ systems and thereby a potential for improvements.

CO₂-based systems constitute the state of the art technologies in cold and moderate climates and are emerging as well in warmer climates [10–12]. Especially fully integrated systems, which integrate the air conditioning and heating requirements into the system while exploiting the peculiarities offered by the refrigerant properties of CO₂, show convincing performances and an increased utilization of existing equipment. Most of the studies focus on the heat recovery to cover demands for space heating and hot water preparation on-site or in close vicinity [10–16].

The studies demonstrated the possibilities for integrating on-site heat demands in the refrigeration system. The examples indicated high performances for cases, in which the heat demand and its temperatures matched well with the available heat. On the other hand, highly integrated systems often require storage tanks for balancing the temporal shift between availability and demand. The amount of available excess heat can furthermore exceed the heat demand.

LTDH networks represent an alternative potential customer of low-temperature excess heat. It was therefore suggested by e.g. [9,17,18] to couple the supermarket refrigeration units to LTDH networks. LTDH networks constitute a flexible customer of the available heat and the supermarkets are representing a decentral heat source for LTDH networks, often implying small distances and in many cases an existing connection to the DH networks, [7].

This study therefore focuses on an analysis of the possibilities for the recovery of excess heat from CO₂ supermarket refrigeration units and evaluates the boundary conditions, for which the sector coupling appears economically feasible.

2. Methods

2.1. Possible system layouts

The following subchapters present the different possibilities to recover excess heat from supermarkets for supplying heat to a LTDH network while heating the return stream from 45 °C to 70 °C. The approaches are compared on an annual basis assuming average ambient temperatures of 20 °C, 9 °C and 1 °C for summer, spring/autumn and winter, respectively, and for an average cooling demand of 100 kW throughout the year.

2.1.1. Supply of excess heat during operation at increased gascooler pressure

Figure 1 a) shows the layout of a simple refrigeration plant with one evaporator, an internal heat exchanger, an ejector and the possibility for direct heat recovery. The gascooler pressure and thereby the temperature profile of CO₂ during heat rejection is during normal operation determined by the ambient temperature, e.g. [12,19]. Consequently, the temperature profile and thereby the amount of excess heat that is directly recoverable, varies as well.

The heat that is directly recoverable during normal operation is often rather limited. The gascooler pressure can alternatively be operated at an increased pressure to not only cover the cooling demand of the supermarket but also to actively supply heat to the DH network. Both the amount of heat that is recovered as well as the COP for supplying the heat are dependent on the additional pressure increase [15]. The contributions increase nonlinearly and suggest that there is an optimal marginal pressure increase, yielding a maximum COP.

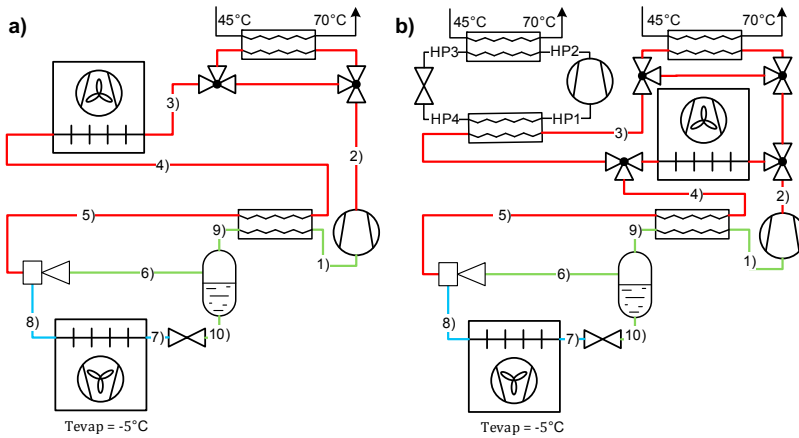


Figure 1: Flow sheets for a standard CO₂ refrigeration system with an ejector and one evaporation temperature with a) direct heat exchange at operation with increased gascooler pressure, b) direct heat exchange and a cascade heat pump in serial connection

Table 1: Assumptions for modelling the CO₂ refrigeration system and the cascade heat pump

	CO ₂ System	Cascade HP
Isentropic efficiency of compressor:	80 %	75 %
Heat loss from the compressor:	5 %	5 %
Efficiency of motor:	95 %	95 %
Lumped isentropic efficiency of ejector:	25 %	-
Effectiveness of internal heat exchanger:	70 %	-
Pinch point temperature differences in HXs:	5 K	5 K
Minimum gascooler outlet temperature:	10 °C	-
Evaporation temperature:	-5 °C	-

In order to analyze the trade-off among additionally supplied heat and the performance, a numerical model was implemented in EES, [20]. The model consists of mass and energy balances for all components, as well as equations modeling their performance. Table 1 summarizes the assumptions for the model of the refrigeration system. The gascooler outlet temperature is determined by the ambient temperature and a pinch point temperature difference of 5 K while the gascooler pressure was set to optimal conditions with respect to cooling COP_c. The coefficient of performance for cooling COP_c = $\dot{Q}_c / \dot{W}_{T_{amb,opt}}$ is defined as the ratio of the cooling rate \dot{Q}_c to the power utilized to operate system optimally according to the ambient temperature $\dot{W}_{T_{amb,opt}}$. The compressor was modelled with an isentropic efficiency for the compression process and an additional efficiency for the motor. Heat losses from the compressor were considered as well.

The model assumes that all heat is rejected by the gascooler to the ambient during standard operation. In order to supply heat to the DH network, the compressor discharge temperature must be high enough to enable cooling of the CO₂ while heating the DH stream from 45 °C to 70 °C and respecting a minimum pinch point temperature difference of 5 K. After the direct heat exchange, the CO₂ is further cooled to the gascooler outlet temperature that is defined by the ambient temperature and the pinch point temperature difference. If the compressor outlet temperature is too low for heating the stream up to 70 °C, the entire heat is rejected through the gascooler.

The performance of supplying the additional heat rate was described by a coefficient of performance COP_{HS,CO₂}, which is defined by the ratio of the heat supplied in the direct heat exchanger \dot{Q}_{dHX} to the additional power that is used to operate the refrigeration system at an increased gascooler pressure. The additional power is defined by the difference between the power during operation at the optimal pressure according to the ambient conditions $\dot{W}_{T_{amb,opt}}$ and the power during operation at an increased gascooler pressure \dot{W}_{comp} while maintaining a constant cooling load.

$$COP_{HS,CO_2} = \frac{\dot{Q}_{dHX}}{\dot{W}_{comp} - \dot{W}_{T_{amb,opt}}} \quad (1)$$

The trends for the additional power, the additional heat rate and the COP will be studied, and a compromise will be chosen as the reference mode for the comparisons.

2.1.2. Supply of excess heat using a cascade heat pump

The heat that is rejected to the environment because it is below the minimum supply temperature can alternatively be used as a heat source for a cascade heat pump, which supplies the district heating network, too. Figure 1 b) shows the system layout and Table 1 summarizes the assumptions for modelling the cascade heat pump.

Utilizing a cascade heat pump enables choosing the gascooler pressure of refrigeration system independently of the ambient conditions. A parameter variation of the gascooler pressure showed that the system performance is optimal for subcritical heat rejection at a condensation pressure of 70 bar, corresponding to a temperature of 28.7 °C. At this operation, the compressor discharge temperature was just high enough to enable direct heat supply.

The coefficient of performance for heat supply in the cascade heat pump scenario $COP_{HS,HP}$ was defined by the ratio of the accumulated supplied heat rate over the power that is additionally invested compared to standard operation for supply of cooling. The supplied heat includes both the heat flow supplied by the cascade heat pump \dot{Q}_{HP} and the direct heat exchange \dot{Q}_{dHX} . The total power is composed by the compressor power of the heat pump \dot{W}_{HP} and the additional power spent in the refrigeration system to operate at a condensation pressure of 70 bar instead of the optimal condensation pressure corresponding to the ambient temperature ($\dot{W}_{pcond=70\text{ bar}} - \dot{W}_{T_{amb,opt}}$).

$$COP_{HS,HP} = \frac{\dot{Q}_{HP} + \dot{Q}_{dHX}}{\dot{W}_{HP} + (\dot{W}_{pcond=70\text{ bar}} - \dot{W}_{T_{amb,opt}})} \quad (2)$$

2.2. Optimization of the cascade heat pump working fluid

This study assumed that the heat supply is realized in a heat exchanger heating the DH stream from 45 ° to 70 °C while respecting a pinch difference of 5 K. This means that the source inlet stream to the evaporator of the cascade heat pump enters at 50 °C, is cooled down to the condensation temperature of approximately 29 °C and condenses at a constant temperature. This temperature profile is nonlinear and it is expected, that a certain mismatch compared to the temperature profile of the cascade heat pump working fluid that evaporates at a constant temperature occurs.

The authors have shown in previous studies that utilizing mixtures constitutes a promising approach to match the temperature profile of the working fluid during evaporation and condensation to the temperature profile of heat sink and source, [5,21,22]. This approach enabled reducing the irreversibilities during heat transfer and thereby improving the performance. The previous studies focused on selecting the working fluid for boundary conditions in which the heat source and sink had a linear temperature glide, while the temperature profile of CO₂ is expected to be nonlinear.

A working fluid screening was conducted as described in [5,21,22]. The model for the cascade heat pump was therefore evaluated for several mixtures, considering all possible binary mixtures of a list of fluids including 14 natural fluids and 4 hydrofluoroolefins (HFOs). The results were analyzed with respect to the thermodynamic performance and to indicators of the investment, such as the volumetric heating capacity VHC or the pressure levels.

2.3. Economic Evaluation

The economic performance is evaluated according to the Danish boundary conditions. The production of district heating with a heat pump includes two key taxes in Denmark. Firstly, there is the excess heat tax which concerns the utilization of any excess heat related to process equipment. It is implemented to counteract tax exemptions that are given to the production of goods by companies. For heat pumps, only the amount of heat produced above a COP of 3 is taxed, and the taxation is 25 % of the heat sale, up to a maximum of 7.40 €/GJ.

$$\text{Excess Heat Tax} = 25 \% \cdot \left(\frac{COP_h - 3}{COP_h} \right) \cdot \text{Heat Sales} \quad (3)$$

The second taxation of interest is the electricity to heat tax. Whenever electricity is used to produce DH there is a surplus tax compared to when electricity is used for process equipment. This will however be reduced in 2020 [23], and the Public Service Obligations (PSO) which are currently imposed on all electricity will also be removed. Together these contributions will drop the current electricity price from ~134 €/MWh to ~94 €/MWh. Heat prices vary a lot

both with regards to geography and season, from the low end which is 27 €/MWh to the gas substitution price of up to about 60 €/MWh, at specific places even higher.

In order to estimate the investment of the cascade heat pump, a specific investment cost per unit of supplied heat of 671 €/kW is assumed [24]. The value of 671 €/kW was related to the construction of industrial heat pumps, which imply a relatively high cost due to case specific engineering and manufacturing. It is assumed that the development of a standard unit could reduce the cost for manufacturing and on-site integration to 400 €/kW, as it can be observed for domestic heat pumps [25]. Estimating the investment cost when using mixtures appears to be more difficult due to the lack of practical experiences with the construction and operation of heat pumps using zeotropic mixtures. Previous studies, [5,22], suggest initial investment costs of competitive solutions using mixtures, comparable to the investment costs for heat pumps using pure fluids or up to 100 % higher. The studies outline the strong dependency on the specific cases. It may furthermore be noted, that the above-mentioned costs included both the cost for acquisition and integration of the heat pump, while the heat pump using mixtures requires the same cost for the integration. For a simplified assessment of the economic performance of a modular cascade heat pump unit, specific investment costs per unit of supplied heat of 600 €/kW were assumed. The cost for connecting the refrigeration system directly to the DH network were estimated with 17,000 €, based on a realized project and neglecting the influence of the capacity. The connection cost for the cascade heat pump solutions are assumed to be included in the above-mentioned estimates. The analysis included furthermore a maintenance cost per unit of supplied heat of 1.60 €/MWh for all scenarios using a cascade heat pump.

The solutions were compared based on the total annual cash flow, which includes the income from the heat sales, all costs for electricity and taxes as well as the levelized investment cost. The comparison was based on a capital recovery factor of 0.08, assuming a lifetime of 20 years and an effective interest rate of 5 %. Lastly, a simple payback time for the investment was calculated by relating the annual net income of each solution to its initial investment cost.

3. Results

3.1. Thermodynamic comparison of heat supply technologies

The first option for supplying heat to a DH network was to operate the supermarket refrigeration system with an increased gascooler pressure to use part of the heat from desuperheating for heating the DH stream from 45 °C to 70 °C, while the remaining part of the heat is rejected to the environment. The results from e.g. [15] have shown the nonlinear dependency between the pressure increase and the additionally recoverable heat and indicated the existence of an optimal COP with respect to heat supply performance.

The first part of the analysis consisted therefore of an analysis of the performance for supplying heat for different gascooler pressures while taking different ambient conditions as reference scenario. Figure 2 shows the trends for the different energy flows and the performance for supplying heat COP_{HS} for the ambient conditions for a) summer, b) autumn/spring and c) winter.

The optimal pressure during normal operation for supply of cooling is defined by the saturation pressures of the gascooler outlet temperature that is determined by the ambient temperature and the assumed pinch point temperature difference. The optimal gascooler pressure for refrigeration operation is 45 bar during winter, 50 bar during autumn/spring and 64 bar during summer. The amount of power required to lift the pressure increases steadily, while the heat flow rates show discontinuities. The heat flows show that the pressure has to be increased up to 80 bar during winter, up to 78 bar during autumn/spring and up to 68 bar during summer to obtain sufficiently high compressor discharge temperatures, enabling direct heat transfer to the network. The absolute pressures that enable heat supply varied depending on the season, due to the different superheating from the internal heat exchanger.

The amount of power that needs to be additionally invested to reach the point at which the direct heat supply is possible, when assuming the optimal operation for supply of cooling as a reference point, is significantly larger during winter and autumn/spring than during summer. The amount of heat that is supplied in the case of just high enough temperatures is in all cases around 33 kW for an average cooling capacity of 100 kW. This yields high COP_{HS} during summer, mainly due to the small amount of additionally required power for the relatively small pressure increase. For the cases of autumn/spring and winter, it may be noted that the COP_{HS} are lower, due to the lower reference pressure of optimal operation for cooling supply.

Increasing the gascooler pressure further, yields an increase of both the amount of supplied heat and the COP before the COP_{HS} shows an optimum around 120 bar for autumn/spring and winter conditions. The amount of supplied heat can be increased even further with higher pressures, while the performance decreases. Under summer conditions, the trend looks different. Above the point at which heat recovery is possible, the performance is high and drops significantly with an increasing pressure, while reaching a plateau between 90 bar and 110 bar, while the amount of supplied heat increases.

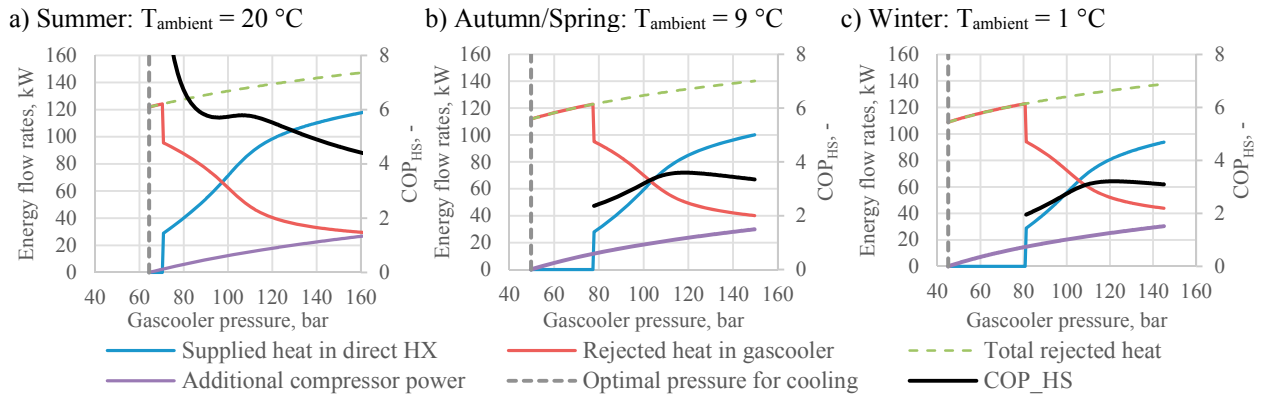


Figure 2: Comparison of the additional power in the refrigeration system ($\dot{W}_{comp} - \dot{W}_{Tamb,opt}$) and the heat flows rejected to environment in the gascooler and to the DH in the direct heat exchanger for a cooling capacity of 100 kW

Table 2: Performance of different scenarios at different boundary conditions for a cooling load of 100 kW

	Operating the refrigeration system at increased pressure			Cascade Heat Pump		
	Summer	Autumn/Spring	Winter	Summer	Autumn/Spring	Winter
$T_{ambient}$	20.0 °C	9.0 °C	1.0 °C	20.0 °C	9.0 °C	1.0 °C
CO₂ refrigeration system:						
$T_{gascooler,exit}$	25.0 °C	14.0 °C	10.0 °C	28.7 °C	28.7 °C	28.7 °C
Optimal gascooler pressure for cooling:	64.3 bar	50.0 bar	45 bar	64.3 bar	50.0 bar	45 bar
Design gascooler pressure for heat supply:	105.0 bar	118.6 bar	120.8 bar	70 bar	70 bar	70 bar
Additional power ($\dot{W}_{comp} - \dot{W}_{Tamb,opt}$):	14.1 kW	23.3 kW	25.3 kW	5.1 kW	15.8 kW	18.9 kW
Heat supply in direct HX \dot{Q}_{dHX} :	81.4 kW	83.8 kW	81.2 kW	32.6 kW	32.6 kW	32.6 kW
Cascade heat pump system:						
Compressor power \dot{W}_{HP} :	-	-	-	23.5 kW	23.5 kW	23.5 kW
Heat supply by cascade HP \dot{Q}_{HP} :	-	-	-	116.5 kW	116.5 kW	116.5 kW
COP of cascade heat pump:	-	-	-	4.9	4.9	4.9
Sum of supplied heat:	81.4 kW	83.8 kW	81.2 kW	149.1 kW	149.1 kW	149.1 kW
COP for heat supply COP_{HS}:	5.8	3.6	3.2	5.2	3.8	3.5

The second considered option for supplying heat to a LTDH network consisted of a cascade heat pump that recovers the part of the heat from the CO₂ system, which is rejected at temperatures that are too low for directly supplying the heat. A parameter variation has shown, that the system performance considering both the heating and the cooling of the entire system is maximal, when the gascooler of the CO₂ refrigeration system is operated at 70 bar, corresponding to subcritical conditions.

Table 2 shows a summary of the performance of the two heat supply technologies. The cascade heat pump using Ammonia as a working fluid operates with a COP of 4.9 and supplies 117 kW, while 33 kW are supplied to the DH

network by direct heat exchange. The additional power that is consumed in the refrigeration system to operate at 70 bar is higher during winter. This results in values for the coefficient of performance for heat supply COP_{HS} of 3.5 in winter, 3.8 in autumn/spring and 5.2 at summer conditions. While the cascade heat pump shows COP_{HS} that are higher than the solution supplying the heat directly with an increased gascooler pressure during winter and autumn/spring, the COP_{HS} is lower at summer conditions. The total amount of supplied heat is almost twice as large for the cascade heat pump solution throughout the year.

3.2. Working fluid optimization of cascade heat pump

In the arrangement of the cascade heat pump, the CO_2 stream entered the evaporator at approximately $50\text{ }^\circ\text{C}$ to evaporate the pure working fluid of the cascade heat pump at around $24\text{ }^\circ\text{C}$. The heat transfer among this enlarged temperature difference corresponds to irreversibilities and constitutes the potential improvements that can be obtained by selecting a mixed working fluid that changes the temperature during evaporation and thereby better matches the temperature profile of the CO_2 during heat rejection.

Table 3 shows the selected screening results and includes different pure fluids with a competitive COP, while Ammonia shows the largest volumetric heating capacity VHC, indicating the most compact compressor. The results show furthermore, that the mixtures can achieve COP as high as 5.7, corresponding to an increase of 15 %.

Figure 3 shows the temperature-heat-diagram for the thermodynamic cycle of Ammonia (left) and 90 % DME / 10 % Hexane (right) and the direct heat transfer. The CO_2 stream cools down while heating part of the DH stream, before cooling further down and condensing while heating the working fluid of the heat pump cycle. Ammonia evaporates and condenses at a constant temperature while the mixture changes temperature in the two-phase zone. Due to the good match between the mixed working fluid of the cascade heat pump and the heat source and sink, the irreversibilities during heat transfer are decreased and the overall performance is improved.

Table 3: Performance of different pure and mixed working fluids for the cascade heat pump

Working Fluid	COP	VHC
	-	kJ/m^3
Propane	4.79	6,519
DME	4.96	4,923
Butane	4.92	2,179
R-1234ze(E)	4.84	4,097
Ammonia	4.93	9,454
90 % DME / 10 % Hexane	5.68	4,186
80 % DME / 20 % DEE	5.48	3,831
10 % Hexane / 90 % R-1234ze(Z)	5.65	1,327

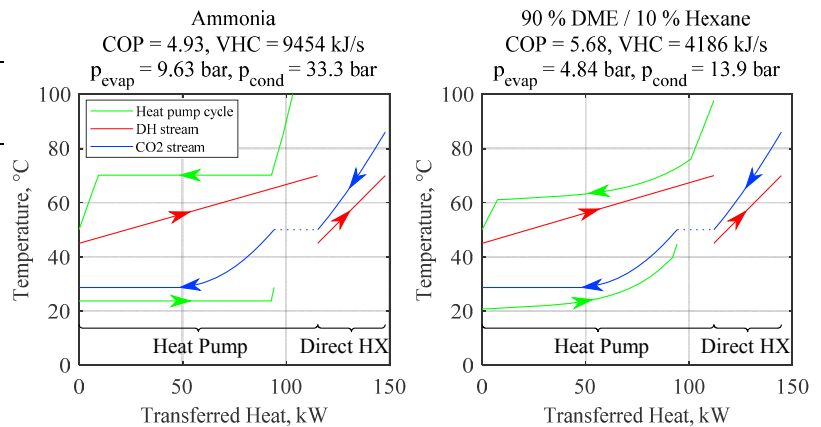


Figure 3: Temperature heat diagram of cascade heat pump working with Ammonia (left) and 90 % DME / 10 % Hexane (right) incl. direct HX

The cascade heat pump using the pure working fluid ammonia consumed 23.5 kW of electrical power for supplying 116.5 kW to the DH network, which corresponds to a COP of 4.93. Utilizing the mixture of 90 % DME / 10 % Hexane, the required power can be reduced to 19.7 kW while supplying 112.0 kW of heat, corresponding to a COP of 5.68.

3.3. Economic evaluation of heat supply technologies

An economic comparison for the case of a refrigeration unit with an average cooling capacity of 100 kW is shown in Figure 4. The approach to operate the CO_2 refrigeration system at an increased gascooler pressure is compared to investing in a cascade heat pump that will work at a higher COP and be able to deliver more heat. The total annual cash flows include the operating cost, the income from the heat sales and the levelized investment cost and correspond

to the annual surplus. The annual cash flows of the options using the cascade heat pump exceed the cash flows for the option to operate the refrigeration system at an increased gascooler pressure for heat prices above 35 €/MWh. The total annual cash flows of the different cascade heat pump solutions are relatively similar. The Danish excess heat taxation impacts the mixture heat pump negatively as the tax per supplied MWh is highest, when delivered at a higher COP. The taxes on the heat sales account for 12 % of the heat sales for the heat pump using a mixture, while accounting for 9 % for the other solutions with a lower COP. The total electricity cost includes 22 % of taxes for all solutions.

The investment cost of the ammonia heat pump was firstly estimated based on the specific cost per supplied heating capacity of 671 €/kW as specified in section 2.3, and the heat pump sizing in Table 2, which results in a total investment of 78,000 €. Considering the development of a modular standard unit, a decrease in manufacturing cost, as well as in cost for installation can be expected. Assuming that the specific investment cost per unit supplied heat can be decreased to 400 €/kW yields an investment of 46,600 €. Assuming a lifetime of 20 years and an effective interest rate of 5 %, the investment costs correspond to an annual cash flow of 6,260 €/year and 3,740 €/year, respectively. Assuming a specific investment cost of 600 €/kW for a standard unit using the mixture 90 % DME / 10 % Hexane, the total investment is expected to be 67,200 €, corresponding to an annual cash flow of 5,390 €/year. The investment for the establishment of the DH substation for the case in which the refrigeration system is directly connected to the DH network was estimated with 17,000 €, corresponding to an annual cash flow of 1,360 €/year.

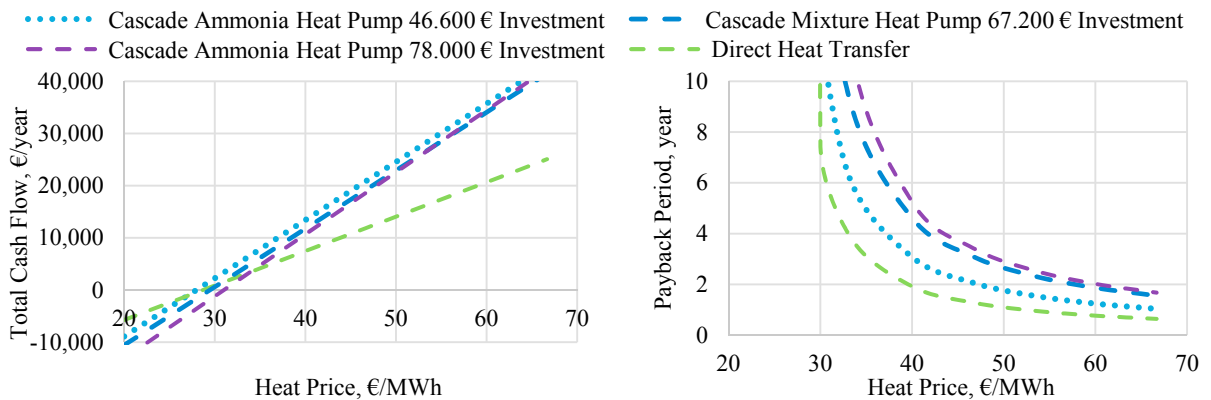


Figure 4: Comparison of total cash flows (left) and simple payback time (right) for the different heat supply technologies

A simple payback period was calculated comparing the investment cost for each solution to its annual income. The second diagram of Figure 4 shows that the lowest payback periods are obtained for the solution in which the heat is directly transferred from the refrigeration system. The payback times for this solution drop below 4 years for 33 €/MWh and reach values below 2 years for heat prices above 40 €/MWh. The solutions using a cascade heat pump show longer payback periods while the standard unit using Ammonia approaches the payback periods of the direct heat recovery. Other performance indicators that account for the entire life time, such as the heat generation cost or the net present value indicate a higher profitability of the cascade heat pump solutions, which is consistent with the findings from [5,22]. The estimation of the investment cost for the establishment of the DH connection implied uncertainties, which have the largest impact on the solution with the direct heat supply from the refrigeration system.

4. Discussion

Both of the presented solutions imply advantages and disadvantages and the considerations as well as uncertainties. The cascade system has shown different beneficial effects, such as the supply of heat to the DH network, the potential to flexibly consume electricity and to improve the performance of the refrigeration system. It may therefore be concluded that such a setup makes sense from a socioeconomic perspective, while the distribution of the benefits to different parties raises difficulties for viable business models. It could be possible, that either the utility company owns and operates the cascade heat pump and is compensated for providing access to a heat sink for the refrigeration system by the supermarket or the supermarket owns the cascade heat pump and sells the heat to the DH network.

In order to conclude further an evaluation of the possibilities to use supermarkets as heat source for DH networks from a socioeconomic point, a comparison to a conventional operation of the DH network and the supermarket refrigeration system would have to be conducted. A central heat pump using the ambient as a heat source has to cover a slightly larger temperature difference but might have better efficiencies due to larger capacities.

It may furthermore be noted, that the external preconditions for acting as a heat supplier are more beneficial during the winter time. During summer, the heat demand and district heating forward temperature requirements are generally lower and the availability of alternative competing heat sources is higher, which may result in lower feed-in tariffs for heat supply to DH networks. Nevertheless, the amount of heat that a supermarket could offer is larger during summer, due to an increased on-site heat demand during the winter period, which generally should be prioritized. Considering these two contradicting effects, a decreased economic potential may be expected. Considering the on-site requirements for heating would generally result in a decreased amount of heat that can be supplied to DH. Since the on-site heat demands are site specific, the impact of this aspect has to be analyzed for specific case studies. The promising performance of the cascade heat pump indicates however, that this solution might be as well promising for covering the on-site heating demands of the supermarket.

The analysis assumed an average cooling demand of the refrigeration system, both during the day and throughout the year. Adding an additional evaporator at the accumulator would enable using the compressors independently of the cooling demand and enable a continuous heat supply. Especially systems equipped with parallel compression would benefit from installing additional evaporators, due to increase utilization of the equipment [17].

5. Conclusions

The study analyzed two different possibilities to recover excess heat from CO₂ refrigeration units from supermarkets for supply of LTDH networks. The two analyzed approaches were either operating the refrigeration system at an increased gascooler pressure to directly transfer the heat or installing a cascade heat pump that recovers the heat that is rejected at temperatures being too low for recovering it directly. It was furthermore studied if it is thermodynamically and economically viable to employ a zeotropic working fluid mixture in the cascade heat pump.

The results showed that the direct heat transfer appears to be thermodynamically promising during the summer months, when the system operates at already high gascooler pressures and the required power to reach the point of operation that enables heat recovery is low. At autumn/spring and winter periods, the cascade heat pump solution showed higher thermodynamic performances. The optimization of the working fluid of the cascade heat pump showed, that a mixture of 90 % DME / 10 % Hexane is expected to yield a COP that is 15 % higher than for using Ammonia. The cascade heat pump could supply more heat at an increased performance during winter and autumn/spring and the economic evaluation showed that the increased incomes could compensate the additional investment, when considering the entire lifetime of the investment. The direct heat supply solution showed the lowest payback times, while the additional investment for the mixture did not cause much longer payback times.

The economic analysis furthermore showed that the recovery of excess heat appears to be an economically viable solution, while the cascade heat pump is more promising for DH prices above 35 €/MWh to 40 €/MWh. The payback periods for the cascade heat pump reached values below 4 years at a DH price of 37 €/MWh under the assumption that a standard unit with low specific investment cost could be produced. Based on the economic analysis it may be concluded that the presented solutions could become economically promising if the required equipment can be supplied as cost efficient standard units.

Acknowledgements

This research project was funded by The Danish Council for Strategic Research in Sustainable Energy and Environment, under the project title: “THERMCYC -- Advanced thermodynamic cycles utilising low-temperature heat sources”.

References

- [1] Lund H, Werner S, Wiltshire R, Svendsen S, Thorsen JE, Hvelplund F, et al. 4th Generation District Heating (4GDH). Integrating

- smart thermal grids into future sustainable energy systems. *Energy* 2014;68:1–11. doi:10.1016/j.energy.2014.02.089.
- [2] Ommen T, Markussen WB, Elmegaard B. Lowering district heating temperatures - Impact to system performance in current and future Danish energy scenarios. *Energy* 2016;94:273–91. doi:10.1016/j.energy.2015.10.063.
- [3] Ommen T, Eric J, Brix W, Elmegaard B. Performance of ultra low temperature district heating systems with utility plant and booster heat pumps. *Energy* 2017. doi:https://doi.org/10.1016/j.energy.2017.05.165.
- [4] Köfinger M, Basciotti D, Schmidt RR, Meissner E, Doczekal C, Giovannini A. Low temperature district heating in Austria: Energetic, ecologic and economic comparison of four case studies. *Energy* 2016. doi:10.1016/j.energy.2015.12.103.
- [5] Zühlsdorf B, Meesenburg W, Ommen TS, Thorsen JE, Markussen WB, Elmegaard B. Improving the performance of booster heat pumps using zeotropic mixtures. *Energy* 2018;154:390–402. doi:https://doi.org/10.1016/j.energy.2018.04.137.
- [6] Bühler F, Petrović S, Karlsson K, Elmegaard B. Industrial excess heat for district heating in Denmark. *Appl Energy* 2017;205:991–1001. doi:10.1016/j.apenergy.2017.08.032.
- [7] Bühler F, Petrović S, Holm FM, Karlsson K, Elmegaard B. Spatiotemporal and economic analysis of industrial excess heat as a resource for district heating. *Energy* 2018;151:715–28. doi:10.1016/j.energy.2018.03.059.
- [8] Bühler F, Petrović S, Ommen T, Holm F, Pieper H, Elmegaard B. Identification and Evaluation of Cases for Excess Heat Utilisation Using GIS. *Energies* 2018;11:762. doi:10.3390/en11040762.
- [9] Lund R, Persson U. Mapping of potential heat sources for heat pumps for district heating in Denmark. *Energy* 2016;110:129–38. doi:10.1016/j.energy.2015.12.127.
- [10] Gullo P, Hafner A, Cortella G. Multi-ejector R744 booster refrigerating plant and air conditioning system integration - A theoretical evaluation of energy benefits for supermarket applications. *Int J Refrig* 2017;75:164–76. doi:10.1016/j.ijrefrig.2016.12.009.
- [11] Pardiñas Á, Hafner A, Banasiak K. Novel integrated CO₂vapour compression racks for supermarkets. Thermodynamic analysis of possible system configurations and influence of operational conditions. *Appl Therm Eng* 2018;131:1008–25. doi:10.1016/j.applthermaleng.2017.12.015.
- [12] Hafner A, Försterling S, Banasiak K. Multi-ejector concept for R-744 supermarket refrigeration. *Int J Refrig* 2014;43:1–13. doi:10.1016/j.ijrefrig.2013.10.015.
- [13] Arias J, Lundqvist P. Heat recovery and floating condensing in supermarkets. *Energy Build* 2006;38:73–81. doi:10.1016/j.enbuild.2005.05.003.
- [14] Kauko H, Kvalsvik KH, Hafner A. How to build a new eco-friendly supermarket - Report 3 - SUPERSMART 2016. <http://www.supersmart-supermarket.info/> (accessed May 22, 2018).
- [15] Nöding M, Fidorra N, Gräber M, Köhler J. Operation Strategy for Heat Recovery of Transcritical CO₂ Refrigeration Systems with Heat Storages. *Proc. ECOS 2016, Portoroz, Slovenia: 2016*.
- [16] Sawalha S. Investigation of heat recovery in CO₂trans-critical solution for supermarket refrigeration. *Int J Refrig* 2013;36:145–56. doi:10.1016/j.ijrefrig.2012.10.020.
- [17] Funder-Kristensen T, Finn L, Larsen S, Thorsen JE. Integration of the hidden refrigeration capacity as heat pump in smart energy systems. *12th IEA Heat pump Conf., Rotterdam: 2017, p. 1–10*.
- [18] Adrianto LR, Grandjean P-A, Sawalha S. Heat Recovery from CO₂ Refrigeration System in Supermarkets to District Heating Network. *Proc. 13th IIR Gustav Lorentzen Conf. Nat. Refrig., Valencia: 2018. doi:doi:10.18462/iir.gl.2018.1385*.
- [19] Nekså P. CO₂ heat pump systems. *Int J Refrig* 2002;25:421–7. doi:10.1016/S0140-7007(01)00033-0.
- [20] Klein SA. *Engineering Equation Solver 2017*. <http://fchart.com/>.
- [21] Zühlsdorf B, Jensen JK, Cignitti S, Madsen C, Elmegaard B. Analysis of temperature glide matching of heat pumps with zeotropic working fluid mixtures for different temperature glides. *Energy* 2018;153:650–60. doi:https://doi.org/10.1016/j.energy.2018.04.048.
- [22] Zühlsdorf B, Bühler F, Mancini R, Cignitti S, Elmegaard B. High Temperature Heat Pump Integration using Zeotropic Working Fluids for Spray Drying Facilities. *12th IEA Heat pump Conf., Rotterdam: 2017, p. 1–11*.
- [23] Regeringen - Energi Forsynings- og Klimaministeriet. *Energi - til et grønt Danmark 2018*. http://efkm.dk/media/11873/energiudspil_2018.pdf (accessed May 29, 2018).
- [24] Danish Energy Agency, Energinet. *Technology Data for Energy Plants for Electricity and District heating generation 2018*. <https://ens.dk/en/our-services/projections-and-models/technology-data> (accessed June 7, 2018).
- [25] Danish Energy Agency, Energinet. *Technology Data for Individual Heating Installations 2018*. <https://ens.dk/en/our-services/projections-and-models/technology-data> (accessed July 11, 2018).



16th International Symposium on District Heating and Cooling, DHC2018,
9–12 September 2018, Hamburg, Germany

Techno-economic Analysis Of Integrated Energy Systems At Urban District Level – A Swedish Case Study

Monica Arnaudo^{a*}, Osama Ali Zaalouk^b, Monika Topel^a, Björn Laumert^a

^aRoyal Institute of Technology, Brinellvägen 68, Stockholm 11428, Sweden

^bEurope Power Solutions, Brinellvägen 68, Stockholm 11428, Sweden

Abstract

Within the Nordic countries, distributed heat and power supply technologies, like domestic scale heat pumps and photovoltaics, are challenging the current centralized district energy infrastructure. An increasing number of customers decide to disconnect from the traditional heating network by comparing the bill to the potential economic savings which can be generated by a residential heat pump system. However, this approach can be considered valid only on a short-term perspective. This paper presents a new approach to compare the techno-economic performance of alternative technologies, based on their lifetime average cost of generation. The proposed analysis is able to determine the optimal energy infrastructure at urban district level. Within this solution, operators, city planners and users will have a solid reference for their decision making process on resources investment. From a first step analysis of a few Swedish case studies, it was found that a district heating based system is more techno-economically efficient compared to the distributed alternative. By comparing the district heating production cost to its final price, a significant profit margin for the utility was qualitatively highlighted. Thus, from a customer perspective, on the medium run, the district heating tariff can be adapted and the estimated savings from switching to a residential heat pump system can be nullified.

© 2018 The Authors. Published by Elsevier Ltd.

This is an open access article under the CC BY-NC-ND license (<https://creativecommons.org/licenses/by-nc-nd/4.0/>)

Selection and peer-review under responsibility of the scientific committee of the 16th International Symposium on District Heating and Cooling, DHC2018.

Keywords: district heating, heat pumps, leveled cost of energy, distributed generation

* Monica Arnaudo. Tel.: +46-762964027

E-mail address: monica.arnaudo@energy.kth.se

1. Introduction

Two major trends are shaping the current energy transition, namely the increasing share of renewables and the increasing penetration of distributed supply technologies. Within the Nordic Countries, hydro- and wind-power based solutions are predicted to dominate the power supply mix by 2050 [1]. While being beneficial to the environment, this phenomenon is affecting the stability of the energy system by raising the levels of unpredictability and variability of the power supply. Distributed technologies, like domestic scale heat pumps (dsHPs) and photovoltaics (PV), come both as part of the renewables complexity but also as one of the potential solutions to the power fluctuation issue.

At the same time, centralized technologies are also re-evaluated as cost-efficient solutions for providing flexibility to the supply-demand balancing process. By linking the heat and the electricity sectors, cogeneration plants for district heating (DH) networks are analyzed as competitors with respect to the distributed dsHPs option [2]. Briefly, DH is considered as a centralized system where one or multiple generation units provide heat to a water network reaching each customer through a substation [3]. A heat pump (HP) is a system able to bring heat from a relatively low-temperature resource (the ground for instance) to a higher temperature one (the heating circuit of a building) [4]. Given this framework, the main question relates to which system configuration would be the most beneficial in terms of technical, environmental and economic impact. A second related question would be which indicators should be used in order to quantify and compare the benefit itself.

When planning the energy infrastructure of a new urban area, previous literature exists comparing DH and dsHPs. The Danish community is intensively working for assessing the future potential of DH. In [5] and [6] the latter is compared to different alternatives, among which dsHPs, in terms of fuel demand, CO₂ emissions and absolute costs. Differently from the present work, a national level perspective is adopted and the cost estimation is referenced to a specific year. The study performed by [7] also discounts the cost analysis to one year. The focus is on low-heat demand buildings and the distributed options are considered as a single category with no technology differentiation. The techno-economic comparison study in [8] is performed with respect to the DH price tariff proposed by the operator, which, according to the authors of this work, prevents a fair determination of the optimal system infrastructure. Within the Swedish context, techno-economic estimations are reported in [12] and [13]. The objective is to develop a new DH tariff model based on the heat generation cost. The DH tariff is considered also in the report provided by [14].

Within the present work, four main types of approaches are collected and briefly analyzed. From the comparison among a techno-economic analysis, a thermo-economic analysis, an equivalent coefficient of performance estimation and a primary energy factor calculation, the first option is selected as the most relevant approach for the objective of the study. Furthermore, in order to investigate the environmental impact, a carbon emission factor is included as well. The overall approach is applied to the techno-economic performance comparison between an energy infrastructure based on a DH technology and an alternative solution based on distributed dsHPs. Two neighborhoods within the Stockholm area are used as reference real cases in terms of design and data: Hammarby Sjöstad (HS) and the aggregation of Högdalen, Farsta and Alvsjö (HFA). The average cost of heat generation is estimated for different scenarios based on centralized and distributed technologies over their economic lifetime. The real cost of generation is highlighted and proposed as an indicator for planning new energy infrastructures. By excluding the DH utility profit from the comparison and by considering the discounted average cost over the lifetime, the present study aims at proposing a new approach for assessing the optimal configuration of an energy system at urban district level. City planners, operators and policy makers can thus direct their resources towards an optimal techno-economic infrastructure. Users can embrace a better understanding of the energy cost structure and thus plan their choices on a longer-term scenario.

2. Methodology

This section first discusses the performance indicators, which are selected in order to answer the questions proposed within this study. The main scenarios for the performance comparison are presented in paragraph 2.2. The different case studies are detailed through both technical and economic parameters. Finally, in paragraph 2.5, the simulation models for the techno-economic analysis are introduced.

2.1. Performance indicators

Four main types of approaches to estimate performance indicators for energy systems are here highlighted:

- Techno-economic analysis (TcEA)
- Thermo-economic analysis (TrEA)
- Coefficient of performance estimation (CP)
- Primary energy factor estimation (PEF)

In order to specifically compare the performance of DH to dsHPs, a thermodynamic CP approach is proposed in [3]. Concerning the DH system, the analysis focuses on a cogeneration plant as supply unit. The latter can be interpreted as a virtual HP, as described in [15]. The coefficient of performance (COP) of the virtual power plant is defined as the inverse of the specific electrical power loss and it can be compared to the conventional COP of HPs. Reference [3] proposes an additional option where dsHPs and cogeneration-DH can be implemented as a hybrid system. Besides a growing interest at industrial level, the CP analysis is still scarcely used and documented. In addition, the complexity to adapt the virtual COP calculation to different technologies is not negligible.

At European level, the PEF approach is discussed as a method to assess the competitiveness of energy systems [16]. For instance, reference [17] draws conclusions on the comparison between dsHPs and alternative technologies, including DH, in terms of their long term sustainability. However, the PEF method is influenced by strong country based assumptions. The Swedish context, in particular, is not currently making use of this method ([18][19]).

The CP and PEF approaches do not include cost estimations. This is the main reason for assigning to them a lower level of priority within a context where the decision making process is strongly linked to economic assessments.

The TrEA is an alternative approach for assessing the competitiveness of an energy supply system. Different types of energy can be considered more valuable than others depending on the capacity to reverse the process, which has led to their transformation. A cost can be associated to the latter, so that different heat and power supply technologies can be compared in terms of energy quality (exergy) [20]. Within a TrEA rules and assumptions are introduced in order to estimate both the irreversibility and the economic cost which are generated during an energy input-output process [21]. References [22]–[24] use exergy and TrEA to optimize DH systems when compared to alternative technologies at user level. The main drawback of the TrEA is related to its complexity, which compromises its acceptance at industry and sometimes even academic level.

The TcEA approach is usually based on the estimation of the Levelized Cost of Energy (LCOE) [25]. The latter is a widely used figure for estimating the average cost of electric power generation over the lifetime of power plants [25]. This indicator is quite well documented and brings to transparent results, which can be explained by a clear statement of the assumptions. Furthermore, the LCOE can be applied to several types of technologies and it can be handled in complexity by including different levels of details. Thus, the TcEA appears to be an effective choice for the approach adopted within this study. When the heat generation is considered, the Levelized Cost of Heat (LCOH) is calculated [12]. The formula (1) is applied to each selected technology:

$$LCOH = \frac{\sum_{t=1}^n [(CAPEX_t + OPEX_t + Fuel_t) * (1+r)^{-t}]}{\sum_{t=1}^n Q_{th} * (1+r)^{-t}} \quad (1)$$

The investment (CAPEX), operation and maintenance (OPEX) and fuel costs are estimated on an annual basis through the economic lifetime n of the technologies. These costs are averaged on the corresponding heat generation Q_{th} . The discount rate r is assumed as a constant parameter. When different technologies are combined within the same system, the overall LCOH should be calculated as the weighted sum based on the contribution of each option.

As environmental indicator, the CO₂ emissions associated with the fuels are estimated by using pre-calculated emission factors [26]–[28]. When it comes to the electricity supply mix, the Swedish context is used as a reference. In Table 1, the emission factors included in this study are shown. The described performance indicators are estimated considering new urban areas to be built from green field. The link to already existing neighborhoods is exclusively used in terms of scale and reference data.

Table 1. Emission factors for different types of fuels

Fuel	Unit	CO ₂ factor
Waste	gr/kWh	100
Biomass	gr/kWh	17
Oil	gr/kWh	274
Electricity	gr/kWh	46

2.2. Scenarios definition

A scenario is here introduced as a set of parameters defining a specific case study. Different scenarios are based on three design categories: technology for heat generation and distribution, heating load scale (community size) and fuels.

Figure 1 shows two case studies, which are characterized by different technologies for the heat generation and distribution. The electricity grid is represented as well because of the interaction with the heat carrier due to the chosen technologies. Notice that in case A only the heat supply pipes are illustrated. The buildings are residential multi-apartments. The number of units is conceptually reduced to four for the sake of clarity.

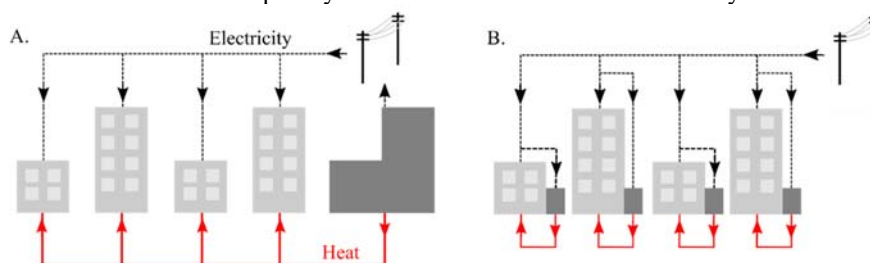


Figure 1. District heating (A) and domestic scale HP (B)

The infrastructure of case A is a DH network with a single supply unit. In this specific representation, a cogeneration plant is considered. As a first sub-case, the latter can be fueled by waste or by biomass. These two resources bring to contrasting result in terms of costs and environmental impact (see section 3). In both sub-cases, oil boilers, flue gas condensation and a hot water tank storage are integrated respectively to cover peak demand, pre-heating and off-design conditions. The technology of large scale HPs (lsHPs) is used as an alternative option within case A. Thus, electricity becomes the relevant fuel in terms of annual costs and environmental emissions. Within this study, the main source for the lsHP is sewage water recovered by a waste water treatment plant. Two real plants are used as reference in terms of design: Högdalenverket for the cogeneration plants and Hammarbyverket for the lsHPs ([29], [30]). Case B of Figure 1 represents the scenario where the same neighborhood of case A is heated through dsHPs distributed at building level. A further sub-set of cases is developed by considering two different community sizes. HS is ranked within the small-scale level with a design peak heat load of about 50 MW. In order to highlight the economy of scale of the selected technologies, the aggregation of the three Swedish neighborhoods of HFA is analyzed across the previously described scenarios. The design peak heat load for HFA is around 400 MW.

A sum up of the case studies, with reference to the size of HS, is reported in Table 2. The set of cases for HFA is indicated by the number 2 (Case 2a, b, c, d). In all cases, the heat load includes both the space heating and the domestic hot water (DHW) needs at building level. In some cases, two or three buildings are grouped together.

Table 2. Case studies with Hammarby Sjöstad as reference size.

Case	Baseload Technologies	Fuels
1a	DH + cogeneration	Waste
1b	DH + cogeneration	Biomass
1c	DH + lsHPs	Electricity
1d	dsHPs	Electricity

2.3. Technical parameters

The cogeneration plant within the cases 1a, 1b, 2a and 2b is a backpressure technology and it is sized to cover 40% of the peak heat load. The flue gases condensation is integrated in order to preheat the DH water temperature from its actual return value to around 40°C. A pressurized water tank is used to compensate for the off-design conditions. An oil-fueled boiler is sized on the remaining 60% part of the load in order to cover the peaks and the potential unavailability of the thermal storage. The cogeneration plant layout and the main technical design parameters for the HS and HFA cases are shown in Figure 2 and Table 3 respectively. The thermodynamic conditions of the steam cycle are based on data provided by the industrial partners. Within this analysis, the cogeneration plant is considered in continuous operation by covering the heat demand when required and charging the water tank with the excess generation. The DH network is characterized by underground pipes, which reach each building (or group of buildings) through a substation. The latter is of the indirect type with no domestic hot water storage. The emission system inside the apartments is a radiator technology with mean temperature around 45°C. The electrical energy required by the plant itself is subtracted from the production.

The lsHP technology of case 1c and 2c is sized as the cogeneration plant previously described. Within the HFA case, multiple units are combined to cover the design heat capacity. The HP source is the sewage water recovered from a waste water treatment plant located nearby. An average COP of 3.5 is assumed.

A dsHP is designed based on an average reference building extracted from the HS neighborhood. The related peak load is around 140 kW.

Because of this assumption, the final results are to be regarded as an average over the selected community. The HP is of the ground source type with a design heat capacity of 80 kW [31] (around 55% of the peak load). An average COP of 3.2 is assumed [5]. A thermal energy storage (TES) unit is integrated to cover the load within a demand response (DR) program. The TES is a stratified water tank and is equipped with an auxiliary internal electrical coil. An independent electrical heater (EH) is sized to cover the peak load (around 60 kW). The system layout and the main technical design parameters are shown in

Figure 3 and Table 4 respectively.

The emission system is again a radiator technology with mean temperature around 45°C. The DR program is based on a time-of-use tariff. Price-signals are sent to the system, which is set to “off” during peak hours (6-8am, 6-9pm) and to “on” during the rest of the day. The TES unit is designed to balance the operation. An independent electrical heater and a TES integrated electrical coil are included in order to guarantee that the heat demand is covered during the peaks and off-design conditions.

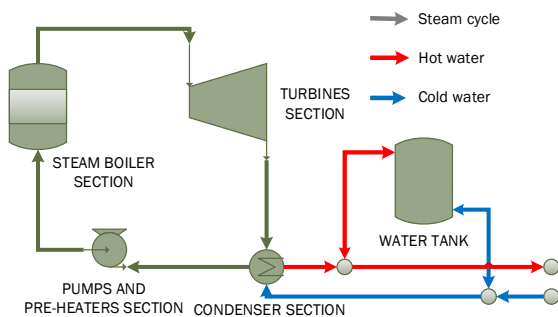


Figure 2. Conceptual layout of a cogeneration plant

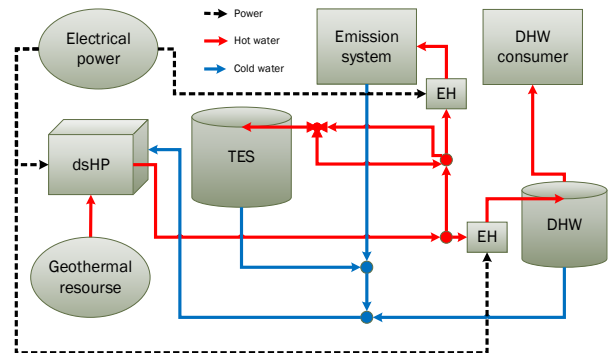


Figure 3. Conceptual layout for a ground source dsHP

Table 3. Main technical design parameters for the cogeneration plant and the DH network for HS and HFA

Design parameters	Units	HS	HFA
Peak heat load	MW	50	400
Cogeneration plant heat capacity	MW	20	175
Steam cycle inlet temperature	°C	520	520
Steam cycle inlet pressure	bar	90	90
Oil boilers overall capacity	MW	30	225
DH supply temperature	°C	70	70
DH return temperature	°C	40	40
DH network pipe length	km	15	120

Table 4. Main technical design parameters for the system of dsHP, TES and backup heaters

Design parameters	Units	HS
Peak heat load	kW	140
dsHP heat capacity	kW	79
dsHP max outlet temperature	°C	70
EH heat capacity	kW	61

2.4. Economic parameters

In order to estimate the LCOH according to equation (1), a literature review and discussions with industrial project partners were carried on. Table 5 and Table 6 report the assumed figures for the main technologies adopted in Case 1a and Case 1-2d. Concerning Table 5, the operation and maintenance costs for the network are extracted from the discussion presented in [3]. These costs are reported as percentage of the capital investment.

Table 5. Economic input parameters for a 50MW waste fuelled cogeneration plant and the corresponding DH network

Design parameters	Units	Waste cog.-DH	Refs.
r	%	8	[12]
lifetime	years	30	[12]
CAPEX plant	sek/kW	108600	[32]
CAPEX network	sek/m	10319	[33]
OPEX fixed	sek/kW	3140	[32]
OPEX variable	sek/MWh	40	[32]
Fuel (waste)	sek/MWh	-130	[32]

Within this analysis, the cogeneration plant costs are entirely allocated on the heat generation. The net electricity sold to the grid is considered as a revenue at a fixed spot market price of 0.375 sek/kwh [34]. The reference figures for the peak boilers, the water tank and the case studies 1b (biomass-based technology), 1c (1sHP) and 2a-c can be found in the same or similar literature, as reported in Table 5 ([5], [32], [35], [36]). It is important to notice that the specific costs scale down by increasing the capacity range and that the biomass-based technology is overall more expensive than the waste incineration option.

Table 6 shows the figures assumed for the case of a ground source dsHP. The drilling costs are included in the capital investment. From discussions with industrial project partners, the operation and maintenance costs are overall considered negligible and thus dominated by the electricity consumption cost. Since the dsHP is involved in a DR program based on a time-of-use electricity tariff, during off-peak hours the electricity bill cost is assumed to be reduced to half of its actual value.

Table 6. Economic input parameters for a dsHP

Design parameters	Units	dsHP	Refs.
r	%	4	[12]
lifetime	years	15	[14]
CAPEX	sek/kW	14560	[37]
OPEX fixed	-	-	-
OPEX variable	öre/kWh	48	[38]

2.5. Models

The models for the thermal performance simulation of the cogeneration plant, the lsHP and the geothermal dsHP are implemented in the TRNSYS [32] environment. The latter is a software for pseudo-dynamic performance simulation of energy systems. A quite developed library of black-box components is available. In addition, the user is able to integrate missing features when necessary.

A yearly simulation with one-hour time step is considered in all scenarios. The objective is to determine how the pre-heating, base- and peak-load options cover the given load, within each sub-case.

The heat load is extracted from real data as a time series curve. Case 1 refers to a representative multi-apartments residential building within HS. The information is extracted from the user account. The neighborhood performance is the result of a scale up process. Case 2 refers to the aggregated performance of HFA. The information is extracted from data provided by the operator. Because of the Swedish context, the weather related parameters refer to Stockholm in terms of location. All the performance data are historical and are related to year 2016.

As an illustration of the results from the TRNSYS simulations, Case 1a and 1d are here discussed for a reference winter day. No degradation factor is considered over the lifetime.

As it can be seen in Figure 4, the load curve is mainly covered by preheating from the flue gas condensers and by the operation of the steam condenser section of the cogeneration plant. Notice that the curves add on each other. The daily load trend is characterized by two peaks, one in the morning and one in the evening, which are considered to be fully covered by the oil boiler. The performance of the latter is estimated in order to exactly compensate the peaks. The water tank is used to respond to the load changes in terms of mass flow rate imposed by the users' substations. In the specific case of Figure 4, no TES charging is happening. On a yearly basis, the steam condenser section covers around 74% of the total load. Around 17% comes from the boiler, while the remaining part is covered by the flue gas condensation and the water tank.

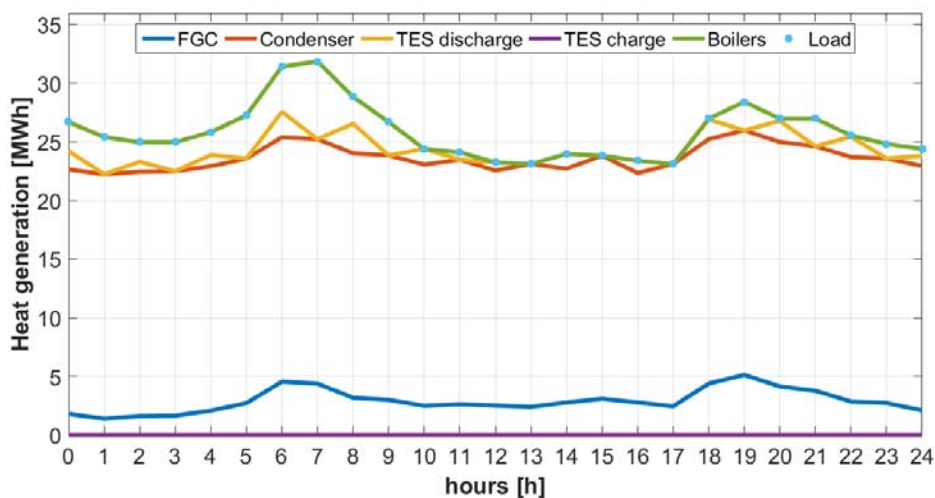


Figure 4. A reference winter day performance for the cogeneration plant of Case 1a

Concerning Case 1d, the daily operation based on the DR program is clearly shown in Figure 5.

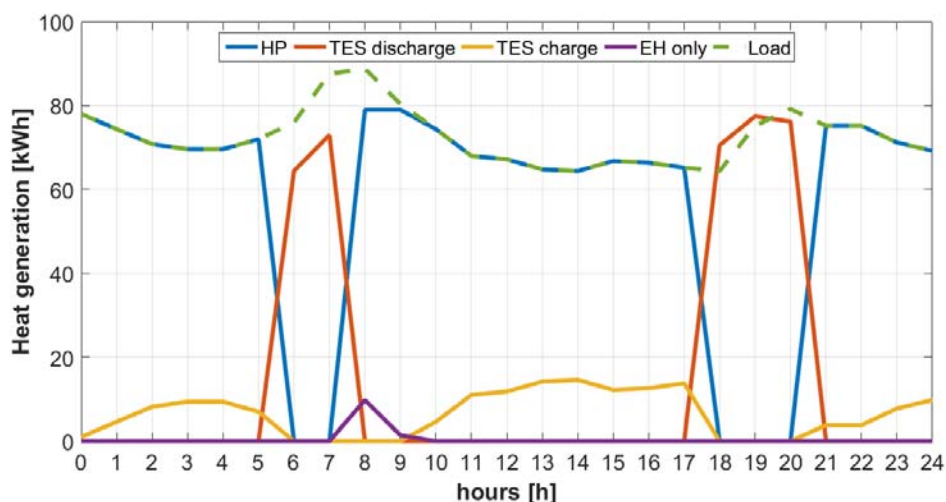


Figure 5. A reference winter day performance for the dsHP of Case 1d

The time-of-use tariff for electricity is imposed by a step function, which sets the dsHP “off” between h6-8 am and h6-9 pm. This is a simplified assumption based on the real possibility to stipulate a contract with variable tariff [39].

The dsHP covers most of the load and can also provide heat to the TES unit for charging. If a peak demand phenomenon occurs outside the set time range, an independent electrical heater is activated. When the HP is forced to the “off” mode, the TES is responsible for covering the load. As it can be noticed, this is not an easy task. Based on the TES state of charge, the unit can sometimes under-perform and sometimes over-perform. This situation might affect the comfort condition for the user. The investigation of the latter is out of the scope of this study. On a yearly basis, the dsHP covers around 74% of the total load. The TES unit contributes as much as around 21%, while the remaining part comes from the electrical heaters.

3. Results and discussions

A sum up of the results for the different scenarios of this study is presented in Table 7 and Table 8 for Case 1 and Case 2 respectively. The estimated figures are to be considered as preliminary values, which indicate a direction of study, namely the comparison of different technologies performance based on their generation cost. The validity of the results is cross checked with the studies presented in [2] and [8] and through discussions with project partners.

Concerning Case 1 (Table 7), it can be observed that a strong contrasting outcome is related to the use of a different fuel for the cogeneration plant feeding the DH network. Waste incineration for heat recovery is considered a convenient process as an alternative solution to its disposal. Therefore, its implementation is economically incentivized. Thus, the operational costs associated with Case 1a are low enough to reduce the final LCOH of about 40% with respect to the biomass-based Case 1b. However, the environmental impact leads to an opposite conclusion concerning the advantages of the two technologies. Overall, the waste incineration option is characterized by a significantly higher carbon emission performance with respect to all the other cases.

Table 7. LCOH and CO₂ results for the HS referenced scenario (Case 1)

Indicators	Units	Case 1a	Case 1b	Case 1c	Case 1d
		DH + waste cog.	DH + bio cog.	DH + lsHPs	dsHPs
LCOH	sek/kWh	0.45	0.62	0.32	0.52
CO ₂	kt	42	15	11	9

Case 1c represents the most interesting solution at a community scale like HS. The main reason is linked to the much lower operating costs compared to the cogeneration plant cases. When DH systems with multiple supply units are considered, these two options are combined in order to profit or save from the variability of electricity prices. Concerning the CO₂ emissions, the Swedish electricity supply mix is characterized by a high share of low or no-carbon emission technologies. This is the reason for the environmental friendly performance of Case 1c and 1d.

When it comes to the LCOH value for Case 1d, it is important to remember that this estimation is made for an average building type, which is assumed as representative for the whole neighborhood. Within this frame and given the assumptions described in Section 2, it can be concluded that the option of distributed dsHP should be in general considered as less techno-economically convenient compared to the DH alternatives. The main reason for this outcome is related to the higher investment cost spread on a shorter economical life of the technology. Furthermore, the cogeneration process brings the opportunity of performing full heat recovery while still profiting from power generation. The option of lsHP is more cost-efficient, given the economy of scale. The introduced type of DR program is not sufficient to justify the choice of a dsHP instead of a DH substation. The only exception, within Case 1, is given by Case 1b which is affected by relatively higher investment and operating costs.

This is a relevant conclusion in the light of comparing the heat production cost of both technologies rather than considering the tariff imposed by the DH operator. The DH final heat price is based on a benchmarking study of the alternative technologies. From the perspective of one or few users, it can be convenient to install a dsHP, thus reducing the heat bill with respect to the current DH tariff. However, on a longer term perspective which includes more users choosing or switching to the alternative technology (dsHP), the DH tariff can change, nullifying the estimated savings. This conclusion assumes that the DH utility has no decisional constraints on the profit margin range, which can be thus reduced to maintain the competitiveness. In the opposite scenario, the alternative technology could take over.

The results of this study are compared to the statistics reported in [14]. Figure 6 shows the generation costs of a DH option compared to the alternative option of geothermal HPs with different levels of interest rates and economic lifetime ranges. The values in Figure 6 include the DH utility profit and the HP connection share, which are not considered in the present study.

Figure 7 shows the results of the LCOH for Case 1 with the costs break-down between capital investment and operation and maintenance. In Case 1a, the incentive on the fuel leads to a reduction of the result (striped texture).

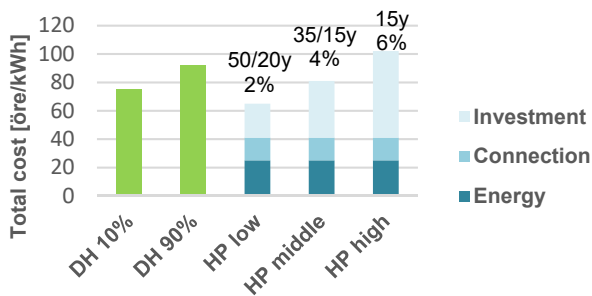


Figure 6. Comparison of generation costs extracted from [14]

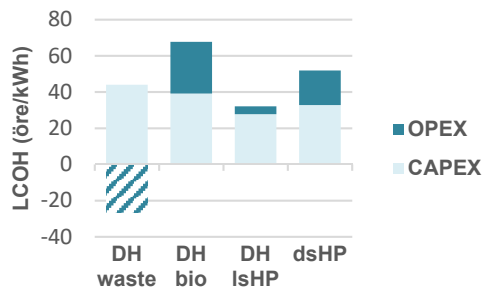


Figure 7. Generation costs from this study for Cases 1a, b, c, d

By comparing Figure 6 and Figure 7, the first outcome is the impact of the profit margin on the DH final heat cost. This observation confirms the previous discussion on the DH tariff composition. The result should be considered as an estimation of order of magnitudes. The precise profit calculation belongs to the business model of the operator. Concerning the HP, it can be noticed that the LCOH value is lower, which is due to two main reasons related to this study. First, the connection costs are not included and, second, the revenues from the DR program are taken into account. Besides these assumptions, the result is considered within the range of validity.

Case 2 refers to the larger scale neighborhood of HFA. The relevance of this scenario is related to the possibility to show the impact of the economy of scale, especially for the DH-based cases. Table 8 shows the results for the second set of case studies within this work.

Table 8. LCOH and CO₂ results for the HFA referenced scenario (Case 2)

Indicators	Units	Case 2a	Case 2b	Case 2c	Case 2d
		DH + waste cog.	DH + bio cog.	DH + IsHPs	dsHPs
LCOH	sek/kWh	0.09	0.35	0.20	0.52
CO ₂	kt	435	158	160	74

When comparing to Case 1, the LCOH value of the waste incineration scenario highlights the strong impact of the economic incentive for this type of fuel. Case 2b benefits more from the scale phenomenon than Case 2c. Thanks to a more efficient allocation of the costs, the DH biomass option gets in line with the other DH cases when compared to the dsHP scenario. Besides the impact of the economy of scale, similar comments as for Case 1 can be applied when dealing with the comparison between a centralized and a distributed energy infrastructure.

4. Conclusion

A techno-economic performance analysis is applied to compare different options of centralized and distributed heat supply technologies. The average cost of heat generation over the lifetime is estimated for three district heating solutions and a distributed domestic scale heat pump option. The same case studies are also scaled-up to highlight the impact of the economy of scale.

The first district heating case is based on a waste incineration technology, which is characterized by significantly lower fuel costs. The second option is a biomass-fueled solution, which is more expensive but brings an advantage in terms of CO₂ emissions. Large-scale heat pumps are used in the third case study, which represents the most interesting scenario at relatively small community scale. The last option is based on distributed domestic scale heat pumps. The results from the techno-economic analysis show that this solution cannot overcome the benefits of a district heating technology. The advantages derived from heat recovery, economy of scale and fuel diversification are even more evident at a larger community size.

Given the discussed boundary conditions and assumptions, the results of this study are considered as a preliminary overview. A direction of research is indicated by proposing future work improvements of the current analysis. For instance, the different proposed cases can be combined with each other to increase the flexibility of the system. A closer look on the user comfort conditions should be included. The heat pump technologies, both at large and domestic scale, should be considered at their full potential by combining the heating and cooling options. Finally, a further optimization of the size of the main technologies would influence the investment costs.

Acknowledgements

The authors would like to thank the industrial and academic partners for the fruitful discussions about district heating networks (Stockholm Exergi), heat pumps (KTH-ETT) and perspective of the customers (ElectricITY).

References

- [1] IEA, "Nordic Energy Technology Perspectives 2016," *Energy Technol. Policy Div.*, no. April, p. 269, 2016.
- [2] S. Werner, "District Heating and Cooling in Sweden," *Energy*, vol. 126, pp. 419–129, 2017.
- [3] S. Frederiksen and S. Werner, *District Heating and Cooling*, First Edit. Lund: Dimograf, 2013.
- [4] Energy Saving Trust, "Domestic Ground Source Heat Pumps: Design and installation of closed-loop systems – A guide for specifiers, their advisors and potential users," p. 22, 2007.
- [5] H. Lund, B. Möller, B. V. Mathiesen, and A. Dyrelund, "The role of district heating in future renewable energy systems," *Energy*, vol. 35, no. 3, pp. 1381–1390, 2010.
- [6] O. Gudmundsson, J. E. Thorsen, and L. Zhang, "Cost analysis of district heating compared to its competing technologies," *WIT Trans. Ecol. Environ.*, vol. 176, pp. 107–118, 2013.
- [7] A. F. Sandvall, E. O. Ahlgren, and T. Ekvall, "Cost-efficiency of urban heating strategies – Modelling scale effects of low-energy building heat supply," *Energy Strateg. Rev.*, vol. 18, pp. 212–223, 2017.

- [8] A. Dalla Rosa and J. E. Christensen, “Low-energy district heating in energy-efficient building areas,” *Energy*, vol. 36, no. 12, pp. 6890–6899, 2011.
- [9] R. Lazzarin and M. Noro, “Local or district heating by natural gas: Which is better from energetic, environmental and economic point of views?,” *Appl. Therm. Eng.*, vol. 26, no. 2–3, pp. 244–250, 2006.
- [10] F. Busato, R. M. Lazzarin, and M. Noro, “Ten years history of a real gas driven heat pump plant: Energetic, economic and maintenance issues based on a case study,” *Appl. Therm. Eng.*, vol. 31, no. 10, pp. 1648–1654, 2011.
- [11] F. Mauthner and S. Herkel, “Technical Report Subtask C – Part C1,” no. January, pp. 1–31, 2016.
- [12] H. Li, F. Wallin, and J. Song, “A dynamic pricing mechanism for district heating,” 2017.
- [13] J. Song, H. Li, and F. Wallin, “Cost Comparison between District Heating and Alternatives during the Price Model Restructuring Process,” *Energy Procedia*, vol. 105, pp. 3922–3927, 2017.
- [14] Värmemarknad Sverige, “Slutrapport - Vår gemensamma värmemarknad,” 2017.
- [15] R. Lowe, “Combined heat and power considered as a virtual steam cycle heat pump,” *Energy Policy*, vol. 39, no. 9, pp. 5528–5534, 2011.
- [16] A. Esser and F. Sensfuss, “Final report Evaluation of primary energy factor calculation options for electricity,” Karlsruhe (Germany), 2016.
- [17] B. Vidrih, A. Kitanovski, and A. Poredo, “Eligibility of a Heat Pump Based on the Primary Energy Factor,” pp. 1–13, 2017.
- [18] T. Persson, “Energimyndighetens syn på vikttnings- och primärenergifaktorer,” vol. 1, no. 202100, pp. 1–5, 2015.
- [19] E. Latõšov, A. Volkova, A. Siirde, J. Kurnitski, and M. Thalfeldt, “Primary energy factor for district heating networks in European Union member states,” *Energy Procedia*, vol. 116, pp. 69–77, 2017.
- [20] Y. M. El Sayed, *The thermoeconomics of energy conversion*. 2003.
- [21] C. Torres Cuadra and A. Valero Capilla, “Thermoeconomics,” Centro de Investigación de Recursos y Consumos Energéticos, 2005.
- [22] V. Verda, R. Borchiellini, and M. Cali, “A thermoeconomic approach for the analysis of district heating systems,” *Int. J. Appl. Thermodyn.*, vol. 4, no. 4, pp. 183–190, 2001.
- [23] V. Verda and A. Krona, “Thermoeconomic approach for the analysis of low temperature district heating systems,” in *THE 25TH INTERNATIONAL CONFERENCE ON EFFICIENCY, COST, OPTIMIZATION, SIMULATION AND ENVIRONMENTAL IMPACT OF ENERGY SYSTEMS*, 2012.
- [24] A. Krona, “Energetic and thermoeconomic approach for optimal planning of district energy systems,” Politecnico di Torino, 2013.
- [25] IEA, “Projected Costs of Generating Electricity,” Paris, 2015.
- [26] O. Eriksson and G. Finnveden, “Energy Recovery from Waste Incineration—The Importance of Technology Data and System Boundaries on CO2 Emissions,” *Energies*, vol. 10, no. 4, p. 539, 2017.
- [27] T. Duveau and N. Tewes, “Climate Scorecard Sweden,” Germany, 2009.
- [28] A. Moro and L. Lonza, “Electricity carbon intensity in European Member States: Impacts on GHG emissions of electric vehicles,” *Transp. Res. Part D Transp. Environ.*, no. November 2016, pp. 0–1, 2017.
- [29] Fortum Värme, “Högdalenverket Miljörapport 2016.” 2017.
- [30] Fortum, “Hammarbyverket,” Stockholm, 2016.
- [31] Thermia, “Thermia Mega Tekniska data.”
- [32] I. Nohlgren, M. Jansson, and J. Rodin, “Electricity from new and future plants 2014,” no. October, 2014.
- [33] International Energy Agency, “District Heating,” *ETSAP - Energy Technol. Syst. Anal. Program.*, no. January, p. 7, 2013.
- [34] NordPool, “Price Chart,” 2018. [Online]. Available: <https://www.nordpoolgroup.com/Market-data1/#/nordic/chart>. [Accessed: 07-May-2018].
- [35] Danish Energy Authority and Energinet.dk, *Technology Data for Energy Plants*, vol. 978-87-784. 2012.
- [36] D. F. Dominković, R. Lund, and B. V Mathiesen, “Large Scale Heat Pumps as a Link Between Intermittent Electrical Energy Sources and District Heating Sector,” no. April, p. 2014, 2016.
- [37] C. Boissavy, “Cost and Return on Investment for Geothermal Heat Pump Systems in France,” *World Geotherm. Congr. 2015*, no. April, pp. 1–9, 2015.
- [38] Energimarknadsinspektionen, “Elpriskollen,” 2018. [Online]. Available: <https://www.ei.se/en/Elpriskollen/Avtalsok/?avtalsstypid=13&forbrukning=40000&postnr=12068>. [Accessed: 07-May-2018].
- [39] Vattenfall, “Så här fungerar rörligt elpris,” 2018. [Online]. Available: <https://www.vattenfall.se/elavtal/elpriser/rorligt-elpris/>. [Accessed: 26-May-2018].



16th International Symposium on District Heating and Cooling, DHC2018,
9–12 September 2018, Hamburg, Germany

District heating leakage measurement: Development of methods

E. Filippini^a, I. Marini^{a*}, M. Ongari^a, E. Pedretti^a

A2A Calore e Servizi S.r.l., via Lamarmora 230, Brescia, 25124, Italy

Abstract

A2A Calore e Servizi carries out maintenance programs; one of the main activities is leak detection performed according to different procedures. The first method was based on pressure measurements and then it has evolved in a direct measurement of water loss. A new method has been tested; fixed metering devices have been installed. According to the law of mass conservation, the mass difference is a calculation of the water lost in the area. This procedure allows reliable continuous leak measurements, simplifying operational activities and giving immediate results on field.

© 2018 The Authors. Published by Elsevier Ltd.

This is an open access article under the CC BY-NC-ND license (<https://creativecommons.org/licenses/by-nc-nd/4.0/>)

Selection and peer-review under responsibility of the scientific committee of the 16th International Symposium on District Heating and Cooling, DHC2018.

Keywords: district heating network; leakage measurement; flow meters; maintenance strategy.

1. Introduction

A2A Calore e Servizi (ACS) is the main district heating (DH) company in Northern Italy and it manages the DH networks of Brescia, Bergamo and Milan. These three systems differ one to the other because of the individual characteristics, such as construction technologies, materials, lengths and heat production.

The first system to operate is the one in Brescia; it started functioning in 1972 and it is widely developed in the city; in fact, it is around 670 km long (trench length) and supplies heat to more than 21.000 connections (more than 70% of the municipal area connections).

* Corresponding author. Tel.: +390303554228; fax: +390303554084.

E-mail address: ilaria.marini@a2a.eu

ACS performs several activities, such as designing, coordinating interventions and maintenance. The latter has a vital importance, especially for wide and old networks, as the one in Brescia.

The leak detection process consists of different steps: leak identification, its localisation and estimation of water loss. Although leak detection can be achieved using different methods, the correct localisation and the estimation of water loss are more complex, but these elements are extremely useful for efficient maintenance. Actually, it is essential to identify, locate leakages and estimate the magnitude of water loss to organize a careful maintenance strategy in order to ensure the correct operation of the system and a longer lifespan [1]. In the last years, ACS has developed and tested several methods to detect leaks, each of whom is briefly described in the following paragraphs.

2. The DH system in Brescia

The DH network in Brescia has an important development and a yearly average of about 1.000 GWh of supplied heat; it is a single system, meaning that it cannot be hydraulically divided in smaller systems. The supply pipeline temperature can reach at maximum 130°C in winter and 90°C in summer, while for the return, temperature is almost constant all year long, and is around 60°C; the maximum operative pressure of the network is 16 bar.

Since the network was partially constructed in the early '70s, pipes' characteristics have been evolving since that moment; nowadays the network is composed of three different types of pipe.

From 1972 to 1979, steel pipes were installed in concrete ducts and sustained by rollers or metallic saddles; this type of pipe represents around 20% of the entire network length. From 1979 to 1985, the "wanit" technology was employed, now it constitutes less than 2% of the network length. According to this method, pipes were laid in preinsulated sheathes, composed by two concentric fibrocement pipes with a layer of polyurethane in the middle. The remaining 78% of network length consists of preinsulated pipe and is made of steel covered by external casings: an inner layer of polyurethane foam and a layer of polyethylene.

The production plant consists of a waste to energy plant and a CHP plant, both located in the southern part of the network, boilers are located in other part of the city and they are switched on during peaks.

3. Leak detection method

Planning effective maintenance is fundamental; thus, measuring the amount of water lost by each leakage provides information regarding the priority of the interventions to perform. Normally, the first monitored parameter is the amount of daily make-up water, but that describes the entire network scenario, thus, it can only be used as trend indicator. To understand where to perform fixing and maintenance activities it is necessary to have more information regarding the location and the magnitude of each leakage; hence, a system able to provide this information has been experimented in Brescia DH network implementing pressure tests, a tool already in use.

Pressure tests are routine maintenance activities, performed during warm seasons (mid-April – mid-October) on the 80% – 90% of the entire network. They consist in choosing an area to test, dividing the examined area from the rest of the network and in evaluating its pressure drop trend for less than half an hour; the pressure drop speed could give information about the leak size. To perform these tests it is necessary to operate on site on valves; in order to do so, at least a temporary working site has to be created and managed. Operators in charge of these activities have gained experience and sensitiveness, however this procedure does not provide necessary information to complete a list of interventions, but it can be used as preliminary test.

Therefore, it was decided to develop procedures, which would allow a more accurate measurement of leakages; thus, a method had been designed to define replicable approaches. This was based on measurements of pressure drop while the test area was separated from the rest of the network and on weighting the discharged volume of water; these parameters were used to estimate the bulk modulus of the area [2]. The registration of data allowed subsequent calculations of the amount of water loss in the examined area; in fact, to obtain an indirect estimation of water loss magnitude the orifice flow equation was applied, whose results could be estimated again only by calculations. The orifice flow equation was applied assuming that the DH network is compressible and it has its own bulk modulus; this parameter is calculated based on pressure and volume variation, as stated previously, hence, the higher the water loss,

the higher the overestimation of this coefficient. Moreover, regarding the estimation of the leak, it is supposed that water loss can be compared to the flow that passes through an orifice, so it is possible to apply the orifice flow equation to have an approximate calculation of the amount of water loss and the size of the leak [3]. This approach required particular care during operational activities and, in addition, data could be obtained only after calculations and not immediately.

A further improvement was the employment of portable flow metering devices, which allowed an instantaneous and direct measurement of water loss. Even though, it was possible to have instantaneous measurements, that was feasible only for a short period of time, less than half an hour, and it was still mandatory operating on site with the creation of temporary working sites.

At this point, it appeared important to improve and optimize detection procedures; not all the methods described above allowed making immediate estimations of leaks size and magnitude, as mentioned; that was possible only after calculations and it was allowed only to estimate the total area of the leaks in the examined zone. Furthermore, data could be recorded only for short periods, hence, during warm seasons it was possible to monitor each area only once per year. In addition, it must be noted that operational activities have to be taken into account: most of the times, these tests were performed on streets, requiring the creation of temporary working sites, traffic management, high safety measures and temporary interruption of service for clients.

4. Fixed metering devices

In 2016, two fixed metering devices were operating in two areas of the Brescia DH network, one device monitors around 100 km of pipes, while the other around 105 km of pipes. These fixed devices consist of roadside cabinets containing a supply and a return pipe where valves, flow-metering devices and air vents are installed (as shown in Figure 1).

The operating tools inside the cabinet are thermal energy meters and related static flow sensors; they calculate energy and measure flow, power and temperature; these results can be read both directly on the display tool and remotely. Flow measurements are based on bidirectional ultrasonic technique and on transit time method: two sound signals are sent, against and with flow direction; the sound signal sent with the flow direction reaches the opposite transducer first, hence the time difference between the two elements can be used to calculate the flow velocity and then translated as volume. At this point, heat meters compute energy and mass based on measurements of temperature and volume. It was chosen to install the same type of heat meters that are normally employed in consumers' substations, in order to have solid, easy to find and reliable instrumentations.

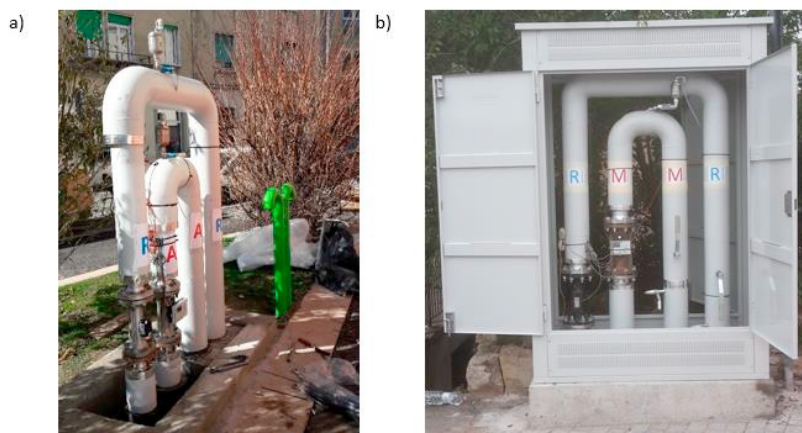


Figure 1: a: roadside cabinet under construction, b: roadside cabinet in operation.

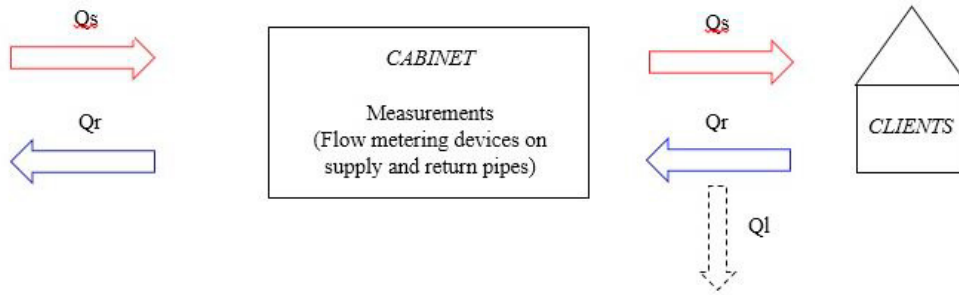


Figure 2: Scheme of the mass conservation theory applied to the employment of fixed metering device.

$$Q_s = Q_r + Q_l \quad (1)$$

Nomenclature

Q_s	supply mass flow
Q_r	return mass flow
Q_l	mass flow of the leak

4.1. Background theory

The idea behind the construction of these tools is based on the theory of mass conservation; the same amount of water should enter and go out of the examined area, as shown in Figure 2 and Equation (1).

In order to apply this theory, the chosen area has to be connected to the rest of the network by a single branch (both supply and return), by opening and closing selected valves, this way it can behave as a branch and can be monitored easily. The difference between supply and return flow is the amount of leak (Q_l).

It must be noted that analyses have to be based on mass flow; hence, it is possible to compare supply and return data, while volumetric flow rate depends on temperature and then it cannot be examined together.

4.2. Laboratory tests

By design, any size of flow metering device has a nominal flow and a related measurement error. To verify these data, flow meters undergone laboratory tests to monitor and evaluate the range of error and their behavior; these tests were performed in an ACS laboratory.

A test bed was built and it consisted in a series of three meters, as shown in Figure 3: a device to test, a tap (behaving as a loss in the system), another device to test and a calibrated device. This test bed has run for few days monitoring two scenarios: in the first scenario, the tap was closed (no water loss), while in the second scenario the tap was open (system with water loss).

Tests have confirmed the error ranges reported in the instruction manuals and, in all the cases, measured values were lower than the design ones; errors obtained after laboratory analyses were lower than 0,5% in both scenarios, thus they were classified as negligible.

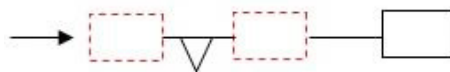


Figure 3: Scheme representing the test bed.

Nomenclature

	Flow metering device to test
	Calibrated flow metering device
	Pipe
	Tap simulating water loss

4.3. Cabinet features

Flow metering devices can operate continuously only during warm seasons (mid-April – mid-October) when flow is lower and supply temperature is more constant, in winter they can be used for instantaneous measurements. They operate as bypasses and, since most of them are above - ground installations, it was preferred to create size-limited tools, and hence, all the designed instrumentation was dimensioned according to summer flows to limit measurement error of metering devices and costs. The investment is in the range between 15.000 and 25.000 €.

A supply pipe connects instruments inside the cabinet to the main network, allowing water to pass through the metering device before running again in the pipe that goes to clients; for the return, a pipe allows water flow to be measured inside the cabinet and then it flows back to the main pipeline, as shown in Figure 4.

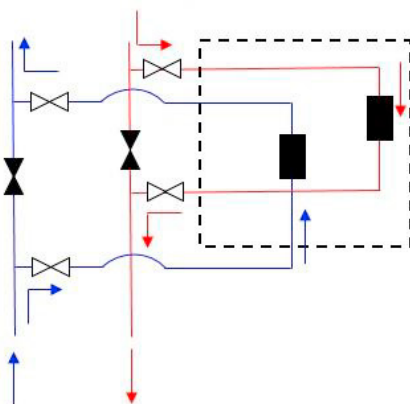


Figure 4: Hydraulic scheme of a typical roadside cabinet

Nomenclature

	Return line
	Supply line
	Valve (open)
	Valve (closed)
	Flow metering device
	Cabinet area
	Direction of flow, red supply flow, blue return flow

Flow sensors measure volumetric flow rate in m^3/h and temperature in Celsius degree, this way the calculator in the heat meter can compute mass flow and energy, as stated in paragraph 4.

Water flow measurements are recorded continually during warm seasons (i.e. around for 5 months), readings are saved automatically and they can be downloaded easily; normally operators download data once per month. Records can be

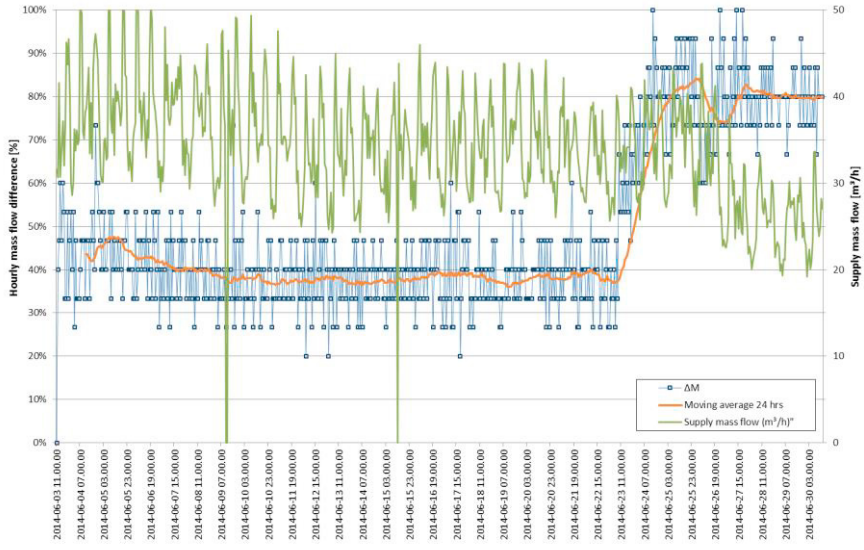


Figure 5: Hourly recorded data

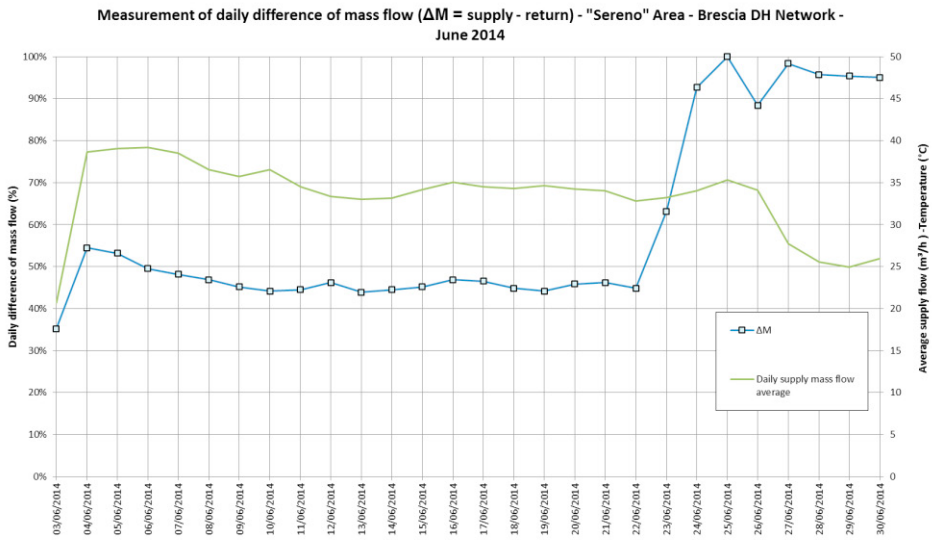


Figure 6: Daily recorded data

saved both on hourly (instantaneous) and daily (sum of the 24 hours) basis. It can be observed, in Figure 5, that instantaneous readings are strongly influenced by the sensitivity of measurement devices, temperature and ordinary hourly flow fluctuations. As visible, hourly measurements are characterized by important variations, although it is possible to easily identify the daily trend (plotted in orange); Figure 6 represents data on a daily basis and, differently from the previous figure, this approach provides more constant data, able to describe the trend effectively; thus, daily basis was chosen.

It must be noted that, most of the times, to activate these devices it is necessary to create a temporary working site, but differently from the previous methods, here it is necessary only to activate and deactivate the metering systems, thus, twice a year and for a shorter period, without service interruptions for customers. Furthermore, for previous

methods, the work of three operators, at least, was necessary for each test, while fixed metering devices require at least three operators twice a year, during activation and deactivation phases, and another operator once per month to download data.

5. Monitoring results

After the installation of the first flow metering devices, it was possible to monitor the trend of water flowing in the areas under test; the following paragraphs show the results obtained for the “*Oltremella Sud*” area since 2014 and for the “*Sereno*” area since 2016.

Data registered by roadside cabinets were validated by measurements recorded by portable meter device and it was observed that fixed metering devices were able to identify water losses lower than 5 t/d.

5.1. *Sereno*

This flow-metering device was activated for the first time in June 2014; it monitors 105 km of pipe (around 8% of the entire network). The following graph (Figure 7) represents the trend from June 2014 to October 2017; it is visible that the trend is recorded only during warm seasons (mid-April – mid-October), the analysis should focus on daily difference of mass flow, which is related to the other represented parameters: supply and return temperatures and supply average flow. The daily difference of mass flow is calculated as the difference between supply mass in tons and return mass in tons that are measured by flow meters and divided by the maximum value of water loss recorded in the examined period.

During measurements recorded in 2014, it is possible to observe a peak around mid-August, as reported in Figure 7, which represents a leak that was fixed quite quickly, approximately in one week, because of its magnitude. Similarly, as represented in Figure 8, the trend of the following year defines a leak, from April to mid-June; in this case, the peak is not as high as it was in the previous year but the repair of the leak is clearly visible, the mass difference goes from 67% the 15th of June to 20% the 19th of June. Moreover, it can be observed that, in the first period, the daily difference of mass flow is above 60% of the maximum value of the year, while after mid-June it is halved, around 30%.

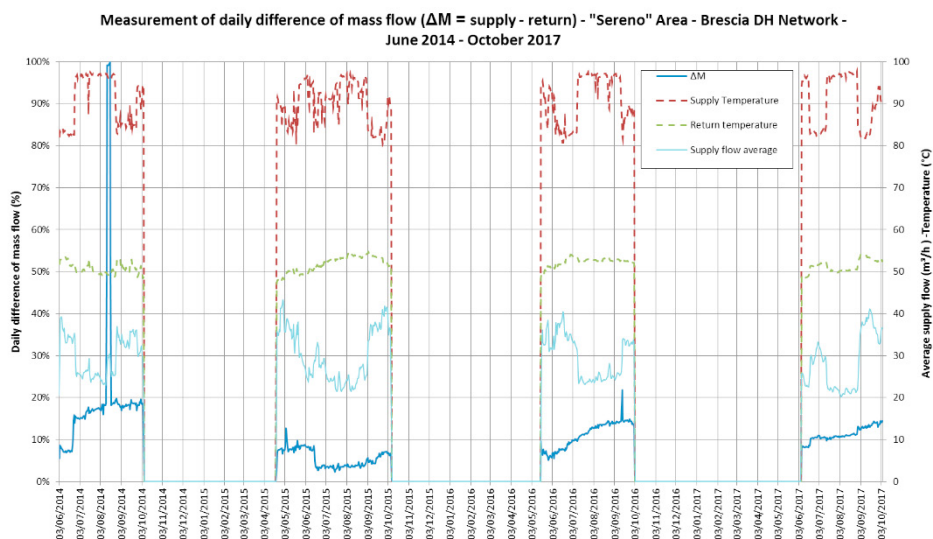


Figure 7: Graph representing measurements of daily difference mass flow, average supply flow, supply and return temperature in the “*Sereno*” area, June 2014 – October 2017.

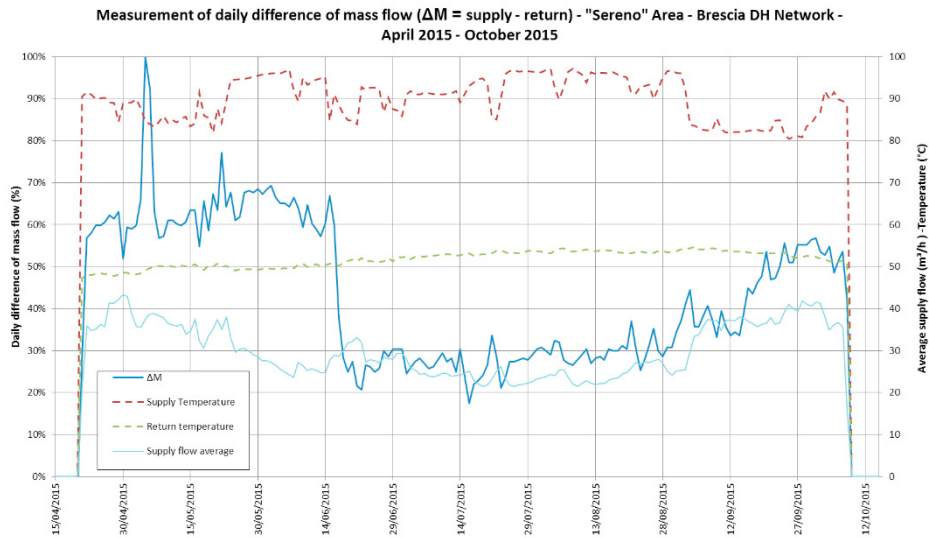


Figure 8: Graph representing measurements of daily difference mass flow, average supply flow, supply and return temperature in the “*Sereno*” area, April – October 2015.

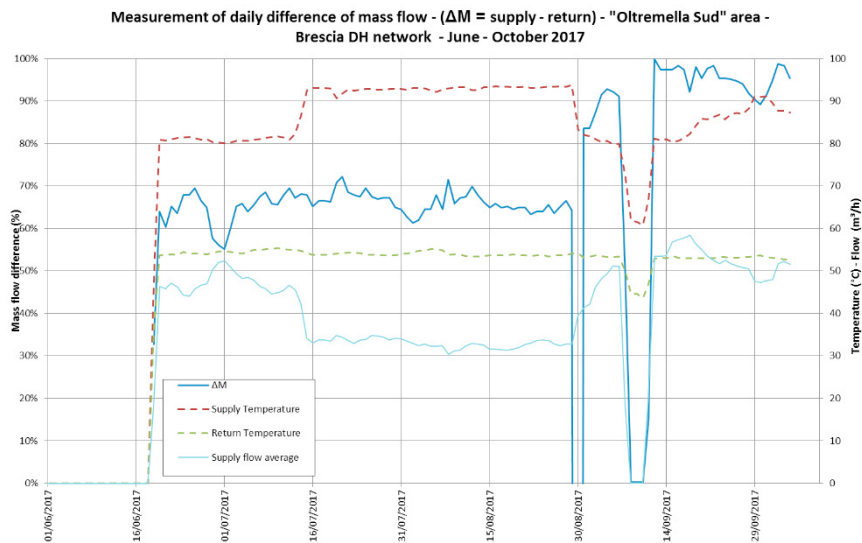


Figure 9: Graph representing measurements of daily difference mass flow, average supply flow, supply and return temperature in the “*Oltremella Sud*” area, June – October 2017.

5.2. Oltremella Sud

This flow-metering device monitors around 100 km of pipe (around 7% of the Brescia DH network) and it has been operating since 2016. The graphs represented in Figure 9 show the trend of the daily difference of mass flow, the supply average flow, the supply and return temperature during the warm season 2017.

This device has been operating only for two warm seasons, furthermore, it must be noted that data describing daily difference of mass flow in 2016 are not reliable, in fact, that year there were problems during some fixing operations performed on the network. Data describing 2017 identifies a water loss in the second part of the season, from end of

August to October when values are higher than 80%. It can be observed that the second part of the period is characterized also by two minimums; regarding these two values, it is important to specify that they correspond to devices switching off during maintenance operations.

6. Discussion and following steps

The employment of fixed flow-metering devices have improved leak detection process; in fact, these tools allow measurements (about 5 months, continuously) of the quantities of the supply and return water in selected areas; the “*Sereno*” and “*Oltremella Sud*” flow meters monitor about 15% of the Brescia DH network. As stated previously, these tools can work continuously only during warm seasons (mid-April – mid-October) when supply temperature is more constant and the amount of supply and return flow are lower than in winter periods.

At the moment, these measurements are not readable remotely, they need to be downloaded on site and they can provide the sum of total amount of water lost in an examined area; in fact, the value of mass difference is related to the entire analyzed area. It must be added that flow-metering tools can restrict the area to inspect providing data almost immediately, if necessary and moreover by creating subsections, it is possible to identify the area with higher water loss. Before their installation, it was not possible to individuate the area without operating on site on valves and this approach did not even allow having an immediate feedback regarding the presence of a leak.

The measured data do not require processing nor particular calculations, thus, their analyses can be done quite quickly and readings can be downloaded every time it is necessary. As shown in the previous graphs (Figure 7, 8 and 9) the trend of the daily difference of mass flow is an important parameter that can give information regarding both water losses and operations on the network, as stated in the description of the “*Sereno*” and “*Oltremella Sud*” areas. The available data could give also information regarding the quantity of energy supplied and lost (estimated by calculations from water loss) in the examined area, as plotted in Figure 10.

At the beginning of May 2018, ACS activated another flow-metering cabinet “*P.le Cremona*”; the area monitored by this new device is Brescia downtown, about 25 km of pipes. This zone represents only about 1% of Brescia DH network, but this is one of the eldest area, characterized by a very high rate of water loss thus, having the possibility to monitor it continuously would improve maintenance efforts. In the last months, some experiments on data radio transmissions employing LoRaWAN protocol have being tested.

ACS is finalizing the design of another device in “*Chiesanuova*” area, which should be tested by the end of summer 2018; this new device should monitor about 54 km of the network. At that point, the total inspected area would be slightly higher than 20% of the pipeline of the city network, as summarized in Table 1, giving an important improvement in the yearly maintenance strategy.

7. Conclusions

ACS performs several activities, one of the main is leak detection; this process is fundamental to ensure the correct operation of the system and a longer lifespan of the network. Leak detection requires an effective analysis on the amount of water lost, thus ACS has been developing several procedures to provide this information.

These experimentations aimed at the identification of a method able to provide, continuously, the amount of water lost in an area, minimizing the operations on the network and avoiding the interruption of the service to customers.

Table 1. Area description. Data in brackets refer to the entire network length and the total number of customers

Name of the area	Length (pipes) [km]	Daily supply average flow (summer) [m ³ /h]	Number of customers [n]	Nominal flow meter [m ³ /h]	Year of activation
Sereno	101,72	35	1.506	40	2014
Oltremella Sud	105,07	47	1.459	60	2016
P.le Cremona	24,32	23	534	25	2018
Chiesanuova	54,54	45	548	60	Expected: end of summer 2018
Total	285,65 (21,3%)		4.047 (19,2%)		

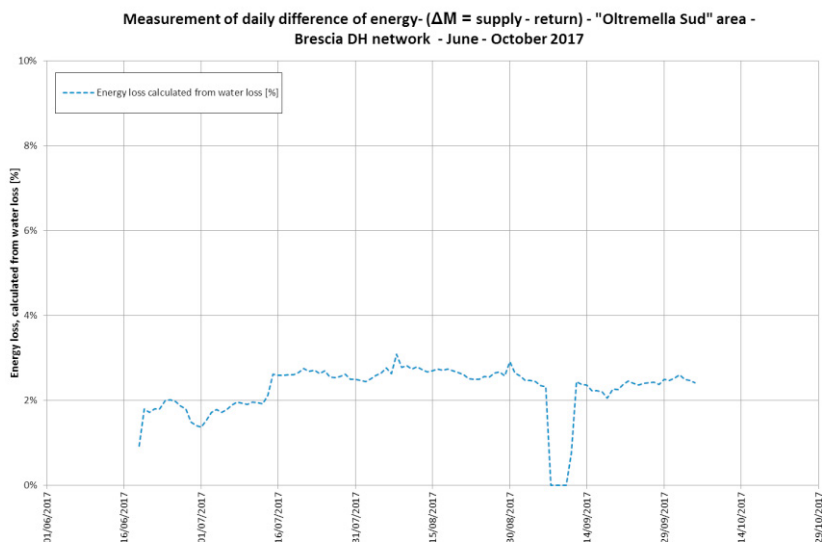


Figure 10: Graph representing the energy loss calculated from water loss in the “Oltremella Sud” area, June – October 2017

Pressure tests were initially employed, they can identify the presence of water loss in the examined area, but they cannot provide the necessary information to classify a leak, such as number of losses, location and magnitude; thus, they are used as preliminary tests. Later, a method based on the application of the orifice flow equation was tested successfully; it was observed that these practices could be performed only for short periods, about half an hour, requiring several operations on site and data processing. Then, portable flow metering devices were applied, this method allowed having instantaneous and direct measurements of water loss, but it was possible only for short periods.

All the methods described above could be performed only for less than one hour, requiring the creation of a working site, often, the interruption of service for customers and processing of the measured data; thus, a new method requiring less operational activities and continuous measurement was implemented.

Fixed metering devices are able to monitor continuously, during warm season (from mid-April to mid-October), the amount of water loss (allowing then the calculations of energy loss) in the area where the roadside cabinet is installed. The theory behind this application is based on mass conservation: the same amount of water entering the area has to flow out, if these quantities differ, there is a leakage. Fixed metering devices consist of roadside cabinets equipped with valves, air vents and flow meters that calculate energy and measure flow, power and temperature; readings are saved automatically and they can be downloaded easily, normally operators do it once per month.

In 2016, two flow-metering devices were in operation, monitoring two areas of the Brescia DH network, in May 2018 a new device was activated and another one is under construction. At the moment, about 17% of the city DH network is monitored continuously during warm season, providing necessary information for maintenance programs.

In fact, the installation of these devices have improved leak detection processes, allowing continuous monitoring of the quantities of supply and return water flow during warm season; they can provide information immediately, when necessary, regarding the presence of one or more leaks, without requiring processing nor particular calculations. The next step is testing and implementing radio data transmission to allow remote readings.

ACS aims at further implementing the employment of fixed metering devices to ensure effective operation of the DH systems it manages, both the old one, as in Brescia, and the more recent, as in Milan.

References

- [1] Frederiksen Svend, Werner Sven, “District heating and cooling”, Studentlitteratur, (2013), AB, Lund.
- [2] Astori P., “Dispense del corso di Impianti aerospaziali”, Politecnico di Milano, Milano, (2005), pp. 3.6 – 3.9.
- [3] Filippini Ettore, and Ongari Marco. “Method for the quantification of a leakage in a district heating network”, (2014), The 14th International Symposium on District Heating and Cooling.



16th International Symposium on District Heating and Cooling, DHC2018,
9–12 September 2018, Hamburg, Germany

Prospects for absorption chillers in Finnish energy systems

Heidi Saastamoinen*, Satu Paiho

VTT Technical Research Centre of Finland Ltd, P.O. Box 1000, FI-02044 VTT

Abstract

Increasing trend in space cooling together with demand of CO₂ emission reduction in energy production directs towards environmentally friendlier cooling options. Absorption chillers utilize waste heat in cold production and could, therefore, fit to this need. Finland has a well established district heating system and growing district cooling markets. The trend is towards renewable options in both heat and electricity production. In this study, after introducing basics of absorption chillers, cooling trends in Finland are discussed and prospects of absorption chillers in Finnish district and building energy systems are defined. A number of potential applications are identified and discussed. After an extensive review of literature, the authors conclude that solar driven absorption chiller applications have not been widely examined in Finnish conditions. Particularly absorption systems in trigeneration systems could be feasible also in Finland. Still, further technical and economic analyses for all potential applications are needed.

© 2018 The Authors. Published by Elsevier Ltd.

This is an open access article under the CC BY-NC-ND license (<https://creativecommons.org/licenses/by-nc-nd/4.0/>)

Selection and peer-review under responsibility of the scientific committee of the 16th International Symposium on District Heating and Cooling, DHC2018.

Keywords: absorption chillers, energy systems, buildings, Finland

1. Introduction

Globally, space cooling is the fastest-growing end use in buildings, even if it is a significantly small portion of energy demand in buildings today (roughly 5%) [1]. Even if energy needs for cooling can be reduced with building envelope solutions by minimizing heat gains in summer using thermal mass, efficient glazing, insulation, shading, reflective surfaces and natural ventilation [2], there still remains needs for the active cooling solutions as well.

* Corresponding author. Tel.: +358-40-568-9860

E-mail address: heidi.saastamoinen@vtt.fi

Statistics have not been compiled on energy consumption for household air conditioning nor on the applications in use although the sector is growing rapidly. IEA suggests that air conditioning accounts for around 9% of household electricity consumption in IEA countries [3]. According to Santamouris [4], globally the Climate Change, increase of population and potential economic growth increases the cooling energy demand. At country level, higher family income, decrease in electricity and equipment price, warmer climatic zone and high local standards for thermal quality of buildings and high requirements for minimum efficiency of air conditioners increase the penetration of air conditioners [4].

The thermal energy demand for cooling per m^2 is not necessarily directly dependent on the climatic condition since buildings in colder climates are usually better insulated [5]. Correspondingly, the demand for high quality room air and possibility to adjust the room temperature freely has increased also in Finland. This increases the interest to chiller applications in new construction production and for buildings under renovation, especially in office buildings, commercial buildings and other public buildings. According to Airaksinen et al. [6] current demand for cooling energy in Finnish buildings is 850-2100 GWh and it is steadily increasing.

The European Commission Energy Roadmap 2050 [7] states that the coal-free future determines the reduction of primary energy production which is approximated to be up to 20% by 2030 and up to 41% by 2050. This means that the energy savings has to be made in all sectors of economy. Thus, although cooling sector is increasing, the increase in production should not increase the primary energy demand. Absorption chillers use very little electricity compared to mechanical chillers because they use waste heat instead of electric motor or engine to produce the needed compression [8]. Therefore, they could settle part of the problem by increasing the cooling production with variable heat sources in flexible configurations.

An EU Strategy on Heating and Cooling [9] recommends the exploitation of tri-generation (simultaneous generation of heating, cooling and power). Absorption chillers could provide savings in electricity production together with combined heat and power production especially during the summer, when space heating is not needed. Absorption chillers can also be powered by solar heat [10,11] which can ease achieving the 55% share of renewable energy according to European Commission Energy Roadmap 2050 [7].

The cost for cooling is closely related to prevailing electricity and fuel prices. The integration of the absorption cooling in the energy system becomes more profitable, if waste heat and natural water sources are available. These kind of conditions can be found in most of the Finnish suburban areas, since Finland has long history in combined heat and power production with local biomass fuels as well as long coastline at the Baltic Sea and inland waters.

Absorption chillers can be widely utilized both in district-level (e.g., [13–15]) and in building-level (e.g., [11,16]) energy systems. Its prospects in Finnish energy systems has not been evaluated. This article aims to support wider rollout of absorption chillers in Finland through introducing recent cooling trends and reviewing potential absorption chiller applications.

2. Absorption cooling

The absorption refrigeration is a non-mechanical option to utilize waste heat (hot air, hot water, steam or hot exhaust) from process applications for cooling. They are typically powered by heat from a district heating, heat recovery or cogeneration heat, but also sun is used as a heat source for refrigeration. Chiller capacities are usually several hundred kW [11,17]. Although the efficiency of absorption cycle is low compared to other commercially used cooling cycles, the energy input for the absorption is free, since the aim is to exploit produced heat that would otherwise be unused. Most absorption systems need an internal solution pump that consumes little electric power. However, this consumption is very small compared to an electric motor-driven compression cycle chiller. Therefore, technology is interesting in the point of view of saving energy.

Basic absorption chiller consists of generator, absorber, evaporator, and condenser [18]. In order to avoid the mechanical work [19], thermal heat input from the surroundings to the solution of refrigerant and absorbent is used to induce the compression. The refrigerant and the absorbent have different boiling temperatures. The input heat energy is used to boil the refrigerant out of the solution while the absorbent stays liquid. The refrigerant continues its way as vapor to the condenser where it cools down to high-pressure liquid due to cooling water. The liquid absorbent instead passes through the solution heat exchanger back to the absorber. After the condenser, the refrigerant liquid passes through an expansion device to the evaporator, where it provides cooling to external heat and again become vapor.

Refrigerant vapor then passes into absorber where it condenses to liquid and dilutes the absorbent. This solution is pumped back to the generator closing the thermal compression cycle [13,19].

The construction, workability, effectiveness and costs of the absorption chiller are highly dependent on properties of the working fluid solution [13,19]. **Error! Reference source not found.** The most common working pairs commercially are H₂O-LiBr and NH₃-H₂O (e.g., [20,21]). In literature, absorption equipment is determined by the number of effects and stages (e.g., [22]). The term effect refers to the number of times the driving heat is used (number of generators) and the term stage refers the number of basic cycles [19]. Single-effect systems are widely used in absorption cooling projects. However, since the coefficient of performance (COP) of the single-effect systems is low, double-effect or triple-effect systems are more feasible for commercial use [21]. The multiple stage cycles expand the workable area of the basic cycle [22]. The absorption chillers can be fired indirectly with heat recovered from another process such as solar collectors, district heating network or a boiler. This heat is delivered to the generator with heat exchanger. The directly fired chiller obtains the heat input from combustion [19].

Absorption machines are manufactured in small and large scale. The technical information of chillers can be found from the webpages of manufacturers AGO, Carrier, Climatewell, Broad, EAW, Ebara, Kawasaki, LG, SolarNext, Robur, Rotartica, SorTech, Thermax (Trane), Yazaki, and York. Most of the manufacturers produce chillers in small scale for air-conditioning. These chillers are usually water fired. However, for instance, Carrier, Ebara, Kawasaki, Thermax, Yazaki, York® and AGO also produce large-scale units for industrial cooling and storage, and for large public buildings. Yazaki produces water fired chillers up to 175 kW cooling capacity, but chillers with larger capacity are gas fired. Thermax, AGO, and Carrier produce steam and water powered large-scale chillers.

3. Cooling trends in Finland

3.1. Cooling demand is increasing

According to IEA [1], there has globally been 4% annual increase in space cooling since 1990. Energy consumption for cooling is expected to increase sharply by 2050 by almost 150% globally [2]. Finnish Meteorological Institute [23] estimates that the need for cooling energy is going to increase 13-19% due to climate change by the year 2030 in Finland. They approximate that annual average temperature in Finland will increase 1.2-1.5 °C by 2030 depending on the region. However, these calculations do not take into account the changes in building regulations. During the past decades, energy efficiency of buildings in Finland has increased due to prevailing regulation [24] and, thus, the heating demand has decreased and need for air conditioning and cooling increased [6]. In addition, the public demand for higher quality for indoor conditions has increased.

According to European Commission [9], the cooling demand for all single-family houses is more than twice as high as that of all multi-family buildings. In Finland, 50% of citizens lived in single-family houses in the end of 2015 [25]. There has been 25-fold increase in the number of heat pumps in Finland since 2000 [26]. The annual increase is about 60,000 units. A huge majority of these, about 45,000, is small (0-6 kW) air-to-air heat pumps which are installed mainly to single-family houses. Partly this is due to the people's willingness to decrease heating costs but an equally important aspect is the opportunity to space cooling during the summer periods.

According to Airaksinen et al. [6] cooling demand in Finland depends on the economic growth, energy system development, as well as amount and quality of buildings and urban development. They present four scenarios: BAU, LAMA, HAJA, and DUO. If the economic growth stays at current rate (BAU) or decelerates (LAMA), present energy systems and regional structure stays and reconstruction of buildings is emphasized. If economic growth is moderate (HAJA), migration is uniform in the country and more single-family houses are build. This increases the use of individual cooling systems. If the economic growth is fast (DUO), city areas are going to grow and more high-level apartment houses are build. Airaksinen et al. [6] refers to the statistics of Helen Ltd, in which the consumption of cooling energy of an office buildings has varied between 1-5 kWh/m²/year. According to scenarios by Airaksinen et al., the cooling demand in 2030 in Finnish residential buildings varies between 0.5-12 kWh/m² and in office buildings 6-39 kWh/m² depending on the construction year and solar shading. This mean that the cooling demand for office buildings is going to increase tremendously. According to BAU scenario, the total yearly cooling demand for buildings in Finland is going to increase from 1300 GWh to 1700 GWh by 2030.

According to the RESCUE project [27], the normalized specific district cooling market was 33 kWh/capita in 2011 in Finland, which means 178 GWh in total. This share was the third largest in the EU after Sweden and Norway. According to Airaksinen et al. [6], the market has grown to 190 GWh in recent years. They approximate that by 2030 the district cooling delivery is going to increase 6% every year on average to 490 GWh. RESCUE estimated that the cooling market in Finland is 11 TWh [27], which is more than 20 times as much as the estimate for the growth in the district cooling. This means that there is potential for absorption chillers also in decentralized market.

Werner [28] estimates that the average specific cooling demand in Finland is 45 kWh/m² in the service sector, 20 kWh/m² in the residential sector and 28 kWh/m² in total. Multiplying these numbers with the total floor areas of the named building types and summarizing these two gives 8.8 TWh for the total cooling demand, which is in good agreement with RESCUE [27], although Werner [28] states that there are remarkable differences in different cooling demand estimations based on the assumptions used.

3.2. District cooling capacity increases moderately

Finland has a well-established district heating system and, thus, steady growing district cooling market. In fact, although the climate is colder in Nordic countries, they have taken the leading position in development of district cooling in Europe [27]. According to Finnish Energy [29], during the year 2017 223,439 MWh district cooling was provided in Finland to 491 customers by 9 Energy companies. Majority (65%) of the available buildings in district cooling network were located in the capital area. The location affects the profitability of district cooling investment since centralized solution cannot compete with price with other cooling options in sparsely populated areas. In addition, natural water systems can be utilized in cold production in Nordic countries. The most commonly used district cooling technology in Finland was heat pump (60%), followed by free cooling (25%) and absorption cooling (10%). District heat providers extend the network depending on the customer need, and new buildings invest in the district cooling option for subsequent joining to the network [30]. According to the statistics of Finnish Energy [29] from the year 2015, the absorption heat pump is only in use at Helen, former Helsingin Energia, where sea water is used for the condenser.

According to Finnish Energy [29], buildings using district cooling gain a number of benefits, such as the air- and structure-borne noises and vibration caused by cooling equipment are eliminated, the space for cooling equipment becomes free for other use, condensing units spoiling the façade of the building are no longer required, and the repair and maintenance of cooling equipment are no longer necessary. In addition, the possibility of connecting to district energy networks can provide urban households with a more cost-effective and less carbon-intensive cooling supply than would be available through individual cooling systems [1].

Recent statistics [31] show that annual sold district cooling energy in Finland has been between around 130-220 MWh with increasing trend (Figure 1). For example, Helen has plans to expand district cooling to new residential areas by 2020 [32]. In order to help buildings in connecting to district cooling networks, Finnish Energy [33] has defined common quality requirements, recommendations and guidelines.

Typically, the price in connecting to district cooling is three-folded [34], including: 1) a contract payment, 2) an annual fee (a fixed capacity payment), and 3) an energy fee. In summer 2014, the energy fee was 31.11 €/MWh in Helen's network in Helsinki and 36.42 €/MWh in Fortum Power and Heat's network in Espoo. Usually, the energy fee is much smaller during the winter time.

A good district cooling system can have a temperature difference of 10°C between the supply and return water flows when a good district heating system can have a difference of 50°C [35]. For instance, in the region of Turku, the delivery temperature for district cold is 7°C and return water temperature is 17°C [36]. This leads to around 4-5 times larger flow (and larger pipe dimensions) to distribute the same energy capacity in a district cooling network. So, the initial investments for a district cooling system are larger than for a district heating system. On the other hand, the production costs are much lower.

Typically, losses in Finnish district heating networks vary between 5-8% in dense urban areas and between 10–15 % in less populated areas [37]. Losses in district cooling networks have not been reported. A Swedish calculation study [38] reports a maximum cooling loss below 2% of the total delivered energy during the season for any analyzed network configuration.

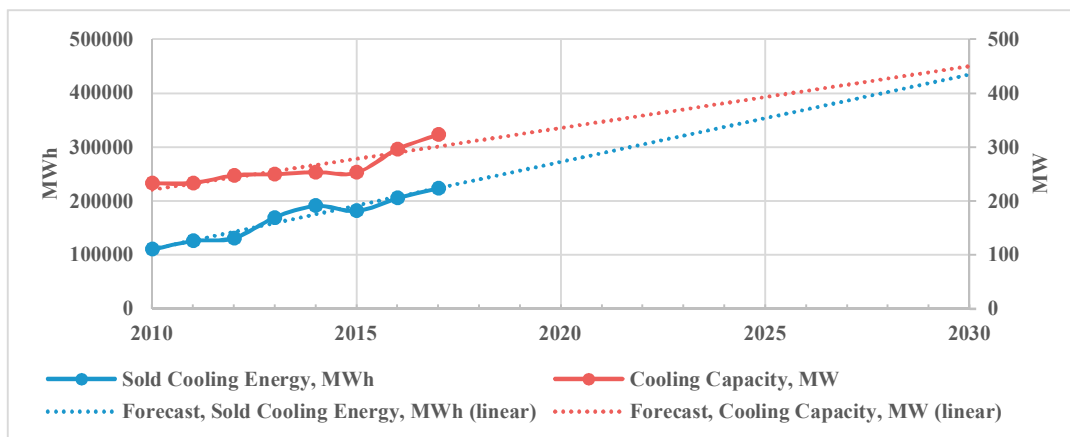


Figure 1. Sold district cooling energy and available district cooling capacity in Finland (modified from the data from [31]) including the forecast for 2030.

4. Opportunities for absorption chillers in Finnish energy solutions

The first absorption chiller in Finland was district heat operated single-effect chiller at Pitäjämäki, Helsinki [13]. Another former absorption chiller produced cold using surplus heat from brewery in Teivaanmäki, Lahti [39], but was closed when the brewery was closed. Two existing applications can be found in Finland. Helen uses sea water heat exchangers to produce condensing water for absorption cooling together with free cooling system [40]. Three out of six seawater heat exchangers are used for condensing water productions. Finnish company Savo-Solar produces solar absorbers for thermal systems and they have been tested for office heating and absorption cooling in Mikkeli [41,42].

4.1. Solar driven absorption systems

Cooling demand usually increases along with the solar intensity, which increases the feasibility of solar cooling systems (e.g., [43,44]). Although Finland is located approximately between latitudes 60 and 70, yearly solar irradiation in Southern Finland is close to countries like Germany and Belgium [45–47]. The electricity production differences can be even lower since the efficiency of commonly used PV-panels increases in lower temperatures [45]. Solar power is produced mainly in small scale in Finland and typical systems are off-grid solutions installed to summer cottages to supply energy for few applications [45] or solutions to increase renewable energy share of one-family and apartment houses. Turnkey solar energy packages are sold to households by energy producing companies [48–50]. The increase of electricity use in single-family house cooling could be covered by solar energy.

Today, solar thermal systems in Finland are still rare. One reason is relatively low price of heat compared to Central-Europe. For instance in 2013, national average prices for district heat in Finland was 16.3 €/GJ whereas for instance in Germany it was 21.2 €/GJ [51]. Small applications are installed occasionally. Sundial Oy [52] estimates that thermal collectors are installed approximately 4000 m²/year in Finland. However, an increasing trend in solar thermal installations is seen in Europe [53], and this trend might reach Finland as well. Thus, absorption cooling with solar thermal energy input would become considerable option to reach the European Commission's yearly target to increase the renewable energy share in cooling systems by at least 1% of the final consumption every year.

Solar thermal systems in Finland have been analyzed [54,55] and their feasibility estimated [56]. It is concluded, that the installed solar thermal systems have been generally feasible, if the system is sized accurately, solar collectors have high efficiency and the collectors are installed to the right direction [56]. However, it is still estimated that with solar photovoltaic panels and air to water heat pump systems less energy is wasted, since the spare electricity can be more easily utilized compared to spare heat [54].

Still ongoing development of the solar absorption cycles hinder their market entry, and thus the cost reduction of applications. Solar absorption cycles have been widely experimentally tested in the air-conditioning of buildings [16,18,57,58]. Majority of these studies deal with climatic conditions not relevant to Finland and are located in much

lower latitudes than for example Helsinki (60°N, 25°E) in Finland. Hwang et al. [59] lists the critical barriers for wide use of the solar cooling technology that include low energy conversion efficiency, high cost of solar collectors and thermal cooling technologies, the cost of installation, and intermittent nature of the solar energy production. Weber et al. [60] point out also the lack of standardization of systems. Aliane et al. [61] suggest that combination of further domestic services with the solar cooling installation could keep the absorption cooling system feasible. They also conclude that the implementation of solar cooling system requires holistic overall design of the configuration not only the collector and cooling system, but also energy storage, auxiliary heating and cooling devices and the heat rejection systems. Agyenim et al. [62] tested 4.5kW LiBr/H₂O chiller with a 1000 litre cold storage tank at the Cardiff University. They found that the absorption technology (the performance) was competitive with available air-conditioning systems. However, due to its high cost the technology was not commercially competitive.

In Finland, cooling towers are not needed for serving to reject the heat from the chiller coolant water due to natural sources of cold water. Thus, the investment to free cooling combined with the absorption chiller coolant water proposed by Ali et al. [63] could be less expensive in Finland. Albers [64] observed that spray water consumption during the months of moderate ambient temperatures (typical to Finland) can be reduced more than 80% due to the increased thermal efficiency of the thermally driven chiller. However, Eicker and Pietruschka [65] remind that in moderate climate conditions with low cooling demand, the system costs are high. Winter period can also cause damage in the equipment needed for solar powered absorption chiller [64].

Finnish company Savo-Solar produces direct solar absorbers for thermal systems. Their collectors have been used in hybrid district heating plants, office heating and domestic heating. Reda et al. [42] made an energy assessment for two solar cooling systems with Savo-Solar collectors, storage tank, and an absorption chiller. They found that for an office cooling application in Finland, large building roof area has to be available. They also found that the collector, storage tank and absorption chiller connected in parallel, so that both the collector and the tank supplies the chiller, had better performance than a system in which the components were connected in series. The profitability analysis was not made in these studies.

4.2. CHP and absorption chiller

Similarly to other Northern European countries district heating is common in Finland [20]. It covers 46% of Finnish heat demand [66] having largest percentage share of the used heating systems and is used in most of the cities and villages. It is energy efficient way to produce heat since most of the heat (3/4) is produced in combined heat and power (CHP) plants. Approximately 1/3 of the district heating is produced by biomass [66]. The increase of heat consumption in Finland especially during the summer time would make the electricity production in existing CHP plants more profitable. This kind of combined cooling, heat and power (CCHP) production is commonly called also trigeneration. Because heat demand is seasonal and low during summer, cooling production through an absorption chiller enables additional revenue for a CCHP [32]. Considerable energy saving, high trigeneration efficiency as well as proper payback time is obtained for integration of CHP site with absorption chiller [67]. Both economic and environmental benefits are obtained in the integration of absorption technology with municipal solid waste-fired power plant [68].

Trygg and Amini [69] studied combining absorption cooling with existing compression cooling in the system in Norrköping, Sweden, which can be compared to Finnish urban areas by its boundaries for cooling. In Norrköping, cooling is produced with CHP plant and oil-fired boiler. District cooling is produced for shopping centers, the library, offices, and university. Cooling is also produced locally for seven large industries. In the study, absorption cooling is introduced as an option for compression cooling, which is the main source of Finnish district cooling. It was observed that if only the energy systems are compared, with and without the option for absorption cooling, the costs for cooling production decrease only slightly when absorption is introduced. However, if European electricity prices are taken into account in the simulation, the absorption become a respectable option. This is explained with the heat demand depending on the season. Cooling is needed during the summer, when the heat demand is low and, thus, heat can be used for cooling with low cost.

Fahlén et al. [14] studied the potential of absorption cooling in district heating system in Göteborg, Sweden, another city comparable to Finnish cities. They conclude that absorption cooling could contribute to more resource-efficient energy systems by increasing the heat utilization in CHP production especially during the times for lowest heat demand (June, July and August) in Nordic countries. According to their study utilization of absorption cooling

decreases CO₂ emission compared to compression cooling, if waste heat is used for absorption. If absorption cooling increases the need for CHP plant operation, the CO₂ reduction depends on the alternative use of the needed fuel.

5. Discussion

The potential to increase cooling in Finnish buildings is significantly higher than the amount of current applications. In addition, demand for cooling is increasing and almost all new office buildings have a cooling application installed. The increasing demand for cooling energy should be produced without significant increase in primary energy consumption. In ecological point of view, thermal cooling has significant advantages compared to conventional compression chillers especially when used in centralized application and combined with free cooling [70]. Shifting from compression to absorption cooling decreases the electricity demand and rounds out the peaks in the demand especially during the summer, and thereby, decreases CO₂ emissions.

The costs for the absorption cooling (€/kW) depend highly on the price of the equipment and on the price of the heat and electricity. The costs for cooling decreases along with the cooling capacity of the equipment. According to survey to equipment suppliers few years ago, the price for cooling decreases from approximately 300 €/kW to 100 €/kW when the capacity of the equipment increases from 100 kW to 1200 kW. Brückner et al. [71] analyses that absorption chillers are economically feasible only for the enthusiast consumer type investors meaning early adopters with now not seeking for profit. For real estate, more than 2500 h operating hours per year is needed and for industrial application, the cost of the technology needs to come down for economically feasible investment.

More input energy is needed for absorption compared to compression. If the costs for cold production is compared by calculating the price of input energy for the systems, compression appears to be the more cost effective option in many cases. The price of electricity needs to be significantly higher than the price of heat, to make absorption more profitable option [70]. This is especially clear in small and medium scale. However, in many applications considered for absorption, the heat would otherwise be wasted, and thus the absorption is also financially an attractive option.

It is estimated that the future district heating in Finland enables trigeneration (simultaneous production of electricity, heating and cooling) [72]. Even the Energy Efficiency Directive requires member states to examine their opportunities for utilizing cogeneration, district heating and district cooling, and to take the necessary measures to promote cogeneration if this proves the most advantageous alternative according to a cost-benefit analysis [73]. Already now, there are examples of such implementations in Finland. Wider adaption of absorption chillers in trigeneration would enable cooling production without significant increase in CO₂ emissions since there is no need for extra electricity [74].

If the waste heat is produced in CHP plant that utilizes fossil fuels, such as coal, the useful heat is taxable and the tax depends on the heating value of the fuel and on the generated CO₂ emissions [75]. Waste heat from Finnish industries can also be used in decentralized absorption cooling or cooling at the industry site especially in summer time. There is a long history for instance in pulp and paper production and metal production in Finland and the sector for liquid fuel production is increasing.

The energy performance of building directive (EPBD) recast (EN 15603) [76] requires that all new building should be nearly zero-energy buildings (nZEBs) by the end of year 2020. The Directive 2010/31/EU also defines a 'nearly zero-energy building' as a building that has a very high energy performance and that the nearly zero or very low amount of energy required should be covered to a very significant extent by energy from renewable sources, including energy from renewable sources produced on-site or nearby. Producing the energy nearby jointly for a number of buildings or for a whole neighborhood also increases the wider rollout of district cooling.

Further analyses of e.g. waste heat potential in Finland, solar thermal applications as supporting systems for district-heated buildings enabling high-temperature district heating utilization with low-temperature technologies, as well as differences of energy, cost and emission of possible district cooling technologies would bring interesting outlooks to the topic of absorption chillers in Finnish energy systems.

6. Conclusions

It is estimated that the cooling demand in Finnish buildings will increase. This can be partly met with passive building design solutions, mainly related to the building facades. However, there remains a need for active cooling

technologies. Absorption chillers are utilized in many such solutions both in district-level and in building-level cooling solutions. This article dealt with their outlooks in Finnish energy systems.

Well-established district heating system in Finland enables absorption cooling both at district level as well as at building level so that the district heat is connected to customer's absorption cooling application. During the summer, CHP systems lack heat consumers while cooling demand increases. Absorption chillers can increase the head load by utilizing the waste heat in cold production and thus enable cost reductions in CHP systems.

Solar heating has been used in several systems in Finland and available technology is applicable to Finnish environment. However, solar thermal cooling is not yet utilized in Finland even if major cooling demands and irradiation occur simultaneously. If the price of the equipment reduce, the solar thermal cooling systems will more easily become reality in Finnish markets.

Today, using absorption chillers in Finnish energy systems is limited. However, clearly there exists new and increasing opportunities both due to increasing cooling demands and by more efficient utilization of waste and solar heat.

Acknowledgements

This study was performed as part of VTT's Ingrid research program under the theme "Flexibility in energy systems". The authors are grateful for the financial support.

References

- [1] International Energy Agency (IEA). Energy Technology Perspectives 2016. Towards Sustainable Urban Energy Systems. Paris: OECD Publishing; 2015. doi:10.1787/energy_tech-2014-en.
- [2] International Energy Agency (IEA). Technology Roadmap. Energy efficient building envelopes. 2013. doi:10.1007/SpringerReference_7300.
- [3] International Energy Agency (IEA). Energy Use in the New Millennium ENERGY - Trends in IEA Countries 2007:168. doi:10.1787/9789264034303-en.
- [4] Santamouris M. Cooling the buildings – past, present and future. Energy Build 2016;128:617–38. doi:10.1016/j.enbuild.2016.07.034.
- [5] Andrews D, Krook Riekkola A, Tzimas E, Serpa J, Carlsson J, Pardo-Garcia N, et al. Background Report on EU-27 District Heating and Cooling Potentials, Barriers, Best Practice and Measures of Promotion. Joint Research Centre; 2012. doi:10.2790/47209.
- [6] Airaksinen M, Vainio T, Vesanen T, Ala-kotila P, Ala-kotila P. Rakennusten jäähdytysmarkkinat. VTT Res Rep 2015:48.
- [7] Energy Roadmap 2050. EUR-Lex-52011DC0885 n.d.
- [8] Johnson-Controls. Application opportunities for absorption chillers 2008:20.
- [9] European Commission. Communication from the Commission to the European Parliament, the Council, the European Economic and Social Committee and the Committee of the Regions on an EU Strategy for Heating and Cooling. Comm Staff Work Doc 2016. doi:10.1017/CBO9781107415324.004.
- [10] Al-Alili A, Hwang Y, Radermacher R. Review of solar thermal air conditioning technologies. Int J Refrig 2014;39:4–22. doi:10.1016/j.ijrefrig.2013.11.028.
- [11] Taha Al-zubaydi AY. Solar Air Conditioning and Refrigeration with Absorption Chillers Technology in Australia—An Overview on Researches and Applications. J Adv Sci Eng Res 2011;1:23–41.
- [12] Lund H, Werner S, Wiltshire R, Svendsen S, Thorsen JE, Hvelplund F, et al. 4th Generation District Heating (4GDH). Energy 2014;68:1–11. doi:10.1016/j.energy.2014.02.089.
- [13] Koljonen T, Sipilä K. Uudemman absorptiojäähdytystekniikan soveltaminen kaukojäähdytyksessä [Modern absorption technology for district cooling]. Espoo: 1998.
- [14] Fahlen E, Trygg L, Ahlgren EO. Assessment of absorption cooling as a district heating system strategy - A case study. Energy Convers Manag 2012;60:115–24. doi:10.1016/j.enconman.2012.02.009.
- [15] Deng J, Wang RZ, Han GY. A review of thermally activated cooling technologies for combined cooling, heating and power systems. Prog Energy Combust Sci 2011;37:172–203. doi:10.1016/j.pecs.2010.05.003.
- [16] Lizarte R, Izquierdo M, Marcos JD, Palacios E. An innovative solar-driven directly air-cooled LiBr-H₂O absorption chiller prototype for residential use. Energy Build 2012;47:1–11. doi:10.1016/j.enbuild.2011.11.011.
- [17] Delorme M, Six R, Mugnier D, Quinette J-Y, Richler N, Heunemann F, et al. Climasol: Solar air conditioning guide. 2004.

- [18] Wang RZ, Ge TS, Chen CJ, Ma Q, Xiong ZQ. Solar sorption cooling systems for residential applications: Options and guidelines. *Int J Refrig* 2009;32:638–60. doi:10.1016/j.ijrefrig.2009.02.005.
- [19] Labus JM, Bruno CC, Coronas A. Review on absorption technology with emphasis on small capacity absorption machines. *Therm Sci* 2013;17:739–62. doi:10.2298/TSCI120319016L.
- [20] IEA. *Transition to Sustainable Buildings. Strategies and Opportunities to 2050*. 2013. doi:10.1787/9789264202955-en.
- [21] Kalkan N, Young EA, Celiktas A. Solar thermal air conditioning technology reducing the footprint of solar thermal air conditioning. *Renew Sustain Energy Rev* 2012;16:6352–83. doi:10.1016/j.rser.2012.07.014.
- [22] Xu ZY, Wang RZ. Absorption refrigeration cycles: Categorized based on the cycle construction. *Int J Refrig* 2016;62:114–36. doi:10.1016/j.ijrefrig.2015.10.007.
- [23] Jylhä K, Kalamees T, Tietäväinen H, Ruosteenoja K, Jokisalo J, Hyvönen R, et al. *Rakennusten energialaskennan testivuosi 2012 ja arviot ilmastomuutoksen vaikutuksista (Test reference year 2012 for building energy demand and impacts of climate change)*. 2012.
- [24] Ympäristöministeriö. *D3 Suomen rakentamismääräyskokoelma - Rakennusten energiatehokkuus, määräykset ja Ohjeet 2012*. Code Build Regul 2012:1–14.
- [25] Statistics Finland. *Suomen virallinen tilasto (SVT): Rakennukset ja kesämökkit [Verkköjulkaisu]*. ISSN=1798-677X. 2015, Liitetaulukko 1. Rakennukset, asunnot ja henkilöt talotyypin ja kerrosluvun mukaan 31.12.2015. 2015. http://www.stat.fi/til/rakke/2015/rakke_2015_2016-05-26_tau_001_fi.html (accessed September 29, 2016).
- [26] Finnish Heat Pump Association - SULPU. *Heat pump statistics (in Finnish)*. 2014.
- [27] RESCUE project. *Work Package 2. EU district cooling market and trends*. 2014.
- [28] Werner S. European space cooling demands. *Energy* 2016;110:148–56. doi:10.1016/j.energy.2015.11.028.
- [29] Finnish Energy. *Kaukojäähdytys n.d.* https://energia.fi/ajankohtaista_ja_materiaalipankki/materiaalipankki/kaukojaahdytystilasto.html (accessed April 26, 2018).
- [30] Vainio T, Lindroos T, Pursiheimo E, Vesanen T, Sipilä K, Airaksinen M, et al. *Tehokas CHP, kaukolämpö ja -jäähdytys Suomessa 2010–2025* 2015:63.
- [31] Finnish Energy. *Kaukojäähdytys 2016 graafeina n.d.* https://energia.fi/ajankohtaista_ja_materiaalipankki/materiaalipankki/kaukojaahdytys_2016_graafeina.html#material-view (accessed April 26, 2018).
- [32] UNEP. *District Energy in Cities: Unlocking the Potential of Energy Efficiency and Renewable Energy*. Paris: 2015.
- [33] Finnish Energy. *Rakennusten kaukojäähdytys Yhtenäiset laatuvaatimukset, suositukset ja ohjeet (in Finnish)*. 2014.
- [34] Nuutinen T. *District cooling in old apartment buildings (in Finnish)*. Metropolia University of Applied Sciences, 2015.
- [35] RESCUE project. *Guidelines with impact calculator*. 2015.
- [36] Lyytikäinen L. *Customer needs survey of two-way district heating network in new residential area*. Lappeenranta University of Technology, 2015.
- [37] Finnish Energy. *Kaukolämpöverkko n.d.* <http://energia.fi/energia-ja-ymparisto/kaukolampo-ja-kaukojaahdytys/kaukolampoverkko> (accessed October 5, 2016).
- [38] Calance MA. *Energy Losses Study on District Cooling Pipes. Steady-state Modeling and Simulation*. University of Gävle, 2014.
- [39] Salmi J. *Adsorptiojäähdyttimen käytön kannattavuus kaukolämpöjärjestelmässä*. Lappeenranta University of Technology, 2013.
- [40] Itkonen V. *Salmisaaren hiililuolan kaukojäähdytyskompressorin toimintakuvaus ja säätösuunnittelu*. Metropolia, 2017.
- [41] Sipilä K, Reda F, Pasonen R, Löf A, Viot M, Pischow K, et al. *Solar heating and cooling in Northern and Central Europe. Pilot plants in Finland and Germany*. Espoo: 2017.
- [42] Reda F, Viot M, Sipilä K, Helm M. *Energy assessment of solar cooling thermally driven system configurations for an office building in a Nordic country*. *Appl Energy* 2016;166:27–43. doi:10.1016/j.apenergy.2015.12.119.
- [43] Bataineh K, Taamneh Y. *Review and recent improvements of solar sorption cooling systems*. *Energy Build* 2016;128:22–37. doi:10.1016/j.enbuild.2016.06.075.
- [44] Otanicar T, Taylor RA, Phelan PE. *Prospects for solar cooling - An economic and environmental assessment*. *Sol Energy* 2012;86:1287–99. doi:10.1016/j.solener.2012.01.020.
- [45] Sipilä K, Pasonen R, Mäki K, Alanen R. *Arctic solar energy solutions*. 2012.
- [46] Kitunen J. *Aurinkosähkön soveltuvuus hajautettuun energiantuotantoon Suomessa*. Master Thesis, Tampere Univ Technol 2007.
- [47] Solpros AY. *Aurinkoenergia Suomen olosuhteissa ja sen potentiaali ilmastomuutoksen torjunnassa*. 2001.
- [48] Fortum. *Aurinkopaneelit asennettuina ja käyttövalmiina n.d.* <https://www.fortum.fi/countries/fi/energiansaasto-jaratkaisut/aurinkopaneelit-aurinkopaketti/pages/default.aspx?ad=search&gclid=CPH9sub81s4CFSXicgodsmINiA> (accessed August 22, 2016).

- [49] Vattenfall. Laadukkaat aurinkopaneelit Vattenfallilta n.d. <http://www.vattenfall.fi/fi/aurinkopaneeli.htm?gclid=COLczKWC184CFcn0cgodrpsNpA&gclid=COiW5aWC184CFU GTGAodB7oFOA> (accessed August 22, 2016).
- [50] Helen. Aurinkopaneelipaketit n.d. <https://www.helen.fi/sahko/taloyhtiot/aurinkopaneelipaketit/> (accessed August 22, 2016).
- [51] Werner S. European district heating price series. 2016.
- [52] Sundial Oy. Aurinkolämpö n.d. <http://www.sundial.fi/aurinko.php?page=aurinko1> (accessed May 25, 2018).
- [53] ESTIF. Solar Thermal Markets 2015;2016:5.
- [54] Piiroinen S. Aurinkolämmön ja -sähkön vertailu Comparison between solar thermal and photovoltaic 2017.
- [55] Komulainen K. Aurinkolämpö - teknologia ja mahdollisuudet. Jyväskylä University, 2006.
- [56] Auvinen K. Aurinkolämpöjärjestelmien hintatasot ja kannattavuus 2016. <http://www.finsolar.net/aurinkoenergia-hankintaohjeita/aurinkolampojarjestelmien-hintatasot-ja-kannattavuus-suomessa/?print=pdf> (accessed May 28, 2018).
- [57] Rodriguez Hidalgo MC, Rodriguez Aumente P, Izquierdo Millan M, Lecuona Neumann A, Salgado Mangual R. Energy and carbon emission savings in Spanish housing air-conditioning using solar driven absorption system. *Appl Therm Eng* 2008;28:1734–44. doi:10.1016/j.applthermaleng.2007.11.013.
- [58] Rosiek S, Batlles FJ. Shallow geothermal energy applied to a solar-assisted air-conditioning system in southern Spain: Two-year experience. *Appl Energy* 2012;100:267–76. doi:10.1016/j.apenergy.2012.05.041.
- [59] Hwang Y, Radermacher R, Alili A Al, Kubo I. Review of Solar Cooling Technologies. *HVAC&R Res* 2008;14:507–28. doi:10.1080/10789669.2008.10391022.
- [60] Weber C, Berger M, Mehling F, Heinrich A, Núñez T. Solar cooling with water-ammonia absorption chillers and concentrating solar collector - Operational experience. *Int J Refrig* 2014;39:57–76. doi:10.1016/j.ijrefrig.2013.08.022.
- [61] Aliane A, Abboudi S, Seladji C, Guendouz B. An illustrated review on solar absorption cooling experimental studies. *Renew Sustain Energy Rev* 2016;65:443–58. doi:10.1016/j.rser.2016.07.012.
- [62] Agyenim F, Knight I, Rhodes M. Design and experimental testing of the performance of an outdoor LiBr/H₂O solar thermal absorption cooling system with a cold store. *Sol Energy* 2010;84:735–44. doi:10.1016/j.solener.2010.01.013.
- [63] Ali AHH, Noeres P, Pollerberg C. Performance assessment of an integrated free cooling and solar powered single-effect lithium bromide-water absorption chiller. *Sol Energy* 2008;82:1021–30. doi:10.1016/j.solener.2008.04.011.
- [64] Albers J. New absorption chiller and control strategy for the solar assisted cooling system at the German federal environment agency. *Int J Refrig* 2013;39:48–56. doi:10.1016/j.ijrefrig.2013.08.015.
- [65] Eicker U, Pietruschka D, Pesch R. Heat rejection and primary energy efficiency of solar driven absorption cooling systems. *Int J Refrig* 2012;35:729–38. doi:10.1016/j.ijrefrig.2012.01.012.
- [66] Finnish Energy. Kaukolämmitys n.d. <http://energia.fi/koti-ja-lammitys/kaukolammitys> (accessed September 15, 2016).
- [67] Ghaebi H, Karimkashi S, Saidi MH. Integration of an absorption chiller in a total CHP site for utilizing its cooling production potential based on R-curve concept. *Int J Refrig* 2012;35:1384–92. doi:10.1016/j.ijrefrig.2012.03.021.
- [68] Udomsri S, Martin AR, Martin V. Thermally driven cooling coupled with municipal solid waste-fired power plant: Application of combined heat, cooling and power in tropical urban areas. *Appl Energy* 2011;88:1532–42. doi:10.1016/j.apenergy.2010.12.020.
- [69] Trygg L, Amiri S. European perspective on absorption cooling in a combined heat and power system - A case study of energy utility and industries in Sweden. *Appl Energy* 2007;84:1319–37. doi:10.1016/j.apenergy.2006.09.016.
- [70] Berliner Energieagentur GmbH. SUMMERHEAT-Meeting cooling demands in SUMMER by applying HEAT from cogeneration. Europe 2009.
- [71] Brückner S, Liu S, Miró L, Radspieler M, Cabeza LF, Lävemann E. Industrial waste heat recovery technologies: An economic analysis of heat transformation technologies. *Appl Energy* 2015;151:157–67. doi:10.1016/j.apenergy.2015.01.147.
- [72] Paiho S, Reda F. Towards next generation district heating in Finland. *Renew Sustain Energy Rev* 2016;65:915–24. doi:10.1016/j.rser.2016.07.049.
- [73] Finnish Government. Finnish National Energy and Climate Strategy 2013.
- [74] Pardo Garcia N, Vatopoulos K, Krook Riekkola A, Perez Lopez A, Olsen L. Best available technologies for the heat and cooling market in the European Union. JRC Scientific and Policy Reports. 2012. doi:10.2790/5813.
- [75] Ministry of Finance. Energiaverotus n.d. <http://vm.fi/energiaverotus> (accessed September 30, 2016).
- [76] Official Journal of the European Union. Directive 2010/31/EU of the European Parliament and of the Council of 19 May 2010 on the energy performance of buildings (recast). *Off J Eur Union* 2010;13–35.



16th International Symposium on District Heating and Cooling, DHC2018,
9–12 September 2018, Hamburg, Germany

Electricity Adjustment by Aggregation Control of Multiple District Heating and Cooling Systems

Kohei Tomita^{a,*}, Masakazu Ito^b, Yasuhiro Hayashi^a, Takahiro Yagi^c, Tatsuya Tsukada^c

^aGraduate School of Advanced Science and Engineering, Waseda University, 3-4-1 Okubo, Shinjuku-ku, Tokyo 169-8555, Japan

^bAdvanced Collaborative Research Organization for Smart Society, Waseda University, 3-4-1 Okubo, Shinjuku-ku, Tokyo 169-8555, Japan

^cTokyo Gas Co., Ltd., 1-5-20 Kaigan, Minato-ku, Tokyo 105-8527, Japan

Abstract

Introduction of wind energy is proceeding all over the world. However, output fluctuation due to inherent intermittency reduce stability of the power system. Therefore, electricity adjustment (EA) auction was introduced in Japan recently. In this auction, power grid companies make a one-year contract with various power generation companies and procure electric power at the time of supply-demand tightness. One candidate for the auction is a District Heating and Cooling system (DHC) with a Combined Heat and Power (CHP). To investigate the usefulness of using DHCs for the EA, two operations are defined in this paper: normal operation and EA capacity (EAC) provision operation. The EAC provision operation always keeps the EAC of contract so that it can provide EA according to directives from the power grid company. In the previous study, the usefulness of the EA by a single DHC was evaluated. In order to realize more efficient EA, aggregation control of multiple DHCs is proposed. For this control, the EACs by each DHC are combined to ensure the EAC of aggregator's contract. At first, two DHCs are modeled assuming actual DHCs. Using these models, the running costs of the normal operation (Op.1) and the EAC provision operation (Op.2) of each DHC are calculated by the particle swarm optimization (PSO). Furthermore, an additional cost for the EAC provision operation are estimated by calculating the difference between the running costs of the two operations. The assigned EACs to each DHC are determined so that the sum of the additional costs of each DHC is minimized. Finally, by comparing additional costs of the conventional single control to that of the aggregation control, it was found that the total additional cost of the proposed method was reduced. In case of 6,000 kW of the total EAC of contract, reduced cost rate was 54.3%. By using this proposed method, the operator can more efficiently operate DHCs for EA, and further stability of the power system can be expected.

© 2018 The Authors. Published by Elsevier Ltd.

This is an open access article under the CC BY-NC-ND license (<https://creativecommons.org/licenses/by-nc-nd/4.0/>)

Selection and peer-review under responsibility of the scientific committee of the 16th International Symposium on District Heating and Cooling, DHC2018.

* Corresponding author. Tel.: +81-3-5286-3000.

E-mail address: kohei_ka_pi787@toki.waseda.jp

Keywords: Aggregation Control, Electricity Adjustment, Multiple District Heating and Cooling Systems, Combined Heat and Power

Nomenclature

CHP	Combined heat and power	$f_{i,n,j}$	Function convert an input i to an output j of device n
DHC	District heating and cooling system	$x_{n,j}$	Inputs and outputs from device n
EA	Electricity adjustment	$p(t)$	Purchased or sold electricity
EAC	Electricity adjustment capacity	$g(t)$	Gas consumption
Op. 1	Normal operation	$p_s(t)$	Station load
Op. 2	EAC provision operation	$cap_{target}(t)$	Capacity target for EA
PSO	Particle swarm optimization	$cap_n(t)$	Capacity of the device n
RE	Renewable energy	$cw_d(t), s_d(t)$	Cold demand, steam demand
		p_g, p_p	Price of gas, price of electricity

1. Introduction

Introduction of renewable energies (REs) is proceeding to prevent global warming [1]. The capacity of photovoltaic power alone increased by 75 GW during 2016 [2]. In addition, the World Wide Fund presents a scenario that all energy is provided by RE by 2050 [3]. However, output of renewable energy fluctuate depends on weather conditions. This output fluctuation is due to inherent intermittency reduce stability of the power system [4]. Therefore, electricity adjustment (EA) markets were launched in some countries [5-8]. In Japan, the EA market auction was launched in 2016. In this auction, power grid companies make a one-year contract with various power generation companies. The power generation companies determine the electricity adjustment capacity (EAC) for the contract with the power grid companies. Then, they need to keep EAC of the contract so that they can provide EA according to directives from the power grid companies. One candidate for the auction is a District Heating and Cooling system (DHC) with a Combined Heat and Power (CHP).

The CHP is an economical and environmental system to provide heat and electricity [9, 10]. Therefore, Andersen et al. described that the integration of CHPs and intermittent REs is important for realizing a sustainable energy society [11]. In fact, many researches on CHP plants aimed at contribution to power systems are carried out. [12-15].

DHCs consist of devices for providing heat and cold energy, and satisfy district heat and cold demand. From the 1880's, DHCs often installed with CHPs in order to improve efficiency. Moreover, from the 1980's, DHCs often installed with large-scale CHPs that can be applied to power systems [16]. Therefore, DHC is attracting attention as a resource for a sustainable future [17, 18]. In addition, the number of DHC has increased in many countries including Japan, mainly in Europe [19-21]. A lot of research on DHCs have also been carried out. For example, Sakawa et al. proposed optimal operation planning methods of a DHC through genetic algorithms [22]. Casisi et al. proposed an optimization model of a DH with CHPs assuming an actual city [23], and Ameri et al. proposed a model that determined the optimal capacity and operation of DHC with CCHP [24]. In addition, researches considered the electricity market were also carried out. Wang et al. and Rolfsman optimized the operation of a DH with CHPs considering electricity price [25, 26].

When using DHCs for the EA market auction, two running costs are important. They are standby cost for the EA (EAC provision cost) and fuel cost to do the EA. In the Japanese EA market auction, the fuel costs consumed for the EA are paid by the power grid company. Consequently, the EA cost cannot be a discussion here. Therefore, the EAC provision cost represent an additional cost for the EA. However, there was no previous research to calculate the total cost including the EAC provision cost when using a DHC for the EA. For this reason, our previous study showed the usefulness of using a single DHC for the EA by calculating the total cost assuming an actual DHC [27].

In this paper, considering large number of DHCs are installed, aggregation control of multiple DHCs is proposed to realize more efficient EA. For this control, the EACs by each DHC are combined to ensure EAC of aggregator's

contract. Also, the aggregator determines the assigned EAC ratio to each DHC per year or per day to minimize the yearly or daily total EAC provision cost. Firstly, operation, evaluation and control methods of DHCs for the EA are explained in Chapter 1 and 2. Secondly, DHC models assuming actual DHCs and problems are formulated in chapter 3, and other simulation conditions are explained in chapter 4. Then, the annual EAC provision costs by single control and aggregation control are calculated by the particle swarm optimization (PSO) and compared in chapter 5, and results are discussed in chapter 6. Finally, a summary of this research is described in chapter 7.

2. Operation and evaluation of a DHC for EA

2.1. Methods for operating a DHC

The original use of a DHC is to satisfy regional heat and cold demand. Fig. 1 shows an image of the use of DHCs. DHCs run on city gas and electricity to satisfy each regional heat and cold demand. Furthermore, recent DHCs are able to generate electricity and sell it for minimizing running costs because they often installed with CHPs in order to improve efficiency. In this research, methods for operating a DHC for EA is examined by utilizing these characteristics.

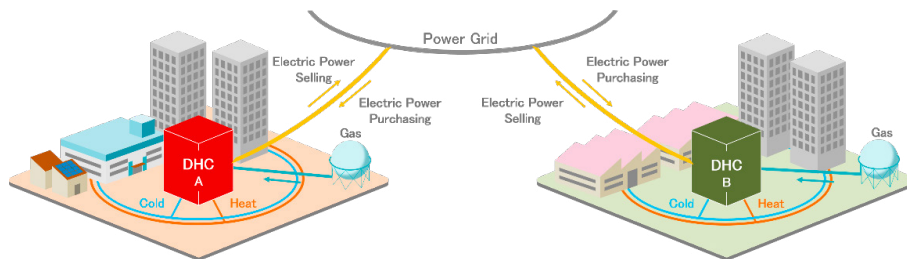


Fig. 1. An image of the use of DHCs.

Two operations are defined in this paper: normal operation (Op. 1) and electricity adjustment capacity (EAC) provision operation (Op. 2). Op. 1 is an operation of DHC without considering EA market auction. Op. 1 satisfies district heat and cold demand. Meanwhile, Op. 2 is an operation of DHC contracting EA with the power grid company through the EA market auction. Op. 2, in addition to satisfying district heat and cold demand, always keeps more EAC than the EAC of contract so that it can provide EA according to directives from the power grid company. Additionally, transmission power in each operation is illustrated in Fig. 2 (a) and (b). The EAC is determined by the difference between the maximum transmission power and the actual transmission power as shown in Fig. 2 (b).

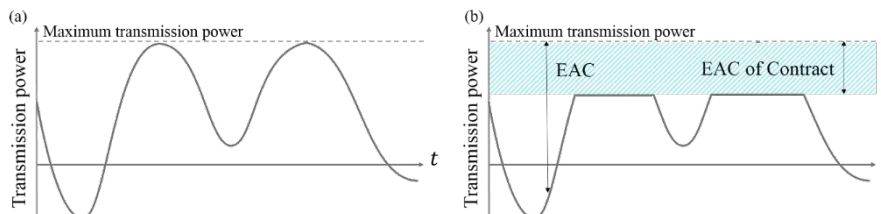


Fig. 2. (a) Transmission power in normal operation (Op. 1); (b) Transmission power in EAC provision operation (Op. 2).

2.2. Methods for evaluating cost

Three costs are defined in this paper: running cost of Op. 1, running cost of Op. 2 and EAC provision cost. First, running cost of each operation (Op. 1, Op. 2) is calculated by the running cost minimum operation determination method shown in our previous study [28]. In addition, the particle swarm optimization (PSO) which is one of the metaheuristics is used in this method [29, 30]. Second, EAC provision cost is calculated by subtracting the running

cost of Op. 1 from the running cost of Op. 2. Therefore, this cost represents the additional cost when DHC is operated for EA. For this reason, EAC provision cost is used as an evaluation index for economic efficiency in this paper. Fig. 3 shows the EAC provision cost calculation flow.

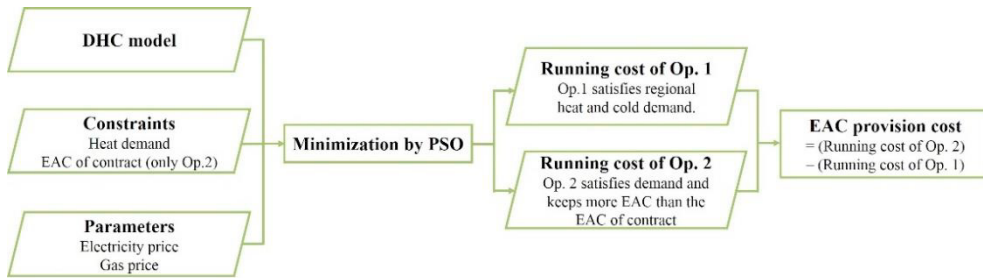


Fig. 3. The EAC provision cost calculation flow.

3. Control methods of multiple DHCs

This chapter explains methods to control multiple DHCs. As an example, a control method for two DHCs is explained here.

3.1. Single control

In the single control, the EAC of the contract of each DHC is arbitrarily determined on a yearly basis without considering the EAC of the other DHC. Fig. 4 (a) shows an image of the single control. For example, DHC A contracts with a power grid company with 5,000 kW EAC of contract, and performs Op. 2. Likewise, if there is DHC B, it arbitrarily determines the EAC of contract, contracts with a power grid company, and performs Op. 2.

3.2. Aggregation control

The aggregation control combines DHC's EACs to ensure the total EAC of contract that is arbitrarily determined. Also, the aggregator determines the assigned EAC ratio which is a ratio of an EAC for the DHC A to an EAC for the DHC B per year or per day so that the total EAC provision cost per year (Yearly Aggregation Control) or per day (Daily Aggregation Control) is minimized. Fig. 4 (b) shows an image of the aggregation control. For example, when the EAC of aggregator's contract is 5,000 kW, the DHC A and B share the total EAC of contract, and each DHC performs Op. 2. The aggregator optimizes the assigned EAC ratio to each DHC so that the total EAC provision cost per year or day is minimized.

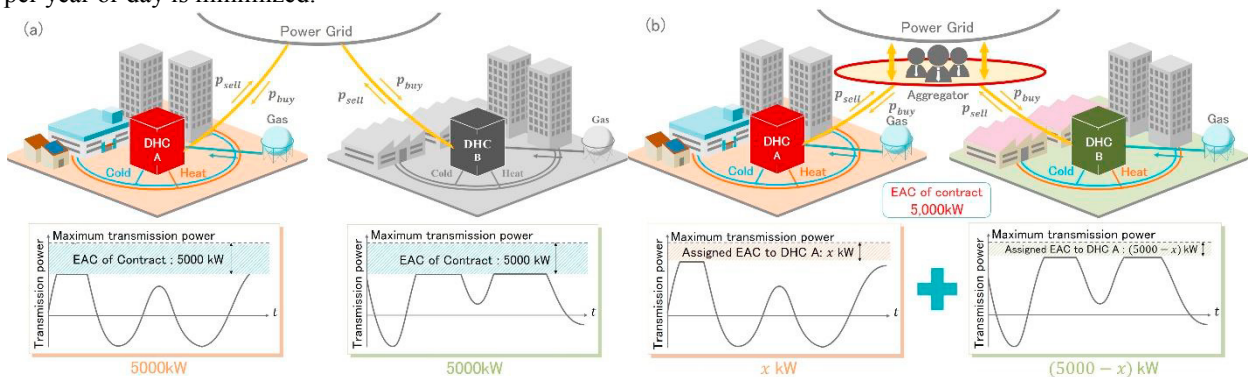


Fig. 4. (a) An image of the single control. (b) An image of the aggregation control.

3. Modeling the DHCs

3.1. Assumptions for the DHC models

This chapter explains modeling of two DHCs used in this research. These DHC models are based on existing DHC in Japan and consist of devices for heat, cold and electricity demand as shown in Fig. 5 (a) and (b). Each device of DHC includes nonlinear efficiency, upper and lower limit output, and starting and stopping time as shown in Table 1 and 2. Since the simulation is carried out at one hour intervals, the starting and stopping time is set as 0 h for the device that can start and stop within 30 minutes.

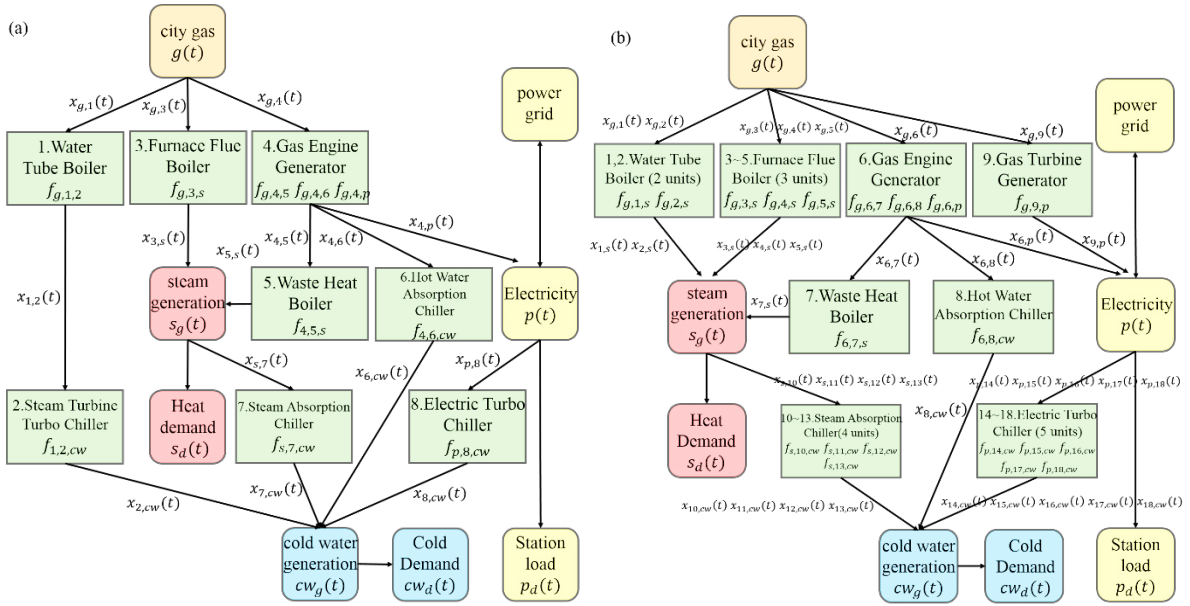


Fig. 5. (a) The DHC A model. (b) The DHC B model.

3.2. DHC A model

The DHC A model consists of eight devices as shown in Fig. 5 (a), which also shows the relationships between them. Heat energy is provided by devices. 3 and 5, cold energy is provided by devices. 1, 2, 6, 7 and 8, and station load is assumed. In addition, the station load is assumed to be constant at 4,000 kW. A gas engine generator (No. 4) provides electricity to the power system and heat energy to devices. 5 and 6, which together comprise the CHP system. Devices. 1, 3, and 4 run on city gas, and device. 8 runs on electricity that is provided by device. 4 and the power system.

3.3. Formulation of DHC A model

Based on the DHC A model in Fig. 5 (a), the problem for calculating the running cost of Op. 1 and the running cost of Op. 2 is formulated. Functions $f_{i,n,j}$ represents functions that convert an input i to an output j of the device n . Parameters $x_{i,n}$ represents inputs to the equipment n . Parameters $x_{n,j}$ represents outputs from the device n . Eq. (1) is the objective function that minimizes the running cost of the day, calculated by the gas consumption and the purchased or sold electricity. Parameter $p(t)$ takes a positive value when purchasing, and takes a negative value when selling. Eqs. (2) - (4) are constraints of heat demand, cold demand and EA. Eqs. (5) and (6) represents the gas consumption and the transmitted power. According to Table 1, Eqs. (7) and (8) represent starting time constraints of the device.

$$Cost = \sum_{t=1}^{24} (p_g \times g(t) + p_p \times p(t)) \rightarrow \text{Minimize} \quad (1)$$

$$x_{3,s}(t) + x_{5,s}(t) - x_{s,7}(t) \geq s_d(t) \quad (2)$$

$$x_{2,cw}(t) + x_{6,cw}(t) + x_{7,cw}(t) + x_{8,cw}(t) \geq cw_d(t) \quad (3)$$

$$cap_{target}(t) \leq \sum_n cap_n(t) \quad (n = 4, 8) \quad (4)$$

$$g(t) = x_{g,1}(t) + x_{g,3}(t) + x_{g,4}(t) \quad (5)$$

$$p(t) = x_{4,p}(t) - x_{p,8}(t) - p_s(t) \quad (6)$$

$$\text{if } x_{n,j}(t - t_n^{start}, \dots, t - 1) = 0 \text{ and } x_{n,j}(t) \neq 0 \quad (7)$$

$$x_{i,n}(t - t_n^{start}, \dots, t - 1) = x_{i,n}^{start} \quad (8)$$

$$t_1^{start} = 2, t_2^{start} = t_3^{start} = 1, t_n^{start} = 0 \quad (n = 4, 5, 6, 7, 8)$$

$$x_{g,1}^{start} = x_{g,1}^{min} / 2, x_{g,3}^{start} = x_{g,3}^{min} / 2, x_{1,2}^{start} = x_{1,2}^{min}$$

Table 1. Device of DHC A data.

Device number and name	Lower output limit	Upper output limit	Starting time	Stopping time
1. Water tube boiler	24.3 ton/h	97.2 ton/h	2h	0h
2. Steam turbine turbo chiller	63.25 GJ/h	253 GJ/h	1h	0h
3. Furnace flue boiler	5.4 ton/h	46.8 ton/h	1h	0h
4. Gas engine generator	3,485 kW	15,700 kW	0h	0h
5. Waste heat boiler	2.25 ton/h	10 ton/h	0h	0h
6. Hot water absorption chiller	2.15 GJ/h	9.0 GJ/h	0h	0h
7. Steam absorption chiller	9.45 GJ/h	75.6 GJ/h	0h	0h
8. Electric turbo chiller	4.4 GJ/h	21.4 GJ/h	0h	0h

3.4. DHC B model

The DHC B model consists of eight types of eighteen devices as shown in Fig. 6 (b), which expresses the relationships between them. Heat energy is provided by devices. 1, 2, 3, 4, 5 and 7, cold energy is provided by devices. 8, 10, 11, 12, 13, 14, 15, 16, 17 and 18, and station load is assumed. In addition, the station load is assumed to be constant at 4,000 kW. A gas engine generator (No. 6) provides electricity to the power system and heat energy to devices. 7 and 8, which together comprise the CHP system. Device. 1, 2, 3, 4, 5, 6 and 9 run on city gas, and devices. 14, 15, 16, 17 and 18 runs on electricity that is provided by device. 6 and the power system.

3.5. Formulation of DHC B model

Based on the DHC B model in Fig. 5 (b), the problem for calculating the running cost of Op. 1 and the running cost of Op. 2 is formulated. Eq. (9) is the objective function that minimizes the running cost of the day, calculated by the gas consumption and the purchased or sold electricity. Eqs. (10) - (12) are constraints of heat demand, cold demand and EA. Eqs. (13) and (14) represents the gas consumption and the transmitted power. According to Table 2, the DHC B has no starting and stopping time constraint of the device.

$$Cost = \sum_{t=1}^{24} (p_g \times g(t) + p_p \times p(t)) \rightarrow \text{Minimize} \quad (9)$$

$$\sum_{n=1}^5 x_{n,s}(t) + x_{7,s}(t) - \sum_{n=10}^{13} x_{s,n}(t) \geq s_d(t) \tag{10}$$

$$x_{8,cw}(t) + \sum_{n=10}^{13} x_{n,cw}(t) + \sum_{n=14}^{18} x_{n,cw}(t) \geq cw_d(t) \tag{11}$$

$$cap_{target}(t) \leq \sum_n cap_n(t) \quad (n = 6, 9, 14, 15, 16, 17, 18) \tag{12}$$

$$g(t) = \sum_{n=1}^6 x_{g,n}(t) + x_{g,9}(t) \tag{13}$$

$$p(t) = x_{6,p}(t) + x_{9,p}(t) - \sum_{n=14}^{18} x_{p,n}(t) - p_s(t) \tag{14}$$

Table 2. Equipment of DHC B data.

Device number and name	Lower output limit	Upper output limit	Starting time	Stopping time
1, 2. Water tube boiler	8.06 ton/h	40.3 ton/h	0h	0h
3, 4. Furnace flue boiler	2.14 ton/h	10.7 ton/h	0h	0h
5. Furnace flue boiler	4.28 ton/h	21.4 ton/h	0h	0h
6. Gas engine generator	3,900 kW	7,800 kW	0h	0h
7. Waste heat boiler	2.8 ton/h	4.1 ton/h	0h	0h
8. Hot water absorption chiller	1.34 GJ/h	6.71 GJ/h	0h	0h
9. Gas turbine generator	1,300 kW	2,000 kW	0h	0h
10, 11. Steam absorption chiller	1.58 GJ/h	15.8 GJ/h	0h	0h
12, 13. Steam absorption chiller	3.16 GJ/h	31.6 GJ/h	0h	0h
14~18. Electric turbo chiller	1.58 GJ/h	15.8 GJ/h	0h	0h

4. Condition for numerical simulations

The values taken for price, amount of EAC, and station load are listed in Table 3. The prices are an example. The EAC of DHC A is 1,000 kW to 8,000 kW in 1,000 kW increments. The EAC of DHC B is 1,000 kW to 5,000 kW in 1,000 kW increments. Both DHCs have station loads of 4,000 kW. Figs. 6 and 7 represent heat and cold demand of each DHC on weekdays, holidays and Saturdays in winter, summer and the other seasons. Table 4 lists the number of days of each day of each season.

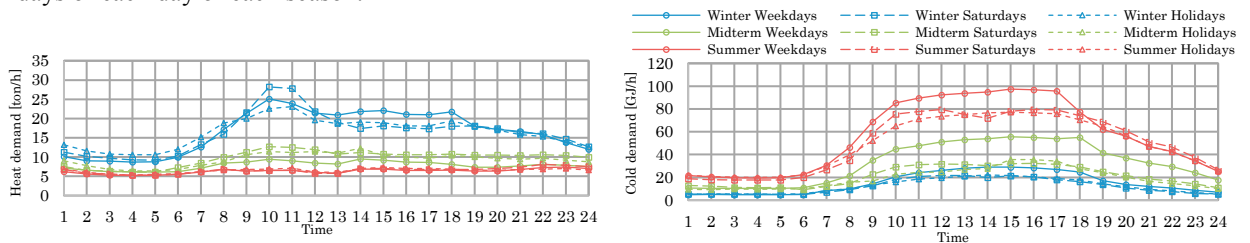


Fig. 6. Heat and cold demand of DHC A.

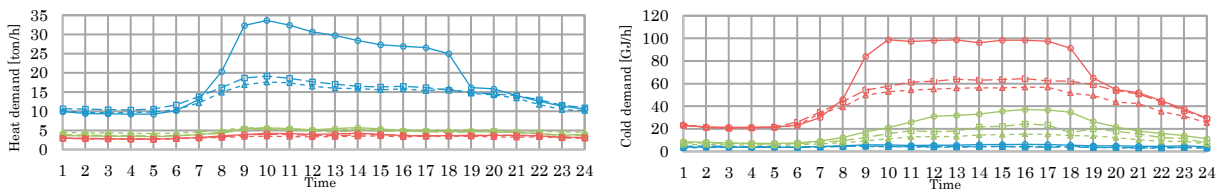


Fig. 7. Heat and cold demand of DHC B.

Table 3. Parameters for the numerical simulations

Name	Value
p_g	90 [yen/m ³]
p_p	17 [yen/kWh] (to buy), 12 [yen/kWh] (to sell)
Number of DHCs	2
cap_{target}	Total; 2,000~10,000 [kW]; 2,000 [kW] DHC A; 1,000~8,000 [kW]; 1,000 [kW] interval interval DHC B; 1,000~5,000 [kW]; 1,000 [kW] interval

Table 4. Lists the number of days of each day of each season.

	Winter (Dec, Jan, Feb)	Midterm (Mar, Apr, May, Sep, Oct, Nov)	Summer (Jun, Jul, Aug)
Weekdays	60	121	64
Saturdays	14	26	13
Holidays	17	36	15

5. Results

5.1. EAC provision costs of each DHCs

Fig. 8 (a) and (b) show the EAC provision costs of DHC A and B that are calculated by subtracting the running cost of Op. 1 from the running cost of Op. 2 and divided by the running cost of Op.1. The EAC provision cost of DHC A is almost zero on a winter Saturday and a winter holiday. And, the EAC provision cost of DHC B is almost zero on any day in winter, midterm holiday, summer weekday and summer holiday. In this way, the EAC provision cost of each DHC is different because the configuration of each DHC and the heat and cold demand are different.

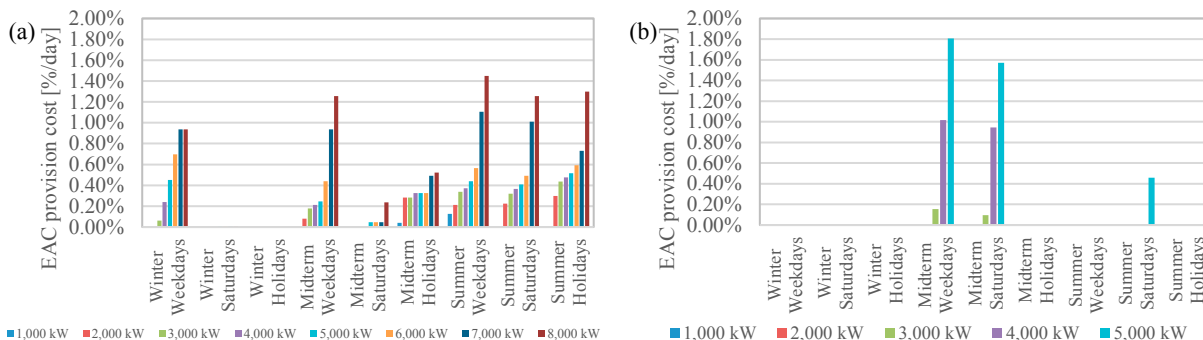


Fig. 8. (a) EAC provision costs for each type of day in DHC A (b) EAC provision costs for each type of day in DHC B.

5.2. Annual EAC provision costs by single and aggregation control

By using the results of section 5.1 and the Table 4, the annual EAC provision costs by single and aggregation control of multiple DHCs are calculated. Fig. 9 (a) shows the annual EAC provision cost rate by single and aggregation control of multiple DHCs. It is annual EAC provision cost is divided by the annual running cost of Op. 1. The values of the single control are sum of the annual EAC provision cost rate of the two DHCs operated for half of the EAC of aggregator’s contract. That is, 5,000 kW EAC of Contract is assigned to the two DHCs in case of 10,000 kW in the figure. Fig. 9 (b) shows the annual reduced cost rate by aggregation control compared with single control. The annual EAC provision costs were reduced in all cases of the EAC of aggregator’s contract by daily aggregation control. For example, when the EAC of aggregator’s contract is 6,000 kW, reduced cost rate was 54.3%.

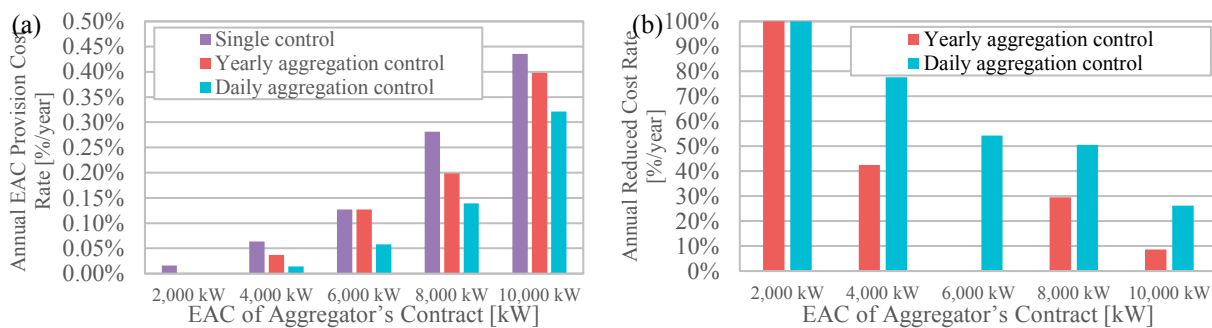


Fig. 9. (a) Annual EAC Provision Cost Rate (b) Annual Reduced Cost by aggregation control.

6. Discussions

Fig. 10 (a) and (b) show the assigned EAC to each DHC for yearly and daily aggregation control in cases of 6,000 kW and 10,000 kW of EAC of aggregator's contract. Ratios of the assigned EACs of each DHC are different depends on days and seasons. The ratios are determined to minimize sum of the EAC provision cost of the DHCs. For example, in case of 6,000 kW EAC of aggregator's contract, the ratio of assigned EAC to DHC A in midterm weekdays and Saturday is high because the EAC provision cost of DHC B is higher than that of DHC A in midterm weekdays and Saturday that can be found in Fig. 8.

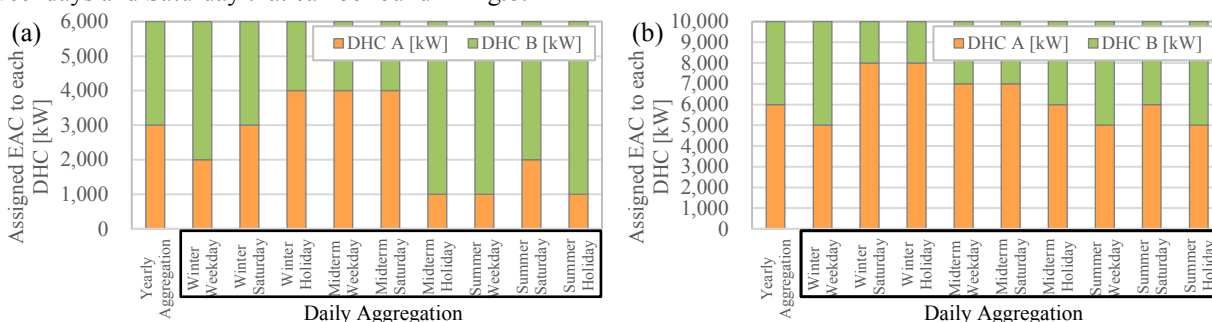


Fig. 10. (a) Assigned EAC to each DHC when it is 6,000 kW (b) Assigned EAC to each DHC when it is 10,000 kW

7. Conclusions

Renewable energies have inherent fluctuation effecting the power system stability. Therefore, the electricity adjustment (EA) market auction was launched in order to increase power system stability. The district heating and cooling (DHC) is operated for not only satisfying the heat and cold demand but also supplying electricity by using the combined heat and power (CHP). For this reason, the possibility of contributions to the power system is expected to be high. However, participation of the DHC in the EA market had not been discussed well. Our previous research showed the usefulness of the EA by single control of the DHC in the EA market. In this paper, in order to realize more efficient EA, aggregation control by multiple DHCs was proposed. The control combines DHC's electricity adjustment capacities (EACs) to ensure the total EAC of contract. Also, the aggregator determines the assigned EAC ratio which is a ratio of an EAC for each DHC per year or per day so that the total EAC provision cost per year (Yearly Aggregation Control) or per day (Daily Aggregation Control) is minimized. At first, two DHCs were modeled assuming actual DHCs. Using these models, the running costs of the normal operation (Op. 1) and the EAC provision operation (Op. 2) of each DHC were calculated by the particle swarm optimization (PSO). And then, the annual EAC provision cost by single and aggregation control of multiple DHCs was calculated. As a result, the annual EAC provision cost was reduced by aggregation control compared with single control. For

example, in case of 6,000 kW EAC of contract, reduced cost rate was 54.3% by daily aggregation control. The operators of DHCs can more efficiently operate DHCs for EA by using proposed aggregation control. Eventually, further stability of the power system can be expected.

References

- [1] Midterm-term renewable energy market report 2016. International Energy Agency: (2016)
- [2] Renewables 2017 global status report. REN21: (2017)
- [3] The energy report 100% renewable energy by 2050. The World Wildlife Fund for nature: (2011)
- [4] Anne Sjoerd Brouwer, Machteld van den Broek, Ad Seebregts, André Faaij. "Impacts of large-scale Intermittent Renewable Energy Sources on electricity systems, and how these can be modeled." *Renewable and Sustainable Energy Reviews* 33 (2014): 443-466
- [5] Maurer, Luiz T. A, Barroso. Luiz A. "Electricity auctions: An overview of efficient practices." *Journal of Economics* 10(3) (2011): 1-180.
- [6] Mathew J. Morey. "Power Market Auction Design: Rules and Lessons in Market Based Control for the New Electricity Industry." Prepared for Edison Electric Institute (2001)
- [7] Andrew L. Ott. "Experience with PJM Market Operation, System Design, and Implementation Andrew." *IEEE Transactions on Power Systems* 18(2) (2003): 528-534
- [8] Barillas, A, Cohen, R, Sukthaworn, N. "Lessons from the First Capacity Market Auction in Great Britain." 12th International Conference on the European Energy Market (2015)
- [9] P. J. Mago, N. Fumo, L. M. Chamra. "Performance analysis of CCHP and CHP systems operating following the thermal and electric load." *International journal of energy research* 33 (2009) 852-864
- [10] Wu, D. W, Wang, R. Z. "Combined cooling, heating and power: A review." *Progress in Energy and Combustion Science* 32(5-6) (2006): 459-495
- [11] Andersen, Anders N, Lund, Henrik. "New CHP partnerships offering balancing of fluctuating renewable electricity productions" *Journal of Cleaner Production* 15(3) (2007): 288-293
- [12] Fragaki, Aikaterini, Andersen, Anders N. "Conditions for aggregation of CHP plants in the UK electricity market and exploration of plant size." *Applied Energy* 88(11) (2011): 3930-3940
- [13] Jarre, Matteo, Noussan, Michel, Poggio, Alberto. "Operational analysis of natural gas combined cycle CHP plants: Energy performance and pollutant emissions." *Applied Thermal Engineering* 100 (2016): 304-314
- [14] Streckiene, G, Martinaitis, V, Andersen, A N, Katz, J. "Feasibility of CHP-plants with thermal stores in the German spot market." *Applied Energy* 86(11) (2009): 2308-2316
- [15] Aghaei, J, Alizadeh, M I. "Multi-objective self-scheduling of CHP (combined heat and power)-based microgrids considering demand response programs and ESSs (energy storage systems)." *Energy* 55 (2013): 1044-1054
- [16] Henrik Lund, Sven Werner, Robin Wiltshire, Svend Svendsen, Jan Eric Thorsen, Frede Hvelplund, Brian Vad Mathiesen. "4th Generation District Heating (4GDH) Integrating smart thermal grids into future sustainable energy systems." *Energy* 68 (2014): 1-11
- [17] Werner, Sven. "International review of district heating and cooling." *Energy* 137 (2017): 617-631
- [18] Lake, A, Rezaei, B, Beyerlein, S. "Review of district heating and cooling systems for a sustainable future." *Renewable & Sustainable Energy Reviews* 67 (2017): 417-425
- [19] Colmenar-santos, Antonio, Rosales-asensio, Enrique, Borge-diez, David, Blanes-peiró, Jorge-juan. "District heating and cogeneration in the EU-28 : Current situation , potential and proposed energy strategy for its generalisation." *Renewable and Sustainable Energy Reviews* 62 (2016): 621-639
- [20] Werner, Sven. "District heating and cooling in Sweden." *Energy* 126 (2017): 419-429
- [21] Sayegh, M A, Danielewicz, J, Nannou, T, Miniewicz, M, Jadwiszczak, P, Piekarska, K, Jouhara, H. "Trends of European research and development in district heating technologies." *Renewable and Sustainable Energy Reviews* 68 (2017): 1183-1192
- [22] Sakawa, M, Kato, K, Ushiro, S. "Operational planning of district heating and cooling plants through genetic algorithms for mixed 0-1 linear programming." *European Journal of Operational Research* 137(3) (2002): 677-687
- [23] Casisi, M, Pinamonti, P, Reini, M. "Optimal lay-out and operation of combined heat & power (CHP) distributed generation systems." *Energy* 34(12) (2009): 2175-2183
- [24] Ameri, M, Besharati, Z. "Optimal design and operation of district heating and cooling networks with CCHP systems in a residential complex." *Energy* 34(12) (2009): 2175-2183
- [25] Wang, Haichao, Yin, Wusong, Abdollahi, Elnaz, Lahdelma, Risto, Jiao, Wenling. "Modelling and optimization of CHP based district heating system with renewable energy production and energy storage." *Applied Energy* 159 (2015): 401-421
- [26] Bjorn Rolfsman. "Combined heat-and-power plants and district heating in a deregulated electricity market." *Applied Energy* 78 (2004): 37-52
- [27] Ito, Masakazu, Takano, Akihisa, Shinji, Takao, Yagi, Takahiro, Hayashi, Yasuhiro. "Electricity adjustment for capacity market auction by a district heating and cooling system." *Applied Energy* 206 (2017): 623-633
- [28] Akihisa Takano, Yasuhiro Hayashi, Masakazu Ito, Takao Shinji, Masayuki Tadokoro "Cost Analysis of Demand Response Incentive for District Heating and Cooling." *The International Conference on Electrical Engineering* (2016)
- [29] J.Kennedy, R.Eberhart. "Particle Swarm Optimization." *IEEE International Conference on Neural Networks* 4 (1995): 1942-1948
- [30] Zue-Lee Gaing. "Particle swarm optimization to solving the economic dispatch considering the generator constraints." *IEEE Transactions on Power Systems* 18(3) (2003): 1187-1195



Available online at www.sciencedirect.com

ScienceDirect

Energy Procedia 149 (2018) 327–336

Energy

Procedia

www.elsevier.com/locate/procedia

16th International Symposium on District Heating and Cooling, DHC2018,
9–12 September 2018, Hamburg, Germany

Differential Impacts of Additional Consumers on DH-Systems – Analysis for Absorption Chillers

Felix Panitz, Vera Volmer*, Karin Rühling

Institute of Power Engineering, Chair of Building Energy Systems and Heat Supply, Technische Universität Dresden, 01062 Dresden, Germany

Abstract

The purpose of this paper is the evaluation of absorption chillers (ACh) acting as additional heat consumers in district heating (DH) networks. The focus is on the ACh-effects on an upstream DH system: network (heat losses, electricity demand of pumps) and heat generator (heat generation, electricity generation, fuel demand). Simulations for real DH systems with different network topologies are performed to determine additional efforts in the network caused by the ACh. Furthermore, effects on heat generation are shown. As real CHP-data of the partners is sensitive, a construed example is used. Characteristic seasonal key figures for the impact of an additional heat consumer are calculated via operational optimization. Afterwards, effects on network and heat generation are combined to overall primary energy effects of ACh. Finally, primary energy efficiency of cold production by district heat driven ACh is evaluated and compared to cold production by compression chillers.

© 2018 The Authors. Published by Elsevier Ltd.

This is an open access article under the CC BY-NC-ND license (<https://creativecommons.org/licenses/by-nc-nd/4.0/>)

Selection and peer-review under responsibility of the scientific committee of the 16th International Symposium on District Heating and Cooling, DHC2018.

Keywords: absorption chillers, district heating, heat losses, pumping electricity, optimization of generator operation

* Corresponding author. Tel.: +49-351-463-34477; fax: +49-351-463-37076.

E-mail address: vera.volmer@tu-dresden.de

1876-6102 © 2018 The Authors. Published by Elsevier Ltd.

This is an open access article under the CC BY-NC-ND license (<https://creativecommons.org/licenses/by-nc-nd/4.0/>)

Selection and peer-review under responsibility of the scientific committee of the 16th International Symposium on District Heating and Cooling, DHC2018.

10.1016/j.egypro.2018.08.196

1. Introduction

Absorption chillers (ACh) have always been an interesting and tempting option to create a higher heat demand in district heating (DH) systems. Part loads in DH systems during summer time can partly be compensated with acyclic occurring cold demand and therefore heat demand of ACh.

However, older generations of ACh require high driving temperatures. In some cases, supply temperatures of DH networks are therefore increased throughout the network and hence increase heat losses. Return temperatures of old ACh are high (about 80 °C), increase the temperature of the return line of the DH system and thus heat losses and electricity demand of DH pumps raise up. Furthermore, providing heat at a high temperature level has a negative effect on the efficiency of CHP plant and is often contrary to long-term strategies of DH companies such as “low-ex” networks and integration of renewable sources.

Nomenclature

Symbols		Abbreviations		Indices		
e_{Pu}	specific electricity demand	kW_{el}/kW_{th}	ACh	absorption chiller	a	ambient
P	electrical power	kW_{el}	CHP	combined heat and power	avg	average
Q	thermal energy	kWh_{th}	COP	coefficient of performance	Con	consumer
\dot{Q}	thermal power	kW_{th}	DH	district heating	el	electrical
\dot{q}_L	specific thermal loss	kW_{th}/kW_{th}			Gen	generation
W	electrical energy	kWh_{el}			L	loss
					Pu	pump
					th	thermal
					0	cold
					*	<u>with ACh</u>

In the project “FAKS - Feldtest Absorptionskältetechnik für KWKK-Systeme” a new generation of ACh called “Hummel” (bumblebee) or “Biene” (bee) is installed in several DH systems in Germany. The new ACh achieves a lower temperature level of the driving heat. Typically, return temperatures in the range of 60 °C to 70 °C are realized, depending on the respective DH and cooling system. Local electricity and heat demand of these ACh cooling systems were measured and are therefore relatively easy to analyze as done in [1]. Depending on the installation, long-term-values of thermal efficiency vary from 0.5 kWh_0/kWh_{th} to 0.75 kWh_0/kWh_{th} . Electrical efficiency reaches values from 3 kWh_0/kWh_{el} to 30 kWh_0/kWh_{el} . For this paper, typical average values of 0.7 kWh_0/kWh_{th} (thermal) and 10 kWh_0/kWh_{el} (electrical) are used for all calculations.

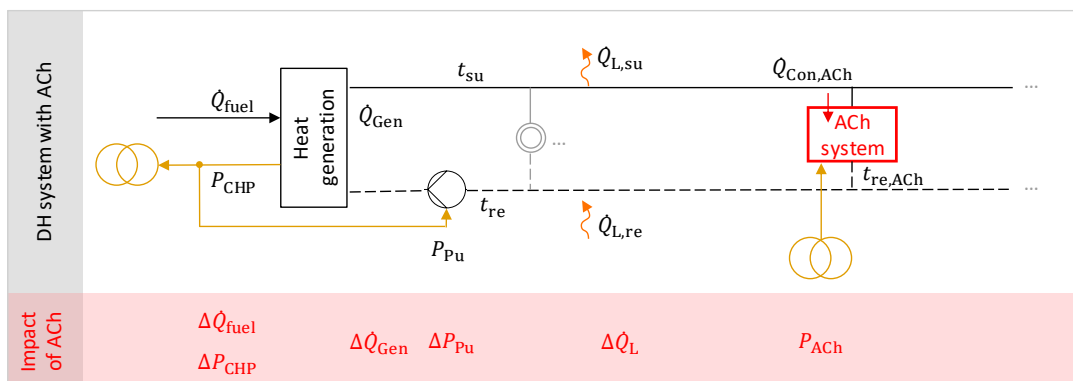


Fig. 1. Influence of an additional ACh integrated in a DH system

The focus of this paper is on the ACh-effects, both for old and new generation, on an upstream DH system as shown in Fig. 1: network with heat losses \dot{Q}_L and electricity demand of pumps P_{Pu} and heat generator with heat generation \dot{Q}_{DH} , electricity generation P_{CHP} as well as fuel demand \dot{Q}_{fuel} . Changes in these values caused by the ACh (red colored symbols in Fig. 1) can hardly be measured and therefore must be estimated model-based.

In this paper, an important basic assumption is that the upstream DH system is not (differentially) changed due to the additional load: No pipe-diameters are enlarged and no additional heat generators are installed. For a fair comparative evaluation of heat and electricity the same assumption has to be made for additional electricity demand for both ACh and compression chiller: No additional renewables are installed, so the additional electricity demand is provided by the existing power plant fleet. Therefore, the additional electricity is produced by the last power station in merit order which currently still is a conventional plant. With these assumptions, results focus on short-term effects.

2. Effect on upstream DH network

2.1. General approach

Network effects will be demonstrated for four ACh installations (called HENK, ROKK, KFWK, ESTW). The method will be presented for HENK, an ACh installation located in a large scale and highly meshed DH network with a peak load of 637 MW. Two heat generator locations, called CHP1 and CHP2, supply the DH network. Linear distances between heat supply stations and ACh are about 3.6 km (CHP2) and 9.5 km (CHP1).

Network simulations for five characteristic load distributions in the DH system (Table 1) have been evaluated regarding heat losses and pumping electricity. In each case, simulations without the consumer ACh (reference case) and with the consumer ACh have been performed. Differences between the results show the impact of the ACh. Due to the low heat load of the investigated ACh these differences will be small and therefore high accuracy of the simulations is necessary.

In all scenarios the ACh has a heat load of 175 kW. The DH return temperature of the ACh is 77 °C and rather representing an older generation of ACh. The supply temperature of the DH system is already sufficient for the ACh and thus is the same in both simulations. Simulations have been executed by the DH company using in-house network data and the simulation tool SIR 3S®.

Table 1. Parameter of the chosen simulation scenarios.

Supply Station & ambient temperature	CHP1+2 / -14°C	CHP1+2 / +1°C	CHP1 / +15°C	CHP1 / +30°C	CHP2 / +30°C
Supply temperature at heat generator	120 °C	92 °C	92 °C	92 °C	92 °C
Return temperature at heat generator	60 °C	58 °C	60 °C	64 °C	64 °C
Thermal load	637 MW	394 MW	105 MW	39 MW	38 MW

2.2. Heat losses

Simulations produce total heat loss of the system without ACh (\dot{Q}_L) and with ACh (\dot{Q}_L^*). Their difference is $\Delta\dot{Q}_L$ which describes the additional heat losses caused by the ACh. $\Delta\dot{Q}_L$ is small in comparison to \dot{Q}_L due to the small heat demand of the ACh. For evaluation purposes specific values are used: The additional heat loss, caused by the ACh, is related to the additional consumer heat demand $\dot{Q}_{Con,ACh}$.

$$\dot{q}_{L,ACh} = \frac{\Delta\dot{Q}_L}{\dot{Q}_{Con,ACh}} \quad (1)$$

Afterwards it is compared to the network's average specific heat loss in the simulation without ACh (overall heat loss \dot{Q}_L related to the overall consumer heat demand $\dot{Q}_{Con,all}$)

$$\dot{q}_{L,avg} = \frac{\dot{Q}_L}{\dot{Q}_{Con,all}} \quad (2)$$

Results for all five scenarios are shown in Fig. 2. Specific additional heat losses caused by ACh are significantly smaller than those of the average consumer although the ACh's return temperature is relatively high. Only the value at CHP1 / +15 °C shows nearly the same values as for the average. One possible reason is that the ACh causes nearby branches not to cool down as much as without ACh. Because of data security reasons unfortunately the authors had no opportunity to investigate local simulation effects in the network in detail.

All in all, heat losses caused by the ACh are not a very relevant aspect for the DH provider as long as the supply temperature does not have to be increased. General lifts of the DH supply temperature for operating an ACh can have much higher relevance but did not occur for the installed new ACh generation, as its required temperature level is rather low.

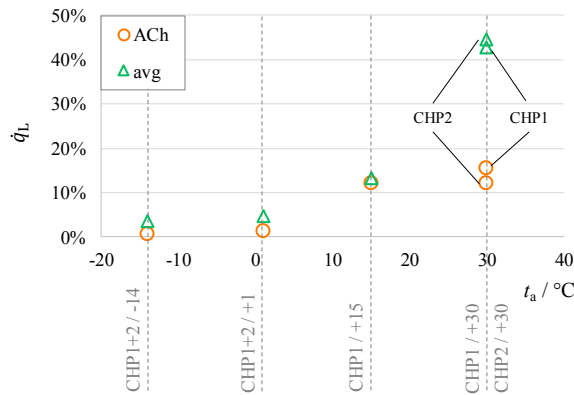


Fig. 2. Heat losses caused by the ACh (heat load 175 kW, return temperature 77 °C) and average heat losses in an existing DH system.

2.3. Hydraulic losses / pumping electricity

Analogously to the heat losses, results of the additional pumping electricity ΔP_{Pu} are shown in Fig. 3 in specific values

$$e_{Pu,ACh} = \frac{\Delta P_{Pu}}{\dot{Q}_{Con,ACh}} \quad (3)$$

and are compared to the average specific pumping electricity

$$e_{Pu,avg} = \frac{P_{Pu}}{\dot{Q}_{Con,all}} \quad (4)$$

Specific pumping electricity is especially high at CHP1 / +15 °C, because the network's volume flow is particularly high during that time. Specific additional pumping electricity of ACh in Fig. 3 is always higher than the network's average. On the one hand, this is caused by the low temperature spread of the ACh. On the other hand, the additional

volume flow has an impact on the circuit of the network with the highest resistance (index circuit) and as a result not only the volume flow but the required head of the central DH pumps increases. The latter is also the reason why additional pumping electricity is extremely depending on load distribution and ACh-location in the network. So although average specific electricity demand from 1 °C to 15 °C decreases by more than half, the specific electricity demand of ACh is even increasing. Even same load and load distributions can lead to different results (scenario CHP1 / +30 °C and CHP2 / +30 °C) due to different heat generation locations.

Pumping electricity demand of the ACh in the investigated network with the given return temperature of 77 °C cannot be neglected as values reach 0.055 kW_{el}/kW_{th}. This is equivalent to an electrical COP of the cold of 12.7 kWh₀/kW_{h_{el}} only for heat transport (with local electricity demand of the cold system not even included in the calculation)!

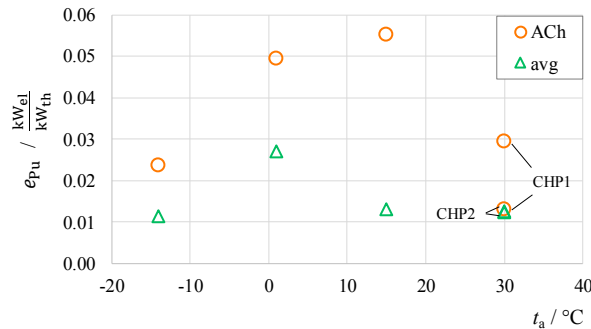


Fig. 3. Pumping electricity demand for ACh-heat (heat load 175 kW, return temperature 77 °C) and average demand in an existing DH system.

2.4. Lower return temperatures and comparison with other ACh installations in DH systems

Simulations from the DH partner from HENK have only been performed for 77 °C ACh return temperature. But as said before the new generation of ACh achieves lower temperatures. The annual average ACh return temperature for HENK is about 68 °C. Based on the simulation results the authors estimated the effects for other ACh return temperatures (Fig. 4): Heat losses at other return temperatures than the simulated one are “roughly” calculated by postulating a simplified network branch structure. Pumping electricity can be transformed as volume-flow related electricity demand remains nearly constant.

For a return temperature of 68 °C, specific additional heat loss as well as additional pumping electricity are significantly lower. Heat losses can especially be reduced in spring and summer. Influence of the return temperature on pumping electricity is high as a lower return temperature leads to lower volume flow. However, pumping electricity values still reach significant values of about 0.03 kW_{el}/kW_{th}. Higher supply temperature of the network also reduces the ACh volume flow and therefore decreases return temperature’s impact on pumping electricity (as can be seen for CHP1+2/ -14).

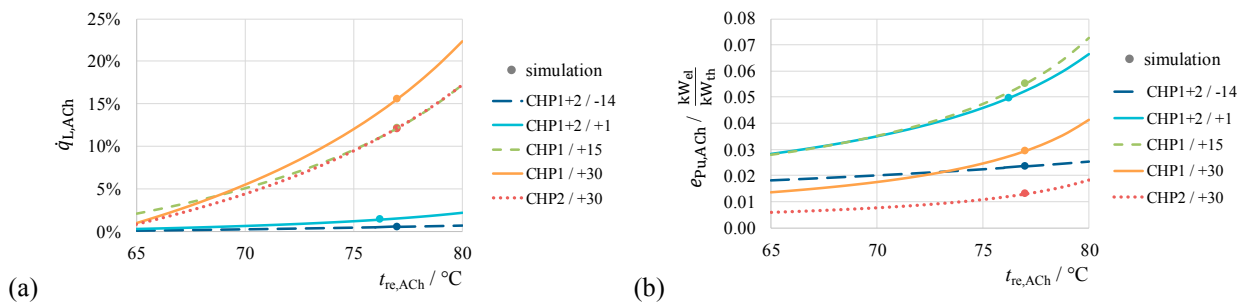


Fig. 4. Network effects for different ACh return temperatures (a) specific additional heat loss (b) specific additional pumping electricity.

Table 2. Information about DH systems with ACh installations.

Name of installation	HENK	ROKK	KFWK	ESTW
Nominal load of network	637 MW _{th}	65 MW _{th}	440 MW _{th}	70 MW _{th}
Network length	315 km	54 km	174 km	120 km
Distance ACh to heat supply	3.6 km/ 9.6 km	0.8 km	0 km	0 km

Network effects in HENK are compared with results from other installations in ROKK, KFWK and ESTW (Fig. 5). These installations are described in Table 2. Highest additional heat losses occur in HENK due to the long distances to the supply stations. As installations in KFWK and ESTW are directly located after a supply station no additional heat losses occur. KFWK values are only shown for the heating period as the heat supply station is deactivated in summertime. Other supply stations in the KFWK network provide the heat in summertime but no information about the network effects were handed over to the authors.

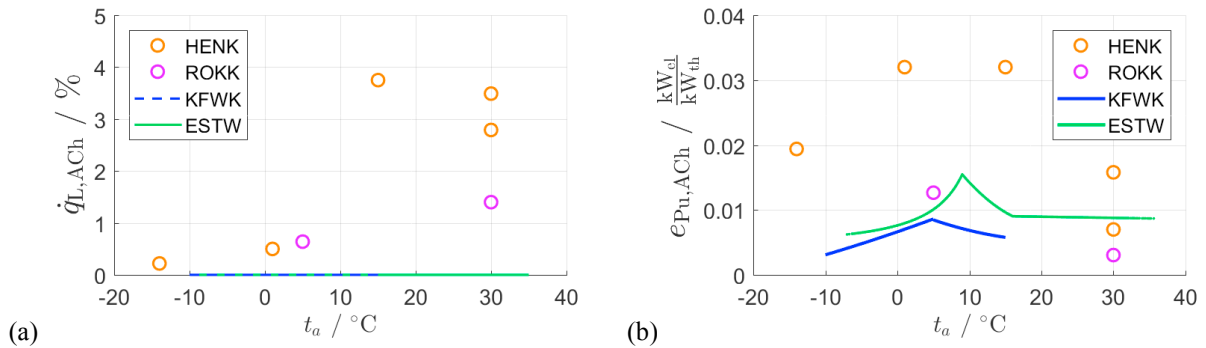


Fig. 5. Network effects for ACh return temperature of 68 °C for different installations
(a) specific additional heat loss (b) specific additional pumping electricity.

Pumping electricity as well shows very high values in HENK compared to the other installations. Reasons are the high distances and the hydraulically highly burdened network.

3. Effect on heat generation

3.1. Motivation / heat generation set-up

Every ACh as an additional heat consumer has significant influence on the energy balance on the heat generation. An additional heat demand $\Delta\dot{Q}_{Gen}$ in a DH system usually causes

- higher CHP output, i.e. electrical output ΔP_{CHP} but also additional fuel demand $\Delta\dot{Q}_{fuel,CHP}$ and
- perhaps higher gas boiler request, i.e. additional fuel demand $\Delta\dot{Q}_{fuel,boiler}$.

Additional use of the gas boiler should be minimized for primary energy and cost efficiency reasons.

Due to sensitivity of real CHP generation data of the project partners, method and calculated effects are presented by a construed example. When comparing real DH system configurations, the sets of heat generators (amount, size) are various and installed plants have very specific characteristics (depending on plant-type, efficiency, part load behavior etc.). That's why the results do not allow general conclusions. The construed set-up in Fig. 6 contains

- gas and steam turbine “GuD1” from [2], scaled to nominal heat load of 16.25 MW_{th}
- gas boiler
- heat storage in common size (equivalent to about 5-7 hours of heat supply in summer)

- moderate switch-on costs
- load profile of DH system ROKK.

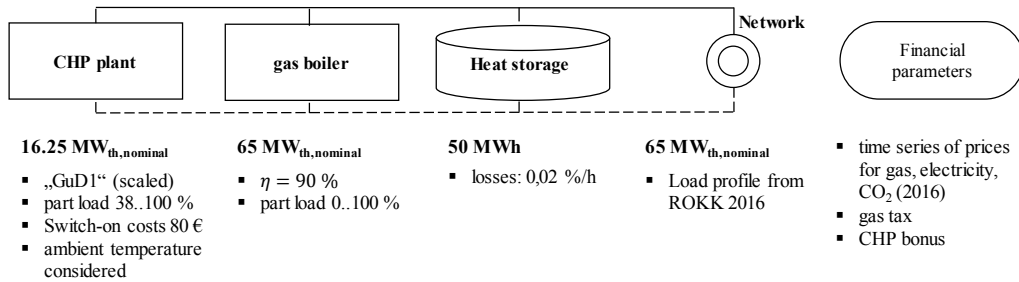


Fig. 6. Investigated heat generation set-up.

3.2. Optimization of generator operation

Real operation of the heat generators in interaction with the storage and spot market prices for gas and electricity follows the criteria “supply guarantee” and “cost optimization”. The optimized operation is mathematically realized by solving a Mixed-Integer-Linear-Programming (MILP) problem. For performance reasons simulation period was limited to one week. Four representative weeks have been chosen (Fig. 7 and table 3).

For each week, calculations without ACh (A) and with ACh (B) have been done. A fictive additional constant heat supply of $\Delta\dot{Q}_{Gen} = 175 \text{ kW}_{th}$ for the ACh is assumed. For the analysis of the ACh impact only the difference of the two calculations (B)-(A) is of interest. Since this difference is really small, high calculation accuracy of the simulations (A) and (B) is required.

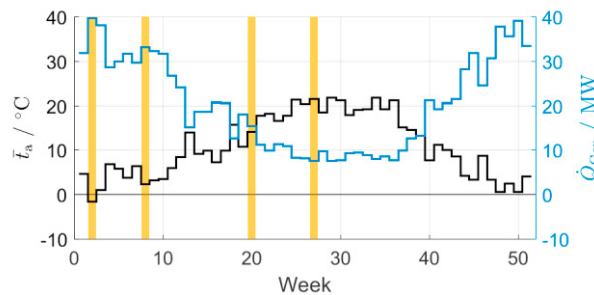


Fig. 7. Chosen weeks for heat generation simulations (orange); ambient temperature and heat load.

Table 3. Parameters of chosen heat generation weeks.

	winter I	winter II	spring	summer
Week	2	8	20	27
\bar{T}_a	-1.6 °C	2.3 °C	14.1 °C	21.5 °C
\bar{Q}_{Gen}	39.7 MW	33.2 MW	15.4 MW	7.5 MW
Load percentage	61.1 %	51.1 %	23.7 %	11.6 %

3.3. Results / characteristic key figures

The impact of the additional heat demand can easily be characterized by (differential) key figures: For evaluating the calculated effort of the additional heat demand (ΔW_{CHP} , $\Delta Q_{\text{fuel,CHP}}$, $\Delta Q_{\text{fuel,boiler}}$) it is useful to introduce a differential primary energy factor

$$f_{\text{P,Gen,ACh}} = \frac{\Delta Q_{\text{P,Gen}}}{\Delta Q_{\text{Gen}}} \quad (5)$$

which represents the additional primary energy $\Delta Q_{\text{P,Gen}}$ related to the additional heat demand ΔQ_{Gen} . This value can be compared with the average primary energy factor of the overall heat generation

$$f_{\text{P,Gen,avg}} = \frac{Q_{\text{P,Gen}}}{Q_{\text{Gen}}} \quad (6)$$

Primary energy $Q_{\text{P,Gen}}$ and $\Delta Q_{\text{P,Gen}}$ is calculated using the power bonus method (primary energy factors for gas 1.1 and electricity displacement mix 2.8). Hereafter, negative values of f_{P} are permitted for scientific analysis of the results.

Further helpful differential key figures are CHP coefficient

$$\sigma_{\text{CHP,ACh}} = \frac{\Delta W_{\text{CHP}}}{\Delta Q_{\text{Gen,CHP}}} \quad (7)$$

and the CHP ratio

$$x_{\text{CHP,ACh}} = \frac{\Delta Q_{\text{Gen,CHP}}}{\Delta Q_{\text{Gen}}} \quad (8)$$

Fig. 8 shows the primary energy factors for the additional heat (ACh) and overall heat (avg) for all four simulated weeks. Differential primary energy factor is always higher than the average value: In winter time the additional heat generation is provided only by the gas boiler, which means that $x_{\text{CHP,ACh}} = 0$; in spring this value reaches 63 %. This follows from the fact that the CHP-plant is already running at maximum power or a further increase of CHP-power is not cost effective due to low electricity prices.

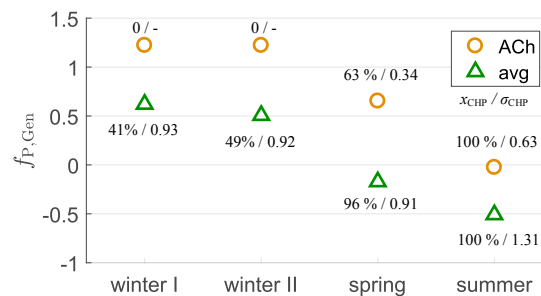


Fig. 8. Differential primary energy factors of heat generation and comparison to average/overall primary energy factors.

Although in the summer-week the whole additional heat demand is produced by CHP the primary energy factor of the additional heat is higher than the overall value. Here, providing the additional heat demand via CHP is cost efficient. But the CHP-plant produces the additional heat with a significant lower CHP coefficient of $\sigma_{\text{CHP,ACh}} = 0.63$ compared to the average value of $\sigma_{\text{CHP,avg}} = 1.31$. That means the CHP-plant is slightly increasing its load-point from a quite optimal point to a slightly worse point (according to σ).

It is equally imaginable that in other heat generation and heat load constellations the additional heat is produced with a better CHP coefficient than the average. Thus, lower primary energy factors of the additional heat could be achieved.

4. Overall impact of ACh: Evaluation of consumer heat and produced cold

Results of the real network HENK and the key figures of heat production from construed heat generation set-up are now combined to evaluate the overall effort. HENK scenarios are, according to the aim of a rough estimation, assigned to the presented heat generation weeks as shown in Table 4.

Table 4. Combinations of HENK network simulations scenarios and heat generation weeks.

Network simulation scenarios HENK	CHP1+2 / -14°C	CHP1+2 / +1°C	CHP1 / +15°C	CHP1 / +30°C	CHP2 / +30°C
Allocated heat generation week	winter I	winter II	spring	summer	summer

Primary energy effort is now presented for the consumer heat in Fig. 9 (a). Values of ACh are higher than average values, so the additional heat consumer ACh will slightly increase the primary energy factor of the DH system.

In consideration of local thermal and electrical efficiency of the ACh cooling system, primary energy effort for the produced ACh cold is calculated and presented in Fig. 9 (b). Local electricity demand of ACh as well as compression chiller is evaluated with a primary energy factor of 2.8 (last power station in merit order). The primary energy factor of the cold of the ACh is compared to compressions chillers with typical annual COP_{el} (blue area). It demonstrates that for the investigated constellation the summer operation of the ACh would have better primary efficiency than a compression chiller solution. Differences in return temperatures look small due to the high primary energy factors for the chosen generation set-up. But transition from 77 °C to 68 °C can lower the primary energy factor of the cold especially in spring and summer by about 0.1 to 0.15.

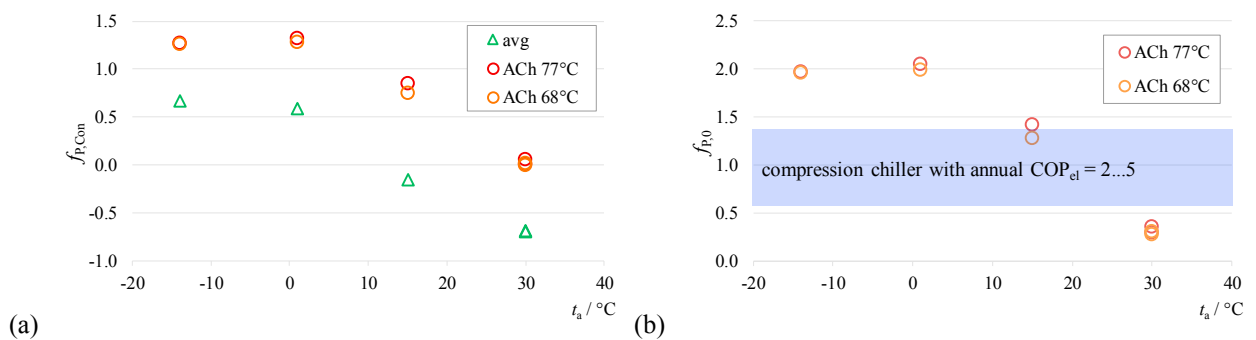


Fig. 9. Primary energy factors of the (a) additional consumer heat (b) additional cold production.

5. Conclusion

The paper shows a method to quantify the effects of additional ACh in existing DH networks. While additional heat losses in the network are small, additional pumping electricity should not be neglected in the given example. Especially heat generation set-up and operation have big influence on the primary efficiency of ACh-operation if the

whole impact chain is taken into account. Results are only valid for the chosen example and will vary widely in reality. DH system companies should apply the method with their realistic models of network and heat generator operation to evaluate the ecological and economic sense of ACh in their DH network. Furthermore, long-term strategies for the DH system have to be taken into account. Future aimed supply and return temperature levels of DH system in the lifetime of the ACh installations have to be considered as well.

Acknowledgements

This project was founded by the Federal Ministry for Economic Affairs and Energy (FKZ: 03ET1171B).

References

- [1] Paitazoglou, Christopher, and Stefan Petersen. "Energy efficient cooling with new absorption chiller technology in solar cooling systems and CHPC-plants." *6 th International Conference ENERGY in BUILDINGS 2017* (2017)
- [2] Rühling, Karin, and Sebastian Groß. "Erhaltung der Marktfähigkeit von KWK Anlagen mittels Einbindung von Umweltenergie". *AGFW* (2016). ISBN 978389990577.



16th International Symposium on District Heating and Cooling, DHC2018,
9–12 September 2018, Hamburg, Germany

Technical improvement potential of large district heating network: application to the Case of Tallinn, Estonia

Eduard Latõšov^{a*}, Anna Volkova^a, Aleksandr Hlebnikov^b, Andres Siirde^a

^aTallinn University of Technology, Department of Energy Technology, Ehitajate tee 5, Tallinn, 19086, Estonia

^bAS Utilitas Tallinn, Punane 36, 13619 Tallinn, Estonia

Abstract

District heating (DH) operators should relentlessly improve district heating networks (DHNs) for staying competitive in the energy market and for offering better service to consumers in comparison to local heating. Tallinn DHN started providing heat to consumers from the year 1959 and evolves according to external condition. Major changes have been made to about 440 km of the DH network due to the fast city development and the implementation of the DH operators' development strategy since early 1990s. In order to maintain the proper technical condition of the DH network and to reduce heat loss from the DHN, the pipelines are well-maintained, renovated and repaired. The improvement analysis of large DHN and renovation influence on DH network parameters is presented in the paper. Technically possible future improvement scenarios for the Tallinn DH network were determined. The methodology for the Tallinn DHN improvement potential evaluation includes an analysis performed to replace the existing pipelines with the same internal diameter size and optimised diameter pre-insulated pipes.

© 2018 The Authors. Published by Elsevier Ltd.

This is an open access article under the CC BY-NC-ND license (<https://creativecommons.org/licenses/by-nc-nd/4.0/>)

Selection and peer-review under responsibility of the scientific committee of the 16th International Symposium on District Heating and Cooling, DHC2018.

Keywords: low temperature; optimisation; pipelines; large-scale district heating system; DH; heat transfer coefficient, pipes

1. Introduction

District heating (DH) has been widely used in space heating and domestic hot water supply for many decades [1]. As shown in the latest overview of the existing district heating systems (DHS), in the Heat Roadmap Europe Study 2050 Across the EU Member States, 60 million (12%) citizens, 141 (28%) cities and 287 (57%) regions are connected to DH [2]. Currently, there are many promising opportunities for DH in terms of future developments in the energy sector; however, this also means that DH must be updated and subjected to major improvements [3].

A DHS consists of three main aspects: production, distribution and consumption. Over the past two decades, the distribution aspect has been carefully examined, most analyses were conducted on network geometry optimisation, hydraulic network simulation methods, [4] and overall parameter optimisation [5,6]. Some optimisations were carried out with multiple heat sources, in order to optimise heating costs [7,8]. There are several studies concerning the evaluation of the DHN improvement

* Corresponding author. Tel.: +372 53359298.

E-mail address: eduard.latosov@ttu.ee

potential through network piping system renovation and optimisation. Zeng has proposed the optimisation scheme in order to determine the optimal pipe diameter of the district heating and cooling piping network [9]. Dalla Rosa et al. have investigated the impact of various pipe designs on the energy saving potential [10].

The DH sector plays a very important role in achieving Estonia's renewable energy goals. In 2016, around 70% of heat consumed in Estonia was supplied by DH.

Tallinn district heating network (DHN) is the largest network in Estonia that has been supplying consumers with heat since 1959, and is developing in accordance with the external conditions. Major changes have been made to about 440 km of the DH network due to the fast city development and the implementation of the DH operators' development strategy since early 1990s.

In order to maintain the proper technical condition and to reduce heat loss from the DHN, the pipelines are well-maintained, renovated and repaired. Hlebnikov et al., have presented an assessment of the Tallinn DHN general condition in [11]. In [12] Volkova et al. have presented the development analysis of the entire district heating system with a focus on heat generation. A general Tallinn DHS development evaluation was demonstrated in [13].

In this study, technically possible future improvement scenarios for the Tallinn DHN were determined. Current conditions of Tallinn DHN are presented in the second section. The methodology for the Tallinn DHN improvement potential evaluation includes an analysis performed to replace the existing pipelines with the same internal diameter size and optimised diameter pre-insulated pipes. A detailed description of this method is presented in the third section. The scenarios for the improvement of the Tallinn DHN are demonstrated in the fourth section.

2. Current conditions of Tallinn district heating network

Tallinn DHN started providing heat to consumers in the year 1959 and is evolving according to external condition. There are huge changes in about 445 km DHN, due to rapid Tallinn city development and implementation of DH operator development strategy starting from the beginning of the 1990s.

In the last ten years, the portfolio of heating equipment of Tallinn DHN has considerably expanded. In 2009, the first biofuel cogeneration plant was opened. Before that, heat was produced using natural gas. A part of the heat was produced in natural gas boilers as part of cogeneration at the Iru power plant. As of today (from the second half of 2017), three CHP plants that run on local fuel types (Iru Waste Incineration Plant, Tallinn CHP 1 and Tallinn CHP 2) cover the base load. The share of the heat produced from local fuel types is about half the total heat produced.

Tallinn DHN was formed by connecting the DHNs of East and West-Tallinn in 2011. Tallinn DHN is conditionally divided into three regions (Fig. 1):

- Lasnamäe district extends from Laagna Pump Station to Maardu. At zero temperatures, the DH is provided by Tallinn and Iru Power Plants;
- Central district extends from Laagna Pump Station to Spordi Boiler House. At zero temperatures, the DH is provided by Mustamäe Boiler House as well as Tallinn and Iru Power Plants;
- Lääne district extends from Spordi Boiler House to the west (the districts of Kristiine, Mustamäe, Õismäe, Põhja-Tallinn). At zero temperatures, the DH is provided by Mustamäe and Kristiine Boiler Houses.



Fig. 1. Tallinn DHN

According to the data of 2017, the length of the district heating pipeline in operation was 426 km. In the past five years, the length of the pipeline in operation increased by 6.3% [14].

In 2017, the share of the renovated pipeline in operation was 43% and the share of the pre-insulated pipeline, 38%. The share of the overhead pipelines (not renovated) is small and remains below 5%.

The main reason for the increase in the share of renovated insulated heating pipeline can be explained by the fact, that insulation of 11 km long pipeline (DN = 1,200 mm, built between 1980 and 1992) was replaced with prefabricated polyurethane (PUR) foam shells [15]. The renovated heating pipeline connects Tallinn consumers with Tallinn and Iru Power Plants. It was preferable to renovate, not to install new pre-insulated pipelines mainly due to the good condition of the DHN pipeline metal.

In the past five years (2013-2017), 66 km of heating pipelines has been replaced, renovated, or built, which in 2017 accounted for 16% of Tallinn DHN pipelines.

The main range of the heating pipeline (53%) is from DN80 to DN200 mm. The largest share is formed by DN80, or 13% of the total length. The average diameter in 2017 was 222.5 mm.

The average age of the pipeline in Tallinn DHN has been relatively stable in recent years (23 to 25 years) and shows a slight decrease trend (Fig.2).



Fig. 2. Average age of Tallinn DHN pipelines

The average age stability and even the decrease is an indirect indicator that characterises the network operator's activity in maintaining and improving the condition of the DHN.

The variations in the average internal diameter and the area of the heating pipes during last 5 years are shown in Fig.3. An increase in the internal area of the DHN pipeline (if the average diameter does not increase) indicates the growth of the heat pipe length, for example, due to the expansion of DH. The average diameter of Tallinn DHN has steadily decreased in recent years (by 3.5% in 2013-2017). However, due to the expansion of the DHN, the average internal area of the pipeline increased by 2.5%.

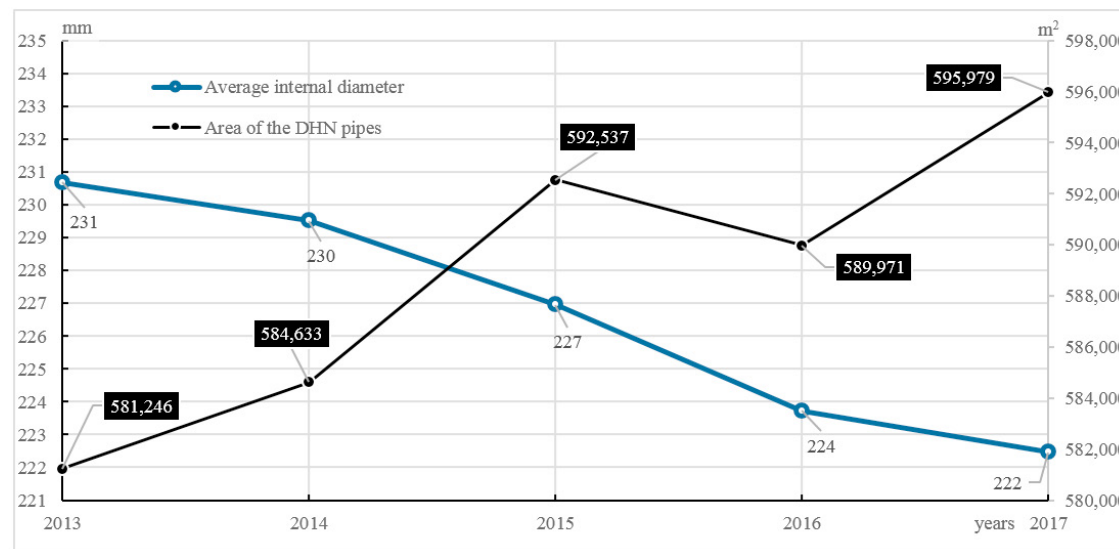


Fig. 3. Average internal diameter and the area of the DHN pipes

The heat loss in the DHN pipeline depends on a number of factors. The main factors affecting the absolute value of heat loss are the condition of the DHN (thermal conductivity of the heating pipeline) and climatic conditions (mainly outdoor temperature, which affects the temperature of the heat carrier in the DHN) [16].

The relative heat loss in the DHN pipeline also depends on the amount of heat consumed from the DHN. In the summer months, the heat loss in the DHN reaches an average of 18,000 MWh. In the winter, the monthly average heat loss can reach

50,000 MWh. In spite of the fact that in the summer months there is less heat loss in absolute value, the relative heat loss, as a rule, is more than three times higher than in the winter months.

3. DHN improvement potential methodology

3.1. Evaluation of DHN current technical condition

To better understand the technical condition of the DHN and to compare it with other DHNs, an analysis of the main indicators/specific factors of Tallinn DHN area was performed.

Calculating the temperature integral of DHN, the following was taken into account:

- the duration of the months;
- the average monthly ambient temperature;
- the dependence of the region-based supply and return water from the ambient temperature (temperature graphs).

The technical condition of the DHN is best characterised by the overall heat transfer coefficient, depending on the internal diameter of the pipeline. This indicator is independent of the specifics of the operation of the DHN and is characterised by the general technical condition of the DHN [16].

The heat transfer coefficient can be calculated using equation (1).

$$K = \frac{Q_{hl}}{L \cdot 2\pi \cdot D_a \cdot G} \quad [\text{W/m}^2\text{K}] \quad (1)$$

where

- K is overall heat transfer coefficient, $\text{W/m}^2\text{K}$;
- Q_{hl} is DHN heat loss, Wh;
- L is network rout length, m;
- D_a is DHN average diameter, m;
- G is degree hours, $^{\circ}\text{Ch}$.

The heat transfer coefficient can be used to compare heating networks. The smaller the coefficient of overall heat transfer and the closer it lies to the parameters of the pre-insulated heating pipelines (whereas the coefficients of overall total heat transfer of the pre-insulated district heating pipelines with different inner diameters are known), the better the DHN. For the evaluation of Tallinn DHN this parameter was compared with Swedish new and old DHNs [17].

Other significant parameters for the evaluation of DHN current technical conditions are relative heat supply in the pipeline per unit length as well as heat output in the heating pipeline per unit volume. These parameters can be calculated, using equations (2-3).

$$Q_L = \frac{Q}{L} \quad [\text{MWh/m}] \quad (2)$$

where

- Q_L is specific heat supply per length, MWh/m ;
- Q is heat output, MWh .

$$Q_V = \frac{Q}{L \cdot \pi \left(\frac{D_a}{2}\right)^2} \quad [\text{MWh/m}^3] \quad (3)$$

where

- Q_V is the specific heat supply per volume, MWh/m^3 .

3.2. Evaluation of DHN improvement potential

Due to the implementation of a remote metering system in Tallinn DHN, various specific characteristics are available and using NetSim modeling software it was possible to establish DHN model, for optimisation of DHN. The model has been developed and balanced over the years. Due to this development, the results are consistent with the real indicators of the monitoring system, which shows high accuracy and reliability of the calculations.

In practice, selection of an optimal DHN pipeline is a task within the scope of technical and economic optimisation. When selecting a particular pipeline, the following must be considered:

- type of DHN pipeline element, i.e., whether it is a straight pipe, with a branch or, for example, with an inlet;
- length of the pipeline to be replaced/selected (strength characteristics);
- difference in the pressure required to operate the boiler room;
- amount of electricity consumed by the network pumps;

- heat loss due to the diameter of the pipeline;
- heat load of the pipeline to be replaced/selected, i.e., whether heat consumption from the given pipeline is increasing (new developments, new consumers) or decreasing (fewer consumers, implementing energy saving measures).

A particular section of the pipeline should be selected before construction or actual replacement, taking into account all abovementioned factors.

The main criterion for the selection is finding the optimum in terms of investment, heat loss, and pumping capacity. Pipelines with larger diameters are more expensive, and the resulting heat loss is higher, but pressure loss and pumping costs are lower. The dimensioning of the DHN is strongly related to the hydraulic conditions [18]. At the same time, large-scale heating networks of trunk lines are usually designed taking into account the recommended friction losses that is calculated with equation (4)

$$R = \frac{\Delta P}{L} \quad [\text{Pa/m}] \quad (4)$$

where

R is friction losses, Pa/m;

ΔP is pressure loss in DHN, Pa.

The R values used will vary depending on the country. For example, in China, the recommended R value is 30–70 Pa/m[19], in Finland, it is less than 1 bar/km, i.e., 100 Pa/m[20] and even higher according to the recommendations of the Swedish District Heating Association[17] (Fig.4)

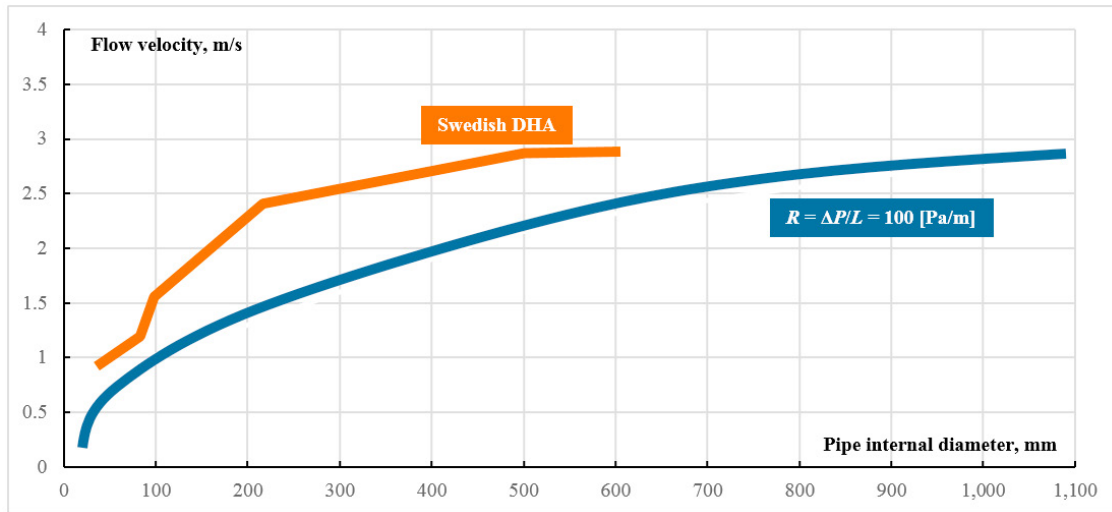


Fig. 4. Design flow velocity depending on the pipe internal diameter according to various recommendations

For the estimation of the load on the pipe, it was considered the following conditionally optimal/recommended speeds: the optimisation condition: $R = 100$ Pa/m has been applied. This condition is described by the equation (5).

$$Y = 0,7754 \ln(X) - 2,5818, \quad (5)$$

where

Y is the recommended flow velocity, m/s;

X is the pipe internal diameter, m.

When modeling, the parameters of all the pipelines of Tallinn DHN were found, including flow rates in the operation of the DHN at an ambient temperature of -22 °C. The achieved speeds were compared with the recommended speed and the real/recommended speed ratio was calculated in percentages. When this ratio is close to 100%, it means, that pipeline are well-optimised (optimum load). If the ratio is small, then the particular pipe section is relatively less loaded.

For the evaluation of improvement potential for DHN two types of calculations have been made:

- Modelling of the main parameters, assuming that all non-renovated heating pipelines are renovated and their internal diameters remain the same as the pipelines to be replaced;
- Modelling of the main parameters, assuming that in addition to the replacement of the non-renovated heating pipelines with pre-insulated pipelines, their internal diameters are optimised according to the optimisation condition $R = 100$ Pa/m.

4. Results

4.1. Evaluation of Tallinn DHB current technical conditions

Based on the method, described in section 3.1., Tallinn DHN was evaluated. Fig.5. summarises the dependence of the heat transfer coefficient from the inner diameter for Tallinn DHN and its districts. The results are compared with overall heat transfer coefficient of new and old DHN in Sweden, as well as the parameters of the pre-insulated pipelines (class II, with a thermal conductivity of 0.035 W/(mK) and a thermal conductivity of 0.027 W/(mK)). The specific heat supply per DHN pipelines length (Q_L) and volume (Q_V) is shown in Fig.6

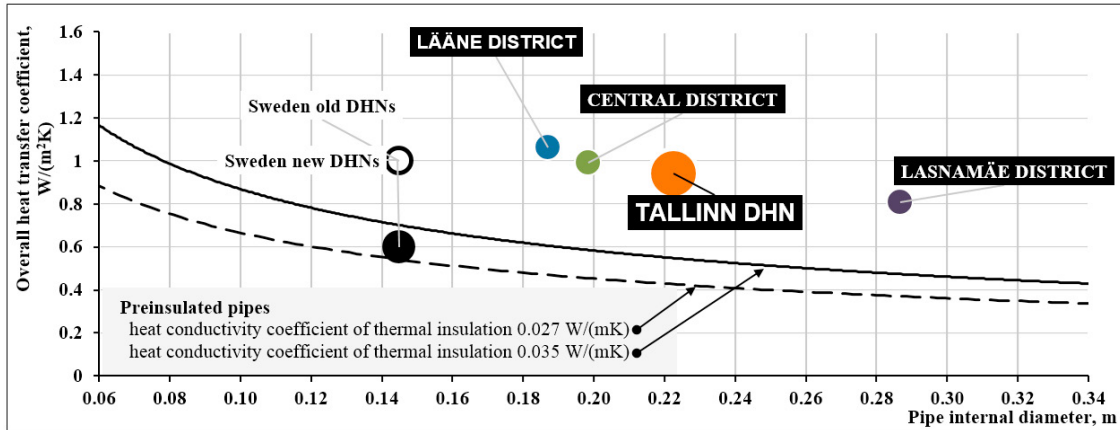


Fig. 5. Heat transfer coefficients of Tallinn DHN and its districts as well as their comparison with Swedish networks and new pre-insulated heating pipelines

It shows that overall heat transfer coefficient of Tallinn DHN is close to the same parameter of old Swedish DHNs, but pipe average internal diameter is much higher, than in Swedish DHN.

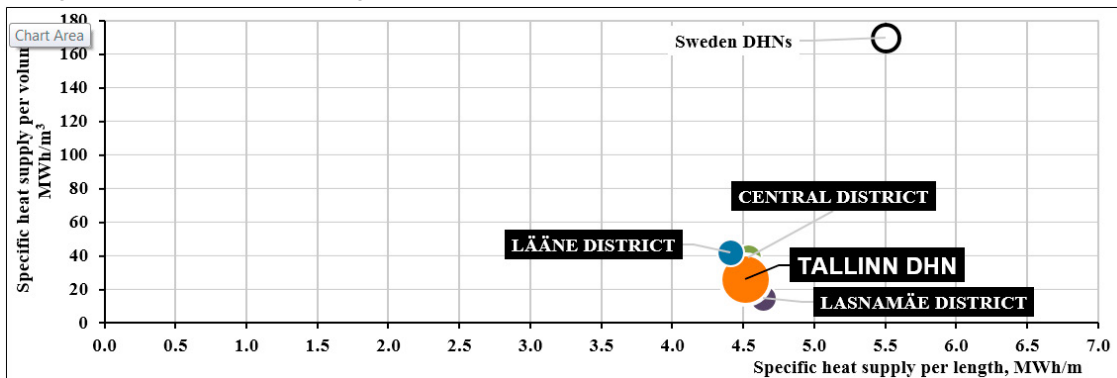


Fig. 6. Specific heat supply per length and volume of the DHN pipelines

The average heat supply of the Swedish networks per meter of the DHN pipeline is higher than in Tallinn. This can be attributed to the common configuration of Tallinn DHN, which consists of a long transmission pipeline sections connecting the districts with high consumption density, particularly, the pipeline between Lasnamäe and Maardu.

As a rule, the dimensions of the Swedish heating networks are more closely aligned to the ideal conditions due to optimisation. On the one hand, it is good, as a smaller amount of water circulating in the pipeline is required to transmit the same amount of energy, and the diameters of the heating pipelines is lower than in comparable circumstances; therefore, the heat losses are also smaller. However, focusing too much on optimisation results may cause difficulties in the expansion of the DHN as the transmission pipeline capacity does not suffice to satisfy the needs for new consumers. Larger speeds also require a higher capacity of circulation pumps, resulting in higher electricity costs.

4.2. DHN improvement potential

The aggregate results of the calculations, according method, described in the Section 3.2. are shown in Fig.7. The figure shows the length of the lines cumulatively according to the load level.

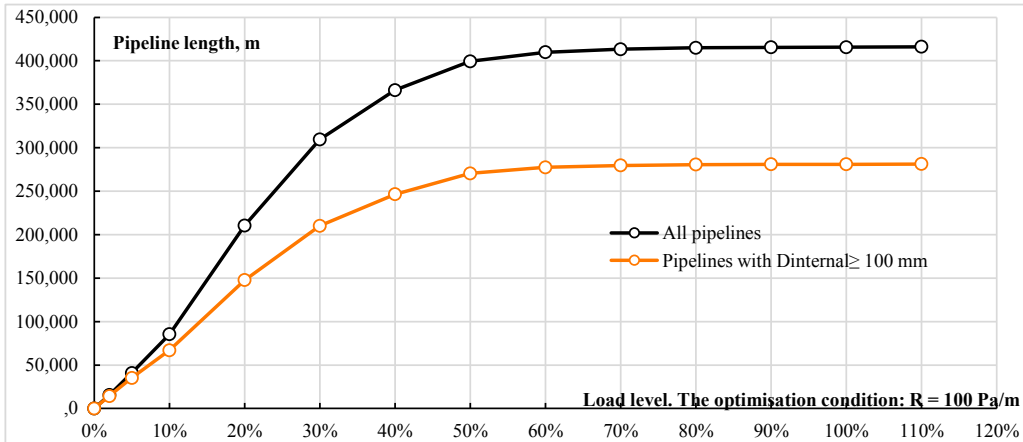


Fig. 7. Cumulative length of Tallinn DHN depending on the load level

The figure shows that most of the low-loaded (less than 10%) heating network sections have an internal diameter of more than 100 mm. The pipeline with the load under 10% accounts for 20% of the total length of the pipeline used. The load of half of the pipeline used is below 20%.

This means that the speed in the DHN is relatively low (lower pumping costs); at the same time, there is a larger volume of water and heat loss in the DHN (a larger external surface of the pipeline). Low speeds indicate the possibility of expanding the DHN (connection of new consumers) and the technical potential to reduce the supply and return temperature (lower temperatures require a higher flow of water for the same amount of energy, i.e., higher speed of water in the pipeline). Renovation of Tallinn DHN can reduce heat loss and, consequently, fuel consumption and environmental impact.

The results of technically possible improvement potential, replacing the existing pipelines with the same internal diameter size and optimised diameter pre-insulated pipes, show that the replacement of old pipelines with pre-insulated heating pipelines with the same internal diameter can reduce heat loss by 40%. If, in addition, to optimise the pipelines that need to be replaced, according to the optimisation condition $R = 100$ Pa/m, the reduction of heat loss will be 60% (Fig. 8).

After replacing the existing non-reconstructed heating pipeline with a pre-insulated pipeline, the overall heat transfer coefficient of the DHN remains almost the same as compared to the heat transfer coefficient of pre-insulated heating pipeline of class II, where the thermal insulation material has a heat conductivity of 0.027 W/(mK).

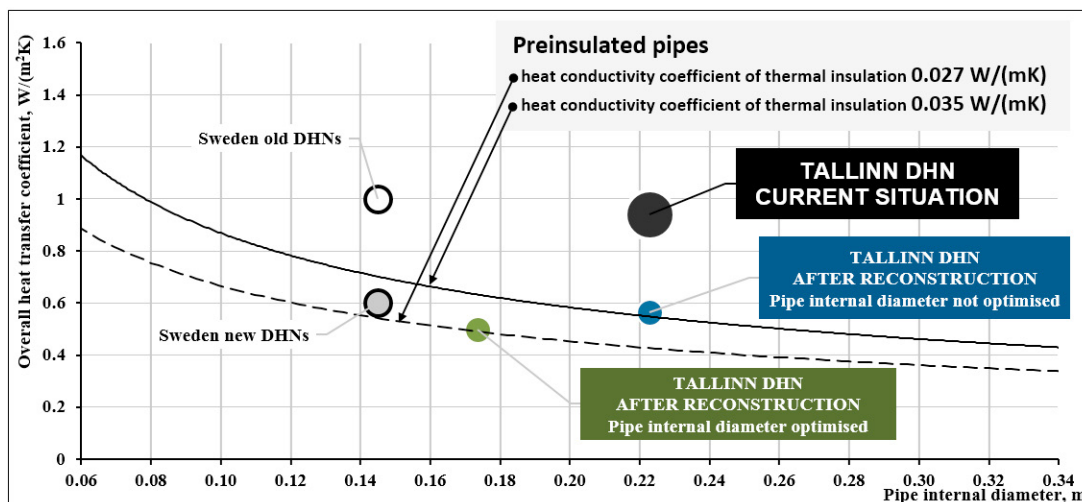


Fig. 8. Heat transfer coefficients of Tallinn DHN (current, not optimised, reconstructed, and reconstructed with diameter optimisation) and their comparison with Swedish networks and new pre-insulated heat pipes

Heat loss decreases even more when reducing the internal diameter. As a result, it is possible to reduce the temperature of the water supplied by the heater suppliers, which, in turn, has a positive effect on the reduction of heat loss.

By optimising the diameters of the pipelines that need to be reconstructed according to the current consumption, the indicators of Tallinn DHN can be approximated to the generalised values of the new Swedish networks. The potential reduction

of heat loss in the future is can be doubled (the comparison is based on the normalised indicators for the DHN in 2016) and the weighted thermal transfer factor remains within the range of 0.5-0.6 W (m²K), with the current range fluctuating from 0.9 to 1.0 W/(m²K).

5. Conclusions

The paper presents evaluation methodology for developing large-scale Tallinn DHN technical conditions and its improvement. Analysing current technical conditions of studied DHN, heat transfer coefficient and specific heat supply per pipe length and volume were evaluated and compared with good practice examples. The average heat supply per length and volume are much lower, then in the good practice example (Swedish DHN). It can be explained by the common configuration of Tallinn DHN, which consists of the long transmission pipeline sections connecting the districts with high consumption density.

The results of DHN improvement potential calculations have shown that the speed in Tallinn DHN is relatively low, that leads to lower pumping costs form one side but at the same time to higher heat loss in the DHN. Low speeds indicate the possibility of expanding the DHN and the technical potential for reduction of supply and return temperature in DHN.

Tallinn DHN modelling results show that the replacement of old pipelines with pre-insulated heating pipelines with the same internal diameter can reduce heat loss by 40%, but with optimized internal diameter by 60%.

Acknowledgements

This work was supported by Estonian Ministry of Education and Research (base funding project B55).

References

- [1] A. Lake, B. Rezaie, S. Beyerlein. "Review of district heating and cooling systems for a sustainable future." *Renewable and Sustainable Energy Reviews* 67 (2017): 417–425, doi:10.1016/j.rser.2016.09.061.
- [2] H. Connolly, D., Mathiesen, B.V., Østergaard, P.A., Möller, B., Nielsen, S., Lund. "Heat Roadmap Europe 2050", Study for the EU27, (2013).
- [3] S. Werner. "International review of district heating and cooling." *Energy* (2017): 1–15, doi:10.1016/j.energy.2017.04.045.
- [4] H. Arce, S. Herrero, S. López, M. Rämä, K. Klobut, J.A. Febres. "Models for fast modelling of district heating and cooling networks." *Renewable and Sustainable Energy Reviews* (2017): 1–11, doi:10.1016/j.rser.2017.06.109.
- [5] H. Averfalk, S. Werner. "Essential improvements in future district heating systems." *Energy Procedia*. 116 (2017): 217–225, doi:10.1016/j.egypro.2017.05.069.
- [6] D. Balić, D. Maljković, D. Lončar. "Multi-criteria analysis of district heating system operation strategy." *Energy Conversion and Management* 144 (2017): 414–428, doi:10.1016/j.enconman.2017.04.072.
- [7] M. Vesterlund, A. Toffolo, J. Dahl. "Optimization of multi-source complex district heating network, a case study." *Energy* 126 (2017) 53–63, doi:10.1016/j.energy.2017.03.018.
- [8] G. Sandou, S. Font, S. Tebbani, A. Hiret, C. Mondon. "OPTIMIZATION AND CONTROL OF A DISTRICT HEATING NETWORK." *IFAC Proceedings Volumes* 38 (2005): 397–402, doi:10.3182/20050703-6-CZ-1902.00466.
- [9] J. Zeng, J. Han, G. Zhang. "Diameter optimization of district heating and cooling piping network based on hourly load." *Applied Thermal Engineering* 107 (2016): 750–757, doi:10.1016/j.applthermaleng.2016.07.037.
- [10] A. Dalla Rosa, H. Li, S. Svendsen. "Method for optimal design of pipes for low-energy district heating, with focus on heat losses." *Energy* 36 (2011): 2407–2418, doi:10.1016/j.energy.2011.01.024.
- [11] A. Hlebnikov, A. Volkova, O. Džuba, A. Poobus, U. Kask. "Damages of the Tallinn district heating networks and indicative parameters for an estimation of the networks general condition." *Environmental and Climate Technologies* 5 (2010): 49–55, doi:10.2478/v10145-010-0034-3.
- [12] A. Volkova, V. Mashatin, A. Hlebnikov, A. Siirde. "Methodology for the improvement of large district heating networks." *Environmental and Climate Technologies* 10 (2012), doi:10.2478/v10145-012-0009-7.
- [13] A. Volkova, V. Mašatin, A. Siirde. "Methodology for evaluating the transition process dynamics towards 4th generation district heating networks", *Energy* 150 (2018): 253–261, doi:10.1016/j.energy.2018.02.123.
- [14] Utilitas A/S report, 2017.
- [15] V. Masatin, A. Volkova, A. Hlebnikov, E. Latšov. "Improvement of District Heating Network Energy Efficiency by Pipe Insulation Renovation with PUR Foam Shells." *Energy Procedia* (2017), doi:10.1016/j.egypro.2017.04.064.
- [16] V. Masatin, E. Latšov, A. Volkova. "Evaluation Factor for District Heating Network Heat Loss with Respect to Network Geometry." *Energy Procedia*, (2016): doi:10.1016/j.egypro.2016.09.069.
- [17] S. Fredriksen, Svend, Werner. "District Heating and Cooling". (2014), ISBN-10: 9144085303
- [18] M. Cali, R. Borchellini. "District heating networks calculation and optimization." *Exergy, Energy System Analysis, and Optimization*, (2013).
- [19] Ministry of Housing and Urban-Rural Development of the People's Republic of China., "Design Code for City Heating Network (CJJ34-2010)." Architecture & Building Press, (2010) Beijing, China.
- [20] X.L. and R.L. Haichao Wang, Lin Duanmu. "Optimizing the District Heating Primary Network from the Perspective of Economic-Specific Pressure Loss." *Energies* 10(8) (2017): 1095.



16th International Symposium on District Heating and Cooling, DHC2018,
9–12 September 2018, Hamburg, Germany

Ranking Abnormal Substations by Power Signature Dispersion

Ece Calikus, Sławomir Nowaczyk, Anita Sant'Anna, Stefan Byttner

*Halmstad University, Department of Intelligent Systems and Digital Design,
Kristian IV:s väg 3, Halmstad, 301 18 Halmstad*

Abstract

The relation between heat demand and outdoor temperature (heat power signature) is a typical feature used to diagnose abnormal heat demand. Prior work is mainly based on setting thresholds, either statistically or manually, in order to identify outliers in the power signature. However, setting the correct threshold is a difficult task since heat demand is unique for each building. Too loose thresholds may allow outliers to go unspotted, while too tight thresholds can cause too many false alarms.

Moreover, just the number of outliers does not reflect the dispersion level in the power signature. However, high dispersion is often caused by fault or configuration problems and should be considered while modeling abnormal heat demand.

In this work, we present a novel method for ranking substations by measuring both dispersion and outliers in the power signature. We use robust regression to estimate a linear regression model. Observations that fall outside of the threshold in this model are considered outliers. Dispersion is measured using coefficient of determination R^2 , which is a statistical measure of how close the data are to the fitted regression line.

Our method first produces two different lists by ranking substations using number of outliers and dispersion separately. Then, we merge the two lists into one using the Borda Count method. Substations appearing on the top of the list should indicate higher abnormality in heat demand compared to the ones on the bottom. We have applied our model on data from substations connected to two district heating networks in the south of Sweden. Three different approaches i.e. outlier-based, dispersion-based and aggregated methods are compared against the rankings based on return temperatures. The results show that our method significantly outperforms the state-of-the-art outlier-based method.

© 2018 The Authors. Published by Elsevier Ltd.

This is an open access article under the CC BY-NC-ND license (<https://creativecommons.org/licenses/by-nc-nd/4.0/>)

Selection and peer-review under responsibility of the scientific committee of the 16th International Symposium on District Heating and Cooling, DHC2018.

Keywords: Anomaly ranking, abnormal heat demand, power signature, district heating, fault detection

1. Introduction

Decreasing distribution temperatures is one of the most important steps to increase efficiency in district heating (DH) systems and plays vital role for the integration of 100% renewable energy supply [1]. Current distribution setups have high supply and return temperatures which lead to large heat losses in the network and inefficient use of heat sources.

One of the factors contributing to this situation is abnormal heat demand caused by faults in customer heating systems and substations [2 - 4]. In many cases, such problems do not directly cause noticeable decrease in customer comfort; however, they influence the performance of the network as a whole, leading to higher return temperatures and flow rates. Low temperatures in district heating can only be achieved if such abnormal demands are detected and eliminated.

Heat power signature models estimate the heat consumption of a building as a function of external climate data. They are typically presented as plots of total heat demand versus ambient temperature, showcasing the unique characteristics of each building (both physical and related to the behavior of the occupants). Many previous studies have been analyzing heat power signatures to diagnose abnormal heat demand.

Most methods are based on detecting outliers in the power signature by, either manually or statistically, setting a threshold on the power signature. However, setting a correct one is not always possible, since loose thresholds often allow outliers to go undetected, while too tight thresholds tend to cause too many false alarms [3, 5].

On the other hand, outliers are not the only symptom for abnormality in the power signature. High dispersion is also an indication of a problem such as faults or poor control [4], therefore must be taken into account. Existing methods that are based on counting outliers are not able to take dispersion into account. Combining both types of indicators requires a new approach.

In this work, we propose a novel method for ranking buildings by measuring both dispersion and outliers in their heat power signature and present large-scale analysis of district heating customers. Our method first produces two different lists by ranking substations using number of outliers and dispersion separately. Then, we merge the two lists into one using the Borda Count method.

Three different approaches, i.e., outlier-based, dispersion-based, and aggregated are evaluated against average and maximum return temperatures measured all the buildings in five different categories connected to two district heating networks in south of Sweden.

Based on those results, we conclude that outliers alone are not enough to identify abnormal heat demand in the buildings. The importance of also considering dispersion is clearly visible in analyzing high temperatures. The state-of-the-art outlier-based approach does not perform well alone for ranking abnormal buildings and it is significantly outperformed by dispersion-based and aggregated methods.

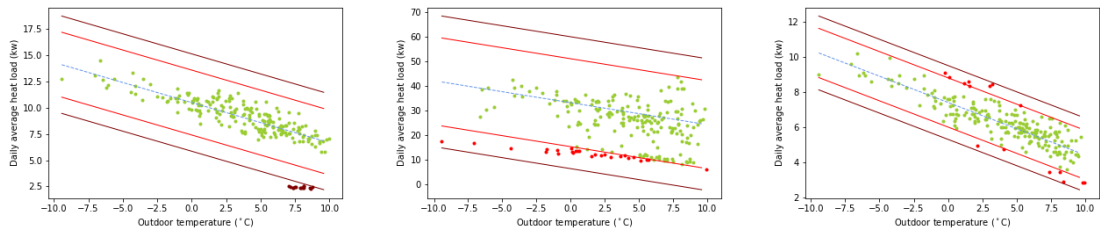
2. Related Work

The energy signature (ES) is a well-known method for the analysis of building energy consumption. It has been widely used for characterizing energy or heat demand behaviors of buildings in various studies.

[6] used ES methods for weather correction which aims to normalize energy consumption so that it becomes the representative of a building's expected long-term performance. In [7], a similar approach is applied to the entire DH network. Single heat power signature per year was plotted from heat load measurements of all the buildings connected to the network in order to compare different heat seasons.

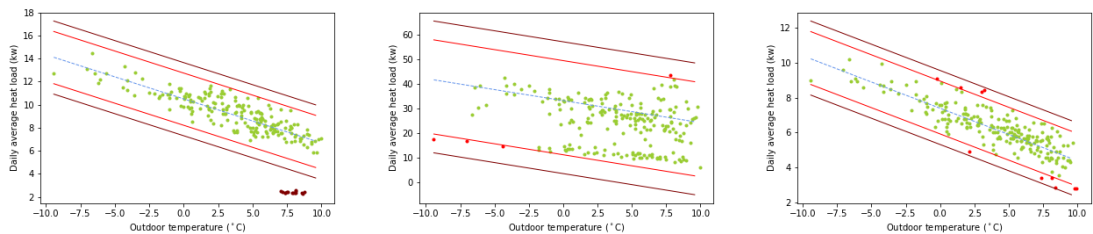
ES based methods have also been applied for the estimation of the amount of heat losses due to transmission and ventilation by quantifying the buildings' total heat loss coefficient [8 - 14]. In addition, they have been investigated to correctly estimate balance temperature in order to separate demand from space heating and domestic hot water [15].

ES methods provide useful information on buildings' energy performance in DH systems by analyzing correlation between the average heating power and outdoor temperature. Therefore, they have also been analyzed for the detection of anomalies or deviations in heat demand behaviors [4, 16]. Those approaches commonly implement outlier detection methods based on thresholding strategies to estimate errors in the energy signatures [3, 17-20].



(a) Abnormal Building: $T_a = 45^\circ\text{C}$, $T_m = 77^\circ\text{C}$ (b) Abnormal Building: $T_a = 57^\circ\text{C}$, $T_m = 72^\circ\text{C}$ (c) Normal Building: $T_a = 27^\circ\text{C}$, $T_m = 30^\circ\text{C}$

Figure 1: Thresholds based on standard deviation of the residuals.



(a) Abnormal Building: $T_a = 45^\circ\text{C}$, $T_m = 77^\circ\text{C}$ (b) Abnormal Building: $T_a = 57^\circ\text{C}$, $T_m = 72^\circ\text{C}$ (c) Normal Building: $T_a = 27^\circ\text{C}$, $T_m = 30^\circ\text{C}$

Figure 2: Thresholds based on median absolute deviation of the residuals.

However, defining the correct threshold is a difficult task. Identifying thresholds manually requires extensive human effort and domain knowledge. It is extremely time-consuming considering the number of buildings in a DH network. On the other hand, automatic determination of thresholds using statistical models is also very challenging since it requires finding an optimum strategy which will maximize the outlier detection performance while limiting false alarms. We demonstrate the difficulty of this task in Figure 1 and 2 by comparing two commonly used statistical thresholding strategies.

Those strategies are applied to the power signatures of three buildings estimated by linear regression. Two of the buildings are selected as abnormal examples whose return temperatures are high, and one is normal having low return temperature measurements. In Figure 1, thresholds are defined based on standard deviation (σ) of the residuals. The wider and the tighter thresholds respectively correspond to 3σ and 2σ above and below the regression line. The second strategy applies modified z-scores [21] which are computed using median absolute deviation of the residuals. The threshold is set so that modified z-scores do not exceed 3.5 for the wider case, and not exceed 2.5 for the tighter threshold.

The wider thresholds in both cases are able to identify outliers in the first abnormal buildings, but they fail detecting the second building showing high dispersion. Tighter thresholds are instead able to detect outliers in both the anomalous building; however, they also mistakenly mark some of the data in normal building as outliers, which leads to a high false alarm rate.

3. Method

In our approach, we rank buildings by measuring the “degree of abnormality” on heat power signatures with three different methods, i.e., outlier-based, dispersion-based and aggregated ranking. Power signatures of the buildings are estimated using robust regression in order to eliminate the influence of the outliers on model estimation.

3.1. Robust Regression

Ordinary Least Squares (OLS), a typical approach used to estimate energy signatures, is highly sensitive to outliers. Since parameter estimation is based on the minimization of squared error, even the presence of few outliers can have distorting influence and makes results of regression analysis including confidence intervals, prediction intervals, R² values, t-statistics, p-values, etc. unreliable [21].

Robust regression methods try to overcome those issues by providing robust estimates when outliers are present in the data. In our work, we apply Random Sample Consensus (RANSAC) algorithm [22] to do robust estimation of model parameters of power signatures in the presence of outliers. RANSAC is an iterative approach which fits the regression line to subsets of data until the model with most inliers and the smallest residuals on the inliers is chosen. The process continues unless either user-defined fixed number of iterations or threshold for the minimum number of samples that would be accepted as inliers to generate a final model is reached.

RANSAC has been shown to be a very robust approach for parameter estimation, i.e., it can estimate the parameters with a high degree of accuracy even when a significant number of outliers are present in the data set [23]. However, there are several drawbacks that should be taken into account while applying this approach. For example, we do not have prior knowledge on the ratio of outliers in power signature for every building in our data set. Therefore, setting stopping criterion such as maximum number of iterations or inliers is not trivial. In our case, we set the ratio of outliers to 20% when fitting the regression line since having false positives does not wildly affect parameter estimation. We estimate the regression line and residuals with this method. However, we employed a different approach to compute the final number of outliers in order to avoid high number of false alarms produced by RANSAC and also computed R² measures removing those outliers.

In order to demonstrate the benefits of using robust models in this problem, we conducted an experiment comparing goodness-of-fit of each power signature estimated by traditional OLS and RANSAC method.

First, OLS and RANSAC methods are separately fitted to each power signature. Then, we measure R² scores of all the models estimated by OLS and RANSAC. In order to avoid influence of outliers, R² scores are computed on observations excluding outliers determined by both OLS and the RANSAC. We use a statistical threshold on residuals to detect outliers which is explained in section 3.2 explicitly.

According to R² results, RANSAC method has better goodness-of-fit score on 61% of the all power signatures. We also conduct Student's t-test [24] to conclude whether R² scores are significantly lower in the models estimated by OLS in comparison to RANSAC algorithm.

The null hypothesis is $H_0: \mu_1 - \mu_2 \geq 0$, alternative hypothesis is $H_a: \mu_1 - \mu_2 < 0$ and significance level is $\alpha = 0.05$. The t-statistics of single-tailed test is $T = -2.349835$ and $p = 0.00944$. The p-value (0.00944) is lower than significance level (0.05). Therefore, at 5% level of significance, the test provides sufficient evidence that the power signatures estimated by OLS have lower goodness-of-fit than the ones estimated by RANSAC algorithm.

Furthermore, we demonstrate that the estimation of power signatures between those two methods differs significantly for a large portion of substations. Figure 3 shows an example substation where the two methods result in significantly different models. Crucially, in our dataset, there are 250 more buildings that have higher difference between R² values from OLS and RANSAC than the example building represented in Figure 3. In other words, for almost 30% of the buildings, the importance of using robust regression is even more significant than for the example.

3.2. Outlier-based ranking

In the literature, a widely applied measure for determining the “degree of abnormality” in buildings is the “number of outliers” in the power signature.

“Number of outliers” is determined by setting a statistical threshold on the distribution of the residuals. Under the normality assumption, 95.45% and 99.73% of the values lie within two (2σ) and three (3σ) standard deviations of the mean, respectively. However, the presence of outliers and the effect of other factors on power signature lead to violation of the assumption of normally distributed residuals.

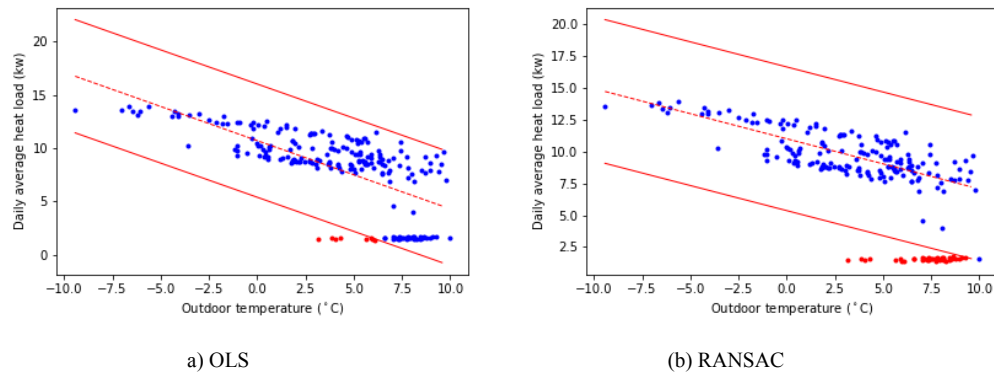


Figure 3: Difference between OLS and RANSAC in the presence of outliers

For non-normally distributed data, only 75% of the distribution's values are guaranteed to lie within (2σ) of the mean and 89% within (3σ) , according to Chebyshev's inequality [25]. Considering that, we set the threshold to (3σ) around the mean of the residuals in order to ensure an upper-bound of approximately 11% on the false positive rate.

Given outdoor temperature x_i in power signature, let y_i be the actual heat load, \hat{y}_i be the predicted heat load, $r_i = \hat{y}_i - y_i$ be the residual and μ and σ , be the mean and standard deviation of the distribution of the residuals $D(\mu, \sigma)$. Then, the outliers are determined as follows:

$$f(x_i, y_i) = \begin{cases} \text{outlier,} & \text{if } r_i - \mu \geq 3\sigma \\ \text{inlier,} & \text{otherwise} \end{cases} \quad r_i \sim D(\mu, \sigma) \quad (1)$$

Finally, all the buildings are sorted based on “the number of outliers” in decreasing order so that buildings that have “higher degree of abnormality” are placed higher in the list.

3.3. Dispersion ranking

In the second approach, the dispersion in the heat power signature is used as "degree of abnormality". In order to measure it, we use coefficient of determination (R^2). This is a statistical metric that evaluates the scatter of the data points around the fitted regression line. Since power signatures with lower R^2 values are more dispersed, we therefore define them as having higher “degree of abnormality”.

As stated earlier, the outliers can also influence R^2 , in particular, they can lead to low scores although the linearity of the model is satisfied. We reduce the effect of such misleading examples by removing the outliers detected with the thresholding strategy before calculating the R^2 scores. Then, the final ranking is produced by sorting all the buildings according to their R^2 values.

3.4. Aggregated approach

The Borda Count method [26] is a traditional voting method that was developed in the 18th-century and broadly applied as aggregation strategy to combine rankings produced by different algorithms.

Given a particular ranking as a sorted list of elements, the method works by assigning a score to each member of the list according to its relative position. Once the method is applied to different rankings, the final aggregated ranking is a sorted list based on the sum of scores of each element. This method can be seen as equivalent to combining ranks by their mean [27].

4. Results

4.1. Data

The dataset used in this study is comprised of smart meter readings from buildings connected to the district heating systems in Helsingborg and Ängelholm in the South-West of Sweden. The data set consists of hourly measurements of heat, flow, supply, and return temperatures on the primary side of the substations from the whole year 2016. In this study, we only use the heat measurements of the buildings in five customer categories: multi-dwelling buildings, industrial demands, health-care social services, public administration buildings, and commercial buildings. The number of buildings is approximately 1700.

Problems in smart meter devices can cause missing or erroneous readings in customer records. Therefore, we apply a data preprocessing step to deal with incorrect meter readings. Customers that have missing heat load or return temperature measurements for at least one consecutive day are excluded from the analysis. Shorter periods of missing values are filled using linear interpolation of surrounding values. Meter readings that have identical values for more than one day are also excluded. As a result, we include 896 buildings in this study.

For the buildings with good quality of data, heat power signatures are extracted based on the daily average heat load and average daily outdoor temperatures. We only consider days when the average outdoor temperature is below 10°C. It has been shown that when the space heating is not the main source of the heat demand in a building, there is no strong correlation between outdoor temperature and the temperature difference between supply and return pipes. Instead of examining balance temperature for each signature, we simply set it to 10 °C as stated in [3].

4.2. Evaluation

In this section, we conduct experiments to evaluate our novel method, which measures both dispersion and outliers by comparing with dispersion-based and outlier-based methods individually. Each method separately produces a ranking of the most anomalous buildings, and we evaluate those rankings using return temperature measurements of the buildings. For each building, we calculate average (denoted T_a) and maximum (denoted T_m) return temperatures measured on the same dates as the heat loads in the power signatures. Clearly, both are relevant from the optimization of DH networks perspective, but they capture different aspects. While T_a values indicate long-term return temperature behavior, the T_m captures the most extreme operation of a building.

We present two different strategies to evaluate that buildings which have high rankings are actually problematic. The first strategy, “accuracy at the top” shows the ratio of abnormal buildings, compared to normal ones, near the top of the ranking. We compute “accuracy of top N buildings” as $(N_{abnormal}/(N_{normal} + N_{abnormal}))$ where N_{normal} and $N_{abnormal}$ are number of normal and abnormal buildings, respectively, among the top N ranked buildings. Buildings that have T_a higher than 35°C or T_m higher than 45°C are considered to be abnormal in this strategy.

The second strategy, “average temperature at the top”, shows the average T_a and T_m values of top ranked buildings. We compute average T_a (\hat{T}_a) and average T_m (\hat{T}_m) of top N buildings as follow:

$$\hat{T}_a = \frac{\sum_{n=1}^N T_{a_n}}{N} \quad (2)$$

$$\hat{T}_m = \frac{\sum_{n=1}^N T_{m_n}}{N} \quad (3)$$

Figure 4 shows accuracies at top N buildings according their T_a and T_m values. Dispersion-based method and aggregated method show very similar performance in T_a accuracy (cf. Figure 4(a)). However, aggregated method converges at the level of 94% (red line), while dispersion-based method settles at 92% (blue line).

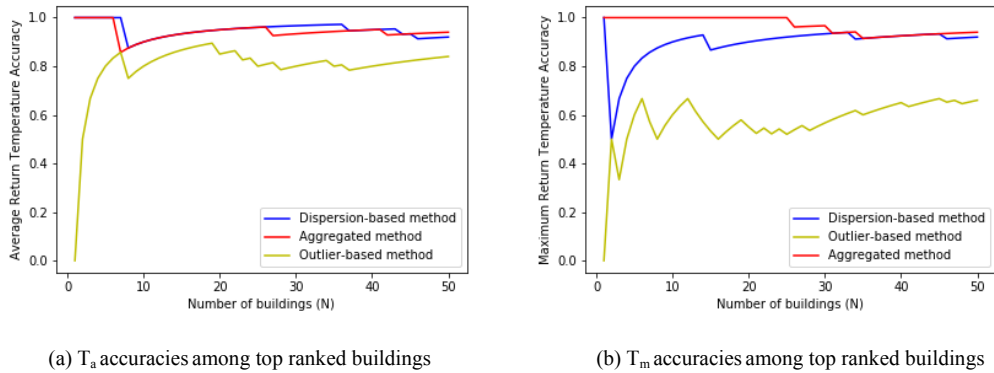


Figure 4: Accuracies at the top

There are minor differences along the way, but they are not significant. On the other hand, the outlier-based method achieves significantly lower accuracy of 83% (yellow line), and actually fails to detect the most severely abnormal building.

In terms of accuracy based on T_m , the aggregated approach significantly outperforms both dispersion-based and outlier-based methods. It perfectly identifies (achieving 100% accuracy) the top 27 abnormal buildings, and flattens at 94% similar (cf. red line in Figure 4b). Dispersion-based approach is hindered by several false positives near the top of the ranking, but its accuracy increases with the number of customers and reaches to 92% (blue line). The outlier-based approach, again, shows by far the worst performance, with final accuracy of only 66% (yellow line).

In Figure 5, the results of average temperatures at the top are shown. Dispersion-based (blue line) and aggregated (yellow line) methods start and get flattened at the same temperature in both cases (cf. Figure 5(a) and Figure 5(b)). Dispersion-based method shows slightly higher \hat{T}_a until top 10 buildings (cf. blue line in Figure 5(a)), while aggregated method is almost constantly better at \hat{T}_m until convergence (cf. red line in Figure 5(a)). Buildings that got higher rankings by the outlier-based approach show significantly lower return temperatures (cf. yellow line in Figure 5(a) and Figure 5(b)).

We present two different results, since they capture different types of abnormality, both of which can be important. It is crucial to notice that our proposed method outperforms state-of-the-art in either case. In particular, the buildings that are experiencing long-term problems are likely to be characterized by large T_a , while abrupt failures will cause unusually high T_m ; however, those latter ones may not affect T_a significantly if they are quickly fixed. An anomaly detection method needs to detect both kinds of problems -- and as shown in Figures 4 and 5, the proposed method exactly provides that.

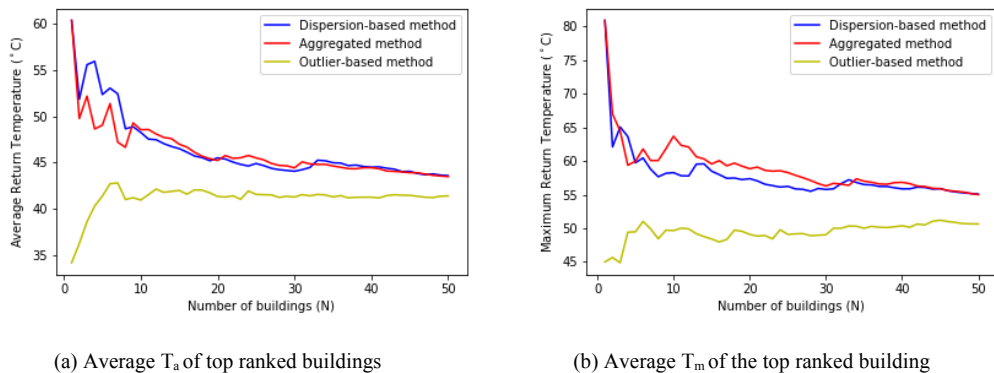


Figure 5: Average temperature at the top.

5. Conclusion

In this work, we postulate that ranking abnormal buildings should be done based on power signatures estimated using robust regression and needs to include measuring both dispersion and outliers. We propose a novel method for doing that, based on combining building rankings to measure their “degree of abnormality”.

We've conducted experiments on large-scale data from substations connected to two district heating networks in south of Sweden. We have compared our method against the state-of-the-art outlier-based approach. Return temperatures of the buildings have been taken as reference for two different types of evaluation which we referred as “accuracy at the top” and “average temperature at the top”. The first one has shown the ratio of abnormal buildings ranked on the top, while the second one has shown average return temperatures of top abnormal buildings.

The results demonstrate that dispersion-based and aggregated methods significantly outperform the state-of-the-art approach.

References

- [1] H. Lund, S. Werner, R. Wiltshire, S. Svendsen, J. E. Thorsen, F. Hvelplund, B. V. Mathiesen, 4th generation district heating (4gdh): Integrating smart thermal grids into future sustainable energy systems, *Energy* 68 (2014) 1–11.
- [2] H. Gadd, S. Werner, Heat load patterns in district heating substations, *Applied energy* 108 (2013) 176–183.
- [3] H. Gadd, S. Werner, Achieving low return temperatures from district heating substations, *Applied energy* 136 (2014) 59–67.
- [4] H. Gadd, S. Werner, Fault detection in district heating substations, *Applied Energy* 117 (2015) 51–59.
- [5] F. Sandin, J. Gustafsson, J. Delsing, R. Eklund, Basic methods for automated fault detection and energy data validation in existing district heating systems, In *International Symposium on District Heating and Cooling: 03/09/2012-04/09/2012*, District Energy Development Center, 2012.
- [6] L. Lundström, Adaptive weather correction of energy consumption data, *Energy Procedia* 105 (2017) 3397–3402.
- [7] M. Noussan, M. Jarre, A. Poggio, Real operation data analysis on district heating load patterns, *Energy* 129 (2017) 70–78.
- [8] L. Belussi, L. Danza, I. Meroni, F. Salamone, Energy performance assessment with empirical methods: Application of energy signature, *OptoElectronics Review* 23 (1) (2015) 85–89.
- [9] I. Allard, T. Olofsson, G. Nair, Energy performance indicators in the swedish building procurement process, *Sustainability* 9 (10) (2017) 1877–14.
- [10] G. Nordström, H. Johnsson, S. Lidelöv, Using the energy signature method to estimate the effective u-value of buildings, in: *Sustainability in Energy and Buildings*, Springer, 2013, pp. 35–44.
- [11] S. Danov, J. Carbonell, J. Cipriano, J. Mart'ı-Herrero, Approaches to evaluate building energy performance from daily consumption data considering dynamic and solar gain effects, *Energy and Buildings* 57 (2013) 110–118.
- [12] C. Ghiaus, Experimental estimation of building energy performance by robust regression, *Energy and buildings*, 38 (6) (2006) 582–587.
- [13] J.-U. Sjögren, S. Andersson, T. Olofsson, Sensitivity of the total heat loss coefficient determined by the energy signature approach to different time periods and gained energy, *Energy and Buildings* 41 (7) (2009) 801–808.
- [14] J.-U. Sjögren, S. Andersson, T. Olofsson, An approach to evaluate the energy performance of buildings based on incomplete monthly data, *Energy and Buildings* 39 (8) (2007) 945–953.
- [15] Averfalk H, Werner S. Novel low temperature heat distribution technology. *Energy*. 2018 Jan 2.
- [16] L. Pistore, G. Pernigotto, F. Cappelletti, P. Romagnoni, A. Gasparella, From energy signature to cluster analysis: an integrated approach.
- [17] L. Farinaccio, R. Zmeureanu, Using a pattern recognition approach to disaggregate the total electricity consumption in a house into the major enduses, *Energy and Buildings* 30 (3) (1999) 245–259.
- [18] L. Danza, L. Belussi, I. Meroni, M. Mililli, F. Salamone, Hourly calculation method of air source heat pump behavior, *Buildings* 6 (2) (2016) 16.
- [19] L. Belussi, L. Danza, Method for the prediction of malfunctions of buildings through real energy consumption analysis: Holistic and multidisciplinary approach of energy signature, *Energy and Buildings* 55 (2012) 715–720.
- [20] Acquaviva A, Apiletti D, Attanasio A, Baralis E, Bottaccioli L, Castagnetti FB, Cerquitelli T, Chiusano S, Macii E, Martellacci D, Patti E. Energy signature analysis: Knowledge at your fingertips. In *Big Data (BigData Congress)*, 2015 IEEE International Congress on 2015 Jun 27 (pp. 543-550). IEEE.
- [21] R. Maronna, R. D. Martin, V. Yohai, *Robust statistics*, Vol. 1, John Wiley & Sons, Chichester. ISBN, 2006.
- [22] Fischler MA, Bolles RC. Random sample consensus: a paradigm for model fitting with applications to image analysis and automated cartography. In *Readings in computer vision 1987* (pp. 726-740). [23] D. R. Kisku, P. Gupta, J. K. Sing, *Advances in biometrics for secure human authentication and recognition*, CRC Press, 2013.
- [24] G. W. Snedecor, *Statistical Methods*: NY George W. Snedecor and William G. Cochran, Iowa State University Press, 1967.
- [25] G. Grimmett, D. Stirzaker, *Probability and random processes*, 2001.
- [26] J. C. de Borda, M'emoire sur les 'elections au scrutin.
- [27] P. A. Jaskowiak, D. Moulavi, A. C. Furtado, R. J. Campello, A. Zimek, J. Sander, On strategies for building effective ensembles of relative clustering validity criteria, *Knowledge and Information Systems* 47 (2) (2016) 329–354



16th International Symposium on District Heating and Cooling, DHC2018,
9–12 September 2018, Hamburg, Germany

Heat pumps with district heating for the UK's domestic heating: individual versus district level

Zhikun Wang^{a,*}

^aUniversity College London, UCL Energy Institute, Central House, 14 Upper Woburn Place, London, London WC1H 0NN, United Kingdom

Abstract

The UK has set ambitious targets to reduce carbon emissions, improve energy efficiency and affordability, encourage renewable energy generation, and reduce dependency on imported fossil fuels. Heating is the most essential component of the UK's current residential energy consumption, and it is mostly supplied through the direct burning of natural gas. With constantly changing market conditions and political regulatory frameworks, technology assessments and cost-effective planning strategies are critical for long-term energy and environmental policy designing. Electric heat pumps with decarbonised electricity are proposed as promising technologies that could replace gas heating and contribute to the UK's future low-carbon heat mix. District heating has been transforming over generations in order to better utilise renewables or resources that otherwise would be wasted. Both technologies have been well developed, with abundant scientific research and industrial experiences in some European countries over the past few decades. However, the market shares of heat pumps and district heating networks are low in the UK. This paper explores empirical heat consumption from smart meter data in different types of dwellings in the UK and the role of heat pumps and district heating for different types of dwellings on different scales. This study investigates heat pumps in individual households versus district heating networks through a levelised cost model, to present their comparative environmental and economic advantages. This study shows that economies of scale arise in the UK's district heating networks with large heat pumps, but the costs of heat are significantly higher than individual gas boilers.

© 2018 The Authors. Published by Elsevier Ltd.

This is an open access article under the CC BY-NC-ND license (<https://creativecommons.org/licenses/by-nc-nd/4.0/>)

Selection and peer-review under responsibility of the scientific committee of the 16th International Symposium on District Heating and Cooling, DHC2018.

Keywords: heat demand; heat pumps; district heating; levelised cost of heat

* Corresponding author. Tel.: +44 (0)20 7679 8186.

E-mail address: zhikun.wang.10@ucl.ac.uk

1. Introduction and background

The UK has set objectives to deep-decarbonise its economy while improving energy affordability and eliminating fuel poverty, promoting energy efficiency, and reducing dependency on imported fossil fuels, with goals to reduce greenhouse gas emissions by 80% by the year 2050 compared to 1990 levels [1]. To meet these targets, carbon emissions from the building sector will need to be reduced to almost zero [2]. It is possible to achieve deep cuts in carbon emissions from British dwellings with the potential for future improvements in building performance, decarbonising the electricity, and re-engineering the heat supply [3]. Renewable electricity together with high-efficiency, low-carbon heat technologies are expected to play an essential role in meeting the UK's heat demand and energy and environmental targets, while bringing health, wellbeing, and economic benefits. With heat technologies continually upgrading and improving, evaluating technologies' advantages and performance is essential to determine the direction of long-term heat decarbonisation and to develop low-carbon heat infrastructure.

Heat demand is the largest demand in the electricity, heating, and cooling sectors regarding both annual and peak hourly demands in the UK [4]. Currently, nearly half of the final energy demand in the UK is consumed to provide heat across the economy [5]. Gas is the most important energy carrier, and individual gas boilers are the principal way of supplying domestic heat demand in over 85% of British households [6]. Residential heat demand varies in different types of dwellings. There are about 27.5 million dwellings in the UK, including five main dwelling types: terraced (28%), semi-detached (26%), flat (20%), detached (17%), and bungalow (9%), and the estimated domestic gas demand is more than three times higher than domestic electricity demand annually [7].

In recent years, there has been an increasing trend for electricity generation from renewables, and better utilisation of waste energy. This promotes the opportunity for the electrification of the heating sector and a shift away from fossil fuels. Electric heat pumps could play a central role in the UK's future approach to heating, together with the decarbonised electricity grid. Additionally, heat pumps can be integrated into district heating networks, which may provide additional carbon emissions reduction potential. Integrating flexible heat pumps into district heating networks has been recognised as a crucial step in transitioning to a 100% renewable energy system cost-effectively [8]. In the UK, the Building Regulations [9] require new buildings to consider district heating as well as the integration of heat pumps. Recently, the Clean Growth Strategy [10] has set out a series of proposals to phase out fossil fuel heating in buildings off the gas grid during the 2020s, build and extend heat networks across the country, and invest in the development of low-carbon heat technologies and energy efficiency measures.

However, although heat pumps and district heating have been widely deployed in Europe, they are still niche options in the UK. Currently, only about 0.2% of the UK's total heat demand is supplied by electric heat pumps [11]. There are less than 2,000 operating district heating networks across the country, and around three-quarters of them are small networks, which are supplying heat to less than a hundred dwellings [12]. It is suggested that the economic viability of district heating networks in the UK depends on a series of factors, including upfront infrastructure costs, volatility of energy prices, and uncertain energy policies [13]. Moreover, there is a great deal of uncertainty regarding the decarbonisation of the electricity grid, demand variations, and future market shares of heat pumps and heat networks [14]. Currently, due to higher upfront costs and longer payback periods compared to gas boilers, district heating networks integrated with heat pumps are considered risky technology in the UK [15].

There are very few empirical studies regarding the operation of heat pumps in the UK's buildings and heat networks. There is a need for research on potential competing heat technologies and detailed analyses of the comparative advantages of deploying heat pumps and district heating in different types of buildings on different scales. This paper aims to provide an empirical analysis of domestic heat demand in different types of dwellings in the UK and conduct economic and environmental assessments of the application of heat pumps and district heating networks on different scales, from individual buildings to the district level.

2. Methodology

2.1 Empirical data analysis: domestic heat demand

Understanding how much and when heat is consumed is fundamental to evaluating heat supplying technologies and designing cost-effective strategies to meet heat demand. This study analyses empirical residential heat consumption, including space heating and domestic hot water demand, for the five main types of dwellings through smart meter data [7], and investigates hourly heat load profiles over a year to estimate variations in total heat demand as well as peak demand. Due to the low installation rate of heat meters and the predominate gas boiler market share in the UK, natural gas consumption data is analysed as a proxy to evaluate heat demand based on the national average gas boiler efficiency (80.54%) according to [7].

Smart meter data from the Energy Demand Research Project (EDRP) is used for this study. The EDRP was a set of large-scale trials implemented by four major energy suppliers to explore customer responses and individuals' energy consumption with smart meters across Britain from 2007 to 2010 [16]. This study analyses the subset data from EDF Energy, which includes half-hourly electricity and gas smart meter data from 1,879 households in England. This study examines households that used gas boilers as the primary technology for their central space heating and domestic hot water. Half-hourly natural gas consumption

data are summed into hourly data, and the annual heat demand from 591 households with different dwelling types is estimated after the data extraction and cleaning processes. Hourly heat load profile is constructed to study peak hourly heat demand over the year of 2009, as winter 2009/2010 was one of the coldest over the last three decades [17].

2.2. Modelling: economic and environmental assessment of heat pumps and district heating

Technology cost assessments are fundamental to inform decision making and policy designing by quantifying and evaluating the trade-offs of how to meet energy demand while mitigating carbon emissions in a cost-effective way. Levelised Cost of Energy (LCOE) is a useful method in modelling to compare the generating costs of energy through alternative technologies, especially for technologies with different operating lifetimes and costing structures. The LCOE method was initially developed for rate-regulated electricity markets. It is sometimes called a life cycle cost as it takes all cost elements into account to generate energy at the plant level through its whole life cycle from planning, installation, and energy generation to site decommissioning and waste management [18]. The LCOE is a form of net present value (NPV) calculation based on the discounted cash flow method under specific technical and economic assumptions [18]. It is the ratio of the NPV of the total costs of a technology over the NPV of the total amount of energy generated by this technology.

Based on the monitored gas consumption data from the EDRP project and the estimated heat demand for individual dwellings and district heating networks, a simple Levelised Cost of Heat (LCOH) model is developed to assess costs and carbon emissions from different individual heating technologies as well as large heat pumps and district heating networks on different scales. Three types of individual heating technologies are considered: a gas boiler, a ground source heat pump, and an air source heat pump. The model is built based on the equation as shown:

$$\text{LCOH} = \frac{\sum \left[\frac{\text{Capital}_t + \text{O\&M}_t + \text{Fuel}_t + \text{Carbon}_t}{(1+r)^t} \right]}{\sum \left[\frac{\text{MWh}_t}{(1+r)^t} \right]} \quad (1)$$

Where Capital_t is the capital expenditures in the year t , O\&M_t is the operation and maintenance costs. Due to the well-developed gas grid in the UK, this model does not consider the costs to construct the gas networks. This study gathers technology costs and performance data from the government commissioned statistical databases [19 - 21], which are considered to be representative of networks in the UK, in addition to industrial practitioners' databases [22 - 23]. Fuel_t and Carbon_t are the fuel costs and the carbon costs in the year t . This study uses the publicly available annual fuel and carbon prices projected by [5]. $(1+r)^t$ is the discount factor in the year t , with the discount rate r . This study applies 3.5%, corresponding to the 'social cost of capital' [24]. MWh_t is the amount of heat produced in the year t . This study assumes that all heating options start to operate in 2018 to meet households' heat demand, but with different projected future lifetimes. Detailed model input assumptions and cost data are included in the appendix.

Upscaling methods are applied to simulate the aggregated heat demand for district heating networks on different scales that could be supplied through large heat pumps based on the proportions of the five dwelling types in the UK [7]. There are different definitions regarding the size of heat networks in the UK. This study uses the adjusted standards defined by [23] and [25] with five scales:

- Small heat networks (less than 100 residential properties)
- Medium heat networks (between 100 and 500 residential properties)
- Large heat networks (over 500 residential properties)
- Single developments (up to 3,000 homes)
- Medium multi-development scales (up to 20,000 homes)

3. Results and discussions

3.1. Heat demand

Based on monitored gas consumption data and households' metadata, heat demand in the five dwelling types in 2009 was estimated. The average amount of gas consumed in 2009 was approximately 18,900 kWh per household. Figure 1 displays the estimated average annual heat demand from the monitored households. On average, a household consumes approximately 15,200 kWhth of heat a year. As expected, a detached house requires the highest amount of heat among all types of dwellings, with annual heat demand reaching over 18,600 kWhth, while a flat consumes only about 10,400 kWhth. Additionally, this study only considers heat demand supplied by individual gas boilers, and does not consider supplementary heating measures used in those households, such as electric heating or fireplaces due to limited metadata.

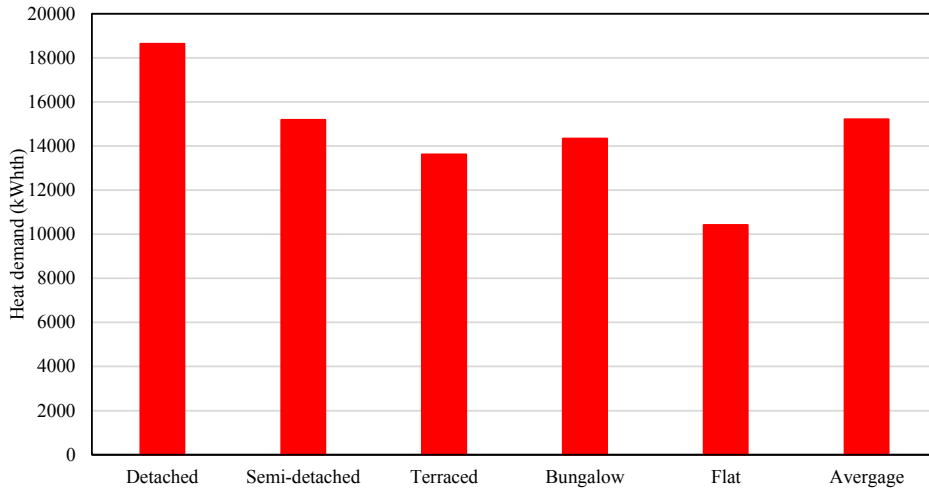


Figure 1. Average annual heat demand in the five main types of residential buildings.

Figure 2 demonstrates the average hourly heat demand profiles per household versus the hourly external temperature over the year of 2009. This figure shows the volatile changes in domestic heat demand over time, with most of the heat demand occurred from November to May. On average, the maximum hourly heat demand reached around 7.5 kWh per household during the coldest periods in the year, which is more than seven times higher than the typical peak hourly heat demand (approximately 1 kWh) during the summer.

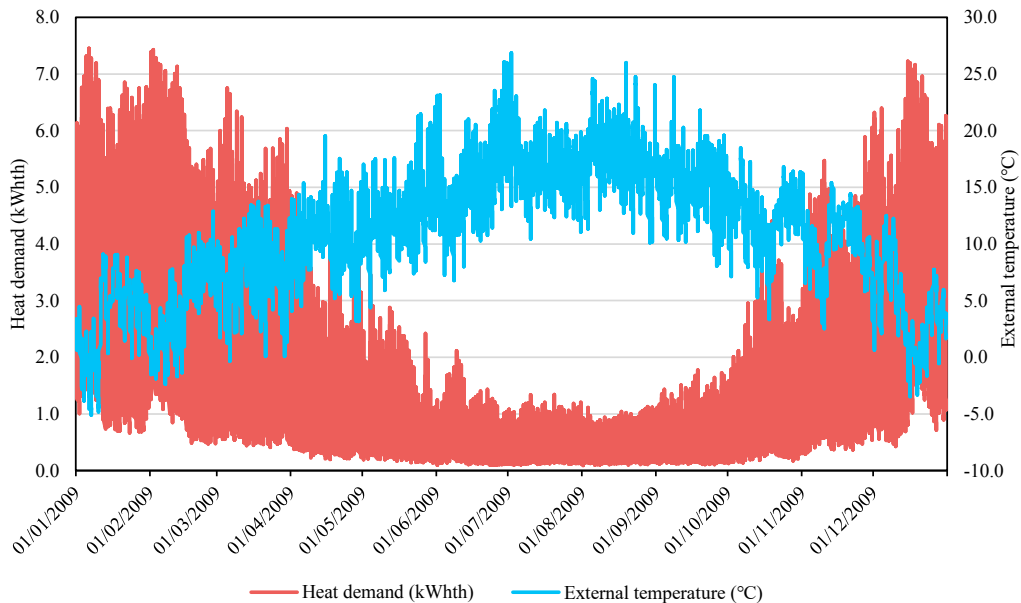


Figure 2. Average hourly heat demand and external temperature in 2009.

3.2. Costs and emissions

3.2.1. Individual heating technologies

The LCOH model is built for different individual heating technologies and district heating networks to meet the heat demand for different types of dwellings. Figure 3 shows the results of the overall LCOH for the five types of individual households, and one household with an averaged heat demand. A 3.5% discount rate is used throughout the technologies' lifetimes. In general, the LCOH is lower in dwellings with a higher annual heat demand, and the difference between the LCOH for a gas boiler and heat pumps becomes larger when heat demand decreases among the five dwelling types. As expected, a gas boiler is the cheapest way to meet heat demand in all individual dwellings, with an overall LCOH of £75/MWhth in a detached house and just over

£90/MWhth in a flat. A ground source heat pump is clearly indicated as the most expensive individual technology for meeting heat demand in all dwelling types. In this study, the LCOH for a flat is indicated as being the highest due to its low annual heat demand, with the LCOH for a ground source heat pump reaching more than £140/MWhth. Meanwhile, based on the average heat demand across all five dwelling types, the LCOH for a gas boiler is just under £80/MWhth, roughly 20% cheaper than an air source heat pump and 30% cheaper than a ground source heat pump.

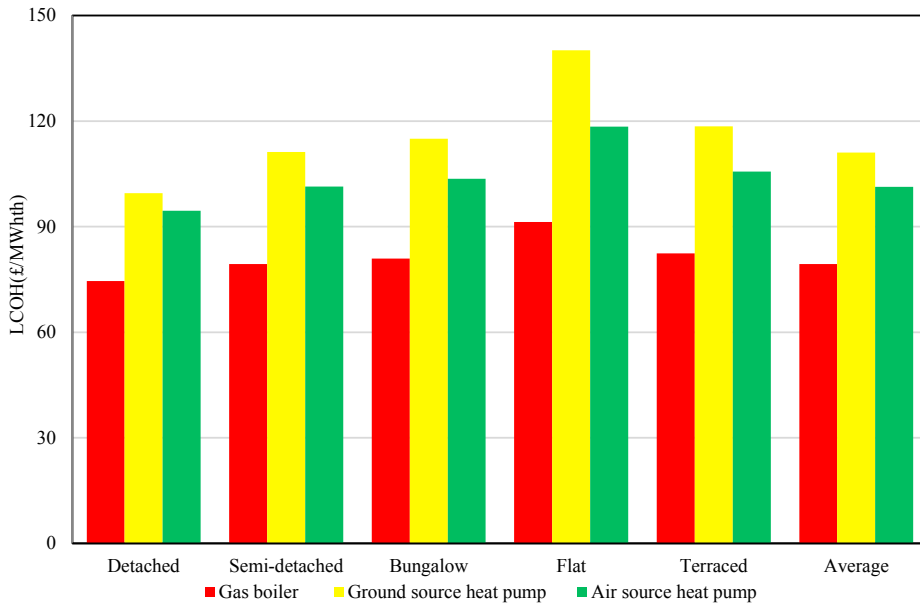


Figure 3. The LCOH for different individual technologies in different dwelling types.

Although heat pumps are more expensive than gas boilers for supplying heat to all individual dwellings, they can significantly reduce carbon emissions from heat for individual households, on the condition that the carbon intensity of the electricity grid in the UK keeps decreasing, as per future projections [5]. Figure 4 indicates the average annual carbon dioxide emissions from different technologies. Based on the carbon content of natural gas and the projected future carbon intensity of electricity in the UK, on average, a gas boiler emits approximately three tonnes of carbon dioxide a year over its technology lifetime. In contrast, a heat pump could reduce more than 80% of carbon emissions while meeting the heat demand, with roughly 0.5 and 0.7 tonnes of annual carbon emissions from a ground source heat pump and an air source heat pump, respectively.

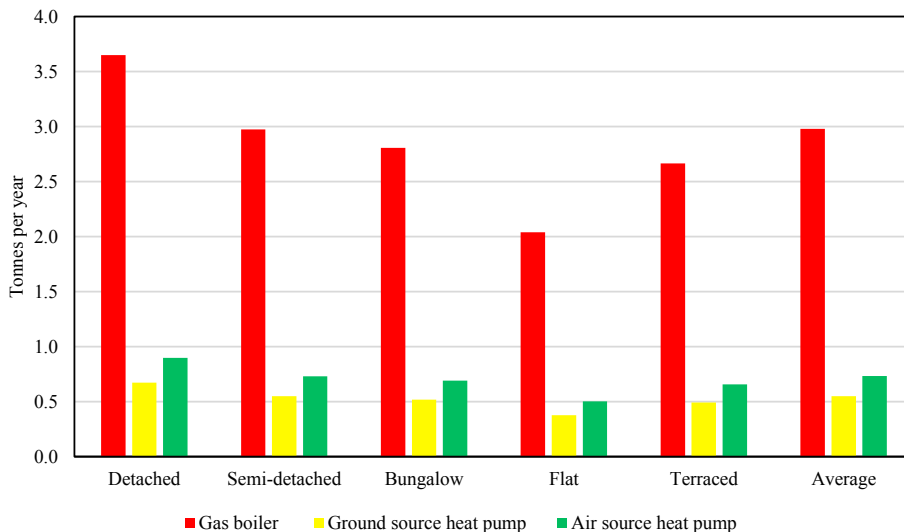


Figure 4. Estimated average annual carbon dioxide emissions from individual heating technologies.

3.2.2. District heating networks integrated with large heat pumps

Based on the five scales of district heating networks defined in section 2.2, the costs of heat are modelled to meet heat demand on the five scales through district heating with large heat pumps, compared to the individual technologies. This study assumes that heat pumps are utilised to generate heat for both space heating and domestic hot water for all dwellings connected to the networks.

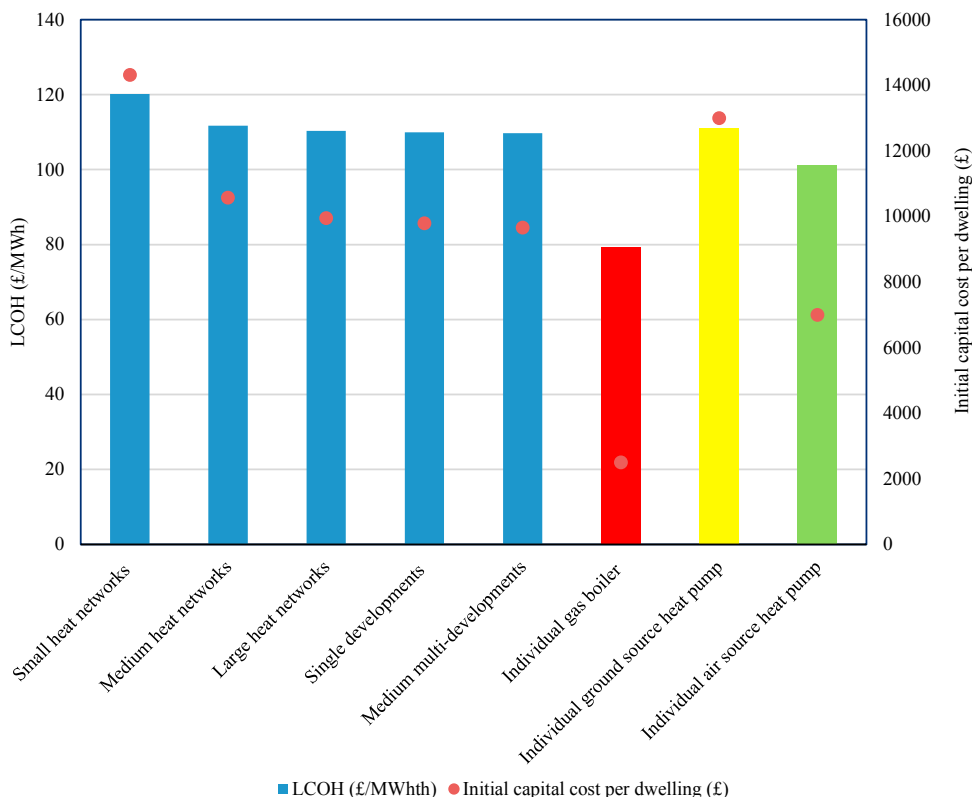


Figure 5. The LCOH and initial capital costs per dwelling for district heating according to five scales, compared to individual heating technologies.

Figure 5 provides an overview of the LCOH (primary vertical axis) and the initial capital costs per dwelling (secondary vertical axis) for district heating networks on the five scales and compared to the three individual technologies. As the figure shows, economies of scale arise in district heating networks, as the overall LCOH decreases steadily from the smallest district heating network to the largest, with the number dropping from over £120/MWh to under £110/MWh. However, the results of LCOH for district heating networks are still significantly more expensive than individual gas boilers due to high capital costs.

Figure 5 also compares the initial capital costs for dwellings with different heating options. As the figure indicates, a small district heating network has the highest initial capital cost per dwelling at approximately £14,300 per dwelling on average, while this number is reduced by around one third to roughly £9,600 per dwelling for the largest district heating scale. Although the LCOH for district heating networks becomes similar to the LCOH for individual ground source heat pumps when the network becomes larger, their initial capital costs per dwelling are still higher than installing individual air source heat pumps.

Figure 6 illustrates the compositions of the overall LCOH according to different cost elements, including capital costs, O&M costs, fuel costs, and carbon costs. For an individual gas boiler, capital cost contributes to less than 20% of the overall LCOH, and fuel cost contributes to more than 60%. An individual ground source heat pump has the highest percentage of capital cost (52%) and the smallest percentage of fuel cost (43%). Meanwhile, among district heating networks, the proportion of capital cost becomes gradually smaller when the scale of the network rises. For a small district heating network (with 100 dwellings), capital cost accounts for about 30% of the overall LCOH, whereas for the largest district heating scale (with 20,000 dwellings), capital cost reduces to about 22% of total LCOH. Due to the projected decreasing carbon intensity of electricity and very low future carbon prices [5] in the UK, carbon costs only contribute to very small proportions of the overall LCOH for all heating options, accounting for less than 5% for gas boilers and less than 1% for heat pumps and district heating networks.

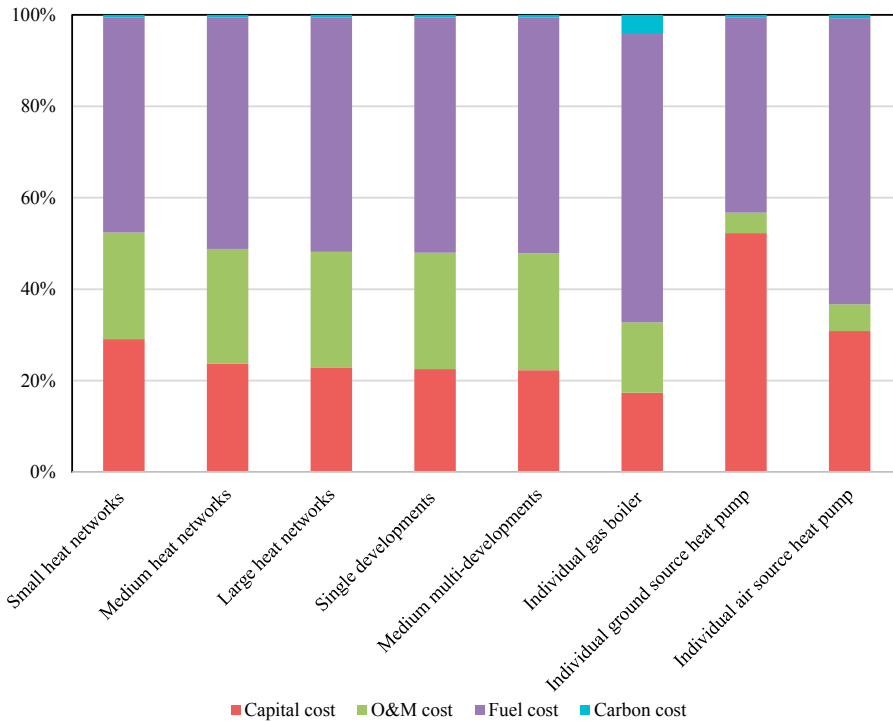


Figure 6: The LCOH cost elements among different heating options.

The levelised cost method is highly sensitive to its assumptions. Sensitivity analysis is conducted to evaluate the correlations between a group of selected independent input factors and the overall LCOH for district heating networks. The LCOH result for a medium scale district heating network is used as a basis, and the selected variables are altered to evaluate their impact on the final LCOH results. Figures 7 and 8 summarise the changes in the overall LCOH when the input assumptions are adjusted. Figure 7 displays the percentage changes in the LCOH when the total heat demand, capital cost, and O&M cost are modified by plus or minus up to 50%. The figure shows that LCOH is more sensitive to heat demand changes than cost factors, as it upsurges by roughly 35% when the total heat demand reduces by half, whereas the overall LCOH decreases by 11% when the total heat demand rises by half. Moreover, when capital cost and O&M cost increase or decrease by 50%, the overall LCOH increases or decreases by 15% and 11%, respectively.

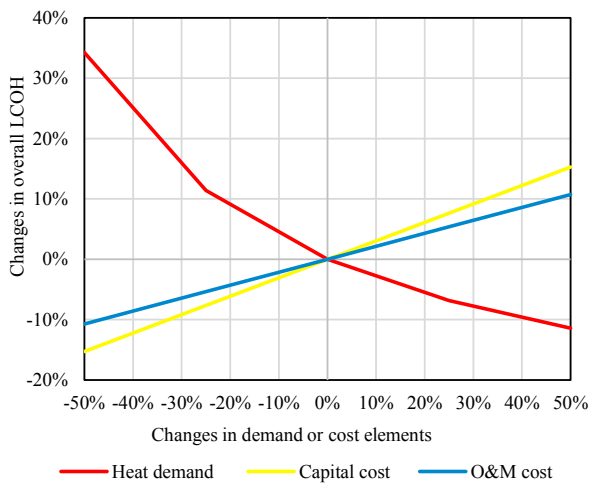


Figure 7: LCOH as the function of heat demand or costs.

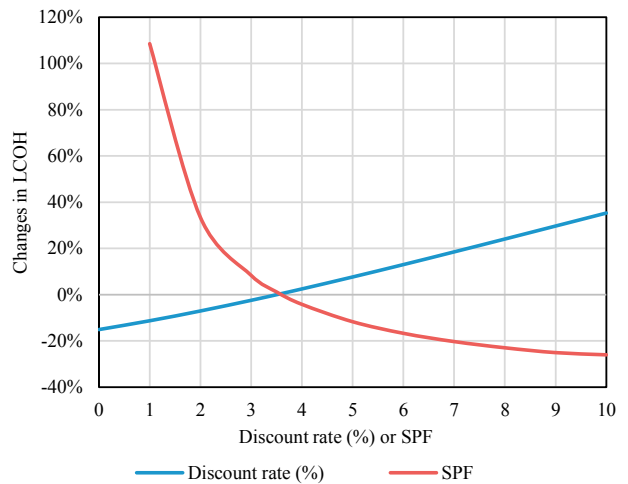


Figure 8: LCOH as the function of discount rate and heat pump efficiency.

The discount rate is crucial, as it determines the net present value and the future costs of technologies over their lifetimes. This study uses 3.5% as a basis, and the number is adjusted from 0% to 10%. As Figure 8 reveals, the overall LCOH drops 15% when the discount rate declines from 3.5% to 0%, and the overall LCOH increases by up to 35% when the discount rate reaches 10%. Moreover, Figure 8 also shows how the overall LCOH changes when the heat pump efficiency (seasonal performance factor, SPF) changes from its initial assumption of 3.6. The LCOH increases significantly, by roughly 110%, when the SPF drops from 3.6 to 1.0, but decreases steadily when the SPF escalates. The overall LCOH could decrease by more than 25%, if the SPF reached 10.

Although the levelised cost method is a useful tool for comparing the costs of different energy generating technologies, some limitations associated with the LCOH are noted. Firstly, the energy costs of the levelised cost method are outputs and assumed to be constant over technologies' lifetimes, and they are not the prices to sell energy. Hence, the levelised cost method does not reflect the short-term or long-term volatilities of energy prices. Secondly, this study modelled the LCOH for the five main dwelling types in the UK. However, the domestic heat demand and technology performance may vary from one dwelling to another, according to numerous features such as building fabrics, ages, designs, sizes, locations and occupants' characteristics. Because of limited metadata, this study does not differentiate heat demand in households regarding their specific features such as floor areas, number of occupants and states of refurbishment.

The results of LCOH are highly sensitive to its assumptions. Accordingly, variations in future heat demand, cost elements or technology performance may considerably influence the results, as the sensitivity analyses have shown. The employed LCOH refers to all costs at the plant level. This study applies secondary technology costs and performance data from different sources, and in reality, these features may vary significantly according to individual dwellings and technologies. Moreover, The LCOH represents a one-time decision that will last for a long period of time. This study uses projected natural gas and electricity prices, carbon taxes and carbon intensities of electricity for the future; however, there are significant uncertainties regarding future taxes, subsidies and renewable shares of electricity generation, and changes in these parameters may cause pronounced impacts on the overall LCOH and carbon emissions. Furthermore, there are substantial uncertainties associated with the UK's future energy and climate policies, especially following the recent Brexit referendum and abrupt changes in exchange rates. Changes in policies may cause significant impacts on many key modelling elements, including technology costs, fuel and carbon prices.

4. Conclusion

To achieve the government's energy and environmental targets, it is imperative to study potential heating options to replace the conventional gas-fired system and reduce carbon emissions. Heat pumps and district heating are established technologies with large-scale deployment in many European countries over the past few decades, but their markets and policy frameworks are immature in the UK, and there are technical, social, and economic barriers for their future deployment. Moreover, the well-developed natural gas networks, the eminently high market share of individual gas boilers and cheap natural gas are the most substantial challenges for the future deployment of electric heat pumps and district heating networks in the UK.

This study quantifies empirical domestic heat consumption through smart meter data from a diverse range of dwellings in the UK. Results show that the domestic heat demand differs in different types of dwellings and changes erratically over time. This study also investigates the cost-competitiveness of heat pumps and district heating compared to individual gas boilers, and demonstrates that economies of scale arise in district heating networks. Although heat pumps with decarbonised electricity could reduce domestic carbon emissions from heat intensively, the levelised costs for heat pumps and district heating are significantly higher than individual gas boilers. The mass electrification of the heating sector and the deployment of the heat networks on large scales will require intensive investment, alterations in supply chain practices, and public acceptance. Further studies are desirable to better understand the role of district heating and heat pumps in the UK's energy system and transform district heating from a strategy into reality.

Acknowledgements

This research was made possible by support from the Engineering and Physical Sciences Research Council (EPSRC) Centre for Doctoral Training in Energy Demand (LoLo), grant numbers EP/L01517X/1 and EP/H009612/1. The author would like to gratefully acknowledge the EDF Energy R&D UK Centre Limited for providing smart meter data and financial support.

Reference

- [1] CCC. Building a low-carbon economy – The UK's contribution to tackling climate change. London, UK: the Committee on Climate Change, 2008.
- [2] DECC. The future of heating: meeting the challenge. London, UK: the Department of Energy and Climate Change, 2013.
- [3] Lowe, R. Technical options and strategies for decarbonizing UK housing. *Building Research & Information*, 2007, Vol. 35, pp. 412-425.
- [4] Connolly, D. Heat Roadmap Europe: Quantitative comparison between the electricity, heating, and cooling sectors for different European countries. *Energy*, 2017, Vol. 139, pp. 580-593.
- [5] BEIS. Updated energy and emission projections. Department for Business, Energy & Industrial Strategy, 2018.
- [6] Delta-ee. IEA HPP Annex 42 Heat Pumps in Smart Grids. Delta Energy and Environment, 2014.

- [7] ECUK. Energy consumption in the UK. Department for Business, Energy & Industrial Strategy, 2017.
- [8] Conolly, D. & Mathiesen, B. V. A technical and economic analysis of one potential pathway to a 100% renewable energy system. *International Journal of Sustainable Energy Planning and Management*, 2017, Vol. 1, pp. 7-28.
- [9] The Building Regulations. The Building Regulations &c. (Amendment) Regulations [Online]. London, UK: Department for Communities and Local Government. Building regulations: divisional circular letters and Building regulation. Available: <https://www.gov.uk/government/publications/the-building-c-amendment-regulations-2014> [Accessed 8th May 2018], 2014.
- [10] BEIS. The Clean Growth Strategy. Leading the way to a low carbon future. London, UK: Department for Business, Energy and Industrial Strategy, 2017.
- [11] Hannon, M. J. Raising the temperature of the UK heat pump market: Learning lessons from Finland. *Energy Policy*, 2015. Vol. 85, pp. 369-375.
- [12] IEA. Heat Pumps in Smart Grids: Market overview – Country report for the United Kingdom. The Netherlands: International Energy Agency, 2017.
- [13] Kelly, S. & Pollitt, M. An assessment of the present and future opportunities for combined heat and power with district heating (CHP-DH) in the United Kingdom. *Energy Policy*, 2010, Vol. 38, pp. 6936-6945.
- [14] Chaudry, M., Abeysekera, M., Hosseini, S. H. R., Jenkins, N. & Wu, J. Uncertainties in decarbonising heat in the UK. *Energy Policy*, 2015, Vol. 87, pp. 623-640.
- [15] Hawkey, D., Webb, J. & Winskel, M. Organisation and governance of urban energy systems: district heating and cooling in the UK. *Journal of Cleaner Production*, 2013, Vol. 50, pp. 22-31.
- [16] AECOM. Energy Demand Research Project: Final Analysis. Hertfordshire, UK: AECOM and Ofgem, 2011.
- [17] Met Office. Met Office Winter 2009/2010. Available: <https://www.metoffice.gov.uk/about-us/who/how/case-studies/winter09-10> [Accessed 8th May 2018], 2016.
- [18] IEA, NEA & OECD. Projected costs of generating electricity. Paris, France, International Energy Agency, Nuclear Energy Agency and Organisation for Economic Co-operation and Development, 2015.
- [19] DECC & AECOM. Assessment of the costs, performance, and characteristics of UK heat networks. London, UK: Department of Energy and Climate Change, 2015.
- [20] DECC. Heat pumps in district heating. London, UK: Department of Energy and Climate Change, 2016.
- [21] DECC & Sweett Group. Research on the costs and performance of heating and cooling technologies. London, UK: The Department of Energy and Climate Change, 2013.
- [22] Pöyry. The potential and costs of district heating networks. A Report to the Department of Energy and Climate Change. Oxford, UK: Pöyry Energy Limited, 2009.
- [23] Greater London Authority. District heating manual for London. London, UK: Greater London Authority and Arup, 2013.
- [24] HM Treasury. The Green Book: appraisal and evaluation in central government [Online]. Available: <https://www.gov.uk/government/publications/the-green-book-appraisal-and-evaluation-in-central-government> [Accessed 8th May 2018], 2018.
- [25] DECC. Summary evidence on District Heating Networks in the UK. the Department of Energy & Climate Change, 2013.

Appendix

A.1. Individual heating technology key assumptions

	Gas boiler	Ground source heat pump	Air source heat pump
Capital cost (£)	2500	13000	7000
O&M cost (£/year)	180	75	90
Efficiency (%)	94	400	300
Life time (year)	15	20	20
Carbon intensity (kg/kWh)	0.184	BEIS projection [5]	BEIS projection [5]

A.2. Key modelling assumptions for large heat pumps and district heating networks

District heating	Unit	Value
Large heat pump capital cost	£/kW	1500
Large heat pump O&M cost	£/kW	1
Large heat pump lifetime	Years	25
Large heat pump efficiency (SPF)	%	360
Average length of internal pipework per dwelling	m	13.3
Network parasitic electricity consumption	% of heat demand	1.9%
Network lifetime	year	50
Assumed main network (buried pipes) length	m	1000
Distribution loss	%	20%
Main network (buried pipes)	£/m	468
Network (internal pipes)	£/m	169
Substation cost per kW capacity	£/kW	35
Domestic HIUs per dwelling	£	1075
Heat meter cost per building	£	3343
Heat meter cost per dwelling	£	579
Heat network maintenance	£/MWh	0.6
HIUs maintenance cost	£/MWh	9
Heat meter maintenance	£/MWh	3.4
Labour for metering, billing and revenue	£/MWh	16.9



16th International Symposium on District Heating and Cooling, DHC2018,
9–12 September 2018, Hamburg, Germany

Concept and Measurement Results of Two Decentralized Solar Thermal Feed-in Substations

M. Heymann^a, T. Rosemann^a, K. Rühling^{a,1}, T. Tietze^b, B. Hafner^c

^a*Technische Universität Dresden, Professorship of Building Energy Systems and Heat Supply, 01062 Dresden, Germany*

^b*DREWAG NETZ GmbH, Rosenstraße 32, 01067 Dresden, Germany*

^c*Viessmann Werke GmbH & Co. KG, 35107 Allendorf, Germany*

Abstract

Decentralized feed-in of solar thermal gains can contribute to the decarbonisation and flexibilisation of modern district heating networks. This paper presents the design, the control concept and measurement results of two solar thermal feed-in substations. Recommendations for future network feed-in substation are derived by analyzing and comparing the operation behavior as well as energy flows. The method used to analyze the different substations and the used characteristic performance parameters are introduced.

© 2018 The Authors. Published by Elsevier Ltd.

This is an open access article under the CC BY-NC-ND license (<https://creativecommons.org/licenses/by-nc-nd/4.0/>)

Selection and peer-review under responsibility of the scientific committee of the 16th International Symposium on District Heating and Cooling, DHC2018.

Keywords: solar thermal, district heating, feed-in, substation

1. Introduction

The development of standards concerning network feed-in substations and their control concepts are the research goals of the ongoing project “Kostenreduktionspotential beim Ausbau der Solarisierung von Fernwärmenetzen durch Standardisierung” (SOLSTAND) [1]. These standards are derived from practical experiences by designing, commissioning and operating pilot plants – including the solar thermal system and the substation itself – as well as simulation studies.

* Corresponding author. Tel.: +49-351-463-32375; fax: +49-351-463-37076.

E-mail address: karin.ruehling@tu-dresden.de

Nomenclature				
Symbols		Abbreviations/Indices		
A	m^2	Area	a	Ambient
a_1, a_2	$W m^{-2}K^{-1},$ $W m^{-2}K^{-2}$	Collector parameter	Col	Collector
COP	-	Coefficient of performance	C	Collector subfield
\dot{G}	$W m^{-2}$	Global irradiation in collector plane	CF i	Collector Field
G	$kWh m^{-2}$	Sum of global irradiation in collector plane	DH	District heating
G_h	$kWh m^{-2}$	Sum of global irradiation horizontal	el	Electrical
\dot{H}	kW	Enthalpy flow rate	F	Feed-in
i	-	Number of feed-in plant (1,2)	FP i	Feed-in plant
\dot{m}	$kg s^{-1}$	Mass flow rate	FS	Flow Sensor
p	bar	Pressure (absolute)	HM	Heat meter
Δp	bar	Pressure difference	loss	Losses
P	kW	Power	LP	Lowest point in system
Q	kWh	Heat, thermal energy	NFS i	Network feed-in substation
\dot{Q}	kW	Heat flow, thermal capacity	PM	Pressure maintenance
W	kWh	electrical energy	LP	Lowest point in system
ζ	-	Efficiency (average in time)	Pu	Pump
η_0	-	Optical collector efficiency	RL	Return line
ν	-	Degree of quality	SL	Supply line
τ	hh:mm:ss	Time	STS	Solar thermal system
			th	Thermal
			theo	Theoretical
			VTC	Vacuum tube collector

This paper presents design, control concept and measurement results of two pilot feed-in plants (FP) for decentralized feed-in of solar thermal yields into district heating networks. The feed-in plant 1 (FP1) is connected to a 2nd generation district heating network (according to IEA DHC Annex X classification [2]) in Dresden. Ambitious conditions for both, target temperature level and pressure difference, are fulfilled by a return to supply line (RL/SL) feed-in design. The high nominal pressure stage of PN 25 requires an indirect connection with a heat exchanger. The network feed-in plant 2 (FP2) is connected to a 3rd generation district heating network in Dresden as well. This small but centralized solar feed-in substation is located directly at the heat transfer station of the secondary district heating network. The solar plant FP2 is directly connected to DH. Both pilot plants are operated with water as heat transfer medium.

The present measurement results include the feed-in operation behavior during one week of May 2018. The calculation or rather measurement of the heat losses and auxiliary power of the pumps allow the evaluation of the efficiency of the monitored network feed-in substations. By comparing the design, the control concepts as well as the operation measurement results first recommendations for future FP-concepts are derived.

2. Description of the two feed-in plants

2.1. General design parameters

The overview of the general design parameters of the feed-in plants FP1 and FP2 are shown in the Table 1. Each feed-in plant is divided into the solar thermal system (STS) including the collector field (CF) and the network feed-in substation (NFS). Both collector fields use water as heat transfer medium because of less investment costs, no negative effects of aging, the option for a direct DH network connection (see FP2) as well as higher thermal capacity compared to water-glycol-mixtures and therefore less auxiliary power consumption of the pumps. The necessary active frost protection is realized by heating the collector field in winter by a RL/RL heat supply from the DH network. The two feed-in plants differ in the following aspects:

Table 1. General design parameter of the investigated network feed-in substations

Parameter	FP1	FP2
in operation since	November 2016	December 2017
DH network temperatures SL/RL	110°C/60°C	75°C/60°C
pressure stage DH	PN25	PN10
	NFS1	NFS2
type of connection to DH	indirect	direct
design heat capacity	30 kW	61 kW
feed-in temperature setpoint	110°C	65 °C RL/RL feed-in
design point feed-in pump delivery height/ volume flow	45 m / 0.5 m ³ /h	6 m / 3.1 m ³ /h
characteristic curve of feed-in pump (max delivery height, max volume flow)	75 m, 3.3 m ³ /h	6 m, 9.0 m ³ /h
	STS1	STS2
gross collector area	83 m ²	143 m ²
inclination angle/ azimuth collector	31°/south	15°/south east
inclination angle/ azimuth vacuum tube	31°/south	45°/south west
collector type	VTC test	VTC Viessmann SPEA
pipe routing	serial	Tichelmann
heat transfer medium	water	water
collector volume per m ² gross collector area	2,33 l/m ²	0,32 l/m ²
connection pipe volume per m ² gross collector area	1,95 l/m ²	1,02 l/m ²
circulation time at design volume flow	43 min	3,6 min

- location of the connection points within the DH network and therefore pressure differences of DH network,
- the level of the DH network temperatures,
- direct or indirect connection to the DH network,
- performance of the installed collectors and
- the circulation time at nominal volume flows.

The FP2 is currently still in the process of operation optimization because of its recent start of operation.

2.2. Schematic and control concept of feed-in plant 1 (FP1)

The network feed-in substation design as well as the control system of the FP1 is described in detail in [3]. The following plant description is a short summary of that paper. The collector field (CF) consists of six in series connected subfields C1...C6 (see Fig. 1) of solar vacuum tube collectors (VTC), working according to the heat pipe principle. The circulation pump in the solar circuit P_{USTS} is a speed-controlled pump group where only one pump is used in main operation at a time and where the other pump is hold as a spare component. A compressor-based pressure maintenance is used and is connected to the system in the supply line via a special designed stagnation cooler.

During the feed-in operation the circulation pump P_{USTS} in the solar circuit is used to control the supply line temperature of the collector field $T_{SL,CF}$. The speed-controlled feed-in pump P_{UDH} has to overcome the time dependent pressure difference Δp_{DH} in the DH network and is used to control the feed-in temperature $T_{SL,DH}$ while also controlling the feed-in volume flow \dot{V}_{DH} as a cascade control (see [3]).

Before switching to the feed-in operation mode the bypass valve V_{a1} will be opened to heat up the medium in the district heating side of the substation. This is supposed to prevent cold plugs in the network. V_{a1} will be closed during normal feed-in. It can be opened during times of partial load/low irradiance to increase the volume flow \dot{V}_{STS} when the speed-controlled pumps reach their minimal flow rate (negative: increase of $T_{RL,CF}$). V_{a2} is used to realize an external unblocking. If necessary, the network operators can withdraw the external release signal to prevent/stop the feed-in by closing the valve and shut off the pumps.

A minimum sensor equipment is necessary for the plant operation. It consists of five temperature sensors ($T_{SL,CF}$, $T_{SL,STS}$, $T_{RL,CF}$ and $T_{SL,DH}$, T_a), the irradiation sensor \dot{G} as well as a heat meter (HM). HM measures the heat fed into the network. The volume

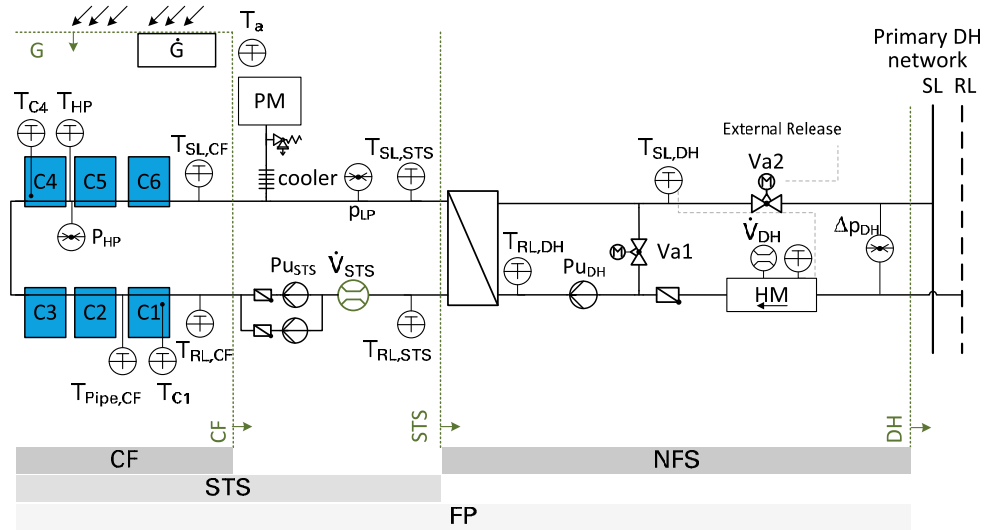


Fig. 1. Simplified schematic of FP1 (decentralized) with energy balance boundaries

flow signal \dot{V}_{DH} of HM is used for a control loop. The monitoring package consists of additional temperature sensors, three pressure sensors (p_{HP} , p_{LP} , Δp_{DH}) and a flow meter \dot{V}_{STS} for the calculation of the energy flows.

2.3. Schematic and control concept of feed-in plant 2 (FP2)

The FP2 (see Fig. 2) is directly connected to a secondary DH network with a nominal pressure stage of PN10 and a nominal target feed-in temperature of 75 °C during summer. Because of the direct connection without a heat exchanger district heating water is used as heat transfer medium. This demands an active first protection during winter season. The collector field has its own backup pressure maintenance, but the goal is to test the usage of the pressure maintenance of the secondary DH network. Solar vacuum tube collectors working according to the heat pipe principle are used in the collector field. This ensures a low heat demand for the active frost protection during the cold seasons. The collector field consists of six subfields C1...C6 which are connected in parallel using the Tichelmann pipe routing with adapted manifold pipe diameter. The inclination and azimuth angle of the collector and vacuum tubes differ because the vacuum tubes can be rotated along their longitudinal axis. The intention is to get higher inclination angles on flat roof installation without a costly substructure.

Within the NFS2 is one speed-controlled pump used to overcome the pressure difference of the collector field, piping and other components. It is hereinafter referenced to as feed-in pump p_{uDH} . The three way distribution valve Va1 is used to switch between

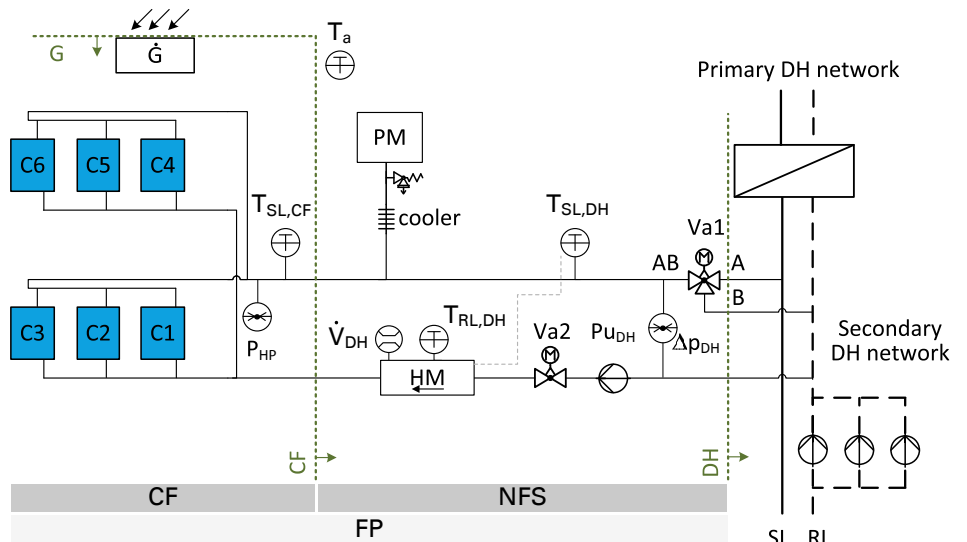


Fig. 2. Simplified schematic of FP2 (centralized) with energy balance boundaries

the RL/RL feed-in (AB-B) and the RL/SL feed-in (AB-A). The RL/RL feed-in is only used for the start-up with low irradiation, the RL/SL feed-in during normal operation. The NFS2 is part of the centralized heat generation unit and the feed-in is realized on the discharge side of the central pump. The pressure difference between the supply and return line is negative during RL/SL feed-in because of the central location within the secondary DH network and the pressure losses of the parallel connected central heat exchanger. Therefore several challenging conditions of the decentralized feed-in like a high and highly volatile pressure difference (see [3], [4]) have not to be taken into account in the design and control concept of the plant. The pressure difference between the two return line connections is zero during the RL/RL feed-in. The control valve Va2 is used to reach low volume flows to maintain the setpoint of the feed-in temperature during RL/SL feed-in with lower irradiation.

The control system of the FP2 is rather simple. The circulation pump of the solar circuit respectively the feed-in pump P_{UDH} is activated when the starting temperature threshold is reached within the collector field. The RL/RL feed-in is used in times of low irradiation e.g. in the starting operation during the morning. The feed-in is switched to RL/SL operation when the switching temperature threshold is reached within the collector field. The matched flow control of the collector field supply line temperature $T_{SL,CF}$ is realized using a split range control for valve Va2 and the feed-in pump P_{UDH} . The setpoint is equal to the supply line temperature of the secondary DH network. When $T_{SL,CF}$ reaches the lower temperature threshold, the feed-in is switched back to RL/RL operation. When reaching even lower collector field supply line temperatures the plant will be deactivated.

3. Analysis and comparison of the operating behavior during the state feed-in of a typical day

3.1. Example for the operating behavior during feed-in of FP1

The exemplary measurement results of the feed-in operation of FP1 (see Fig. 3) starts at 5:18 of 14th of May with sunrise and ends at 20:45 with sunset. During this time range an average irradiation of 524 W/m² and an average ambient temperature of 21.8 °C are measured.

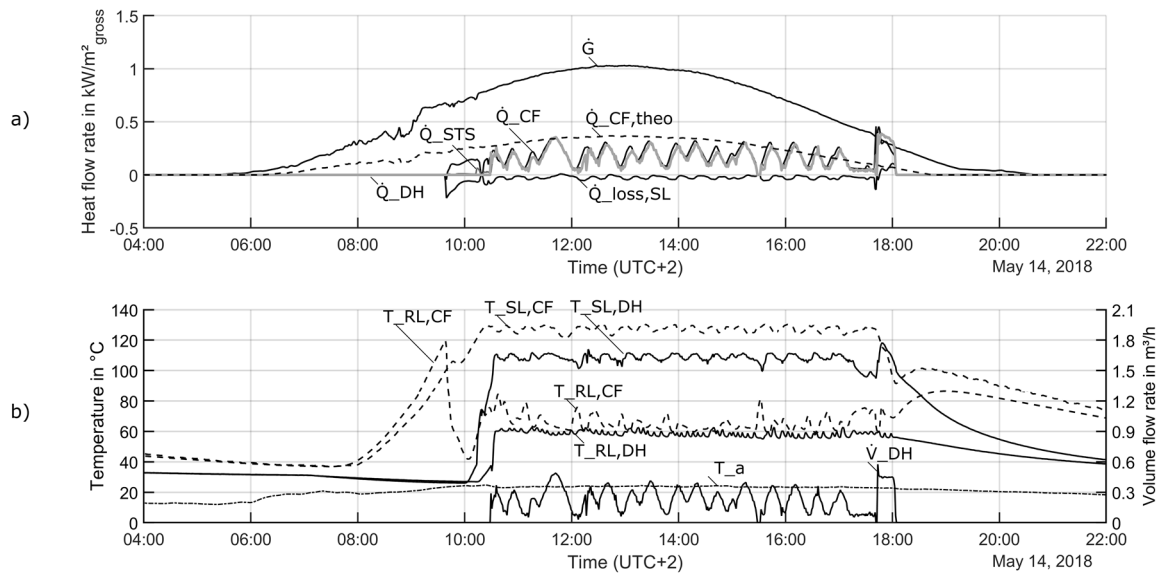


Fig. 3. Measurement results of the specific heat flow rates (a) and temperatures as well as volume flow rates (b) during the feed-in operation of FP1

Time range Description of the operation behavior

- 05:18 - 09:40 The collector field heats up until $T_{CF,SL}$ or $T_{CF,RL}$ exceeds $115\text{ }^{\circ}\text{C}$. Pu_{STS} isn't in operation. The collector field return line temperature $T_{RL,CF}$ is remarkable higher than the collector field supply line temperature mainly due to shading of the subfield C6. The collector field CF1 has a high delay between sunrise and starting operation due to the high thermal capacity (high volume of heat transport medium & DN50 steel manifold pipe) and high target collector temperatures $T_{SL,CF}$.
- 09:40 - 10:30 The Pu_{STS} is turned on and the hot medium is transported to the heat exchanger. Then the Pu_{DH} is activated and the district heating side gets heated up via Va1.
- 10:30 - 17:39 The FP1 is in feed-in operation. The setpoint for the feed-in temperature $T_{SL,DH}$ is controlled very accurate (see Fig. 3 b). The average heat flow of the collector field \dot{Q}_{CF} is clearly lower than the expected theoretical heat flow $\dot{Q}_{CF,theo}$ of the collector curve. This undesirable performance occurs because of the malfunction of the used test collector as well as a too small collector array for this kind of collector (turbulence at the condenser of the VTC isn't always ensured). The oscillation of the heat flows \dot{Q}_{CF} and \dot{Q}_{DH} (see Fig. 3 a) is caused by the low specific volume flow, the oversized connection pipe diameter as well as the long connection pipe² between the collector subfields. This results in a long circulation time in the solar thermal system causing high dead times which are hard to control with classical PID controller (marginal stability).

3.2. Example for the operating behavior during feed-in of the FP2

The exemplary measurement results of the feed-in operation of FP2 are shown in Fig. 4. The plant operates under very similar weather conditions like FP1.

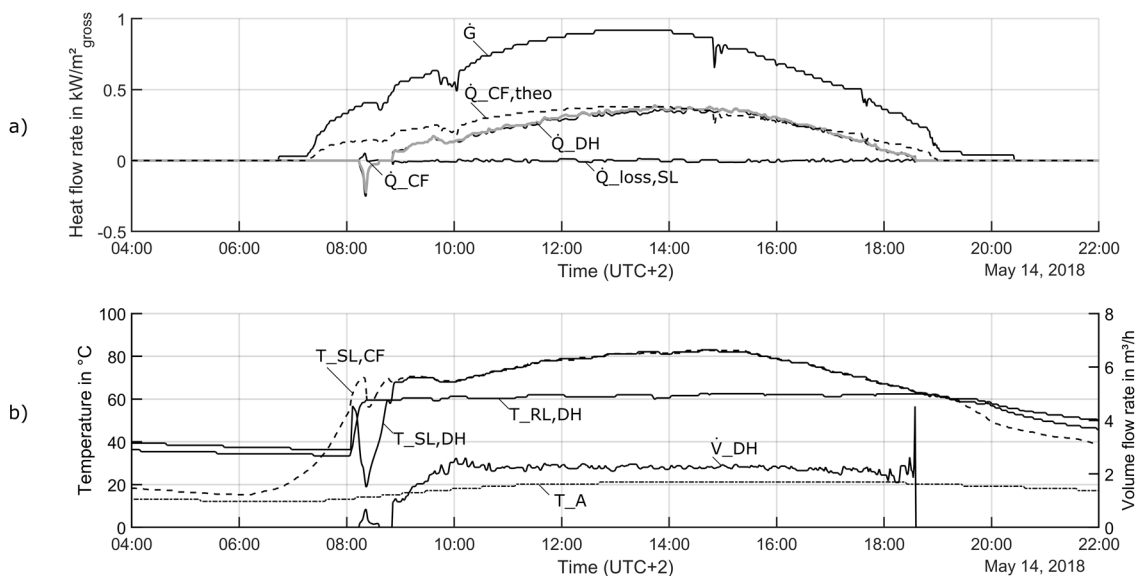


Fig. 4. Measurement results of the specific heat flow rates (a) and temperatures as well as volume flow rates (b) during the feed-in operation of FP2

² These were given by the preinstalled shed roof.

Time range	Description of operation behavior
05:18 - 08:17	The collector field heats up until $T_{CF,SL}$ exceeds 55 °C. P_{UDH} isn't in operation. The CF2 heats up 1.5 h (33 %) faster than CF1 because of lower desired collector field temperatures as well as a lower thermal capacity (see Table 1).
08:17 – 08:47	The feed-in pump P_{UDH} is turned on. The feed-in temperature $T_{SL,DH}$ drops significantly. The temperature drop occurs because of the cold heat transport medium in the return line connection pipe which is flowing through CF2 before the warmer return line medium of the DH network reaches the collectors. Therefore P_{UDH} is turned off.
08:47 – 18:34	P_{UDH} is turned on again and FP2 is in the feed-in operation. The setpoint for the feed-in temperature $T_{SL,DH}$ of 65°C for RL/RL-feed-in is only reached until 11:00. Afterwards the maximum volume flow is reached because of an undersized feed-in pump P_{UDH} and the feed-in temperature rises up to 82,7 °C (RL/VL-feed-in is not activated until now). There is no relevant temperature drop between the collector field supply line temperature $T_{SL,CF}$ and the feed-in temperature $T_{SL,DH}$ because of the short transport time (high flow velocity) resulting in low heat losses of the water in the supply line pipes. This ensures a lower average collector field temperature and respectively higher collector efficiencies. The direct connection to the DH network without a heat exchanger (no temperature difference) lowers the average collector field temperature as well.
08:47 – 12:00	The heat flow of the collector field \dot{Q}_{CF} is clearly lower than the expected theoretical heat flow $\dot{Q}_{CF,theo}$ and the beginning of the feed-in operation. This occurs because of the neglect of the thermal capacity of the collector field in the calculation of the theoretical heat flow $\dot{Q}_{CF,theo}$.
14:00 – 17:00	\dot{Q}_{CF} is almost equal and sometimes slightly higher than the theoretical heat flow $\dot{Q}_{CF,th}$. The real performance of the collector field is therefore rated as good in general.
18:34	The feed-in operation is stopped because of the low collector $T_{SL,CF} < 50$ °C criterion. The feed-in operation of the NSF2 lasted 1,5 h longer than the feed-in operation of the NSF1 because of the lower target collector field temperatures.

3.3. Optimization potential

Summarizing the analysis of the feed-in operation of the two feed-in plants recommendations for an optimized operation are derived and will be implemented as soon as possible. The measurement data of FP1 show the following:

- The test collectors have a significant deviation between the heat flows of the laboratory tests $\dot{Q}_{CF,th}$ and the measured in situ yields \dot{Q}_{CF} . This could be approved with the reconstruction of the collector field using new commercially available and well tested collectors.
- The specific fluid volume of the collectors as well as the specific fluid volume of the connection pipes (see Table 1, CF1) are too high. For high temperature differences in the collector field this causes very low flow velocity and high circulation times as well as thermal losses due to the high thermal capacity. Smaller sized connecting pipes would simplify the target temperature control of the system. This can't be approved without reconstruction of the collector field.

The genera design and control concept of the network feed-in substation NFS1 shows good functionality. For the FP2 the following recommendations of optimization are given:

- The feed-in pump P_{UDH} is undersized. The operator of the FP2 suggests to upgrade this pump to a serial double pump in order to reach higher pressure head as well as volume flows and to rise the pumps fail safety. The latter would avoid longer periods of stagnation during summer and the risk of frost damages during winter in case of pump failure.
- The CF2 has a very good hydraulic balancing. This is achieved through the Tichelmann pipe routing, which leads to longer connection pipes and consequently to higher piping costs and thermal losses. The better design is to use a classic parallel circuit and to achieve the hydraulic balancing by adapting the diameter of the main pipe after each junction. This is a general recommendation for the hydraulic design of a collector field which can't be realized in the operating phase of the FP2.

4. Analysis and Comparison of the energy flows during the state feed-in of a typical week

4.1. Overview of the evaluation period and formula

The two feed-in plants are both located in Dresden, only 6.3 km away. Therefore it is possible to compare the efficiency of the plants under very similar weather conditions. An evaluation period of one week in the late spring season starting at 10.05.2018 and ending at 16.05.2018 was chosen for this purpose

Table 2. Overview of weather conditions and operation results of FP 1 and FP 2 for the evaluation period 10.-16.05.2018

date	Weather		FP1	FP2
parameter	G_h	\bar{T}_a	$\bar{T}_{SL,DH}$	$\bar{T}_{SL,DH}$
considered during	day	feed-in	feed-in	feed-in
unit	kWh/m ² /d	°C	°C	°C
10.05.18 (Start 00:00)	7.3	25,0	107,5	69,2
11.05.18	5.2	18,5	102,5	67,5
12.05.18	6.6	21,6	107,1	70,5
13.05.18	7.5	24,4	107,3	71,1
14.05.18	7.6	21,8	109,0	71,7
15.05.18	3.9	17,9	no feed-in	63,6
16.05.18 (End 24:00)	2.8	15,9	no feed-in	65,7
setpoint temperature			110	65

The operation conditions, which are the sum of horizontal global irradiation, the average ambient temperature between sunrise and sunset as well as the average feed-in temperature $\bar{T}_{SL,DH}$ during the feed-in operation, are shown in Table 2. The regarded week included four sunny days with high irradiation, as well as two cloudy days and one day with unsettled weather. The average feed-in temperature $\bar{T}_{SL,DH}$ of the FP1 during the feed-in operation is slightly smaller than the setpoint temperature. This is explained by the oscillation of the supply line temperature of the collector field (see Fig. 3) and a lowered set point for start and stop of feed-in (90 °C). High temperature amplitudes are controlled by a high \dot{V}_{DH} . But low temperatures can't be prevented. The average feed-in temperature is very low during the 11.05.18 because of a short feed-in operation of only 4 hours. The feed-in temperature setpoint is reached quite accurately on days with sufficient irradiation.

The average feed-in temperature $\bar{T}_{SL,DH}$ of the NFS2 during the feed-in operation is often higher than the setpoint temperature. This is caused by the currently installed feed-in pump P_{UDH} , which is undersized (compare section 3.2). The significant lower feed-in temperature $T_{SL,DH}$ allows operation on two more days compared to FP1.

The different sizes of the systems shall be considered by referring their solar thermal outputs to the energy inputs. This leads to physical quantities that can be interpreted as an average efficiency ζ . Influences of the very different operation conditions can be taken into account by referring to the calculated energy outputs of a simplified comparison model. This leads to degrees of quality ν , rating the measured heat flows to the expected ones.

The limits used for the energy balances are shown in Fig. 1 and Fig. 2. Heat or thermal energy flows are calculated in the section planes G (global irradiation on the collector cross area), CF (heat output of the collector field), STS (heat output reduced by the thermal losses of SL and RL) and DH (thermal output to the district heating network). The small green arrows show the direction of positive heat flows. The heat flows over the balance boundaries $k \in \{CF, STS, DH\}$ are calculated using the enthalpy flows \dot{H} at each section point (see Eq. (1)).

$$Q_k = \int_{\tau_{start}}^{\tau_{end}} (\dot{H}_{SL,k} - \dot{H}_{RL,k}) d\tau \quad \text{with} \quad \dot{H} = \dot{V} \cdot \rho_{FS} \cdot h \quad (1)$$

Two methods are used to calculate the global irradiation in the gross area of the collector plane \dot{G} . For the FP1 horizontal direct and diffuse irradiation is measured and transformed to the inclined collector plane using the Dymola *BuildingSystems* library. Concerning the FP2 an irradiation sensor installed in the collector plane is used.

For the simplified determination of the auxiliary power P_{el} only the energy demand of the feed-in pumps is included. It is measured for the NFS1 and for the NFS2 estimated using a quadratic polynomial derived of the maximal characteristic curve given

by the manufacturer of the pump. A coefficient of performance can be derived according to Eq. (2). The electrical energy consumption is an important issue for decentralized feed- in substations.

To compare the thermal outputs of the two systems and considering their different size, the efficiency is defined according to Eq. (3a-b). The efficiency ζ_{FP} rates the heat which can be fed into the DH network to the global irradiation on the collector gross area. This is dependent upon the quality of the used collectors and the specification of the collector fields. To focus on the efficiency of the network feed-in substation ζ_{NFS} is related to the output of the solar thermal system. In case of the FP2 the thermal outputs Q_{CF} and Q_{STS} are considered to be equal because the absence of an additional temperature sensors and a heat exchanger. In consideration of the very different operation parameters of the two feed-in plants the degree of quality ν_{CF} in Eq. (4) relates the solar heat gains of the feed-in plants the expected gains $Q_{CF,theo}$, which are calculated according to Eq. (5). It can be used to evaluate and compare the performances of the two collector fields and to indicate a general malfunction of the collector fields. Eq. (5) uses the solar thermal collector equation as a simplified reference model to calculate the estimated solar keymark yields (For CF1 preliminary lab results are used).

$$COP = \frac{Q_{DH}}{W_{el}} \quad (2) \quad \zeta_{FP} = \frac{Q_{DH}}{G} \quad (3a) \quad \zeta_{NFS} = \frac{Q_{DH}}{Q_{STS}} \quad (3b) \quad \nu_{CF} = \frac{Q_{CF}}{Q_{CF,theo}} \quad (4)$$

$$Q_{CF,theo} = A \cdot \int_{\tau_{Start}}^{\tau_{end}} \dot{G} \cdot \left(\eta_0 - \frac{a_1}{\dot{G}} \cdot \Delta T - \frac{a_2}{\dot{G}} \cdot \Delta T^2 \right) d\tau \quad \text{with} \quad \Delta T = \frac{T_{RL} + T_{SL}}{2} - T_a \quad (5)$$

4.2. Analysis and Comparison of the energy flows

Fig. 5 shows the energy flow diagrams of FP1 (a) and FP2 (b) for the analyzed week in May 2018. All heat yield results are rated to the collector field heat output Q_{CF} . This allows a direct comparison of the two plants.

The FP1 has significant thermal losses of in total 20.2 % in the return and supply line of the solar thermal system. This mainly results from the high supply line temperatures of the collector field and the large surface of the oversized connection pipes. The thermal losses within the substation NFS1 sum up to only 1 %. Overall 78.8 % of the solar thermal yields of the collector field are fed into the DH network. The electric energy consumption for the feed-in pump P_{UDH} is only 1.1 % which is low, considering the high pressure difference of the primary DH network (see Table 1). The main thermal losses occur in the collector field. The reasons are the reduced yields of the collectors – which will not be investigated further – as well as the high thermal capacity of the collector field which cools down overnight.

The FP2 has very low heat losses in the supply line of the collector field and 98.1 % of the solar thermal yields of the collector field are fed into the DH network. The electric energy consumption for the feed-in pump P_{UDH} is only 0.2 % because of the very low pressure difference of the network.

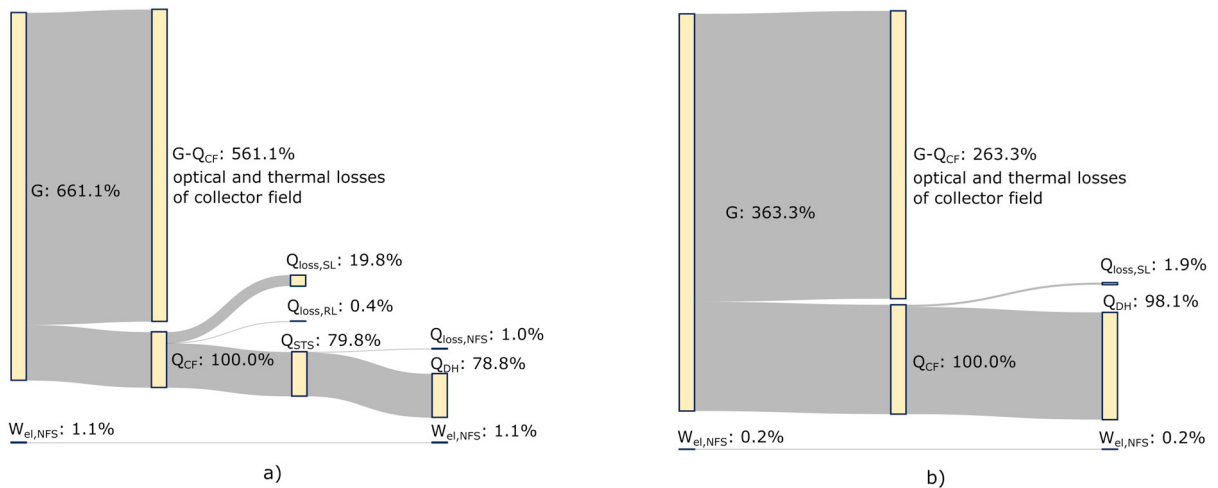


Fig. 5. Energy flow diagrams of the FP1 (a) and the FP2 (b), rated to the heat output of the collector fields Q_{CF}

Table 3. Performance numbers of the feed-in plants during the evaluation period 10.-16.05.2018

Symbol	Description	FP1	FP2
ζ_{FP}	Total efficiency of feed-in plant	11.9 %	27.0 %
ζ_{NFS}	Efficiency of network feed-in substation	98.7 %	98.1 %
ν_{CF}	Degree of quality of collector field	48.6 %	72.3 %
COP	Coefficient of performance	69	522

According to Tab. 3 feed-in plant 1 has a very low overall efficiency of $\zeta_{FP1} = 11.9\%$. This mainly can be explained with the malfunction of the used test collectors (see section 3.1). The degree of quality of the collector field ν_{CF1} is 48.6%. Only the half of the solar thermal gains expected according to the collector parameters can be reached. The second main issue is the thermal loss on the supply line of the collector field (compare Fig. 5a). The efficiency of the network feed-in substation $\zeta_{NFS1} = 98.7\%$ is good. Auxiliary energy consumption of FP1 results in a COP of 69. This value results from the very high requirements regarding the network pressure difference. The feed-in pump of FP1 takes over a part of work from the central circulation pump of the DH network. The feed-in plant 2 has a medium overall efficiency $\zeta_{FP2} = 27\%$. Due to the high degree of quality $\nu_{CF2} = 73.7\%$ and low thermal losses (see Fig. 5b) the medium overall efficiency is caused by the chosen collector. It is characterized by a low ratio of the aperture A_{AP} to gross area A_{gross} and therefore generates a lower specific heat output. The efficiency of the feed-in substation is $\zeta_{NFS2} = 98.1\%$ including the heat losses of the supply line. Actually no losses occur in the substation itself because of the direct connection. The coefficient of performance COP is very good because of the advantageous location of the connection points to the district heating network.

5. Conclusions and prospects

The design and control concept, measurements of the feed-in operation and energy flows of two DH network feed-in pilot plants have been discussed. The FP1 is a decentralized feed-in plant within a primary DH network and therefore challenging operation conditions concerning feed-in temperature, pressure stage and volatile pressure differences in the network. The installed test collectors in combination with the oversized connection pipes of CF1 lead to low collector efficiencies compared to state of the art solar thermal collectors and lead to high thermal losses. In contrast the network feed-in substation NFS1 itself is operating well delivering the heat reliable to the network while maintaining good thermal efficiencies, high control accuracy of the feed-in temperature as well as a low auxiliary power demand.

The FP2 is a directly connected centralized feed-in plant. It has better energetic performance because of the less demanding operation conditions, state of the art solar thermal collectors and a direct connection to the DH network and therefore lower target collector temperatures. A good consistency comparing the solar keymark collector values and the real yields can be shown. The most important optimization measure is to switch to a feed-in pump with higher volume flow.

The presented degrees of efficiency of the feed-in plant and the NFS as well as the degree of quality along with the common coefficient of performance can be used to compare plants in terms of heat losses and energy conversion.

Both feed-in plants have a high optimization potential. The NFS itself are well designed and deliver the heat provided by the collector field reliably to the network. Both network feed-in substation are very valuable in terms of standardization of the substation concepts.

In the final report of the project SOLSTAND two additional pilot plants will be integrated into the measurement – another decentralized feed-in plant as well as a prosumer substation. General recommendations for standardization processes of DH network substation concepts will be derived.

References

- [1] C. Felsmann, K. Rühling and B. Hafner. Kostenreduktionspotential beim Ausbau der Solarisierung von Fernwärmenetzen durch Standardisierung. Projektantrag, TU Dresden, Viessmann Werke GmbH, July 2014.
- [2] A. D. Rosa, H. Li, S. Svendsen, S. Werner, U. Persson, K. Rühling, C. Felsmann, M. Crane, R. Burzynski and C. Bevilacqua. Annex X Final Report: Toward 4th Generation District Heating. Tech. rep.. IEA DHCIHP, 2014
- [3] T. Rosemann, M. Heymann, K. Rühling and B. Hafner. Dh networks - concept, construction and measurement results of a decentralized feed-in substation. *International Conference on Solar Heating and Cooling for Buildings and Industry*, Abu Dhabi, October 2017.
- [4] G. Lennermo, P. Lauenburg. Variation in Differential Pressure at a District Heating Prosumer Substation, 3rd International Solar District Heating Conference, Toulouse, 2015



Available online at www.sciencedirect.com

ScienceDirect

Energy Procedia 149 (2018) 373–379

Energy

Procedia

www.elsevier.com/locate/procedia

16th International Symposium on District Heating and Cooling, DHC2018,
9–12 September 2018, Hamburg, Germany

Heating seasons length and degree days trends in Russian cities during last half century

I. N. Belova, A. S. Ginzburg*, L. A. Krivenok

A.M. Obukhov Institute of Atmospheric Physics, RAS, Pyzhevsky per., 3, Moscow 119017, Russia

Abstract

An analysis of the completeness and compatibility of data from different sources on the energy consumption of Russian cities situated in different climatic zones was conducted. Data obtained from Russian Federal Services and from some cities' authority. Based on these data and ones in public domain, the trends of the characteristics of the heating season were studied. Sufficient plenitude and high quality of these data were established. Almost universal decrease in the duration of the heating period and energy consumption for heating living and public spaces was shown. The similar behavior of heating seasons characteristics trends is well-known for many EU cities. It makes possible to develop the common projections of heating season characteristics trends for EU and Russian large cities.

© 2018 The Authors. Published by Elsevier Ltd.

This is an open access article under the CC BY-NC-ND license (<https://creativecommons.org/licenses/by-nc-nd/4.0/>)

Selection and peer-review under responsibility of the scientific committee of the 16th International Symposium on District Heating and Cooling, DHC2018.

Keywords: heating season length; heating degree days

* Corresponding author. Tel.: +7-910-423-1434.

E-mail address: gin@ifaran.ru

1876-6102 © 2018 The Authors. Published by Elsevier Ltd.

This is an open access article under the CC BY-NC-ND license (<https://creativecommons.org/licenses/by-nc-nd/4.0/>)

Selection and peer-review under responsibility of the scientific committee of the 16th International Symposium on District Heating and Cooling, DHC2018.

10.1016/j.egypro.2018.08.201

Nomenclature

HDD	heating degree days
t_c	base indoor comfort temperature
t_a	atmospheric air temperature
N	number of days with heating

1. Introduction

Major number of midland Russian cities is situated in continental climate with distinct division between cold and warm seasons. Since 1930, when the GOERLO (the Russian abbreviation for “State Commission for Electrification of Russia”) plan had been established, constructing and development of heating and electrification systems became affairs of state and was realized in the all-country scale. Most Russian cities are equipped by the central heating system, which is turning on and off according to the decision accepted by city government. For example, Moscow city district heating system is the largest in the world. Many European cities also widely use district heating and spend approximately of whole urban energy demand for space heating. The objective of this investigation is to analyze the trends of heating period characteristics for large Russian cities in comparison with European ones.

2. Methods and data

The duration of indoor heating periods in various countries and regions of the world is defined in different ways. In Russia, the heating season generally starts on the date when average daily air temperature stably (for 5 days) falls below the level of +8°C in autumn and ends on the date when it stably (for 5 days) rises above this level in spring. Due to climate warming several last winters in Moscow region had the 2-3 weeks periods with mean daily air temperature above +8°C and Moscow city authority switched off city district heating system for about a week. Such gaps are not considered below.

Heating degree day (HDD) is the parameter, which is applied to estimate the energy amount needed to heat indoor living and public spaces [1]. This is the most common climatic indicator of energy consumption for the building heating, which is calculated for a certain period of the year by summing the absolute deviations of the average daily air temperature from the selected base temperature. According to Roshydromet (Russian Met Office) Second Assessment Report [2], in Russia as in many other countries the basic comfort temperature $t_c = 18$ °C (see for example [2, 3, 4]).

HDD is calculated as follows:

$$HDD = \sum_{i=1}^N (t_c - t_{ai}) \quad (1)$$

where N is the number of days within heating period, when t_a bellow 8 °C.

European Energy Agency presented population weighed HDD date for EU cities [5] for the period from 1951 to 2015. In [5] stated that in the middle and second half of the 20th century (until about the 80s), the temperature regime of the heating periods in Europe remained practically unchanged. Over the past three decades, European heating demands have been perennially decreasing.

Fig. 1 shows population weighed HDD data in the EU cities over the past decades. It is shown linear trends for two periods – 1951-2015 and 1966-2015 to compare with date used for Russian cities.

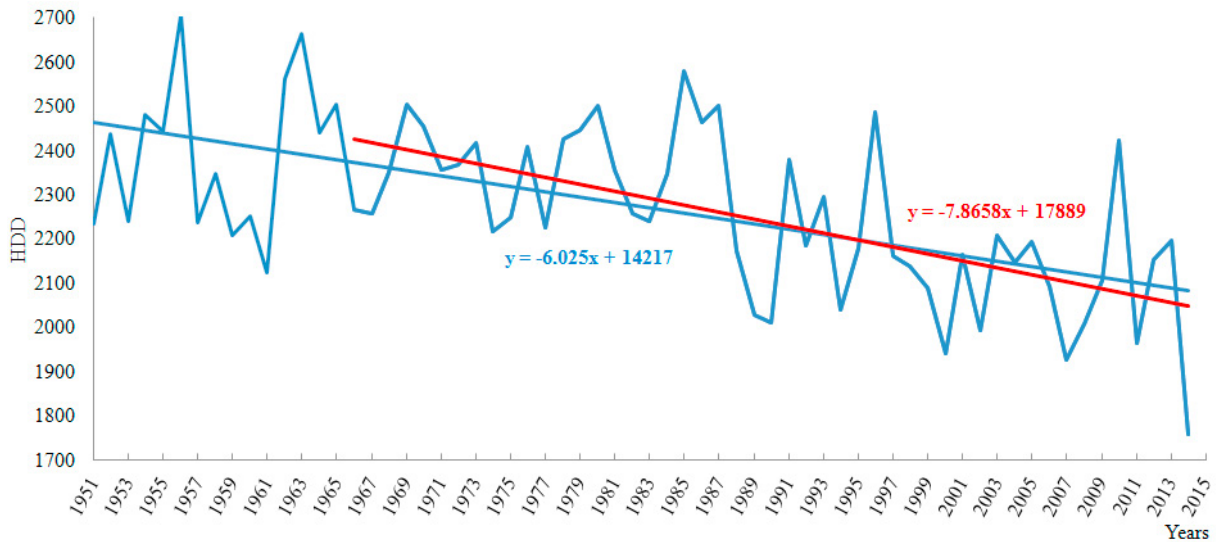


Fig. 1. HDD with linear trends in European Union cities according to the European Energy Agency data [5]

Using Russian meteorological data for the period from 1966 to 2015, we present the HDD patterns for six Russian large cities situated in different parts of Russia. These megalopolises were chosen as typical for Russia.

Since Moscow is both a capital of the Russian Federation and the one of the largest megalopolis not only in Russia, but in the world as well, this city is used as a main comparison object. Based on their geographical location, cities are represented by two groups: midland and coastal. The climate of Moscow is humid continental with warm summers and cold long-lasting winters.

Samara has a continental arid climate, and the average annual temperature is relatively like those in Moscow (+5.7 °C, +5.8 °C respectively).

Novosibirsk is the largest megalopolis of Siberia and is located on the same latitude as Moscow, it has continental climate (more continental than Moscow's one) with severe winters.

Saint Petersburg is located northward of the capital of Russia and has a moderate transitional from the continental to the marine climate.

Vladivostok has a monsoon climate, and the duration of winter is much more comparable to that in Moscow due to Pacific Ocean influence.

The climate of Krasnodar is transitional, from moderately continental to humid subtropical climate. This city was chosen as the southern city with largest population, closed to the geographical longitude of Moscow.



Fig. 2. Geographical location of selected cities (©Google Earth)

The research was carried out for cities of midland cities - Moscow, Samara, Novosibirsk and coastal cities - Saint Petersburg, Krasnodar, and Vladivostok.

Data for heating period length and HDD calculation were obtained from Roshydromet of Russia and from Russian Federation Federal State Statistic Service on official request of Institute of Atmospheric Physics RAS. Based on these data and meteorological data from open sources, the trends of the heating seasons characteristics were studied for largest Russian cities in different climatic zones.

3. Results

The meteorological data for each selected city heating seasons length during last half of century and its linear trends for six selected Russian cities presented in table 1.

Table 1 Heating seasons length in Russian cities and its trends.

City	The average heating season length (days)	Heating season length trend (days per year)
Moscow	201	0.30
Samara	198	0.34
Novosibirsk	223	0.51
Saint Petersburg	210	0.44
Krasnodar	143	0.41
Vladivostok	193	0.17

According to these data heating season lengths in all selected cities became shorter during last decades. Climatic trends of surface air temperature significantly affect the trends of the heating period durations for the whole period of 1966–2015. Table 1 shows that Novosibirsk – the most continental city – has longest heating period and this period is decreasing during last half of century faster than in other Russian cities, presented in table 1. Shortest

heating season in Krasnodar - city near the Black Sea coast, and the slowest decrease of heating season duration in Vladivostok – city on the Pacific coast.

HDD annual data and its linear trends for six Russian cities and for European cities on average during last half of century are shown in table 2. and fig. 3-8.

Table 2. The heating degree days values during 1966–2015 years for the cities of Moscow, Samara, Novosibirsk, Saint Petersburg, Krasnodar, and Vladivostok and population weighted EU data.

City	The average value of heating degree days (HDD)	The HDD trend slope (HDD per year)
Moscow	4129	13.55
Samara	4502	14.96
Novosibirsk	5768	18.6
Saint Petersburg	4088	15.26
Krasnodar	2270	10.73
Vladivostok	4808	5.26
EU	2236	7.87

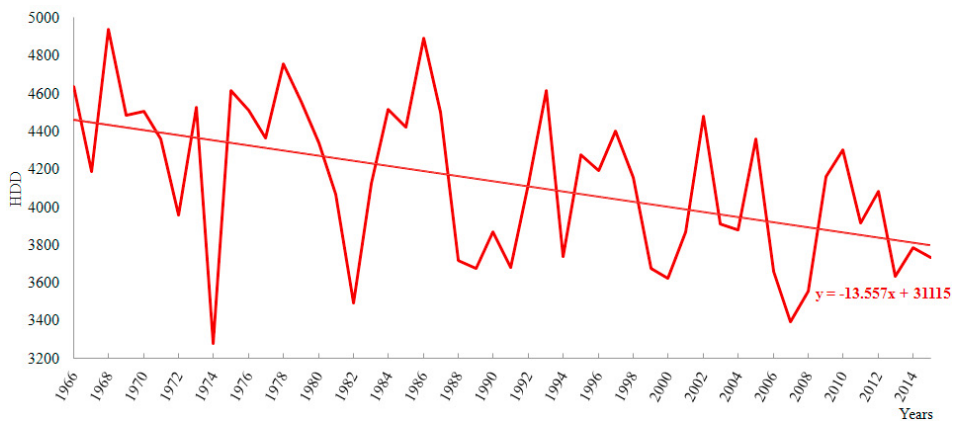


Fig. 3. HDD data with linear trend for Moscow from 1966 to 2015.

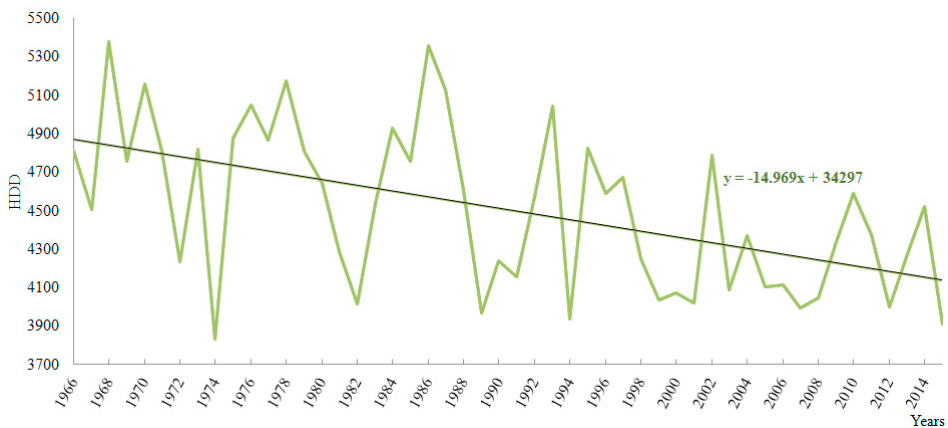


Fig. 4. HDD data with linear trend for Samara from 1966 to 2015.

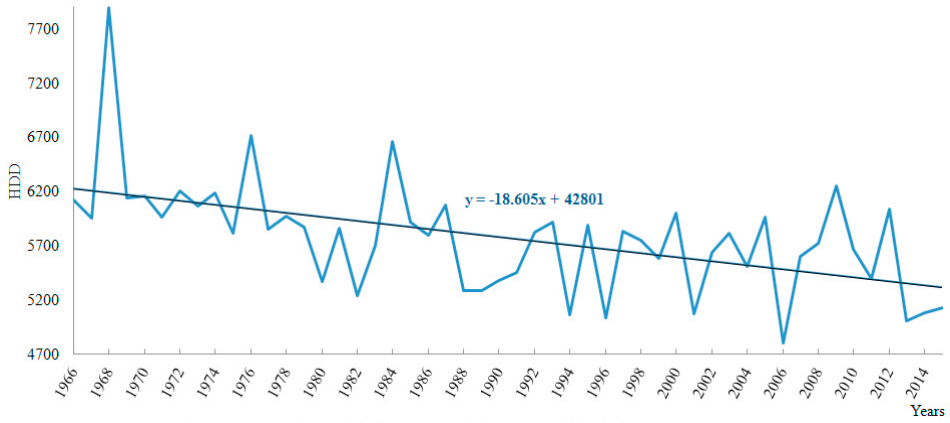


Fig. 5. HDD data with linear trend for Novosibirsk from 1966 to 2015.

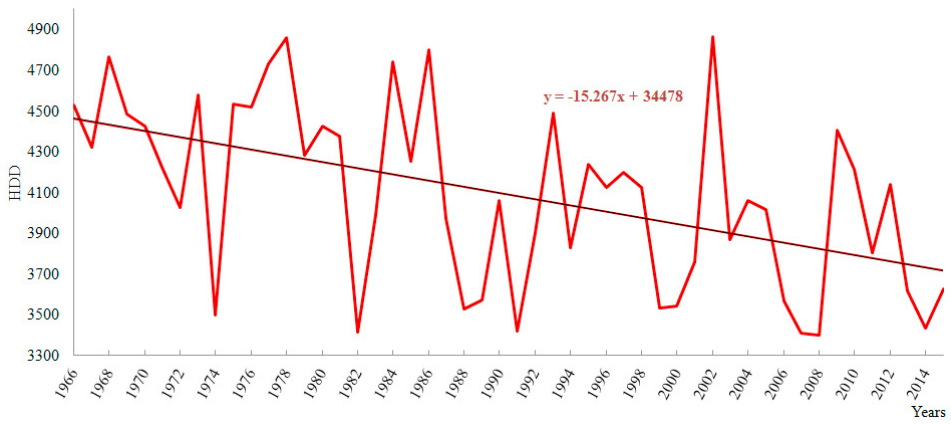


Fig. 6. HDD data with linear trend for St. Petersburg from 1966 to 2015.

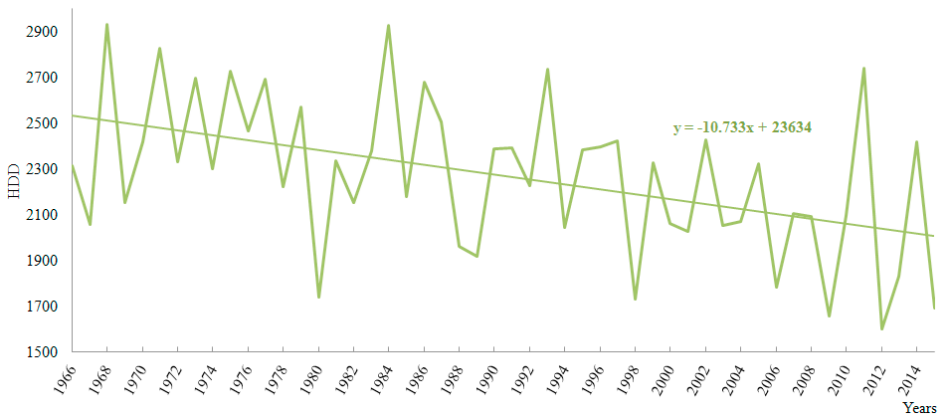


Fig. 7. HDD data with linear trend for Krasnodar from 1966 to 2015.

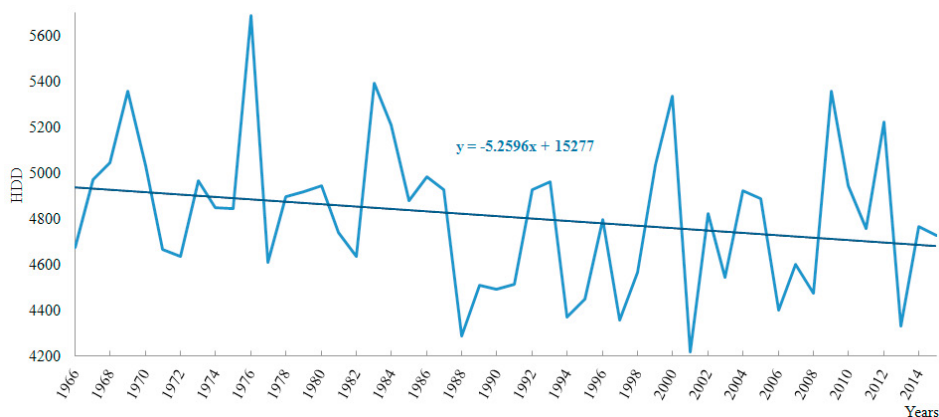


Fig. 8. HDD data with linear trend for Vladivostok from 1966 to 2015.

4. Conclusions

Sufficient plenitude and high quality of official data provided Russian governmental agencies were established. Based on these data, as well as on open ones, the trends of the heating season characteristics for three midland and three coastal large cities of Russia were studied. All these cities showed the decreasing of heating period length and energy needs for space heating.

As for heating season duration, that Novosibirsk has the longest one with biggest decreasing trend, Krasnodar has the shortest heating season duration (close to European cities) and Vladivostok has the slowest heating season duration decreasing.

For most selected Russian cities HDD amount decreases faster than in European cities on average. The only for city of Vladivostok situated on the Pacific coast the HDD trend slope is about 5 HDD per year compare to about 8 HDD per year for European cities on average.

The similarity of heating season characteristics behavior in Europe and Russia makes possible to develop the common projections of heating seasons trends for EU and Russian large cities based on climate modeling results.

Acknowledgements

This study supported by Russian Science Foundation (project No 16-17-00114).

References

- [1] Klimenko V. V. , Ginzburg A. S., Demchenko P. F., Tereshin A. G., Belova I. N., and Kasilova E. V. "Impact of urbanization and climate warming on energy consumption in large." *Doklady Physics* 61(10) (2016): 521–525, doi: 10.1134/S1028335816100050.
- [2] Kattsov V. M, and Semenov S. M. "The Second Roshydromet Assessment Report on Climate Change and its Consequences in the Russian Federation. General Summary" (2014) Moscow, Planeta
- [3] Ginzburg A. S., Reshetar O. A., and Belova I. N. "Impact of climatic factors on energy consumption during the heating season." *Journal Thermal Engineering* 63(9) (2016): 621–627, doi: 10.1134/S0040601516080061.
- [4] The Manual for Energy Statistics in Households Luxembourg: Publications Office of the European Union (2013) doi:10.2785/45686.
- [5] Heating and cooling degree days. European Environment Agency (2016).



16th International Symposium on District Heating and Cooling, DHC2018,
9–12 September 2018, Hamburg, Germany

Risks and opportunities for bottleneck measures in Swedish district heating networks

Lisa Brange^{a*}, Marcus Thern^a, Kerstin Sernhed^a

^aLund University, Faculty of Engineering, Energy Sciences Box 118, SE-221 00 Lund, Sweden

Abstract

Heat supply bottlenecks are common in district heating (DH) networks and makes the DH network work in a non-optimal way, why it is beneficial to address them. The purpose of this paper is thus to investigate risks, opportunities, added values and issues coupled to various bottleneck measures. This is made by in depth interviews with DH companies and through DH network simulations. The results showed numerous risks and opportunities coupled to each bottleneck measure investigated, and are meant to highlight more effective measures, to help increase the competitiveness of and improve the environmental performance of DH.

© 2018 The Authors. Published by Elsevier Ltd.

This is an open access article under the CC BY-NC-ND license (<https://creativecommons.org/licenses/by-nc-nd/4.0/>)

Selection and peer-review under responsibility of the scientific committee of the 16th International Symposium on District Heating and Cooling, DHC2018.

Keywords: District heating development; Bottlenecks; Optimization; Supply temperature; Pump; Pipe area; Substations; Local heat supply; Demand side management

1. Introduction

District heating (DH) is an important part of a sustainable European energy system [1]. It is thus important that DH systems work in the best possible way. Even if DH in itself can help improve environmental issues, optimization and adaption within the DH systems is also needed to achieve a more sustainable system [2], [3]. One issue that is currently much debated is the supply temperature in DH systems. A lower supply temperature in DH systems could help reduce

* Corresponding author. Tel.: +46 46 222 33 20; fax: +46 46 222 47 17

E-mail address: lisa.brange@energy.lth.se

heat losses in the pipes [4], increase the competitiveness of DH [5] and also help facilitate the introduction of prosumers, for example by solar panels and excess heat from cooling systems [6]. A lower supply temperature is also very advantageous from a cost perspective [7]. Bottlenecks in the DH network however tend to increase the supply temperature as supply temperature is one of the main ways to regulate a DH system [8].

Bottlenecks in DH systems are in this study defined as pipes with too low a pipe diameter to keep a sufficient differential pressure (Δp) in the areas beyond the pipe. If bottlenecks were addressed wherever possible, the supply temperature could probably be lowered, with all the benefits with a lower temperature as a result. To go through and display various measures to solve bottlenecks is thus an important part of DH system optimization. In a wider perspective, also the area with the lowest Δp in the DH network may be seen as a bottleneck for network optimization, making the results in this study more universally useful.

The present study is part of a larger project on bottleneck problems. Within this project, two articles are published, hereafter called study 1 [9] and study 2 [7]. Study 1 describes different measures possible to take to eliminate or reduce bottlenecks and also what the bottleneck situation in Swedish DH networks looks like, according to a survey. The results in study 1 show that bottleneck problems are common in DH networks. It also shows which are the most common causes of bottlenecks in Swedish DH network and which measures that are used to overcome bottleneck problems. Study 2 includes a simulation study and a cost study of the bottleneck measures most often used according to study 1. The results in study 2 show what to regard when introducing a bottleneck measure in different DH network configurations and also what parameters affect the cost and how much it varies. Apart from these studies, there is not much research performed on bottlenecks in DH systems. There are a few studies that describe DH network simulation programs that can be used to find bottlenecks but not focusing how to address them [10], [11]. Studies also investigate the different measures respectively but not from a bottleneck perspective. No other studies than study 1 and study 2 take a holistic approach and compare the measures to each other, why the research described in this paper fills a knowledge gap. The purpose of the present paper is to investigate risks, opportunities, added values and issues coupled to the chosen bottleneck measures. This is performed by a qualitative interview study and a simulation study. The interview study focuses on finding as many factors as possible coupled to each bottleneck measure and also emphasizes economy and bottleneck origin. The simulation study focuses on technical effects resulting from bottleneck measures. The simulations are performed for different seasons, partly to see if the DH network reacts in the same way during all the seasons and partly to be able to pinpoint if specific effects were of a greater importance during some seasons. The measures chosen to work with in the present paper were the same as the ones dealt with in study 2: increased supply temperature, a bigger pipe area, more pumping, increased cooling in substations, local heat supply (LHS) and demand side management (DSM). These are the measures most used according to the results in study 1.

Nomenclature

DH	District heating
ΔP	Differential pressure
LHS	Local heat supply
DSM	Demand side management
DOT	Dimensioning outdoor temperature
CHP	Combined heat and power

2. Methodology

2.1. Interviews

A qualitative method was chosen, to be able to cover as many aspects as possible of bottlenecks. A total of six in-depth, semi structured interviews were performed. The semi structured layout enabled the opportunity to ask follow-up questions for better understanding. The interviews took approximately 1-2 hours to conduct and were conducted face-to-face by the same interviewer.

The companies chosen to be interviewed were of various sizes, had different owner structures and had different answers to the survey questions in study 1. This approach was chosen to get an as broad as possible range of answers in the interviews. The one thing that the companies had in common was that they had experienced some sort of bottleneck problem. In the later interviews less and less new facts appeared in the answers and the interview study could thus be seen as saturated for the purpose of this study. The interviews were conducted during the autumn of 2016 and the early spring of 2017.

The interviewees were persons involved in and/or responsible for the development of the DH network. These persons were chosen by the companies themselves when asked who would know most about the DH network development and bottleneck measures. Some interviews involved two persons, one more involved in management and leadership work and one more involved in the technical development of the network.

The interviews were recorded and thereafter concluded in written text. The notes were sent to the respective companies for fact check. If something was unclear in the recordings, this was also checked via email or telephone with respective interviewee.

2.2. Simulations

In order to see technical effects coupled to the bottleneck measures more clearly, simulations were performed for different seasons. The aim of the season simulations was partly to identify common effects for all seasons and partly to highlight effects that may be negligible during one season but important in another. In study 2, the measures were simulated for the dimensioning outdoor temperature (DOT) case of -16°C . These simulations were performed in a fictitious DH network called the Pasture, thought to be situated in the outskirts of Malmö in southern Sweden, and were made for different network configurations. The measures were in the present study simulated in the same network configuration as for the original scenario in study 2. The simulations were in the present paper, as in study 2, performed in NetSim, a DH simulation program also used in other studies, such as [12] and [6]. The mathematical and physical algorithms for the simulations can be found in the manual [13].

The simulations for each season were first performed without any measures and then for one measure at a time. The measures were dimensioned and simulated in the same way as for the original scenario in study 2, where they were used to increase the lowest dP from 0 to 100 kPa. This means that for the increased supply temperature measure the supply temperature was increased by 4°C , for the bigger pipe area measure 513 m of pipe were exchanged to one with a bigger pipe area, for the more pumping measures the maximum power output of the new pump was 5 kW and the maximum power output of the existing pump was 41 kW, for the increased cooling measure the five buildings with the highest overflow was addressed, for the LHS measure the LHS had a power output of 550 kW and for the DSM measure the heat demand of the four buildings with the lowest dP was lowered to 62 %. DSM was however assumed not to be able to be used during the summer because the heat demand then would consist of only domestic hot water [8]. The seasons simulated were mild winter (1°C outdoor temperature, 3°C ground temperature and 5.7 MW heat demand in the Pasture), spring/autumn (9°C outdoor temperature, 8°C ground temperature and 3.4 MW heat demand in the Pasture) and summer (17°C outdoor temperature, 8°C ground temperature and 1.6 MW heat demand in the Pasture). The outdoor temperatures were generated from the last 10 years (2007-2017) of temperature data for Malmö, collected from the Swedish Meteorological and Hydrological institute [14]. The ground temperatures were set to the same as in [6] and were the ground temperatures used by the local DH company. The supply temperatures during the seasons were generated from a simulation model of the Malmö DH network. The consumer return temperatures and heat power demand were regulated with standard curves, used and calibrated by the local DH company, describing how these parameters varied with the outdoor temperature. For the consumers with the highest average return temperatures, the return temperature curve had to be somewhat adapted for the spring/autumn and summer seasons for the simulations to function. The curves were however the same for the simulations both with and without measures why this should not have affected the result. The dP was regulated to be 100 kPa in the node with the lowest dP, to ensure a sufficient heat delivery. The pressure maintenance was set to 400 kPa instead of 300 kPa as in study 2, to be able to keep the pressure above critical limits.

3. Results and analysis

3.1. Identified causes of bottleneck problems

The mentioned causes of bottlenecks in the interviews were expansion and/or densification of the DH network, the location of the production unit, interconnection between DH networks, change of municipal plans, single events (e.g. power failure), and plain calculation errors. Expansion, densification and interconnection often becomes a problem because it was not taken into account when the DH network was built. The location of the production units could pose a problem because many cities in Sweden do not allow for DH production units to be situated in the center of the city any more, due to environmental permits and local environmental issues.

When analyzing the causes behind DH bottlenecks, the main problem seemed to be difficulties to accurately predict the future, which is a difficult problem to solve. Even if there are municipal plans for future building and expansion, these could be changed. Furthermore, district heating pipes often have a longer lifetime than the municipal plans are accounting for. Most likely, bottlenecks will thus be present in DH networks also in the future.

3.2. Utility views on the economy of bottleneck measures

The interviews showed that there are different views on the costs and the economy of the different bottleneck measures. Some of the differences could be explained by different prerequisites for the companies, but also by differences regarding which costs and savings that were included for the measures. On the whole, there seemed to be a lack of lifecycle perspective on the costs and savings among the companies. This was reflected in that only the most visible costs, such as investment costs, were accounted for whereas for example operational costs, required time and possible savings were neglected.

According to study 2, a higher supply temperature is a very expensive solution, except for very small DH systems. Despite this, a higher supply temperature was often considered a cheap bottleneck measure, even if the risk of this inducing a lower electrical efficiency in combined heat and power (CHP) plants also was mentioned. This would however depend on how the CHP is operated. It was also mentioned that if this measure was needed for a longer time period, it would instead become an expensive solution.

A bigger pipe area was often considered a rather expensive solution, where the most expensive part was the earthwork.

The time factor was also mentioned for the more pumping measure, in that more pumping was cheaper if the measure was only needed a short time. It could also be cheaper to install a new pump station to increase the dP in a smaller part of the network instead of pumping more with the main pumps, as the electricity demand for the main pumps plus a distributed pump would be smaller than the electricity demand for only one pump in the network. The economy of this however depended on the cost of the pumping station.

Increased cooling was seen as a rather cheap solution from the DH company point of view as the substations were consumer owned. The cost of fixing the substation would thus be with the consumers. The only cost for the companies would then be to analyze data and inform the consumer, which was not seen as expensive. It was however mentioned that this work is time consuming which is also a kind of cost. If the company instead would need to be completely or partially responsible for fixing the substations, this measure could become more expensive. It was also stated that there is a lot of possible savings with correctly functioning substations and thus a lower return temperature, why it could be cost effective for the companies to fix the substations themselves if the consumer is not willing to do that. This approach could however pose problems regarding injustice between consumers. Another factor mentioned with better cooling in substations was that the incomes for the company could be lowered. This should however not be a problem if the tariff is correctly dimensioned. The increased cooling measure would also cause an overall more effective DH system, causing lower costs for the DH company.

The views about the economy of LHS also differed, partly depending on the size and function of the LHS. A mere peak load heat boiler was a cheap option but if a larger average load plant would instead be used, the LHS measure would be more expensive.

The economy of DSM seemed to depend partly on how many consumers that was needed in order address the bottleneck problem, with few strategic consumers being cheaper than many consumers. The cost also depended on

how the buildings were equipped. Another cost driver was the labor costs related to how long time it took to implement the DSM measures. A risk that DSM could lead to less heat demand was also mentioned, which could lower the incomes for the DH company. This would however mainly be a problem if the tariff did not account for the actual costs, for example costs related to heat power and flow. Furthermore, DSM does not necessarily lead to less total heat demand as the peak heat demand could be either shifted to another hour or be completely reduced. As for the increased cooling measure, DSM would also render an overall more effective DH system, causing lower costs for the DH company.

3.3. *Choosing a bottleneck measure*

The interviews showed very diverse answers to the question of how the companies choose measures to handle bottleneck problems. Parameters that affected which bottleneck that was chosen were economy, robustness of measure, redundancy of measure, future plans, time factors, local conditions and directives from management. The absolutely most important parameter considered by companies when choosing between bottleneck measures was the economy. Time factors referred to both for how long time per year the bottleneck was a problem, how quickly a measure was needed and when future plans were planned to be executed.

An example of local condition affecting the bottleneck measure choice was the age and condition of the existing pipe leading to the bottleneck area. Furthermore, it could be more complicated to build new pipes in the inner city than in the outskirts, due to crowded streets and also crowded ground beneath the streets. Regarding more pumping, too high dPs could limit the possibility to pump more with the main pumps. One local condition favoring LHS could be if suitable DH production was already available in the right location. The ownership of the substations could be a parameter when considering better cooling in substations. The substations in the DH networks belonging to the interviewed companies were all consumer owned, which according to the answers rendered this measure more difficult to perform.

Directives from the management could, according to the answers, marginally affect which bottleneck measure that was chosen, but often the responsibility was with the organization or person responsible for the development of the DH network. When there were directives, they most often concerned the economy. There were however some exceptions. One example was a policy that stated that it was the responsibility of the company to deliver enough heat and the consumers should be able to withdraw as much as they wanted from the network. This resulted in only the measures a bigger pipe area or more pumping being used as bottleneck measures. Other examples were environmental aspects regarding earthwork affecting the decision process and management driven programs about for example the return temperature.

3.4. *Interview results for risks and opportunities for bottleneck measures*

The summary of the risks and opportunities coupled to the bottleneck measures is showed in Table 1. The measure is stated to the left in the table and the risks and opportunities coupled to this measure are then listed to the right. The interview answers showed very different risks and opportunities coupled to the measures, which could partly be explained by different situations in different DH networks but also by varying knowledge about bottlenecks and bottleneck measures.

One interesting thing discussed with a higher supply temperature was that the possibility to increase the supply temperature may decrease in the future if more low temperature networks would be implemented. But it could also be hard to decrease the supply temperature in existing DH networks because the pipes and consumer systems are dimensioned according to a higher supply temperature.

Regarding a bigger pipe area, an interesting strategy was to strengthen the DH network with a ring structure pipe in a later stage rather than building a pipe of larger dimension from the beginning. A ring structure pipe would also help increase the redundancy in the network and could be a strategy when dealing with increasing future loads.

The main risk mentioned with more pumping as a measure was if the pump for some reason would stop working. One solution was to install two smaller pumps instead of one big. A pump failure could however sometimes be solved by a higher supply temperature, which decreased the total risk picture.

Table 1. Risks and opportunities for bottleneck measures according to the interviews.

	Risks	Opportunities
Higher supply temperature	<ul style="list-style-type: none"> More wear on the pipes Reduced efficiency in heat pumps, CHP units and for prosumers More heat losses in the network Risk of more fluctuations in the network Higher safety risks 	<ul style="list-style-type: none"> Simplicity Quick fix Less pumping power demand Start of new production units could be avoided Possible to optimise other parameters i.e. pumping and fuel order
Bigger pipe area	<ul style="list-style-type: none"> Higher/too high temperature loss in the pipe during the summer Customer base not developing as predicted Risk with groundwork and digging, connected to for example personal safety and uncertainties 	<ul style="list-style-type: none"> Robustness Low maintenance demand Higher redundancy in DH network (ring feed) Possibility to connect more consumers Better leak detectors on newer pipes Better possibility to use the existing production in economic order Established solution leading to well-known risks
More pumping	<ul style="list-style-type: none"> Pump failure Outcome of pumping in ring structure networks is hard to predict An intervention in the pipes are necessary for new pumps More maintenance demand 	<ul style="list-style-type: none"> Help to control the flow and supply temperature Solution to altitude problems New measuring point, which is beneficial for a better control of the DH network Smaller safety margins regarding supply temperature would be needed Good temporary solution when waiting for an area expansion
Increased cooling	<ul style="list-style-type: none"> Ownership structure of the substations (when they are consumer owned) Doubts concerning the robustness Time consuming 	<ul style="list-style-type: none"> Increased customer contact More efficient system and optimized DH network Increased opportunity to lower the supply temperature Increased opportunity to receive waste heat Higher efficiency in flue gas condensation, heat pumps and CHP units Lower electricity demand in pumps Lower heat losses
LHS	<ul style="list-style-type: none"> Increased maintenance demand Difficult permit processes Risks for humans depending on location and the fuel used Risk of overusing the production unit due to simplicity, instead of using production units with better environmental and economic performance Long start-up time depending on fuel Could be environmentally less favourable depending on the fuel used Vulnerable to power failures Prosumers being unreliable 	<ul style="list-style-type: none"> Higher redundancy and operational reliability for the network Start-up of other production units could be avoided New measuring point, which is beneficial for a better control of the DH network Smaller safety margins regarding supply temperature and pump work would be required Possibility to use prosumers
DSM	<ul style="list-style-type: none"> New technique for DH companies Doubts concerning the robustness Education of staff or new staff would be needed Dissatisfied consumers if their comfort is affected Changed system boundaries where the DH company gets responsibility further into the building Improper control could lead to unstable heat curves 	<ul style="list-style-type: none"> Increased consumer contact Start-up of new production could be avoided Investments in new peak load production could be avoided Less dP variation More even operational situation Smaller safety margins regarding supply temperature and pump work would be needed Better control of the indoor temperature Possibility to allocate heat shortages to larger part of the network Improved energy efficiency depending on method

The most mentioned risk and negative aspect with increased cooling in substations was the difficulty to convince DH consumers to revise and maintain their substations. Since the most common ownership structure in Sweden is for the consumers to own the substations, the maintenance responsibility lies with them. If the consumers have little or nothing to win personally with a lower return temperature, it may be hard to convince them to do anything requiring an investment. This was mentioned also for companies with an existing flow tax, as this was often too low to motivate consumers to act. The majority of the companies had some sort of service agreement available for the consumers. The consumers with a service agreement were often not causing problems related to cooling in the DH network to the same extent. This further added complexity to the issue, because it would be unfair if the DH company would do investments

for free in substations not covered by service agreements. The way to deal with this issue differed amongst the DH companies. A change of the price model to one that included a flow fee could be one way to solve the problem. Sometimes, the companies considered themselves obliged to maintain substations if the impact on the network was big enough. A possibility could also be for the company to help to some extent with the investment or refer to the consumer agreement if maintenance was mentioned there.

It seemed like an increased cooling measure would be easier to perform if the DH company owned the substations. Some disadvantages were however discussed coupled to owning of the substations, for example that the investment costs for buying all the substations in the DH network would be large, that the company would have a bigger responsibility further into the buildings and that more personnel would be needed. A positive aspect of a better cooling mentioned was a possibility of that a higher waste heat utilization, even if this depended on the possibility to lower also the supply temperature, which may not always be possible if the bottleneck is to be solved by this measure.

Regarding LHS, temporary heat boilers could be used until a pipe was built, which could be a way to handle the time factor. One problem mentioned with LHS was that if the heat supply unit was to be cheap, it had to be run on solid fuel, which would be harder to get a permit for due to more deliveries and dust problems and also require more maintenance in the form of for example on-site staff and supervision. Smaller LHS units (<10 MW) however needed only a simplified permit process.

Regarding prosumers as LHS, they could help increase the dP in the network during very cold temperatures by satisfying all or part of their own heat demand. Prosumers could furthermore be a cheap and relatively easy way to provide local heat in remote areas. It could however be unrealistic to use prosumers as the single bottleneck solution as their supply security could not be assured. The possible difficulties for prosumers to deliver heat of high enough supply temperature could further hinder prosumers as the only bottleneck solution.

The companies that had used DSM had often not used it in a fully developed way but as pilot studies or projects. DSM was however seen as a very interesting measure and one reason might be that it could be important for DH companies to offer DSM solutions to consumers before they individually start to use DSM. The latter could for example lead to an uncharacteristic and more uneven heat load curve. The redundancy of DSM as a bottleneck measure was also questioned. The redundancy would however increase if a big enough amount of consumers were included in the DSM measure. An alternative to DSM mentioned was to use thermal energy storages, either small distributed consumer owned or large company owned, which would have the same effect on the DH network.

3.5. Simulation results for risks and opportunities for bottleneck measures

The overall result for the season simulations can be seen in Table 2. All effects in the table were the same for all seasons. If some effect stood out during a specific season, it is described in the following text. The analysis was based on equations found in Frederiksen and Werner, describing heat losses from a pipe and temperature losses from a pipe [8]. The local supply temperature refers to the supply temperature reaching the consumers.

The parameters mainly affecting the heat losses and temperature losses from a pipe were the difference between the water temperature in the pipes and the ambient temperature, the diameter of the pipes, the flow velocity and the total amount of heat being transported in the pipes. An increased difference between the water temperature in the pipes and the ambient temperature resulted in increased heat losses and vice versa. This effect was relevant for the higher supply temperature measure (increased heat losses) and for the increased cooling measure (decreased heat losses). A larger pipe diameter resulted in an increased heat transfer area to the surroundings and a lower flow velocity, which increased the heat losses. This effect was relevant for the bigger pipe area measure. A lower flow velocity resulted in increased temperature losses and thus a lower local supply temperature. This effect was relevant for all of the measures except for more pumping. A lower amount of heat being transported in the pipes resulted in decreased heat losses. This effect was relevant for the increased cooling, LHS and DSM measures. A note is that a lower flow velocity also results in a lower heat transfer coefficient which decreases the heat losses, but this is not accounted for in NetSim.

For all measures except for a higher supply temperature, it was possible to lower the supply temperature for all the seasons tested. This possibility would result in lower heat losses and lower costs and all benefits that comes with a lower supply temperature. It is however possible that the lowest dP location changes places when the supply temperature is lowered, which should be accounted for to avoid dP problems in the network.

Table 2. Risks and opportunities according to the simulations.

	Risks	Opportunities
Higher supply temperature	Increased heat losses	Increased local supply temperature
Bigger pipe area	Increased heat losses Decreased local supply temperature	Possibility of lower supply temperature
More pumping	Change of lowest dP location	Possibility of lower supply temperature
Increased cooling	Decreased local supply temperature	Possibility of lower supply temperature Decreased heat losses
LHS	Change of lowest dP location Decreased local supply temperature	Possibility of lower supply temperature Decreased heat losses Increased local supply temperature
DSM	Decreased local supply temperature	Possibility of lower supply temperature Decreased heat losses

An opportunity with a higher supply temperature was that the lowest local supply temperature increased. This effect was however counteracted by higher temperature losses due to the lower flow velocity and the larger difference between the water temperature and the ambient temperature. The lowest local supply temperature was thus not increased by 4°C, as the initial supply temperature, but by 0.85-1.7°C for the different seasons.

For a bigger pipe area, the lowest local supply temperatures were only minimally lowered. This could be explained by the fact that the exchanged pipe section were rather short. If longer pipes were to be exchanged, a bigger pipe area could pose a risk of lower local supply temperatures, especially during the summer when the supply temperature is lower from the beginning and the flow velocity is low. This effect is however counteracted by more energy needed to be transported in the pipes, due to the higher heat losses in a bigger pipe, which induces a higher flow velocity and thus higher local supply temperatures. This effect has a higher impact when the heat losses constitutes a larger part of the total heat demand, i.e. during the summer. The lowered heat transfer coefficient for bigger pipes would also lower the heat losses. This means that when changing the pipe area, the resulting local supply temperatures should be carefully evaluated.

For the measure consisting of more pumping, the dP at the consumers before the pump became lowest in the DH network when using the new distributed pump. When increasing the load in the existing initial pump, this was not an issue.

For the increased cooling measure, the lowest local supply temperature was much more affected than by other flow reducing measures. This was because the consumers with the most critical supply temperature were involved in the measure. The lower local supply temperature was mainly a problem during the summer when the supply temperature was lowered from above 58 °C to below 53 °C. This was also hard to counteract by an increased initial supply temperature, because it would lead to a lower flow velocity, which would induce more temperature losses. The low local supply temperature would instead be needed to be increased by for example summer bypasses.

For the LHS, the lowest dP location was changed, which could result in a suboptimal DH network operation if there are not enough measuring points. Depending on location, LHS could help keep the supply temperature up in critical areas. In the Pasture, the critical supply temperature and dP areas were not the same and the LHS unit was located according to the dP. The lowest local supply temperature was thus somewhat decreased and the supply temperature close to the LHS was increased.

Even if the DSM measure led to marginally lower heat losses, the relative heat losses increased for this measure. In the Pasture, the lowest local supply temperature was almost not affected at all by the DSM measure, even if the flow velocity was lowered. This depended on the location of the DSM consumers, not being close to the most critical supply temperature area.

4. Discussion

The interviews show that the companies were very interested in and often had projects and tests about more consumer oriented and local measures to increase the local dP, such as increased cooling at substations, DSM and LHS. A lot of DH research is also currently oriented towards these areas. This indicates that the view of DH is

transferring from a centrally controlled technology system towards a system where all parts, including consumers, are important.

An interesting aspect in the interview results was that the economy is seen as the most important factor when choosing bottleneck measure for all companies interviewed. Many of the risks and opportunities listed by the companies however affect the economy why they also should be accounted for in these calculations, which seems not to be the case today. The simulations for example show that the supply temperature could be lowered for all seasons and all measures, except for an increase of the supply temperature, which could mean great savings for the DH company.

Regarding the increased cooling measure, there was often more sufficient cooling among the consumers covered by a service agreement, which means that the maintenance of their substations was the DH company's responsibility. This could give an argument for the DH companies to own the substations, which is seldom the case today. It would then be easier to maintain and control the substations. There are however also disadvantages with ownership and responsibility of equipment located further into the consumers' buildings. Another option to improve the cooling could be for DH companies' to review their service agreements and how they are marketed to customers, to get more customers covered by such a service agreement.

One of the main causes of bottlenecks in DH networks was that the DH network and the customer base grows more than planned for. An interesting answer regarding the strategy to handle this was that one company built a smaller pipe in an earlier stage of construction of new areas. When the heat demand increased, the company strengthened the connection to the new areas with a ring pipe. This was a strategy to handle some of the problem of correctly predicting the future but also created extra redundancy in the DH network. Since the most expensive part of installing a new pipe is the earthwork, this method could however also become unnecessary costly.

Both DSM and increased cooling could induce lower incomes for the DH company due to lower energy use, which was a common concern. This may result in companies hesitating to implement these measures, even if they would mean a more optimally working DH network, less environmental impact, more sustainable cities and also lower costs for the DH company. The lower incomes should however not pose a problem if a price model that correctly reflects the costs for producing and distributing the DH is used. Such a tariff could include a flow fee and a heat power fee.

Regarding the results for the interview study, it is possible that more interviews would have given a broader range of answers. Most answers were however already given in the last interviews, why the interview study was assessed as saturated. No quantitative conclusions have been drawn from the interview study and the results are thought to be seen as examples of how Swedish DH companies think about bottlenecks and give examples of risks and opportunities coupled to the measures.

The results in this study has given rise to new questions and suggestions for research areas. For example, the most common reason for bottleneck problems seems to be difficulties to correctly predict the future. An investigation of the best way to predict the future and which strategies that are available and works best to handle this problem would thus be interesting to study. Is it for example better to build an oversized pipe from the beginning or is it better to complement with ring structure pipes in a later stage? There are also a lot of parameters affecting which bottleneck measure that was chosen. A study on how to assess and evaluate these parameters in relation to each other would thus be a valuable element in the understanding of bottleneck measures. A total economical assessment of all measures and an annual energy and carbon dioxide balance would further add to this understanding.

5. Conclusions

The present study was performed to investigate risks, opportunities, issues and added values coupled to different bottleneck measures. This was made by in depth interviews and DH network simulations. The main results are described in the bulleted list below.

- There are very different views among Swedish DH companies on bottlenecks and their risks, opportunities and economy. This may to some extent depend on different network conditions from the beginning but also on varying knowledge about bottlenecks, bottleneck measures and their economy.
- Bottlenecks in DH networks are very hard to completely avoid because the origin is often difficulties to correctly predict the future.

- Parameters that affected the choice of bottleneck measure were economy, robustness of measure, redundancy of measure, future plans, time factors, local conditions and directives from management.
- Economic concern is the most important factor for DH companies when choosing bottleneck measure. There however seems to be a lack of lifecycle perspective on the economy of the measures, why many of the risks and opportunities that may affect the economy of bottleneck measures are presently not accounted for.
- To avoid problems connected to lower incomes for measures such as better cooling or DSM, it is important that the DH pricing is correct and that the costly parameters are included in the tariff. Such a tariff could include a flow fee and a heat power fee.
- If the DH companies owned the substations, improvement of the cooling in substations would probably be a more accessible measure to use.
- All bottleneck measures except an increased supply temperature render in possibilities to decrease supply temperatures during other seasons than for DOT.
- One risk of using bottleneck measures is that bottleneck measures may increase the temperature loss in pipes, which especially during the summer months may result in too low local supply temperatures.
- Bottleneck measures may move the point with the lowest dP.
- The heat losses are increased for the higher supply temperature and a bigger pipe area measures.
- The heat losses are decreased for the increased cooling, LHS and DSM measures.
- The relative heat losses are increased for the DSM measure.

Acknowledgements

This work was performed with financial support from E.ON Energilösningar AB.

References

- [1] "Communication From the Commission to the European Parliament, the Council, the European Economic and Social Committee and the Committee of the Regions - An EU Strategy on Heating and Cooling," European Commission, Brussels, 2016.
- [2] H. Lund, S. Werner, R. Wiltshire, S. Svendsen, J. E. Thorsen, F. Hvelplund och B. Vad Mathiesen, "4th Generation District Heating (4GDH): Integrating smart thermal grids into future sustainable energy systems," *Energy*, vol. 68, pp. 1-11, 2014.
- [3] Y. Li, Y. Rezugui och H. Zhu, "District heating and cooling optimization and enhancement – Towards integration of renewables, storage and smart grid," *Renewable and Sustainable Energy Reviews*, vol. 72, pp. 281-294, 2017.
- [4] J. E. Thorsen, C. H. Christiansen, M. Brand, P. K. Olesen och C. T. Larsen, "Experiences On Low-Temperature District Heating In Lystrup – Denmark," in *Proceedings of International Conference on District Energy, 2011*, 2011.
- [5] H. Kauko, K. Husevåg Kvalsvik, D. Rohde, N. Nord och Å. Utne, "Dynamic modeling of local district heating grids with prosumers: A case study for Norway," *Energy*, vol. 151, pp. 261-271, 2018.
- [6] L. Brange, J. Englund och P. Lauenburg, "Prosumers in district heating networks – A Swedish case study," *Applied Energy*, vol. 164, p. 492–500, 2016.
- [7] L. Brange, P. Lauenburg, K. Sernhed och M. Thern, "Bottlenecks in district heating networks and how to eliminate them – A simulation and cost study," *Energy*, vol. 137, pp. 607-616, 2017.
- [8] S. Frederiksen och S. Werner, *District Heating and Cooling*, Lund: Studentlitteratur AB, 2013.
- [9] L. Brange, J. Englund, K. Sernhed, M. Thern och P. Lauenburg, "Bottlenecks in district heating systems and how to address them," *Energy Procedia*, vol. 116, pp. 249-259, 2017.
- [10] M. Vesterlund och J. Dahl, "A method for the simulation and optimization of district heating systems with meshed networks," *Energy Conversion and Management*, vol. 89, pp. 555-567, 2015.
- [11] M. Vesterlund, A. Toffolo och J. Dahl, "Optimization of multi-source complex district heating network, a case study," *Energy*, vol. 126, pp. 53-63, 2017.
- [12] L. Brand, A. Calvén, J. Englund, H. Landersjö och P. Lauenburg, "Smart district heating networks – A simulation study of prosumers' impact on technical parameters in distribution networks," *Applied Energy*, vol. 129, pp. 69-88, 2014.
- [13] Vitec, "An onlinemanual from Vitec NETSIM," Vitec, 27 09 2013. [Online]. Available: <http://doc.energy.vitec.net/ManualData/ve/en/vitechelp.asp?produkt=NetSim&folder=netsim>. [Used 07 05 2018].
- [14] SMHI, "Öppna data - Meteorologiska observationer (Open data - meteorological observations)," SMHI (Swedish Meteorological and Hydrological Institute), [Online]. Available: <http://opendata-download-metobs.smhi.se/explore/?parameter=1>. [Used 08 05 2018].



16th International Symposium on District Heating and Cooling, DHC2018,
9–12 September 2018, Hamburg, Germany

Performance assessment of a multi-source heat production system with storage for district heating

M.N. Descamps, G. Leoncini, M. Vallée*, C. Paulus

CEA, LITEN, 17 rue des Martyrs, F-38054 Grenoble, France

Abstract

This work contributes to the development of a multi-vector flexibility management platform, combining electric, heat and gas optimization at district level. The multi-vector flexibility management platform will be validated both experimentally and by simulation, on a set of demonstration scenarios. Each scenario refers to an eco-district topology with a given distribution network of energy, a consumer side and a multi-source heat production plant, consisting of a gas boiler, a solar collector, and a heat pump. In addition, a thermal storage in the form of a water tank is connected to the network. A key aspect is the ability to optimize such a system at district level, with the performance of the individual components depending on operating temperatures and environmental conditions, and varying primary energy prices. By simulating the distribution network with a dynamic model, the non-linear influence of various parameters on the system can be investigated.

In particular, the current study focuses on the operation of the multi-source heat production system and thermal storage. A 1D model of the multi-source heat production (gas, solar and heat pump), the thermal storage, and a global consumer is performed using the equation-based object-oriented language Modelica along with the simulation platform Dymola. The model is run with standard controls from district heating provider, i.e. constant or linear controls. For a given consumer load, a set of key performance indicators (KPI) are used to assess the performance of the system, e.g. energy share from renewables and storage utilization rate. The sensitivity to the model's input is analyzed as well. The results can be used as reference to apply optimal control schemes and study the influence on the corresponding KPIs.

© 2018 The Authors. Published by Elsevier Ltd.

This is an open access article under the CC BY-NC-ND license (<https://creativecommons.org/licenses/by-nc-nd/4.0/>)

Selection and peer-review under responsibility of the scientific committee of the 16th International Symposium on District Heating and Cooling, DHC2018.

* Corresponding author.

E-mail address: mathieu.vallee@cea.fr

Keywords: Hybrid District Heating; Power to Heat; Dynamic Simulation

1. Introduction

District heating networks (DHN) have long been coupled to electricity and gas networks via conversion units such as heat pumps for instance. However the trend is to have an even higher integration of the energy networks, leading to the concept of Hybrid Energy Networks (HEN). Advanced control strategies are required to manage the energy generation, storage and consumption with a high share of renewable energy sources, whilst ensuring cost efficiency. In this context, planning tools based on optimization algorithms are used. The performance of such tools is assessed by comparing an optimal situation to a reference situation. This can only be done by means of numerical simulations, which can generate reproducible and controllable conditions for the operation of a DHN. It should be noted that it can be challenging to validate and calibrate the components of a DHN simulation, due to the lack of high quality measured data [1].

Therefore the purpose of the current study is to develop a methodology for DHN simulations calibrated on experimental data. The DHN simulations will later be linked to an optimization module for the flexible management of a HEN. The experimental data is collected from the micro DHN facility of CEA-INES, which can be used for the validation of DHN simulation as well as the implementation of optimal control strategies in real time.

The proposed methodology relies on a dynamic simulation of the heating network with the equation-based object oriented language Modelica. A set of KPIs are defined and evaluated. The present work aims more specifically at defining a reference setup, and therefore focuses on targeted KPIs for a non-optimal energy management strategy. This strategy is implemented via a set of logical rules applied at each time step, and tested for the satisfaction of a prescribed building heat load for a year. Different scenarios are taken into account to study the influence of the multi-source heat plant sizing. In a subsequent work, the flexible management of the system will be demonstrated by comparing an optimal strategy to the current one.

Nomenclature

COP	Coefficient Of Performance
DHN	District Heating Network
DHW	Domestic Hot Water
GB	Gas Boiler
HP	Heat Pump
HEN	Hybrid Energy Network
mflow	Mass flow rate (kg/s)
KPI	Key Performance Indicator
SH	Space Heating
T _{min} ,	Minimum and maximum temperature in the thermal storage tank (C)
T _{max} ,	Maximum and maximum temperature in the thermal storage tank (C)
T _{stor_top}	Temperature at the top of the storage tank (C)
T _{stor_bot}	Temperature at the bottom of the storage tank (C)
c _p	Specific heat capacity of water (J/kg/K)
P _{stor_demand}	Heat load on the thermal storage tank applied by the consumer and the solar field (kW)
P _{stor_max}	Thermal storage tank critical power above which the gas boiler is used (kW)

2. Case study

2.1. Heating network

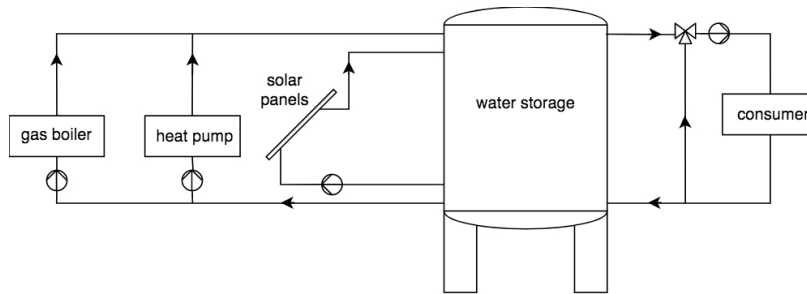


Fig. 1: Heating network considered in the present study

A small scale heating network system is considered as a case study. The benefit of this approach is that it allows to use the micro district heating network of CEA-INES [2] to partially validate the heating network model. The focus is on the management of the energy production, with flexibility through storage at district level, as opposed to e.g. demand side management, which is not considered here. A simplified network layout is used (Fig. 1), whereby all heat production units run in parallel, and the consumer side is represented by a single heat exchanger which aggregates all the heat loads coming from virtual buildings. A water tank is used as thermal storage for this system. The heat is distributed to the consumer via the distribution pipes, through which heat loss with the environment occur.

The case study will be sized to comply with the scale of the micro district heating network of CEA-INES. In particular, the maximum heat load applied on the consumer side will be limited to 50 kW in this study. Despite its simplicity and scale, this case study is suitable to assess some key concepts of district heating systems, such as the integration of renewable energy sources, the coupling between the heating network and electricity grid, or the control strategy to reach an optimum operation of the network. The outcome of the study can be up-scaled or adapted to existing eco-districts.

2.2. Control strategy

Each heat generator (gas boiler and heat pump) operates at a fixed supply temperature (i.e. set point) and variable mass flow rate. The consumer supply temperature set point is satisfied by using a three-way valve, which acts as a bypass between the thermal storage and the consumer (see Fig. 1). The storage temperature should therefore be larger than the consumer supply temperature. The solar thermal system is used at fixed flow operational mode, which means the feed-in pump of the solar field operates at constant volumetric flow for a solar irradiation above a given threshold. For the purpose of this study, the detail hydraulics of the solar field is not required. Instead, the output power of the solar field is used.

The overall control strategy combines the requirement to satisfy the consumer demand to the constraints on the thermal storage tank. The following rules are listed:

- The power coming from the solar panels is not a control variable (passive components from the operator point of view),

- The heat pump is used for the base load, therefore has priority over the gas boiler to satisfy the demand, up to its maximum power,

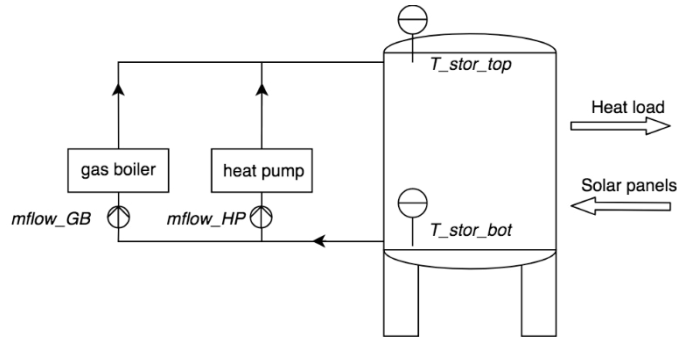


Fig. 2: Reduced functional heating network layout considered

- The gas boiler is used for peak load, i.e. to provide the remaining power when the heat pump is at maximum power and the demand is not satisfied,
 - The temperature at the top of the storage tank should stay within a range $[T_{min}, T_{max}]$.
- By aggregating the heat load coming from the solar field and the buildings, a reduced functional model of the case study can be proposed (Fig. 2)

It can be seen that the thermal storage tank is equivalent to a heat consumer with its own demand, which corresponds the building heat load from which the solar field production is subtracted. Consequently, the heat load demand used in the control strategy is the thermal storage power demand, calculated as

$$P_{stor_demand} = (mflow_GB + mflow_HP) * c_p * (T_{stor_top} - T_{stor_bot}) \quad (1)$$

In addition, the heat plant is required to provide power whenever the temperature in the storage falls below T_{min} . In this case, the heat pump operates by default at its maximum capacity. The gas boiler operates to provide some extra power which is scaled to the maximum flow rate allowable as follows:

$$P_{stor_max} = max_flowrate * c_p * (T_{min} - T_{stor_top}) \quad (2)$$

In other words, when the temperature of the storage tank is too low, the control strategy maximizes the power provided by the heat plant to bring it back above T_{min} , without necessarily using both the heat pump and the gas boiler at maximum capacity.

Indeed, preliminary tests have shown that if both the heat pump and gas boiler operate at their maximum power to fulfill the minimum storage temperature constraint, then in practice the heat plant operates at maximum capacity for a large part of the year, which is not efficient.

A flow chart representing the control strategy is displayed in Fig. 3. The strategy is only based on instantaneous inputs.

The implementation of the control strategy is carried out using smooth operator functions instead of logical relation

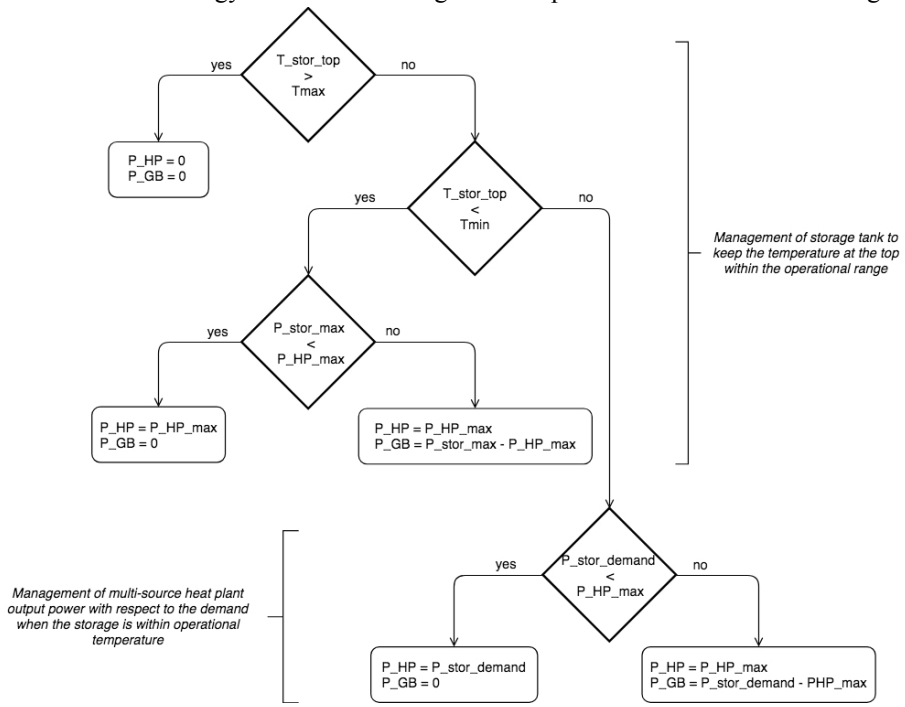


Fig. 3: Control strategy for the management of the multi-source heat plant and storage

events. The benefit of this approach is that it avoids event triggering processes which are not computationally efficient. As a reminder, the heating network simulator will run alongside other modules such as an electric simulator, an optimizer, a prediction module, in cycles of 15 min. Therefore, it is critical to achieve a good performance of each module. The drawback of the use of smooth operator function is that the priority rules need to be implemented with care, especially in the acausal environment chosen for the model (presented in section 3.1).

2.3. Scenarios

The energy produced by the multi-source heat plant is consumed by a set of residential buildings, all identical. In the following, the multi-source heat plant and thermal storage are sized according to different scenarios using available data [3], [4], [5]. A summary of the reference system is shown in Table 1.

Table 1: Reference building characteristics

System parameters	Value
Two storey single family building	
Total floor area	140 m ²
SH load at design outdoor temperature [3]	8400 kWh/a
SH peak load estimation [6]	4.2 kW
DHW peak load with diversity factor [5]	3 kW
Design inlet temperature of the heating system [3]	40 C
Design outlet temperature of the heating system [3]	35 C

The reference building has a peak load of DHW and SH of 7.2 kW, which includes the diversity factor, i.e. the fact that DHW draw-off peaks are not synchronized among several houses. In order to match the heat load limit mentioned in section 2.1, it is assumed that 7 reference buildings are connected to the district heating network, accounting for approximately 50 kW of consumer peak load.

With these figures, the multi-source heat plant is designed to provide a maximum of 60 kW, which should satisfy the SH and the DHW at district level, i.e. taking account of the pipe heat loss. The distribution pipe length, insulation and diameter are representative of what is installed on the experimental facility.

Different scenarios are investigated with respect to the sizing of the heat generators and thermal storage (Table 2).

Table 2: Sizing of the multi-source heat plant for different scenarios

Component	Scenario 0	Scenario 1	Scenario 2	Scenario 3
Gas boiler	45 kW	35 kW	45 kW	45 kW
Heat pump heating capacity	15 kW	25 kW	15 kW	15 kW
Water tank	15 m ³	15 m ³	10 m ³	15 m ³
Solar field	50 m ²	50 m ²	50 m ²	25 m ²

It should be noted that because cooling loads are not considered here, a careful sizing of the solar field and thermal storage should be undertaken. The risk is that in the summer months, the combination of a low consumer demand and high solar production leads to temperatures above the operational constraint inside the thermal storage tank. For the scenarios proposed, it has been verified that the operational constraints are respected. Interestingly, the methodology developed in the current study can also be used to design and size a multi-source production heat plant.

The chosen set point temperatures for the scenarios are shown in Table 3.

Table 3: Set point and critical temperature for the scenarios

Temperature	Value (C)
Gas boiler supply	80
Heat pump supply	80
Consumer supply	60
Storage top max	85
Storage top min	70

3. Methodology

3.1. Dynamic distribution network model

A dynamic network model based on the layout shown in Fig. 1 is built using the equation-based object-oriented language Modelica along the Dymola simulation platform and an in-house model library [7].

On the production side, the solar field is represented by a component which computes the solar heat gain based on ASHRAE Standard 93. The gas boiler is represented by a heat generator component which models heat and momentum balances. It takes as input the supply temperature downstream of the heat generator and outputs the power. The heat pump is represented by a component with a performance curve based on Carnot efficiency. The water from the cold source enters the evaporator at 12 C. The cold water circuit is not modelled in this work.

The distribution pipes are represented by a component which implements the method of characteristics to integrate the transport equation along a fluid particle's path.

The water tank is represented by a vessel component with perfect temperature stratification. The insulation properties are taken from the experimental facility specifications. From the heat production side, the hot water enters

the tank from the top, and leaves colder from the bottom. On the consumer side, the hot water leaves the top of the tank, and returns colder at the bottom of the tank.

The consumer is modelled by prescribing a heat flux from a time-series table. The 3 way valve that sets the consumer supply temperature is adjusted via a Proportional Integral controller.

3.2. Validation of the model using experimental data

The tank and gas boiler components are validated using experimental data from the micro district heating network of CEA-INES. The micro-DHN consists in a two-tube district heating network of about 200 m long, supplying heat to real buildings (offices and clean room) and to an emulated building. The main production unit of this micro-DHN is a condensing gas boiler of 280 kW. A solar field of 300 m² (about 210 kW) with various thermal solar panels technologies is also supplying heat to the network either in a centralized or in a decentralized manner. The network is also equipped with a hot storage tank of 40 m³.

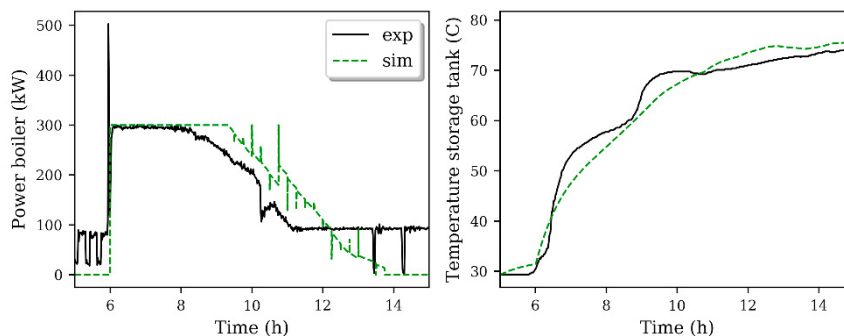


Fig. 4: Response to a sudden increase of set point of the gas boiler at $t=6h$ and comparison between experimental data and simulation using Modelica (Left) Output power of the gas boiler (Right) Temperature at the top of the storage tank

The data used for the validation corresponds to a sudden increase of temperature inside the water tank following the activation of the gas boiler. The inputs to the simulation are:

- The maximum power of the boiler;
- The gas boiler set point temperature profile, which is in the range 72 to 76 C;
- The experimental heat load applied to the thermal storage tank by the solar field and an external heat consumer.

Fig. 4 shows that the dynamics of the system is reasonably well captured. The simulated gas boiler power increases suddenly to its maximum value, then decreases along the same rate as the experimental data, although with a delay of 1h. This could be due to some unaccounted heat load on the experimental set. Furthermore, the simulated temperature in the storage tank is in good agreement with the experimental data. An extensive set of data can be used to calibrate or validate other components of the heating network simulation, which will be carried out in a future work.

3.3. Key performance indicators

In the current study, several KPIs are defined, with a focus on the heating network (Table 4). The electrical energy used for the compressor of the heat pump is calculated based on the COP of the heat pump, which is an output of the simulation. It should be noted that in the calculation of the primary energy consumption, a primary energy factor of 2.5 is included for the electricity [8], and the gas boiler is assumed ideal with an efficiency of 1. The maximum accumulated energy in the storage tank is calculated for a temperature range between the zero enthalpy temperature of 0 C and 100 C as a maximum temperature.

Since the results from the current study are used as a reference to compare with alternative control strategies in a subsequent work, the KPI's listed in Table 4 are absolute quantifiers, i.e. they are not relative to a reference case.

Table 4 : Key performance indicators

KPI	Description
Thermal energy share (HP, GB, solar)	Ratio of the annual thermal energy produced by the heat pump, gas boiler and solar field to the total thermal energy produced
Primary energy ratio	Ratio of the annual energy demand to annual primary energy production (electricity and gas)
Storage average capacity	Annual average ratio of the energy accumulated in the storage to the maximum energy capacity of the storage

4. Results and discussion

The heat loads for SH and DHW are generated prior to the network simulation using the methodology developed in IEA SHC – Task 32 [3].

SH load profile of the reference building (section 2.3) is generated using TRNSYS transient system simulation software with a weather file input corresponding to Chambéry (France). As part of this simulation, the average DHW energy in kWh is calculated for the cold water temperature of the building using the average DHW load profile mentioned above. The simulation is run for 1 year, using a time step of 15 min.

The heat load curve and heat load diagram for one house are shown in Fig. 5. The consumer peak load is about 5 kW for one house, or 35 kW for the 7 houses, which is less than the design value, hence the multi-source heat plant is slightly over-sized.

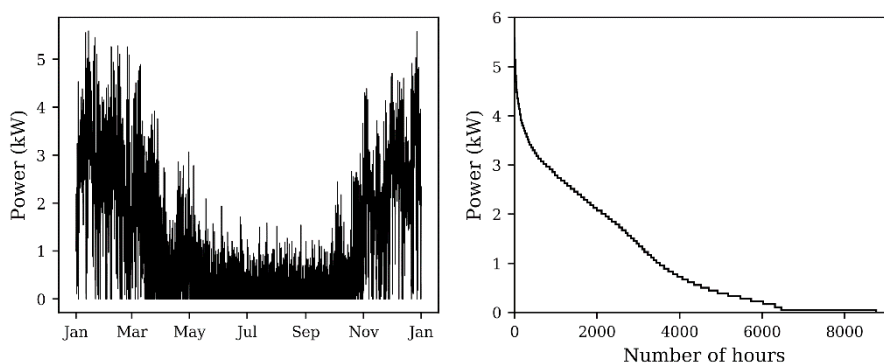


Fig. 5: Annual heat load (space heating and domestic hot water) for one residential buildings. (a) Time series; (b) Heat load diagram

The heat production profile and diagram for scenario 0 is shown in Fig. 6. As prescribed in the control strategy, the heat pump provides a base load, and the gas boiler is used to provide the excess power during peak demand. The configuration chosen, with the thermal storage acting as a buffer between the heat plant and the consumer, means that the production and consumption peaks are not synchronized. As a consequence, there is a mismatch of the heat load diagrams between the production (heat pump, gas boiler, and solar) and the DHN demand (Fig. 6 bottom). However the energy balance over the year is respected within 2%. The annual energy at district level is around 99000 kWh for scenario 0, which is 14140 kWh per house for SH and DHW including distribution heat loss.

The temperature at the top of the storage tank remains above 70 C, whereas the consumer supply temperature is fluctuating around 60 C, with higher temperature in the summer months, as shown in Fig. 7. This could be improved

by tuning the setting of the PI controller and reviewing the thermal storage control (e.g adding schedule constraints for the summer months).

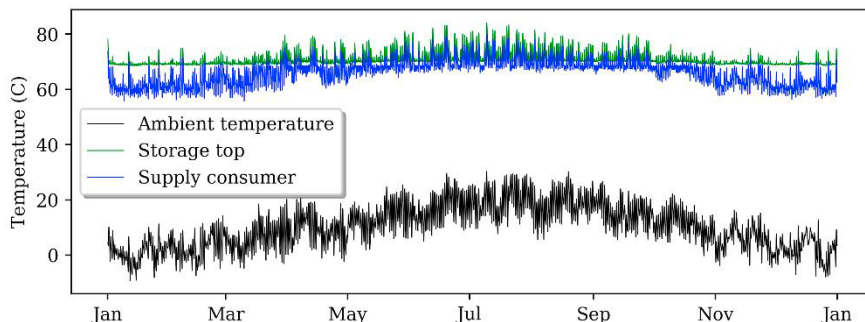


Fig. 6: Heat plant load profile for scenario 0

The KPIs are shown in Table 5 for the different scenarios. When the size of the storage tank is decreased, its average capacity increases, which means it is easier to charge it to full capacity (scenarios 0 and 2). However there is no impact on the energy share of the generators, which is a sign that the control strategy is not able to leverage the thermal storage. The energy share of the HP increases when its nominal power increases, as expected (scenarios 0 and 1), and it also increases when the solar field surface is decreased (scenarios 0 and 3), because the HP is then used more often to keep the storage tank at a sufficient temperature in the absence of sufficient solar power. The primary energy ratio is quite low for all scenarios, which is mainly due to the low COP of the heat pump (around 2.1 for temperature levels of the study).

Overall, what the KPI values of Table 5 reflect is the absence of a predictive strategy in the energy management. Therefore, the current set of results can be used as a reference to compare against an optimal control strategy which would take full advantage of the storage for demand peak shaving.

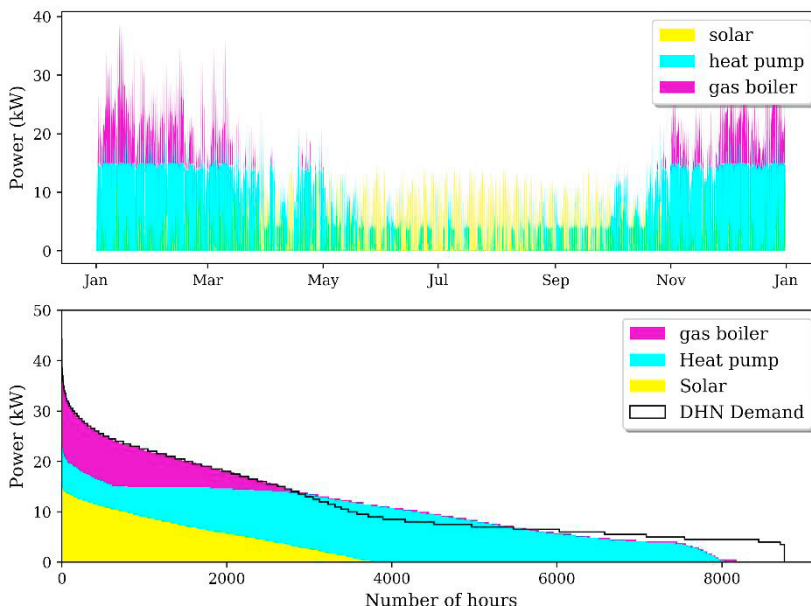


Fig. 7: Temperature profiles for scenario 0

Table 5 : Calculated KPIs for the different scenarios

Key performance indicator	Scenario 0	Scenario 1	Scenario 2	Scenario 3
Storage capacity	47%	47%	82%	46%
Energy share HP	59%	73%	59%	69%
Energy share GB	18%	4%	18%	19%
Energy share solar	23%	23%	23%	12%
Primary energy ratio	0.35	0.30	0.35	0.30

5. Conclusion and future work

This study proposes a methodology to simulate a heating network and evaluate KPIs, in order to contribute to the development of a HEN flexibility management platform. A thermal storage tank and a multi-source heat plant consisting of a heat pump, a gas boiler and a solar field are specified for a small scale district heating network. A dynamic network simulation was run on a set of scenarios for a control strategy based on logical rules. The analysis of the KPIs confirm that in the absence of any predictive feature, the control strategy is non-optimal. The study can be replicated on other district configurations for a range of scenarios.

In a future work, the DHN simulation will be linked to an optimization module to compare the results to the non-optimal case. In this perspective; the heating network simulation will be modified to include machine learning models, using historical data from the solar field of CEA-INES to train and test the models. The price of primary energy will be included in the analysis. Furthermore, the experimental micro DHN of CEA-INES will be used to test in live conditions the optimal control strategy.

Acknowledgements

The authors gratefully acknowledge the financial support of the funded PENTAGON project by the European Commission, granted in the Horizon 2020 no.731125.

References

- [1] D. Coakley, P. Raftery et M. Keane, «A review of methods to match building energy simulation models to measured data,» *Renewable and Sustainable Energy Reviews*, vol. 37, pp. 123-141, 2014.
- [2] N. Lamaison, C. Tantolin et C. Paulus, «Experimental Solar District Heating Network Operation at CEA INES,» in *poster of the 5th International Solar District Heating Conference*, Graz, Austria, 2018.
- [3] R. Heimrath et M. Haller, «Project report A2 of subtask A : the reference heating system, the template solar system,» IEA SHC Task 32, 2007.
- [4] U. Jordan et K. Vajen, «Realistic domestic hot-water profiles,» IEA SHC Task 26, 2001.
- [5] U. Jordan et K. Vajen, «DHWcalc : Program to generate domestic hot water profiles with statistical means for user defined conditions,» chez *ISES Solar World Congress*, Orlando, US, 2005.
- [6] M. Airaksinen et M. Vuolle, «Heating energy and peak-power demand in a standard and low energy building,» *Energies*, vol. 6, pp. 235-250, 2013.
- [7] L. Giraud, R. Bavière, M. Vallée et C. Paulus, «Presentation, Validation, and Application of the DistrictHeating Modelica Library,» in *Proceedings of the 11th International Modelica Conference*, Versailles, France, 2015.
- [8] International Institute for Sustainability Analysis and Strategy, «Development of the primary energy factor of electricity generation in the EU-28 from 2010-2013,» Darmstadt, 2015, available at : http://www.iinas.org/tl_files/iinas/downloads/GEMIS/2015_PEF_EU-28_Electricity_2010-2013.pdf (accessed July 2018)



16th International Symposium on District Heating and Cooling, DHC2018,
9–12 September 2018, Hamburg, Germany

Method for allocation of carbon dioxide emissions from waste incineration which includes energy recovery

Danica Djuric Ilic^{a,*}, Louise Ödlund (former Trygg)^a

^a*Division of Energy Systems, Department of Management and Engineering, Linköping University, SE-581 83 Linköping, Sweden*

Abstract

Presently, waste is regarded as any other fuel in the Swedish district heating (DH) plants where it is treated in combination with energy recovery. Consequently, all carbon dioxide (CO₂) emissions that occur during waste treatment are allocated to DH producers even though two simultaneous services are provided – waste treatment and energy recovery. As the focus today is on phasing out fossil fuels from Swedish DH sector, energy recovery from waste turns out to be less desirable than heat production using biofuel and renewable electricity. This article discusses whether the existing allocation method of CO₂ emissions contributes to sustainable development and if it does not, to recommend a new method that will. To do this type of assessment, we used the principles from Framework for Strategic Sustainable Development. Results showed that the existing allocation method does not consider the problem of waste generation. The method shifts the responsibility from waste producers to DH customers. To prevent this ‘burden shifting’, a broader system perspective and an upstream approach should be applied. In addition, the method should be designed in ways that would give incentives to responsible stakeholders to act properly, which requires identifying the reasons why waste is not being recycled and to find a way to apply the allocation. Considering resource efficiency, waste treatment through combustion should always include energy recovery. To encourage energy recovery, the produced heat should not be burdened with CO₂ emissions.

© 2018 The Authors. Published by Elsevier Ltd.

This is an open access article under the CC BY-NC-ND license (<https://creativecommons.org/licenses/by-nc-nd/4.0/>)

Selection and peer-review under responsibility of the scientific committee of the 16th International Symposium on District Heating and Cooling, DHC2018.

Keywords: District heating, waste incineration, allocation method, case study

Abbreviations

CO₂ - carbon dioxide; CO₂eq - greenhouse gas emissions presented as CO₂ equivalent; DH - district heating; FSSD - Framework for Strategic Sustainable Development.

1. Introduction

District heating (DH) has several benefits [1], including the ‘economy of scope’, which refers to the possibility to use a secondary energy supply and fuels that are difficult to handle. Secondary energy supply comes from excess heat produced, for example, through industrial processes, thermal power stations, waste treatment, and electricity users (such as computer data centres). Sweden is a country with a well-developed DH sector (more than a half of the heat market), which opens up a possibility for building an effective national energy system with a high utilisation of secondary energy. Despite this fact, approximately two-thirds of the total primary energy used in Sweden in 2014 (e.g., approximately 1.3 EJ of 2 EJ) have been lost as excess heat [2]. Therefore, it should be a priority to use this excess heat before using electricity or direct fuels combustion for heating/DH production.

However, presently, DH derived from energy recovery from treating waste is considered to be negative in different climate and environmental evaluation systems. Two influential systems for evaluating the environmental impact of DH in Sweden are emission estimates according to the *Värmemarknadskommittén* (Heat Market Committee) agreement and certification of buildings in the environmental building certification system, *Miljöbyggnad*. The *Värmemarknadskommittén* agreement [3] is between the Swedish District Heating Association and the major trade associations for property owners in Sweden. The idea with the agreement is that the assessment of the climate impact and resource efficiency of DH production should be done in an orderly and common way for all DH networks in Sweden. The rules are handled by *Värmemarknadskommittén*, where representatives of DH and property owners participate. The environmental building certification system (*Miljöbyggnad*) is a well-established and frequently applied system for certification of buildings in Sweden, developed exclusively for Swedish conditions. One of the assessment criteria in the certification system is energy generation, where fuel used for heating has a major impact [4,5]. In both systems, waste is regarded as any other fuel used for DH production. Even though, during waste incineration two simultaneous services are provided – waste treatment and energy recovery. Waste is seen as a mixture of wood and coal, which is fired only to meet the DH demand. As the focus today is on phasing out the fossil fuels in the energy sector, energy recovery from waste is evaluated as bad for the climate compared to biofuel and renewable electricity used for heating/DH production.

1.1. Objective and scope of the study

The aim of the study is to recommend a method for allocation of carbon dioxide (CO₂) emissions from waste treatment in Swedish DH systems, which would help to establish a sustainable future. The study aims only to allocate the emissions between two simultaneous services – waste treatment and energy recovery. That is, the study does not aim to identify recipients of emissions that are not allocated to energy recovery and does not include recommendations on how allocation should be applied in practice.

2. Case study description

The analyzed system consists of Swedish DH sector (approximately 500 DH networks) and the waste generation and management system. In 2014 DH in Sweden accounted for more than 55% of the heat market. A large share of DH in Sweden is produced from biomass and excess heat (including the excess heat from waste treatment) [6]. Since the year 2002, when the Swedish parliament introduced landfill bans for combustible waste, the amount of the waste treated in combination with energy recovering start to increase [6, 7]. In 2015, approximately 5.8 million tonnes of the waste (40% municipal, 37% industrial, and 23% imported waste) was treated in Swedish DH plants (mostly combined heat and power plants) [8].

The Swedish waste management system is a part of the European waste management system and as such is highly subordinate to the European Energy and Climate policy [9]. The Swedish waste generation and management system consists of several stakeholders, such as product development companies, manufacturing companies, product users, stakeholders involved during the transportation of the products and the waste, as well as stakeholders involved in waste collection and disposal. The stakeholders interact with each other and their actions or decisions influence waste generation and treatment. For a more detailed description of the system see Djuric Ilic et al., [10].

3. Methodology

The topic was addressed by conducting a traditional literature review and by applying a framework called Framework for Strategic Sustainable Development (FSSD).

3.1. Framework for Strategic Sustainable Development (FSSD)

FSSD is an interpretation of Brundtland's definition of sustainable development: '... a development that meets the needs of the present without compromising the ability of future generations to meet their own needs' [11]. Development of FSSD was initiated by the international organization The Natural Step [12,13] in 1989. FSSD consists of sustainable principles that should be used as boundary conditions for the sustainable development. The sustainable principles cover all elements of social and ecological sustainability: 'In a sustainable society, nature is not subject to systematically increasing (1) concentrations of substances extracted from the Earth's crust, (2) concentrations of substances produced by society, (3) degradation by physical means, and, (4-8) in that society, people are not subject to conditions that systematically undermine their capacity to meet their needs' [12,13]. The last principle (the social principle) has lately been elaborated into five social principles [14,15]. Ny et al. [16] strongly recommend applying the FSSD when dealing with complex systems, such as management of materials, products, and waste. Applying the FSSD (1) enables avoiding sub-optimisation and future problems easier, (2) enables more effective management of system boundaries and trade-offs, and (4) opens up a possibility for developing strategic collaborations across disciplines and between stakeholders that may have different values and preferences (such as sectors, departments, and organisations) [17,16,18]. The FSSD includes a model that comprises the following five levels: system level, success level, strategic guidelines level, actions level, and tools level.

3.1.1 The system level

Identification of the system components, boundaries and surroundings, as well as identification of interactions between the system and system surroundings should be relevant in relation to the specific research question. Furthermore, it is important to consider how the system may change over time, especially in studies that include a long-term perspective [19, 20, 21], such as studies about sustainable development. System boundaries can be specified in different dimensions and may include different contents [22]. According to Tillman et al. [22], there are three approaches that can be applied when defining the contents of a system: process tree, technological whole system (includes even processes outside the process tree), and socio-economic whole system (includes economic and social factors). In many cases, the processes and the factors outside the process tree have more influence on the results than the factors within the process tree. However, Tillman et al. [22] recognised that the socio-economic whole system is rarely possible to apply because of its size, complexity, and many uncertain assumptions.

3.1.2 The success level

One of the principles to deal with sustainable development of a complex system is to apply backcasting [13, 17]. Backcasting starts with an imagined outcome in the future (the 'success') and continues by exploring strategic pathways to realize that outcome. Defining the desirable future by previously presented sustainable principles opens up a possibility for developing many future scenarios within the constraints of the principles

3.1.3 The strategic guidelines, actions, and tools levels

There are several principles that need to be considered when designing strategic pathways to reach the imagined sustainable future. Some of them are: to prefer an 'upstream approach', to apply 'step-by-step' approach to reduce the risk for being surprised by unpredictable trade-offs, to use 'flexible platforms' (flexible stepping stones for further activities), to prefer the actions that ensure return on investment (since less profitable strategies may slow down further development) and to consider social aspects by encouraging all actors in the system to act correctly. When designing strategic pathways, it is extremely important to attack problems by focusing on upstream of the cause-effect chains (i.e., to apply the 'upstream approach'). This means that the problems in the system should be solved by dealing with the cause of the problems (the primary problems) rather than by dealing with symptoms (the secondary problems that arise latter in the life cycle). By applying the 'upstream approach', possible future problems can be avoided. Furthermore, the complexity of the system is usually lowest at the beginning of a system (e.g., a life cycle), which makes it easier to introduce changes at those earlier stages [23, 13]. The last two steps in the FSSD is

to suggest actions and tools that may be used in line with the strategic guidelines. For a detailed description see Robèrt et al. [23, 13] and Broman and Robèrt [17].

3.2. Applying the FSSD

The analyzed system is described in section 2 (the system level). The system consists of Swedish DH sector and the waste generation and management system. The waste system is not geographically limited to Sweden, since a part of the waste that is treated in Sweden is imported from other countries. There are two sustainable goals (the success level) related to the analysed system: (1) to reduce the waste and (2) to use secondary energy supply (excess heat that otherwise would be lost) before using electricity or direct fuel combustion for DH production. UN DESA [25] stresses the importance to always deal with sustainability issues on a global level. Thus, due to the import of products and waste from other countries, when considering the possible strategies to reach the desirable outcomes, a global perspective was applied by discussing the sustainability issues in the exported countries as well.

Two well-known strategies that are developed to steer towards waste reduction are circular economy and waste hierarchy. The circular economy refers to a possibility for materials from old products to have a second life as recycled materials in new products [26]. The waste hierarchy is a framework for handling of waste, which shows in which order different measures related to the waste generation and disposal should be performed [27, 28]. The waste hierarchy presents the measures from the most favourable to the least favourable in following order: prevention, reuse, material recycling, energy recovery, and landfill disposal.

A strategy related to the sustainable development of the DH sector is the DH hierarchy. The fundamental idea of DH to meet customers' heating demands by using local fuels or excess heat that would otherwise be wasted [1]. Related to this, the DH hierarchy presents the possible sources for DH production from the most favourable to the least favourable: excess heat (from, e.g., industrial processes and waste treatments); inexhaustible renewable sources (geothermal and solar); exhaustible renewable resources (biomass); fossil fuels; and electricity [1].

Based on the sustainable principles and principles for sustainable development (see sections 3.1 and 3.1.3), following criteria were applied to recommend the allocation method which would steer towards sustainability:

- The allocation method should not lead to sub-optimization
- The allocation method must consider resource efficiency (the second sustainable principle, see section 3.1)
- The allocation method must apply an upstream approach
- The allocation method must consider social aspects (There is a lack of studies that consider waste prevention in relation to Life Cycle Assessment [29], despite the fact that social aspects can be decisive factors in implementing sustainable development measures [13]. Therefore, it is important for the allocation method to guide the stakeholders within the system into a behavior that would lead to global sustainable development.)

The waste delivered to DH producers was divided into different parts depending on the waste supplier. After this, each part of the waste is discussed based on the following questions:

1. Which stakeholders are involved in the life cycle of that part of the waste?
2. Which of the stakeholders can contribute to reducing the emissions from that part of the waste?
3. Which allocation method between two simultaneous services (waste treatment and energy recovering) would be most appropriate for that part of the waste, considering the previously selected criteria?

4. Recommending the allocation methods of carbon dioxide emissions from waste treatment that includes energy recycling

At present, waste is regarded as any other fuel in Swedish DH plants where it is treated in combination with energy recovery [30]. Consequently, all CO₂ emissions which occur during the waste treatment allocates to the energy recovery (the DH producers), even though two simultaneous services are provided, waste treatment and energy recovery [31]. Several studies analyzed a possibility to allocate emissions in another way [61, 62, 63, 64, 65], however, most of them do not apply upstream approach and do not consider social aspects. Applying the upstream approach involves detecting and managing the primary problems that cause other problems later in the system. Which problems are detected as the primary problems depends on the system boundaries. If in the present study system boundary includes only the plant where the waste is treated, the answer is that the primary problem are CO₂

emissions from the plant. Such an approach can lead to sub-optimization and adversely affect global sustainable development. If wider system boundaries are applied, the answer to the question is that the waste, or rather our actions that lead to waste generation, are the primary problems. Thus, the upstream approach involves measures aimed at waste production and producers. After discovering the primary problems, it is important to detect the responsible stakeholders (i.e. the polluters) and to apply the "Polluter Pays Principle" which means that the stakeholders that cause damage to the environment pay the socio-economic costs. Such a measure would give them incentives to act and to reduce the problems that they cause. In order to detect these stakeholders, the waste delivered to DH producers was divided into different parts depending on who is the waste supplier: waste which is rejected from material recycling industry, municipal waste, industrial waste, and imported waste.

4.1. Recommendation for allocation methods for waste that is rejected from material recycling industry

There is a part of the waste that is not recycled even though it has been sorted and sent to the material recycling industry. There are several reasons for rejecting the waste from the material recycling industry: (1) the waste cannot be recycled anymore, (2) the waste is not sorted properly, (3) it is unprofitable to perform the recycling, (4) is not environmentally friendly to perform the recycling because of energy-intensive recycling processes, and (5) the recycled material has no market.

According to the waste hierarchy (see section 3.2), after the waste is rejected from the material recycling industry, the second most advantageous alternative is waste incineration. Because of this, waste disposal in comparison with energy recovery can be considered as the primary service. Therefore, heat from waste treatment can be considered as excess heat from the process. Such an approach leads to the conclusion that all CO₂ emissions should be allocated to the waste disposal service and thus the excess heat from the process should not be charged with the emissions.

In order for the allocation method to be inspiring (i.e., to give incentives to the responsible stakeholders to 'do the right thing'), two challenges must be overcome: the challenge of assessing which stakeholder can help the waste not be rejected and the challenge of practically applying the allocation method itself.

To avoid the rejection of the waste because it is not properly sorted, the producers should include clear information on how the product should be sorted. In addition, the material recycling industry can include central sorting within its operations.

In some cases, it is unprofitable or technically impossible to recycle the waste. One of the reasons for this is that the quality of the recycled material decreases every time it is recycled [32]. Certain materials (such as aluminum) can be recycled many times before a quality deterioration is noted. However, quality of some materials significantly deteriorates after just a few recovery cycles [32]. Plastic, for example, can only be recycled three to four times before the quality deteriorates beyond usefulness [33, 34]. Similarly, paper quality deteriorates after just a few recyclings [32]. According to [35], there are two groups of problems related to the issue when it is impossible to recycle the waste: the problems related to delivered materials and the problems related to the recycling technology. An example of the problems related to materials is when the waste consists of a mixture of plastics (e.g., colored and non-colored plastics) [33, 36, 37]. Examples of problems related to the technology are the equipment's capacity and the inability to identify the specific plastic types [34]. These problems can be overcome by investing in a better recycling process, such as combination of automatic equipment and manual operators [35, 38, 39] or alternatively by implementing a labeling standard that would facilitate the sorting of the waste [40]. In this case, policy makers can play a decisive role. If the recycling process is expensive due to the complexity of the product, manufacturers and product developers can help solve the problem by making the product easier to repair, remanufacture, upgrade, and reuse [41, 42, 38]. This is also discussed in the next section.

According to the European Commission [26], the factor that probably represents the largest obstacle to increasing material recycling is the undeveloped market for recycled raw materials. This undeveloped market is the result of insufficient demand due to uncertainty related to the quality of the recycled material. Only about 5% of the plastic material used in the EU is recycled plastic [26]. The stakeholders that can help solve the problem are product developers who choose the raw material and product users who can indirectly affect the product developers' and producers' decisions. The role that these stakeholders can play is discussed in more detail in the next section. As mentioned, the reason that product developers and manufacturers more often choose a virgin material is that a

recycled material usually has poorer quality. In addition, as mentioned, material quality degrades every time it is recycled. Therefore, to be competitive, a material recycling company must deliver products to its customers with the right quality and quantity and at the right time [43]. To facilitate this, quality standards for recycled raw materials should be developed, and access to data on these materials should be improved. Important stakeholder that can contribute to this are policy makers. One possible action is to introduce a tax on virgin raw materials [44].

4.2. Recommendation for allocation methods for the municipal waste

Municipal waste that contains fossil materials can be divided into two different groups: waste that cannot be recycled and waste that is not sorted for recycling. According to Sundberg [32] and Gode et al. [45] there will always be a need for energy recovery to take care of: materials that cannot be recycled, waste from complex products, and contaminated materials that we do not want to get back into society (e.g. waste containing organic toxins, bacteria, such as diapers and hospital waste). Destruction of the non-recycled waste can be considered as a primary service in comparison to energy recovery; therefore, heat from the waste treatment can be considered as excess heat, so CO₂ emissions should not be allocated to the energy recovery service. Which actor could contribute to reducing this waste depends on several factors. The reasons why materials cannot be recycled can be different. One is that the material can no longer be recycled due to the deterioration in quality (explained in the previous section). Other examples are plastics that contain additives that destroy the quality of the plastic such as materials that includes toxic coloring agents or materials that are a mixture of two or more materials [33, 36, 37]. Product developers have a large possibility to reduce this type of waste.

According to Schögl et al. [46] and Shapira et al. [47], a comprehensive approach covering different sustainability criteria should be applied in the early stages of product development. The environmental impact that a product has over its life cycle is largely determined by decisions made during the design process. This illustrates the responsibility of product developers to design products with lower environmental impact. From this point of view, the choice of raw materials is one of the characteristics that can play a crucial role [43]. To reduce the waste from products that due to their complexity cannot be recycled (e.g., electronic devices such as computers and mobile phones), it is important to make products more durable and easier to repair, remanufacture, upgrade, and reuse [26]. Product developers have this responsibility [42, 43, 48, 49, 50].

Even policy makers can influence product design (e.g., choice of material through different taxes) as well as product users who are the ‘starting point’ for a product design [51], since they can ‘send a signal’ to product developers through, for example, rejecting products that consist of materials that cannot be recycled.

There is also a waste that can be recycled but which is not sorted. In 2014, approximately 36% of municipal waste in Sweden (about 1.6 million tonnes) was recycled. However, according to Avfall Sverige [52], the potential for recycling of household waste is much higher: about 60% to 80% depending on whether food is already sorted. Rousta and Ekström [53] conducted an analysis of environmental, economic, and social aspects of incorrect sorting of waste in a medium-sized Swedish city and concluded that approximately 68% of household waste sent to combustion plants could be sorted and sent to material recycling. It indicates that stakeholders who can contribute most to better recycling of the waste are primarily product users.

4.3. Recommendation for allocation methods for the industrial waste

Industrial waste consists of packaging or of the rest of the material used during the production processes. If material cannot be recycled because it consists of contaminated and toxic material, the ability to reduce that waste is limited and depends mostly on the type of industry. On the other hand, there is even a part of the industrial waste that could be recycled but was not sorted. That problem can be solved by including sorting as a part of the industrial processes. Long-term energy strategies in industry are of the utmost importance for implementing both technical and behavioral measures [54, 55, 56]. Despite this fact, several studies [57, 58, 59] have shown that long-term energy strategies on a business level have rarely been adopted, mostly because companies focus their efforts on their core business activities. A lack of a long-term energy strategy in a company indicates that it is most likely that the company does not have strategies for sorting the waste included in the production processes. To give the industry an incentive

to act properly by including sorting as part of their manufacturing processes, CO₂ emissions from waste management should be allocated to the industrial companies.

4.4. Recommendation for allocation methods for the imported waste

It remains unclear whether combustion of the imported waste in Swedish DH networks are a sustainable measure. The media is often critical when discussing this issue. On the other hand, there are advocates who emphasise that the energy recovery of imported waste reduces landfill and consequently greenhouse gases (e.g., methane) in Europe.

As sustainability must be considered from a global perspective [25], imports of waste lead to sustainable development if the alternative waste treatment in the exporting country results in higher greenhouse gas emissions than the waste treatment in the country that imports the waste. However, import/export of the waste under such a criterion presents only a flexible platform (see section 3.1.3) for further steps in sustainable development for both countries. In the long term, the exporting country should develop its own waste management system in line with the waste hierarchy. The country that imports waste can use waste heat from the waste treatment for DH production instead of using fuel directly (see description of DH production hierarchy in section 3.2). But in the future, when imported waste decreases, the boilers that combust waste can combust biomass instead.

According to [60], greenhouse gas emissions during transportation of the waste are usually insignificant compared to the reduction of greenhouse gas emissions due to energy recovery when landfill is the other option. Therefore, the impact on global greenhouse gas emissions when the waste is imported mainly depends on the alternative waste treatment in the country that exports waste. When waste is imported from the UK and Italy (where landfill is the most common waste management), global greenhouse gas emissions reduce by about 250 kg CO₂eq and 550 kg CO₂eq per tonne of waste. When the waste is imported from Poland, the reduction is 1100 kg CO₂eq per tonne of waste [60]. These numbers include methane from landfills. Due to this, the allocation method from the imported waste should consider alternative treatment of the waste in the exporting country. If the exporting country has a landfill ban, such as Norway, then there is no other alternative to combustion. Therefore, the same allocation method should be applied as for municipal waste (i.e., no emissions should be allocated to energy recovery service). Such allocation would provide an incentive for the exporting country to develop its own waste management systems in line with the waste hierarchy such as developing its own material recycling infrastructure.

If the exporting country has no a landfill ban, such as Great Britain, it is reasonable to allocate that fraction of combustion emissions that exceeds the greenhouse effect from the landfill option to energy recovery. Most often, combustion emissions are lower than greenhouse gases from landfills (e.g., landfills in Great Britain, Poland, and Italy) and in such cases no emissions should be allocated to energy recovery. The allocation method may also include greenhouse gas emissions from the waste transportation. In that case, emissions allocated to energy recovery would be as high as emissions during transport if the waste is imported from a country with a landfill ban. If the waste is imported from a country without a landfill ban, emissions allocated to energy recovery would be the sum of greenhouse gas emissions that occur during the transportation and that fraction of combustion emissions that exceeds the greenhouse effect from the landfill.

5. Conclusion

The existing method for allocation, where all CO₂ emissions from the waste treatment are allocated to energy recovery service does not consider the problem of waste generation. Therefore, a new method is required.

The new allocation method should apply an upstream approach and encourage all stakeholders in the system to act properly. It should give incentives (1) to production developers and producers to choose the right raw material and build products less complicated to repair and recycle, (2) to producer users to choose the right product and sort their waste better, (3) to material recycling industries to improve their processes, (4) to industrial companies to reduce the industrial waste by including waste sorting for recycling, (5) to district heating producers to always include energy recovery when performing waste treatment and to use excess heat from the energy recovery rather than electricity and direct fuel combustion. Since reducing the waste should be a priority, the emissions should be allocated to the stakeholders which contribute to the waste generation. To contribute to sustainable development, the allocation method should be combined with other measures, such as developing quality standards for recycled raw

materials or implementing a labeling standard that would facilitate the sorting of the waste. The same allocation method should be applied for waste imported from a country with a landfill ban. If the waste is imported from a country without a landfill ban, emissions allocated to energy recovery should be the sum of greenhouse gas emissions that occur during the transportation and the fraction of combustion emissions that exceeds the greenhouse effect from the landfill.

The study has its foundation in Swedish conditions. Since DH systems have local characters the recommendations about how to allocate CO₂ emissions can be useful only for countries with similar local conditions related to the DH sector as Sweden. Two of the most important local conditions which have the largest influence are that the biofuels and renewable electricity are the alternative ways of heat production, and that similar climate and environmental evaluation systems exist. On the other hand, the recommendations related to the possible measures on the waste generation side of the system, i.e. the measures which may lead to the waste reduction, are general and can be applied on a global level.

Acknowledgements

The research was financially supported by energy companies Göteborg Energi, Göteborg, Sweden and Tekniska Verken, Linköping, Sweden. The financial support is acknowledged.

References

- [1] Frederiksen, Svend, and Werner, Sven. "District heating and cooling." Studentlitteratur, Stockholm (2013)
- [2] Werner, Sven. "Energiförsörjning – En introduktion till vårt energisystem." Studentlitteratur AB, Lund (2016)
- [3] Värmemarknadskommittén. "Överenskommelse i värmemarknadskommittén 2013." (2013)
- [4] Miljöbyggnads Tekniska råd. "Miljöbyggnads bedömningskriterier för nyproduktion, Manual 2.2." (2014)
- [5] Miljöbyggnads Tekniska råd. "Miljöbyggnads bedömningskriterier för befintlig byggnad, Manual 2.2." (2014)
- [6] Werner, Sven. "District heating and cooling in Sweden." *Energy* 126 (2017): 419-429.
- [7] Furtenback, Örjan. "Demand for waste as fuel in the Swedish district heating sector: a production function approach." *Waste Management* 29(1) (2009): 285-292.
- [8] Avfall Sverige. "Svensk Avfallshantering." (2016).
- [9] Naturvårdsverket. "Från avfallshantering till resurshushållning - Sveriges avfallsplan 2012–2017." Naturvårdsverket. Rapport 6502 (2012).
- [10] Djuric Ilic, Danica; Eriksson, Ola; Ödlung, Louise; Åberg, Magnus. "No zero burden assumption in a circular economy." *Journal of Cleaner Production* 182 (2018): 352-362.
- [11] Brundtland, Gro. "Our Common Future: The World Commission on Environment and Development." Oxford University Press, Oxford. (1987)
- [12] The Natural Step, (2015). Available at: <http://www.thenaturalstep.org>
- [13] Robèrt, K.-H., Broman, G., Waldron, D., Ny, H., Byggeth, S., Cook, D., Johansson, L., Oldmark, J., Basile, G., Haraldsson, H., MacDonald, J. "Strategic leadership towards Sustainability." Blekinge Institute of Technology, Karlskrona, Sweden, Fourth Edition. (2007)
- [14] Missimer, M., Robèrt, K.-H., Broman, G. "A strategic approach to social sustainability – Part 1: exploring the social system." *Journal of Cleaner Production* 140(1) (2017): 32-41.
- [15] Missimer, M., Robèrt, K.-H., Broman, G. "A strategic approach to social sustainability – Part 2: principle-based definition." *Journal of Cleaner Production*, 140(1) (2017): 42-52.
- [16] Ny, H., MacDonald, J.P., Broman, G., Yamamoto, R., Karl-Henrik, R. "Sustainability Constraints as System Boundaries – An approach to making life-cycle management strategic." *Journal for Industrial Ecology* 10(1-2) (2006): 61-77.
- [17] Broman, G.I. and Robèrt, K.-H. "A framework for strategic sustainable development." *Journal of Cleaner Production* 140(1) (2017): 17-31.
- [18] Byggeth, S. and Hochschorner, E. "Handling trade-offs in Ecodesign tools for sustainable product development and procurement." *Journal of Cleaner Production* 14(15-16) (2006): 1420-1430.
- [19] Churchman, C.W. "The Systems Approach." Dell, New York. (1968).

- [20] Bertalanffy, L., Von. "The History and Status of General Systems Theory." *The Academy of Management Journal* 15 (1972): 407-426.
- [21] Ingelstam, L. "System – att tänka över samhälle och teknik." Swedish Energy and Lars Ingelstam, Kristianstad, Sweden (in Swedish). (2002).
- [22] Tillman, A.-M., Ekvall, T., Baumann, H., and Rydberg, T. "Choice of system boundaries in life cycle assessment." *Journal of Cleaner Production* 2 (1) (1994).
- [23] Robèrt, K.-H. "Tools and concepts for sustainable development, how do they relate to a general framework for sustainable development, and to each other?" *Journal of Cleaner Production* 8(3) (2000): 243-254.
- [24] Robèrt, K.-H., Schmidt-Bleek, B., Aloisi de Larderel, J., Basile, G., Jansen, J.L., Kuehr, R., Price Thomas, P., Suzuki, M., Hawken, P., Wackernagel, M. "Strategic sustainable development e selection, design and synergies of applied tools." *Journal of Cleaner Production* 10(3) (2002): 197-214.
- [25] United Nations Department of Economic and Social Affairs (UN DESA). "Guidance in Preparing a National Sustainable Development Strategy: Managing Sustainable Development in the New Millennium." Background Paper No. 13. (2002).
- [26] European Commission. "Closing the loop - An EU action plan for the Circular Economy." Communication from the commission to the European Parliament, The council, the European economic and social committee and the committee of the regions, Brussels (2015).
- [27] European Waste Directive 2006/12/EC of the European Parliament and of the Council of 5 April 2006 on waste
- [28] European Parliament and the Council of the European Union, 2008. Directive 2008/98/EC of the European Parliament and the Council of the European Union. Official Journal of the European Union. (2008)
- [29] Laurent, A., Bakas, I., Clavreul, J., Christensen, T.H. "Review of LCA studies of solid waste management systems - Part I: Lessons learned and perspectives." *Waste Management* 34 (2013): 573–588
- [30] IEA. *Energy Statistics Manual*. International Energy Agency (IEA), Head of Publications Service, Paris, France (2005).
- [31] IPCC. "Guidelines for National Greenhouse Gas Inventories" Prepared by the National Greenhouse Gas Inventories Programme, Eggleston H.S., Buendia L., Miwa K., Ngara T. and Tanabe K. (eds). Published: IGES, Japan (2006).
- [32] Sundberg, J. "Ökad materialåtervinning – Vad är energiutvinningens roll?" *Avfall Sverige*. Rapport E2013:08 (2013).
- [33] Gupta, P. "Fuels from plastics waste." *Popular Plastics & Packaging*, 56 (2011): 28-33.
- [34] Eriksson, O. and Finnveden, G. "Plastic waste as a fuel - CO₂-neutral or not?" *Energy & Environmental Science* 2 (2009): 907-914.
- [35] Elo K., Karlsson J., Lydebrant K., Sundin E. "Automation of Plastic Recycling – A case study" Sixth international symposium on EcoDesign: Environmental Conscious Design and Inverse Manufacturing, Sapporo, Japan (2009): 935-940.
- [36] Dodbiba, G. and Fujita, T. "Progress in separating plastic materials for recycling." *Physical Separation in Science & Engineering* 13 (2004): 165-182
- [37] Froelich, D., Maris, E., Haoues, N., Chemineau, L., Renard, H., Abraham, F., Lassartesses, R. "State of the art of plastic sorting and recycling: Feedback to vehicle design." *Minerals Engineering* 20 (2007): 902-912
- [38] Elo K. and Sundin E. "Requirements and needs of automatic material recycling of flat panel displays" *Green Care innovation*, Vienna, Austria, paper 107. (2010)
- [39] Elo K. and Sundin E. "Conceptual process development of automatic disassembly of flat panel displays for material recycling." *International conference in remanufacturing*, Glasgow, United Kingdom, (2011): 188-197.
- [40] Ahmad, S.R. "Marking of products with fluorescent tracers in binary combinations for automatic identification and sorting." *Assembly Automation* 20 (2000): 58-65.
- [41] World Trade Organization. "Market access for non-agricultural products - Negotiating NTBs Related to Remanufacturing and refurbishing." US (2005)
- [42] Sundin, E., Lindahl M., Ijomah, W. "Product design for product/service systems." *Journal of Manufacturing Technology Management* 20(5) (2009): 723-753.
- [43] Elo, K. "Automation in the recycling industry recycling of plastics and large liquid crystal displays." Licentiate thesis No.1583. Linköping studies and technology, Linköping (2013).

- [44] Rutkowski, J.E. and Rutkowski, E.W. "Recycling in Brasil: Paper and Plastic Supply Chain." *Resources* 6(3) (2017): 1-15.
- [45] Gode, J., Fredén, J., Adolfsson, I., Ekvall, T. "Värdering av fjärrvärmens resurseffektivitet och miljöpåverkan." Fjärrsyn, Svensk Fjärrvärme. Rapport 2013:3. (2013)
- [46] Schögl, J.-P., Baumgartner, R.J., Hofer, D. "Improving sustainability performance in early phases of product design: A checklist for sustainable product development tested in the automotive industry." *Journal of Cleaner Production* 140(3) (2017): 1602–1617.
- [47] Shapira, H., Ketchie, A., Nehe, M. "The integration of Design Thinking and Strategic Sustainable Development." *Journal of Cleaner Production* 140(1) (2017): 277–287.
- [48] Sodhi, M. och Knihgt, W.A. "Product Design for Disassembly and Bulk Recycling." *CIRP Annals - Manufacturing Technology* 47 (1998): 115-118
- [49] Bogue, R. "Design for disassembly: a critical twenty-first century discipline." *Assembly Automation* 27 (2007): 285-289
- [50] Suga, T. and Hosoda, N. "Active disassembly and reversible interconnection." *IEEE International Symposium on Electronics and the Environment* (2000)
- [51] Ashby, M.F. "Materials and the Environment – Eco-Informed Material Choice." Butterworth-Heinemann – an imprint of Elsevier USA (2013).
- [52] Avfall Sverige. "Svensk Avfallshantering 2015." Avfall Sverige. Malmö, Sverige (2015).
- [53] Rousta, K. and Ekström, K.M. "Assessing Incorrect Household Waste Sorting in a Medium-Sized Swedish City." *Sustainability* 5(10) (2013): 4349-436
- [54] McKane, A., Williams, R., Perry, W.T.L. "Setting the standard for industrial energy efficiency retrieved." (2007). December 9, 2009, from. <http://industrial-energy.lbl.gov/node/399>
- [55] Caffal, C. "Energy Management in Industry. In: Analysis Series 17." Centre for the Analysis and Dissemination of Demonstrated Energy Technologies (CADDET), Sittard, The Netherlands (1996).
- [56] Rohdin, P., Thollander, P. "Barriers to and driving forces for energy efficiency in the non-energy intensive manufacturing industry in Sweden." *Energy* 31(12) (2006): 1836-1844.
- [57] Thollander, Patrik, and Ottosson, Mikael. "Energy management practices in Swedish energy-intensive industries." *Journal of Cleaner Production* 18(12) (2010): 1125-1133.
- [58] Thollander, Patrik, and Ottosson, Mikael. "An energy efficient Swedish pulp and paper industry - Exploring barriers to and driving forces for cost-effective energy efficiency investments." *Energy Efficiency* 1(1) (2008): 21-34.
- [59] Thollander, P, Solding, P, Söderström, M. "Energy management in industrial SMEs." In: *Proceedings of the 5th European conference on economic and management of energy in industry (ECEMEI-5)*, (2009) 1-9.
- [60] Profu AB. "Perspectives on future waste treatment - Waste management in Sweden from 2013 onwards." Profu, Gothenburg, Sweden. (2013) Available at: www.wasterefinery.se
- [61] Gode, J., Ekvall, T., Martinsson, F., Särnholm, E., Green, J. "Primärenergi i avfall och restvärme." Svensk Fjärrvärme AB. Rapport 2012:5 (2012)
- [62] Martinsson, F., Gode, J., Ekvall, T. "Kraftvärmeallokeringar – en översikt." Svensk Fjärrvärme AB. Rapport 2012:8 (2012)
- [63] Gode, J., Fredén, J., Adolfsson, I., Ekvall, T. "Värdering av fjärrvärmens resurseffektivitet och miljöpåverkan." Fjärrsyn, Svensk Fjärrvärme. Rapport 2013:3 (2013)
- [64] Johansson, I. "Praktisk bedömning av allokeringsmetoder för avfallsförbränning." Avfall Sverige Utveckling. Rapport E2013:07 (2013)
- [65] Johansson, I. and von Bahr, B. "Ekonomisk allokering av emissioner och resurser vid avfallsförbränning med energiutvinning." Avfall Sverige. Rapport E2014:06 (2014)



16th International Symposium on District Heating and Cooling, DHC2018,
9–12 September 2018, Hamburg, Germany

Analysing district heating potential with linear heat density. A case study from Hamburg.

Ivan Dochev^a, Irene Peters^a, Hannes Seller^a, Georg K. Schuchardt^b

^a *HafenCity University, Überseeallee 16, Hamburg 20457, Germany*

^b *Klimaschutz- und Energieagentur Niedersachsen, Osterstr. 60, Hannover 30159, Germany*

Abstract

District heating (DH) can play a key role for a sustainable urban energy supply, especially in the presence of a building stock with high heat demands and several decades of useful life ahead. The economic viability of DH depends, among other things, on the distances between heat generators and customers and hence is not automatically given for each urban context.

Many decision support tools for energy planning are currently being developed, which, though differing in complexity, always contain some kind of heat atlas, or heat cadastre – a thematic map representing spatially disaggregated heat demand. We propose extending this approach, combining built environment and urban space layout so that heat demands can be connected to heat infrastructure. Specifically, we analyse the linear heat density (the annual heat demand per metre of grid length) in order to inform strategic heat planning. We use a heat demand atlas, the street layout of the city of Hamburg and an algorithm based on graph theory to group buildings according to their closest street segment and then generate hypothetical heating grid layouts, which connect all buildings within a group. These hypothetical grids represent potential small heating grids or likely modules of a grid. We then transfer the heat demand information from the heat demand atlas to these hypothetical heating grids. That way, we create a dataset containing aggregated groups of buildings, their heat demand and a plausible assumption as to the grid layout and length required to connect them. We then use this dataset in a case study of Hamburg, Germany to (i) identify where potential expansions of existing and construction of new DH grids could take place, (ii) estimate effects of increasing the connection density within urban areas currently supplied by DH and (iii) simulate grid expansions while preserving the current average linear heat density.

© 2018 The Authors. Published by Elsevier Ltd.

This is an open access article under the CC BY-NC-ND license (<https://creativecommons.org/licenses/by-nc-nd/4.0/>)

Selection and peer-review under responsibility of the scientific committee of the 16th International Symposium on District Heating and Cooling, DHC2018.

Keywords: Heat Density, Graph Theory, District Heating Expansion Potential

1. Introduction

District heating is recognized as a key technology for sustainable heat supply [1], even in areas with low energy buildings [2]. As district heating has a strong spatial element (due to the heat losses occurring in heat transport), it is no surprise that recent years have seen the emergence of GIS based tools for heat energy planning. Many municipalities develop a heat demand atlas (or heat “cadastre”) of their jurisdictions. These atlases are often based on urban energy demand models (UBEMs) [3], which in their simplest form are building stock models with energy-relevant data. In the following, we illustrate an expansion of the currently dominating approach such that the potential for district heating grids can be mapped and visualized.

2. Methodology

In this paper we use a UBEM, prepared as part of the GEWISS Project Hamburg [4]. It is based on the digital cadastre of the city of Hamburg (ALKIS), the building typology of the German Institute for Housing and Environment (IWU) for residential buildings [5] and the German VDI 3807 guideline [6] for non-residential buildings. Similar to many other building energy models [3,7] we use the ‘archetype’ approach, making use of building ‘archetypes’ which are allocated to cadastral objects. The ‘archetypes’ are typical buildings with energetic properties, usually derived from building samples. Buildings in the ALKIS are represented with a footprint geometry and attributes stored in a database. By allocating archetypes to cadastral objects, an estimation is made of the energetic characteristics of the cadastral objects. The quality of the estimation depends upon how well a building corresponds to its allocated ‘archetype’. The allocation of the ‘archetypes’ to cadastral objects is based upon characteristics of the buildings found in the cadastre that do not include energetic properties but are considered as proxies (obviously, if energetic properties were available for the cadastral objects, the archetypes would be unnecessary).

2.1. Modelling Residential buildings

We use the archetypes of the IWU for the residential buildings. The typology classifies the buildings into a matrix of 5 construction types, 12 construction epochs and 3 retrofit levels (baseline, standard 2014 energy retrofit and passive-house retrofit). For construction epoch, we use the building age found in the digital cadastre. To assign a construction type, we use the floor count and a building type classification found in the ALKIS. Estimating the level of retrofit is a bit of a challenge. We use available information on construction permits and building energy certificates to arrive at a plausible estimation. From our field studies for the GEWISS project we learnt that energy certification of individual buildings which are part of a housing cooperative (which make up large parts of the Hamburg building stock) is in many cases a signal that neighbouring buildings owned by the same cooperative are also retrofitted. Since ownership data is not available we use the plot structure to estimate where such cases could occur. Plots containing a building with an energy certificate are treated as ‘retrofitted’ and all buildings within the same plot receive the same status. Our second source of information on retrofit level – construction permits – is also available only at the plot level. This method is prone to errors, but it constitutes our best guess. Moreover, the exact type and depth of the retrofit is not known and we estimate a dichotomous – ‘yes’ or ‘no’. Given that the energy certificates are from the period 2002-2016 and the construction permits from 2014-2017, the retrofitted buildings most probably vary in their retrofitting. This, however, we cannot mirror with the defined retrofit levels of the IWU typology. We also consider it as too fine modelling for the purpose of our heat demand atlas and the amount of uncertainty associated with the archetype approach in general. With the allocation of the IWU archetypes and a dichotomous retrofit level a specific heat demand value in kWh/(m²*a) is assigned to each residential building in the cadastre. This value we then multiply with the residential floor area, which is the heat demand reference area for these buildings. The residential floor area we consider being equal to 80% of the gross floor area of any building. Mixed-use buildings we treat as half residential and half non-residential.

2.2. Modelling Non-residential buildings

Estimating the energetic properties of the non-residential building stock poses more of a challenge. Not only is there a lack of data on building retrofits, but building age itself is available for only a small portion of these buildings. The latter is perhaps less of a problem, since age correlates less with heat demand in the non-residential building sector as it does in the residential sector. Non-residential buildings are more heterogeneous in use, geometry and materials and hence are not as easily classified into ‘archetypes’. Due to a lack of important information we adopt a simplified approach and use specific heat consumption values from the German VDI 3807 guideline. These values are medians from samples of real measurements. They are grouped in ‘archetypes’ based only on building use, e.g. administrative buildings, schools, office buildings etc. and two refurbishment levels (“baseline” and “renovated”). The reference area for non-residential buildings in the typology we use (from the VDI 3807 guideline) is the gross floor area which we derive from the digital cadastre using floor count and footprint area without the need for further calculations.

2.3. Heat Demand Atlas Validation

We perform a two-step validation of the heat demand atlas. Since total heat demand is highly dependent on the size of a building, we first validate the estimation of the reference floor area. For the residential buildings, an external validation is possible using data from the 2011 census at the *Stadtteil*¹ level [8]. This data includes total residential floor area for each *Stadtteil*. We sum up the areas of the individual buildings from the heat demand atlas at the same geographic level (*Stadtteil*) and correlate the result with the census data (Fig.1. (a)). The fit of the regression line is very good with a high coefficient of determination ($r^2=0.99$). The equation with an intercept of zero shows that our model yields an estimated floor area that exceeds the census data by 5%. This is to be expected, given that our heat demand atlas is based on cadastral data from 2018, while the census data is from 2011 and the city of Hamburg has a vibrant real estate market with a lot of new construction every year (for German standards). Externally validating the non-residential floor area is not possible in this way, because the census gathers data only on the residential buildings. Using gross floor area as the reference area for the non-residential buildings reduces the risk of errors with these buildings. An issue exists however, which we still consider problematic – a building with multiple structures or bodies but a single mutual footprint (e.g. a shopping centre with two residential towers). With these buildings, the gross floor area, as we calculate it, would equal the footprint area times the number of floors, which will be an overestimation in many cases. Although this applies to only a small fraction of the building stock, it has very large impacts on some buildings, with total floor areas being off by a factor of 2 or 3. Surprisingly, using 3D data does not solve this problem. The 3D model of Hamburg (available freely online) in both Level of Detail 1 and 2 uses the footprint geometry of the ALKIS as basis and the issue gets propagated. While we are exploring ways to solve this issue, we neglect it for the purpose of this paper, as the effects are mostly local and isolated.

The second validation (Fig.1. (b)) of the heat demand atlas we perform at the city level, where we compare the estimated heat demand to monitored consumption values averaged over the years 2014, 2015 and 2016 [9–11]. It is well known that heat demand (estimates based primarily on transmission losses through the building shell) can greatly differ from real consumption. Therefore, caution has to be observed when comparing the two. In our case, however, the heat demand atlas uses consumption-corrected values for the residential buildings and consumption-based values for the non-residential buildings; hence, the heat demand atlas is comparable with the energy consumption statistics. We adjusted each year’s consumption to the long-term average for the Hamburg climate zone using a tool by the IWU based on degree-days from the German Meteorological Service [12] and averaged the result over the three years. We arrive at 17.3 TWh energy consumption for heating and domestic hot water for the entire building stock, excluding heat needed for industrial processes. The estimated heat demand from the heat demand atlas is 19.8 TWh (13% higher). For the residential buildings, this includes useful energy plus system losses without conversion losses so that it resembles the demand a building requires at its substation/heat transfer station.

¹ An administrative division, roughly equivalent to a neighbourhood. Our case study city of Hamburg is comprised of a circa 100 such *Stadtteile*.

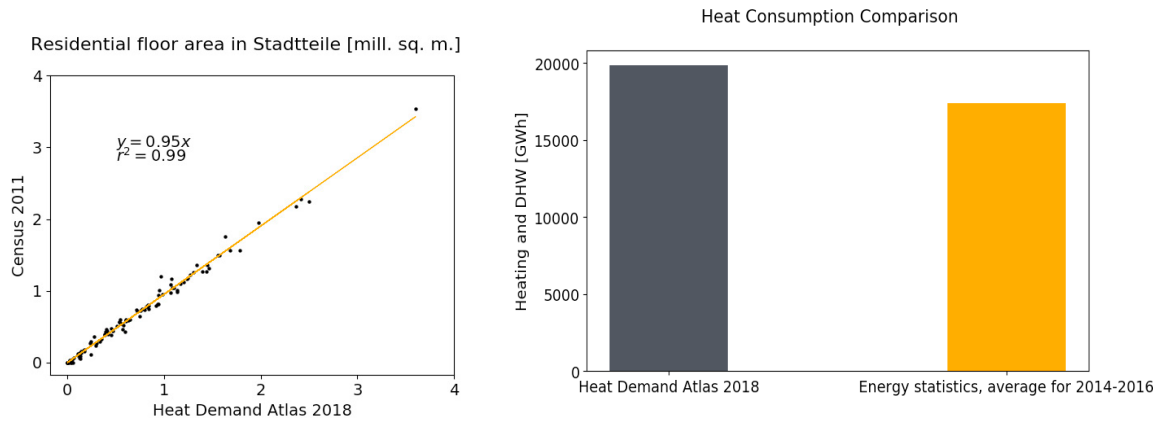


Fig. 1. (a) Correlation of residential floor area between estimations of our heat demand atlas and census 2011 at the *Stadtteil* level; (b) Heat Demand Atlas total heat demand compared to consumption values

The consumption-based specific heat demand of the non-residential buildings as given in the VDI 3807 includes also conversion losses. Note that the energy statistics for Hamburg do not differentiate between heat demand for space heating and domestic hot water (DHW) and so we had to use the estimated national split of end-energy into use categories [13] to estimate the amount of energy consumption only for heating and hot water. Generally, the heat demand atlas performs well. Both floor areas and total consumption come close to values provided in external sources. We decided not to adjust the heat demand totals with the 13% overestimate out of reasons of transparency of the numbers. The overestimation leads to slightly higher heat density, which we account for by considering more conservative cut-off values for it. Of course, total consumption at the city level averages out many of the discrepancies at lower levels. Since we could not validate the heat demand at various levels of aggregation, we consider the atlas good at city and district scales and assume a moderate performance at smaller neighbourhood or urban block scales. For individual buildings, the heat demand atlas can show large discrepancies, not only due to user behaviour problems but also due to the renovation level.

2.4. Linear heat density

Heat density (or Areal Heat Density) in the context of heat planning is usually defined as energy demand per hectare or square meter of urban space. It is used in many heat demand atlases, e.g. the Pan European Thermal Atlas (Peta) or the Saarland heat cadaster [14,15]. We propose using an alternative measure – linear heat density. Linear heat density of a heating grid is defined as the ratio between heat demand (or delivered heat if an existing grid) and heating grid length (supply and return pipes counted as one, also “trench length”). It can come in different units, we use MWh per meter and year - MWh/(m*a). Both types of density are used as indicators for the economic viability of a heating grid. The higher the density, the more heat can be delivered and sold over a unit of the grid, reducing losses and investment costs. Both density types give an important orientation as to a grid’s viability [16,17], although by far not the only decision parameter for the construction of a heating grid. Nevertheless, linear heat density has the advantage (over Areal Heat Density) that non-relevant urban spaces do not enter the measure. The usual problem with the Areal Heat Density (as in yearly energy per hectare of urban space) is the definition of the urban space, when it is actually used as a proxy for the needed grid length. Since the linear heat density directly uses grid length, we consider it as the superior measure of the two. Arriving at a measure for linear heat density requires, however, calculating the grid length. For existing grids, this is straightforward, but since our goal is to estimate potential for heating grid expansion, we need an estimation of the length of a potential new heating grid in areas without one. This we call *hypothetical grid modelling*.

2.5. Hypothetical Heating Grid Modelling

We use the term “hypothetical grid modelling” to refer to the generation of a 2D polyline geometry that connects a number of buildings to each other. An example can be found in [18]. The focus lies on estimating a plausible length and routing of pipelines. Apart from the need for geometry, linear heat density requires a defined building stock for a heating grid. In order to allow a more fine-grained spatial analysis that can be useful also at a local level, we divide the building stock into building groups and generate hypothetical grids for each group (see [19] for the importance of spatial resolution in energy system modelling). These building groups we consider as the buildings served by small heating grids or as groups of buildings served by a larger grid. By mapping the linear heat density for groups we can better analyse the areas which have potential for heating grids. The building groups are based on the plot structure and street layout of the city. The plot structure we consider, since it mirrors property-rights and it is likely that buildings within a single plot would be part of the same heating grid or heat supply solution. Since urban infrastructure and heat supply pipelines in particular usually traverse public spaces or streets we consider the street layout as a good starting point for estimating pipeline routes. We use the street centerlines from a 2D street model [20] and we group the building stock of Hamburg first into buildings with mutual plots and then mutual street segments. A street segment is a part of a street between two junctions.

After defining the building groups, we generate a 2D polyline geometry that connects the buildings in the group to each other, resembling a heating grid. There are a number of different heating grid layouts – radial, circular or multi-circular [21]. The radial grid layout has a main supply pipeline and individual substations/heat transfer stations connect to it. The circular grid layout is similar, but the main pipeline is in the form of a ring. With the multi-circular layout, the main pipeline has multiple rings. For the purposes of the hypothetical grid modelling, we use the radial grid layout, since the building groups are rather small and a ring layout is rarely used at this scale. Furthermore the groups we consider also as grid segments, therefore multiple radial layouts of building groups can be connected and thus form a ring layout. We model the grid layouts with each street segment being the radial, main pipeline. Of course, this is a form of simplification, but one that plausibly represents heating grid layouts. Next, we model the connections from the main pipeline (represented by the geometry of the street segment) to the buildings. We convert each building to a point. Most buildings in the ALKIS have a geographic location associated with their addresses, which in most cases represent the location of the entrance to the building. For the buildings that have this geographic location of the address point i , we use it to represent the possible geographic location of a substation/heat transfer station. For all others we use the centroid point of the geometry. We also project i onto a 2-meter buffer around the building and obtain a point j directly in front of the entrance to each building. This point j we use so that connecting pipes coming from the main pipeline do not (or at least more rarely) enter the buildings at all possible angles. The point j we connect to i (Fig. 2). We then use j to locate the nearest point along the street segment s . However, simply connecting each j to s fails in many locations where it would make more sense to connect a couple of buildings to each other first and then connect the group to the main pipeline. In order to have an algorithm that can decide this based on the concrete spatial constellation, we use an approach from graph theory – a minimum spanning tree (MST) [22]. An MST is a graph that connects each node from a set of nodes n that has a minimal length compared to all other graphs that span n . We use all the points j , s and the vertices of the street segment v as the set of nodes n and create an MST connecting all of them in an optimal (minimal length) way.

The geometry we create by converting the edges of the MST to polylines in 2D space. Since, in reality, optimal solutions are rarely possible, we reweight the distances between nodes so that the algorithm considers some practical aspects.

Firstly, in order to ensure that the main pipeline, represented by all the points s and v is always a continuous pipeline we decrease the distance between each of these points. Secondly, we increase the distances between buildings in different plots with a factor of 2. Note the horizontal distances between the nodes j for each building. In a non-weighted distance matrix each separate connection j to s would mean a non-minimal tree, since the optimal way would be to connect each point j to another point j on the same side of the street and then only one of them to the street segment. However, due to the weighting of the distances the algorithm considers the distance of j to another j as “longer” due to the factor of 2 stemming from the two being in different plots. This means the algorithm prefers connecting a building to the main pipeline or to a building within the same plot. This is in line with the general logic that cascaded

connections of multiple buildings are somewhat problematic when it comes to obtaining passage rights for the infrastructure from plot owners. Of course, buildings within the same plot, assumed as having one owner, are not subject to this problem. Generally, these rules can be applied without the use of a MST.

However, since the urban fabric is rather heterogeneous, having strict rules leads to illogical constellations of pipeline routes in some places. For this reason, we use the MST algorithm. It provides flexibility and introduces a tendency towards some rules, but retains the ability to break them if the spatial constellation demands it. In practical terms, the weighting allows the algorithm to connect a building (a) to another one (b) from a different plot, rather than the main pipeline, if a is more than twice as far away from the main pipeline as from b . These rules are a simplification of reality, but we consider them plausible when it comes to pipeline lengths and routes.

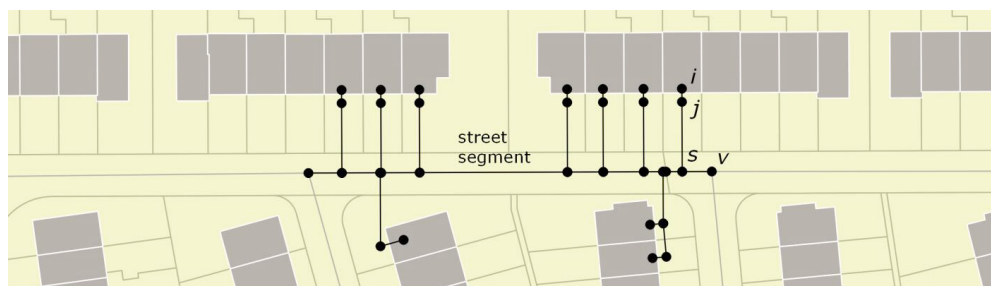


Fig. 2. Nodes of a hypothetical heating grid.

2.6. Hypothetical grids validation

We now compare the lengths of the generated hypothetical grids with lengths of existing grids of different sizes. In this way we estimate the plausibility of the algorithm. We use a vector polyline geometry of the existing main district heating grid of Hamburg, provided by the BUE. Hamburg has a large district heating grid and multiple smaller ones, we use the large one for a city-scale comparison and two smaller ones for a local scale comparison. We spatially intersect the buildings with the pipelines and obtain a subset of the building stock that is connected to each grid. We then use this subset of buildings as the input into our algorithm and generate hypothetical grids for it. We then compare the sum of the length of the hypothetical grids to the actual length of the existing grid. Note that the existing large grid has long main supply pipelines in the western part of the city that connect the coal-fired cogeneration-plant “Wedel” to the city centre. Since our algorithm is designed to estimate linear heat density it cannot directly tackle such specifics as the location of large power plants. Therefore, for the comparison, we manually take out some grid segments from the existing grids and compare only the areas that include a supplied building stock. The total length of the existing grid without these segments is 754 km (773 km with them). The generated hypothetical grids for the same building stock have a total length of 775 km, which is 3% higher than the 754 km of the existing grid (Table 1). This is probably due to the hypothetical grids using street segments, some parts of which are unnecessary and lead to rings within the grid. Having inner rings in the grid layout is observable for existing grids, but to a lesser extent compared to the hypothetical ones. Nevertheless, we consider this a good approximation that allows the use of the algorithm for city-scale analysis of densities and lengths.

Next, we test the performance at a local scale. For this, we compare the lengths of two existing small heating grids to the sum of hypothetical grids for the two respective building stocks (Fig. 3 and Table 1.). The first of the smaller grids is in an area of mainly single-family houses, while the second is in an area with large apartment blocks. In this way, we attempt to validate the results also in different urban settings. Although the grid lengths are close to the existing ones, there are discrepancies when it comes to the layouts of the hypothetical grids. In the area with single-family houses, the pipeline routes of the hypothetical grids are closer to the routes of the existing grids. We expected this, since the algorithm is heavily depending upon the street layout and it is logical that it performs better in areas where the existing grids also follow this pattern. Nevertheless, in the second area, the grids also have overall plausible layouts. Note that the hypothetical grids do not connect all buildings in the two examples. This is the case, since the algorithm divides the building stock into smaller sets of buildings and aims at connecting only them. We defined the

algorithm in this way so that it divides the building stock into sub-stocks for which densities can be estimated, rather than create a single grid for a whole input building stock. The latter would mean that densities are averaged out between the different areas of a city, which doesn't allow the analysis of different areas within a city. Overall we consider the algorithm to be useful for estimating linear heat densities. It is not however suited for the planning of a particular grid with exact routing and pipe dimensioning or similar more “concrete” planning tasks.

Table 1. Comparison of total grid lengths of existing grids and the corresponding hypothetical grids.

Type of grid used for validation	Length (Existing) [km]	Length (Hypothetical) [km]	Deviation in %
Main district heating grid	754.0	775.0	+3%
Small grid with single-family houses	16.4	14.4	-13.3%
Medium sized grid with multifamily buildings	21.0	20.4	-3%

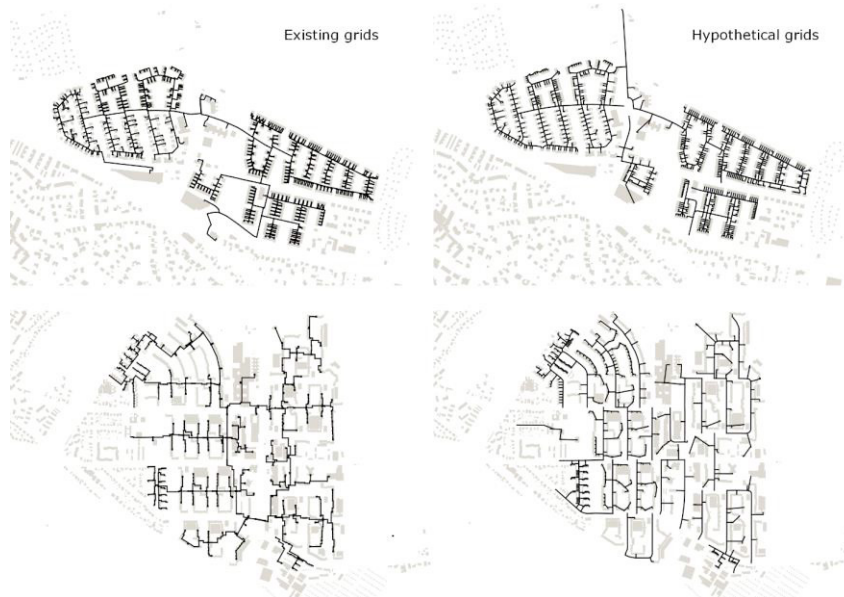


Fig. 3. Existing and hypothetical heating grids.

3. Case study Hamburg

After validating the proposed algorithm, in this section, we apply it to the city of Hamburg in order to show how it can be used for exploring different planning issues. Running the hypothetical heating grids algorithm for the entire building stock of Hamburg together with the street layout resulted in 18 000 building groups and a hypothetical grid for each of these groups. Generally, a value of 1.5 MWh/(m²a) as a cut-off for grid viability is considered a rule of thumb [19,23]. This is an orientation value. It means grids with lower density are less viable since potential investment costs and grid losses become too great in relation to the delivered heat. We adopt a more conservative approach and consider a cut-off value of 2.5. Not surprisingly the central parts of the city showed the highest grid density, but there were numerous other areas with high density and therefore potential for district heating, even given our conservatively chosen cut-off.

3.1. Grid expansion and new grids

Hypothetical grid modelling is especially useful in conjunction with other data to address different planning questions. In this section we overlay the higher density hypothetical grids (>2.5 MWh/(m²a)) with the existing grids

(Fig. 4 left) and urban areas planned for new residential construction [24] (Fig. 4 right). The first map allows the localization of areas, close to the existing grids with high linear heat density, which constitute areas for potential expansion (e.g. the orange ovals in the figure). The second map brings also another aspect into play – finding areas, where new developments can be used as triggers for new grids that combine new and existing buildings.

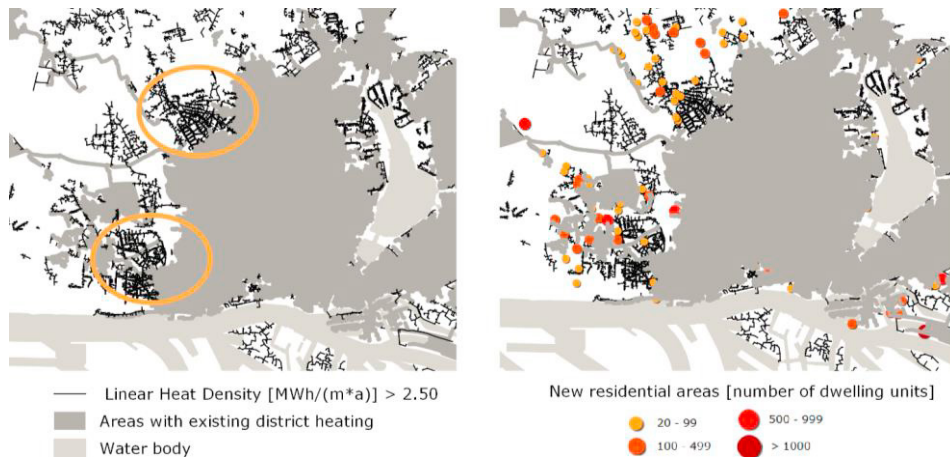


Fig. 4. Hamburg city centre. Analysing potential areas for grid expansion in combination with planned new residential areas.

3.2. Connection density within currently supplied areas

Another application of the hypothetical heating grids is analysing possible unused potential within areas with existing grids. There are many buildings in Hamburg that use other forms of heat supply, although in an area with an existing heating grid. In this case the hypothetical heating grids can be used to analyse the impact of connecting **all** buildings within already supplied areas. Currently the total length of all heating grids is 1 200 km with 4.4 TWh average early heat consumption [11] (corrected with degree days and averaged over the period 2014-2016). This leads to a linear density of 3.7 MWh/(m*a). We defined all buildings within a 40m buffer around the existing grids as “buildings within areas with existing district heating”. We then ran the hypothetical grids with this subset of buildings as inputs. The results show a total grid length of 1800 km (+50%), a total heat demand (consumption-corrected) of 7.5 TWh (+59%) and an average density of 4.2 MWh/(m*a) (+12%). This means that there is considerable potential within these areas – currently around 22% of the demand is covered by district heating (4.4 TWh from the estimated 19.8 TWh of the atlas), while this could potentially be 7.5 TWh or 38% and it would also lead to a higher average density. Note that the hypothetical heating grids tend to overestimate lengths at this scale and one could possibly connect these buildings with less new pipeline length.

3.3. Grid expansion simulation

Lastly, we use a simple simulation algorithm to locate grid expansions using the hypothetical grids. We take as input the areas with existing heating grids as polygons (using the 40m buffer to convert the polylines into polygons). We then rank all the hypothetical grids outside these areas according to their distance to an existing grid area. We iterate over the hypothetical grids and if a hypothetical grid has a linear heat density over the current city average of 3.8 MWh/(m*a) we connect the hypothetical to the existing grid using a straight line. Note that the linear heat density of each hypothetical grid is updated with the segment needed to connect it to the closest existing grid **before** the comparison with the city average. We then update the existing grids so that the hypothetical grid from the previous step is counted as “existing”. We proceed with this expansion logic for all hypothetical grids. The results are presented in Fig. 5. The simulated expansions amount to 484 km and a total yearly heat demand of 3174 GWh/a (72% of the current district heating consumption) with a density of 6.5 MWh/(m*a), which is significantly higher than the current

average. These numbers suggest high potential outside currently supplied areas. Spatially, the expansions are dispersed in different areas of the city. This simulation uses a simplified logic and the entire simulated expansion is most likely not plausible. Nevertheless, this simulation provides an overview of where potentials in urban space lie and is a way of generating ideas about possible future developments.

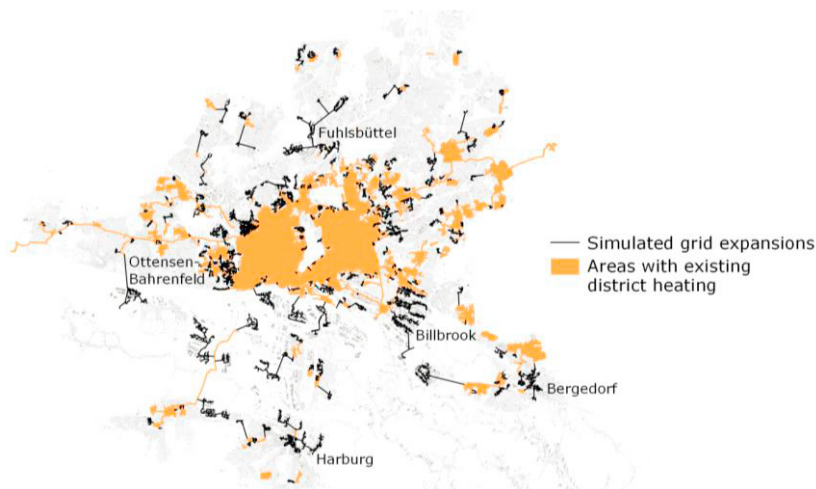


Fig. 5. Grid expansion simulation

4. Conclusion

The goal of the method presented here is to estimate linear heat density in urban space. The linear heat density we consider as a signal for economic viability. Mapping and presenting it can be a way of motivating, giving ideas to or simply bringing together relevant public and private actors. This can support efforts for sustainable heat supply, in this case, the use of district heating. The hypothetical grid modelling we presented is a conceptually straightforward and easily implemented way for estimating linear heat density. Using only a heat demand atlas and the street network as inputs, we managed to map the linear heat density of the entire city of Hamburg. Both the heat demand atlas and the estimated grid lengths we validated against real-world data, which showed a good fit. Of course, the application of this hypothetical linear heat density has its limitations. Important aspects concerning the construction of district heating grids are omitted – e.g. situation of the underground and costs connected with different types of construction. Furthermore, we do not analyse actual economic viability but use the ratio of heat demand and grid length (linear heat density) as a proxy for it. This has the disadvantage that external economic factors (e.g. energy prices) are not considered. On the other hand, district heating grids are a long-term infrastructure that has to be planned with certain economic robustness. Since linear heat density is relatively fixed and not as volatile as energy prices, we consider it plausible to use it as a proxy. Additionally, expected heat deliveries over the coming decades could be a more important parameter than current energy prices, as they also implicate resource efficiency independent of prices. Also, for the decision and potential to construct heating grids, there are other aspects than economics. Institutional issues such as existing heat delivery contracts and plot easements can stand in the way of heating grid expansions. Therefore, it is important to use this method for its specific purpose – mapping and presenting linear heat density as a way of communicating potentials in urban space and providing orientation of economic viability of district heating grids.

Acknowledgements

This research paper was prepared as part of the GEWISS Project Hamburg, funded by the German Federal Ministry for Economic Affairs and Energy (BMWi). It is based in large parts on the Master Thesis of the first author, which was supported by the Hamburg Ministry for Environment and Energy (BUE).

References

- [1] Agora Energiewende. *Heat Transition 2030: Key technologies for reaching the intermediate and long-term climate targets in the building sector*. Available at: https://www.agora-energiewende.de/fileadmin/Projekte/2016/Sektoruebergreifende_EW/Heat-Transition-2030_Summary-WEB.pdf; 2017 [accessed 17.04.2018].
- [2] Sandvall AF, Ahlgren EO, Ekvall T. Cost-efficiency of urban heating strategies – Modelling scale effects of low-energy building heat supply. *Energy Strategy Reviews* 2017;18:212–23, doi:10.1016/j.esr.2017.10.003.
- [3] Reinhart CF, Cerezo CD. Urban building energy modeling – A review of a nascent field. *Building and Environment* 2016;97:196–202, doi:10.1016/j.buildenv.2015.12.001.
- [4] GEWISS Project. *GEWISS Geographisches Wärmeinformations- und Simulationssystem [Geographical Heat Information and Simulation System]*. Available at: <http://gewiss.haw-hamburg.de/>; 2018.
- [5] Loga T, Stein B, Diefenbach N, Born R. *Deutsche Wohngebäudetypologie [German residential building typology]: Beispielhafte Maßnahmen zur Verbesserung der Energieeffizienz von typischen Wohngebäuden*; 2015.
- [6] The Association of German Engineers. *Characteristic consumption values for buildings: Characteristic heating-energy, electrical-energy and water consumption values*; 91.140.10, 91.140.50, 91.140.60. Berlin: Beuth Verlag; 2018. Available at: http://www.vdi.eu/nc/guidelines/vdi_3807_blatt_2-verbrauchs-kennwerte_fuer_gebaeude_verbrauchs-kennwerte_fuer_heizenergie_strom_und_wasser [accessed 16.05.2018].
- [7] Li W, Zhou Y, Cetin K, Eom J, Wang Y, Chen G, Zhang X. Modelling urban building energy use: A review of modelling approaches and procedures. *Energy* 2017;141:2445–57, doi:10.1016/j.energy.2017.11.071.
- [8] Statistics Office for Hamburg and Schleswig-Holstein. *Stadtteil Profile 2015*. Available at: https://www.statistik-nord.de/fileadmin/Dokumente/Datenbanken_und_Karten/Stadtteilprofile/Stadtteilprofile-Berichtsjahre-2007-2015.xlsx; 2015 [accessed 16.05.2018].
- [9] Statistics Office for Hamburg and Schleswig-Holstein. *Energiebilanz und CO₂-Bilanzen für Hamburg 2014 [Energy and CO₂ balance for Hamburg 2014]*. Available at: https://www.statistik-nord.de/fileadmin/Dokumente/Sonderver%C3%B6ffentlichungen/Energie-_und_CO2-Bilanz_Hamburg/EB_CO2_HH_2014.pdf; 2016 [accessed 17.07.2018].
- [10] Statistics Office for Hamburg and Schleswig-Holstein. *Energiebilanz und CO₂-Bilanzen für Hamburg 2015 [Energy balance and CO₂ balance for Hamburg 2015]*. Available at: https://www.statistik-nord.de/fileadmin/Dokumente/Sonderver%C3%B6ffentlichungen/Energie-_und_CO2-Bilanz_Hamburg/EB_CO2_HH_2015.pdf; 2017 [accessed 17.07.2018].
- [11] Statistics Office for Hamburg and Schleswig-Holstein. *Energiebilanz und CO₂-Bilanzen für Hamburg 2016 [Energy balance and CO₂ balance for Hamburg 2016]*. Available at: https://www.statistik-nord.de/fileadmin/Dokumente/Sonderver%C3%B6ffentlichungen/Energie-_und_CO2-Bilanz_Hamburg/EB_CO2_HH_2016.pdf; 2018 [accessed 17.07.2018].
- [12] Institut Wohnen und Umwelt. *Gradtagszahlen Deutschland [Degree days in Germany]: Klimadaten auf Basis von Deutscher Wetterdienst, Offenbach - www.dwd.de*. Available at: http://t3.iwu.de/fileadmin/user_upload/dateien/energie/werkzeuge/Gradtagszahlen_Deutschland.xls; 2018 [accessed 30.05.2018].
- [13] Arbeitsgemeinschaft Energiebilanzen e.V. *Anwendungsbilanzen für die Endenergiesektoren in Deutschland in den Jahren 2013 bis 2016 [Final energy consumption by sector and type of use in Germany in the period 2013 2016]*. Available at: https://ag-energiebilanzen.de/#ageb_-_zusammenfassender_bericht_fu_r_die_endenergiesektoren_2013_-_2016; 2017 [accessed 17.07.2018].
- [14] Heat Roadmap Europe 4 Project. *Pan-European Thermal Atlas 4.2*. funded by the Horizon 2020 Programme of the European Union. Available at: <http://heatroadmap.eu/peta4.php>; 2017 [accessed 17.07.2018].
- [15] Institut für ZukunftsEnergieSysteme. *Wärmekataster Saarland [Heat Demand Cadastre Saarland]*. Available at: http://geoportal.saarland.de/mapbender/frames/index_ext.php?gui_id=Template_GDZ&WMC=3761#; 2017 [accessed 17.07.2018].
- [16] Andreas Pfnür, Bernadetta Winiewska, Bettina Mailach, Bert Oschatz. *Dezentrale vs. zentrale Wärmeversorgung im deutschen Wärmemarkt [Decentralized vs centralized heat supply in the German heating market]: Vergleichende Studie aus energetischer und ökonomischer Sicht*. Arbeitspapiere zur immobilienwirtschaftlichen Forschung und Praxis. Darmstadt: Technische Universität Darmstadt, Forschungscenter Betriebliche Immobilienwirtschaft; 2016.
- [17] Jalil-Vega F, Hawkes AD. Spatially resolved model for studying decarbonisation pathways for heat supply and infrastructure trade-offs. *Applied Energy* 2018;210:1051–72, doi:10.1016/j.apenergy.2017.05.091.
- [18] Dochev I. *Significance of the accuracy of building heat demand estimations for the planning of heating grids*. Hamburg; 2017.
- [19] Jalil-Vega F, Hawkes AD. The effect of spatial resolution on outcomes from energy systems modelling of heat decarbonisation. *Energy* 2018;155:339–50, doi:10.1016/j.energy.2018.04.160.
- [20] Hamburg Ministry for Economic Affairs, Transport and Innovation. *Strasseninformationsdatenbank Hamburg [Hamburg Street-Information-Database]*. Available at: http://daten-hamburg.de/transport_verkehr/strassen_und_wegenetz/Strassen_und_Wegenetz_HH_2017-02-28.zip; 2017 [accessed 22.05.2018].
- [21] Dötsch C, Taschenberger J, Schönberg I. *Leitfaden Nahwärme [Guidelines for small-scale district heating]*. Stuttgart: Fraunhofer-IRB-Verl; 1998.
- [22] Kruskal JB. On the shortest spanning subtree of a graph and the traveling salesman problem. *Proceedings of the American Mathematical Society* 1956;48–50, doi:10.1090/S0002-9939-1956-0078686-7.
- [23] Nast M, Harald D, Hartmann H, Kelm T, Kilburg S, Mangold D, Winter H. *Evaluierung von Einzelmaßnahmen zur Nutzung erneuerbarer Energien im Wärmemarkt (Marktanreizprogramm) im Zeitraum Januar 2007-2008 [Evaluation of single measures for the use of renewable energy sources in the heating market]*. Available at: [http://www.dlr.de/tt/Portaldata/41/Resources/dokumente/institut/system/publications/MAP-Endbericht_2007-2008_\(ohne_Anhang\).pdf](http://www.dlr.de/tt/Portaldata/41/Resources/dokumente/institut/system/publications/MAP-Endbericht_2007-2008_(ohne_Anhang).pdf); 2009 [accessed 22.05.2018].
- [24] Hamburg Ministry for Urban Development and Housing. *Wohnungsbauflächenpotenziale [Planned Residential Building Areas]*. Available at: <http://metaver.de/trefferanzeige?docuid=8223B7BD-D194-4230-B436-1607D3BF3BC5>; 2017 [accessed 22.05.2018].



Available online at www.sciencedirect.com

ScienceDirect

Energy Procedia 149 (2018) 420–426

Energy

Procedia

www.elsevier.com/locate/procedia

16th International Symposium on District Heating and Cooling, DHC2018,
9–12 September 2018, Hamburg, Germany

Optimizing Efficiency of Biomass—Fired Organic Rankine Cycle with Concentrated Solar Power in Denmark

Andreas Zourellis^{a*}, Bengt Perers^b, Jes Donneborg^c and Jelica Matoricz^d

^{a,c,d} Aalborg CSP A/S, Hjulmagervej 55, 9000 Aalborg, Denmark

^b Department of Civil Engineering, Technical University of Nordvej Building 119, 2800 Kgs. Lyngby, Denmark

Abstract

A first of its kind concentrated solar power (CSP) installation has been integrated together with a biomass heat and power (CHP) plant using an organic rankine cycle (ORC) unit. The plant has been deployed in the northern part of Jutland in Denmark, right next to the city of Brønderslev. The plant has been supplying heat to the local district heating network since the end of 2016. Aalborg CSP has developed and built the CSP plant consisting of parabolic trough collectors with an aperture reflecting area of 26,920 m². The CSP plant is able to deliver 16.6 MWth at its peak while it can supply the district heating or the ORC with approximately 16,000 MWh of heat annually. This paper serves as a description of the technical aspects of the system with specific focus on the CSP field as well as present the first measured performance from the Summer of 2017.

© 2018 The Authors. Published by Elsevier Ltd.

This is an open access article under the CC BY-NC-ND license (<https://creativecommons.org/licenses/by-nc-nd/4.0/>)

Selection and peer-review under responsibility of the scientific committee of the 16th International Symposium on District Heating and Cooling, DHC2018.

Keywords: Solar Energy, Concentrated Solar Power, CSP, Concentrated Solar Heat, CSH, Solar-Thermal, Integrated Energy System, Organic Rankine Cycle, ORC, Biomass

* Corresponding author. Tel.: +45 50 30 00 25

E-mail address: azo@aalborgcsp.com

1. Introduction

Solar energy is abundant and increasingly utilized in domestic systems to supply space heating and cooling. However, over the last couple of decades the world energy demand has increased dramatically due to both industrial growth and population increase.

1.1 Concentrated Solar Power in Denmark

Concentrated solar power (CSP) plants have so far mainly been built to produce electricity for export to the grid, however, numerous advantages have been identified in industrial setting as well. Due to the technology’s flexibility to produce high and mid temperature heat, it provides an ideal solar-thermal solution for industrial purposes. Parabolic trough CSP plants are typically found in countries around the solar belt, but economic viability has also been proven in a place with limited solar resources, in Denmark, where efficiency of the system was monitored and compared with flat solar-thermal panels. The report concluded that CSP produces more energy per square meter above 50 °C, provides a better economy over the system’s 25-years lifetime and ensures a year-round energy production even in Nordic climate conditions compared to flat panel systems [1]. It has also be seen that even when operating in higher temperature the parabolic trough collectors maintain a high heat yield per square meter or aperture area [2], [3]. That is because the heat is concentrated in a central receiver tube enclosed in a vacuum glass envelope.

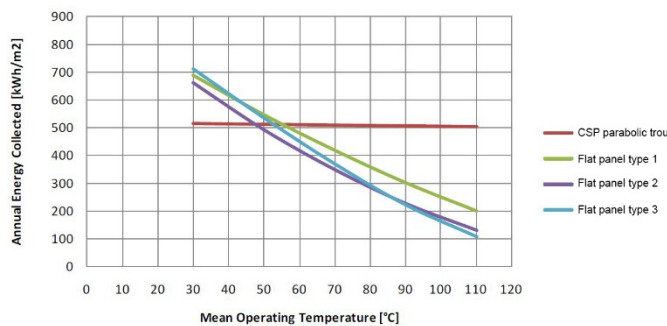


Figure 1: Parabolic trough collector performance vs. flat plate collectors in low heating temperatures

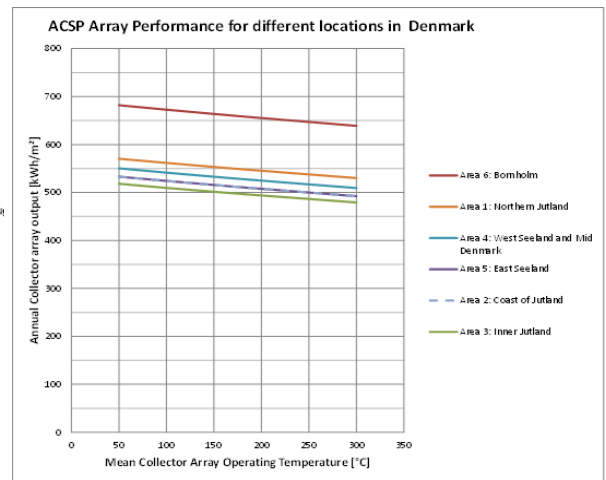


Figure 2: Parabolic trough collector performance in different Danish regions and high temperatures [3]

2. Technology description

2.1. Parabolic Trough Collectors (PTC)

The parabolic troughs reflect the rays of the sun onto a receiver pipe filled with heat transfer fluid. The receiver pipe is located in the central focal point of the troughs. In the receiver pipe, the fluid is heated up and pumped into the heat consumer.

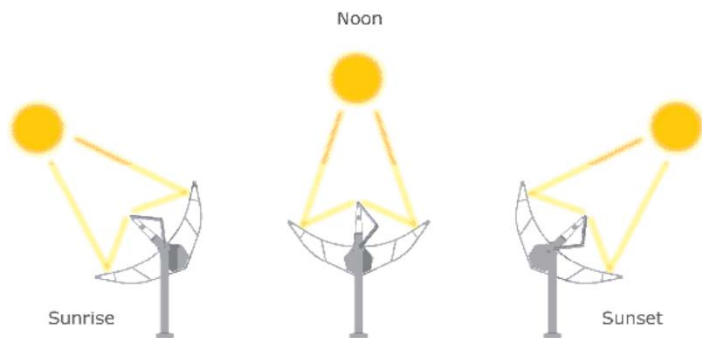


Figure 3: Sun tracking technology enabling the parabolic troughs to follow the sun's position throughout the day

placement. The PTCs track and follow the sun in a tracking window of $\pm 0.15^\circ$ from the present solar position. The rotation is ensured by a gear and a hydraulic system.

2.2. The system

In December 2016, a world first CSP plant went into operation in the northern part of Denmark (town of Brønderslev). The plant's uniqueness lies in the fact that it was designed to be integrated with a biomass-fired Organic Rankine Cycle (ORC) which is currently still under the last stages of commissioning. This combined solution is the first large-scale system in the world to demonstrate how CSP, with an integrated energy system design can optimize efficiency of ORC even in areas with less sunshine, in this case Denmark.



Figure 4: Image of the concentrated solar power plant in Brønderslev, Denmark

The CSP technology is the most effective solar heating method for high temperature ranges. The parabolic troughs has a special glass vacuum tube guaranteeing some of the markets lowest heat losses thus providing stable energy production even at middle temperatures as the receiver pipe has very low heat losses to the ambient.

The parabolic trough uses a custom-made sun-tracking technology, where a computer calculates and calibrates the troughs into the required position to receive optimal radiation throughout the day. The sun-tracking technology achieves a very high efficiency per m^2 of aperture mirror area, thereby optimizing the use of land intended for technology

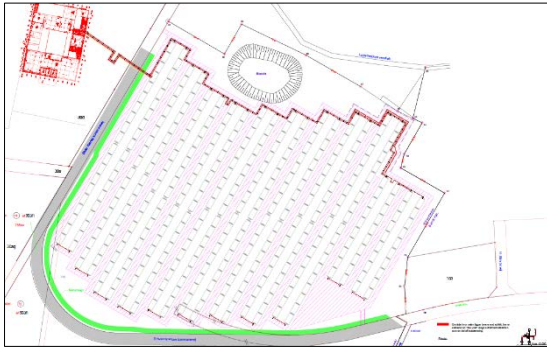


Figure 5: Top view of the solar field layout



Figure 6: Photo of the AAL-Trough™ 3.0 model - third generation of Aalborg CSP's parabolic trough technology

The solar energy plant was delivered by Danish renewable energy specialist Aalborg CSP, and it is based on the company's own CSP parabolic trough technology, also called the AAL-Trough™. The plant consists of 40 rows of 125m U-shaped mirrors with an aperture area of 26,929 m². These 40 rows are divided in 10 loops. Each loop has an inlet and outlet connection to the main pipe, meaning that the cold thermal oil will flow through 4 rows (i.e. 500m) until it gets the right temperature and finally leaves the loop. In order to fit within the land boundaries the loops were bended into half, saving cost for extra piping at the same time. As seen in Figure 5 the solar field is tilted 29° from the North-South axis due to specific land availability.

The curved mirrors collect the sunrays throughout the day and reflect them onto a receiver pipe, which sums up to 5 kilometer receiver tubes. This receiver pipe is surrounded by a special glass vacuum tube and inside this runs - only heated by the sun - thermal oil with temperatures up to 312 °C. This high temperature is able to drive an electric turbine to produce electricity, but the flexibility of the system also allows production of lower temperatures for district heating purposes.

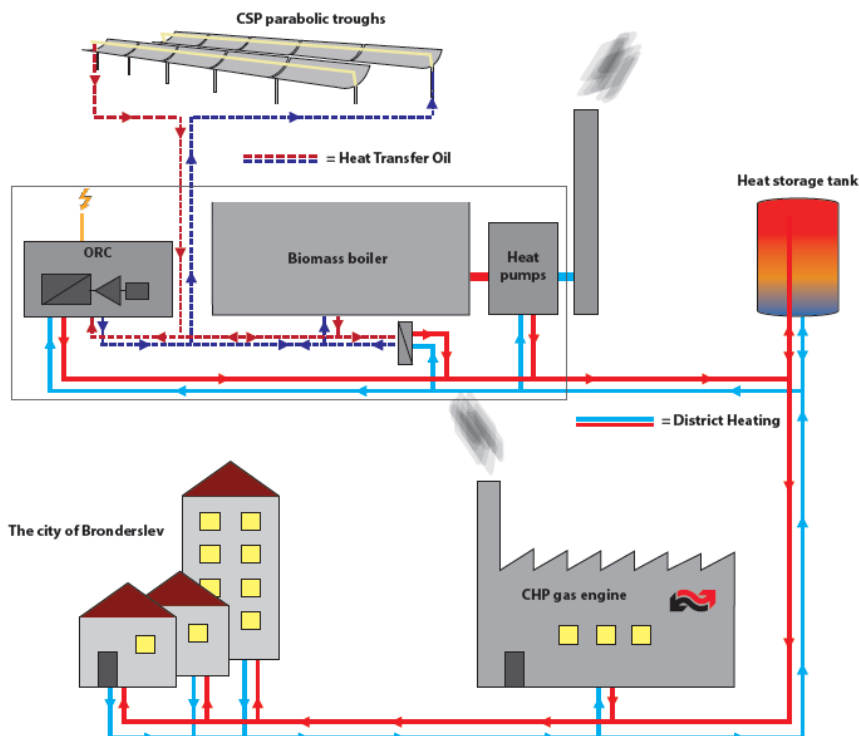


Figure 7: Flow chart of the energy distribution at the hybrid plant of Brønderslev

The solar heating system can thus alternate between providing heat and power or deliver heat exclusively. To maximize yield of energy, the waste heat is utilized and sent to the district heating circuit whereas electrical power is generated at peak price periods.

In Figure 7, it can be seen that the CSP field is delivering hot thermal oil to both the ORC unit and the oil-to-water heat exchanger which delivers the heat to the district heating network to the city of Brønderslev. The CSP solar field has a thermal peak effect of 16.6 MWth and is expected to deliver approximately 16,000 MWh of heat in an average weather year.

Apart from the solar field, there are two biomass boilers each of a maximum capacity of 10 MWth running with wood chips as fuel.

Both the CSP field and the biomass boilers are working in conjunction to supply with sufficient heat the ORC unit, which in full load is supposed to deliver 4MWe. The dissipated heat from the ORC condenser is used to provide additional heat to the district heating network. Therefore, one might notice that the hybrid system is designed in a sustainable and efficient way, avoiding to unnecessarily waste heat to the ambient. The biomass boiler house embeds a 2 MWth heat pump as well, to make use of waste heat from the biomass chimney and supply the district heating as supplementary source. In order to guarantee that the total energy demand is covered at any time, a CHP gas engine is placed as final backup

The achievement of the world’s first CSP system combined with a biomass-ORC plant is supported by the Danish Government’s Energy Technology Development and Demonstration Programme (EUDP).

3. Monitoring and validating performance during the first solar season

As aforementioned, the peak performance of the plant is set to reach 16.6 MWth and the annual yield is expected to be 16,000 MWh of thermal energy. Since the CSP-plant went into operation in the end of 2016, it has been meeting the expected operational goals.

In figure 8, the CSP performance in different seasons is illustrated. It is interesting to see that the time moves from Summer to Autumn, Spring and Winter the thermal power output curve shifts down. This is happening due to the lower solar altitude from month to month. As an example Figure 8 shows the expected thermal output for a day in January, April, July and October, based on an average weather year issued by the Danish Meteorological Institute [4]. Usually, when a PTC field tracking axis is not declining from the North-South axis then the profile of the thermal output curve has two symmetrical peaks (i.e. one in the morning and one in the afternoon). In the present case it should also be mentioned that the thermal peak in the morning hours is always higher than the one in the afternoon. This is explained from the tilted tracking axis in Brønderslev which deviates 29° from the North-South. Therefore, the optical losses are lower before solar noon, because of the lower incidence angle. The incidence angle is the angle in which the solar beams hit the surface of the reflecting mirrors in relation to the normal incidence. The lower the incidence angle is, the lower the optical losses are and thus the higher the thermal output is. The incidence angle of a day in May can be seen in Figure 9.

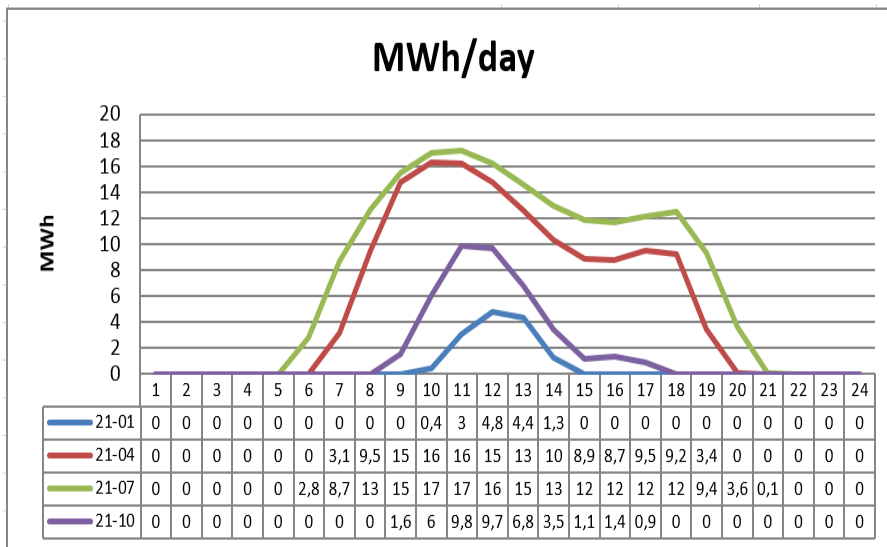


Figure 8: Seasonal variation on CSP thermal power output curve

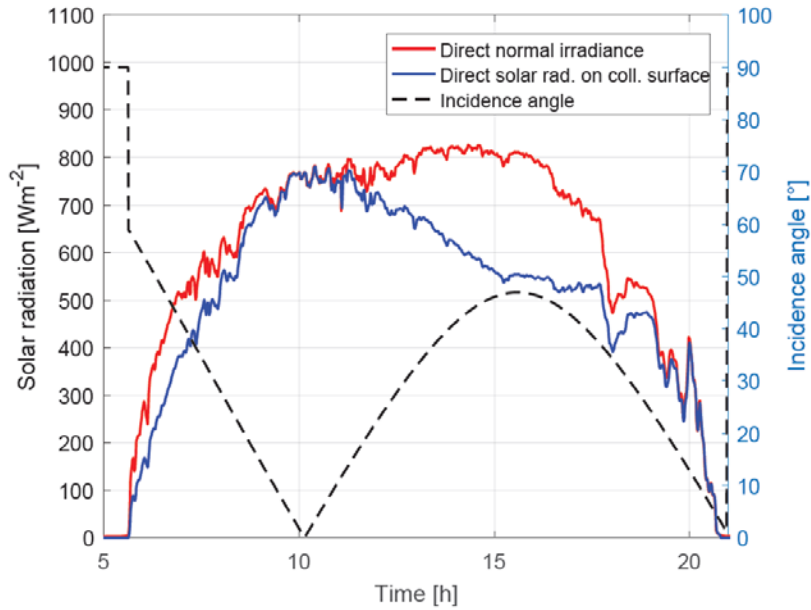


Figure 9: Incidence angle effect on thermal power output curve [2]

Figure 9 shows the effect of turning the tracking axis from exactly North South direction. The daily profile is then changed and may be adapted to the highest electricity price that at present often is in the mornings at around 8-10 [3].

The solar plant performance was monitored and cross checked during its first summer period from May 2017 to September 2017. Figure 10 illustrates the modeled versus the measured performance in kWh of heat produced per day and as it can be clearly seen the two series of data come in very good agreement when they get the same daily beam radiation as input.

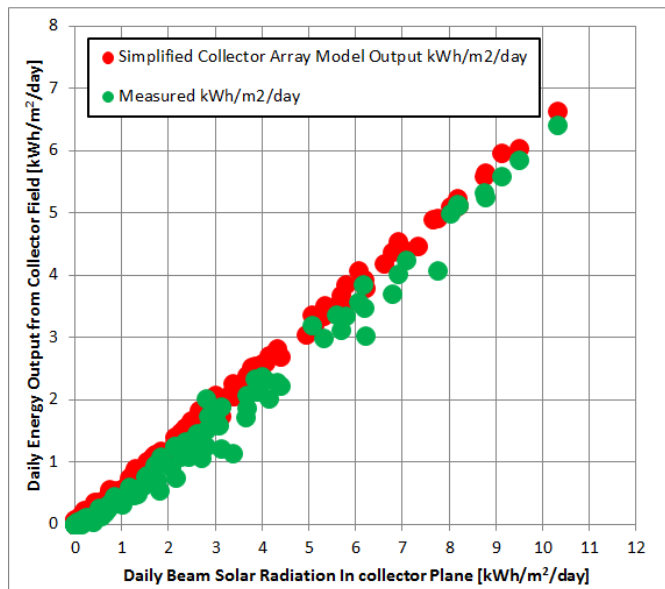


Figure 10: Validation of measured vs. computed performance for summer 2017, Perers et.al [3]

The same procedure has been followed and is presented here for a whole day of solar heat production in May. In Figure 11 the measured and calculated thermal performance of the field are presented with a yellow and a black line respectively and it becomes apparent that they are almost identical. All the heat produced by the field at that moment was delivered to the district heating network. The monitored forward water temperature to the district heating grid was also in very good agreement with the calculated one and averaging at around 80°C. With blue and red, the measured and calculated outlet temperature of the thermal oil is shown to be peaking at around 180°C. At that moment the ORC unit was still under construction and there was not need to operate at a higher temperature than that.

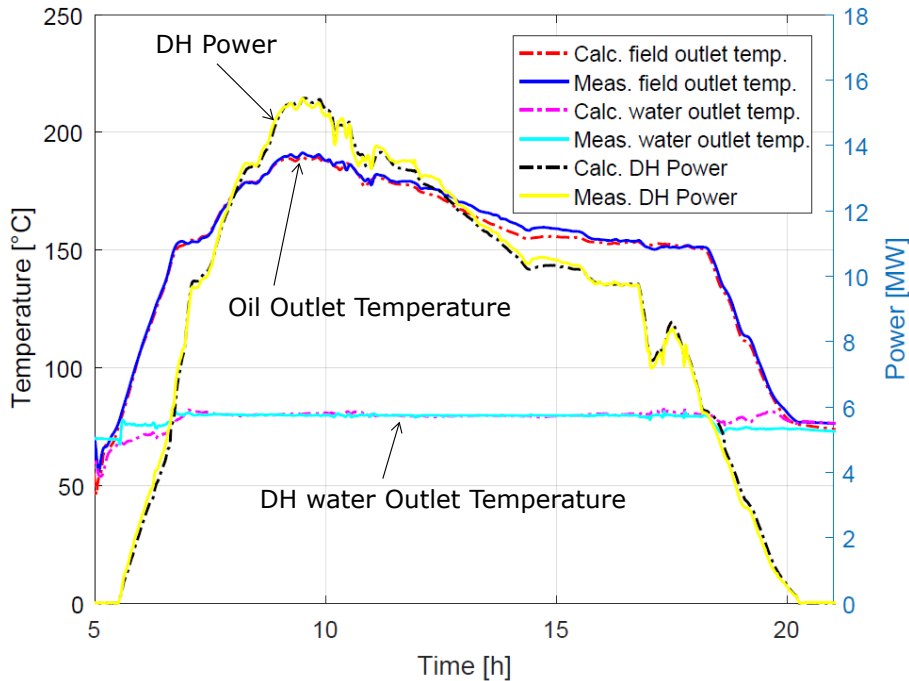


Figure 11: Measured and calculated performance of solar field [3].

Acknowledgements

The first author really appreciates the assistance from the Technical University of Denmark and especially Senior researcher Bengt Perers whose effort and continuous technical support was essential. Special thanks are expressed to Simon Furbo, Zhiyong Tian Alejandro de la Vega Fernandez for contributing in the performance analysis.

References

- [1] B. Perers, S. Furbo and D. Janne, "Thermal performance of concentrating tracking solar collectors," Technical University of Denmark (DTU) Civil Engineering Report R-292 (UK) Department of Civil Engineering, Denmark, 2013.
- [2] Fernandez A. Analyses of Brønderslev solar energy plant by use of TRNSYS. DTU master thesis; 2017.
- [3] B. Perers, S. Furbo, Z. Tian, J.H. Rothmann, J. Juul, T. Neergaard, P.V. Jensen, J.R. Jensen, P.A. Sørensen, N. From, "Performance of the 27000 m² parabolic trough collector field, combined with Biomass ORC Cogeneration of Electricity, Brønderslev Denmark", Solar District Heating Conference 2018, Graz, Austria, 2018
- [4] Danmarks Meteorologiske Institut, www.dmi.dk



16th International Symposium on District Heating and Cooling, DHC2018,
9–12 September 2018, Hamburg, Germany

LowExTra - Feasibility of a Multi-Conductor District Heating System

Elisa Dunkelberg^{a*}, Andreas Schneller^b, Max Bachmann^c, Martin Kriegel^c

^a*Institute for Ecological Economy Research, Potsdamer Straße 105, Berlin, 10785, Germany*

^b*adelphi research gemeinnützige GmbH, Alt-Moabit 91, Berlin, 10559, Germany*

^c*Technical University of Berlin, Marchstraße 4, Berlin, 10587, Germany*

Abstract

District heating (DH) systems can be a promising technology for a low-carbon heat supply if the share of renewable heat and waste heat will be increased. However, the level of integration from low temperature (renewable) heat sources is currently limited by the system temperatures of the heating grid. To develop a solution for this challenge, this paper examines the feasibility of a multi-conductor DH-grid concept which was investigated from technical and economic perspectives. The analysis of the dynamic grid and plant simulations show that a share of over 40 percent renewable and waste heat can be reached in the test area of a built-in district in Berlin. Different designs of the heat supply units lead to similar overall costs and can be competitive compared to decentralized heating concepts with comparably high level of renewable and waste heat. However, in Germany, due to the currently low natural gas price, gas boilers are often still the option with the lowest heat production costs for the existing building stock. Therefore, political action is needed to increase the feasibility for a successful low-carbon transition and to overcome obstacles for innovative low-temperature (LowEx) DH-systems.

© 2018 The Authors. Published by Elsevier Ltd.

This is an open access article under the CC BY-NC-ND license (<https://creativecommons.org/licenses/by-nc-nd/4.0/>)

Selection and peer-review under responsibility of the scientific committee of the 16th International Symposium on District Heating and Cooling, DHC2018.

Keywords: multi-conductor; low temperature; district heating; decentral feed-in; renewable heat; climate action; waste heat utilisation

* Corresponding author. Tel.: +49–30–884 594-36; fax: +49–30–882 54 39.

E-mail address: elisa.dunkelberg@ioew.de

1. Introduction

About 80% of the worldwide energy consumption and CO₂ emissions are emitted in cities [1]. In temperate and cold climate zones the provision of heat produces a significant share of urban emissions; e.g. in Berlin, the building stock emits half of the city's CO₂ emissions [2]. Thus, in order to fulfil the targets of the Paris Agreement it is essential to transform the urban heating sector in order to provide heat with a considerable share of renewable energies [3;4]. The first important pillar for a transition of the heating sector is a comprehensive modernization of the building stock in order to decrease the energy consumption [3;5]. The second important pillar is the structural transition of the heating supply sector to more climate-friendly forms of heat generation by switching from fossil fuels to renewable heat and waste heat.

District heating (DH) systems enable producers to use renewable and waste heat sources such as wastewater heat, large-scale solar thermal systems or geothermal heat by matching the regional available supply with the respective demand [6;7;8]. Therefore, numerous studies have concluded that DH will play an important role for future sustainable energy system [9;10;11]. However, most of the renewable heat sources as well as many waste heat sources provide low-temperature heat, while DH usually operates on high supply and return temperatures [7;12]. Furthermore, there are obstacles for energy refurbishment measures; many European cities have a relevant number of buildings protected as historic monuments. In Berlin a sixth of building stock are listed buildings [13]. For the future, it is necessary that the energy demand and the temperature requirements of a high share of buildings decreases significantly. However, in neighbourhoods characterized by the existing stock of buildings with high energy demand, there will very likely be a coexistence of refurbished buildings that can use low-temperature heat and buildings that still need high temperature heat. Since the consumer with the highest temperature demand in the supply area determines the temperature for DH systems [14], solutions are needed to deal with this temperature diversity in neighbourhoods.

To develop an innovative solution for this challenge, this paper introduces a multi-conductor DH-grid approach and presents the results of a feasibility analysis from technical and economical perspectives. In contrast to conventional networks with two pipes, the multi-conductor heating network is designed with several conductors, each with different temperatures. This means that the temperature level of the heating network is no longer determined solely by the consumer with the highest temperature requirements but can be optimally adapted to the existing consumer and producer structure. An important feature of this novel heat network is the decentralised integration of regenerative energy sources and waste heat at low temperature levels so that the consumer can also be a producer and, as a prosumer, feed in heat from own heating plants.

2. Methodology

2.1. Feasibility analysis from technical and economical perspective

The technical and economical feasibility of the future-oriented multi-conductor heating network was investigated using the example of an urban neighbourhood. An iterative approach served to identify technical designs of the network itself and producer scenarios with low overall costs. Therefore, the initial design of the generation park was subsequently adapted in such a way that the total costs are as low as possible.

In a first step the technical design of the multi-conductor network was developed specifically for the study area. A modelling of the heat producers and their producer profiles, the consumers and their consumption profiles, as well as the network itself served as the basis for the technical design of the network. For the simulation, the modelling language Modelica and its implementation environment Dymola were chosen. In order for a LowEx multi-conductor heat network to react flexibly with regard to the supply and removal of heat, an adapted hydraulic network concept is required. A detailed description of the methodological approach and of the results of the hydraulic feasibility analysis can be found in [14].

In a second step the network itself and the producer scenarios created on the basis of modelling were examined with regard to the total costs and the producer-specific heat production costs. The annuity method, a dynamic method of investment analysis, that takes financial parameters such as interest rates, inflation and price changes into consideration, was applied. The chosen observation period is 20 years. The total annual costs and heat generation costs were calculated on the basis of the investment costs, operating and consumption costs for the heat generation

plants, the grid itself and the transfer stations. Initial energy prices refer to the prices in Germany in 2015, price-increase rates are 2.6% for natural gas, 2.3% for light fuel oil, 0.6% for electricity and 1.5% for biomethane. A detailed description of the methodology and the assumptions can be found in [15].

2.2. Characterization of the study area

An urban neighbourhood was chosen as a model area for the multi-conductor network, since greenhouse gas emissions from the heat supply are particularly high in cities and therefore especially relevant for effective mitigation strategies. In addition, grid-bound heat is particularly profitable in densely populated areas where there is a high consumption density. Furthermore, the focus of the feasibility study was on the existing building stock, as it is responsible for the majority of the heat consumption. At last, due to different renovation conditions, there are rather different temperature requirements by the consumers in existing or mixed areas when compared to in purely new construction areas. Generally spoken, a multi-conductor network with more than two conductors only makes sense if a consumer structure with significantly different temperature requirements exists in an area.

Based on these considerations, a district in Berlin Pankow was selected as the study area. The district of Pankow was found at the end of the 19th century with the construction of densely packed tenement buildings, which in the course of time were modernized by different intensity and standards. The chosen city district consists out of 59 single-family and two-family homes, and 31 apartment buildings as well as a shopping centre and a school and several non-residential buildings. Fossil fuels such as natural gas and heating oil are currently predominantly used for heating in both single-family and multi-family houses. Using a software building simulation the total heat requirement in the district was determined to 17.1 GWh/a in 2015 [14].

3. Technical design and control of a multi-conductor heating network

The number of conductors that were determined is based on the existing consumer structure. In the study area, a total of six consumer classes were defined on the basis of their design temperatures. Among them are buildings with radiators with operating temperatures of 90/70 °C, 75/65 °C, 70/55 °C and 60/45 °C as well as buildings with surface heating systems with an operating temperature of 45/35 °C. In addition, the hot drinking water requirements of the buildings are also indicated as consumers. For hygienic reasons, the temperature for providing hot drinking water is above 60 °C at all times of year. The number of temperature levels required to meet the demand was set at four. The consumer groups 90/70 °C and hot drinking water as well as the consumer types 75/65 °C and 70/55 °C were each combined in one conductor. For each conductor, the temperatures result from the heating curves of the type of consumer with the highest temperature requirements in each case.

In order to implement a multi-conductor heat network, different heat sources are required in one district, which can provide heat at the temperature levels required by the consumer structure. Possible generation plants that supply heat for heating networks include combined heat and power plants (CHP), gas-fired boilers for peak loads, solar thermal plants, low temperature waste heat from industrial and commercial sources (e.g. bakeries, laundries, compressed air production, data centres) as well as environmental heat (air, geothermal energy, river water and waste water). For the use of environmental and some types of waste heat, heat pumps are required to transfer the heat to a usable temperature level of more than 50 °C.

Producer types can be characterised by the attainable flow temperatures and their adjustability. With regard to the adjustability, a distinction is made between non-adjustable and adjustable producers. Adjustability describes to what extent it is possible and practical to operate a generation plant flexibly depending on the heat demand in the grid. Adjustable generators can feed their power into the grid at any time. Non-adjustable generators provide their power depending on external factors. Examples of adjustable representatives of the category include gas boilers and heat pumps, and representatives of the non-adjustable category include solar thermal or waste heat processes. Heat from renewable energies or waste heat is generally available at lower temperatures compared to conventional district heating and can in many cases be characterised as not adjustable (Table 1).

Table 1. Characterization of heat sources according to achievable temperature levels and controllability.

Generating plant	Attainable temperature level	Adjustability
CHP	< 100 °C	Adjustable
Gas-fired boilers	< 100 °C	Adjustable
Solar thermal energy	< 100 °C	Not adjustable
Heating pumps	< 60 °C	Adjustable
Outside air, soil, groundwater	< 60 °C	Not adjustable
Exhaust air, sewage water	< 60 °C	Not adjustable
Bakery	> 100 °C	Not adjustable

For climate policy reasons, in most cases heat from non-adjustable sources should be prioritised for feeding-in, since it often has a lower primary energy factor than heat from adjustable generators (e.g. solar thermal energy, waste water heat). However, in order to guarantee supply reliability in a heating network, it is necessary to maintain a sufficiently high adjustable heating power at the corresponding temperature levels. In order for a LowEx multi-conductor heat network to react flexibly with regard to the supply and removal of heat, a new hydraulic network concept is required and has been developed. The temperature and pressure level in the network is highest in conductor L1 and lowest in the lowermost conductor (see Figure 1 for a three-conductor DH system). Consumers and producers are connected between two adjacent conductors. In addition, by using at least one tank per conductor, the individual conductors are hydraulically decoupled from one another. The aim of using the tanks is to decouple consumption and generation over time. This makes it possible to operate adjustable generator plants according to demand. The tanks have been modelled using a customized version of the expansion vessel provided by the buildings library developed by the Lawrence Berkeley National Laboratory. This model was extended by a signal output for the tank volume. The pressure inside the tank is set to be constant. The hydraulic separator has been modelled using a discretized pipe model and a mass flow sensor between each grid level.

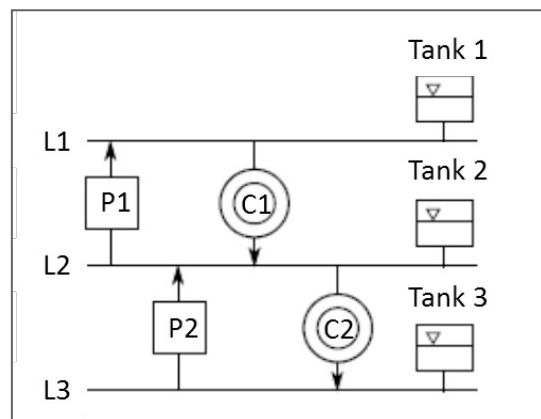


Figure 1. Sketch of multi-conductor heating network with three conductor (L = line, P = producer, C = consumer)

The respective load condition of the individual conductors in the heating network can be determined at the filling level of the tanks. If the consumption of conductor L1 to conductor L2 is greater than generation, the fluid level of tank 1 decreases, but if generation is greater than the consumption, the fluid level of tank 1 rises. This information can be used to determine the load situation in the heating network at a central point and is therefore important for regulating the adjustable generators. Adjustable generators can be regulated in their entire power spectrum, whereas non-adjustable generators can only be prevented from feeding into the grid. The primary aim of this grid control is to adapt generation to consumption without determining the exact consumption of each consumer on a decentralised basis. Generation that is not adapted to consumption can lead to an under- or over-supply of the heating network;

this means that central generator control is also absolutely essential in a LowEx multi-conductor heat network. Furthermore, a centrally controlled producer regulation control makes it possible to prioritise efficient producers allowing for making the best possible use of the energy potential of a production park, for reducing CO₂ emissions, and for improving the overall efficiency of the production plants. Further information on the hydraulic concepts and the control concept can be found in [14].

4. Feasibility of a multi-conductor heat network from an economic perspective

The economic analyses refer to a four-conductor DH-system and various producer scenarios. While a centralised scenario called Grid-Central includes only a few large heat generation plants, a scenario called Grid-Decentral represents a producer structure with many small system installations (mainly heat pumps). At last, a scenario called Grid-RE-Ambitious incorporates the highest amounts of renewable heat and waste heat by integrating several small heat pumps, two big wastewater heat pumps and a solar thermal plant with 1,200 m² of collector area. The total annual costs and heat generation costs were calculated on the basis of the investment costs, operating and consumption costs for the heat generation plants, the grid itself and the transfer stations (cf. Table 2 and 3).

Table 2. Type and number of heat generation plants in the LowEx scenarios

System type/output	Grid-Central	Grid-Decentral	Grid - RE Ambitious
Solar thermal energy 300 m ²		3	
Solar thermal energy 600 m ²			2
Solar thermal energy 900 m ²	1		
Solar thermal energy 1800 m ²			1
Air-heat pumps – Apartment buildings 1960-1990, 101 kW			9
Air-heat pumps - One/two family houses <1960, 34 kW			3
Geothermal heat pumps - Apartment buildings 1960-1990, 101 kW		5	
Geothermal heat pumps - Apartment buildings <1960, 123 kW		4	
Geothermal heat pumps - One/two family houses <1960, 34 kW		14	
Bakery, 9,9 MWh MWh/a		2	2
Wastewater heat, 2.000 MWh/a	2		2
Natural gas CHP, 600 kWel	1	1	2
Gas-fired boilers, 2.600 kW	1		
Gas-fired boilers, 2.050 kW	2	2	1
Gas-fired boilers, 1.000 kW		2	2
Gas-fired boilers, 750 kW	1	1	2
Storage facility, 1650 m ³			1

Table 3. Costs of heat generation plants and the grid

System type/output	Investment costs [€]	Subsidies [€]	Operating costs per year [€]	Consumption costs [ct/kWh]
Solar thermal energy 300 m ²	179.200	42.500	863	0
Solar thermal energy 600 m ²	323.400	84.500	1.550	0
Solar thermal energy 900 m ²	453.000	126.500	2.175	0
Solar thermal energy 1800 m ²	892.000	252.500	4.275	0
Air-heat pumps, 101 kW	70.980	4.500	773	6,7
Air-heat pumps, 34 kW	35.240	2.000	225	7,1
Geothermal heat pumps, 101 kW	76.220	10.500	1.817	5,0

System type/output	Investment costs [€]	Subsidies [€]	Operating costs per year [€]	Consumption costs [ct/kWh]
Geothermal heat pumps, 123 kW	127.870	10.500	2.531	5,0
Geothermal heat pumps, 34 kW	41.980	5.000	615	5,4
Bakery, 9,9 MWh MWh/a	10.850	750	225	0
Wastewater heat, 2.000 MWh/a	666.606	200.000	16.581	3,9
Natural gas- CHP unit, 600 kWel	423.720		22.537	5,1
Gas-fired boilers, 2.600 kW	159.350		3.120	5,0
Gas-fired boilers, 2.050 kW	126.350		2.460	5,0
Gas-fired boilers, 1.000 kW	63.350		1.200	5,0
Gas-fired boilers, 750 kW	48.350		900	5,1
Storage facility, 1650 m ³	27.833			
Grid, 3.166 m	1.785.855	190.000	63.117	0,2

The heat supply system must be economically viable from the perspective of all actors involved in the heat supply, i.e. for the network operators, the heat producers, and the heat consumers. From the point of view of energy suppliers, it makes sense to design the generation park in such a way that the total costs of the generation park and the grid, including investment costs and running costs, are as low as possible. In order to attract heat consumers, the heat price, which can be derived from the heat generation costs, should also be of a similar magnitude such as options for individual building supply (e.g. a decentralised gas boiler or a heat pump).

In the case of solar thermal systems, the heat generation costs for larger systems are significantly lower than for small systems. Solar thermal systems should also be dimensioned to suit the heat requirements in the district, so that as much of the generated heat as possible can be used. In the case of an installation without seasonal storage, the dimensioning depends on the summer load of the quarter. Heat generation costs of solar systems vary strongly depending on the dimension, type of collector, roof orientation and inclination. The solar thermal plants considered here result in heat generation costs of about 9 to 11 ct/kWh, only a combination with a seasonal storage allows the heat generation costs to be reduced to less than 6 ct/kWh. Relatively low heat generation costs of about 7 to 9 ct/kWh can be achieved with commercial waste heat, for example from bakeries or waste water heat, so that the integration of such heat sources makes economic sense. With heat pumps, the achieved heat generation costs depend less on the size of the systems than on the annual performance factor and the annual service life of the systems. However, due to the relatively high investment costs for heat pumps, the running times should be as long as possible. Since the annual operating hours for connecting heat pumps to the grid are generally higher than for purely object-related operation, the heat generation costs for heat pumps that are connected to the grid are lower: 7 to 10 ct/kWh with a grid connection and 10 to 13 ct/kWh without a grid connection, depending on the system type. However, due to the heat quantity of certain temperatures determined by the consumer structure, it is not possible to integrate any amount of heat from heat pumps into the LowEx-multi-conductor heating network. The overall costs and average heat generation costs of the system therefore increase if there is so much heat pump power in the system that its heat can only be absorbed by the grid in small quantities.

Economic analyses for the entire heat supply system show that producer structures with many small system installations (decentralised scenario) lead to comparable total costs as those with a few large installations (centralised scenario), provided the heat quantities from the various heat sources are of a similar size (see Figure 2). Total costs and average heat generation costs are significantly higher if an ambitious concept is to be implemented that maximises the share of renewable heat and waste heat on the basis of existing potential and consumer structure. The ambitious scenario has a 40% share of renewable heat and waste heat. The higher total costs are mainly due to the significantly higher installed capacity of heat pumps (incl. waste water heat pump) compared to the other scenarios. As a result, the annual full load hours of the heat pumps in this scenario are much lower. In order to achieve a cost-efficient overall system, a central player is therefore required to decide on the integration and feeding volume of the heat generation plants.

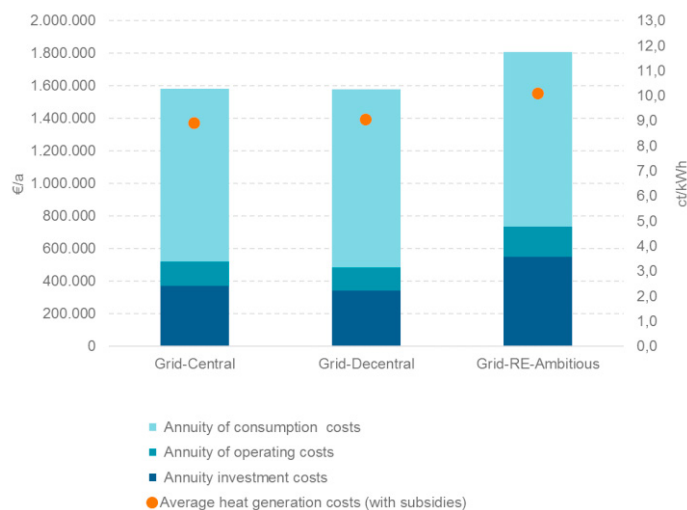


Figure 2. Total annuity costs and average heat generation costs for three generator structures with LowEx multi-conductor heat grid.

The average heat generation costs of 9 to 10 ct/kWh (over 20 years) achieved in the centralised and decentralised scenarios for the entire heat supply system are, under favourable conditions, competitive compared to scenarios with a comparatively high share of renewable energies for individual buildings. Favourable framework conditions relate to technical aspects such as low network losses but also an increase in gas prices. However, for some consumer groups, especially older, unrenovated apartment buildings, the heat generation costs of the LowEx multi-conductor heating network are higher than those of individual gas or oil boilers in the building. Since the share of consumption-related costs in the supply of gas and oil boilers to individual buildings is significantly higher than in the scenarios with the LowEx multi-conductor heating network, a gas-based supply to individual buildings however reacts much more sensitively to higher gas price increases. A heat supply concept with a LowEx multi-conductor network can therefore be described as more stable in the face of price increases of fossil fuels.

Several aspects have to be considered from an economic perspective regarding the technical design of the network. The heat losses in the grid are a highly relevant influencing factor for the efficiency and competitiveness of the LowEx multi-conductor heating network. The technical simulations showed a network loss of 3 % of the generated heat for the area under study. Under these circumstances, the total costs for the area under study with grid-connected heat supply can be reduced compared to individual building supply with a comparable share of renewable energies. However, if the grid loss increases by a few percent, under the assumed economic boundary conditions the grid-connected heat supply loses its advantage in terms of total costs compared to a building-specific heat supply. From a technical point of view, an increase in the number of conductors in the grid can lead to an optimum supply of consumer groups from individual heat sources. However, the number of conductors is limited due to economic reasons, as the investment costs increase as the number of conductors increases. If the number of conductors doubles, network operators estimate that grid investment costs will increase by about 30 to 50 %. In relation to the total costs of heat supply, the consumption-related costs outweigh the others, so that the annuities of the total costs increase by only about 2 to 3 % if the number of conductors is doubled. Under certain circumstances, however, these additional costs can lead to the grid-connected supply being more expensive than a building-specific heat supply. A detailed description of the economic analyses from the perspective of the different actors involved (producers, grid operators, customers) can be found in [15].

5. Conclusion

The examined multi-conductor district heat supply system can cost-effectively integrate renewable energies and waste heat and is therefore in line with the climate and energy policy objectives at the German and EU level, which foresee extensive decarbonisation of the heating sector by 2050. The results of the technical and economic analyses

show that multi-conductor networks are feasible and can be implemented with an adjusted network and control concept and that existing potentials for renewable heat and waste heat can be utilised by integrating different heat sources. The multi-conductor concept is particularly suitable for urban areas with a heterogeneous consumer structure and a large number of available heat sources. In order to hydraulically decouple the individual conductors from one another, there must at least be one tank per conductor. Investments costs of a four-conductor network are about 30 % higher compared to a conventional grid with two pipelines. Consumption costs however are comparably low and a heat supply concept with a LowEx multi-conductor network can be described as more economical sustainable in the face of possible price increases of fossil fuels.

In order for innovative heating concepts to play a significant role, timely adjustments to the European and German regulatory framework are necessary. Since gas boilers are for many households still the most cost-efficient technology to provide heat, the political framework has to be adjusted in order to increase the competitiveness of the presented multi-conductor network. The continuous lack of internalisation of environmental costs associated with low fossil fuel prices represents a major obstacle to the transformation towards a climate-friendly heat supply and specifically to the feasibility of LowEx multi-conductor networks. Higher costs of gas or oil-fired heat supply systems, for example through a CO₂ tax, would directly improve the competitiveness of various climate-friendly heat supply options, and thus also a LowEx multi-conductor heating network with a high share of renewable energy. In addition, possible instruments for increasing the competitiveness of heat from a LowEx multi-conductor network in comparison with individual fossil boilers could also include targeted financial support programmes for grid solutions with a high proportion of renewable energies and waste heat [16].

Acknowledgements

The authors owe thanks to the LowExTra research team, namely Julika Weiß, Swantje Gähns, Bernd Hirschl, Steven Salecki, Kora Töpfer, Leonard Frank, Amelie Thürmer, Nicolas Bach, Sabine Schroeder, Stefan Brandt, Bahar Saeb Gilani, and Benjamin Zielke. We are grateful to the German Federal Ministry for Economic Affairs and Energy (BMWi) for funding the LowExTra research project (Funding Code: 03ET1237). Please find further information on the project website: www.lowextra.de.

References

- [1] The World Bank, 2010. Cities and Climate Change: An Urgent Agenda. Vol. 10. Washington DC.
- [2] Hirschl, B., Reusswig, F., Weiß, J., et al., 2015. Entwurf fuer ein Berliner Energie- und Klimaschutzprogramm (BEK). IOEW, Berlin.
- [3] Weiß, Julika, Elisa Dunkelberg and Bernd Hirschl. "Implementing the Heating Sector Transition in Our Cities - Challenges and Problem-Solving Approaches Based on the Example of Municipalities in Germany". In: Droege, Peter et al. Urban Energy Transition (2018): 271-279.
- [4] Ecofys, 2012. Towards Nearly zero-Energy Buildings. (Definition of common principles under the EPDB).
- [5] Schubert, S., 2016. Ausbau von Waermenetzen vs. energetische Sanierung? - Umgang mit konkurrierenden Strategien zur Umsetzung der "Wärmewende" auf kommunaler Ebene. In: Schubert, (Ed.), Raumforschung und Raumordnung. 74(3), pp. 259–271.
- [6] Paar, A.; Herbert, F.; Pehnt, M. et al. (2013): Transformationsstrategien Fernwaerme, TRAFO. Frankfurt am Main: AGFW. www.eneff-stadt.info (Accessed 27 January 2018).
- [7] Li, H., Svendsen S., Rosa, A.D., 2014. Toward 4th generation district heating: Experience and potential of lowtemperature district heating. The 14th International Symposium on District Heating and Cooling, September.
- [8] Galindo Fernandez, M.; Roger-Lacan, C.; Gähns, U. et al. (2016): Efficient District Heating and Cooling Systems in the EU Case Studies Analysis, Replicable Key Success Factors and Potential Policy Solutions.
- [9] Connolly, D., Mathiesen, B.V., Østergaard, P.A., et al., 2012. Heat Roadmap Europe: First Pre-study for EU27.
- [10] Connolly, D., Mathiesen, B.V., Østergaard, P.A., et al., 2013. Heat Roadmap Europe: Second Pre-Study.
- [11] Connolly, D., Lund, H., Mathiesen, B.V., et al., 2014. Heat Roadmap Europe: Combining District Heating with Heat Savings to Decarbonise the EU Energy System. In: Energy Policy 2014. Vol. 65, pp. 475–489.
- [12] Lund, H., Werner, S., Wiltshire, R., et al., 2014. 4th Generation District heating (4GDH). Integrating smart thermal grids into future sustainable energy systems. In: Energy.68, pp. 1–11.
- [13] Reusswig, F., Hirschl, B., Lass, W., et al., 2014. Klimaneutrales Berlin 2050. Machbarkeitsstudie, Hauptbericht. Berlin, Potsdam.
- [14] HRI. Herrmann-Rietschel-Institut. Schlussbericht LowExTra Niedrig-Exergie-Trassen zum Speichern und Verteilen von Wärme. 2018.
- [15] Dunkelberg, E.; Weiß, J.; Gähns, S.; Salecki, S. (2018): Ökonomische Bewertung von Mehrleiter-Wärmenetzen zur Nutzung von Niedertemperaturwärme. Institut für ökologische Wirtschaftsforschung, Berlin, forthcoming.
- [16] Schneller, A.; Frank, L.; Kahlenborn, W. (2018): Waermenetze 4.0 im Kontext der Wärmewende. Strategiepapier für die Dekarbonisierung der leitungsgebundenen Wärmeversorgung. Berlin: adelphi.



16th International Symposium on District Heating and Cooling, DHC2018,
9–12 September 2018, Hamburg, Germany

Numerical Investigations on District Heating Pipelines Under Combined Axial And Lateral Loading

Tim Gerlach*¹, Martin Achmus¹, Mauricio Terceros¹

¹*Institute for Geotechnical Engineering, Leibniz University Hannover, Appelstr. 9A, 30167 Hanover, Germany*

Abstract

Within the design process of district heating networks, the soil resistances in axial and lateral pipeline direction are commonly treated independently as friction resistance and bedding pressure. However, at curved segments or near elbows, these resistances occur simultaneously and affect each other. The state of knowledge regarding this topic is summarized, and it is shown that only limited information exists for this case of loading.

Therefore, a three-dimensional finite element model was developed, using the sophisticated concept of hypoplasticity as an advanced constitutive model for the bedding material. This soil model is able to account for dilatancy, barotropy and pycnotropy of granular soils. Subsequently, variations of the loading direction were performed for a reference system. The investigations give a good insight into the behaviour of district heating pipelines under combined loading, showing the interdependency of skin friction resistance and bedding pressure. We present a design approach which incorporates interaction terms, derived from the presented investigations. Results gained from these investigation are then transferred to the academic district heating network design tool IGtH-Heat, to evaluate in which manner the incorporation of coupling terms between bedding and friction resistance influences the pipe-soil interaction. Additionally, a temperature dependent formulation of maximum friction resistance is adopted to incorporate the effects of radial pipe displacement. Thereby we demonstrate that the predicted pipeline's displacement significantly change when these effects are taken into account. Using this new formulation, model predictions are compared to data from full scale field measurements.

© 2018 The Authors. Published by Elsevier Ltd.

This is an open access article under the CC BY-NC-ND license (<https://creativecommons.org/licenses/by-nc-nd/4.0/>)

Selection and peer-review under responsibility of the scientific committee of the 16th International Symposium on District Heating and Cooling, DHC2018.

* Corresponding author. Tel.: +49-511-762-3529; fax: 49-511-762-5105.

E-mail address: gerlach@igth.uni-hannover.de

Keywords: Soil-structure interaction; numerical modelling; buried pipelines; combined loading

1. Introduction

Nowadays, an efficient handling of resources is of special importance for our society. In consequence, the energy from former unused industrial waste heat gets increasingly utilized. Through combined heat and power, the heat waste gets transported by district heating networks to public buildings or private households. For transportation, preinsulated pipelines are predominantly used. They consist of three components that serve different purposes: the steel medium pipe transports the hot water and bears the primary portion of the load, while the outer layer (HDPE) protects the insulation material from water, harmful solids, and mechanical influences. The primary function of the polyurethane rigid foam is the insulation of the pipeline. As a side-effect, it also transfers loads between the medium and the casing pipe. Traditionally, a feed and a return line are installed at the same depth. The pipeline and the filling zone are usually filled with sand, that gets compacted in several layers.

During the operation of district heating networks, changes of the media temperature lead to periodic varying loading conditions. Hereby, the free movement of the pipe, which tends to elongate and shorten under temperature load, is hindered by the adjacent soil. The resistance of the soil can be divided into axial friction resistance and lateral bedding resistance. While both components have already been investigated independently of each other by several authors, the knowledge concerning interaction effects is limited. However, it is evident from figure 1, that near curves or elbow segments both bedding and friction resistances get mobilized and may affect each other.

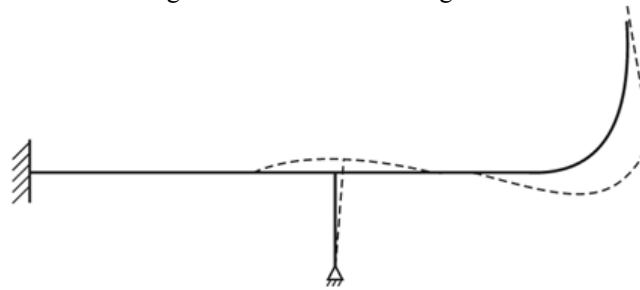


Figure 1: Displacement of temperature loaded, buried district heating system [1]

2. State of the art

2.1. Axial friction resistance

In common design practice in Germany [2], the maximum friction resistance is estimated from:

$$F_{R,\mu} = \mu \cdot (F_N' + F_G') \quad (1)$$

Herein $F_{R,\mu}$ denotes the maximum resistance force per meter length, μ is the friction coefficient and F_N' and F_G' are the integrated normal stresses around the pipes circumference and the sum weight force of the filled pipeline, respectively. To incorporate the effects resulting from changes of operating temperature, the coefficient of contact friction is taken to $\mu = 0.4$ for increasing temperature conditions. During unloading (decrease of temperature), a value of $\mu = 0.2$ shall be applied [2]. However, the coefficient of contact friction is a material specific constant.

In general, the estimation of the maximum resistance force is based on Coulomb's friction law [3]. Following *Coulomb*, the maximum shear stress that can be mobilized between the pipe's mantle and the surrounding soil is proportional to the current normal stress. The constant of proportionality is the coefficient of contact friction μ . Neglecting the shear stresses in circumferential direction, the maximum resistance force that soil can exert on the pipeline due to axial relative displacement can be calculated from equation 1, wherein

$$F_N' = \sigma_0 * \pi * D_a * \frac{1+k_0}{2}. \quad (2)$$

Herein D_a denotes the outer diameter of the pipeline and k_0 is the coefficient of earth pressure at rest. Assuming the groundwater level to be beneath the bottom of the pipeline, the overburden stress at the centre of the pipeline is considered as the average normal stress σ_0 :

$$\sigma_0 = \gamma * H. \quad (3)$$

The coefficient of earth pressure at rest can be estimated by the use of *Jaky's* formula [4]:

$$k_0 = 1 - \sin(\varphi'). \quad (4)$$

Gramm [5] recommended an increased coefficient of earth pressure at rest, resulting from the densification process during the installation of the pipeline. Values between $0.5 < k_0 < 0.85$ are proposed, dependent on the intensity of densification.

The second term in brackets of equation 1 denotes the sum weight force of the pipeline:

$$F_G' = 2 * \pi * r_m * s * \gamma_s + \pi * r_i^2 * \gamma_w, \quad (5)$$

where r_m and r_i are the mean and the inner radius of the medium pipe, respectively. The wall thickness is denoted with s and γ_s and γ_w are the steel and water unit weights.

2.2. Radial pipe expansion

A change of media temperature leads to thermal strains within the pipeline. They evolve in both axial and radial pipe direction, while for the design, solely the axial strains are directly considered. As mentioned before, effects from radial expansion are only accounted for by using different coefficients of contact friction. Actually, the coefficient of contact friction is a constant and the increased friction, observed for pipelines subjected to a rise of temperature, results from higher contact normal stresses.

An increase of friction resistance was experimentally observed by several authors. Within full scale field tests by *HEW* (1987) [6], two DN700 pipelines of 19.65m length were installed and tested under different thermal conditions. Overburden heights of 0.8m and 1.15m were realized. Within 57 tests a dependency on medium temperature as well as on ambient temperature was observed. The maximum friction force at $T=136^\circ\text{C}$ medium temperature was about four times greater compared to $T=18^\circ\text{C}$. Further experimental investigations were made by *Gietzelt et al.* (1991) [7]. Pipelines of different diameter were tested in a 25m long trench with concrete walls. For an increase of temperature of $\Delta T=100\text{K}$ a two times greater resistance force was measured. *Huber and Wijewickreme* (2014) [8] presented results from experimental tests using a pipeline with an outer diameter of $D=520\text{mm}$. Inside a chamber $3.8\text{m} * 2.5\text{m} * 2.5\text{m}$, pipelines with different medium temperatures were axially displaced until failure. For $\Delta T=50\text{K}$ an increase of maximum resistance force could be observed. An about 10% higher value was measured, which is only a small increase compared to the aforementioned investigations.

Within the investigations on radial pipeline extension by *Achmus* (1995) [9], first the ratio between changes of media temperature to mantle temperature was evaluated. Assuming rotational symmetry of heat flux, the mantle temperature was calculated using the method of fictive heat sources and sinks. In a next step, the radial displacement was evaluated. For the steel pipe and the mantle, the theory of thin-walled shells and for the insulation the shell theory in plain strain conditions was considered. The same methodology was also used by *Beilke* (1993) [10].

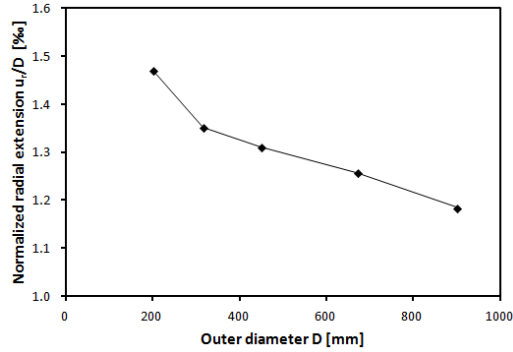


Figure 2: Normalized radial extension dependent on diameter for $\Delta T=120K$ [9].

For an increase of medium temperature $\Delta T=120K$, the radial displacements normalized on diameter are depicted in Figure 2 for different pipeline diameters. Due to the high stiffness of the steel pipe compared to the other materials involved, changes of inner pressure and initial soil stress state were found to have only minor influence on the radial expansion.

Based on this work, an improved numerical model was presented by *Gerlach & Achmus* (2016) [11] using the sophisticated HSsmall model to describe the complex stress-strain behavior of the bedding material. The HSsmall accounts for an increased stiffness of soil in the small strain region, which leads to slightly higher increase factors κ . Based on comprehensive parametric studies, a corrective term was established to describe the changes of maximum friction force for arbitrary geometric conditions and soil properties. Due to the incorporation of small strain stiffness, the relation between media temperature and increase of resistance was found to be nonlinear.

2.3. Bedding resistance

The second main reaction component of the subsoil is the lateral resistance force F_B , or the average bedding pressure p_m , dependent on the lateral deflection y .

The first publication on this subject was presented by *Audibert & Nyman* (1977). They carried out a laboratory test series where the influence of soil density, pipe diameter and embedment ratio was investigated. A detailed description of the test setup can be found in [12]. The scope of laboratory investigations included three different diameters, the distinction between loose and dense sand and the variation of cover ratio. Additionally, one field test was carried out. As a schematic result, *Audibert & Nyman* pointed out two kinds of failure mechanisms dependent on the embedment depth. This was possible due to a transparent plexiglas window, which made the inspection of the soil movement possible. It was found that for shallow burials, less than three times of the pipe's diameter, two wedges are formed. A passive wedge can be observed in front of the pipe (in direction of displacement). Behind the pipe, a smaller, nearly vertical wedge is forming an active zone. With increasing burial depth, the lower bounds of the wedges become steeper and a separating zone forms between the two wedges, in which no vertical movement of the soil is observed.

Another goal was to find an analytical representation for the soil resistance-displacement relationship. A nonlinear curve which represents the relation of bedding resistance p over displacement y from the initial state to the maximal displacement y_u was found. At y_u , the soil reaction force reaches its maximum value p_u . According to *Audibert & Nyman*, the normalized bedding resistance \tilde{p} over the normalized displacement \tilde{y} can be approximated by:

$$\tilde{p} = \frac{\tilde{y}}{A_{lat} + (1 - A_{lat}) \cdot \tilde{y}}. \quad (6)$$

A_{lat} denotes the form factor that defines the initial stiffness and was found to be in the range of 0.145 – 0.2. The two normalized parameters are defined as:

$$\tilde{p} = \frac{P}{P_u} \quad \text{and} \quad \tilde{y} = \frac{y}{y_u} \quad (7)$$

So, to predict the bedding resistance for any state of displacement the maximum bedding resistance p_u and the maximum displacement y_u are needed. The maximum of bedding resistance can be obtained from:

$$p_u = \gamma \cdot H \cdot N_u \quad (8)$$

Herein, N_u is a bearing capacity factor found by *Brinch Hansen* (1961) [13]. This factor can be taken from a chart, depending on the angle of internal friction and the cover ratio. *Audibert & Nyman* found a good agreement between their experimental laboratory and field tests carried out by *Brinch Hansen*.

Many design recommendations refer to their work, e.g. the most comprehensive code for district heating networks by *AGFW* [2]. Distinction is made between dense and loose sand. For loose sand holds:

$$N_u = \left[-12.34138 \cdot e^{-0.07628616 \cdot \frac{H}{D_a}} + 17.31058 \right], \quad (9)$$

$$y_u = 0.020 \cdot (h + D_a) \quad (10)$$

Further experimental work was carried out by *Trautmann & O' Rourke* (1985) [14]. A total of 30 lateral loading tests were performed. The relation between normalized bedding resistance \tilde{p} over normalized displacement \tilde{y} was found similar to *Audibert & Nyman*, while the bearing capacity factors are much lower.

This could be identified by *Achmus* [9] as an effect of diameter. Within his finite element modelling in plane strain conditions, the influences of cover ratio, distance to the border of the trench, and pipe diameter were investigated. It is pointed out that the diameter of the pipe obeys a functional relation of the bearing capacity factor. This gives an explanation for the differing values of the bearing capacity factor as determined by *Audibert & Nyman*, who mainly investigated pipes with diameters of $D = 25\text{mm}$ and $D = 60\text{mm}$, and *Trautmann & O' Rourke*, who used pipes with $D = 102\text{mm}$ and $D = 324\text{mm}$.

2.4. Interaction

In the previous subsections we presented the descriptions of resistance components, holding if both of them are treated independently. Briefly, if solely pure axial or pure lateral pipe displacements are considered. As depicted in figure 1, this assumption does not match the real displacement paths of several pipeline segments, especially at and near curved sections. Here, the displacement is a combination of both local directions and thus, the occurring bedding and friction resistances may affect each other.

This interaction was investigated experimentally and numerically by a few authors. Thereby, the simplification was made that only a bidirectional movement of a rigid pipeline was taken into account and a possible rotation or bending was neglected. The angle of attack θ defines the angle between the pipelines displacement vector norm and the axial direction, e.g. $\theta = 0^\circ$ describes pure axial movement. *Hsu et al.* (2001, 2006) presented results from experimental investigations in loose [15] and dense [16] sand. Within their scope of work, pipelines with different diameters were subjected to oblique displacement in a testing box. Regardless of deposit density, diameter and embedment ratio, it was found that the maximum bedding resistance is lowered by a simultaneous occurrence of axial displacement, while the maximum friction resistance is increased by the bedding reaction in lateral direction.

Further investigations were carried out by *Daiyan et al.* (2011) [17], who considered a small scale model in combination with a centrifuge and finite element modeling. They found the maximum bedding resistance to be up to 30% reduced in comparison with pure lateral loading. A more significant influence was observed for the axial component: For an oblique angle of $\theta \approx 40^\circ$, the friction resistance was about 2.5 times higher compared to pure axial displacement. In addition, a two part failure mechanism was proposed. While for small oblique angles the failure occurs in circumference of the pipeline, with greater angles it turns into bearing failure through the subsoil.

3. Numerical modeling

3.1. Model

The presented investigations give a first insight into the impact of interaction effects due to bidirectional loading. However, for the development of an approach of practical usability, more comprehensive studies are necessary. Therefore, a three dimensional finite element model using the commercial software package ABAQUS [18] was established. The reference model consists of a rigid pipeline with an outer diameter of $D = 0.25m$ (DN150), the overburden height is $h = 0.8m$. The adjacent soil is assumed to be a homogenous loose sand ($D_r = 0.4$), so that no layering or influences of the trench walls are considered. For the soil domain, continuum elements with linear shape functions come into use. Within the soil layer a size bias is used so that the size of the elements is increasing with the distance from the pipe. Hence, the region near the pipe can be discretized finer than the elements at a larger distance where the mesh density can usually be reduced because of lower stress gradients. The resulting finite element model is depicted in figure 3.

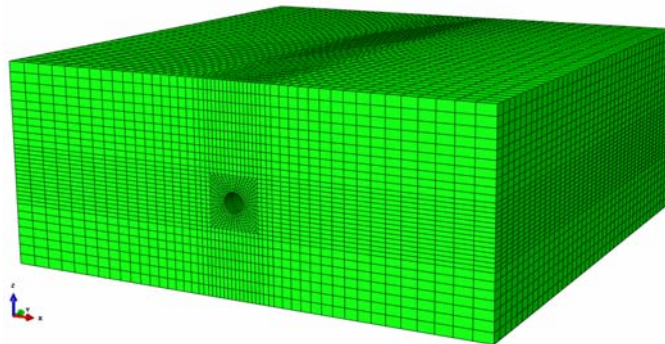


Figure 3: Finite element mesh used for the calculations

The constitutive law of hypoplasticity is used to describe the soil stress-strain behaviour. An implementation of hypoplasticity as an ABAQUS compatible user material (umat) is employed [19]. The hypoplastic material law is a rate-type model which accounts for the complex non-linear soil behaviour by just one (rather sophisticated) tensorial equation. In its form by *von Wolffersdorff*, the hypoplastic material law needs eight parameters [20]. It uses the stress state and the void ratio of a non-cohesive material as state variables and accounts for stress-dependence of soil stiffness and soil strength, thereby reflecting contractancy or dilatancy of soils under shearing in a realistic manner. For further description of the hypoplastic material model [20] is recommended while the considered set of material constants can be found in [21]. For a mean effective stress of $\sigma_m = 20kPa$, the angle of internal friction is $\varphi' \approx 35^\circ$.

A relative displacement between the pipe and the surrounding soil occurs under oblique pipe movement. To enable the possibility of relative slipping within the finite element model, a contact condition is defined. The frictional contact is established using the simple friction law according to Coulomb. Following the guideline recommendations, the coefficient of contact friction is set to $\mu = 0.4$.

The calculation consists of three phases. In the first phase solely the soil domain is present in order to establish the geostatic stress state. In the following step, the pipeline as well as the contact condition are activated. During the final phase, the pipeline gets displaced with a predefined oblique angle by a reference node. The resulting contact

forces are extracted only from the middle third of the model to exclude possible boundary effects from the solution.

3.2. Results

Within a parametric study, 13 different oblique angles were considered. The results gained from the finite element model are depicted in figure 4 (grey lines) in terms of force-displacement curves. The left diagram shows the evolution of friction force over axial pipeline displacement. It is obvious that the coincident occurrence of both resistance components has a significant influence on the axial friction resistance. Due to the mobilization of bedding pressures, the average normal stress acting on the pipeline gets increased. This increased average normal stress, multiplied with the coefficient of friction, results in higher friction forces compared to the case of pure axial displacement. For small oblique angles, the increase of friction resistance is almost linearly related to the increase of bedding pressure. If the oblique angle becomes larger, the failure mechanism changes, as also observed by *Daiyan et al.*, and the shear failure through the subsoil leads to a complex state of stress and soil disturbance. Then, the formulation of interdependency between bedding and friction resistance becomes more complex. This can be explained by the fact that, besides the (horizontal) bedding pressure, also the vertical stress state in the pipelines circumference changes and affect the average normal stress.

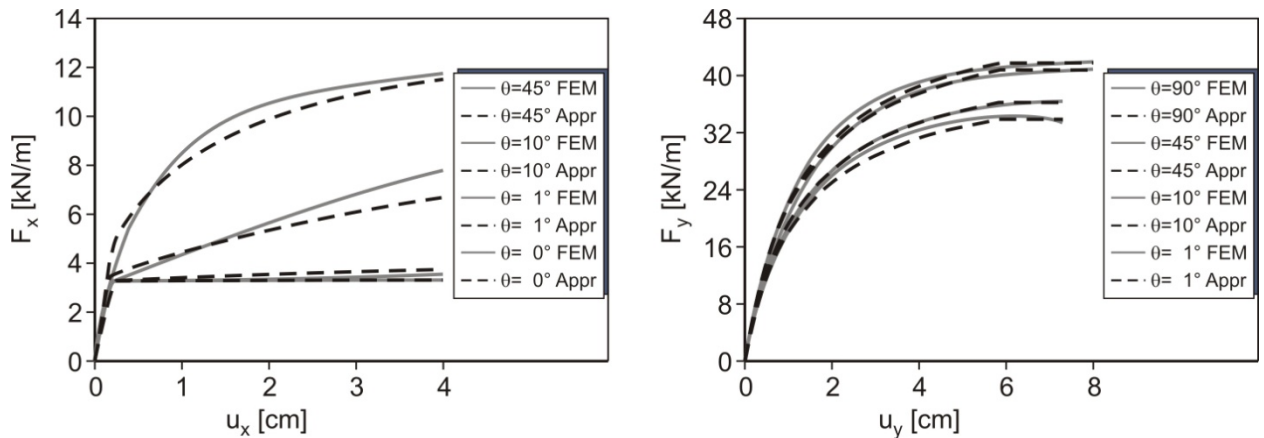


Figure 4: Force-displacement curves for different oblique angles

In contrast to the friction resistance, the impact of interaction on the bedding pressure is less pronounced. Figure 4 (right) shows the relation of bedding reaction force over lateral pipeline displacement. For small oblique angles, a reduction of maximum bedding force of about 20% can be observed. However, to reach these magnitudes of lateral displacement under small oblique angles, axial displacements are needed that are far beyond practical order. Nevertheless, the effects on bedding pressure are also considered in the following derivation of an improved description of spring stiffnesses.

3.3. Design approach

To incorporate the effects of interaction and radial pipeline expansion to the formulation of bedding and friction stiffness, we firstly refer to the procedure of *Audibert & Nyman* to describe the evolution of bedding resistance (cf. equations 6-10). Additionally, we take the oblique angle dependent reduction of maximum bedding force into account:

$$F_{B,u}(\theta) = \chi(\theta) \cdot (\gamma \cdot H \cdot N_u \cdot D), \tag{11}$$

with:

$$\chi(\theta) = \min((0.006 \cdot \theta + 0.807), (-0.0000108 \cdot \theta^2 + 0.00199 \cdot \theta + 0.907)), \quad (12)$$

Herein, χ is calibrated against the results from the numerical model and reflects also the transition between the two failure mechanisms. As depicted in figure 5, a good agreement between the numerical results and the predicted maximum bedding force could be achieved.

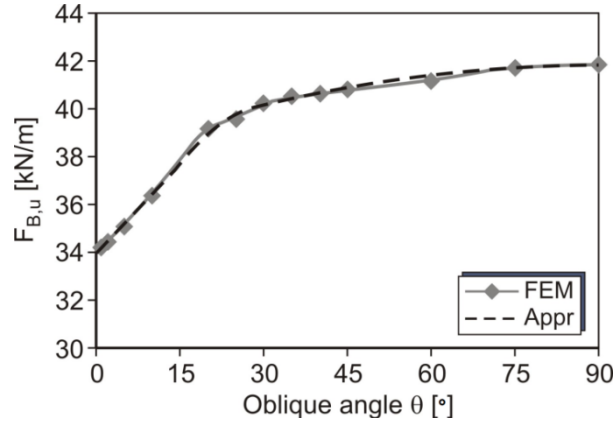


Figure 5: Maximum bedding force in dependency of oblique angle

The formulation of frictional spring stiffness needs to account for both interaction effects and radial pipe expansion. Therefore, we substitute F_N' , the integrated normal stresses around the pipes circumference, by its oblique angle and media temperature dependent counterpart. Equation 1 can then be rewritten:

$$F_{R,\mu} = \mu \cdot (F_N'(\theta, T) + F_G'). \quad (13)$$

The substituted term can be decomposed in two parts:

$$F_N'(\theta, T) = \zeta \cdot F_B(\theta) + \kappa_T(T) \cdot F_N'. \quad (14)$$

To account for interaction effects, ζ denotes the amount of actual, oblique angle dependent bedding force F_B , that increases the average radial stress state. For the reference system, a value of $\zeta = 0.55$ was found to be in good agreement with the finite element results (cf. figure 4). F_N' in the second term refers to unmodified equation 2, multiplied with κ_T , denoting the ratio of initial average radial stress to the average radial stress dependent on the actual temperature :

$$\kappa_T(T) = \frac{\Delta\sigma_r(T)}{\sigma_0} + 1. \quad (15)$$

For the derivation of the change of radial stress $\Delta\sigma_r(T)$, we adopt the elastic solution of a plate with hole:

$$\Delta\sigma_r(T) = \frac{E'(\sigma_0)}{1+\nu} \cdot \frac{\Delta r(T)}{0.5 \cdot D_a}. \quad (16)$$

Herein, ν is the Poisson's ratio and $E'(\sigma_0)$ the stress dependent Young's modulus:

$$E'(\sigma_0) = \kappa \cdot 100kPa \cdot \left(\frac{\sigma_0}{100kPa} \right)^\lambda \cdot \frac{(1+\nu) \cdot (1-2 \cdot \nu)}{1-\nu} \quad (17)$$

κ and λ are material dependent constants to account for stress dependent stiffness of soil and can be determined by oedometric tests. Finally, the change of pipeline diameter (here: radius) can be estimated from the temperature increment and mantle displacement for a temperature rise of $T = 120K$, as proposed by *Achmus* (cf. figure 2):

$$\Delta r(T) = \frac{T_i - T_{i-1}}{120K} \cdot u_{r, \Delta T=120K} \quad (18)$$

For simplification, we assume that the interaction independent part of friction resistance increases linearly up to $x_u = 0.01D$.

4. Holistic simulation using IGtH-Heat

The presented design approach was implemented into the academic district heating network design tool IGtH-Heat, which adopts the temperature-loaded pipeline as beams according to Bernoulli's theory and the soil reaction as nonlinear springs. Due to this nonlinearity, Newton-Raphson method is used to solve the set of equations. For validation, data from a full scale field testing network were provided by our research partner *AGFW*. The test site is located in Chemnitz (Germany) and consists of four geometrically identical pipeline systems. Its geometry is depicted in figure 6.

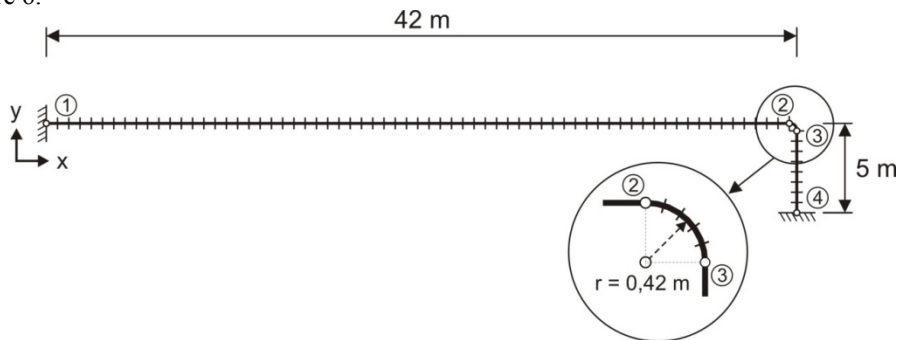


Figure 6: Geometry of the testing pipeline in Chemnitz (Germany)

The pipeline is a DN150 ($D = 0,15m$) embedded in medium-fine sand ($d_{10} = 0.08m$; $U = 2.4$; $D_r = 0.4$). The overburden height is $h = 0.8m$. Geotechnical investigations were carried out in field and laboratory and resulted in a coefficient of earth pressure of $k_0 = 0.5$, a soil unit weight of $\gamma' = 15.2kN/m^3$, stress dependent constants of $\kappa = 210$ and $\lambda = 0.5$ as well as an a peak friction angle of $\varphi' = 35.5^\circ$. The coefficient of contact friction was evaluated by direct shear tests to be $\mu = 0.415$. The remaining inputs are based on (2).

To compare the IGtH-Heat prediction with field data, the initial heating phase is considered. Therein, the media temperature rises from $T = 13.2^\circ C$ to $T = 88.0^\circ C$. In consequence, the same loading was adopted for the design calculation. The axial displacements are compared at $x = 40m$. In the test side, an axial movement of $u = 23.5mm$ was measured. In IGtH-Heat, firstly a calculation was carried out under neglect of interaction effects or influences from radial expansion. Thereby, a displacement of $u = 26.6mm$ resulted, which is a deviation of approximately 13%. Subsequently, the media temperature dependent formulation of frictional spring stiffness was taken into account, leading to a calculated displacement of $u = 25.4mm$, which represents a deviation of 8%. In the final validation step, interaction effects were accounted for in addition. The resulting displacement was $u = 24.8mm$ or in terms of deviation: 5.5%. Thus, the deviation could be more than halved based on the proposed design approach for lateral and axial spring stiffness.

4. Conclusion and perspective

Within the paper at hand, the interaction of the soils reaction components bedding pressure and friction resistance was investigated. Therefore, after a brief introduction, the state of knowledge was summarized. In the following, a three dimensional finite element was introduced, using the sophisticated hypoplastic material model to describe the stress-strain behavior of the soil. For a reference system, the oblique angle was varied in a wide range. Based on these results, new formulations for both reaction components were proposed. In addition, the temperature dependent radial pipeline extension and the resulting stress changes within the soil were incorporated.

Finally, these design approaches were implemented into the academic design code IGtH-Heat. Therewith, calculations were carried out in order to compare them to field data. It was shown, that by the use of the new formulations, the deviation between prediction and measurement could be more than halved (13% -> 5.5%).

In future work we intend to extend the numerical modeling to different geometric properties in terms of diameter and embedment depth as well as a variation of soils deposit density.

Acknowledgements

The presented research work was funded by the German Federal Ministry of Economic Affairs and Energy under Grant number 03ET1335B. The support is gratefully acknowledged.

References

- [1] Achmus, Martin and Weidlich, Ingo. "Interaktion zwischen Fernwärmeleitungen und dem umgebenden Boden". *Bautechnik* 93 (2016), 663-671. (in German)
- [2] AGFW e.V. "Verlegung und Statik von Kunststoffmantelrohren (KMR) für Fernwärmenetze" (2007). (in German)
- [3] Coulomb, C. A. "Essai sur une application des regles des maximis et minimis a quelques problems de statique relatifs, a la architecture". *Mem. Acad. Roy. Div.Sav.* 7. 1776, 343–387. (in French)
- [4] Jaky, J. "Pressure in silos", London (1948), Vol. 1, 2nd ICSMFE. 1948, 103-107.
- [5] Gramm, G. "Statik und Festigkeit des Kunststoffmantelrohres". *3R International* Jg. 22, Nr.7/8. (1983), 355–357. (in German)
- [6] HEW. "Fernwärmehtransportleitung Karoline-Wedel Kunststoffmantelrohr DN 700". Hannover, (1987). (in German)
- [7] Gietzelt, M., et al. "Ermittlung der Reibungskräfte an erdverlegten wärmeleitenden Leitungen zur Sicherstellung wirtschaftlicher Konstruktionen". (1991). (in German)
- [8] Huber, M. and Wijewickreme, D. "Thermal Influence on Axial Pullout Resistance of Buried District Heating Pipes". Stockholm, Sweden, (2014). *14th International Symposium on District Heating and Cooling*.
- [9] Achmus, Martin. "Zur Berechnung der Beanspruchungen und Verschiebungen erdverlegter Fernwärmeleitungen". Hannover: Institut für Grundbau, Bodenmechanik und Energiewasserbau, (1995). (in German)
- [10] Beilke, O. Interaktionsverhalten des Bauwerks "Fernwärmeleitung-Bettungsmaterial". Institut für Grundbau, Bodenmechanik und Energiewasserbau, (1993). (in German)
- [11] Gerlach, Tim and Achmus, Martin. "On the influence of thermally induced radial pipe extension on the axial friction resistance". *Energy Procedia*. (2017), Vol. 116, pp. 351-364.
- [12] Audibert, Jean ME and Nyman, Kenneth J. "Soil restraint against horizontal motion of pipes". *Journal of the Geotechnical Engineering Division*. (1977), Vol. 103, pp. 1119-1142.
- [13] Hansen, N.B. and Christensen, N.H. "The Ultimate Resistance of Rigid Piles Against Transversal Forces: Model Tests with Transversally Loaded Rigid Piles in Sand". Geoteknisk Institut (1961).
- [14] Trautmann, Charles H. and O'Rourke, Thomas D. "Lateral force-displacement response of buried pipe". *Journal of Geotechnical Engineering*. 9 (1985) Vol. 111, pp. 1077–1092.
- [15] Hsu, T. W., Chen, Y. J., & Wu, C. Y. "Soil friction restraint of oblique pipelines in loose sand". *Journal of transportation engineering*. (2001), Vol. 127(1), pp. 82-87.
- [16] Hsu, T. W., Chen, Y. J., & Hung, W. C. "Soil restraint to oblique movement of buried pipes in dense sand". *Journal of Transportation Engineering*. (2006), Vol. 132(2), pp. 175-181.
- [17] Daiyan, N., Kenny, S., Phillips, R., & Popescu, R. "Investigating pipeline–soil interaction under axial–lateral relative movements in sand". *Canadian Geotechnical Journal*. (2011), Vol. 48(11), pp. 1683-1695.
- [18] Hibbitt, D., Karlsson, B., & Sorensen, P. "ABAQUS 6.11: a computer software for finite element analysis" Dassault Systems, (2011)
- [19] G. Gudenus, A. Amorosi, A. Gens, I. Herle, D. Kolymbas, D. Mašin, D. Muir Wood, R. Nova, A. Niemunis, M. Pastor, C. Tamagnini, and G. Viggiani. "The soilmodels.info project". *International Journal for Numerical and Analytical Methods in Geomechanics*. (2008), Vol. 12, 32, pp. 1571-1572.
- [20] von Wolffersdorff, P. A. "A hypoplastic relation for granular materials with a predefined limit state surface". *Mechanics of Cohesive-frictional Materials*. (1996), Vol. 1(3), pp. 251-271.
- [21] tom Würden, Florian. "Untersuchungen zum räumlichen aktiven Erddruck auf starre vertikale Bauteile im nichtbindigen Boden": Institut für Grundbau, Bodenmechanik und Energiewasserbau (IGBE), (2010). (in German)



16th International Symposium on District Heating and Cooling, DHC2018,
9–12 September 2018, Hamburg, Germany

The role of district heating in coupling of the future renewable energy sectors

Oddgeir Gudmundsson^{a*}, Jan Eric Thorsen, Marek Brand

^a*Danfoss A/S, Nordborgvej 81, 6430 Nordborg, Denmark*

Abstract

For the last decades energy efficiency initiatives have avoided enormous amounts of energy consumption, to the favor of the environment and consumer expenditures. Although there is still a big potential for further energy efficiency improvements it is time to move further and start preparing the whole energy system for the challenge of oversupply from intermittent renewable energy sources, particularly in the power sector. In 2015 the maximum one-hour power oversupply from wind turbines alone in Denmark happened the 26th of June, peaking at around 900 MW and the oversupply over a 15-hour period was 10 GWh. Known solutions to make use of oversupply in the power sector are power export, energy storage and halting the power generation. The power export needs to rely on sufficient capacity at local interconnectors, power demand in the importing country and there is an economic gain in the export. Energy storages can range from storing of power in batteries, pumped hydro, synthetic fuels to fuel displacing at other energy sectors. The last option is stopping the turbines, which should be avoided. The optimum energy storage would have large capacity, fast charging, high recovery efficiency and low cost. Scoring high on all criteria's can be difficult when focusing on a single energy sector. By widening the perspective and start taking advantages of synergies between the energy sectors there is a possibility to score high on all three criteria's. In this paper the potential of utilizing synergies between the power and heat sectors will be explored by considering the projections for the Danish energy system in 2025. The result of the analysis shows the optimum energy storage of renewable power is achieved through fuel displacement in the heating sector in combination with utility sized heat pumps, electric boilers and large thermal storages.

© 2018 The Authors. Published by Elsevier Ltd.

This is an open access article under the CC BY-NC-ND license (<https://creativecommons.org/licenses/by-nc-nd/4.0/>)

Selection and peer-review under responsibility of the scientific committee of the 16th International Symposium on District Heating and Cooling, DHC2018.

* Corresponding author. Tel.: +45 74882527; fax: +45 74 7449 0949
E-mail address: og@danfoss.com

Keywords: district heating; power; cost efficient; renewables; energy efficiency; coupling of energy sectors

1. Introduction

District energy is the nominator for district heating, which has been utilized since 1880, and district cooling, which has been gaining ground in the last two decades. As district energy systems are by nature infrastructure for energy transfer they are fuel independent, meaning that if the heat or cool are at the right temperature levels it is irrelevant how it was produced. This fact puts district energy systems in an advantageous place in the green and renewable energy system of the future as it can integrate the various energy sectors and significantly increase their overall energy efficiencies. The commonly mentioned heat sources for district heating are combined heat and power (CHP) together with the utilization of heat from waste incinerations and various industrial surplus heat sources as well as the inclusion of geothermal and solar thermal heat.

As district heating is the focus of this article it is worth to note that the history of district heating (DH) goes quite some years back. During the years it has developed to fulfil the demands as they came up, typically driven by the demand for reduced investment and heat costs, but also lower equipment space demands, concerns of energy efficiency, environment, longer life-time, and lower fire risks. The development has been categorized in 4 generations which each indicate major changes in the technology [1]. Currently most DH schemes being operated are categorized as being at the stage of 3rd generation DH technology starting its transition to the 4th generation DH [1] to address the challenge of the future non-fossil and renewable based energy system and integrating the different energy sectors. The major improvements with the 4GDH are the lower operational temperature, smart system control and focus on energy efficiency and incorporating more renewable and surplus heat sources in the local surroundings, either by direct usage or through temperature boosting using large scale heat pumps.

The synergy between the energy sectors is further one key point of the 4GDH as district heating provides the means to store large amounts of energy for long time periods in an environmental friendly way at a very low cost. The synergies district heating has with the other energy sectors can be on various forms such as utilizing excess power production during periods of high wind and solar intensity and utilizing excess heat from industrial processes of converting solid biomass into biogas and/or liquid biofuels for the transportation sector or long-term energy storage for power generation through fuel displacement.

When talking about synergies between the energy using sectors it will inevitably be focused on the power sector, due to the highest energy quality and difficulties to store large amounts of power.

Nomenclature

DH	district heating
CHP	combined heat and power
P2P	power-to-power

2. Comparison of the energy sectors yearly demand profiles

When considering the energy demands it is important to note the difference in the consumption profile between the different forms of energy demand, see Figure 1. If excluding power consumption for space conditioning the power demand is essentially instantaneous demand, independent at the period of the year. Electric appliances are either turned on or off, which lead to clear system daily variations but only moderate variations between months, see top figure in Figure 1. The transport sector behaves similar as the power sector, with clear daily variations and moderate monthly variations, see middle figure in Figure 1. The heating and cooling sector which is compromised by two general use cases, space conditioning and domestic hot water (DHW) demands, has a completely different behavior. The demand from space conditioning has seasonal behavior as the energy demand for space conditioning is dependent on the outdoor temperature. The DHW demand on the other hand has clear daily variations but limited monthly variations. The bottom figure in Figure 1 shows the combined DHW and space heating behavior across a year.

Figure 1 shows that the power and transportation sector energy demand has monthly variations by 20-30% over the year, the energy demand of the heating sector is varying by factor 10.

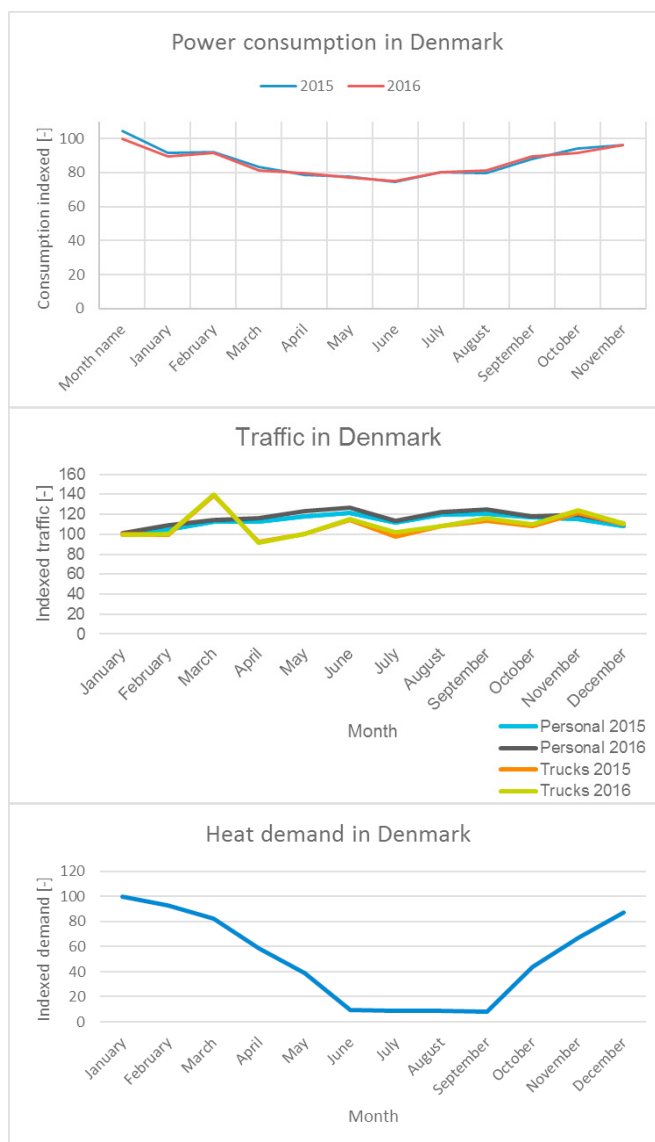


Figure 1. Top: Monthly power consumption in Denmark for the years 2015-2016, normalized for January [2]. Middle: Traffic per month in Denmark. Both the personal and truck traffic is normalized to January respectively [3]. Bottom: Heat demand per month in Denmark 2015, normalized to January.

3. Power sector

The main challenge of the power sector is expected to be increased share of renewable power, mainly wind power, see Figure 2 to the right. According to Energinet’s projections the traditional power demand in Denmark is projected to be stable around 32.000 GWh/year for the coming decades, when considering both increase in traditional loads as well as expected energy efficiency measures [4]. On top of increase in traditional loads it is expected that new loads will be data centers, in the short run, and the electrification of the transport sector in the long run. The power demand from data centers

will inevitably be part of the base load but the electrified transport sector will add new variable demands. To some extent the electrified transport sector has been suggest to be used as electric sinks or even electric storages in periods of high share of renewable power.

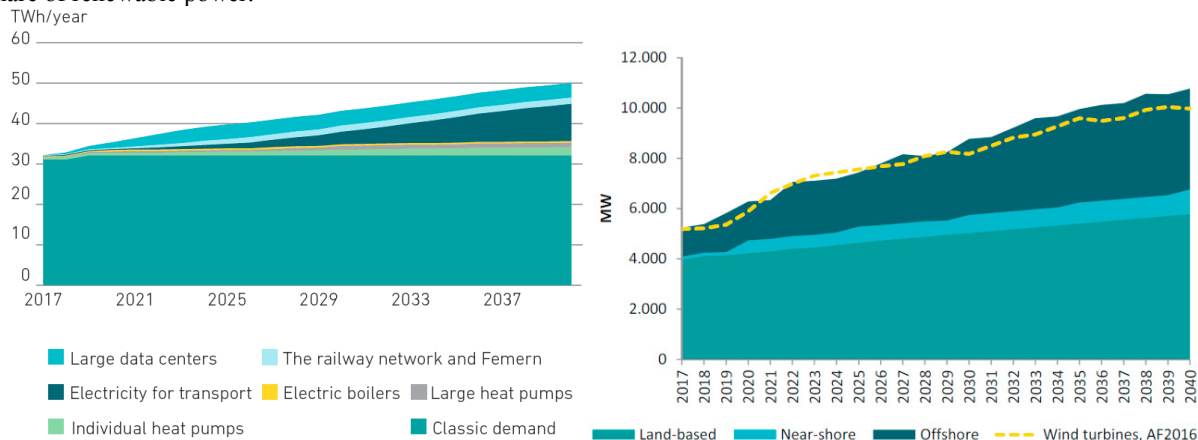


Figure 2. Left: Projected power demand in the Denmark. Right: Projected development of power capacity from wind turbines, yellow dotted line indicates projections made in 2016 [4].

In relation to synergies with the heating sector it has historically been in relation to combined heat and power plants, where the waste heat from the power generation was supplied to the district heating system. In the future renewable based power sector the role of district heating is expected to expand significantly. Firstly, in the role of energy storage provider and secondly in the role of grid balancing user.

3.1. Maximizing renewable power in the power sector

With the ambition of a green energy system the share of intermittent energy sources, wind and solar, will increase. The challenge with intermittent sources is that they do not have constant and reliable supply, as an example in 2015 the 5.070 MW installed wind capacity in Denmark had yearly utilization factor of only 32%, for solar power the utilization factor was approximately 14%. This fact clearly implies that to achieve a dominant share of renewables in the overall demand a significant over capacity is needed, which can cause problems by itself during periods of excessive renewable power generation. As an example, in 2015 there were multiple periods where the power generation from wind turbines exceeded the total power demand, the most severe excess power generation in 2015 occurred between 7:00-8:00 26th of July with power generated by wind exceeding the demand by 985 MW, see the top figure in Figure 3. In the period from 03:00-17:00 26th of July the cumulative excess wind power amounted to staggering 10.098 MWh [5]. During the period the price of electricity dropped significantly on the Nordic electric spot market and the average spot price over the period was around 17% of the average price of the excess power in 2015 [6]. Which clearly signals that the law of supply and demand is working well, leading to low prices at periods of excessive supply.

The impact of the projected installed wind power capacity can be analyzed by looking in the condition in 2015, which had wind capacity of 5.070 MW and oversupply of 148 GWh, and scaling up the wind power according to the projections in Figure 2. In 2025 the installed wind power capacity is expected to be 7.400 MW with an estimated oversupply of 1.960 GWh, more than 13-fold compared to 2015. As shown in the bottom figure in Figure 3 the amount and periods with excess power will grow significantly compared to 2015, top figure.

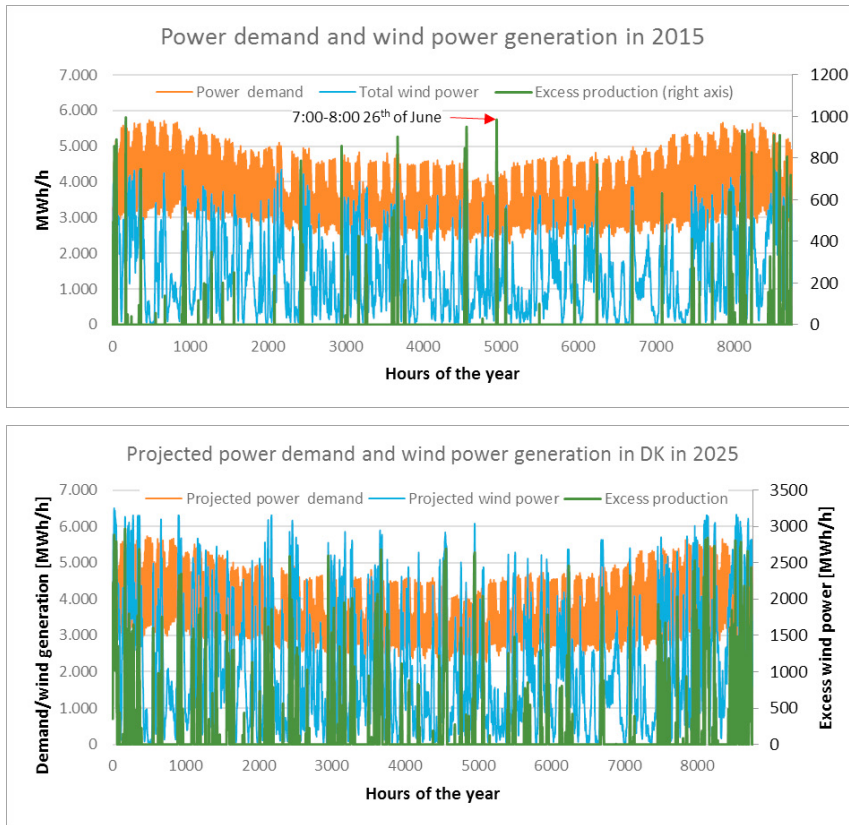


Figure 3. Top: Power demand and wind power generated in 2015. Bottom: 2015 power demand and projected 2025 wind power generated.

In addition to the wind power there is expected an increased power generation from photovoltaics, see Figure 4. However, as the solar power is not expected to have significant growth until after 2025 it is not considered in this study, but the general impact will be increased oversupply at certain periods.

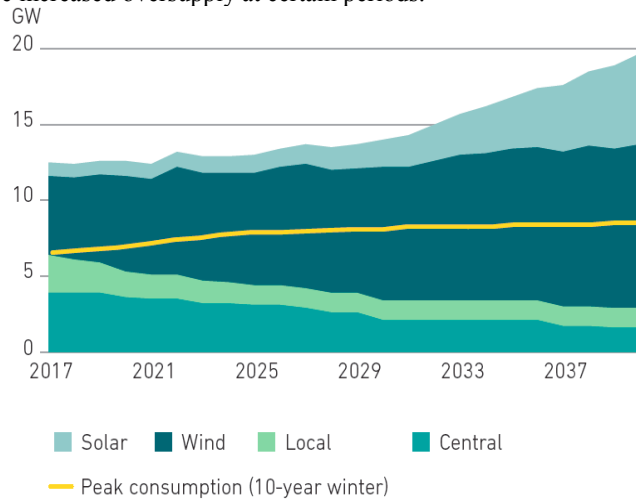


Figure 4. Peak power generation capacity in Denmark in 2017 and projection to 2040 [4].

4. Exploiting synergies between sectors

In a smart energy system, the optimum solution is achieved by exploiting synergies between the energy sectors. However, to be able to take advantages of the synergies it is important to identify the circumstances within each sector and the means that can be used for that purpose.

4.1. Exporting of excess power

Although the amount of excess power is unlikely to surpass the capacity of interconnectors between Denmark and its neighboring countries power export may not be the most economical way of utilizing the excess power. If it possible to generate higher value domestically than is achieved through export it should be done. In this respect it is important to keep in mind that the selling price of electricity in the Nordpool spot market is determined by the market, i.e. it is determined by the supply and demand, see Figure 5. In 2015 the selling price at periods of excess power generation was on average 60-70% of the yearly average price per MWh on the Nordpool power exchange spot market, at the period of maximum oversupply the export price was less than 10% of the average price [6]. Considering similar trends with buildup of renewable power industries, wind and solar, in the neighboring countries, Germany and Sweden, the trend of significant lower than average prices for renewable power will likely increase, which will put focus on local usage of excess power. Local usage could be power storage through batteries, power for the transportation sector, manufacturing of synthetic fuels or heat generation in district heating systems.

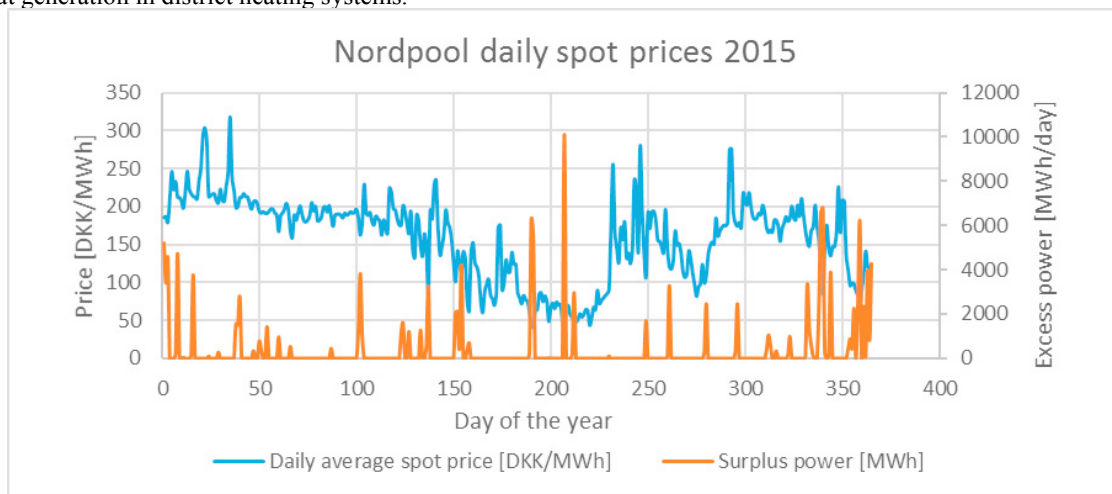


Figure 5. Excess wind power and daily average Nordpool spot prices.

4.2. Batteries

In this paper the term battery is defined as any technology that is storing a power in a medium for the purpose of generating power at later stages. The energy storing method can for example be based on a chemical, compressed medium and elevated medium potentials and virtual batteries. Figure 6 gives an overview of traditional battery technologies in terms of the power rating and discharging time. By viewing the figure in respect to the expected amounts of hourly excess power generation in the future renewable energy systems only few technologies are really applicable.

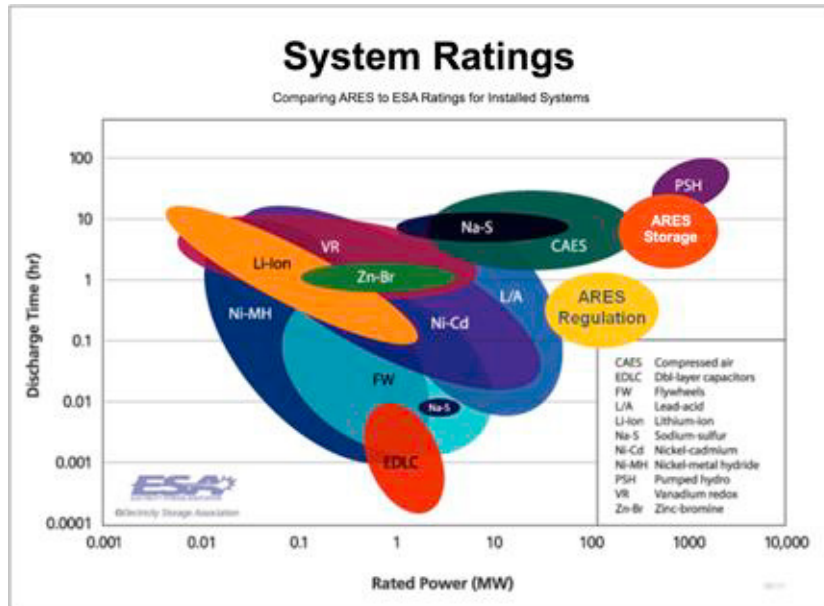


Figure 6. Typical power rating and discharge periods of typical power storage systems [7].

Chemical based batteries in a utility size are very capital expensive per capacity and hence require intense charging/discharging cycles to achieve cost efficient usage. Due to the high cost and environmental concerns chemical batteries might not be a sustainable solution for systems with immense over generation for short period of time followed by no excess supply for longer periods. The biggest batteries today have charging/dispensing rate of around 50 MW and 300 MWh capacity [8], which is not even close to the Danish oversupply peak of 985 MW and 10.098 MWh 26th of July in 2015.

Batteries like compressed air energy storage (CAES), advanced rail energy storage (ARES) and pumped-storage hydroelectricity (PSH) required certain geographical features to be applicable. Assuming the right conditions are available the potential capacity can be couple of factors greater than is achieved in todays chemical batteries. The round-trip efficiency of CAES is in the range of 60% and ARES and PSH in the range of 70%-85%.

4.3. Decentralized batteries – transport sector

With the high reliability of modern electricity grids, 99,99% uptime in case of the Danish power system [9] It can be stated that the only decentralized batteries that will make sense are batteries that would be needed anyhow due to non-connected units, like batteries in the transport industry. In that respect there have been ongoing discussions about the role of electric cars in enabling renewable energy and balancing the supply and the demand. The challenge with this approach is that first of all it will add to base demand, which will inevitably increase the base power generation capacity to compensate for the increase demand, secondly it is not logical to expect that the cars will always be plugged in and available for participating in the power market, thirdly the available battery capacity to be manipulated per car will likely be at max 60% at the time it is connected. To get an idea on the impact electric cars can have to absorb excess power in the power grid in 2025 the assumptions in Figure 7 are used.

Assumptions:

Battery capacity: 50 kWh
 Minimum acceptable charging level: 40%
 Daily electricity demand: 7,1 kWh
 Charging period:
 - 80% of cars charged between 19:00-7:00
 - 20% of cars charged between 7:00-19:00
 Charging rate: 3,6 kW
 500.000 electric cars (20% of DK)

**Potentials:**

500.000 electric cars (20% of cars in DK)
 Total capacity: 25 GWh
 Max effective charging capacity: 15 GWh
 Average effective charging capacity: 7,5 GWh
 Daily demand: 3,5 GWh
 Max night time charging rate: 1.440 MW
 Max day time charging rate: 360 MW

Figure 7. Assumptions used to access the impact of electric cars in DK.

The following results are based on that the electric cars are only charged above 40% in case there is excess power available in the system, if there is no excess power available they are only charged to 40%. For this assumption to hold a smart charger that is communicating with the power system would be required. By taking the assumptions above and run them over a year in correlation with estimated excess wind power from renewables in Denmark in 2025 it was estimated the electric cars could absorb 798 GWh of the 1.956 GWh of expected excess power in the grid in 2025. This would be a best-case scenario considering that 1st of January 2017 there were only 8.930 electric cars [9] in the fleet of 2.465.000 personal cars in Denmark [11] and new registered cars in 2016 and 2017 were 222.000 per year [12]. In respect to the rest of Europe the average share of electric cars of new car registrations in 2017 was <1% [13].

As the ambition of the world is to become fossil free only the load shifting potential of electric vehicles is considered. For the sake the curious reader the power-to-power (P2P) round efficiency from displacing fuels in the transport sector is estimated to be in the range of 105%-155% given an oil power plant with 45% efficiency. The efficiency might be somewhat higher if additional energy savings could be achieved at the refinery plants.

Although fuel displacement is not considered relevant for the transport sector the electrification of the transport sector brings in another opportunity, which is load shifting through utility management of the batteries. Assuming it would be acceptable to discharge the batteries down to a minimum of 40% at periods of no excess renewable power and recharge at periods of excess power higher share of excess power could be absorbed. In this study the additional potential was estimated to be 148 GWh. In reality it would be less, as not all car owners might want to participate in such market and the capacity available at any given time would generally be lower than the best-case scenario considered here, due not all cars being connected to the grid as systematically as assumed in this study.

4.4. Virtual batteries - fuel displacement in the heating sector

There are two options when it comes to fuel displacement a) by using the excess power for manufacturing hydrogen through electrolysis and feed the hydrogen into an existing gas pipeline and b) by displacing fuels in industries that are currently burning fuels for heat or power generation. For fuel displacement the district heating industry is an obvious case example. At periods of excess power supply heat can be generating using heat pumps and electric boilers and used either directly to displace the applied fuel and in case of excess heat generation the heat can be stored in short term to seasonal thermal storages. Through fuel displacement via heat pumps and virtual batteries it is possible to get very high P2P efficiencies.

Case example – Wood chips:

A biomass CHP plant has 28% power efficiency and 55% heat efficiency in cogeneration mode, in a heat only mode it is assumed the heat efficiency is 85%. In the event of excess power supply 100 power units are used in a heat pump with COP of 3,5. The heat pump would in this case displace fuels in the biomass plant operating in a heat only mode, resulting in displacement of $350 \text{ units} / 84\% = 417 \text{ units}$ of input fuels. At later stage those 417 displaced fuel units could be burned with power generation efficiency of 28%, resulting in the 117 units of power being generated. The P2P efficiency in this case would be 117%.

Case example – Natural gas:

Another example could be where natural gas is displaced from a heat only boiler and then burned at later stage at a large high efficient combined cycle gas turbine plant with power generating efficiency of 60%. Assuming that the gas heat only boiler has efficiency of 105% the heat pump the 100 power units could displace 333 units of input fuels. When those

displaced fuel units are burned in the efficient power plant 200 power units could be generated. The P2P efficiency in this case would be 200%.

From the two cases above it is clear that if there is a possibility to displace fuels by renewable power in existing systems very high P2P round efficiencies can be achieved.

5. Synthetic fuels for storing power

Alternative to storing power in batteries, real and virtual, would be to go for synthetic fuel production. Synthetic fuels produced at periods of excess power can be used for long term energy storage and converted back to power when there is a lack of renewable power in the power system. The main challenges with this approach are high plant investment costs and conversion losses, both during synthetic fuel production and when converting them back to power. The most likely synthetic fuel to be produced with excess power is hydrogen through electrolysis. The expected efficiency of electrolysis can be in the range of 60-70% [13]. The efficiency when the hydrogen would be used for power generation could be 50-60%, similar as combined cycle power plants [15], leading to P2P efficiencies in the range of 30-42%. It should be noted that both in the electrolysis and the following power generating process excess heat could be captured and used for district heating purposes, this would although lead to lower P2P efficiencies. In addition of being a clean heat the avoided fuel consumption in the district heating systems could be used for power generation purposes when there is a lack of wind power in the system, hence effectively taking over the functionality of synthetic fuels for power generation.

6. Conclusions

The share of intermittent renewables is increasing fast in the energy sector. The nature of the renewables will both bring opportunities as well as challenges to the energy systems. The main foreseeable challenge, as well as opportunity, will be the excess power generation in the power sector, which this paper focuses on. In relation to the excess power that is expected to be generated at periods of high winds and sunny days a luxury challenge/question rises, which is what should be done with the excess power? The answer to the question will depend on the system boundaries. The choice of system boundary in this paper was the country the energy is generated in. The following bullets present the main results from the study.

- Although the power export should in principle be the obvious solution to utilize excess power generated it has the drawback that the value of the power is dependent on the market conditions, supply and demand. When looking on the Nordpool electric spot prices it is clear that the value of the electricity is lower at periods of high share of renewable power than when there is limited or no renewable power in the system. Due to this fact it may be of higher value to store the power within the system boundaries for later usage.
- Under the assumption that the political aim is to make the transport industry fossil free the possibility of fuel displacement in the transport industry is irrelevant. The assumed 20% share of electric cars in the Danish 2025 car fleet is estimated to hold 148 GWh power load shifting capabilities. In respect to the yearly traditional power demand of 33.5 TWh it can be considered insignificant.
- With utilization of virtual batteries, which is basically fuel displacement in the heating sector, it would be possible to achieve less storage of large amount of power for long periods. In combination with heat pumps and thermal storages the power storage potential could be up to 200% of the excess power, or up to 11,6% of the yearly traditional power demand. The feasible storage potential will although be lower and dependent on the required investment in heat pumps, electric boilers and thermal storages.
- The last considered option was synthetic fuel production. From the expected P2P round efficiency of only 30-42% it should be considered the least attractive method for utilization of excess power.

The indications from this study is that the most sensible usage of the excess power in the Danish 2025 power system is to use it to displace fuels in the district heating systems. However, before a definite conclusion can be drawn it will be needed to make an investment analysis for the different alternatives.

Although the power sector has been the main focus in the paper there are interesting synergy potentials between the heating and transport sector in the coming renewable transport sector era. The synergy will be through utilization of waste heat when producing biomass based fuels or other synthetic fuels.

Recommended future studies will be to expand this analysis to take into account the investment costs required to achieve fuel displacements in the heating sector as well as in the synthetic fuel production scenario.

References

- [1] Lund, Henrik et. al., “4th Generation District Heating (4GDH) - Integrating smart thermal grids into future sustainable energy systems,” *Energy*, vol. 68, pp. 1-11, 2014.
- [2] Energi Data Service, “Consumption per Municipality,” <https://www.energidataservice.dk/en/dataset/communityconsumption>. [Accessed 30 May 2018].
- [3] Vejdirektoratet. http://www.vejdirektoratet.dk/DA/viden_og_data/statistik/Sider/default.aspx. [Accessed 30 May 2018].
- [4] JAE-KNY/MDA, “Energinet's analysis assumptions 2017,” Energinet, Copenhagen, 2017.
- [5] P.-F. Bach, “Download Hourly Time Series,” www.pfbach.dk/. [Accessed 30 May 2018].
- [6] Nordpool, “Historical Market Data”. www.nordpoolgroup.com/historical-market-data/. [Accessed 30 May 2018].
- [7] Energy Storage Association, “Energy Storage Association”. www.energystorage.org. [Accessed 30 May 2018].
- [8] Brown, Peter, “Mitsubishi Installs 50MW Energy Storage System to Japanese Power Company” <http://electronics360.globalspec.com/article/6402/mitsubishi-installs-50mw-energy-storage-system-to-japanese-power-company>. [Accessed 30 May 2018].
- [9] State of Green, “Denmark's electricity grid leading in Europe” <https://stateofgreen.com/en/profiles/invest-in-denmark/news/denmark-s-electricity-grid-leading-in-europe>. [Accessed 30 May 2018].
- [10] Dahlin, Ulrik, “Nu falder antallet af elbiler i Danmark,” *Information.dk*, 24 February 2017. www.information.dk/indland/2017/02/falder-antallet-elbiler-danmark. [Accessed 29 May 2018].
- [11] Dansk Transport Authority, “Nøgletal om vejtransport” www.vejdirektoratet.dk/DA/viden_og_data/statistik/trafikken%20i%20tal/Noegletal_om_vejtransport/Sider/default.aspx. [Accessed 30 May 2018].
- [12] Danmark statistik, “Nyregistrerede og brugte biler” <https://www.dst.dk/da/Statistik/emner/priser-og-forbrug/biler/nyregistrerede-og-brugte-biler>. [Accessed 30 May 2018].
- [13] European Alternative Fuel Observatory - European Commission, “Electric cars in Europe”. www.eafo.eu/Europe. [Accessed 30 May 2018].
- [14] Danish Energy Agency, “Technology Data for Renewable Fuels” Energinet, Copenhagen, June, 2017.
- [15] Danish Energy Agency, “Technology Data for Energy Plants for Electricity and District heating generation” Energinet, Copenhagen, March, 2018.



16th International Symposium on District Heating and Cooling, DHC2018,
9–12 September 2018, Hamburg, Germany

Improving district heat sustainability and competitiveness with heat pumps in the future Nordic energy system

Kristo Helin^{a,*}, Sanna Syri^a, Behnam Zakeri^{a,b}

^aDepartment of Mechanical Engineering, School of Engineering, Aalto University, Otakaari 4, 02150 Espoo, Finland

^bSustainable Energy Planning, Department of Planning, Aalborg University, A. C. Meyers Vænge 15, 2450 Copenhagen, Denmark

Abstract

District heating (DH) in Nordic countries largely relies on efficient large-scale combined heat and power (CHP) production. The currently low electricity market price has diminished the economic competitiveness of CHP production. Production of DH increasingly happens in thermal heat-only boilers, increasing long-term environmental impacts. An alternative is the use of large-scale heat pumps (LHPs). Utilization of LHPs in hours of low electricity price could be economically advantageous to producers, reduce carbon emissions from burning fuels, and aid in balancing the production and consumption of electricity in a future energy system where electricity production from variable renewable energy is increasing rapidly.

© 2018 The Authors. Published by Elsevier Ltd.

This is an open access article under the CC BY-NC-ND license (<https://creativecommons.org/licenses/by-nc-nd/4.0/>)

Selection and peer-review under responsibility of the scientific committee of the 16th International Symposium on District Heating and Cooling, DHC2018.

Keywords: heat pump; district heat; energy system modeling; variable renewable energy; CHP

1. Introduction

Nordic district heating (DH) is in large part produced in efficient, large-scale combined heat and power (CHP) plants. For peak and backup operation and small networks, likewise common heat-only boilers (HOBs) are

* Corresponding author. Tel.: +358505607256.

E-mail address: kristo.helin@aalto.fi

preferred. This dynamic is set to change, if the market price of electricity in the Nordic countries (Finland, Sweden, Denmark, and Norway) remains at a low level. The current price level is not sufficient for long-term investments in a large share of existing CHP plants [1]. We expect this to lead to a trend of replacing ageing DH CHP plants with HOBs in the Nordic countries, and this has already been noted in Finland [1] and Denmark [2].

As the relative profitability of CHP in DH production is decreasing due to a low market price of electricity, the same reason is increasing the relative profitability of large-scale heat pumps (LHPs), which produce heat with electricity. Although they are already in use in Nordic DH networks [3], their operational environment is greatly improved with a low price level of electricity. Moreover, even if the price of electricity on average does increase (as expected by many authorities (see e.g. [4–6])), the ongoing rapid growth in the share of variable renewable energy (VRE) based electricity production is expected to bring about more volatility and seasonality into electricity prices, accentuating price peaks and valleys [7]. This will open the possibility for DH producers with LHP capacity to benefit not only from price highs with CHP electricity production, but also from price lows that make heat production from LHPs more economical than from HOBs.

Electricity production in the Nordic countries has notably low carbon emissions. This is due to the technology mix utilized: in 2015, most of electricity production was divided between hydro (58%), nuclear (19%), CHP (11%), and wind power (9%) [8–12]. Due to the marginal cost based pricing system in the Nordic electricity market, the hourly emissions of electricity production (per megawatt-hour) are tied to the amount of hourly production.

Production of DH, in contrast with electricity production, is mostly based on burning fuels, fossil or renewable. In 2015, main technologies utilized were CHP (54% of production), and HOB (estimated at 30% of production) [9], [11], [13–15]. Because there is necessarily only limited trade between DH networks, the networks are limited to the same set of fuels at all times. On the national level, the fossil fuel share in DH production is around 55%, 15%, 40%, and 5% in Finland, Sweden, Denmark, and Norway, respectively, as collected in [16]. Corresponding total DH productions were 35, 52, 35, and 7 TWh, respectively [8], [9], [11], [15].

In the future, an increasing number of DH networks could utilize LHPs in DH production. These LHPs can have a coefficient of performance (COP) of over 3 [17], meaning they can provide thermal energy three times as much as they consume as electricity. In this vision, DH networks would become linked to the electricity market, and they would be able to utilize low-CO₂ and low-priced electricity for heat production when it is available [18].

While the addition of a single LHP to a DH network is a pure investment consideration, the addition of a large total capacity of LHPs to DH networks may affect the whole electricity market. Due to marginal pricing in the Nordic electricity market, the price of electricity (theoretically) increases with each additional megawatt-hour of demand. For example, 500–1000 MW_e of LHP capacity operating simultaneously will increase the total electricity demand corresponding to the total production of a medium-to-large power plant, necessarily affecting the hourly market price. Implications of this dynamic are discussed in depth in [19]. It is important to model the electricity market, along with DH production, in order to understand the system level effects of a large increase in DH LHP utilization.

In this work, we focus on the electricity market perspective of increasing LHP capacity in Nordic DH networks. Our goal is to quantify how a sizeable increase in LHP electricity consumption in the cheapest hours of the year would affect the overall operation of the electricity market and the operation of DH networks. We assess the effects of LHP capacity additions in scenarios with differing electricity production capacities and yearly electricity demands. Our results show that LHPs have the potential to decrease the cost of DH production, to decrease fuel use in the whole Nordic electricity and DH system, and counteract the low price level in the Nordic electricity market.

Nomenclature

CHP	Combined heat and power
COP	Coefficient of performance (heat pumps)
DH	District heating
HOB	Heat-only boiler
LHP	Large-scale heat pump
VRE	Variable renewable energy

2. Literature review

District heat became a part of the energy systems of Nordic countries aided by a wide range of possibilities, including efficient CHP heat and electricity production, utilization of communal waste, and a reduction of dependency on foreign fuels [16]. With these and other standpoints in mind, all Nordic countries support DH utilization with political and/or economic measures.

With a start (historically) as more of an electricity and oil saving heating device than a large-scale heating option, heat pumps had a harder time becoming widespread in the Nordic heating market than DH (see e.g. [20]). Especially the utilization of LHPs in DH systems is quite rare (currently about 1300 MW_{th} [21], a total of 600 MW_{th} of units listed in [22]), even though at least one such operation has existed in Sweden already since the 1970s [17].

Heat pump utilization for heating is different in nature from heat production with thermal processes in more conventional ways. Instead of direct heat production (as in an electric boiler), an LHP transfers heat from a heat source to a higher temperature, consuming electricity in the process. An LHPs COP, which describes the heat transferred per electricity consumed, is highest with the smallest temperature differences between the heated and cooled streams. For this reason, LHPs are installed near a heat source of sufficient size, stability and temperature. The availability of such heat sources is a requirement for investment in LHPs. Lund and Persson [23] have studied the sizes and locations of potential DH LHP heat sources in Denmark, showing that there are potential heat sources nearby almost all DH networks. However, local potentials relative to heat demand favor smaller networks. Lund and Persson have considered such LHP heat sources as industrial excess heat, supermarkets, waste water, ground water and water in rivers, lakes, and seas. Corresponding heat sources can be expected to be suitable also in other Nordic countries due to similar climates.

The potential of LHP heat production in the DH system of Greater Copenhagen has been assessed by Bach et al. [24] using the Balmorel modeling tool. Their results indicate clear potential for LHP usage with the LHP capacity of 260 MW_{th}, corresponding to around 10% of current yearly heat demand in the network with ca. 3500 full load hours. According to the authors' 2025 scenario, the LHPs will have ca. 4000 full load hours. The authors additionally make tests to determine whether the COP of heat pumps needs to be modeled seasonally, or whether a constant value may be used. Based on the results, a constant COP value is sufficient for high level modeling, such as this work.

Schweiger et al. [18] estimate the technical and economic potential of power-to-heat in Swedish district heating to 2 TWh/a in their (year 2050) scenario with 70 TWh/a wind power. They analyze the potential with electric boilers, and state that with LHPs the potential would be lower by a factor of 2–4, because DH demand is a notable limiting factor. A thermal storage with a capacity corresponding to 25% of daily demand is found to improve the potential by 9%. Hast et al. [25] also report that total DH production costs can be reduced with heat storage in a network with a large LHP (20 MW_{th}) relative to network peak demand (ca. 115 MW_{th}). Lund et al. [2] find clear socio-economic benefits from adding an LHP capacity between 2 and 4 GW_{th} to the Danish energy system. They state that LHPs for DH are not currently a feasible investment due to the Danish tax structure, and call for regulatory changes to encourage investment. The investment cost of for a small LHP unit is estimated in [26] to be 0.7 M€/MW_{th}. The corresponding estimates are 0.15 M€/MW_{th} for a small electric boiler, and 0.7 M€/MW_{th} for a small wood chip boiler.

Levihn [17] offers practical insight into the DH network in Stockholm, where heat pumps have long been in use, integrated to CHP plants. The insights include that the combination of LHPs and CHP allows wide heat production optimization based on electricity price, and that a COP of 3.3–3.5 can be achieved in the DH network that has a 65–115 °C supply interval.

3. Modeling method

We model the Nordic electricity market using the Enerallt electricity and DH model, which has been discussed in detail in [27]. New implementations to the model regarding the modeling of hydro power production and the pricing of CHP electricity production were presented in [28]. In the following, we present briefly the key operating principles of the Enerallt model.

Enerallt simulates the electricity market and DH production in the Nordic area on an hourly level. The simulation considers price areas or countries set up by the user and the electric interconnection capacities between them. In the version of Enerallt used in this work, the exchange of electricity between the Nordic countries and the external power markets is modeled as a set of fixed profiles from the reference year (here 2014). Enerallt is an especially capable model for modeling the hydro-dominated Nordic power market. With it, we can assess the effects of specific power production and consumption changes to the overall Nordic market.

3.1. District heating modeling

The DH demand of each modeled area is divided for different fuels and technologies based on plant capacities (for technologies) and historical fuel shares (for fuels). This is done because each area may contain numerous separate DH networks, which are tied to specific fuels and technologies. The division of DH demand is meant to capture this inflexibility as accurately as possible.

After the division, DH production is planned hourly for the whole year. Heating demand divided for HOBs is produced with HOBs, and the demand divided for CHP is produced by CHP plants and compensated with HOBs where necessary. Before these technologies are used, there is the possibility to produce heat from variable sources, here LHPs.

For CHP, it is not known at the time of DH planning if the electricity produced will be cleared in the market (if the area price is sufficiently high). The marginal cost of CHP electricity is additionally fuel (and area) dependent. Thus, the actual CHP production (cleared in the market) differs from the planned one both in amount and fuel distribution.

The share of CHP heat that is planned in the DH modeling, but is not purchased in the market, is replaced with HOB heat. On the other hand, if CHP electricity production is not planned (i.e. not all CHP heating capacity is needed), large CHP plants will offer their electricity production capacity to the electricity market as condensing power. It should be noted that without heat storage implemented (which is the case in this work), this methodology is electricity market focused, and the fuel mix changes resulting from the inflexibility of CHP production are not always realistic. However, this minor issue is mostly relevant in emission comparisons between DH technology scenarios.

3.2. Electricity market modeling

The electricity market simulation is made in a way that closely resembles the operation of the Nordpool Spot market. The simulation is carried out in three main steps, consecutively for each hour. First, the electricity demand is determined for each area. This includes LHP electricity demand from the DH modeling step. The electricity demand is not dependent on the price of electricity. Next, electricity supply (i.e. sell bids to the market) is determined. This happens by consolidating the marginal price and capacity combinations of the power production technologies. Third, the electricity market is simulated by determining first the system price of electricity, followed by the area price determination that considers the interconnection capacities between countries or price areas. As a result of this last calculation, also the production technologies, transmission line use, and other market outcome features become clear.

The method of hydro power modeling has a large impact on simulations of the Nordic electricity market. In this work, hydro power capacity is categorized based on country and storage capacity. Each category of capacity follows the reference year (here 2014) system price profile, which has been scaled first for each storage capacity category to reflect possibility to delay production, and then for each country to reflect the potential for profit with the available inflow. The latter scaling is done by running the model iteratively to find price levels that lead to the expected hydro power total yearly production in each country. A detailed description of the method used is available in [28].

4. Scenarios

We show the impact of LHPs on the electricity market and DH production in three different scenarios, which are projections of the electricity production and consumption developments in the Nordic area from year 2014 to 2030.

The base scenarios (without LHP capacity) have been presented in an earlier work [28]. From here on, we will use the word “scenario” for describing all “cases” (simulations with a specific LHP capacity) that are based on the same base scenario. Because LHP operation is very dependent on the price level on the electricity market, we assess the impact of LHPs in three scenarios with different qualities. The first is Scenario 2014, modeled with available data from that year. The second is Scenario 2030A, where wind power capacity has more than doubled from 2014, and nuclear capacity has increased, among other changes. Electricity and heating demands are unchanged. The third scenario is Scenario 2030B, which is identical to 2030A, except that electricity demand has increased from 2014 by 43 TWh (from national forecasts [4], [29–31]). The demand of DH is kept constant between the scenarios in order to show the effects of the LHPs clearly. In reality, according to the IEA Nordic Energy Technology Perspectives 2016 report [6], DH demand will fall in 2013–2050 about 1% annually, on average. Because of the tight connection between DH and CHP, we keep also CHP capacities constant over the scenarios. Nordic-level information about the scenarios is shown in Table 1. Detailed descriptions of the scenarios can be found in [28].

The LHP capacity to the base scenario is added identically in all cases. The capacity is set for a number of periods of 12+ hours so that the capacity is available for a total of 4000 hours with the lowest possible average system price, with the system prices of the appropriate base scenario with no LHP capacity. The purpose of this is to simulate LHP utilization in hours in which CHP production would be the least profitable or feasible. The LHPs are set to produce heat in connection with (and with priority over) existing CHP plants.

Table 1. Key attributes of the modeled scenarios.

	2014	2030
Hydro power	50,317 MW _e	51,843 MW _e
Nuclear power	11,200 MW _e	12,300 MW _e
CHP	15,280 MW _e	15,280 MW _e
–Of which large plants	9,484 MW _e	9,484 MW _e
Condensing power	9,146 MW _e	0 MW _e
Wind power	10,600 MW _e	28,800 MW _e
Solar power	627 MW _e	985 MW _e
Electricity demand	377 TWh	377 TWh (in 2030A) 420 TWh (in 2030B)
Carbon emission price	5 €/tCO ₂	20 €/tCO ₂

4. Results and discussion

In this section, we present results from adding 0–2000 MW_e of LHP capacity into the scenarios described in the previous section. We analyze the effects of LHP capacity increases in a logical manner, starting from effects on electricity production, moving on to effects on the electricity market, and to discussing the effects on the technologies and costs of heat production in the three scenarios. Finally, we analyze the sustainability of LHPs in the Nordic area.

In Figure 1, we show electricity production in CHP and condensing power plants in the Nordic countries in each scenario with a range of added LHP capacity. Clearly, total electricity production will increase by the consumption of the LHPs. This increase is approximately 3 TWh with 1000 MW_e of HP capacity, and 5 TWh with 2000 MW_e of HP capacity in all scenarios.

The increase in electricity production happens in condensing and CHP electricity production in Scenarios 2014 and 2030B. In Scenario 2030A, there is unused nuclear power capacity in the low electricity price hours because of the high share of VRE electricity production with low marginal costs. Thus, the increase in electricity consumption leads to an increase in nuclear power production specifically, due to its low marginal cost of production.

The total CHP power production decreases in each scenario with increasing LHP capacities. An exception to this observation is Scenario 2030B with 0–1000 MW_e of LHP capacity. There, CHP power production does decrease in

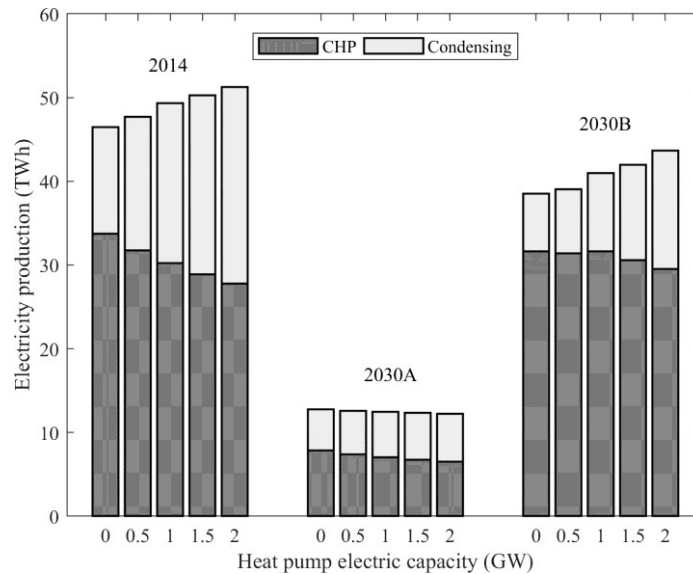


Figure 1. Production of CHP and condensing mode electricity in the three scenarios with different amounts of large-scale heat pump capacity. The base scenario is indicated at the top of each group of bars.

the hours when LHPs are running (like in the other scenarios), but this increases the average yearly electricity price so much that CHP production increases in other hours. These opposing changes in production approximately cancel each other out. The electricity price increase is not limited to the hours in which LHPs are running due to the myopic hydro production modeling method.

Regarding the changes in condensing and CHP power production shown in Figure 1, it should be noted that we do not consider DH heat storage or thermal inertia in this paper. Thus, CHP electricity production is restricted to satisfying the DH demand on each single hour. Compared to reality, this causes the model to overestimate the share of condensing power at the expense of CHP electricity production.

The system price of electricity is important in an effort to understand the dynamics of the Nordic electricity market concerning LHP capacity increases. In Figure 2, the system price is shown for each scenario with a set of LHP electric capacities. In the figure, the median system price and the range from the 25th to the 75th percentiles of hourly electricity prices during the modeled year are shown for each case. The implications of Figure 2 are tightly linked to those of Figure 1. For Scenario 2014, the system price increases steadily with increasing LHP capacities. This steadiness of change is interestingly visible also in Figure 1. For Scenario 2030B, the price increase is steeper, and perhaps surprisingly not linear. For Scenario 2030A, the price increase is practically nonexistent, with nuclear power remaining as the typical marginal price setting technology. It should be noted that in practice Scenario 2030A is discussed here as a scenario that is indicative of a more general oversupply situation. The authors of this paper do not believe such a low price level would be in practice possible without subsequent corrective adjustments in the market. However, modeling these adjustments is outside the scope of this work, and the scenario is included due to its value as an indicative scenario.

As is visible from the above discussion, the analyzed changes in heat and electricity production have interrelations that are not trivial. As examples, LHP capacity addition may cause an average price increase that causes the amount of CHP electricity production to increase. At the same time, this price increase would make LHP heat production less profitable. The consequences of these types of interrelations depend on the proportions of the studied system: the capacity of LHPs vs CHP, the share of CHP of total yearly heat production, the fuel mix of the CHP and condensing power plants, the fuels' relative prices, and other similar relationships. The issue of LHP operation affecting the electricity price (and hence, the profitability of the LHPs) is handled in a simple manner here, as LHP operation hours in all cases are chosen from the lowest price hours in the scenario without LHPs.

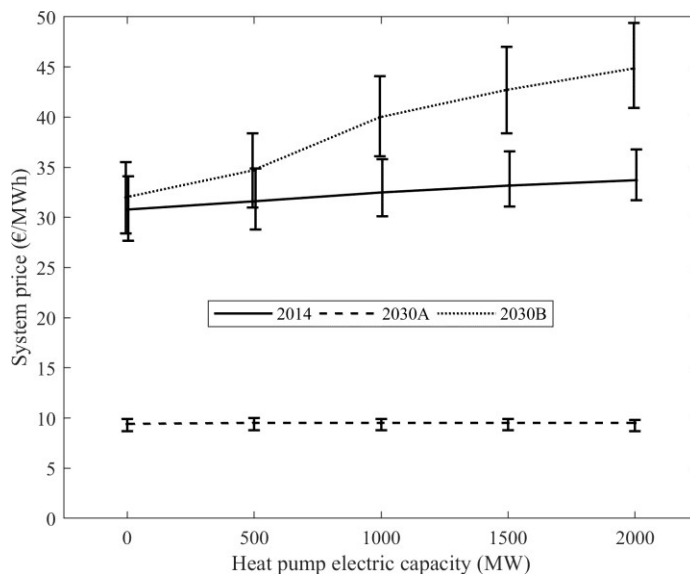


Figure 2. The median system price in the scenarios with different large-scale heat pump capacities. The vertical bars represent price variation during the year, specifically the 25th and 75th percentiles of the hourly system price.

In Figure 3, the total cost of heat production in the whole Nordic area is calculated for each scenario and case. In the calculation, variable heat production costs are considered for all plants. For LHPs, these are the cost of electricity plus an additional cost of 2 €/MWh_{th} for DH production (see [26]). For CHP, revenue from electricity sales is calculated separately from costs. For both CHP and LHP, the price of electricity is the area price of the hour of consumption or production. The total cost of heat production with CHP electricity revenue subtracted is shown with a white circle. Investment costs are not considered in the calculations.

It is seen from Figure 3 that the effects of LHPs on heat production costs are not decidedly linear. The only linearity in the figure that is common to all scenarios is the fact that the net cost of heat production decreases in each scenario with the addition of LHP capacity. The mechanism for the decreasing total cost varies in the scenarios. In Scenario 2014, the cost of CHP heat production decreases (due to the decrease in production), but it decreases more than the reduction of revenues from CHP electricity (due to the increasing system price). In Scenario 2030A, a straightforward cost decrease is seen due to the low cost of LHP heat production, which in turn is caused by the low price of electricity. In Scenario 2030B, the cost of heat production (not considering revenues) stays relatively unchanged compared to Scenario 2014 with different LHP capacities. However, revenue from CHP electricity increases with the LHP capacity (as the system price increases), causing the decline in the total heat production cost.

Next, we discuss the results regarding the sustainability of DH from two viewpoints: i) fuel consumption and CO₂ emissions, and ii) the long-term viability of the technology and fuel mix. The latter viewpoint is related to economic and system infrastructure issues, of which the economic side has been discussed above.

Our results indicate CO₂ emission reductions, if the fuel mix does not change. The total fuel consumption in DH and electricity production in the Nordic area is decreased by the addition of 2000 MW_e of LHP capacity by 5, 18, and 7 TWh (2%, 10%, and 3%) for Scenarios 2014, 2030A, and 2030B, respectively. This implies a significant potential for CO₂ emission reductions. The overall emission reductions in electricity and DH production depend on how the marginal power production fuels change because of LHP operation. The main fuels are coal, peat, natural gas, and biomass. As biomass is supported with financial mechanisms in all countries considered, we can assume that the fuel use reductions will be largely targeted at fossil fuels, such as coal. Because we have not modeled thermal inertia or heat storage of DH networks in this work, the current results do not realistically represent the dynamic of fuel mix changes from the LHP capacity additions.

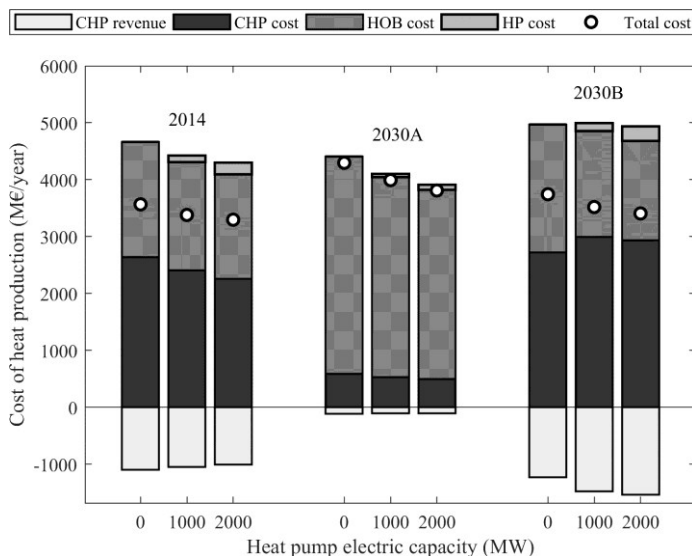


Figure 3. Costs of heat production from CHP, heat-only boiler, and large-scale heat pump units in the scenarios with different large-scale heat pump capacities. The revenue from CHP electricity production is shown separately from CHP heat production costs as a negative cost. The total net cost of heat production is marked with a white circle. The base scenario is indicated at the top of each group of bars.

The utilization of LHPs can be argued to increase the robustness of DH as a part of a low-CO₂ energy system. The diversification of heat production to power-to-heat technologies will improve flexibility of production in DH networks. This creates robustness against fuel and electricity price fluctuations in the future. From the perspective of the electricity and DH system, the interconnection of the two sectors is a vital early step in progressing towards a “smart energy system” as envisioned in [32]. The interconnection of the sectors may in the future add flexibility to electricity demand (e.g. through utilizing heat storages) and help in integrating a higher share of VRE in energy production than would be possible without its flexible use in the DH sector.

5. Conclusions

In this work, we analyzed three heat and electricity production scenarios for the Nordic area. We simulated the addition of varying amounts of DH LHP capacity to each scenario to investigate the effects this has on the electricity market and DH production. In our analysis, the LHPs were added to networks with existing CHP plants. Heat production by LHP was prioritized over CHP in 4000 hours with low electricity prices, where CHP production was less profitable or infeasible in the scenario without LHPs.

According to our results, the addition of LHPs into the DH systems decreases DH production operating costs in all examined scenarios by 8–12%, with taxes on LHP excluded. However, the market price of electricity increases at the same time by 0–40%, with the highest increase occurring in our high electricity demand scenario 2030B. As a result, the revenues of CHP plants increase relative to a unit of heat production. The electricity price increase is a positive impact for the Nordic electricity market that is currently experiencing a period of low electricity prices, which hinders investment in new electricity production capacity.

When LHP heat production is added to a base scenario, CHP heat and electricity production typically decreases. This is not the case in Scenario 2030B, where with low LHP capacities the decrease is compensated by higher production in hours without LHP heat production. This is due to an overall increase in the price of electricity. Because we did not consider thermal inertia and heat storage in this work, condensing production is overall higher than it would be in reality, at the expense of CHP electricity production. Regardless of the decrease of CHP energy

production, the total fuel consumption in the Nordic electricity and DH system decreases in all examined scenarios due to the addition of LHP capacity. This is made possible by the high COP (3.0) of the LHPs. The decrease in total fuel consumption (7–18 TWh in 2030) indicates significant potential for emission reductions.

In addition to the described benefits, LHPs strengthen the interconnection between the electricity and DH markets. This is seen as an important development in research into future energy systems (e.g. [32]). The interconnection allows the usage of VRE and other inflexible electricity production for heating, increasing the potential for low-CO₂ DH production beyond biomass utilization. The diversification of technologies also has benefits for DH networks through added robustness against future energy market trends. For example, periods of low electricity price will become increasingly common with the growing share of VRE in total electricity production. Networks with LHP capacity can benefit from such periods. There is also potential for additional revenues from LHP operation from intra-day or balancing electricity markets, which are not analyzed in this work.

As next steps for future research, heat inertia and storage should be included in the model used in this work. Additionally, LHP operating hours should be set incrementally and iteratively to the scenarios to improve the representation of the production planning done in DH networks.

In this paper, we have shown that LHP utilization has a selection of potential benefits to the future Nordic energy system, from economic and environmental benefits in DH production to the improvement of electricity system flexibility. Based on this, we suggest that policymakers should ensure that taxation or political barriers do not impair the feasibility of new LHP projects.

Acknowledgements

This work has been completed with funding by the RenewFIN project of the Academy of Finland. The contribution by Behnam Zakeri has been partly supported by the RE-INVEST project “Renewable Energy Investment Strategies – A two-dimensional interconnectivity approach” funded by Innovation Fund Denmark.

References

- [1] Pöyry Management Consulting Oy. Suomen sähkötehon riittävyys ja kapasiteettirakenteen kehitys vuoteen 2030 (The adequacy of electric power in Finland and the development of the capacity structure until year 2030), 2015.
- [2] Lund, Rasmus, Danica Djuric Ilic, and Louise Trygg. “Socioeconomic potential for introducing large-scale heat pumps in district heating in Denmark.” *Journal of Cleaner Production* 139 (2016): 219–229, doi:10.1016/j.jclepro.2016.07.135.
- [3] Averfalk, Helge, Paul Ingvarsson, Urban Persson, Mei Gong, and Sven Werner. “Large heat pumps in Swedish district heating systems.” *Renewable and Sustainable Energy Reviews* 79 (2017): 1275–1284, doi:10.1016/j.rser.2017.05.135.
- [4] Finnish Ministry of Economic Affairs and Employment. Government report on the national energy and climate strategy for 2030.
- [5] Statnett. Long-term market analysis – The nordic region and europe 2016–2040 (2016).
- [6] International Energy Agency. Nordic energy technology perspectives 2016 (IEA Publications, 2016).
- [7] Martin de Lagarde, Cyril, and Frédéric Lantz. “How renewable production depresses electricity prices: Evidence from the German market.” *Energy Policy* 117 (2018): 263–277, doi:10.1016/j.enpol.2018.02.048.
- [8] Statistics Finland. Official Statistics of Finland.
- [9] Danish Energy Agency. Energy Statistics 2015.
- [10] Statistics Norway. Statistics Norway – Electricity.
- [11] Statistics Norway. Production and consumption of energy, energy balance, 2014-2015, final figures.
- [12] Statistics Sweden. Annual energy statistics.
- [13] Statistics Finland. Production of electricity and heat.
- [14] Finnish Energy. Kaukolämpötilasto 2015 (District heat statistic 2015), 2016.
- [15] Statistics Sweden. Sveriges officiella statistik: Statistiska meddelanden (Official statistics of Sweden: Statistical communication) (2016).
- [16] Sandberg, Eli, Daniel Møller Sneum, and Erik Trømborg. “Framework conditions for Nordic district heating - Similarities and differences, and why Norway sticks out.” *Energy* 149 (2018): 105–119, doi:10.1016/j.energy.2018.01.148.
- [17] Levihn, Fabian. “CHP and heat pumps to balance renewable power production: Lessons from the district heating network in Stockholm.” *Energy* 137 (2017): 670–678, doi:10.1016/j.energy.2017.01.118.
- [18] Schweiger, Gerald, Jonatan Rantzer, Karin Ericsson, and Patrick Lauenburg. “The potential of power-to-heat in Swedish district heating systems.” *Energy* 137 (2017): 661–669, doi:10.1016/j.energy.2017.02.075.
- [19] Arango, Santiago, and Erik Larsen. “Cycles in deregulated electricity markets: Empirical evidence from two decades.” *Energy Policy* 39(5) (2011): 2457–2466, doi:10.1016/j.enpol.2011.02.010.
- [20] Nyborg, Sophie, and Inge Røpke. “Heat pumps in Denmark—From ugly duckling to white swan.” *Energy Research & Social Science* 9 (2015): 166–177, doi:10.1016/j.erss.2015.08.021.
- [21] David, Andrei. Large heat pumps in European district heating systems, 2016.
- [22] Valor Partners Oy. Large heat pumps in district heating systems, 2016.

- [23] Lund, Rasmus, and Urban Persson. “Mapping of potential heat sources for heat pumps for district heating in Denmark.” *Energy* 110 (2016): 129–138, doi:10.1016/j.energy.2015.12.127.
- [24] Bach, Bjarne, Jesper Werling, Torben Ommen, Marie Münster, Juan M. Morales, and Brian Elmegaard. “Integration of large-scale heat pumps in the district heating systems of Greater Copenhagen.” *Energy* 107 (2016): 321–334, doi:10.1016/j.energy.2016.04.029.
- [25] Hast, Aira, Samuli Rinne, Sanna Syri, and Juha Kiviluoma. “The role of heat storages in facilitating the adaptation of district heating systems to large amount of variable renewable electricity.” *Energy* 137 (2017): 775–788, doi:10.1016/j.energy.2017.05.113.
- [26] Danish Energy Agency. *Technology Data for Energy Plants for electricity and District heating generation*, 2018.
- [27] Zakeri, Behnam, Vilma Virasjoki, Sanna Syri, David Connolly, Brian V. Mathiesen, and Manuel Welsch. “Impact of Germany’s energy transition on the Nordic power market – A market-based multi-region energy system model.” *Energy* 115, Part 3 (2016): 1640–1662, doi:https://doi.org/10.1016/j.energy.2016.07.083.
- [28] Helin, Kristo, Behnam Zakeri, and Sanna Syri. “Is District Heating Combined Heat and Power at Risk in the Nordic Area?—An Electricity Market Perspective.” *Energies* 11(5) (2018): 1256, doi:10.3390/en11051256.
- [29] Danish Energy Agency. *Basisfremskrivning 2017 (Basic projection 2017)* (2017).
- [30] Norwegian Ministry of Petroleum and Energy. *Kraft til endring – Energipolitikken mot 2030 (Power for change – Energy policy towards 2030)* (2016).
- [31] Swedish Energy Agency. *Scenarier över Sveriges energisystem 2016 (Scenarios of the energy system of Sweden 2016)* (2017).
- [32] Mathiesen, B. V., H. Lund, D. Connolly, H. Wenzel, P. A. Østergaard, et al. “Smart Energy Systems for coherent 100% renewable energy and transport solutions.” *Applied Energy* 145 (2015): 139–154, doi:https://doi.org/10.1016/j.apenergy.2015.01.075.



16th International Symposium on District Heating and Cooling, DHC2018,
9–12 September 2018, Hamburg, Germany

“NeckarPark Stuttgart”: District heat from wastewater

H. Erhorn^a, J. Görres^b, M. Illner^{a*}, J.-P. Bruhn^b, A. Bergmann^a

^aFraunhofer Institute for Building Physics IBP, Nobelstr. 12, Stuttgart, 70569, Germany

^bLandeshauptstadt Stuttgart Amt für Umweltschutz, Gaisburgstr. 4, Stuttgart, 70182, Germany

Abstract

The 22-hectare area of the former freight station is currently Stuttgart's largest urban development project. In addition to commercial and service areas, around 850 residential units are to be built on a net floor area totaling 220,000 m². The energy concept includes heat recovery from wastewater with a capacity of 2.1 megawatts, which is extracted from a nearby sewer. The energy concept is supplemented by cogeneration units. In the NeckarPark district a low-temperature four-pipe heating grid, which is built by the state capital Stuttgart and operated by the city-owned energy supplier (Stadtwerke Stuttgart), provides heat to the buildings.

© 2018 The Authors. Published by Elsevier Ltd.

This is an open access article under the CC BY-NC-ND license (<https://creativecommons.org/licenses/by-nc-nd/4.0/>)

Selection and peer-review under responsibility of the scientific committee of the 16th International Symposium on District Heating and Cooling, DHC2018.

Keywords: Urban district heating, wastewater heat recovery, heat pumps, cogeneration units

1. Introduction

Following a Swiss study [1], 15% of the thermal energy supplied to buildings is lost through the sewer system. In new and well-insulated buildings distinguished by low energy consumption this value can even rise to 30%, which makes the sewer one of the largest sources of heat loss in energy-efficient buildings [1]. After use, the domestic hot

* Corresponding author. Phone: +49 711 970-3471; fax: +49 711 970-3399.

E-mail address: Micha.Illner@ibp.fraunhofer.de

water is discharged into the sewer system, thus turning domestic wastewater into a carrier of heat [2] with a huge potential.

According to data published by the IEE project ‘Stratego’ [3] 5% of the heat demand of towns and cities with more than 10,000 inhabitants can be covered through heat that is extracted from sewage water by means of large heat pumps. In Fig. 1 the heat potential of urban sewage systems that can be exploited by means of heat pumps is shown for nine European countries, indicating its international relevance.

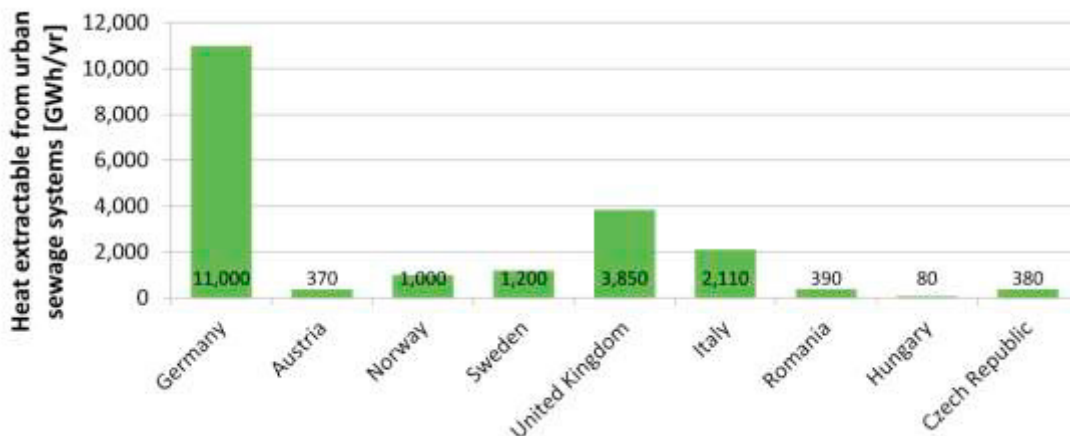


Fig. 1. Heat extractable from urban sewage systems by means of heat pumps (Source: Fraunhofer IBP, using data from [3] and [4])

For extracting heat or cold from a sewage system, three different technological solutions are currently used. When applying the first technology, sewer-integrated heat exchangers are placed directly inside the sewer tunnel. The heat-exchanger system consists of heat-exchanging surfaces through which an intermediate medium flows. Pipes transport the intermediate medium to the heat pump. Depending on heating or cooling requirements, the elements can extract heat from or supply heat to the wastewater. The second commonly used technology is heat recovery from sieved wastewater. In this system, the raw wastewater flowing in the sewer is first fed to a sieving stage in which solids are separated. This is necessary in order to protect the downstream heat exchanger from blockages and to make it as compact and cost-effective as possible. Subsequently, the wastewater is passed through the heat exchanger and then returned to the sewage system. As a third technology to use wastewater heat recovery, collecting shaft heat exchangers can be installed. In a specially constructed shaft the wastewater is filtered and collected. The heat exchanger installed inside the shaft is then able to extract heat from or supply heat to the wastewater. After that the wastewater is fed back into the sewer system. The shaft itself is always filled with wastewater up to a certain limit to ensure continuous heat transfer, even if only small quantities of wastewater are available. The present paper focuses on sewer-integrated heat exchangers.

2. Main text

As a member of the European Covenant of Mayors and with the energy concept “Urbanization of energy transition in Stuttgart”, the city has set itself the goal of reducing Stuttgart's energy consumption by 20% by 2020 (compared to 1990), and improving the renewable share of energy use in the city area to 20%.

Stricter energy requirements are contractually agreed when awarding city property to new construction projects planned by private builders. Private renovation projects are promoted through an urban energy-saving program and builders are advised neutrally and inexpensively by the Energieberatungszentrum Stuttgart (EBZ), a center for energy consulting, which was founded in 1999. In the 1990s, the city gained experience with the Burgholzhof residential area in terms of urban development and the progressive energy design of larger conversion areas towards new, forward-looking urban districts. Building owners were obliged to build low-energy houses and connect them to

a solar supported local heating supply. This procedure is now also being applied to the new NeckarPark district, but wastewater is being used as a heat source instead.

2.1. Wastewater heat potential in Stuttgart

As an alternative heat source to the substitution of fossil energy sources, wastewater heat is an interesting option, especially for municipalities - after all, any wastewater must be supplied to the municipality for disposal. The municipalities thus have the sole right to use the wastewater produced in their territory. In order to be able to evaluate the possibilities of using wastewater for heating and cooling in Stuttgart, the city commissioned a wastewater heat potential study.

The analysis of the temperature in the aeration tank of the Stuttgart main sewage treatment plant shows that even during cold periods the temperature level does not drop below 12 °C. Only short-term meltwater runoffs lead to temporary drops in temperature. However, these drops are acceptable for wastewater heat utilization, since the temperature of the outside air is above freezing point during this period (usually in spring) and thus the full output of the heating systems is not required.

In winter, the temperatures in the aeration tank of Stuttgart's main sewage treatment plant are about 2 degrees warmer than in comparable sewage treatment plants in Baden-Württemberg. This phenomenon can be explained by the fact that the wastewater flows into a canal upstream of the wastewater treatment plant, which passes under a vineyard over a length of 2,750 meters. The surrounding rock can function as a seasonal heat store. If the wastewater that flows into Stuttgart's main sewage treatment plant (1,300 l/s dry weather discharge) was cooled by 2 degrees, almost 11 MW of heating capacity and around 17 GWh/a of heat could be generated.

Suitable sewers for wastewater heat recovery should have an average dry weather discharge of at least 15 l/s and a diameter of DN 800 or larger. To ensure economical wastewater heat utilization, the distance between the property to be supplied and the sewer should not exceed 300 m (preferably, 150 m). A wastewater heat potential map for Stuttgart was prepared on the basis of these wastewater, energy and economic limit criteria (Fig. 2.). In addition to suitable sewers, the municipal buildings are also listed as heat demand points. In relation to the total length of the sewer network, 7% of Stuttgart's wastewater collectors are suitable for heat and cold utilization. The majority of these (88%) can be used without restrictions.

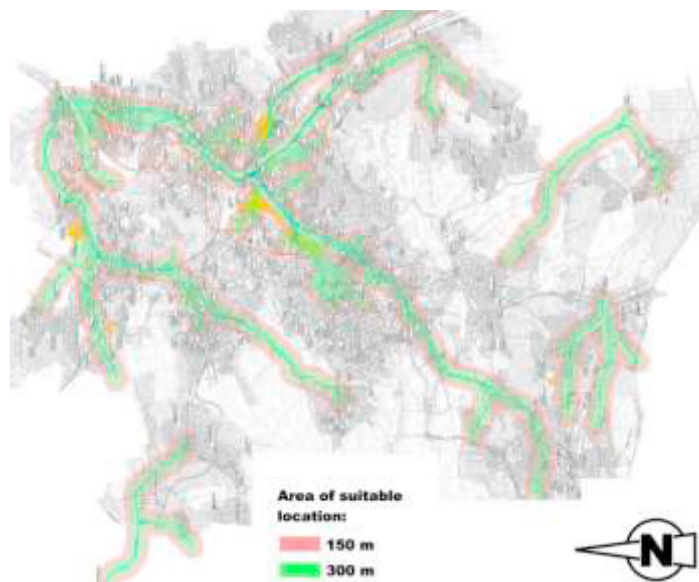


Fig. 2. Wastewater heat potential map (Source: Landeshauptstadt Stuttgart, Tiefbauamt, Stadtentwässerung)

2.2. Development area NeckarPark

One of Stuttgart's most important development areas at present is the 22-hectare wasteland area of the former Bad Cannstatt freight terminal (Fig.3.(a)). Deutsche Bahn used the site until the late 1980s. The city of Stuttgart bought the site in 2001. According to the urban development framework plan "NeckarPark", 850 apartments are to be built on the area; service providers, commercial enterprises and hotels are also to be established (Fig.3.(b)). In total, the development will comprise 220,000 m² of net floor area, of which approx. 70,000 m² for residential buildings.

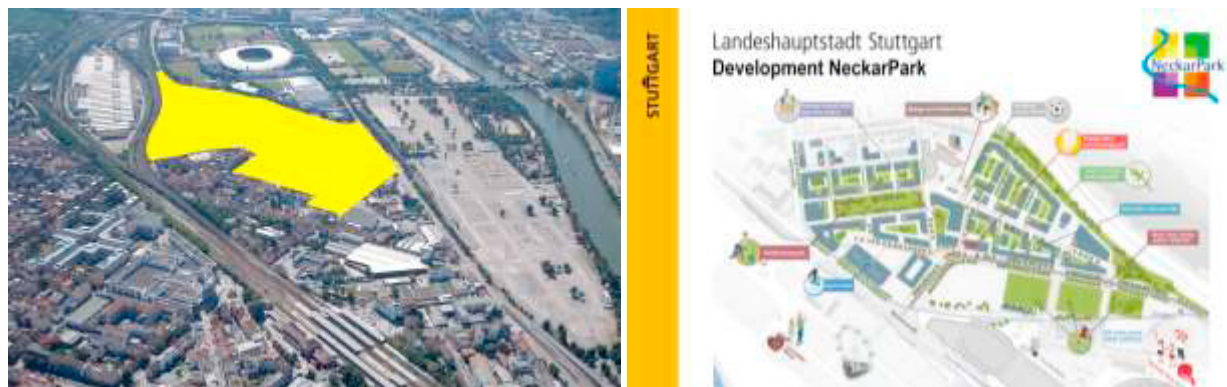


Fig. 3. (a) Development area NeckarPark; (b) Construction site sign of the NeckarPark (Source: Landeshauptstadt Stuttgart)

As specified in the NeckarPark development plan, the building owners are obliged to construct residential buildings as KfW efficiency houses 55, which is under discussion as the probably nearly zero-energy building standard in Germany from 2021 onwards. For non-residential buildings, corresponding energy-efficient requirements are also set out in the contracts covering the sale of municipal property. Even with high building concentration, this concept will result in a low heat density. Traditional district heating involving high supply temperatures and corresponding pipe losses often proves to be inefficient and uneconomical for supplying heat to such low-energy areas. The maximum heat demand of the NeckarPark is estimated at 12 MW and 13 GWh/a, based on a detailed type-building calculation performed with the 'District Energy Concept Advisor'[5] (Fig. 4) within the scope of the research project.



Fig. 4. Detailed type-building calculation using the 'District Energy Concept Advisor'

2.3. Energy concept NeckarPark

The development of the NeckarPark as a nearly zero energy district allows the predominant use of surface heating elements like concrete core activation, underfloor and wall heating. This makes it possible to significantly reduce the

flow temperatures of the heating supply (35 °C) while keeping the heat losses of an upstream local heating network low, thus making extensive use of the low-temperature heat source of wastewater heat. The required heat is extracted from a nearby sewer. In order to assess its performance, a two-year measuring phase was carried out. The maximum flow rate of the channel is 2,500 l/s, in dry weather 200 l/s. This results in a calculated extraction capacity of 838 kW/K for dry weather flow. For instance, the analysis of the temperature distribution shows that the wastewater in the sewer never gets colder than 6 °C and never falls below 8 °C for longer than 12 hours [6]. Throughout the whole year, the wastewater temperature is between 6 °C and 8 °C only during 29 hours, in total. Thus, in addition to the higher thermal conductivity, the thermal use of wastewater offers far better temperature conditions than the use of near-surface geothermal energy.

A further boundary condition for the design of wastewater heat utilization is to determine the temperature up to which the wastewater may be cooled or heated. Here, the biochemical processes of wastewater treatment in the sewage treatment plant are of particular importance. The minimum setpoint temperature for wastewater treatment is 10°C. The main sewage treatment plant discharges 6.5 times more wastewater than the sewer at NeckarPark. In the NeckarPark, wastewater heat exchangers (Fig. 5.(a)) with a total extraction capacity of 2.1 MW were installed in the sewer to recover the wastewater heat. This requires a heat exchanger of about 1 km in length in relation to a wastewater collector with standard dimensions. This means that the use of wastewater heat in the Neckar Park is ten times greater than in existing plants in Germany. The sewer at the NeckarPark with a diameter of DN 2400 was dimensioned so large that a heat exchanger can be laid in two parallel, wide bands at the sewer bottom, which shortens the installation length of the heat exchanger to 280 m. A flushing shield (Fig. 5.(b)) is operated periodically to flush away any deposits that might reduce the efficiency of the wastewater heat exchanger. The installation of the heat exchanger and the flushing shield was finalized in June 2018.



Fig. 5. (a) Sewer-integrated wastewater heat exchanger; (b) Flushing shield in the duct (Source: Landeshauptstadt Stuttgart)

The local heating network in the NeckarPark is designed as a 4-wire network: two wires are responsible for the high-temperature heat supply (75 °C supply, 50 °C return) for domestic hot water, the other two wires cover the low-temperature supply (43 °C supply, 28 °C return) for space heating purposes.

Low-temperature heat generation is mainly provided by the three heat pumps, with a total thermal output of 2.6 MW, connected to the wastewater heat exchanger (Fig. 6.) High-temperature heat can be coupled into the low-temperature network to cover peak loads. The cogeneration plants with 0.4 MW_{th} and 0.2 MW_{el} as well as the peak-load gas condensing boilers (5.5 MW) will generate high-temperature heat.

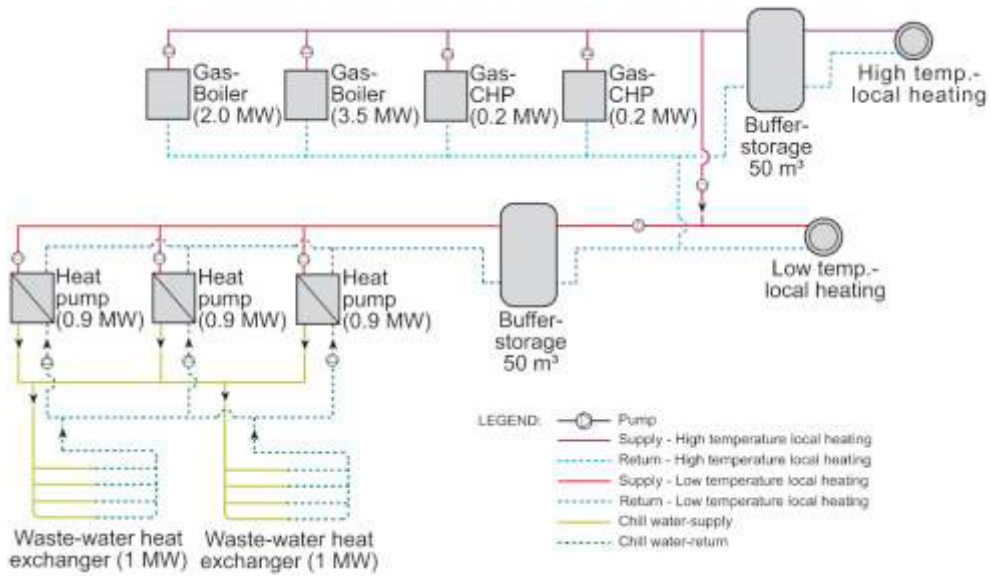


Fig. 6. Scheme of heat generation in the NeckarPark (Source: Fraunhofer IBP, Stuttgart)

In order to keep the high-temperature heat demand as low as possible and thus make maximum use of wastewater heat recovery, the domestic hot water in the buildings is preheated via the low-temperature network. Starting from a cold water temperature of 10 °C, this reduces the need for high-temperature heat by around 50%.

Based on the current state of knowledge, a rough simulation of energy generation in the NeckarPark has shown that 67% of the predicted total heat demand (13 GWh/yr) of the NeckarPark is covered by the heat pumps, while the CHPs contribute 19% and the gas condensing boilers 14%. The monthly distribution of the heat generation is shown in Fig. 7.

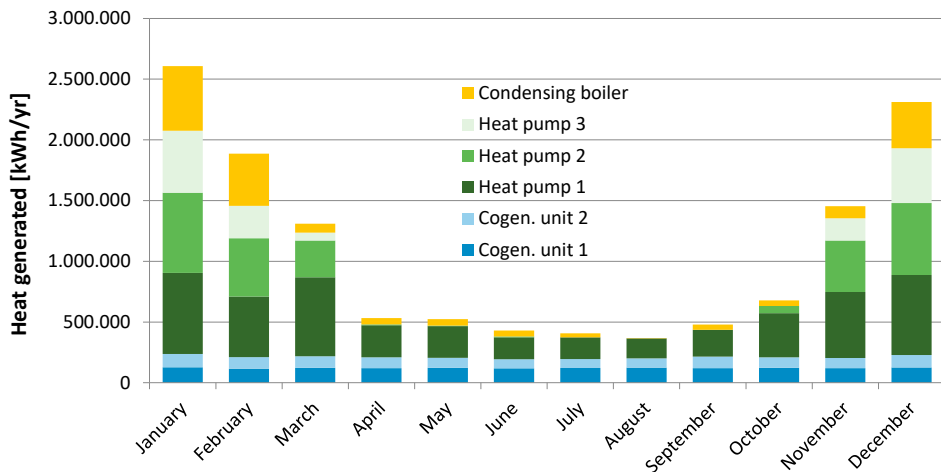


Fig. 7. Results of the rough simulation of energy generation in the NeckarPark (Source: IBS Ingenieuresellschaft mbH, Bietigheim-Biss.)

The electricity yield of PV systems is used to compensate for the auxiliary energy required for the local heating grid. To ensure the realization of the PV-systems, the property buyers had to contractually commit themselves to equip all roof surfaces with PV systems. This does not apply to roof surfaces:

- that are either shaded between 9-16 o'clock in the time from April to October
- that use solar radiation in another way to generate energy (e.g. through solar thermal systems)
- whose basic functions prevent the use of solar systems (e.g. roof terraces and roof gardens)
- on which no continuous module area of at least 50 m² in total can be achieved.

According to the calculations performed by the City of Stuttgart, the heat is provided by a price of 12 cents/kWh. This calculation takes all capital, operating and energy costs into account. The project in the NeckarPark district shows that the predominant supply of heat from wastewater to a highly efficient urban district is possible on economic terms. With its size, the district provides a practical example for other cities.

Acknowledgements

The R&D project is funded by the German Federal Ministry of Economics and Energy (support code: 03ET1156A&B) in the funding priority "Energieeffiziente Wärme- und Kältenetze – EnEff:Stadt".

In addition to the institutions acting as authors, the project in the NeckarPark is accompanied by the engineering office "Ingenieurbüro Schuler" from Bietigheim-Bissingen (responsible for planning the heating centre and the local heating network) and the engineering office "Klinger und Partner" from Stuttgart (responsible for planning the sewer and the wastewater heat exchanger). The Stadtwerke Stuttgart (public utility company) are also a project partner and will later be responsible for the operation of the heating system and the local heating network.

References

- [1] Schmid, Felix. "Sewage water: interesting heat source for heat pumps and chillers" *Swiss Energy Agency for Infrastructure Plants. Zurich, Switzerland, 2009.*
- [2] Frijns, Jos, Hofman, Jan and Nederlof, Maarten. "The potential of (waste) water as energy carrier." *Energy Conversion and Management 65 (2013): 357-363*, doi: 10.1016/j.enconman.2012.08.023.
- [3] Möller, Bernd. "Mapping the Renewable Heat Sources in Europe." Stratego Enhanced heating & cooling plans project. Work Package 2, Background Report 9. Project No: IEE/12/650
- [4] Hermann, Laurenz et al. "Heating with wastewater heat. Best practice catalogue." WasteWaterHeat project. Project No: EIE/05/145/2005
- [5] Erhorn-Kluttig, Heike. et al. "Der Energiekonzept-Berater für Stadtquartiere – Ein Potenzialbewertungstool aus der Forschungsinitiative EnEff:Stadt [The District Energy Concept Adviser – A tool for assessing the potential out of the research initiative Energy Efficient Cities]." Published by Fraunhofer IRB Verlag (2014) ISBN 978-3-8167-9139-3
- [6] Görres, Jürgen, Erhorn, Hans, Schäfer, Nino, Bergmann Antje. "Energieeffizienz in Gebäuden, Jahrbuch 2015 [Energy efficiency in buildings, yearbook 2015] Jürgen Pöschk (Publishers) VME Verlag (2015) ISBN 978-3-936062-11-3



16th International Symposium on District Heating and Cooling, DHC2018,
9–12 September 2018, Hamburg, Germany

Transformation of an existing into a Fourth Generation Heating Network

Britta Kleinertz^{a*}, Dr. Götz Brühl^b, Frank Veitengruber^a,
Dr. Christoph Pellinger^a, Dr. Serafin von Roon^a

^aResearch Center for Energy Economics, Am Blütenanger 71, 80995 Munich, Germany

^bStadtwerke Rosenheim GmbH & Co. KG, Bayerstraße 5, 83022 Rosenheim, Germany

Abstract

Various concepts for reduction of grid losses and innovative heat supply concepts are compared. Line-wise intra-year variation is highly economical in networks with low domestic hot water demand. Intra-day variation to charge decentral storages once a day requires higher flow temperatures, which in the considered network even increases overall losses. The two considered heat generation concepts are a low temperature network with decentral heat pumps and a Heat Dispatch Centre, where heat pump, biomass-gasification with combined heat and power and supply from primary network are connected in series. Running costs, specific emissions and Primary Energy Factor are considerably lower for the Heat Dispatch Centre, but due to lower investments and maintenance costs for the low temperature network it results in 2 €ct lower heat generation price of 11.5 €ct/kWh (incl. 20 % investment funding).

© 2018 The Authors. Published by Elsevier Ltd.

This is an open access article under the CC BY-NC-ND license (<https://creativecommons.org/licenses/by-nc-nd/4.0/>)

Selection and peer-review under responsibility of the scientific committee of the 16th International Symposium on District Heating and Cooling, DHC2018.

Keywords: District heating network, Fourth Generation District Heating, Variable supply temperatures, Heat Dispatch Centre

* Corresponding author. Tel.: +49- 89-158 121 39; Fax: +49-89-158 121 10.

E-mail address: bkleinertz@ffe.de

1. Introduction

In the following subsections the general concept of fourth generation district heating is shortly described. After that from the limitations of renewable energies, the importance of temperature levels when investigating thermal energy supply is deduced. In section 2 the characteristics of single lines of an exemplary district heating network (DHN) are described to derive possible adaptations of supply temperature (section 3) in order to limit losses and to assess different heat supply concepts (4). In section 5 the overall results are discussed towards giving an outlook on the relevance and limitations of the preliminary findings. Further research questions are derived in section 6.

Nomenclature

4GDH	Fourth Generation District Heating
CHP	Combined Heat and Power
DHN	District Heating Network
DHW	Domestic Hot Water
PN	Primary Network

1.1. Fourth Generation District Heating

A fourth generation district heating (4GDH) network is a network that distributes heat at temperatures of 20 – 95 °C in a highly efficient way. Moreover, the heat is primarily supplied from renewable energy sources and waste heat. In addition, adequate network monitoring enables the identification of losses and intelligent sector coupling with the electricity supply network. The term "fourth generation district heating" expresses that from the first generation the temperature levels of heat supply as well as its efficiency and the share of renewable heat sources have changed in several development steps. [1], [2], [3].

1.2. Limitations of renewable heating sources and the importance of temperature

As stated before the main heating sources for 4GDH are waste heat and renewable energies. All of these energy sources have their own limitations when focusing on a reliable thermal energy supply.

- **Solarthermal energy:** Generated heat load and reached temperature level are entirely dependent on environmental conditions and therefore underlie strong variations. Especially in winter heat generation is low.
- **Heat pump:** For the usage of heat pumps an adequate environmental or waste heat source has to be available in the area of heat demand. Furthermore, the efficiency of heat pumps is mainly dependent on the temperature difference between heat source and heat sink temperature [4]. In order to reach high supply temperatures with heat pumps these are usually connected in series [5].
- **Waste heat:** It is estimated that in Germany the potential for useable waste heat at a temperature level above 60 °C is 476 PJ [6]. Still, especially high temperature waste heat generally results from industrial processes, which are far away from domestic consumers. Also the availability underlies seasonal and daily fluctuations.
- **Biomass heat:** As biomass can be burned in different heat generation units such as combined heat and power (CHP) or thermal power stations, no limitations regarding the provision of heat in 4GDH systems apply. However, due to its applicability for material use and conversion to syngas/ methane connected to usage in high temperature processes (especially industrial applications), biomass resources available for low-temperature heat provision are highly limited.

Summarized, biomass is the only regenerative thermal energy source which can constantly supply heat at high temperatures. Nevertheless, its limited resources make the usage of other renewable energy sources or a combination of several sources mandatory.

2. Description of the considered district heating network

The results given are an excerpt of the project “Fourth Generation District Heating” [7]. Several possible improvements of the existing network-based heat supply of a district are investigated. As a new public building will be built closely to the existing network, a concept for heat supply for the overall area is considered in this study leading to an overall heating demand of about 4 GWh.

Because the existing district consists of areas with three different types of usage, the overall area can be differentiated into four sub-areas, which are provided by different lines from the heating central. Most relevant characteristics of the different lines, namely a southern, a northern, a centrally placed kitchen and a public building line, are described in Table 1. It becomes clear that heat demand and especially domestic hot water (DHW) demand highly differ between the buildings by line.

Table 1: Overview on characteristics of consumers in the DHN by line

	Usage	Heating demand and profile	Domestic Hot Water Demand
Southern line (800 m, 8 buildings)	Housing and working buildings	High demand in winter	Continuous all year round demand, concentrated in the morning and the evening
Kitchen line (130 m, 1 building)	Kitchen and cafeteria	Medium demand in winter (waste heat from open kitchen)	Continuous all year round demand, concentrated around midday for cooking and cleaning
Northern line (1050 m, 7 buildings)	Several workshops and garages	Medium heat demand, only frost protection heating in several garages	Low demand, main demand in the afternoon for several showers in one of the garages
Public building line (500 m, 1 building)	Mainly seminar rooms	Expected low demand due to current energy efficiency building construction obligations	Low demand, therefore decentral provision by instantaneous water heaters or low-temperature circulation line with decentral DHW stations

3. Evaluation of measures to decrease thermal losses

For this study the aim was to decrease the required temperature by line in order to decrease thermal losses and increase the potential for the integration of renewable heating sources. In section 3.1 energetic and economic effects of an overall decrease in supply temperature is assessed. Afterwards possible energy and cost savings resulting from an intra-day variation of supply temperatures in summer are determined (section 3.2).

3.1. Variation of supply temperature per network line

When determining temperatures for heat supply systems the most important factors are technical and regulative limitations. Usually heating curves are implemented in heating systems, so that a decrease in outside temperatures leads to an increase in heating system temperatures. The set flow and return temperatures by line and season are stated in Table 2. These temperatures are based on the following assumptions:

- General assumptions:
 - In winter (here: days with outside temperatures below 0°C) the supplied temperatures have to be increased in order to limit flow rates and resulting pressure losses.
 - For network-based DHW provision a flow temperature of 70 °C has to be maintained in order to fulfil hygienic requirements.
 - In summer the return temperature increases, because only DHW from the building circulation line is heated.
- Assumptions for individual lines:
 - For the garages in one branch of the northern line, lower target temperatures are required. Therefore, these buildings are connected to the return of the northern line and allow a decrease in return temperature of the line.
 - Due to low DHW demand in summer in northern and public building line, these are uncoupled from the DHN.

- In order to increase the temperature difference between flow and return in the heat central, the public building line is connected to the return of the other lines. This is enabled by the low-energy standard of the public building and the assumed DHW provision either by DHW stations or by decentral boiler systems.

Table 2: Overview on set temperature levels depending on weather conditions differentiated by line (occurrence of seasonal heating derived from 2017 weather data)

	Set temperatures in °C						
	Losses coefficient	Winter ($T_{\text{outside}} < 0$ °C) about 1.300 hours		Transition period ($T_{\text{outside}} > 0$ °C and < 16 °C) about 5.400 hours		Summer (no heating demand) about 2.060 hours	
		Flow	Return	Flow	Return	Flow	Return
Southern and kitchen line	185 W/K	75	50	70	50	70	55
Northern line	240 W/K	75	40	70	40	12*	12*
Public building line	115 W/K	50	30	50	30	12*	12*

*equal to outside temperature

In order to calculate the reduction in thermal losses, the new scenarios are compared to a reference scenario, which is a constant flow temperature in all lines of 75 °C and a return of 50 °C in the heating period or 55 °C in the non-heating period. Generally, losses of a DHN (Q_{losses}) can be calculated from the difference in temperature between DHN and surrounding ($\Delta T_{\text{DHN-outside temperature}}$), the heat transmission coefficient (U) and the length of the DHN (l) according to formulae (1). Because only the temperature difference between system and surrounding temperature is changed, the relative change in system temperatures (flow and return) is equal to the change in losses. Relative reductions in thermal losses by line are stated in Table 3.

$$\dot{Q}_{\text{losses}} = \Delta T_{\text{DHN-outside temperature}} U l \quad (1)$$

Table 3: Relative decrease in losses due to variation of flow and return temperature

Line	Winter	Transition period	Summer
Southern and kitchen line	0 %	4 %	4 %
Northern line	8 %	12 %	100 %
Public building line	32 %	36 %	100 %

Due to constantly required high temperatures for hygienic DHW provision in southern and kitchen line, the only relevant savings can be reached in northern and university line. While the reduction in losses in the heating and transition period directly leads to cost savings (CS) according to formulae (2), the decrease in costs for energy provision in the northern line in summer has to be compared to the additional costs caused by DHW provision from decentral boiler systems according to formulae (3). In the calculations an efficiency of the heat exchangers ($\eta_{\text{heat exchanger}}$) of 99 %, an average district heating price ($C_{\text{heat prov}}$) of 7.34 €/kWh [8], an efficiency of an electric boiler (η_{Boiler}) of 97 % [9] and an electricity price (C_{electr}) of 29.28 €/kWh (2017 [10]) are used. In both cases it is assumed that the specific electricity or respectively heat cost is not dependent on the overall electricity respectively heat demand and that the average outside temperature is at 12°C.

Because the actual DHW demand (Q_{DHW}) in the northern line is unknown, a sensitivity analysis of the cost savings depending on the actual DHW demand was executed. The resulting savings are presented in Table 4.

$$CS_{\text{heating period}} = \left(\frac{Q_{\text{losses,ref}} - Q_{\text{losses,new}}}{\eta_{\text{heat exchanger}}} \right) \cdot C_{\text{heat prov}} \quad (2)$$

$$CS_{non-heating\ period} = (Q_{losses,ref} + Q_{DHW} - Q_{losses,new}) \cdot C_{heat\ prov} - \frac{Q_{DHW}}{\eta_{boiler}} \cdot C_{electr} \quad (3)$$

Table 4: Cost savings due to temperature adaptation – in northern and public building line in summer compared to decentral DHW provision (¹according to [11])

Line	DHW demand	Winter	Transition period	Summer
Southern and kitchen line	50 kW	0 €	372 €	142 €
Northern line	5 kW	229 €	1,429 €	2,310 €
	10 kW			-763 €
Public building line	6.37 ¹ kW	444 €	2,076 €	- 1,075 €

Generally, savings in the southern and kitchen line are low but easy to achieve. While in the transition period relative savings in the public building line are three times higher than in the northern building line, absolute cost savings are only 45 % higher. This is caused by the higher thermal loss coefficient of the northern line. In summer the usage of decentral boiler systems is only economical in the northern line in case of a low DHW demand of about 5 kW. The higher variable cost of DHW generation from electric boilers overcompensates the cost related to thermal losses in the network. This equally applies to the university line, where lower system temperatures lead to lower losses and therefore even higher additional costs when electric heating is applied. The cost-wise break-even point between thermal energy provisions from the grid and from decentral boiler systems in non-heating period in the northern line is at a DHW demand of 8,35 kW.

3.2. Decrease of thermal losses due to intra-day temperature variation

Especially in summer high losses occur in DHN, because the provision of DHW requires high flow temperatures for hygienic reasons, while the overall thermal energy demand is low. In residential buildings the DHW demand is highly concentrated in the morning and the evening [12], while in DHN the heat is supplied evenly all-day long. Currently, three measures to decrease thermal losses of DHN are considered in research:

- Usage of chemical or organic substances in order to prevent growing of legionella
- Decreasing necessary temperatures by usage of DHW stations per flat or per tapping point
- Intra-day variation of DHN supply temperatures for selective charging of decentral storage tanks

In contrast to the first option, which is currently still in the research state, the other two are already implemented. For the considered existing network, the implementation of decentral DHW stations would require extensive construction works and costs. Additionally, the existing heating infrastructure needs system temperatures of over 70 °C about half year round, making the investment only useable at summer time. Therefore, the concept is considered as non-viable in the existing network but applicable to the public building heating system.

For the determination of economic benefits of intra-day variations of supply temperatures in the southern and kitchen line, an exemplary day for an average building is investigated. From the available data an average daily DHW demand (including circulation losses) per southern-line building of 170 kWh can be derived.

The suitable storage size is derived from formulae (4) an allowed temperature variation of the storages of $T_{storage,max} = 90^{\circ}\text{C}$ and $T_{storage,min} = 60^{\circ}\text{C}$, for specific heat capacity (c_p) and density of water of (ρ_{water}) values of water at 75°C are used.

$$V_{Storage} = \frac{Q_{DHW}}{(T_{storage\ max} - T_{storage\ min}) \cdot c_p \cdot \rho_{water}} \quad (4)$$

For the calculation of cost savings resulting from an intra-day variation formulae (5) is seen as appropriate, where $Q_{losses,new}$ includes the network losses as well as decentral storage losses, $t_{live\ time\ storage}$ is the livetime of the storage tanks (20 years [13]) and $C_{Storage}$ is the cost of all storage tanks. The decrease in electricity demand for pumps caused by intra-day variation in supply is neglected.

$$CS_{summer} = (Q_{losses,ref} - Q_{losses,new}) \cdot C_{heat\ provision} \cdot t_{livetime\ storage} - C_{Storage} \quad (5)$$

Compared to the heat demand in winter, the DHW demand is low, therefore it can be estimated that a flow rate charging the decentral storages within one hour is achievable. Because decentral storages must be heated up to 90 °C to provide storage capacity for DHW thermal losses in the network need to be newly calculated. It is assumed that the network is heated up to 90°C once a day and then cools out over the rest of the day. In Table 5 required storage sizes and characteristics depending on the set loading frequency are stated as well as estimated losses.

Table 5: Losses of the system with decentral storage tank and resulting costs difference depending on loading frequency

Line	Daily	Daily twice
Storage volume	5,000 l	2,500 l
Storage loss coefficient	12,2 kWh/day	8,6 kWh/d
Storage costs	3.700 €	2.300 €
Network losses	351 kWh/day	398 kWh/day
Overall losses network and decentral storages	484 kWh/day	459 kWh/day

In the reference case of continuous heat provision at 75°C thermal losses per day of 376 kWh occur. These are lower than the losses calculated for intra-day variations in supply temperatures. Therefore, the usage of intra-day variation in supply temperatures cannot be economically viable for these set parameters. It is possible to decrease the maximum temperature of the storage tank and by this limit thermal network losses. Still, in this case the storage volume increases as well as storage costs and storage losses.

4. Description and evaluation of different heat supply concepts

After an overview on project requirements and available renewable energy sources is given (section 4.1), the two considered supply systems low-temperature DHN connected to decentral heat pumps (4.2) and Heat Dispatch Center (section 4.3) are described and resulting heat supply costs are evaluated (section 0). A more detailed analysis regarding dependencies on boundary conditions such as electricity prices and development of heat demand in the area will be available on the project homepage [7] from November 2018.

4.1. Boundary conditions

The project conditions require that 50 % of the heat shall be supplied by renewable energies or waste heat, with a maximum of half of it supplied from biomass. Generated electricity from renewable generation units may not be marketed according to the Renewable Energy Sources Act (EEG). [14]

Investigations in the surrounding of the considered network show that there is no waste heat available. Neither is the ground water quality suitable nor the available free surface area large enough to use close-to-the-surface geothermal energy. In 2020 a sewer pipe will be laid centered through the considered area. From the expected flow rate of 25 l/s a thermal energy supply of about 300 kW can be derived.

Measurements of heat demand in the individual buildings over the past winter serve as a basis to derive adequate load profiles per building for the weather year 2017. The thermal load of the public building is predicted with the simulation tool Sophena [11]. Employing a regression analysis of the data generated from Sophena the load curve for the weather year 2017 is generated.

The specific CO₂ emissions (excluding upstream chain) and Primary Energy Factors of the different energy supply sources is stated in Table 6.

Table 6: Set specific CO₂-emissions and primary energy factor for different heat supply technologies [15]¹, ² calculated from primary grid supply composition, ³ with CHP allocation according to electricity benefit method (further information see [16]), [17]⁴, [18]⁵, [19]⁶

	Specific CO ₂ emissions	Primary energy factors (non-renewable)
Natural gas	202 g/kWh ¹	1.1 ⁵
Primary grid	77 g/kWh ^{1,2}	0 ⁶
Wood	0 g/kWh	0.2 ⁵
Electricity from gasifier + CHP	0 g/kWh	0.2 ³
Electricity from grid	489 g/kWh ⁴	1.8 ⁵

In order to connect the buildings to either of the innovative supply concepts several network adaptations have to be implemented. The costs for these are kept constant for both supply concepts and add up to about 1,310,000 €. Funding is expected to lie at 20 % for all investments.

4.2. Low temperature DHN with decentral heat pumps

With the aim of reducing thermal supply losses and increasing the integration of low heat energy sources, the research on and construction of low temperature networks has increased. In order to supply the existing building stock or to provide DHW, in those buildings the low temperature heat serves as heat source for a heat pump. A well-known example is the DHN in Dollnstein [20].

In this case study the central heat pump is expected to lift the return temperature from 30 to 50 °C at a COP of 4 in order to directly supply the temperatures for the public building. Overall costs for the sewage water heat pump (machine, construction) are 270,000 €/t with maintenance costs at 6,200 €/a. The COPs of all individual heat pumps is expected to be at 7.7 [21], costs for these by individual buildings [22] are expected as the following:

- All buildings in the southern line are assumed to have the same maximum load. This leads to 8 heat pumps with individual heat load of 75 kW, each with a cost of 20,950 €.
- The kitchen line consists of one building with 1 heat pump with a heat load of 95 kW and a cost of 22,142 €.
- The garages in the northern line, which are only heated for frost protection, are supplied directly by the flow, while the buildings with heat demand are expected to have the same maximum load curve. This leads to 7 heat pumps with an individual heat load of 75 kW and a cost of 20,950 €.

Including an installation cost per heat pump of 3.000 € the initial invest sums up to 389,291 €. Maintenance costs per heat pump can be expected to lie at 2.5% per year [13], resulting in yearly costs of 8,530 €/year. As stated in section 4.1 heat from the waste water stream is limited to 300 kW, which would not be sufficient to supply the whole area with heat. The remaining thermal energy demand at 50 °C for the local heat network is directly provided by the primary heating network.

4.3. Heat Dispatch Center

The concept Heat Dispatch Centre is based on the idea that every energy source provides heat at the temperature where it is efficient. High temperature heat sources (e.g. CHP) are used to upgrade the temperature level of low-temperature components (e.g. heat pumps). By this the energy supply from the high temperature sources is decreased and low temperature sources are integrated into the heat supply. Here a brief description of the Heat Dispatch Center and the generated simulation tool is provided. A more detailed description will be available at the project homepage [7] from November 2018.

In the considered network the combination of the sewage water heat pump with the gasifier + CHP and primary grid is investigated (see Figure 1). In order to allow an efficient use of the heat pump it is used to increase the temperature level of the return from all lines to about 60 °C. The energy demand for increasing the temperature further up to the required flow temperatures of 75 °C/ 70 °C is provided by gasifier + CHP and primary network. Additionally, the primary network serves as back-up for heat supply at times of high demand and as main heat source in summer. This series interconnection is enabled by one medium temperature storage (about 30 – 60 °C) and a high temperature storage (about 75 °C).

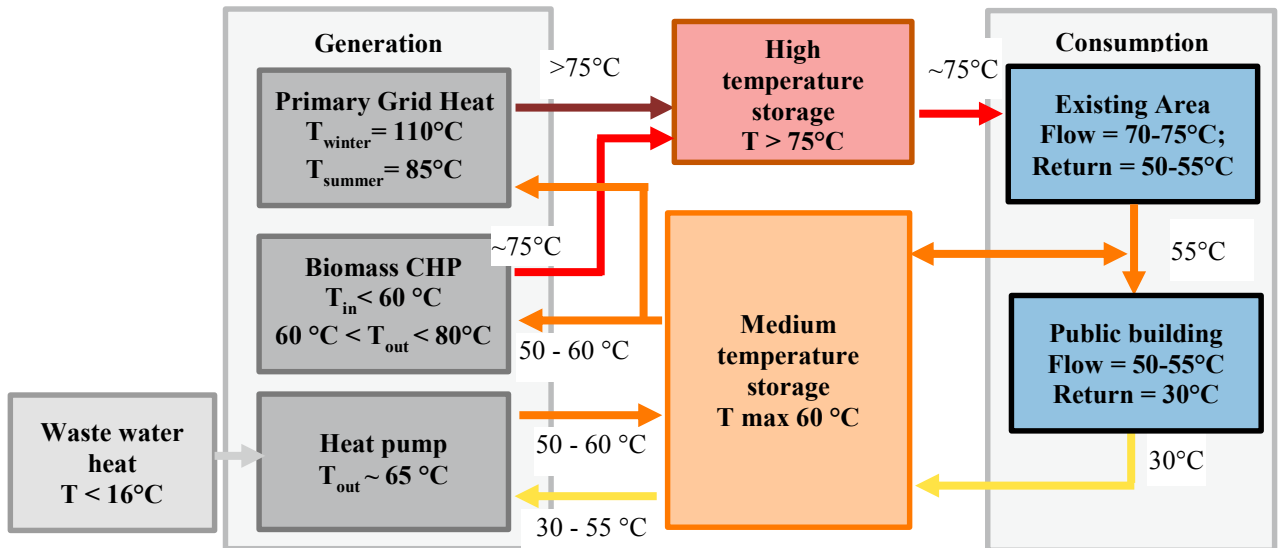


Figure 1: Interconnection of heat generation and storage units in the Heat Dispatch Center and connected consumers considering energy flows and temperature levels

The electricity demand of the heat pump is covered by the CHP as the opportunity cost for selling the electricity is lower than the achievable electricity price, additional generation is sold at the electricity market. Economic parameters of the heat pump are the same as for the first concept. A biomass gasifier connected to a CHP unit with a thermal load of 380 kW and an electric load of 120 kW was considered. The overall cost of the Heat Dispatch Center including gasifier, CHP and auxiliaries, connection to primary grid, monitoring and control units including installation costs is expected to lie at 1,150,000 €. Preliminary evaluations show that storage volumes of 20 m³ for high and 50 m³ for medium temperature storage are suitable, leading to overall costs of 51,000 €. Costs for domestic transfer stations are about 340,000 € including installation costs.

Further relevant specific prices are wood including transport at 305 €/t (heat capacity 4.3 MWh/t), waste disposal 1,300 €/t and nitrogen costs 270 €/bundle.

Developed simulation tool

Several simulation tools for district heating systems exist. These do not allow evaluations, such as the interconnection of different heat supply units on subsequent temperature levels. In order to determine capacities and economic efficiency depending on overall system configuration and generation prioritization, a Microsoft® Excel based simplified DHN simulation tool was developed. For every hour of the reference year 2017 the state of the two storage tanks and the provision of heat from the different supply units is calculated.

4.4. Preliminary results for heat supply concepts

Energetic, economic and ecologic results for the two innovative supply concepts are stated in Table 7. As a reference a gas boiler system can be expected to generate heat at a cost of 8,5 €/kWh, when investments are neglected (efficiency 90 %, gas price 6.86 €/kWh [23]). This gas system would lead to specific emissions of 224 g CO₂/kWh.

Table 7: Energetic, economic and ecologic results for the different thermal energy supply systems

Energy supply concept	Low temperature network connected to building individual heat pumps	Heat Dispatch Centre
Heat generation costs	11.5 ct/kWh with and 12 ct/kWh without funding of 20 % on invest	13.5 ct/kWh with and 14 ct/kWh without funding of 20 % on invest
Specific CO ₂ -Emissions	162 g/kWh	19 g/kWh
Primary Energy Factor	0.5	0.12

A cost analysis shows that the cost for heat generation in the Heat Dispatch Center is dominated by the cost for the biomass gasification + CHP unit. This includes the investment as well as the maintenance and variable costs. About 48 % of the heat is provided by the CHP unit, 28 % by the heat pump and 24 % by the primary heating network.

The annual costs of the low temperatures district heating network are highly dominated by electricity costs, the high electricity demand also leads to the comparatively high specific CO₂ emissions and primary energy factor. Heat from the primary grid provides about 40 % of the energy is provided from the primary grid, 35 % from the environment and 25 % is based on electricity.

5. Discussion of the results

Here firstly the results from the evaluation of concepts to decrease thermal losses are discussed (section 5.1), then the findings for the two different heat supply concepts is contrasted (section 5.2).

5.1. Methodology and results to decrease thermal losses

In this study intra-year and intra-day variations in supply temperatures are assessed, for this simplifications were made. Here some of them are discussed regarding their effect on the results and ideas for improvements are given.

With the heat loss coefficients from supplied data yearly losses of 12 % relative to the overall heat generation can be calculated. This value is comparatively low, which indicates that the network is well insulated or the values are not correct. Hence, for the derivation of realistic savings the loss coefficients need to be verified. Higher thermal loss coefficients would make variations in supply temperatures more economical. In contrast to this intra-day variation could become even less viable. Costs and savings for temperature variation in the public building line need to be recalculated when the actual amount of tapping points in the building is known and the savings can be compared to the additional cost for decentral water stations.

The change to electric boilers was only calculated considering a building-central boiler system. Due to the age and insulation standard of the circulation lines in the buildings a cost-comparison with decentral boilers would be adequate.

When investigating the existing network more in detail, it shows that the southern as well as the northern supply line include branches in which none of the buildings generate DHW from the DHN. Therefore, these buildings could be integrated into the return of the other buildings, which would be beneficial to a further decrease in an overall return temperature. In two buildings connected to the southern line instantaneous water heaters are installed for the provision of heat. Accordingly, this branches could be disconnected to the southern network in summer.

5.2. Innovative thermal energy provision

Although preliminary results indicate that the low-temperature heating network is more economical, further investigations regarding the actual generation costs are required. While the prices for storages were neglected for the low-temperature system, these might be necessary for actual implementation of the concept. Vast potential to increase the economic viability of the Heat Dispatch Centre exist. One step to improve economic viability is to increase the share of heat from the primary heating network and decrease the share of heat supply from comparatively expensive biomass. This analysis and further in-detail investigations will be published at [7].

6. Conclusion and Outlook

In the feasibility study the aim was to approximately assess the economic viability of innovative heat supply systems. Up to now in industrial and residential applications the focus was less on required temperature levels and more on thermal loads. Also often the actual temperature demand of consumers connected to grid based thermal energy supply is unknown. Caused by this, high temperatures are used although they are not required. In order to enable an efficient thermal energy supply based on renewable energies the actual energy demands per network line have to be carefully assessed and compared to alternative supply concepts. Moreover, the implementation of concepts employing heat supply units connected in series instead of in parallel should be further investigated.

References

- [1] District energy in cities - Unlocking the Potential of Energy Efficiency and Renewable Energy. Paris, Frankreich: United Nations Environmental Programm - Division of Technology, Industry and Economics, 2015
- [2] Pehnt, Martin et al.: Wärmenetzsysteme 4.0 - Endbericht - Kurzstudie zur Umsetzung der Maßnahme "Modellvorhaben erneuerbare Energien in hocheffizienten Niedertemperaturwärmenetzen". Heidelberg, Berlin, Düsseldorf, Köln: Adelphi, 2017.
- [3] Lund, Henrik et al.: 4th Generation District Heating (4GDH) - Integrating smart thermal grids into future sustainable energy systems. In: Energy 68 (2014) 1-11; Amsterdam, Netherlands: Elsevier, 2014.
- [4] Braungardt, Simon et al.: Elektrisch angetriebene Wärmepumpen - Aktuelle Ergebnisse aus Forschung und Feldtests. Eggenstein-Leopoldshafen: BINE Informationsdienst, 2013.
- [5] Arpagaus, Cordin: Multi-temperature heat pumps: A literature review. Buchs, Schweiz: Institute for Energy Systems, NTB University of Applied Sciences of Technology Buchs, 2016.
- [6] IFEU; GEF: Transformationsstrategien Fernwärme - TRAFÖ - Ein Gemeinschaftsprojekt von ifeu-Institut, GEF Ingenieur AG und AGFW. Frankfurt am Main: Der Energieeffizienzverband für Wärme, Kälte und KWK e.V. (AGFW), 2013
- [7] Kleinertz, Britta; Brühl, Götz et al 2018: Project "Fourth generation district heating – Feasibility study for a district heating network 4.0 in Rosenheim" Forschungsgesellschaft für Energiewirtschaft mbH (FfE), 2017 – sponsored by Bundesamt für Wirtschaft und Ausfuhrkontrolle <https://www.ffegmbh.de/kompetenzen/energiekonzepte/746-waermenetze-4-0-machbarkeitsstudie-fuer-ein-innovatives-waermenetz-der-vierten-generation-in-rosenheim>
- [8] Preis für Fernwärme nach Anschlusswert in Deutschland in den Jahren 1992 bis 2017: <https://de.statista.com/statistik/daten/studie/250114/umfrage/preis-fuer-fernwaerme-nach-anschlusswert-in-deutschland/>; Hamburg: Statista GmbH, 2018.
- [9] Durchlauferhitzer - Schock für Warmduscher in: Stiftung Warentest 01/2015. Berlin: Stiftung Warentest, 2015
- [10] BDEW - Strompreisanalyse Mai 2018 - Haushalt und Industrie. Berlin: BDEW - Bundesverband der Energie- und Wasserwirtschaft, 2018.
- [11] C.A.R.M.E.N. e.V.:(2017). Sophena (1.1) [Software]. Abgerufen von <https://www.carmen-ev.de/infothek/downloads/sophena/2008-download-von-sophena>. Straubing: 2017
- [12] DIN Deutsches Institut für Normung e.V. (DIN): DIN EN 15450 - Heizungsanlagen in Gebäuden - Planung von Heizungsanlagen mit Wärmepumpen. Berlin: Beuth Verlag GmbH, 2007
- [13] VDI 2067 - Blatt 1 - Wirtschaftlichkeit gebäudetechnischer Anlagen - Grundlagen und Kostenberechnung. Ausgefertigt am 2000, Version vom 2012-09; Düsseldorf: Verein Deutscher Ingenieure (VDI), 2012.
- [14] Merkblatt zu den technischen Anforderungen an ein Wärmenetzsystem 4.0 - Modellvorhaben Wärmenetzsysteme 4.0. Eschborn: Bundesamt für Wirtschaft und Ausfuhrkontrolle, 2018.
- [15] 2006 IPCC Guidelines for National Greenhouse Gas Inventories - Energy - Stationary Combustion. Kamiyamaguchi Hayama, Kanagawa: Institute for Global Environmental Strategies, 2006.
- [16] Wiesemeyer, Karin; Schwentzek, Marco; Corradini, Roger; Mauch, Wolfgang: Allokationsmethoden für spezifische CO₂-Emissionen von Strom und Wärme aus KWK-Anlagen in: Energiewirtschaftliche Tagesfragen 60. Jg. (2010) Heft 9. Essen: etv Energieverlag GmbH, 2010
- [17] Entwicklung des CO₂-Emissionsfaktors für den Strommix in Deutschland in den Jahren 1990 bis 2017 (in Gramm pro Kilowattstunde): <https://de.statista.com/statistik/daten/studie/38897/umfrage/co2-emissionsfaktor-fuer-den-strommix-in-deutschland-seit-1990/>; Hamburg: Statista GmbH, 2018 (überarbeitet: 2018).
- [18] DIN V 18599-1:2011-12 - Energy efficiency of buildings - Calculation of the net, final and primary energy demand for heating, cooling, ventilation, domestic hot water and lighting - Part 1: General balancing procedures, terms and definitions, zoning and evaluation of energy sources. Berlin: DIN Deutsches Institut für Normung e.V. (DIN), 2011
- [19] Broschüre - Fernwärme für Rosenheim. Rosenheim: Stadtwerke Rosenheim GmbH & Co. KG, 2016.
- [20] Ramm, Tobias et al.: Energy storage and integrated energy approach for district heating systems. Amsterdam: Elsevier B.V., 2017.
- [21] Fricke, Manfred: Großwärmepumpen: ein wichtiges Bauteil für Fernwärmenetze. Berliner Energietage: OCHSNER Energie Technik, 2016.
- [22] Wolf, S.; Fahl, U.; Blesl, M.; Voß, A.: Analyse des Potenzials von Industriewärmepumpen in Deutschland - Forschungsbericht. Stuttgart: Institut für Energiewirtschaft und Rationelle Energieanwendung (IER), 2014
- [23] Energiedaten - Nationale und Internationale Entwicklungen - Stand 05.05.2017. Berlin: Bundesministerium für Wirtschaft und Technologie (BMWi), 2017



16th International Symposium on District Heating and Cooling, DHC2018,
9–12 September 2018, Hamburg, Germany

Transition to the 4th generation district heating - possibilities, bottlenecks, and challenges

Haoran Li^{a*}, Natasa Nord^a

^aNorwegian University of Science and Technology, Kolbjørn Hejes v 1B, Trondheim, NO-7491, Norway

Abstract

The 4th generation district heating (DH) will be available in the coming years. However, the transition from the current 2nd or 3rd generation DH is a challenging task. This article reviewed the technical issues associated with the transition: supplying low temperature to buildings, integrating various heat sources and thermal storages, and developing smart DH systems. Possibilities, bottlenecks, and challenges of the transition were discussed. The conclusion was that the transformation should be conducted carefully and gradually. Comprehensive consideration such as the energy status, system conditions, and operation customs must be taken into account.

© 2018 The Authors. Published by Elsevier Ltd.

This is an open access article under the CC BY-NC-ND license (<https://creativecommons.org/licenses/by-nc-nd/4.0/>)

Selection and peer-review under responsibility of the scientific committee of the 16th International Symposium on District Heating and Cooling, DHC2018.

Keywords: 4th generation district heating, transition, challenges, low temperature district heating, various heat sources, thermal storage, smart district heating system;

1. Introduction

District heating (DH) is an energy service, which moves the heat from available heat sources to customers. The fundamental idea of DH is to use local fuel or heat resources, which would otherwise be wasted, to satisfy local customer heat demands, by using heat distribution networks [1].

* Corresponding author. Tel.: +47-48670533.

E-mail address: haoranli@ntnu.no

In historical development of DH, three generations of DH developed successively. The 1st generation DH systems used steam as the heat carrier. Typical components were steam pipes in concrete ducts, steam traps, and compensators. Almost all DH systems established until 1930 used this technology. The 2nd generation DH systems used pressurized hot water as the heat carrier, with supply temperatures mostly higher than 100°C. Typical components were water pipes in concrete ducts, large tube-and-shell heat exchangers, and material-intensive, large, and heavy valves. These systems emerged in the 1930s and dominated all new systems until the 1970s. The 3rd generation DH systems still use pressurized water as the heat carrier, but the supply temperatures are often below 100 °C. Typical components are prefabricated, pre-insulated pipes directly buried into the ground, compact substations using plate stainless steel heat exchangers, and material lean components. The systems was introduced in the 1970s and took a major share of all extensions in the 1980s and beyond [2].

The direction of development for these three generations has been in favor of lower distribution temperature, material-lean components, and prefabrication. On the basis of the trends identified above, the future DH technology should include lower distribution temperatures, assembly-oriented components, and more flexible materials [1]. The revolutionary temperature level, with supply temperature below 50~60°C, will become the most important feature of the 4th generation DH. The energy supply system, end users, and occupants will benefit from the low temperature level. A brief summary of those benefits are shown in Table 1.

Table 1. Major advantages with lower distribution temperatures.

Objects	Advantages	References
Flue gas condensation from combustion of biomass and waste	Higher output capacity (25~40%) from direct condensation of the fuel moisture in biomass fuels and waste	[1]
Geothermal energy and industrial residual heat with medium temperature	Higher output capacity (50~100%) from available medium-temperature (70~100°C) water flow	[1]
Solar energy	Higher output capacity from connected solar heat collectors	[1]
Steam based combined heat and power (CHP) plant	Higher power-to-heat ratios in the same CHP plant design, results more electricity generation at the same heat demand	[1]
Heat pump (HP)	Higher coefficient of performance, since both pressure and temperature can be lower in the HP condenser	[3]
Heat storage	Increased capacities in water-based heat storages managing both supply and demand variations, reduce heat losses from thermal storage units	[1, 3]
Network	Higher distribution efficiency due to less heat loss from the network	[3]
Network	Lower risk of pipe leakages due to thermal stress, and the corresponding maintenance costs are reduced as well	[3]
Network	Possibility to use plastic pipes in distribution areas with low pressures	[3]
Network	Lower risk of water boiling in the network, which means lower risk of two-phase-flow in pumps and fast moving water walls	[3]
Building	Better match the future building heat demand and heat temperature requirement	[3]
Occupant	Eliminate the potential risk of scalding human skin due to water leakages	[3]

In addition, the 4th generation DH will take advantage of various heat sources, different level thermal storages, modern measuring equipment, and advanced information technology, to make itself more flexible, reliable, intelligent, and competitive.

This article reviews the technical issues associated with transition to the future DH. The studies on transition to the low temperature DH (LTDH) systems are summarized in Section 2.1. The knowledge of integrating various heat sources and thermal storages are presented in Section 2.2 and Section 2.3, respectively. The idea of smart DH system is shown in Section 2.4. Further, some facing challenges and possible solutions for the future DH are discussed in Section 3. Finally, the conclusions for transition to the future DH are proposed in Section 4.

2. Transition to the future district heating

Characterized by low temperature, various heat sources, thermal energy storage (TES), intelligent management, and integration with smart energy system, the 4th generation DH will be available in the coming years. However, the transition from the current 2nd or 3rd generation DH to the future 4th generation DH is a challenging task. This section reviews the following technical issues associated with transition to the 4th generation DH: supplying low temperature to new and existing buildings, integrating various heat sources including renewable sources and recycled sources, different TES technologies, and smart DH systems. In addition, the bottlenecks and challenges of the transition are presented together with potentials solutions.

2.1. Transition to the low temperature district heating system

2.1.1. Temperature level of the current system

For the DH system using pressurized hot water as the heat carrier, the water is heated up to the supply temperature at the heat supply units, and cooled down to the return temperature at the customer substations. The supply temperature is decided by the heat provider, while the return temperature is the aggregated result from all cooling processes at the customer substations. The supply and return network temperatures are not standardized, they will depend on the local conditions [1].

An overview of annual average temperature level of 142 Swedish and 207 Danish DH systems is provided in Fig. 1 [4]. Fig. 1 shows that Swedish and Danish DH systems can be regarded as the 3rd generation DH system with respect to their temperature levels. The average network temperatures in Sweden and Denmark are compared with six other European DH systems in Fig. 2. Fig. 2 shows that the temperature levels of Riga, Warsaw, and Poznan DH systems are similar to the Swedish and Danish systems and they can be also classified as the 3rd generation DH system. However, for Geneva and Brescia systems, the temperature level are relative high, with annual average supply temperatures close to or above 100°C, and with return temperatures range from around 60°C to 80°C. Therefore, these systems may be regarded as the 2nd generation DH system [5].

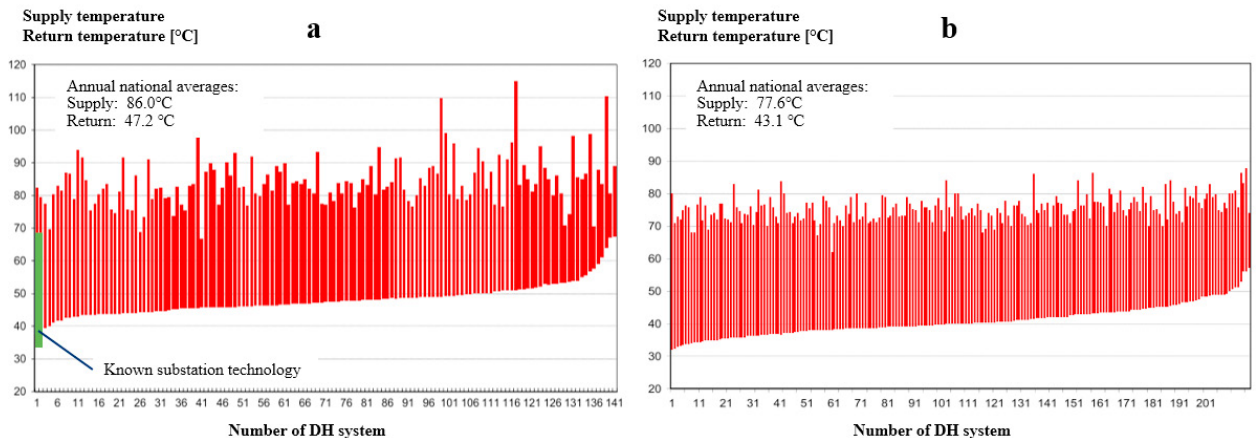


Fig. 1. Overview of heat distribution temperatures in different DH systems. (a) 142 Swedish DH systems, (b) 207 Danish DH systems [4]

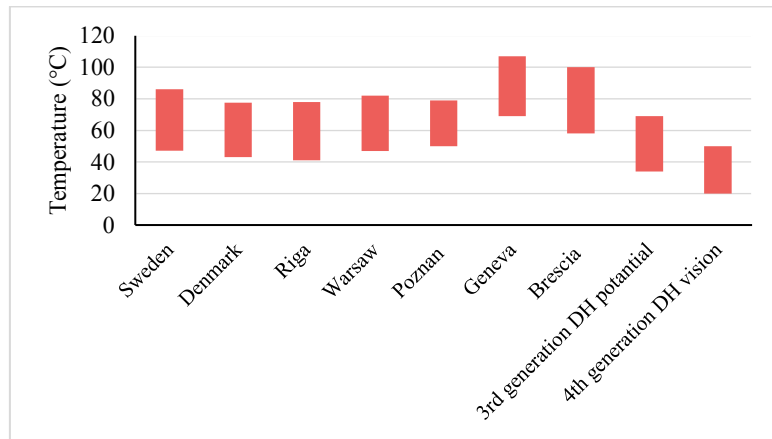


Fig. 2. Typical distribution temperatures for various systems

2.1.2. Transition to the low temperature district heating system

The possibilities to achieve lower temperature level are summarized in the final report of International Energy Agency Technology Collaboration on District Heating and Cooling including Combined Heat and Power (IEA DHC) Annex XI - Transformation Roadmap from High to Low Temperature District Heating Systems [5]. In this report, the transition processes to the low temperature DH are explained in two steps. In the first step, the temperature potential of the current DH system will be fulfilled, with the measures of eliminating system errors and improving system control. In the second step, the temperature level will be further reduced, by the means of enhancing the heat transfer performance of heat exchangers, and improving the design of substations. The renovation of buildings will be conducted along the two steps when it is necessary. These necessary actions for the transition are explained in the text below.

Eliminating system errors and improving system control is a highly important task to reduce the temperature in a DH system. The green bar at the left of Fig. 1 (a) shows the theoretical annual supply and return temperatures of 69 and 34°C for a typical error-free substation with the current substation technology [1]. During 2009, the Marstal DH system in Denmark had an annual average supply and return temperature of 74 and 36°C, very near to the theoretical temperature level. The Marstal DH management has thus proved that it is possible to operate a DH system very near to the theoretical supply and return temperatures [1]. However, Most Swedish DH systems have substantially higher return temperature than their potentials, especially the systems located to the right of Fig. 1 (a). The causes and possible solutions for the difference between actual and theoretical return temperature are summarized in Table 2.

Table 2. Causes and possible solutions for the difference between actual and theatrical return temperature.

Causes		Possible solutions	References
Short-circuit flows	Intentional short-circuit flows to maintain a minimum supply temperature, or to avoid network work freezing	Suitable controlled by thermostatic valves, or introduce innovative systems to avoid bypass flow	[1, 6]
	Unintentional short-circuit flows from remnants of construction, or from the connection mistake	Improve the construction quality	
Low supply temperature	Substation control with high flows to compensate the low supply temperature	Apply intentional short-circuit flows, or use three pipe system with two supply pipes and one return pipe	[1, 5]
Errors in customer heating systems	Missing thermostatic valves in space heating (SH) system, missing hot water circulation in domestic hot water (DHW) system, and using three-way diverting valves in the SH system	Add thermostatic valves in SH system, put the temperature sensor of DHW near or in the heat exchanger, and replace three-way diverting valves with two-way valves	[1, 5]

Causes	Possible solutions	References
	Too small heat emitting surfaces in SH, ventilation and DHW system, which results in a large flow and low cooling	Choose suitable heat emitting surfaces
Errors in customer substations	Set point errors, sometimes the secondary set point temperature is higher than the primary supply temperature, giving full primary flow	Intelligent control which can ignore impossible control situations
	Malfunction errors, such as leaking valves, defective valve motors, and malfunctioning temperature transmitters, fouled heat transfer areas for heat exchangers	Use high quality equipment, apply fault detection technology, and regular maintenance
	Design errors, such as too large valves, wrongly assembled temperature transmitters, and wrong valve motors chosen, parallel flow installations for heat exchangers, and wrong heat exchanger size chosen, deviations from recommended substation configurations	Improve the design quality, apply the prefabricated equipment

Domestic hot water (DHW) preparation requires certain temperature levels and thereby influence the substation layout and component sizes. The Number of Thermal Units (NTU) indicates the heat transfer ability of heat exchangers. With a fixed heat exchange capacity, larger NTU allows a heat exchanger to operate with lower temperature difference. Meanwhile, larger NTU implies an increased heat exchanger area, which leads to an increased investment cost. For a heat exchanger for DHW preparation, the NTU value is 3.2, with the primary and secondary inlet/outlet temperature as 60°C/25°C and 10°C/50°C, which are recommended by Euroheat and Power [8]. For the low temperature systems with the primary and secondary inlet/outlet temperature as 50°C/20°C and 14°C/47°C, the NTU value should be doubled to 7.6 [5].

For the ultra-low-temperature DH systems, whose supply temperature can be 46°C most of the year, supplementary heating devices are recommended to guarantee comfortable and hygienic DHW [9-11]. Some examples for such application are shown in Fig. 3. In Fig. 3 (a), the DHW is stored in the storage tank and used directly. The DHW is preheated by the DH and further heated by the electric heater. The layout difference between Fig. 3 (a) and Fig. 3 (b) is that Fig. 3 (b) has a heat exchanger after the storage tank, and the DH water is stored in the tank. In Fig. 3 (c), the DHW is preheated by DH through a heat exchanger. The temperature could be comfortable for taking a shower, but considering the requirement for hotter DHW for washing purposes in the kitchen, an instantaneous electric heater is installed on the DHW pipe to the kitchen taps. Fig. 3 (d) has the same layout as Fig. 3 (c), except that an electric heater is used to heat up the total DHW flow. In Fig. 3 (e), a micro HP and a storage tank are installed before the heat exchanger, and one stream of the DH supply is used as the heat source for the HP.

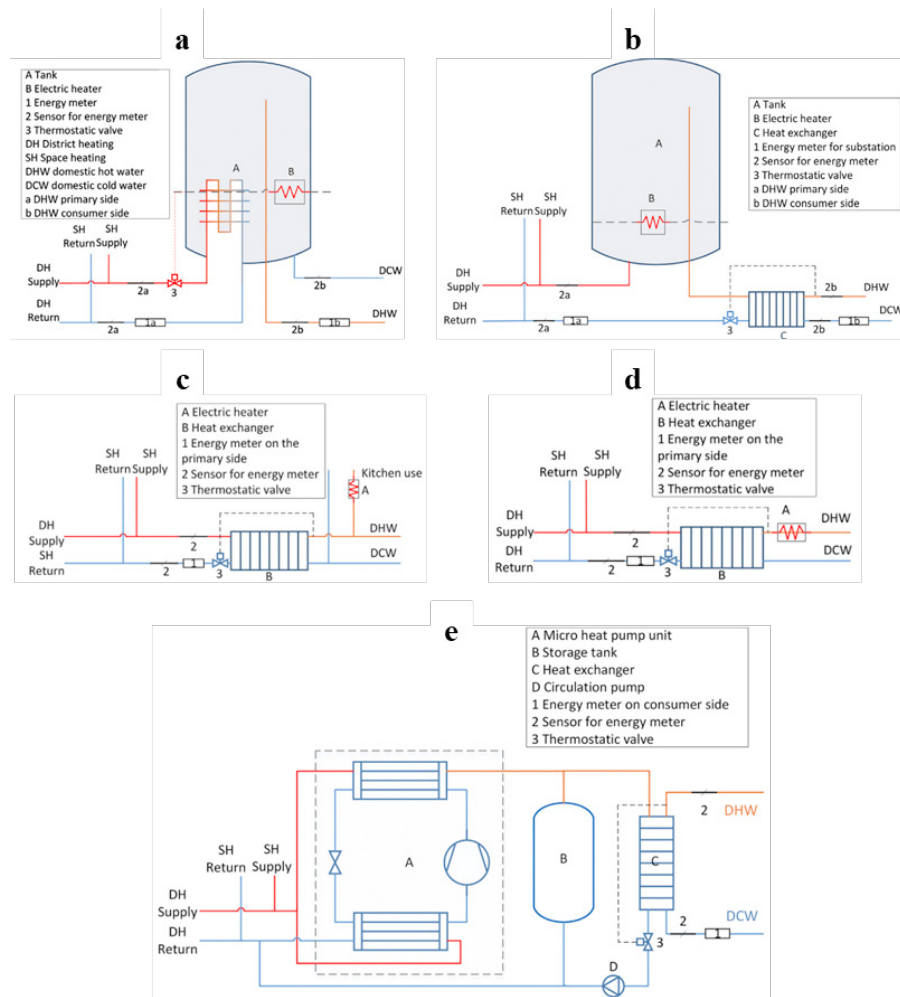


Fig. 3. Different layouts of substations for DHW with supplementary heating devices. (a) substation with tank, (b) substation with tank and heat exchanger, (c) substation with heat exchanger and supplementary heater for kitchen use, (d) substation with heat exchanger and supplementary heater for the total DHW flow, (e) substation with HP, tank and heat exchanger [10].

Building space heat (SH) demand will change in the future and thereby the temperature requirements will change. For newly built buildings and future buildings, 50°C supply temperature to the SH system is enough, with floor heating or low-temperature radiators, and there is still the option to boost the supply temperature during the coldest periods. In fact, the DH supply temperature can be even lower, but it needs supplementary heating system to heat up DHW as explained previously [12].

Low-energy buildings comprise only a small share of the building stock, while the majority are older buildings with considerably higher heat demand. The older buildings will continue to make up a large share of the building stock for many years (for Denmark and Norway, the share will be about 85-90% [13] and 50% [14] in 2030, respectively). Existing buildings are usually equipped with SH systems designed with supply temperatures around 70°C or higher and thereby a reduction of the supply temperature would be expected to cause discomfort for the occupants [12]. However, studies show that houses from the 70s or 80s without any renovation are possible to be heated with the low supply temperature of 50°C most of the year, and only limited time the supply temperature has to be above 60°C. If original windows of the houses are replaced, it is possible to decrease the supply temperature below 60°C for almost the entire year. Further, when the renovated houses replace their SH systems with low-temperature radiators, they may be supplied year around with the supply temperature of 50°C [12, 15].

2.2. Integrating various heat sources into district heating system

There is a huge potential to supply DH systems with heat from various renewable sources, such as industrial waste heat (IWH), solar thermal energy, and geothermal energy. The main advantage of LTDH system is its easier integration and higher efficiency when utilize renewable energy and waste heat (REWH). When the temperature of REWH is higher than the return temperature of a DH system, the resource can be used directly, otherwise the temperature must be upgraded with a HP [16].

Availability is one critical aspect of REWH. Some resources, such as solar and wind, are intermittent and not dispatchable. The hourly and seasonal distribution of those resources may be counter to the distribution of heat demands. In addition, some resources, such as IWH, may be subject to interruptions due to the operating hours of industrial facilities [16]. One common solution is to combine REWH with TES and dispatchable heat sources [1, 17–19].

2.2.1. Methods for heat sources feed-in

There are mainly three ways to feed-in heat sources into DH grids: 1) extraction from the return line and feed-in into the supply line, 2) extraction from the return line and feed-in into the return line, and 3) extraction from the supply line and feed-in into the supply line. The features, advantages, and disadvantages of those variants are summarized in Table 3 [14].

Table 3. The features, advantages and disadvantages of various connection variants.

Connection variants	Features	Advantages	Disadvantages
Extraction from the return line and feed-in into the supply line	The temperature difference is dependent on operating conditions and grid operator. The pressure difference is high, and depends on the actual location in the grid	The return temperature is unchanged, which avoids temperature the strain on return pipes, and the influence of heat extraction efficiency of other heat sources	High energy demand for the mandatory feed-in pumps
Extraction from the return line and feed-in into the return line	The temperature rise is commonly set by the DH operator, the pressure difference is relatively low	It is preferable for heat sources with high efficiencies for lower temperatures	The return temperature is raised, which increases the grid heat loss, and influence the efficiency of other heat sources
Extraction from the supply line and feed-in into the supply line	The temperature increase is prescribed by the grid operator, the pressure difference is relatively low	—	The supply temperature is raised, which increases the grid heat loss, and influence the efficiency of other heat sources

2.2.2. Heat recycling from industrial processes

Recycling heat from industrial processes represents one of the main strategic opportunity for DH, in line with the basic idea of using heat that would otherwise be wasted. In Sweden, recycling of IWH makes up around 6% of the total energy supply to DH networks in 2010. For Danish DH systems, the proportion is about 2%~3%. The DH system in Gothenburg, Sweden, obtains 1112 GWh waste heat from two oil refineries. This gave approximately 27% of heating demand in 2010 [1].

The IWHs are heterogeneous and of various grades. The high-grade IWHs, such as steam and combustible gas, mostly be exploited within the factory, for power generation. However, the low-grade IWHs, with the temperature mostly between 30°C and 200°C, are likely discarded into the environment. There are several technical issues for recycling IWH for DH use: the long distance delivery of IWH to end users, and peak load-shaving of DH system [20].

Long distance delivery for waste heat: Industrial plants are usually far away from DH users, the recommended radius for IWH based DH is 5~10 km for a small-scale town and 20~30 km for a large-or-medium-scale city, due to the investment of transmission network and heat loss during the transmission. However, such a radius might vary with different economic conditions [21].

To decrease the energy use of distribution pumps and thereby the distribution losses, the temperature difference between the supply and return temperature should be increased. As the advantages of LTDH, the reasonable solution is to reduce the return temperature. Several potential techniques to obtain higher temperature difference are shown in Fig. 4, which includes cascade heating technology, absorption heat pump (AHP) technology, and HP technology.

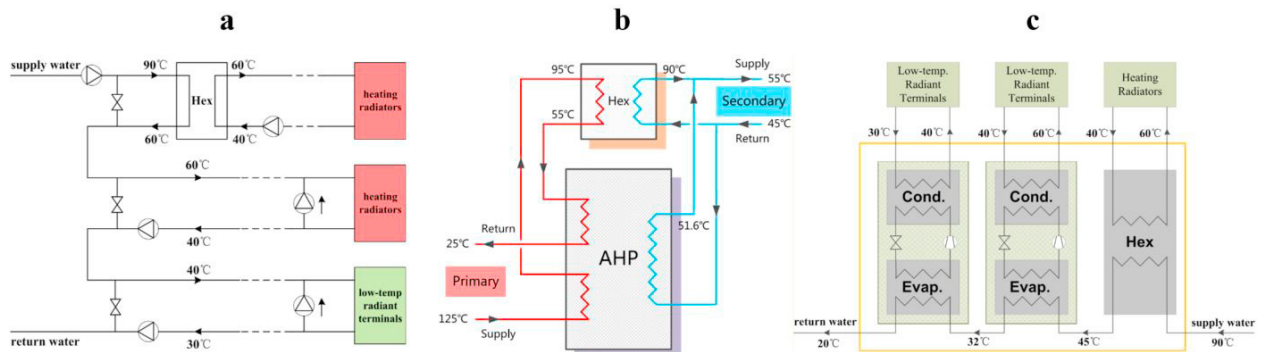


Fig. 4. Scheme of different IWH transition techniques. (a) typical cascade heating system, (b) substation/building entrance AHP system, (c) substation/building entrance electrically driven HP system [20].

In Fig. 4 (a), cascade heating technology supplies heat to the indirectly connected radiators, directly connected radiators, and directly connected low-temperature heating terminals (e.g. floor heating), in sequence. Commonly, the return temperature can be reduced to 30°C or even less by this technology. In Fig. 4 (b), water on the primary side firstly flows into AHP to drive the machine, AHP extracts heat from return water of heat exchanger. After AHP, the water go through the heat exchanger and AHP successively. The final return water can be 25°C. The limitation of this technology is the supply temperature should be high enough to drive AHP. In Fig. 4 (c), supply water firstly transfers heat to heating radiators through a heat exchanger, afterword, the water provides heat to several low-temperature heating terminals by HPs, until the final return temperature become 20°C or even lower [21].

Peak load-shaving in DH systems: An IWH based DH system is complex with respect to the coordination between IWH productions and DH heat demands. Waste heat from industrial processes is constantly fluctuating, and may even come to a temporary stop, depending on the production schedules [21]. However, the heat demand of a DH system changes continuously and smoothly according to the weather conditions [21] and the occupant behaviors [22].

For the above reason, IWH can never serve as the sole heat source, specific control and peak load-shaving strategies should be applied, as shown in In Fig. 5. In Fig. 5 (a), IWH is able to serve the maximum heat load, and cooling towers (CTs) have to operate all the time except the coldest days to release heat to the environment. Opposite, in Fig. 5 (c), IWH serves as the base load. Thus, the peak load-shaving strategies have to be implemented to make up the difference between the total load and the base load. Fig. 5 (b) illustrates a case between these extremes, in which both the CTs and peak-shaving strategies are necessary. To achieve a high IWH recovery ratio, it is appropriate for the IWH to serve as the base load as in Fig. 5 (c). Fig. 5 (d) shows an ideal operation strategy, which takes the fluctuation of IWH into consideration. In this case, IWH together with other heat sources provide the base load, and the peak load-shaving strategy works at the coldest time in winter [21].

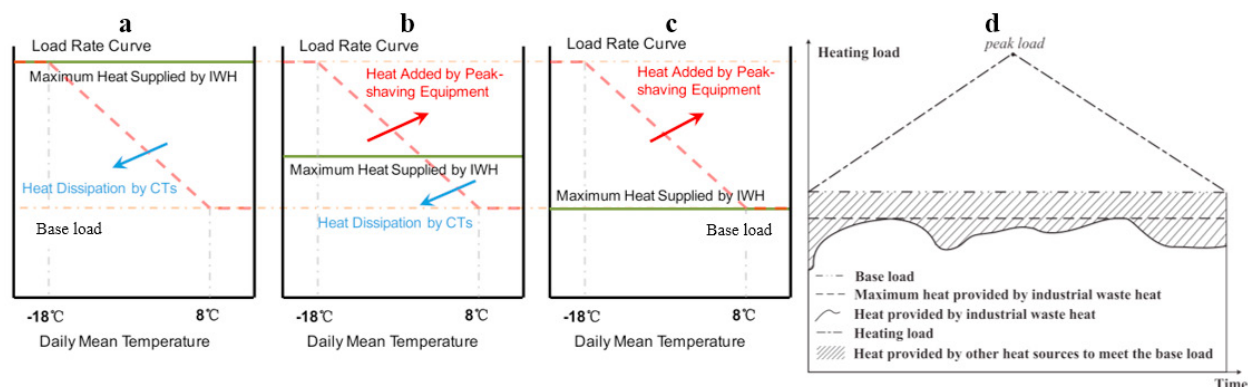


Fig. 5. Regulation and peak load-shaving of IWH based DH system. (a) IWH is able to serve the maximum heat load, (b) a moderate operation strategy with both the peak load-shaving equipment and CTs, (c) IWH serves as the base load, (d) an ideal operation strategy taking the fluctuation of IWH into consideration [20].

2.2.3. Solar district heating

In an international context, solar DH is still in development stage, and it is difficult to ascertain its long-term prospects. There have been interesting developments in a number of countries in Europe, especially in Austria, Denmark, Germany, and Sweden. Recently, companies from these countries have succeeded in contracting for large plants in Asia [1].

The contribution of solar heat to the total heat load can be various from system to system. A large solar thermal plant can be used as a preheater with solar fraction up to 5%. A 100%-coverage of the summer heat load is usually reached with a solar fraction of about 15% on an annual basis. Solar fraction of up to 50% of the annual heat load have been demonstrated for systems using large seasonal heat storages, charging the summer solar heat for the heating period in winter [23].

Solar DH can be provided in a centralized manner with a large array of ground-based collectors, or in a decentralized manner with rooftop-mounted collectors on the buildings that are connected to a DH network, mixed alternatives are also possible, depend on the situation of the projects [1, 19]. Several typical applications of solar DH are presented in Table 4.

Table 4. Typical applications of solar DH.

Location	Solar fraction/ Solar capacity (%/MW _{th})	Other heat sources	DH supply/return temperature (°C)	Thermal storage	Type of integration	Reference
Vallda Heberg (Sweden)	10~20/ 0.2~2	Wood-pellet boiler	—	Buffer storage tank	Centralized	[23]
Crailsheim (Germany)	20~50/ 2~20	Main DH system	65/40	Inter-seasonal borehole heat storage	Centralized	[23]
Gothenburg (Sweden)	100/ 0.2~2	Main DH system	65~100/-	No heat storage	Decentralized	[23]
Büdingen (Germany)	15~20/ 0.5~50	Biomass boiler	75~80/50	—	Centralized	[23]
Braedstrup (Denmark)	10~50/ 0.5~50	CHP, HP and electro- boiler	70~75/30	Multifunctional heat storage	Centralized	[23]
Wels (Austria)	10/ 0.5~10	Main DH system	70~120/-	No heat storage	Decentralized	[23]
Marstal (Denmark)	30/ 13	Oil boiler	—	Two small and one large buffer storages	Centralized	[1]

Location	Solar fraction/ Solar capacity (%/MW _{th})	Other heat sources	DH supply/return temperature (°C)	Thermal storage	Type of integration	Reference
Lyckebo (Sweden)	-/ 3	Biomass boiler	—	Rock cavern hot water storage	Centralized	[1]

The major technical limitation for solar DH is the low energy production density, which means the large areas for placing the solar collectors. In the future, solar thermal energy will continue to be a complementary option [23]. However, the developing technology will bring some possibilities for DH. In the decentralized solar DH systems, there is a possibility that buildings can be either ‘importers’ or ‘exporters’ of solar heat energy, or both, depending on the time of the year. Flexibility in this respect offers a prospect for maximizing the use of solar energy, but makes its management difficult. There is another possibility that a large, inter-seasonal storage can be combined with the decentralized solar energy, so that in the summer season all (or most) connected buildings act as ‘exporters’.

2.2.4. Geothermal district heating

Geothermal energy has enormous potentials; meanwhile, utilization of geothermal energy produces minimal environmental impact. To varying degrees, exploitable geothermal energy is available all around the world. In spite of the impressive size of this energy source, it currently accounts for only a small fraction of the world energy supply. Intensive initial cost, exploration risk, and human-induced earthquakes are the major obstacle to utilize geothermal energy. In addition, there is also the resource problem- once a geothermal well is set up at a given location, the amount of extracted heat tends to decay gradually, makes it felt to a significant degree after one or few decades, while the DH network is still functioning [1].

Deep geothermal systems use heat from 500~5000 m depth; shallow geothermal systems provide heat from less than 300 m depth. High temperature geothermal energy can be used in conventional ways for electricity generation and for direct heat utilization. Ambient heat stored at shallow depths, and aquifer thermal energy stores in ground water layers can be extracted with ground source heat pump (GSHP) and applied for SH and DHW [24].

Several typical applications of geothermal DH are presented in Table 5.

Table 5. Typical applications of geothermal DH.

Location	Type of system	Geothermal fraction /Geothermal capacity (%/MW _{th})	Other heat sources	Geothermal or DH temperature (°C)	Reference
Paris (France)	1.5~1.8 km depth wells	-/ 250	Fossil fuel boilers	Geo: 70	[25]
Ferrara (Italy)	1 km depth wells	80/ 14	Waste-to-energy plant, backup stations, solar heating station, thermal storage, and organic rankine cycle electricity generation	Geo: 100~105	[25]
Beijing (China)	3 km depth wells	100/ -	No other heat source	Geo: 75	[25]
Ontario (Canada)	213 m depth boreholes	—	—	—	[26]
Malmö (Sweden)	90 m depth wells	-/ 1.3	GSHP, boiler	—	[26]
Bucharest (Romani)	70 and 170 m depth wells	100/ 0.39	GSHP	DH: 40/35	[26]

2.3. Thermal energy storages in district heating system

TES can be divided into inter-seasonal storage and short-term storage. Inter-seasonal storage is still in a development phase, while, short-term storage can be made with well-proven technology. However, the dividing line is not sharp; the largest facilities used for short-term storage in large networks could provide inter-seasonal storage in

small systems [1]. In addition, as the end users of DH systems- buildings can also function as TES, due to their thermal inertia. Sometimes, building inertia TES is able to moderate short-term daily net load variations to the same degree compared with hot water tank, while, with much lower investment cost [27].

One purpose of short-term storage is to shift loads away from peak demand hours to lower demand hours. Another purpose is to provide rapid heat or cold supply to meet sudden load changes, which is not capable for heat generating equipment, or to avoid losses associated with quick starts and stops of the generating equipment. A further function of short-term heat storage is to allow for boosted electric power output from some type of CHP plants, which are characterized by a reduced output at increased heat extraction [1, 28].

The objective of inter-seasonal storage is usually either to store collected solar heat for winter heating, or to act as the heating and cooling source as well as thermal storage for GSHP [29].

There are three available technologies for TES: sensible heat storage, latent heat storage, and chemical storage. Sensible heat storage is a comparatively mature technology that has been implemented and evaluated in many large-scale demonstration projects. Latent heat and chemical storage have much higher energy storage densities than sensible storage, and seldom suffer from heat loss problems. However, the latter two technologies are currently still in the stages of material investigations and lab-scale experiments [30]. The detail comparison of those three technologies are shown in Table 6.

Table 6. Comparison of the three available technologies for TES [30].

	Sensible	Latent	Chemical
Storage medium	Water, gravel, pebble, soil...	Organics, inorganics	Metal chlorides, metal hydrides...
Type	Water, rock, and ground based system	Active and passive storage	Thermal sorption and chemical reaction
Advantage	Environmentally friendly, cheap material, relative simple system, easily control, and reliable	Higher energy density than sensible heat storage, and provide thermal energy at constant temperature	Highest energy density, compact system, and negligible heat losses
Disadvantage	Low energy density, huge volumes required, self-discharge and heat losses problem, high cost of site construction, and geological requirements	Lack of thermal stability, crystallization corrosion, and high cost of storage material	Poor heat and mass transfer property under high density condition, uncertain cyclability, and high cost of storage material
Present status	Large-scale demonstration projects	Laboratory-scale prototypes	Laboratory-scale prototypes
Future work	Optimization of control strategy to advance the solar fraction and reduce the power consumption, optimization of storage temperature to reduce heat losses, and simulation of ground based system with the consideration of affecting factors	Screening for better suited phase change material materials with higher heat of fusion, optimal study on store process and concept, and further thermodynamic and kinetic study, noble reaction cycle	Optimization of the particle size and reaction bed structure to get constant heat output, optimization of temperature level during charging/discharging process, screening for more suitable and economical materials, and further thermodynamic and kinetic study, noble reaction cycle

2.4. Smart district heating system

The transformation toward the future renewable energy system poses challenge for all the sub-systems. Facing the challenge, all the sub-systems should benefit from the use of modern information and communication technologies, and uprated themselves to become smart systems [31].

The smart DH system consists of three essential parts: physical network (PN), internet of things (IoT), and intelligent decision system (IDS). PN includes pipes, heating equipment, local meters, and control devices. IoT is the network of sensors, data collecting and transmission devices, and other items, which enables these objects to be connected and exchange data. IDS makes the optimal decisions based on collected data, heat demands, and system responds [32]. One example for the smart DH concept is shown in Fig. 6.

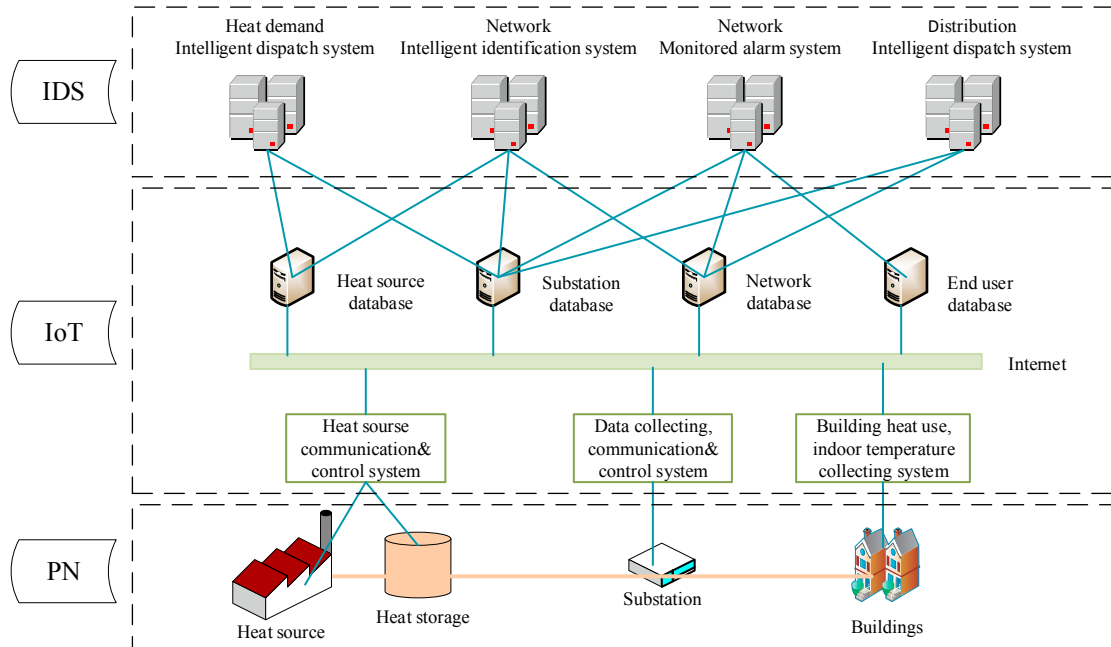


Fig. 6. Concept of smart DH system [33].

The final goal of the smart DH system is to become an essential part of the future smart and renewable energy system. In the future energy system, the focus is on the integration of the electricity, heating, cooling, and transport sectors, and on the use of flexibility in demands and various storages of different sectors. To enable this, the smart DH system must be able to coordinate with other sectors in the energy system [2, 34].

3. Facing challenges for the future district heating system

3.1. Heat losses through distribution network

Reducing heat losses in DH networks is one of the main challenges for the future DH system, because it will reduce the primary energy use and infrastructure investments. Heat loss in DH networks accounts for a relatively high share of heat supply [35], and it will become more significant for the future DH with decreased heat demand.

Real measurement data for heat losses for several DH systems are organized in Table 7. Except the three Swedish cases, all the cases are LTDH demonstration projects. From Table 7, it is obviously that the heat loss in DH networks should not be underestimated, even for the systems with the low temperature and newly upgraded networks. Ten of thirteen systems have a heat losses over 15%, and seven systems have a heat losses over 20%. For the system in Rotskär, the heat losses are up to 32%.

Table 7. Heat losses and detail information of several DH systems.

Location	Construction or upgrade year	Linear heat density MWh/(m·a)	Supply/Return temperature (°C)	Heat loss share (%)	Reference
Slough (UK)	2009–2010	0.319	52/32	28	[14]
Taastrup (Denmark)	2012	—	55/40	13~14	[14]
Lystrup (Denmark)	2008–2009	0.31	55/25	17	[36]
Samsø island (Denmark)	2005	—	—	20~24	[36]
Spjald (Denmark)	1998	0.57	65/32~39	26	[5]
Tarm (Denmark)	1995	0.66	65 /36	17	[5]

Location	Construction or upgrade year	Linear heat density MWh/(m·a)	Supply/Return temperature (°C)	Heat loss share (%)	Reference
Bramminge (Denmark)	—	—	68/-	20	[5]
Middelfart (Denmark)	—	0.72	68/44	19	[5]
Munich (Germany)	2006	1.43	55/30	3	[3]
Okotok (Canada)	2005~2007	0.7	40/35	5~13	[3]
Prästmarken (Sweden)	1995~2004	0.5	75/50	24	[37]
Munksundet (Sweden)	1997	0.84	70/40	22	[37]
Rotskär (Sweden)	2002	0.49	80/-	32	[37]

Some potential solutions to reduce the distribution heat loss are summarized in Table 8.

Table 8. Potential solutions to reduce the distribution heat loss.

Object	Solutions	Limitation	Project applications	Reference
Network	Install pipes inside buildings, to decrease the length of network and utilize heat loss for SH	Not welcomed by DH companies and customers	Peter Freuchenvvej	[37]
Network	House-to-house connection, to decrease the length of service pipes	Not welcomed by DH companies and customers	Cederborg, Nordgren, Gudmundsson	[37]
Network	Three or four media pipes, to shut down one or two pipes in summer	—	Experiment in Nykøbing Falster	[37]
Network	Use booster pumps, to reduce the dimension of pipes	—	Widely used	[37, 38]
Network	Apply branched network with bypass units instead of looped network	Results in high return temperature	Widely used	[38]
Pipe	Improve the insulation of pipes	—	Widely used	[37]
Pipe	Pre-insulated twin pipes or triple pipes	—	Widely used	[1, 37, 39]
Pipe	Prevent over dimensioning of pipes	—	Widely used	[38]
Pipe	Use buffer tanks for DHW production, to reduce the dimension of pipes	Legionella problem with LTDH system	Widely used	[38]
DH system	Leakage detection to avoid hot water loss	—	Widely used	[40]
Substation	Fault detection to avoid any malfunction	—	Widely used	[1, 4, 7]

3.2. Decreased heat demands in the future district heating

The competitiveness of DH systems may be decreased when heat demands are expected to decrease in the future. One study, based on 83 DH systems in European cities shows that there is a lower risk for reduced competitiveness for large cities and inner city areas, however, the areas with low heat density will lose competitiveness in the future [41].

The experiences gained from different projects show that DH systems with low heat demand density require careful plan and design to achieve good economy. In some cases, innovative solutions have been applied and gained extra rewards. With those solutions, it is believed that DH may supply the areas with heat density of 10 kWh/(m²·a), or linear heat density of 0.3 MWh/(m·a) [37]. Some potential measures to apply DH in low heat density areas are shown in Table 9.

Table 9. Potential measures to apply DH to low heat density areas.

Classification	Solutions	Limitation	Reference
Heat source	Use IWH, waste incineration and other cheap heat sources	—	[41]
System design	Optimized network layout with less pipeline length, to get higher linear heat density	—	[42]

Classification	Solutions	Limitation	Reference
System design	Low pressure and low temperature systems with direct connection of SH system	Hydraulic interaction between DH system and SH system	[1, 37]
System design	Reduce pipe dimensions by applying DHW tanks	Legionella problem with LTDH system	[37]
System design	Reduce pipe dimensions by applying booster pumps	—	[37]
System design	House-to-house connection to decrease the length of service pipes	Not welcomed by DH companies and customers	[37]
System design	Three or four media pipes, to shut down one or two pipes in summer	—	[37]
System design	Install pipes inside the buildings, to decrease the length of network and utilize heat loss for SH	Not welcomed by DH companies and customers	[37]
System design	Increase the degree of connection		[37]
Pipe	Improve the insulation of pipes		[37]
Pipe	Pre-insulated twin pipes or triple pipes		[37]
Pipe	Prevent over dimensioning of pipes		[38]
DH system	Leakage detection to avoid hot water loss		[40]
Substation	Fault detection to avoid any malfunction		[1, 4, 7]
Civil works	Reduce the ground cover		[37]
New loads	Supply household equipment previously supplied by electricity	Conflict with traditional practices	[37]

4. Conclusion

Transition to the 4th generation DH is a challenge issue. The process requires the upgrades of DH system and the collaboration with other energy systems. In addition, buildings may also need some refurbishment to coordinate the changes of those systems. The final goal of the transition is to make the future DH system more flexible, reliable, intelligent, and competitive, and become an essential part of the future smart and renewable energy system.

The upgrades of DH system involve the physical system as well as the virtual system. For the physical system, the transition will focus on lowering the system temperature levels, and integrating various heat sources and thermal storages. Two steps will be conducted to lower the temperature level. The first step is to achieve the temperature potentials of the current DH system by the means of eliminating system errors and improving system control. The second step is to further reduce the temperature levels through enhancing heat transfer performance of heat exchangers and improving system design. The renovation of buildings may also be conducted through those two steps when it is necessary. Various heat sources and different level TESs will be integrated into the future DH system. Transition to 4th generation DH should take into consideration all the consisting issues such as way of heat feed-in, type of heat sources and TESs, distribution heat losses, the design of DH system, and operation strategies. Finally, the decisions should be made depending on the local natural and economic conditions.

For the virtual system, transition to 4th generation DH will be based on the intelligent physical system, which is able to measure, transmit information, collect data, and control. In addition, IDS will become more powerful with advanced functions in the future DH system, such as the reliability assessment, accident analysis, accident alarm, operation evaluation, operation supervision, and operation optimization.

The large share of distribution heat loss and the decreasing heat demand are two challenges the future DH systems are going to face. The potential solutions involve innovating system design, upgrading physical and virtual system, integrating cheap heat sources, and introducing new heat loads.

The conclusion of this study is that even enjoying the developing trend of the 4th generation DH, transition to 4th generation DH should be conducted carefully and gradually. Comprehensive consideration must be taken into, focus on the energy status, condition of existing systems, and the operation custom in different areas or countries. In addition, the technologies for the future system need further development, and the operation as well as management strategies should be innovated.

Acknowledgements

The authors gratefully acknowledge the support from the Research Council of Norway through the research project Understanding behaviour of district heating systems integrating distributed sources under FRIPRO/FRINATEK program (the project number 262707).

References

- [1] S. Frederiksen, S. Werner, District Heating and Cooling, Studentlitteratur, 2013.
- [2] H. Lund, S. Werner, R. Wiltshire, S. Svendsen, J.E. Thorsen, F. Hvelplund, B.V. Mathiesen, 4th Generation District Heating (4GDH) Integrating smart thermal grids into future sustainable energy systems, *Energy*, 68 (2014) 1–11.
- [3] A.D. Rosa, H. Li, S. Svendsen, S. Werner, U. Persson, K. Ruehling, C. Felsmann, M. Crane, R. Burzynski, C. Bevilacqua, Annex X Final report: Towards 4th Generation DH Experiences with and Potential of Low Temperature DH, in, IEA DHC/CHP, 2014.
- [4] H. Gadd, S. Werner, Achieving low return temperatures from district heating substations, *Applied energy*, 136 (2014) 59–67.
- [5] H. Averfalk, S. Werner, C. Felsmann, K. Rühling, R. Wiltshire, S. Svendsen, H. Li, J. Faessler, F. Mermoud, L. Quiquerez, Annex XI final report: Transformation Roadmap from High to Low Temperature District Heating Systems, in, IEA DHC/CHP, 2017.
- [6] D. Schmidt, A. Kallert, M. Blesl, S. Svendsen, H.W. Li, N. Nord, K. Sipilä, Low Temperature District Heating for Future Energy Systems, in: *Energy Procedia*, 2017, pp. 26–38.
- [7] K. Yliniemi, Fault detection in district heating substations, in, Luleå tekniska universitet, 2005.
- [8] Euroheat & Power: Home, in.
- [9] X. Yang, H. Li, S. Svendsen, Energy, economy and exergy evaluations of the solutions for supplying domestic hot water from low-temperature district heating in Denmark, *Energy conversion and management*, 122 (2016) 142–152.
- [10] X. Yang, H. Li, S. Svendsen, Evaluations of different domestic hot water preparing methods with ultra-low-temperature district heating, *Energy*, 109 (2016) 248–259.
- [11] X. Yang, S. Svendsen, Achieving low return temperature for domestic hot water preparation by ultra-low-temperature district heating, *Energy Procedia*, 116 (2017) 426–437.
- [12] M. Brand, S. Svendsen, Renewable-based low-temperature district heating for existing buildings in various stages of refurbishment, *Energy*, 62 (2013) 311–319.
- [13] H. Lund, B. Möller, B.V. Mathiesen, A. Dyrelund, The role of district heating in future renewable energy systems, *Energy*, 35 (2010) 1381–1390.
- [14] IEA, Future low temperature district heating design guidebook, in: D. Schmidt, A. Kallert (Eds.), International Energy Agency Technology Collaboration Programme on District Heating and Cooling including Combined Heat and Power, AGFW-Project Company Stresemannallee, Germany, 2017.
- [15] N. Nord, M. Ingebretsen, I. Tryggestad, Possibilities for Transition of Existing Residential Buildings to Low Temperature District Heating System in Norway, in: *Proceedings of the 12th REHVA World Congress*, Aalborg, Denmark, 2016, pp. 22–25.
- [16] M. Spurr, T.S.E. Moe, M. Lehtmetts, Annex X Final Report: Economic and Design Optimization in Integrating Renewable Energy and Waste Heat with District Energy Systems, in, 2014.
- [17] F.M. Rad, A.S. Fung, Solar community heating and cooling system with borehole thermal energy storage – Review of systems, *Renewable and Sustainable Energy Reviews*, 60 (2016) 1550–1561.
- [18] C. Winterscheid, J.-O. Dalenbäck, S. Holler, Integration of solar thermal systems in existing district heating systems, *Energy*, 137 (2017) 579–585.
- [19] M. Rämä, S. Mohammadi, Comparison of distributed and centralised integration of solar heat in a district heating system, *Energy*, 137 (2017) 649–660.
- [20] H. Fang, J. Xia, Y. Jiang, Key issues and solutions in a district heating system using low-grade industrial waste heat, *Energy*, 86 (2015) 589–602.
- [21] H. Fang, J. Xia, K. Zhu, Y. Su, Y. Jiang, Industrial waste heat utilization for low temperature district heating, *Energy policy*, 62 (2013) 236–246.

- [22] N. Nord, T. Tereshchenko, L.H. Qvistgaard, I.S. Tryggestad, Influence of occupant behavior and operation on performance of a residential Zero Emission Building in Norway, *Energy and Buildings*, 159 (2018) 75-88.
- [23] T. Pauschinger, Solar thermal energy for district heating, *Advanced District Heating and Cooling (DHC) Systems*. Woodhead Publishing Series in Energy, (2015) 99-120.
- [24] R.E.T.D.I.A.a.t.R.E.W.P.o.t.I.E. Agency, Renewables for heating and cooling, in, Paris, France, 2007.
- [25] R. Bertani, 4 - Deep geothermal energy for heating and cooling A2 - Stryi-Hipp, Gerhard, in: *Renewable Heating and Cooling*, Woodhead Publishing, 2016, pp. 67-88.
- [26] J.F. Urchueguia, 5 - Shallow geothermal and ambient heat technologies for renewable heating A2 - Stryi-Hipp, Gerhard, in: *Renewable Heating and Cooling*, Woodhead Publishing, 2016, pp. 89-118.
- [27] D. Romanchenko, J. Kensby, M. Odenberger, F. Johnsson, Thermal energy storage in district heating: Centralised storage vs. storage in thermal inertia of buildings, *Energy Conversion and Management*, 162 (2018) 26-38.
- [28] V. Verda, F. Colella, Primary energy savings through thermal storage in district heating networks, *Energy*, 36 (2011) 4278-4286.
- [29] A.V. Novo, J.R. Bayon, D. Castro-Fresno, J. Rodriguez-Hernandez, Review of seasonal heat storage in large basins: Water tanks and gravel-water pits, *Applied Energy*, 87 (2010) 390-397.
- [30] J. Xu, R.Z. Wang, Y. Li, A review of available technologies for seasonal thermal energy storage, *Solar Energy*, 103 (2014) 610-638.
- [31] H. Lund, *Renewable energy systems: a smart energy systems approach to the choice and modeling of 100% renewable solutions*, Academic Press, 2014.
- [32] X. Fang, Requirement of smart heating for heating enterprises and related enterprises, *Gas & heat*, 38 (2018).
- [33] P. Zou, *Heating Engineering*, China Architecture & Building Press, Beijing, 2018.
- [34] B.V. Mathiesen, H. Lund, D. Connolly, H. Wenzel, P.A. Østergaard, B. Möller, S. Nielsen, I. Ridjan, P. Karnøe, K. Sperling, Smart Energy Systems for coherent 100% renewable energy and transport solutions, *Applied Energy*, 145 (2015) 139-154.
- [35] R. Lund, S. Mohammadi, Choice of insulation standard for pipe networks in 4 th generation district heating systems, *Applied Thermal Engineering*, 98 (2016) 256-264.
- [36] A. Dalla Rosa, The Development of a New District Heating Concept, in, Ph. D. thesis, Technical University of Denmark, Kgs. Lyngby, Denmark. Google Scholar, 2012.
- [37] H. Zinko, B. Bøhm, H. Kristjansson, U. Ottosson, M. Rämä, K. Sipilä, District heating distribution in areas with low heat demand density, in: H. Zinko (Ed.), IEA 2008.
- [38] H.Å. Tol, S. Svendsen, Improving the dimensioning of piping networks and network layouts in low-energy district heating systems connected to low-energy buildings: A case study in Roskilde, Denmark, *Energy*, 38 (2012) 276-290.
- [39] A. Dalla Rosa, H. Li, S. Svendsen, Method for optimal design of pipes for low-energy district heating, with focus on heat losses, *Energy*, 36 (2011) 2407-2418.
- [40] S. Zhou, Z. O'Neill, C. O'Neill, A review of leakage detection methods for district heating networks, *Applied Thermal Engineering*, (2018).
- [41] U. Persson, S. Werner, Heat distribution and the future competitiveness of district heating, *Applied Energy*, 88 (2011) 568-576.
- [42] N. Nord, E.K.L. Nielsen, H. Kauko, T. Tereshchenko, Challenges and potentials for low-temperature district heating implementation in Norway, *Energy*, 151 (2018) 889-902.



Available online at www.sciencedirect.com

ScienceDirect

Energy Procedia 149 (2018) 499–508

Energy

Procedia

www.elsevier.com/locate/procedia

16th International Symposium on District Heating and Cooling, DHC2018,
9–12 September 2018, Hamburg, Germany

Design of a Smart Thermal Grid in the Wilhelmsburg district of Hamburg: Challenges and approaches

Peter Lorenzen^{a,b,*}, Philipp Janßen^a, Michael Winkel^b, Dörte Klose^b, Paul Kernstock^a,
Joel Schrage^b, Franz Schubert^a

^aHamburg University for Applied Sciences, Berliner Tor 5, Hamburg, 20099, Germany

^bHamburg Energie GmbH, Billhorner Deich 2, Hamburg, 20539, Germany

Abstract

The paper presents the design of a smart thermal grid in the Wilhelmsburg district of Hamburg. It is emphasized how technical and economical concepts are cross-linked and how district heating systems can become more flexible and efficient by focusing on the whole lifecycle process from customer acquisition over implementation up to operation. Technical concepts for centralized and decentralized generation, grid design and consumer integration are shown. Currently some of these are in the process of implementation, e.g. a grid coupling point, power house expansion, and flexible customers using 3-pipe connections and smart substations.

© 2018 The Authors. Published by Elsevier Ltd.

This is an open access article under the CC BY-NC-ND license (<https://creativecommons.org/licenses/by-nc-nd/4.0/>)

Selection and peer-review under responsibility of the scientific committee of the 16th International Symposium on District Heating and Cooling, DHC2018.

Keywords: Smart Thermal Grid; Renewable Heat Generation; Flexible Operation; Efficiency

* Corresponding author. Tel.: +49-40-42812-5803.

E-mail address: peter.lorenzen@haw-hamburg.de

1. Introduction

European [1] as well as German [2] climate goals aim to significantly reduce primary energy consumption in the heating sector. Figure 1 shows the goals of the German “Energiewende” concerning electricity and heat. The primary goal for heating—reduction of the primary energy demand by 80 %—must be achieved in three different areas: Generation (efficient, renewable and integrated), distribution (efficient) and demand side (reduced). In the electricity sector, 80 % generation from renewable sources should be accomplished. Using wind and photovoltaics causes high fluctuations in electrical generation. This volatility can be compensated by flexible operated combined heat and power (CHP) units or heat pumps in combination with heat storages. As a result, the heating sector is required to provide an increasing share of flexibility and efficiency.

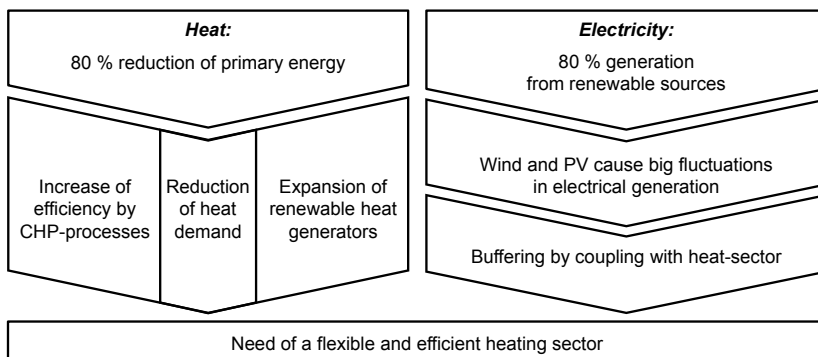


Fig. 1. Goals of the German “Energiewende” until 2050.

Modern district heating systems (DHS) are considered a key component to achieve the reduction of primary energy [3], while they must be transformed to fit the features of newer generations. As described in [4] with every new DHS generation temperature levels decrease while the number of different generators increases. Latest DHS, grids of the 4th generation, integrate a variety of renewable generation, see figure 2. This leads to decentralization, fluctuation and complexity on the generation side.

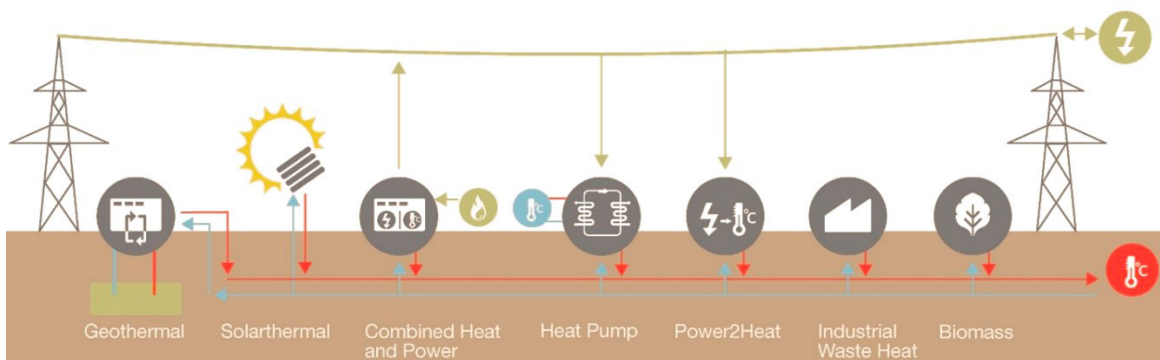


Fig. 2. State of the art technologies for renewable heat generation.

In order to achieve a flexible operation in future energy systems, it is necessary to utilize heat storage and make consumption as flexible as possible to use the energy when it is available. Since DHS are circulatory systems, it is crucial at which temperature the thermal energy is returned. Considering a constant mass flow: the lower the return temperature of this residual heat, the more heat was used by the customer [5]. All in all, comprehensive solutions considering all sectors seem to be promising. For heat, these are addressed by smart thermal grids (STGs) [6]. An

STG is the counterpart to electrical smart grids. Their challenge is to balance generation and demand extremely fast. Additionally, a second key in the inertial DHS is handling low and varying temperatures. STGs provide technical approaches based on information and communication technologies as well as new hydraulic concepts to overcome these challenges. The following sections showcase STG concepts and their realization in an existing DHS in Wilhelmsburg.

2. A smart thermal grid in the Wilhelmsburg district of Hamburg

In the course of the research project “Smart Heat Grid Hamburg” (SHGH), the transformation of a 3rd generation DHS into an STG in Wilhelmsburg is developed and evaluated including the lifecycle process from customer acquisition over implementation up to operation.

2.1. History of the district heating system in Wilhelmsburg

The starting point for the implementation of the STG are the district heating systems “Energieverbund” and “Energiebunker” of Hamburg Energie GmbH. Both systems have been developed in the context of the International Building Exhibition as innovative prototypes for district heating. The Energieverbund was designed as an open heating grid. Customers can feed in surplus heat from regenerative sources into the flow-pipe of the heating grid. The grid operator is buying the surplus heat for a variable feed-in price. All other heat comes from a power house with a biogas CHP unit and gas-fired boilers for peak load. As part of the Energiebunker project an ancient anti-aircraft bunker from the Second World War was transferred into an energy bunker. Core idea of the system is to use a 2000 m³ thermal storage for peak shaving. Heat is produced by one solar thermal unit on the roof, biogas and natural gas CHP units and by industrial waste heat. Gas-fired boilers are used for peak load and redundancy. The grid supplies a residential area built at the turn of the nineteenth century. Due to competition with conventional single house supply and no compulsory connection, the biggest challenge was customer acquisition. Nevertheless, both grids are growing continuously. Their interconnection is planned.

2.2. Research objectives of Smart Heat Grid Hamburg

As described above, system efficiency and flexibility can be raised with communication technologies connecting relevant actors and processes of the district heating system. The needed infrastructure (plant and information technology and hydraulics) will be determined. The project is dedicated to six main goals [7]:

- In the first step, hydraulic concepts are developed. Fields of application will be analyzed for several renewable and current-fed generators. During this step, the entire network infrastructure will be used to increase efficiency and flexibility. One possibility to achieve higher flexibility is given by an active integration of the secondary side (thermal load management).
- These concepts can only be realized in a cost-effective way by combination with highly standardized measurement and control concepts.
- An existing simulation environment shall be expanded to provide a platform for the development and testing of algorithms on the one hand. On the other hand, it can be used as a planning tool to develop constructive concepts. In addition, a link between simulation and the control system will enable an actual usage in operation.
- The developed operating concepts shall enable a competitive generation market under ecological conditions. In addition to the generator coordination, the secondary side should be integrated as well to provide more flexibility by e.g. thermal load management. In the generator scheduling phase, monitoring of the heat grid stress and, if necessary, an adjustment of the existing generators (redispatch) is carried out. The main objective of the operation concepts is to optimize the overall operation, meaning ecological, economic und thermodynamic measures.
- Concepts of real-time operations monitoring shall ensure that all processes are performing as planned. Therefore, the state must be detected and key figures for real time evaluation of the system have to be formed. A central

monitoring will detect errors by aggregating data (operations analytics). A concept will be designed on how automatic optimization measures can be derived from real time data and historical data. Defects and manipulations will also be tracked and reported.

- To implement the aspects mentioned above, concepts for a proper market integration have to be developed. Overlapping interests with external shareholders or other third parties have to be identified. Therefore, concepts offering incentives for efficient and flexible thermal consumption or production have to be developed. Additionally, the legal and economic framework has to be considered. Finally, all results and methods should be generalized and as a result become transferable to other DHC systems.

3. Concepts for smart thermal grid elements

Hydraulic as well as control concepts are split into generation integration, grid design and customer integration. Each has to achieve two main goals: increase flexibility and efficiency. The former divides up into temperature level and energetic flexibility. Efficiency could be increased by minimizing operation temperatures as well as by implementing improved comprehensive control strategies.

3.1. Generation integration

Power from renewable energies is highly dependent from site and time, e.g. at geothermal plants, solar thermal plants or heat pumps. Applying a decentralized prosumer approach allows the integration of several smaller renewable sources, especially in urban environments. Since the prosumer's role is shifted from consumer to producer during operation, bidirectional substations are needed. These require a higher grade of communication technology which further creates a higher level of transparency in system operation and efficiency in real time. These integration concepts are presented in the subchapter grid concepts.

Since a decentralized approach is not suited for all generation units, e.g. CHP plants or gas boilers, these can be placed in central power houses. Figure 3.a shows a concept using a parallel generator-storage set-up [8]. In this concept all generation units must reach the same supply temperature. No temperature flexibility is available. Therefore, this concept fits mostly for generators based on combustion processes and limits the use of renewable generation. Nevertheless, the energy flexibility is maximized because the storage is accessible from every generator. The only temperature influencer is a motorized valve lowering the generation temperature to the grid supply temperature. The latter is controlled on ambient temperature basis.

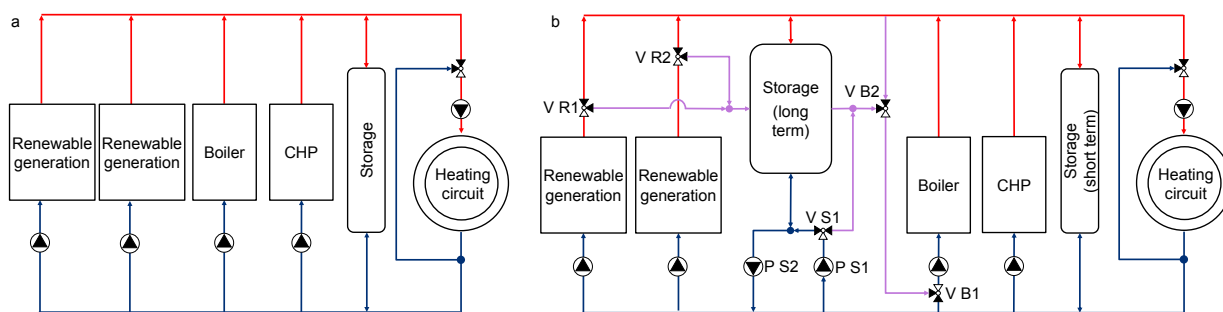


Fig. 3. (a) Generation with high temperature level; (b) Generation with different temperature levels

If generation units can't reach the grid supply temperature, e.g. solar thermal plant or industrial waste heat, another hydraulic concept, shown in Figure 3.b, is needed. The power house supports generation on different, variable flow temperature levels. It is an advancement of [9]. In this scheme a short-term and a long(er)-term storage is used. The former uncouples load and generation. The latter uncouples the generation unit's temperature levels supporting a mean variable temperature level (magenta). As a result, renewable generators can supply the high flow temperature level

(valves R1 & R2) as well as the medium temperature level depended on their momentary capabilities. Pump S1 controls the unloading of the long-term storage. Depending on the return temperature, valve R1 can switch between the low and the medium temperature level. Pump S2 controls storage loading. Loading by renewables should use the lowest expected temperature level as medium temperature level. The long-term storage is one element in the merit order of all generators. Some generators are controlled by schedules. Some generators react on the state of charge of the short term storage. The short term storage is used as an indicator, for the current ratio of demand and generation. If the temperature of the long term storage or the generators is not adequate, the boilers are used for temperature boosting using valves B1 and B2. It is also possible to load the long-term storage top with the boiler by switching valve B2 to the medium temperature level and B1 into the storage-boiler position. In conclusion, the highest energy and temperature flexibility is provided because all generated energy—even on low temperature levels—is used and different, useful temperature levels can be realized. Furthermore, the concept is easily expandable with additional temperature levels at the long-term storage.

3.2. Grid concepts

As part of the evolution to more renewable generation, low temperatures on both flow and return side are needed. In addition, temperature levels depend on consumer requirements. Especially building stock requires high supply temperatures and will also return high temperatures, whereas newer buildings can be supplied with lower temperatures. Urban districts are often very heterogeneous in their structure. But on a more detailed level are homogenous accommodations. In that case, an interaction of accommodations with new buildings and accommodations with building stock can achieve an additional benefit. One example is a cascade of those areas. To guarantee the needed temperature level, controllable grid coupling points are needed.

From a grids perspective, the connection types consumer (supply), producer (feed in) and prosumer (supply and feed-in changes during operation) are possible. Their general grid connection concepts are shown in Figure 4.a. More advanced concepts with an additional medium temperature pipe are possible. Since this depends on the customer's hydraulics, they are explained in the next section. A single point of feed-in is the most basic approach and described by the "Power house 1" standard scheme. Pump P1 is controlled by the differential pressure between flow and return. The needed temperature is realized with a motorized 3-way valve. If there are additional feed-in points, the differential pressure control must be changed to a fixed volume flow control ("Power house 2"). In a bidirectional coupling point between two or more grids both concepts have to be combined ("Prosumer / DH subsystem").

The connection of several grids, with different temperature and pressure levels can be done using the coupling point concepts shown in Figure 4.b. The storage integration realizes a flexible and independent grid operation and increases the inertia. The concept allows grid cascades and the integration of additional temperature levels.

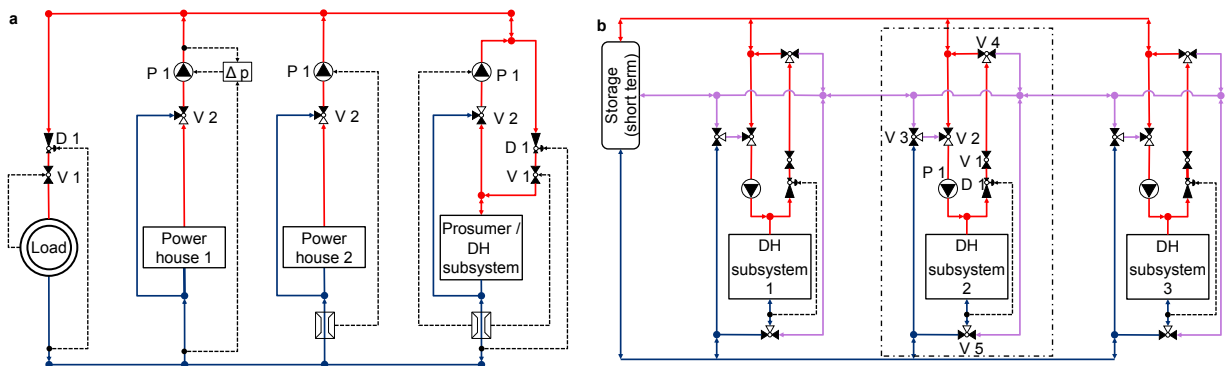


Fig. 4. (a) General connection concepts; (b) Grid coupling point.

3.3. Customer integration

A reduction of either return or flow temperatures requires an integrated customer substation design. In general, their hydraulic design allows variations as direct or indirect system approach. The latter uses a heat exchanger for decoupling the grid's and the consumer's water circuit. In residential areas indirect systems are frequently used. But today's implementations are mostly operated in an inefficient and inflexible way. Mandatory for the development of a flexible customer is the access to the customer's flexibility. Both, the quantification of the existing amount of flexibility as well as the later use of it are crucial. Therefore, the creation of transparency meaning measureable and controllable consumer substations is intended. SHGH identified the most promising approach as a shift of ownership in DHS substations: The grid operator installs and operates all central elements, mainly heat storages, decentralized at the customer's site. On this basis a concept for a smart substation is developed. Since its overall hydraulic concept is state of the art, the innovation arises by additional temperature, flow and pressure sensors as well as new controllers. By connecting the controllers to the grid control software, new, comprehensive control strategies are available. These allow not only remote substation control, but also new hydraulic concepts for a flexible customer, shown in Figure 5.

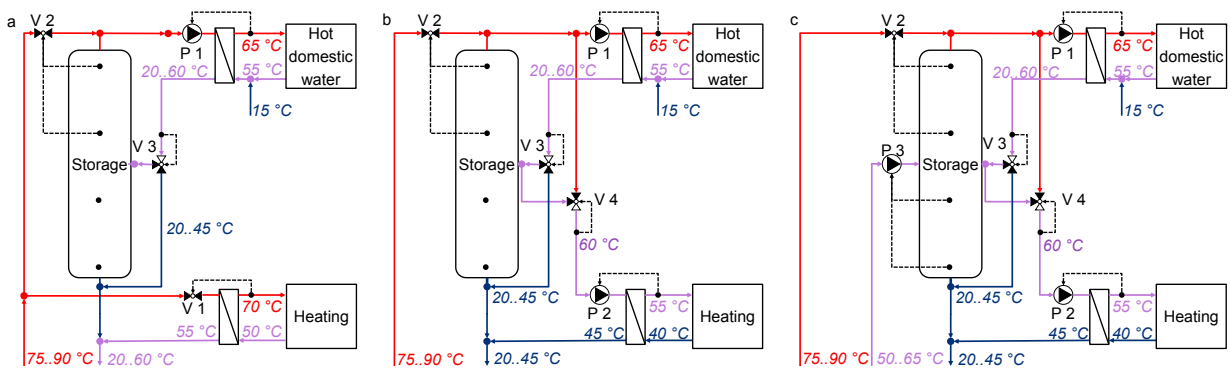


Fig. 5. Flexible customers: (a) flexible domestic hot water heating; (b) additional flexible space heating; (c) three pipe connection.

In relation to the common DHS consumer, who operates his heat storage on his own, a flexible customer is actively controlled by the grid operator which increases energy and temperature flexibility within the grid. The basic, state of the art hydraulic concept is shown in Figure 5.a. A new variant which will be analyzed and tested is shown in figure 5.b. It is only usable in buildings requiring heating circuit temperatures around 55 °C, e.g. for floor heating. This temperature can partly be provided by the domestic hot water circulation, which must exceed 65 °C as required by regulations. If the temperature or the amount of energy are too low, it is possible to add the grid flow (valve V4).

At some points in the district heating system it is possible to implement a three pipe connection, shown in Figure 5.c. This concept is a cascade from at least two or more buildings. The installation point depends on the return temperature from building one. It must exceed 50 °C, better up to 65 °C. Similar to the domestic hot water heating circuit cascade, the high return temperature can be used for supplying newer buildings that only require lower temperatures. By adding a medium temperature level (third pipe) to the storage, it is similar to the power house concept with different temperature levels. The third pipe is connected to a high return temperature pipe from any other building. Pump P3 allows to store the medium temperature in the middle of the storage. The high temperature is controlled by a valve. It uses the flow grid pressure for supply. The high temperature level is either used for the hot domestic water or for the heating circuit. Pump P1 controls the temperature of the hot domestic water. If the return temperature exceeds 55 °C (in case of circulation) valve V3 loads the storage. If the return temperature is below 55 °C it is fed to the grid. The supply for the heating circuit uses mostly the medium or higher temperatures. Pump P2 is controlled by the heating circuits flow temperature. If the medium temperature is not high enough for space heating, valve V4 increases it, using the grid flow.

With these concepts, a more efficient and flexible storage operation is realizable. The flexible customer deployment will be done in two different test buildings in the DHS of Wilhelmsburg. SHGH will adjust, optimize these and will share the experience within operation.

4. Proof of technical concepts

All described concepts will be proofed either in laboratory and/or by simulation before realization of prototypes.

4.1. Testing station

The Hamburg University for Applied Sciences has a substation testing laboratory divided into generation, substation and thermal load module. The generation module consists of two electrical heating units with 9 kW thermal power each, a hydraulic compensator and a hydraulic temperature control, realizing the target temperature by mixing flow and return. The heat load module uses a fan cooling system to simulate a scheduled heat demand with a total power of up to 25 kW. Both are connected with the substation module. The commonly used heating circuit controller will be replaced by a custom solution, allowing parameter variation and evaluation of the measurement results. Since the test bed offers more constant conditions and defined parameters without needing to deliver thermal energy to real customers, it is used for model validation and control strategy development.

4.2. Simulation

To investigate and evaluate future thermal grid scenarios a numerical simulation should be used. To accurately represent STGs and to be able to simulate grids with a high number of interlinked hardware and software components, a distributed simulation platform is being developed. Evaluation shall be possible by simulation of whole grids implementing STG concepts as well as plugging simulated components or plants into the real grid topology. During runtime of real and simulated components as well as part of post simulation processing, the platform shall be able to perform operation analysis, implement algorithms for optimization and operation management and lastly simulate and evaluate the concept of a district heating market place trading supply and demand of participants present on the grid. As result of a precedent tools analysis, present high-level simulation platforms could not fit these preliminaries because they are mostly designed to compute simulations sequentially. Low-level platforms and tools as well as high-level programming languages in combination with suitable libraries to build a distributed simulator were investigated to match a defined set of requirements including and beyond the above mentioned were contrasted. As a results, the platform is designed as a distributed back end architecture with a centralized coordination service as well as relational and time series databases and a flexible number of services that perform computation. A web front end is developed to provide client independent and concurrent accessibility.

For energy system and grid models, which are both large and highly detailed technical models, simulation speed is crucial and can be aimed by computational efficiency of the simulating routines themselves on the one hand or by parallelization and distribution on multiple computers and processors on the other. At the same time technical components in energy grids can be distributed in a computational meaning. Based on this, the platform implements grid components in multiple processes. Their model computation is parallelized by means of multi-threading. This makes it possible to parallelize a computational step by both computing independent parts of the system and compute independent physical regimes of those systems (e.g. hydraulics and temperature) concurrently.

4.3. Realization

After a concept is simulated or tested at the testing station, it will be realized. Two of the presented generation concepts are implemented in existing power houses. The realization at the Energieverbund is already finished. Since the adjustments planned for the Energiebunker require more planning and simulation, the concept is currently being proofed. The implementation will start in summer 2018. The coupling point planning process begins in June 2018. The initial operation is planned for 2019. Customer concepts such as a smart substation and the flexible customer are

already implemented. The flexible customer using the introduced three pipe concept will be realized in 2019. After single plant operation evaluation and optimization, their system impacts will be evaluated and optimized, too. Besides this, developments for a roll out must be made. These are discussed in the next section.

5. Interconnections

To achieve the research goals mentioned above, technical concepts were developed. These represent modules in an overall complex STG, linked to other, non-hydraulic or non-thermodynamic sectors. On the one hand they have to be technically combined with the right operation system using communication technology. On the other hand, they must be included in each customer's contracts. Since a wide rollout requires economic profitability, the current section discusses some possible measures to achieve this goal.

5.1. Information technology and operation system

In the DHS in Wilhelmsburg all substations are hard wired to the nearest power house. All data is observable and controllable with an over-all operational platform called "hype". Data evaluation detects issues lowering the system efficiency. In addition, the data is used for continuous optimization and planning processes. The system is controlled using specific operational states and generation schedules. To realize upcoming developments as a dynamic heat market, algorithms have to be developed, that detect the system's overall state and increase the system's efficiency as well as the system's flexibility.

5.2. Customer contracts

Besides the development of new technical concepts for DHSs, revised contract standards must be defined. Therefore, new prototype contract models are under development. Finally these will be modularly incorporated into existing heat supply contracts and their technical connection conditions. By means of predefined processes, contract negotiations get much simpler and quicker. Exemplary contract modules are: Shift of delivery-limit, performance-limit and line of ownership. These modules incentivize investments into efficiency by customers. Furthermore, the shift of ownership aims on operating customer's buffer tanks which can be used in a grid-serving and intelligent manner, e.g. increasing flexibility. This is emphasized since more and more housing associations also tend to ask for "all-round packages within DHS" with additional complete customer-side construction and operation up to the risers of the heating circuit. Such contracts pass operational management responsibility to the DHS supplier. They offer opportunities for the DHS supplier to maximize influence on the overall efficiency and flexibility and to enhance the customer satisfaction. Furthermore, contract modules providing boiler operation service enable a transition period which allows boiler operation by a DHS supplier until the DHS connection can be realized. This is key for customer acquisition since DHS expansion is a years-taking process. This strategy enables potential of stock buildings in advance. As a result district heating expansion becomes more predictable, reliable and cost-efficient.

5.3. Economics

In general, the implementation of all actions mentioned above has to be economically profitable. Nevertheless, STGs face tough market conditions in Germany due to several reasons. Two of these are mentioned in the following section. First, in most cases decentralized heat generation units in the building stock using fossil fuels (especially natural gas boilers) offer very competitive pricing conditions, focusing on operating and investment costs. A predefined share of renewable energy is compulsory just for newly constructed buildings, while renovating heat generation systems are not affected. As a DHS connection often requires high investment costs, compared to gas boiler installation, building owners tend to invest in the latter benefitting from shorter amortization periods. These barriers could be lowered e.g. by higher taxes on fossil fuels for heating purposes or, vice versa, lower taxes on electricity consumed by heat pumps. Furthermore, some regions established a compulsory connection for all buildings in a certain area. Despite this leads to reliable and cost-effective planning process, it is criticized by some consumers due to its

monopoly-like structure. Second, current DHS market conditions have not undergone a liberalization yet. Thus, a liberalized grid structure with competing heat products (e.g. renewable or standard heat) from different generation companies is not established yet. The liberalized market design might lead to a cost effective integration of renewable energies into the German heat supply. Summing up, DHS and/or STG should form a vital part of the German heat supply in the following years, although higher economic incentives are required.

6. Discussion

The main challenge in transitioning an existing into a 4th Generation DHS is raising efficiency and flexibility. First means lowering temperatures and optimizing consumer system operation. Both enable more renewable heat generators to feed-in since these operate much more decentralized than their fossil fuel competitors, while generating thermal energy at lower temperatures. To integrate these distributed generators hydraulic concepts were presented. Currently, implementation, testing and evaluation of these are ongoing. For example, to connect DHS subsystems operating on different temperatures a coupling point was developed. Yet, the customer side remains to be the key success factor in the transition to lower temperature grids. First results show that the comprehensive rollout of the concepts mentioned above mainly depends on economic and legal reasons.

First outcomes concerning profitability analysis and customer models show that efficiency in general is not incentivized in the current market framework with divergent interests of building owners, residents and suppliers. For example, there are no explicit legal requirements with reference to temperature levels of newly built houses connected to a DHS. Under these circumstances optimizing and operating substations and in-house heating systems in a way that supports flexible and efficient grid operation in DHS remains unrewarding. Nevertheless, measures like economic incentives, penalties or a shift of ownership are possible to lower this barrier.

Economic incentives and penalties lead to additional revenues and costs, which result from the reduction of the return temperature, and must be allocated according to cause and effect. Thus, the increased current efficiency due to the reduction of the return temperature must also be reflected in lower heat production costs. The prospect of a lower performance and working price gives the customer the decisive investment incentive.

The shift of ownership implies the operation of customer substations and his heating circuits by the grid operator. Since buildings in Hamburg are mainly multifamily houses which are not owner-occupied the grid operator must implement a higher service level for the tenants, which could be compensated by an elevated level of standardization and automation. As a result, the operation of the in-house distribution system as well as the domestic hot water heating can be monitored and controlled remotely. Failures can be detected before the tenants are affected. In combination with an intelligent storage management, the short-term flexibility of the system can be increased.

On the technical side the prototypes for these concepts exist. The main challenge is not given by the implementation of a single concept but their interaction and their comprehensive integration. Standardized modules concerning generation, distribution and supply have to be connected via communication technology. Control, planning and evaluation algorithms have to be developed and implemented.

A general challenge is given by the expansion of DHSs to building stock. Due to different regulatory conditions, natural gas boilers are highly competitive compared with DHSs. The building stock has no incentive to achieve low primary energy factors, but in contrast to that benefits from a low gas price. The customers' interests are mainly driven by low prices and simple management in contrast to climate protection goals. These barriers could be conquered e.g. by higher taxes on fossil fuel consumption for heating purposes or inversely by a lower tax burden on electricity consumed by heat pumps. DHSs require a long-term financial commitment that fits poorly with a focus on short-term returns on investment, as district heating pipes, substations and generation plants require high initial capital expenditure and financing. For reasons of climate protection municipalities are in general able to legally impose a compulsory connection and mandatory supply contract concerning the use of DHSs for all properties in the given area. A decisive factor is the particular state law, since the legal authorization usually lies in the municipal regulations of the federal states. In general, compulsory connections are seen negative due to the danger of monopoly structures with one single supplier company. To tackle this concern and raise the competition for innovative concepts, a separation of grid operator and supplier could be advisable. While the grid operator is responsible to construct the grid infrastructure—including peak generation and metering as well as a market place for different suppliers—the suppliers

could close deals for several years. Within this timespan, they are responsible for the efficiency of customer sites and their flexibility. Flexibility in the system could be financed by dynamic prices in long term, day ahead or intraday trading. The described market design will be simulated in the next steps of the Smart Heat Grid Hamburg project.

7. Conclusion

The paper presents the challenges of the transition to 4th generation of district heating systems in Hamburg, Germany. Technical concepts to raise efficiency and flexibility at the generation, distribution and customer side were shown. Some of these are in the process of implementation, e.g. a three-pipe-connection, flexible customers and a smart substation prototype. Currently, the biggest technical challenge is given by implementing the interconnection of these different concepts using information infrastructure including general standardization. Nevertheless, the main barriers are not given by technical issues, since all concepts add nearly no economic value. As a result, statutory changes have to be undergone. These can be compulsory connections, taxes on fossil fuels for heating or the introduction of liberalized DHS markets.

Acknowledgements

The authors acknowledge the financial support by the Federal Ministry for Economic Affairs and Energy of Germany in the project “EnEff:Wärme - Smart Heat Grid Hamburg” (project number 03ET1458A-C). We also would like to thank our project partners from eNeG GmbH who provide great expertise that moves our research project forward.

References

- [1] European Commission. “A policy framework for climate and energy in the period from 2020 to 2030” *Directorate-General Energy*, Brussels (2014).
- [2] German Government (Bundesregierung). “Energiekonzept für eine umweltschonende, zuverlässige und bezahlbare Energieversorgung” *Federal Ministry for Economics and Technology, Federal Ministry for the Environment, Nature Conservation and Nuclear Safety*, Berlin (2010).
- [3] “Klimaschutzplan 2050: Klimaschutzpolitische Grundsätze und Ziele der Bundesregierung“ *Federal Ministry for the Environment, Nature Conservation and Nuclear Safety* Berlin, (2016): 45.
- [4] Lund H, Werner S, Wiltshire R, Svendsen S, Thorsen J, Hvelplund F, Vad Mathiesen B. “4th Generation District Heating (4GDH): integrating smart thermal grids into future sustainable energy systems” *Energy Journal* 68 (2014): 1-11.
- [5] Knierim R, „Rücklauftemperatur: Ungehobener Schatz für Versorger und Kunden“, *Heft 3 EUROHeat & Power* (2007): 56 - 65.
- [6] Connolly D, Lund H, Mathiesen BV, Østergaard PA, Möller B, Nielsen S, et al. “Smart energy systems: holistic and integrated energy systems for the era of 100% renewable Energy” *Aalborg University*, Denmark (2013).
- [7] Lorenzen P, et al. “Smart Heat Grid Hamburg: A project description” <http://hamburgenergie.de/smartheatgridhamburg>, Hamburg (2017)
- [8] Sudeikat J, Thomsen M, Rathjen C, Klammer M, Weigel M, Berkel A, Lorenzen P, Bergsträßer W, Köhler JK, Heitmann O. “EnEff:Wärme - Smart Power Hamburg: Abschlussbericht zum Verbundprojekt: Teilvorhaben der Hamburg Energie GmbH” *Leibniz-Informationszentrum Technik und Naturwissenschaften Universitätsbibliothek*, Hamburg (2016): 232
- [9] Beck JP, Lorenzen P, Janßen P, „Smart Heat Grid Hamburg: Anforderungen an Energiezentralen im Kontext von Wärmenetzen der 4ten Generation“, *Jahrestagung der BDEW-Landesgruppe Norddeutschland und DVGW-Landesgruppe Nord*, Hamburg (2018)



16th International Symposium on District Heating and Cooling, DHC2018,
9–12 September 2018, Hamburg, Germany

Combined Optimization of District Heating and Electric Power Networks

Jona Maurer^{a,*}, Christoph Elsner^a, Stefan Krebs^a, Sören Hohmann^a

^a*Institute of Control Systems, Karlsruhe Institute of Technology, Wilhelm-Jordan-Weg, Karlsruhe, 76131, Germany*

Abstract

The main contribution of this work is the development of a network operation approach for integrated electric power and district heating networks based on social welfare optimization. Thereby demand-side management and economic dispatch are obtained simultaneously by taking into account consumers, flexible consumers, producers and renewable energy sources and the operational restrictions of both networks. The optimal operation is based on a transactive control approach which is identical to a nonlinear model predictive control problem here. Both energy networks are modeled in an accurate way leading to a nonlinear programming problem. Additionally an extension to the node method is presented.

© 2018 The Authors. Published by Elsevier Ltd.

This is an open access article under the CC BY-NC-ND license (<https://creativecommons.org/licenses/by-nc-nd/4.0/>)

Selection and peer-review under responsibility of the scientific committee of the 16th International Symposium on District Heating and Cooling, DHC2018.

Keywords: District Heating Networks; Node Method; Electric Power Systems; Multi-Carrier Energy Systems; Multi Energy Systems; Energy Internet; Model Predictive Control; Transactive Control; Social Welfare Optimization.

1. Introduction

The energy transition is replacing conventional power plants by renewable energy sources (RES) around the world [1]. Due to the volatile character of these RES new storages and flexibility options are necessary for reliable network

* Corresponding author. Tel.: +49 721 608 43179; fax: +49 721 608 42707.

E-mail address: jona.maurer@kit.edu

operation. One major flexibility option is found in sector coupling. District heating networks (DHN), which will play a dominant role in the future energy system [2], bring relevant storage capacities [3] and by using demand-side management, thermal inertia of buildings can be used as well [4]. To profit from these flexibility options it is necessary to operate the electric power network and the district heating networks in a coordinated way. However, these networks are operated separately at the moment. A second important development is the digitalization which brings up new devices in the energy system as home energy management systems and smart meters. These devices bring the possibility to let flexible consumers and producers automatically trade energy as it is done e.g. in a local community in Brooklyn [5]. Further projects [6] have proven that flexibility provision between multiple energy domains can be handled by software agents of flexible consumers. Case studies demonstrated that marginal temperature differences in buildings, which are hardly realized by the owners, can in sum lead to relevant shifting of electrical demand in the range of several hours [6].

Nomenclature

\mathbb{K}	Set of all time steps k within the prediction horizon n_p
\mathbb{S}_I	Set of all nodes i
$\mathbb{S}_{I,el/ht}$	Set of all nodes i of the electric power / district heating network
\mathbb{S}_L	Set of all pipes l
$\mathbb{S}_{L_i,ht,out/in}$	Set of all pipes l with water (mass flow) flowing into / out of the node i
\mathbb{S}_N	Set of all grid participants n
\mathbb{S}_{N_i}	Set of all grid participants n at node i
$\mathbb{S}_{N_i,el/ht}$	Set of all grid participants n at node i in the electric power / district heating network
$\mathbb{S}_{N_i,ht,out/in}$	Set of all grid participants n in the DHN with water entering from / flowing to node i
$\mathbb{S}_{N,conv}$	Set of all energy converting grid participants n connected to both energy domains
$\mathbb{S}_{N,prod,el/ht}$	Set of all producers n in the electric power / district heating network
$\mathbb{S}_{N,cons,el/ht}$	Set of all flexible consumers n in the electric power / district heating network
i, q	Index of nodes
l	Index of pipelines
s	Index of the supply network of the district heating network
r	Index of the return network of the district heating network
in/out	Index of temperatures of water masses entering/leaving a pipeline/grid participant
n	Index of grid participants
el/ht	Index describing the electric power/district heating network

Thus, a new approach is presented in this paper which enables combined optimization of district heating and electric power networks based on social welfare optimization. Thereby the bids of flexible consumers and producers in both energy domains are taken into account and optimized simultaneously. This leads to a form of transactive control [7] for coupled electrical and district heating systems. In [7] transactive control is described as the implementation of transactive energy, where transactive energy itself is defined as: “a set of economic and control mechanisms that allows the dynamic balance of supply and demand across the entire electrical infrastructure using value as a key operational parameter”. Until now the term transactive energy has mainly been used in connection with the electrical infrastructure. One of the main ideas behind this work, also expressed in [8], is to expand this approach to coupled electrical and district heating systems. A further discussion of the state of the art literature is found on the following page. The basic idea of the transactive control approach used in this work is depicted in Fig. 1, which consist of images from [9], and comprises the following steps:

- 1) At time step k_0 flexible consumers and producers send their bids for the next k_0+1, \dots, k_0+n_p time steps to the coordinator. Herein n_p describes the number of future time steps taken into account, also described as the prediction horizon in the context of model predictive control (MPC). The bids are functions of benefit

per power demand $b(P(k)), b(\Phi(k))$ for flexible consumers and price per power infeed $c(P(k)), c(\Phi(k))$ for producers. Herein P describes the electric power and Φ the heat power.

- 2) The coordinator solves an optimization problem based on social welfare optimization, taking into account the network models and restrictions as well as predicted values of the power infeed of RES and the power demand of conventional consumers. These passive grid participants (RES and consumers) whose behavior is only modeled by predictions of the grid operator are colored blue in Fig. 1. The results of this optimization are the prices the producers should be paid and the benefits/prices the flexible consumers are willing to pay in the following time steps k_0+1, \dots, k_0+n_p .
- 3) The prices and benefits calculated in 2) are then send to flexible consumers and producers by the coordinator.
- 4) Now the producers/flexible consumers will adapt their power demand/power infeed during the next time step k_0+1 based on the power that results from matching the price/benefit with their previous bid.
- 5) Then producers and flexible consumers will adapt their bids for the next time steps k_0+2, \dots, k_0+1+n_p and send them to the coordinator.

Steps 2) until 5) are permanently repeated over a moving horizon. Therefore, this form of control equals a form of model predictive control with dynamic subsystems. Thereby producers and flexible consumers in both networks can adopt their bids to the power needed in the system. As already implemented today, it is required to have a form of unit commitment and primary frequency control in the power grid and a form of pump control in the district heating networks. This new approach can then be seen as a form of market-based flexibility provision which optimizes network operation and guarantees a stable network operation at the same time.

The state of research comprises some approaches for the combined dispatch of electric power and district heating networks. Some papers focus on solving the optimal power flow for a single time step [10], [11]. Most of the approaches which optimize a sequence of time steps use simple models for the electric power or district heating networks, where the networks are modeled as a single node [12], [13], [14], [15] and [16]. Others neglect the dynamics as time delays induced by transport [17]. The papers which can be compared the best with this work are presented in the following. In [18], an approach for combined heat and power dispatch for combined heat and power plants (CHP), conventional power plants and wind farm curtailment is presented. It is based on a dynamic district heating model and DC power flow constraints leading to a mixed integer nonlinear optimization problem. The authors of [19] use the optimality condition decomposition approach to split up the combined dispatch of electric power and district heating networks. A DC power flow model is used to represent the electric power grid and a dynamic model of the district heating network is implemented. Both works presented neglect the possibility of demand-side management through flexible consumers and use DC power flow models for the power network. As the AC power flow serves a higher accuracy of the relevant physics in the distribution grid, where most of the RES are installed, it is used here.

The main contribution of this work is the development of a new form of coordinated optimal operation of coupled electric power and district heating networks based on social welfare optimization between flexible consumers and producers. In other words, economic dispatch and demand-side management are obtained in an integrated way for both energy networks based on transactive control. This comes along with a high detailed modeling of the energy networks and the transactive grid participants of the integrated energy system. Additionally an extension of the node method is presented which is used for the modeling of the district heating network.

The rest of this paper is structured as follows. First, the modeling of the energy networks, the consumers, flexible consumers, energy converters and producers is presented. Then, in chapter 3 the resulting control problem is formulated. Finally the conclusion of this work is presented in chapter 4.

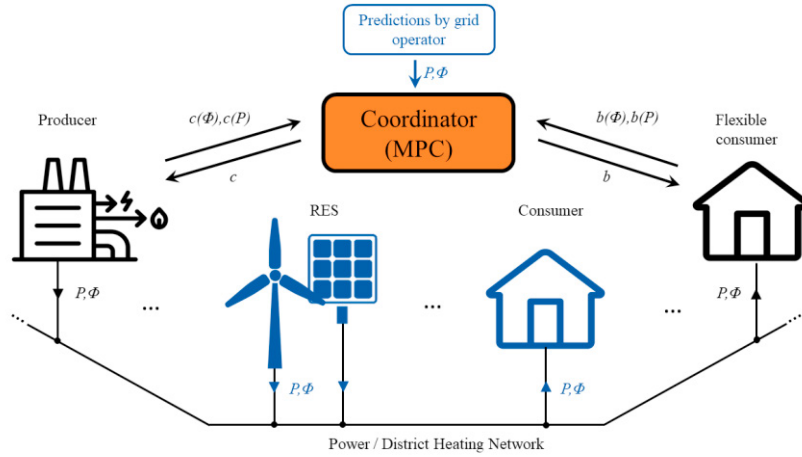


Fig. 1: Overview of the information flow between the different entities in this approach

2. Modeling

In this section, the modeling of the electric power network, the DHN, the network participants and the energy converters is presented. The modeling is done in time-discrete form as there are discrete market offers and measured data.

2.1. Electric Power Network

The electric power system model is based on the power flow equations. In this work the power flow on all phases is assumed to be symmetrical, thus a single-phase standard π transmission line model is used. It comes in series with an optional ideal phase shifting transformer model, as described in [20]. The complex powers flowing between bus i and all its neighbors q must be equal to the apparent power S_i injected or withdrawn from bus i . This leads to the following power flow equation [21]:

$$\sum_{q \in \mathbb{S}_{I,el}} S_{iq}(k) = S_i(k) = (P_i(k) + jQ_i(k)) = U_i(k) \sum_{q \in \mathbb{S}_{I,el}} Y_{iq}^*(k) U_q^*(k). \quad (1)$$

The power flows between the node i and its neighbors q can be expressed by the voltages U_i at bus i and U_q at the neighboring buses and the corresponding branch admittances Y_{iq} . Equation (1) is formulated for all buses, which results in a set of nonlinear, algebraic equations. Herein every node brings four variables. The first two are the real and reactive power P_i or Q_i which are injected or withdrawn at node i . The second two represent the voltage amplitude $|U_i|$ and phase θ_i at that node. Logically the set of nonlinear equations can be solved when two of the four variables of each node are known. For the optimization problem, described in detail in section 3, all buses except one are modeled as PQ buses which means the power infeed or output is given. One bus is modeled as a slack bus where the voltage amplitude and phase are known. The generator connected to this bus is used to compensate the difference between the power infeed into the network and the sum of the power demand and the network losses.

2.2. District Heating Network

The DHN model is based on hydraulic and thermal equations, which are described in the following paragraphs. Besides the mathematical network description is based on the graph theory.

2.2.1. Hydraulic Model

The relevant variables are pressure and mass flow for the hydraulic model. Pressure changes travel with the velocity of sound [22], so transient effects can be neglected as their time constants are much smaller than the time steps used for the optimization. Therefore, a stationary model is used. Additionally, the fluid flow is assumed to be an ideal plug flow. In every node the continuity of flow is applied, which is expressed as

$$\mathbf{A}(k) \dot{\mathbf{m}}_l(k) = \dot{\mathbf{m}}_n(k) \quad (2)$$

where \mathbf{A} is the network incidence matrix, $\dot{\mathbf{m}}_l$ is the vector of the mass flows in the pipes and $\dot{\mathbf{m}}_n$ is the vector of the mass flows injected or extracted by the network participants. The continuity of flow postulates that the mass flow which enters a node must be equal to the mass flow that leaves the node.

The mass flows rejected from the network are defined by the flexible consumers and consumers, see section 3 and can be calculated from

$$\dot{m}_n(k) = \frac{\Phi_n(k)}{c_p (T_{n,in}(k) - T_{n,out}(k))} \quad (3)$$

where Φ_n describes the power demand of the flexible consumer or consumer, c_p defines the specific heat capacity of water, $T_{n,in}$ describes the input temperature at the consumer or flexible consumer and $T_{n,out}$ its output temperature. The injected mass flows are determined by the operation points of the pumps, which are usually located near the producers. These operation points can be assumed given as they are determined by the network operators.

Additionally, a loop pressure equation is applied which describes head losses in a network loop. Head loss Δp is the pressure change due to pipe friction. It is stated that the sum of head losses around a closed loop must be equal to zero. Using the loop incidence matrix \mathbf{B} the loop pressure equation for a network is expressed, as in [23], by

$$\mathbf{B}(k) \Delta \mathbf{p}(k) = \mathbf{B}(k) \mathbf{K} \dot{\mathbf{m}}_l^2(k) = \mathbf{0} \quad (4)$$

where the head loss is Δp and \mathbf{K} is the vector of the resistance coefficient of each pipe. These resistance coefficients of the different pipelines K_l depend on pipe parameters and the friction factor λ .

2.2.2. Thermal Model

The thermal model is used to determine the temperatures in the network. It is dependent on the mass flows which have to be calculated before by the hydraulic model described in the previous section. The thermal dynamics are considered due to the low flow velocities between 0.8 m/s and 3 m/s in the pipes [24]. The temperatures, which are calculated by the thermal model, are the participant outlet temperature, the node temperature and the pipe outlet temperature. The former is depending on the participant type and is calculated by a family of characteristics for consumers and flexible consumers

$$T_{n,out}(k) = f(T_{i,s}(k), T_a(k), \Phi_n(k)). \quad (5)$$

Here the ambient temperature is defined by T_a . Besides the outlet temperature of a producer is calculated by

$$T_{n,out}(k) = T_{i,r}(k) + \frac{\Phi_n(k)}{c_p \dot{m}_n(k)}. \quad (6)$$

The node temperature T_i is determined in (7) by a mixing of the incoming mass flows and its temperatures as in [11]. Note that the incoming mass flows at node i are the mass flows leaving the respective pipelines and grid participants.

$$\left(\sum_{l \in \mathbb{S}_{Li,jt,in}} \dot{m}_l(k) + \sum_{n \in \mathbb{S}_{Ni,jt,in}} \dot{m}_n(k) \right) T_i(k) = \sum_{l \in \mathbb{S}_{Li,jt,out}} \dot{m}_l(k) T_{l,out,3}(k) + \sum_{n \in \mathbb{S}_{Ni,jt,out}} \dot{m}_n(k) T_{n,out}(k) \quad (7)$$

In (7) \mathbb{S}_{L_i} is the set of either incoming or outgoing pipe mass flows, \mathbb{S}_{N_i} the set of either incoming or outgoing participant mass flows, T_l the pipe mass flow temperature and T_n the participant mass flow temperature. The mixing is assumed to be ideal. The thermal dynamics in the network is determined by the node method [25]. The node method obtains the outlet temperature of a pipe by approximating the pipe as a dead-time element embedded between an inlet and outlet node. Thereby the output temperature $T_{l,out}$ is calculated in three steps, marked with the indices 1 to 3. In a first step the lossless output temperature of a pipeline $T_{l,out,1}$ is determined, see (8). The lossless output temperature is calculated as the weighted sum of the outflowing plugs in every time step, see also Fig. 2. Thereby (9) - (12) serve the necessary constants R , S , γ and ϵ . The second step, described in (13), is used to calculate the output temperature $T_{l,out,2}$ dependent on the temperature change due to heat exchange of the water with the steel core of the pipeline. Finally, in a third step the output temperature $T_{l,out,3}$ is calculated by (14). Herein the losses due to heat loss through the pipe walls are taken into account. The lossless outlet temperature $T_{l,out,1}$ is expressed as

$$T_{l,out,1}(k) = \frac{1}{\dot{m}_l(k)\Delta k} \left[\left((R_l(k) - \rho A_l t_l) T_i(k - \gamma_l(k)) \right) + \sum_{\kappa=k-\epsilon_l(k)+1}^{k-\gamma_l(k)-1} \left(\dot{m}_l(\kappa)\Delta k T_i(\kappa) \right) + \left(\dot{m}_l(k)\Delta k + \rho A_l t_l - S(k) \right) T_i(k - \epsilon_l(k)) \right]. \quad (8)$$

Therein $\rho A_l t_l$ describes the total mass of water in the pipeline l , where the density of water is described by ρ , the cross section of the pipeline and its length are defined by A_l and t_l . The constant γ_l serves to describe the plug which just left the pipe in this time step while ϵ_l describes the plug which has first left the pipe in this time step. They are calculated by finding the following integer minima:

$$\gamma_l(k) = \min_x \left\{ x \text{ s.t. } \sum_{\kappa=0}^x \left(\dot{m}_l(k - \kappa)\Delta k \right) \geq \rho A_l t_l, x \geq 0, x \in \mathbb{Z} \right\} \quad (9)$$

$$\epsilon_l(k) = \min_z \left\{ z \text{ s.t. } \sum_{\kappa=1}^z \left(\dot{m}_l(k - \kappa)\Delta k \right) \geq \rho A_l t_l, z \geq 0, z \in \mathbb{Z} \right\} \quad (10)$$

The constants R and S describe water masses as depicted in Fig. 2:

$$R_l(k) = \sum_{\kappa=0}^{\gamma_l(k)} \left(\dot{m}_l(k - \kappa)\Delta k \right) \quad (11)$$

$$S_l(k) = \begin{cases} \sum_{\kappa=0}^{\epsilon_l(k)-1} \left(\dot{m}_l(k - \kappa)\Delta k \right), & \text{if } \epsilon_l(k) \geq \gamma_l(k) + 1, \\ R_l(k), & \text{otherwise.} \end{cases} \quad (12)$$

In a second step, the outlet temperature is calculated resulting from the temperature exchange of the water with the steel core of the pipeline. Thereby it is assumed that the heat exchange will lead to an equal temperature of the water temperature at the output $T_{l,out,2}$ and the steel mass T_c :

$$T_{l,out,2}(k) = \frac{T_{l,out,1}(k)\dot{m}_l(k)c_p\Delta k + C_l T_c(k-1)}{C_l + \dot{m}_l(k)c_p\Delta k} = T_c(k). \quad (13)$$

Herein C_l describes the heat capacity of the steel core of the pipe and T_c describes the temperature of the lumped steel core of the pipeline. The last step of the node method calculates the resulting outlet temperature after taking into account the losses through the pipeline isolation $T_{l,out,3}$. The heat losses are dependent on the thermal loss coefficient h_l of a pipe, the ambient temperature T_a and the time the water stays in the pipe which is dependent on the constants derived from (9) and (11):

$$T_{l,out,3}(k) = T_a(k) + (T_{l,out,2}(k) - T_a(k)) \exp\left[-\frac{h_l t_l(k)}{A_l \rho c_p}\right]. \quad (14)$$

In this equation the time the water stays in the pipeline t_l is calculated by the weighted sum of all the different times the different plugs have been in the pipeline before they leave it. This time can be calculated from:

$$t_l(k) = \frac{1}{\dot{m}_l(k)\Delta k} \left[\gamma_l(k)(R_l(k) - \rho A_l t_l) + \sum_{\kappa=k-\epsilon_l(k)+1}^{k-\gamma_l(k)-1} ((k-\kappa)\dot{m}_l(\kappa)\Delta k) + \epsilon_l(k)(\dot{m}_l(k)\Delta k + \rho A_l t_l - S(k)) \right] \Delta k. \quad (15)$$

This equation is different from the approach in [25] and newly presented here. It has strong analogies to the ideas which lead to (8). This form of calculation also calculates t_l exact in the case of non-constant mass flows.

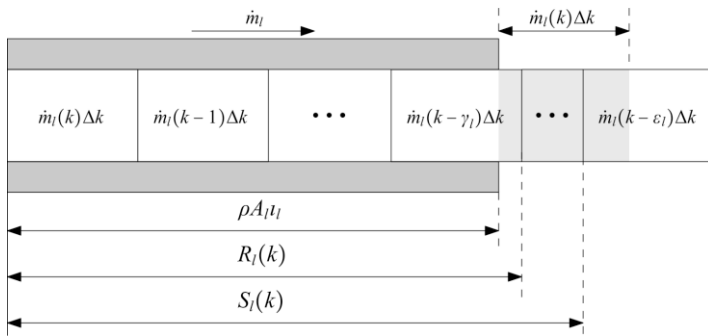


Fig. 2: Scheme of a pipeline and the relevant variables in the node method

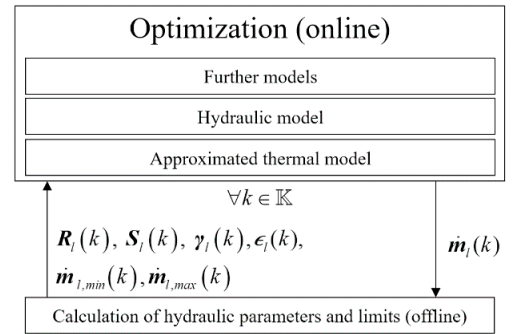


Fig. 3: Online and offline computations in the control problem

2.3. Active Grid Participants

Active grid participants are flexible consumers and producers. Storages can also be taken into account by this approach. As the time steps regarded here are much smaller than the charging or discharging time of these, they can be taken into account as producers or flexible consumers for every time step. The same concept is used to model prosumers. The flexible consumers are described with the following benefit per power demand functions. The benefit, also understandable as the price a consumer is willing to pay, of a flexible consumer in the electric power network is expressed as

$$b_{n,el}(k) = \zeta_{n,el}(k)P_n(k) - \delta_{n,el}(k)P_n^2(k) \quad (16)$$

while the benefit of a flexible consumer in the DHN is

$$b_{n,ht}(k) = \zeta_{n,ht}(k)\Phi_n(k) - \delta_{n,ht}(k)\Phi_n^2(k) \quad (17)$$

where P_n is the active power demand, Φ_n is the heat power demand and ζ_n and δ_n define positive cost parameters. In contrast a producer is described by its price per power infeed $c(P)$. The price per power infeed are stated in (18) and (19) for producers of the electric power or the district heating network, where α_n , β_n and ψ_n are positive cost parameters.

$$c_{n,el}(P_n)(k) = \alpha_{n,el}(k) + \beta_{n,el}(k)P_n(k) + \psi_{n,el}(k)P_n^2(k) \quad (18)$$

$$c_{n,ht}(\Phi_n)(k) = \alpha_{n,ht}(k) + \beta_{n,ht}(k)\Phi_n(k) + \psi_{n,ht}(k)\Phi_n^2(k) \quad (19)$$

The cost parameters used in (16) - (19) result from the bids the flexible consumers or producers send to the coordinator in every time step, see step 1) in the introduction.

2.4. Passive Grid Participants

Passive grid participants are consumers and RES which are defined by given load or generator profiles. Unlike active grid participants their behavior is not adaptable. In the electric power network, the passive grid participants are modeled as PQ nodes.

2.5. Energy Converters

Energy converters between the electric power and heat networks are modeled with a constant power-to-heat ratio η_n . The full equation used to describe a CHP or a heat pump (HP) is stated in (30). Different energy converters are described by different values of η_n .

3. Control Problem

In this work, the control approach is an MPC approach which can also be described as a transactive control approach in this context. MPC is a very powerful approach in using predictions, equality and inequality constraints. In this context, the predicted values are the consumed power of the consumers and the power infeed of the RES, provided by the grid operator, as well as the power infeed of the producers and the power demand of the flexible consumers in both energy networks, which come to the coordinator in the form of bids. These predictions come from different sources as depicted in Fig. 1. During every time step k_0 the following nonlinear programming problem (20) - (37) is solved by the coordinator to determine the optimal prices and benefits of the next time steps k_0+1, \dots, k_0+n_p which are then sent to the active grid participants. The objective function (20) is defined by the social welfare of all active grid participants in the electric and district heating networks for all time steps over the prediction horizon n_p . Hence, the global minimum is equal to the operation point in which flexible consumers and producers are most likely to be content with in regard of the market situation. The network models and the models of the energy converters are represented by the equality constraints (21) - (30). The output temperatures of the grid participants in the district heating network are defined by (28) and (29). The inequality constraints (31) - (36) ensure that the operational restrictions, which ensure safe network operation of the power grid are respected. The optimization problem is given by

$$\min_{P_n, \Phi_n} \sum_{k \in \mathbb{K}} \left(\left(\sum_{n \in \mathbb{S}_{N,prod,el}} c_{n,el}(P_n(k), k) + \sum_{n \in \mathbb{S}_{N,prod,ht}} c_{n,ht}(\Phi_n(k), k) \right) - \left(\sum_{n \in \mathbb{S}_{N,cons,el}} b_{n,el}(P_n(k), k) + \sum_{n \in \mathbb{S}_{N,cons,ht}} b_{n,ht}(\Phi_n(k), k) \right) \right) \tag{20}$$

with respect to

$$\sum_{n \in \mathbb{S}_{Ni,el}} P_n(k) + \sum_{n \in \mathbb{S}_{Ni,el}} jQ_n(k) = U_i(k) \sum_{q \in \mathbb{S}_{I,el}} Y_{i,q}^* U_q^*(k) \quad \forall k \in \mathbb{K}, i \wedge q \in \mathbb{S}_{I,el}, \tag{21}$$

$$\left(\sum_{l \in \mathbb{S}_{Li,ht,in}} \dot{m}_l(k) + \sum_{n \in \mathbb{S}_{Ni,ht,in}} \dot{m}_n(k) \right) T_i(k) = \sum_{l \in \mathbb{S}_{Li,ht,out}} \dot{m}_l(k) T_{l,out,3}(k) + \sum_{n \in \mathbb{S}_{Ni,ht,out}} \dot{m}_n(k) T_{n,out}(k) \tag{22}$$

$\forall k \in \mathbb{K}, i \in \mathbb{S}_{I,ht},$

$$A(k) \dot{m}_i(k) = \dot{m}_n(k) \quad \forall k \in \mathbb{K}, \tag{23}$$

$$B(k) K \dot{m}_i^2(k) = 0 \quad \forall k \in \mathbb{K}, \tag{24}$$

$$T_{l,out,1}(k) = \frac{1}{\dot{m}_l(k)\Delta k} \left[((R_l(k) - \rho A_l t_l) T_i(k - \gamma_l(k))) + \sum_{\kappa=k-\epsilon_l(k)+1}^{k-\gamma_l(k)-1} (\dot{m}_l(\kappa)\Delta k T_i(\kappa)) \right. \\ \left. + (\dot{m}_l(k)\Delta k + \rho A_l t_l - S(k)) T_i(k - \epsilon_l(k)) \right] \quad \forall k \in \mathbb{K}, l \in \mathbb{S}_{L,ht}, \quad (25)$$

$$T_{l,out,2}(k) = \frac{T_{l,out,1}(k) m_l(k) c_p \Delta k + C_l T_c(k-1)}{C_l + m_l(k) c_p \Delta k} = T_c(k) \quad \forall k \in \mathbb{K}, l \in \mathbb{S}_{L,ht}, \quad (26)$$

$$T_{l,out,3}(k) = T_a(k) + (T_{l,out,2}(k) - T_a(k)) \exp\left[-\frac{h_l t_l(k)}{A_l \rho c_p}\right] \quad \forall k \in \mathbb{K}, l \in \mathbb{S}_{L,ht}, \quad (27)$$

$$T_{n,out}(k) = f(T_{i,s}(k), T_a(k), \Phi_n(k)) \quad \forall k \in \mathbb{K}, i \in \mathbb{S}_{I,ht}, n \in \mathbb{S}_{N,cons,ht}, \quad (28)$$

$$T_{n,out}(k) = T_{i,r}(k) + \frac{\Phi_n(k)}{c_p \dot{m}_n(k)} \quad \forall k \in \mathbb{K}, i \in \mathbb{S}_{I,ht}, n \in \mathbb{S}_{N,prod,ht}, \quad (29)$$

$$\Phi_n(k) = \eta_n P_n(k) \quad \forall k \in \mathbb{K}, n \in \mathbb{S}_{N,comb}, \quad (30)$$

$$T_{i,min} \leq T_i(k) \leq T_{i,max} \quad \forall k \in \mathbb{K}, i \in \mathbb{S}_{I,ht}, \quad (31)$$

$$\Phi_{n,min}(k) \leq \Phi_n(k) \leq \Phi_{n,max}(k) \quad \forall k \in \mathbb{K}, n \in \mathbb{S}_{N,ht}, \quad (32)$$

$$\dot{m}_{n,min}(k) \leq \dot{m}_n(k) \leq \dot{m}_{n,max}(k) \quad \forall k \in \mathbb{K}, n \in \mathbb{S}_{N,ht}, \quad (33)$$

$$0.9 |U_N| \leq |U_i|(k) \leq 1.1 |U_N| \quad \forall k \in \mathbb{K}, i \in \mathbb{S}_{I,el}, \quad (34)$$

$$P_{n,min}(k) \leq P_n(k) \leq P_{n,max}(k) \quad \forall k \in \mathbb{K}, n \in \mathbb{S}_{N,el}, \quad (35)$$

$$Q_{n,min}(k) \leq Q_n(k) \leq Q_{n,max}(k) \quad \forall k \in \mathbb{K}, n \in \mathbb{S}_{N,el}, \quad (36)$$

$$\dot{m}_{l,min}(k) \leq \dot{m}_l(k) \leq \dot{m}_{l,max}(k) \quad \forall k \in \mathbb{K}, l \in \mathbb{S}_{L,ht}, \quad (37)$$

As visualized in Fig. 3 the thermal model is not fully integrated in the optimization to prevent the long computation times of a mixed integer optimization. Instead, after the optimization in every time step, the constants R_l , S_l , γ_l and ϵ_l used in the thermal model and the limits of mass flows of all pipes $\dot{m}_{l,min}$ and $\dot{m}_{l,max}$ are calculated offline. These new values are then used in the optimization during the next time step. Thereby the latest mass flows in the pipelines \dot{m}_l resulting from the optimization are considered to assure high accuracy. The constants R_l , S_l , γ_l and ϵ_l are calculated from (9) - (12) while the limits of mass flows of the pipes $\dot{m}_{l,min}$ and $\dot{m}_{l,max}$ are calculated by adding or subtracting the boundary value $\Delta \dot{m}_l$ to the actual values. If the mass flows in the pipes \dot{m}_l would be kept constant and not variable as implemented by (37), then the mass flows of the grid participants and thereby their power consumption or infeed would also be determined mainly by (22), even if (23) and (24) would be neglected.

4. Conclusion

An approach is presented which enables demand-side management and economic dispatch of flexible consumers and producers in the electric power and district heating network at the same time. This is done by optimizing the social welfare of all market participants. As this is done over a moving horizon, bringing together control and market mechanisms, this approach describes a form of transactive control for coupled electric power and district heating networks. The electric power network is modeled by the AC power flow equations while the heating network is modeled by the node method. For the node method a new formula is introduced which enables an accurate calculation of the time the water plugs stay in the pipeline in the case of varying mass flows. To prevent the high computational effort of the resulting mixed integer nonlinear programming problem an iterative approach is introduced, leading to a nonlinear programming problem and a very fast computable offline calculation. The presented approach optimizes the social welfare while maintaining network restrictions for stable operation of the entire multi-carrier energy system.

Acknowledgements

The authors gratefully acknowledge funding by the German Federal Ministry of Education and Research (BMBF) within the Kopernikus Project ENSURE ‘New ENergy grid StructURes for the German Energiewende’.

References

- [1] REN21, “Renewables 2017, global status report,” Renewable Energy Policy Network for the 21st Century, Tech. Rep., 2017.
- [2] H. Lund, B. Möller, B. Mathiesen, and A. Dyrelund, “The role of district heating in future renewable energy systems,” *Energy*, vol. 35, no. 3, pp. 1381 – 1390, 2010.
- [3] M. Wiegels, B. Böhm, and K. Sipilae, “Dynamic heat storage optimisation and demand side management,” International Energy Agency, Tech. Rep., 2005.
- [4] J. Kensby, A. Trüschel, and J.-O. Dalenbäck, “Potential of residential buildings as thermal energy storage in district heating systems - results from a pilot test,” *Applied Energy*, vol. 137, pp. 773 – 781, 2015.
- [5] F. Hasse, A. von Perfall, T. Hillebrand, E. Smole, L. Lay, and M. Charlet, “Blockchain - Chance für Energieverbraucher? Kurzstudie für die Verbraucherzentrale NRW, Düsseldorf [Blockchain – A Chance for Energy Consumers?],” Tech. Rep., 2016.
- [6] K. Kok and S. Widergren, “A society of devices: Integrating intelligent distributed resources with transactive energy,” *IEEE Power and Energy Magazine*, vol. 14, no. 3, pp. 34–45, 2016.
- [7] T. G. A. Council, “Gridwise transactive energy framework,” The GridWise Architecture Council, Tech. Rep., 2015.
- [8] N. Good, E. A. M. Ceseña, and P. Mancarella, “Ten questions concerning smart districts,” *Building and Environment*, vol. 118, pp. 362–376, 2017.
- [9] F. Rinaldi, M. Domingo, E. Schuster, and M. Aman, “Cogeneration, wind turbine, solar panel, home.” [Online]. Available: <https://thenounproject.com/>
- [10] M. Geidl and G. Andersson, “Optimal power flow of multiple energy carriers,” *IEEE Transactions on Power Systems*, vol. 22, no. 1, pp. 145–155, 2007.
- [11] X. Liu, J. Wu, N. Jenkins, and A. Bagdanavicius, “Combined analysis of electricity and heat networks,” *Applied Energy*, vol. 162, pp. 1238–1250, 2016.
- [12] G. Gambino, F. Verrilli, D. Meola, M. Himanka, G. Palmieri, C. Del Vecchio, and L. Glielmo, “Model predictive control for optimization of combined heat and electric power microgrid,” *IFAC Proceedings Volumes*, vol. 47, no. 3, pp. 2201–2206, 2014.
- [13] N. Good, E. A. M. Ceseña, C. Heltorp, and P. Mancarella, “A transactive energy modelling and assessment framework for demand response business cases in smart distributed multi-energy systems,” *Energy*, 2018.
- [14] J. Zheng, Z. Zhou, J. Zhao, and J. Wang, “Integrated heat and power dispatch truly utilizing thermal inertia of district heating network for wind power integration,” *Applied Energy*, vol. 211, pp. 865 – 874, 2018.
- [15] T. Guo, M. I. Henwood, and M. Van Ooijen, “An algorithm for combined heat and power economic dispatch,” *IEEE Transactions on Power Systems*, vol. 11, no. 4, pp. 1778–1784, 1996.
- [16] J. Maurer, P. S. Sauter, M. Kluwe, and S. Hohmann, “Optimal energy management of low level multi-carrier distribution grids,” *Proceedings on 2016 IEEE International Conference on Power System Technology (POWERCON)*, pp. 1–6, 2016.
- [17] Z. Pan, Q. Guo, and H. Sun, “Feasible region method based integrated heat and electricity dispatch considering building thermal inertia,” *Applied Energy*, vol. 192, pp. 395 – 407, 2017.
- [18] Z. Li, W. Wu, M. Shahidehpour, J. Wang, and B. Zhang, “Combined heat and power dispatch considering pipeline energy storage of district heating network,” *IEEE Transactions on Sustainable Energy*, vol. 7, no. 1, pp. 12–22, Jan 2016.
- [19] J. Huang, Z. Li, and Q. Wu, “Coordinated dispatch of electric power and district heating networks: A decentralized solution using optimality condition decomposition,” *Applied Energy*, vol. 206, pp. 1508 – 1522, 2017.
- [20] R. Zimmerman and C. E. Murillo-Sanchez, “Matpower: Steady-state operations, planning, and analysis tools for power systems research and education,” *IEEE Transactions on Power Systems*, vol. 26, no. 1, pp. 12–19, Feb 2011.
- [21] W. F. Tinney and C. Hart, “Power flow solution by newton’s method,” *IEEE Transactions on Power Apparatus and Systems*, vol. 1, no. 11, pp. 1449–1460, Nov 1967.
- [22] G. Scholz, *Rohrleitungs- und Apparatebau: Planungshandbuch für Industrie- und Fernwärmeversorgung [Piping and apparatus construction, planning manual for industrial and district heating supply]*. Springer-Verlag, 2012.
- [23] D. Surek, *Technische Strömungsmechanik : Für Studium, Examen und Praxis [Technical fluid mechanics: For study, exam and practice]*. Wiesbaden: Springer Vieweg, 2017.
- [24] B. Glück, *Heizwassernetze für Wohn- und Industriegebiete [Heating water networks for residential and industrial areas]*. Verlag für Bauwesen, 1985.
- [25] A. Benonysson, “Dynamic modelling and operational optimization of district heating systems,” Ph.D. dissertation, Technical University of Denmark, Lyngby, 1991.



16th International Symposium on District Heating and Cooling, DHC2018,
9–12 September 2018, Hamburg, Germany

Estimation of the energy-saving effect of introducing a heat source water network system with single-loop piping utilizing hot spring heat

Minako Nabeshima^{a*}, Naoyoshi Koh^a, Masaki Nakao^b, Masahito Mike^c

^a *Graduateschool of Engineering, Osaka City University, Osaka, Japan*

^b *The OCU Advanced Research Institute for Natural Science and Technology, Osaka City University, Osaka, Japan*

^c *Sogo Setsubi Consulting Co., Ltd, Tokyo, Japan*

Abstract

The introduction of a heat source water network system using heat from hot spring and drainage water for hot water supply in accommodation facilities in hot spring areas is expected to contribute to increased energy efficiency. In this study, the relationship between the temperature of the heat source water and the energy efficiency of heat pump water heaters introduced in hot spring facilities connected to a single-loop heat source water network was analyzed. The primary energy consumption of the heat source water network system was compared with that of a centralized heat supply system by conducting a dynamic simulation using Modelica in the Dymola environment. The yearly average coefficients of performance of the proposed heat source water network and centralized heat supply systems were estimated to be 4.56 and 3.24, respectively. The seasonal performance of the proposed system was also investigated based on measurement data. In December, it was estimated that the heat source water network system would achieve a 17.6% reduction in primary energy consumption in comparison with the centralized heat supply system. However, in August, it was estimated that the primary energy consumption of the heat source water network system would be 8.9% higher than that of the centralized system.

© 2018 The Authors. Published by Elsevier Ltd.

This is an open access article under the CC BY-NC-ND license (<https://creativecommons.org/licenses/by-nc-nd/4.0/>)

Selection and peer-review under responsibility of the scientific committee of the 16th International Symposium on District Heating and Cooling, DHC2018.

* Corresponding author. Tel.: +81-6-6605-2719; fax: +81-6-6605-2719.

E-mail address: nabeshima@eng.osaka-cu.ac.jp

Keywords: heat pump; coefficient of performance; primary energy consumption; drainage water; heat recovery

1. Introduction

1.1. Background and motivation

In Japan, more than 27,000 hot spring wells are distributed throughout the country, approximately 52% of which have temperatures exceeding 42 °C. The potential for hot spring heat to be used as thermal energy is considered to be high. However, some accommodation facilities containing high-temperature hot spring wells often adjust the temperature of the hot spring water to within a usable range of approximately 40 °C by discharging heat into the air or adding water and thus do not use the hot spring heat effectively. This means that there is unused heat in the hot spring area that could be utilized to improve the energy efficiency of accommodation facilities in the area.

In accommodation facilities in hot spring areas, water from the hot springs is supplied to the hot spring baths, and the tap water supplied to faucets in the facility is heated through heat exchange with the hot spring water or using other water heating methods. At present, many facilities use hot water boilers that run on fossil fuel for their hot tap water supply. In an area where the use of hot spring water to supply a hot spring bath is limited, another heat source is necessary to maintain the water temperature in the bath because the spring water is recycled in a loop with a filtration device. Surprisingly, the demand for hot tap and spring water heating in facilities in hot spring areas is high. In hot spring districts in Japan, some facilities have their own hot spring wells with plenty of hot spring water, whereas others purchase hot spring water; notably, heat interchange among facilities is seldom implemented in these regions.

The heat of hot spring and drainage water at temperatures of less than 100 °C can be utilized as a heat source for water source heat pumps (HPs). This paper discusses how to utilize the unused heat from hot springs to supply hot spring and tap water to the entire community with lower power consumption than in conventional methods. As stated previously, many accommodation facilities in hot spring districts use fossil fuels for hot water supply, though some have turned to high-efficiency HP systems that utilize hot spring heat as a heat source by using heat exchangers (HEXs). An HP system that has a high coefficient of performance (COP) can emit less CO₂ than a conventional boiler system. In the future, HP systems are expected to gradually become more popular, despite their higher initial costs. Therefore, research on the effective utilization of hot spring heat based on the assumption that facilities are already equipped with HP water heaters is needed.

Nomenclature

HP	Heat Pump
COP	Coefficient of Performance
HEX	Heat Exchanger

1.2. Concept for the utilization of the heat of hot spring and waste water

This study focused on the unused heat of hot springs, that is, the heat of the hot spring and drainage water. This paper suggests a method of implementing a multiple-heat source network system with unidirectional single-loop piping to promote overall improved energy efficiency in the hot spring area. The proposed system was evaluated through dynamic one-dimensional (1D) simulation using Modelica. The purpose of this study was to verify the energy saving effect of implementing a multiple-heat source water network that can exchange unutilized hot spring heat among different facilities in the network in comparison with a conventional centralized heat supply system.

The proposed system recovers heat from drainage and hot spring water within each facility, and the recovered heat is used as the heat source for water source HPs used to supply hot water to the facility. Then the facility discharges surplus heat to the network piping or charges heat from the network if their heat supply is otherwise insufficient. It was assumed in this study that each facility connected to the unidirectional network uses a water source HP for hot

water supply and that heat charged from this network is used as a heat source of the HPs. From the viewpoint of temperature, the network is a type of unidirectional low-temperature network (LTN) for district hot water supply but with only a single pipe, which differs from the fourth-generation district heating and cooling (DHC) system with two pipes: a warm line for heating and a cold line for cooling [1].

One important feature of the heat source water network proposed in this study is that it uses not only heat recovery from each hot spring source but also a mechanism of drainage water heat recovery. Because the hot water discharged from a hot spring bath has a stable temperature of approximately 38 °C, even in a hot spring area containing few hot spring sources with low water temperatures, the improvement of the overall system COP can be expected.

In areas where the excavation of new hot spring wells is restricted for the sake of resource management, a centralized hot spring management method is often adopted. In such areas, a number of facilities do not have their own hot spring wells, and these facilities must purchase hot tap and spring water from management associations, which transport the water to the facilities via tank trucks or underground piping. There are approximately 90 locations that have introduced such a centralized supply system for hot tap and spring water; these include Tohyako in Hokkaido and Kusatsu in Gunma Prefecture. At Yunohama Onsen in Yamagata Prefecture, hot spring water is distributed to 50 facilities from a centralized plant. Additionally, centralized hot water supply equipment was introduced in 2017 with the aim of utilizing unused heat from hot springs by employing HP water heaters [2]. In the Yunohama Onsen system, hot water with a temperature of 65 °C is produced by exhaust heat recovery-type HPs using hot spring water with a temperature of 60 °C, and this hot water is distributed to 13 facilities. The total piping length in this system is about 3.5 km. The reductions in the energy cost and CO₂ emissions achieved since implementing this system are currently being investigated. This previous work demonstrates the steps being taken toward the utilization of unused hot spring heat in the hot spring area for a more sustainable community.

In hot spring areas containing high concentrations of high-temperature hot spring wells with abundant hot spring water, centralized control systems have often been adopted to supply hot tap and spring water to each facility. For this type of system, the initial cost of the piping and heat insulation work is relatively high. However, because the water temperature of the heat source water sent to each facility is close to the temperature of the soil surrounding the underground piping, heat loss is not expected to be a serious problem, even in non-insulated piping. Thus, this system can be applied even in areas where hot spring wells are distributed among multiple facilities. Hot water supply systems using multiple hot spring heat sources are expected to use less energy than conventional methods; however, there have been few cases of domestic introduction, and the effects in these cases have not been examined.

1.3. Previous works

Recently, the LTN system has been studied for DHC. Hai Wang et al. [3] proposed a general district energy planning method that can achieve mutual interconnection and interchange among thermal grids. In their paper, multi-source and multi-user were connected together with a warm line and a cold line, which is a two-pipe system. A novel bidirectional LTN system, which uses a single circuit for DHC, defined as a fifth-generation DHC has been studied in terms of its thermodynamic performance and operation optimization by Wetter's research group at Lawrence Berkeley National Laboratory [4, 5]. In [4], the control concept based on a temperature set point optimization and agent-based control was proposed. In [5], a diversity criterion was developed to understand when the bidirectional system may be a more energy-efficient alternative to modern individual building systems. They targeted only DHC excluding hot water supply.

Nakagawa and Koizumi [6] have proposed a hybrid HP system for the utilization of hot spring heat and have studied the effects of the system in Idaho Spring, Colorado. The hybrid system coupled with water from mines and hot springs can be used to cool buildings and melt snow. Nakagawa and Koizumi [6] also estimated the heat loss from the piping due to the traveled distance and the thickness of the pipe, but they did not describe the behavior or energy efficiency of the HP.

In our previous study [7], the effect of introducing a heat source water network connecting several facilities in the hot spring area was verified. This is a bidirectional LTN system, depicted in Fig. 1-a, which uses a single-loop of combined tow pipes, one acting as a warm line and the other as a cold line. The ends of the pipes are connected, and the heat source water circulates. Each facility charges its HP with heat from the warm line and returns the water to the

cold line; heat from the hot spring is then discharged to the cold line, and the reheated water is returned to the warm line. In this previous work, the energy efficiency effect of a single-loop bidirectional water source heat network composed of six facilities was determined by 1D dynamic simulation. The hot water supply load of each facility was defined based on actual measurement data. The simulation results confirmed that using such a single-loop water source heat network can reduce the primary energy consumption by 16.9 GJ/day in comparison with using a hot water boiler supply system and 8.9 GJ/day in comparison with using a centralized heat supply system. In this previous study, although the simulation results demonstrate the good energy saving performance of the single-loop heat source water network, this system still has the following problems: (1) the system prioritizes inputs to the network rather than use at each facility, and (2) the cost of introducing the new piping and pumps required for this bidirectional system is high.

Therefore, this paper proposes a unidirectional single-loop heat source water network (Fig. 1-b). In this system, heat from a hot spring is used preferentially at each facility as heat source water for the HP water heaters and to preheat makeup water. Surplus heat is then charged to the network. The heat source water is used in multiple stages among the facilities in the network. The use of a single pipe means that the heat source water temperature in the network is lower than that in the two-pipe system, but it has some advantages, including the relatively low cost of introducing the required piping and connections between each facility and the network.

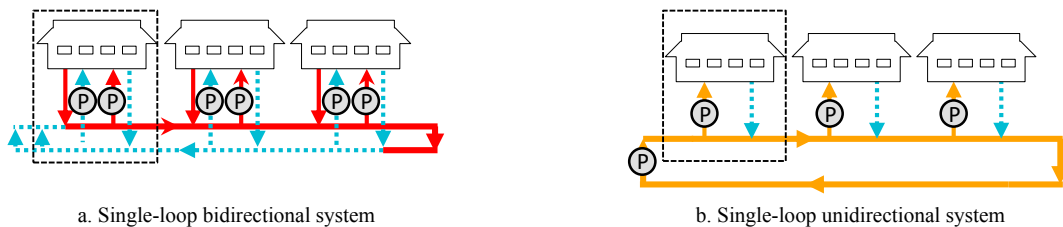


Fig. 1. Comparison of piping system

2. Methodology

2.1. Details of the system

As a case study, a network of six facilities connected by a single-loop heat source water system (Fig. 2-a) was considered. Two of the six facilities, Nos. 1 and 2 in Fig. 2-a, have their own hot spring wells, and the others buy hot spring water from the management association. Fig. 3 shows an outline of the onsite heat source water piping within a facility containing a hot spring well. The concept of the onsite heat source water piping within these facilities is a cascading heat utilization, which works as follows. First, heat source water flowing through the pipe transfers heat to drainage water from bathrooms in the facility and raises the temperature before the water reaches the HP water heater. As a result, the temperature of the heat source water supplied to the HP water heater rises, which improves the COP; thus, a reduction in power consumption can be expected. Regarding fluctuations in the demand for hot water, the hot water storage tank is able to make the appropriate adjustments. After the HP water heater, the heat source water decreases in temperature, which can exchange heat with hot spring water. Because the temperature of the heat source water at this time is higher than the temperature of the tap water, it can be used to preheat the makeup water. Additionally, sending the preheated tap water to the HP water heater enables the reduction of the energy consumption required to heat the hot water supply. In this way, the onsite heat source water piping within a facility is built to utilize hot spring heat to reduce the power consumption of the HP water heater. The surplus heat produced by the HP in the facility is charged to the heat source water in the network piping, which is exchanged with other facilities by the grid pump.

Fig. 2-b shows the centralized heat supply system used to distribute hot water and hot spring water to each facility as a basis of comparison. In the centralized heat supply system, a heat source plant is set up in one location in a hot spring area with hot spring accommodation facilities. Concentrating the heat source plant has some merits, such as the effective use and stable supply of energy, the economic improvement of equipment, and the prevention of air pollution. The centralized heat supply system is thought to be suitable for areas containing hot spring source wells with abundant upwelling high-temperature waters, such as Kusatsu Onsen in Japan.

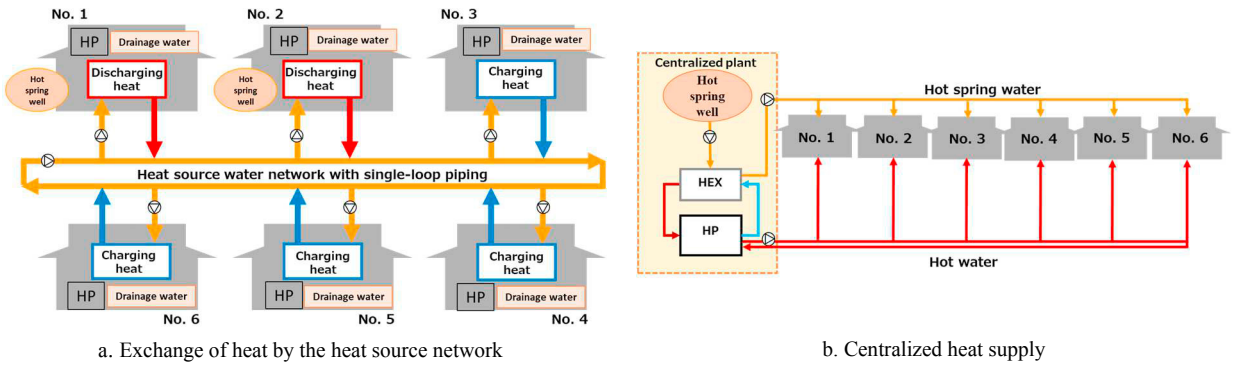


Fig. 2. Example of the proposed heat supply system for six users and the conventional system used as a basis for comparison

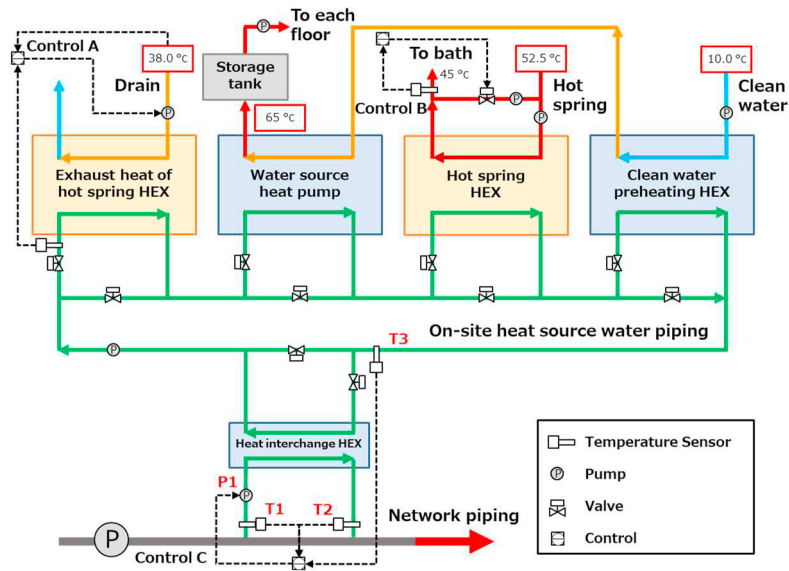


Fig. 3. Onsite heat source piping system used in facilities containing hot spring wells in the proposed heat source network

2.2. Models for simulation

In environment of the physical modeling tool Dymola, models of the water source HP, heat exchanger (HEX), piping, constant flow pump, and controller from Buildings Library 3.0 [8] developed by Lawrence Berkeley National Laboratory, University of California were used to develop models of the hot spring heat utilization heat source water network system and the centralized heat supply system. For details of each physical model, see the Buildings Library [9]. An overview of each of the models is given below.

- HP water heater

The COP of the HP was calculated using the following model:

$$COP = \eta_{PL} COP_{carnot} \eta_{carnot,0} \tag{1}$$

$$\eta_{carnot,0} = COP_0 / COP_{carnot,0} \tag{2}$$

$$COP_{carnot,0} = T_{con_out,0} / (T_{con_out,0} - T_{eva_out,0}) \tag{3}$$

$$COP_{carnot} = T_{con_out} / (T_{con_out} - T_{eva_out}) \tag{4}$$

$$\eta_{PL} = a_1 + a_2 y_{PL} + a_3 y_{PL}^2 + \dots \tag{5}$$

$$\sum a_j = 1 \tag{6}$$

The parameter values are given in the table below. This model describes the partial load characteristics of an actual HP water heater with a rated power of 109.8 kW and a rated COP of 4.7 under hot water inlet and outlet temperatures of 30 and 70 °C respectively. The regression coefficient a_j of the model was determined based on manufacturer data. The model does not consider the heat capacity of the equipment.

Parameter	Definition	Unit
η_{PL}	Ratio of the COP at a partial load to the Carnot COP	-
η_{carnot}	Ratio of the rated COP to the Carnot COP	-
COP, COP_0	COPs at a partial load and the rated load	-
COP_{carnot}	COP of the Carnot cycle	-
y_{PL}	Partial load ratio	-
a_j	Regression parameters	-
$T_{eva\ out}$	Temperature of evaporator outlet, approximate heat source water temperature of HP outlet	°C
$T_{con\ out}$	Temperature of condenser outlet, approximate hot water temperature of HP outlet	°C
0	Subscripted 0 indicates parameters under rated power conditions	-

- Pipe

For the pipe model, the 1D thermal conduction equation was solved. Because spatial differentiation is not necessary to solve the 1D heat conduction equation when using a lumped parameter model, it was assumed in this model that the temperature varies linearly over the discretized elements representing the pipe. The pipe model was customized to consider heat loss due to convective heat transfer inside the piping, the heat capacity of the fluid, and the pipe heat capacity. The centralized heat supply system must be able to insulate the piping to supply high-temperature hot springs and hot water. Additionally, it was assumed that the underground piping of the heat source water network is not insulated and the piping inside facility is completely insulated. The burial depth of the heat source water network piping is 600 mm, and the heat capacity of the soil was not considered. To calculate the heat loss of the buried piping, the soil temperature was represented using the thermal boundary condition at a position 600 mm outside of a 100A pipe.

- Pump

The pump model does not consider equipment pressure loss or discharges at a constant flow rate. The daily cumulative power consumption of the network circulation pump and each pump inside the facilities were calculated from the operating time and the power consumption at the rated operation. Regarding the network circulation pump capacity, the pressure loss in the piping was defined as twice the pressure loss of the straight pipe portion calculated based on the rated flow rate.

- Control

The temperature measurement points labeled T1, T2, and T3 in Fig. 3 were used to control the on/off state of the pull-in pump P1 by Control C in Fig. 3. When the temperature differences between T1 and T2 and between T1 and T3 are both at least 3 °C, P1 is operated to withdraw heat source water for heat exchange.

3. Case Study

3.1. Baseline data of hot water demand and given conditions

Conditions such as the source temperature, hot water temperature, and hot water demand were set based on actual measurements conducted for two types of accommodation facilities in the Shima Onsen area of Gunma Prefecture from 2014 to 2015 [10]. One is a mid-sized facility with 80 rooms and its own hot spring source wells. The other has 15 rooms and does not possess its own hot spring source well but buys hot spring water from the hot spring management association.

In this study, the seasonal primary energy saving effect was investigated by comparing the results obtained using data representative of typical days in each season to set the conditions of six facilities connected to the heat source water network. Table 1 gives the hot water heat demand and hot spring water demand of each facility in December as an illustrative example. In this case study, the six facilities numbered Nos. 1–6 are connected to the heat source

network, and the conditions set for Nos. 1 and 3 correspond to the hourly demand obtained from the actual measurement of the abovementioned medium- and small-scale facilities, respectively. Regarding the other facilities, the hot water heat demand, hot spring water demand, and drainage quantity were set to multiples of those for No. 1 or 3 according to the number of rooms in each facility.

The temperature of the hot spring water was set to 52.5 °C in the facilities that possess their own source wells (Nos. 1 and 2), and hot spring water is available for heat exchange for temperatures of up to 45 °C. The other facilities (Nos. 3–6) do not have their own hot spring source wells and purchase hot spring water at 35 °C from hot spring associations, so it is necessary to heat this water to 45 °C.

Nos. 1 and 2 were assumed to have only one HP water heater each, whereas the other facilities were given two types of HP water heaters: one for hot water supply and the other for heating hot spring water. The hot water outlet temperature was set to 65 °C. Regarding heat recovery from the drainage water, the waste water temperature was set to a constant value of 38 °C. For the centralized heat supply system considered as a basis of comparison, the hot water heat supply of the system was set to the total hot water heat demand of the six facilities in the heat source water network system, and the hot spring water supply was set to the sum of the total hot water heat demand and hot spring water demand of the six facilities in the heat source water network system. For example, in December, the hot water heat supply was set to 49.5 GJ/day, and the hot spring water supply was set to 951 t/day (= 240 t/day + 711 t/day). Table 2 gives the seasonal values of the total hot water heat demand of the six facilities. There was no seasonal change in the hot spring water demand.

Table 1. Demand settings for each facility in December

Hotel ID number	Number of rooms	Hot water heat demand	Purchased hot spring water (35 °C)	Own hot spring water (52.5 °C)	Waste water (38 °C) for heat recovery
		GJ/day	t/day	t/day	t/day
1	80	12.0	0	237	296
2	160	24.0	0	474	593
3	15	2.25	40.0	0	74
4	15	2.25	40.0	0	74
5	15	2.25	40.0	0	74
6	45	6.75	120.0	0	222
Sum	330	49.5	240	711	1,333

Table 2. Total daily hot water demand of six facilities in each season [GJ/day]

Apr.	Aug.	Oct.	Dec.
45.8	31.9	38.9	49.5

Table 3. Soil and clean water temperatures based on measurement data [°C]

Daily averaged value	Apr.	Aug.	Oct.	Dec.
Soil temp.	12.2	24.7	17.7	11.6
Makeup water temp. of HP inlet	11.3	19.5	14.9	10.1

Table 4. Given characteristics of piping (100A polyvinyl chloride pipe)

Parameter	Value	Unit
Heat capacity of pipe	1.17×10^3	J/(kgK)
Density of pipe	1.43×10^3	kg/m ³
Diameter of pipe	Outside: 114, Inside: 100	mm
Insulation for pipe: glass wool	0.033	W/(mK)
Thickness of insulation	0.1	m
Thermal conductivity of soil	0.2558	W/(mK)

Table 3 shows the soil temperature and the HP makeup water temperature under the given conditions. All the conditions were measured every hour, and the data between the measurements were linearly interpolated. Table 4

gives the parameters for the piping used in the heat source water network and the centralized heat supply system. The heat source water network piping is a unidirectional single loop with a total length of 1000 m buried at a soil depth of 0.6 m. In the case of the centralized heat supply system, the piping for the hot spring water distributed over the six facilities is 500 m in length, and the facilities are arranged at intervals along this piping. The distance between Nos. 1 and 2 is 90 m, and the distance between the remaining facilities is 80 m. Circulation piping for the hot water supply was set to 1000 m in length.

4. Results

Numerical simulation was conducted in the Dymola environment with the Modelica Buildings library. Fig. 4 shows the heat balance between the hot water demand and the HP production heat at Nos. 1 and 3. The hot water demand schedule was determined based on the original unit for the design of the accommodation facilities. With the hot water tank at each facility utilized, the HP for hot water was set to operate at the rated power for 22 h/day. The rated power of the HP heating capability was determined so as to satisfy the hot water demand each day.

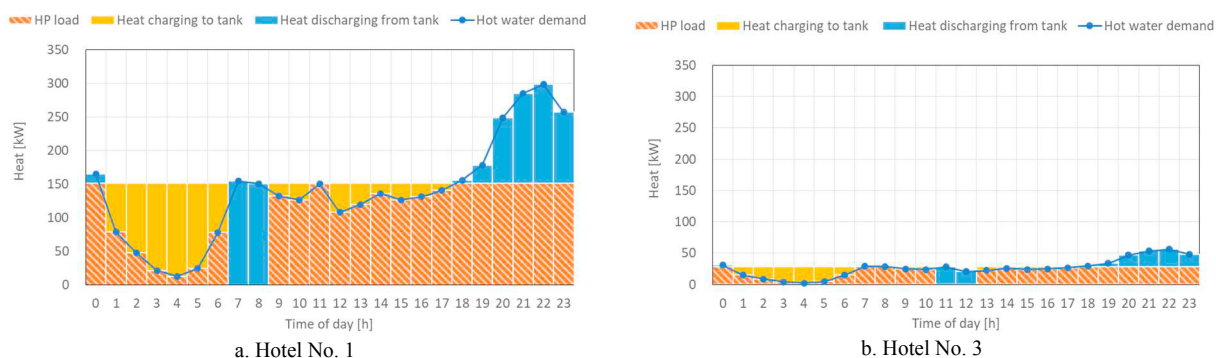


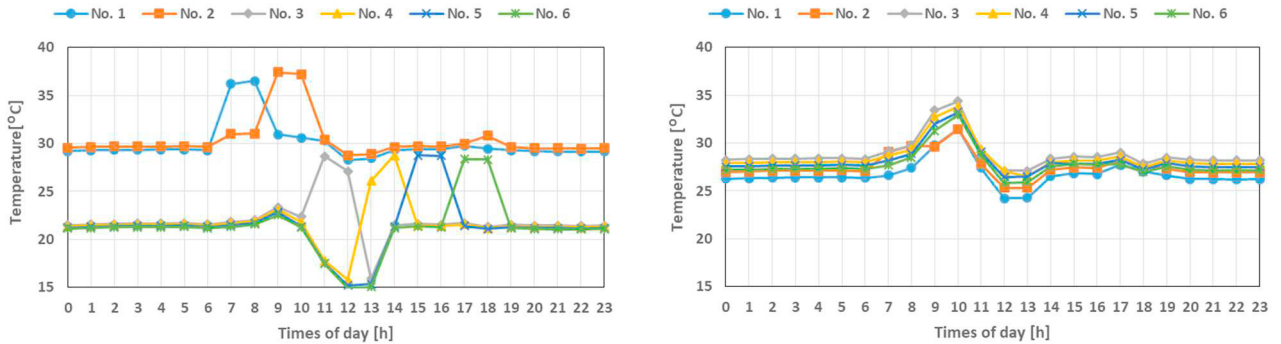
Fig. 4. Behavior of HP and heat balance in each facility

The temperature results for the heat source network in December are shown in Fig. 5. Fig. 5-a shows the estimated temperature of the heat source water inside each facility just before exchanging heat with the heat source water network. Fig. 5-b shows the heat source water temperature in the network piping just before exchanging heat with the heat source water inside each facility. The highest daily average value of the heat source water temperature was 30.4 °C, which was recorded inside No. 2, one of the facilities with a hot spring source well. The lowest daily average value of the heat source water temperature was 21.2 °C, which was recorded inside No. 6, a facility without a source well. There is a 9.2 °C difference between Nos. 2 and 6, which leads to a difference in the COPs of the corresponding HP water heaters. The highest daily average COP of the HP water heaters was 4.85 at No. 2, and the lowest was 4.39 at No. 6. The heat source water temperature inside each facility rises over the 2 h during which the HP is not operated. Fig. 5-b shows the results for the heat source water temperature of the network, which demonstrate that this temperature is kept stable in the range of 25–35 °C throughout the day. Because the temperatures of the heat source water inside Nos. 1 and 2 are higher than that inside the network, these hotels mainly discharge heat to the network. In contrast, Nos. 3–6 mainly draw heat from the network.

Fig. 6-a shows the heat source temperature at the HP inlet for the two considered systems. The yearly average heat source water temperatures of the network and centralized systems were estimated to be 24.4 and 15.1 °C, respectively. Fig. 6-b shows the average COP of the HP water heaters for the two systems, the yearly averages of which were estimated to be 4.56 and 3.24, respectively. The reason the COP of the centralized system was lower than that of the network system is that heat source water in the centralized system is heated by only exchanging heat with the hot spring source water whereas that in the network system is heated by exchanging heat with both hot spring water and waste water at each facility.

Fig. 7 shows the primary energy consumption of the two considered systems. The primary energy consumption of the heat source water network reached a peak of 41 GJ/day in December when the hot water demand was the largest,

and the reduction in energy consumption was estimated to be 17.6% relative to that of the centralized heat supply system, which was 50 GJ/day. In contrast, in August, when the hot water demand was the smallest, the primary energy consumption of the heat source water network was estimated to be 8.9% higher than that of the centralized system. Although the power consumption of the HPs in August was estimated to be 9.4% lower for the network than for the centralized system, that of the circulation pump for the heat source water in the network was estimated to be 1.6 times that of the centralized plant, offsetting the benefit achieved by reducing the HP consumption. This demonstrates that the total energy consumption of the network may be higher than that of the centralized system in summer when the hot water demand is low. In April and October, the network achieved a power consumption reduction of 13.5% and 4%, respectively, relative to the centralized system.



a. Average heat source water temperatures inside the facilities b. Average heat source water temperatures of the network

Fig. 5. Temperature of the heat source water of the network and inside each facility in December



a. Average heat source water temperature of HP inlet b. Average COP of HP water heater
 Fig. 6. HP performances of the system, CNT: centralized heat supply system, NTW: heat source water network, each season

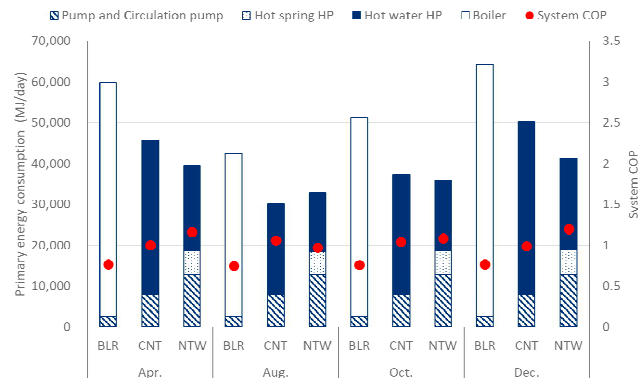


Fig. 7. Primary energy consumption
 BLR: individual boiler system, CNT: centralized heat supply system, NTW: heat source water network

In comparison with the individual boiler system, the centralized heat supply and heat source water network systems achieve power consumption reductions of 25.5% and 30.6%, respectively. The COPs of the boiler, centralized, and network systems including auxiliary machineries based on the primary energy consumption in December were estimated to be 0.77, 0.99, and 1.20, respectively. It was thus demonstrated that the energy saving performance of the

proposed hot spring heat utilization networked system is superior to the other system from the perspective of primary energy consumption performance.

5. Conclusions

In this study, a heat source water network system for utilizing hot spring heat was proposed, and a feasibility study on the heat source water network system was conducted using a model network of six facilities simulated in Modelica to estimate the energy saving effect of the network relative to conventional hot water supply systems. The results of this study demonstrate that the proposed heat source water network system comprising multiple connected HP hot water heaters can utilize the heat from multiple hot springs to supply each facility in the network and optimize the primary energy consumption of the entire community.

The main results can be summarized as follows.

- (1) The yearly average COP of the heat source water network and centralized heat supply systems when applied to the considered community of facilities were estimated to be 4.56 and 3.24, respectively.
- (2) In comparison with the centralized heat supply system, the proposed network system was confirmed to conserve energy except in August. The reduction in energy consumption was particularly high at 17.6% in December. However, in August, the use of the network system was estimated to increase the primary energy consumption by 8.9% in comparison with the centralized system.
- (3) The system COPs including auxiliary machineries based on the primary energy consumption in December were estimated to be 0.77 for the boiler system, 0.99 for the centralized heat supply system, and 1.20 for the heat source water network system.

Finally, comparing the initial costs of the two systems, the proposed network system and the centralized system, we found that there is a cost benefit for the former because the heat source water network system assumes piping without insulation, owing to the similar temperature of the heat source water and the temperature underground.

Acknowledgements

This paper is based on results obtained from a project commissioned by the New Energy and Industrial Technology Development Organization (NEDO).

References

- [1] Henrik Lund, Sven Werner, Robin Wiltshire, Svend Svendsen, Jan Eric Thorsen, Frede Hvelplund, Brian Vad Mathiesen. "4th Generation District Heating (4GDH): Integrating smart thermal grids into future sustainable energy systems" *Energy* 68 (2014): 1-11.
- [2] Yunohama Gensen Setsubi Hoyu Co. ,Ltd., "Heat Pump Thermal Storage Dissemination Contribution Award" *Cool and Hot* 52 (2017): 69. (In Japanese)
- [3] Hai Wang, Hua Menga, Weiding Long. "A District Energy Planning Method with Mutual Interconnection and Interchange of Thermal Grids" *Procedia Engineering*, 205, (2017): 1412-1419.
- [4] Felix Bünnig, Michael Wettera, Marcus Fuchs, Dirk Müller. "Bidirectional low temperature district energy systems with agent-based control: Performance comparison and operation optimization" *Applied Energy* 209 (2018): 502-515, doi:10.1016/j.apenergy.2017.10.072
- [5] Rebecca Zarin Pass, Michael Wetter, Mary Ann Piette. "A thermodynamic analysis of a novel bidirectional district heating and cooling network" *Energy*, 144 (2018): 20-30, doi:10.1016/j.energy.2017.11.122
- [6] Nakagawa, M., Koizumi, Y. "Geothermal heat pump system assisted by geothermal hot spring." *Geoth. Energ. Sci.* 4 (2016): 1-10, doi:10.5194/gtes-4-1-2016.
- [7] Koichi Sawabe, Masahito Mike, Sana Sawada, Naoyoshi Koh, Minako Nabeshima, Masatoshi Nishioka, Masaki Nakao. "Construction of Heat Source Water Network System with Hot Spring and Drainage (Part3) Estimates of Energy Consumption Reduction Effect by the System Introduced" *Annual Conference Proceedings of SHASE* (2016): 189-192, doi:10.18948/shasetaikai.2016.10.0_189. (In Japanese)
- [8] Michael Wetter, Wangda Zuo, Thierry S. Nouidui, Xiufeng PangSorrrell, Steve. "Modelica Buildings library" *Journal of Building Performance Simulation* 7(4) (2014): 253-270.
- [9] Modelica Buildings library <<https://simulationresearch.lbl.gov/modelica/>> [accessed on: 01-10-2017]
- [10] Naoyoshi Koh, Masahito Mike, Koichi Sawabe, Sana Sawada, Minako Nabeshima, Masatoshi Nishioka, Masaki Nakao. "Construction of heat source water network system with hot spring and drainage (Part2) Survey of hot spring, hot water demand and drainage temperature in accommodation facilities" *Annual Conference Proceedings of SHASE* (2016): 185-188, doi:10.18948/shasetaikai.2016.10.0_185. (In Japanese)



16th International Symposium on District Heating and Cooling, DHC2018,
9–12 September 2018, Hamburg, Germany

Renewables, storage, intelligent control: how to address complexity and dynamics in smart district heating systems?

Keith O'Donovan¹, Basak Falay¹, Ingo Leusbrock¹

¹ AEE – Institute for Sustainable Technologies, Department of Thermal Energy Technologies and Hybrid Systems, Group of “On-Grid Energy Supply and System Analysis”, Feldgasse 19, 8200 Gleisdorf, Austria

Abstract

The design of future district heating network will focus on two major aspects: The first of which is boosting the share of renewable heat in overall energy mix, and the second of which is to achieve lower network operating temperatures, thus increasing the potential for integrating new alternative heat sources. Renewable heat sources by their nature are highly fluctuating and require thermal storage and sophisticated control strategies to be utilized efficiently. Static modelling and simulation tools are incapable of capturing the dynamic effects and necessary control strategies that come with such complex systems. The work in this paper will outline how Dymola, a Modelica based simulation tool is capable of handling such complexity. The first section will outline an automated workflow to translate CAD drawings into functioning Dymola models. The next sections will upgrade a small heating network model to a future system with the addition of a large thermal storage tank, solar collectors and prosumers. The last section will demonstrate a concept to achieve lower network operating temperatures by simulating the network with a branch supplied by the return pipeline. The addition of the storage tank and solar showed an increase of the combined biomass and solar from 82% to 93% over the reference time frame. The second use case demonstrated a 12% reduction in network heat losses for a given week by implementing the lower temperature branch.

© 2018 The Authors. Published by Elsevier Ltd.

This is an open access article under the CC BY-NC-ND license (<https://creativecommons.org/licenses/by-nc-nd/4.0/>)

Selection and peer-review under responsibility of the scientific committee of the 16th International Symposium on District Heating and Cooling, DHC2018.

Keywords: District Heating, Modelling, Dynamic Simulation, Dymola, Modelica, Storage, Solar Thermal, Control, Low Temperature Networks.

1. Main text

1.1 Introduction

Until recent times, the classic district heating networks could be characterized by high temperature, pressurized water or steam driven heat, produced almost exclusively by coal, oil or gas based fuels. The associated network operating control strategies were relatively simple, with typically one or two centralized heating plants covering the entire network heating demand. Supply temperatures and heat production rates were regulated based on heuristic methods based on long term weather forecasting and “rule of thumb” approximations. As a consequence, production plants spend a large amount of time operating in an inefficient way with unnecessary plant start-ups and shut downs occurring to match the network demand.

The design and operation of district heating networks has since seen a major overhaul, with a focus on large scale integration of fluctuating renewable heat sources with the aim of achieving a fully decarbonised, flexible heat supply. Future district heating systems also strive towards lowering network temperatures in order to maximise potential of alternative heat sources in the network such as solar, geothermal and industrial waste heat as well as to reduce heat losses in the distribution lines and increase the coefficient of performance of any heat pumps integrated into the network [1].

Previous research has shown that district heating and cooling infrastructure has the potential to play a key role in the transition towards fully decarbonised, flexible, sustainable energy systems [2, 3]. Multiple options exist for increasing energy system flexibility, including combining the heating grid with other energy domains such as electrical and gas networks, increasing supply and demand flexibility through integrating of large thermal energy storage technologies and increasing the transmission capacity of the national grid as well as interconnections to other countries.

The integration of all of these technologies and flexibility measures leads to an inevitable increase in network complexity. Future district heating networks will see a large number of additional decentralised heat sources, many of which will need to be coupled with storage for short or long term periods to match the instantaneous heating demand. Despite the rapidly growing list of opportunities, the planning and efficient operation of such networks presents an immense challenge.

Many of the standard simulation tools and methods for analysing heating networks are unsuitable for addressing such complexity, because they often rely on simplified models, static relationships and single-domain approaches [4]. One consequence of this among others, is that they are frequently unable to capture the dynamic behaviour of such complex systems and the interaction between included components. It is therefore necessary to adapt to sophisticated, dynamic simulation tools and control strategies.

Recent advances in object-oriented, physical modelling of energy systems has led to potential for developing novel tools for system planning and operation control that focus specifically on these new challenges. The modelling language Modelica is a promising candidate to become standard for industry and academia in the field of dynamic modelling, and in particular, modelling of multi-domain systems [5]. Modelica is a well-established modelling language in industry (7% of German power production is based on Modelica models [6] and academia). A general distinction can be drawn between block diagram modelling (also known as causal modelling) using imperative programming languages and equation-based modelling (also known as acausal modelling). Equation-based languages are most advantageous for:

- representing the physical structure of systems as it enables the modeller to model the system directly by means of physical equations. The causality of how to solve the equations is not decided during the modelling stage, which means that the usual need for manual conversion of equations to a block diagram is removed.
- reusability, extensibility, adaptability of models and
- being simple to code and read.
- are preferable for optimization tasks [7]

In the first section of this paper, we describe a framework for modelling and simulating such networks using Dymola as a simulation environment with an example focusing on converting an existing network to a 4th generation district heating system. The impacts of thermal energy storage, large scale solar thermal collector fields and prosumers will be demonstrated. The second use case will outline a method to convert a branch of the chosen network to a low temperature branch by supplying its consumers with heat from the return pipeline.

We will thus highlight the differences between standard tools for planning and design of the systems with our approach and show the added value in terms of accuracy and representation of dynamics, which will become a vital feature of future DH systems.

1.1. Network Modelling and Simulation Workflow

To manually build a district heating network simulation model of any significant level of detail would be an arduous and time consuming task, not to mention highly prone to human error. A better approach is to implement an automated work flow to go from a CAD drawing of the network plan all the way to executable Modelica code. This is done in a number of steps:

1. Assuming the network representation has embedded GIS data, one can export main pipeline, producer and consumer coordinates from the CAD using Python scripts.
2. Using the Python Package, NetworkX, pipes and consumers can be represented as a collection of connected “edges” and “nodes” respectively. Both have a dictionary format which stores data and parameters such as coordinates, loads, temperatures, pipe diameters, and insulation thickness’ etc.
3. Another Python script translates this plan to executable Modelica code which can be interpreted by Dymola which allocates the models to each consumer, producer and pipe.

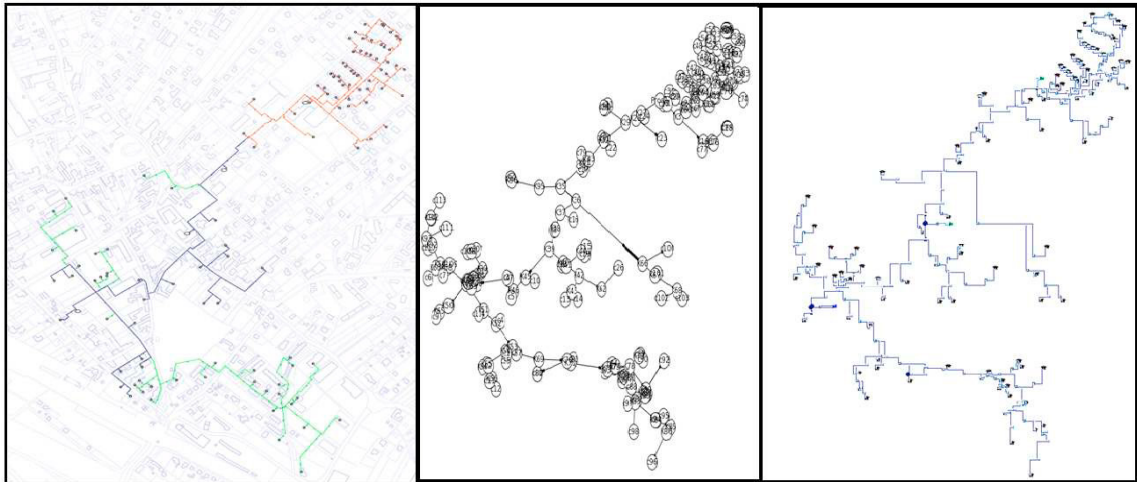


Fig 1: Left: Network Plan in CAD format; Middle: NetworkX representation in Python; Right: Network Translated to Dymola Model

Dymola is supported by a wide array of open source and commercial libraries containing detailed components for heating network building and simulation. A dynamic pipe model developed by van der Heijde et al. [8] will be incorporated in the use cases here to accurately capture heat wave propagation throughout the network.

Any additional data relating to network operating temperature or demand profiles are read typically from txt files directly from Dymola. Dymola's intuitive block diagram layout and wide range of logical operator allow for relative ease in implementing simple control strategies in the model environment. A very useful step to aid in the interpretation of the obtained results would be to produce a visualization. This can be done as a post processing step outside of Dymola by importing the results back into the Python representation of the network. Color coding can be applied to each element in the network at a given time step, to represent any result variable of interest, for example – pressure and temperature distributions in the pipeline, instantaneous consumers loads, heat loss distributions and more. By compiling the images at every time step in the simulation, an animation can be created to see the propagation of temperature and pressure waves throughout the network. A similar study on network visualization methodology using Dymola has previously been carried out here [9].

The entire workflow including pre and post processing steps are outlined in the flow chart in Fig 2 below:

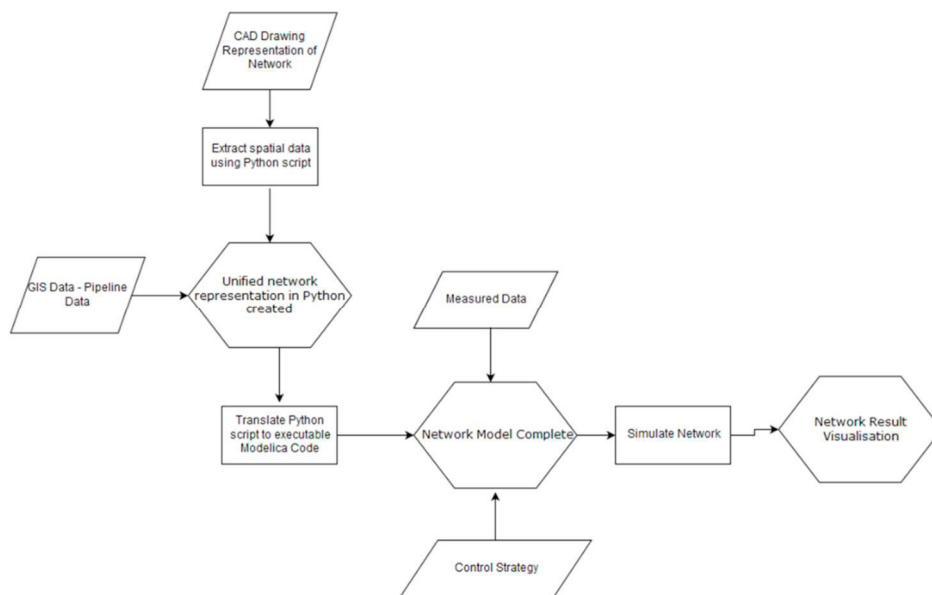


Figure 2: Network Modelling Workflow

1.2. Case Study 1: Upgrading an Existing Heating Network to a 4th Generation Network:

The following example demonstrates the capabilities of Modelica in modelling and simulating a DHN by taking an existing network and upgrading it to a typical 3-4th generation network with the addition of small and large scale solar collectors. The results aim to demonstrate the capability of Dymola of capturing a number of complex dynamic effects.

Base Case

The base case represents one supplying a small town in Austria with some future planned network extensions already in place. The specifications for this base case do not reflect exactly those of the network, but serve rather as a potential future situation. The simulated network consists of:

- 116 consumers – nominal load 8.5MW
- Mean supply return temperatures 88/55°C
- Three production sites:
 - Base load supplied by Biomass plant – capacity 3.5MW
 - Peak load supplied by a gas boiler of capacity 2MW
 - Constant 300kW_{th} from CHP in the south east.
- Approx. 7km of pipeline.

Consumer load profiles were used from existing load data from the year 2015. The main pressure control is implemented at the Biomass plant in the south east which provides a pressure drop such that the minimum pressure drop in the network at some critical consumer (usually the furthest away) is at least 0.5bar. The required mass flow is then computed indirectly as a function of the pressure drop.

Upgraded Network

The upgraded case was kept like above with the addition of:

- Three large consumers converted to prosumers with a total area of 150m² of solar thermal collectors.
- Large solar thermal collector field 1350m² added and coupled to storage.
- 750 m³ thermal storage tank next to the Biomass plant.

The purpose of the storage tank is to allow for increased hours of the biomass plant, thus increasing its operating efficiency. Excess heat from the Biomass plant is stored in the tank during periods of low demand and discharged during times of high demand. Aside from increasing the output of the biomass, the additional heat from the tank will help reduce the dependency of the gas boiler during periods of high demand, thus reducing the overall CO₂ emission levels.

A stratified tank model developed by Modelica Buildings Library (Berkley), is used for the simulation. A control strategy is implemented to assess when to charge and discharge the tank based on current network demand levels and minimum and maximum permissible tank temperatures. The biomass plant was configured to run at a constant output of 3MW with any surplus heat used to charge the tank during times of low demand. At times of higher demand, the tank is then discharged into the network cover the remaining load. Only when the tank is fully discharged and total net load is above 3MW is the gas boiler switched on. The idea is reduce the dependency on the gas boiler while also operating the biomass boiler at a more efficient output level. The tank is considered to be fully charged when the temperature of the storage medium reaches that of the network supply right through. The tank is considered to be fully discharged when the temperature of the storage medium reaches that of the network return temperature right through.

For the solar facilities, a weather data file is read at every simulation time step with the global irradiance, G , angle of incidence, θ and ambient air temperature T_{amb} serving as inputs to the collector model.

The collector model itself assumes a flat plate collector with a collector area, A , in a horizontal configuration. An average collector temperature of 70 degrees is specified and the collected heat can therefore be calculated from Eq. (1).

$$Q_{solar} = \eta AG \tag{1}$$

Where η is the collector efficiency calculated from Eq. (2)

$$\eta = F \left(a_0 - \frac{a_1(T_{collector,avg} - T_{amb})}{\max(G, 0.0001)} - \frac{a_2(T_{collector,avg} - T_{amb})^2}{\max(G, 0.0001)} \right) \tag{2}$$

Where F is a function of the angle of incidence θ , a_0 , a_1 and a_2 are constants and properties of the collector itself. The mass flow is achieved via a circulation pump which only switches on once the irradiance exceeds a specified minimum value G_{min} . The prosumers consume the solar heat instantaneously to meet their total heating demand. During periods of net demand, the deficit is taken from the network while during periods of negative net demand, the excess solar heat is fed directly into the grid.

Results

A detailed simulation was ran over a four month period from late winter into spring (Jan 1st to April 30th). Spring time was chosen to observe a period with significant heating demand with growing solar thermal potential throughout the period. To observe the daily heat flows in and out of the storage as well as the heat production at the additional solar collector sites, a two week period of the results are presented below in simulated plots in Figure 3. The top graph illustrates the total network load over a one week period with clear times of tank charging and discharging shaded. The corresponding state of charge of the stratified tank can be overserved in the lower plot with the temperature distribution shown throughout.

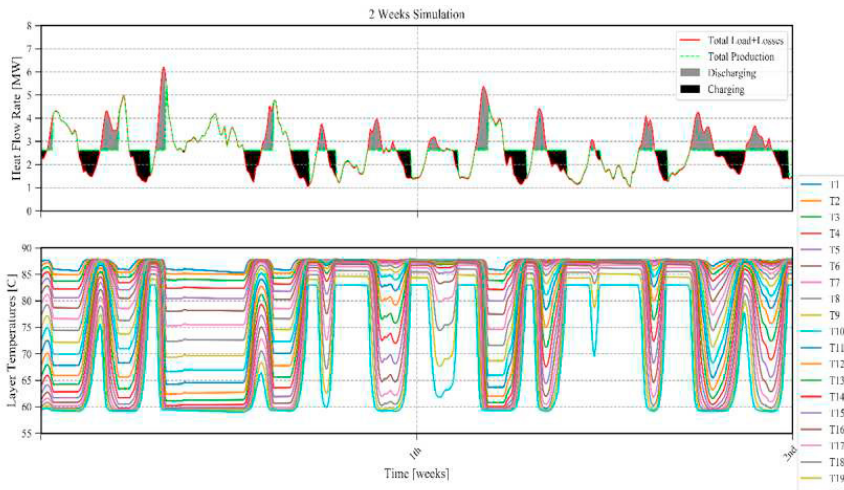


Figure 3: Top: Two week of simulation with total production with indicated energy to and from the storage component; Bottom: Temperature distribution in the tank

The plot below illustrates the hourly solar production at one of the prosumers with regions of net negative load being fed back into the net:

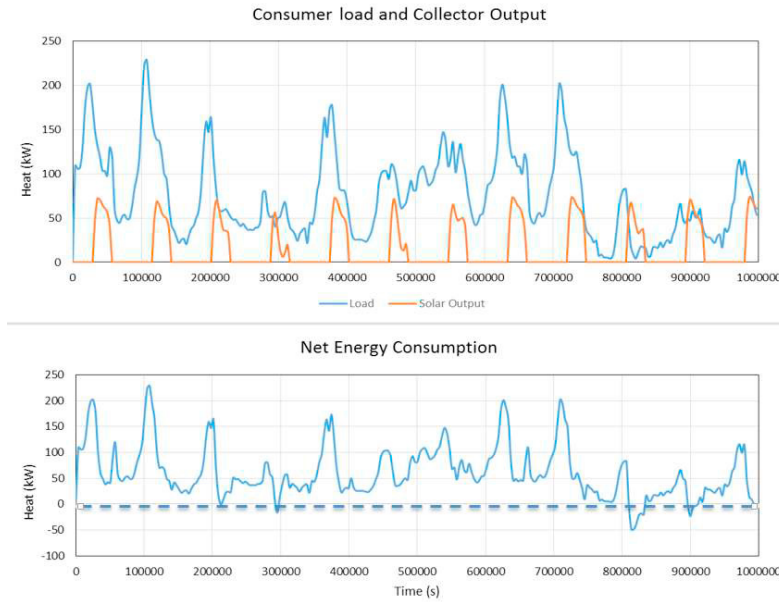


Figure 4: 12 days result plot of 300kW prosumer with 150m² Collector: Output vs Consumption

The bar chart in Figure 5 gives a breakdown of the energy mix over the given period for three different scenarios:

- i. Base case with no solar or buffer storage
- ii. Upgraded case with only solar installations present
- iii. Upgraded case with buffer storage and solar installations present

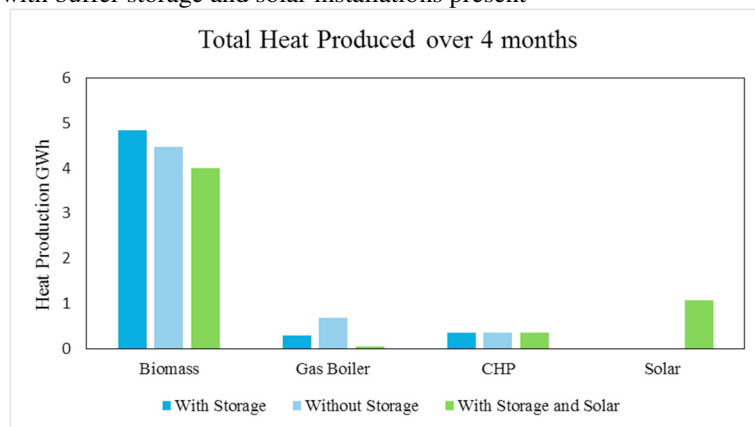


Figure 5: Total Energy Consumption Jan-April Period for Base case and upgraded scenarios

The dependency of the gas boiler is significantly reduced with the addition of the storage tank, with its output being reduced from 671MWh down to 291MWh over the four month period. With the addition of the solar collectors, its output is further reduced to just 48MWh over the given period. The heat output from the CHP is fixed and not affected by the implementation of storage or solar components. The corresponding percentage breakdown for the period for the three different scenarios is given in Figure 6.

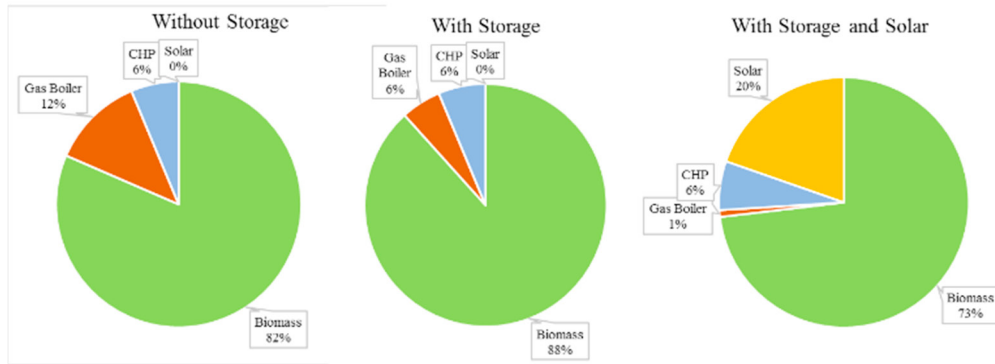


Figure 6: Energy Mix for Base Case and Upgraded scenarios

The solar energy produced here was fed directly into the grid which is favourable over such a Winter/Spring period with a reasonably high heat demand. The 1,500m² of solar collector surface added here accounted for approximately 20% of the overall heat demand of the network over the given period. For a summer period simulation, further control strategies will need to be implemented to store as much excess solar heat as possible, which can be discharged at times of higher demand in autumn and Winter.

1.3. Case Study 2: Low temperature supply concept – Supplying from the Return Pipeline.

This case study will demonstrate an innovative method to lower the network operating temperatures in a small branch of the network by connecting a number of consumers via the return pipeline of the network, thus lowering the overall network heat losses while allowing for additional network capacity without the need to increase the pressure level. The branch to be supplied by the return pipe line consists of 20 consumers, approx. 1.2km of supply pipeline and a total nominal load of 1.5MW. The set condition imposed on the network is to achieve a minimum temperature of 60 degrees at each consumer substation. The actual network return temperature is varying about 50-60 degrees depending on location and time of year. In order to meet the required supply temperature, an additional pipeline is connected to enable partial mixing with fluid from the main supply pipeline when necessary. The mixing and subsequent temperature at the substation is regulated by a PID controlled valve. To ensure adequate circulation, pumps are implemented to the return side of the consumers to raise the fluid pressure back to that at the connection points back into the main return pipeline. The associated pumping costs will be examined. The working principal is illustrated below.

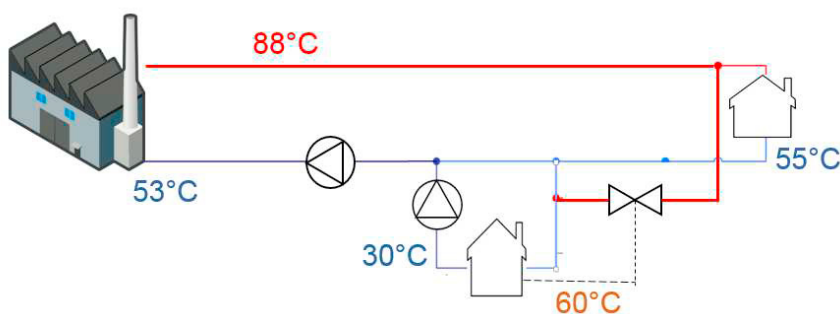


Figure 7: Supplying a consumer connected to the return pipeline - working principal

Results

A week long simulation study was carried out during a typical winter week to compare the differences with and without the branch being supplied from the return pipeline. In Figure 8, the top plot shows a significant reduction in total network distribution heat losses with the branch being supplied from the return. The total energy savings from heat losses over the week period amounted to 3.75MWh which is approximately 12% for the given week.

The bottom plot shows a reduction in mean return temperature as it returns back to the biomass plant with a drop from approx. 58°C to 42°C degrees over the simulation period.

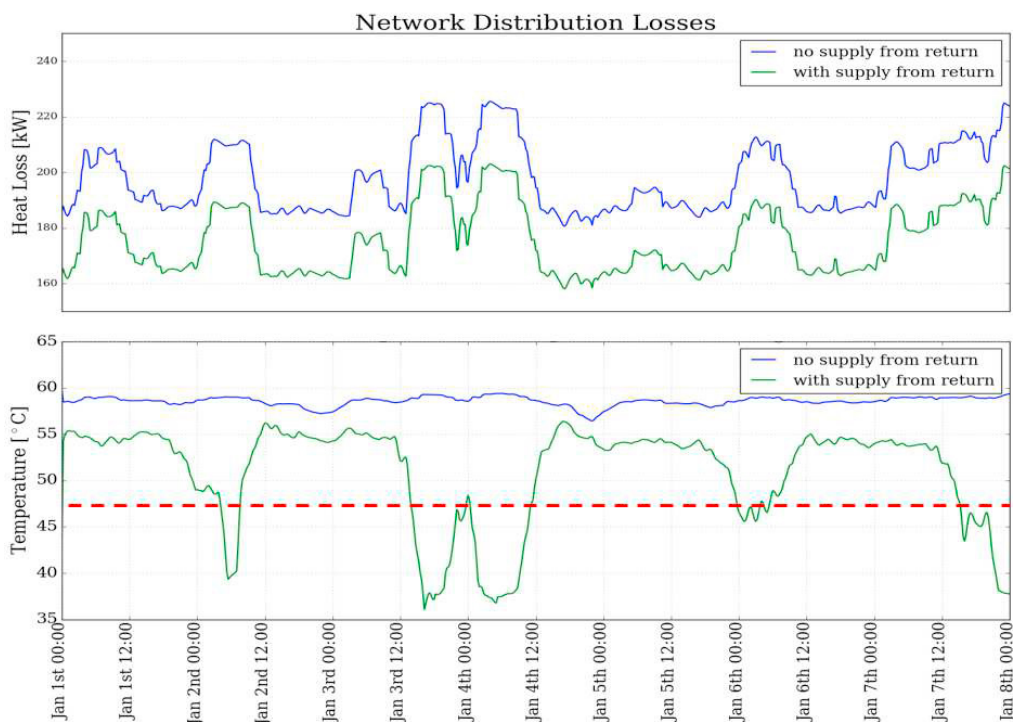


Figure 8: Supply from return result comparison. Top: total network distribution losses. Bottom: Comparison of return temperatures at Biomass production plant

The associated additional pumping energy was also accounted for which amounted to 0.27MWh to maintain the imposed minimum pressure drop of 0.5bar across all consumers while retaining adequate flow circulation throughout the whole network.

The outlined approach above can be used to achieve at least partially lower temperature conditions in existing networks where the targeted consumers are adequately equipped to operate at low temperature conditions.

Conclusions:

We have shown that dynamic modelling in combination with suitable additional scripting tools offers great flexibility and potential to address challenges in the modelling and later control of 4th generation district heating system. We have demonstrated how the impacts of thermal energy storage, large scale solar thermal collector fields and prosumers can be included and how low-temperature branches supplied by the heat from the return pipeline can be evaluated. The next steps in this line of development will be the inclusion of MPC strategies and the reduction of complexity by aggregation to reduce computing time.

References

- [1] Lund, Hendrik, Möller, Bernhard, and Vad Mathiesen, Brian. "The Role of District Heating in Future Energy Systems." *Energy Journal* 35(3) (2010): 1381-1390.
- [2] Lund, Hendrik. et al. "4th Generation District Heating (4GDH) Integrating smart thermal grids into future sustainable energy systems", *Energy Journal* 68 (2014): 1–11.
- [3] Schweiger G, et al. "The potential of power-to-heat in Swedish district heating systems", *Energy Journal* 2017, <http://dx.doi.org/10.1016/j.energy.2017.02.075>
- [4] J. Allegrini, et al. 2015: "A review of modelling approaches and tools for the simulation of district-scale energy systems" *Renewable and Sustainable Energy Reviews*, vol. 52, 1391-1404.
- [5] Fritzson, P. 2015: "Principles of Object-Oriented Modeling and Simulation with Modelica 3.3" 2nd edition. Wiley-IEEE Press, Piscataway, NJ.
- [6] M. Wetter and C. van Treeck, "BIM/GIS and Modelica Framework for building and community energy system design and operation." Presentation of IBPSA Project 1, 2016.
- [7] Schweiger, G. et al. 2017: "District heating and cooling systems – framework for Modelica-based simulation and dynamic optimization, *Energy*, <https://doi.org/10.1016/j.energy.2017.05.115>.
- [8] van der Heijde, Bram & Fuchs, Marcus & Tugores, Carles & Schweiger, Gerald & Sartor, Kevin & Basciotti, Daniele & Mueller, Dirk & Nytsch-Geusen, Christoph & Wetter, Michael & Helsen, L. (2017). "Dynamic equation-based thermo-hydraulic pipe model for district heating and cooling systems". *Energy Conversion and Management*. 151. 158-169. 10.1016/j.enconman.2017.08.072.
- [9] Fuchs M., Streblov R., and Müller D., (2015). Visualising Simulation Results from Modelica Fluid Models Using Graph Drawing in Python. Proceedings of the 11th International Modelica Conference September 21-23, 2015, Versailles, France.



16th International Symposium on District Heating and Cooling, DHC2018,
9–12 September 2018, Hamburg, Germany

Improving the operation of a district heating and a district cooling network

Johannes Oltmanns^{a,b,*}, Martin Freystein^c, Frank Dammal^{a,b}, Peter Stephan^{a,b}

^a*Institute for Technical Thermodynamics, Technische Universität Darmstadt, Alarich-Weiss-Str. 10,
64287 Darmstadt, Germany*

^b*Darmstadt Graduate School of Excellence Energy Science and Engineering, Technische Universität Darmstadt,
Otto-Berndt-Str. 3, 64287 Darmstadt, Germany*

^c*ENTEKA AG, Frankfurter Str. 110, 64293 Darmstadt, Germany*

Abstract

Ongoing research activities at TU Darmstadt aim at improving the energy efficiency of its Campus “Lichtwiese”. In accordance with the national climate protection goals, CO₂ emissions shall be reduced by 80 percent until 2050 compared to the level of 1990. The district heating and cooling networks and the combined heat and power (CHP) generation play a key role in the university’s energy efficiency strategy. The following components for future development are represented in a thermal model of the campus: (1) The cooling supply is switched from compression to absorption chillers supplied with CHP heat, in order to increase the operating time of the CHP plants, especially in the summer. (2) Thermal energy storage along with a predictive control algorithm for the operation of the energy system is implemented to increase the flexibility of the energy supply. This approach also allows to increase the operating time of the CHP plants. (3) The district heating network temperatures, currently depending solely on ambient temperatures, can be reduced considering the heat supply temperature inside the buildings. Thereby, the efficiency of the heat distribution is increased and alternative heat sources can be integrated more easily in the future.

* Corresponding author. Tel.: +49 6151 1622691.

E-mail address: oltmanns@ttd.tu-darmstadt.de

These components are combined in four different scenarios in order to understand their impact on possible CO₂ emissions and primary energy savings compared to the reference scenario. The components can generate significant efficiency gains at reasonable cost and make a contribution to reach the university's climate protection goals.

© 2018 The Authors. Published by Elsevier Ltd.

This is an open access article under the CC BY-NC-ND license (<https://creativecommons.org/licenses/by-nc-nd/4.0/>)

Selection and peer-review under responsibility of the scientific committee of the 16th International Symposium on District Heating and Cooling, DHC2018.

Keywords: District heating operation improvement; combined heat and power; heat demand forecast; thermal energy storage; network temperature reduction

Nomenclature

<i>Symbols</i>		$P_{el,CHP}$	Electric power generation CHP in kW
f_{CO_2}	Total CO ₂ emissions in optimization scenario in tCO ₂	$P_{el,grid}$	Grid electric power demand in kW
$CO_{2,gas}$	CO ₂ emission factor gas in tCO ₂ /MWh	$P_{el,tot}$	Total electric power demand in kW
$CO_{2,grid}$	CO ₂ emission factor grid electric power in tCO ₂ /MWh	t	Point in time in hours
\dot{Q}_{NL}	Thermal network losses in kW	Δt	Time step for simulation (1 hour)
Q_{TES}	Storage heat content in MWh	T_g	Ground temperature in °C
$\dot{Q}_{TES,in}$	Heat flow charging storage in kW	$T_{amb,thr}$	Heating threshold ambient temperature in °C
$\dot{Q}_{TES,out}$	Heat flow discharging storage in kW	T_S	Network supply temperature in °C
$\dot{Q}_{th,CHP}$	Heat generation CHP in kW	η_{TES}	Storage efficiency
$\dot{Q}_{th,boiler}$	Heat generation boilers in kW	$\eta_{tot,CHP}$	Total efficiency CHP
$\dot{Q}_{th,ME}$	Heat demand mechanical engineering in kW	$\sigma_{P,CHP}$	CHP coefficient
$\dot{Q}_{th,tot}$	Total heat demand in kW	<i>Abbreviations</i>	
		4GDH	4 th Generation District Heating
		CHP	Combined Heat and Power
		HPS	Heat and Power Station
		TRY	Test Reference Year

1. Introduction

In order to reach climate protection goals, energy transition and efficiency must not only be tackled on a national, but also on a local level, especially for building heating and cooling purposes. District heating and cooling will play a major role in local energy efficiency strategies in the future, because they are able to connect heat sources and sinks over greater distances, e.g. industrial plants emitting waste heat and residential buildings with heat demand [1]. In order to prepare district energy systems for future changes in energy supply as well as demand, the networks have to be transformed to 4th Generation District Heating (4GDH) as defined in [2]. The idea of 4GDH is to improve the possibility to integrate fluctuating, decentralized and low-temperature heat sources into a district heating system, such as renewable sources or waste heat from industry or data centers. Therefore, network temperatures have to be lowered [3], thermal storage has to be implemented [4] and intelligent control strategies have to be developed [5]. In this paper, we use the case of TU Darmstadt's Campus "Lichtwiese" to evaluate components that make it possible to transform an existing district energy system to 4GDH. We set up four scenarios to compare the impact of the different components in terms of CO₂ emissions and primary energy input to the reference scenario of the 2016 state of the system.

2. The TU Darmstadt Campus Lichtwiese district heating and district cooling networks

TU Darmstadt's Campus Lichtwiese is a typical university campus erected on the outskirts of Darmstadt in the 1960s and expanded repeatedly. In 2016, it comprised 40 buildings with a total net internal area of more than 200000 m² for lecture halls, offices, laboratories, workshops and auxiliary buildings, such as a dining hall and the university heat and power station (HPS). Most buildings were constructed in the 1960s and 1970s, but in recent years, construction activity has increased again and several modern buildings with low energy and temperature demand were added. As of 2016, heat for the campus is supplied using three gas engine combined heat and power (CHP) plants (2 MW_{th} each) as well as six gas boilers (9.3 MW_{th} each). The CHP plants also provide electric power (1.9 MW_{el} each) and generate about 60 % of the electric energy needed at the university. In 2017, the campus energy system was expanded by the construction of a district cooling network.

Currently, an absorption chiller (1 MW) and an additional CHP plant (3.3 MW_{el} / 3.0 MW_{th}) as well as thermal storage are under construction. The campus heat demand is about 23 GWh/a, its electric energy demand 32 GWh/a and its cooling demand 18.5 GWh/a.

TU Darmstadt owns a district heating system with a total length of 28 km, 6.5 km of which connect Campus Lichtwiese (Fig. 1). The district heating supply temperature varies between 65 °C and 110 °C, the return temperature between 45 °C and 75 °C. The new district cooling network operates with a supply temperature of 6 °C and a return temperature of 12 °C. The HPS situated on Campus Lichtwiese does not only supply the campus itself with heat and power, but also other university sites and additional public buildings in the city center of Darmstadt. District cooling on the other hand is only available on campus.

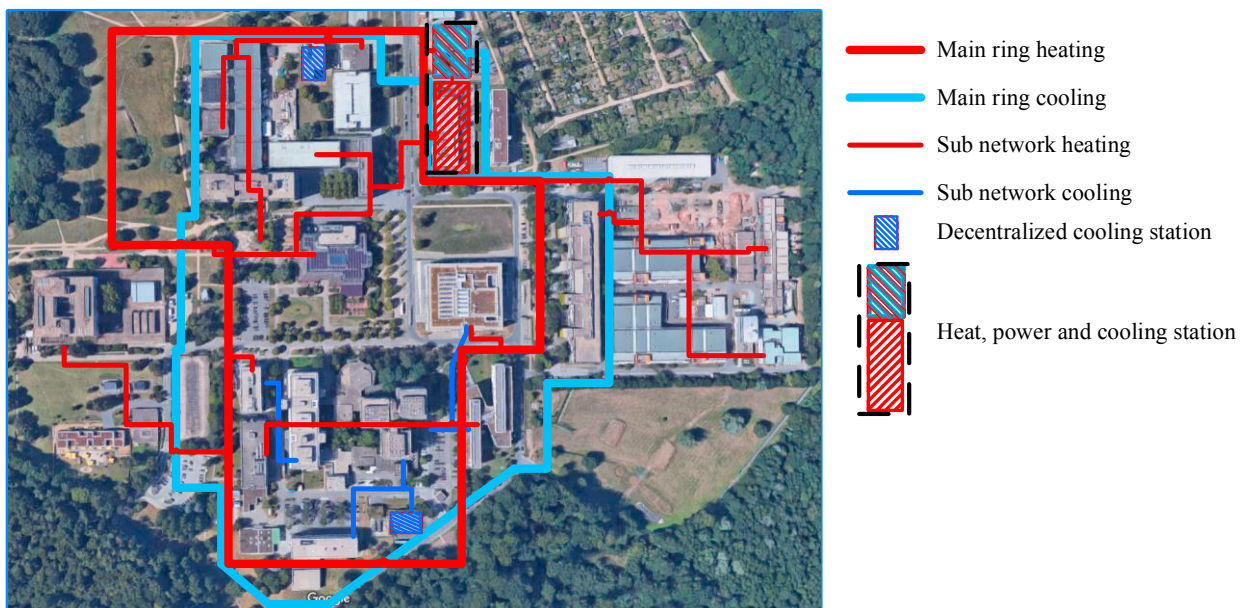


Fig. 1: Campus Lichtwiese District Heating and District Cooling network (adapted from Google Maps)

3. Modeling approach and energy demand profiles

To quantify the impact of possible future adaptations in the energy system, we develop a model of Campus Lichtwiese including heating and cooling generation as well as networks. For modeling purposes, we use MATLAB/Simulink including the CARNOT Toolbox [6].

3.1. District heating model input data

On the heating side, the model serves to calculate network heat losses, temperature distribution across the network, and primary energy input as well as CO₂ emissions to supply the necessary heat and power. Since we focus on the

generation and distribution side of the system, we do not include physical representations of the buildings but rather use hourly heat demand and return flow temperature profiles of each building as model input. Additionally, we use the network supply temperature at the HPS. We calculate the hydraulic losses within the network. The losses in the network itself are small compared to the losses inside the buildings where heat exchangers and room heaters generate the main part of the hydraulic losses. Therefore, we use the literature value of 0.5 % of the building heat demand [7] to account for the electric power demand of the network pump that results from hydraulic losses.

3.2. Standardized profiles for building heat demand and return flow temperatures

Heat demand and return flow temperatures depend on weather conditions, therefore simulation results from different years cannot easily be compared to each other. Accordingly, we transform single year heat demand and temperature profiles to standardized profiles using the test reference year (TRY) weather data [8]. This makes the results of the study independent from weather influences of one specific year. We develop regression models for each building to explain daily heat demand and daily average return temperatures depending on average ambient temperatures. To account for the building heat storage capacity, we consider a weighted ambient temperature including the influence of the three previous days. The regression model we selected is a piecewise function separated at the heating threshold ambient temperature $T_{amb,thr} = 15\text{ °C}$ (Fig. 2). Above this temperature, heat demand only serves for hot water preparation and does not depend on the ambient temperature anymore. We create different regression models for weekdays and weekends since heat demand patterns slightly differ between these cases. We validate the profiles using them to predict heat demand and temperature profiles for real ambient temperatures and comparing them to the measured data (Fig. 3). The annual average deviation between measurement and model in 2017 is about 2-3 %, depending on the building.

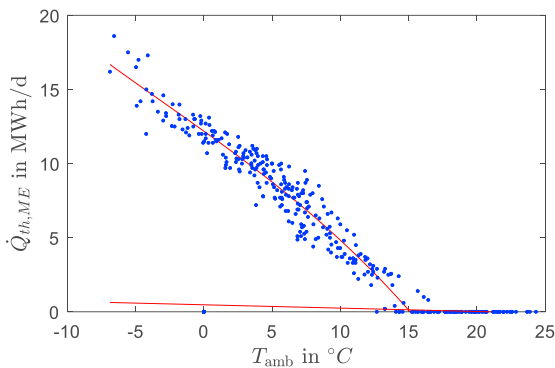


Fig. 2: Regression model for mechanical engineering building

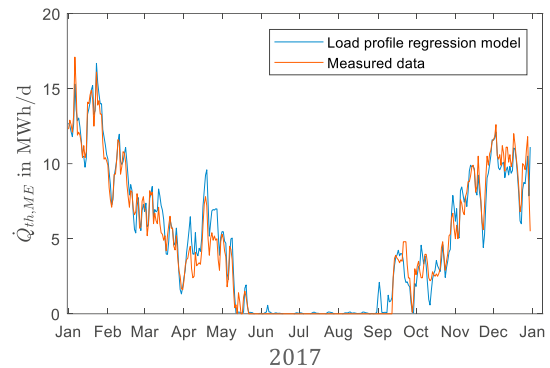


Fig. 3: Regression model validation for mechanical engineering building

3.3. District cooling model input data

Along with the model for the district heating system, we dispose of a model for the district cooling system. We do not yet have detailed information on the cooling demand of individual buildings but rely on one aggregated load profile for the whole campus. The main cooling demand originates from the data center and from experiments in chemical or material research. For the data center, the cooling demand is approximately $\dot{Q}_{cool} = 500\text{ kW}$. For the other main users, we calculate the cooling demand using supply and return temperatures which are available in the university's building control system. For all remaining buildings, we estimate the cooling demand calculating the impact of internal and external heat sources according to VDI 2078 [9]. We combine all sources available to generate an overall annual load profile for the campus. Considering the fact that detailed cooling load profiles are not available for all buildings, it does not make sense to establish a detailed model of the cooling network representing the physical setup in detail. Instead, we opted for an aggregated modeling approach and do not calculate temperature and mass flow distribution in the network but only cooling energy. We also neglect thermal losses in district cooling as network temperatures are in the range of the ground temperature ($T_g = 10\text{ °C}$ for Darmstadt) and losses due to heat input into the network are very small. On the other hand, hydraulic losses play a more important role in district cooling than they do in district

heating. Due to the same reasons as mentioned for the heating case, also here we consider a literature value of 2 % of the cooling demand [7] as the electric power demand for the district cooling network pump.

3.4. Electric power input data

To account for the overall electric power demand, we rely on measurement data recorded at the transformers on Campus Lichtwiese in 2016. TU Darmstadt electric power bills show that this campus represents about half the university's electric power demand, so we double the measurement data available to account for the total electric power demand we feed into our model.

3.5. Cost calculation

Along with primary energy input and CO₂ emissions, our model is also able to calculate the operational costs of the energy generation. Because costs depend highly on the specific regulatory framework in Germany, we will not present cost related results in this paper.

4. Modeling future network components

We now want to introduce the future network components we investigate to improve the campus energy system. Some of these components are already in the course of implementation; others serve as ideas for future adaptations of the system. In this context, we concentrate on the potential savings of CO₂ emissions and primary energy input in operation. CO₂ emissions and primary energy input to produce new equipment are not considered.

4.1. Summer use of CHP heat via absorption chillers

Centralized cooling via absorption chillers is already in the course of implementation. TU Darmstadt is currently installing a 1 MW absorption chiller that connects heating and cooling generation using CHP heat as its input. This makes it possible to increase CHP heat and power generation, especially in the summer, when formerly heat demand was too low to operate the CHP plants and electric power had to be supplied by the grid. To reflect the system integration, we merge the models for heating and cooling into one combined simulation model. Although absorption cooling provides a significant part of the cooling demand in the future system, compression cooling will keep on playing an important role during wintertime, when the CHP plants are running at full load. Using the absorption cooling machines would mean to use boiler heat for cooling purposes, which is not favorable in terms of primary energy input or CO₂ emissions. Therefore, we consider absorption cooling only when excess CHP capacity is available after supplying the heating demand.

4.2. Integration of a central heat storage

Integrating a central heat storage serves to increase the share of CHP heat and power generation and control the maximum peak in the heat and power plant's gas demand. The storage technology we consider is a stratified sensible water storage, which can store heat at temperatures up to about 150 °C at the network's pressure level (5.3 bar) and at very low cost. In order to investigate the potential of improved operating strategies, we consider a storage volume of 2,200 m³, which allows storing heat for about 12-24 hours in spring and fall, depending on the heat load demand and the required temperatures. The storage is used to store CHP heat exclusively due to the high efficiency of the combined generation compared to the alternative of grid electric power and boiler heat.

We integrate the heat storage into our system using an intelligent prediction and optimization algorithm. The goal of the optimization is to supply the necessary heat load using the available generation and storage units in a way that minimizes CO₂ emissions. Before we can optimize the system operation, we first need to predict the overall heat load over the time horizon for which we want to create flexibility, in our case 24 hours. A longer horizon would only make sense if we considered a much bigger storage in order to not only disconnect heat supply and demand on a daily basis but also account for differences between weekdays and weekends or even seasonal patterns. If we did not predict the heat demand for our time horizon and were to optimize the system's operation for each point in time individually, the storage would be discharged whenever possible. This would be the optimal solution for each individual step but not

the global optimum for a whole day. We carry out the heat load prediction in a separate, simplified and linearized model calculating only heat generation instead of the detailed temperature and mass flow calculation of the main model. Additionally, the prediction model uses a multiple polynomial regression model to account for the network heat losses instead of a detailed simulation of these losses.

In order to be able to find global optima and to reduce simulation time, we apply a linear optimization algorithm. Our objective function states:

$$f_{CO_2} = CO_{2,gas} \cdot \frac{Q_{th,CHP} + W_{el,CHP}}{\eta_{tot,CHP}} + CO_{2,gas} \cdot \frac{Q_{boiler}}{\eta_{boiler}} + CO_{2,grid} \cdot W_{el,grid} \quad [t_{CO_2}] \quad (1)$$

We have to obey the following constraints:

$$\dot{Q}_{th,CHP}(t) + \dot{Q}_{th,boiler}(t) - \dot{Q}_{TES,in}(t) + \dot{Q}_{TES,out}(t) = \dot{Q}_{th,tot}(t) + \dot{Q}_{NL}(t) \quad [kW] \quad (2)$$

$$P_{el,CHP}(t) + P_{el,grid}(t) = P_{el,tot}(t) \quad [kW] \quad (3)$$

$$Q_{TES}(t - \Delta t) \cdot \eta_{TES} + \dot{Q}_{TES,in}(t - \Delta t) \cdot \Delta t - \dot{Q}_{TES,out}(t - \Delta t) \cdot \Delta t = Q_{TES}(t) \quad [MWh] \quad (4)$$

$$\dot{Q}_{th,CHP}(t) \cdot \sigma_{P,CHP} = P_{el,CHP}(t) \quad [kW] \quad (5)$$

$$P_{el,CHP} \leq P_{el,tot} \quad [kW] \quad (6)$$

For each hourly time step, we predict and optimize the operation for the next 24 hours, but only use the result for one step and return to do the same exercise again after simulating one step in the main model using the optimization result (receding horizon).

4.3. Decrease of network temperatures

Lowering the district heating network temperatures is the last approach we investigate to improve the Campus Lichtwiese energy system. As stated in numerous publications on 4th Generation District Heating [2,3,10,11], lower network temperatures are the key factor to prepare district heating for a sustainable future. Lower temperatures decrease heat losses in the network itself and, very importantly, make it possible to integrate low temperature renewable heat sources such as solar, geothermal, or waste heat. Waste heat integration from industrial processes or data centers is especially interesting because it saves energy twice, for heating as well as for cooling of the processes considered [12]. Nowadays, such concepts often fail due to a lack of adequate sinks for waste heat with suitable heat and temperature demand. The lower the network temperatures get, the easier it becomes to use a district heating network to distribute heat from alternative energy sources. On the supply side, temperature depends on the temperature demand of the most critical building and can be controlled centrally in the heat and power station. To determine necessary temperatures at Campus Lichtwiese, we compare primary side supply temperatures to secondary side supply temperatures increased by 4 K to account for the necessary temperature difference at the heat exchangers. This comparison reveals that throughout the year, primary side supply temperatures are 5-20 K higher than secondary side supply temperatures at the most critical building even after considering heat exchanger losses and are decreased before reaching the room heaters via a return flow addition. Therefore, even without energetic renovation of the buildings or the installation of new heaters, network supply temperatures could be decreased considerably (Fig. 4). On the return side, preliminary investigations for representative buildings have revealed that building return temperatures could be decreased by 10-15 K with only small adaptations on the heat transfer system inside the buildings. In the context of this study, we consider a return temperature reduction of 10 K for all buildings.

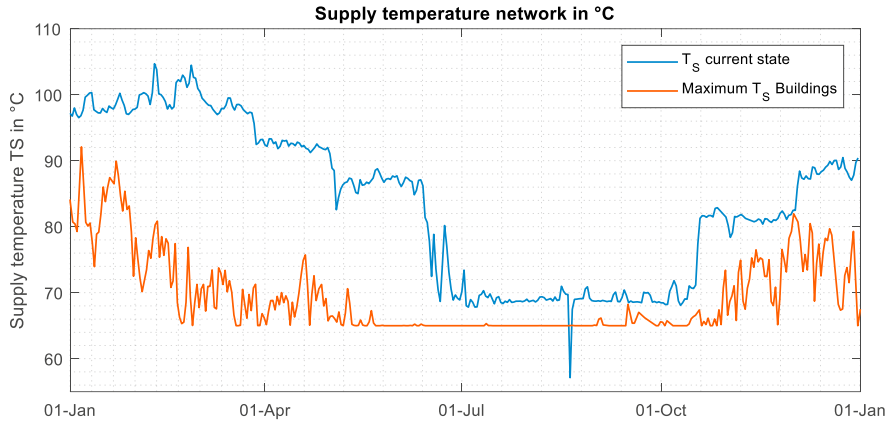


Fig. 4: Comparison of primary and secondary side supply temperatures

5. System adaptation scenarios

To compare the impact of the different future components, we set up five different scenarios:

- Reference scenario: The reference scenario is based on the 2016 campus energy system setup without absorption cooling, thermal storage, unrefurbished CHP plants and high network temperatures (*ref*)
- Absorption chiller scenario: Fully connected system with new CHP plants and cooling generation based on CHP heat via absorption chillers (*absorp*)
- Temperature reduction: New CHP plants, decreased supply temperatures and exploitation of return flow temperature reduction potential (ΔT)
- TES scenario: New CHP plants and integration of a heat storage as well as application of a predictive optimization algorithm for the operation of the energy system (*TES*)
- Combination scenario: Combination of all proposed components (*comb*)

Table 1 shows which ones of the future network components are integrated in which scenario:

Table 1. Investigated scenarios

	Old CHP	New CHP	High Temp.	Low Temp.	Absorp. Chiller	TES
<i>ref</i>	X		X			
<i>absorp</i>		X	X		X	
ΔT		X		X		
<i>TES</i>		X	X			X
<i>comb</i>		X		X	X	X

For the calculation of primary energy input and CO₂ emissions, we use the factors listed in Table 2:

Table 2. Primary energy and CO₂ emission factors

Factor	Value	Source
Primary energy factor grid electric power	1.8	[13]
Primary energy factor gas	1.1	[14]
CO ₂ emissions factor grid electric power	0.527 t _{CO2} /MWh	[15]
CO ₂ emissions factor gas	0.202 t _{CO2} /MWh	[16]

6. Results and Discussion

As we explained in chapter 1, the HPS supplies heat and power not only to Campus Lichtwiese itself, but also to other sites around the city. In order to model the supply side, we need to consider the entire thermal and electric energy demand of all buildings connected to the district heating system. However, to show the impact of our future components correctly, it makes sense to concentrate on the results for Campus Lichtwiese where they are applied. Therefore, based on simulation results, we calculate the share for Lichtwiese in primary energy input and CO₂ emissions based on the distribution of heat, cooling and electric energy demand between Lichtwiese and the rest of the university energy system. Fig. 5 shows the primary energy savings and Fig. 6 the CO₂ emissions savings for Campus Lichtwiese in the four scenarios we considered compared to the 2016 reference case.

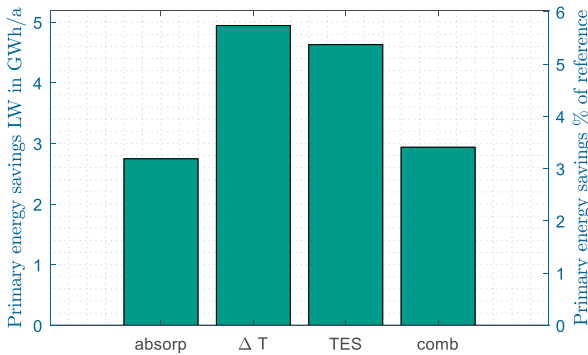


Fig. 5: Comparison of the yearly primary energy input

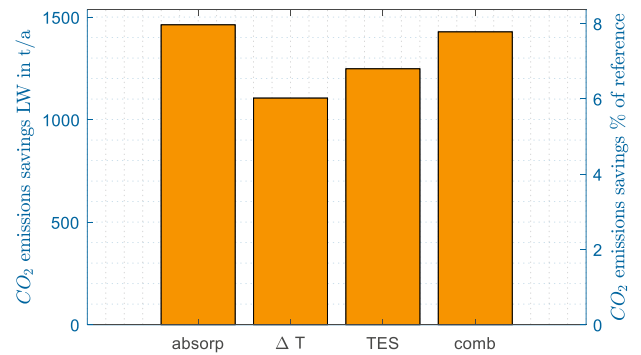


Fig. 6: Comparison of the yearly CO₂ emissions

Uncertainties in the results arise from uncertainties in the input data. We dispose of data on heat demand with a resolution of 100 kWh/h, but we are not able to validate our data appropriately since generation data from our heat and power station is not available. Although data availability on cooling demand is also still limited, this will soon become easier because along with the district cooling ring a more detailed building-wise metering of cooling demand was installed.

The results show that all improvement scenarios allow cutting primary energy input by about 5 % and CO₂ emissions by up to 8 % compared to the 2016 reference case. We now want to take a closer look at the differences between the scenarios. Load profiles presented in this section represent TU Darmstadt as a whole but conclusions drawn from them apply to Campus Lichtwiese equally.

Although reduction potential is quite similar across all scenarios, the strategies applied to improve the system differ, especially between the absorption chiller (*absorp*) and the temperature reduction (ΔT) scenario. The absorption chiller scenario focuses on the integration of new equipment on the generation side to increase the efficiency of the energy supply, while the temperature reduction scenario decreases the heat demand by lowering network temperatures. The

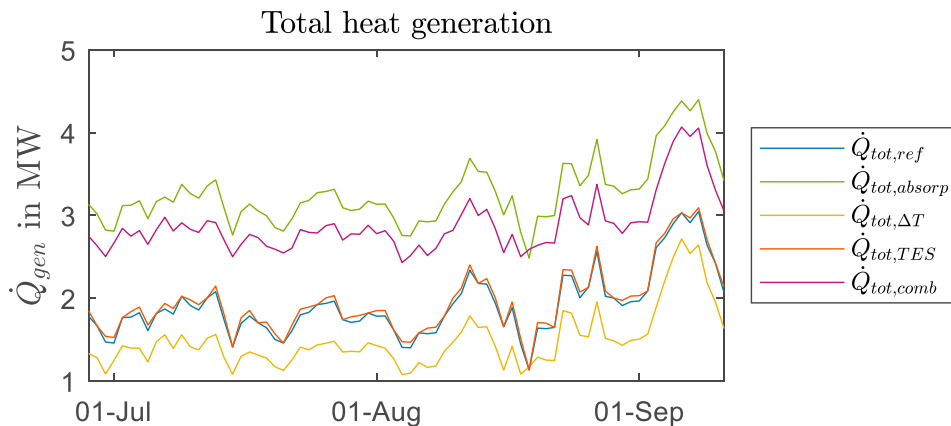


Fig. 7: TU Darmstadt total heat generation July-September

effects of these different approaches become clear when looking at the summer period of the total heat generation (Fig. 7).

In the absorption chiller scenario, heat generation increases compared to the reference scenario due to the additional heat demand for absorption cooling. On the other hand, in the temperature reduction scenario, network losses are decreased and therefore heat generation is lower than in the reference case. We reveal the major disadvantage of the decrease in heat demand due to lower network temperatures in Fig. 8: it leads to a major increase in summer grid electric power demand.

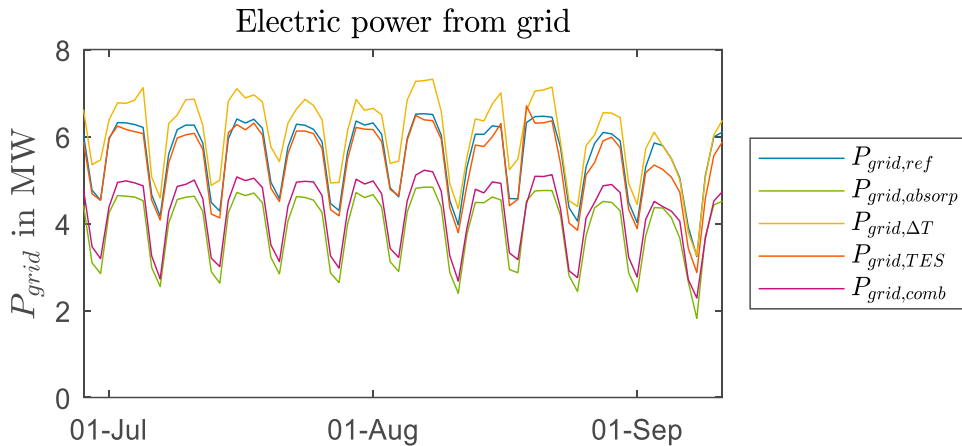


Fig. 8: Grid electric power demand TU Darmstadt July-September

In terms of primary energy input, the temperature reduction scenario is favorable, because the primary energy factor for grid electric power is only 60 % higher than the one for gas (Fig. 5). The CO₂ emissions factor for grid electric power is 160 % higher than the one for gas, so on the CO₂ emissions side, the increased grid electric power demand in the temperature reduction scenario has a lot more of a negative impact (Fig. 6).

In wintertime, the differences are a lot smaller. Absorption cooling is not running because the entire CHP capacity is necessary to supply the district heating demand and network losses represent a much smaller share in the overall heat generation. Therefore, in the winter months, differences between the scenarios in terms of heat generation are almost negligible (Fig. 9).

Storage integration and operation optimization (TES scenario) only have an impact in short periods in the spring and in the fall (Fig. 10). In wintertime, the CHP plants run at full load and no extra capacity is available to store heat. In the summer, heat demand is always lower than the CHP capacity, so the storage remains fully charged.

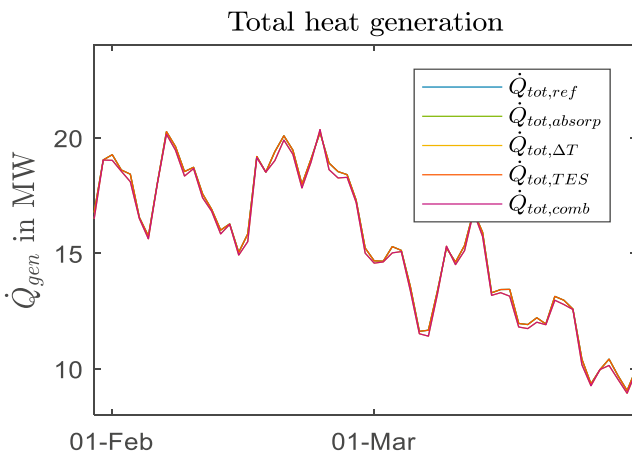


Fig. 9: Total heat generation TU Darmstadt February-March

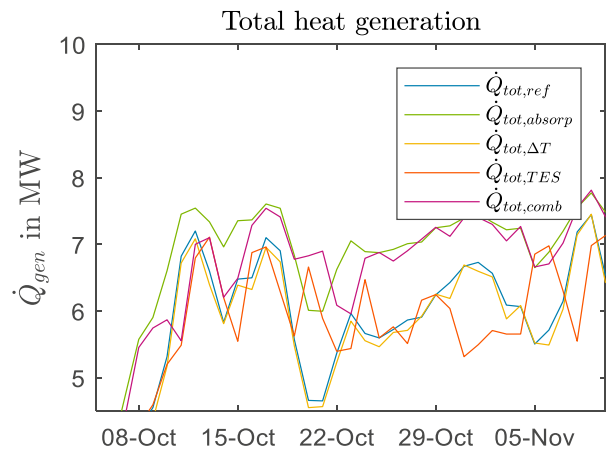


Fig. 10: Total heat generation TU Darmstadt October-November

The results show that we cannot lower yearly gas demand peaks in the current setup of the system. The maximum peak appears in February when the CHP plants already operate at full capacity (Fig. 9). In order to have an impact on the yearly maximum peak, it would be necessary to accept to store boiler heat as well. The results also show that a combination of all future components (combination scenario *comb*) does not lead to the best solution in terms of primary energy input and CO₂ emissions, but rather represents a tradeoff between the previously discussed scenarios due to the effects we just explained (Fig. 5 and Fig. 6).

7. Conclusion and Outlook

The goal of this study was to compare different scenarios to improve the operation of the district heating and district cooling at TU Darmstadt. All scenarios create reductions compared to the reference scenario in terms of the indicators we investigated. Comparing the scenarios among each other, a district heating network temperature reduction leads to lower primary energy input and higher CO₂ emissions while the integration of absorption cooling has the opposite effect. This is due to the major bottleneck in the system: the electric power demand. As long as the electric power demand remains the same, decreases in heat demand will always lead to higher grid electric power demand that generates high primary energy demand and CO₂ emissions. This will only change if the share of renewables in the electric power mix is increased considerably or if electric power demand is decreased on the local level, especially in the summer. We shall also not forget that a network temperature reduction does not only affect heat generation but is a prerequisite for the integration of waste heat and renewables into the system. Future improvements in the system are therefore strongly connected to further reductions in network temperatures.

The model and the simulation results we presented in this paper give us a good understanding of the Campus Lichtwiese energy system. In the future, we will build upon these results and perform sensitivity analyses on key parameters considered as predetermined in this context, such as the heat storage size or the prediction horizon for the optimization. This will make it possible for us to understand if more flexibility through extended storage periods of weeks or even seasonal storage could generate additional benefits. In addition to this, we want use our model to determine the impact of an integration of decentralized heat sources on the system as a whole, such as waste heat from the university's data center located on campus.

8. Acknowledgement

The Technische Universität Darmstadt is funded for this research by the German Federal Ministry of Economic Affairs and Energy (BMWi) in the project “EnEff:Stadt Campus Lichtwiese” (03ET1356A). Further financial support comes from the DFG in the framework of the Graduate School of Excellence Energy Science and Engineering (GSC 1070).

References

- [1] Bühler F, Petrović S, Karlsson K, Elmegaard B. Industrial excess heat for district heating in Denmark. *Applied Energy* 2017;205:991–1001.
- [2] Lund H, Werner S, Wiltshire R, Svendsen S, Thorsen JE, Hvelplund F, Mathiesen BV. 4th Generation District Heating (4GDH). *Energy* 2014;68:1–11.
- [3] Rämä M, Sipilä K. Transition to low temperature distribution in existing systems. *Energy Procedia* 2017;116:58–68.
- [4] Verda V, Colella F. Primary energy savings through thermal storage in district heating networks. *Energy* 2011;36:4278–86.
- [5] Rosemann T, Löser J, Rühling K. A New DH Control Algorithm for a Combined Supply and Feed-In Substation and Testing Through Hardware-In-The-Loop. *Energy Procedia* 2017;116:416–25.
- [6] Solar-Institute Juelich of the FH Aachen. *CARNOT Toolbox Version 6.1*; 2016.
- [7] Frederiksen S, Werner S. *District heating and cooling*. Lund: Studentlitteratur; 2013.
- [8] Deutscher Wetterdienst. *Ortsgenaue Testreferenzjahre von Deutschland für mittlere, extreme und zukünftige Witterungsverhältnisse*. Offenbach; 2017.
- [9] Verein Deutscher Ingenieure. *VDI 2078: Calculation of thermal loads and room temperatures*. Berlin: Beuth Verlag; 2015.
- [10] Schmidt D, Kallert A, Blesl M, Svendsen S, Li H, Nord N, Sipilä K. Low Temperature District Heating for Future Energy Systems. *Energy Procedia* 2017;116:26–38.
- [11] Nord N, Løve Nielsen EK, Kauko H, Tereshchenko T. Challenges and potentials for low-temperature district heating implementation in Norway. *Energy* 2018;151:889–902.
- [12] Wahlroos M, Pärssinen M, Manner J, Syri S. Utilizing data center waste heat in district heating – Impacts on energy efficiency and prospects for low-temperature district heating networks. *Energy* 2017;140:1228–38.
- [13] Bundesrepublik Deutschland. *Verordnung über energiesparenden Wärmeschutz und energiesparende Anlagentechnik bei Gebäuden: EnEV*; 2014.
- [14] Deutsches Institut für Normung e.V. *DIN V 18599-1: Energetische Bewertung von Gebäuden*. Berlin: Beuth Verlag; 2011.
- [15] Umweltbundesamt. *Entwicklung der spezifischen Kohlendioxid-Emissionen des deutschen Strommix in den Jahren 1990 - 2016*. Dessau; 2017.
- [16] Umweltbundesamt. *CO₂-Emissionsfaktoren für fossile Brennstoffe*. Dessau; 2016.



16th International Symposium on District Heating and Cooling, DHC2018,
9–12 September 2018, Hamburg, Germany

Introduction of small-scale 4th generation district heating system. Methodology approach

Ieva Pakere^{a*}, Francesco Romagnoli^a, Dagnija Blumberga^a

^a*Institute of Energy Systems and Environment, Riga Technical University, Azenes street 12/1, Riga*

Abstract

In nowadays, increased energy efficiency in buildings and reduced thermal energy consumption requires innovative solutions and appropriate district heating system development planning process. 4th generation district heating system is one of the key solutions for improved overall system efficiency by decreased heat losses, improved heat generation efficiency, more efficient use of renewable energy sources and other advantages. The article describes the approach and the methodology for development of strategy to transform the existing DH system to 4GDH system particularly in cases with low DH systems loads. Two factors (low heat load and low temperatures) are becoming more and more actual.

The article analyses the transformation process of the particular small-scale DH system in a parish located in the East part of Latvia. As a result, several transformation scenarios are identified. The technical solutions include replacement of a boiler, heating network reconstruction, heat supply temperature lowering and solar panel installation. Further technical analyses is carried out for system development evaluation and strategy implementation. Results shows that it is essential to evaluate the future energy efficiency measures in buildings when such small scale system is evaluated as it results in lower heat density and higher specific heat losses.

© 2018 The Authors. Published by Elsevier Ltd.

This is an open access article under the CC BY-NC-ND license (<https://creativecommons.org/licenses/by-nc-nd/4.0/>)

Selection and peer-review under responsibility of the scientific committee of the 16th International Symposium on District Heating and Cooling, DHC2018.

Keywords: 4th generation district heating, energy planning, solar power, primary energy, shrinking municipalities

Nomenclature

DH- district heating

4GDH – 4th Generation District Heating

PEF –Primary Energy Factor

PEF_{solar} –Primary Energy Factor for system with integrated PV panels;

E_j – the amount of the primary energy for heat production consumed;

E_{el} – the amount of primary energy for power consumption coverage;

$f_{p,j}$ - the primary energy factor related to an energy source;

$f_{p,el}$ - the primary energy factor for the power plants;

E_{del} - the amount of energy delivered to the consumers.

1876-6102 © 2018 The Authors. Published by Elsevier Ltd.

This is an open access article under the CC BY-NC-ND license (<https://creativecommons.org/licenses/by-nc-nd/4.0/>)

Selection and peer-review under responsibility of the scientific committee of the 16th International Symposium on District Heating and Cooling, DHC2018.

10.1016/j.egypro.2018.08.219

1. Introduction

Introduction of 4th Generation District Heating (4GDH) System with lower heat transfer media temperature and integrated renewable energy sources is one of the key solutions for sustainable development of existing district heating (DH) systems. In nowadays, increased energy efficiency in buildings and reduced thermal energy consumption requires innovative solutions and appropriate system development planning process [1]. Therefore, there is several other reasons for decreased heating loads such as shrinking municipalities and prosumers approach. This requires searching for economically and environmentally beneficial solutions for development of such changing DH systems. Lowered heating network temperature is one of the key aspects for improved overall efficiency by decreased heat losses, improved heat generation efficiency, more efficient use of renewable energy sources and other advantages [2, 3].

When planning lowered heat transfer temperature in the new housing areas it is relatively simple to adjust the internal space heating and domestic hot water preparation system according the required temperature levels in design phase. However, when implementing LTDH in existing buildings it requires innovative technical solutions to ensure the necessary thermal comfort [4].

Jengsten et.al [5] has studied the actual supply temperatures and heat transfer areas of radiators in Gotheburg. Those are the key parameter, which should be taken into account when lowering the supply temperature in buildings with a radiator space heating. Authors conclude that buildings in the particular district require energy efficiency measures for the heat demand reduction as well as an increase of the radiators' heat transfer surfaces to enable lower operating temperatures. Nevertheless, another study by Tunzi et.al. [6] proposes the method for the optimal regulation of the existing radiator system according the optimal temperature level which can allow reducing the space heating supply temperature without any other particular system adjustments.

Kofingher et.al. [7] offer to implement the energy-cascades between different types of buildings in order to lower the return water temperature. This is possible when aligning the DH return flow from high-temperature consumers with the supply flow for low-temperature consumers. Authors conclude that energy cascades can ensure the return flow reduction up to 10K and improve the overall system efficiency.

As system approach is essential to develop smart DH system, several authors have studied the transition process from traditional DH system to more efficient 4GDH system [8,9]. Ziemele et.al [10] has developed the multi-perspective methodology to compare different DH system development scenarios to move toward 4GDH. The methodology allows evaluating the development perspectives from the different interested parties' point of view. The methodology of transition process dynamic analyses evaluation has been proposed by Volkova et.al [11]. Authors focuses on transition process monitoring in past and present in order to identify the weak links in the system.

Municipalities are one of stakeholders who has important role in DH transformation course. Therefore, the DH system development strategy can be a significant changing point to create the energy efficient energy supply system [12-13].

The article describes the methodology for development of strategy to transform the existing DH system to 4GDH system. The main focus group is municipality who has the opportunities to support innovative solutions. The methodology includes several modules, which allows identifying most suitable development scenarios. The particular scenarios are compared with the existing DH system scenario (Base scenario) in order to evaluate the technical feasibility.

2. Methodology

The transformation of the existing DH system to 4GDH requires careful planning process from the involved stakeholders. The municipalities are one of main interested parties of this system development. Therefore, local authorities should follow the methodology to achieve effective heat supply in accordance with specific local conditions.

As a first step, it is important to analyse the overall heat supply system of the municipality to obtain the information about main networks, building structures, heat densities, heat production plants etc. Such analyses can also include the building age, depreciation periods and the upcoming investments. Therefore, it is important to identify the main stakeholders and key actors that have an impact on the overall DH system development.

When the general overview of the particular urban or rural area is obtained, the next step is to search for the most suitable long-term development path of heat supply. When comparing different technological solutions it is necessary to consider if the framework conditions will change in future, what are the economical, ecological, and social implications involved.

When the common guiding principles for DH transformation are designed, the particular district as a pilot case study can be chose. There are several selection criteria such as high energy efficiency and renewable energy implementation potential, suitable framework conditions, need for reconstructions etc.

Further, more detailed analyses needs to be carried out for the particular pilot case in order to set the goals, develop strategies and evaluate technical alternatives. The onsite measures, input data analyses and mathematical model development are the main methods used for such investigation. Figure 1 shows the methodology for pilot case analyses. The main input data for this stage are building state of modernisation, total and specific heat and power consumption. In addition, the heat production data is required (CO₂ emissions, type of heat supply, production efficiency etc. technical information). The energy balance sheet is one of the main outputs that should include both heat demand and CO₂ emissions.

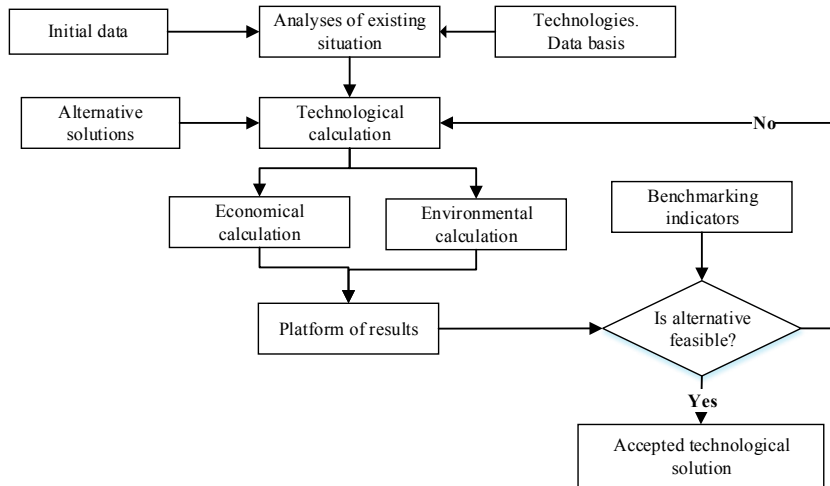


Fig.1. Pilot case investigation methodology

The transformation potential and different development alternatives can be determined after the technological calculations of the particular pilot case. In order to compare those alternatives, different indicators can be used. For particular pilot case analyses, primary energy factor has been calculated. Primary energy factor (PEF) is an energy indicator used for quantifying the primary energy use of a system [14]. PEF is defined as follows:

$$PEF = \frac{\sum_j E_{h,j} f_{p,h} + E_{el} f_{p,el}}{E_{del}} \quad (1)$$

where

E_j – the amount of the primary energy for heat production consumed, MWh;

E_{el} – the amount of primary energy for power consumption coverage, MWh;

$f_{p,j}$ - the primary energy factor related to an energy source;

$f_{p,el}$ - the primary energy factor for the power plants;

E_{del} - the amount of energy delivered to the consumers MWh.

Table 1. Primary energy factors used for scenario evaluation

Energy source	Primary energy factor
Biomass	0.2
Power from grid	1.5
Power from solar energy	0

Table 2 shows the primary energy factors used for calculations. PEF are compared and those are further justified in order to find the most feasible technical solution, which can be then implemented, into the particular district.

3. Results

The methodology is applied and tested on the particular DH system in Latvia. The chosen case study is a parish located in the East part of country. Due to decreasing number of inhabitants and recently accomplished energy efficiency measures in building it was necessary to redesign the existing inefficient DH system. Detailed analyses according methodology described above has been applied for the particular parish. As a result, several transformation scenarios are identified. The technical solutions include replacement of boiler, heating network reconstruction, heat supply temperature lowering and solar panel installation. Further technical analyses is carried out for system development evaluation and strategy implementation.

The DH network scheme of the parish can be seen in Fig.2. The DH network has been redesign completely in order to increase the heat density and reduce heat losses. In order to optimize the heat pipe length, four private houses has been switched from the DH network to individual heating system. In addition, the location of boiler house has been changed and new pellet boiler house is integrated into the system.

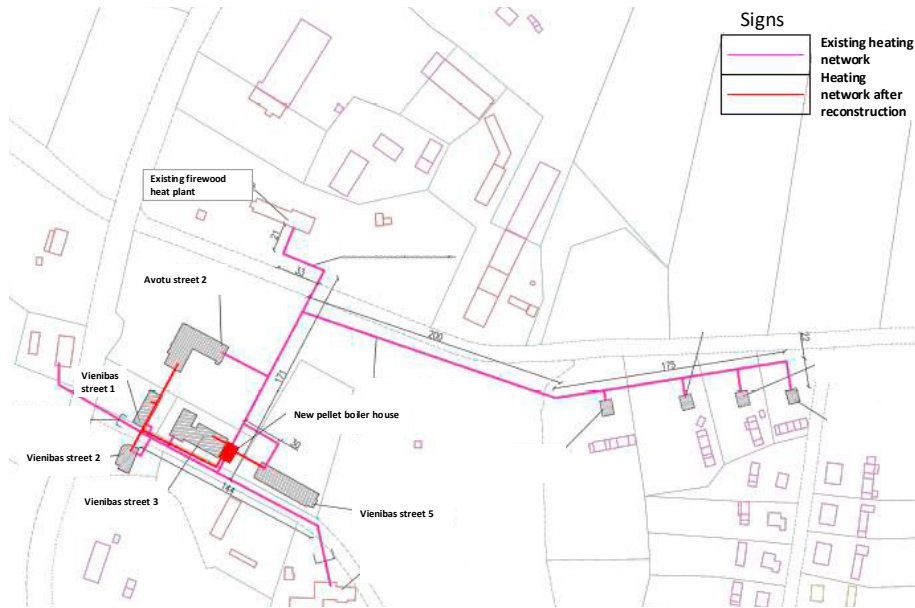


Fig.2. Pilot case DH network before and after reconstruction

After the DH network reconstruction only five buildings will be connected to the system. The heat density increases from 1.1 MWh/m to 2.8 MWh/m after reconstruction. Table 2 shows the overview of the building types, area and specific heat consumption for space heating. Most of buildings experienced energy efficiency measures recently, therefore only apartment building has high specific heat consumption compared to standard in Latvia that is 80 kWh/m² per year. Therefore, two different scenarios are analyzed for further development of scenarios. In Base scenario the heat consumptions remains constant. In energy efficient (EEF) scenario it is assumed that heat losses from apartment building will be reduced due to insulation works and the specific heat consumption will decrease by 60% to 80 kWh/m².

Table 2. Overview of buildings connected to DH system after reconstruction

Nr.	Address	Type	Insulated	Area, m ²	Specific heat consumption, kWh/m ²
1	Avotu street 2	Kindergarten	Yes	1614	75
		Mail			
		Local authority			
2	Vieniabas street 2	Shop	Yes	229	88
3	Vieniabas street 1	Recreational, utility room	No	277	65
4	Vieniabas street 3	Cultural house	Yes	723	125
5	Vieniabas street 5	Apartment building	No	1224	192

Figure 3 shows the heat load duration curves for both scenarios. It can be seen that heat capacity in EEF scenario reduces to 150 kW by comparing to 200 kW in Base scenario. In the particular parish heat is provided only for space heating and there is no heat load in summer period.

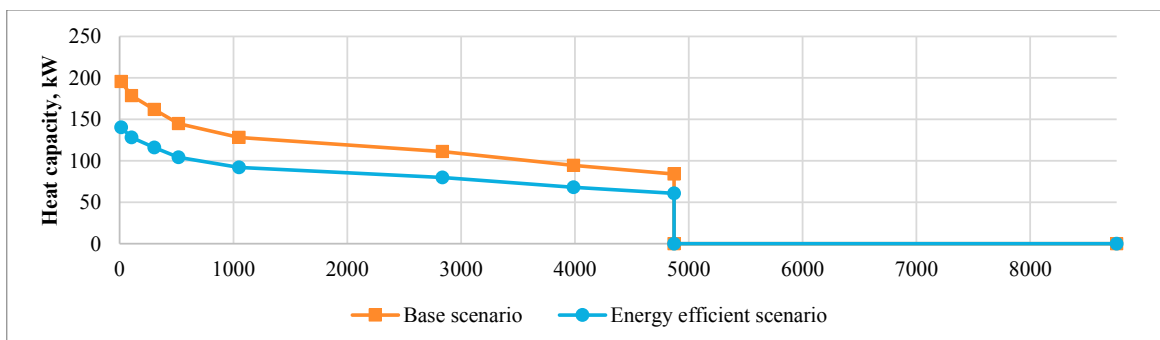


Fig.3. Heat load duration curve

An essential aspect to approach 4GDH is to lower heating network temperature. Therefore, it is considered to reduce supply and return water temperature from 90°C/60 °C to 60°C/35°C. The heating network temperature curve is shown in Figure 4. It has been considered that heating system in renovated buildings remains the same as before the renovation. Therefore, the surface area of installed heating elements would allow to reduce the supply water temperature without any other additional change of operational parameters [6]. In case of apartment building in BS when no energy efficiency measures are considered, it would require to consider energy cascade [7] or other solutions for supply temperature lowering to be possible.

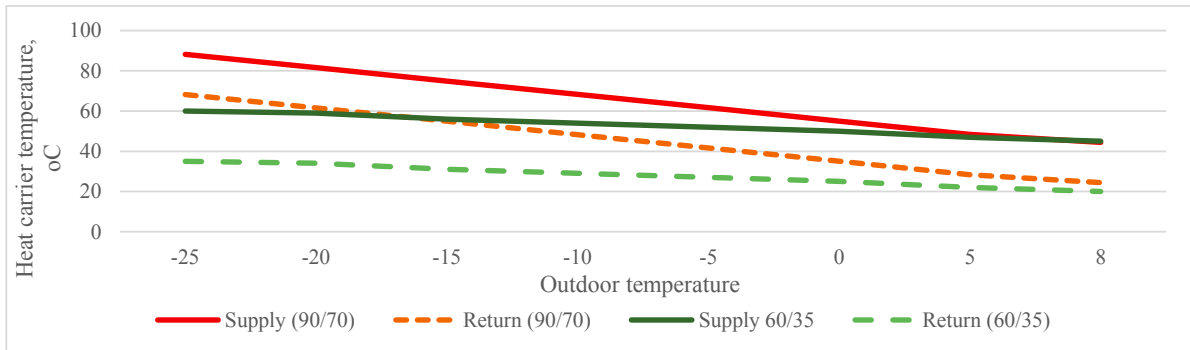


Fig.4. Heat carrier temperature curves for standard and low temperature system

Therefore, four different technical alternatives regarding building heat consumption and temperature levels in DH network have been identified for the further development of particular parish. In order to compare and evaluate those alternatives, the heat losses and heat density have been used as technical indicators.

In addition, it has been considered to install the PV panels for power production and building power consumption coverage. The total power consumption in buildings and boiler house is 33 MWh per year. It would require 9 kW of PV panel to cover such consumption in summer period (see Figure 5). The assumed PV efficiency is 15% and annual solar radiation is 973 kWh/m².

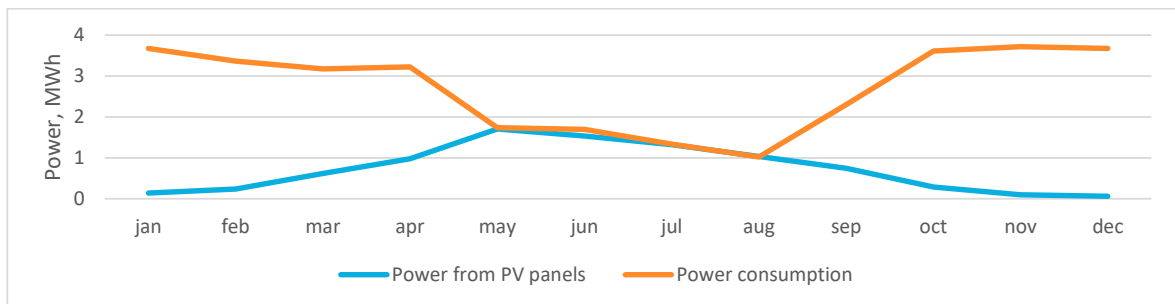


Fig.5. Power consumption and solar power production duration

Table 3 shows the results of technical calculations. It can be seen that in EEF scenario, when energy efficiency measures are considered, the heat consumption and heat density decreases, therefore specific heat losses in heating network increases. Reduced heating network temperature is a solution for optimal operation of DH system in such conditions.

Table 3. Technical calculation for different scenarios

Scenario	Heat consumption, MWh per year	Heat density, MWh/m	Heat losses, MWh	Heat losses, %	Power consumption, MWh	Solar power, MWh	PEF	PEF _{Solar}
BS (90/60)	491	2.8	41.3	8%	33	8.7	0.322	0.347
BS (60/35)	491	2.8	34.5	7%			0.319	0.344
EEF (90/60)	347	2	41.3	12%			0.350	0.384
EEF (60/35)	347	2	34.5	10%			0.345	0.380

In order to compare the scenarios when PV are installed for power production, the primary energy factor is calculated for all scenarios (PEF –without solar power and PEF_{solar} – with solar power considered). Results shows that lowest value is for base scenario with lowered temperature regime and solar panel installation as primary energy is low and delivered energy remains high. Therefore, PEF for EEF scenarios is higher than for BS scenarios as heat consumption decreases and the specific heat losses are higher.

4. Conclusions

The article provides the methodology for municipalities to transform the existing DH system to 4GDH system with lower heat supply temperature and integrated alternative energy sources. Therefore, the main steps of the transformation process is to evaluate the overall DH system of particular region/city, identify the most suitable transformation path and further select the relevant district/area for pilot case study which needs to be analyzed more detailed. The example of such analyses has been provided in the article with the comparison of different technological alternatives for particular parish. The analyzed example is a small-scale DH system with few buildings connected in order to achieve optimal heat density and operational conditions.

The calculation of technical indicators allows evaluating the possible development scenarios, which includes the energy efficiency measures, reduction of heat supply temperature and installation of solar PV panels for power production for self-consumption coverage. The heat losses, heat density and primary energy factor have been calculated for all scenarios.

The results shows that when energy efficiency measures are considered, the overall heat consumption reduces by around 30%. This effect the heat density of network and it decreases from 2.8 to 2 MWh/m. Therefore, in considered EEF scenario, the specific heat losses increases from 8% to 12%, but reducing the heat supply temperature from 90°C to 60°C allows decreasing the specific heat losses to 10% level.

For the particular parish it is considered to install the 9kW PV panel power station for self-consumptions coverage of buildings and boiler house. Therefore, such power station can cover around 27% of total power consumption. The calculated primary energy factor allows comparing the primary energy consumption with and without integrated solar panels. Integration of solar panels reduces the PEF by around 7% in BS scenarios and by 9% in EEF scenarios.

Therefore, the methodology allows identifying and evaluating potential technical solutions for particular district to approach 4GDH concept. The municipality should than ensure the suitable conditions for the implementation of desirable solution in pilot case district. However, afterward it requires monitoring the results of particular pilot case to evaluate the achievement or identify improvements for the further transformation process and application to larger scale (region or district).

Acknowledgement

This work is supported by the European Commission through the EU INTERREG Baltic Sea Region Project Number #R063 „Low Temperature District Heating for the Baltic Sea Region” (LowTEMP).



References

- Schmidt D., Ballert A., Blesl M., Jsvendsen S., Li H., Nord N., Sipilä K. Low Temperature District Heating for Future Energy Systems. Energy Procedia 2017- 116, 2017: 26-38.
- Elmegaard B., Ommen T.S., Markussen M., Iversen J. Integration of space heating and hot water supply in low temperature district heating. Energy and Buildings 2016- 124: 255-264.
- Averfalk H., Werner S. Essential improvements in future district heating systems. Energy Procedia 2017- 116:17-225.
- Rämä M., Sipilä K. Transition to low temperature distribution in existing systems. Energy Procedia 2017- 116, 2017:58-68.
- Jangsten M., Kensby J., Dalenbäck O., Trüschel A. Survey of radiator temperatures in buildings supplied by district heating. Energy 2017- 137: 292-301.
- Tunzi M., Skaarup Østergaard D., Svendsen S., Boukhanouf R., Cooper E. Method to investigate and plan the application of low temperature district heating to existing hydraulic radiator systems in existing buildings. Energy 2016-113:413-421.
- Köfinger M., Basciotti D., Schmidt R. Reduction of return temperatures in urban district heating systems by the implementation of energy-cascades. Energy Procedia 2017- 116: 438-451.
- Delmastro C., Martinsson F., Dulac J., Corgnati S.P. Sustainable urban heat strategies: Perspectives from integrated district energy choices and energy conservation in buildings. Case studies in Torino and Stockholm. Energy 2017-138: 1209-20.
- Baptista D.N.P., Simoes M., Silva C.A., Figueira J. Designing a municipal sustainable energy strategy using multi-criteria decision analysis. Journal of Cleaner Production 2018- 176: 251-260.
- Ziemele J., Kubule A., Blumberga D. Multi-perspective Methodology to Assess the Transition to 4th Generation District Heating Systems. Energy Procedia 2017- 113: 17-21.
- Volkova A., Mašatin V., Siirde A. Methodology for evaluating the transition process dynamics towards 4th generation district heating networks. Energy 2018- 150: 253-261.
- Beihmanis K., Rosa M. Energy Management system implementation in Latvian municipalities: from theory to practice. Energy Procedia 2016-95: 66-70.
- Fenton P., Gustafsson S., Ivner J., Palm J. Sustainable Energy and Climate Strategies: lessons from planning processes in five municipalities. Journal of Cleaner Production 2015-98:213-221.
- Latšov E., Volkova A., Siirde A., Kurnitski J., Thalfeldt M. Primary energy factor for district heating networks in European Union member states, Energy Procedia 2017- 116: 69-77.



16th International Symposium on District Heating and Cooling, DHC2018,
9–12 September 2018, Hamburg, Germany

Methodology to evaluate and map the potential of waste heat from sewage water by using internationally available open data

Pelda J.^{a*}, Holler, S.^a

^aHAWK, Rudolf-Diesel-Straße 12, 37075 Göttingen

Abstract

The integration of waste heat from industrial processes has been identified as a major research area in the European Union strategy on heating and cooling. In fact, the waste heat potential of combined cycle gas turbine power stations or energy-from-waste plants is well known. Plenty of district heating networks, in markets of different maturity across the world, make use of this technology. This work contributes to the wider integration of low-grade waste heat from sewage water systems by providing an open data methodology that can be easily adapted to various types of cities and district heating systems under changing boundary conditions. The methodology provides an easy calculation of waste heat potential for a city using population density and geographic information system data. The methodology identifies suitable sites for the integration of heat sources into district heating systems or building heating. It is based upon open-source technology and open data that helps to map waste heat sources spatially. Graph theory is key to generating a generic sewage network needed to carry out the methodology. The methodology will be applied and validated at an example city in Germany.

© 2018 The Authors. Published by Elsevier Ltd.

This is an open access article under the CC BY-NC-ND license (<https://creativecommons.org/licenses/by-nc-nd/4.0/>)

Selection and peer-review under responsibility of the scientific committee of the 16th International Symposium on District Heating and Cooling, DHC2018.

Keywords: waste heat; district heating; sewer; spatial allocation; heat recovery; open-source

* Corresponding author. Tel.: +49-551-5032-185; fax: +49-551-5032-200185.

E-mail address: Johannes.pelda@hawk.de

1. Introduction

The potential of district heating systems to reduce greenhouse gas emissions through more efficient use of primary energy is considerable. Increasing fossil fuel prices, the need to reduce greenhouse gas emissions, and partly decreasing heat demand of buildings due to improved building insulation envelopes put alternative and renewable ways of supplying district-heating systems with energy into focus in current research. Besides these aspects, district heating systems also contain great potential to give flexibility to electricity systems that are marked by the increasing fluctuations of renewable energy sources.

Decentralized, flexible combined heat and power (CHP) stations as well as power-to-heat (PtH) technologies support the interaction between district-heating systems and the electricity market. Characterized by their highly flexible operation mode, they can increase the available control energy of electricity grids. Regarding PtH, heat pumps (HPs) combined with environmental or waste heat sources have been discovered to be the most efficient technology from an economic and ecological perspective [4–6]. Heat pumps promise a wide range of uses through their exploitation of waste heat.

The technology to recover waste heat from sewage networks or even low-grade heat sources is simple and proven. [7] speaks of 500 wastewater heat pumps in operation world-wide. They are utilizing thermal ratings from 10 kW to 20 MW with a source temperature between 10 °C and 25 °C all year round.

Wastewater carries a lot of low-grade heat with it and does not vary its temperature level within seasons significantly as several measuring points in the sewer of Bologna show. It was found that the daily temperature fluctuations vary in the order of 2-3 °C. The yearly level of temperature varies between 10 °C and 22 °C for the city of Bologna. [8] Practical experiences show that a minimum dry weather flow rate from 0.01 m³/s must be given to recover waste heat from sewage [9, 10]. A range between 0.015 m³/s and 0.03 m³/s is mentioned by [11]. A minimum of 0.03 m³/s is also supported by [12].

There has been much research on the potential and usage of waste heat via HP. Methodologies exist that help to quantify the spatial distribution of waste heat from industrial processes [13–17]. Technologies to exploit the potential of low- to high-level temperature sources for heat recovery are available and their operational mode well-known [18–20]. By contrast, there is little research determining the potential of utilizing waste heat from sewage networks quantitative, qualitative and spatial [21]. One paper could be found that analyses the spatial congruence between heat demand and waste heat sources to determine locations for heat-recovery in Tokyo based on geographic information system (GIS) data from the Tokyo Metropolitan Government [22].

There is a lack of methodologies for spatial analysis of waste heat potential from sewage systems. The research question that arises from the current state of the art is the following: how can a methodology quantify the highly distributed potential of waste heat from sewage systems, qualify it and allocate it to its sources?

This paper introduces a novel methodology that accesses the waste heat potential of sewage systems on a local highly resolved level. The primary focus of this work is the mapping of the very likely route of wastewater to the wastewater treatment plant by using open data and open-source technology. It provides an algorithm that is able to quantify, qualify and spatially allocate the waste heat potential of sewage systems on an urban district level, in all cases where real data from the sewage system does not exist or is not publicly available. The methodology is applied on an example city in Germany, where GIS data from the sewage network is provided to quantify and verify the accuracy of the presented methodology.

Nomenclature

CHP	Combined heat and power
EU	European Union
GEB	Göttinger Entsorgungsbetriebe
GIS	Geographic information system
IEA	International Energy Agency
HP	Heat pump
N	Node

PtH	Power to heat
UK	United Kingdom
WWTP	Wastewater treatment plant
WWV	Wastewater volume
WU	Water usage
PD	Population density

2. Methodology

The methodology combines different open data sources and generates a generic network by open-source technology [23]. The generic network designed by algorithm matches the real sewage network to a certain extent. Therefore, the generic network makes it possible to spot suitable locations for exploitation of waste heat from sewers without having the original GIS data of the sewer. Overall, the methodology allocates population density to street networks and calculates the wastewater volume flow (WWV) for each street. WWV results from the product of population density (PD) and the country-specific water usage (WU) (2.1). Finally, an algorithm determines the shortest paths from each street to the wastewater treatment plant and accumulates the wastewater volume flows along these paths. The paths form a graph with edges and nodes.

The methodology assumes the following:

- Water consumption is equivalent to the amount of wastewater.
- Specific water consumption is the statistical average at national level.
- Rainwater accumulates discontinuously and is therefore neglected.
- The path of the sewage system is said to be the shortest path along the street network from wastewater occurrences to the wastewater treatment plant. Obstacles (e.g. rivers, bridges, train tracks), pumps, geodesic heights are not taken into account in the first step.

To determine the maximum wastewater flow WWV_n has to be adjusted either by a flow coefficient used for the construction of the sewer system or by a load profile. According to [24], the water consumption can be calculated with the general flow formula $f(h)$. The $f(h)$ differs by the size of the city. It is said that the smaller the city, the more water is tapped simultaneously [24, 164 et. seq., 25, p. 30]. Figure 1 shows the load factor for urban areas from different literature [1–3]. Load factor 1 and load factor 3 proceed the same way and are in the range between 0.20 [1] and 1.66 [1]. For the calculation the figures from [1] are taken. Compared to [8, 26] a maximum load factor of 1.60 seems to be reasonable for maximum flow. WWV_n is then evenly distributed to all nodes of the graph that are spatial within WWV_n occurrences.

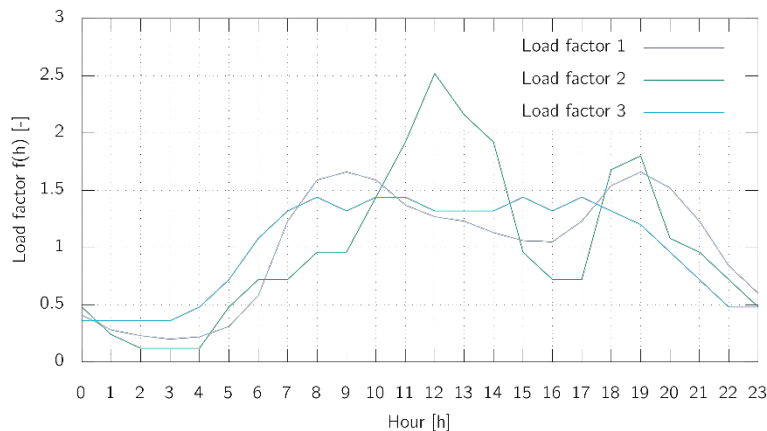


Figure 1 The load factor determines the hourly average water consumption using the average water usage per day [1–3].

3. Data sources

With this research project, a newly created database contains relevant information, needed to quantify the waste heat potential from wastewater in versatile developed cities in different countries. The database shows exclusively figures from countries within IEA DHC member states, which are in the focus of the research project. The database shows quantitatively the water consumption per inhabitant specific to each IEA DHC member state, as well as quantitative data about the amount of wastewater from different building types (e.g. schools, offices, public buildings). To obtain the water consumption per inhabitant several sources were used (see Table 1). The year of origin of the collected data from the different sources varies between 1997 and 2014.

Table 1 Sources for the key figure “water consumption per inhabitants” for different countries. Countries marked by * show the sum of water consumption by households and services. Key figures marked by ** show the sum of households and small businesses.

Country	Source
Australia, Japan, South Korea, USA	[27]
Canada	[28]
Belgium, Czech Republic, Denmark, Great Britain*, Greece*, Hungary*, Netherlands*, Norway, Poland*, Portugal, Spain, Sweden, Switzerland	[29]
New Zealand, Austria	[30]
Austria, Finland, France, Luxemburg	[31]
Turkey	[32]
Italy*	[33]
Slovakia	[34]
Ireland*	[35]
Germany**	[36]
Estonia	[37]

Figure 2 shows the water consumption of the considered states. In most countries, only the household’s water consumption entered into the data, but not rainwater. The numbers of water consumption were gathered many years ago (1997 – 2014), and this may lead to deviations from the real value. In particular, water saving campaigns within the countries and usage of improved technology towards water saving can influence the average water consumption.

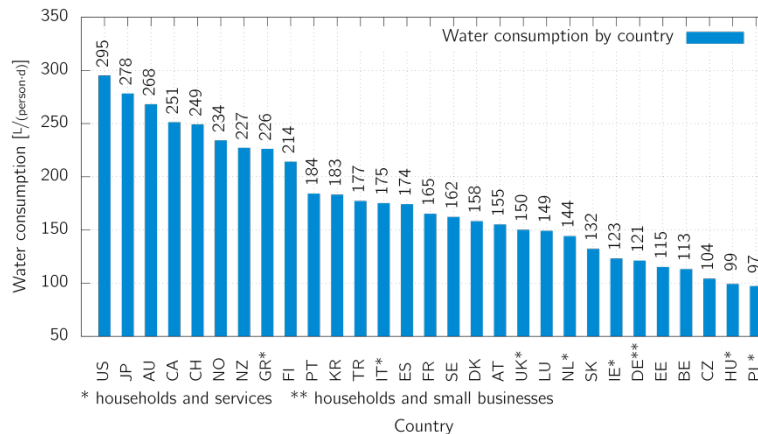


Figure 2 Overview of water consumption by country

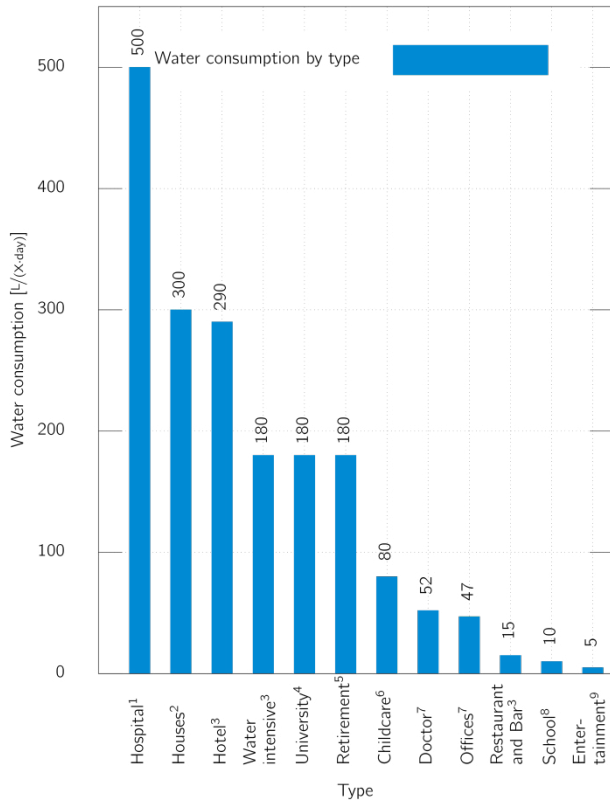


Figure 3 Water consumption by different building types. The amount of water usage depends on the reference value x. (¹ x = bed, ² x = person, ³ x = guest, ⁴ n.a., ⁵ x = patient + personell, ⁶ x = child, ⁷ x = employee, ⁸ x = pupil, ⁹ x = seat)

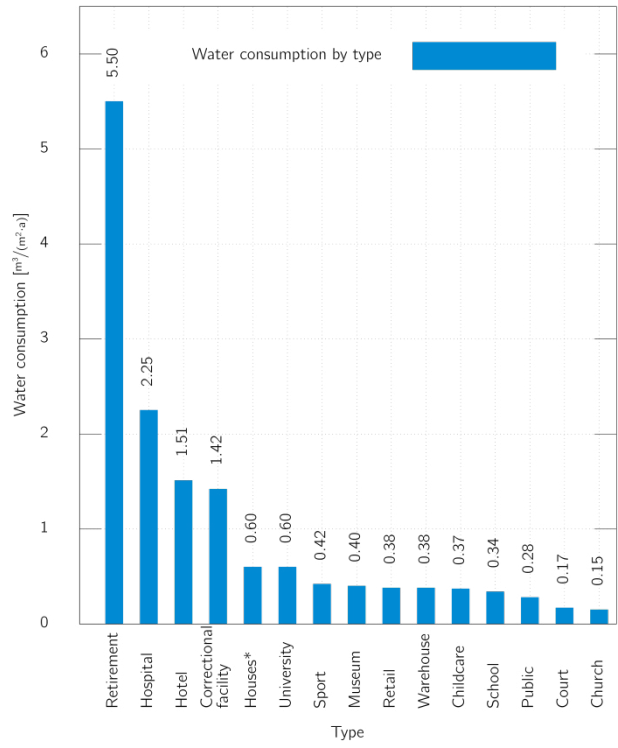


Figure 4 Water consumption by different building types (* used during daytime)

[25, 38, 39] give key figures of the amount of water consumption by different building types. Figure 3 shows the data related to various reference values, such as water consumption per bed, per guest, per person and so forth. These numbers must be adapted at local level. Figure 4 points out the water consumption per square meter. To ease the process of estimating the wastewater flow, the methodology focusses on building types with known water consumption per square meter and year. Their water consumption can then be counted up with the area of the buildings given in the GIS data and finally allocated to the nearest node of the graph.

Since 2011, the European Union (EU) requires all member states to carry out population, building and housing censuses every ten years. This means that existing administrative registers are used as data sources, supplemented in certain areas by a combination of complete surveys and sample surveys [40]. For Germany, the resolution of these data is inhabitants per 10,000 m². In this dataset areas are marked with -1 when no data exist or no information is available due to restricted areas.

The geographic information system provides the spatial data needed to build up the artificial sewage network and to estimate the amount of wastewater at building level. GIS data were taken from [41, 42].

4. Application of the methodology to an example city in Germany

To test the methodology for accuracy and applicability the results of the algorithm are compared to the sewage network of the city of Göttingen.

Göttingen is a city with approximately 120,000 inhabitants. It is located in the centre of Germany and belongs to the Federal State of Lower Saxony. The sewage network covers the whole city as well as some outlying districts.

The sewage network is altogether 1,320 km long and is divided into 360 km of sewer and 360 km rainwater channel. The pipe diameter differs between 0.15 m and 2.00 m. Five pumps in the sewer and one pump in the rainwater channel are installed. The average water consumption between 2015 and 2017 was approximately 0.42 m³/s. [43]

GEB Göttinger Entsorgungsbetriebe (GEB) provided GIS data of the real sewage network for verifying the results of the calculation based on the methodology. The GIS data hold information about the pipes' length, nominal diameter, start height and end height. With Equation 4.1 the maximal water flow rate of the pipes is estimated through their nominal diameter.

$$Q = \frac{\pi \cdot d^2}{4} \cdot \left(-2 \cdot \lg \left[\frac{2,51 \cdot \nu}{d \cdot \sqrt{2g \cdot d \cdot J_E}} + \frac{k_b}{3,71 \cdot d} \right] \cdot \sqrt{2g \cdot d \cdot J_E} \right) \quad (4.1)$$

Q	Flow rate [m ³ /s]
d	Nominal diameter [m]
ν	Kinematic viscosity of waste water: $1,31 \cdot 10^{-6}$ m ² /s
g	Acceleration of gravity: 9,81 m/s ²
J_E	Energy line gradient (corresponds to bottom gradient JSO with full filling and stationary uniform discharge)
J_{SO}	Sole slope: Difference in height of two points of the river bed in relation to the length of the river between the points

5. Results

The overlay of the GIS data on the sewer of the city of Göttingen with the generic designed network shows that within the area of Göttingen the novel methodology has the potential to match the route of the sewage system to the wastewater treatment plant to a certain extent.

A closer look at the system is given in Figure 5, which magnifies the area of the city of Göttingen with sewage network pipes' nominal diameter between 0.80 m and 2.00 m and a wastewater flow of the generic network between 0.01 m³/s and 0.28 m³/s. As mentioned above these flow rates are considered to be economic and ecological feasible

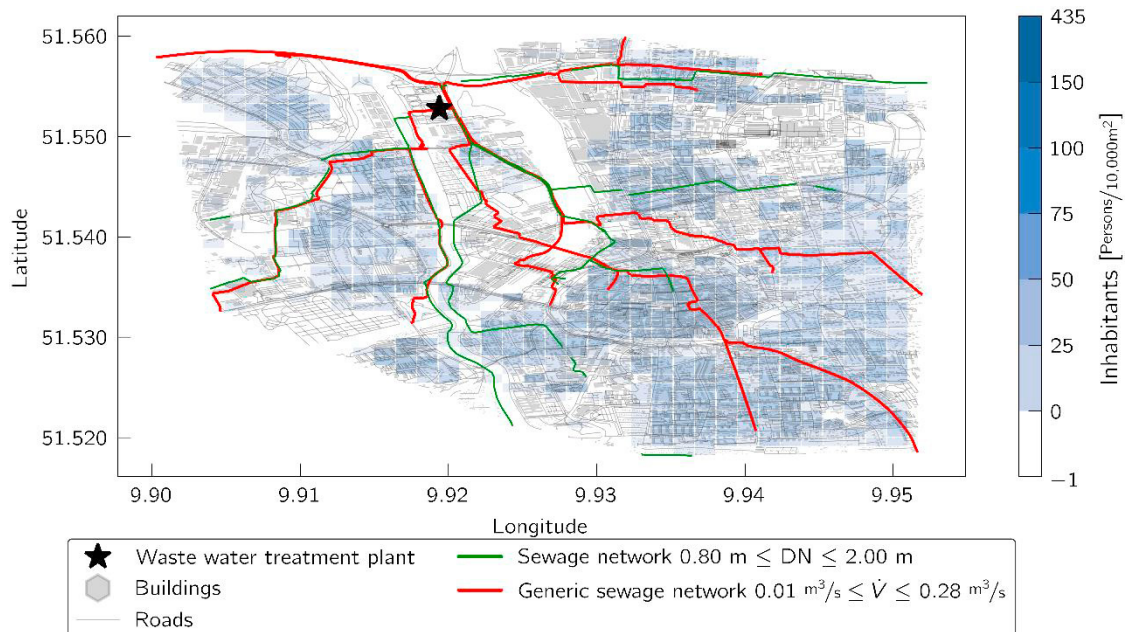


Figure 5 Partial map of the city of Göttingen filtered by a nominal diameter from 0.80 m to 2.00 m of the sewage network and a wastewater flow of 0.01 m³/s to 0.28 m³/s of the generic network.

for waste heat exploitation of sewer. Preliminary studies of GEB confirm the minimum dry weather flow rate by $0.01 \text{ m}^3/\text{s}$ or a nominal diameter of 0.80 m . The map demonstrates largely the same course for the pipes in the selected range. By evaluating the results visually by compass direction the map shows a high correlation of the generic network to the sewer. At a closer look, some generic routes are identical to the sewer; exceptions also occur which mostly run parallel to the sewer. The red line in the top left corner runs along a highway feeder road, which was built long after the sewage channel had been constructed elsewhere. However, the algorithm laid the generic sewage pipe on the shortest path to the wastewater treatment plant, in this case the highway feeder road. On the contrary, the routing of the sewage network is parallel to the y axis and turns to the right in the middle of the map. This pipe is not displayed, as its nominal diameter is out of range. The map also shows differences in the length of both networks within the displayed range, which can be explained by the historical growth of the sewage network and therefore its alternate routing to the wastewater treatment plant. Historically the shortest path to the wastewater treatment plant was not the optimal solution connecting new districts to the sewer. Compounding the problem, the generation of the generic network does not take pumps and geodetic height into account.

Figure 6 shows a partial map of the city of Göttingen to get a closer look on heavily developed urban areas. It turns out that with increasing density of population and denser street network the generic network becomes more

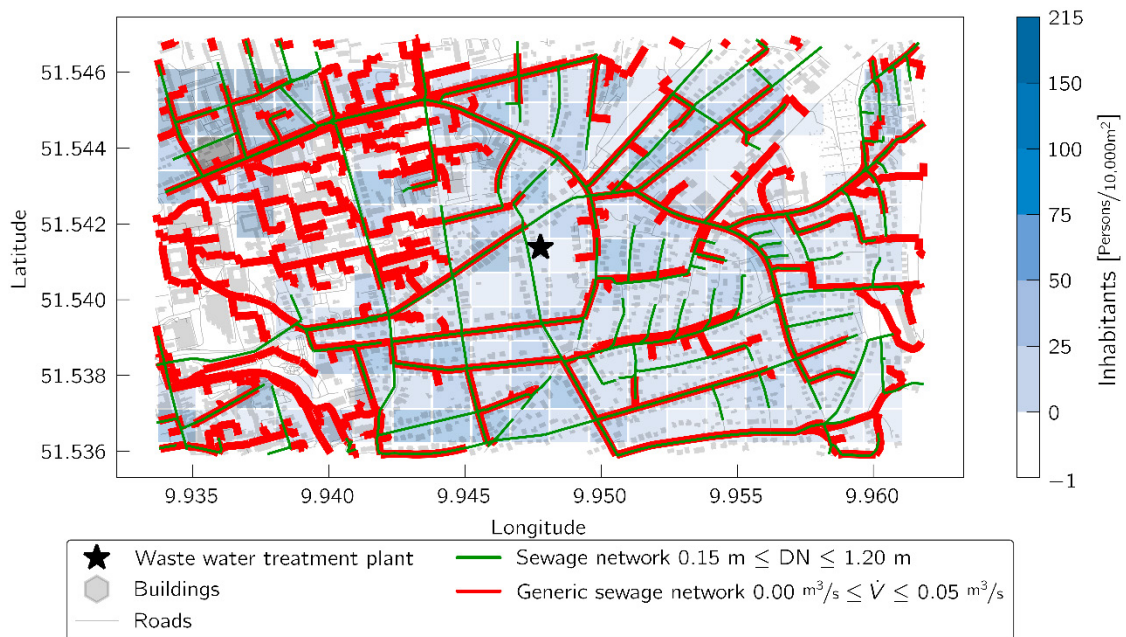


Figure 6 Partial map of the city of Göttingen, showing all existing pipes within.

accurate. This is because every building is connected to the sewer, which normally runs in front of the building. This can be approved by getting a better insight into the overall accuracy between the generic network and the sewer with the following analysis.

Figure 7 shows the match of the routing of both networks. Therefore, the edges of both networks are transformed into points, whereas each edge consists of two points: the start point and the end point. Finally, the rasters of inhabitants cluster the two point clouds along the scale of its amount of inhabitants. The congruity between both networks is calculated as follows:

Figure 7 shows that the amount of nodes of the generic network within a raster field have high congruity compared to the amount of nodes of the sewage system, as a match of one indicates a match to 100 %. It is obvious that at raster fields with inhabitants around the average and thus a high distribution within the area of Göttingen, the congruity between the generic network and the real network is high, whereas in raster fields with no information (-1 inhabitants/10,000 m²) or great numbers of inhabitants (> 150 inhabitants/10,000 m²), the deviation increases. One has to keep in mind that the occurrences of rasters with values of inhabitants higher than 150 inhabitants/10,000m² is little.

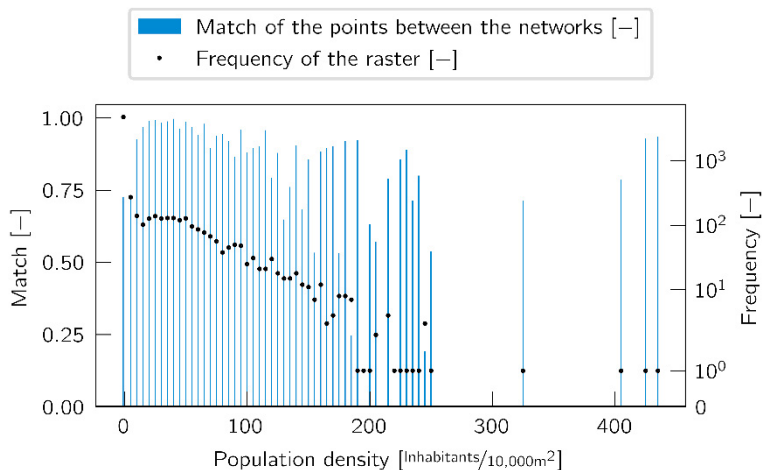


Figure 7 Matching of all points of the generic sewage network to the points of the sewage network over the population density. The frequency gives significance to the scale of the population density.

6. Conclusion

The results at the example city show that the methodology effectively calculates the path from wastewater sources to the wastewater treatment plant as well as the wastewater volumetric flow. It was found that the sewage system overlays the road network more accurately within areas that have a population density close to the average, and thus the methodology is more accurate in this range. The volumetric flows calculated via the methodology could not be verified directly with the volumetric flow of the sewage network due to lack of measurement points in the sewage system. Nevertheless, deducing the volumetric flow from the nominal diameter using Equation 4.1, the maximal flow rates of the sewage network can be compared to the flow rate of the generic networks. The comparison with the nominal diameter of the sewage network showed that the calculated volumetric flow seems to be highly underestimated. Reasons for this are in particular the missing allocation of building types to their specific water consumption and the differences in calculating flow rates of sewage networks. The generic system calculates the maximum average flow rate at daily peak, neglecting rainwater. The sewage network, however, is designed for a 90 % full load considering rainwater and its flow rate is deduced from its nominal diameter. The mapping of the results also shows major differences in the routing of pipes with higher volumetric flow and pipes that are in areas of low population density. Nevertheless, the methodology is accurate in relation to the length of pipes with least deviation in volumetric flow rate compared to the sewage system. Consequently, the methodology is capable of determining the length and usually the location of pipes.

For further research, these discrepancies should be categorized by the reason of their origin. With measured data of water consumption in the example city, the underestimated flow rates can be adjusted to the real water consumption. Considering local conditions will improve the assumption concerning the water demand of specific building types. In particular, multi-storey buildings tend to be underestimated as the algorithm uses key figures depending on square meters. GIS data provide property areas which do not mention storey levels. The use of further attributes of the GIS data such as street types, tunnels and maximum allowed speed can help to improve the

algorithm and enhance the accuracy of routing. The development of a probability of routing along these street types improves the algorithm's ability to find the most accurate route.

Despite small inaccuracies, the methodology is capable of presenting a good estimation of spatially distributed wastewater flows of the sewage system in the example city; it helps to assess the potential of waste heat sources of sewages quantitatively, qualitatively and spatially. As a result, the methodology can show not only the wastewater flows and their spatial distribution in cities but also the potential of utilizing waste heat from sewers.

Acknowledgements

Many thanks to the International Energy Agency (IEA) who are funding this research within the Technology Collaboration Programme on District Heating and Cooling including Combined Heat and Power named ANNEX XII. The research is about a methodology to evaluate and map the potential of waste heat from sewage water by using internationally available open data (MEMPHIS). It focuses on waste heat from small and medium industries as well as sewage networks and elaborates a tool to map potentials spatially. In addition, many thanks to the Göttinger Entsorgungsbetriebe (GEB) for supporting the project with their technical knowledge and providing their GIS data. Thanks to the open-source community, who provide professional tools and helped with programming challenges. Their work enables the project results to be freely distributed and utilized without costs. Personal thanks to Ciara Higgins for edit and her help improving the paper's readability.

References

- [1] *Arbeitsblatt W 410*, W 410, 2008.
- [2] W. Gujer, *Siedlungswasserwirtschaft: Mit 84 Tabellen*, 3rd ed. Berlin, Heidelberg: Springer, 2007.
- [3] J. Mutschmann and F. Stimmelmayer, *Taschenbuch der Wasserversorgung*, 14th ed. Wiesbaden: Vieweg, 2007.
- [4] R. Lund, D. D. Ilic, and L. Trygg, "Socioeconomic potential for introducing large-scale heat pumps in district heating in Denmark," *Journal of Cleaner Production*, vol. 139, pp. 219–229, 2016.
- [5] H. Ü. Yilmaz, D. Keles, A. Chiodi, R. Hartel, and M. Mikulić, "Analysis of the power-to-heat potential in the European energy system," *Energy Strategy Reviews*, vol. 20, pp. 6–19, 2018.
- [6] A. Bloess, W.-P. Schill, and A. Zerrahn, "Power-to-heat for renewable energy integration: A review of technologies, modeling approaches, and flexibility potentials," *Applied Energy*, vol. 212, pp. 1611–1626, 2018.
- [7] F. Schmid, "Sewage Water: Interesting heat source for heat pumps and chillers," in *Advances and Prospects in Technology, Application and Markets*, Zurich, 2008.
- [8] S. S. Cipolla and M. Maglionico, "Heat recovery from urban wastewater: Analysis of the variability of flow rate and temperature," (en), *Energy and Buildings*, vol. 69, pp. 122–130, 2014.
- [9] AWEL Zürich, "Heizen und Kühlen mit Abwasser: Leitfaden für die Planung, Bewilligung und Realisierung von Anlagen zur Abwasserenergienutzung," 2010.
- [10] M. Biesalski, "Moderne Wärmetauschertechnologie aus Baden-Württemberg – ein Exportprodukt," 2010.
- [11] S. Fiore and G. Genon, "Heat Recovery from Municipal Wastewater: Evaluation and Proposals," *Environmental Engineering and Management Journal*, no. Vol. 13, No. 7, 1595-1604, <http://omicron.ch.tuiasi.ro/EEMJ/>, 2014.
- [12] F. Schmid, "Sewage Water: Interesting Source for Heat Pumps," 2009.
- [13] S. Brueckner, L. Miró, L. F. Cabeza, M. Pehnt, and E. Laevemann, "Methods to estimate the industrial waste heat potential of regions – A categorization and literature review," *Renewable and Sustainable Energy Reviews*, vol. 38, pp. 164–171, 2014.
- [14] F. Bühler, S. Petrović, F. M. Holm, K. Karlsson, and B. Elmegaard, "Spatiotemporal and economic analysis of industrial excess heat as a resource for district heating," *Energy*, vol. 151, pp. 715–728, 2018.
- [15] R. Lund and U. Persson, "Mapping of potential heat sources for heat pumps for district heating in Denmark," *Energy*, vol. 110, pp. 129–138, 2016.
- [16] L. Miró, S. Brückner, and L. F. Cabeza, "Mapping and discussing Industrial Waste Heat (IWH) potentials for different countries," *Renewable and Sustainable Energy Reviews*, vol. 51, pp. 847–855, 2015.
- [17] A. Luo, H. Fang, J. Xia, B. Lin, and Y. Jiang, "Mapping potentials of low-grade industrial waste heat in Northern China," *Resources, Conservation and Recycling*, vol. 125, pp. 335–348, 2017.

- [18] F. Huang, J. Zheng, J. M. Baleynaud, and J. Lu, “Heat recovery potentials and technologies in industrial zones,” *Journal of the Energy Institute*, vol. 90, no. 6, pp. 951–961, 2017.
- [19] A. Bertrand, R. Aggoune, and F. Maréchal, “In-building waste water heat recovery: An urban-scale method for the characterisation of water streams and the assessment of energy savings and costs,” *Applied Energy*, vol. 192, pp. 110–125, 2017.
- [20] F. Meggers and H. Leibundgut, “The potential of wastewater heat and exergy: Decentralized high-temperature recovery with a heat pump,” *Energy and Buildings*, vol. 43, no. 4, pp. 879–886, 2011.
- [21] R. Kollmann *et al.*, “Renewable energy from wastewater - Practical aspects of integrating a wastewater treatment plant into local energy supply concepts,” (en), *Journal of Cleaner Production*, vol. 155, pp. 119–129, 2017.
- [22] T. Ichinose and H. Kawahara, “Regional feasibility study on district sewage heat supply in Tokyo with geographic information system,” *Sustainable Cities and Society*, vol. 32, pp. 235–246, 2017.
- [23] *Anaconda Software Distribution: Computer software*, 2018.
- [24] P. Klingel, *Modellierung von Wasserverteilungssystemen*. Wiesbaden: Springer Fachmedien Wiesbaden, 2018.
- [25] R. Neunteufel, L. Richard, and R. Perfler, “Studie Wasserverbrauch und Wasserbedarf,” Universität für Bodenkultur Wien, Wien, 2010.
- [26] B. Molino, G. Rasulo, and L. Tagliatalata, “Peak coefficients of household potable water supply,” *Water Resource Management*, no. 4, pp. 283–291, 1991.
- [27] François de Dardel, *Domestic water consumption*. [Online] Available: <http://dardel.info/EauConsumption.html>. Accessed on: Feb. 07 2018.
- [28] Government of Canada, *Residential water use*. [Online] Available: <https://www.canada.ca/en/environment-climate-change/services/environmental-indicators/residential-water-use.html>. Accessed on: Feb. 07 2018.
- [29] eurostat, *Use of water by the domestic sector*. [Online] Available: [http://ec.europa.eu/eurostat/statistics-explained/index.php/File:Use_of_water_by_the_domestic_sector_\(households_and_services\)_%E2%80%94_a_ll_sources,_2003%E2%80%9313_\(%C2%B9\)_\(m%C2%B3_per_inhabitant\)_YB16-de.png#file](http://ec.europa.eu/eurostat/statistics-explained/index.php/File:Use_of_water_by_the_domestic_sector_(households_and_services)_%E2%80%94_a_ll_sources,_2003%E2%80%9313_(%C2%B9)_(m%C2%B3_per_inhabitant)_YB16-de.png#file). Accessed on: Feb. 07 2018.
- [30] *Water Use | LEARNZ*. [Online] Available: <http://www.learnz.org.nz/water172/bg-standard-f/water-use>. Accessed on: May 14 2018.
- [31] M. P. Vall, “Umwelt und Energie: Abwasser in den europäischen Staaten,” *Statistik kurz gefasst*, no. 14, 2001.
- [32] Business Monitor International, “Turkey - Water Report,” 2015.
- [33] I.Stat, *Acqua - Consumo per uso domestico 2011*. [Online] Available: http://dati.istat.it/Index.aspx?DataSetCode=DCCV_INDACQDOM. Accessed on: Feb. 07 2018.
- [34] Ministry of the Environment of the Slovak Republic, “National ISPA Strategy of the Slovak Republic: Environment,” 2000.
- [35] Expert commission on domestic public water services, Ed., “Report on the Funding of Domestic Public Water Services in Ireland,” 2016.
- [36] DESTATIS, *Wasserwirtschaft: Öffentliche Wasserversorgung in Deutschland von 2013*. [Online] Available: https://www.destatis.de/DE/ZahlenFakten/GesamtwirtschaftUmwelt/Umwelt/UmweltstatistischeErhebungen/Wasserwirtschaft/Tabellen/Wasserabgabe_2013.html;jsessionid=0B8631E92F696649BA1F1999CB12F7EE.cae1. Accessed on: Feb. 07 2018.
- [37] P. Banhard, “Water Pricing and Policy in Estonia: Presentation for the First Conference of the NIS Water Senior Officials,” 2001.
- [38] A. Hamann, *Grundlagen der Abwasserwärmenutzung: Leitfaden für Architekten, Ingenieure und Stadtplaner*. Stuttgart: Fraunhofer IRB Verlag, 2015.
- [39] TWW, “Kennwerte Wasserverbrauch,”
- [40] Statistische Ämter des Bundes und der Länder, *ZENSUS2011 - Methode*. [Online] Available: https://www.zensus2011.de/DE/Zensus2011/Methode/Methode_node.html. Accessed on: May 18 2018.
- [41] G. Boeing, “OSMnx: New methods for acquiring, constructing, analyzing, and visualizing complex street networks,” *Computers, Environment and Urban Systems*, vol. 65, pp. 126–139, 2017.
- [42] Geofabrik, *GEOFABRIK*. [Online] Available: <http://www.geofabrik.de/>. Accessed on: May 22 2018.
- [43] M. Reinhardt, R. Boll, R. Rohlfig, and J. Müller, “Wärmenutzung aus Abwasser der Stadt Göttingen und Nutzung der Wasserkraft auf der KA Göttingen: Machbarkeitsstudie,” Hannover, 2009. Accessed on: May 23 2018.



16th International Symposium on District Heating and Cooling, DHC2018,
9–12 September 2018, Hamburg, Germany

Performance of Different Back-up Technologies for Micro-Scale Solar Hybrid District Heating Systems with Long-term Thermal Energy Storage

A. Rosato*, G. Ciampi, A. Ciervo, S. Sibilio

University of Campania Luigi Vanvitelli, Department of Architecture and Industrial Design, via San Lorenzo, Aversa, 81031, Italy

Abstract

In this paper the performance of a solar heating network devoted to satisfying the heating demand of a micro-scale district composed of 6 typical single-family houses and 3 typical schools under the climatic conditions of Naples (south of Italy) is investigated by means of the dynamic simulation software TRNSYS over a 5-year period. The proposed system is composed of a solar collectors array, a short-term thermal energy storage, a long-term double U-pipe vertical borehole thermal energy storage and a heat distribution network. Three different technologies are investigated as back-up devices to be included in the district heating system: (i) a natural gas-fired boiler, (ii) a vapor-compression electric heat pump and (iii) a natural gas-fuelled internal combustion engine-based micro-cogeneration unit.

The simulation results are compared with those associated to a conventional heating system in terms of primary energy consumption, operating costs as well as simple pay-back period in order to identify the best option in terms of back-up system and assess the potential energy and economic benefits associated to each technology.

© 2018 The Authors. Published by Elsevier Ltd.

This is an open access article under the CC BY-NC-ND license (<https://creativecommons.org/licenses/by-nc-nd/4.0/>)

Selection and peer-review under responsibility of the scientific committee of the 16th International Symposium on District Heating and Cooling, DHC2018.

Keywords: Solar energy; Back-up system; Micro-cogeneration; District heating; Borehole thermal energy storage; TRNSYS.

* Corresponding author. Tel.: +39 0815010845; fax: +39-0815010845.

E-mail address: antonio.rosato@unicampania.it

1. Introduction

Solar energy has received extensive study and numerous applications throughout the world for producing heat and/or electricity in residential and commercial sectors. With the trend of decreasing specific investment cost for solar systems and the increasing price of conventional fuels, solar energy may become cost-competitive even in small-scale or micro-scale District Heating (DH) networks [1]. One of the longstanding barriers to solar energy technology lies in the noticeable misalignment between energy supply and consumption; long-term storage allows for thermal energy storage over weeks and months, with it being a challenging key technology for solving the time-discrepancy problem of solar energy utilization. Based on a comprehensive literature review, Rad and Fung [2] concluded that Borehole Thermal Energy Storage (BTES) has the most favorable condition for long-term energy storage thanks to the large amounts of energy involvement and relatively low cost of storage media.

However, difficulties emerge with the increasing penetration of intermittent energy sources characterized by a stochastic behavior; when such sources are not available, in fact, other generation units have to compensate the lack of energy and, consequently, sufficient reserve margins must be ensured. Several technologies can be integrated into a solar district heating network; in particular, the integration of cogenerated heat is one of the key point of the 2012/27/EU Energy Efficiency Directive issued by the European Union (EU) [3-5]. However, selecting the technology and capacity of back-up unit in an optimal district heat production system is a dynamic issue to be solved based on the scale and variation of heat demand, the local availability and costs of energy sources, the investment cost of each technology, etc. Therefore the best solution is not always straightforward, leading to the need of simulation tools to select the optimal design according to specific criteria.

Few papers are available in literature focusing on micro-scale renewable hybrid district heating systems. Buoro et al. [6] investigated the integration between distributed energy supply system, solar thermal plant and heat storage for a district composed of 9 industrial facilities located in the north-east of Italy. The work of Kallert et al. [7] focused on modeling, simulation and exergetic analysis of a low temperature DH network including short- and long-term storages as well as different heat generation units (solar thermal collectors, ground source heat pumps and natural gas-fired cogeneration devices); the plant was investigated while serving a small building group of 10 residential low energy residences characterized by an energy demand for new buildings according to German regulation EnEV 2009 [8]. Marguerite et al. [9] presented the results of a multi-criteria evaluation of different design scenarios for a micro-DH network in Vienna (Austria) serving two energy efficient office buildings (supplied by solar thermal collectors and heat pumps) and one standard office building (equipped with gas boilers). To our knowledge, there is not a single scientific paper which specifically addresses the potential of the joint use of micro-scale solar district heating networks and micro-cogeneration units under the climatic conditions of Italy.

In this paper a micro-scale solar district heating system based on the utilization of a seasonal borehole thermal energy storage is modeled, simulated and analyzed by means of the TRaNsient SYStems (TRNSYS) software platform (version 17) [10] over a 5-year period. The system is devoted to satisfying the heating demand and domestic hot water requirements of a district consisting of 6 typical single-family houses and 3 typical schools under the climatic conditions of Naples (south of Italy). The plant is mainly composed of a flat-plate solar collectors field, a short-term thermal energy storage, a seasonal double U-pipe vertical borehole thermal energy storage and a heat distribution network. A back-up system is also included in the plant layout in order to take into account the intermittent nature of the solar source; in particular, three different technologies are investigated as back-up devices: (i) a 26.6 kW_{th} natural gas-fired boiler, (ii) a 11.7 kW_{th} natural gas-fuelled internal combustion engine-based micro-cogeneration unit combined operating together with a 26.6 kW_{th} natural gas-fired boiler and (iii) a vapor-compression electric heat pump with a nominal output of 24.4 kW_{th} combined with a 26.6 kW_{th} natural gas-fired boiler. The primary energy consumption and operating costs of the proposed system have been evaluated based on the simulation results and compared with those associated to a conventional heating system consisting of a number of individual natural gas-fired boilers installed inside the single buildings. The main aim of the paper is assessing the potential energy and economic benefits associated to the utilization of different back-up technologies and, therefore, the potential improvements that can be achieved by optimizing the design of the proposed solar district heating system.

2. Description of the district

The district served by the proposed plant is composed of 6 typical Italian single-family residences and 3 typical schools located in Naples (latitude = 40° 51' 46" 80 N; longitude = 14° 16' 36" 12 E). Three different typologies of residential buildings (A, B and C) and three different schools (Nursery (N), Nursery School (NS) and Elementary School (ES)) have been considered. In particular, the district is composed of 2 residential buildings for each typology. Table 1 summarizes the main characteristics of end-users composing the district.

Table 1. Geometrical characteristics of buildings.

	Residential building typology			School building typology		
	A	B	C	N	NS	ES
Number of buildings (-)	2	2	2	1	1	1
Floor area (m²)	60	78	114	780	670	1340
Windows' area (m²)	84	102	230	387	743	670
Volume (m³)	230	370	448	2480	2203	4470
Maximum number of simultaneous occupants (-)	3	4	5	98	115	145

In order to be compliant with Italian legislation requirements [11], the thermal transmittance of the building envelopes has been equated to the given threshold values (2.40 W/m²K for windows, 0.36 W/m²K for roofs, 0.40 W/m²K for floors, 0.38 W/m²K for external vertical walls), whatever the building typology is. For each residential building typology, a specific annual stochastic profile (composed of 365 different daily stochastic profiles) at one-minute time resolution has been considered for defining both the number of active occupants as well as the electric power demand as a function of the time; these profiles have been obtained by using the models developed by Richardson and Thomson [12]; the total electric energy demand for the 6 residential buildings is equal to 14.98 MWh/y due to the operation of lighting systems as well as domestic appliances (a fridge, a freezer, a cordless phone, an iron, a vacuum, a PC, a printer, two TVs, a microwave, a dish washer, a washing machine for each residential building). The annual electric demand profile at one-minute time resolution for schools has been derived by considering the operation of lighting systems, 3 printers as well as 3 PCs for each school building from Monday to Friday (according to the schools' timetable) between September 15th and June 30th (except dates and periods of school holidays); a total electric energy demand of 12.46 MWh/y is obtained for the 3 school buildings. Several sets of yearly load profiles for the domestic hot water demand have been specified within the IEA-SHC Task 26 [13]. In this study, a demand profile with an average basic load of 100 l/day in the time scale of 1 minute has been used for both building typologies A and B, while a demand profile with an average basic load of 200 l/day in the time scale of 1 min has been used for building typology C. The total energy demand for the production of DHW at 45 °C associated to the 6 residential buildings is equal to 8.97 MWh/y. The DHW demand has been neglected for the school buildings.

3. Description of the proposed district heating system

The schematic of the proposed plant is reported in Figure 1. In this figure, the following main components of the system can be identified: end-users (6 residential buildings and 3 school buildings), solar collectors (SC), heat dissipator (HD), short-term thermal energy storage (STTES), borehole thermal energy storage (BTES) with vertical double-U-pipes borehole heat exchangers, back-up system (BS), heat exchangers (HE1 and HE2), local individual boilers (B), fan-coils (FC), pumps (P), 3-way valves and pipes. In the figure, the following three main circuits are highlighted: SC circuit (light blue); BTES circuit (orange); heat distribution network (red).

The solar energy captured by the solar thermal collectors is first transferred, through a heat exchanger (HE1), into the short-term thermal energy storage; dissipation of solar thermal energy surplus is obtained by blowing air across a finned coil heat exchanger when the solar collectors outlet temperature is higher than 95°C. From the STTES, if there is a heating demand, the solar energy is transferred through another heat exchanger (HE2) into the distribution network, and then to the end-users for space heating. Each building is equipped with a group of fan-coils, supplied by the STTES. If the solar energy is not immediately required for heating purposes, it can be moved from short-term

thermal energy storage to the long-term thermal energy storage system during the whole year (“BTES charging mode”). During the heating season, thermal energy stored in the BTES field can return into the STTES (“BTES discharging mode”) to provide additional thermal energy.

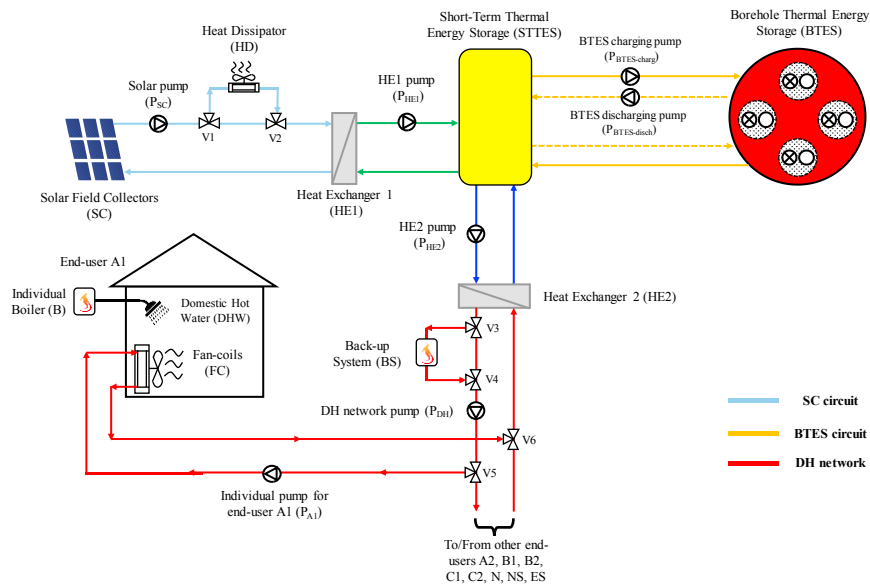


Fig. 1. Schematic of the proposed central solar heating plant with seasonal thermal energy storage.

During the charging, the flow direction is from the center to the boundaries of the BTES to obtain high temperatures in the center and lower ones at the boundaries of the storage; the flow direction is reversed during the discharging phase. The set-point for the DH supply temperature is 55°C . In order to supplement the space heating demand when the solar energy recovered and stored in the short- and long-term storages cannot meet the energy requirements, a back-up system is used. In particular, the following three different alternative cases involving different technologies have been investigated in this paper:

- case 1) $26.6 \text{ kW}_{\text{th}}$ Main natural gas-fired Boiler (MB);
- case 2) $11.7 \text{ kW}_{\text{th}}$ natural gas-fuelled internal combustion engine-based micro-cogeneration (MCHP) unit (nominal electric output of 6.0 kW) series-connected with the Main natural gas-fired Boiler (also used in the case 1);
- case 3) vapor compression Electric Heat Pump (EHP), with a nominal thermal output of $24.4 \text{ kW}_{\text{th}}$, series-connected with the Main natural gas-fired Boiler (also utilized in the case 1).

The MCHP unit as well as the electric heat pump have been combined with the boiler (case 2 and 3, respectively) in order to guarantee the capability of the system in maintaining the desired temperature level (55°C) at the inlet of the distribution network at any case. Figure 2 describes in more detail the configurations of back-up system investigated in this paper.

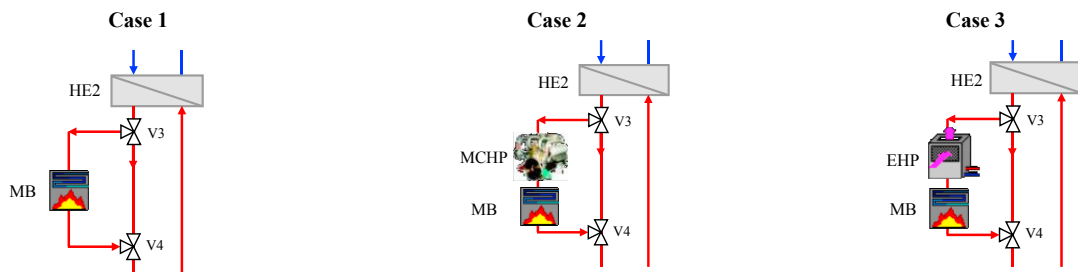


Fig. 2. Configurations of the back-up system (BS).

An additional individual natural gas-fired boiler has also been installed inside each single building specifically devoted to the domestic hot water production. All the electric requirements are satisfied with the electric energy supplied by the central national grid. In Table 2 the main characteristics of each component of the proposed plant are indicated. The area of solar collectors, the volume of both the STTES and BTES, the number of BTES boreholes, the thermal conductivity of both grout and soil as well as the U-pipe spacing have been determined by the authors based on the results of a sensitivity analysis performed in previous studies [14] focused on the same urban district.

Table 2. Main characteristics of plant components.

Solar Collector (SC) [15]						
Collector typology/model	Number of collectors	Aperture area of a single collector (m ²)	Tilted angle	Azimuth	Orientation	
Flat plate/ FSK 2.5	39	2.31	30°	0°	South	
Short-term Thermal Energy Storage (STTES)						
Typology				Volume (m ³)		
Vertical cylindrical storage tank				9.0		
Boreholes Thermal Energy Storage (BTES)						
Borehole radius (m)	Inner/outer radius of U-tube pipe (m)	Thermal conductivity of soil (W/mK)	Thermal conductivity of grout (W/mK)	Volume (m ³)	Number/depth of boreholes (-)/(m)	U-pipe/borehole spacing (m)
0.15	0.01372/0.01669	3.0	5.0	352.4	4/20.1	0.050/2.25
Main back-up Boiler (MB) [16] and individual Boiler (B) [16]						
Fuel	Maximum thermal output (kW)			Efficiency at rated capacity (-)		
Natural gas	26.6			0.9213		
Micro-cogeneration unit (MCHP) [17]						
Engine type	Displacement (cm ³)	Fuel	Rated electric output (kW)	Rated thermal output (kW)	Electric efficiency η_{el} at maximum load (%)	Thermal efficiency η_{th} at maximum load (%)
Reciprocating internal combustion engine	952	Natural gas	6.0 kW	11.7	28.8	56.2
Vapor compression Electric Heat Pump (EHP) [18]						
Nominal thermal output (kW)			COefficient of Performance at nominal conditions (-)			
24.4			3.05			

3.1. Simulation models

The TRAnSient SYStems (TRNSYS) software platform [10] has been used to model and simulate the proposed plant. Table 3 highlights the component modules (called “Types”) selected for this project.

Table 3. “Types” used in the TRNSYS project.

Buildings	Solar collectors	STTES	BTES	MB	MCHP	EHP	B	FC	P	Climatic data	3-way valves	Pipes
Type 56	Type 1b	Type 534	Type 557a	Type 700	Type 907	Type 941	Type 659a	Type 753e	Type 656	Type 15	Type 647	Type 31

The simulation models have been calibrated and enhanced by manufactures performance data or information available in current scientific literature according to the common characteristics of the components used in practice prior to performing the simulations. The Type 534 used to model the STTES is based on the assumption that the tanks can be divided into N fully-mixed equal sub-volumes; for each sub-volume, the mass and energy balances are considered transient state, making it possible to calculate the thermal stratification in the component. In this paper, the STTES has been modelled with 10 isothermal temperature layers to better represent the stratification in the tank, where the top layer is 1 and the bottom layer is 10. The Type 557a, adopted to model the BTES, is considered to be the state-of-the-art in dynamic simulation of ground heat exchanger that interacts thermally with the ground and has been used by several researchers for simulating energy systems with BTES [19]. The model assumes that the

boreholes are placed uniformly within a cylindrical storage volume of ground; there is a convective heat transfer within the pipes, and a conductive heat transfer to the storage volume.

The Main natural gas-fired Boiler (MB) can regulate its thermal output between 5.32 kW and 26.6 kW. This component has been modelled by using the Type 700 and calculating its thermal efficiency η_{MB} through the following equation (according to the manufacturer performance data [16]) as a function of its thermal output $P_{MB,th,out}$:

$$\eta_{MB} = 0.0015 \cdot P_{MB,th,out} + 0.8814 \quad (1)$$

The individual boilers installed inside the buildings for DHW production have been modelled with the Type 659a by assuming a constant thermal efficiency of 90%, whatever their thermal output is.

The micro-cogeneration device under investigation [17] can operate under both thermal and electric load following control strategies. In case of electric load following operation, the cogeneration system produces electricity by varying the power supplied through the inverter on the basis of the user's power demand in that instant. In case of thermal load following logic, the device operates according to an external temperature signal coming from a specific thermostat: when this temperature is lower than the set-point value, the unit operates providing its maximum electric and thermal outputs; when the temperature from the thermostat exceeds the set-point value, the unit switches in stand-by mode operation; any unused excess of current that is not self-used is sent to the power line on the basis of the net metering contract. In this paper the MCHP unit is operated under the thermal load following logic and it is modelled by means of the Type 907. In particular, a simplified state-state model has been used by assuming that the device provides its nominal thermal (11.7 kW) and electric (6.0 kW) outputs at nominal efficiencies ($\eta_{th} = 56.6\%$, $\eta_{el} = 28.8\%$) while in operation.

The Type 941 is used to simulate the vapor-compression electric heat pump. In particular, the performance of the EHP has been modelled based on manufacturer data [18] by assuming the values of COP as a function of ambient temperature as well as temperature of the fluid at the condenser inlet as indicated in the Figure 3.

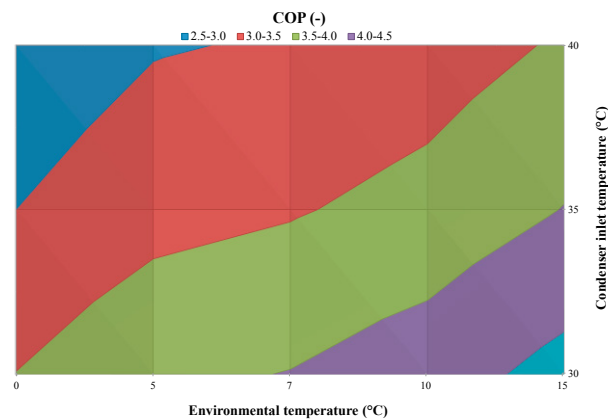


Fig. 3. Values COP as a function of the ambient temperature as well as the condenser inlet temperature [18].

3.2. Control logics

The duration of the heating period has been assumed from 15th November up to 31st March. The DH network pump operates continuously with a flow rate varying between 497.7 kg/h and 18,015.7 kg/h (depending on the number of buildings requiring thermal energy for space heating) during the heating season. When there is no heat demand, the DH network pump operates with the minimum flow rate to avoid a significant temperature drop in the district heating network. The flow rate on the source side of the heat exchanger HE2 is set to the same value of the load side. The heat carrier fluid flows through the air handlers only in cases when there is a call for heat triggered by

a thermostat installed in each building. The room temperature is targeted to be kept at 20°C (deadband = 1°C) only in case of at least one occupant being inside the building, otherwise the indoor air temperature is not controlled; when the room temperature is lower than 19.5°C, it calls for heat from the STTES; the call for heat signal will be disabled when the room temperature reaches 20.5°C.

The solar energy recover is mainly based on the comparison between the current values of temperature at node 10 (lower part) of STTES and the temperature of the fluid exiting the solar collectors field. The BTES charging/discharging is controlled based on the current values of the temperature at nodes 1 (upper part) and 10 (lower part) of STTES, the temperature in the center of BTES field as well as the room target temperature (20°C).

The DHW temperature is assumed to be produced at 45°C.

The set-point for the DH supply temperature is 55°C; therefore the control logic of the back-up systems under investigation has been defined accordingly as reported in Table 4 (where $T_{in,MB}$ is the temperature at the inlet of the MB, $T_{out,MB}$ is the temperature at the outlet of the MB, \dot{m}_{FC} is the mass flow rate of heat carrier fluid entering the fan-coils, $T_{out,HE2,cold}$ is the inlet temperature at the HE2 load side, $T_{out,MCHP}$ and $T_{out,EHP}$ are the outlet temperature of the MCHP device and the outlet temperature of the EHP unit, respectively).

Table 4. Control logic of the back-up systems.

	Main Boiler		MCHP/EHP	
	ON	OFF	ON	OFF
Case 1	Heating period		-	-
Case 2	AND	$\dot{m}_{FC} = 0$ OR	Heating period AND $\dot{m}_{FC} \neq 0$ AND $T_{out,HE2,cold} < 50^\circ\text{C}$	$\dot{m}_{FC} = 0$ OR $T_{out,MCHP} \geq 55^\circ\text{C}$
Case 3	$\dot{m}_{FC} \neq 0$ AND $T_{in,MB} < 50^\circ\text{C}$	$T_{out,MB} \geq 55^\circ\text{C}$	Heating period AND $\dot{m}_{FC} \neq 0$ AND $T_{out,HE2,cold} < 50^\circ\text{C}$	$\dot{m}_{FC} = 0$ OR $T_{out,EHP} \geq 55^\circ\text{C}$

4. Description of the reference heating system

A typical/simple conventional heating system has been considered to be compared with the proposed plant. In the reference system, each building is equipped only with a natural gas-fired boiler (characterized by a constant efficiency of 90%) used for both space heating and domestic hot water production (without using solar collectors). All the electric requirements are satisfied with the electric energy supplied by the central national grid.

5. Methods of analysis

In this paper the performance of the proposed plant has been investigated upon varying the back-up technologies by means of the software TRNSYS over a 5-year period. The simulation results have been analyzed and compared with those associated to the conventional heating system assumed as reference. The comparison has been performed from energy and economic points of view as detailed below.

The energy comparison between the proposed and conventional systems has been performed in terms of primary energy consumption by means of the index named Primary Energy Saving (PES):

$$PES = \left(E_{p,TOT}^{CS} - E_{p,TOT}^{CSHPSS} \right) / E_{p,TOT}^{CS} \quad (2)$$

where $E_{p,TOT}^{CSHPSS}$ is the primary energy associated to the proposed system and $E_{p,TOT}^{CS}$ is the primary energy associated to the conventional system. The power plant average efficiency η_{pp} is assumed equal to 0.42, including transmission losses, according to the Italian scenario [20].

The economic analysis has been performed in terms of both capital and operating costs.

The capital cost of the proposed plant has been evaluated according to the following formula:

$$CC_{CSHPSS} = CC_{SC} + CC_{STTES} + CC_{BTES} + CC_{DH} + CC_{Pumps} + CC_{BS} + \sum_1^6 CC_B \quad (3)$$

where CC_{SC} is the capital cost of the solar collectors, CC_{STTES} is the capital cost of the short-term thermal energy storage, CC_{BTES} is the capital cost of the long-term thermal energy storage, CC_{DH} is the capital cost of the distribution network, CC_{Pumps} is the capital cost of the pumps of the plant, CC_{BS} is the capital cost of the back-up system, CC_B is the capital cost of a single individual boiler. CC_{SC} has been assumed equal to 169.00 €/m² according to the values suggested by Ramos et al [21]. The capital cost associated to the distribution network has been considered equal to 10.55 €/m according to the Italian price list of public works for Naples [22]. The capital costs associated to the pumps of the plant have been considered equal to 4000 €/pump [23]. The values of CC_{STTES} and CC_{BTES} have been evaluated by using the specific cost functions suggested by Pahud [24] based on which CC_{STTES} depends on the volume of the thermal energy storage, while CC_{BTES} is affected by the number of boreholes, the depth of boreholes, the borehole spacing, the depth of the top soil layer covering the thermal storage, the ground area as well as the length of the connection between the boreholes. CC_B and CC_{MB} have been assumed equal to 759.0 € according to manufacturer data [16]. The capital costs for the MCHP unit and the EHP unit are assumed equal to 18,000.0 € [17] and 2,700.0 € [18], respectively. The maintenance costs have been neglected in this study.

The operating costs of the proposed system have been compared with those of the conventional system by means of the following parameter:

$$\Delta OC = \left(OC^{CS} - OC^{CSHPSS} \right) / OC^{CS} \quad (4)$$

where OC^{CSHPSS} are the operating costs associated to the proposed system and OC^{CS} are the operating costs associated to the conventional system.

The tariffs of both the electric energy as well as the natural gas have been kept up-to-date according to the Italian scenario [25]. The unit cost of natural gas ranges from 0.466 €/Sm³ to 0.848 €/Sm³ in Naples. The unit cost of electric energy purchased from the Italian grid is a function of the hour of the day, the day of the week, the level of cumulated electric energy consumption as well as the region where the plant is located; it ranges from 0.121 €/kWh to 0.301 €/kWh in Naples [25]. The unit cost of natural gas for cogenerative use is cheaper than other applications; in particular a tax rebate on natural gas consumption is adopted by the Italian Government in case of MCHP units [26]. The price of the electric energy sold to the Italian grid is a function of the hour of the day, the day of the week, the level of cumulated electric energy consumption as well as the region where the plant is located [27]. In order to evaluate the feasibility of the proposed system, the Simple Pay-Back (SPB) period has been evaluated according to [20]. This economic parameter represents the amount of time required to recover the extra cost of the proposed system (thanks to the reduction of operating costs) in comparison to the reference system. In calculating the values of SPB periods, the Italian economic incentives for promoting the use of renewable energy-based technologies associated to thermal energy production have been taken into account [28] as well as the Government Capital Grants (GCG) on the purchase of the cogeneration units (equal to the 40% of the capital cost of the MCHP device [29]).

6. Results and discussion

The simulation results highlighted that the yearly thermal energy demand for heating purposes is 13.54 MWh/year for the 6 residential buildings and 11.11 MWh/year for the 3 school buildings.

With respect to the operation of the proposed plant, firstly it should be noticed that the values of PES and ΔOC increase with the time assuming the maximum values during the 5th year of operation, whatever the back-up solution is; in particular, they mainly increase from the 1st to the 2nd year of operation and then become substantially constant. This is thanks to the fact that the average temperature of the long-term thermal energy storage becomes higher and higher, allowing for a more effective exploitation of solar energy.

Figures 4a and 4b describe the main simulation results associated to the three different plant configurations under investigation in this paper. In particular, figure 4a reports the values of PES^{5th-year} and $\Delta OC^{5th-year}$ referring to the 5th year of simulation together with the capital costs and the values of SPB, while figure 4b is highlighting the main energy flows associated to the plant components during the 5th year of operation. Figure 4a shows that the values of PES^{5th-year} and $\Delta OC^{5th-year}$ are always positive, whatever the plant configuration is; this means that all the proposed

configurations are able to reduce the primary energy consumption as well as the operating costs in comparison to the reference heating system. In particular, the values of $PES^{5th-year}$ vary between 5.4% and 8.5%, while $\Delta OC^{5th-year}$ is in the range 14.0-24.3%. The maximum values of both $PES^{5th-year}$ (8.5%) is obtained in the case of the EHP is used as back-up unit; the largest value of $\Delta OC^{5th-year}$ (24.3%) is achieved when the MCHP device is included in the plant configuration mainly thanks to the facts that (i) the overall electric energy demand is covered for a significant percentage (around 17%) by the electric output of micro-cogeneration unit (a small amount is also exported to the central grid), thus allowing to reduce the electricity import from the central grid (Figure 4b), and (ii) the unit cost of natural gas for cogenerative uses in Italy is lower than that one associated to other applications. The configuration including only the natural gas-fired boiler as back-up system is that one characterized by the lowest values of both $PES^{5th-year}$ (5.4%) and $\Delta OC^{5th-year}$ (14%): this is related to the facts that (i) the entire electric load is satisfied by the electric energy imported from the central grid and (ii) the EHP is able to satisfy the same thermal energy demand of end-users more efficiently than the boiler. Figure 4a shows that the configuration including the micro-cogeneration device is that one characterized by the largest capital cost (even if the government capital grants associated to the purchase of the MCHP unit are taken into account), but it is able to guarantee the minimum SPB (26.9 years) thanks to the reduced operating costs (also related to the economic incentives adopted by the Italian Government). However, it should be highlighted that the simple pay-back period is relevant at any case and it would not be economically acceptable for the configuration with the MCHP without the support mechanisms of Italian government. Figure 4b also shows that during the 5th year the efficiency of BTES (ratio between the energy extracted and energy injected) is around 26%, while the solar fraction (ratio between the thermal energy demand of end-users and solar energy recovered from solar collectors) is around 34%, whatever the back-up system is.

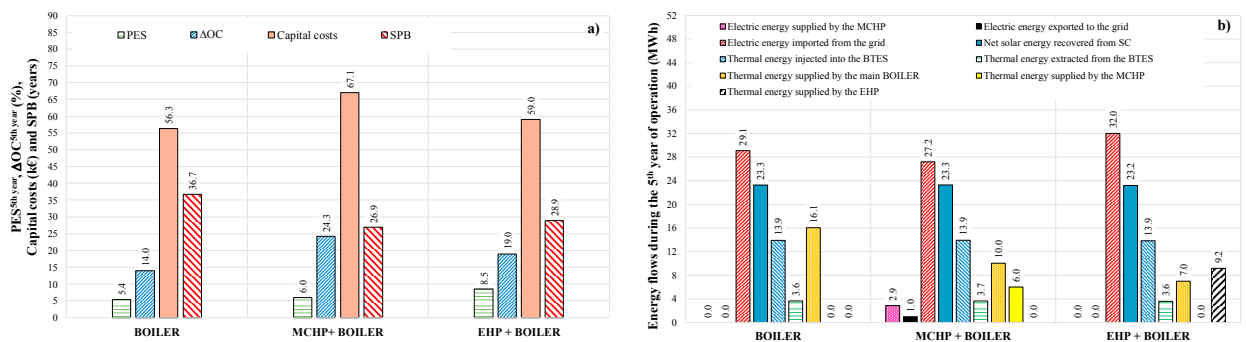


Fig. 4. (a) $PES^{5th-year}$, $\Delta OC^{5th-year}$, capital costs and SPB; (b) Energy flows during the 5th year of simulation.

7. Conclusion

In this paper the performance of a micro-scale solar district heating system located in Naples (south of Italy) has been simulated and analyzed by considering three different plant configurations in terms of back-up system to be used to supplement the intermittent nature of solar source: 1) natural gas-fired boiler only; 2) natural gas-fuelled MCHP unit combined with natural gas-fired boiler; 3) vapor-compression electric heat pump combined with natural gas-fired boiler. The simulation results highlighted that: (a) the proposed solar district heating network is always able to reduce both the primary energy consumption as well as the operating costs with respect to a conventional heating plant assumed as reference, whatever the back-up system is; (b) the configuration with the EHP as back-up unit is characterized by the largest reduction of primary energy consumption (8.5%) thanks to its high energy conversion efficiency; (c) the configuration including the MCHP device as back-up unit is potentially able to obtain the maximum reduction in terms of operating costs (24.3%) allowing to achieve the minimum SPB (26.9 years), mainly thanks to the economic incentives adopted by the Italian government to support the diffusion of micro-cogeneration technology.

References

- [1] Le Truong, N., Dodoo, A., Gustavsson, L. “Effects of energy efficiency measures in district-heated buildings on energy supply”, *Energy* 142 (2018): 1114-1127.
- [2] Rad, F. M., Fung, A. S. “Solar community heating and cooling system with borehole thermal energy storage – Review of systems”, *Renewable Sustainable Energy Reviews* 60 (2016): 1550-1561.
- [3] Directive 2012/27/EU on Energy Efficiency, Amending Directives 2009/125/EC and 2010/30/EU and Repealing Directives 2004/8/EC and 2006/32/EC. OJ L315, 14 November 2012.
- [4] Rosato, A., Sibilio, S., Angrisani, G., Canelli, M., Roselli, C., Sasso, M., Tariello, F. “The micro-cogeneration and emission control and related utilization field”, *Lecture Notes in Energy* 33 (2017): 795-834.
- [5] Sibilio, S., Rosato, A. “Energy technologies for building supply systems: MCHP”, *Energy Performance of Buildings: Energy Efficiency and Built Environment in Temperate Climates* (2015): 291-318.
- [6] Buoro, D., Pinamonti, P., Rein, M., “Optimization of a Distributed Cogeneration System with solar district heating”, *Applied Energy* 124 (2014): 298-308.
- [7] Kallert, A., Schmidt, D., Bläse, T. “Exergy-based analysis of renewable multi-generation units for small scale low temperature district heating supply”, *Energy Procedia* 116 (2017): 13-25.
- [8] German regulation EnEV 2009, <http://www.buildup.eu/en/practices/publications/german-energy-saving-ordinance-2009-enev-2009>.
- [9] Marguerite, C., Schmidt, R.R., Pardo-Garcia, N., Abdurafikov, R. “Simulation based multi-criteria evaluation of design scenarios for an industrial waste heat based micro district heating network supplying standard and low-energy buildings”, *Energy Procedia* 116 (2017): 128-137.
- [10] TRNSYS. The transient energy system simulation tool. Available from <http://www.trnsys.com>.
- [11] Italian Decree, DM 26/06/2015, http://www.gazzettaufficiale.it/do/atto/serie_generale/caricaPdf?cdimg=15A0519800100010110002&dgu=2015-07-15&art.dataPubblicazioneGazzetta=2015-07-15&art.codiceRedazionale=15A05198&art.num=1&art.tiposerie=SG.
- [12] Richardson, I., Thomson, M., Infield, D., Clifford, C. “Domestic electricity use: a high-resolution energy demand model”, *Energy Buildings* 42(10) (2012): 1878-1887.
- [13] Jordan, U. and Vajen, K. Realistic Domestic Hot-Water Profiles in Different Time Scales (2001). <http://sel.me.wisc.edu/trnsys/trnlib/iea-shc-task26/iea-shc-task26-load-profiles-description-jordan.pdf>.
- [14] Ciampi, G., Ciervo, A., Rosato, A., Sibilio, S., Di Nardo, A. “Parametric Simulation Analysis of a Centralized Solar Heating System with Long-term Thermal Energy Storage Serving a District of Residential and School Buildings in Italy”, *3rd AIGE/IIETA International Conference and 12th AIGE 2018*, Reggio Calabria-Messina, June 14-16, 2018, 1-8.
- [15] Kloben, <http://www.kloben.it/products/view/3>.
- [16] Vaillant, <https://www.vaillant.it/home/prodotti/atmotec-exclusive-vmw-9664.html>.
- [17] AISIN SEIKI, TECNOCASA CLIMATIZZAZIONE, www.tecno-casa.com/EN/Default.aspx?level0%4prodotti&level1%4mchp
- [18] CLINT, <http://www.clint.it/index.php?m%400&m2%401&lang%4en>.
- [19] Yang, L., Entchev, E., Rosato, A., Sibilio, S. “Smart thermal grid with integration of distributed and centralized solar energy systems”, *Energy* 122 (2017): 471-481.
- [20] Angrisani, G., Canelli, M., Roselli, C., Russo, A., Sasso, M., Tariello, F. A small scale polygeneration system based on compression/absorption heat pump, *Applied Thermal Engineering* 114 (2017): 1393-1402.
- [21] Ramos, A., Chatzopoulou, M.A., Guarracino, I., Freeman, J., Markides, C. M. “Hybrid photovoltaic-thermal solar systems for combined heating, cooling and power provision in the urban environment”, *Energy Conversion and Management* 150 (2017): 838-850.
- [22] Price list of public works for the Campania region, http://www.lavoripubblici.regione.campania.it/joomla/index.php?option=com_jdownloads&Itemid=105&view=viewcategory&catid=111.
- [23] Wilo, <https://wilo.com/en/index.html>.
- [24] Pahud, D. “Central solar heating plants with seasonal duct storage and short-term water storage: design guidelines obtained by dynamic system simulations”, *Solar Energy* 69(6) (2000): 495-509.
- [25] Italian Regulatory Authority for Energy, Networks and Environment, <https://www.arera.it/it/inglese/index.htm>.
- [26] Sibilio, S., Rosato, A., Ciampi, G., Scorpino, M., Akisawa, A. “Building-integrated trigeneration system: Energy, environmental and economic dynamic performance assessment for Italian residential applications”, *Renewable and Sustainable Energy Reviews* 68 (2017): 920-933.
- [27] GSE, <https://www.gse.it/servizi-per-te/fotovoltaico/scambio-sul-posto>.
- [28] Ciampi, G., Rosato, A., Sergio, S. “Thermo-economic sensitivity analysis by dynamic simulations of a small Italian solar district heating system with a seasonal borehole thermal energy storage”, *Energy* 143 (2018): 757-771.
- [29] Arteconi, A., Brandoni, C., Polonara, F. “Distributed generation and trigeneration: energy saving opportunities in Italian supermarket sector”, *Applied Thermal Engineering* 29 (2009): 1735-1743.



16th International Symposium on District Heating and Cooling, DHC2018,
9–12 September 2018, Hamburg, Germany

Online Leakage Attribution to Exclusion Areas Prototype Application

Bernd Rüger^{a*}, Dennis Pierl^b, Marina Guber^c, Jun Yin^d, Michael Baur^a,
Heinz Eberhard^a, Frank Klawonn^d, Kai Michels^b

^a*SWM Services GmbH, Emmy-Noether-Straße 2, München, 80992, Germany*

^b*Institut für Automatisierungstechnik (Universität Bremen), Otto-Hahn-Allee 1, Bremen, 28359, Germany*

^c*Munich University of Applied Sciences, Lothstraße 34, München, 80335, Germany*

^d*Institut für Information Engineering (Ostfalia Hochschule Wolfenbüttel), Salzdhalmmer Straße 46/48, Wolfenbüttel, 38302, Germany*

Abstract

Localisation of leakages within district heating networks is a challenging but highly essential task. In case of a leakage, especially in sudden cases, there occur miscellaneous adverse effects. In any case, the lost medium must be fed back to the network. If the amount of lost medium is too large, it is inevitable to shut down the network. This can be prevented by the use of exclusion areas if these can separate the damaged parts of the network. However, in order to effectively use these exclusion areas, the leakage must be attributed to one or more exclusion areas as quickly as possible.

One possible approach is based on the propagation of the pressure wave, which may arise as an initial reaction to the occurrence of a leakage. The first step of the prototype presented here is to recognise the leakage entry based on the measurement data. Subsequently, all pressure measurement data are evaluated to find the point in time at which these pressures dropped due to leakage. It is not possible to deduct the leakage position on the basis of these times directly as the data quality meets the operational requirements but is far too low. The prototype can use these time points despite their big errors. For all possible leakage positions the theoretical wave propagation is calculated taking into account the valve states. The leakage is attributed to the exclusion area where the theoretical wave propagation fits best.

Leakages within a real district heating network were simulated to test and evaluate the prototype. For example, about five percent of the transport medium of the network was replenished within a time span of one and a half hours. We present the results of the prototype based on these real data.

© 2018 The Authors. Published by Elsevier Ltd.

This is an open access article under the CC BY-NC-ND license (<https://creativecommons.org/licenses/by-nc-nd/4.0/>)

Selection and peer-review under responsibility of the scientific committee of the 16th International Symposium on District Heating and Cooling, DHC2018.

* Corresponding author. Tel.: +49 / (0)89 2361 - 3347; fax: +49 / (0)89 2361 - 70 3347.

E-mail address: rueger.bernd@swm.de

Keywords: district heating network; fault detection; leak detection; leakage localisation; leakage attribution; Pressure wave; Model-based data evaluation

1. Introduction

For the detection and the localisation of leakages within hydraulic networks or in district heating networks in particular a large variety of methods exists. Some of these methods require at least a rough pre-localisation like thermography or measuring of structure-borne noise which is emitted by the fluid flowing through the breach in case of a leakage. In order to apply these methods, additional measurement equipment is necessary to be able to measure the physical effects resulting from a leakage. Another approach would be the usage of already existent measurement equipment which is needed for operational purposes of the network. Usually, there exist various measurement devices for pressure as well as for flow distributed within a district heating network. As a leakage will always influence and change both, the pressures and the flow state within the pipes, the usage of these available measurement values is plausible.

District heating networks are normally closed systems consisting of two network parts, the supply and the return network. Within the supply network the hot transport medium, mostly water or in some cases steam, is flowing from a supply (here a thermal power plant) towards the consumers. The purpose of the return network is to bring the medium back to the thermal power plant. This is the most common structure of district heating networks. All medium entering the supply network is fed back through the return network in case of standard operation. From this it follows that the law of conservation of mass holds for such district heating networks. If a leakage occurs, medium is leaving the network which will result in a difference between to supply and the return mass flow. Because of the change in the flow state through the pipeline system the pressures within the network will change as well. Especially in case of a large and fast change in the flow state transient effects like the formation of pressure waves may occur. These pressure waves travel through the network with the speed of sound specific for the transport medium and, if recognisable by the pressure measurement devices, may be used for the estimation of the damaged spot in the pipe. This method was already proposed and tested in [1]. Furthermore, pressure wave-based as well as other measurement data driven leakage detection systems for hydraulic networks and systems in general have already been part of research such as in [2], [3] or [4].

Within this work a combination of a flow monitoring system, which interprets the flow measurement signals for supply and return network at the thermal power plant for leakage occurrence detection, and a pressure wave-based localisation algorithm, which estimates the exclusion area in which the damaged spot is situated, is presented.

2. Fundamentals

Media circulation in a district heating network is separated by heat exchangers from the thermal power plant and the customers. The recirculation pump moves the medium in the network and ensures a minimum differential pressure between the supply and the return network at the customers. In this network a minimum pressure is kept by a pressure maintenance pump. In case of a leakage this pump maintains the pressure in the network at a given value as long as enough medium from an equalizing tank can be refilled to the network.

Supply, return and consumption mass flow are equal in an undamaged network. If a leakage occurs, there are dynamic transitions at first. Normally, these transitions decay and a new steady state is established. Medium is lost in damaged district heating networks all the time, which must be refilled. Assuming heat demand of the consumers to be independent from leakages, consumption mass flows are the same before a leakage occurrence and after reaching a new steady state. However, supply and return mass flow will change as follows:

- Leakage in supply network – Supply mass flow rises to the sum of the consumption and the refill mass flow. Return mass flow stays equal to consumption mass flow.
- Leakage in return network – Supply mass flow stays equal to the consumption mass flow. Return mass flow drops to consumption mass flow minus refill mass flow.

If this holds true for real measurement data, it can be useful to narrow down the position of a leakage or to attribute it e.g. to an exclusion area because only half of the network has to be considered.

An exclusion area is a network part which may have intersections but can be separated from the rest of the network easily. Exclusion areas border on each other in manholes where remote controllable motor driven valves are installed in the supply and the return network. All valves bordering an exclusion area can be operated at the same time by a single command. These valves may only be opened if the differential pressure across them is small enough. Hence, there is at least one pressure measurement in the supply network and one in the return network of each exclusion area installed. The measured values are transmitted to the dispatcher to allow remote control. Normally there is more than one measurement in the supply or return network of an exclusion area as further parts may be separated inside exclusion areas manually.

The topology of the exclusion areas of a real district heating network of the company Stadtwerke München is shown in Fig. 5 (upper left). It is not to scale and does not show correct lengths or areas. Nevertheless, all exclusion areas and possible connections between them are displayed correctly. The network is supplied from one single point and shows three lines. Two of the lines are connected to each other directly or via exclusion areas of linking lines, respectively. Compared to other networks only a few meshes are present. Each line consists of several exclusion areas which are numbered for each line separately starting at the supply. Including the supply there are 28 exclusion areas in total. The network has a total length of 95.7 km and a volume of 7709 m³. The length of the pipes in exclusion areas differs significantly and ranges between 4 m and 15.6 km. Likewise, the volumes range from 1 to 917 m³. The exclusion areas number 3 and 10 in line 2 are extraordinarily small because they are both located inside a manhole. These exclusion areas are not used in operation very often.

3. Measurement data description

Real measurement data is most important for the development of procedures for narrowing down the localisation of leakages or for their attribution to exclusion areas. Technical infrastructure was installed during a project funded by the Bundesministerium für Wirtschaft und Energie (BMWi). It allows recording all data of the given district heating network in parallel to normal operation in the best possible quality. This was realized with standard systems and no changes were made with respect to the hardware of measurements or the transmission technology.

Unfortunately, no real leakages occurred within the network since infrastructure installation. However operational tasks like preservation and maintenance works have been conducted at pipes of this network. These pipes were separated from the network and emptied during these tasks. Thereafter the pipes were refilled after completion of the maintenance works. Generally, the return network is employed for refilling. Hereby the filling cycle appears similar to a leakage to the residual network. Therefore corresponding data is named artificial leakage or simply leakage. Two measurement data sets are available:

- 27.07.2017 – Exclusion area 6 of line 1 was separated from the residual network and a larger pipe of that exclusion area was emptied (290 m³, 3.8 % net volume). Refilling after maintenance work took place via the return network in exclusion area 5 of line 1. All connections between exclusion area 6 of line 1 and exclusion area 2 of the linking line were closed the whole time.
- 01.08.2017 – Four refill events were conducted. In the first, second and fourth event the supply network was employed for refilling. This is only possible as a network part after a mixing station was refilled. A mixing station reduces pressure and temperature in the supply network after the station by mixing medium of return network and supply network before the station. This enables direct feed of network parts with lower maximum pressure and/or temperature. If the temperature in the supply network is low enough, it can be employed for refilling. The first and the second event took place in exclusion area 6 of line 1. The fourth event took place in exclusion area 4 of line 2.

4. Leakage detection based on refill mass flow

The pressure value at a damaged spot drops if a leakage occurs. This pressure drop spreads from that spot into the network by the speed of sound. With a given maximum distance to the supply of e.g. 10 km the pressure wave needs less than 10 seconds to arrive there. The pressure maintenance pump reacts directly to this and refills medium to hold the pressure. Leakage entry leads to a rise of refill mass flow within a matter of a few seconds after leakage occurrence which can be used to detect the leakage (see Fig. 1). To recognize a leakage based on pressure measurement values is much more complicated as these values change with different operating conditions.

Fig. 1 (upper part) shows the refill mass flow over time on the 27.07.2017. It has been calculated as sum of the supply mass flows of the three lines minus the sum of their return mass flows. At that point in time these measurements were operated since quite a long time and were not especially calibrated. The refill mass flow is in a range between 0 and 75 t/h during normal operation (green area) and is superimposed by large noise. If calibrated the refill mass flow should be close to 0 t/h on average. The refill mass flow is much higher in the time period between 17:45 and 19:30 h (yellow area). At begin and end of the filling cycle the refill mass flow rises and drops fast respectively. A maximum value of about 250 t/h is reached and kept for about one hour. In total about 290 m³ are refilled.

Fig. 1 (lower part) shows the refill mass flow between 17:35 and 17:59 h. It is not rising continuously. Four steps can be identified (blue areas). The reason for this is that the valve is opened in four steps to avoid a too big pressure drop. A real leakage would not do this but as it is an operational task shutting down of the thermal power plant due to pressure falling below a minimum value should be avoided. A pressure wave can occur at each of the four steps.

Refill mass flow on the 01.08.2017 is evaluated in the same manner. At that day there were four events. Three of these can be detected by an increased refill mass flow. The third event cannot be identified as it is too small compared to noise.

Table 1 allows the comparison of the values for key parameters of the four steps and the four events. Refill mass flow rises by about 17 t/h in the minimum and 75 t/h in the maximum case. It is not rising abruptly but rather with a gradient between 9 t/h/min and 100 t/h/min. The pressure wave triggered by leakage entry is expected to be more distinct if the rise in refill mass flow is large and occurs with a steep gradient.

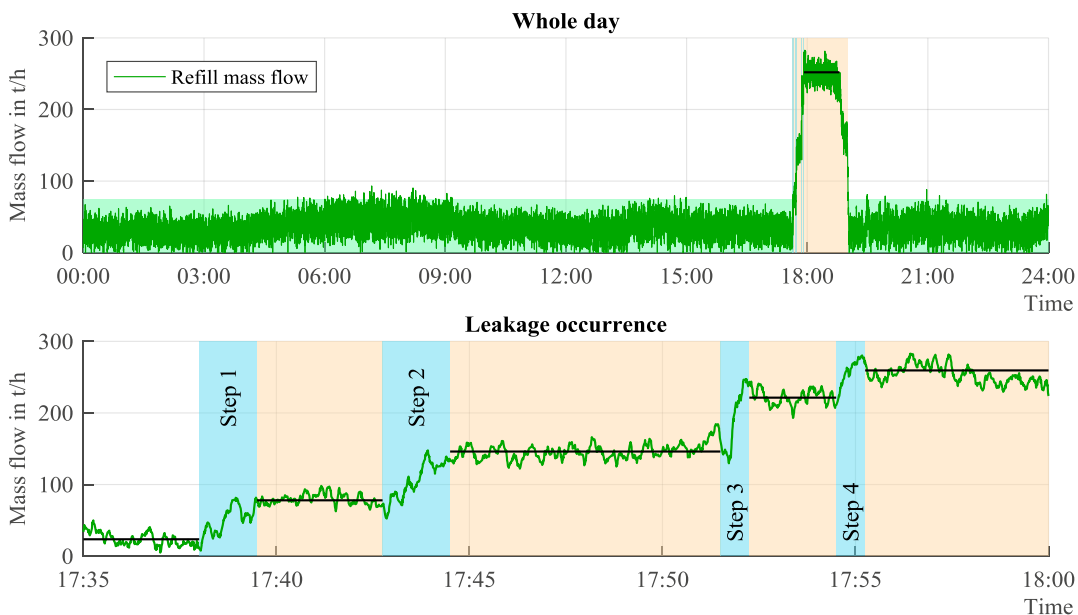


Fig. 1. Total refill mass flow calculated from flow measurements over time on the 27.07.2017.

Table 1. Key parameters and values of the artificial leakages (four steps on the 27.07.2017; four events on the 01.08.2017)

Date	Event	Begin	Refill in t/h	End	Refill in t/h	Δ Refill in t/h	Gradient in t/h/min
27.07.2017	step 1	17:38:00	23.54	17:39:30	77.96	54.42	36.28
	step 2	17:42:45	77.96	17:44:30	146.11	68.15	38.94
	step 3	17:51:30	146.11	17:52:15	221.35	75.24	100.32
	step 4	17:54:30	221.35	17:55:15	251.94	30.59	40.79
01.08.2017	event 1	08:22:30	45.33	08:24:30	62.77	17.44	8.72
	event 2	09:02:00	46.13	09:09:30	113.50	67.37	8.98
	event 3	N/A	N/A	N/A	N/A	N/A	N/A
	event 4	13:48:00	36.28	13:50:30	71.86	35.58	14.23

5. Attribution to supply or return network

Earlier in this paper changes of supply and return mass flows during leakages were considered. Hence Fig. 2 shows these mass flows over time on the 27.07.2017. The return mass flow drops clearly during the filling cycle (yellow area) whereas the supply mass flow stays unchanged. This matches perfectly to the considerations as the pipe was refilled via return network. If this is observed it can be used to reduce search space for leakage position to return network only.

Fig. 3 shows the mass flows over time on the 01.08.2017. During events 2 and 4 (yellow areas) supply mass flows rise and return mass flows stay unchanged. This is not easy to decide due to the constant and synchronic changes of both mass flow values and because these leakages have much smaller refill mass flow values compared to the one on the 27.07.2017. Most important is the change at the end of filling cycle when the refill mass flow drops abruptly. This again matches perfectly to the considerations at the beginning of the paper as in both events medium was taken out from supply network. If this is observed it can be used to reduce search space for leakage position to supply network only. Event 1 cannot be evaluated as refill mass flow change is too small compared to noise.

Correlation between changes in mass flows and leakage position in supply and return network respectively cannot be used shortly after leakage occurrence if only a small refill mass flow is present. Refill mass flow often rises in a time span of several minutes. Hence supply and return mass flow drift away from each other. But it cannot be decided if supply mass flow rises or return mass flow drops due to the constant and synchronic changes of both mass flows values. This can only be decided after the end of the events with the abrupt drop of the refill mass flows. But maybe more sophisticated algorithms can be developed to support this decision.

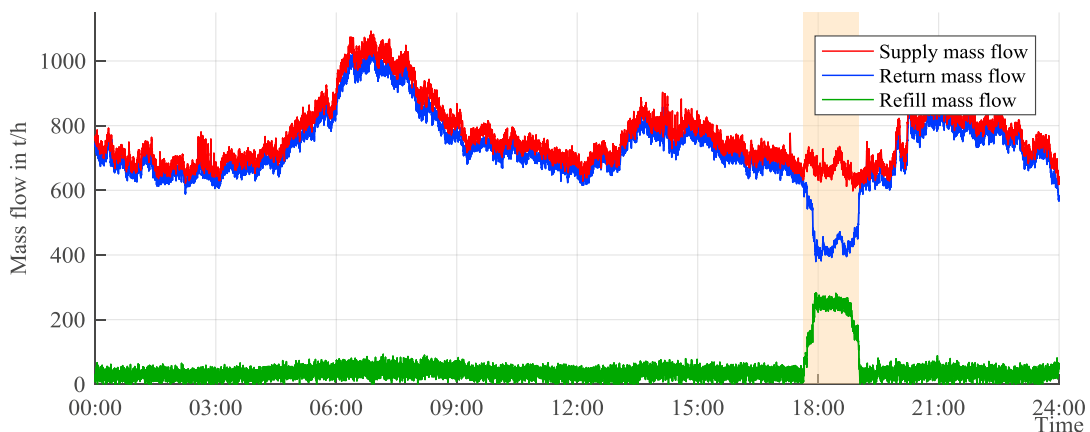


Fig. 2. Total supply, return and refill mass flow over time on the 27.07.2017 (whole day).

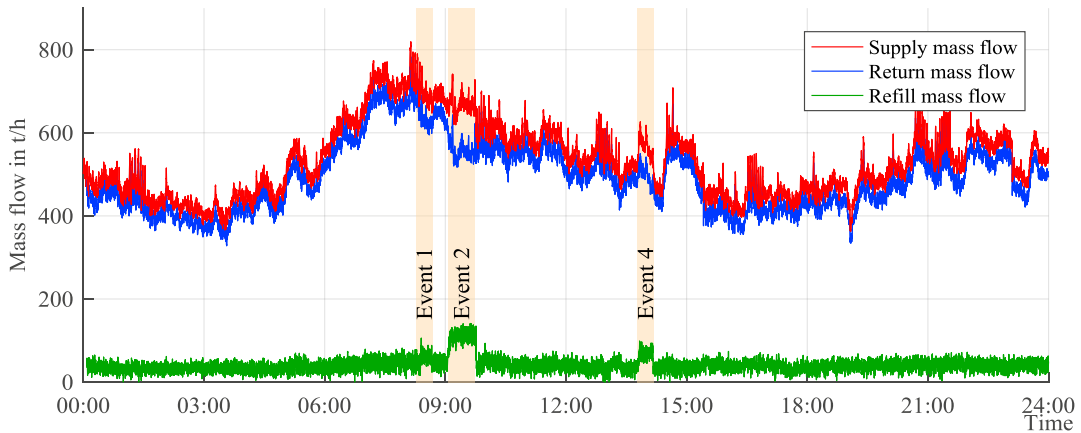


Fig. 3. Total supply, return and refill mass flow over time on the 01.08.2017 (whole day).

6. Attribution to exclusion areas based on negative pressure wave

If a leakage is large and develops fast enough a distinct and abrupt drop of measured pressure values will occur. This pressure drop spreads from the damaged spot into the network by the speed of sound and results in a negative pressure wave. Due to different distances the pressure wave arrives at different points in time at different measurement locations. In [1] leakage position is determined based on those points in time. Like in [1] a direct localisation of the leakage based on the points in time when the pressure wave reaches measurement devices was considered. Fig. 5 (lower left) shows the results for step 3 on the 27.07.2017 [5]. Only measurements in return network of good quality were examined as pressure wave is more distinct there. Points in time where the pressure wave reaches the measurements were identified automatically by different algorithms. The best results are shown here. Fig. 5 (lower left) shows the results in relation to the topology. Colour of measurements correlates to time differences. No causal relationship between damage/filling spot and measurement location is visible. Furthermore measurements cannot be grouped and no systematic is visible.

The question here is why it is that difficult to conduct a leakage attribution resp. a localisation based on the points in time. In [1] a special measurement technology was installed which records measurement values every 300 ms. The measurement technology installed in the district heating network at hand does not provide measurement data with a fixed time interval. Instead the transmission of data is performed spontaneously whenever the measured value changes by a given quantum compared to the value transmitted last. This quantum was changed to 1 bit, so with every change in the least significant bit a new measurement value will be transmitted. Because of the equipment used and the transmission chain with e.g. programmable logic controllers (PLC) the recorded data cannot be transferred at any rate and speed. PLC's usually have cycle time of about 250 ms. And depending on the measurement device and the transmission path a varying maximum amount of data can be sent.

The distance in time of the measurement values may vary. If the pressure does not change no new measurement value is transferred. If the pressure changes drastically within a longer period of time new measurement values are transferred as often as possible during this period. Therefore it could make a difference if recorded measurement data before, during or after the occurrence of a leakage is evaluated. Prior to as well as after a leakage the pressures in the network normally do not fluctuate too much. But in the event of a leakage there are large changes.

A histogram of the distance in time between the single data points for all available measurement data of step 3 on the 27.07.2017 prior to, during and in the aftermath of the occurrence of the leakage was evaluated. The distribution differs marginally. A possible reason for this could be the fact that the pressures within the network change permanently thus measurement data is recorded und transferred at the maximum possible rate all the time. But this was not further investigated. Crucial is the fact that more than 60 % of the data points are more than 2 seconds apart from each other. Furthermore 40 % of the data points are more than 5 seconds apart. On the other hand data points

with less than 200 ms of distance in time barely exist. Only about 5 % of the data points are less than 400 ms apart from each other. Hence the quality of the available measurement data is significantly worse compared to the one in [1]. But from the point of view of the owner of a district heating network it would better if no new or additional measurement and transmission technology with significantly better properties is needed as this normally means higher costs.

7. Improved leakage attribution to exclusion areas by pressure wave calculations

One main question is if available measurement data in total maybe still hold sufficient information to generate a rating for the exclusion areas. This rating should depend on the probability for the exclusion area to contain the damaged spot. In the considered district heating network 119 pressure measurements in 28 exclusion areas are existent (whereby some measurements are omitted because of insufficient quality).

Fig. 4 illustrates the concept of the rating algorithm. As first step the points in time at which all pressures drop are extracted from the real measurement data. If all points in time are plotted on a time axis this results in a specific leakage profile or leakage fingerprint (green time axes shown in Fig. 4).

In a second step theoretical pressure waves for all possible leakage positions within the network are calculated. The points in time at which these pressure waves reach the measurement devices depend on distance between device and wave origin and speed of sound for the flowing fluid. For each possible leakage position these points in time are as well plotted on time axes respectively. This results in a large amount of calculated pressure wave profiles. In Fig. 4 this is shown for 3 leakage positions exemplarily. Both the sequence and distance of the points in time at which the theoretical pressure waves reach the measurement devices vary. As example the point in time for measurement device 2 is exemplarily marked in all calculated pressure wave profiles.

Third step is to compare leakage fingerprint with each single calculated pressure wave profile separately. For each measurement device the absolute deviation between measured and calculated point in time is determined and subsequently summed up. Hereby the two time axis compared to each other must be shifted so that the sum of the deviations becomes minimal. The smaller the value of the summed up deviations is the better leakage fingerprint fits to the calculated pressure wave profile. This approach was applied to all nodes of the network model of the considered district heating network. The computed sums of deviations for all nodes are assigned to their appropriate exclusion area. Based on this a condensed value for each exclusion area is computed.

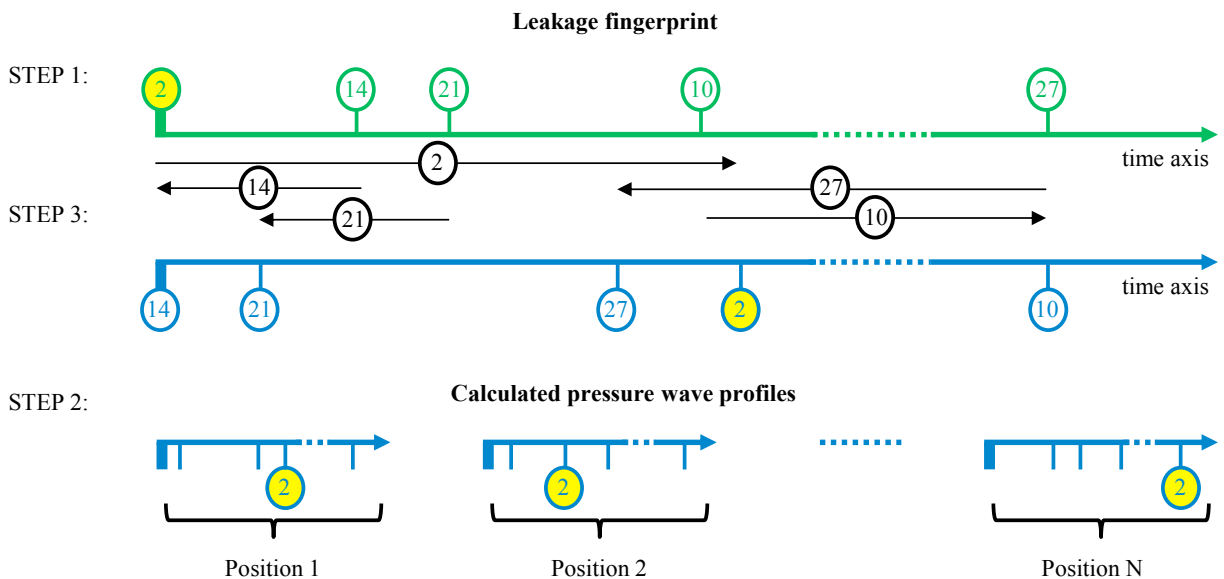


Fig. 4. Rating algorithm steps: 1) Extract fingerprint from measured data, 2) Calculate wave profiles and 3) match them.

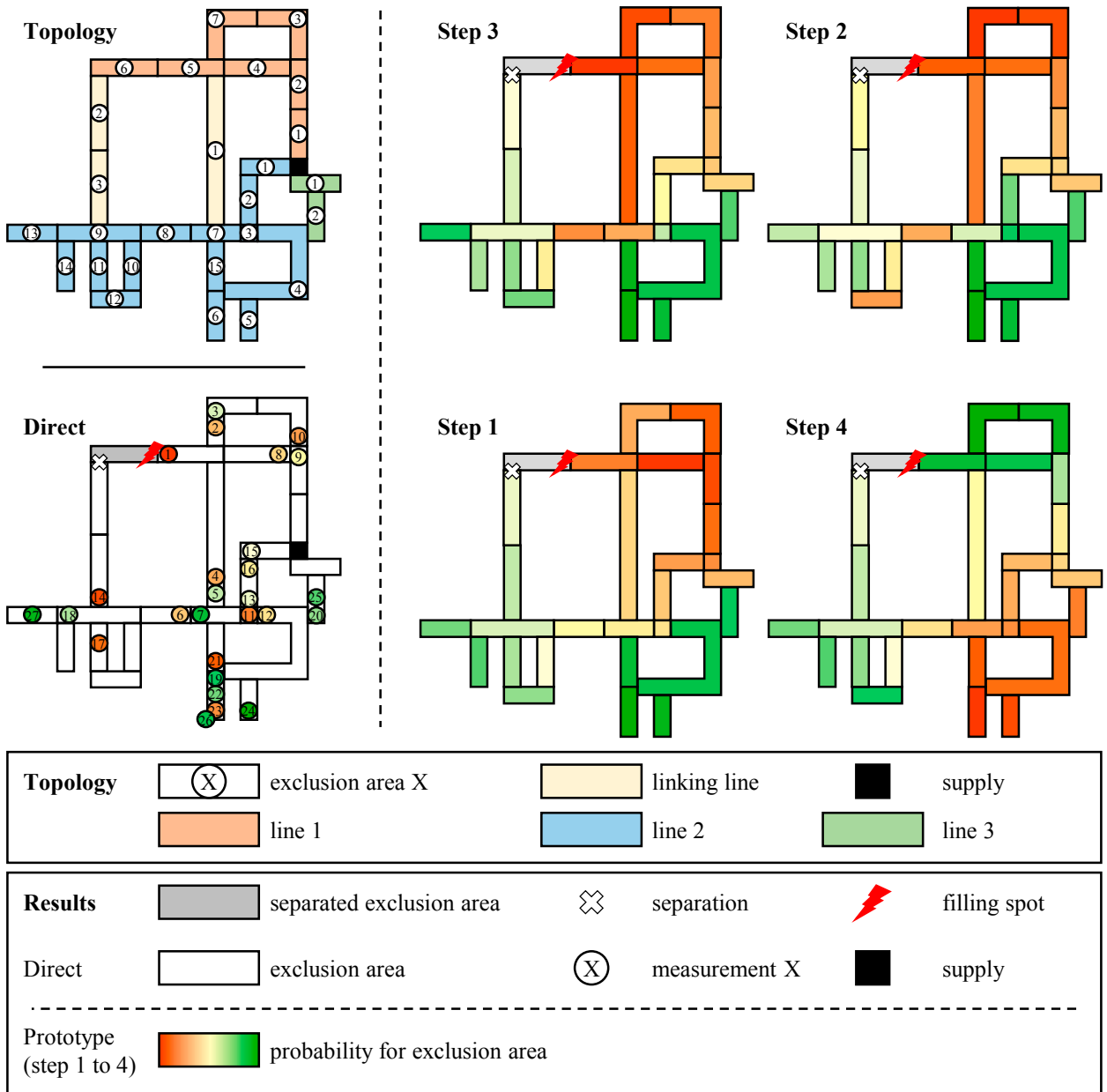


Fig. 5. Network topology, visualisation of the determined points in time where the pressure drops for all measurements (direct) and result of the prototype for all steps on the 27.07.2017 (= colour coded probability for exclusion areas to contain the damaged spot)

The final result can either be represented in the form a table sorted descending by the value of the sum of deviations or as a coloured map of the topology of the network. Fig. 5 (upper middle) shows the result for the evaluation of the most distinct pressure wave (step 3 on the 27.07.2017). Colour correlates to the probability that the exclusion area contains the damaged spot (red = highest; green = lowest). Indeed there is correlation between the exclusion area predicted by the algorithm and the location of the filling spot. Exclusion area 6 in line 1 was separated and is coloured in grey. The filling was performed via exclusion area 5 in line 1 which is ranked 1st by the algorithm. All neighbouring exclusion areas are ranked next and colour distribution in the topology shows a

plausible causal relationship. The further an exclusion area is situated with respect to the damaged spot the worse the calculated pressure waves match leakage fingerprint.

Fig. 5 shows the results for the evaluation of all pressure waves (steps 3, 2, 1 and 4 on the 27.07.2017). The order is chosen according to the gradient and as steps 2, 1 and 4 show the same one additionally to the extent of the leakage. This order matches the quality of the results. The pressure wave shape was found to be less distinct in that order too. And as the algorithm uses leakage fingerprint results must be influenced by this. Steps 3, 2 and 1 deliver acceptable results whereas step 4 is pointing to a totally wrong network part.

A rating was calculated by the algorithm described for all pressure waves (steps 3, 2, 1 and 4 on the 27.07.2017). The more distinct the pressure wave is, the smaller the summed up deviations become. E.g. smallest value for step 3 is 65.11 and for step 4 it is 2882.91 which is a significant difference. This can be used as additional information on how reliable the coloured map is. For step 3 the correct exclusion area is ranked 1st with the lowest rating of 65.1. For step 2 it is ranked 3rd with a much higher rating of 1517.9. For step 1 it is ranked 5th with a similar rating. For step 4 it is ranked 25th with almost the highest rating of 3326.8.

8. Conclusions

- Within the scope of the project „EnEff:Wärme – Eingrenzung von Leckagen auf Basis eines analytischen Fernwärmenetzmodells“ funded by the BMWi a district heating network of the company Stadtwerke München was revised so that measurement data can be recorded at the best possible quality. But still the typical operational hardware is employed.
- On the 27.07.2017 a filling cycle of a previously for maintenance work separated and emptied part of the network was performed. The share of this part of the network’s volume is about 3.8 %. The filling cycle took about 1:15 h. The valve was opened in four steps at the start of the filling cycle. The whole process could be tracked on the basis of the refill mass flow. For all four steps a pressure wave occurred which was evaluated. On the 01.08.2017 four single events took place. Three of these filling cycles could be recognised based on the refill mass flow. Only for events 2 and 4 the pressures drop over time was evaluated as event 1 has a very small leakage extent. The pressure drop is in both cases very slow and no distinct pressure wave is visible.
- The assumptions on how supply and return mass flow behave for the new steady state after the occurrence of a leakage could be approved on the basis of measurement data. If supply mass flow rises while return mass flow stays constant leakage is located in supply network. If supply mass flow stays constant and return mass flow drops leakage is located in return network. Unfortunately it is not easy to use that relationship if there are only few data points after leakage occurrence available and if leakage gradient is small compared to normal changes of the mass flows. Information about leakage location in supply or return network may enable algorithms to work more precise and faster.
- The attribution of the leakage to one exclusion area on the basis of the points in time at which the pressure wave reaches the pressure measurement devices is not possible directly. This is due to the measurement data quality. For more than 60 % of the data points the distance in time is greater than 2 seconds and for 40 % it is 5 seconds. This is independent of time: before, during or after a leakage.
- For all nodes of the network theoretical pressure waves were calculated. The times these waves need to reach all pressure measurement devices can subsequently be compared to leakage fingerprint. The absolute deviation between them can be used to determine which theoretical pressure wave matches to leakage fingerprint best. The smaller the deviation the more probable it is that the real pressure wave’s origin is at that particular node of the network. The results for the single nodes are condensed for each exclusion areas. This results in a rating for all exclusion areas.
- The applicability of the described method depends on how distinct the pressure wave is. This depends on both the extent and the gradient of the leakage. Suggested reference point: gradient should be at least 40 t/h/min and extent of the leakage should be at least 50 t/h. This is a limitation for practical use. However there are certain types of leakages where this method fits perfectly: e.g. if a fibre-glass reinforced plastic pipe breaks at a coupling.
- For the data on the 27.07.2017 the actual affected exclusion area was rated on the first place for step 3, on third place for step 2, on fifth place for step 1 and 25th place for step 4.

- Until now the analysis of the measurement data was performed offline. The work on installing a prototype which performs the data analysis online without supervision of an operator is currently going on. For testing purposes the data on the 27.07.2017 is passed to the prototype as if it was actual data. The complete toolchain for evaluation already exists and a rating is generated and displayed. It is planned to deploy the prototype until June 2018. In July 2018 another maintenance work is planned which can be used to test the prototype online. As this is a work in progress the applied algorithms and parameters may still change to achieve better results.

Acknowledgements

Funding by the BMWi is gratefully acknowledged. Good collaboration with Projektträger Jülich (PTJ) shall be mentioned. Furthermore this work would not have been possible without fruitful discussions, support, participation and contributions of several employees of the company Stadtwerke München and of several students in the project.

Gefördert durch:



Bundesministerium
für Wirtschaft
und Energie

aufgrund eines Beschlusses
des Deutschen Bundestages

References

- [1] Valinčius, Mindaugas, Mindaugas Vaišnoras, and Algirdas Kaliatka. "Study and demonstration of pressure wave-based leak detection in a district heating network." *Structure and Infrastructure Engineering* 14:2 (2018): 151-162.
- [2] Chuanhu, Ge, Wang Guizeng, and Ye Hao. "Analysis of the smallest detectable leakage flow rate of negative pressure wave-based leak detection systems for liquid pipelines." *Computers and Chemical Engineering* 32 (2008): 1669-1680.
- [3] Ostapkowicz, Paweł. "Leak detection in liquid transmission pipelines using simplified pressure analysis techniques employing a minimum of standard and non-standard measuring devices." *Engineering Structures* 113 (2016): 194-205.
- [4] Arifin, B.M.S., Zukui Li, Sirish L. Shah, Gordon A. Meyer, Amanda Colin. "A novel data-driven leak detection and localization algorithm using the Kantorovich distance." *Computers and Chemical Engineering* 108 (2018): 300-313.
- [5] Yin, J. "Localization of leakages in a district heating network by evaluation of pressure measurement data." *Master's Thesis*, Institut für Wirtschaftsinformatik (Technische Universität Braunschweig), Universitätsplatz 2, Braunschweig, 38106, Germany (2018).



16th International Symposium on District Heating and Cooling, DHC2018,
9–12 September 2018, Hamburg, Germany

Design Aspects for Large-scale Pit and Aquifer Thermal Energy Storage for District Heating and Cooling

Thomas Schmidt^a, Thomas Pauschinger^a, Per Alex Sørensen^b, Aart Snijders^c,
Reda Djebbar^{d*}, Raymond Boulter^d, Jeff Thornton^e

^aSteinbeis Research Institute for Solar and Sustainable Thermal Energy Systems (Solites), Meitnerstr. 8, 70563 Stuttgart, Germany

^bPlanEnergi Nordjylland, Jyllandsgade 1, 9520 Skørping, Denmark

^cIFTech International, Mooieweg 238, NL 6836 AM, Arnhem, The Netherlands

^dNatural Resources Canada – CanmetENERGY (NRCan), 1 Haanel Drive, Building 5A, Nepean, Ontario K1A 1M1, Canada

^eTESS, 22 N. Carroll Street – Suite 370, Madison WI 53703, USA

Abstract

Large-scale seasonal thermal energy storage (TES) can help maximize renewable energy integration into district heating and cooling (DHC) systems. However, expertise and concrete projects in the field is limited and there is currently a lack of reliable and adequate analysis tools and cost data to assess the technical-economic potential of aquifer thermal energy storage (ATES) or pit thermal energy storage (PTES). This paper provides a review summary for current ATES and PTES systems, including design concepts, application criteria, specific cost comparisons of various storage systems, as well as a summary of applicable modelling and design tools currently available.

© 2018 The Authors. Published by Elsevier Ltd.

This is an open access article under the CC BY-NC-ND license (<https://creativecommons.org/licenses/by-nc-nd/4.0/>)

Selection and peer-review under responsibility of the scientific committee of the 16th International Symposium on District Heating and Cooling, DHC2018.

Keywords: Aquifer Thermal Energy Storage (ATES); Pit Thermal Energy Storage (PTES); Large-scale Thermal Energy Storage; District Heating and Cooling

* Corresponding author. Tel.: +1 (613) 996-8828; fax: +1 (613) 996-9416.

E-mail address: Reda.Djebbar@Canada.ca

Nomenclature

ATES	Aquifer Thermal Energy Storage	PP	Polypropylene
BTES	Borehole Thermal Energy Storage	PTES	Pit Thermal Energy Storage
CHP	Combined Heat and Power	RES	Renewable Energy Sources
DHC	District Heating and Cooling	SDH	Solar District Heating
HDPE	High-density Polyethylene	STES	Seasonal Thermal Energy Storage
IEA	International Energy Agency	TES	Thermal Energy Storage
PE	Polyethylene	TTES	Tank Thermal Energy Storage
PEX	Cross-linked Polyethylene	UTES	Underground Thermal Energy Storage

1. Introduction

Modern district heating and cooling (DHC) systems are a key technology for the energy transition to a green economy, because they enable at a large scale to couple the heat and electricity sector and hence to increase the flexibility of the overall energy system. In so-called smart DHC systems, large-scale thermal energy storages (TES) render possible the integration of high shares of renewable energy sources (RES), to integrate excess electricity from RES and to optimize combined heat and power plants (CHP).

The research in the IEA project ‘Integrated Cost-effective Large-scale Thermal Energy Storage for Smart District Heating and Cooling’ (IEA DHC Annex XII Project 3, Contract No. XII-03) contributes towards the development of data, information and analysis tools to encourage the use of cost-effective large-scale underground thermal energy storage (UTES) in DHC systems. The TES technologies of interest for this international collaboration are aquifer and pit thermal energy storage (ATES and PTES), where ATES use naturally occurring self-contained layers of ground water, so called aquifers, for heat and cold storage and PTES are made of an artificial pool filled with storage material and closed by a lid. These TES types offer cost-effective solutions for large-scale applications. Where applicable, these TES types have a significant cost advantage compared to conventional heat stores. Cost levels of less than 50 €/m³ have been reached and are in particular interesting for DHC applications with a low number of storage cycles (e.g. long-term or seasonal storage of cold or heat).

Four main concepts for large-scale UTES have been developed and demonstrated in the last decades (see Figure 1).

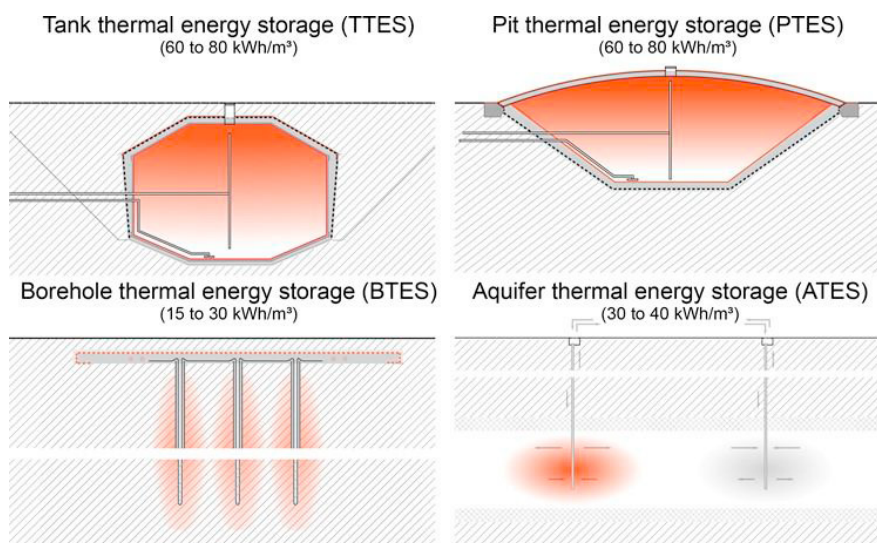


Fig. 1. Overview of available Underground Thermal Energy Storage (UTES) concepts [1].

Each of these concepts has different capabilities with respect to storage capacity, storage efficiency, possible capacity rates for charging and discharging, requirements on local ground conditions and on system boundary conditions (e.g. temperature levels). The most suitable TES concept for a specific project has always to be found by a technical-economical assessment for the specific boundary conditions. The assessment has to consider all relevant boundary conditions like local (hydro-) geological situation, system integration, required storage capacity, temperature levels, power rates, number of storage cycles per year, legal restrictions, etc. For all concepts a geological investigation has to be made in the pre-design phase. The highest requirements with respect to this are made by ATES and BTES. Also legal requirements have to be checked. In most countries the usage of the ground for heat storage has to be approved by the local water authorities to make sure that no water protection areas are affected. This can also become necessary if only the ground surrounding a storage tank or pit is heated up by thermal losses.

In the following ATES and PTES concepts are treated in more detail. More information on other storage concepts can be found in [1] or [2].

2. ATES design concepts

An aquifer is a subsurface geologic feature that is capable of yielding large quantities of water (e.g. a layer of sand, gravel, sandstone or fractured rock). While aquifers are geographically limited in area around the world, they are typically located under large population areas such as the east coast of the US and river deltas such as the Netherlands.

The IEA Implementing Agreement on Energy Conservation through Energy Storage (ECES) supported several research and development activities on ATES commencing in the early 1980s. Cold storage for cooling buildings with “cold” stored in the winter proved the most promising in temperate and northern climates: the natural underground temperature is typically only 0 to 10 °C warmer than the required storage temperature for cooling. This allows sizing an ATES system to meet (part of) the cooling demand with direct cooling, i.e. without running a chiller. High-temperature aquifer storage of surplus heat from combined cycle power plants have also been demonstrated [3, 4, 5].

Figure 2 displays the **basic principle** of an ATES system that is used for both cooling and heating, the most common application of ATES. In summer, groundwater is extracted from the cold well(s) and used for cooling purposes, depleting the cold store over the cooling season. The warmed return water is injected in the warm well(s) to recharge the warm store. In winter the process is reversed: water is pumped from the warm well(s) and applied as a low temperature heat source for one or more heat pumps. After the heat transfer the chilled water from the heat pump(s) is injected into the cold well(s), recharging the cold store for use the following summer.

All the water extracted from the cold store is re-injected into the warm store. There is no net extraction of groundwater, so although ATES systems operate at high flow rates, there is no consumptive use of groundwater.

ATES systems require three primary site-specific physical characteristics:

- An aquifer capable of yielding high flow rates from wells.
- Seasonally variable (and preferably, relatively balanced) heating and cooling requirements.
- Relatively large thermal loads, typically greater than 250 kW heating and cooling load.

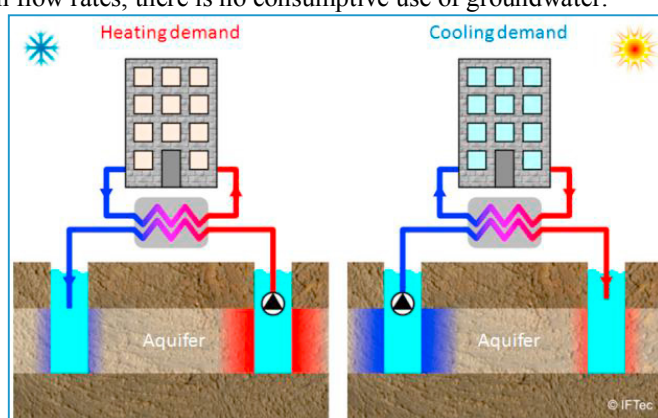


Fig. 2. Principle of ATES in heating (winter) and cooling (summer) mode [6,7]

As of the end of 2017, an estimated 3,000 ATES projects were in operation in Europe. The number of ATES projects integrated in a local DHC network has exceeded 100. These are larger scale ATES projects (storage capacity 1 MW or more) with a distribution network serving two or more buildings or industries.

Utility scale ATEs projects consist of a well field with several groundwater production/recharge wells, groundwater transport/distribution piping, heat pumps as well as warm and chilled water distribution piping. These systems provide heating or cooling, or simultaneous heating and cooling to several buildings. The groundwater circuit is hydraulically separated from the heating and cooling circuits inside the buildings by plate heat exchangers.

From the thermal energy distribution perspective, several system configurations can be distinguished (Table 1.).

Table 1. Distribution system configurations

Heat pump location	Distribution groundwater	Distribution chilled and warm water
1. In centralized plant room for all buildings together.	Between well field and central plant room. Single, uninsulated piping (water is flowing either from warm to cold wells or from cold to warm wells).	Supply and return piping for warm and chilled water between central plant room and buildings, and inside buildings. Four-pipe system, insulated.
2. In central plant room per building (also group of houses/apartment block). Remark: Best suited for ATEs application.	Between well field and buildings. Two- or four-pipe system, piping not insulated.	Supply and return piping for warm and chilled water inside buildings. Four-pipe system, insulated. Remark: DHW make-up might be integrated in building plant room.
3. Distributed heat pumps in the buildings. Remark: Central heat exchanger per building is recommended for hydraulic separation ATEs and building circuit.	Between well field and buildings. Two pipe system (supply and return), piping not insulated.	Two-pipe system (supply and return) inside buildings between heat exchanger and distributed heat pumps. Piping insulated. Supply and return piping for warm and chilled water after heat pumps. Two- or four-pipe system.

Figures 3 and 4 depict the **conceptual design** of an ATEs integrated with a local DHC network. A two-pipe groundwater loop with active building connections is applied in this example. The principle of operation for a building in winter mode and the ATEs system in winter mode (ATEs system heating mode and charging operation for the cold ATEs wells) is displayed in Figure 3. Note that with this winter mode configuration:

- Some buildings can still be in cooling mode while the other buildings are in heating mode. In heating mode of the ATEs system, the net flow in the groundwater loop will be from the warm wells to the cold wells.
- The warm well discharge temperature indicated in Figure 3 is resulting from the summer operation.

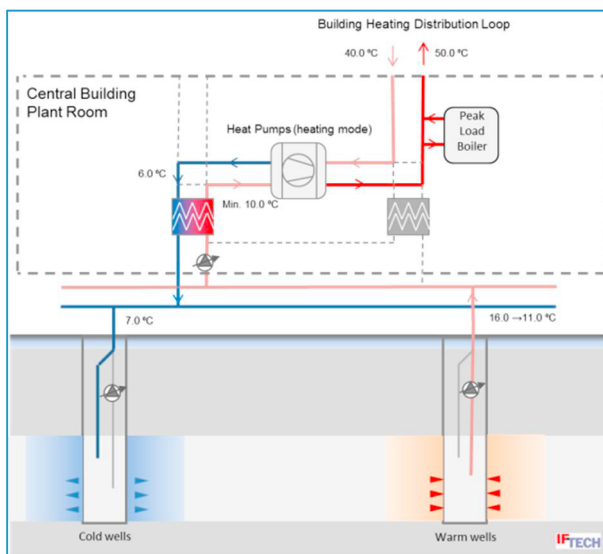


Fig. 3. ATEs system in heating mode (winter operation)

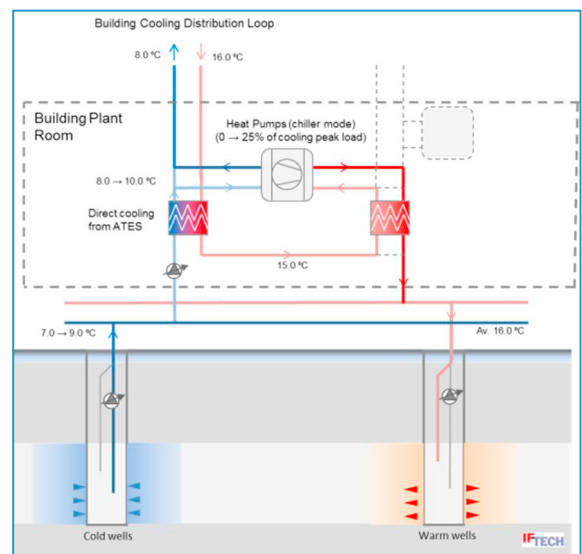


Fig. 4. ATEs system in cooling mode (summer operation)

The principle of operation for a building in summer mode and the ATES system in summer operation mode is displayed in Figure 4. In cooling mode (discharging operation for the cold ATES wells) groundwater is pumped from the cold wells to the warm wells. Direct cooling to a building in cooling mode is supplied by thermal energy exchange over a plate heat exchanger. At the start of the cooling season, when the cold wells are fully charged, the extraction temperature from the cold wells will be close to the charging temperature. As a result of the temperature drop over the plate heat exchanger (in this example 1.0 °C) both during charging and discharging, the temperature supplied to the building distribution loop will be 8.0 °C. During summer operation the extraction temperature from the ATES wells will gradually rise. The heat pump(s) in the building plant room are utilized in chiller mode for additional cooling in order to have a guaranteed cooling capacity and temperature.

3. PTES design concepts

The main driver in the development of PTES in Denmark has been the price for stored solar heat. In the 1990s the overall objective was to construct long-term thermal storages for a price below 200 DKK/m³ (27 €/m³) including in- and outlet, connection pipes, heat exchangers and pumps, valves etc. in the storage circle.

To reach this objective the total construction and the different parts of the construction have to be economically optimized.

The total construction for large pit storages (>50,000 m³ water equivalent) is cheapest if it is made from soil excavated with a soil balance such that no material has to be added or to be removed from the building site.



Fig. 5. Principle sketch of a pit heat storage cross section.

To make this possible, the excavated soil has to be of a quality that can be utilized as banks, see Figure 5. Too much silt in the soil can be a problem and a geotechnical investigation has to confirm that the excavated soil can be utilized as banks.

Insulation is expensive and use of insulation material must be optimized. Calculations carried out by Danish Technical University in the 1990s for a 100,000 m³ PTES showed that insulation on the banks and on the bottom is not economically feasible. The lid insulation should be similar to 39 cm of mineral wool and it was not economical feasible to extend the lid insulation to cover the top of the banks. This result depends of course on the temperatures in the storage, cost of insulation and other boundary conditions and has in principle to be recalculated when conditions are changed.

Storage medium is water since it is inexpensive, does not harm nature, has high thermal capacity and allows stratification pumping and high charge and discharge capacity. Since the thermal capacity for water is app. 1.16 kWh/(m³*K) and for soil and rock 0.8-0.9 kWh/(m³*K) filling of gravel or stones in the storage will reduce the thermal capacity. However, water can be corrosive because of content of oxygen and bacteria. Therefore, the water in the Danish PTES storages is treated like water in the district heating network (pH 9.8, removal of lime and removal of salts).

For tightening the storage polymer **liners** with high thermal resistance is used. Polymer liners as Polypropylene (PP) and polyethylene (PE) are relatively cheap and easy to install with well documented welding and testing techniques. Therefore, they are widely used for geo-membranes. The welding process is shown in Figure 6.

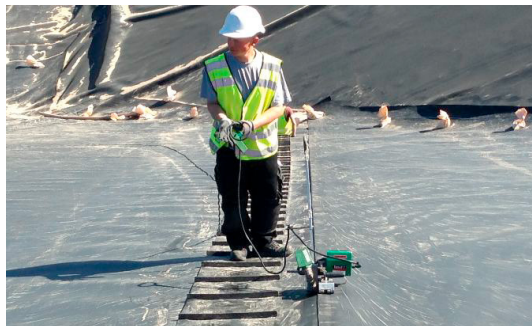
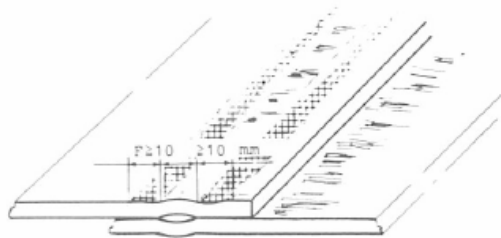


Fig. 6. Double welding of a HDPE liner. The welding can be tested by applying pressurized air to the air channel between the welding seams.

The major issue regarding polymer liners is the temperature resistance, where 90 °C is the maximum. Another disadvantage compared to metal liners is the water vapor permeability. For polymer liners the water vapor permeability is strongly temperature dependent. HDPE liners have the lowest water vapor permeability compared to other geo-membranes. At 20 °C the water vapor permeability is around 0.03 g/(m²*day) for a 1 mm liner. For temperatures above 60 °C it is difficult to get data from the suppliers, but experiments have shown a water vapor permeability for a 2.5 mm liner of app. 1.5 g/(m²*day) at 80 °C.

The lid is floating on the water. This is to avoid an expensive structural system and to avoid using steam or nitrogen as corrosion protection between lid and water. The lid construction has been continuously developed since the early 1990s. Until now a solution with two alternative insulation materials (Nomalén and LECA) have been implemented in the Danish full-scale storages.

Nomalén is a PE/PEX product sold in mats of for instance 200x600x10 cm. The floating lid is mounted with weight pipes making rain water flow to a pumping sump in the middle of the storage. The lid is constructed with layers of bottom liner, ventilation net, insulation, ventilation net and top liner with ventilation valves, see Figure 7. This design concept has been implemented in the Danish cities Marstal (75,000 m³) and Dronninglund (60,000 m³).

LECA is expanded clay, and the solution with LECA is also mounted with weight pipes, but the layers in the lid construction is bottom liner, LECA and top liner including ventilation pipes. This design concept has been implemented in the Danish cities Gram (122,000 m³), Vojens (203,000 m³) and Toftlund (85,000 m³).

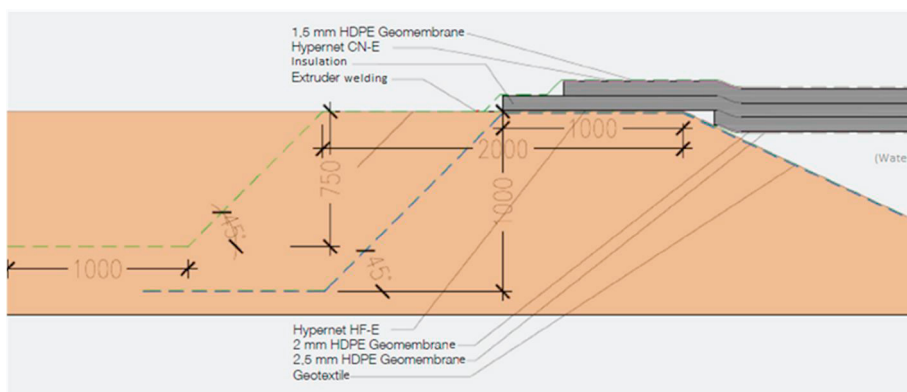


Fig. 7. Cross section of the edge of the floating cover [8].

4. System integration

A deliberated integration into the overall energy supply system is essential for an efficient operation of a large-scale TES. This includes a suitable hydraulic system layout as well as a careful design of not only the storage but also other system components like additional heat or cold producers, DH network, heat transfer substations up to the point

of building installations. In particular the process control system has to make use of the storage services in the best possible way, depending on the specific objectives like e.g. maximization of renewable energy share or CHP electricity production.

Temperatures levels, quality of stratification and return temperatures of the heating network do strongly influence the efficiency of a TES. Those parameters do not only depend on the storage, but also to a large extent on the connected energy system. Hence, during storage design an accurate prediction of the entire system characteristics is needed. Operation temperatures of the storage throughout the year and charging and discharging power rates have to be predicted, along with the DH network return temperatures, as they have a key role for the performances of the storage. Together with the maximum charging temperatures they define the usable temperature difference and accordingly the thermal capacity of a TES. For some storage concepts also additional components like short-term buffer tanks or heat pumps can be economically reasonable supplements.

5. Application areas

Today ATES, PTES and other UTES can be applied in all application areas where large thermal storage capacities are required at moderate or low temperature levels ($< 90\text{ }^{\circ}\text{C}$). Large-scale TES can have different roles in energy supply systems. The major ones are

- Buffer storage for short-term heat storage and / or peak shifting
- Long-term or seasonal storage of e.g. solar thermal or surplus heat
- Energy management of multiple heat producers like e.g. CHP, solar thermal, heat pumps, industrial surplus heat etc.
- Cold storage of e.g. ambient cold (air, surface water) or evaporator cold from heat pumps

In the following, some possible applications are described exemplarily. A number of realized project examples are described more detailed in [1].

In **solar district heating** (SDH) systems with seasonal thermal energy storage (STES), large solar thermal collector areas produce heat mostly in the summer period. Solar heat that is not used directly is charged into the seasonal storage for a heat supply in the following heating season. STES enables SDH systems to supply shares of 50 % and more of the yearly DH heat demand by solar energy.

Large-scale TES in connection to **CHP plants** allow for a separation of the electricity from the heat production. The CHP units can operate when economic conditions in the electricity grid are favorable independently of the actual heat demand. Surplus heat can be charged into the TES for later use when electricity prices are low and the CHP is switched off. In these periods no expensive backup boilers have to be operated.

In **power-to-heat** applications, surplus renewable electricity can be transferred into heat. In connection to large-scale TES more heat than actually needed can be produced and stored. In larger applications, regulation services can be offered to the electricity market, which offers additional business opportunities.

So-called **smart district heating** systems have been implemented in a number of Danish district heating systems in the past years. They often consist of the four main components: large-scale solar thermal system, CHP plant, electrical heat pump and / or direct electrical heater and large-scale TES. In the summer period solar heat is produced by the solar thermal collectors. Surplus solar heat is stored into the TES. In the winter period the solar heat is discharged. In addition, the heat pump produces heat in periods with low electricity prices and uses the colder parts of the TES as heat source. The CHP plant produces heat in periods with high electricity prices, independently from the actual heat demand. The Smart District Heating concept also allows for selling regulation services to the electricity market.

Industrial waste heat is often available on a rather constant power level throughout the year, whereas heat demand usually follows the seasonal weather variations. TES can level out this discrepancy and offers the possibility for much higher amounts of waste heat to be used compared to a direct waste heat usage only.

In **cooling** applications, e.g. ambient cold from ambient air or surface or sea water can be charged into a TES in the winter period for cold supply in the summer period. From the economical point of view these systems are often very interesting, as no cold has to be produced by a cooling machine but only freely available ambient cold is used. Besides the electricity for some circulation pumps, no further operational cost incur. **Combined heating and cooling**

applications work similarly for the cooling part, besides the fact that the cold source is the evaporator side of a heat pump in this case. The heat that is charged into the TES during the cooling season is used as a heat source for the heat pump in the following heating season. Because of the favorable economics, quite some local DHC systems with heat pumps and UTES are in operation already.

6. Cost

Construction costs of the four storage concepts vary significantly. Figure 8 presents the investment cost data of realized large-scale TES plants. For comparing different storage concepts and storage materials, the specific storage costs are related to the water equivalent storage volume. The listed storages are operated at maximum storage temperatures between 50 °C and 95 °C and are integrated into solar district heating plants as seasonal storages.

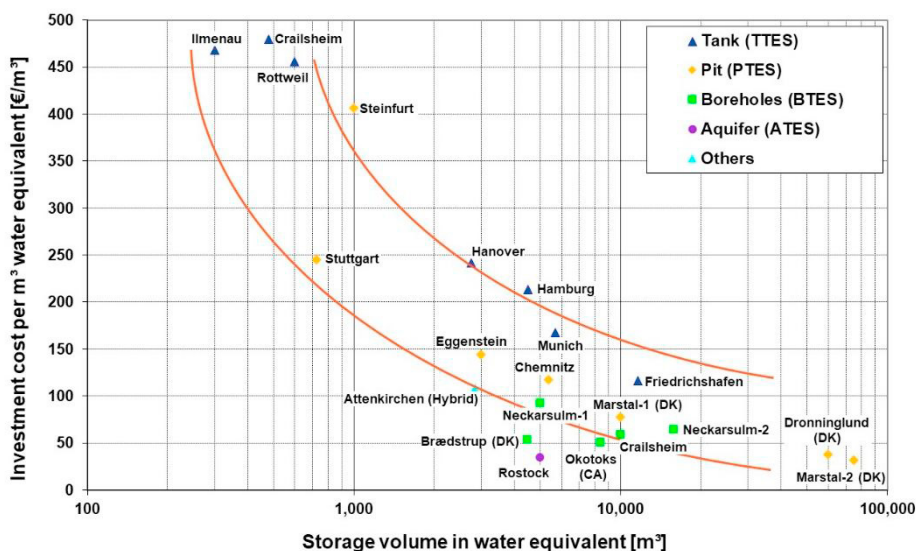


Fig. 8. Specific investment cost for large-scale thermal energy storages (including design, without VAT).

Figure 8 illustrates the cost decrease with increasing storage volumes. Appropriate sizes for large-scale UTES are above 2000 m³ water equivalent. Here the investment costs vary between 40 and 250 €/m³. Generally, TTES have higher specific investment costs than other UTES types. On the other hand, they offer advantages regarding the thermodynamic behavior and they can be built almost independently from the local ground conditions. The lowest costs can be reached with ATES and BTES. However, they often need additional equipment for operation like e.g. buffer storages or water treatment and they have the highest requirements on the local ground conditions.

The economy of a storage system depends not only on the storage costs, but also on the thermal performance of the storage and the connected system. Hence each system has to be evaluated separately. To determine the economy of a storage system, the investment, maintenance and operational costs have to be related to its thermal performance in the overall system.

7. Design tools

With their high capital costs, transient storage temperature behavior, and possible long-term heat build-up impact in the surrounding soil, proposed TES solutions often require detailed modelling to assess the thermal and economic performance of the design over the anticipated lifetime of the equipment. But it is often not enough to just study the TES system individually without also considering its impact on the balance of the system. For example, in a design where the TES system is being charged by a combined heat and power plant, being able to accurately predict the storage temperatures can be critical when deciding when and how to operate the power producing components

(turbines, fuel cells etc.). A modelling platform that can accurately analyze the available TES technologies, as well as their interaction with power producing components, heat rejection devices, solar energy components, controllers and heat distribution networks, becomes a valuable tool to the designers, operators and investors. For this IEA task, the TRNSYS software package [9] was chosen for the simulation engine.

TRNSYS is a transient system simulation package that has been developed and supported for over 40 years and features an extensive library of commercial and research grade component models covering a wide range of applications. TRNSYS is powerful modelling platform that has been used extensively in IEA projects due to its inherent flexible nature and ability for users to easily add content to the package. For this IEA project, TRNSYS was chosen because it contains state-of-the-art component models for many of the TES technologies under consideration and it has the balance of system models required to integrate the TES models into real-world applications. A quick discussion of the available TES technologies in TRNSYS follows.

- **TTES:** There are storage tank models in TRNSYS for spherical, cylindrical, rectangular parallelepiped, conical and inverted pyramid storage geometries. These models typically rely on 1-dimensional finite difference approaches using horizontal isothermal temperature nodes within the storage to solve the inter-dependent set of coupled differential equations. The models are well validated and are extremely flexible with where insulation is placed, where fluid enters and exits the tanks, where auxiliary energy can be added to the fluid, etc. These models usually assume constant volume storage but there are several versions with variable volume.
- **PTES:** There are several options in TRNSYS for the analysis of pit thermal energy systems. Most of the TTES models described above also have a soil “wrapper” model that can be used to effectively bury the tank in the ground. These soil wrappers are typically either 2-dimensional (radial and vertical direction) or 3-dimensional (x, y and z directions) finite-difference conduction solution models. These models are used iteratively with the storage tank models to pass temperature and energy flow information back and forth between the models. In addition, a highly detailed model of an inverted, truncated pit storage system (tank + soil) has been developed by the authors and is being validated against a measured data set with very promising results.
- **ATES:** There are two approaches being used to study ATES systems in TRNSYS currently. The first relies on a model called TRNAST [10] that solves the case of two de-coupled wells (the wells do not interact thermally). This model has been used to study ATES systems for many years and usually does a nice job provided the injection and extraction wells are far enough apart that they do not interfere with each other. The second solution is relatively new and involves the pairing of the popular ModFlow groundwater modelling package [11] with TRNSYS. The user describes the detailed ATES sub-surface conditions and design using ModFlow and the balance of the system using TRNSYS (heat distribution system, heat generation equipment, controls etc.). Because the timescale for the balance of system components in TRNSYS can be on the order of minutes or seconds, and the timescale for the aquifer is often on the order of days, weeks, or even months, the solution methodology can be slightly de-coupled (if desired to help speed up the simulations) where the ModFlow program is only called every ‘n’ TRNSYS timesteps (where n is an integer ≥ 1). Between ModFlow calls, the TRNSYS balance of system components use the temperature of the aquifer from the previous ModFlow solution. This new approach using ModFlow/TRNSYS is currently being validated against two multi-year measured data sets from commercial ATES applications in Europe.
- **BTES:** There are several BTES options in TRNSYS with the most popular being a modified version of the DST solution methodology from Lund University in Sweden [12]. This model is for U-tube and concentric tube borehole systems using a cylindrical approach and has been extensively validated over a wide range of commercial and residential applications. The DST model in TRNSYS has been recently updated to allow for fluid flow into different ‘rings’ of the stratified ground field.

8. Summary

As part of the IEA DHC Technology Collaboration Programme a research project to address general technical issues on large-scale seasonal thermal energy storage applications has been initiated. These issues include the lack of reliable up-to-date data and information, in particular proven concepts, cost data, technology suppliers and experiences from realized projects. Expertise and concrete projects in the field of seasonal thermal energy storage is limited

internationally and there is currently a lack of reliable and adequate analysis tools to assess the technical-economic potential of aquifer thermal energy storage (ATES) or pit thermal energy storage (PTES) integration in DHC systems. The first deliverable of this IEA-DHC funded project is the development of a review report for ATES and PTES technologies [1] including up-to-date cost data and cost functions showing the cost of larger scale ATES and PTES systems versus storage system size. In countries such as Denmark and the Netherlands, cost-effective concepts for ATES and PTES have been developed in the past decade and realized in numerous local DHC projects. These TES technologies have been demonstrated within the frame of national R&D programs and more recently as non-subsidized projects by industry. Excerpts from the review report, which will be published by the IEA-DHC and is introduced and presented in this paper, provide a summary of the report sections related to ATES and PTES design concepts, cost of ATES and potential application areas as well as an introduction of relevant design tools being used by the authors for completing technical economic feasibility studies for district heating and cooling systems with integrated ATES and PTES systems. The data, information and general knowledge summarized in the report and in this paper is directed to operators of DHC systems and other stakeholders interested in transforming their systems to smart DHC systems incorporating seasonal storage.

Acknowledgements

This project has been independently funded by the International Energy Agency Technology Collaboration Programme on District Heating and Cooling including Combined Heat and Power (IEA DHC). The authors gratefully acknowledge this support. Any views expressed in this publication are not necessarily those of IEA DHC. Neither the authors nor IEA DHC can take any responsibility for the use of the information within this publication or for any errors or omissions it may contain.

References

- [1] Pauschinger, Thomas (ed), Thomas Schmidt, Per Alex Sørensen, Aart Snijders, Reda Djebbar, Raymond Boulter and Jeff Thornton. "Integrated Cost-effective Large-scale Thermal Energy Storage for Smart District Heating and Cooling." *Deliverable within IEA DHC Annex XII Project 3, Contract No. XII-03* (2018)
- [2] Schmidt, Thomas and Dirk Mangold. "Large scale solar thermal energy storage - status quo and perspectives." *Solar District Heating Conference. April 9-10 2013*. Malmö, Sweden (2013)
- [3] Sanner, Burkhard (ed.). "High Temperature Underground Thermal Energy Storage - State-of-the-art and Prospects." *Giessener Geologische Schriften Nr. 67*. University of Giessen, Germany (1999)
- [4] Richlak, U., Beuster, H., Kabus, F. " Saisonale Speicherung von Überschusswärme eines Gas- und Dampfturbinenkraftwerkes im Aquifer - Monitoring und Optimierung des Betriebes des Aquiferspeichers Neubrandenburg bei steigenden Speichertemperaturen." , *Report to Research Project BMWi 0329838C*, Neubrandenburger Stadtwerke GmbH and Geothermie Neubrandenburg GmbH, Neubrandenburg, Germany (2011)
- [5] Sanner, B., Knoblich, K. "Thermische Untergrundspeicherung auf höherem Temperaturniveau: Begleitforschung mit Messprogramm Aquiferspeicher Reichstag. ", Institut für Angewandte Geowissenschaften, University of Giessen, Germany (2004)
- [6] B. Nordell, A. Snijders, and L. Stiles. "The use of aquifers as thermal energy storage (TES) systems. Advances in Thermal Energy Storage Systems.", 87-115, Woodhead Publishing Series in Energy: Number 66, Elsevier book, Cambridge, UK (2015).
- [7] J.S. Dickinson, N.Buik, M.C. Matthews and A.L. Snijders. "Aquifer thermal energy storage: theoretical and operational analysis". *Géotechnique* 59, No.3 (2009).
- [8] Vang-Jensen, Morten. "Seasonal Pit Heat Storages – Guideline for Materials and Construction." <http://Task45.iea-shc.org/fact-sheets>. (2014)
- [9] TRNSYS. "A TRAnsient SYStems Simulation Program." *Solar Energy Laboratory, University of Wisconsin*, Madison, USA (2018)
- [10] Schmidt, Thomas. "TRNASt - Aquifer Thermal Energy Storage - Two well model for TRNSYS." Manual. *Solites - Steinbeis Research Institute for Solar and Sustainable Thermal Energy Systems*, Stuttgart, Germany (2005)
- [11] Langevin, Christian D.; Hughes, Joseph D.; Banta, Edward R.; Niswonger, Richard G.; Panday, Sorab; Provost, Alden M. "Documentation for the MODFLOW 6 Groundwater Flow Model." *U.S. Geological Survey Techniques and Methods, book 6, chap. A55, 197 p.*, <https://doi.org/10.3133/tm6A55>. (2017)
- [12] Hellström, Göran. "Duct Ground Heat Storage Model, Manual for Computer Code", *Department of Mathematical Physics, University of Lund*, Sweden. (1989)



16th International Symposium on District Heating and Cooling, DHC2018,
9–12 September 2018, Hamburg, Germany

Low Temperature District Heating for Future Energy Systems

Dietrich Schmidt^a *

^a *Fraunhofer Institute for Energy Economics and Energy System Technology
Königstor 59, DE-34119 Kassel, Germany*

Abstract

A reduction of emissions in the energy sector is essential for meeting international goals for climate change mitigation. Here, district heating (DH) can contribute significantly to a more efficient use of energy resources as well as better integration of renewable energy into the heating sector (e.g. geothermal heat, solar heat, heat from biomass combustion or waste incineration), and surplus heat (e.g. industrial waste heat). The more efficient use of all energy resources and the use of renewable energy are measures which lead to a reduced utilization of fossil energy, and thereby a reduction of greenhouse gas (GHG) emissions. Within this context, it is mandatory to consider the entire energy chain to achieve a good overall system performance. In this perspective low temperature district heating offers suitable technology solutions.

The paper presents and discusses the final output of the international co-operative work in the framework of the International Energy Agency (IEA), the District Heating and Cooling including Combined Heat and Power (DHC|CHP) Annex TS1. The material collected and summarized in the recently published guidebook [1] show that low temperature district heating is a key enabling technology to increase the integration of renewable and waste energy for heating and cooling. Low temperature district heating is one of the most cost efficient technology solutions to achieve 100 % renewable and GHG emission-free energy systems on a community level.

© 2018 The Authors. Published by Elsevier Ltd.

This is an open access article under the CC BY-NC-ND license (<https://creativecommons.org/licenses/by-nc-nd/4.0/>)

Selection and peer-review under responsibility of the scientific committee of the 16th International Symposium on District Heating and Cooling, DHC2018.

Keywords: Low Exergy Communities; Low Temperature Supply Structures and District Heating;

* Corresponding author. Tel.: : +49-561-804-1871; fax: +49-561-804-3187.

E-mail address: dietrich.schmidt@iee.fraunhofer.de

1. Introduction

The reduction of emissions within the energy sector is a mandatory to meet the set national and international goals for climate mitigation. Studies, as [2] pointing out that district heating could play an important role in a cost effective de-carbonization of the heating sector and will have a vital role in our future energy system. In turn, the IEA DHC Annex TS1 aims to identify holistic and innovative approaches to communal low temperature heat supply. It is a framework that promotes the discussion of future heating networks with an international group of experts. The goal is to obtain a common development direction for the wide application of low temperature district heating systems in the near future [3].

The Annex TS1 is intended to provide solutions for both expanding and rebuilding existing networks and new DH networks. It is strongly targeted at DH technologies and the economic boundary conditions of this field of technology. The area of application under consideration is the usage of low temperature district heating technology on a community level. This requires a comprehensive view of all process steps: From heat generation over distribution to consumption within the built environment. The approach includes taking energy (e.g. primary energy, delivered energy, etc.) and exergy into account. This allows an overall optimization of energy and exergy performance of new district heating systems and the assessment of conversion measures (from high temperature DH to low temperature DH) for existing DH systems.

The main objective of the described research activity is to demonstrate and validate the potential of low temperature district heating as one of the most cost efficient technology solution to achieve 100 % renewable and GHG emission-free energy systems on a community level. This is reached by providing tools, guidelines, recommendations, best-practice examples and background material for designers and decision makers in the fields of building, energy production/supply and politics in the recently published guidebook [1].

During the course of the Annex activities, the aim was to develop and improve means for increasing the overall energy and exergy efficiency of communities through the use of low temperature district heating. Therefore, the compilation of existing know-how for developing new district heating concepts and for implementing the results in existing grids is necessary. In this way, low temperature DH can become the least expensive way of realizing the future of fossil free energy systems in the heating sector. In this context, new business cases and models could support the wider implementation of new and especially innovative low temperature DH systems. Next to this technology, developments for reduced DH network costs are necessary. It seems to be sensible to focus on the motivation for investments into new networks and the renovation of existing networks [3].

2. District Heating and Cooling Technologies

As already stated above, low temperature district heating (LTDH) based on renewable energy can substantially reduce total greenhouse gas emissions and secure energy supply for future development of society [4]. It has the ability to supply heat for space heating (SH) and domestic hot water (DHW) for various types of buildings, to distribute heat with low heat losses and ability to recycle heat from low-temperature waste heat and renewable energy sources. From various research and development of LTDH projects, it has been shown that it is both technically feasible and economically sound to change current high/medium temperature district heating system to LTDH for both new and existing building areas [5]. During the course of the Annex TS1 project promising technologies for LTDH application have been collected and identified to meet the goals of future renewable based community energy systems. Innovative technologies and advanced system concepts in LTDH are reported for heat generation, distribution and end user utilization [1].

2.1. District Heating Pipes

The heat loss in a DH system occurs in different places in the heat generation, distribution and utilization, appearing in different forms. The success of LTDH largely relies on substantially reduced distribution heat loss. DH network heat loss is determined by multiple factors: geometrical condition (network dimension, length and ground conditions/properties), DH pipes (type of pipes, insulation materials/conditions) and DH operation (heating load, temperature level, bypass operation and other factors such as leakages) [6]. There are different types of pipes used in DH. Some of them are in the commercial market like single pipe and twin pipe. To reduce network heat loss, small pipe diameters and high performance pipe insulation is recommended in the distribution network and service pipes and presented in [1].

2.2. Energy Efficient District Heating Network

The pipes length between in plant and the consumer vary in traditional DH networks, which results in changing differential pressure. The consumers close to the plant has larger available differential pressure, whereas the consumers away from the plant have smaller available differential pressure. One solution to reduce the valve throttling and potential hydraulic imbalance when the valves were malfunctioned is to apply a ring shape network topology. Unlike the traditional network, a topology based on ring network equalizes the pressure differences between the supply and return pipes [3], [7], [8]. Other issues for an efficient network design are solutions for avoiding bypasses, both in the building systems and as street bypasses. One of those is the so-called comfortable bathroom concept, where the bypass water is directed to the bathroom and cooled down to 25°C in a floor heating system before it flows back to the return pipe [1], [3], [9].

2.3. Domestic Hot Water Preparation in LTDH

An important issue in LTDH schemes is the hygienic preparation of domestic hot water (DHW) and the Legionella treatment. There are several regulations and guideline for the DHW preparation, which have been analyzed and summarized in the guidebook [1]. Suitable DHW units and their connections into DH systems are presented [10] as well as the different treatment solutions for Legionella growth prevention [1], [11], [12].

2.4. Control of Space Heating

It has been proven that LTDH can meet space heating (SH) demand for both low-energy buildings and existing buildings with floor heating [9]. For existing buildings with the existing radiators, LTDH can meet SH demand for a certain amount of time of the year, while the supply temperature needs to be increased during cold winter period. To ensure consumer thermal comfort while saving energy and reducing network return temperature, the hydronic system in the SH loop need to be properly designed and functioning via a direct or indirect connection and proper control [1]. Another control issue is the control of the mass flow. The mass flow control concept refers to a system where both the primary and secondary side flows are adjusted with inverter-controlled pumps instead of control valves in networks [7], [8].

3. Interfaces and Communities

For a wider implementation of district heating schemes not only issues on the technology need to be solved. Especially the design of interfaces in the communities is regarded. The challenge of the improved interfaces in district heating systems may be explained via so-called hard and soft issues:

- The hard issues cover the following topics: District heating network structures, requirements for consumer substations and buildings, and connection principles for distributed heat sources.

- The soft issues cover the following topics: Technical and economical modelling of the distribution system, optimization between demand and generation side, innovative control concepts and energy measurement, transition of the existing DH grid to the LTDH grid, and new pricing and business models.

During the course of the project promising models, concepts, and technologies to meet the goals of future renewable based community energy systems have been collected and identified. The interfaces issue is highly relevant for a successful implementation of the LTDH and thereby enabling transition to the renewable energy society and secure energy supply for future development of society. By introducing better interfaces between the demand and supply, DH systems can be transformed into a smart grid energy system on a district level. Questions as the prediction of future DH demands, the successful integration of renewable or excess heat sources and pricing or business models are outlined in [1].

4. Calculation Tools or District Heating Systems

During the course of the work within Annex TS1 a methodology for assessing and analyzing procedures for the optimization of local energy systems with focus on DH has been identified and adapted. Furthermore, a simplified planning tool for DH is developed and advanced tools for design and performance analysis of local energy systems, which are based on DH, are further developed. The presentation of tools is part of the full report [1], [13]. For the evaluation of existing local and DHC models, a classification form was created together with Annex TS1 participants to conduct a survey on planning tools for DH.

Table 1. Classification categories for the evaluation of planning tools for district heating (based on [13])

Analytical Approach	Demand Categories
Energy System Model	Households
Thermodynamic Model	Commercial
	Industry
Target Audience	Transportation/mobility
Municipal Authorities	
Professional Planners	Final Energy Consumption
Internal Use, R&D	Electricity
	Heat
Level of Detail	Transport/mobility
Geographical Scope	
Time Horizon	Variables
	Costs
Model Type	Energy
Simulation Model	Exergy
Optimization Model	Temperature

Input from Annex participants (in total twelve planning tools) could be gathered and evaluated to formulate requirements for the development of a simplified DH planning tool and to further develop an existing advanced tool (TIMES Local). Based on this, a new simplified planning for DH has been outlined and developed: Easy District Analysis (EDA). EDA is a simplified DH planning tool for urban planners for the energetic, ecological and economic analysis as well as the evaluation of urban districts. In the following the results of the survey on local and DHC models are described and evaluated. The developed Easy District Analysis (EDA) tool is then presented and applied to a case study of an urban district consisting of 140 multi-family houses. Based on the survey results on local and DHC models, twelve planning tools for DH are listed in the following.

Table 2. Overview of planning tools from the survey on local and DH models (based on [13])

Energy System Models		
EnergyPLAN	KOPTI	LowEx-CAT
SIMUL_E.NET	TIMES Local	
Thermodynamic Models		
HeatNET	LowEx-CAT	NET Local
SIMUL_E.NET	spHeat	Termis
Others		
District ECA	EME Forecast	Exergy Pass Online

Initially, a classification form for local and DHC models was developed and distributed to tool developers. After obtaining the completed classification forms from the Annex TS1 participants, the planning tools were assessed in seven categories: analytical approach (energy system model, thermodynamic model, other), target group of users (municipal authorities, professional planners, R&D), level of detail (geographical scope, time horizon), model type (simulation, optimization), demand categories (households, commercial, industry, transportation), final energy consumption (electricity, heat, transport) and used variables (costs, energy, exergy, temperature).

The planning tools were divided according to their analytical approach into energy system and thermodynamic models. Energy system models cover the whole energy supply chain from primary energy sources to delivered energy. However, they usually do not consider the thermodynamics of district heating (e.g. interactions on thermodynamic level of processes with requirements of predefined temperature levels). Thermodynamic models are thus required. There are also planning tools that did not fit into the categories stated above. These were classified as ‘others’ (e.g. EME Forecast) [1].

To conclude, the evaluation has shown some promising approaches for low temperature DH. However, there was none found to be appropriate for the objective of a simplified, holistic tool for low-ex DH. By evaluating the selected planning tools for DH schemes, requirements can be derived for the development of a simplified planning tool.

4.1. Easy District Analysis (EDA) - A Simplified Tool

Easy District Analysis (EDA) is a simplified tool for urban planners and utilities for the energetic, ecological and economic analysis as well as the evaluation of districts with regard to low temperature heating to enable comparisons with other heat supply options. EDA is a simplified tool rather in terms of the required amount of input data than in terms of the complexity of calculation. This means with little information on a district energy system that is being analyzed, an annual load profile is generated in hourly resolution (taking simultaneity of demand into account) to enable the integration of intermittent renewable energy (e.g. solar thermal) into the district heating system and to consider storage options [1], [13].

The focus of the EDA tool lies on the evaluation of the impact of different grid temperatures (e.g. standard DH vs. low temperature DH) and of different operation modes (technical vs. economic operation) on the use of DH technologies, primary energy consumption, carbon emissions and heat production costs. To enable the easy district analysis, a load curve of space heat and domestic hot water is generated. The design of the cogeneration plant and boiler is based on the load curve and preset full load hours. Solar collector surface can be designed on e.g. solar fraction. After the capacities of technologies are calculated, the use of different DH supply options can be compared in terms of technical and economic operation. Technical operation leads to minimum carbon emissions, whereas economic operation means the hourly cost-effective operation of DH technologies based on fuel costs and varying

revenues from electricity feed. Economic conditions, such as the development of the electricity baseload price, hinder the realization of the carbon mitigation potential of CHP DH supply to its full extent [13].

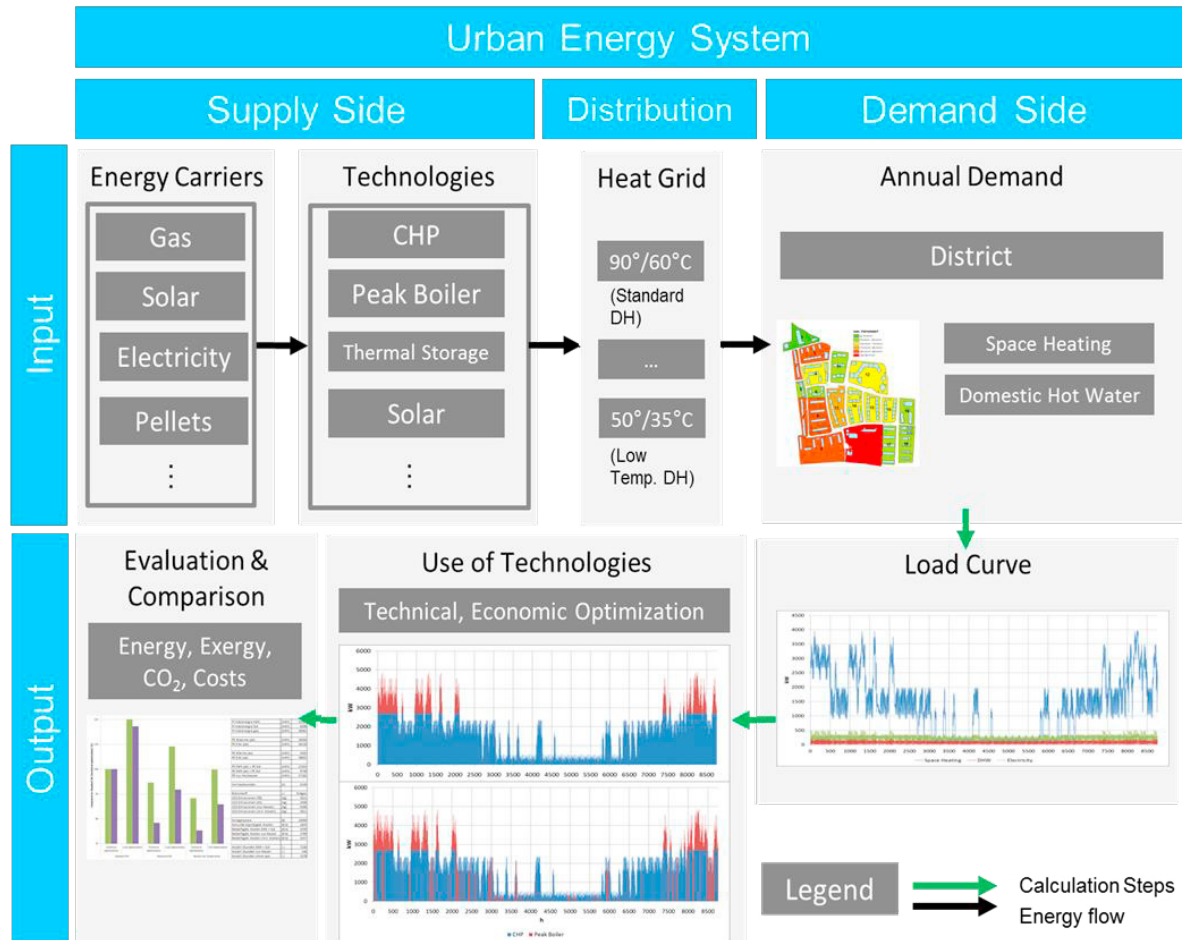


Fig. 1. Approach for a simplified tool to evaluate energy supply options for districts: Easy District Analysis (EDA) [1]

5. Application of Low Temperature District Heating to Community Case Studies

Core objective for the description of case studies was to identify and collect innovative demonstration concepts as examples of success stories for communities interested in developing low temperature district heating systems. Demonstrated cases include use of advanced technologies and interaction between different components within the systems. Based on these experiences, principles and lessons learned in designing these systems are given. Measurement data from community projects are also used in validation of the models and tools developed.

There were a total of eight case studies from Germany, Denmark, Finland, Norway and Great Britain. The district heating systems were of very different sizes, from miniature to city wide systems. Network lengths were from 165 m to 140,000 m. The connected buildings were detached, terraced and block houses, and mostly low energy or passive houses. Sources of heat were solar collectors, heat pumps, CHP plants, excess heat from industry or the systems were connected to a larger network close by with heat exchangers. The temperature levels recorded were typical for low-temperature systems, varying from 40 to 60 °C in supply and 25 to 40 °C in return. Savings and increased efficiencies were observed in every case studied [1].

Table 3. Summary of the case study systems of IEA DHC Annex TS1 (based on [14])

Case system	Heat demand	Temperatures
Slough (UK)	49.6 MWh/year	52/32 °C
Ludwigsburg (Germany)	825 MWh/year	40/25 °C
Wüstenrot (Germany)	376 MWh/year	40/30 °C
Kassel (Germany)	1,827 MWh/year	40/30 °C
Hyvinkää (Finland)	630/1,371 MWh/year	65/35 °C
Sønderby (Denmark)	975 MWh/year	55/40 °C
Ulstein (Norway)	20,000 MWh/year	4-9 °C
Middelfart (Denmark)	118,000 MWh/year	64.6/40 °C

Greenwatt Way in Slough (UK) has a system of 10 dwellings with 845 m² heated floor area, supplied by a miniature district heating system with a trench length of 165 m. Heat supply consist of 20 m² solar thermal collectors, two 17 kW ground source heat pumps with 14 boreholes, two 20 kW air source heat pumps and a 30 kW biomass boiler as well as a 8 m³ thermal storage tank. The total capacity of the controllable heat sources is 105 kW with added capacity from solar thermal collectors and the storage unit. The heat pumps can work in series so that at first stage water is heated up to 45 °C and at the second stage up to 55 °C. Each house is fitted with a substation with direct connection for space heating and with a heat exchanger for domestic hot water. Radiators are dimensioned for 55/35 °C temperatures. Domestic hot water is supplied at 43 °C. Relative monthly heat losses were 60 % at highest in summer and 20 % at lowest in winter.

An energy efficient district heating system in Sonnenberg district of Ludwigsburg (Germany) was studied as a case system. Target of the project was to develop a simulation environment for studying integration of distributed renewable heat sources in existing and new systems. A new low temperature (40/25 °C) extension to the existing (70/40 °C) district heating network has been established. The heat supply consists of a 350 kW gas CHP plant and a 200 kW geothermal heat pump. The project started in 1/2012 and ended in 3/2015.

The Wüstenrot (Germany) case study represents a plus energy community. It consists of 24 mostly single family houses, built almost according to local passive house standard. All buildings have large solar panel systems on the roof-tops and battery storages. The heat demand of the buildings is supplied by decentralized heat pumps and heat storages, which in turn are connected to a centralized geothermal system. This system consists of a cold water district heating network delivering low temperature water from a novel agro-thermal collector to the heat pumps within the buildings. The concept includes activation of agricultural fields as geothermal collectors by ploughing tubes in 2 m depth, the distance between the tubes being 0.5 to 1.0 m. The cold water network can be also used for direct cooling of the buildings in summer time. Total duration of the monitoring activity was planned to be 3-4 years. The heat pump COP was 4.8 in average with variation between 2.5 to 6.5. The project ran from 11/2012 to 6/2016.

The case study “Zum Feldlager” in Kassel (Germany) is a low temperature district heating system supplying heat for 127 buildings by utilizing solar collectors, a centralized ground heat pump with boreholes utilized also as seasonal heat storage. Heat storage is loaded by unglazed solar collectors (swimming pool absorbers as the low-cost option). The supply temperature in the district heating network is 40 °C. Connection for the space heating is implemented using heat exchangers, but for the preparation of domestic hot water there are different options; thermal solar collectors (e.g. flat-plate collectors) or an electric heating element complementing district heating. Aim is to find an optimal balance between the economy, use of electric heating, available solar output and distribution heat losses in the network.

A district heating system in Hyvinkää (Finland) building fair (2013) area was a case study for investigating low temperature district heating. The building fair area consists of 40 consumers within an area of 17 ha. In the implemented system, about half of them are connected to district heating system, the rest having a building specific heating system; e.g. combination of solar PV and collectors or a heat pump. Results of simulations showed that the majority of the solar energy is used for the domestic hot water, covering about half of its annual heating needs. Low temperature variation for distribution resulted in lower heat losses, but approximately doubled consumption of electricity in pumping.

The demonstration project in Sønderby (Denmark) was a full scale renovation of a part of an existing district heating system enabling a change from traditional distribution temperatures to a low temperature system. The area included 75 single family houses with the living area of 110 to 212 m² each, built in 1997-1998 with underfloor heating systems. The houses originally had hot water tanks for domestic hot water supply (110 l or 150 l in volume). In the demonstration project, the old inefficient pipes within the network were replaced by better insulated pipes and the old water storage tank substations were replaced with heat exchanger substations. The low-temperature network in the area uses return pipeline in the medium-temperature network from the neighboring Taastrup district heating network as heat supply. The supply temperature averaged at 48 °C with heat from the return pipeline covering about 80 % of the total heat supply. The remaining heat was supplied by warmer water from the feed pipeline in the neighboring network. The results showed that it is possible to provide consumers a supply temperature of 50 - 53 °C, which is sufficient for space heating and domestic hot water supply. Heat losses in the old medium temperature system were approximately 41 % while in the new system reached heat losses of 13 – 14 %. One advantage of the concept is the increased available capacity for the existing district heating system without any investment on production.

In Ulstein (Norway) fjord district heating is based on utilization of the “free” heat from the sea by using decentralized heat pumps. A common heat exchanger is utilized to take the heat from the sea. The sea heat with low temperature is then distributed to energy substations. Both heating and cooling are distributed by using the same pipe network without insulation. The local energy substation could be used for one or few buildings. This solution with utilization of sea heat and decentralized heat pumps is suitable for places located at coast. Including the reserve capacity, the plant should deliver about 20 GWh heating and 5 GWh cooling.

Middelfart (Denmark) district heating company has succeeded in lowering supply and return temperatures in their system from an average of 80.6/47.6 °C to 64.6 /40.0 °C during 2015. The district heating network in question is 139 km long in pipe length and services approximately 5000 customers. The heat supply consists of surplus heat from an oil refinery, a CHP plant and a waste incineration plant. The annual heat consumption is approximately 480,000 GJ. The district heating company has taken part in the development and testing of software tools that have helped in reducing the also return temperature in district heating network. Furthermore, the company has demonstrated a process that district heating companies can follow when aiming for a low temperature distribution. During the process the network heat losses in Middelfart have been reduced by 25 % and the economic benefits were estimated to be approximately 5.5 million DKK (0.7 million EUR). The economic savings obtained from the temperature reduction consist of savings due to lower heat loss and savings from a return temperature tariff that is paid to the local heat supplier.

6. Summary

DHC Annex TS1 was a three year international research project and aims to identify holistic and innovative approaches to communal low temperature heat supply by using district heating. It is a framework that promotes the discussion of future but also existing heating networks with an international group of experts. The goal is to obtain a common development direction for the wide application of low temperature district heating systems in the near future. The gathered research [1] which has been collected within this Annex should contribute to establishing DH as a significant factor for the development of 100% renewable energy based communal energy systems in

international research communities and in practice. The Annex TS1 project provided solutions for both expanding and rebuilding existing networks and new DH networks. It is strongly targeted at DH technologies and the economic boundary conditions of this field of technology. The area of application under consideration is the usage of low temperature district heating technology on a community level. In connecting the demand side (community/building stock) and the generation side (different energy sources which are suitable to be fed in the DH grids), this technology provides benefits and challenges at various levels. The scientific basis for the development of assessment methods provides the low exergy (LowEx) approach. This approach promotes the efficient and demand adapted supply (e.g. at different temperature levels) and the use of renewable energy sources. The Annex TS1 provides a framework for the exchange of research results from international initiatives and national research projects and allows, in a novel way, the gathering, compiling and presenting of information concerning low temperature district heating. 12 research institutions from 8 countries participated in this international research activity [1], [15].

As part of the project promising technologies for low temperature district heating application have been collected and identified to meet the goals of future renewable based community energy systems. Background materials and cutting edge knowledge on district heating pipe systems, network designs, hygienic domestic hot water preparation in low temperature supply schemes, space heating controls and the integration of small scale decentralized heat sources is provided in the report for designers as well as decision makers in the building and district energy sector.

The analysis of the future heat demand showed that the district heating would still be needed for most of the buildings in 2050, indicating that the low temperature district heating is a promising heat supply for the future and for many buildings. Considering that there is enough available heat from renewables and waste heat sources at the low temperature level, the low temperature district heating will be of high relevance in the future. For future development of the district heating and a high reliability of the low temperature district heating, statistical data and knowledge on the heat losses and how operation or temperature levels may contribute to the distribution losses are highly necessary.

For the identification of integral and innovative approaches to low temperature heat supply at municipal level, an overview of a number of existing evaluation methods is provided. The planning tools are assessed in seven categories: analytical approach, target group of users, level of detail, model type, demand categories, final energy consumption and used variables within the assessment. The evaluation of the collected tools has shown some promising approaches for low temperature district heating. However, none has been found to be fully appropriate for the objective of a simplified, holistic tool for the evaluation of low temperature district heating. By evaluating the selected planning tools for district heating schemes, requirements have been derived for the development of a simplified planning tool. The so-called Easy District Analysis tool has been developed, based on the identified requirements for a simplified district heating planning tool. The intended target groups of the tool are urban planners and planners in utility companies. The tool is intended to be used in the pre-planning phase of a district energy system. The focus of the tool is on the evaluation of the impact of different grid temperatures and of different operation modes of district heating schemes. The assessment is based on the parameters primary energy consumption, carbon emissions and heat production costs.

In the description of different case studies innovative demonstration concepts as examples of success stories for communities interested in developing low temperature district heating systems are displayed. Demonstrated cases include the use of advanced technologies and the interaction between different components within the systems. Based on these experiences, principles and lessons learned in designing these systems are given. There were a total of eight case studies from Germany, Denmark, Finland, Norway and Great Britain. The district heating systems were of very different sizes, from smaller building groups to city wide systems. Taking into account the size of the supply area, the network lengths vary from 165 m to 140,000 m. The connected buildings were residential buildings of different sizes, and mostly low energy or passive houses. Sources of heat were solar collectors, heat pumps, combined-heat-and-power-plants, excess heat from industry or the systems were connected to a larger network close by with heat exchangers. The temperature levels recorded were typical for low-temperature systems, varying from

40 to 60 °C in supply and 25 to 40 °C in return. Savings and increased efficiencies were observed in every case studied.

The material collected and summarized in the guidebook [1] show that low temperature district heating is a key enabling technology to increase the integration of renewable and waste energy for heating and cooling. More research and development work is needed to assess the practical and wider implementation of low temperature district heating schemes for various cases and locations. Especially ways to overcome the hindering reasons need to be identified. This supports more discussions to get low temperature heating systems built and in operation.

Acknowledgements

This article is the result of cooperative research work of many experts from various countries. We would like to gratefully acknowledge all those who have contributed to the IEA DHC Annex TS1 project by taking part in the writing process of the final report and the numerous discussions. This cooperative research work is funded by various national sources and from industry partner. All participants and authors would like to thank for the given financial support. A list of the participants within Annex TS1 and their corresponding countries can be found in [1].

References

- [1] Schmidt, D., Kallert, A. (Editors) (2017) "Future Low Temperature District Heating Design Guidebook". Final report of IEA DHC Annex TS1 Low Temperature District Heating for Future Energy Systems. AGFW-Project Company. Frankfurt am Main, Germany.
- [2] Gerhardt, N., Sandau, F., Becker, S., Scholz, A., Schumacher, P., Schmidt, D. (2017). Wärmewende 2030 - Schlüsseltechnologien zur Erreichung der mittellund langfristigen Klimaschutzziele im Gebäudesektor. Study by order of Agora Energiewende. Fraunhofer IWES/IBP Kassel, Germany.
- [3] Schmidt, D., Kallert, A., Blesl, M., Svendsen, S., Li, H., Nord, N., Sipilä, K., Low Temperature District Heating for Future Energy Systems. Energy Procedia, 116 (2017), pp. 26-38.
- [4] Lund, H. Wiltshire, R., Svendsen, S., Thorsen, J.E., Hvelplund, F., Mathiesen, B., 4th Generation district heating (4GDH) integrating smart thermal grids into future sustainable energy systems, Energy, 68 (2014) 1-11.
- [5] Dalla Rosa, A., Li, H., Svendsen, S., Method for optimal design of pipes for low-energy district heating, with focus on heat losses, Energy 2011 (36), pp.2407-2418
- [6] Li, H. (2015). Energy efficient district heating, Handbook of Clean Energy Systems. John Wiley & Sons Ltd, Hoboken, United States
- [7] Kuosa, M, et.al, Study of a district heating system with the ring network technology and plate heat exchangers in a consumer substation, Energy and Building, 80 (2014), pp.276-289
- [8] Laajalehto T., Kuosa M., Mäkilä T., Lampinen M., Lahdelma R., Energy efficiency improvements utilising mass flow control and a ring topology in a district heating network, Applied Thermal Engineering 69 (2014), pp.86-95
- [9] Brand M., Heating and Domestic Hot Water Systems in Buildings Supplied by Low-Temperature District Heating, PhD Thesis Department of Civil Engineering 2014.
- [10] District heating application handbook, Danfoss Co. Ltd. www.danfoss.com
- [11] Yang, X., Li, H., Svendsen, S., Analysis and research on promising solutions of low temperature district heating without risk of legionella. DHC 14 Stockholm, 2014
- [12] Yang, X., Li, H., Svendsen, S., Alternative solutions for inhibiting Legionella in domestic hot water systems based on low-temperature district heating. Building Service Engineering Research & Technology. 2015
- [13] Blesl, M. and Stehle, M. (Editors) (2017). ANNEX TS1: Low Temperature District Heating for Future Energy Systems – Subtask A: Methods and Planning Tools. Final subtask A report of the IEA DHC Annex TS1: Low Temperature District Heating for Future Energy Systems, Institute of Energy Economics and Rational Energy Use (IER), University of Stuttgart, Germany.
- [14] Rämä, M. and Sipilä, K. (Editors) (2016). ANNEX TS1: Low Temperature District Heating for Future Energy Systems – Subtask D: Case studies and demonstrations. Final subtask D report of the IEA DHC Annex TS1: Low Temperature District Heating for Future Energy Systems, VTT Technical Research Center of Finland, Espoo, Finland.
- [15] Homepage of the IEA District heating and Cooling, including the integration of CHP, Implementing agreement: www.iea-dhc.org.



16th International Symposium on District Heating and Cooling, DHC2018,
9–12 September 2018, Hamburg, Germany

Thermal and hydraulic investigation of large-scale solar collector field

Nirendra Lal Shrestha^{a*}, Ophelia Frotscher^a, Thorsten Urbaneck^a, Thomas Oppelt^a,
Thomas Göschel^b, Ulf Uhlig^b, Holger Frey^b

^aChemnitz University of Technology, Faculty of Mechanical Engineering, Professorship Technical Thermodynamics, 09107 Chemnitz, Germany
^binetz gmbH, Augustusburger Straße 1, 09111 Chemnitz, Germany

Abstract

Large collector fields are increasingly being integrated into district heating systems. Due to the operation mode of these networks, the solar system must provide the desired supply temperature. Therefore, knowledge of thermal-hydraulic behavior and energy efficiency are very important for planning, operation and control. The study presents the investigation of two large-scale solar collector fields in Chemnitz (Germany). For the detailed study of heat transfer and hydraulic behavior of the field, mobile monitoring has been installed on selected rows in addition to the conventional monitoring system. The measurement results show that large collector fields with differently sized rows, consisting of a large number of collectors with a dividing manifold (below) and a combining manifold (above) connected to a large row, can be operated with a variable flow rate (matched flow). With the provided measured values, comparison of the desired/actual values and the calculation of absolute and relative parameters are performed. The Brühl solar district heating system has been in operation since summer 2016 and meets the expectations of thermal performance and efficiencies.

© 2018 The Authors. Published by Elsevier Ltd.

This is an open access article under the CC BY-NC-ND license (<https://creativecommons.org/licenses/by-nc-nd/4.0/>)

Selection and peer-review under responsibility of the scientific committee of the 16th International Symposium on District Heating and Cooling, DHC2018.

Keywords: collector; field; solar thermal system; monitoring; efficiency; hydraulic; performance; operation; measurement

* Corresponding author. Tel.: +49 37153132637; fax: +49 371531832637.

E-mail address: nirendra-lal.shrestha@mb.tu-chemnitz.de

Nomenclature			
a_0	conversion factor, -	FM	flow meter
a_1	linear heat loss coefficient, $W/(K \cdot m^2)$	g	global radiation
a_2	quadratic heat loss coefficient, $W/(K^2 \cdot m^2)$	in	inlet
c	specific heat capacity, $kJ/(kg \cdot K)$	m	mean
f_0	safety factor for other uncertainties, -	max	maximum
f_P	safety factor taking into account heat loss from pipes, -	meas	measured value
f_U	safety factor taking into account measurement uncertainty, -	min	minimum
G	global radiation, W/m^2	N	row in the north field
H	daily global radiation, kWh/m^2	NF	north field
p	pressure, Pa	nom	nominal
Q	thermal energy, kWh	Pa	sensor, ambient pressure
\dot{Q}	thermal power, kW	r	return
T	temperature, °C, K	rad	radiation
\dot{v}	specific flow rate, $l/(m^2 \cdot h)$	s	supply
\dot{V}	flow rate, m^3/h	S	row in the south field
η	efficiency, -	SF	south field
ρ	density, kg/m^3	SHCT45	Solar Heating and Cooling Task 45
a	ambient	Ta	sensor, ambient temperature
cm	combining manifold	TC	thermocouple
coll	collector	Trad1	sensor, outside temperature with influence of sky radiation
diag	diagonal	Trad2	sensor, outside temperature with influence of ground radiation
dm	dividing manifold	w	water
Ecoll	sensor, solar radiation on collector surface	Ww	sensor, wind velocity
Fa	sensor, outside air humidity		

1. Introduction

From 2011 to 2014, the Professorship Technical Thermodynamics at the Chemnitz University of Technology and the *inetz* company (district heating operator) developed a highly efficient district heating system with solar thermal system and combined heat and power for the urban quarter Brühl in Chemnitz (Germany) considering of complex urban development conditions [1], [2], [3]. The system was built between 2015 and 2016. In summer 2016, the solar plant was put into operation. The monitoring and analysis are carried out as part of the project “Solar district heating for the Brühl district in Chemnitz – accompanying research (SolFW)” which is located in the 6th energy research program of the German federal government [1].

This article refers to the operation of large collector fields. The collector field operated with variable flow should provide heat at the desired supply temperature¹. The heat can then be directly fed into the network or used for charging the storage. For reliable operation, it is necessary to know the thermal and hydraulic conditions. In the system presented here, the questions are not trivial, as there is an irregular structure of the fields (in contrast to [5]). Moreover, many large collectors are connected in parallel. From practice, there are only a few results available [5, 6]. In this article, the energy efficiency of the collector fields is also considered together with the thermal-hydraulic behavior (for e.g. collector’s efficiency, thermal power output).

¹ The first known large-scale plant is located in Marstal (Denmark) [4]. There, this type of operation mode has been practiced since 1996 using large-scale collectors with harp absorbers by Arcon (12.5 m²).

2. Collector fields layout

The structure of the south and north solar collector field (ground-mounted) is shown in Fig. 1. Large-sized flat plate collectors from Wagner Solar [7] were used. The collector fields (Table 1) differ in number and length of the rows and in number and type of collectors installed. In order to ensure an optimal use of the field, two different sizes of collectors were installed in the system (WGK 80 and WGK 133 with three and five meander pipes, respectively). Each field is part of a collector circuit with independent operation. Each row (Fig. 2) consists of parallel-connected collectors, which have a common dividing and combining manifold. That means, each row forms an additional mesh system with the meanders in the collectors (Tichelmann circuit). Here is a difference to large-sized flat plate collectors which are internally fitted with harp absorbers. These collectors have been installed in the Danish large plants since the 1990s and each row consists of a series of harps. The sum of the pressure losses of all the collectors in the row gives the pressure loss of a row.

The operation of the system with variable flow rates (Table 1) should ensure an adjustable supply temperature (70...80 °C). Therefore, the rows are hydraulically balanced with regulating valves.

The special feature of the Brühl solar system [2], [3] is that water is used as heat transfer medium throughout the system. This means that no heat exchangers are used between the collector and the consumer. As a result, the following advantages can be achieved: improvement of the heat transfer in the collector and the venting, reduction of the temperature losses along the supply line, thereby increasing the collector output and yield, simplification of the safety technology. On the other hand, there are disadvantages of active frost protection, which are associated with low-temperature heat consumption and complex operation. In order to be able to evaluate this concept, first of all the thermal-hydraulic behavior and the operating results must be analyzed.

The measurement of the parameters of the plant is carried out by the project partner *inetz* through the conventional monitoring system. In addition, for the detailed measurement of the parameters to determine heat transfer and hydraulic behavior of the plant, mobile monitoring is installed in both fields (Fig. 2). Here, two rows (S6, S7, N5 and N6) with different numbers of collectors (Table 2) are fitted with the corresponding measuring equipment in both fields. The temperature sensors (Thermocouples, TC) were mounted at various positions on the dividing and combining manifolds² as well as on the absorber plate. The flowmeters were installed in the return pipes. Furthermore, environmental sensors were installed. The recording of the measurement is done for every minute, ensuring a high resolution of dynamic processes.

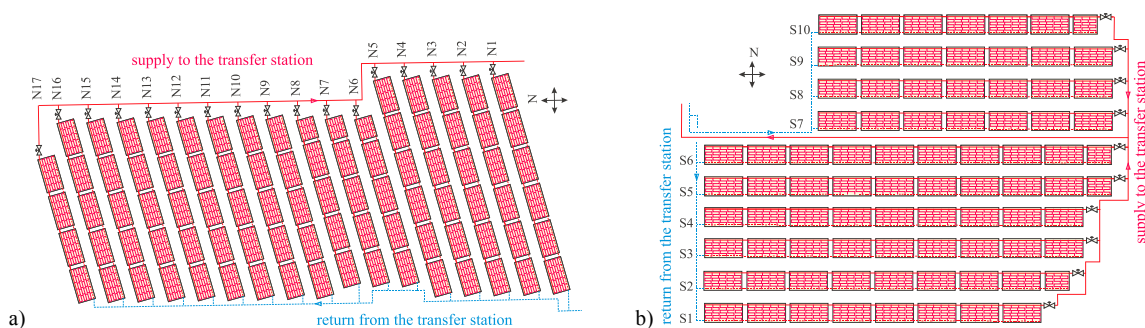


Fig. 1. Layout of the Brühl solar collector fields (a) north field; (b) south field.

² The mean collector temperature ($T_{m, coll, diag}$) is determined by averaging the temperature in the dividing and combining manifolds according to Fig. 2. Due to the surface temperature sensors, the heat transfer at the pipes influences the measurement of the heat transfer fluid's temperature. If the flow distribution in all the meander pipes in row is equal, then the temperature differences also match. The determination of the mean collector temperature is then relatively accurate. In the case of non-uniform temperature distributions in the meanders, deviations occur and the mean temperature ($T_{m, coll, diag}$) deviates from the actual mean value.

3. Analysis of the hydraulic behavior

3.1. Flow distribution and pressure loss in row

Fig. 3 shows the flow distribution in the meander pipes for the rows S6, S7, N5 and N6. The crosses represent the calculated flow rates in the meander pipes, respectively and the dashed line represents the desired flow rate with a uniform distribution. The maximum deviation occurs always in the last meander pipe. The flow distribution takes a parabolic form. The meander pipes in the center of the row have always the lowest flow rate. Despite the approximately parabolic distribution, the flow rate in the first meander do not reach the same values as those at the end of the row. This asymmetry results from the influences of the T-pieces. There are dividing and combining flows in the manifolds.

In row S6 (Fig. 3, red), the meanders 14 to 34 have an almost identical flow rate. Due to the low flow rates, the flow regimes lie in the transition region from turbulent to laminar flow. Therefore, the pressure losses are low and such a plateau is formed. The series connection of the collectors and the flow rate in the row also provides different pressure losses (Table 3). The deviation of the pressure losses in the meander pipes is also shown in Table 3.

Table 1. Parameters of the collector fields and specification of the operating range of the fields (matched flow), specific flow rate.

Parameter	North field	South field
Aperture area [m ²], fields	1086.08	1006.91
Aperture area, [m ²], total	2092.99	
No. of WGK 133AR/80AR [-]	86/3	79/4
No. of rows [-]	17	10
Interconnection of the rows	Parallel	
	No further subdivision	Additionally subdivided into two meshes
Min. / max. number of meander pipes per	20/30	33/48
Collector row distance [m]	3.74	
Collector tilt angle [°]	35	
Field azimuth [°]	-30	0
$\dot{v}_{nom.}$ [l/(m ² ·h)]	15.00	
$\dot{v}_{min.} / \dot{v}_{max.}$ [l/(m ² ·h)]	11.12/23.00	9.03/24.80

Table 2. Parameters of the investigated rows with mobile monitoring.

Parameter	N5	N6	S6	S7
Aperture area [m ²]	74.22	56.90	118.75	86.59
Number of collectors WGK 13 /WGK 80	6/0	4/1	9/1	7/0
Number of meanders	30	23	48	35

3.2. Temperature distribution in row

A higher/lower flow rate means a lower/higher supply temperature during operation at nominal conditions. In the mobile monitoring, the temperatures in the combining manifolds T_{cm} and in the distributing manifolds T_{dm} (Fig. 2) are measured in the rows S6, S7, N5 and N6. The following diagrams in Fig. 4 depict the mean collector temperature and the mean temperature in row (line). The row S6 with the highest number of collectors (10 collectors, 48 meander pipes) shows approximately a parabolic shape. The collector temperature is in a range of 3 K (minimum measured value 62.75 °C, maximum measured value 65.78 °C). The temperature increase in the first four collectors is approximately linear. The seventh collector has the highest mean temperature. Then, temperature decreases again. The mirrored behavior of the temperatures in row (Fig. 4 a) indicates that the calculated flow distribution for the row S6 is correct at least qualitatively.

Row S7 (Fig. 4 b) depicts a similar temperature distribution as of the row S6, whereby the difference between the minimum and maximum values being only 1.43 K. This effect can be attributed to a more uniform flow distribution (Fig. 3), which results from a lower number of meanders.

The rows N5 and N6 (Fig. 4 c, d) show a small temperature deviation over the row. The lowest value occurs in the first collector. However, in row N6, the mean collector temperature in collector 5 does not drop. It must be remembered that the number of five collectors or measuring points is not adequate for a statement about the temperature behavior over the entire row with 23 meander pipes.

The tendency of the temperature curves nevertheless supports the calculation results of the flow rates, as the temperature is indirectly proportional to the flow rate. In addition, the deviation from the mean value increases both in the calculation of the flow rates and also in the observation of the mean collectors temperature. From this it can be concluded that the flow distribution is more uniform with a small number of meander pipes. However, the construction of large rows with up to 119 m² area can also be approved from a technical point of view.

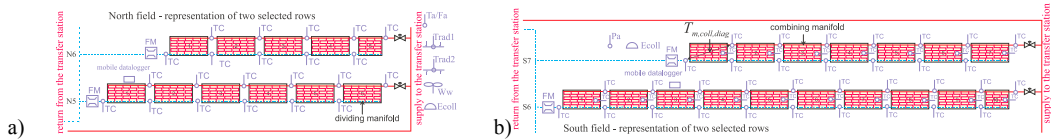


Fig. 2. Schematic representation of the mobile monitoring in the (a) north field and (b) south field.

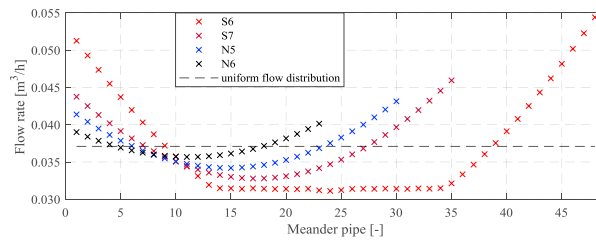


Fig. 3. Calculated flow rate per meander pipe for the rows S6, S7, N5 and N6 in comparison to a uniform flow distribution for nominal conditions with 15 l/(m²·h).

Table 3. Calculated pressure losses for the rows with nominal conditions of 15 (l/m²·h), fluctuations of pressure losses in the meander pipes.

	N5	N6	S6	S7
Pressure loss [mbar]	103.65	77.86	226.04	129.30
Min./max. deviation [%]	-8.2/+17.0	-4.1/+8.6	-15.9/+43.5	-12.2/+24.9

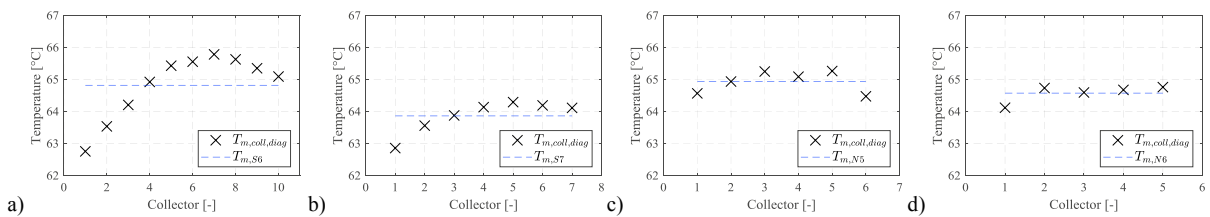


Fig. 4. Mean collector temperature for a) S6, b) S7, c) N5 and d) N6, averaging in the time 12:00 – 13:00, test day 15.10.2017.

3.3. Flow distribution and pressure loss in the field

The calculation of the pressure losses is very crucial for the design of a field. The pressure loss of a row depends strongly on the row length and the flow distribution (Fig. 5). Due to this reason, the flow distributions and pressure losses for an increased and reduced flow rate are calculated (Fig. 5). The maximum flow rate in both collector fields is approx. 25 m³/h. During operation the flow rate is controlled accordingly within a range of 30 to 167 % of the nominal flow rate (15 l/(m²·h)). As expected, the pressure losses increase with the increase of flow rates (Fig. 5). Also the deviations of the flow rates in the meander pipes increase (Fig. 6). However, the distribution of flow rates at

167 % is much more unfavorable than at 100 %³. In order to reach the desired supply temperature, the balancing valves are set for a flow distribution with 15 l/(m²·h). Due to the effects above presented, the operation should be kept as far as possible within the design range.

The flow distribution in the collector fields after hydronic balancing and with uniform flow distribution are shown in Fig. 7. The distribution in the north field shows a typical behavior, as described by *Eismann* [8]. The flow rate is higher than the average value in the rows which are close to the entrance of the return line in the field. Then the flow rate drops further. This explains the influence of the different row lengths and the associated pressure losses. In row N8, the calculated flow rate is higher than that of a uniform distribution. In row N9, both values are approximately the same. Subsequently, the calculated flow rates are below the values for a uniform distribution. In row N16, the difference between the two values is higher than in row N17. The distribution in the south field indicates a noticeable difference between the two sub-meshes of rows S1 to S6 with eight to ten collectors and S7 to S10 with seven collectors. Therefore, the flow rates of the rows S7 to S10 are above the desired values and rows S1 to S6 are below. Table 4 depicts the pressure loss in the fields and the maximum deviations of the pressure loss in a row to the respective uniform flow.

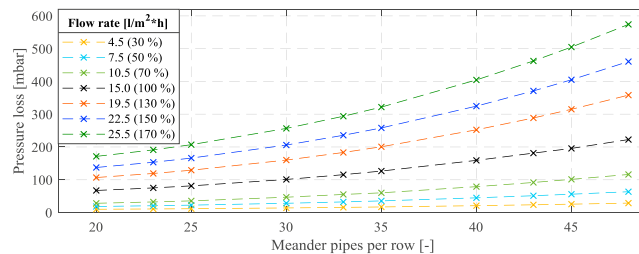


Fig. 5. Pressure losses over the row's length as a function of the specific flow rate and the number of meander pipes.

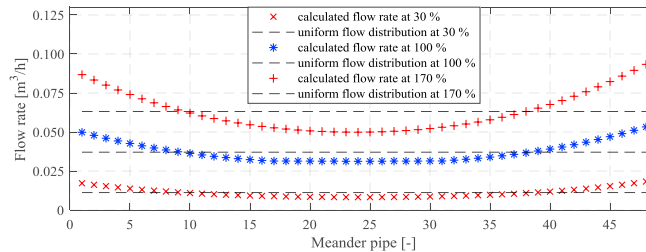


Fig. 6. Calculated flow distribution through the meanders in row S6 at a flow rate of 30 % 4.5 l/(m²·h), 100 % 15 l/(m²·h) and 170 % 25.5 l/(m²·h) as well as representation of the average values.

Fig. 8 illustrates the trend of the specific flow rates for each field and both the investigated rows after the hydronic balancing. In this case the specific flow rate of the field should be the desired value (blue). The measured specific flow rate in row S7 (yellow) is significantly higher than that of the field (Fig. 8 b). In contrast, the specific flow rate in row S6 (orange) is very close to the desired value. In the north field (Fig. 8 a), the deviation is relatively small for both rows. Table 5 depicts the maximum deviations of the rows to the respective desired values.

However, by evaluating the flow rate from the mobile monitoring, clear deviations were found in rows N5, N6 and S7 even at 15 l/(m²·h) (Fig. 8).

Row S6 is the first row starting from the entry of the return flow into the field (Fig. 1). Despite the high length of the row, the flow rate is identical to the planning values. This is because of the good setting of the valves. Row S7 is in a sub-mesh including the short rows S7-S10. Row S7 has the shortest connection to the supply and return line

³ In this case, there is also an asymmetrical distribution due to the pressure loss coefficient of the T-pieces. The form of the flow distribution changes from the parabolic shape (30 %) via the parabola with plateau (100 %) to reformation of the parabolic form (170 %).

(Fig. 1). The short row length and the proximity to the field inlet enable the increased flow rate of the row⁴. An insufficient setting of the balancing valve at the supply line of the row is also responsible for this higher flow rate.

Rows N5 and N6 are connected directly one after the other. They differ significantly in their length. The pressure loss occurs mainly in the rows. This explains the marginal increase of flow in row N6.

The measurements are by no means contradictory to the hydraulic calculation. It must be checked whether a fine-adjustment of the balancing valves leads to an improvement of the flow distribution. If the field planning permits, the use of long rows near the field entrance is expected to be favorable.

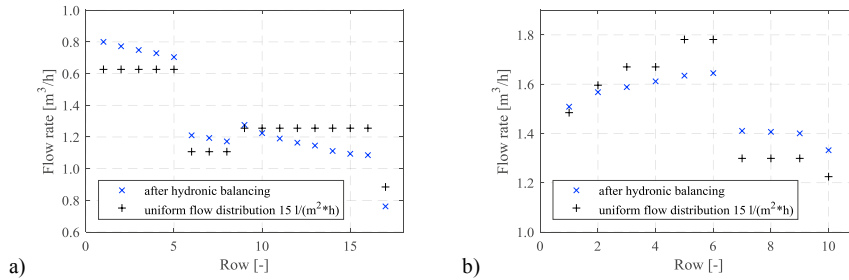


Fig. 7. Flow distribution in pressure balance and with uniform distribution in (a) north field and (b) south field.

Table 4. Pressure loss in the collector field and maximum deviation of the pressure loss in a row referred to a uniform flow distribution.

	North field	South field
Pressure loss [mbar]	123.17	199.04
Max. deviation [%], positive / row	7.54 / N1	8.85 / S10
Max. deviation [%], negative / row	8.85 / N16	7.97 / S5

Table 5. Specific flow rate of the row, deviation referred to a uniform flow distribution.

	N5	N6	S6	S7
Max. deviation [l/(m²*h)], absolute/relative value	-0.58/-3.7	+0.43/+2.7	±0.21/±1.2	+1.72/+10.2

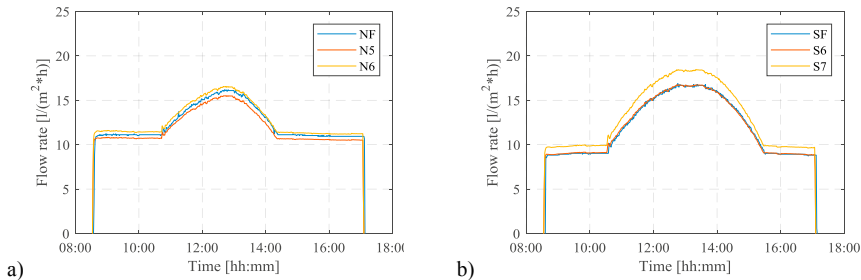


Fig. 8. Specific flow rate, measured values for (a) the north field and rows N5 and N6, (b) the south field and rows S6 and S7, test day 15.10.17.

4. Field thermal performance

4.1. Basic principles

The thermal power output of a collector is determined according to Eq. 1. Density and specific heat capacity of the water are characteristic properties and are dependent on the temperature.

⁴ Other studies have shown that with the rows of equal length, the first row has a higher flow.

$$\dot{Q}_{coll} = \rho_W \dot{V}_{coll} c_{p,W} (T_{coll,out} - T_{coll,in}) \quad (1)$$

Capacitive effects of the collector and the heat transfer fluid (water) are neglected in this investigation. Therefore, quasi-stationary conditions are applied to all the analysis in this paper. Eq. 1 can also be applied to rows and fields [9]. So, additional heat losses for e.g. pipes are included.

The collector efficiency function is given by Eq. 2. It incorporates the parameters from the collector test. Therefore, this value is to be understood as a desired value. This equation can also be applied to a field or the particular rows. Then the field or the row is assumed to behave like the collector under test. In the mobile monitoring, the temperatures in the rows (N5, N6, S6 and S7) and the global solar irradiation on collector plane are determined. These measurements give a second interesting possibility for calculating the desired value as defined by Eq. 3. The averaged collector efficiency is determined by Eq. 2.

$$\eta_{coll,cal} = a_0 - a_1 \frac{(T_{coll,m} - T_a)}{G_{g,coll}} - a_2 \frac{(T_{coll,m} - T_a)^2}{G_{g,coll}} \quad (2)$$

$$\dot{Q}_{coll,S/N} = G_{g,coll,N/S} A_{coll,N/S} \eta_{coll,m}(T_{coll,m,N/S}) \quad (3)$$

The thermal power output according to Eq. 1 (actual value) can be used for measuring efficiency⁵ (Eq. 4). The denominator represents available irradiation.

$$\eta_{coll,meas} = \frac{\dot{Q}_{coll}}{\dot{Q}_{rad}} = \frac{\rho_W \dot{V}_{coll} c_{p,W} (T_{coll,out} - T_{coll,in})}{A_{coll} G_{g,coll}} \quad (4)$$

Since the energy transport processes are very complex and fields are constructed differently, within the IEA SHC Task 45 [10], *Nielson* and *Daniel* have developed a method to calculate the guaranteed power output (Eq. 5) of large solar systems. Analogous to Eq. 4, the solar radiation and the temperature difference to the ambient are incorporated. In addition, however, there are various safety factors which take into account the real boundary conditions (e.g. heat losses of the pipes, measurement uncertainties). The determination of the power output (Eq. 5) is based on the definition of efficiency (Eq. 2). Analogous to Eq. 4, the efficiency of the field can be calculated by Eq. 6.

$$\dot{Q}_{SHCT45} = A_{coll} [a_0 G_g - a_1 (T_m - T_a) - a_2 (T_m - T_a)^2] f_P f_U f_o \quad (5)$$

$$\eta_{coll,SHCT45} = \frac{\dot{Q}_{SHCT45}}{\dot{Q}_{rad}} \quad (6)$$

The collector parameters required here were determined by TÜV Rheinland in accordance with EN 12975 and are listed in Table 6 [11]. Table 6 also contains the safety factors.

Table 6. Collector parameter from the collector test and safety factors according to the calculation procedure, IEA SHC Task 45.

a_0 [-]	a_1 [W/(m ² ·K)]	a_2 [W/(m ² ·K ²)]	f_P [-]	f_U [-]	f_o [-]
0.857	3.083	0.013	0.970	0.900	0.950

4.2. Field thermal power output and collector efficiency

Fig. 9 illustrates the thermal power output (red), the supply and return temperatures (green/blue) of the fields and the field flow rate (black). It can be seen that when the supply temperature reaches about 76 °C (adjustable value), the

⁵ Also here, quasi-stationary conditions are required. Thus, the start-up and shut-down processes have been eliminated in the calculation. Furthermore, optical losses due to certain angular dependencies of the radiation should not occur.

flow rate is regulated (increased) to maintain the desired supply temperature provided by the planned operating concept. Due to the different irradiation conditions, the north field is connected earlier to the system. Despite maximum power output being approximately the same, the orientation of the fields results in different daily yields (Table 7).

A comparison of the measured field efficiencies with the calculated desired values is presented in Fig. 10. These values are shown depending on the mean field temperature. With increasing operating temperature (Fig. 9) and radiation, the efficiency values rise in the morning. The plant is at first operated with minimum flow rate and after with adjusted flow rate (matched flow). During the adjustment of the flow rate, the measured efficiency for the south field increases from approx. 41 % to approx. 63 %. In the north field, an increase of approx. 47 % to approx. 64 % can be seen⁶. These increases are visible in Fig. 10 as surges. After that, the fields are operated with maximum flow rate. In Fig. 10, the profiles show a small increase. In these situations, a comparison between the desired and the actual values is suitable:

- relative low changes of temperature and irradiation over time in the field and this is a prerequisite for the quasi-stationary approach,
- approximately perpendicular irradiation with a low angular dependence of the optical losses,
- high flow rate of the field with a particular flow distribution in the meander pipes (see above), with a relatively high heat transfer in the absorber pipe and with a good venting.

These statements support the comparison of the desired and actual values in Fig. 10 (north field from 11:10 to 13:10, south field from 12:20 to 14:20, CEST). The measured values (point cloud) have a slightly steeper rise compared to the calculated values. Fig. 10 also shows that the calculated collector efficiency according to Eq. 2 (green) lies in the range above the measured efficiencies (blue). The inclusion of the safety factors in Eq. 5 corrects the calculation values. The measured values of both fields are above the desired values of task 45. Therefore, the guaranteed conditions are met.

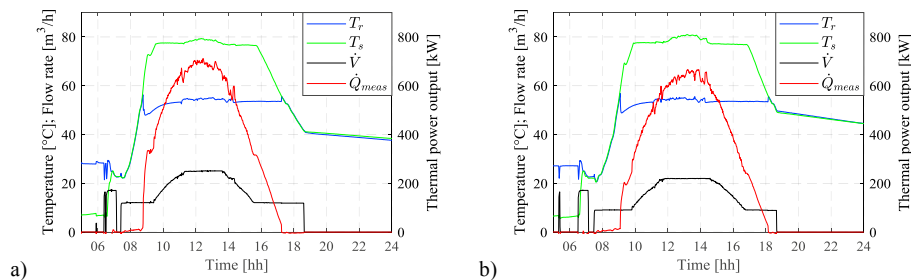


Fig. 9. Measurement results for a) the north field and b) the south field, test day 18.04.2018

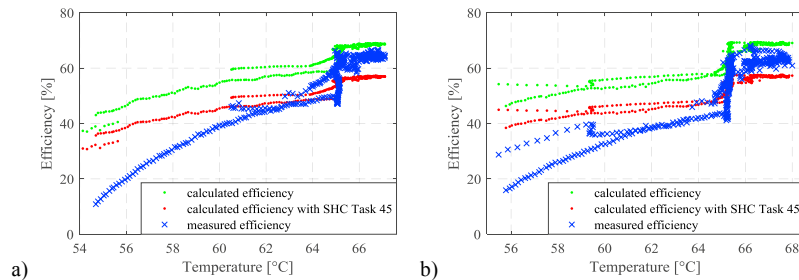


Fig. 10. Field efficiencies (Eq. 2, Eq. 6, Eq.4) depending on the mean field temperature, a) north field, b) south field, test day 18.04.2018

⁶ The measured efficiencies are partly below the calculated values. The following effects are responsible for this tendency: limited capacitive effects, higher optical losses due to slanted solar radiation, relatively low flow rate with a poor heat transfer in the meander pipes.

Table 7. Overview of the investigated data for the test days 19.06.2017 and 18.04.2018

	19.06.2017		18.04.2018	
	North field	South field	North field	South field
$G_{g,Max}$ [W/m ²]	995,80	994,60	1010,7	1029,7
H_g [kWh/m ²]	8,07	8,05	7,31	7,62
Q_d [kWh/m ²]	4,15	4,20	3,63	3,80
$\eta_{coll,meas,m}$ (actual value) [%]	64,11	64,33	63,69	63,63
$\eta_{coll,cal,m}$ (desired value) [%]	68,45	69,15	68,31	68,93
$\eta_{coll,SHCT45,m}$ (desired value) [%]	56,84	57,35	56,65	57,16
Mean temp. diff. to the ambient [%]	44,68	44,13	44,60	45,70

5. Conclusions

Two large collector fields were investigated in terms of thermal and hydraulic behavior. The fields consist of differently sized rows which are hydraulically balanced. A large number of collectors with a dividing manifold (below) and a combining manifold (above) were connected to relatively large rows.

For large collector fields, a well-chosen number of meander pipes and good setting of the regulating valve in each collector row seems to be a reliable solution to achieve a uniform flow distribution. The results show that the desired values of the efficiencies, calculated according to the SHC Task 45, can be achieved.

The operation with variable flow rate works as planned. In normal operation⁷, water is suitable excellently because various properties (e.g. viscosity, density) are significantly better compared to glycol-water mixtures. The results and interrelations shown here can be transferred to other solar district heating systems. The consistently positive results confirm the concept, i.e. the construction of large rows with the selected flat plate collector and the operation.

Acknowledgements

The project underlying this report is funded by the German Federal Ministry for Economic Affairs and Energy under the code 0325871 following a decision by the German parliament. Special thanks also go to the Project Management Jülich for supporting the project. The sole responsibility for the report's contents lies with the authors.

References

- [1] Urbaneck, T. et al. <http://www.solfw.de>. Project website, April 2018.
- [2] Urbaneck, T., Oppelt, T., Platzer, B., Frey, H., Uhlig, U., Göschel, T., Zimmermann, D., Rabe, D. "Solar District Heating in East Germany – Transformation in a Cogeneration Dominated City." *Energy Procedia*, Vol. 70 (2015): 587–594. DOI: 10.1016/j.egypro.2015.02.090.
- [3] Urbaneck, T., Oppelt, T., Shrestha, N. Lal, Platzer, B., Göschel, T., Uhlig, U., Frey, H. "Technische Umsetzung der solaren Fernwärme Brühl." *EuroHeat&Power*, VWEW Energieverlag 46. Jg. Vol 11, (2017): 20-23. – ISSN 0949-166X.
- [4] Heller, A., Dahm, J. "The Marstal Central Solar Heating Plant: Design and Evaluation." *ISES Solar World Congress*, Israel, (1999): 180-187.
- [5] Bava, F., Dragsted, J., Furbo, S. "A numerical model to evaluate the flow distribution in a large solar collector field." *Sol. Energy* 143 (2017): 31-42. DOI: 10.1016/j.solener.2016.12.029.
- [6] Ohnewein, P. et al. "Hydraulikdesign von parallelen Kollektormodulen in solarthermischen Großanlagen." *Endbericht Parasol*, 2015.
- [7] Wagner Solar. <http://www.wagner-solar.com/de>. April 2018.
- [8] Eismann, R. "Thermohydraulische Dimensionierung von Solaranlage." Wiesbaden: Springer Fachmedien Wiesbaden GmbH, (2017): 67-70.
- [9] Urbaneck, T., Schirmer, U. "Großanlage mit Vakuumröhrenkollektoren – Eine Leistungsbestimmung." 12. Symposium „Thermische Solarenergie." *Staffelstein, Ostbayerisches Technologie Transfer Institut e.V. (OTTI), Regensburg (Hrsg.), Conference Proceedings*, (2016): 183-189. – ISBN 3-934681-20-4.
- [10] Nielsen, J. E., Daniel, T. "Guaranteed power output. IEA Solar Heating and Cooling Programme, Task 45 Large Systems." 2016.
- [11] TÜV Rheinland - DIN CERTCO, Summary of EN 12975 Test Results annex to Solar KEYMARK Certificate, DIN CERTCO, Berlin, 2015.

⁷ The work in the field of active antifreeze is planned and not part of this article.



16th International Symposium on District Heating and Cooling, DHC2018,
9–12 September 2018, Hamburg, Germany

Demonstration of an Overground Hot Water Store in Segmental Construction for District Heating Systems

Thorsten Urbaneck^{a*}, Jan Markus Mücke^a, Fabian Findeisen^a, Markus Gensbaur^b,
Stephan Lang^b, Dominik Bestenlehner^b, Harald Drück^b, Robert Beyer^c, Konrad Pieper^c

^a Chemnitz University of Technology, Department of Mechanical Engineering, Institute of Mechanics and Thermodynamics, Professorship Technical Thermodynamics, 09107 Chemnitz, Germany

^b University of Stuttgart, Institute of Thermodynamics and Thermal Engineering, Research and Testing Centre for Thermal Solar Systems, 70550 Stuttgart, Germany

^c farmatic tank systems, Kolberger Str. 13, 24589 Nortorf, Germany

*thorsten.urbaneck@mb.tu-chemnitz.de

Abstract

Thermal energy stores can significantly improve the efficiency and environment-friendliness of the heat supply by storing heat surpluses and supply heat to the consumer if necessary. Therefore, a high demand for cost-effective storage technologies with low energy losses exists. For hot water storage tanks using the displacement principle significant optimization potentials exist regarding currently at the market available storage technologies, in particular pressure vessels and flat-bottom tanks. A new tank design eliminates disadvantages and offers numerous benefits. A demonstrator with a new design was already built in cooperation with scientific and industrial partners as part of the OBSERW project in Nortorf (Germany). The demonstrator is a small-scale hot water storage tank with a volume of approx. 100 m³. It allows numerous tests with low energy and time effort. The main novelty of the construction is an indoor floating ceiling, with the loading device (e. g. a radial diffuser) attached directly to it. A flexible connection allows the free movement of the floating ceiling between a top and bottom dead centre. This work describes the function of the storage tank and presents first operation experiences.

© 2018 The Authors. Published by Elsevier Ltd.

This is an open access article under the CC BY-NC-ND license (<https://creativecommons.org/licenses/by-nc-nd/4.0/>)

Selection and peer-review under responsibility of the scientific committee of the 16th International Symposium on District Heating and Cooling, DHC2018.

Keywords: district heating; floating ceiling; heat supply; hot water storage tank; segmental construction; solar thermal application; thermal energy storage, cogeneration networks.

1. Introduction

The heat supply in Germany is tied to a very high primary energy demand. As a result, there is significant potential to reduce consumption, increase the energy efficiency of the supply and above all to use renewable energy sources in order to avoid future problems. In contrast to other sectors, technical implementation is initially relatively simple. For example, there are many local and district heating networks that can be used for the transport of heat to the consumer. Thermal energy storage systems play a key role in this context. By decoupling heat generation (e.g. solar thermal energy, combined heat and power, industrial waste heat) from the application (e. g. load in the district heating network), the above-mentioned points, the use of renewable energy sources and the increase in energy efficiency, can be achieved.

The technology for the large-scale storage of hot water and its requirements are not new. In the joint project *Overground Storage in Segmental Construction for Heat Supply Systems* (OBSERW) [1], [2], the parties involved are taking a path that differs significantly from other technical developments. The starting point is formed by large segmented cold water storage tanks [3]. With the construction of the first large cold water storage tank, it was possible to prove that with overground construction technology and the use of enameled and sealed segments respectively with a low material usage, the production costs are lower than with other constructions. This is partly due to faster production and better logistics. Up to now, this design could not be transferred to heat storage systems. Until 2017, there were no findings as to whether sealed segments could withstand temperatures of up to 92 °C or alternating temperature stresses. Other problem areas identified were water vapor and oxygen diffusion as well as thermal bridges.

The OBSERW project focused on overcoming the technical problems mentioned above. The planned construction should cover storage sizes of 500 to 6000 m³. The maximum charging and discharging capacity is 56 MW. The authors aim to achieve low heat losses and good thermal stratification behaviour as well as good integration into local and district heating systems. Furthermore, the store should provide system services (e.g. pressure maintenance). As expected, low investment and operating costs are important for market assertion. The store construction presented allows an unproblematic adjustment of the store size (capacity) for many applications, allowing short to long-term storage cycles to be operated. Within the project, among other tasks, the design was completely revised in comparison to existing flat-bottom tanks and cold water storage tanks. The focus of this article is on constructive development. The participants first had to test the materials on a small scale, then on a larger laboratory scale and finally with the demonstrator (three-stage process). The partial results were published according to the progress of the project [4] to [22]. This contribution is dedicated to the constructive development. The results presented here are intended to provide first proof of comprehensive functionality.

2. Design and functionality of the demonstrator

The OBSERW store (Figure 1 and 2) is a single-zone storage tank (see [9]). The overground tank stands on a foundation. The floor, wall and floating ceiling are insulated to prevent heat losses. The demonstrator can be charged and discharged with two radial diffusers according to the displacement principle. This typically corresponds to the use in cogeneration networks. In such cases, short-term storage is often of interest. The same design can also be used in solar thermal systems with variable or constant flow temperatures. The storage volume can then be increased to 6000 m³. This also enables long-term storage. The thickness of the thermal insulation layer can be adjusted according to the application or requirements. The maximum storage tank temperature is determined by the boiling point of the water due to the ambient pressure at the surface of the water or at the floating ceiling. This means that the storage tank is not designed for classic primary networks with flow temperatures above 100 °C. Such systems are suitable for use in secondary and tertiary areas. By avoiding high temperatures, the following advantages can be achieved via the flat-bottom tank design:

- a fast production of large storage volumes on the basis of bolted segments,
- a relatively good surface to volume ratio,
 - cost-effective design (minimization of the store surface),
 - reduction of heat losses,
 - minimization of piping, instrumentation, etc.,

- avoidance of follow-up measures (see below, e. g. safety measures in the attic [9]).

The following sections deal with the design details of the OBSERW storage tank. The new design (Figure 2) was first implemented with a demonstrator (Figure 1, Table 1). With this implementation and a special test program, the following points were to be investigated:

- feasibility of the construction,
- suitability of the materials and their combination on a technical scale respectively the temperature durability,
- charging and discharging behaviour and thermal stratification quality,
- heat losses,
- improvements regarding the points mentioned above.

Table 1. Key properties of the demonstrator.

Storage tank	
Overall height [m]	7.77
Height of the wall [m]	7.29
Inner diameter [m]	5.12
Minimal height of the floating ceiling [m]	5.59
Maximum height of the floating ceiling [m]	6.29
Thermal insulation width of the foundation [m]	0.21
Thermal insulation width of the wall structure [m]	0.29
Thermal insulation width of the ceiling structure [m]	0.45
Maximum store temperature (planned) [°C]	98
Maximum store temperature (tested) [°C]	92
Radial diffusor	
Maximum flow rate [m ³ /h]	19.44
Shape, type	Free form
Stratification device	
Maximum flow rate [m ³ /h]	1.00
Number of outlets [-]	5



Fig. 1. Demonstrator in Nortorf (Germany).

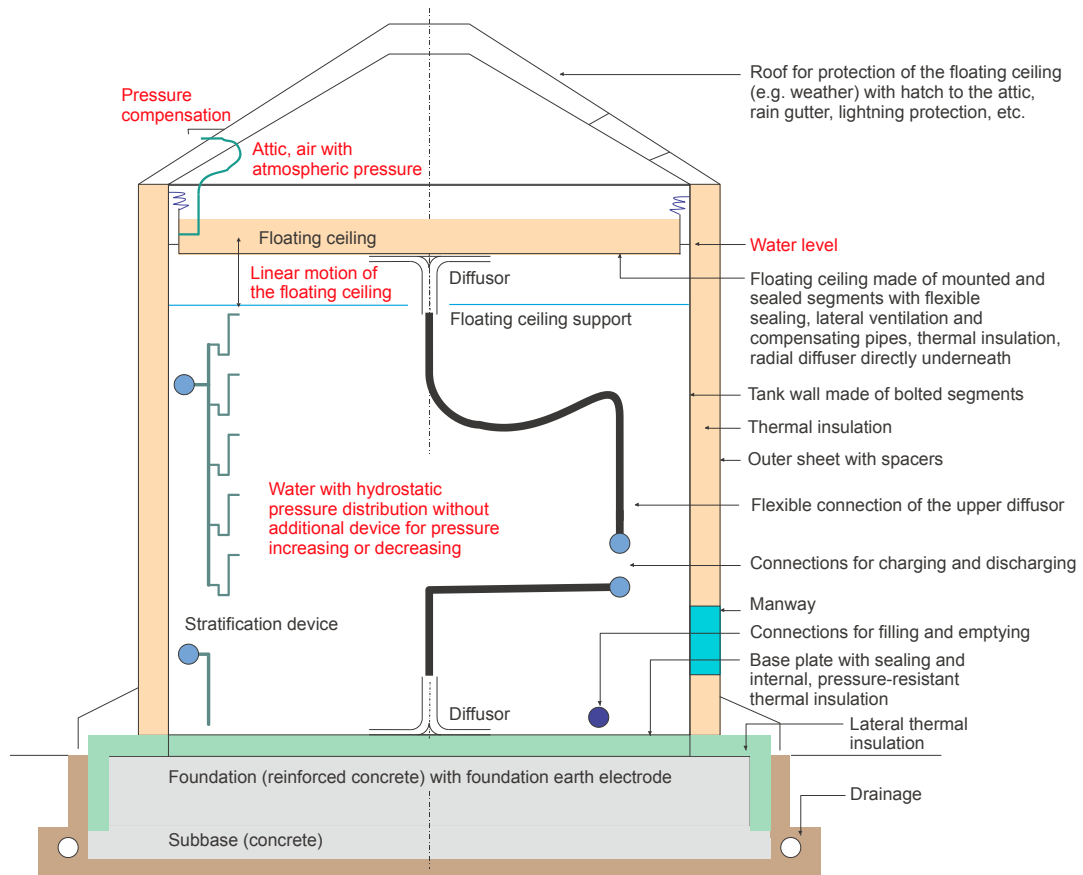


Fig. 2. Schematic structure of the OBSERW storage tank or the demonstrator.

3. Wall construction

The tank wall must fulfil the function of the sealing and structural framework and is manufactured from bolted segments. The steel segments are typically coated to ensure protection against corrosion and a sufficient water quality. Table 2 gives an overview of the coatings tested in the laboratory. In the first laboratory tests, the sealants were also examined with regard to their thermal and mechanical durability [5], [6]. The investigations correlated closely with the surface properties of the segments. The best results could be achieved with Sika sealant Sikasil AS-70.

Table 2. Overview of the used segment coatings.

Name of the surface coating	Manufacturer	Type of material
Proguard CN 200	Ceramic Polymer	Epoxy resin with ceramic particles
Ecofusion® exterior coating	Permastore®	Enamel
Ecofusion® interior coating	Permastore®	Enamel
Fusion® V1100 exterior coating	Permastore®	Epoxy powder
Fusion® V1100 interior coating	Permastore®	Epoxy powder
Painted Epoxy	Permastore®	Epoxy resin
Tankguard Storage	JOTUN®	Epoxy resin

The coatings tested in the laboratory were used on the demonstrator. In addition, segments with an Epoxy HR coating from JOTUN® were installed. All coatings, with the exception of Painted Epoxy, showed no visible changes after approximately one year of operation with temperature stresses of up to 92 °C in some cases. The other coatings

are therefore suitable for use as corrosion protection for the steel segments in hot water storage tanks. Figure 3 shows two exemplary comparisons to the above statements. It can clearly be seen that bubbles have formed on the entire surface of the inner wall of the Painted Epoxy coating. There are also bubbles under the sealant. The water-filled bubbles have partially burst open. The authors assess this as a failure of the coating with a significant effect on the sealing of the segments. The Proguard CN 200 coating, on the other hand, appears unchanged (except for a slight change of colour due to the deposition of rust from the plant).

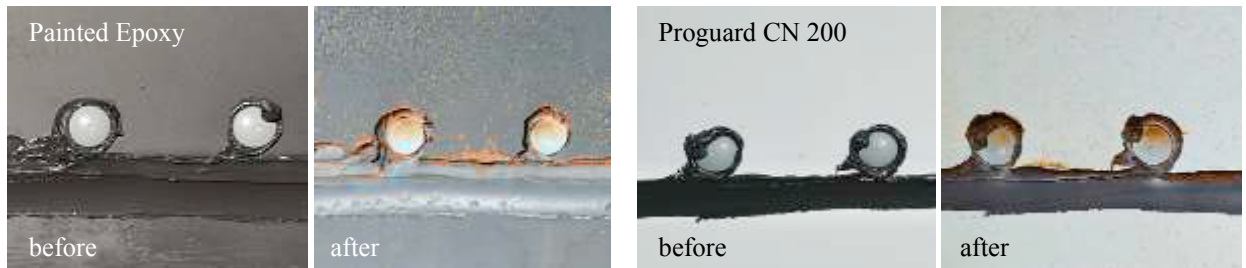


Fig. 3. Exemplary comparison between two coatings at the demonstrator before use and after one year of testing.

At the same time, extensive investigations on thermal insulation materials were carried out. Table 3 shows shortlisted thermal insulation materials for the entire store structure. For technical, economic and ecological reasons, the authors selected a pourable recycling material for the ceiling and wall construction. Rathipur from the company Rathi is a polyurethane granulate (Figure 4a). The thermal insulation material has relatively low material costs.

The screws on the outside of the segments as well as the spacers and other components make the installation of thermal insulation panels difficult. An adaptation to the surface would be very laborious. Intermediate grooves as they occur between the cladding sheet and the screwed wall (Figure 4b) can easily be filled with the bulk material. This means that assembly costs can also be reduced due to the filling technology.

Table 3. Thermal insulation materials, selection of the examined products.

Thermal insulation material	Area	Price [€/m ³]
Polyurethan-recycling-granulate (Rathipur, GranuPUR)	Wall, Ceiling	60...85
Glass wool mats	Wall, Ceiling	50...210
Rock wool flakes (ProtectFill)	Wall, Ceiling	96...144
Foamglas panels (Floorboards T4+)	Foundation	500
Panels of extruded polystyrol (XPS, Styrodur 5000CS)	Foundation	320
Panels of polyisocyanurat (E 40, E 80, B2 145)	Foundation	260...740
Panels of phenolic resin (Kooltherm 1200)	Foundation	480
multiporous insulation panels (WDS Ultra)	Foundation	2500

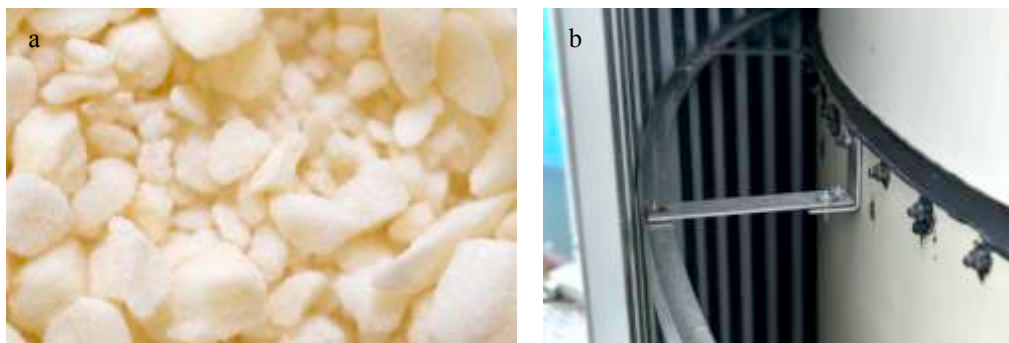


Fig. 4. (a) Rathipur; (b) Structure of the storage wall, cladding sheet, spacers, screwed segments.

In the next stage of the project, practical tests were carried out on the planned wall construction with a newly built test rig for practical testing of multi-layered wall structures (TR-WS) [16], [20]. The results of the investigations were as follows:

- Rathipur is subject to certain fluctuations due to the raw material and the processing, which are, however, not critical with regard to the intended use here.
- Fillings over several meters of height (e.g. in the wall structure of the demonstrator) can be realised without significant changes of the properties.
- The particles are hydrophobic. Long-term tests have shown that particles stored under water do not absorb water for months. Piles in contact with the ambient air dry quickly. According to current information, no significant degradation processes are known.
- The effective thermal conductivity (Figure 5) increases with temperature, which can be observed with most thermal insulating materials. However, the increase is relatively low. The measured values in the test setup of the wall at the Chemnitz University of Technology (TUC) with the TR-WS are higher than in the material value tests of the Institute of Thermodynamics and Thermal Engineering in Stuttgart (ITW). In the vertical position of the structure, convection fluxes occur at the TR-WS which lead to an increase in the effective thermal conductivity. The Installation of two convection barriers (XPS Plates) effectively suppresses these transport processes. The convection barriers are installed horizontally and divide the vertical structure in three approximately 60 cm high sections. According to current knowledge, no significant convection occurs in the horizontal position (ceiling installation). A detailed description of the TR-WS and the carried out tests is given in [16] and [20].
- Despite the effects that lead to an increase in the effective thermal conductivity, the authors consider the thermal insulation material to be suitable.

Table 4. Material properties of Rathipur [16].

Property	
Particle diameter [mm]	approx. 1...16
Mean particle diameter[mm]	5.3
Non-uniformity number [-]	2.7
Mean density (shaken) [kg/m³]	29.0
Outer porosity [%]	53

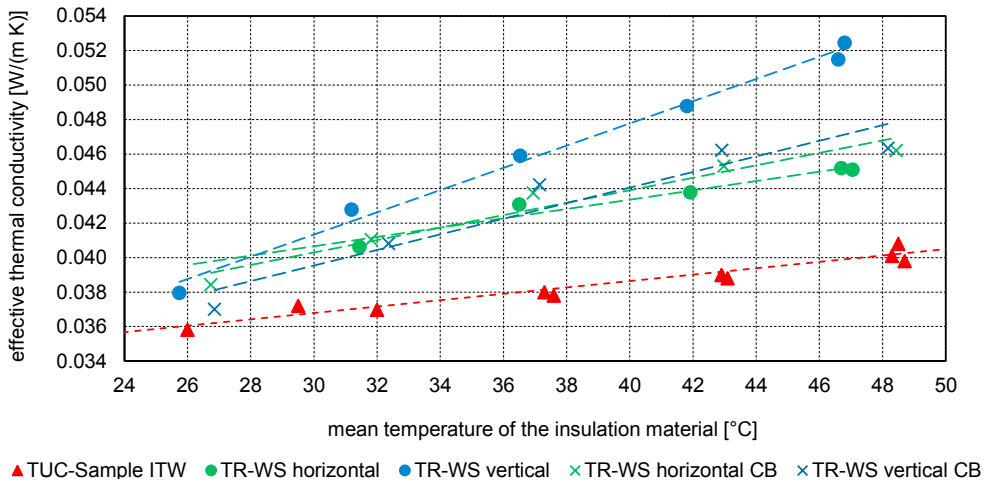


Fig. 5. Effective thermal conductivity of Rathipur as a function of the mean temperature of the thermal insulation material, TUC-Sample ITW: measurement of a relatively small sample with a two-plate apparatus at the ITW (stage 1); TR-WS: Measurement with the test stand for practical tests of multi-layered wall structures at Chemnitz Technical University (stage 2); horizontal: horizontal position of the structure to examine the ceiling structure; vertical: vertical position of the structure to examine the wall structure; CB: Use of convection barriers to suppress natural convection in the wall structure.

Another problem identified was the thermal bridges induced by the spacers for the outer sheet. A variant analysis (Figure 6a) shows that heat losses can be significantly reduced when plastics (e.g. glass fibre reinforced plastic (GRP) or polypropylene) are used. Thermal decoupled stainless steel bars (Figure 4b) are currently mounted on the demonstrator. The heat losses are measurable (Figure 6b). Further work on this topic is planned.

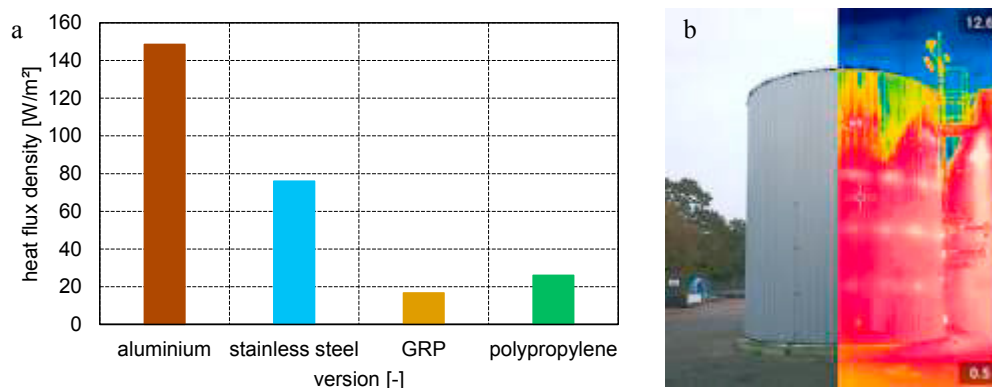


Fig. 6. (a) Representative heat flux densities (heat losses) in the spacers of the wall structure, calculated with the Delphin program; (b) Image taken with a thermal imaging camera to verify the thermal bridges.

4. Construction of the roof and floating ceiling

The following conclusions can be drawn from theoretical considerations (without explanation) on the topic of an indoor floating ceiling:

- A consistent pursuit of the segment design (wall structure) offers advantages with regard to lightweight construction, easy transport, sealing technology, etc.
- The construction of a fixed panel allows the diffuser to be mounted directly underneath the ceiling and low mechanical loads to be absorbed when filled (e. g. when walked on).
- More unusual approaches to edge connections require a longer development time and could not be implemented at the demonstrator during the project phase.
- Therefore, the use of a foil for flexible sealing of the edge area seemed feasible and effective. Due to limited temperature resistance as well as the desired long-term stability, protective measures must be taken in particular for thermal protection: a distanced position, a gas cushion and the use of lips.

The constructive concept [22] was implemented accordingly. The following points describe the implementation as well as the experiences and results:

- The floating ceiling (Figure 2, 7a and 7b) consists of elongated segments that are screwed and sealed.
- Various (temperature-resistant) foils are available for flexible sealing (Figure 7b). Several tests were carried out as short-term experiments in the laboratory. At the demonstrator the foil Alcryn was used. The tested construction allows a height compensation of approximately 70 to 100 cm. The height deflection is based on larger reservoirs. This enables the storage tank to compensate volume changes very well. For test reasons (investigation of the three-dimensional bending behaviour, determination of the height compensation, etc.), the examination regarding waterproofing was initially carried out without thermal insulation. This results in considerable heat losses over the circular space. Because the lip on the underside of the floating ceiling (Figure 7c) cannot completely seal the circular space, hot water enters the circular space. As a result, water vapour condenses on the relatively cold seal. The seal must be partially supported so that the condensate can flow back reliably into the circular space. The development of suitable insulation for this thermal bridge is not yet complete.
- As with the wall structure (see above), Rathipur is used as thermal insulation. The filling process is quick and easy. In addition, XPS panels were laid on the webs of the floating ceiling. This makes the attic accessible and inspectable.

- The upper radial diffuser is located directly on the underside of the floating roof (Figure 7d). This position allows the use of the entire storage capacity compared to other single-zone store constructions. The density current, which is particularly important for high quality thermal stratification, forms very well [10], [11], [12], [15], [19], [21].
- The roof is made of folded sheets. For larger storage tanks, rafters are used. The design guaranteed reliable protection against environmental influences during test operation. The relatively high heat losses over the circular space also resulted in a more intensive absorption of water vapour in the air of the attic. A temporary condensate accumulation was eliminated with a fan. There were no negative effects on the thermal insulation.

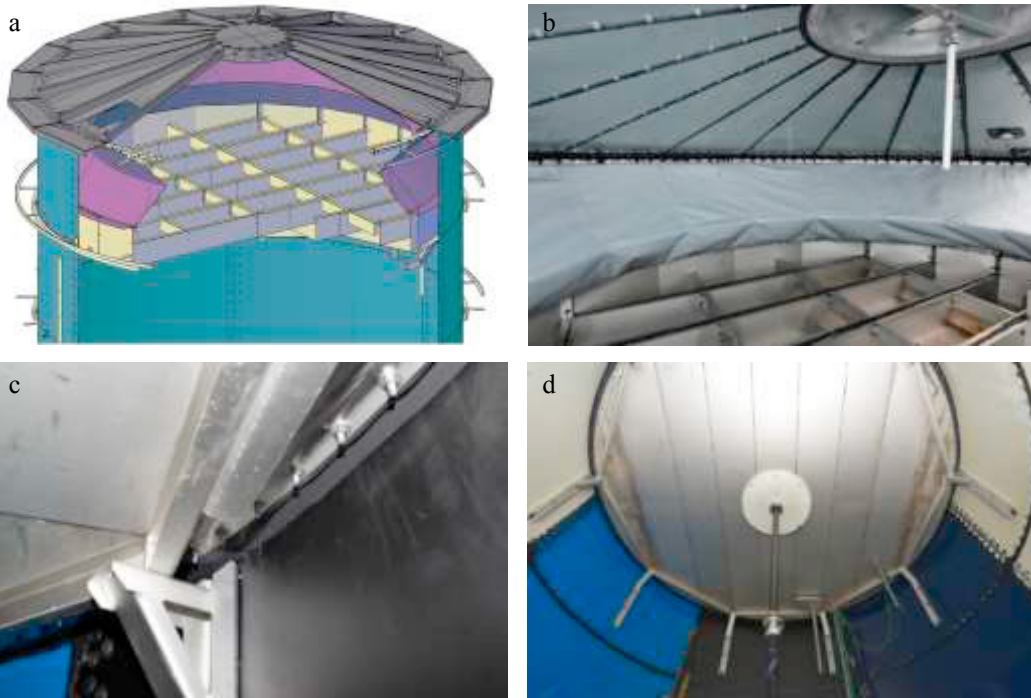


Fig. 7. Demonstrator: (a) Graphic representation of the roof area with floating roof and flexible sealing; (b) Attic, flexible sealing of the floating ceiling, before filling with Rathipur (thermal insulation material), 09.02.2017; (c) Support of the floating ceiling, sealing lip on the underside of the floating ceiling, 14.12.2016; (d) Inside the storage tank, floating ceiling with radial diffusor, 13.07.2017.

5. Construction of the base

Figure 8 shows the structure of the storage tank base. The store wall stands directly on the foundation and is fastened there with screws. The thermal insulation of the wall extends down to the ground. The thermal insulation of the floor is achieved by an internal thermal insulation layer (Figure 8a and 8b). This arrangement is nearly free of thermal bridges and the insulation layers are very close to the storage medium. This way the heat losses could be minimized. The load transfer of the store wall takes place directly at the foundation. The pressure- and temperature-resistant thermal insulation is not stressed three-dimensionally by the storage wall as in other storage constructions. The only mechanical load that the internal thermal insulation must absorb is the static load of the water head. This means that the use of more insulating materials in the future is possible. A stainless steel plate protects the internal insulation against the ingress of storage water. This plate is installed with the same sealing technology as the wall segments (Figure 8c). The entire wall structure continues to expand as the temperature increases and contracts again when the temperature drops. This is why this area is considered particularly demanding. No disadvantages could be determined after the test operation. The authors regard this area as largely resolved.

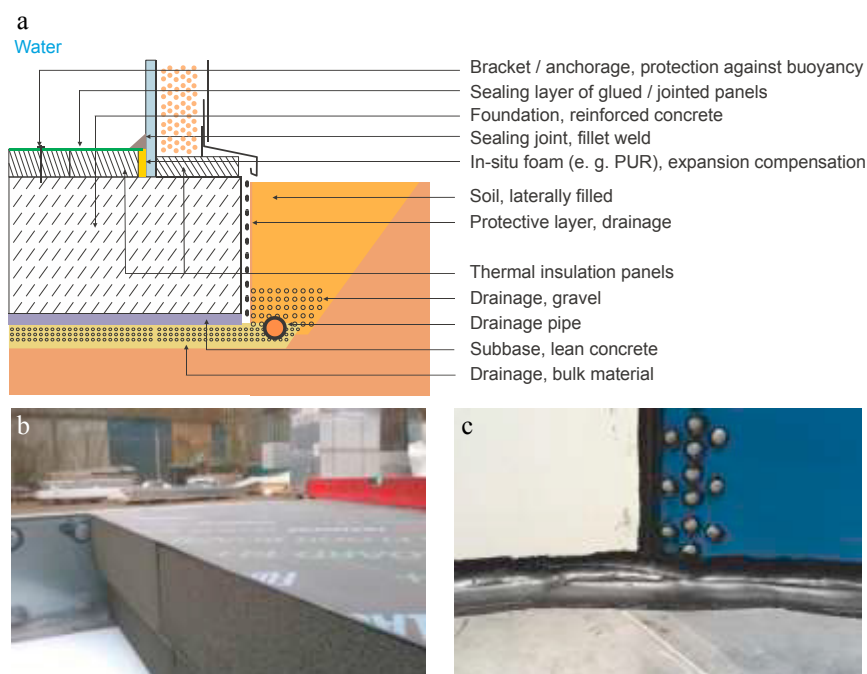


Fig. 8. (a) Construction of the storage tank floor; (b) Starter ring with internal thermal insulation (foam glass plates); (c) Storage tank floor and wall with sealing.

6. Conclusion and outlook

The use of heat storage tanks offers many advantages and key functions. Therefore, thermal energy storage systems must meet high technical requirements (e. g. very low heat losses, best possible stratification quality, very long technical lifespan). The design of the OBSERW storage tank is fundamentally suitable for operation in solar and district heating systems. This was proven in a three-step procedure. The procedure from the small laboratory test to the test with the demonstrator was necessary and purposeful. The main tasks (e. g. material testing, design, operation) were carried out in a network of scientific and industrial partners. This article presented the new constructive approaches in the ceiling, wall and bottom areas. Low construction costs are targeted through the design and construction technology. The fundamental potential for a later application in, for example, local solar heating systems or secondary network areas of classic district heating systems is given. However, the conversion to larger storage tanks is still pending. There are also detailed problems to be solved (e.g. the reduction of thermal bridges and further improvement of the stratification device for very great heights, etc.). This technology also offers a high potential for the export of large-scale storage systems.

Acknowledgements

The realization of the project and the scientific work is supported by the German Federal Ministry for Economic Affairs and Energy (BMWi) on the basis of a decision by the German Bundestag (funding reference: 03ET1230A/B/C). The authors gratefully acknowledge this support and carry the full responsibility for the content of this paper.

References

- [1] Urbaneck, T. et al.: www.obserw.de. Webseite zum Projekt, April 2018
- [2] Bundesministerium für Wirtschaft und Energie (BMWi): <http://forschung-energiespeicher.info>. Energiespeicher Forschungsinitiative der Bundesregierung, 2016

- [3] Urbaneck, T.; Platzer, B.; Schirmer, U.; Uhlig, U.; Göschel, T.; Baumgart, G.; Fiedler, G.; Zimmermann, D.; Wittchen, F.; Schönfelder, V.: Pilotprojekt zur Optimierung von großen Versorgungssystemen auf Basis der Kraft-Wärme-Kälte-Kopplung mittels Kältespeicherung. Technische Universität Chemnitz, Fakultät für Maschinenbau (Hrsg.), Stadtwerke Chemnitz AG (Hrsg.), Chemnitz, 2010, Forschungsbericht, Projektträger Jülich (PTJ), Förderkennzeichen 0327357B/C. - ISBN 3-9811424-4-6
- [4] Urbaneck, T.; Platzer, B.: Overground storages in segmental construction for district heating systems (OBSERW) - Project overview. Greenstock, 13th International Conference on Thermal Energy Storage, Peking (China), 2015.
- [5] Gerschitzka, M.; Marx, R.; Lang, S.; Bauer, D.; Drück, H.: New developments related to thermal insulation materials and installation techniques for over ground seasonal thermal energy stores. Greenstock, 13th International Conference on Thermal Energy Storage, Peking (China), 2015
- [6] Lang, S.; Marx, R.; Gerschitzka, M.; Drück, H.; Urbaneck, T.; Mücke, J.; Hoffmann, F.; Gebhardt, S.; Beyer, R.: Hot water stores in segmental construction: adhesive strength between sealing materials and segment coatings. Book of Abstracts, The Energy and Material Research Conference (EMR2017), Lisbon, Portugal, 2017.
- [7] Lang, S.; Bauer, D.; Drück, H.: Neue Untersuchungen zu Wärmedämmstoffen für thermische Energiespeicher. 5. Fachforum Thermische Energiespeicher, Ostbayerisches Technologie Transfer Institut e.V. (OTTI), Regensburg (Hrsg.), 2016, Tagungsband, S. 53-55.
- [8] Urbaneck, T.; Findeisen, F.; Mücke, J.; Marx, R.; Lang, S.; Bauer, D.; Rohde, T.; Hoffmann, F.; Gebhardt, S.; Fischer, M.; Beyer, R.: Oberirdische Tankspeicher in Segmentbauweise (OBSERW) – Vorstellung des Projektes. 5. Fachforum Thermische Energiespeicher, Ostbayerisches Technologie Transfer Institut e.V. (OTTI), Regensburg (Hrsg.), 2016, Tagungsband, S. 93-100.
- [9] Urbaneck, T.; Platzer, B.; Findeisen, F.: Warmwasserspeicher – Stand der Technik und Entwicklungen. HLH Lüftung/Klima Heizung/Sanitär Gebäudetechnik Springer 67. Jg. (2016) Heft 07-08 S. 16-21. - ISSN 1436-5103
- [10] Findeisen, F.; Urbaneck, T.; Platzer, B.: Radiale Diffusoren in Warmwasserspeichern – Funktionale Optimierung mittels CFD; Teil 1 Grundlagen und Modellierung. HLH Lüftung/Klima Heizung/Sanitär Gebäudetechnik Springer 67. Jg. (2016) Heft 10 S. 20-28. - ISSN 1436-5103
- [11] Findeisen, F.; Urbaneck, T.; Platzer, B.: Radiale Diffusoren in Warmwasserspeichern – Funktionale Optimierung mittels CFD; Teil 2 Optimierung des Be- und Entladeverhaltens. HLH Lüftung/Klima Heizung/Sanitär Gebäudetechnik Springer 68. Jg. (2017) Heft 2 S. 25-33. - ISSN 1436-5103
- [12] Findeisen, F.; Urbaneck, T.; Platzer, B.: Radiale Diffusoren in Warmwasserspeichern – Funktionale Optimierung mittels CFD; Teil 3: Detaillierte Untersuchung des Beladeverhaltens. HLH Lüftung/Klima Heizung/Sanitär Gebäudetechnik Springer 68. Jg. (2017) Heft 6 S. 19-27. - ISSN 1436-5103
- [13] Gerschitzka, M.; Schmidt, D.; Bestenlehner, D.; Marx, R.; Drück, H.: Thermal performance testing of outdoor hot water stores for long-term thermal energy storage. 6th International Conference on Solar Heating and Cooling for Buildings and Industry (SHC 2017), Abu Dhabi (UEA), 2017
- [14] Urbaneck, T.; Findeisen, F.; Mücke, J.; Platzer, B.; Gerschitzka, M.; Lang, S.; Bestenlehner, D.; Drück, H.; Herrmann, T.; Beyer, R.: Development of Overground Hot Water Stores in Segmental Construction for Solar and District Heating Systems Within the Project OBSERW. Proceedings of the 6th International Conference on Solar Heating and Cooling for Buildings and Industry (SHC 2017), Abu Dhabi (UAE), 2017
- [15] Findeisen, F.; Urbaneck, T.; Platzer, B.: Radial Diffusers in Stratified Hot Water Stores: Geometry Optimization with CFD. Proceedings of the 6th International Conference on Solar Heating and Cooling for Buildings and Industry (SHC 2017), Abu Dhabi (UAE), 2017
- [16] Mücke, J.; Urbaneck, T.; Platzer, B.: Versuchsstand zum praxisnahen Test von Wandaufbauten für thermische Energiespeicher – Materialuntersuchung des Einblasdämmstoffs aus Polyurethan-Hartschaum-Partikeln. 24. Energie - Symposium Nutzung regenerativer Energiequellen und Wasserstofftechnik; Luschtinetz, T.; Lehmann, J. (Hrsg.), Stralsund, 2017, Tagungsband, S. 73-81. – ISBN 978-3-9817740-3-0
- [17] Urbaneck, T.; Findeisen, F.; Mücke, J.; Platzer, B.; Gensbaur, M.; Lang, S.; Bestenlehner, D.; Drück, H.; Herrmann, T.; Beyer, R.: Performance of Overground Hot Water Stores in Segmental Construction for Solar and District Heating Systems. 5th International Solar District Heating Conference, Graz (Österreich), 2018, Tagungsband.
- [18] Gensbaur, M.; Gohl, N.; Bestenlehner, D.; Drück, H.: Investigation of the integration of a newly developed overground hot water store in solar district heating system. 5th International Solar District Heating Conference, Graz (Österreich), 2018, Tagungsband.
- [19] Findeisen, F.; Kroll, U.; Urbaneck, T.; Platzer, B.: Radial Diffusers in Stratified Hot Water Stores: Simulation of Three-Dimensional Flow Behavior with CFD. 5th International Solar District Heating Conference, Graz (Österreich), 2018, Tagungsband.
- [20] Mücke, J.; Urbaneck, T.; Platzer, B.: Experimental Identification of Effective Thermal Conductivities in Wall Constructions with Blow-In Insulation for Thermal Energy Storage Tanks in Segmental Construction. 5th International Solar District Heating Conference, Graz (Österreich), 2018.
- [21] Findeisen, F.: Radiale Diffusoren in Warmwasserspeichern - Einfluss des Beladesystems auf Strömungsverhalten und Schichtungsqualität. Diss., TU Chemnitz, Fakultät für Maschinenbau, 2018. – ISBN 978-3-9811424-7-1
- [22] Urbaneck, T.; Findeisen, F.; Platzer, B.: Schwimmdach für thermische Energiespeicher mit integrierten Komponenten. 2016011514183500DE, Patentanmeldung vom 15.01.2016.
- [23] Michejew, M. A.: Grundlagen der Wärmeübertragung. 3. Auflage Berlin. VEB Verlag Technik 1964, 24; 84



16th International Symposium on District Heating and Cooling, DHC2018,
9–12 September 2018, Hamburg, Germany

The effect of discretization on the accuracy of two district heating network models based on finite-difference methods

J. Vivian^{a,*}, P. Monsalvete Álvarez de Uribarri^b, U. Eicker^b, A. Zarrella^a

^aUniversity of Padova, Dept. of Industrial Engineering, Via Venezia 1, Padova, 35131, Italy

^bUniversity of Applied Sciences Stuttgart, Center for Sustainable Energy Technology (*zafh.net*), Schellingstrasse 24, Stuttgart, 70174, Germany

Abstract

District heating and cooling (DHC) networks play a fundamental role in the transition towards a sustainable supply of heating and cooling, due to their ability to integrate any available source of thermal energy and to distribute it to the buildings. However, the use of renewable non-constant sources together with the variable heat demand of the buildings creates instable and pronounced transient operating conditions. In order to analyse the hydraulic and thermal behaviour and the dynamics occurring within these networks, several physical models based on different methods were proposed by previous researchers. Numerical thermal models based on finite difference methods (FDM) were pointed out to suffer from artificial diffusion when simulating the propagation of heat through the network. However, due to a wide and well-known literature on these methods, they are still used by many researchers and are therefore worth being investigated. The present paper analyses the effects of artificial diffusion using two models based on two different first-order approximation schemes. An ideal temperature wave and a dataset from a real DH network were used to evaluate the accuracy of the models using different discretization levels in time and space. As a result, the paper provides a framework to set a proper discretization when simulating a DHC network with FDM-based models considering both the expected accuracy and the computation time as criteria.

© 2018 The Authors. Published by Elsevier Ltd.

This is an open access article under the CC BY-NC-ND license (<https://creativecommons.org/licenses/by-nc-nd/4.0/>)

Selection and peer-review under responsibility of the scientific committee of the 16th International Symposium on District Heating and Cooling, DHC2018.

Keywords: District heating and cooling; models; finite-difference; accuracy

* Corresponding author. Tel.: +39 049 827 6879. E-mail address: jacopo.vivian@unipd.it

1. Introduction

District heating systems are characterized by temperature and velocity fluctuations, especially when unstable heat sources such as waste or solar heat are connected. Furthermore, in many DH systems, a temperature wave is deliberately produced to reduce the flow during peak consumption periods.

In literature two types of models for the simulation of the transient thermal behaviour in district heating systems can be found, namely the element-method and the node-method [1]. The element method finds an explicit solution to the transient heat balance equation by means of different possible finite difference schemes. It was shown that low-order schemes suffer of artificial numerical diffusion, thus resulting in abnormal smoothing of sharp temperature profiles [2] and that higher order schemes may instead bring to overshooting [3]. In the element method, the temperature at each time–step is determined only from the time–step before. The node method, instead, uses temperature values at different time–steps to determine the current temperature situation [2]. Pálsson et al. [1] implemented and tested two models based on the different two methods. The comparison revealed that, unless higher order schemes are used, the node method is superior to the element method at low Courant numbers, which corresponds to a situation with long district heating pipes and sharp temperature gradients which in turn require small time-steps. Furthermore, the computational effort seems to be also lower for the node-method. The application of the node method is however limited to tree-shaped networks [4].

Later on, another experiment was carried out to measure the temperature in a district heating pipeline under transient conditions [5]; both models were used to simulate the propagation of the temperature front and then compared against measured data. The comparison showed that the element-method predicts better the amplitude of the wave when the temperature changes rapidly, whereas the node-method predicts better the delay of the temperature front.

Nevertheless, to obtain acceptable results with the element-method, an adequate discretization in time and space must be done in the pre-processing phase [6].

In this paper we aim at investigating to which extent the performance of the models can be improved by a correct discretization of the network in relationship with the Courant number, and the impact that this discretization has on the accuracy of the results and the computational time.

Nomenclature		Subscripts	
c_p	Specific heat capacity (J/(kg K))	$adim$	dimensionless
Co	Courant number	i	i-th node
e	Error	j	j-th node
f	Performance indicator	g	Undisturbed ground
G	Mass flow rate (kg/s)	in	Inlet
K	Stiffness matrix	min	Minimum
L	Length (m)	n	Number of nodes
M	Mass matrix	out	Outlet
q	Vector of known terms	s	Wave start
T	Temperature (°C)	st	Steady state
T_{CPU}	CPU time (s)	Tr	Transient
U	radial heat transmission coefficient (W/(m ² K))	w	Wave width
v	Velocity (m/s)		
V	Volume (m ³)		
z	Depth (m)		
<i>Abbreviations</i>		<i>Greek symbols</i>	
FDM	Finite difference method(s)	τ	Time (s)
ODE	Ordinary differential equation	Ω	Pipe section perimeter (m)
		ρ	Density of the heat carrier fluid (kg/m ³)
		λ	Thermal conductivity (W/(m K))

2. Models

Both models describe the topology of the network using graph theory. The network is represented by a set of nodes and oriented branches and an adjacency matrix determines their mutual connections. Once the geometry is established, the pressure and temperature profiles are calculated.

When forced convection occurs, the velocity of the heat carrier fluid does not depend on the temperature distribution. Therefore, the hydraulic and thermal sub-models can be uncoupled. This allows the calculation of the mass flow rates and the pressures across the network in a first step; then, given the mass flow rates, the energy balance is performed to find out the temperature distribution.

Both models rely on the following assumptions:

- A slug flow is assumed, which implies that the velocity of the heat carrier fluid is uniform in the radial direction (one dimensional model)
- The heat conduction through the wall pipe along the axial direction is neglected
- The heat transfer in the radial direction considers the convection between the heat carrier fluid and the inner pipe surface, the thermal insulation of the pipe and the thermal resistance of the surrounding ground
- The heat capacity of the surrounding ground is neglected

2.1. NeMo

Due to the incompressible nature of the heat carrier fluid, the hydraulic problem can be described using only two equations: the continuity and the momentum equations. NeMo solves these equations using the SIMPLE method proposed by Patankar and Spalding [7]. The heat propagation in the network is then described by the energy balance performed on the volume of heat carrier fluid around the nodes of the network. The control volume of the *i*-th node corresponds to half of the heat carrier fluid volume of all the branches connected to it.

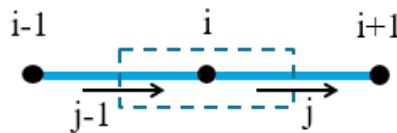


Fig. 1. Control volume of the *i*-th node.

Applying the energy balance to the node shown in Figure 1 leads to Equation (1):

$$\rho V_i c_p \frac{\partial T_i}{\partial \tau} = G_{j-1} c_p T_{j-1} - G_j c_p T_j - \frac{1}{2} (L_j \Omega_j U_j + L_{j-1} \Omega_{j-1} U_{j-1}) (T_i - T_\infty) \quad (1)$$

Where *G* are the mass flow rates, *V* is the volume of heat carrier fluid enclosed in the control volume, *Ω* is the perimeter of the pipe section, *U* is the radial heat transmission coefficient from fluid to the ground and *T_∞* is the undisturbed ground temperature. The temperature of the branches is then associated to the temperature of the corresponding upwind nodes, according to the well-known *upwind scheme*. Therefore, Equation (1) becomes:

$$\rho V_i c_p \frac{T_i^{(\tau)} - T_i^{(\tau-\Delta\tau)}}{\Delta\tau} = G_{j-1} c_p T_{i-1}^{(\tau)} - G_j c_p T_i^{(\tau)} - \frac{1}{2} (L_j \Omega_j U_j + L_{j-1} \Omega_{j-1} U_{j-1}) (T_i^{(\tau)} - T_g) \quad (2)$$

Equation (2) can be represented in matrix form as:

$$M \dot{T} = q - K T \quad (3)$$

Where *M* and *K* are the so-called *mass matrix* and *stiffness matrix*, respectively. The temperature at the inlet node is fixed (*Dirichlet condition*). The first-order ordinary differential equation (ODE) (3) is solved by the ODE solver

ode15s of Matlab, that implements the Numerical Differentiation Formulas (NDF) [8]. The mass matrix is singular as the inlet node is massless according to the Dirichlet condition. The missing mass is attributed to the adjacent node.

2.2. spHeat

Also in spHeat model the hydraulic balance is solved before calculating the temperature distribution. Pressures at the nodes and mass flows along the edges are calculated assuming steady-state conditions using the electrical analogy to formulate the conservation of mass and the conservation of momentum. The pressure losses are calculated using the Darcy-Weisbach equation and the system of non-linear equations is solved by means of the Newton-Raphson method. The energy balance accounts for the transient behaviour of the heat carrier fluid using a finite difference method. Each pipe is discretized into a set of elements of length L . Equation (1) is applied to each of these elements. Then, the temperature at the node is calculated using an explicit formulation, as in Equation (4).

$$\rho V_i c_p \frac{T_i^{(\tau)} - T_i^{(\tau-\Delta\tau)}}{\Delta\tau} = G_{j-1} c_p T_{j-1}^{(\tau-\Delta\tau)} - G_{j1} c_p T_j^{(\tau-\Delta\tau)} - L_i \Omega_i U_i (T_i^{(\tau-\Delta\tau)} - T_g) \quad (4)$$

While in NeMo the time step of the calculation is decided by MATLAB, in spHeat the time step is externally set by the user. Further explanations for the spHeat model can be found in [9].

3. Cases of study

This Paragraph describes the two cases of study (Section 3.1 and 3.2) used to test the accuracy of the models presented above.

3.1. Ideal square temperature wave

The first case study consists of an ideal square wave that propagates through a single pipe. The inlet temperature is 30°C in the first 40 minutes, then it is 50°C for the next 40 minutes and finally drops to 30°C and remains constant for the last 80 minutes. The characteristics of the case study are summarized in Table 1.

Table 1. Parameters and boundary conditions of the pre-insulated pipe.

Parameter	Units	Value
Pipe length, L	M	500
Internal diameter of the pipe, d_i	mm	80.0
External diameter of the pipe, d_e	mm	83.0
Diameter of casing, D	mm	150.0
Thermal conductivity of insulation, λ	W/(m K)	0.033
Thermal conductivity of the ground, λ_g	W/(m K)	2.0
Depth, z	m	1.0
Temperature of the undisturbed ground, T_g	°C	8.0
Initial temperature at inlet node	°C	30.0
Initial temperature at outlet node	°C	30.0
Mass flow rate (constant)	kg/s	2.74

3.2. Real case study: measured data

In the second case study the propagation of the temperature front in a 470 m long pre-insulated pipe, as logged during an experiment that was carried out by Ciuprinskas et al. [10] in the district heating system of Vilnius (Lithuania)

during May 1997. This dataset was already used by other researchers for comparing and validating thermal networks models [5,11]. A schematic view of the experimental site is depicted in Figure 2.

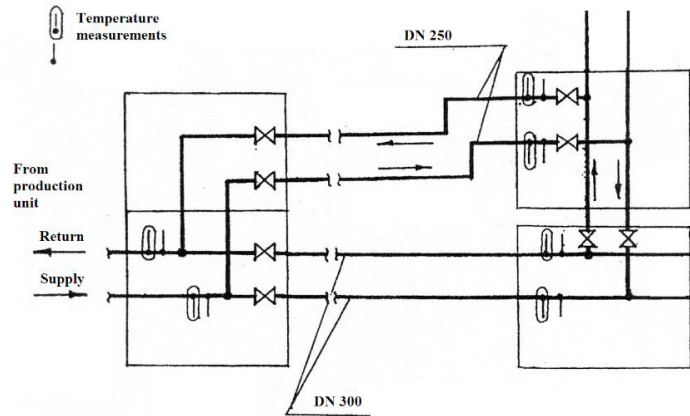


Fig. 2. Schematics of the experimental site (taken from [10]).

The inlet temperature and the mass flow rate of the supply pipe are set as boundary conditions and the resulting outlet temperature profile is compared with the measured values. Due to the very low fluid velocity in the considered period (about 0.036 m/s), it takes hours for the temperature front to reach the outlet of the pipe. This unusual condition affects the accuracy of the models as discussed in Gabrielaitiene [5]. The parameters and the boundary conditions used in the simulations are reported in Table 2. The time-step of simulation is 5 minutes and the sample-time of the dataset is 10 minutes. Values at times between two consecutive loggings were linearly interpolated.

Table 2. Parameters and boundary conditions of the pre-insulated pipe.

Parameter	Units	Value
Pipe length, L	m	470
Internal diameter of the pipe, d_i	mm	312.7
External diameter of the pipe, d_e	mm	323.9
Diameter of casing, D	mm	450.0
Thermal conductivity of insulation, λ	W/(m K)	0.033
Thermal conductivity of the ground, λ_g	W/(m K)	2.0
Depth, z	M	1.0
Temperature of the undisturbed ground, T_∞	°C	8.0
Initial temperature at inlet node	°C	67.7
Initial temperature at outlet node	°C	66.3
Mass flow rate (constant)	kg/s	2.65

4. Methods

The temperature profiles at pipe outlet obtained from the simulations were compared to the theoretical ones (see 3.1) and then to the measured ones (3.2). In order to facilitate the analysis, the dimensionless temperature suggested by [5] was used:

$$T_{out,adim} = \frac{(T_{tr} - T_{st})_{out}}{(T_{tr,max} - T_{st})_{in}} \quad (5)$$

where T_{tr} is the temperature output given by the model and T_{st} is the temperature during steady-state conditions. The normalized temperature T_{adim} is equal to 1 when the wave peak reaches the pipe outlet if no heat loss occurs in between, and is equal to 0 during steady state conditions –i.e. before and after the temperature wave arrives at pipe outlet. The Courant number is a dimensionless number that expresses the ratio between the physical velocity v (velocity of the water stream in each pipe element) and the “velocity of calculation”, i.e. the ratio between the length of each element Δx and the time step $\Delta \tau$ used by the numerical method to update the temperature distribution.

$$Co = \frac{v \Delta \tau}{\Delta x} \quad (6)$$

The Courant number indicates how fast the temperature information travels on the computational grid; the latter is regarded as the most important parameter as far as the performance of numerical methods for convective flow is concerned [1]. In explicit numerical schemes, a necessary condition for stability is $Co < 1$: the step size must be smaller than the time interval it takes for the flow to cross the smallest distance between two adjacent points [12].

Two indicators are used to measure the difference between simulated and actual temperature wave: the time of wave start t_s and the wave width Δt_w . As explained in Sections 3.1 and 3.2, a temperature profile was set at the inlet of a pipe and the resulting temperature profile at pipe outlet was then compared to a reference profile in order to assess the accuracy of the models. The reference temperature wave was represented in the first case study by the ideal temperature profile and in the second case study by the measured temperature profile.

The time of wave start was determined as the moment when the increment of temperature $T_{out,adim}$ between two consecutive steps was bigger than a certain value, set to 0 in the ideal case and to 0.0015 in the single-pipe case.

The wave width was instead determined as the time interval with the outlet temperature $T_{out,adim}$ above a certain value, that was set to 0.05 in the ideal case study and to 0.20 in the second one.

The error in the wave start e_s is the difference between the times at which the temperature front arrives at the pipe outlet with the model and in ideal/measured conditions. Here, for a given time step $\Delta \tau$ used by the solver the error is expressed as a function of the number of nodes n

$$e_s^{(n)} = t_s^{(n)} - t_s^{id} \quad (7)$$

An analogous definition holds true for the error in the wave width, that is the difference between the length (duration) of the wave between modelled and ideal/measured conditions

$$e_w^{(n)} = \Delta t_w^{(n)} - \Delta t_w^{id} \quad (8)$$

In order to evaluate the improvement in accuracy brought by a higher spatial discretization of the pipe, the accuracy improvement Δe was defined as the percent error between the model using n nodes and the error of the model using the minimum number of nodes considered (n_{min}). This indicator was used for both errors (e_s and e_w) as follows:

$$\Delta e_s^{(n)} = \frac{|e_s^{(n)} - e_s^{(n_{min})}|}{|e_s^{(n_{min})}|} \quad (9)$$

$$\Delta e_w^{(n)} = \frac{|e_w^{(n)} - e_w^{(n_{min})}|}{|e_w^{(n_{min})}|} \quad (10)$$

Finally, the indicator f was defined as the ratio between the accuracy improvement and the logarithm of the computational time T_{CPU} needed by the processor to find the solution. This indicator represents the efficiency of the model for each discretization level considered.

$$f_w^{(n)} = \frac{\Delta e_w^{(n)}}{\log_{10} T_{CPU}^{(n)}} \quad (11)$$

$$f_s^{(n)} = \frac{\Delta e_s^{(n)}}{\log_{10} T_{CPU}^{(n)}} \tag{12}$$

5. Results and discussion

5.1. Accuracy of the models: evaluation using an ideal square temperature wave

Figure 3 shows the outlet temperature of the step wave for both models, NeMo and spHeat. In both cases it can be seen that increasing the number of nodes reduces the artificial diffusion and leads to a better approximations of the theoretical wave. By comparing Figure 4(a) and 4(b), it seems that spHeat obtains a better fit on the amplitude of the wave.

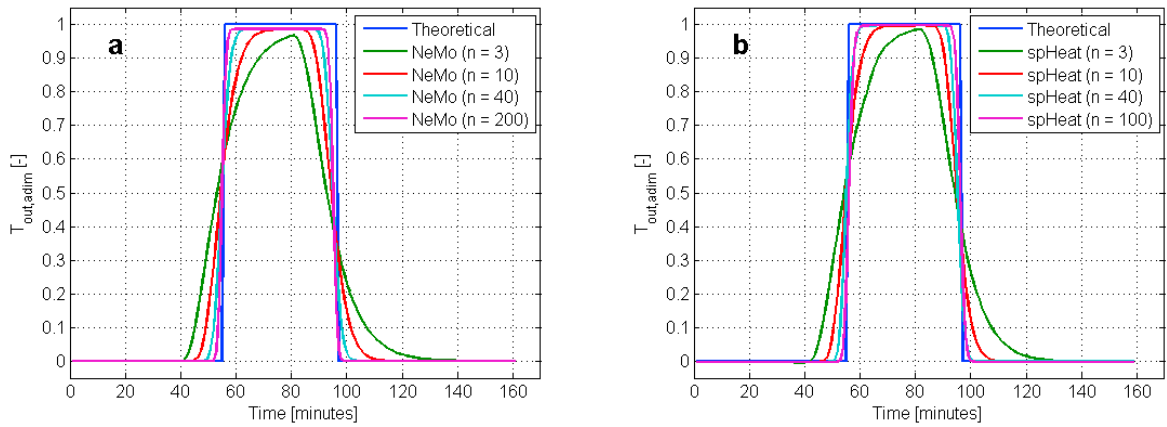


Fig. 3. Normalized temperature profiles with different discretization levels obtained with (a) NeMo and (b) spHeat.

Figure 4 plots the two errors (wave start and wave width) against the mean Courant number. Note that the MATLAB ODE Suite does not allow the user to set the time-step of the solver, but only to set an upper threshold. The solver used by NeMo is *ode15s*, that uses a variable step size. Therefore, the upper step size was fixed to the nominal values of $\Delta\tau = 3$ s and $\Delta\tau = 30$ s, and then after the simulation the average time-step $\Delta\tau$ was printed and used to calculate the mean Co *a posteriori*. In turn, spHeat does allow externally fixing the timestep, keeping it constant (and the Co number with it) during the complete period. On the flip side, spHeat does not support models with more than 100 nodes. Figure 4(a) confirms that, since NeMo is based on an implicit differentiation method, using $Co > 1$ does not imply convergence problems, and both errors decrease asymptotically with increasing Co , i.e. with increasing number of nodes. Figure 4(b) show the results obtained with spHeat. $Co > 1$ is not allowed on this model due to the explicit solution methodology. Nevertheless, the tendencies in the errors are similar to those of NeMo but with the maximum limit. For a given Courant number, the temperature profiles obtained with $\Delta\tau = 3$ s give a lower error than those obtained with $\Delta\tau = 30$ s. This is reasonable because the same Co number with a 10-times lower time-step implies solving the equation 10 times more, i.e. having a finer mesh in space and time.

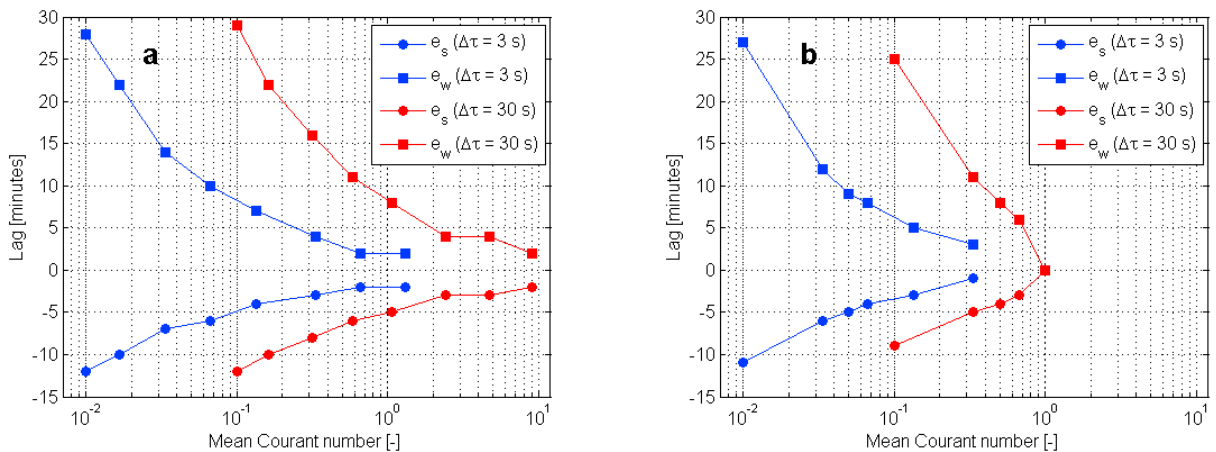


Fig. 4. Errors in wave start (e_s) and wave width (e_w) for (a) NeMo and (b) spHeat.

It must be noticed that spHeat provides a perfect match with the theoretical solution for $Co = 1$. This is specific for this case and is due to the fact that the output temperature in the theoretical solution is very similar to the input temperature. In spHeat when $Co = 1$, the same shape of the wave is propagated along the pipe, i.e. there is absence of diffusion. This is due to the fact that there is no mass or heat exchange between pipe elements. So, the only phenomena considered is the heat loss to the ground.

It is interesting to calculate the accuracy improvement Δe defined in Equations (9-10) and to relate it to the computational time needed by the processor to find the solution. Figure 5 shows that, while the accuracy improvements Δe_s and Δe_w tend to 1, the CPU time grows exponentially. Therefore, choosing a discretization level that gives an acceptable accuracy at a reasonable computational cost seems to be an efficient criterion to determine the discretization level in the pre-processing phase. To which extent the accuracy is “acceptable” and the simulation time is “reasonable” depends on the scope of the simulation and on the time constraints of the user, and can not be generalized here. However, the performance indicator f plotted in Figure 5 demonstrates that a “region” of high efficiency arises from the compromise between accuracy and CPU time.

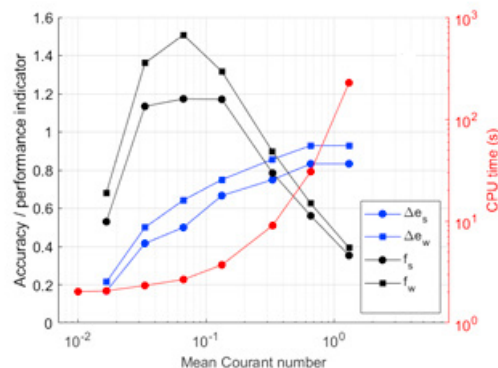


Fig. 5. Performance indicators of the first case study for NeMo simulations.

5.2. Accuracy of the models: evaluation using measured data

Figure 6 shows the temperature profiles measured at pipe outlet in the experiment described in Section 3.2 (dashed line) and those obtained by modelling the same pipe with the finite difference models. The effect of artificial diffusion, that is typical of FDM models based on first-order approximation, seems to drop significantly when a sufficiently high number of nodes is adopted. This consideration holds true for the wave start and for the wave width, whereas

overshoots seem to occur when the mesh gets too fine. In fact, NeMo seems to best approximate the amplitude of the wave with only 21 nodes, and to overestimate the peak for higher number of nodes. This result does not agree neither with the observations of the first case study nor with the theory, as overshoots are expected from models of higher order [3]. However, this overestimation of the peak might be caused by stratification effects that occurred during the experiment due to very low velocity of the flow, as discussed in a previous paper [11] and that are not considered within the models. Therefore, the wave amplitude cannot be used as an indicator of the models accuracy.

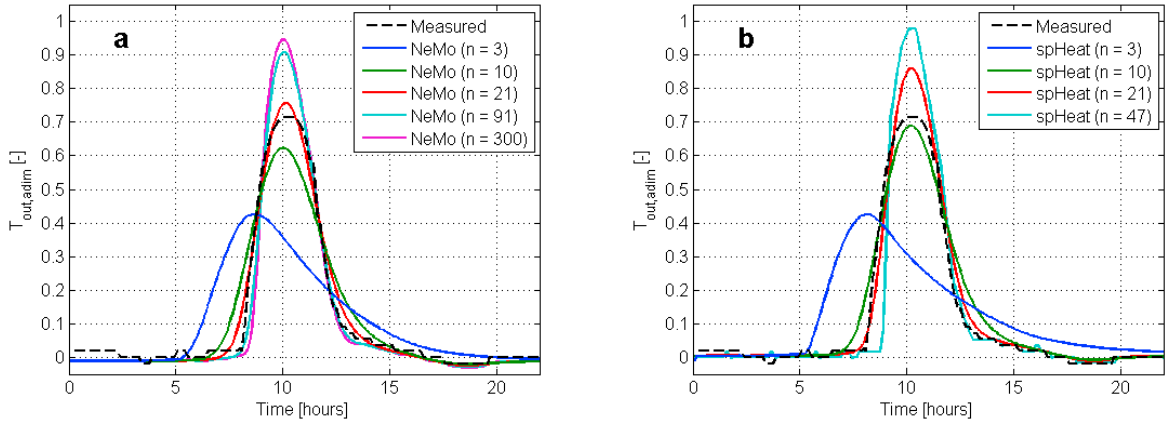


Fig. 6. Normalized temperature profiles obtained by (a) NeMo and (b) spHeat using different discretization of the pipe.

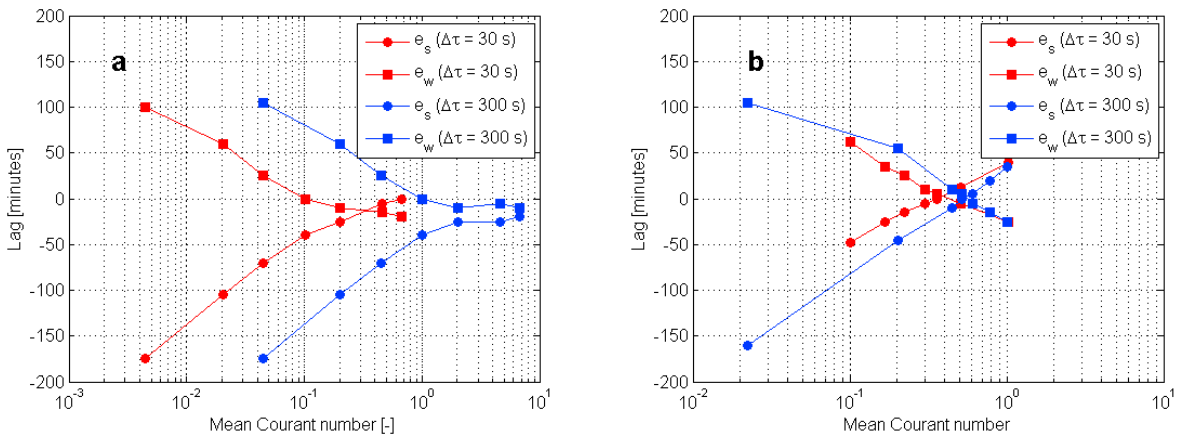


Fig. 7. Errors in wave start and wave width of (a) NeMo and (b) spHeat.

Figure 7(a) shows that the accuracy of NeMo has a similar trend compared to that discussed above for the ideal case study. In particular, the error in wave start shows the same tendency: it drops with increasing Courant number, with the approximation error asymptotically reaching 0 for very dense meshes. For a given Courant number, the lag decreases with increasing number of time steps. The errors in wave width have a similar trend, but above a certain Co the width becomes smaller than the measured one. Accordingly, an optimal accuracy arises at $Co = 0.1$ when the solver uses a 30 s time-step, and at $Co = 1$ when the time-step is 300 s. The explicit solution, Figure 7(b), follows a similar tendency, the error is reduced when the Co number increases but finding an optimum after which the errors start increasing again. In this sense, the implicit solution has the advantage that the best solutions can be found in a range, so the model is more adaptable to changes in the water velocity. This optimum of the explicit solution seems to be dependent also on the time step. As well as in the case of the implicit solution, the smaller the time-step, the

smaller the optimum Co number. Nevertheless, the deviations from the “ideal” behaviour shown in Figures 6(a) and 6(b) suggest that either some errors in the experiment might have occurred, or that the models don’t consider some physical effects that are occurring during the experiments. In fact, the tendency of the error in wave width seems to be in line with the one highlighted for the ideal temperature wave, but shifted downwards.

6. Conclusions

In the present work the effects of numerical diffusion obtained by two district heating network models based on two different first-order approximation schemes were analysed. The main difference between the models is that one (spHeat) uses an explicit method and the other (NeMo) is based on an implicit method. From the analysis of the results, the following conclusions can be drawn:

- Both models show good agreement with the outputs of a theoretical square temperature wave that propagates along a pipe, if the right Courant number is chosen for pipe discretization.
- When comparing the models with measurements of a real district heating pipe, some uncertainties appear and make the comparison less reliable. Nonetheless, both models show good agreement with the experimental data in crucial zones such as the moment when the temperature starts to rise and when it ends its drop.
- The comparison with the experimental data suggests that there is an optimum range of Courant number and the relationship between this and the calculation time step must be further studied.
- While the accuracy of the models increases linearly/asymptotically with the number of elements/nodes set by the user, the computational time has an exponential increase.

A performance indicator such as the one shown in the paper could be used in the pre-processing phase to determine the best trade-off between expected accuracy and computational cost.

Acknowledgements

The research activity of Jacopo Vivian was supported by the Interdepartmental Centre for Energy Technology and Economics “G. Levi Cases” of University of Padua and co-funded by the German Academic Exchange Service (DAAD), Grant Nr. 57210260. The authors gratefully acknowledge the Federal Ministry for Economic Affairs and Energy (BMWi) for providing financial support for the „EnVisaGe-Plus“ project, Grant Nr. 03ET1465A.

References

- [1] Pålsson H, Böhm B. Methods for planning and operating decentralized combined heat and power plants. PhD Thesis. Risø & DTU - Department of Energy Engineering (ET), 2000.
- [2] Benonysson A, Böhm B, Ravn HF. Operational optimization in a district heating system. *Energy Conversion and Management* 1995;36:297–314. doi:[https://doi.org/10.1016/0196-8904\(95\)98895-T](https://doi.org/10.1016/0196-8904(95)98895-T).
- [3] Grosswindhager S., Voigt A., Kozek M. *Linear Finite-Difference Schemes for Energy Transport in District Heating Networks*, Brno, Czech Republic: 2011.
- [4] Gabrielaitiene I, Sundén B, Kacianauskas R, Bohm B. Dynamic modeling of the thermal performance of district heating pipelines. *Advances in Heat Transfer Engineering, Proceedings, Begell House*; 2003, p. 185–192.
- [5] Gabrielaitiene I, Böhm B, Sunden B. Evaluation of Approaches for Modeling Temperature Wave Propagation in District Heating Pipelines. *Heat Transfer Engineering* 2008;29:45–56. doi:[10.1080/01457630701677130](https://doi.org/10.1080/01457630701677130).
- [6] Wang Y, You S, Zhang H, Zheng X, Zheng W, Miao Q, et al. Thermal transient prediction of district heating pipeline: Optimal selection of the time and spatial steps for fast and accurate calculation. *Applied Energy* 2017;206:900–10. doi:[10.1016/j.apenergy.2017.08.061](https://doi.org/10.1016/j.apenergy.2017.08.061).
- [7] Patankar, S. V., Spalding, D.B. A calculation procedure for heat, mass and momentum transfer in three-dimensional parabolic flows. *Int Journal of Heat and Mass Transfer* 1972;15:1787–806.
- [8] Shampine LF, Reichelt MW. The MATLAB ODE Suite. *SIAM Journal on Scientific Computing* 1997;18:1–22. doi:[10.1137/S1064827594276424](https://doi.org/10.1137/S1064827594276424).
- [9] Hassine IB, Eicker U. Impact of load structure variation and solar thermal energy integration on an existing district heating network. *Applied Thermal Engineering* 2013;50:1437–46. doi:<https://doi.org/10.1016/j.applthermaleng.2011.12.037>.
- [10] Ciuprinskas, K., Narbutis, B. Experiments on Heat Losses from District Heating Pipelines. *Energetika* 1999;2:35–40.
- [11] Giraud L, Baviere R, Vallée M, Paulus C. Presentation, Validation and Application of the DistrictHeating Modelica Library, 2015, p. 79–88. doi:[10.3384/ecp1511879](https://doi.org/10.3384/ecp1511879).
- [12] Courant R, Friedrichs K, Lewy H. On the Partial Difference Equations of Mathematical Physics. *IBM Journal of Research and Development* 1967;11:215–34. doi:[10.1147/rd.112.0215](https://doi.org/10.1147/rd.112.0215).



16th International Symposium on District Heating and Cooling, DHC2018,
9–12 September 2018, Hamburg, Germany

GIS-based optimisation for district heating network planning

Stanislav Chicherin^a, Anna Volkova^{b*}, Eduard Latõšov^b

^a*Omsk State Transport University, prospekt Karla Marksa 35, Omsk, 644046, Russian Federation*

^b*Tallinn University of Technology, Department of Energy Technology, Ehitajate tee 5, Tallinn, 19086, Estonia*

Abstract

Geographical features of district heating (DH) networks make geographic information system (GIS)-based tools attractive for the structural planning of local energy systems. Improving a DH network is a complex task, where many parameters should be taken into account, and it can only be achieved if sufficient data is available. An increase in data collection efficiency also contributes to the decision-making process. A GIS-based model of a DH network is proposed for the simultaneous improvement of both pipe routing and energy efficiency. A simple scenario-based formulation is used for combinations of heat investment decisions under uncertainty over specified planning horizons. One of the first steps of the methodology is the development by means of a cyclic decision support optimisation process. The optimisation is carried out within two types of constraints: the spatial (geographical) constraints and consumption profiles. The application of this method is demonstrated by the Omsk DH network analysis. It has been proven that it is possible to combine the DH network simulation with the optimization algorithm in order to illustrate several alternatives in real time. Through the evaluation of energy consumption and the optimisation of DH networks by means of a GIS-based model, the feedback was gathered and shared with the local DH company. Methods of analysis and visualisation for awareness building and decision support have also been demonstrated. The paper highlights the advantages of combining a GIS application with an energy demand forecasting model to create a tool aimed at supporting decision-making.

© 2018 The Authors. Published by Elsevier Ltd.

This is an open access article under the CC BY-NC-ND license (<https://creativecommons.org/licenses/by-nc-nd/4.0/>)

Selection and peer-review under responsibility of the scientific committee of the 16th International Symposium on District Heating and Cooling, DHC2018.

Keywords: multi-criteria analysis; decision support; optimisation; urban planning; pipes; GIS

* Corresponding author. Tel.: +3725582866

E-mail address: anna.volkova@ttu.ee

1. Introduction

At the moment, District Heating (DH) is a popular topic in the energy industry, as it deals with a sustainable and efficient means of delivering heat to buildings. DH challenges include introducing low temperatures, achieving low heat distribution loss, and using renewable and excess energy [1].

The development of DH systems enables the use of renewable heat energy, which may lead to the need for GIS-based planning [2]. GIS-based decision-support tools are rather useful in network sizing in terms of energy [3] and urban planning [4]. They are also used in electric power infrastructure planning, in particular, when it comes to optimising the type of electricity generation or distribution assets, as in [5].

Delangle et al. have developed a methodology to identify the best DH network expansion strategy with the help of modelling and optimisation [6]. Schweiger et al. emphasised that using a certain tool (Modelica®, in this case) is the primary way to speed up the work process [7]. Modelica® library, Apros®, IDA-ICE® Software, and Simulink® are discussed in [8], even though none of the above involve a simple scenario-based formulation for combinations of heat investment decisions under uncertainty over a finite planning horizon.

Ultimately, designing and evaluating DH networks introduces the idea of optimisation and decision-making methods into early stages of urban planning, using complicated multi-stage stochastic programming [9]. Bratoev et al. have studied urban design and planning, and decision-making processes by means of Collaborative Design Platform (CDP) [10]. In order to make it useful for decision-making, Wang et al. suggests optimising the network, prioritising sequence preparation for restoration of DH pipe segments [11].

An increase in the number of buildings, connected to DH in Denmark, forced researchers to combine various energy planning strategies into a spatial decision-support tool, a so-called heat atlas [12]. This works pretty much like GIS mapping [13], monitoring the current state. The new tool, developed by Verrilli et al. is mostly aimed at dealing with operational (not design) strategies [14].

The authors have developed GIS-based methodology for network design optimisation that is suitable for DHN parameters in Russia.

2. Methods

The first network optimisation algorithm is a mixed integer linear programming model implementing the AMPL programming language and the Cplex solver. The algorithm minimises the costs associated only with piping investments, but with high accuracy. Objective function is an equation (1) that is the general equation for the investment costs.

$$C^{inv} = \sum_{j=1}^m [(OMP_d + CCP_d) \cdot \delta_j \cdot L_j] + \sum_{k=1}^v [OMV + CCV] \quad (1)$$

,where

C^{inv} is investment costs (E per year);

OMP is **O**peration & **M**aintenance costs of **P**ipework (euro per unit per year);

OMV is **O**peration & **M**aintenance costs of **V**alve **V**aults (euro per unit per year);

CCP and CCV are **C**apital **C**osts of the **P**ipe and **V**alve **V**ault respectively (euro per unit per year);

δ_j is a binary variable, which equals one, only if two pipelines (supply and return) are assigned a single diameter value corresponding to the standard series;

L_j is the length of the pipe j ;

D -subscript means that a variable depends on a pipe dimension;

m is a number of isolated lengths of a DH network;

v - numbers of valve vaults.

The yearly investment costs are calculated using (2)

$$C_{an}^{inv} = (1 + F_m) \cdot An \cdot C^{inv} \quad (2)$$

,where

F_m is the maintenance factor;

C^{inv} - investment costs of a given device (euro per year);

Annuity for a given investment

$$An = \frac{r(1+r)^N}{(1+r)^N - 1} \quad (3)$$

,where

r is the interest rate;

N is the expected duration for a given investment (years).

Equations (1-2) are applied to the entire piping network. The optimisation is performed within the spatial (geographical) constraints and consumption profile constraint.

Constraints:

$$\sum_{i=1}^n Q_i = IN \quad (4)$$

$$Q_i \leq IN \cdot \delta_j \quad (5)$$

,where

Q_i is the heat demand by i -th node (MW);

IN is the amount of thermal energy at the zero point of flow distribution per unit of time (mostly at the connection point with the DH transmission network) (MW):

$$\sum_{j=1}^m \delta_j \leq 1 \quad (6)$$

The algorithm calculation steps are as follows:

- Plot a temperature graph
- Activate the “Find Path” mode
- Calculate dimensions
- Make adjustments

In many cases, the DH system has to fit in an existing city block, village or small town. Therefore, constraints such as the location coordinates of the buildings, the layout of the roads, space constraints in the existing technical galleries, as well as constraints associated with soil quality must be taken into account during the design stage. An analysis of the existing soil's condition should be conducted to determine the proper type of foundation for the pipes. Soil's data should include the elevation of each boring, groundwater levels, description of soil strata, including the group symbol assigned in accordance with the local regulations, and penetration data. Geologic conditions must make it possible to install the DH network at a reasonable cost, with an extra focus on bedrock formations, unstable soils, and other faults. Excessive traffic on construction sites or after completion of construction can lead to the collapse of the pipeline system. This kind of information is generally not made readily available, and thus is not used by the network optimisation algorithm. A so-called routing algorithm would therefore take over the task of generating a structure with all the buildings, all possible connections and spatial restrictions that can be read by the network optimization algorithm. Typically a pipe, for example, cannot be laid along the shortest path between two buildings, as it could potentially pass right across another building. There are certain routes that have to be followed, as shown below. Finally, specific laws or regulations might ban certain solutions if these solutions do not correspond with the given parameters.

The consumption profiles for the various energy services must be known in order to properly design the layout of the network, pipes, and other equipment. For heating and cooling, it is important to not only know the amount of energy required, but also the temperature level this energy needs to be provided at, and the required capacity. Usually, these profiles are not only difficult to obtain, they also contain major uncertainties due to their stochastic nature.

3. Case Study

The development of the aforementioned model was prompted by the opportunity to design a new DH system for the area chosen by the Municipality of Omsk in accordance with its Municipal Energy Plan. Fig. 1 shows the district with the buildings considered in the case study.



Fig. 1. An aerial image of the chosen area;

A CHP plant located outside the city supplies the heat to a residential area comprised of multi-storey apartment buildings, shops, schools, etc. The primary network is supplied by the high-temperature DH with the temperature 150 /70°C. In this case, the buildings are 3-4-storey high, and heat exchangers are used for domestic hot water (DHW) preparation in 5 buildings. Out of all possible measures to save energy, most have to do with the replacement of windows. After implementing the first energy-saving measures, the municipality decided to proceed with the thermal insulation of the roof and the floor below the building. Supply temperature is thermostatically modulated at 95, but return temperature stays at 70°C.

The main input data is presented in Table 1. Capital and operation & maintenance costs for reference scenario have been provided by the Omsk District Heating Supply Company

Table 1. Reference scenario.

DH network operating parameters	Actual characteristics	Financial assumptions
Energy generated (MW)	4.36	
Energy delivered (MW)	3.57	
Distribution heat losses (MW)	0.79	
Mass flow rate (kg/h)	38.4	
Average velocity (m/s)	1.1	
Supply pressure (bar)	7.1	
Return pressure (bar)	4.0	
Discount rate (%)	2-15	6

Interest rate (%)	7.25	8.25
Electricity price (€/kWh)	0.1-0.5	0.2
Developer connection costs (€/GJ)	5,700-8,000	6,000
DN150 pipe cost (€/m)	4,500-12,000	7,000
DN150 pipe maintenance (€/m)	0-100	40
Capital costs of a valve vault (€)	5,000-1,000,000	350,000
Operation costs of a valve vault (€)	0-10,000	2,000

Names of the objects (Fig. 1) correspond to the names in Fig. 2 and 3. For residential buildings the number of flats or the order number of a substation are given in brackets. The existing pipe sections are shown in yellow.

3. Results

The results are presented in Fig. 2 and 3.

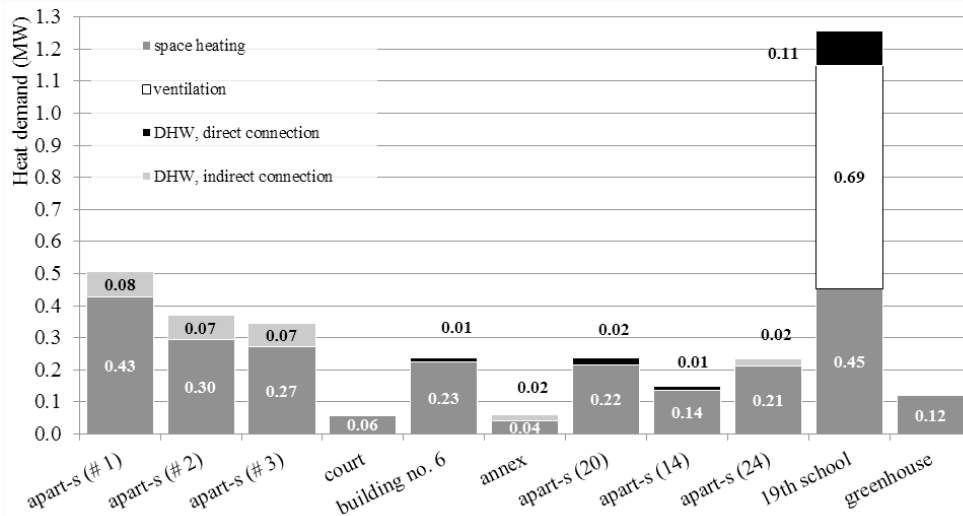


Fig. 2. Heat load characteristics (MW) of buildings in the area.

Fig. 2 shows the heat load profiles for each building. A significant demand for heating characterises school No.19, and the building in the upper-left corner (Fig. 3). It should be noted, that office and public buildings have an insignificant DHW demand. The network calculated is represented by thick lines in Fig. 3. For the hydraulic calculations of the DH system, pressure losses were modelled for each pipe segment and so the path with the greatest pressure loss can be determined. In the example shown, the network optimisation algorithm could locate the central technologies on any existing node, given that there is already a building located at that node. Some nodes are depicted without any buildings; these nodes represent, for example, road crossings: pipes usually follow the roads [15] so they could take a turn at a crossing to connect the two buildings. The suggested route is based on the proposal of a centralised network with a connection located at the top of the Figure. It is assumed that the next network connection is made next to the buildings on the right- and left-hand side, and then going right, where a connection is made with the court and building No. 6. A little lower, the route will connect to more than 1.2 MW.

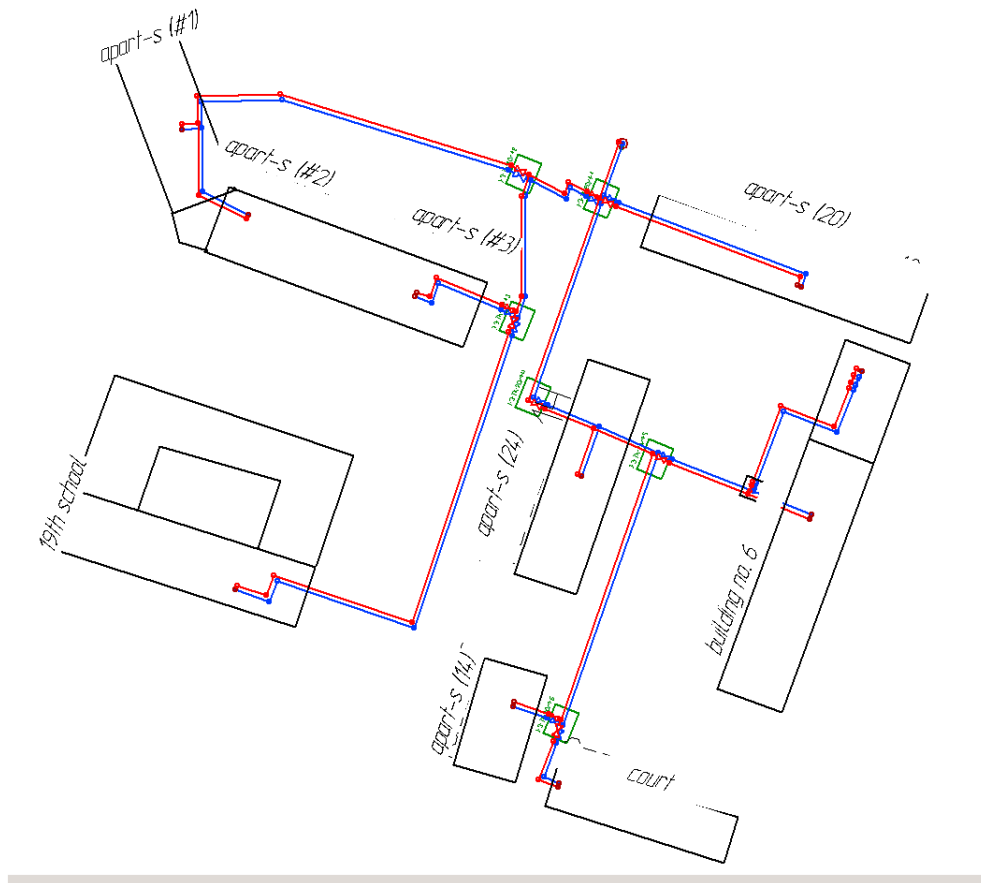


Fig. 3. The proposed DH network.

Using school no. 19 as the anchor site involves the installation of 561 m of isolated length. Therefore, the DH operator has to engage directly with the anchor-user and make sure the heating systems are controlled properly to minimise the risk of overflow in the network and consequent increase in return temperatures. After the optimisation is complete connecting all 11 buildings, including both extension and greenhouse (Fig. 2), it is determined that only 7 valve vaults will be installed, which will lead to a capital investment reduction by 15.786 thousand euro, and a 4.129 thousand euro decrease in operating costs for the case study. As a consequence, the total C^{inv} costs for the heat that must be transported from the DH transmission hub to the neighborhood decrease significantly, for instance, in the previous solution DN 150 is selected for the pipe length from I-3-TK-20/4-4 to I-3-TK-20/4-5 (now DN 100), while DN 50 is selected to connect apartment buildings #1..#3. In the optimised configuration, smaller diameters are installed, which leads to a significant reduction in investments necessary for the DH network, along with a small increase in pumping costs due to higher heat friction loss. A computerised maintenance management system, where pipes and components of the DH network are described and registered in a structured way, provides for more efficient maintenance work [3]. There are, however, some critical problems: this case study, in particular, has shown that the optimisation procedure can increase profits, while also leading to network configurations that are rather sensitive to changes in estimated heat demand patterns. In [10], some sections of the researched area may not be connected to a DN network due to low heat demand density.

4. Conclusions

The models similar to the ones presented in the paper are indicative of scenario development and can be useful in comparing the primary network solutions. The advantage of using this model is that it allows to obtain reliable results using relatively low-quality input data. One of the conclusions of this study is that there are many opportunities for possible expansion of DH in areas with mixed building stock. However, the final results largely depend on the input data, especially the cost of technology and pipelines. Besides, the optimum has to be found for both the requested accuracy (especially for the network optimisation algorithm) and the available input accuracy (e.g., consumption profiles). Another way to use GIS in a DH network is for documentation. Once a network has been documented in a GIS, more features can be added to simplify and increase operational efficiency for several areas, such as maintenance, planning, pipe design and consumer management.

In any case, the financial optimisation aimed at achieving the lowest costs possible vouches for the competitiveness and the advantages of the DH system expansion.

Acknowledgements

This research was supported by the Government of the Russian Federation via Project No. 860 (August 8, 2017 Decree) and by the Estonian Ministry of Education and Research (base funding project B55). The authors would like to thank the Omsk District Heating Supply Company ('Omsk RTS', JSC) for the cooperation and information provided.

References

- [1] Volkova A, Mašatin V, Siirde A. "Methodology for evaluating the transition process dynamics towards 4th generation district heating networks". *Energy* 150 (2018): 253–61.
- [2] Resch B, Sagl G, Törnros T, Bachmaier A, Eggers J-B, Herkel S, et al. "GIS-Based Planning and Modeling for Renewable Energy: Challenges and Future Research Avenues". *International Journal of Geo-Information* 3(2) (2014):662-692.
- [3] Van Hoesen J, Letendre S. "Evaluating potential renewable energy resources in Poultney, Vermont: A GIS-based approach to supporting rural community energy planning". *Renew Energy* 35 (2010):2114–22.
- [4] Pol O, Schmidt R-R. "Advanced District Heating and Cooling (DHC) Systems", (2016) Elsevier Science.
- [5] Eroglu H, Aydin M. "Optimization of electrical power transmission lines' routing using AHP, fuzzy AHP, and GIS". *Turkish Journal of Electrical Engineering and Computer Sciences* 23(5) (2015):1418-1430.
- [6] Delangle A, Lambert RSC, Shah N, Acha S, Markides CN. "Modelling and optimising the marginal expansion of an existing district heating network". *Energy* 140 (2017):209–23.
- [7] Schweiger G, Larsson P-O, Magnusson F, Lauenburg P, Velut S. "District heating and cooling systems – Framework for Modelica-based simulation and dynamic optimization". *Energy* 137 (2017):566–78. doi:10.1016/J.ENERGY.2017.05.115.
- [8] del Hoyo Arce I, Herrero López S, López Perez S, Rämä M, Klobut K, Febres JA. "Models for fast modelling of district heating and cooling networks". *Renew Sustain Energy Rev* 82 (2018):1863–73. doi:10.1016/J.RSER.2017.06.109.
- [9] Lambert RSC, Maier S, Polak JW, Shah N. "Optimal phasing of district heating network investments using multi-stage stochastic programming". *Int J Sustain Energy Plan Manag* 9 (2016):57–74. doi:10.5278/ijsepm.2016.9.5.
- [10] Bratoev I, Bonnet C, A. C, Schubert G, Petzold F, Auer T. "Designing and Evaluating District Heating Networks with Simulation Based Urban Planning". URBANCEQ-2017 Int. Conf. Urban Comf. Environ. Qual. 28-29 Sept. 2017, Genova, Italy, (2017):167–74.
- [11] Wang H, Wang H, Zhou H, Zhu T. "Modeling and optimization for hydraulic performance design in multi-source district heating with fluctuating renewables". *Energy Convers Manag* 156 (2018):113–29. doi:10.1016/J.ENCONMAN.2017.10.078.
- [12] Petrovic SN, Karlsson KB. "Danish heat atlas as a support tool for energy system models". *Energy Convers Manag* 87 (2014):1063–76. doi:10.1016/j.enconman.2014.04.084.
- [13] Wyrwa A, Chen Y. "Mapping Urban Heat Demand with the Use of GIS-Based Tools". *Energies* 10 (2017):1–15.
- [14] Verrilli F, Srinivasan S, Gambino G, Canelli M, Himanka M, Vecchio C Del, et al. "Model Predictive Control-Based Optimal Operations of District Heating System With Thermal Energy Storage and Flexible Loads". *IEEE Trans Autom Sci Eng* 14 (2017):547–57. doi:10.1109/TASE.2016.2618948.
- [15] Chicherin, Stanislav. "Unlocking a potential of district heating network efficient operation and maintenance by minimizing the depth of a trench system". *Bull. Tomsk Polytech. Univ. Geo Assets Eng.* 328(9) (2017):49–56.